A11101 565590

NAT'L INST. OF STAND & TECH R.I.C.

A11105 887643

NIST
PUBLICATIONS

NBS SPECIAL PUBLICATION 651

U.S. DEPARTMENT OF COMMERCE/National Bureau of Standards

Wind and Seismic Effects

Proceedings of the Fourteenth Joint UJNR Panel Conference

QC
100
.U57
651
1983
C.2

NATIONAL BUREAU OF STANDARDS

The National Bureau of Standards[1] was established by an act of Congress on March 3, 1901. The Bureau's overall goal is to strengthen and advance the Nation's science and technology and facilitate their effective application for public benefit. To this end, the Bureau conducts research and provides: (1) a basis for the Nation's physical measurement system, (2) scientific and technological services for industry and government, (3) a technical basis for equity in trade, and (4) technical services to promote public safety. The Bureau's technical work is performed by the National Measurement Laboratory, the National Engineering Laboratory, and the Institute for Computer Sciences and Technology.

THE NATIONAL MEASUREMENT LABORATORY provides the national system of physical and chemical and materials measurement; coordinates the system with measurement systems of other nations and furnishes essential services leading to accurate and uniform physical and chemical measurement throughout the Nation's scientific community, industry, and commerce; conducts materials research leading to improved methods of measurement, standards, and data on the properties of materials needed by industry, commerce, educational institutions, and Government; provides advisory and research services to other Government agencies; develops, produces, and distributes Standard Reference Materials; and provides calibration services. The Laboratory consists of the following centers:

Absolute Physical Quantities[2] — Radiation Research — Chemical Physics — Analytical Chemistry — Materials Science

THE NATIONAL ENGINEERING LABORATORY provides technology and technical services to the public and private sectors to address national needs and to solve national problems; conducts research in engineering and applied science in support of these efforts; builds and maintains competence in the necessary disciplines required to carry out this research and technical service; develops engineering data and measurement capabilities; provides engineering measurement traceability services; develops test methods and proposes engineering standards and code changes; develops and proposes new engineering practices; and develops and improves mechanisms to transfer results of its research to the ultimate user. The Laboratory consists of the following centers:

Applied Mathematics — Electronics and Electrical Engineering[2] — Manufacturing Engineering — Building Technology — Fire Research — Chemical Engineering[2]

THE INSTITUTE FOR COMPUTER SCIENCES AND TECHNOLOGY conducts research and provides scientific and technical services to aid Federal agencies in the selection, acquisition, application, and use of computer technology to improve effectiveness and economy in Government operations in accordance with Public Law 89-306 (40 U.S.C. 759), relevant Executive Orders, and other directives; carries out this mission by managing the Federal Information Processing Standards Program, developing Federal ADP standards guidelines, and managing Federal participation in ADP voluntary standardization activities; provides scientific and technological advisory services and assistance to Federal agencies; and provides the technical foundation for computer-related policies of the Federal Government. The Institute consists of the following centers:

Programming Science and Technology — Computer Systems Engineering.

[1]Headquarters and Laboratories at Gaithersburg, MD, unless otherwise noted; mailing address Washington, DC 20234.
[2]Some divisions within the center are located at Boulder, CO 80303.

NATIONAL BUREAU
OF STANDARDS
LIBRARY
MAY 31 1983

Wind and Seismic Effects

Proceedings of the 14th Joint
Panel Conference of the U.S.-Japan
Cooperative Program in
Natural Resources

Editors:
R.M. Chung
H.S. Lew
W.D. Kovacs

Center for Building Technology
National Engineering Laboratory
National Bureau of Standards
Washington, DC 20234

NBS special publication

U.S. DEPARTMENT OF COMMERCE, Malcolm Baldrige, Secretary
NATIONAL BUREAU OF STANDARDS, Ernest Ambler, Director

Issued April 1983

Library of Congress Catalog Card Number: 83-600713

National Bureau of Standards Special Publication 651
Natl. Bur. Stand. (U.S.), Spec. Publ. 651, 716 pages (April 1983)
CODEN: XNBSAV

U.S. GOVERNMENT PRINTING OFFICE
WASHINGTON: 1983

For sale by the Superintendent of Documents, U.S. Government Printing Office, Washington, DC 20402
Price
(Add 25 percent for other than U.S. mailing)

PREFACE

The U.S.-Japan Cooperative Program in Natural Resources (UJNR) was established in 1964 for the exchange of technical information and experience mutually beneficial to the economics and welfare of both countries. The Panel on Wind and Seismic Effects held its first joint meeting in 1969 in Tokyo, Japan. The joint meeting has been held annually ever since, alternately in Japan and the U.S.

The Fourteenth Joint Meeting was held in Washington, D.C. on May 17-20, 1982. Under five themes, thirty-nine technical papers were presented and discussed. Ten task committees on the Panel also held their meetings during this period. Prior to the joint meeting, the third U.S.-Japan Joint Workshop on Repair and Retrofit of Structures was held on May 13-15, 1982 at San Francisco, California under the sponsorship of Task Committee C - Repair and Retrofit on Existing Structures.

These proceedings include the program of the Fourteenth Joint Meeting, the formal panel resolutions, the technical papers, and the task committee reports. The text of the papers has been edited for clarity.

Preparation of the proceedings was partially supported by funds from the National Science Foundation.

H. S. Lew, Secretary
U.S. Panel on Wind
and Seismic Effects

SI CONVERSION UNITS

In view of the present accepted practice for wind and seismic technology, common units of measurements were used throughout this publication. In recognition of the position of the United States as a signatory to the General Conference on Weights and Measures, which gave official status to the International System of Units (SI) in 1960, the table below is presented to facilitate conversion to SI Units. Readers interested in making further use of the coherent system of SI units are referred to: NBS SP 330, 1977 Edition, The International System of Units; and ASTM Standard for Metric Practice.

TABLE OF CONVERSION FACTORS TO SI UNITS

	Customary Units	International (SI) UNIT	Conversion Approximate
Length	inch (in)	meter (m)[a]	1 in = 0.0254 m*
	foot (ft)	meter (m)	1 ft = 0.3048 m*
Force	pound (lbf)	newton (N)	1 lbf = 4.48 N
	kilogram (kgf)	newton (N)	1 kgf = 9.807 N
Pressure or Stress	pound per square inch (psi)	newton/per square meter	1 psi = 6895 N/m^2
	kip per square inch (ksi)	newton per square meter	1 ksi = 6895 x 10^3 N/m^2
Energy	inch•pound (in-lbf)	joule (J)	1 in•lbf = 0.1130 J
	foot•pound (ft-lbf)	joule (J)	1 ft•lbf = 1.3558 J
Torque or Bending Moment	pound•inch	newton-meter (N•m)	1 lbf•in = 0.1130 N•m
	pound•foot (lbf-ft)	newton-meter (N•m)	1 lbf•ft = 1.3558 N•m
Weight	pound (lb)	kilogram (kg)	1 lb = 0.4536 kg
Unit Weight	pound per cubic foot (pcf)	kilogram per cubic meter (kg/m^3)	1 pcf = 16.018 kg/m^3
Velocity	foot per second (ft/sec)	meter per second (m/s)	1 ft/s = 0.3048 m/s
Acceleration	foot per second square (ft/s^2)	meter per second square (m/s^2)	1 ft/s^2 = 0.3048 m/s^2

[a] Meter may be subdivided. A centimeter (cm) is 1/100 m and a millimeter (mm) is 1/1000 m.

* Exactly

ABSTRACT

The Fourteenth Joint Meeting of the U.S. - Japan Panel on Wind and Seismic Effects was held in Washington, D.C., United States from May 17 through 20, 1982. This publication, the proceedings of the Joint Meeting, includes the program, list of members, formal resolutions, technical papers, and the task committee reports. Subjects covered in the papers presented to the panel include (1) characteristics of strong winds, (2) wind loads on structures and design criteria, (3) earthquake ground motions and dynamic analysis of embankment dams, (4) soil liquefaction studies and methods to improve liquefaction resistance (5) seismic loads on structures and design criteria, (6) stress analyses of pipelines during earthquakes, (7) full-scale seismic experiments, (8) earthquake hazard reduction program, (9) use of the microcomputer for earthquake studies, (10) quantitative evaluation of damages caused by winds and earthquakes, and (11) tsunami research projects.

Keywords: Accelerograph; codes; design criteria; disaster; earthquakes; earthquake hazards; geotechnical engineering; ground failures; liquefaction; pipeline; seismicity; solids; standards; structural engineering; structural response; tsunami; wind loads; and winds.

CONTENTS

	Page
PREFACE	iii
SI CONVERSION	iv
ABSTRACT	v
PROGRAM OF THE JOINT MEETING	vii
OPENING SESSION	x
LIST OF MEMBERS	xvi
PHOTOGRAPHS OF PARTICIPANTS	xxv
FORMAL RESOLUTIONS	xxvi
THEMES AND TECHNICAL PAPERS	1
Theme I: WIND ENGINEERING	1
Effect of Solidity of Trusses on Unsteady Aerodynamic Forces of Stiffening Trusses-Girders T. Okubo, N. Narita, K. Yamamoto, H. Sato	1
Field Studies on the Pasco-Kennewick Cable Stayed Bridge M. C. C. Bampton	20
Wind Load on Solar Water Heaters H. Okada and T. Murota	34
Environmental Monitoring Program for the National Strategic Petroleum Reserve C. B. Barrientos (Manuscript not available)	-
Theme II: EARTHQUAKE ENGINEERING - PART 1	
Estimation of Response Spectral Values as Functions of Magnitude, Distance, and Site Conditions W. B. Joyner and D. M. Boore	53
Reconsideration of the Input Waves for Dynamic Analysis K. Ohtani	75
Some New Processing Techniques for the Imperial Valley 1979 Aftershocks A. G. Brady	81
Dense Instrument Array Observation of the Public Works Research Institute and Analyses of Some Records T. Okubo, T. Arakawa, and K. Kawashima	95
Gravel Drains as a Countermeasure to Liquefaction of the Ground Y. Sasaki and E. Taniguchi	124
Volume Change and Excess Pore Pressure Buildup as a Function of Degree of Saturation of Sands During Resonant Column Testing R. Chung, F. Yokel, and E. Anderson	150
Estimation Procedure of Liquefaction Potential and Its Application to Earthquake Resistant Design T. Iwasaki, T. Arakawa, K. Tokida, and T. Kimata	172

CONTENTS (Continued)

Page

THEME II: EARTHQUAKE ENGINEERING - PART 2

Coupled Hydrodynamic Response Characteristics and Water Pressures of Large Composite Breakwaters 193
T. Uwabe, S. Noda, and H. Tsuchida

Dynamic Analysis of Embankment Sections, Richard B. Russell Dam 218
A. G. Franklin and M. E. Hynes-Griffen

Pipe Stresses During Earthquakes Based on a Two-Dimensional Seismometer Array Observation 242
H. Tsuchida, K. Minami, O. Kiyomiya, and S. Noda

Buckling and Rupture Failure in Pipelines Due to Large Ground Deformations 259
T. Ariman

Experimental Studies on Seismic Behavior of Structural Members Using a Dynamic Structural Testing Facility at PWRI 272
E. Kuribayashi, T. Iwasaki, R. Hagiwara, and T. Hadate

Report of the Urakawa-oki Earthquake of March 21, 1982 325
T. Yasue, T. Iwasaki, Y. Sasaki, H. Asanuma, and T. Nakajima

Linear versus Nonlinear Behavior of Cable Stayed Bridges 343
J. F. Fleming

Behavior of Concrete-Filled Steel Tubes 361
N. Narita, S. Saeki, M. Kanai, and T. Ohsio

Microcomputer for Earthquake Studies 402
S. K. Takahashi and J. V. Tyrrell

THEME III: STORM SURGE

A Tsunami Research Plan for the United States 416
E. Bernard

Digital Data Services for Tsunamis and Engineering Seismology 426
J. Lander

THEME IV: U.S.-JAPAN COOPERATIVE PROGRAM

Construction of a Full-Scale Reinforced Concrete Test Specimen 433
J. K. Wright

Progress Report on the Full-Scale Seismic Experiment of a Seven-Story Reinforced Concrete Building -- Part 1 Pseudo-Dynamic Test Before Repair -- 440
S. Okamoto, S. Nakata, M. Yoshimura, Y. Kigagawa, and T. Kaminosono

Progress Report on the Full-Scale Seismic Experiment of a Seven-Story Reinforced Concrete Building -- Part 2 Pseudo-Dynamic Test Before Repair -- 457
S. Okamoto, S. Nakata, M. Yoshimura, Y. Kigagawa, and T. Kaminosono

Tests of Planar Wall Assemblies Under In-Plane Static Reversing Loads 476
B. J. Morgan, H. Hiraishi, and W. G. Corley

Research Program on the Full-Scale Seismic Experiments of Steel Buildings 489
M. Watabe and H. Yamanouchi

CONTENTS (Continued)

Page

THEME V: TECHNICAL COOPERATION WITH DEVELOPING COUNTRIES

United States Foreign Assistance Program on Tsunami Hazard 507
G. T. Hebenstreit and P. F. Krumpe

Technical Cooperation in Developing Countries On Earthquake Engineering 522
K. Kamimura, M. Watabe, Y. Ishiyama, and Y. Yamazaki

Incremental Expansion and Aseismic Design of Low-Cost Housing in Sites and Services Projects 532
E. Simiu

PAPERS NOT PRESENTED BUT INCLUDED IN THE PROCEEDINGS

Storm Surge Forecasting 538
C. S. Barrientos

Vibratory Cone Penetrometer to Assess the Liquefaction Potential of the Ground 541
Y. Sasaki and Y. Koga

Direct Evaluation Method for Floor Response Spectra 556
M. Watabe

A Procedure for Estimating Indirect Effects of Earthquakes on Economy 565
E. Kuribayashi, T. Iwasaki, and T. Nakajima

Dynamic Tests of Rockfill Dam Models 587
N. Matsumoto, M. Totoda, and M. Shiga

The Connecting Method for Pile Head and Footing of Pile Foundations Subjected to a Horizontal Load 600
N. Narita, H. Asanuma, J. Fukui, and Y. Yamamoto

On the Status of In Situ Strong Ground Motion and Structural Response Investigations 617
C. Rojahn and R. D. Borcherdt

Storm Surge Defense Works and Related Researches in Japan 655
Y. Goda and H. Hashimoto

APPENDIX A - TASK COMMITTEE REPORTS 669

FOURTEENTH JOINT MEETING

OF THE

U.S.-PANEL ON WIND AND SEISMIC EFFECTS

May 17 - 20, 1982

at the

National Bureau of Standards

MONDAY - May 17 Lecture Room B, Administration Building

OPENING SESSION

10:00 A.M. Call to order by Dr. H. S. Lew, Secretary, U.S. Panel
Remarks by Dr. John W. Lyons, Director, National Engineering Laboratory, National Bureau of Standards
Remarks by Mr. Hiroto Ishida, Science Counselor, Embassy of Japan
Remarks by Dr. Edward O. Pfrang, Chairman, U.S. Panel
Remarks by Dr. Tadayoshi Okubo, Chairman, Japanese Panel

10:30 A.M. Introduction of U.S. Panel Members by U.S. Chairman and Japanese Panel Members by Japanese Chairman

10:45 A.M. Election of Conference Chairman

10:50 A.M. Adoption of Agenda

11:00 A.M. Group Photograph

11:30 A.M. Lunch - Dining Room C

THEME I - WIND ENGINEERING

Chairman: Dr. Edward O. Pfrang

1:00 P.M. Effect of Solidity on Unsteady Aerodynamic Forces for Stiffening Trusses - T. Okubo, N. Narita, K. Yamamoto, H. Sato

Speaker: T. Okubo

1:20 P.M. Field Studies on the Pasco-Kennewick Cable Stayed Bridge - M. C. C. Bampton

Speaker: H. Bosh

1:40 P.M. Wind Load on Solar Hot Water Heaters - H. Okada and T. Murota

Speaker: S. Nakata

2:00 P.M. Environmental Monitoring Program for the National Strategic Petroleum Reserve - C. B. Barrientos

Speaker: C. B. Barrientos

2:20 P.M. Discussion

2:40 P.M. Break

THEME II - EARTHQUAKE ENGINEERING: PART 1

Chairman: Dr. Tadayoshi Okubo

3:00 P.M. Estimation of Response Spectra Values as Functions of Magnitude, Distance and Site Conditions - W. B. Joyner and D. M. Boore

Speaker: W. B. Joyner

3:20 P.M. Reconsideration of the Input Waves for Dynamic Analysis - K. Ohtani

Speaker: K. Ohtani

3:40 P.M. Some New Processing Techniques for the Imperial Valley 1979 Aftershocks - A. G. Brady

Speaker: A. G. Brady

4:00 P.M. Dense Instrument Array Observation of the Public Works Research Institute and Analysis of Some Records - T. Okubo, T. Arakawa, and K. Kawashima

Speaker: T. Okubo

4:20 P.M. Discussion

4:40 P.M. Gravel Drains as a Countermeasure to Liquefaction of the Ground - Y. Sasaki and E. Taniguchi

Speaker: E. Taniguchi

5:00 P.M. Volume Change and Pore Pressure Buildup as a Function of Degree of Saturation of Sands During Cyclic Loading - R. Chung, F. Yokel, and E. Anderson

Speaker: R. Chung

5:20 P.M. Estimation Procedure of Liquefaction Potential and Its Application to Earthquake Resistance Design - T. Iwasaki, T. Arakawa, K. Tokida, and T. Kimata

Speaker: T. Iwasaki

5:40 P.M. Discussion

6:00 P.M. Adjorn

TUESDAY - May 18 Lecture Room B, Administration Building

THEME II - EARTHQUAKE ENGINEERING: Part 2

Chairman: Dr. Edward O. Pfrang

9:00 A.M. Coupled Hydrodynamic Response Characteristics and Water Pressures of Large Composite Breakwaters - T. Uwabe, S. Noda, and H. Tsuchida

Speaker: S. Noda

9:20 A.M. Dynamic Analysis of Embankment Sections, Richard B. Russell Dam - A. G. Franklin and M. E. Hynes-Griffen

Speaker: M. E. Hynes-Griffen

9:40 A.M. Pipe Stresses During Earthquakes Based on Two Dimensional Seismometer Array Observation - H. Tsuchida K. Minami O. Kiyomiya, and S. Noda

Speaker: S. Noda

10:00 A.M. Break

10:20 A.M. Buckling and Rupture Failure in Pipelines Due to Large Ground Deformations - T. Ariman

Speaker: T. Ariman

10:40 A.M. Experimental Studies on Seismic Behavior of Structural Members Using a Dynamic Structural Testing Facility at PWRI - E. Kuribayashi, T. Iwasaki, T. Hadate, and R. Hagiwara

Speaker: T. Iwasaki

11:00 A.M. Discussion

11:20 A.M. Report of the Urakawa-oki Earthquake of March 21, 1982 - T. Yasue, T. Iwasaki, Y. Sasaki, H. Asanuma, and T. Nakajima

Speakers: T. Iwasaki
S. Okamoto
K. Ohtani

11:50 A.M. Discussion

12:00 NOON Lunch - Dining Room C

1:30 P.M. Seismic Response of Cable Stayed Bridges - J. Fleming and J. D. Zenk

Speaker: J. Fleming

1:50 P.M. Behavior of Concrete-Filled Steel Tubes - N. Narita, S. Saeki, and M. Kanai

Speaker: T. Okubo

2:10 P.M. Microcomputer for Earthquake Studies - S. K. Takahashi

Speaker: S. K. Takahashi

2:30 P.M. Discussion

2:40 P.M. Break

THEME IV - U.S.-JAPAN COOPERATIVE PROGRAM

Chairman: Dr. Tadayoshi Okubo

3:00 P.M. Construction and Testing of a Full-Scale Reinforced Concrete Specimen - J. K. Wight

Speaker: J. K. Wight

3:20 P.M. A Progress Report on the Full-Scale Seismic Experiment of a Seven-Story Reinforced Concrete Building - S. Okamoto, S. Nakata, T. Kaminosono, M. Yoshimura, and Y. Kitakawa

Part 1. Pseudodynamic Tests Before Repair

Speaker: T. Kaminosono

3:45 P.M. Part 2. Pseudodynamic Tests After Repair

Speaker: S. Nakata

4:10 P.M. Discussion

4:30 P.M. Tests of Planar Wall Assemblies Under In Plane Static Reversing Loads - B. Morgan, H. Hirashi, and W. G. Corley

Speaker: B. Morgan

4:50 P.M. Discussion

5:00 P.M. Research Program on the Full-Scale Seismic Experiments of Steel Buildings - M. Watabe and H. Yamanouchi

Speaker: S. Okamoto

5:20 P.M. Status of U.S. Research Program on Full-Scale Steel Buildings - S. C. Liu

Speaker: S. C. Liu

5:40 P.M. Discussion

6:00 P.M. Adjourn

WEDNESDAY - May 19 Lecture Room B, Administration Building

THEME III - STORM SURGE

Chairman: Dr. Edward O. Pfrang

9:00 A.M. A Tsunami Research Plan for the United States - E. Bernard

Speaker: E. Bernard

9:20 A.M. Digital Data Services for Tsunamis and Engineering Seismology - J. Lander

Speaker: J. Lander

9:40 A.M. Discussion

9:50 A.M. Break

THEME V - TECHNICAL COOPERATION WITH DEVELOPING COUNTRIES

Chairman: Dr. Tadayoshi Okubo

10:10 A.M. United State Foreign Assistance Program on Tsunami Hazard - P. F. Krumpe and G. T. Hebenstreit

Speaker: P. F. Krumpe

10:30 A.M. Technical Cooperation in Developing Countries in Earthquake Engineering - K. Kamimura, M. Watabe, Y. Ishiyawa, and Y. Yamazaki

Speaker: M. Hirosawa

10:50 A.M. Incremental Expansion and Aseismic Design of Low-Cost Housing in Sites and Services Project - E. Simiu and J. M. Courtney

Speaker: E. Simiu

11:10 A.M. Discussion

11:20 A.M. Task Committee Meetings

A. Strong Motion Instrumentation Arrays and Data
C. Repair and Retrofit of Existing Structures
D. Evaluation of Performance of Structures
F. Disaster Prevention Methods for Lifeline Systems
J. Wind and Earthquake Engineering for Transportation Systems

12:00 NOON Lunch - Dining Room C

1:30 P.M. Task Committee Meetings (con't.)

A. Strong Motion Instrumentation Arrays and Data
C. Repair and Retrofit of Existing Structures
D. Evaluation of Performance of Structures
F. Disaster Prevention Methods for Lifeline Systems
J. Wind and Earthquake Engineering for Transportation Systems

3:00 P.M. Break

4:15 P.M. Adjourn

THURSDAY - May 20 Lecture Room B, Administration Building

9:00 A.M. Task Committee Meetings

B. Large-Scale Testing Program
E. Land Use Program for Controlling Natural Hazard Effects
G. Wind Characteristics and Structural Response
H. Soil Behavior and Stability During Earthquakes
I. Storm Surge and Tsunamis

10:30 A.M. Break

10:50 A.M. Task Committee Meetings (con't.)

B. Large-Scale Testing Program
E. Land Use Program for Controlling Natural Hazard Effects
G. Wind Characteristics and Structural Response
H. Soil Behavior and Stability During Earthquakes
I. Storm Surge and Tsunamis
Resolution Committee

12:00 NOON Lunch - Dining Room C

1:30 P.M. Task Committee Reports

A. Strong Motion Instrumentation Arrays and Data
B. Large-Scale Testing Program
C. Repair and Retrofit of Existing Structures
D. Evaluation of Performance of Structures
E. Land Use Program for Controlling Natural Hazard Effects
F. Disaster Prevention Methods for Lifeline Systems
G. Wind Characteristics and Structural Response
H. Soil Behavior and Stability During Earthquakes
I. Storm Surge and Tsunamis
J. Wind and Earthquake Engineering for Transportation Systems

3:10 P.M. Adoption of Final Resolution

3:40 P.M. Break

CLOSING SESSION

4:00 P.M.	Call to Order by Dr. H. S. Lew, Secretary, U.S. Panel Closing Remarks by Dr. Tadayoshi Okubo, Chairman, Japanese Panel Closing Remarks by Dr. Edward O. Pfrang, Chairman, U.S. Panel
4:30 P.M.	Adjourn

U.S. PANEL ON WIND AND SEISMIC EFFECTS

MEMBERSHIP LIST

1982

Dr. Edward O. Pfrang
Chairman
Chief, Structures Division
Center for Building Technology, NEL
National Bureau of Standards
Washington, DC 20234
(301) 921-2196

Dr. H. S. Lew
Secretariat
Leader, Construction Safety
Structures Division
Center for Building Technology, NEL
National Bureau of Standards
Washington, DC 20234
(301) 921-2647

Dr. S. T. Algermissen
Office of Earthquake Studies
Denver Federal Center
Branch of Earthquake Tectonics, USGS
Stop 978, Box 25046
Denver, CO 80225
(303) 234-4014

Dr. Celso Barrientos
EDIS-NOAA-CEAS D213
3300 Whitehaven N.W.
Washington, DC 20235
(301) 634-7379

Dr. Eddie N. Bernard
Deputy Director, Pacific Marine Environmental Laboratory
3711 15th Avenue, NE
Seattle, WA 98105
FTS 399-0199 or (206) 442-0199

Dr. Roger D. Borcherdt
Chief, Branch of Ground Motion and Faulting
Office of Earthquake Studies, USGS
345 Middlefield Road
Menlo Park, CA 94025
(415) 323-8111

Dr. A. Gerald Brady
Physical Scientist
Office of Earthquake Studies, USGS
345 Middlefield Road
Menlo Park, CA 94025
(415) 323-8111

Mr. James D. Cooper
Structures and Applied Mechanics Division
Federal Highway Administration
Office of Research HRS-11
Washington, DC 20590
(202) 557-4315

Mr. Jerry Dodd
Chief, Division of Geology
Bureau of Reclamation
P. O. Box 25007
Denver Federal Center
Denver, CO 80225
(303) 234-3089

Mr. G. Robert Fuller
Architectural and Engineering Division
Department of Housing and Urban Development
Washington, DC 20411
(202) 755-5924

Dr. Michael P. Gaus
Division of Problem-Focused Research Applications
National Science Foundation
1800 G Street, NW
Washington, DC 20550
(202) 632-5700

Mr. Peter E. Gurvin
A/FBO, SA-6
Department of State
Washington, DC 20520
(202) 235-9489

Mr. John J. Healy
Chief, Research and Development Office
Department of the Army
DAEN-RDM
Washington, DC 20314
(202) 272-0260

Dr. William B. Joyner
Geophysicist
Office of Earthquake Studies
Branch of Ground Motion and Faulting, USGS
345 Middlefield Road
Menlo Park, CA 94025
(415) 323-8111

Mr. John W. Kaufman
Aerospace Engineer
Atmospheric Sciences Division, E582
National Aeronautics and Space Administration
Marshall Space Flight Center, AL 35812
(205) 453-3104

Mr. James Lander
Acting Director, National Geophysical & Solar-Terrestrial Data
Center and
Director, World Data Center-A for Solid Earth Geophysics
Environmental Data Service, NOAA
Boulder, CO 80302
FTS 323-6474 or (303) 449-1000, ext. 6474

Dr. E. V. Leyendecker
Leader, Earthquake Hazards Reduction Group
Structures Division
Center for Building Technology, NEL
National Bureau of Standards
Washington, DC 20234
(301) 921-3471

Dr. Shih C. Liu
Program Director
Division of Civil & Environmental Engineering
National Science Foundation
Washington, DC 20550
(202) 632-5700

Dr. Richard D. McConnell
Office of Construction
Veterans Administration
811 Vermont Avenue NW
Washington DC 20420
(202) 389-3103

Dr. William F. Marcuson, III
Chief, Geotechnical Laboratory
Department of the Army
Waterways Experiment Station, Corps of Engineers
P. O. Box 631
Vicksburg, MS 39180
FTS 542-2202 or (601) 636-3111, ext. 2202

Dr. Richard D. Marshall
Leader, Structural Engineering
Structures Division
Center for Building Technology, NEL
National Bureau of Standards
Washington, DC 20234
(301) 921-3471

Mr. John F. Meehan
Principal Structural Engineer
Research Director
Structural Safety Section
Office of the State Architect
Department of General Services
Sacramento, CA 95805

Dr. John B. Scalzi
Program Manager, Division of Problem-Focused Research
Applications
National Science Foundation
1800 G Street NW
Washington, DC 20550
(202) 632-0648

Dr. Joseph T. Schaefer
Chief, Techniques Development Unit
National Severe Storm Forecast Center
National Weather Service. NOAA
601 E. 12th Street, Room 1728 Federal Building
Kansas City, MO 64106
(816) 374-3367

Mr. Charles Scheffey
Director, Office of Research
Federal Highway Administration
Department of Transportation
Washington, DC 20590
(202) 557-5254

Dr. Lawrence C. Shao
Assistant Director for General Reactor Safety Research
Division of Reactor Safety Research
Nuclear Regulatory Commission
Washington, DC 20555
(301) 427-4442

Dr. Lawrence A. Soltis
Research Engineer
Engineered Wood Structures
Forest Products Laboratory
Forest Service
U.S. Department of Agriculture
Madison, WI 53705
(608) 264-5910

Mr. Stanley K. Takahashi
Structures Division
Civil Engineering Laboratory
Naval Construction Battalion Center
Port Huemene, CA 93043
(805) 982-4684

ALTERNATES:

Mr. Michael Changery
National Climatic Center
Federal Building
Asheville, NC 28787
(704) 258-2850 ext. 217

Mr. Ronald J. Morony
Program Manager
Building Technology Research Staff
Department of Housing and Urban Development
Washington, DC 20410
(202) 755-0640

Mr. Drew A. Tiedemann
Bureau of Reclamation
Engineering and Research Center
Denver Federal Center
Denver, CO 80225
(303) 234-3029

JAPAN PANEL ON WIND AND SEISMIC EFFECTS

MEMBERSHIP LIST

1982

Dr. Tadayoshi Okubo
Chairman
Director-General, Public Works Research Institute
Ministry of Construction
Asahi 1-banchi, Toyosato-machi, Tsukuba-gun
Ibaraki-ken 305, JAPAN
0298-64-2211

Dr. Kozo Kaneyasu
Secretary-General
Director, Planning and Research Administration Department
Public Works Research Institute
Ministry of Construction
Asahi 1-banchi, Toyosato-machi, Tsukuba-gun
Ibaraki-ken 305, JAPAN
0298-64-2211

Dr. Masahiko Aihara
Head, Typhoon Research Division
Meteorological Research Institute (MRI)
Japan Meteorological Agency (JMA)
1-1, Nagamine, Yatabe-machi, Tsukuba-gun
Ibaraki-ken 305, JAPAN
0298-51-7111

Mr. Tadashi Arakawa
Head, Ground Vibration Division
Earthquake Disaster Prevention Department
Public Works Research Institute
Ministry of Construction
Asahi 1-banchi, Toyosato-machi, Tsukuba-gun
Ibaraki-ken 305, JAPAN
0298-64-2211

Mr. Hideya Asanuma
Head, Foundation Engineering Division
Structure and Bridge Department
Public Works Research Institute
Ministry of Construction
Asahi 1-banchi, Toyosato-machi, Tsukuba-gun
Ibaraki-ken 305, JAPAN
0298-64-2211

Dr. Yoshimi Goda
Director, Hydraulic Engineering Division
Port and Harbour Research Institute
Ministry of Transport
3-1-1, Nagase, Yokosuka-shi
Kanagawa-ken 239, JAPAN
0468-41-5410

Mr. Hiroshi Hashimoto
Head, Coastal Engineering Division
River Department
Public Works Research Institute
Ministry of Construction
Asahi 1-banchi, Toyosato-machi, Tsukuba-gun
Ibaraki-ken 305, JAPAN
0298-64-2211

Dr. Sadaiku Hattori
Chief, Seismology Division
International Institute of Seismology and
Earthquake Engineering (I.I.S.E.E.)
Building Research Institute
Ministry of Construction
Tatehara 1-banchi, Oh-ho-machi, Tsukuba-gun
Ibaraki-ken 305, JAPAN
0298-64-2151

Dr. Masaya Hirosawa
Director, Structure Department
Building Research Institute
Ministry of Construction
Tatehara 1-banchi, Oh-ho-machi, Tsukuba-gun
Ibaraki-ken 305, JAPAN
0298-64-2151

Dr. Toshio Iwasaki
Head, Earthquake Engineering Division
Earthquake Disaster Prevention Department
Public Works Research Institute
Ministry of Construction
Asahi 1-banchi, Toyosato-machi, Tsukuba-gun
Ibaraki-ken 305, JAPAN
0298-64-2211

Dr. Katsuro Kamimura
Director-General
Building Research Institute
Ministry of Construction
Tatehara 1-banchi, Oh-ho-machi, Tsukuba-gun
Ibaraki-ken 305, JAPAN
0298-64-2151

Dr. Norihisa Matsumoto
Head, Fill Type Dam Division
Dam Department
Public Works Research Institute
Ministry of Construction
Asahi 1-banchi, Toyosato-machi, Tsukuba-gun
Ibaraki-ken 305, JAPAN
0298-64-2211

Dr. Misato Murakami
Director, Earthquake Disaster Prevention Department
Public Works Research Institute
Ministry of Construction
Asahi 1-banchi, Toyosato-machi, Tsukuba-gun
Ibaraki-ken 305, JAPAN
0298-64-2211

Mr. Tatsuo Murota
Head, Building Aerodynamics Section
Structure Engineering Division
Building Research Institute
Ministry of Construction
Tatehara 1-banchi, Oh-ho-machi, Tsukuba-gun
Ibaraki-ken 305, JAPAN
0298-64-2151

Dr. Keikichi Naito
Head, Meteorological Satellite Division
Meteorological Research Institute (MRI)
Japan Meteorological Agency (JMA)
1-1 Nagamice, Yatabe-machi, Tsukuba-gun
Ibaraki-ken 305, JAPAN
0298-51-7111

Dr. Nobuyuki Narita
Director, Structure and Bridge Department
Public Works Research Institute
Ministry of Construction
Asahi 1-banchi, Toyosato-machi, Tsukuba-gun
Ibaraki-ken 305, JAPAN
0298-64-2211

Mr. Setsuo Noda
Chief, Earthquake Resistant Structures Laboratory
Structure Division
Port and Harbour Research Institute
Ministry of Transport
3-1-1, Nagase, Yokosuka-shi
Kanagawa-ken 239, JAPAN
0468-41-5410

Mr. Keiichi Ohtani
Chief, Earthquake Engineering Laboratory
Second Research Division
National Research Center for Disaster Prevention
Science and Technology Agency
3-1, Tennodai, Sakura-mura, Niihari-gun
Ibaraki-ken 305, JAPAN
0298-51-1611

Mr. Shin Okamoto
Head, Housing Construction Division
Production Department
Building Research Institute
Ministry of Construction
Tatehara 1-banchi, Oh-ho-machi, Tsukuba-gun
Ibaraki-ken 305, JAPAN
0298-64-2151

Mr. Shoichi Saeki
Head, Bridge Division
Structure and Bridge Department
Public Works Research Institute
Ministry of Construction
Asahi 1-banchi, Toyosato-machi, Tsukuba-gun
Ibaraki-ken 305, JAPAN
0298-64-2211

Mr. Yasushi Sasaki
Head, Soil Dynamics Division
Construction Method and Equipment Department
Public Works Research Institute
Ministry of Construction
Asahi 1-banchi, Toyosato-machi, Tsukuba-gun
Ibaraki-ken 305, JAPAN
0298-64-2211

Dr. Hiroshi Takahashi
Head, Second Research Division
National Research Center for Disaster Prevention
Science and Technology Agency
3-1, Tennodai, Sakura-mura, Niihari-gun
Ibaraki-ken 305, JAPAN
0298-51-1611

Dr. Hajime Tsuchida
Director, Structure Division
Port and Harbour Research Institute
Ministry of Transport
3-1-1, Nagase, Yokosuka-shi
Kanagawa-ken 305, JAPAN
0468-41-5410

Mr. Eisaku Tsurumi
Head, First Geographic Division
Geographical Survey Institute
Ministry of Construction
Kitazato 1-banchi, Yatabe-machi, Tsukuba-gun
Ibaraki-ken 305, JAPAN
0298-64-1111

Dr. Makoto Watabe
Director, International Institute of Seismology and
Earthquake Engineering (I.I.S.E.E.)
Building Research Institute
Ministry of Construction
Tatehara 1-banchi, Oh-ho-machi, Tsukuba-gun
Ibaraki-ken 305, JAPAN
0298-64-2151

Dr. Hideo Watanabe
Head, Seismology and Volcanology Division
Meteorological Research Institute (MRI)
Japan Meteorological Agency (JMA)
1-1, Nagamine, Yatabe-machi, Tsukuba-gun
Ibaraki-ken 305, JAPAN
0298-51-7111

Mr. Kunio Yamamoto
Head, Structure Division
Structure and Bridge Department
Public Works Research Institute
Ministry of Construction
Asahi 1-banchi, Toyosato-machi, Tsukuba-gun
Ibaraki-ken 305, JAPAN
0298-64-2211

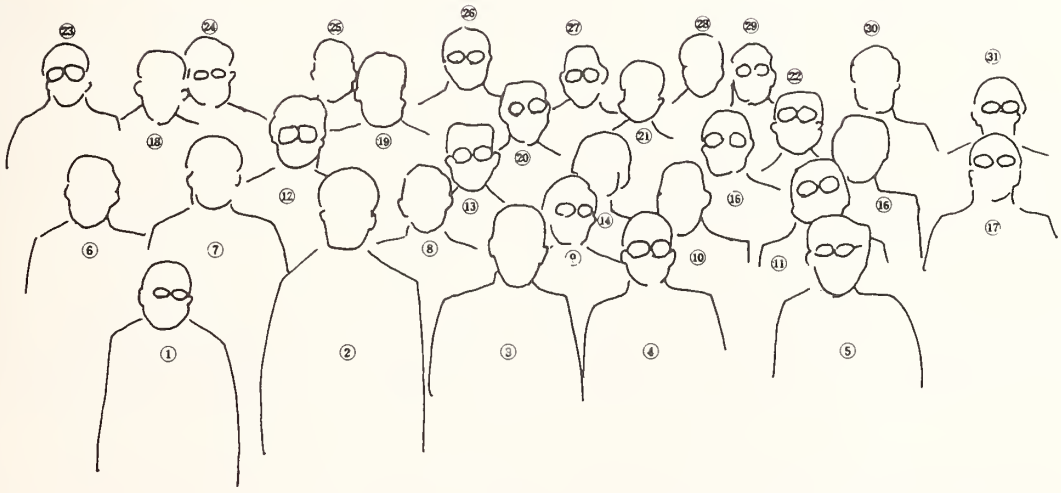

1. C. F. Scheffey
2. E. O. Pfrang
3. R. N. Wright
4. T. Okubo
5. H. Ishida
6. W. E. Joyner
7. C. Barrientos
8. S. Noda
9. S. Okamoto
10. S. Takahashi
11. M. Hirosawa
12. T. Mizuyoma
13. T. Iwasaki
14. M. E. Hynes-Griffen
15. J. B. Scalzi
16. T. Kaminosono
17. M. Kishita
18. H. S. Lew
19. G. R. Fuller
20. S. Nakata
21. K. Ohtani
22. E. Taniguchi
23. E. V. Leyendecker
24. R. D. McConnell
25. P. E. Gurvin
26. J. F. Lander
27. J. F. Costello
28. J. D. Cooper
29. G. T. Hebenstreit
30. A. G. Brady
31. E. Nakamura

RESOLUTIONS OF THE FOURTEENTH JOINT MEETING

U.S.-JAPAN PANEL ON WIND AND SEISMIC EFFECTS

U.J.N.R.

Washington, D.C., U.S.A.

May 17-20, 1982

The following resolutions for future activities of this Panel are hereby adopted:

1. The Fourteenth Joint Meeting provided an extremely valuable exchange of technical information which was beneficial to both countries. In view of the importance of cooperative programs on the subject of wind and seismic effects, the continuation of Joint Panel Meetings is considered essential.

2. The Panel on Wind and Seismic Effects recognizes the importance of the continued exchange of technical information and research data and the promotion of joint research programs including the exchange of personnel and use of available facilities in both countries. Thus, these activities should be strengthened and expanded.

3. The Panel recognizes the accomplishments of the U.S.-Japan Cooperative Program on Large-Scale Testing.

   The Panel continues to endorse the technical content of the Joint Program involving Large-Scale Testing of Steel Structures. Close working relationships should be maintained between the Panel and the Joint Technical Coordinating Committee of the Large-Scale Testing Program.

   The Panel endorses the efforts of Task Committee (B) to examine the use of masonry in both countries and review this construction type for a possible coordinated research program.

   The Panel encourages the exchange of information on large-scale testing facilities and large-scale testing programs in both countries.

4. Because the workshops on Repair and Retrofit of Existing Structures have been so successful, it is recommended that continued exchange of technical information be made on a timely basis by the workshop participants. It is further recommended that workshops be held in the future on codes and standards and construction practices for repair and retrofit of structures.

5. The Panel agrees with the recommendation of Task Committee (D) on Evaluation of Performance of Structures, that workshops be held on "Evaluation of Performance of Existing Buildings for Resistance to Earthquakes." The first workshop is tentatively planned to be held in Tsukuba Science City, Japan, in May 1983, prior to the 15th Joint U.S.-Japan Panel on Wind and Seismic Effects. Specific details and an agenda of the workshop will be established by each side and coordinated by correspondence. A final report is expected to be published in 1985 and reported to the 17th Joint Panel in Japan.

6. The Panel accepts the recommendation of Task Committee (F) to establish planning committees on each side. These planning committees, composed of representatives from government, universities, and the private sector, will cooperate in the formulation of a joint research program on reduction of the severity of the consequences of earthquakes and other natural hazards on lifeline systems. These committees will assist Task Committee (F) in the selection of projects for which support will be promoted.

7. Recognizing the importance of the seismic response and performance of bridge columns and piers, the Panel encourages the continued conduct of coordinated experimental studies on the behavior of large-scale bridge columns to dynamic loading. The Panel further encourages the appointment of at least one technical representative from each side of Task Committee (J) to maintain close coordination of those studies.

8. Recognizing the importance of in-situ measurement of soil properties, the Panel encourages the continuation of a cooperative research plan to evaluate the use and application of in-situ soil testing techniques. Standard penetration and cone penetration tests, for seismic design and analysis, should be specifically evaluated. The Panel recognizes the importance of the U.S.-Japan cooperative program on the response of semi-buried concrete structures due to earthquakes, and therefore the Panel should consider the initiation of the above mentioned cooperative program.

9. The Panel recognizes the importance to mitigate hazards from tsunami, and considers that better coordination between U.S. and Japan is desirable since numerous scientists and engineers in both nations are conducting complimentary studies on this subject. The Panel endorses the recommendation of Task Committee (I) on Storm Surge and Tsunami to organize a workshop on cooperative tsunami programs.

10. Recognizing that wind and seismic disaster mitigation plans benefit disaster-prone countries worldwide, that many developing countries suffer from natural disasters such as extreme winds and earthquakes, and that both the U.S. and Japan has been involved in international technical cooperation programs, the Panel will continue coordinating projects which provide aid to developing countries and maintain the exchange of technical information.

11. The date and location of the 15th Joint Meeting of the Panel on Wind and Seismic Effects will be held in May 1983, at Tsukuba, Japan. Specific dates, program, and itinerary will be proposed by the Japanese Panel with concurrence by the U.S. Panel.

EFFECTS OF SOLIDITY OF TRUSSES ON UNSTEADY AERODYNAMIC FORCES OF STIFFENING TRUSSED-GIRDERS

Tadayoshi Okubo
Nobuyuki Narita
Kunio Yamamoto
Hiroshi Sata

Public Works Research Institute
Ministry of Construction

ABSTRACT

Unsteady aerodynamic forces acting on stiffening trussed-girders are described. The models of stiffening trussed-girders which were used in the previous experiments [1] have trusses of low solidity (about 20 percent). In the present experiment, measurements were made for trusses of various solidity ratios, thus, the effects of solidity on unsteady aerodynamic forces of stiffening trussed-girders were investigated. Furthermore, measures to improve stability to torsional flutter of stiffening trussed-girders of high solidity (about 40 percent) were investigated and some effective measures have been found.

INTRODUCTION

In a previous paper given by the authors in 1981 [1], unsteady aerodynamic forces acting on stiffening trussed-girders which had a single deck and a main truss of low solidity ratio, ϕ (about 20 percent) were described. The girders generally showed good stability to torsional flutter at the angles of attack (α) of 0° and -3°. But the aerodynamic forces at α of 3° tend to cause tortional flutter. It was found that effective countermeasures for suppressing the torsional flutter are: (1) arranging the upper surface of the floor deck at the same height as that of the upper chords; (2) using π section for the floor deck; (3) blocking the parapet on the median; or (4) attaching the flap at outer handrails.

However, long-span bridges with stiffening trussed-girders of high solidity have recently been planned and is under construction by Honshu-Shikoku Bridge Authority, Metropolitan Expressway Public Corporation. For this reason, unsteady aerodynamic forces acting on stiffening trussed-girders of high solidity (about 25 to 50 percent) were measured to investigate the effects of solidity on these unsteady aerodynamic forces. Some measures, which were applied to the model of ϕ of 20 percent for improving aerodynamic stability, were also applied to a stiffening girder of solidity ratio of about 40 percent, to compare their effectiveness. Furthermore, one of the effective measures was applied to stiffening girders of various solidity ratios and the effect was recognized.

METHOD AND CONDITION OF THE EXPERIMENT

METHOD FOR MEASUREMENT OF UNSTEADY AERODYNAMIC FORCES

The method is basically a forced oscillation method [2]. The inertia forces of a model are balanced out mechanically by adjusting the mass and the position of dummy weights to measure only the aerodynamic forces. The measured aerodynamic forces are separated into the component that is in phase with oscillation displacement and that in phase with oscillation velocity. The coefficients of unsteady aerodynamic forces are then obtained.

FLOW AND MODEL

The main dimensions of the wind tunnel used for measuring unsteady aerodynamic forces are shown in table 1.

The experiment was made in a uniform laminar flow. The model of a stiffening trussed-girder with a single deck was used. The height of the main truss is about 1/3 of its width. The cross section of the basic shape model is shown in figure 1. Solidity ratio was changed by attaching the plates of different size to both sides of the stiffening truss (figure 2). For reference, unsteady aerodynamic forces acting on the model of ϕ = 100 percent were measured. In order to improve aerodynamic stability, such measures as attaching the flap (figure 3-3), blocking the parapet on the median (figure 3-2), using π section for the floor deck (figure 3-1), or arranging the upper surface of the floor deck at the same height as that of the upper chord, which are all effective for stiffening trussed-girder of $\phi \simeq 20$ percent, were applied to the models of higher solidity to investigate their effectiveness.

CONDITION OF THE EXPERIMENT

The model was put in oscillation in vertical bending mode or torsional model. Condition of the experiment is shown in table 2 and cases of the experiment are given in table 3.

RESULTS OF THE EXPERIMENT

The coefficients of unsteady aerodynamic forces which have close relations with aerodynamic stability are C^I_{LH} (coefficient of unsteady lift in phase with vertical bending oscillation velocity) and C^I_{MT} (coefficient of unsteady aerodynamic moment in phase with torsional oscillation velocity). When C^I_{LH} is positive, wind-induced oscillations of vertical bending mode (vortex-excited oscillation, galloping) tend to occur. When C^I_{MT} is positive, wind-induced oscillations of torsional mode (vortex- excited oscillation, torsional flutter) tend to occur. When the coefficients are negative, these oscillations are unlikely to happen.

The relations between the coefficients and reduced wind-speed expressed as V/NB (V, wind speed; N, frequency; B, distance between two upper chords of stiffening truss) are shown in figures 4-1 through 4-19. The characteristics of C^I_{LH} and C^I_{MT} with respect to the aerodynamic stability of stiffening trussed-girders are described as follows.

AERODYNAMIC STABILITY TO VERTICAL BENDING OSCILLATION

Test results show that stiffening trussed-girders of ϕ up to 50 percent have stable characteristics in aerodynamic oscillation of vertical bending mode. An example of this is given in figure 4-1 which presents the relation between C^I_{LH} and V/NB of the basic shape (ϕ = 40 percent). When ϕ is increased to 100 percent (figure 4-2), remarkably unstable characteristics appear, i.e., vortex-excited oscillation (V/NB $\simeq$ 2) and galloping (V/NB > 5) tend to occur.

AERODYNAMIC STABILITY TO TORSIONAL OSCILLATION

Solidity Ratio of 40 Percent

The stiffening trussed-girder of basic shape shows stable characteristics at α of 0° and -3°; however, it becomes unstable to torsional flutter at α =3° in the region of V/NB > 8 (figure 4-3). In order to improve the characteristics of basic shape at this angle of attack, blocking the parapet in the median (figure 4-4), attaching the flap (figure 4-6), or using π section for the floor deck (figure 4-7) are found to be effective measures. Such a measure as arranging the upper surface of the floor deck at the same height as that of the upper chord is found ineffective. The critical value of V/NB where a negative C^I_{MT} turns positive becomes smaller (figure 4-5) than that of the basic shape.

Effects of Solidity Ratio

C^I_{MT} at α = 0° of the basic shape whose ϕ is up to 45 percent remains negative in the region of $0 \leq V/NB \leq 12$, thus shows stable characteristics (figures 4-8 through 4-11). But torsional flutter tends to occur in the reigon of V/NB > 7.5 when ϕ = 50 percent (figure 4-12) and vortex-excited oscillation (V/NB $\simeq$ 1) and torsional flutter ($V/NB \geq 2$) tend to occure when ϕ = 100 percent (figure 4-13). C^I_{MT} of the basic shape at α = 3° was not measured except for ϕ = 40 percent; however, from the experimental results on the basic shape whose ϕ are 20 percent [1] and 40 percent (figure 4-3), and from the results on the girder with the flap (figures 4-14 through 4-19), its characteristics can be estimated as follows: the critical value of V/NB where a negative C^I_{MT} turns positive may be at about 8 for $20 \leq \phi \leq 40$ percent. The critical value may become remarably small when ϕ exceeds 45 percent.

The flap, which is one of the effective measures to improve the aerodynamic stability of the basic shape of ϕ = 40 percent, was attached to the basic shape and C^I_{MT} at α of 0° and 3° were

measured for ϕ = 25 percent to 100 percent. As a result, it is found that C^{I}_{MT} remains negative and shows stable characteristics in the region of $0 \leq V/NB \leq 12$ when $\phi \leq 45$ percent (figures 4-14 through 4-17). When ϕ = 50 percent, C^{I}_{MT} remains negative at $\alpha = 0°$; however, torsional flutter tends to happen at $\alpha = 3°$ in the region of V/NB > 6.5 (figure 4-18). When ϕ = 100 percent, vortex-excited oscillation ($V/NB \simeq 1$) and torsional flutter (V/NB > 2) tend to occur at α of 0° and 3°.

CONCLUSION

1. Unsteady aerodynamic forces acting on stiffening trussed-girders of various solidity ratios (ϕ) were measured to investigate the effect of solidity of trusses on aerodynamics stability.

2. Aerodynamic stability to vertical bending oscillations were found to be sufficient up to a ϕ of 50 percent.

3. In the region of ϕ = 20 to 40 percent, the aerodynamic stability of stiffening trussed-girders of basic shape to torsional oscillations rarely changes. No unstable oscillations occur at the angles of attack (α) of -3° and 0° for the value of V/NB up to 12, but torsional flutter tends to happen at $\alpha = 3°$ in the region of V/NB > 8. The stability becomes worse when ϕ exceeds 45 percent.

4. Blocking the parapet on the median, using π section for the floor deck, or attaching the flap are effective measures to improve stability of stiffening trussed-girder of ϕ = 40 percent against torsional flutter at $\alpha = 3°$.

5. When the flap is attached to a stiffening trussed-girder of $\phi \leq 45$ percent, the girder shows stable characteristics to torsional flutter in the region of $0 \leq V/NB \leq 12$. The stability becomes worse when ϕ exceeds 45 percent and torsional flutter tend to occur at $\alpha = 3°$ in the region of V/NB > 6.5 when ϕ = 50 percent.

REFERENCES

[1] Okubo, T., N. Narita, K. Yamamoto, and H. Sato, "Unsteady Aerodynamic Forces for a Suspended Structure With Stiffening Trusses," Thirteenth Joint Metting, Japan-US Panel on Wind and Seismic Effects, UJNR, Tsukuba, Japan, May 19-22, 1981.

[2] Okubo, T. N.Narita, and K. Yakoyama, "Some Approaches for Improving Wind Stability of Cable-Stayed Girder Bridges," Proceedings Fourth International Conference on Wind Effects on Buildings and Structures, 1975.

Table 1. Main Dimensions of the Wind Tunnel

Type	Göttinge	
Dimension	Test Section	
	Width	1000 mm
	Height	2000 mm
	Length	3000 mm
	Contraction Cone	
	Inlet	3000 mm x 5000 mm
	Outlet	1000 mm x 2000 mm
	Contraction Ratio	7.50 : 1.00
	Total Path	55,000 mm
Blower	Type	Axial with Fixed Blades
	Diameter	1500 mm
	Total Pressure	40.0 mm Aq
	Total Wind Volume	70.0 m^3/sec
	Maximum Rotation	1250.0 rpm
	Maximum Power	50.0 kW
Flow	Maximum Wind Speed	30.0 m/sec
	Turbulent Intensity	Less than 0.5%
Supplementary Facilities	Three component balance, support facility for flutter test, Measuring device for unsteady aerodynamic forces, pulse wind generator, gust generator, data processing system	

Table 2. Condition of the Experiment

Mode	Torsion	Vertical Bending
Frequency	4.0 Hz	2.0 Hz
Amplitude	1°	0.01 B
Angle of Attack*	-3°, 0°, 3°	-3°, 0°, 3°
Wind Speed (V/NB)	0-12	0-30

V, wind speed; N, frequency of oscillation; B, distance between two upper chords of stiffening trusses.

* Some angles were omitted.

Table 3. Case of the Experiment

Model No.	Solidity Ratio of Trusses (%)	Feature of Model	Angle of Attack (°)
1	25	Basic shape	0
2	25	With flap (figure 3-3)	0, 3
3	30	Basic shape	0
4	30	With flap	0, 3
5	35	Basic shape	0
6	35	With flap	0, 3
7	40	Basic shape	-3, 0, 3
8	40	With flap	0, 3
9	40	π type floor deck section (figure 3-2)	0, 3
10	40	Blockage of parapet on the median (figure 3-2)	0, 3
11	40	h/d = 0	0, 3
12	45	Basic shape	0
13	45	With flap	0, 3
14	50	Basic shape	0
15	50	With flap	0, 3
16	100	Basic shape	0
17	100	With flap	0, 3

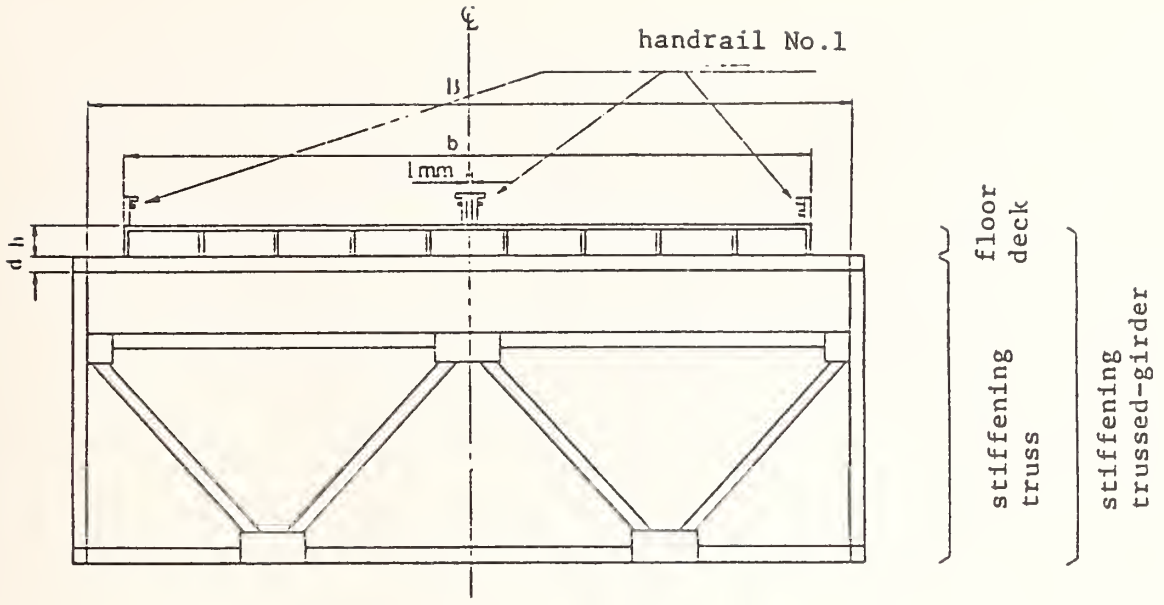

Cross section of stiffening trussed-girder
(Basic Shape; b/B=0.9, h/d=2)

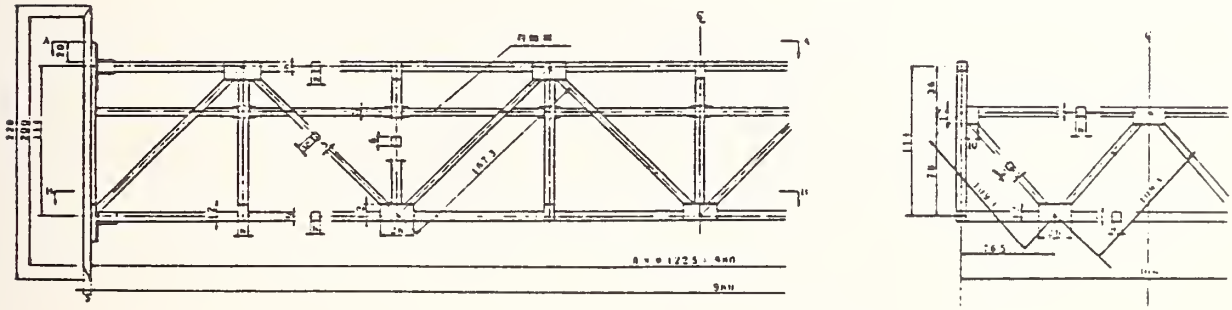

Stiffening truss

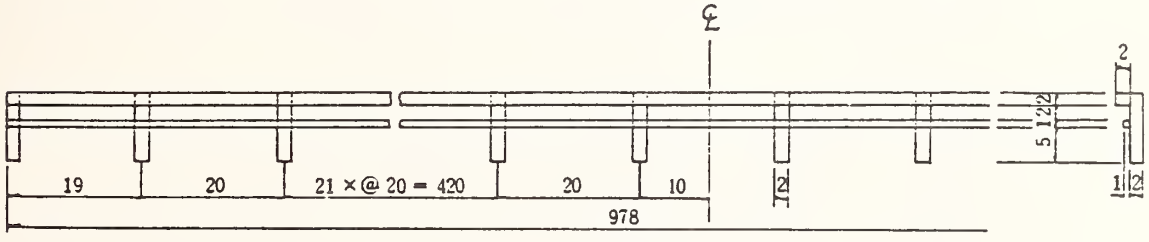

Handrail No.1

Fig.1 Model (Basic Shape)

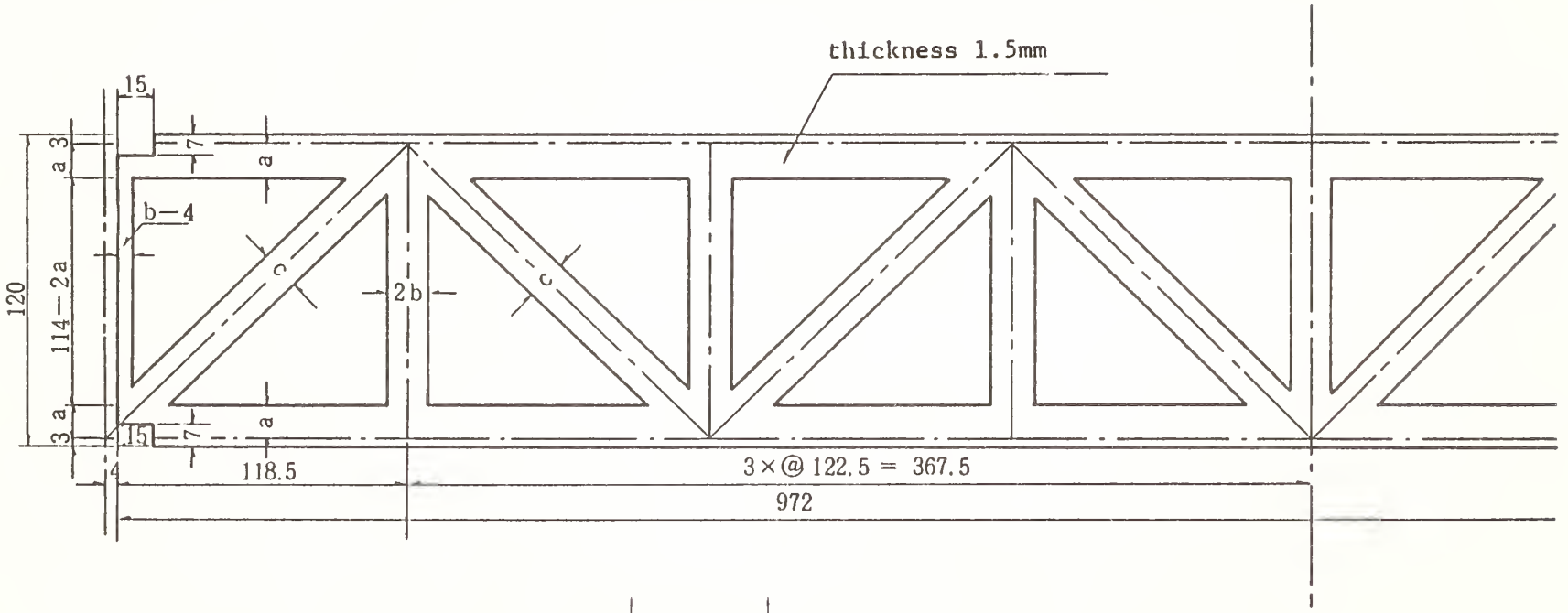

Solidity Ratio(%)	a	b	c
25	4	4	7
30	6	4.5	9
35	8	5	10
40	9	6.5	12
45	11	7	14
50	13	8	16
100	solid plate		

Fig.2 Plates for changing solidity ratio of stiffening truss
(Solidity ratio; 25%~100%)

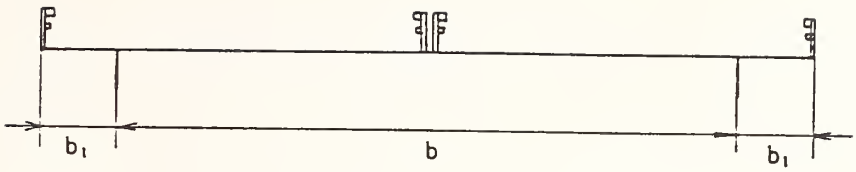

Fig.3-1 π type floor deck (b=0.7B, b_1=0.1B)

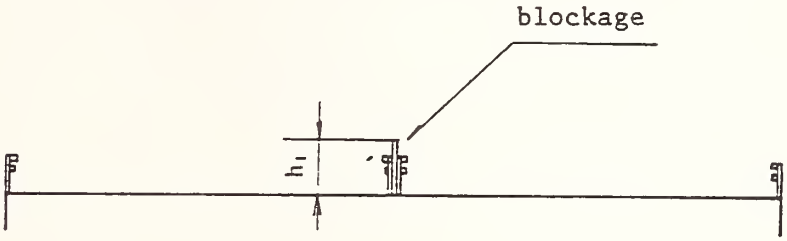

Fig.3-2 Blockage of parapet on the median ($h_1 = \frac{10}{3} d$)

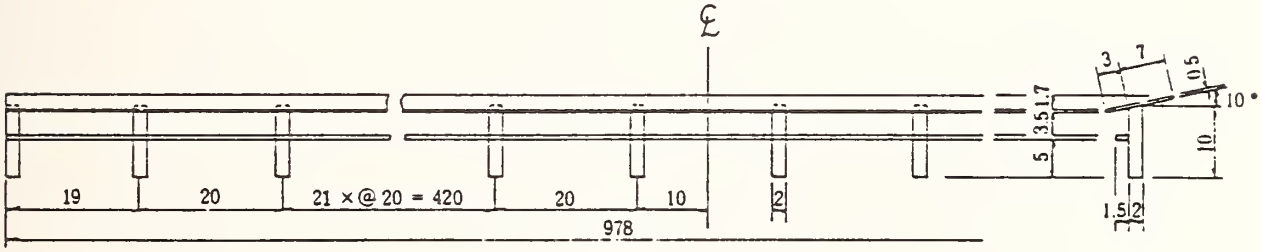

Fig.3-3 Handrail No.3 (with a flap)

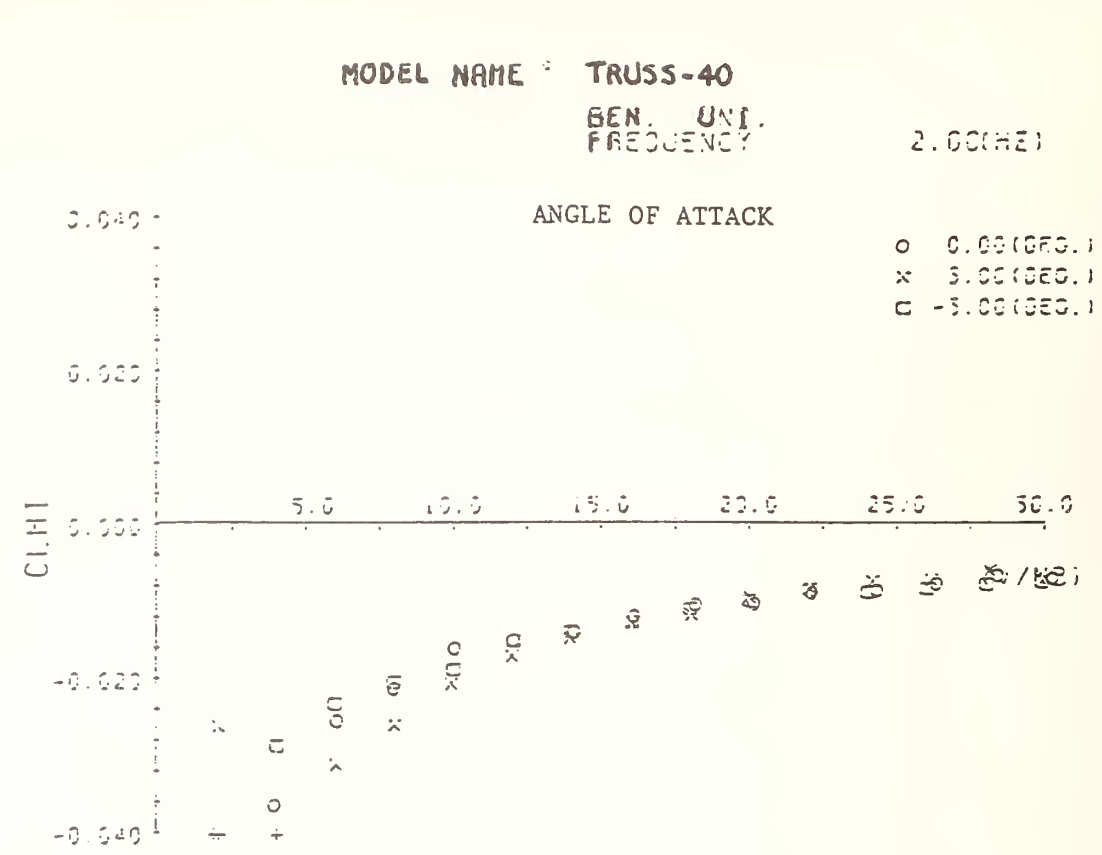

Fig.4-1 C_{LH}^{I} — V/NB (Model No.7)

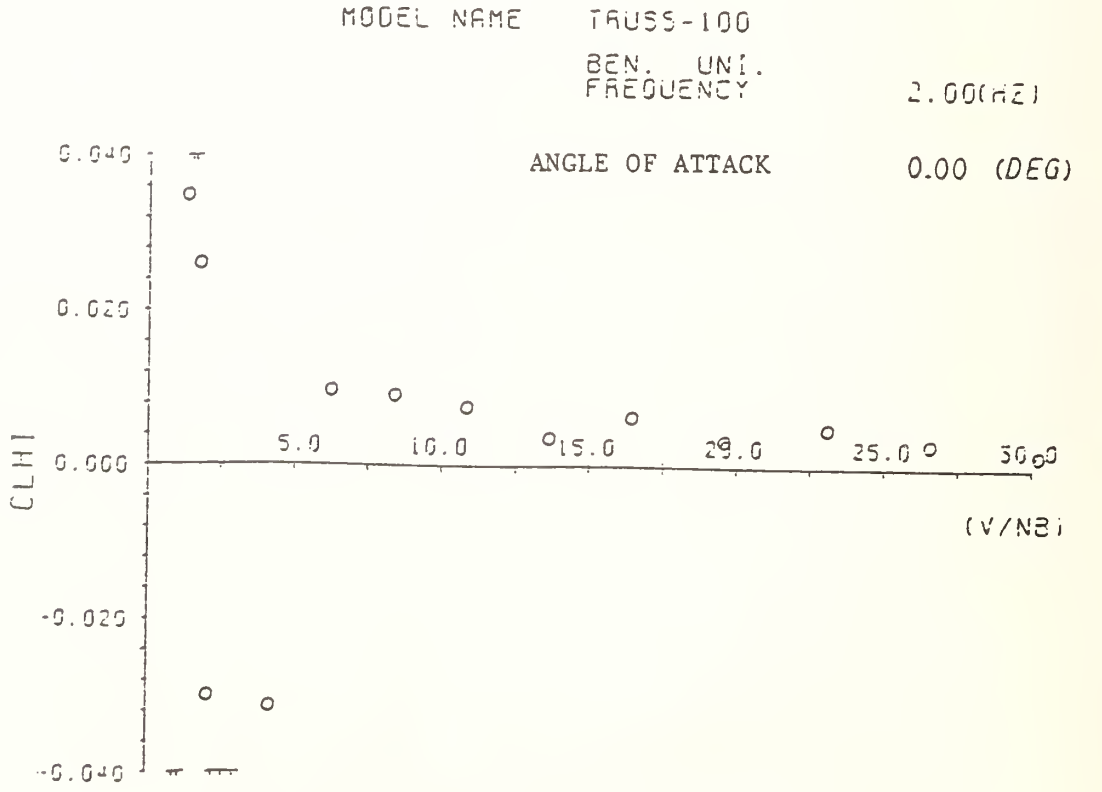

Fig.4-2 C_{LH}^{I} — V/NB (Model No.16)

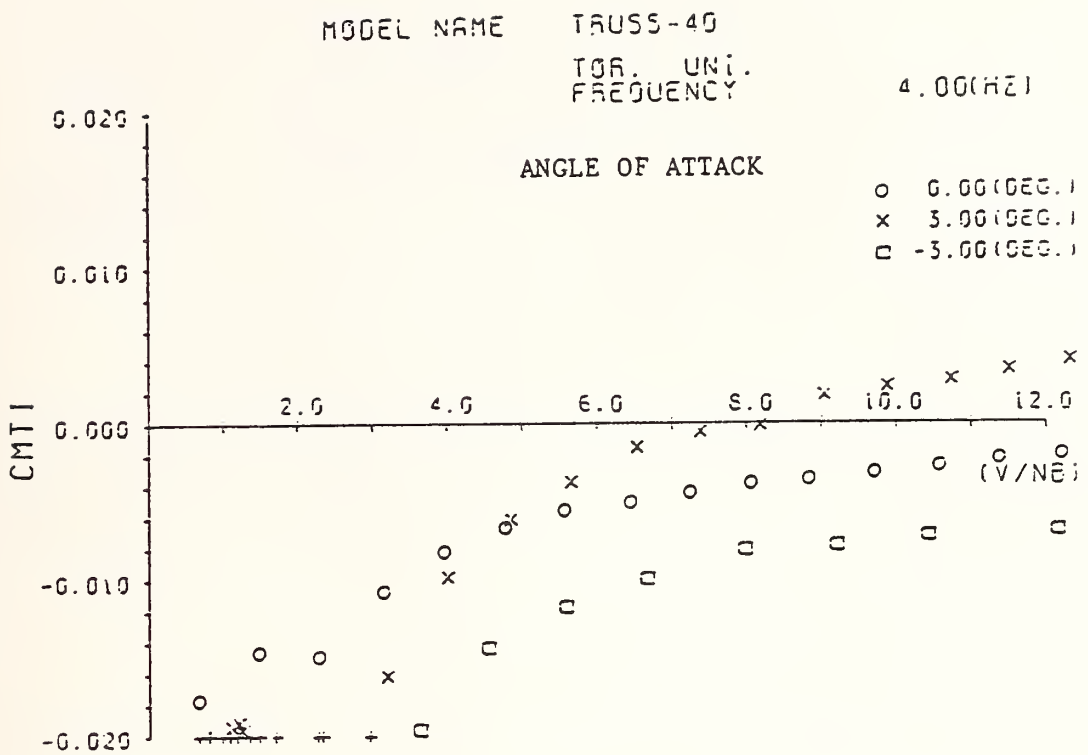

Fig.4-3 C_{MT}^{I} — V/NB (Model No.7)

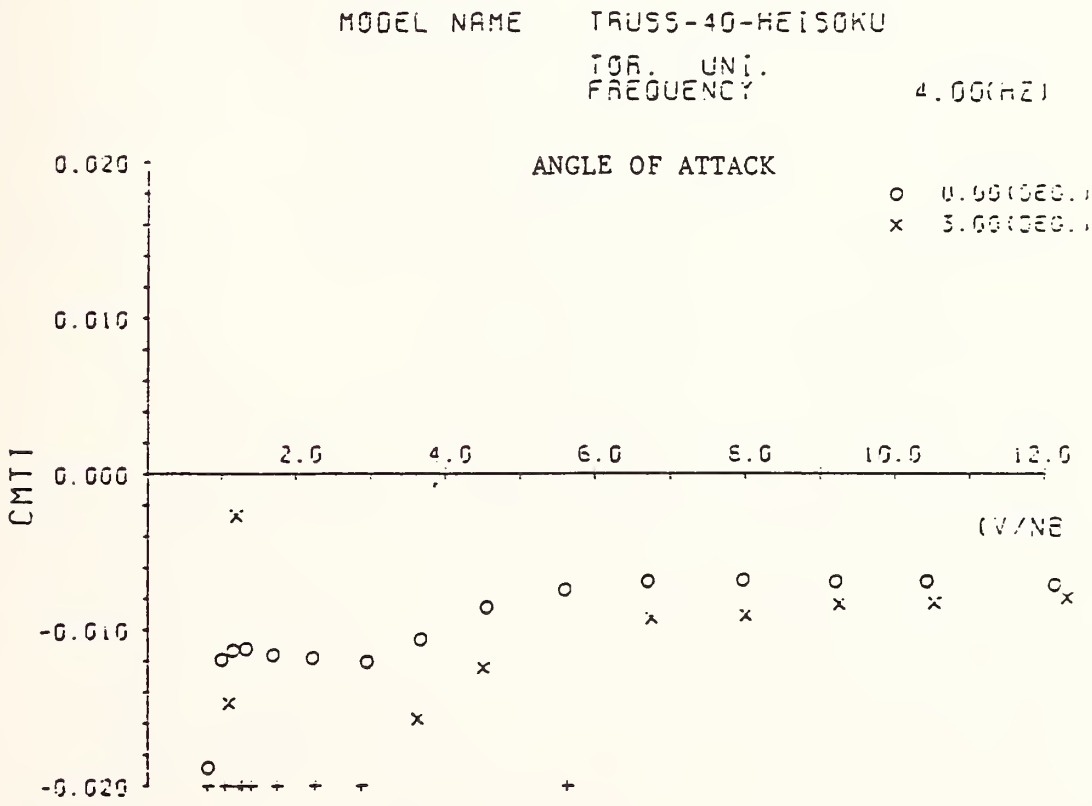

Fig.4-4 C_{MT}^{I} — V/NB (Model No.10)

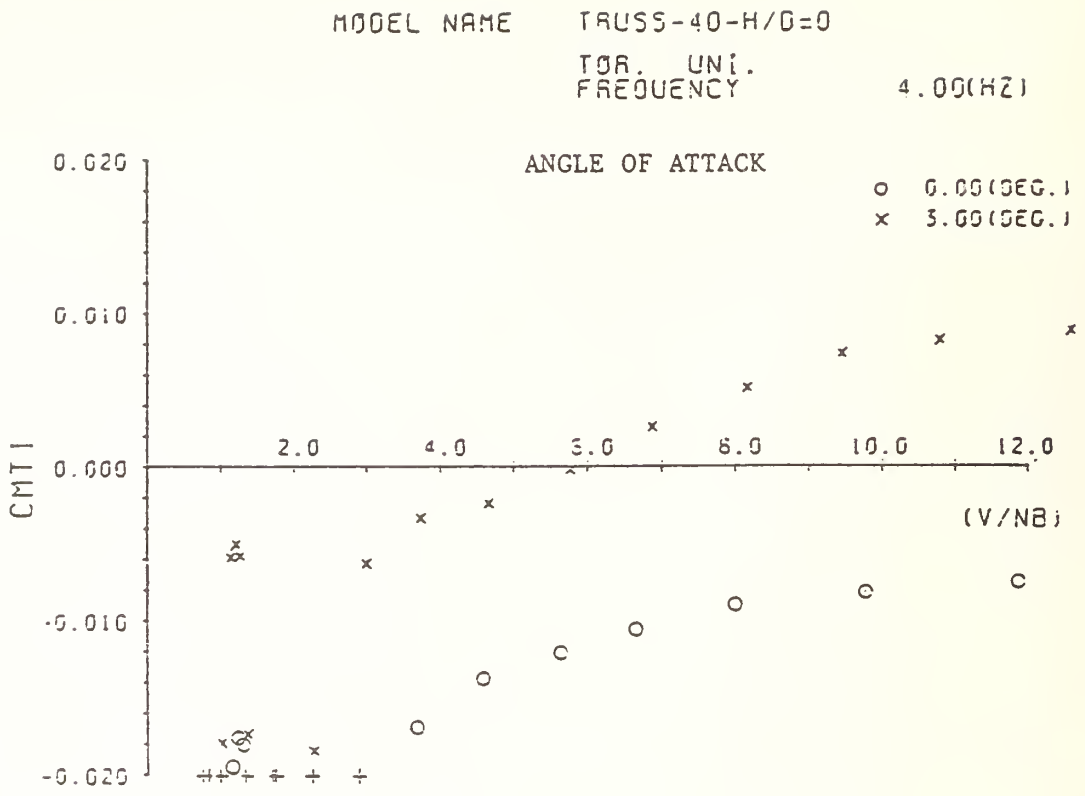

Fig.4-5 C_{MT}^{I} — V/NB (Model No.11)

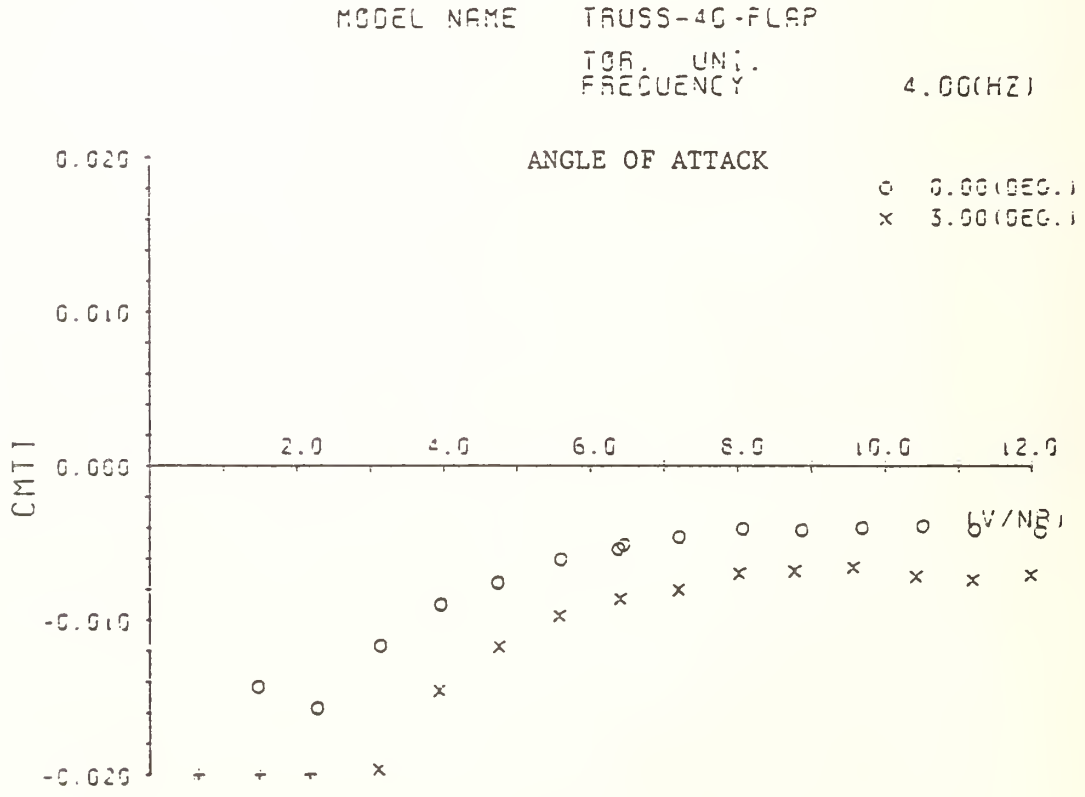

Fig.4-6 C_{MT}^{I} — V/NB (Model No.8)

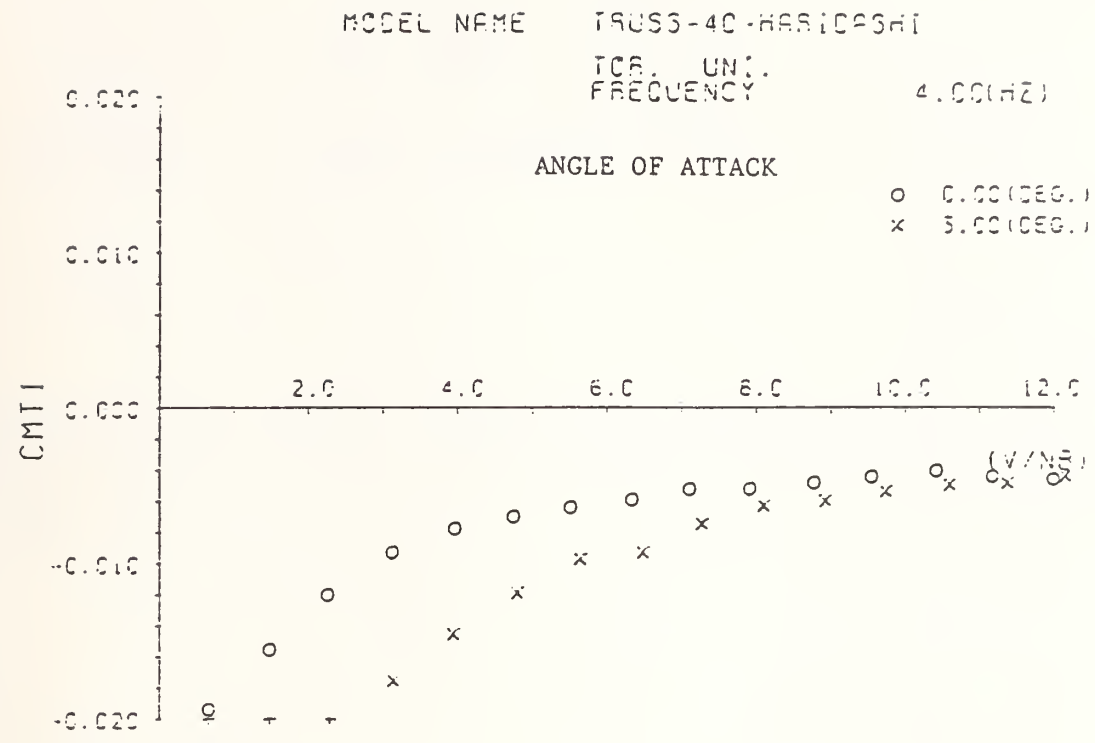

Fig.4-7 C_{MT}^{I} — V/NB (Model No.9)

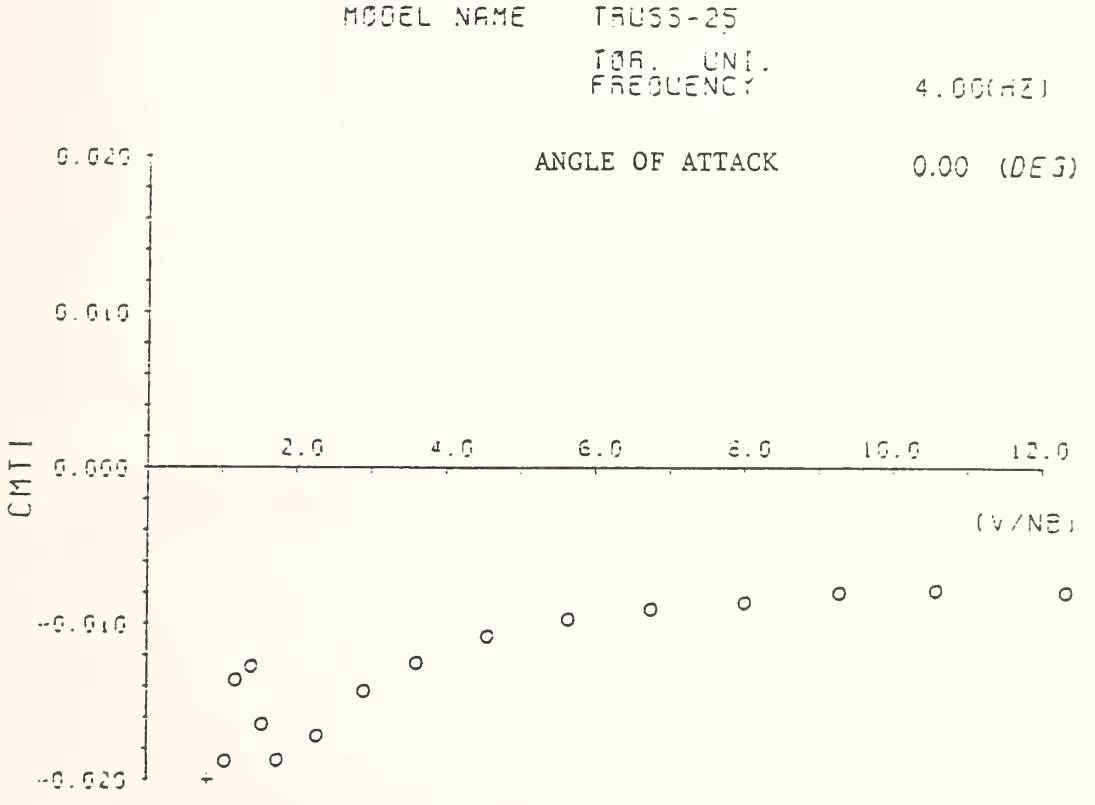

Fig.4-8 C_{MT}^{I} — V/NB (Model No.1)

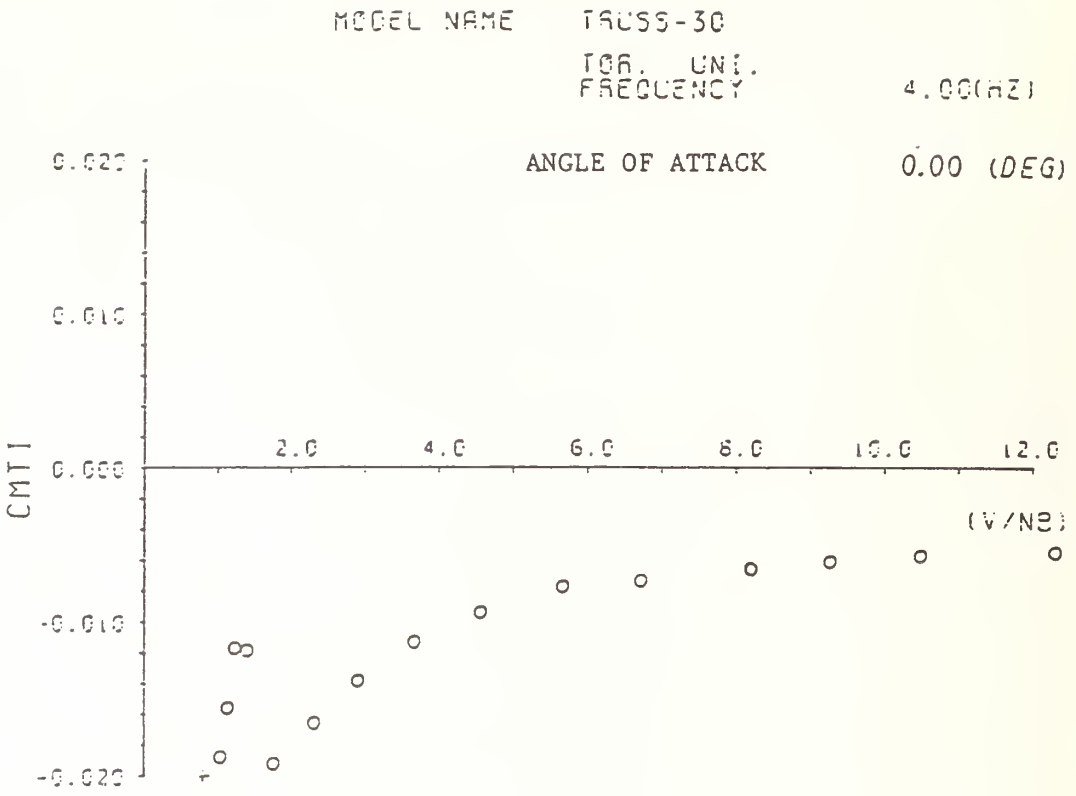

Fig.4-9 C_{MT}^{I} — V/NB (Model No.3)

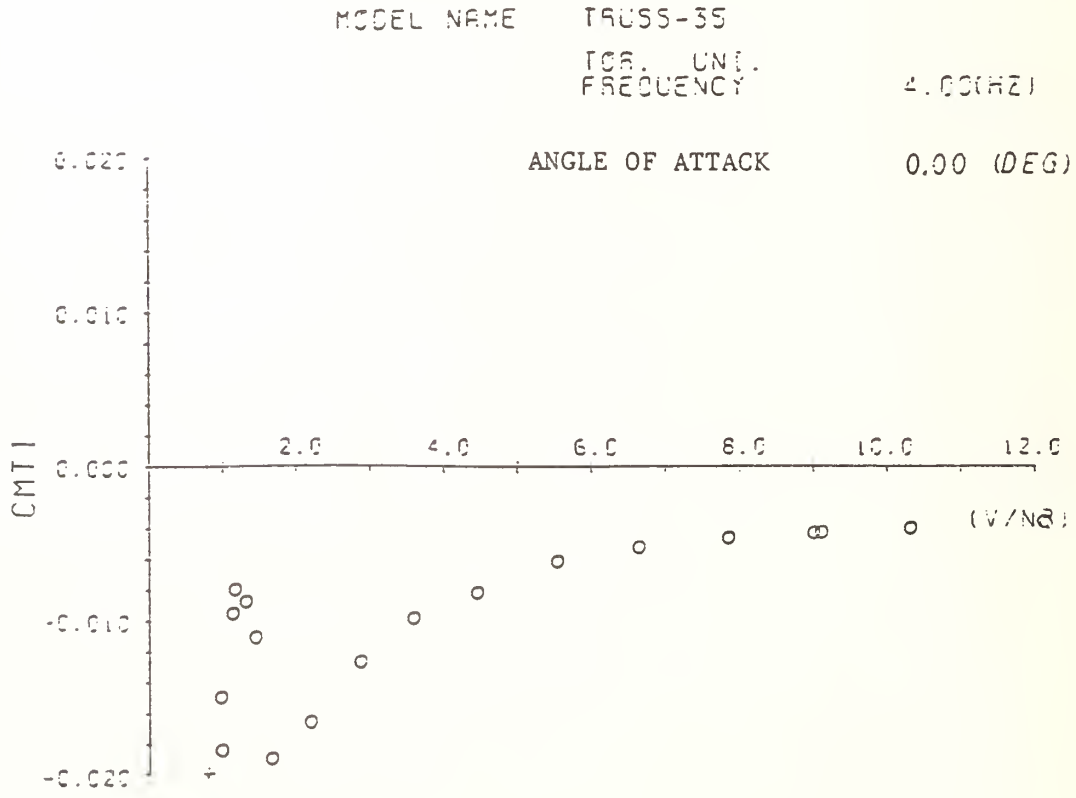

Fig.4-10 C_{MT}^{I} — V/NB (Model No.5)

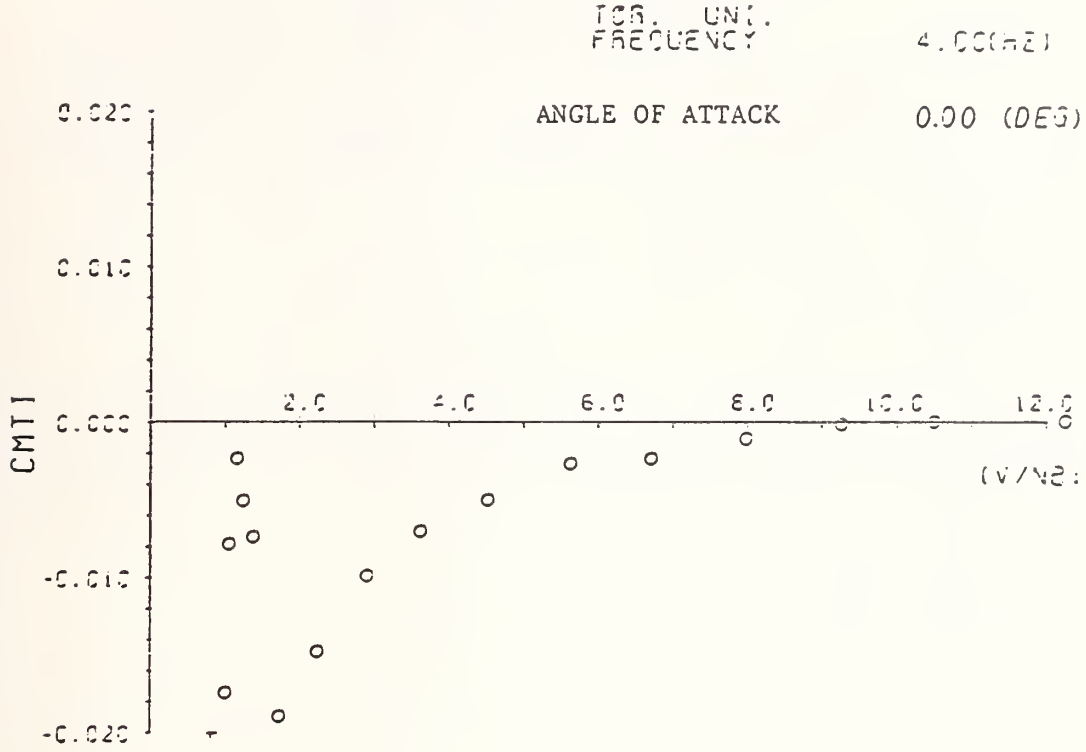

Fig.4-11 C_{MT}^{I} — V/NB (Model No.12)

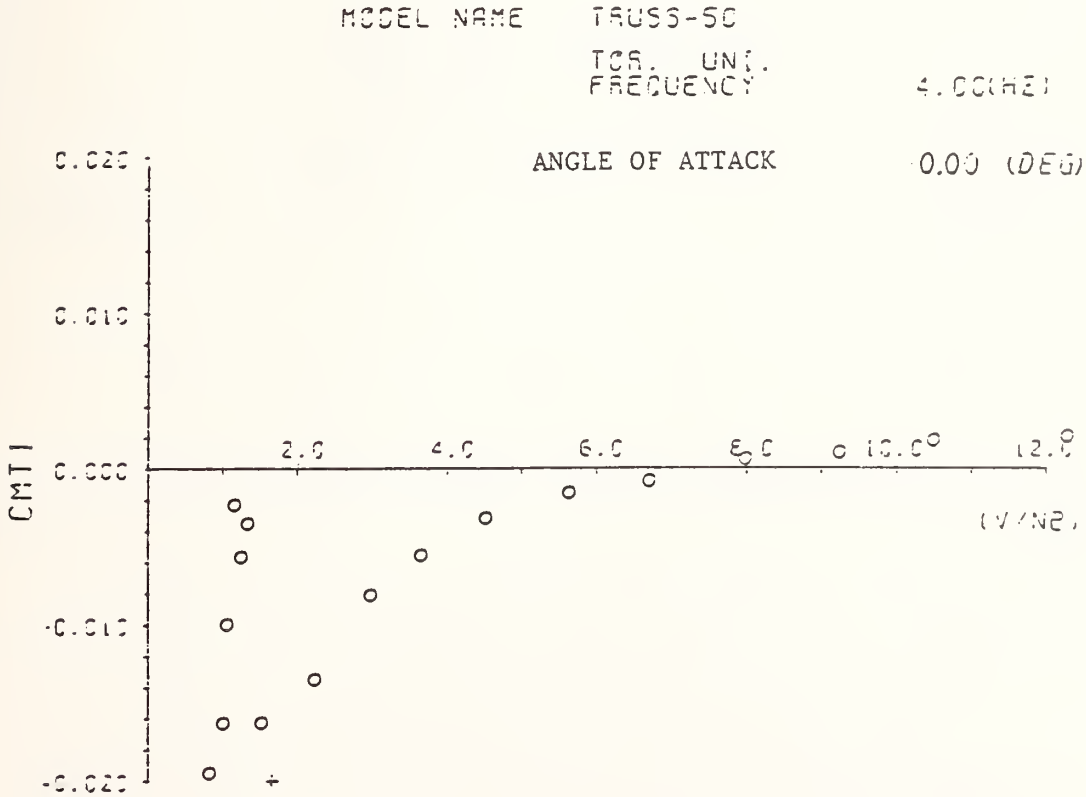

Fig.4-12 C_{MT}^{I} — V/NB (Model No.14)

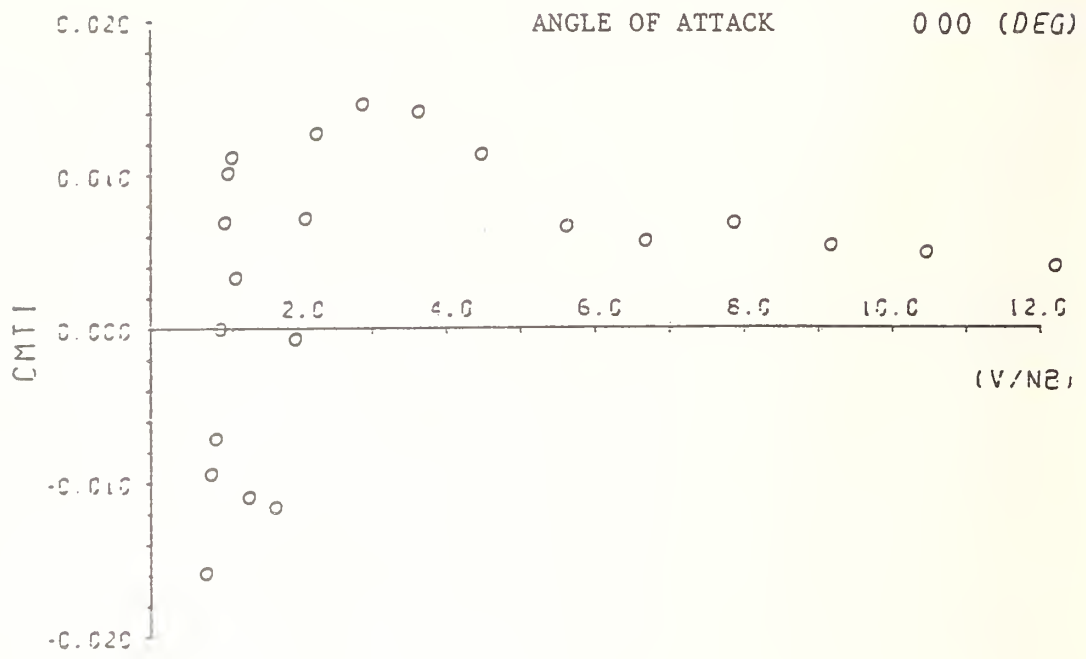

Fig.4-13 C_{MT}^{I} — V/NB (Model No.16)

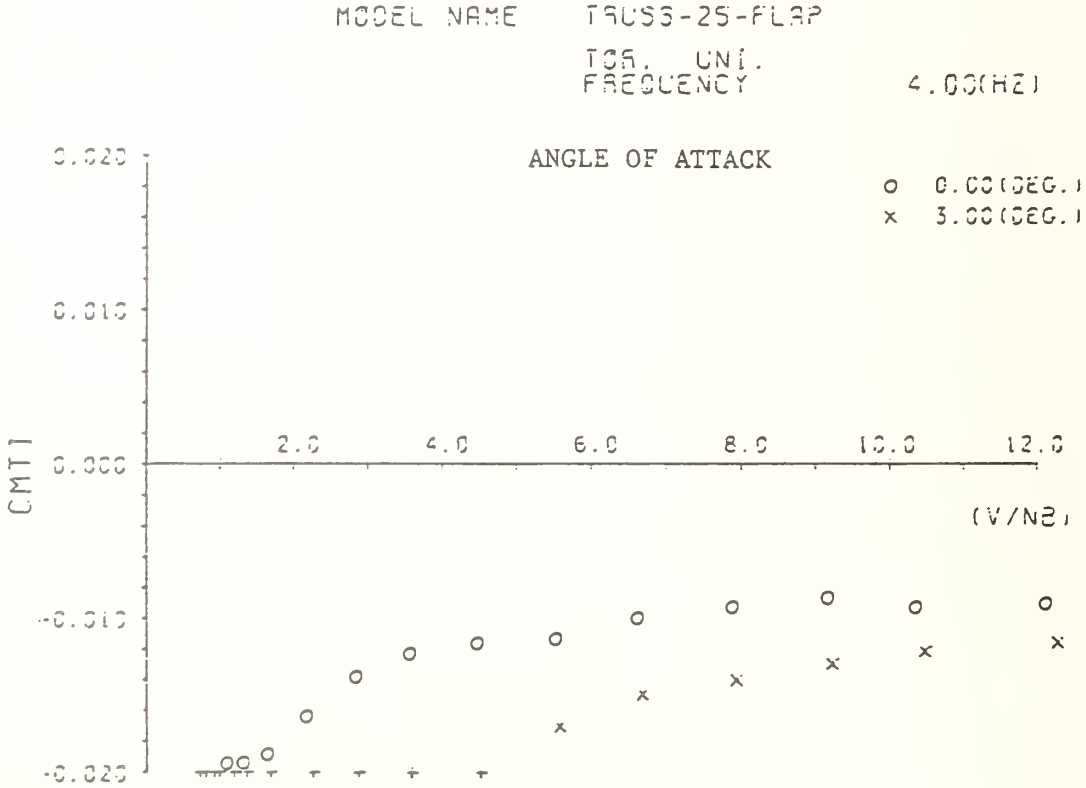

Fig.4-14 C_{MT}^{I} — V/NB (Model No.2)

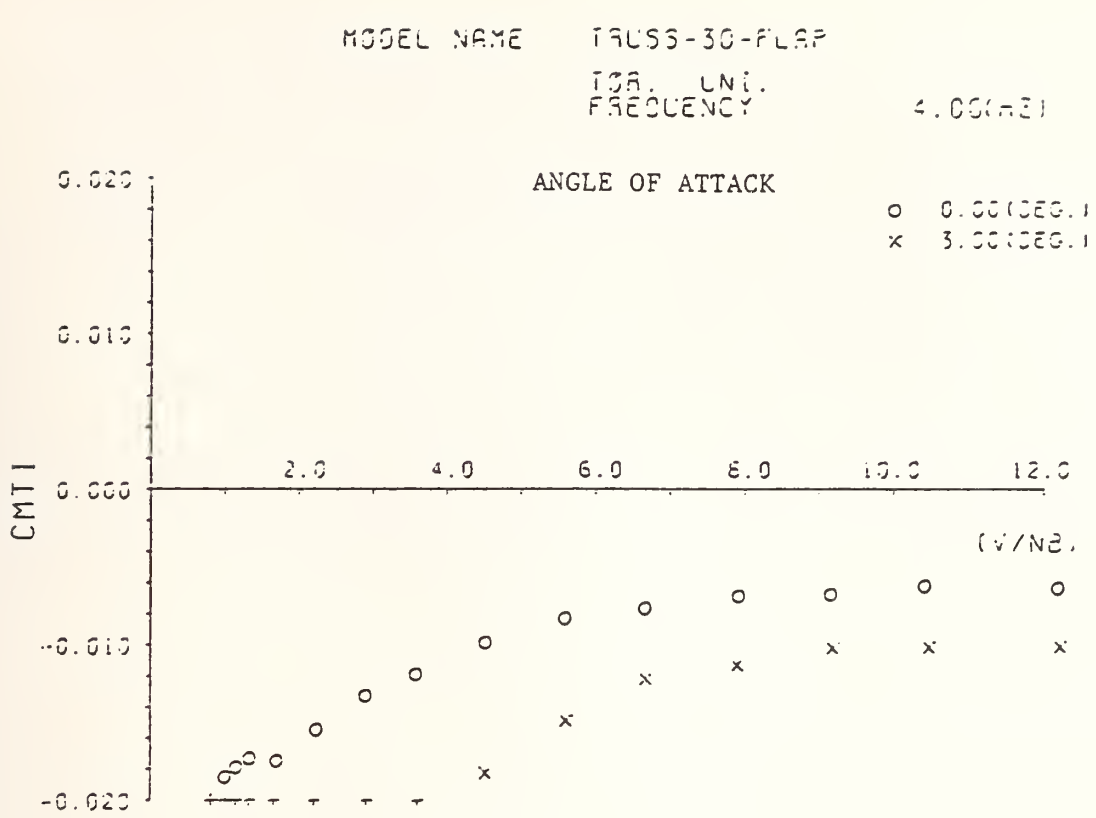

Fig.4-15 C_{MT}^{I} — V/NB (Model No.4)

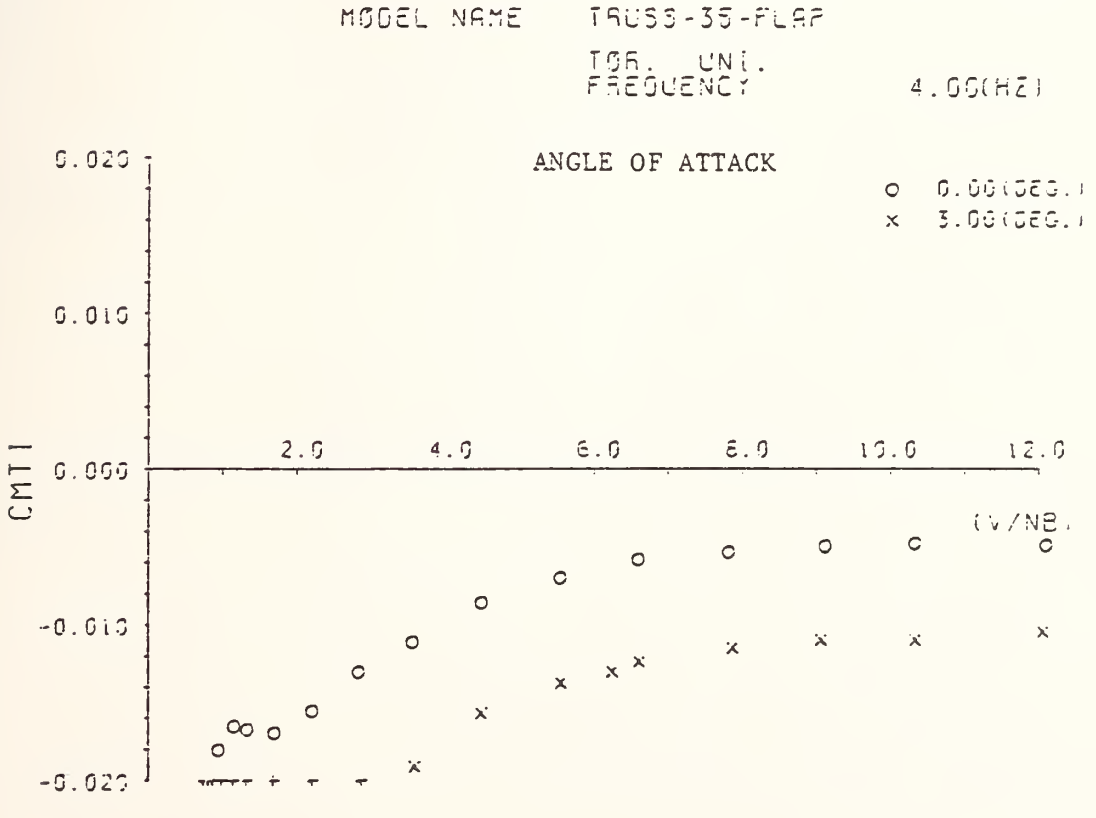

Fig.4-16 C_{MT}^{I} — V/NB (Model No.6)

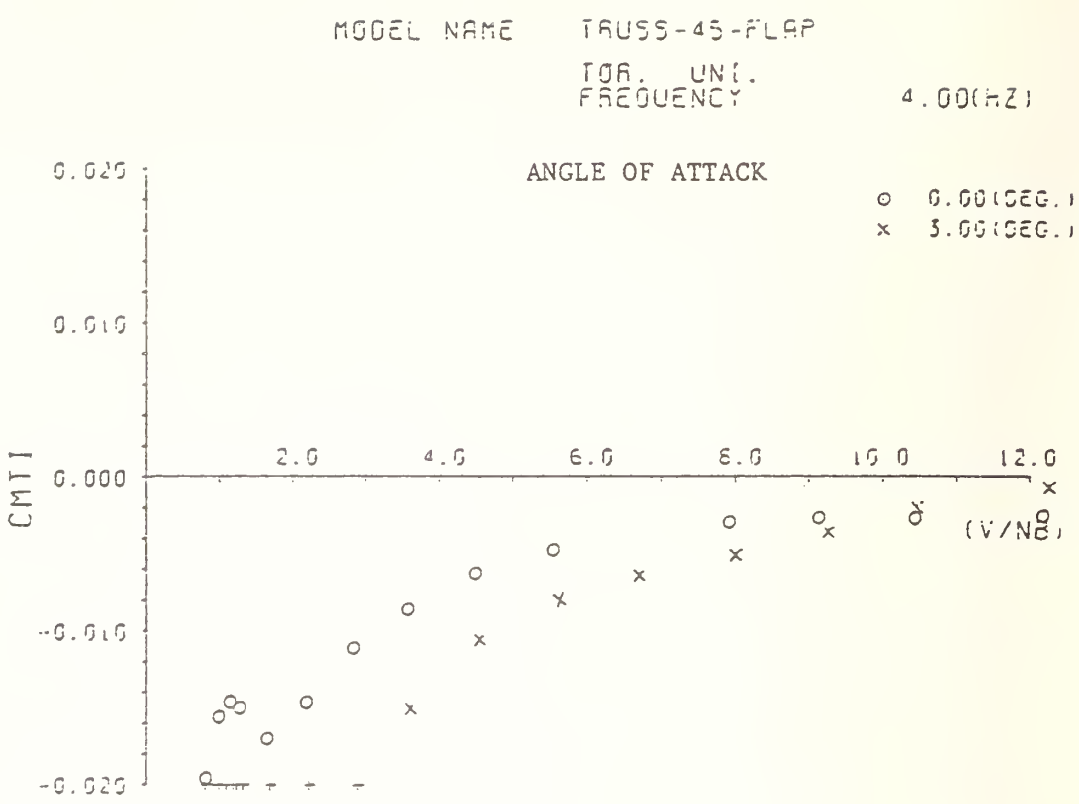

Fig.4-17 C_{MT}^{I} — V/NB (Model No.13)

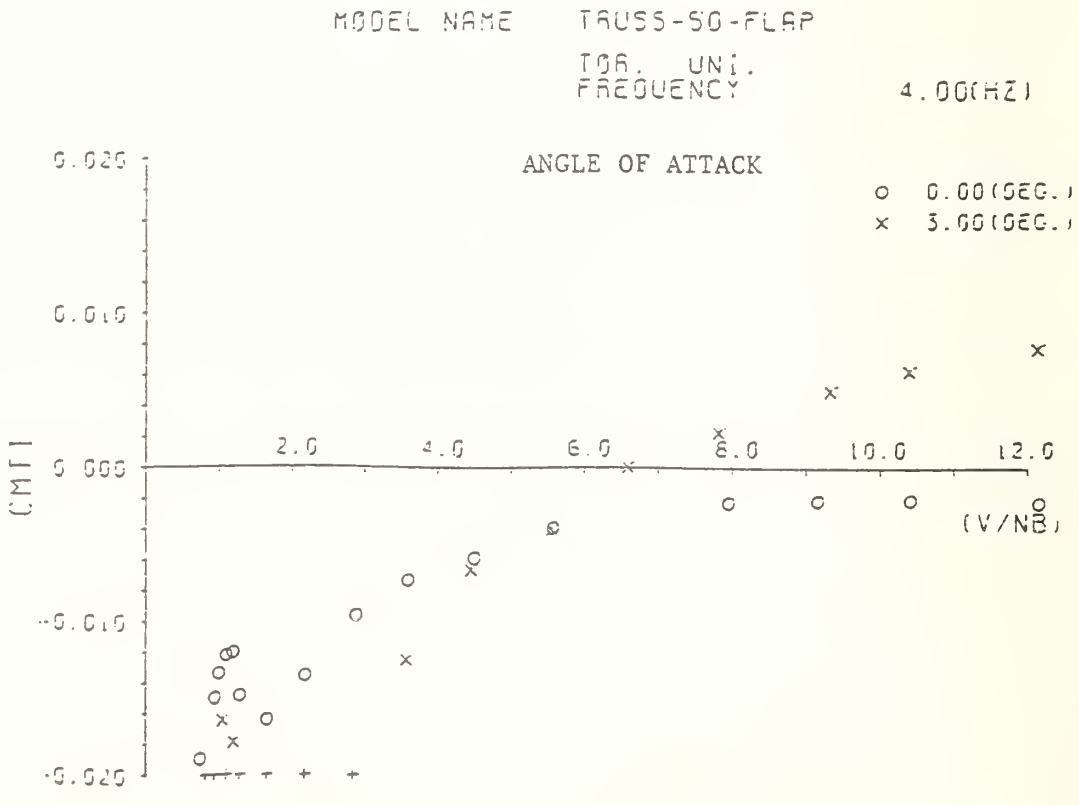

Fig.4-18 C_{MT}^{I} — V/NB (Model No.15)

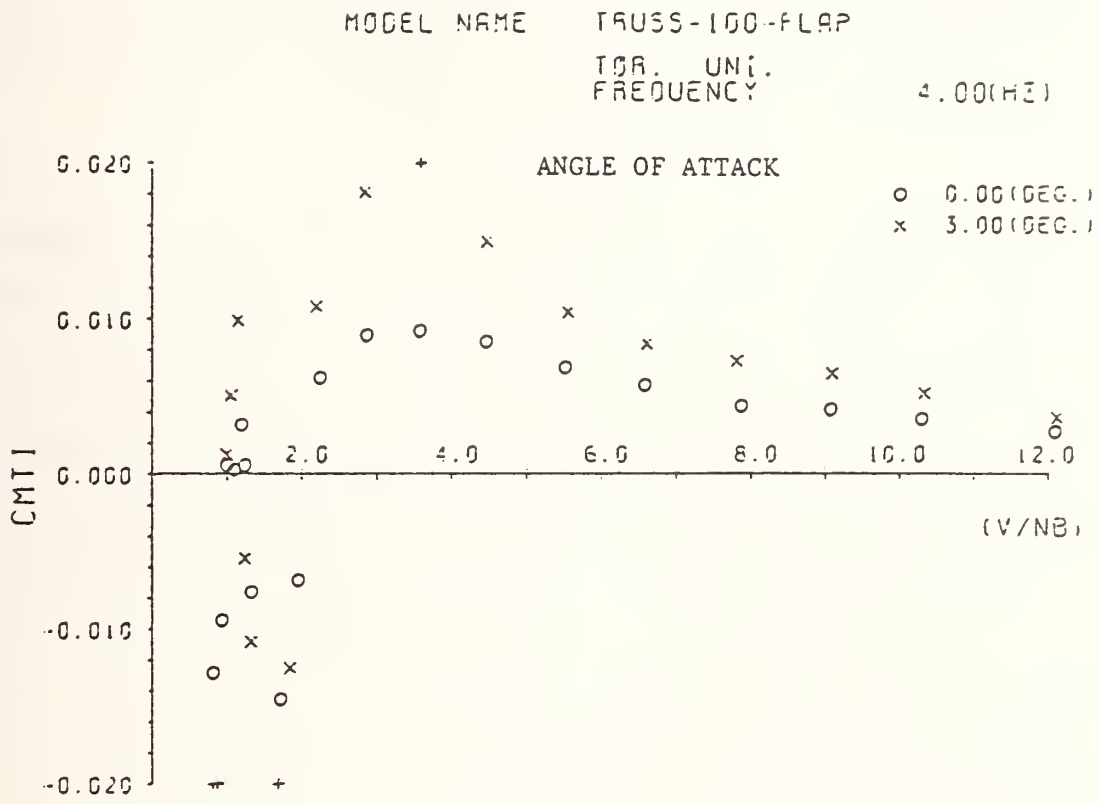

Fig.4-19 C_{MT}^{I} — V/NB (Model No.17)

FIELD STUDIES ON THE PASCO-KENNEWICK CABLE-STAYED BRIDGE

M. C. C. Bampton

Battelle Pacific Northwest Laboratories
Richland, WA

ABSTRACT

This paper briefly describes a recent study to collect bridge motion and natural wind data at the site of the 763 m (2503 ft) Pasco-Kennewick Cable-Stayed Bridge using an automated data collection system. Examples of wind and acceleration spectra as well as coherence and deck frequency measurements are presented. The research was sponsored by the Federal Highway Administration and performed by Battelle Pacific Northwest Laboratories over a 3 year period.

INTRODUCTION

Traditionally, wind tunnel tests on scaled section models have been used to evaluate the aerodynamic stability of long-span bridge designs. This procedure is generally considered to provide conservative (safe) results.

However, there are two areas of uncertainty in wind tunnel tests and the interpretation of their results. The first is related to differences in turbulence characteristics between the real world and the wind tunnel and the effect of these differences on the wind velocities that initiate unstable structural aeroelastic oscillations. The second area of uncertainty is related to the transfer of energy from the wind to the bridge and the dissipation of that energy by the bridge. The Federal Highway Administration has sponsored a study of wind induced motions of the new, cable-stayed bridge between Pasco and Kennewick, Washington to provide prototype information on atmospheric turbulence and the actual response of a bridge to the turbulence.

The specific objective of the study was to determine the responses of an existing, inland, long-span, cable-stayed bridge to the wind. This was accomplished by making detailed measurements of the wind structure and bridge motions during a 2 year period. The contract for this study was awarded to Battelle, Pacific Northwest Laboratories in Richland, WA.

THE BRIDGE SITE

The Pasco-Kennewick Cable-Stayed Bridge was opened to traffic September 16, 1978. It is currently the longest span, cable-stayed bridge in the United States (figure 1). The bridge has a total length of 763 m (2503 ft) and a center span of 229 m (981 ft). Its width is 25 m (81 ft). At the middle of the center span, the vertical clearance between the bridge and the river is 18 m (60

ft). The cables that support the road-bed are hung from concrete towers that extend 74 m (244 ft) above the rivers normal water line.

Pasco, Kennewick, and Richland, collectively referred to as the Tri-Cities, are situated on the Columbia River in South-Central Washington State, just north of the Washington-Oregon border (figure 2). This part of the State has a semiarid climate with southwesterly prevailing winds with an average wind speed of 3.5 m/s (7.9 mph).

In the reach of the river between Pasco and Kennewick, the Columbia flows from the west-northwest. Therefore, the prevailing winds and almost all high winds approach the bridge from its upriver side. The upwind fetch in this direction is relatively unobstructed. There are no isolated surface features that would have a dominant effect on turbulence characteristics.

RESEARCH APPROACH

Preliminary investigations included: review of previous research on wind induced motions with particular emphasis on motions of long-span bridges, study of the reports of wind tunnel tests of a scaled section model of the Pasco-Kennewick Cable-Stayed Bridge, and evaluation of the adequacy of the Federal Highway Administration instrument system provided for use in this study.

The data collection phase of the research included: physical checkout and calibration of the instrument system, selection of locations on the bridge for instrument installation, preparation of mounting brackets and installation of the instruments, maintenance of the instrument system, collection of wind and bridge motion data, and removal and packaging of the instrument system for shipment to the location of the next study.

INSTRUMENTATION

The primary instruments for measurement of bridge motions were paired, servo-type accelerometers, manufactured by Tetra Tech, Inc. They were firmly attached to the road-bed support structures inside weatherproof boxes (figure 3). The accelerometer signals were filtered to remove the effects of extraneous high frequency motions that might have been generated by vehicular traffic.

Twelve accelerometers were distributed along the bridge deck in pairs, one on each side, at six stations (figure 4). In each pair the accelerometers moved in identical directions for pure bending motions, and in opposite directions for torsional motions. Symmetry in the bending motions was assumed to exist about the midpoint between towers. Early accelerometer data were used to check this assumption.

The primary wind instruments used were three-dimensional propeller anemometers, commonly referred to as Gill anemometers. Gill anemometers, manufactured by R. M. Young Co., are a compromise between

the rugged instruments required for high wind speed measurements and the response sensitivity required for turbulence measurements. The three propeller configuration permitted complete description of wind vector, and the 1 m (3 ft) distance constant of these anemometers permitted resolution of turbulent eddies that were small compared to the major structural components of the bridge.

The anemometer supports consisted of an aluminum frame, tensioned from above and below, that held the anemometer 2.5 m (8.2 ft) away from the deck (figure 5). Six anemometers were positioned on the west side of the deck in a logarithmically spaced array (figure 4). Separation between anemometers ranged from 10 to 310 m (33 to 1017 ft) with no two separations the same.

The data acquisition system provided by the Federal Highway Administration was capable of automatically recording data from a maximum of 60 input signals. Signal conditioning was available for 39 input channels leaving 21 spare channels for monitoring system performance. Ten channels of supplementary signal conditioning were used in conjunction with the anemometers to trigger the recording system. A multiplexor stepped through the channels at the rate of 1250 samples per second and passed the signals to the A/D converter. The digitized samples were then stored in a data buffer in 8-bit, offset-binary form prior to being written on one of two tape drives. A trailer, housing the data acquisition system, was located immediately beneath the bridge at the Pasco end.

DATA ANALYSIS

The digitized data were first processed by a tape screening program. This program summarized the data by generating maxima, minima, averages, and standard deviations of each sensor's output for prescribed time periods. The summaries were used as a basis for the selection of data sets to be processed further. In the latter stages of processing pairs of time histories were analyzed simultaneously using Fast Fourier transform techniques to obtain power spectral densities and autocorrelations for individual series, and cross-spectral and cross-covariance estimates for each pair.

Three sets of data were selected for analysis in detail. They were chosen principally on the basis of wind directions (figure 6). One is almost perpendicular to the bridge, one is parallel, and the third is in a quartering direction. Power spectra were computed for the wind components perpendicular and parallel to the span and for the vertical wind component for each of the cases (figure 7). The spectra do not reveal any unusual features in the wind turbulence. The spectral characteristics for each component for the three cases were compared by plotting the spectra on a common graph (figure 8).

The spatial characteristics of the turbulence were examined by computing the coherence in the wind signals produced by pairs of anemometers (figure 9). Coherence is a measure of the correlation between the signals in a small frequency band. By examining the manner in which the coherence decreases as the frequency increases, it is possible to estimate the size of typical turbulent eddies.

The logarithmic plots of deck acceleration spectra show symmetry of response about the midpoint of the bridge (figure 10). This is observed by comparing accelerometer 4 response with that of accelerometer 12, and accelerometer 2 response with that of accelerometer 10. The latter two spectra indicate how reduced the motion is at the deck stations immediately adjacent to the towers. The linear plots of acceleration spectral densities for two of the sensors indicate a tendency for the deck to respond to a parallel wind (March 20) in a torsional mode (0.68 Hz) and to the quartering (March 23) and perpendicular (July 22) winds in a bending mode (0.35 Hz) (figure 11).

The first four mode shapes for the deck were identified consistently throughout the data (figure 12). Relative amplitudes and phases were obtained through transfer functions for the various accelerometers in response to the excitation due to the prevailing wind and vehicular traffic. A fifth mode - second torsion - was identified with difficulty within some of the data. The experimental values for the bridge deck lower frequencies obtained by processing the data tapes were compared with the results of a finite element analysis (figure 13). Agreement for the bending modes was excellent.

The half bandwidth method was used to formulate the estimates of damping at various frequencies. The peak width at 50 percent of the peak amplitude of the power spectra is applied in conjunction with the frequency of the amplitude in question. This method does not recognize the effects of amplitude dependence. The table of damping estimates, obtained by the half bandwidth method, shows a degree of consistency by two of the accelerometers for several frequencies (table 1). These values represent total system damping which includes both structural and aerodynamic contributions. The estimates are reasonable for a concrete bridge structure.

CONCLUSIONS

During the 2 year exposure period, no severe storms or extreme wind conditions were recorded at the site. The cable-stayed bridge shows very little response (0.01 g's) to the recorded winds. For the observed conditions, the bridge demonstrates excellent performance and confirms the aeroelastic stability exhibited in the wind tunnel tests.

The higher speed wind events are generally from the south-southwest to southwest. There are no unusual features related to the turbulence spectra, although computed coherences appear to be higher than reported by previous research. This feature is particularly true for winds parallel to the span.

The deck lower vibration modes and frequencies are well established and damping estimates appear reasonable.

This field study is one of a series of field studies either sponsored by or conducted by the Federal Highway Administration. The results will be used to evaluate and improve both experimental and analytical procedures for predicting the aerodynamic stability of long span bridges.

Table 1. Deck Damping Values by the Half Bandwidth Method

Date	Frequency (Hz)	Damping Factor	
		Accelerometer 8	Accelerometer 6
March 20, 1981	.36	.00432	.0040
	.57	.00365	.0030
	.68	.0023	.0014
	.75	.00258	.0028
March 3, 1980	.36	.0048	.0043
	.50	.0030	.0036
	.68	.0041	.0023
	.77	.0019	.0020
July 22, 1980	.36	.0037	.0040
	.50	.0036	.0035
	.68	.00193	.0020
	.76	.00187	.0031

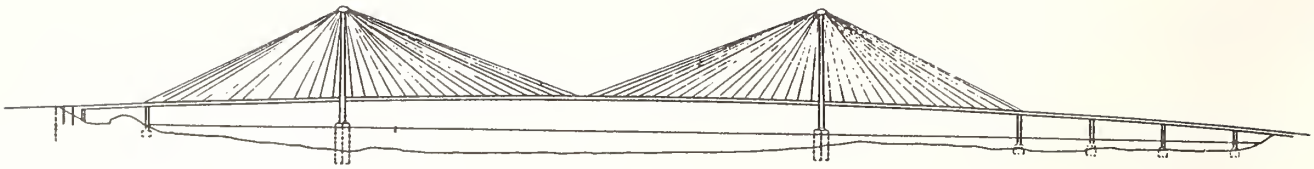

Figure 1.

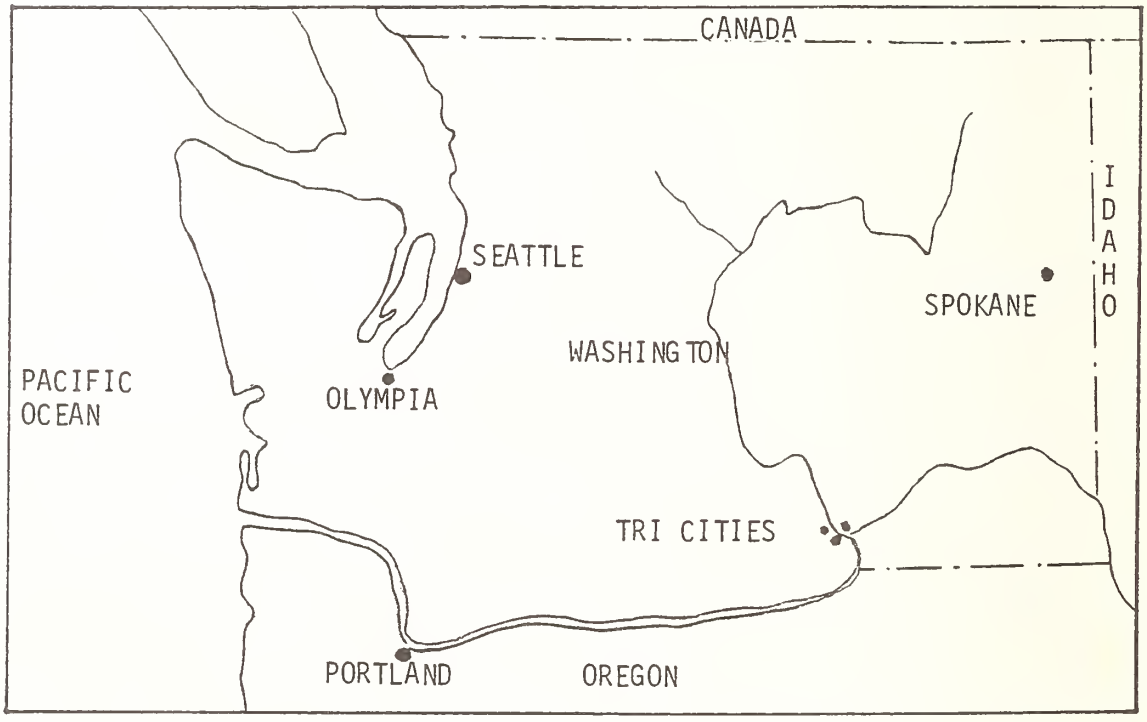

Figure 2.

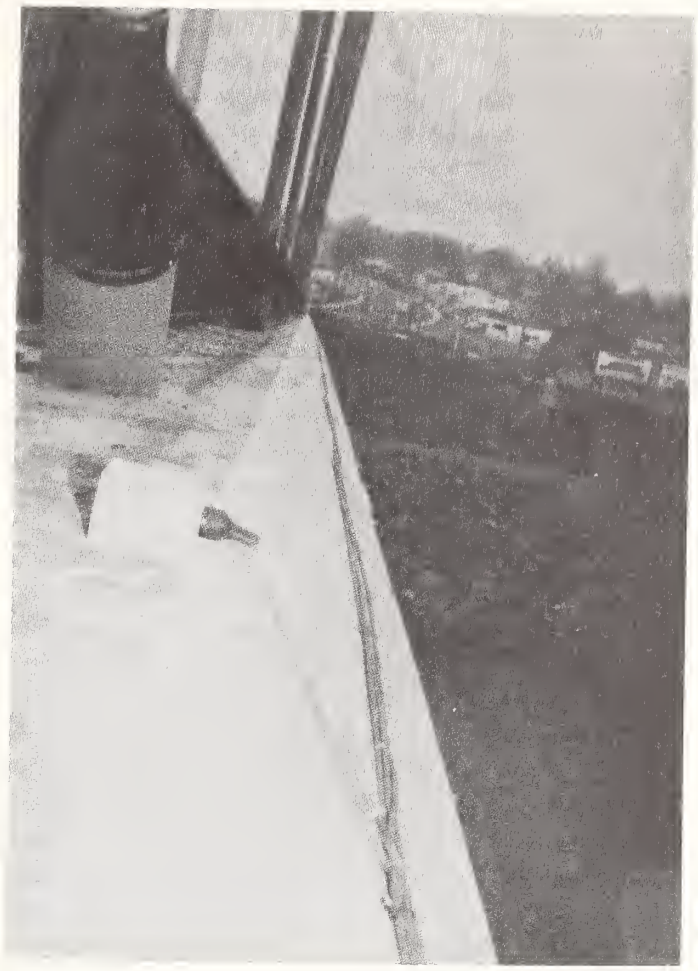

Figure 3.

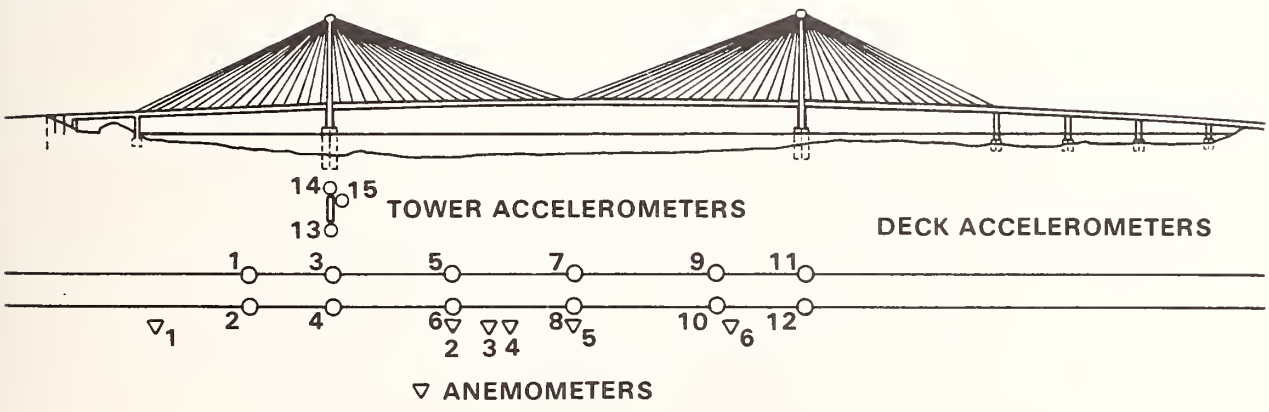

Figure 4.

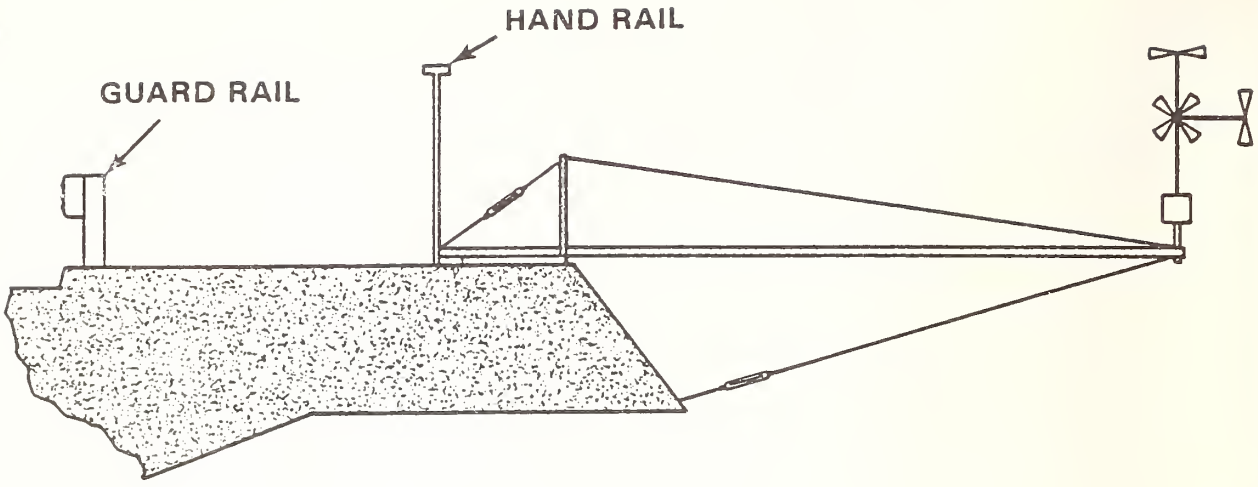

Figure 5.

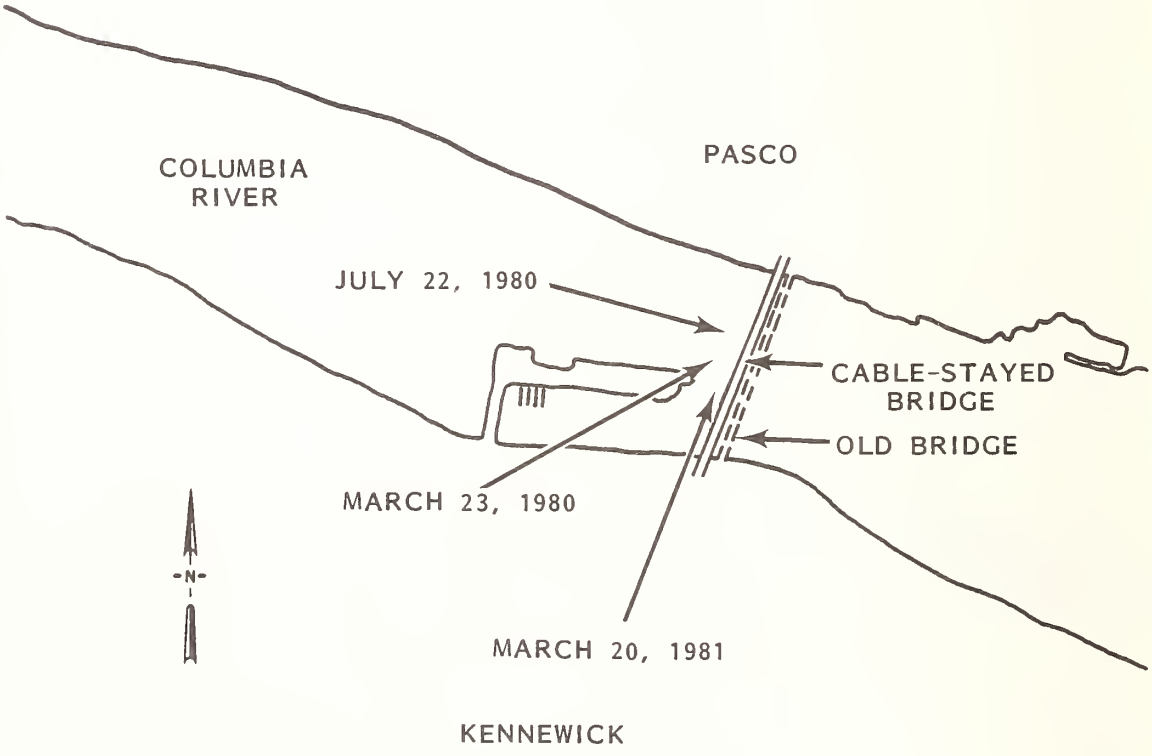

Figure 6.

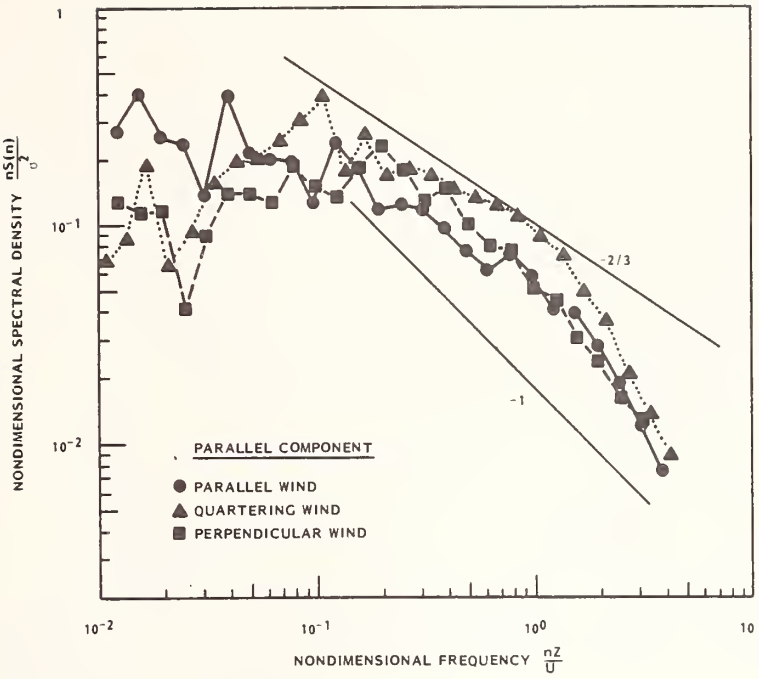

Figure 7.

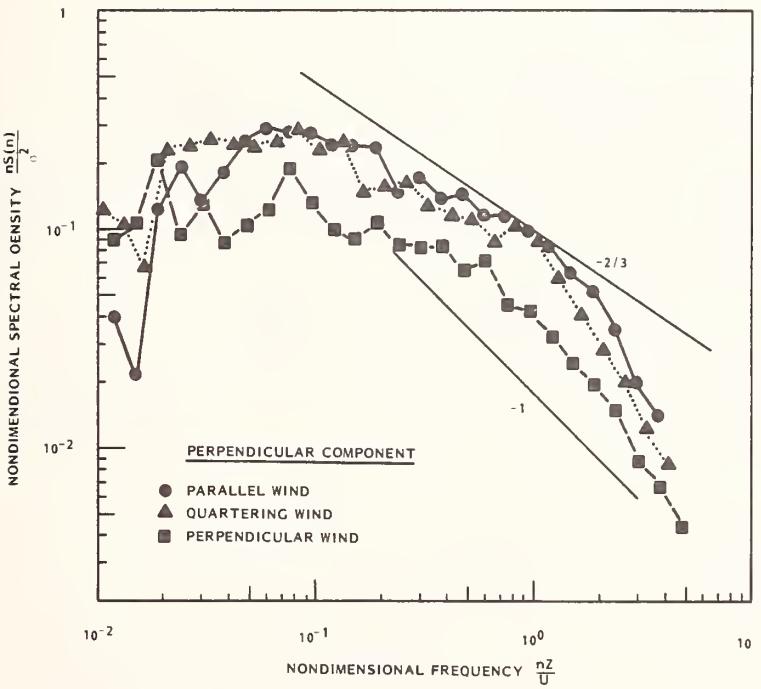

Figure 8.

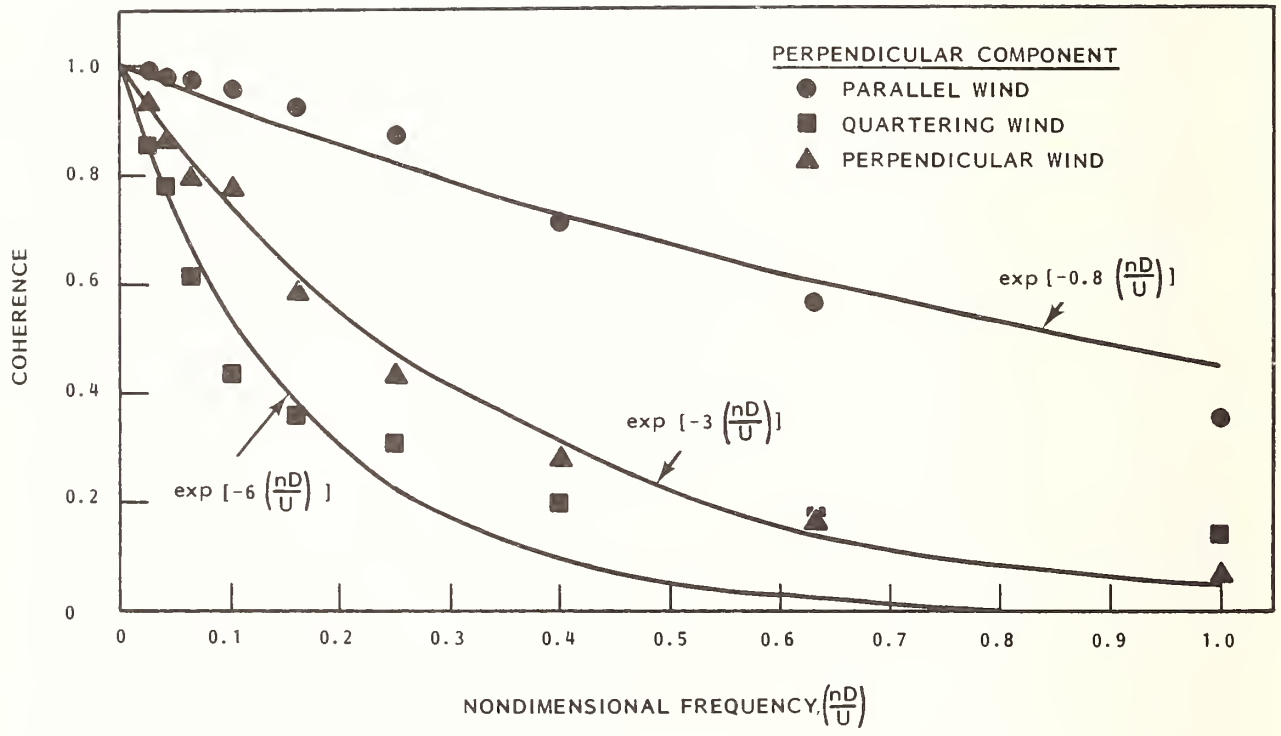
PERPENDICULAR COMPONENT
PARALLEL WIND
QUARTERING WIND
PERPENDICULAR WIND
exp [-0.8 (nD/U)]
exp [-3 (nD/U)]
exp [-6 (nD/U)]
COHERENCE
NONDIMENSIONAL FREQUENCY, (nD/U)
1.0
0.8
0.6
0.4
0.2
0
0.1
0.2
0.3
0.4
0.5
0.6
0.7
0.8
0.9
1.0

Figure 9.

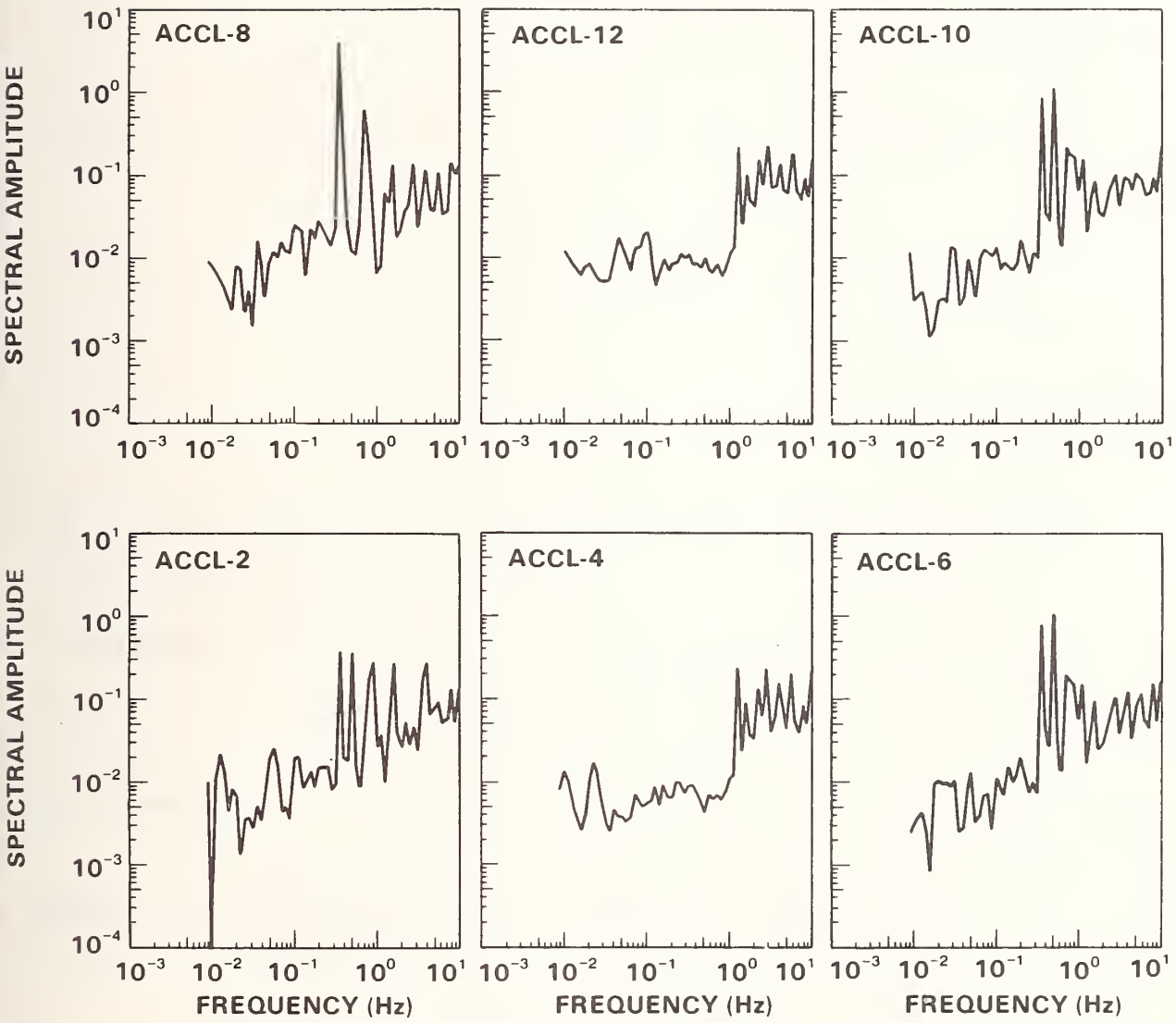
ACCL-8
ACCL-12
ACCL-10
ACCL-2
ACCL-4
ACCL-6
SPECTRAL AMPLITUDE
SPECTRAL AMPLITUDE
FREQUENCY (Hz)
FREQUENCY (Hz)
FREQUENCY (Hz)

Figure 10.

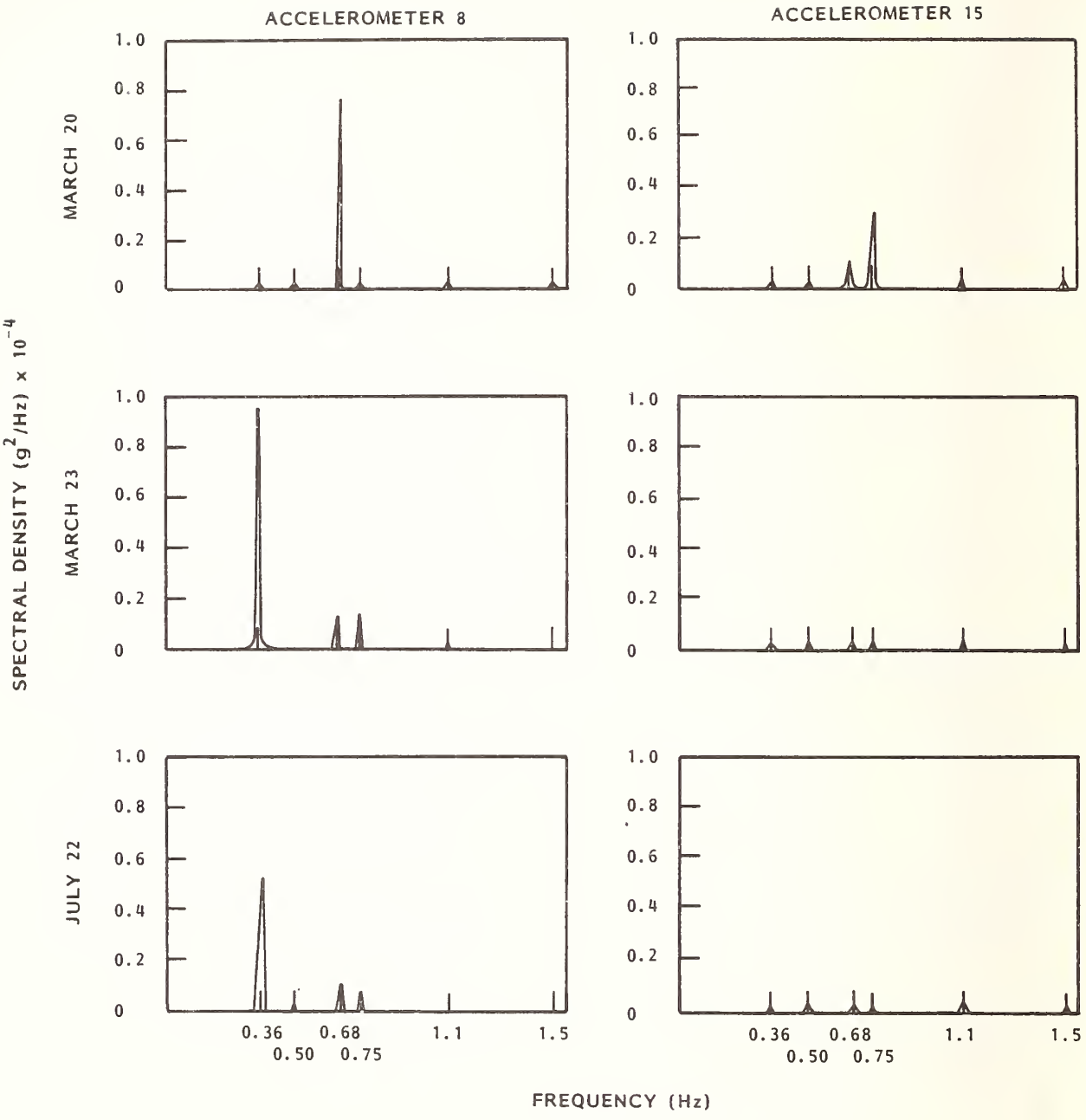
ACCELEROMETER 8
ACCELEROMETER 15
MARCH 20
MARCH 23
JULY 22
SPECTRAL DENSITY (g²/Hz) x 10⁻⁴
1.0
0.8
0.6
0.4
0.2
0
0.36
0.50
0.68
0.75
1.1
1.5
FREQUENCY (Hz)

Figure 11.

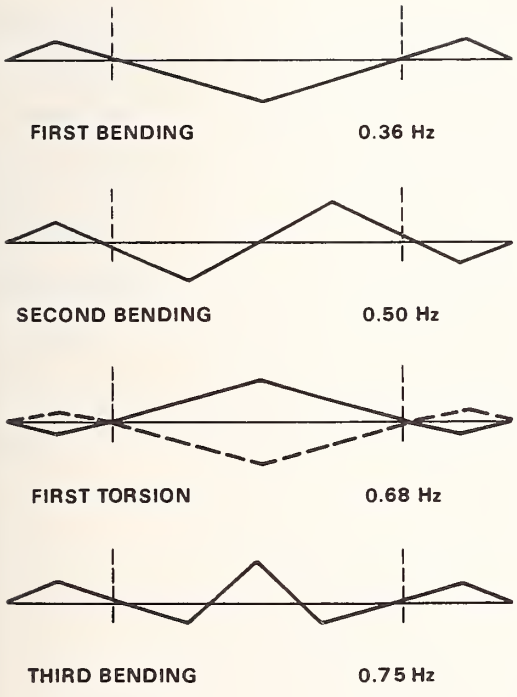

Figure 12.

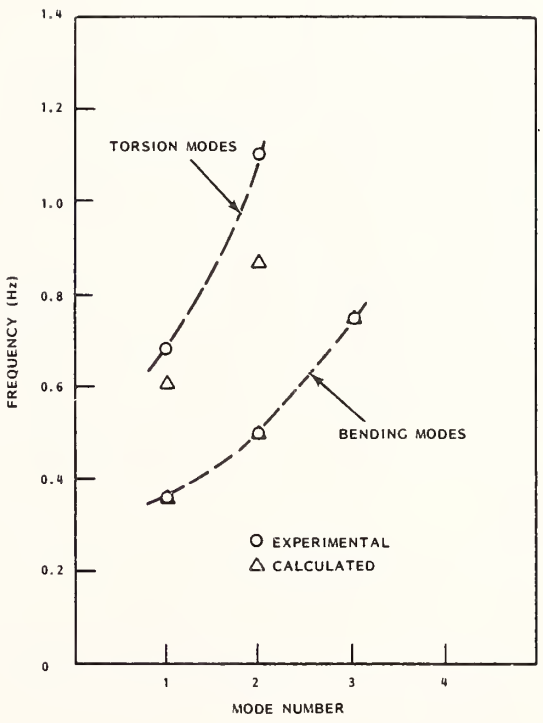

Figure 13.

WIND LOAD ON SOLAR WATER HEATERS

H. Okada
T. Murota

Bulding Research Institute
Ministry of Construction

ABSTRACT

Solar water heaters mounted on house roofs are becoming widely used due to the recent rise of consciousness of saving energy in Japan. This paper describes results of wind tunnel tests conducte to obtain information with regard to wind forces on solar water heaters mounted on house roofs. The effects of heater shape, mounting pattern, roof pitch, roof shape, etc., on wind forces on heaters are discussed.

The paper also describes a field observation of wind forces on a full-scale solar water heater mounted on a cottage.

INTRODUCTION

Recently, solar water heaters are becoming widely used in Japan to save energy. Most of those heaters are mounted on roofs of residential houses where they are sometimes exposed to strong winds. It is therefore of great concern for structural engineers to provide safe installation of the heater against their demolition in winds. It is difficult at present to examine the safety of mounting methods because of the lack of information that can be applied for examination.

As a cooperative research program between the Building Research Institute and Center for Better Living, a series of wind tunnel tests was conducted to obtain information on wind load on solar wate heaters mounted on residential houses and the results of these wind tunnel tests are described in this paper. The cooperative research also started a field observation of wind load on a full-scale solar water heater in October 1981. The full-scale test setup is described herein.

DESCRIPTION OF WIND TUNNEL TEST

TEST PARAMETERS

Main parameters which govern the wind force on solar water heaters mounted on roofs are as follows:

1. shape of heater,
2. shape of house,
3. mounting position and pattern,
4. wind properties (mean wind velocity profile, turbulence intensity, and scale of turbulence)

The following variations were made for each parameter in the investigation:

1. Shape of Heater

In general, solar water heaters are either plate-like (type I) or laid-L-like (type II) in shape with their sizes about 2 m x 2 m or 1 m x 2 m. The number of heaters mounted on residential houses, in most cases, are one for 2 m x 2 m size heaters or two for 1 m x 2 m size heater. Therefore, the following four cases were chosen for the study of this parameter (figure 1):

a. one 2 m x 2 m plate-like heater

b. one 2 m x 2 m laid-L-like heater

c. two 1 m x 2 m plate-like heaters set apart at a distance of 20 cm in parallel direction

d. two 1 m x 2 m laid-L-like heaters set apart at a distance of 20 cm in parallel direction

2. Shape of Residential House

The shape and dimension of the roofs of the residential houses on which the four types of heaters were mounted are given below (figure 2):

plan: 3.15 m (spanwise) x 4.05 m

roof: flat roof and gable roof of 1/10, 2/10, 3/10, 4/10, and 5.8/10 pitch

height of eaves: 3.4 m (one story house) and 6.0 m (two story house)

3. Position and Pattern of Mounting

Four positions and five patterns shown in figures 4 and 5, respectively, were selected for heaters to be placed on roofs. The heaters in positions A and B are located on the center line of a roof slope and positions C and D on the ridge. In pattern (a), the heaters are set on the roof without leaving any space between the back surface of the heater and the roof surface. This pattern can only be utilized on sheet metal roofs. Pattern (b) has a 10 cm gap between the two surfaces and has been used quite frequently. Heaters are mounted using pattern (c) when the ridge of the house is running in the south to north direction. Pattern (d) is applied in such a case that the solar energy cannot be fully supplied if heaters are mounted parallel to the roof slope. Pattern (e) is applied in cases similar to pattern (d) but with small roof area.

4. Wind Properties

Residential houses where solar water heaters are to be installed are located in various districts which consist of a different extent of aerodynamic surface roughness. In general, the smaller is the surface roughness in a district, the larger becomes the force on solar water heaters. Therefore, installation of solar water heaters can be designed on the safe side if the wind force data obtained in a district having a smaller surface roughness is selected. The wind in this experiment was selected

as the one in open rural districts where the mean wind velocity profile can be expressed by a logarithmic formula with the roughness parameter, Z_0, of 14 cm.

From many possible combinations of those parameters stated above, 55 conditions were selected in the program as summarized in table 1.

WIND TUNNEL TEST

1. Wind Tunnel

The wind tunnel used in the test was the Boundary Layer Wind Tunnel at the Building Research Institute, which has a working section of 3.0 m (width) x 2.5 m (height) x 25.0 m (length) and the maximum wind speed of 24 m/s.

2. Wind Tunnel Model

The scale of the model for residential houses and solar water heaters was 1/20. Model dimensions are shown in figures 1 and 2. The maximum blocking ratio, the ratio of the maximum projected area of the model to the cross sectional area of the wind tunnel was 2.8 percent.

Pressure taps of 1 mm diameter hole were made on the upper and lower surfaces of the heater. The number of taps was 24 (12 each on upper and lower surfaces) for type I models and 28 (16 and 12 on upper and lower surfaces, respectively) for type II models.

3. Wind Tunnel Flow

Turbulent boundary layer similar to the one in rural districts was simulated by utilizing roughness blocks and spires arranged on the tunnel floor. Photograph 1 shows the wind tunnel model. Mean wind velocity profile, turbulence intensity profile, and power spectrum of turbulence observed at the model test sites are shown in figures 6, 7, and 8, respectively. The mean wind velocity can be closely approximated to a logarithmic law of the roughness parameter, Z_0, of 0.70 cm.

4. Pressure Measurement

Wind pressures on heater surfaces were led by vinyl tubes to an electric differential pressure transducer through a scanning device (figure 3). Mean components of the pressures were measured in reference to the static pressure in the wind tunnel.

In addition, the dynamic pressure of wind at a point which is 1 m above the tunnel floor and 2 m upstream from the model center was also measured. The "reference" dynamic pressure stated in the next section was calculated by reducing this pressure to the one at the height of the eaves of model residential houses according to the mean wind speed profile.

WIND PRESSURE COEFFICIENT

Assuming that the same pressure as observed at the ith tap also acts on an area around the tap, the mean wind pressure on the upper surface of the heater can be calculated by equation 1:

$$\overline{P}_{up} = \sum_{i}^{up} Pi\ Ai\ /\ A \qquad (1)$$

where

$\overline{P}_{up}$: mean wind pressure on upper surface,

Pi : wind pressure measured at the ith tap,

Ai : area of the upper surface of heaters subjected to pressure Pi and projected to a plane parallel to lower surface (see figure 10),

A : projected area of upper surface of heaters to a plane parallel to lower surface, and

$\sum_{i}^{up}$: summation over taps on upper surface.

Similarly, the mean pressure on the lower surface is calculated by:

$$\overline{P}_{lw} = \sum_{i}^{lw} Pi\ Ai\ /\ A \qquad (2)$$

where

$\overline{P}_{lw}$: mean wind pressure on lower surface, and

$\sum_{i}^{lw}$: summation over taps on lower surface.

Normalizing these pressures by the reference dynamic pressure, q_o, the wind pressure coefficients are obtained as follows:

$$C_{up} = \overline{P}_{up}/q_o \qquad (3)$$

$$C_{lw} = \overline{P}_{lw}/q_o \qquad (4)$$

The positive and negative coefficients are corresponding to the pressure and suction, respectively. Some examples of the wind pressure coefficients on the upper and lower surfaces of heaters are shown in figures 11 and 12. The azimuth angle in these figures is defined in figure 9. These figures show that the coefficients are negative in almost all the range of azimuth angle. They become minimum at azimuth angles of about 135° and 45° for upper and lower surfaces, respectively. The same tendency is observed also in other series.

WIND FORCE COEFFICIENT

The mean wind force on solar water heaters, $\overline{F}$, can be derived from the difference between the mean wind pressure on upper surface $\overline{P}_{up}$ and that on lower surface $\overline{P}_{lw}$:

$$\overline{F} = \overline{P}_{up} - \overline{P}_{lw} \tag{5}$$

Normalizing this by the reference dynamic pressure, q_o, we can obtain the wind coefficient C as follows

$$C = \overline{F}/q_o \tag{6}$$

The positive and negative coefficients are corresponding to the resultant wind forces acting in the downward and upward directions, respectively.

RELATION BETWEEN WIND FORCE COEFFICIENT AND AZIMUTH ANGLE

Typical examples given the variations of wind force coefficient with azimuth angle are shown in figure 13. The wind force coefficients are positive in the range of 0° to 90° azimuth angle and they reach their maximum values of about 45°. On the other hand, they are negative in value in the range of 90° to 180°, and become minimum at around 135°.

In the wind resistant design of heater mounting, the maximum, and especially, the minimum values of wind force coefficients are of great significance. The effects of various parameters on the extreme values of these coefficients are discussed in the following paragraphs.

MOUNTING PATTERN AND ROOF PITCH

Variations of the maximum and minimum force coefficients with roof pitch are given in figure 14 for each mounting pattern. It can be observed from the figure that the extreme values of the wind force coefficients change greatly with the mounting patterns:

pattern (a) : The minimum wind force coefficients are -1.0 to -1.2 and the maxima are negative.

pattern (b) : The maxima are about 0.1 and the minima are about -0.1. These values are much less than others.

pattern (c) : The maxima are about 1.2 and the minima are about -1.6.

pattern (d) : The extreme values change greatly with roof pitch, i.e., the maximum force coefficient increases from 1.0 to a maximum of 1.2 when roof pitch changes from 0° to 10°. It then decreases sharply with the increase of the roof pitch and nearly equals to zero when the roof pitch is 30°. The minimum force coefficient which is about -1.7 for flat roof, increases to zero as the roof pitch increases to 30°.

pattern (e) : The extreme values for this pattern are larger than other mounting patterns tested and the characteristics of the change is the same as that observed in pattern (d). The maximum coefficient increases from 1.2 to 1.4 for the roof pitch ranging from 0° to 15° and decreases to 0.7 when the roof pitch approaches

30°. The minimum coefficient decreases from -1.6 to -2.0 when the roof pitch varies from 0° to 15° and increases to -1.0 when the roof pitch is 30°.

SHAPE OF SOLAR WATER HEATER

The effect of the shape of heaters on the maximum and minimum wind force coefficients is shown in figure 15. The maximum coefficients for type II are found to be greater than those for type I by 0.1 to 0.4 and the minimum coefficients for type II are found to be less than those for type I by up to 0.4.

SLIT

Figure 16 shows the effect of slit on wind force coefficients. The introduction of a 10 mm slit causes the maximum coefficient of both types I and II to decrease by 5 to 10 percent and the minimum coefficients for type II to increase by 20 to 30 percent. No special effect was found on the minimum coefficients for type I.

NUMBER OF STORIES

The maximum and minimum wind force coefficients for heaters mounted on one-story and two-story houses are compared in figure 17. The absolute values of maximum and minima for the one-story house seem to be larger than those for the two-story house, but the difference is very small. The largest difference is about 10 percent at very slight roof slopes.

MOUNTING POSITION

As shown in figure 18, the effect of mounting position on the maximum and minimum wind force coefficients is minor. In the case where heaters are mounted on the outer part of the roof (positions B and D in figure 4), both the maximum and minimum wind force coefficients are found to be less than those where the heaters are mounted on the inner part (positions A and C). The difference is 10 percent at most.

DESCRIPTION OF FULL-SCALE OBSERVATION

Field observation of the wind forces on a full-scale solar water heater mounted on a small house started in October 1981. The house is located in the Construction Test Field, Building Research Institute. The purpose of the observation is to compare the wind force data observed in the field with those obtained by wind tunnel testing. Specifications of the full-scale heater test are given below:

shape : Type II

net area : 2 m x 2 m

mounting pattern : e

mounting position : C

plan of house : 2.7 m (span) x 3.6 m (ridge)

roof : gable roof

roof pitch : 3/10

Photograph 2 is a view of the full-scale test setup. Wind forces on the heater are measured by three load cells inserted between the heater and the roof. The observation will continue for a few years.

CONCLUSIONS

Wind tunnel tests to obtain wind forces on solar water heaters mounted on roofs were conducted. The results are summarized as follows:

1. Wind pressure coefficients for upper and lower surfaces of the heaters are negative (suction) in general.
2. Wind force coefficients of the heaters are positive (downward) when the azimuth angle is 0° to 90° and negative (upward) when it is 90° to 180°. The positive coefficients are of their maxima at about 45° azimuth angle and negative coefficients minima at about 135°.
3. The extreme values of wind force coefficients depend mainly on the mounting patterns, but not so much on the shape of the heaters, the number of stories of the residential houses, and the mounting position. The effects of the roof pitch on wind forces are large for the cases of mounting patterns (d) and (e), but small in other patterns. The effect of slit between heaters are small for type I heaters but for type II heaters the negative wind force coefficients were found to decrease by 20 to 30 percent with the existence of slit.

Table 1. List of Test Series

Series	No.	Heater				House	
		T	g	S	P	R	St
1	1 2 3	I	0	a	A	1 3 5.8	2
2	1 2 3	I	0	b	A	3 4 5.8	2
3	1 2	I	0	c	C	0 3	2
4	1 2 3 4 5 6	I	0	d	A	0 1 2 3 4 5.8	2
5	1 2 3 4 5 6	I	0	e	C	0 1 2 3 4 5.8	2
6	1 2 3	I	10	d	A	1 3 5.8	2
7	1 2 3	I	0	d	A	1 3 5.8	1
8	1 2 3 4 5 6	I	0	d	A	0 1 2 3 4 5.8	2
9	1 2 3	I	0	d	B	1 3 5.8	1
10	1 2	I	0	c	D	0 3	2
11	1 2 3	II	0	b	A	3 4 5.8	2
12	1 2 3 4 5 6	II	0	d	A	0 1 2 3 4 5.8	2
13	1 2 3	II	10	d	A	1 3 5.8	2
14	1 2 3 4 5 6	II	0	d	B	0 1 2 3 4 5.8	2

T : Type of heater
g : Width of slit (mm)
S : Mounting pattern
P : Mounting position
R : Roof pitch
St : Number of Story

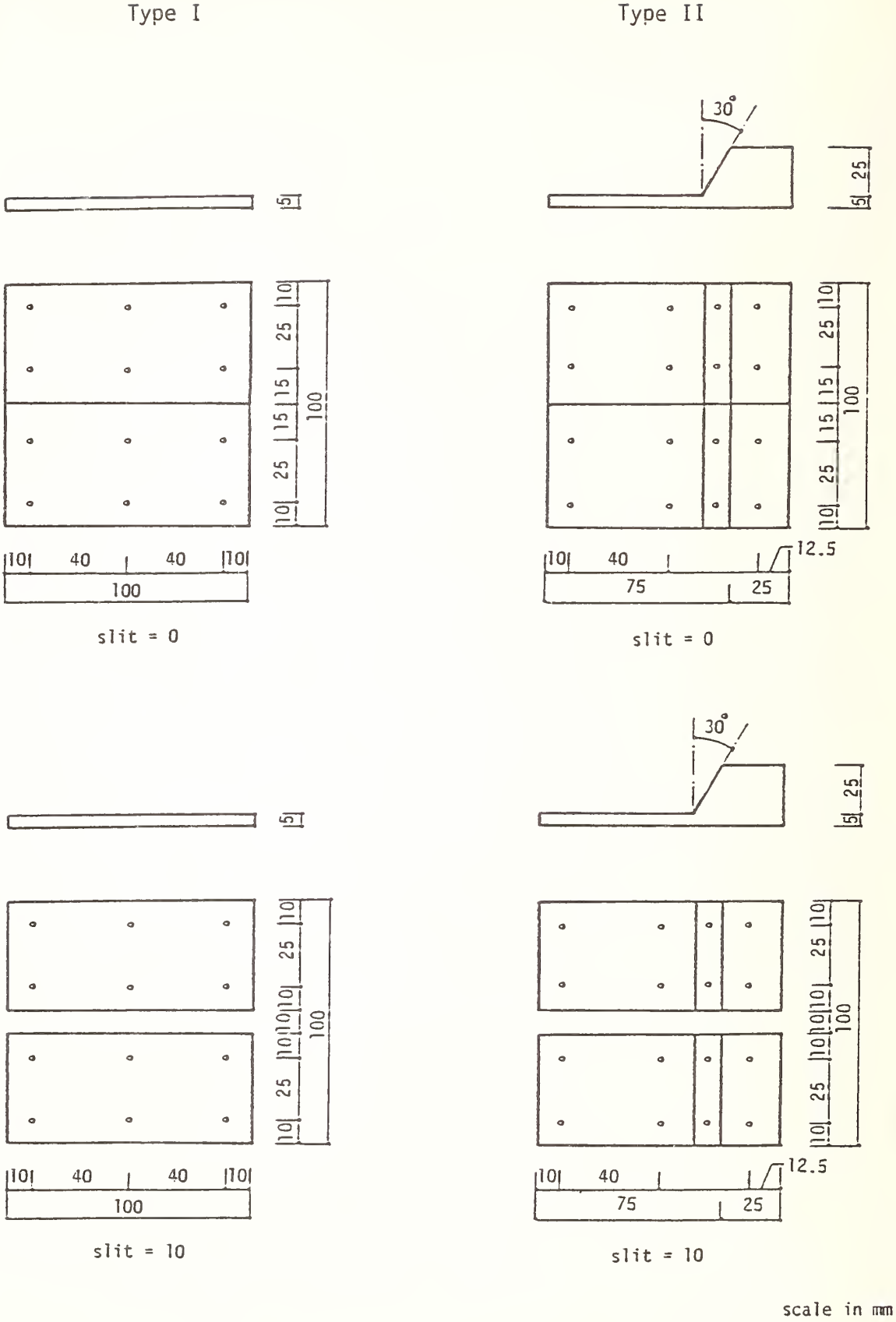

Fig. 1 Types of solar water heaters tested and dimensions of wind tunnel models

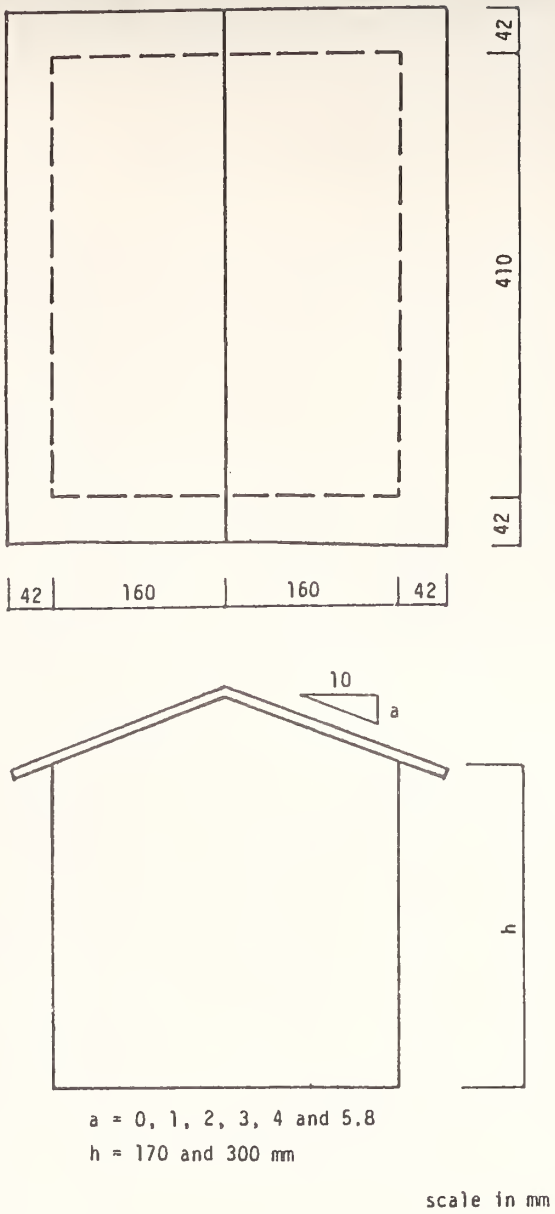

Fig. 2 Shape and size of wind tunnel model houses

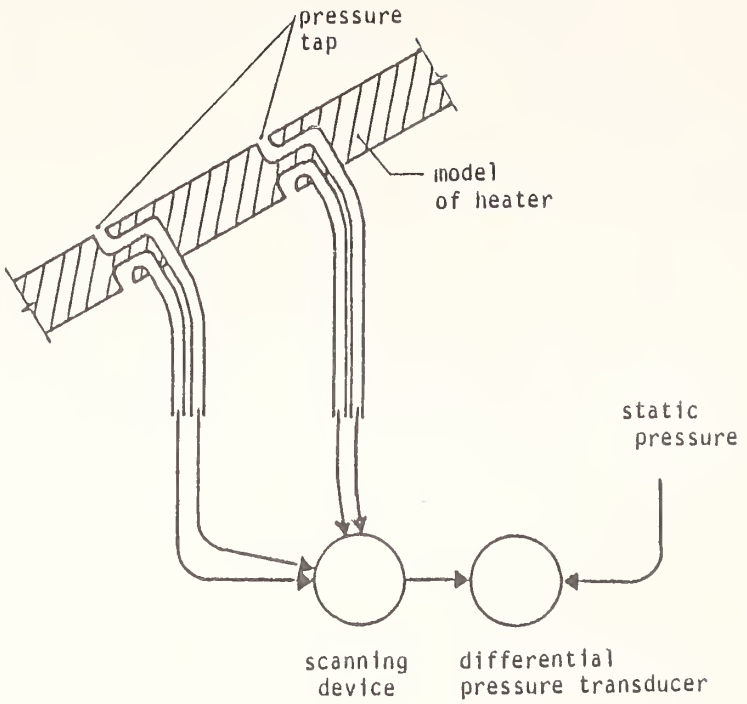

Fig. 3 Wind pressure measurement system

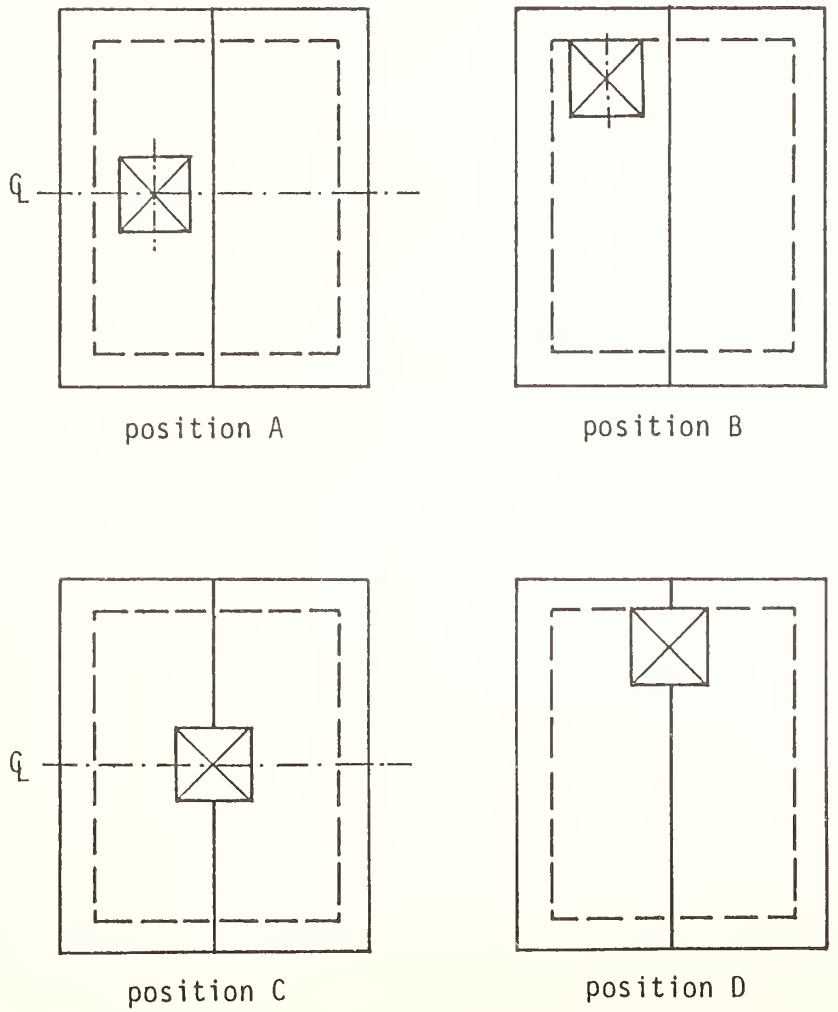

Fig. 4 Mounting position

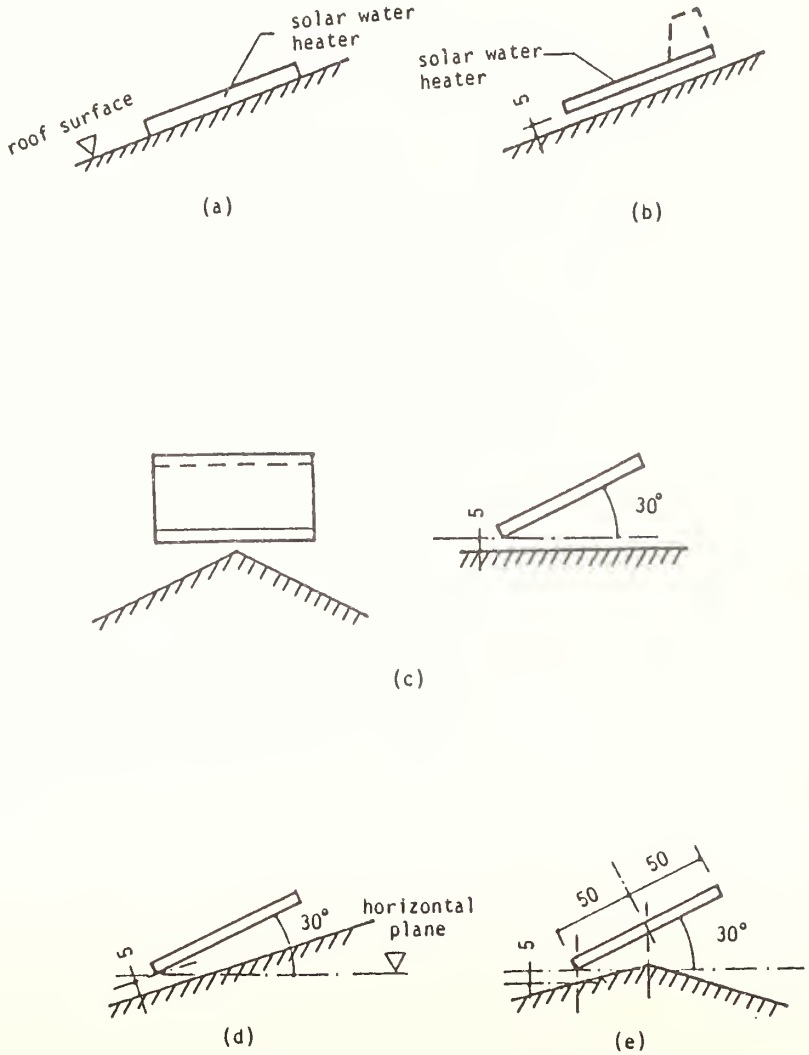

Fig. 5 Mounting pattern

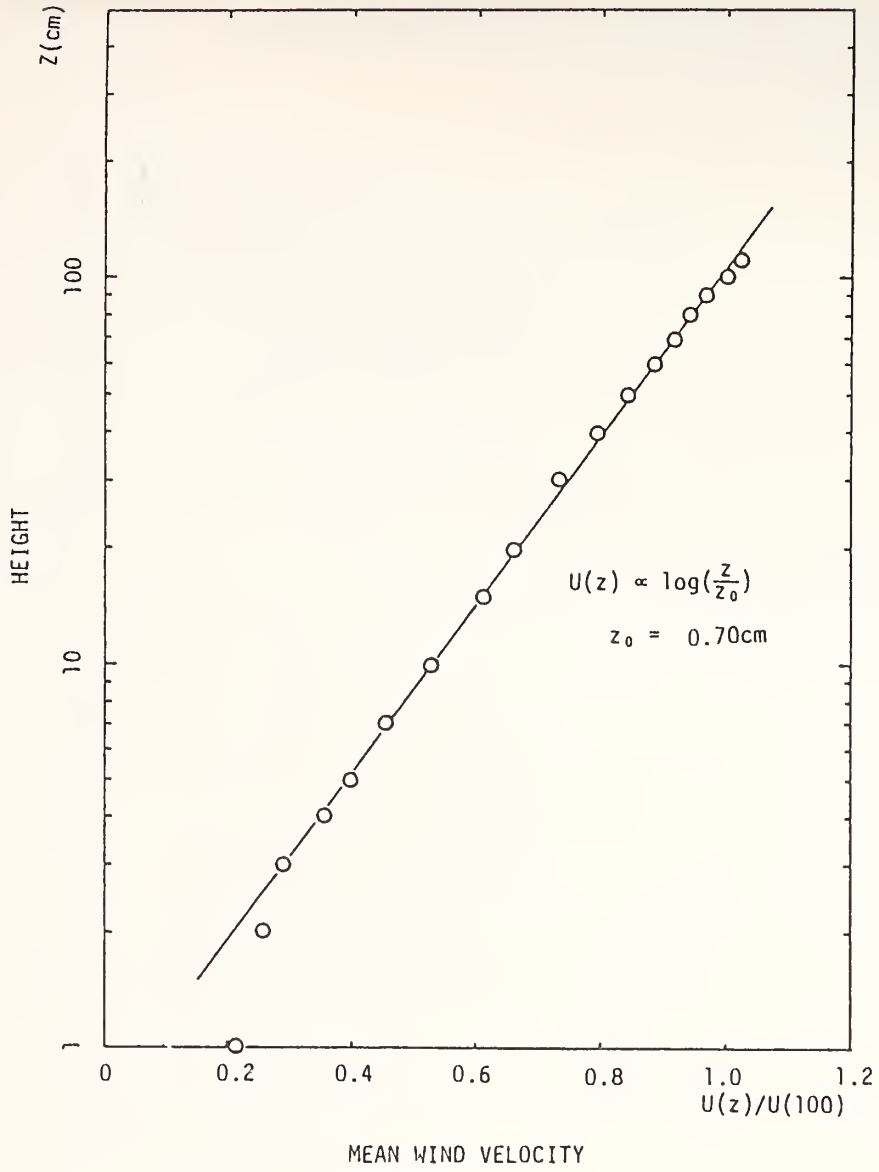

Fig. 6 Mean wind velocity profile

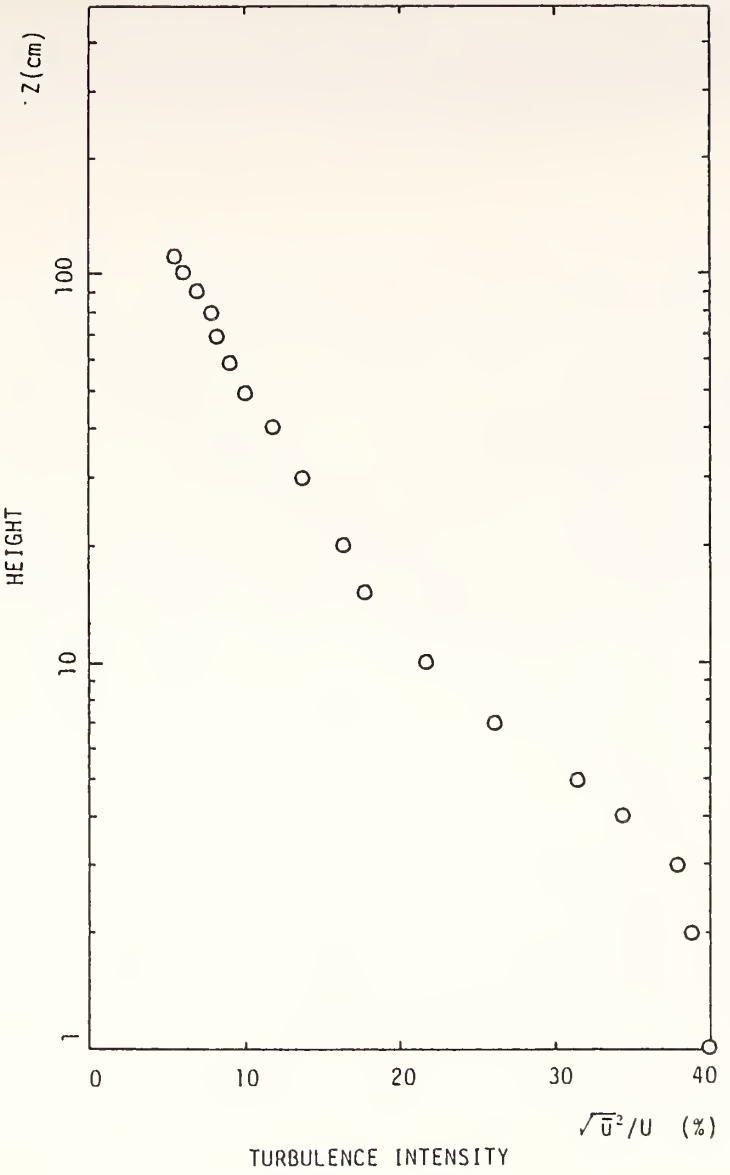

Fig. 7 Turbulence intensity profile

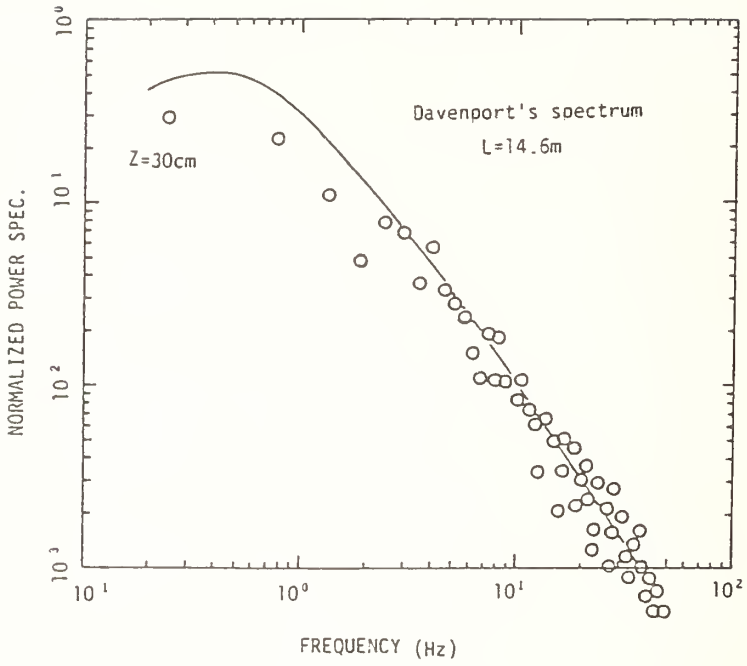

Fig. 8 Power spectrum of turbulence at z=30cm

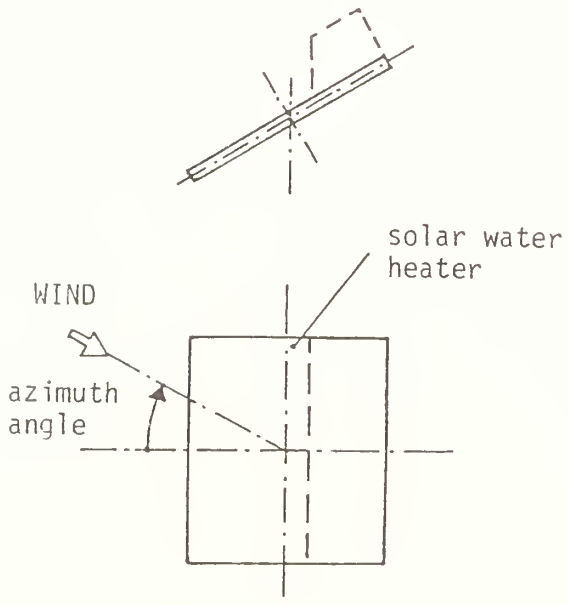

Fig. 9 Difinition of azimuth angle

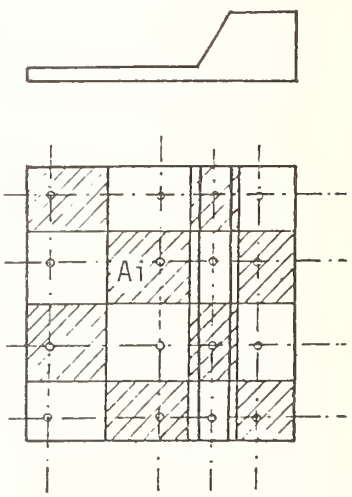

Fig. 10 Difinition of Ai

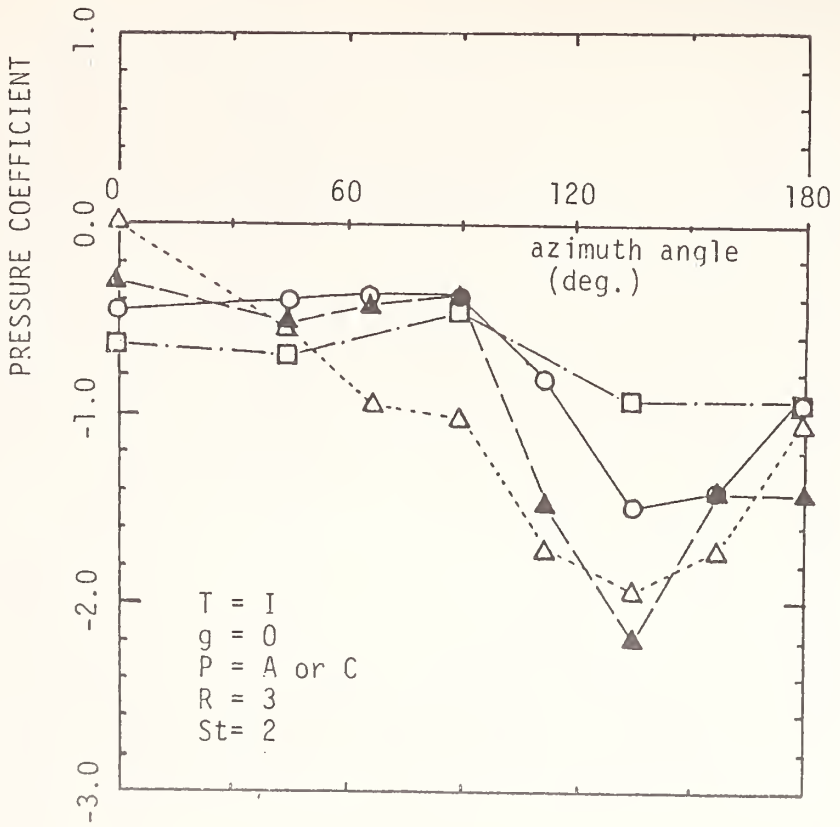

Fig. 11 Variation of upper wind pressure coefficient with azimuth angle
□-·-mounting pattern (b), △·····(c), ○— (d), ▲– –(e)

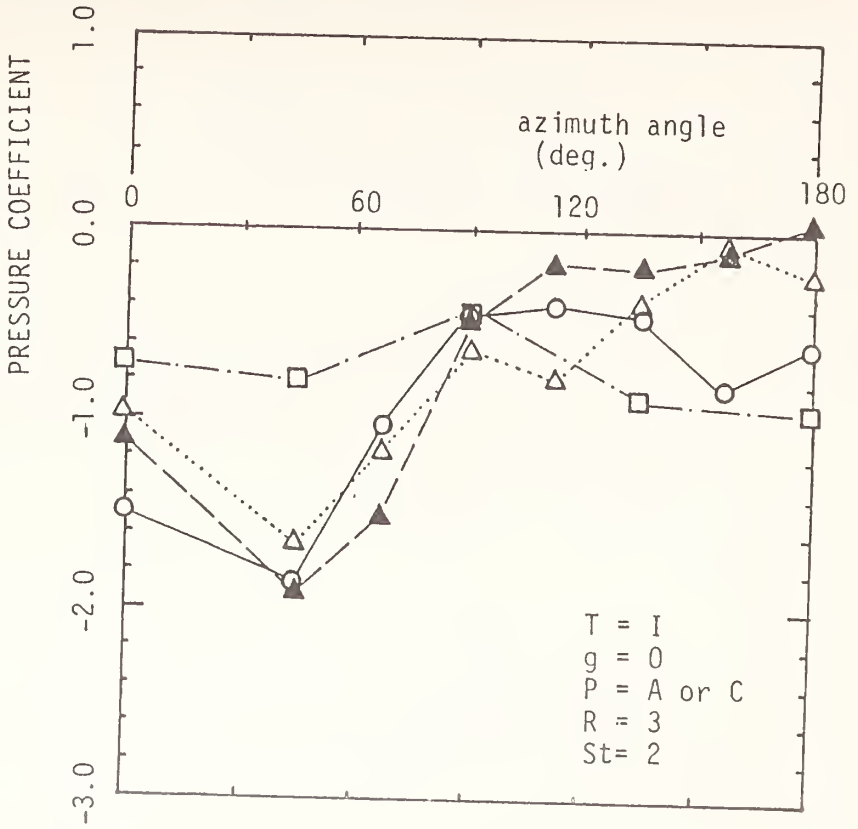

Fig. 12 Variation of lower wind pressure coefficient with azimuth angle
□-·-mounting pattern (b), △·····(c), ○— (d), ▲– –(e)

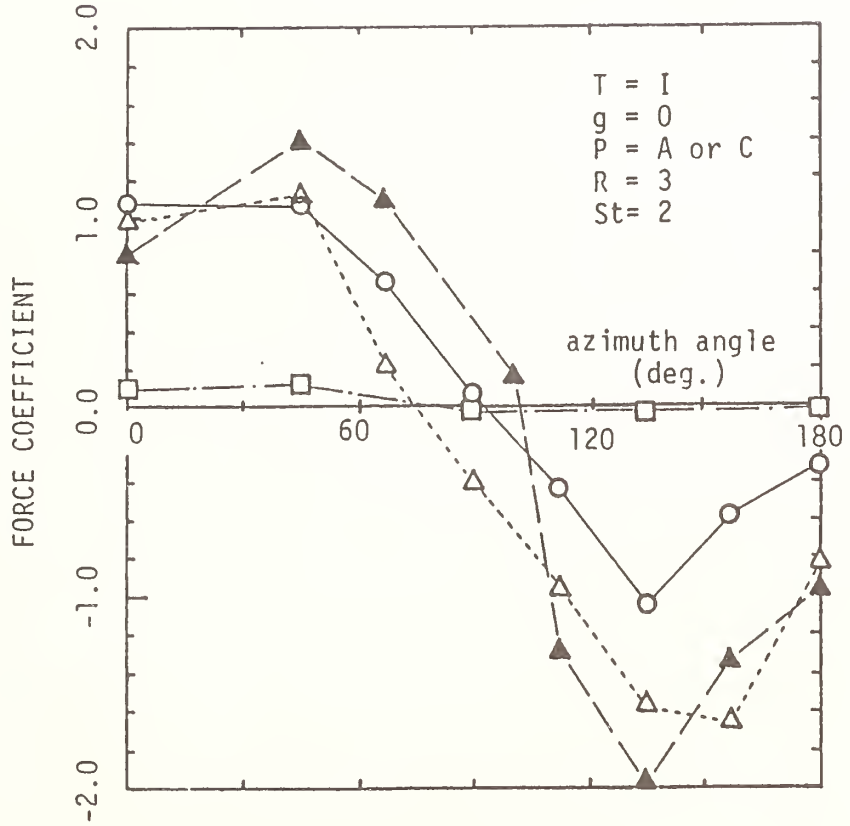

Fig.13 Variation of force coefficient with azimuth angle

□-·- mounting pattern (b), △··· (c), ○— (d), ▲-- (e)

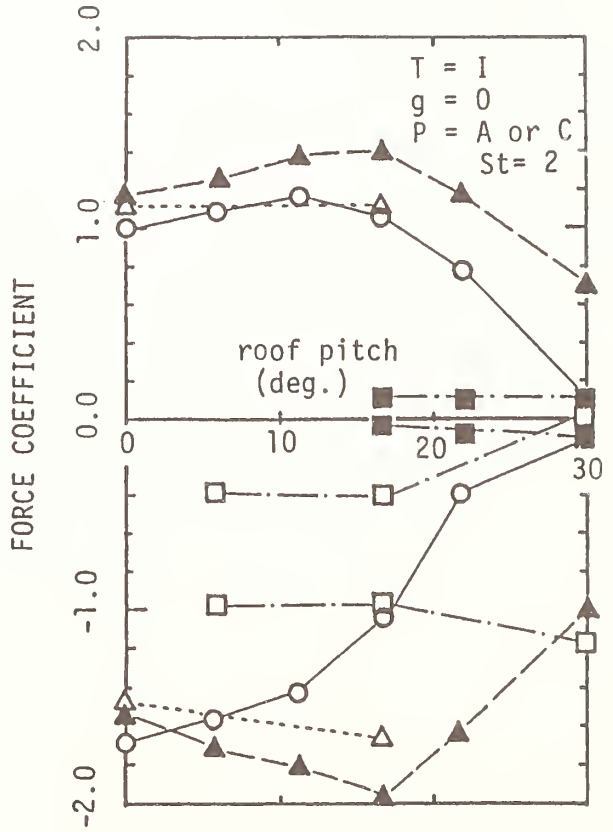

Fig.14 Variation of maximum and minimum force coefficient with roof pitch

□-·- mounting pattern(a), ■-·- (b)
△···· (c), ○— (d), ▲-- (e)

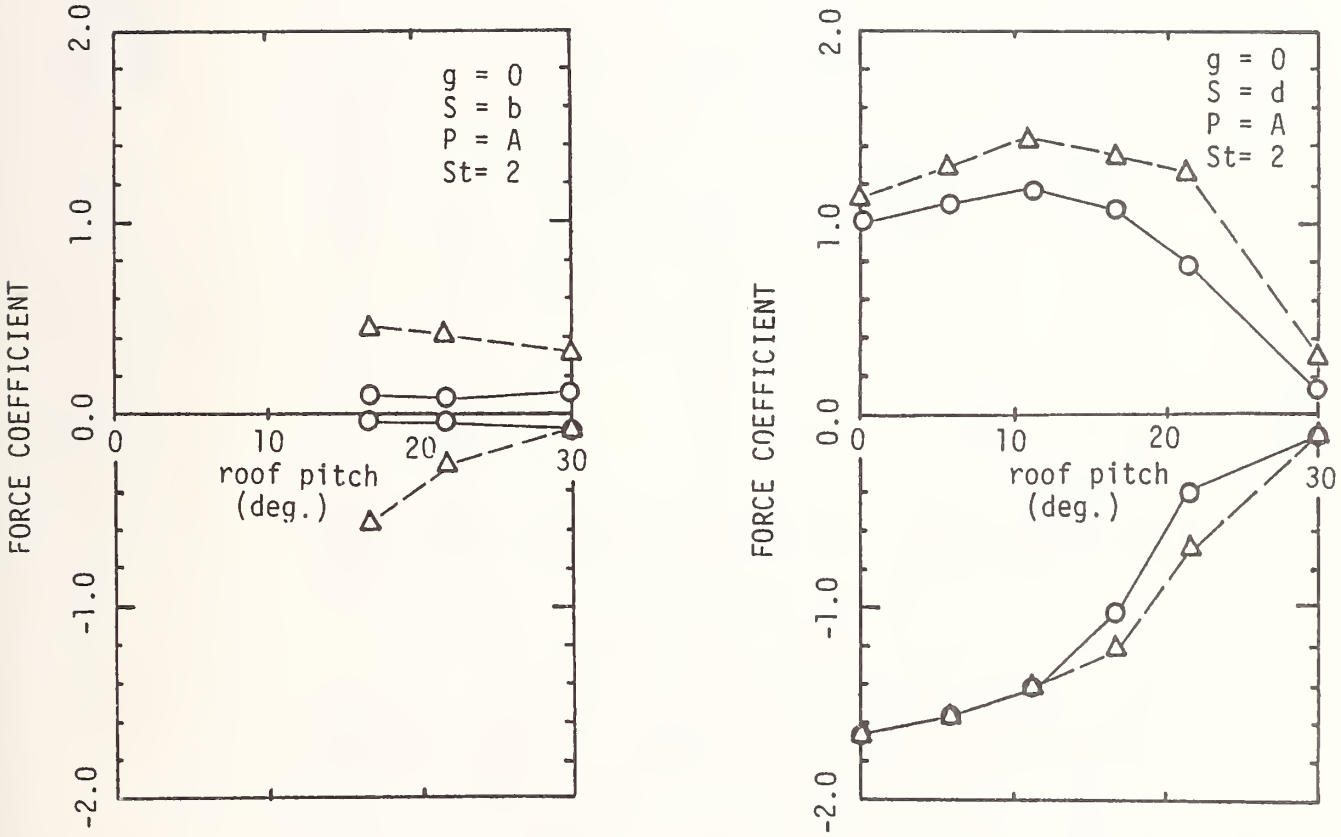

Fig. 15 Maximum and minimum force coefficients for type I and type II

O— type I, △-- type II

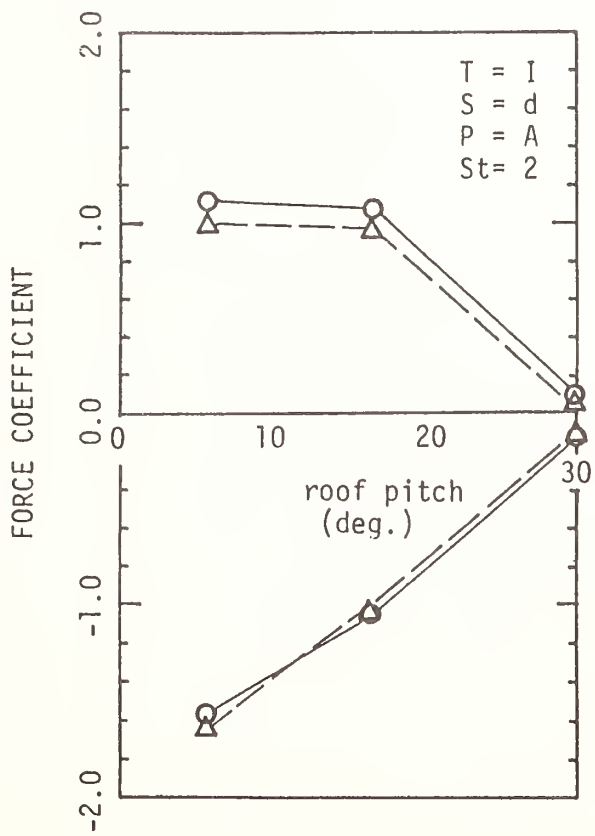

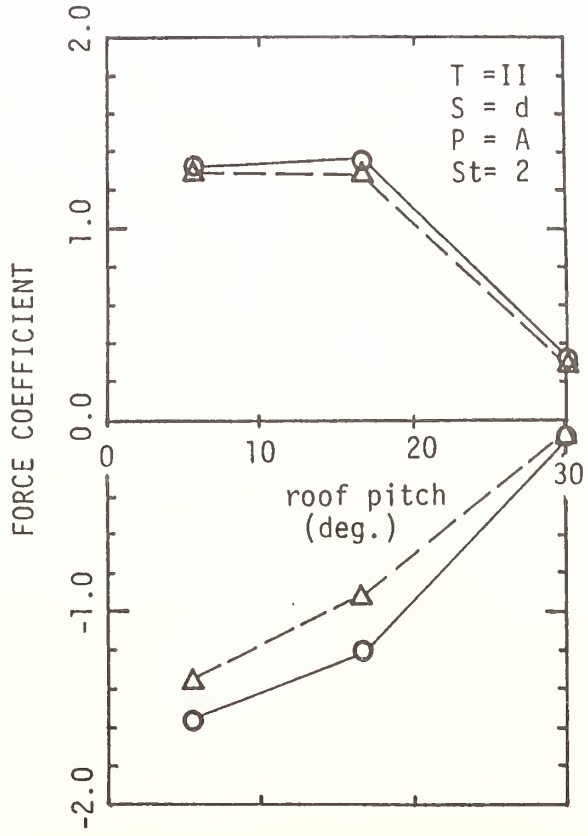

Fig.16 Effect of slit on maximum and minimum force coefficient

△——10mm slit, ○——no slit

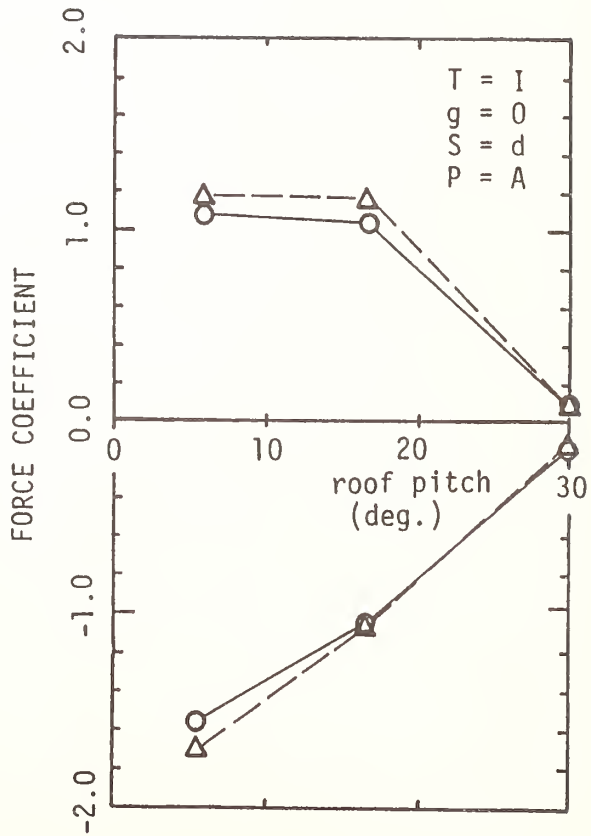

Fig. 17 Effect of number of stories on maximum and minimum force coefficients

△——1 story, ○——2 stories

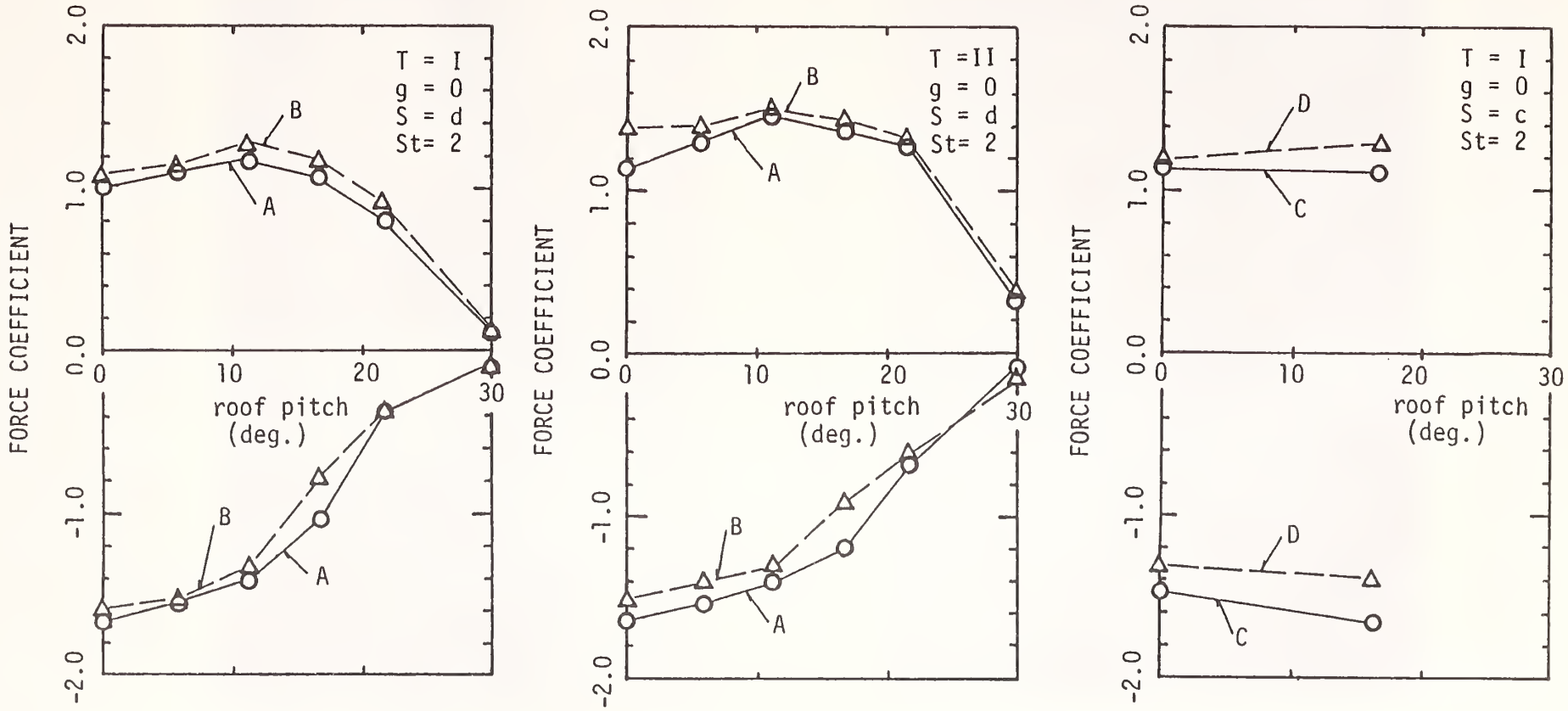

Fig. 18 Effect of mounting position on maximum and minimum force coefficients

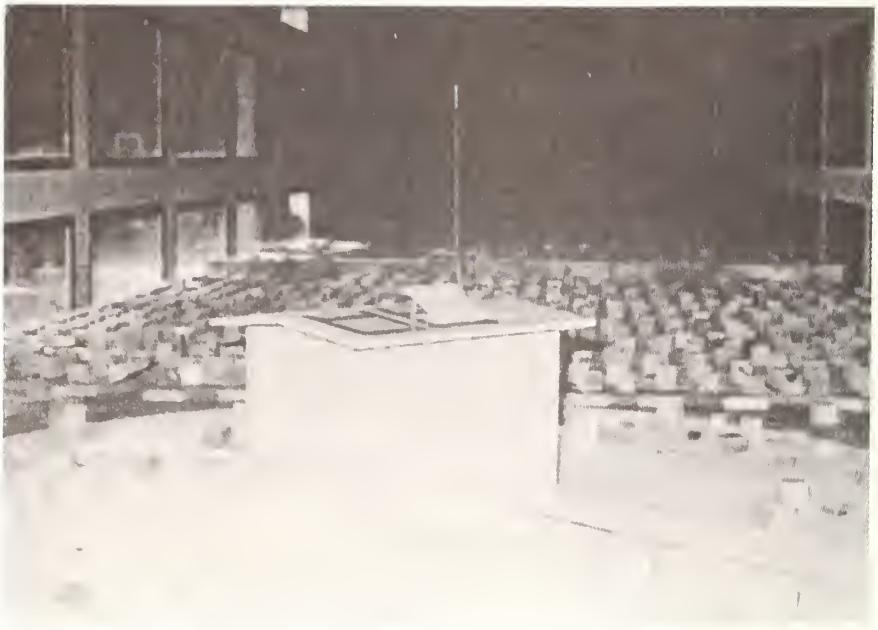

Photo 1 View of a wind tunnel model

Photo 2 View of the full-scale observation

ESTIMATION OF RESPONSE-SPECTRAL VALUES AS FUNCTIONS OF MAGNITUDE, DISTANCE, AND SITE CONDITIONS

W. B. Joyner
D. M. Boore

U.S. Geological Survey
345 Middlefield Road, MS 77
Menlo Park, CA 94025

ABSTRACT

We have developed empirical predictive equations for the horizontal pseudo-velocity response at 5 percent damping for 12 different periods from 0.1 to 4.0 s. Using a multiple linear-regression method similar to the one we used previously for peak horizontal acceleration and velocity, we analyzed response spectra period by period for 64 records of 12 shallow earthquakes in Western North America, including the recent Coyote Lake and Imperial Valley, California, Earthquakes. The resulting predictive equations show amplification of the response values at soil sites for periods greater than or equal to 0.5 s, with maximum amplification exceeding a factor of 2 at 1.5 s. For periods less than 0.5 s there is no statistically significant difference between rock sites and the soil sites represented in the data set. These results are consistent with those of several earlier studies. A particularly significant aspect of the predictive equations is that the response values at different periods are different functions of magnitude (confirming earlier results by McGuire and by Trifunac and Anderson). The slope of the least-squares straight line relating log response to moment magnitude ranges from 0.21 at a period of 0.1 s to greater than 0.5 at periods of 1 s and longer. This result indicates that the conventional practice of scaling a constant spectral shape by peak acceleration will not give accurate answers. The Newmark and Hall method of spectral scaling, using both peak acceleration and peak velocity, largely avoids this error. Comparison of our spectra with the Regulatory Guide 1.60 spectrum anchored at the same value at 0.1 s shows that the Regulatory Guide 1.60 spectrum is exceeded at soil sites for a magnitude of 7.5 at all distances for periods greater than about 0.5 s. Comparison of our spectra for soil sites with the corresponding ATC-3 curve of lateral design force coefficients for the highest seismic zone indicates that the ATC-3 curve is exceeded within about 5 km of a magnitude 6.5 earthquake and within about 20 km of a magnitude 7.5 event. The amount by which it is exceeded is largest in the period range from 0.5 to 2.0 s.

INTRODUCTION

Recently acquired strong motion data make possible improved predictions of near-source earthquake ground motion. In a previous paper (Joyner and Boore, 1981) we used those data in developing prediction equations for peak horizontal acceleration and velocity. The present paper

gives the corresponding predictive equations for horizontal pseudo-velocity response values at 5 percent damping and 12 different periods from 0.1 to 4.0 s. (The pseudo-velocity response is defined as the angular frequency of the oscillator times the maximum relative displacement response.) These equations enable us to predict response spectra directly without the use of a scaling parameter such as peak acceleration or peak velocity. They also enable us to examine the degree to which the shape of response spectra depends on magnitude, distance, and site conditions -- an important issue in engineering seismology in view of the common practice of deriving design spectra by using peak acceleration to scale spectra of constant shape.

METHOD

We fit the response spectral data at each period using a two-step regression analysis. The first step is represented by the equation:

$$\log y_{ij} = a_i - p \log r + b\, r + c\, S_j \qquad (1)$$

where

$S_j = 1$ if site j is a soil site,

$= 0$ if site j is a rock site,

$r = (d_{ij}^2 + h^2)^{1/2}$.

y_{ij} is the pseudo-velocity response value for earthquake i at site j and d_{ij} is the closest distance from recording site j to the vertical projection on the earth's surface of the rupture surface for earthquake i. The parameters a_i, p, b, c, and h are determined by the regression analysis. In the usual case p is taken to be unity and a_i, b, and c are determined by linear regression for successive assumed values of h. The final values are determined by a simple search procedure on h to minimize the sum of squares of residuals. If the final value obtained for b is positive (which would represent negative anelastic attenuation) we set b equal to zero and redo the process with a_i, p, and c as the parameters determined by linear regression. Once the values of a_i are determined they are used in a second regression analysis to determine the magnitude dependence according to the equation:

$$a_i = \alpha + \beta M_i \qquad (2)$$

where M_i is the moment magnitude (Hanks and Kanamori, 1979) of earthquake i. The form chosen for the regression is the equivalent of:

$$y = \frac{k}{r^p} e^{-qr}$$

where k is a function of magnitude and period and q is a function of period.

To estimate σ_y, the standard error of the prediction made by the procedure described here, we use the equation:

$$\sigma_y = (\sigma_s^2 + \sigma_s^2)^{1/2}$$

where

σ_s is the standard deviation of the residuals from the regression analysis of equation (1),

σ_a is the standard deviation of the residuals of the regression analysis of equation (2).

DATA

The data set represents 64 records from 12 earthquakes. This is the data set used earlier (Joyner and Boore, 1981) for peak velocity, augmented by two additional records, a record at Sitka, Alaska, on a rock site 45 km from the M 7.7 Sitka Earthquake of 1972 and a record at Icy Bay, Alaska, on a soil site 25.4 km from the M 7.6 St. Elias Earthquake of 1979. The distribution of the data set in magnitude and distance is shown in figure 1.

At each period we use the larger of the two horizontal response values. In the future we plan to repeat the analysis for the mean of the two horizontal values.

RESULTS

To illustrate the dependence of the response values on magnitude, the results of the regression analysis of equation (2) are shown in figures 2, 3, and 4 for periods of 0.1, 0.5, and 1.0 s, respectively. Note that the slope of the line is greater at longer periods.

The result of the two-stage regression analysis is a predictive equation for pseudo-velocity response

$$\log y = \alpha + \beta M - p \log r + b\, r + c\, S \qquad (3)$$

$$r = (d^2 + h^2)^{1/2}$$

where the symbols are as defined for equation (1) and the parameters α, β, p, b, c, and h are determined for each period by the two-stage regression analysis in the manner previously described.

Our use of a value of h in equation (3) that is independent of magnitude is the equivalent of assuming that the curve showing the attenuation of response with distance has the same shape independent of magnitude or, in other words, that the change in response for a given change in magnitude is the same at every distance. We used the same assumption in our analysis of peak acceleration (Joyner and Boore, 1981). Others (e.g., Campbell, 1981) in analyzing peak acceleration have postulated that the shape of the attenuation curve does in fact change with magnitude and in particular that at small source distances there is less change in peak acceleration for a given change in magnitude than at large distances. We test this proposition for response spectra in the same way we tested it

for peak acceleration and velocity (Joyner and Boore, 1981). We take stations with source distances less than 10 km, which are the ones most sensitive to a magnitude dependent attenuation, and we compute the residuals against the predictive equations based on the assumption of magnitude-independent attenuation. We then plot the residuals against magnitude. If there is support in the data for magnitude-dependent attenuation, it should show as a magnitude dependence in those residuals. The residuals are plotted against magnitude along with the least-squares straight line in figures 5, 6, and 7 for periods of 0.1, 0.5, and 1.0 s, respectively. These plots do not suggest any systematic relationship. The slope of the least-squares straight line in figure 5 indicates a greater change at small distances for a given change in magnitude rather than less. We conclude that there is no support in the data for an attenuation curve with magnitude-dependent shape.

Carrying out the analysis for response at 5 percent damping gives the parameters required by equation (3). These are plotted against period in figure 8. Because we believe that smooth spectra will be more useful, we draw smooth curves for the points in figure 8, and use the smoothed values for all spectra shown. Both raw and smoothed values of the parameters are given in table 1.

Figure 9 shows the spectra for rock and soil sites at zero distance and moment magnitudes of 5.5, 6.5, and 7.5. A large effect of magnitude on spectral shape is indicated by the different spacing at short and long periods between the curves for different magnitudes. The same result is implicit in figure 8 which shows that the magnitude coefficient β ranges from less than 0.25 at the short period end to more than 0.50 at the long period end. Earlier work by McGuire (1974) and by Trifunac and Anderson (1978) demonstrated this general relationship between response values and magnitude.

Figure 9 indicates a dependence of spectral shape on site conditions in that there is an amplification by about a factor of two at soil sites for the longer periods and no amplification at all for the shorter periods. These results are similar to those of several earlier studies and certainly hold for the typical soil site represented in our data set, but caution should be exercised in applying the results, because there is evidence that substantial amplification does occur at short periods for certain site conditions. In the 1979 Coyote Lake Earthquake, records were obtained at a rock site and at a site only 2 km away where 180 m of Quaternary alluvium overlay the rock (Joyner and others, 1981). The pseudo-velocity response at 0.1 s and 5 percent damping was amplified by a factor of 1.9 at the site on alluvium. A likely explanation of the discrepancy is that there is a much greater thickness of low-Q material at the typical soil site, and therefore, more attenuation of high frequencies than at the site referred to above.

Figure 10 shows the spectra for soil sites at magnitude 7.5 and a range of distances. The shape of the spectrum changes significantly between d = 0 and 10 km but relatively little between 10 km and 40 km. The difference in shape between 0 and 10 km reflects the fact that the h values at shorter periods are about twice as great as those for longer periods. A corresponding relationship was found between the h values for peak horizontal acceleration and velocity (Joyner and Boore, 1981).

DISCUSSION

Equation (3) along with the parameter values given in table 1 constitutes a set of equations by which response spectra can be predicted directly without the use of scaling parameters such as peak acceleration or peak velocity. These equations are constrained by data at soil sites over the entire distance range of interest for moment magnitudes less than or equal to 6.5. The data set contains no recording at rock sites with d less than 8 km for earthquakes with magnitude greater than 6.0, and caution should be used in applying the equations to rock sites at shorter distances for earthquakes of larger magnitudes. For distances less than 25 km and magnitudes greater than 6.6 the predictive equations are not constrained by data, and there also the results should be treated with caution. We do not propose use of the predictive equations beyond a moment magnitude of 7.7, the limit of the data set.

The result that the shape of response spectra depends strongly on magnitude indicates that the common practice of using peak acceleration to scale normalized spectra of fixed shape leads to substantial error. The coefficient of magnitude in the predictive equation for peak horizontal acceleration is approximately 0.25 and the corresponding coefficients for the response spectral values at periods greater than 1.0 s are all greater than 0.50. Most of the records used in determining standard spectral shapes are from earthquakes of magnitude less than 7.0; the average might be 6.5 or less. Under these circumstances the practice of scaling a standard spectral shape using peak acceleration would result in an error of about a factor of two at magnitude 7.5 for periods greater than 1.0 s.

The scaling procedure advocated by Newmark and Hall (1969) is largely immune from the errors associated with scaling standard spectral shapes by peak acceleration. They suggested scaling the short period portion of the spectrum by peak acceleration and the intermediate portion (about 0.3 to 2.0 s) by peak velocity. Comparison of the parameter values in figure 8 and table 1 with the corresponding values for peak horizontal acceleration and velocity (Joyner and Boore, 1981) indicates a general similarity between the parameter values for short period response and those for peak acceleration and between the values for longer period response and those for peak velocity.

The design of nuclear power facilities in the United States is largely on the basis of a fixed spectral shape described in Regulatory Guide 1.60 (U.S. Atomic Energy Commission, 1973). It is intended that this spectral shape be scaled by peak acceleration. Regulatory Guide 1.60 specifies that it does not apply to sites which "(1) are relatively close to the epicenter of an expected earthquake or (2) have physical characteristics that could significantly affect the spectral pattern of input motion, such as being underlain by poor soil deposits." No quantitative definitions of "close to the epicenter" or "poor soil deposits" are given. We compare the Regulatory Guide 1.60 spectrum with our spectra in figures 11 and 12. Figure 11 gives spectra for soil sites for a moment magnitude of 6.5 and distances of 0, 10, and 40 km. Figure 12 gives the corresponding spectra for a magnitude of 7.5. The Regulatory Guide 1.60 spectrum is shown by the dashed line and for the purpose of comparison is anchored to each of our spectra at a period of 0.1 s. On figure 11, the Regulatory Guide 1.60 spectrum is exceeded only by our spectrum for zero distance. Even that is not a problem, however, because the Regulatory Guide 1.60 spectrum is not intended for use at "close" distance. In figure 12, we see that for magnitude 7.5 the Regulatory Guide 1.60 spectrum is substantially exceeded at all distances for periods greater than about 0.5 s. Whether this represents a serious problem or not depends of course upon whether there are important structures with periods greater than 0.5 s and upon the safety margins available.

The lateral-force coefficients in the earthquake-resistance provisions of building codes can be related to response spectra. In figures 13 and 14 we compare our spectra with the lateral design force coefficient C_s in the proposed ATC-3 Code (Applied Technology Council, 1978). Figure 13 gives our spectra at soil sites and a range of distances for a magnitude of 6.5, and figure 14 gives the corresponding spectra for magnitude 7.5. The C_s curve from ATC-3, shown in both figures 13 and 14 by the dashed line, is calculated for a response modification factor R of 1.0, for soil type S2 (deep cohesionless or stiff clay soil conditions) and for A_a and A_v values of 0.4, which correspond to the zones of greatest expected ground motion. The comparisons show that the ATC-3 curve is exceeded within about 5 km of a magnitude 6.5 earthquake and within about 20 km of a magnitude 7.5 event. The amount by which it is exceeded is largest in the period range from 0.5 to 2.0 s. The implications of these differences depend among other things upon the safety margins available in the system and can only be properly evaluated by structural engineers.

REFERENCES

[1] Applied Technology Council, 1978, "Tentative Provisions for the Development of Seismic Regulations for Buildings," Applied Technology Publication ATC 3-06, 505 p.

[2] Campbell, K. W., 1981, "Near-source Attenuation of Peak Horizontal Acceleration," Bulletin of Seismological Society of America, Vol. 71, pp. 2039-2070.

[3] Hanks, T. C. and H. Kanamori, 1979, "A Moment Magnitude Scale," Journal of Geophysical Research, Vol. 84, pp. 2348-2350.

[4] Joyner, W. B. and D. M. Boore, 1981, "Peak Horizontal Acceleration and Velocity From Strong-Motion Records Including Records From the 1979 Imperial Valley, California, Earthquake," Bulletin of Seismological Society of America, Vol. 71, pp. 2011-2038.

[5] Joyner, W. B., R. E. Warrick, and T. E. Fumal, 1981, "The Effect of Quaternary Alluvium on Strong Ground Motion in the Coyote Lake, California, Earthquake of 1979," Bulletin of Seismological Society of America, Vol. 71, pp. 1333-1349.

[6] McGuire, R. K., 1974, "Seismic Structural Response Risk Analysis, Incorporating Peak Response Regressions on Earthquake Magnitude and Distance," Research Report R74-51, Department of Civil Engineering, Massachusetts Institute of Technology, 371 p.

[7] Newmark, N. M. and W. J. Hall, 1969, "Seismic Design Criteria for Nuclear Reactor Facilities," Proc. World Conference on Earthquake Engineering, 4th, Santiago, Chile, Vol. 2, pp. B4-37 to B4-50.

[8] Trifunac, M. D. and J. G. Anderson, 1978, "Preliminary Empirical Models for Scaling Pseudo-Relative Velocity Spectra, Appendix A in Methods for Prediction of Strong Earthquake Ground Motion," U.S. Nuclear Regulatory Commission NUREG/CR-0689.

[9] U.S. Atomic Energy Commission, 1973, "Design Response Spectra for Seismic Design of Nuclear Power Plants," Regulatory Guide 1.60, 6 p.

Table 1. Parameters in the Prediction Equations for Pseudo-Velocity Response (cm/s) at 5 Percent Damping

Period s		α	β	h km	p	b km^{-1}	c	σ_y
0.1	raw	0.81	0.210	9.4	1.0	-0.00612	0.0	0.26
	smoothed	0.95	0.210	10.6	1.0	-0.00707	0.0	0.27
0.15	raw	1.07	0.221	11.4	1.0	-0.00766	0.0	0.28
	smoothed	1.09	0.218	10.4	1.0	-0.00661	0.0	0.27
0.2	raw	1.13	0.226	10.8	1.0	-0.00637	0.0	0.27
	smoothed	1.09	0.232	9.7	1.0	-0.00628	0.0	0.27
0.3	raw	0.89	0.276	6.9	1.0	-0.00480	0.0	0.27
	smoothed	0.87	0.280	6.9	1.0	-0.00583	0.0	0.28
0.4	raw	0.39	0.358	4.6	1.0	-0.00519	0.0	0.32
	smoothed	0.41	0.352	5.0	1.0	-0.00551	0.03	0.31
0.5	raw	0.11	0.390	4.7	1.0	-0.00543	0.14	0.33
	smoothed	0.08	0.401	4.5	1.0	-0.00523	0.08	0.33
0.75	raw	-0.52	0.478	3.3	1.0	-0.00451	0.19	0.34
	smoothed	-0.47	0.479	4.4	1.0	-0.00470	0.19	0.36
1.0	raw	-0.72	0.519	5.0	1.0	-0.00548	0.21	0.37
	smoothed	-0.80	0.523	4.4	1.0	-0.00429	0.25	0.36
1.5	raw	-0.93	0.528	5.6	1.0	-0.00310	0.33	0.37
	smoothed	-1.14	0.564	4.4	1.0	-0.00358	0.31	0.36
2.0	raw	-1.44	0.611	5.2	1.0	-0.00327	0.30	0.36
	smoothed	-1.26	0.574	4.4	1.0	-0.00259	0.32	0.36
3.0	raw	-1.37	0.573	3.7	1.0	0.0	0.31	0.33
	smoothed	-1.37	0.576	4.4	1.0	0.0	0.29	0.36
4.0	raw	-1.29	0.554	4.1	0.982	0.0	0.22	0.37
	smoothed	-1.44	0.576	4.4	0.982	0.0	0.25	0.36

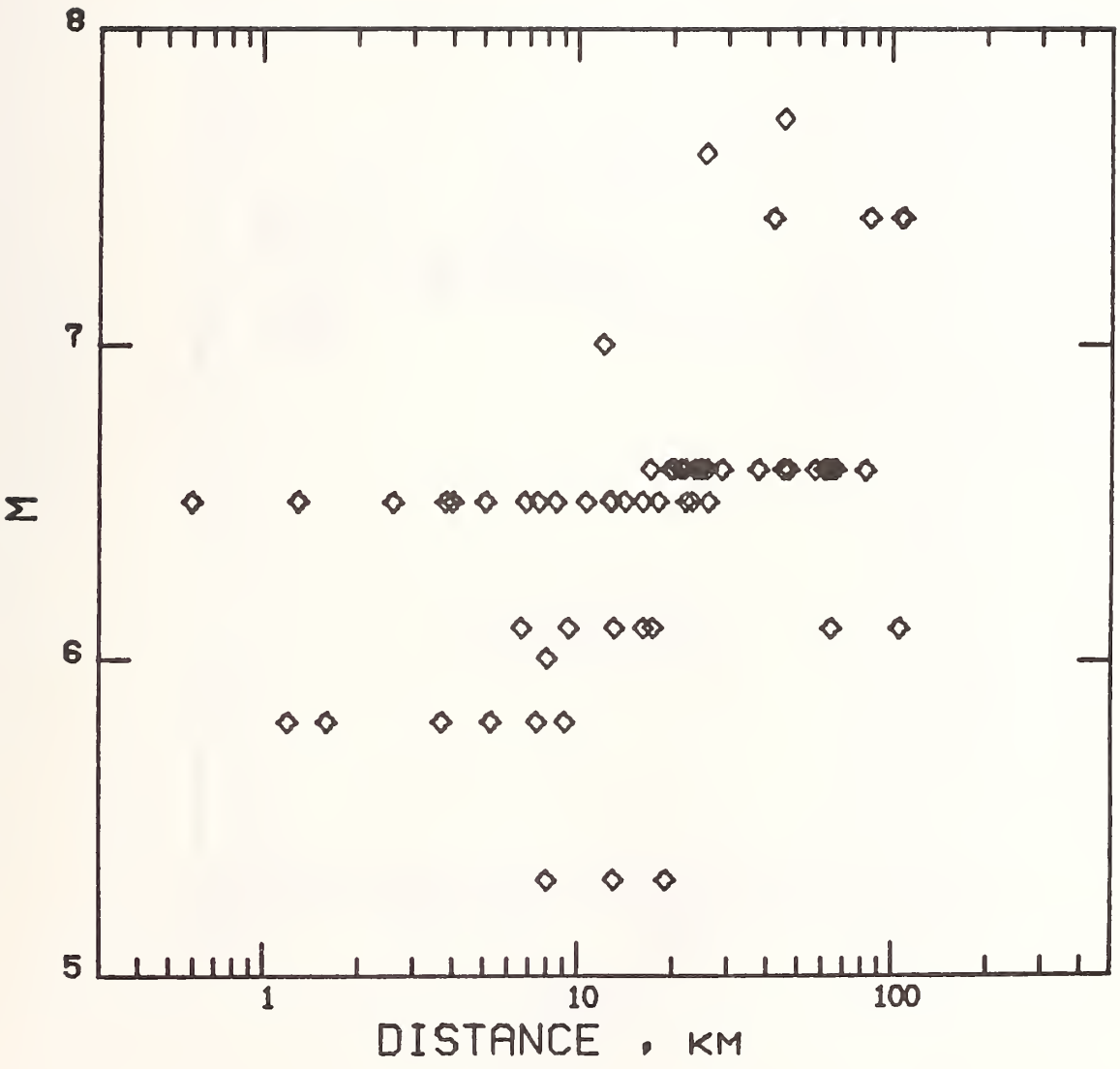

Figure 1. Distribution of the data set in moment magnitude and distance

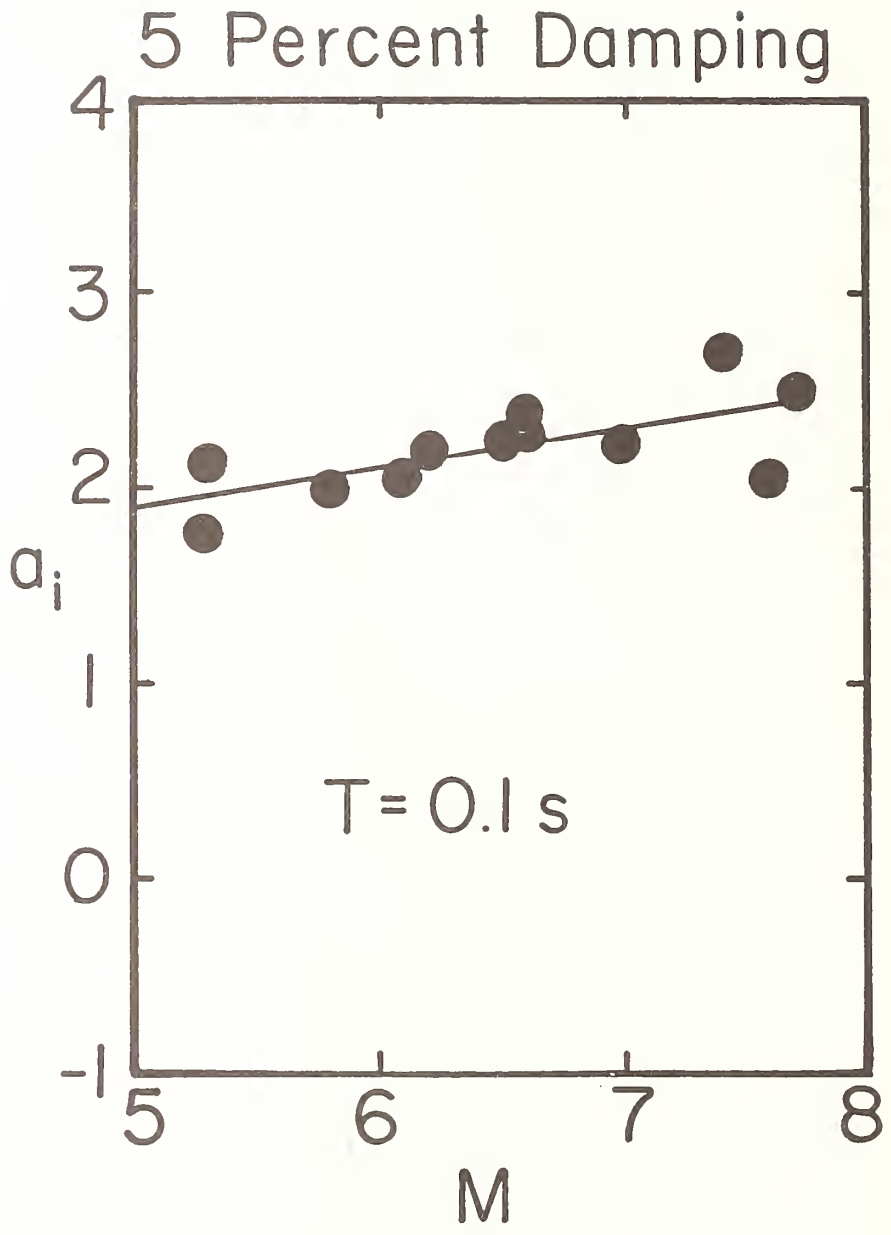

Figure 2. Values of a_i for horizontal pseudo-velocity response (cm/s) at 5 percent damping and 0.1 s period from the regression analysis of equation (1), plotted against moment magnitude

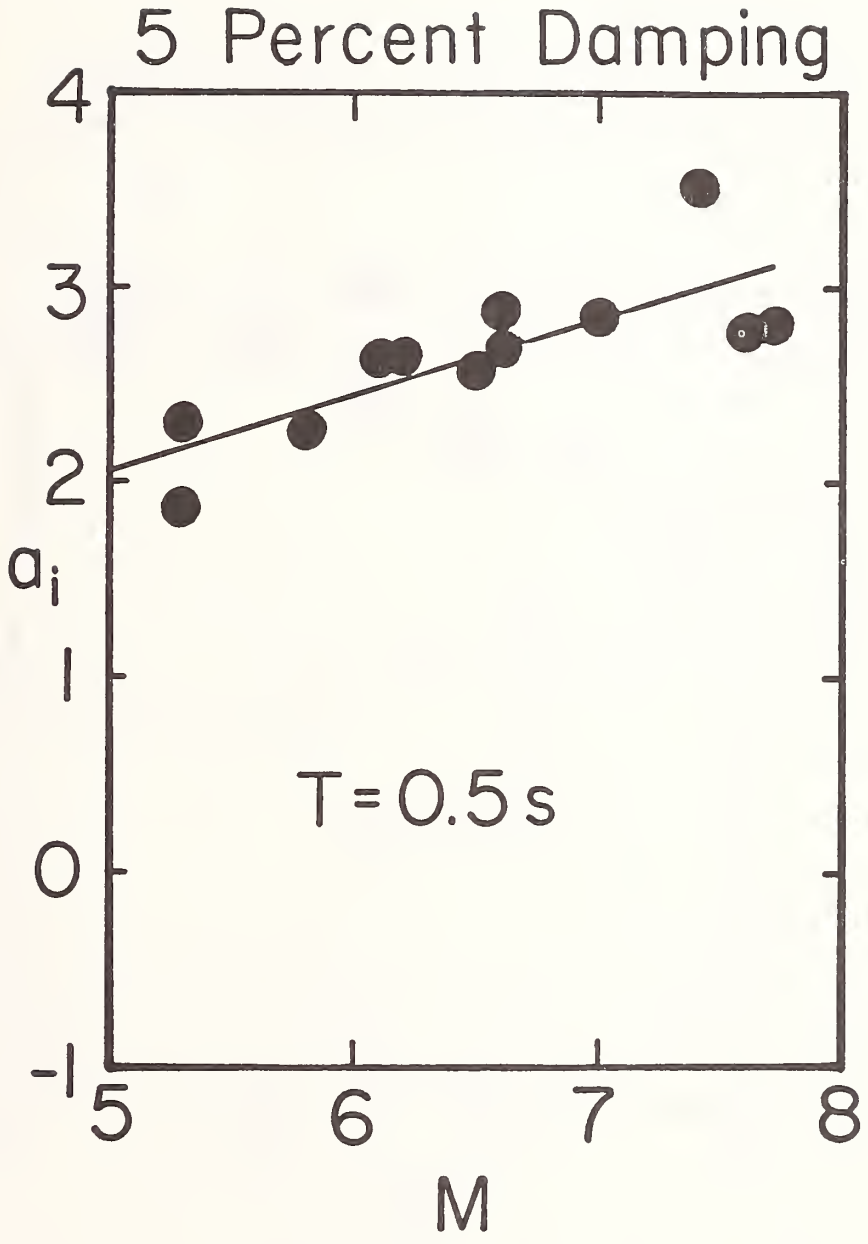

Figure 3. Values of a_i for horizontal pseudo-velocity response (cm/s) at 5 percent damping and 0.5 s period from the regression analysis of equation (1), plotted against moment magnitude

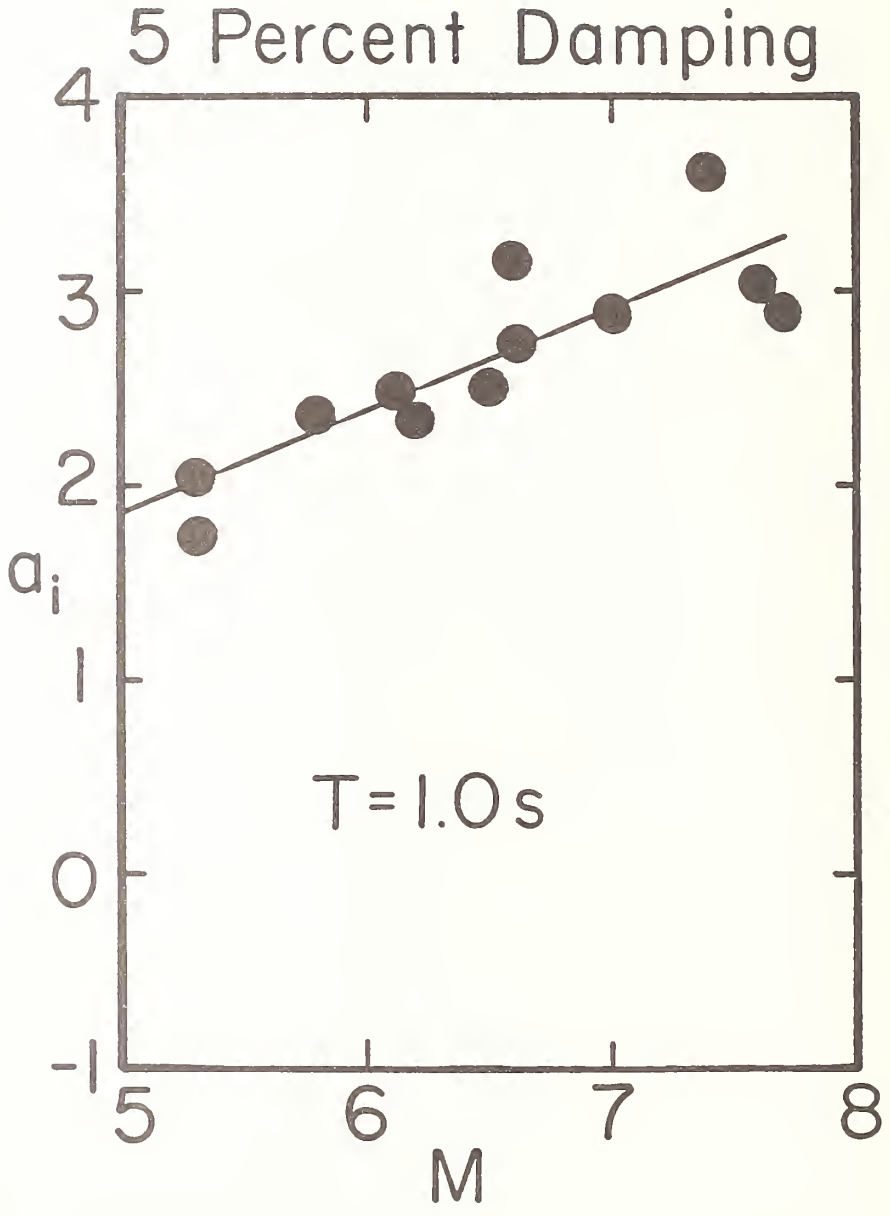

Figure 4. Values of a_i for horizontal pseudo-velocity response (cm/s) at 5 percent damping and 1.0 s period from the regression analysis of equation (1), plotted against moment magnitude

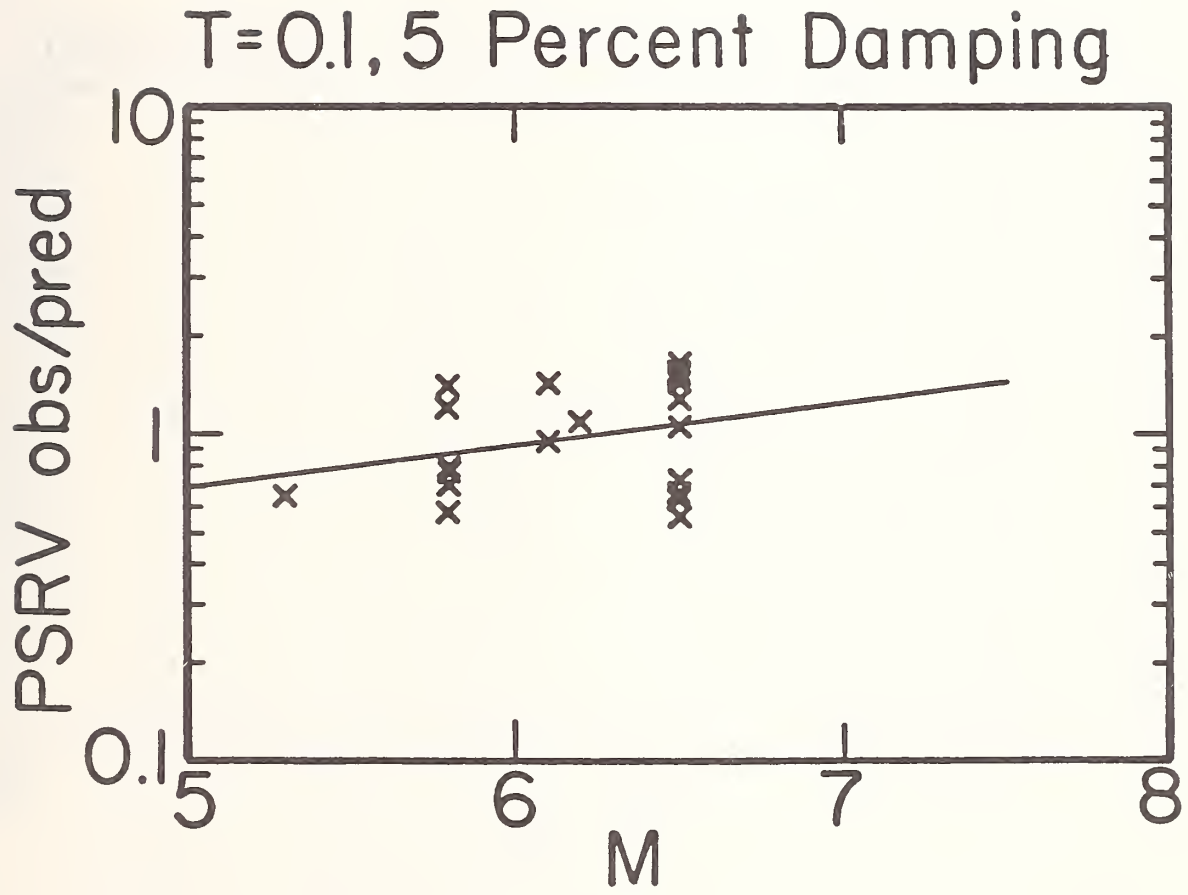

Figure 5. Residuals with respect to equation (3) of the logarithm of horizontal pseudo-velocity response at 5 percent damping and 0.1 s period plotted against moment magnitude for stations with d less than or equal to 10 km, with least-squares straight line superposed.

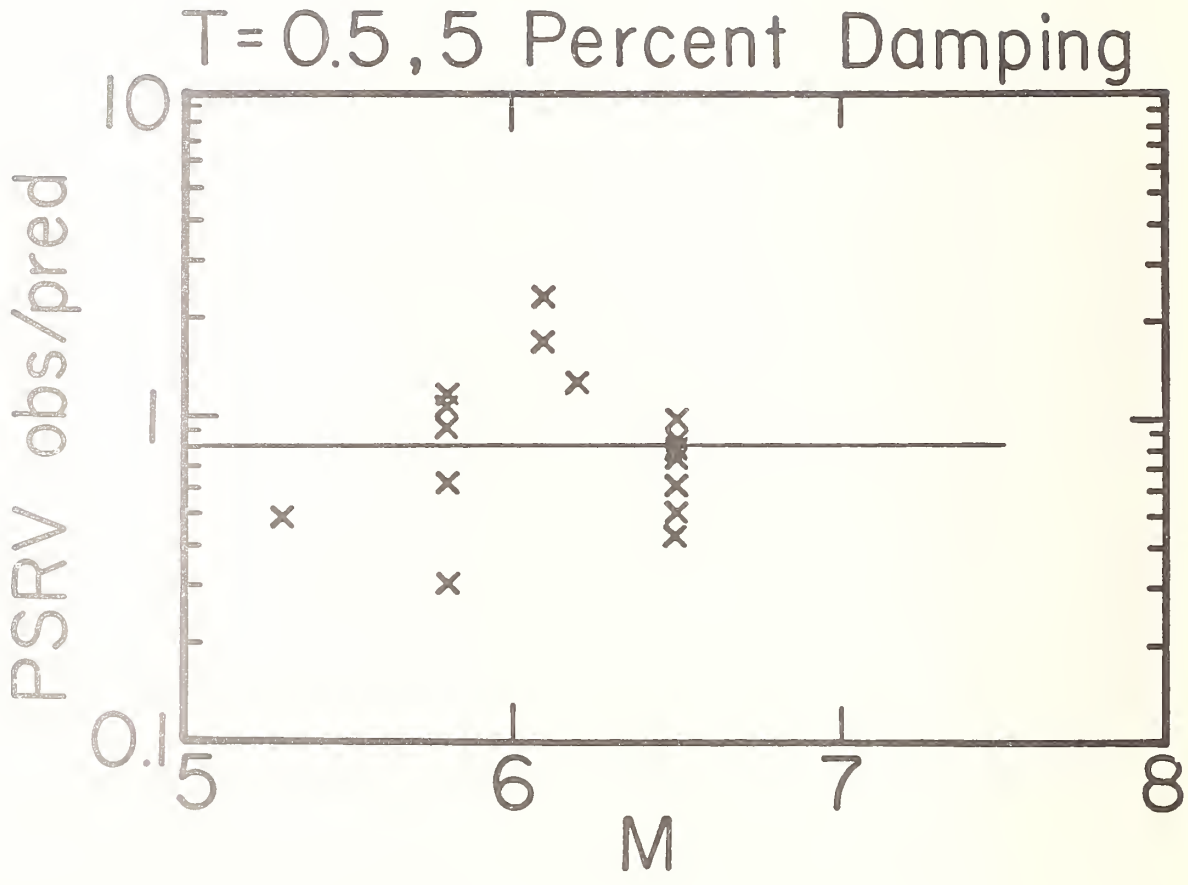

Figure 6. Residuals with respect to equation (3) of the logarithm of horizontal pseudo-velocity response at 5 percent damping and 0.5 s period plotted against moment magnitude for stations with d less than or equal to 10 km, with least-squares straight line superposed

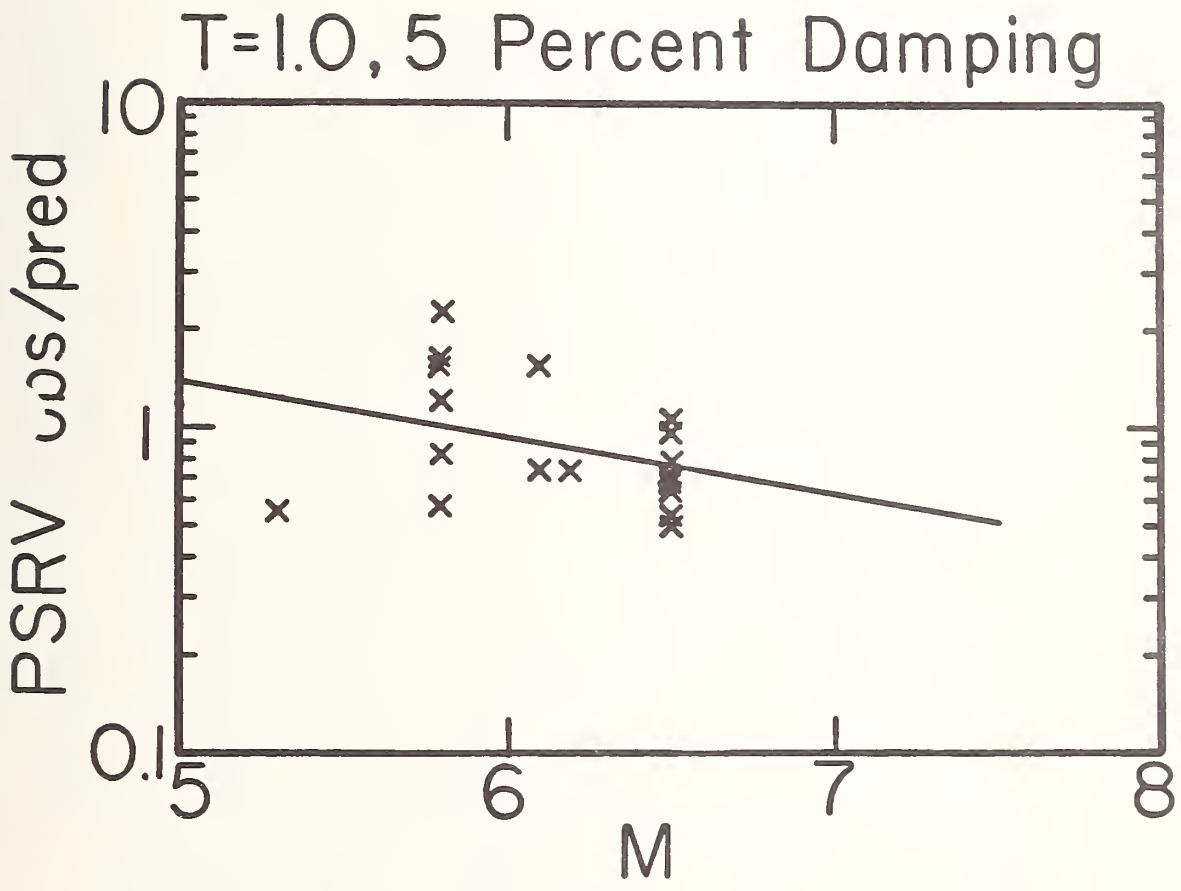

Figure 7. Residuals with respect to equation (3) of the logarithm of horizontal pseudo-velocity response at 5 percent damping and 1.0 s period plotted against moment magnitude for stations with d less than or equal to 10 km, with least-squares straight line superposed

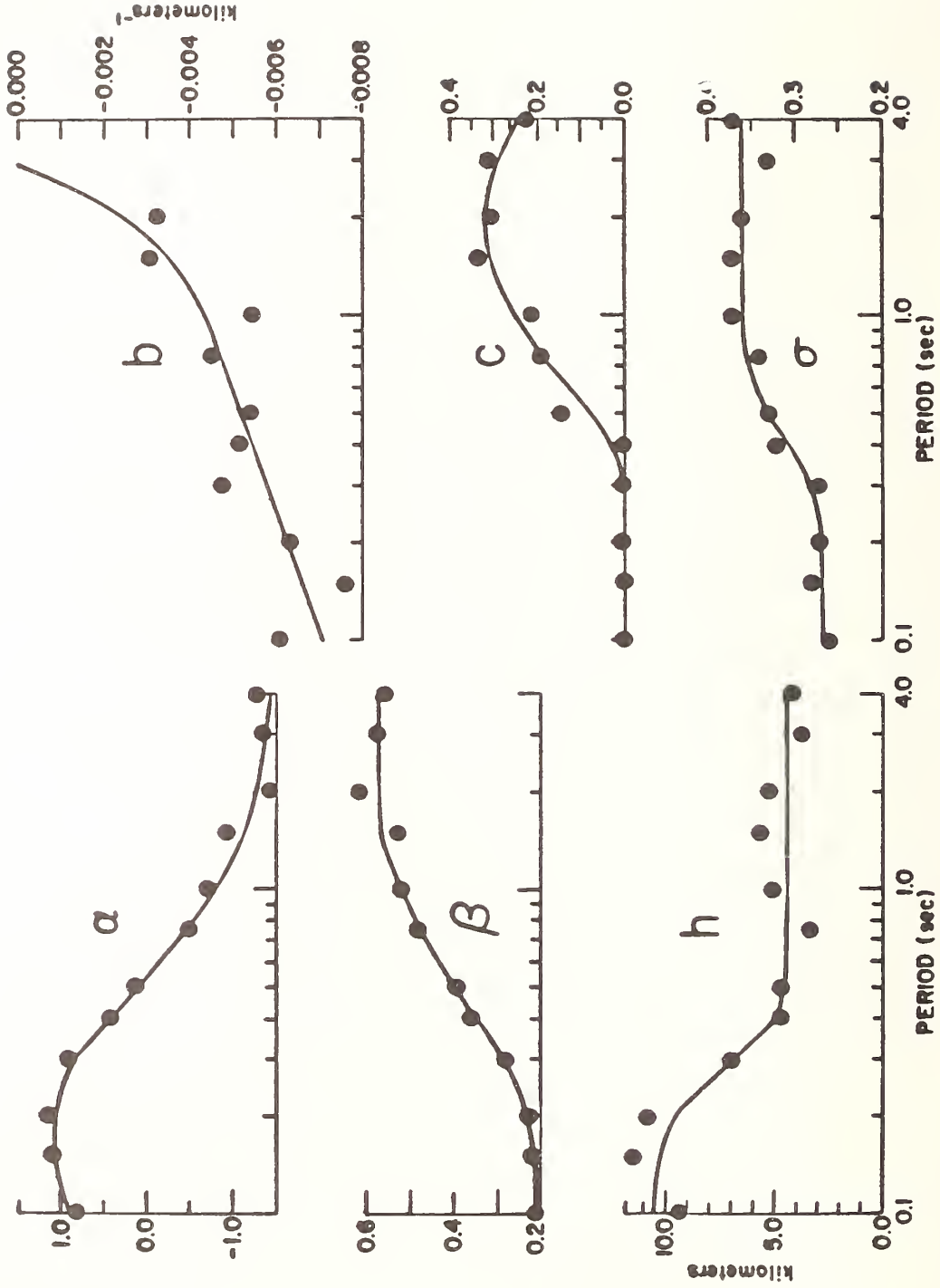

Figure 8. The parameters of equation (3) plotted against period (except for the parameter p, which is given in table 1). The solid circles show the values determined by the two-stage regression analysis and the solid lines show the smoothed values.

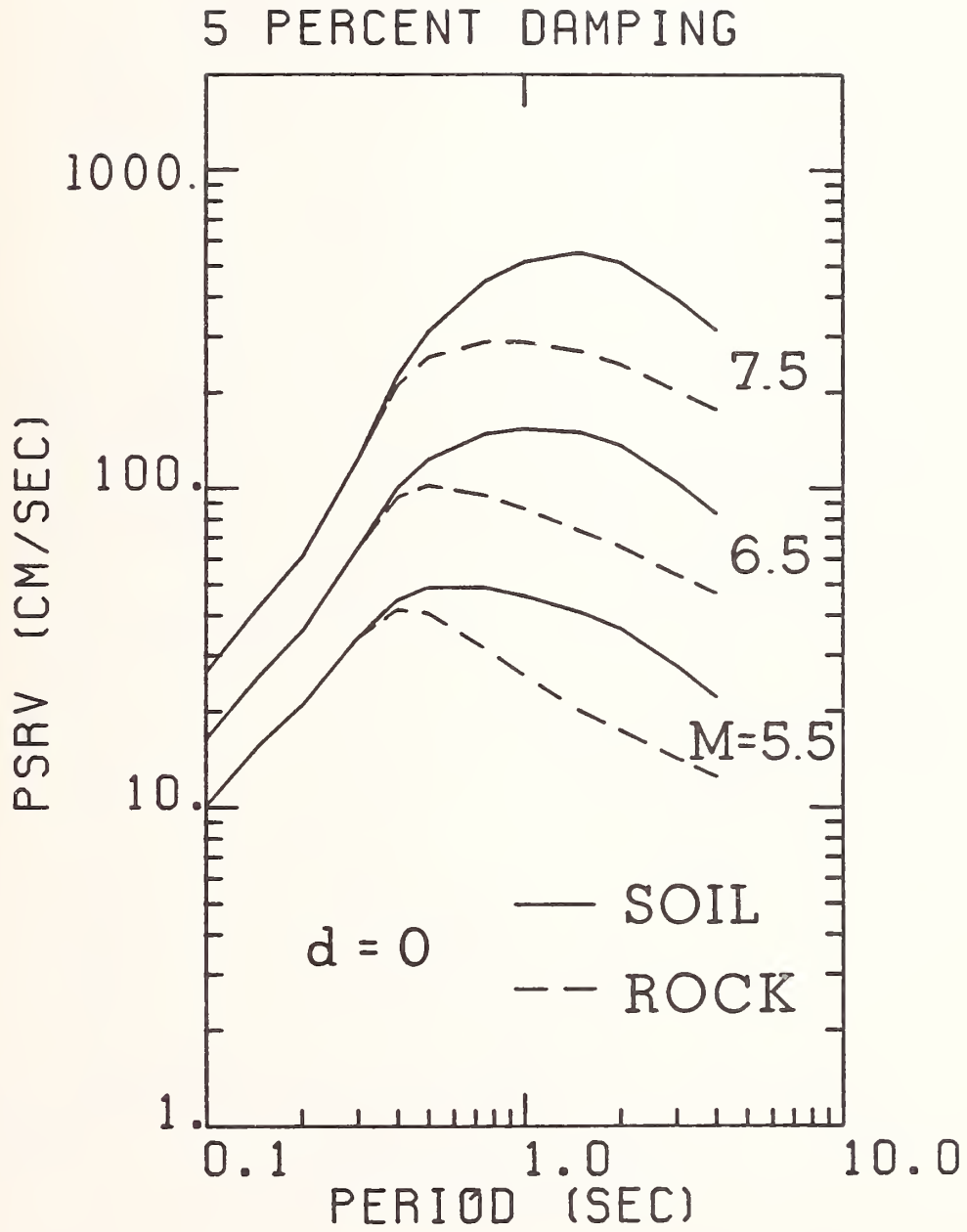

Figure 9. Predicted pseudo-velocity response spectra for 5 percent damping at rock sites (dashed line) and soil sites (solid line) for d equal to zero and moment magnitude equal to 5.5, 6.5, and 7.5

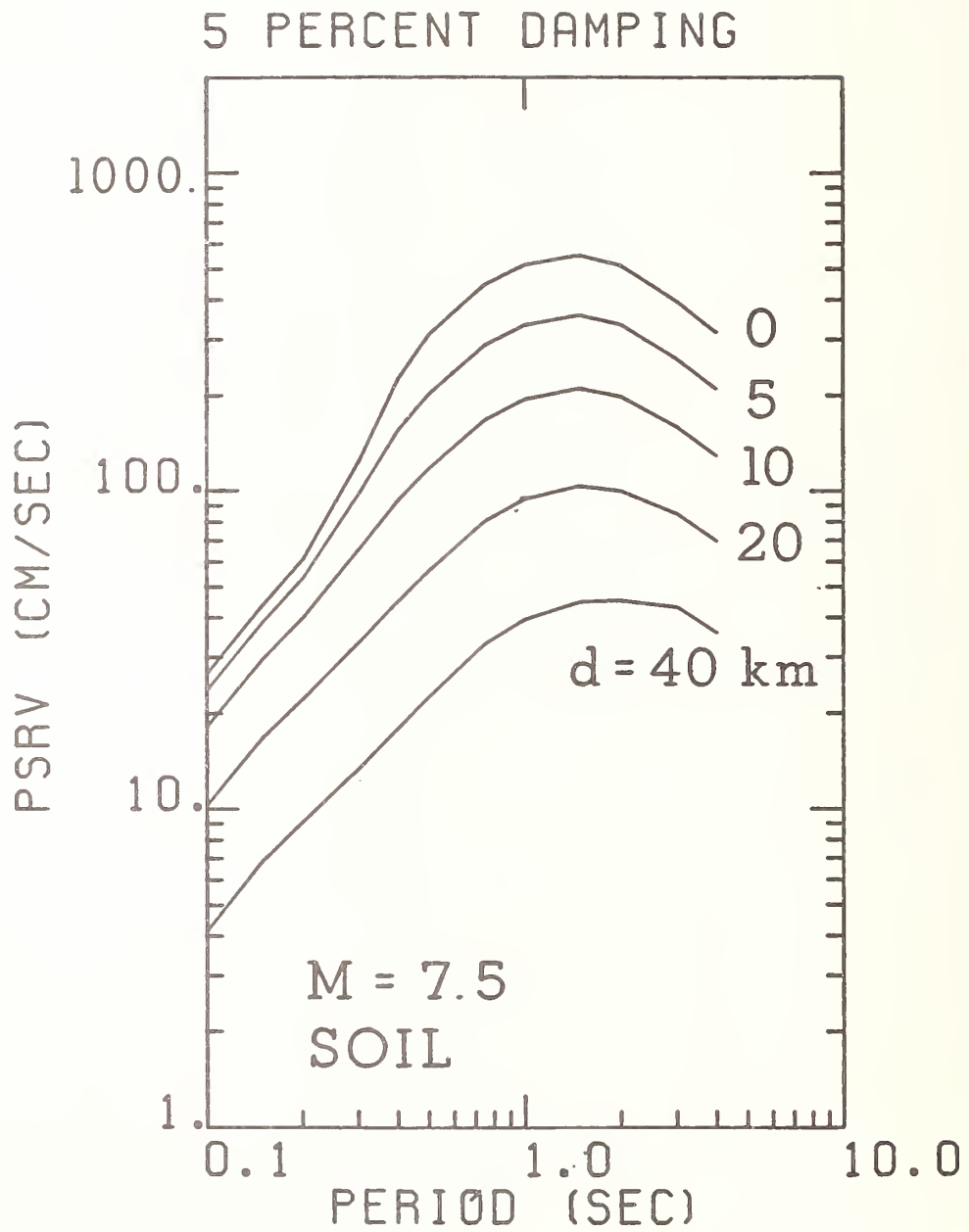

Figure 10. Predicted pseudo-velocity response spectra for 5 percent damping at soil sites for a moment magnitude of 7.5 and d equal to 0, 5, 10, 20, and 40 km

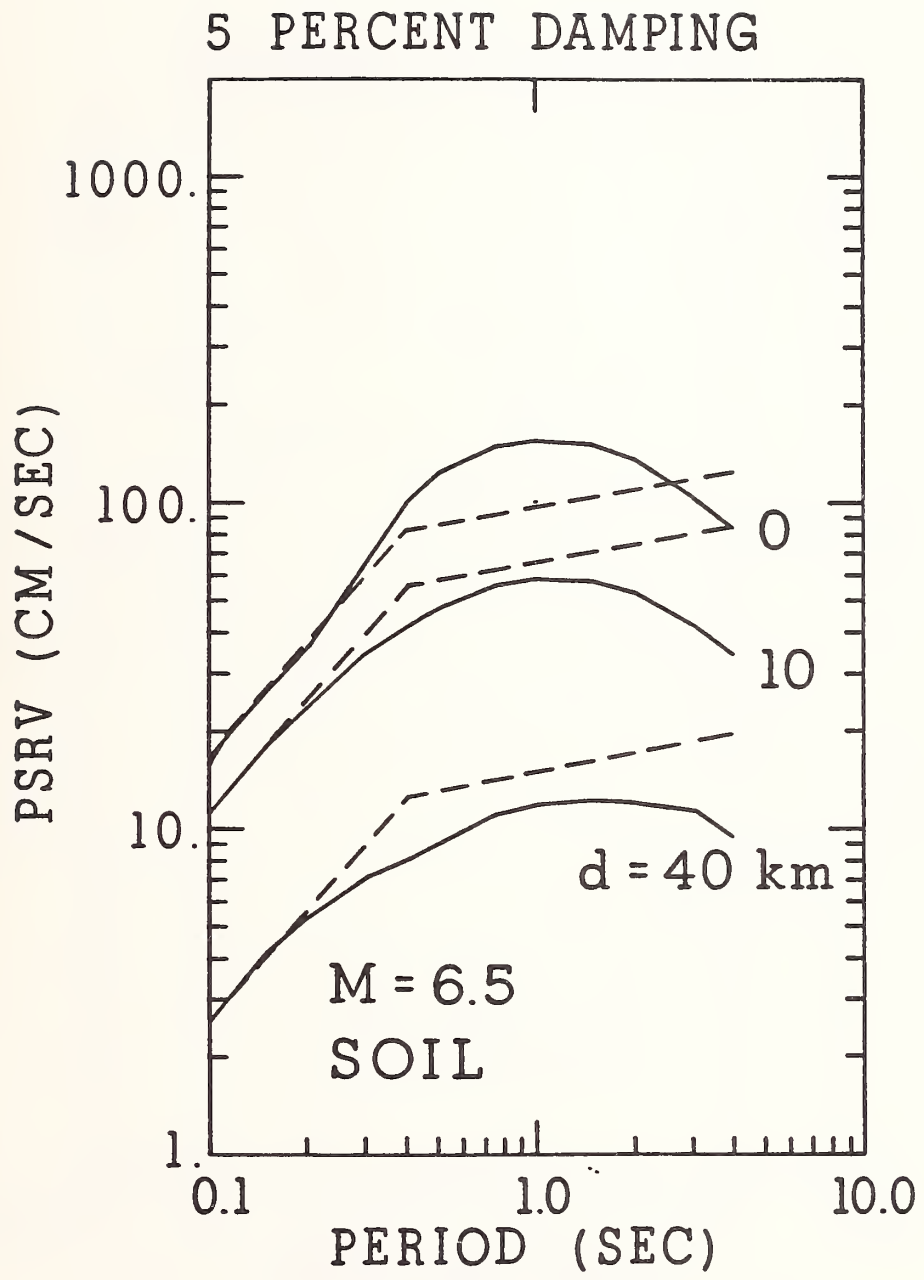

Figure 11. Predicted pseudo-velocity response spectra for 5 percent damping (solid lines) at soil sites for a moment magnitude of 6.5 and d equal to 0, 10, and 40 km compared to the Regulatory Guide 1.60 spectrum (dashed lines) anchored to the predicted spectra at 0.1 s

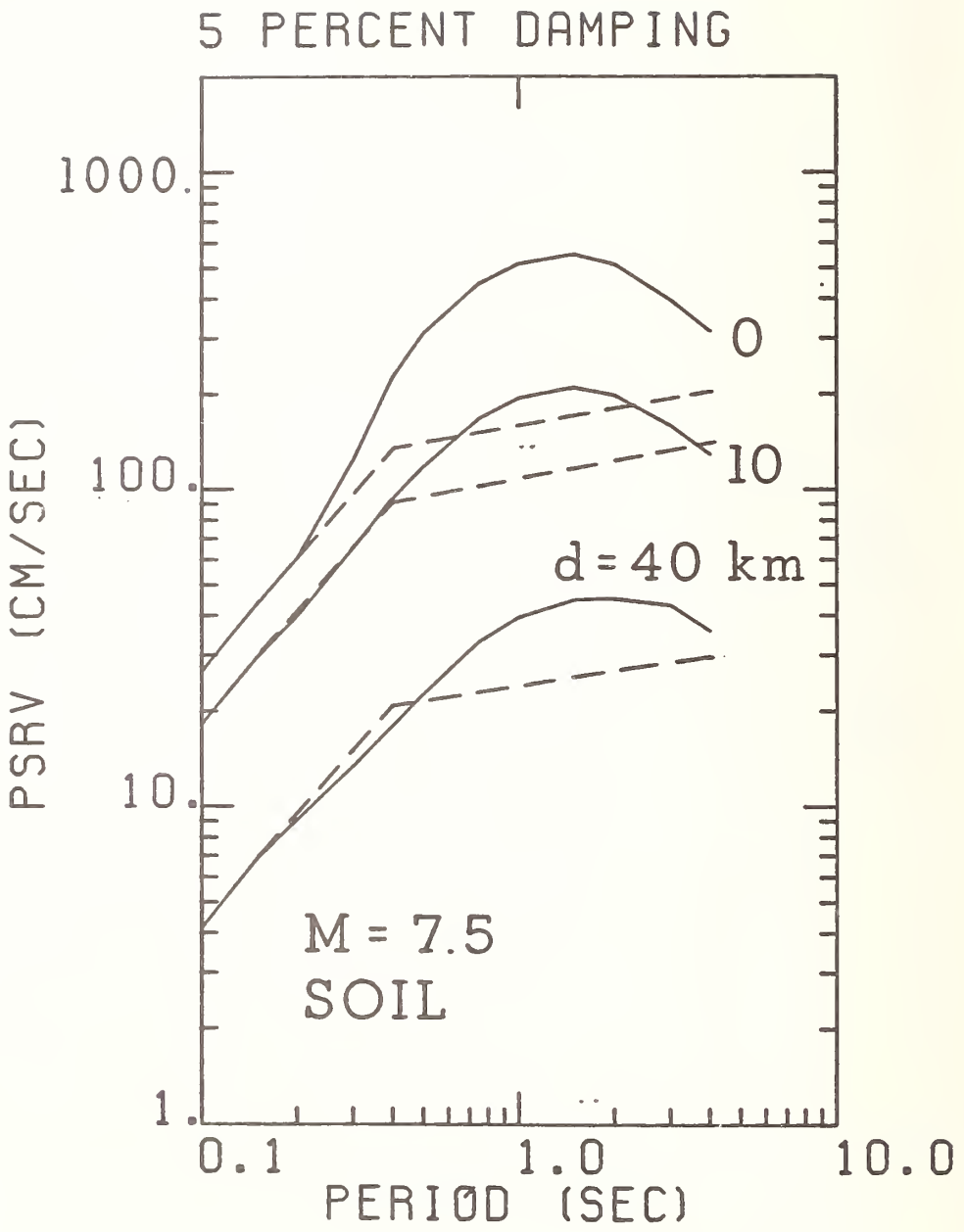

Figure 12. Predicted pseudo-velocity response spectra for 5 percent damping (solid lines) at soil sites for a moment magnitude of 7.5 and d equal to 0, 10, and 40 km compared to the Regulatory Guide 1.60 spectrum (dashed lines) anchored to the predicted spectra at 0.1 s

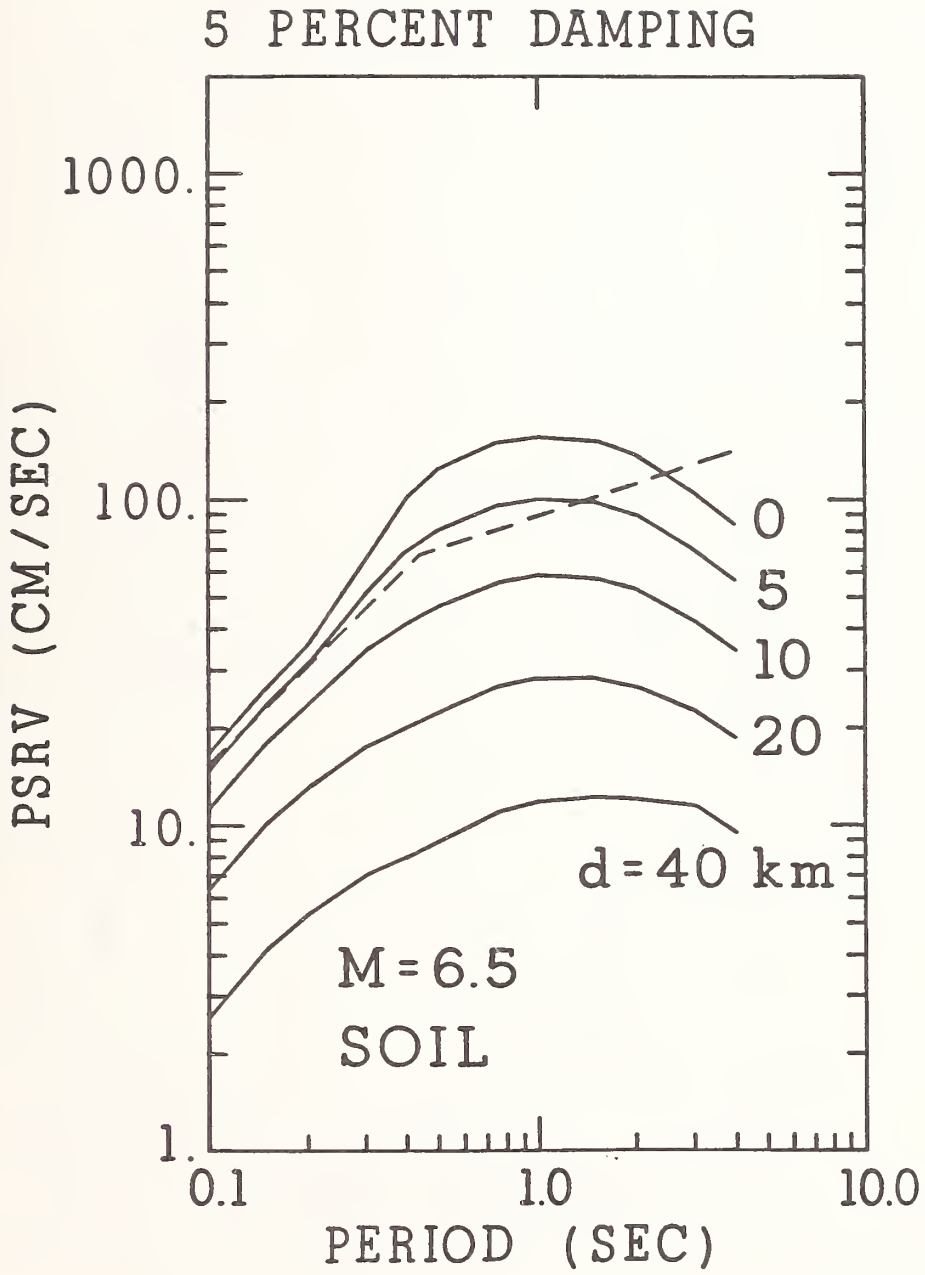

Figure 13. Predicted pseudo-velocity response spectra for 5 percent damping (solid lines) at soil sites for a moment magnitude of 6.5 and d equal to 0, 5, 10, 20, and 40 km compared to the ATC-3 lateral design force coefficient (dashed lines) calculated for a response modification factor R of 1.0, for soil type S2, and for A_a and A_v of 0.4

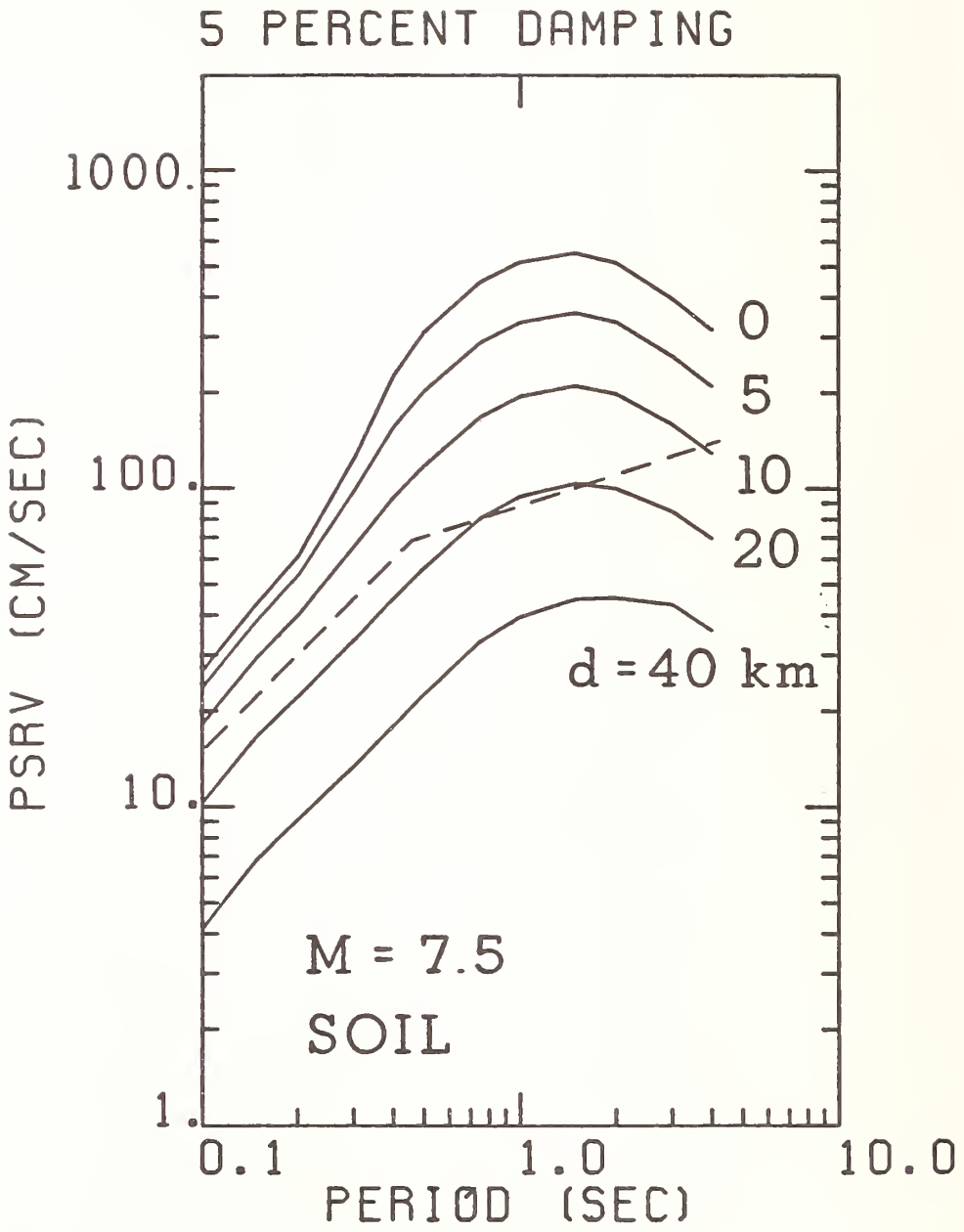

Figure 14. Predicted pseudo-velocity response spectra for 5 percent damping (solid lines) at soil sites for a moment magnitude of 7.5 and d equal to 0, 5, 10, 20, and 40 km compared to the ATC-3 lateral design force coefficient (dashed lines) calculated for a response modification factor R of 1.0, for soil type S2, and for A_a and A_v of 0.4

RECONSIDERATION OF THE INPUT WAVES FOR DYNAMIC ANALYSIS

Keiichi Ohtani

National Research Center for Disaster Prevention
Science and Technology Agency

ABSTRACT

The aseismic design method using dynamic analysis has been well established in Japan. Actual design cases of high rise buildings have been totaled up to about 400 in the past 20 years. In this paper, the present state of aseismic design, especially of the dynamic response analysis is reviewed.

Some problems related to the input waves for design are also discussed, and some future subjects for research and development are proposed.

INTRODUCTION

Building height in Japan has been limited to 31 meters since the Kanto Earthquake. In February 1962, a study to possibly understand fully the design and construction of high rise buildings was initiated by the Building Constructor Society in behalf of the Ministry of Construction. In September 1963, the Archtectural Institute of Japan published its original draft of the "Guideline for Aseismic Design of Tall Buildings." As a result, the "Building Standard Law" of Japan was altered from the building height limitation to building volume limitation in January 1964.

The number of high rise buildings exceeding 45 meters has been increased to about 400 since January 1964. These buildings have been examined thoroughly with regard to aseismic safety using dynamic analysis instead of static analysis, and have received the judge-and-rating to the propriety of their structural design by a committee consisting of a group of specialists. In June 1981, the structural design specified in the "Building Standard Law" was again revised to reflect the accumulation of experiences in using the dynamic analysis in actual design and the results of the earthquake engineering research.

The general trend of the current aseismic design of high rise buildings are discussed and some approaches related to input waves for the design are proposed in this paper.

PRESENT STATE OF ASEISMIC DESIGN OF HIGH RISE BUILDINGS IN JAPAN

The structural design of high rise buildings are carried out in accordance with the "Guideline for Aseismic Design of Tall Buildings," usually employing dynamic response analysis to check the structural safety. The documents and drawings of the structural design are presented by structural designers to the Building Center of Japan (BCJ) and are reviewed by the Evaluation Committee of the High Rise Building Structures of BCJ with regard to the propriety of the structural design.

A summary of the aseismic design of the high rise buildings is given as follows:

The structural systems used are either the S type (steel structure for the main parts) or the SRC type (composite steel and reinforced concrete structure), and the ratio between the two is about 1:2. The number of stories varies from 10 to 60, and in most cases is 14 to 18 for SRC type and, 14 to 30 for S type.

A general method of modeling is to connect the masses of each floor by springs from floor to floor (the idealized lumped mass vibration system). Both shear model and flexual-shear model are used for elastic response analysis, but at present the flexual-shear model is much more widely used than the shear model. In general, the shear model is used for inelastic response analysis. If the flexual-shear is used for elastic analysis, the equivalent shear model which is constructed using the fundamental period and vibration mode of the shear model is used for the inelastic case. The force-deformation curves of the open frame and of the quake resisting wall are determined respectively, and then the curve used for the building design is made by the superposition of these curves. To further simplify the curve, the spring used to represent the story is approximated by either a bilinear or trilinear line.

The approximate relation between fundamental period (T_1) and number of stories (N) is given as follows:

$$T_1 \simeq 0.08N \quad (S)$$

$$\simeq 0.1N \quad (SRC)$$

The relation between "T_1" and "C_B" where C_B, is the design base shear coefficient is given as $C_B = (0.24 \simeq 0.42)/T_1$ whereas the "Guideline" recommends $C_B = (0.18 \sim 0.36)/T_1$. Therefore, the designers have a tendency to design structures using a more severe criterion than that specified by the "Guideline." They expect that satisfactory structural safety margins can be accomplished by selecting larger sections in the design, even if it results in a little waste in the design, since the high rise buildings have not yet experienced any great earthquakes and their safety has not been proven enough in practice.

The earthquake accelerograms from El Centro NS has been used in almost all design cases as the standard excitation, and Taft EW is also used in 80 to 90 percent of the cases. The accelerograms from Tokyo 101 NS, Sendai 501 NS, and Osaka 205 EW, etc., observed in Japanese earthquakes are also used in the design.

The maximum input acceleration varies from 200 to 250 gal for the elastic response analysis and 350 to 400 gal for the inelastic response analysis. However, the use of maximum input velocity in the design method has been increased in recent years. In this approach, maximum velocity of 25 kine

for elastic analysis and 40 kine for inelastic analysis are employed. The maximum angle of story deformation used in the design is in the range of 1/200 to 1/150 for elastic analysis with a higher magnitude of 1/120 to 1/80 for inelastic analysis. Ductility factor for the inelastic design is $\mu \leq 2$.

INPUT WAVES FOR DESIGN

The aseismic design method using the dynamic analysis, which has been used in the actual design of about 400 cases in 20 years, has not been made any revision in those 20 years. By examining carefully through the stages in the actual design, I consider that the method certainly has some problems. The problem of selecting input waves for design is discussed in this section.

ESTABLISHMENT OF INPUT WAVES FOR DESIGN

Earthquake motion is determined by factors such as the scale of the earthquake, the characteristics of the epicenter, the passage of wave propagation, and the condition of rock and soil at the site, etc. Of course, it is extremely difficult to forecast the earthquake motions, which would occur in the future, by considering the above mentioned many factors. Many researchers are studying the forecasting by deterministic or statistical methods, but these methods have not been used in practice yet.

Establishment of the input waves used in the aseismic design (design wave) affects greatly the design results. Methods used to establish the design waves, at the present, are as follows:

(1) To use the observed earthquake accelerograms.

(2) To develop an artificial earthquake using random theory.

(3) To calculate the earthquake motion using theoretical seismology and other engineering knowledge.

However, in the actual design, method (1) has been used almost exclusively, except that other methods were employed during the investigation stage for checking purposes.

In design method (1), the selected accelerograms are affected by the characteristics of the observation site and the magnitude of earthquake one selects. Therefore, there is a question that the earthquake which would occur in the future at the design site would have the same characteristics. To reduce the uncertainty, several earthquake accelerograms are employed as the design waves for the design. Figure 1 shows the velocity response spectra of El Centro NS, Taft EW, and Tokyo 101 NS. These three waves are used very commonly in Japan, and have different dominant periods, i.e., El Centro NS is 2.6 sec, Taft EW is 1.6 sec, and Tokyo 101 NS is 0.8 sec, respectively. If these three waves are employed in the design as a set, these waves are given the same regular response level for the wide frequency zone to make up the frequency characteristics.

In the future, it is necessary that both regularly used and new design waves be examined to minimize the weakness of this approach. The expected method of selecting design waves should include the establishment of wave groups calculated from the seismicity map of the region and the subsurface condition of the site.

FREQUENCY CHARACTERISTICS OF THE DESIGN WAVES

The frequency characteristics of the earthquake accelerograms, which are used very commonly in design are shown in figure 1. It is the question that the frequency characteristics for elastic analysis and for inelastic analysis should be the same or not.

The velocity response spectra of several earthquakes observed at Iwatsuki, Saitama Prefecture are shown in figure 2. Numerals in the figure indicate the magnitude of the earthquakes. The relation between the dominant period and the magnitude is given in figure 3 which indicates that the dominant period has the trend to increase with the magnitude. The dominant period for an earthquake of M = 8 is estimated at about 2 to 2.5 sec.

In the future, it is necessary that the frequency characteristics be changed to calculate the dynamic response for elastic analysis and inelastic analysis. To accomplish this goal, strong motion observations should be continued and strengthened by a network system.

LEVEL OF THE DESIGN WAVES

Essentially, the level of the design waves is determined by the level of seismicity of the construction site. Most commonly, the level of the design waves is determined by the maximum input acceleration. As accumulation of the strong earthquake records increases along with the improvement of accuracy of measurement, the recorded maximum acceleration is also increasing. However, the relation between the recorded maximum acceleration of an earthquake and its associated damage is not very good. If a very strong earthquake of long duration is employed as the design wave, the response should be much greater than the response of a general earthquake.

The use of maximum input velocity is considered as another method of determining the level of the design waves. Both the maximum acceleration and the maximum velocity methods are determined by the peak (the maximum value) in the duration of an earthquake.

It is the question that these two methods used for the evaluation of dynamic behavior in the duration of an earthquake are proper methods or not. The level of the design waves should be determined by the total information through the duration of the earthquake. It therefore should be a useful alternative that the maximum input energy (calculate from the time integration of the energy of an earthquake) is employed to determine the level of the design waves.

CONCLUSION

The current design method used in 400 actual designs of high rise buildings and some questions related to input waves for design are discussed. Although the "Guideline" has recommended that a suitable input excitation must be chosen according to site or foundation condition, the actual state of the design is hardly taking into consideration of this foresaid condition. The development of a "Standard excitation" (design wave) and the method which takes into account of the seismicity and dynamic characteristics of the ground at the site are necessary. Several points of future developments of the input waves are proposed:

(1) To prepare the seismicity map of each region using parameters such as the scale of an earthquake and the focal distance.

(2) To prepare a calculation method considering the above seismicity map and the dynamic characteristics of ground at the site.

(3) To establish the frequency characteristics of an earthquake in accordance with the scale of the earthquake.

(4) To establish an evaluation method for the level of earthquake considering the total information through the duration of the earthquake. For example, the maximum input energy is an effective parameter for the determination of the level of the design waves.

It is a fact that the characteristics of the design waves have significant influence on the results of the structural design. Therefore, it is very important for the structural designer and researchers to continue the consideration of this problem.

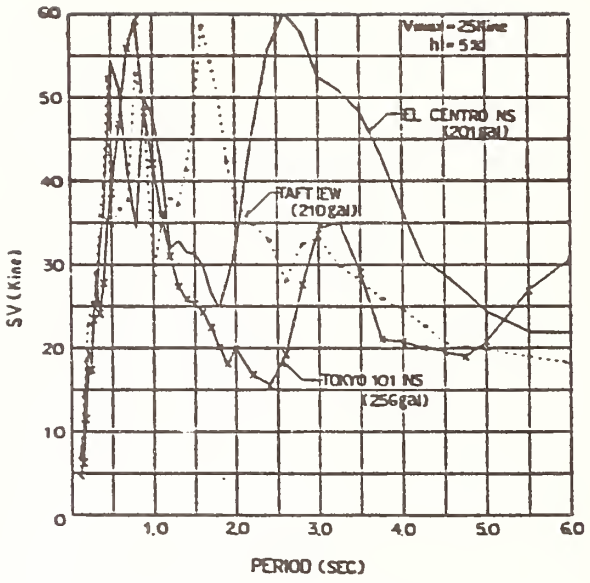

Fig. 1 Velocity response spectra
(V_{max} = 25 kine, h = 5 %)

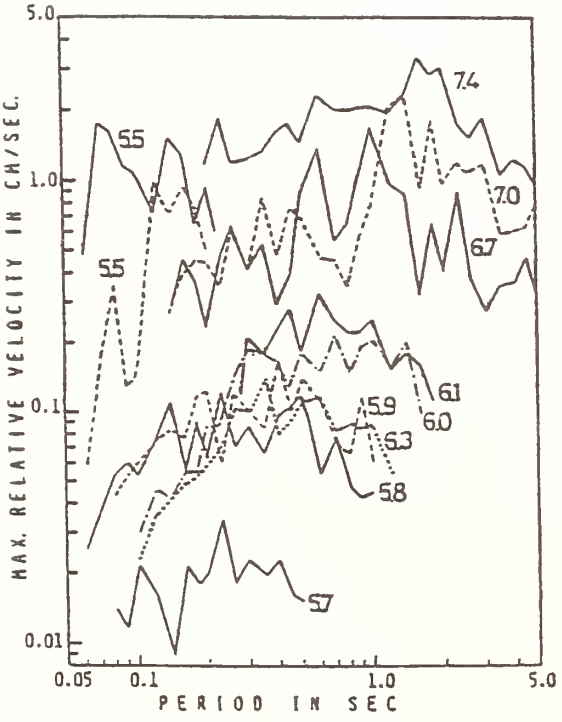

Fig. 2 Velocity response spectra
(no damping)

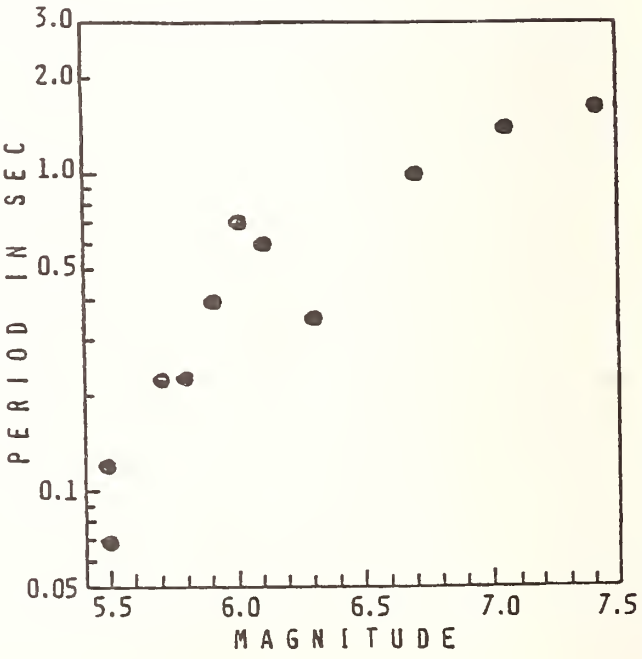

Fig. 3 Relation between dominant period and Magnitude

SOME NEW PROCESSING TECHNIQUES FOR THE IMPERIAL VALLEY 1979 AFTERSHOCKS

A. Gerald Brady

U.S. Geological Survey
Menlo Park, CA

ABSTRACT

This paper describes some of the features of the latest processing improvements that the U.S. Geological Survey (USGS) is currently applying to strong-motion accelerograms from the national network of permanent stations. At the same time it introduces the application of this processing to the set of Imperial Valley aftershocks recorded following the main shock of October 15, 1979. Earlier processing of the 22 main shock recordings provided corrected accelerations, velocity and displacement, response spectra, and Fourier spectra. The digital data has been available on two tapes from NOAA, in Colorado, for 2 years now, and a report containing computer plots has been available, while supplies last, from the USGS in Menlo Park.

The USGS has taken the opportunity provided by the large number of triggerings at 30 permanent stations in the Imperial Valley to update the processing scheme applied particularly to short duration accelerograms with frequencies possibly as high as 50 Hz.

A total of 67 of the aftershock recordings were selected for digitization, from eight events. The number of stations involved is 20, all of which had previously recorded the main shock. A brief outline of the processing steps that have been developed is included, as they have been applied to the best recorded, M 5.0, aftershock. The selection of a long-period filter and its dependence on the need to remove a predominant 4 sec component is discussed. Displacements from those stations on the El Centro Array with radio time have been plotted so as to indicate visually the total processing package.

IDENTIFYING AND SCALING AFTERSHOCK RECORDINGS

The stations in the permanent network are shown in the map of figure 1. All are USGS stations except the following which belong to the California Division of Mines and Geology network: the ground stations at Niland and Westmorland, the bridge overpass on Interstate 8, and the County building in El Centro. The El Centro Array lies approximately perpendicular to the Imperial Fault, spanning 22 km on either side, with station 6 located between the Imperial and Brawley Faults. Four USGS stations lie to the southeast of the array, although the instrument at Meadows was inoperative. Six USGS stations lie on the northwestern side of the array. An additional film recorder, named the Differential Array, is located at the site of the special array of digital instruments within the city of El Centro.

The epicenter of the 1940 event is indicated in addition to the main shock of October 15, 1979. The epicenters of five of the eight aftershocks whose records have been digitized are indicated by crosses. The M 5.0 event labeled E2319 occurred 2-1/2 min after the main shock; the other four all to the northwest surrounding Brawley occurred during the next 24 hr. The three events whose epicenters have not been calculated or plotted occurred in the 2-1/2 min time intervals between the main shock and E2319.

A partial listing of the accelerograms occurring during the first 24 hr is included in table 1. The top section of the table lists those aftershocks occurring in the first 2-1/2 min; the time given, in seconds, is the average triggering time of the contributing records. The stations and their fault distance are listed at the top and bottom of the table. In addition to the stations on the El Centro Array, numbered 1 to 13, are the abbreviations used for the other stations, namely, Superstition Mountain, Parachute Test Facility, Calexico, the Differential Array, Brawley, Bonds Corner, Holtville, Calipatria, and the Salton Sea Wildlife Refuge.

Positively identified records are indicated by an x. Parentheses surrounding an x indicates less than a positive identification, and inclusion of such records in the study of a particular event would have to await more detailed wave form comparisons. Of the 11 aftershocks listed during the first 2-1/2 min, 4 were recorded by at least 6 stations. The total number of records, N, is listed in the right-hand column for each aftershock. This criteria, of at least six records, governed whether a particular aftershock set was digitized. The event identified by the average triggering time of 23 hr, 19 min, 35 sec, M 5.0, has 16 positively identified records and is the subject of the processing steps described in the following. Its location and origin time were determined from the strong-motion data (D. Boore, personal communication):

Epicenter	32° 46.00'N
	115° 26.48'W (± 6 km, horizontally)
Depth	9.52 ± 3 km
Origin time	2319 hr, 29.62 sec, October 15, 1979, UTC
Magnitude M_L	5.0 (PAS)

Scaling of the peak values, and reading of S-t intervals and durations are carried out from the original records at the same time as events are identified (Matthiesen and Porcella, 1980). Figure 2 shows the peak sealed accelerations for those stations whose accelerographs are aligned transverse and parallel to the Imperial Fault. The drop in amplitude of the horizontal peaks at station 10 to the southwest, and stations 3, 2, and 1 to the northeast is partially explained by the fact that these stations lie on the 45° shear wave nodal lines drawn from the plotted epicenter (figure 1).

PROCESSING STEPS

The elements of the processing procedure can be divided into three main groups:

A. Digitization and preparation of uncorrected data, with no alteration to the frequency content of the digitized record.

B. Instrument correction and its preliminary anti-aliasing, to provide equispaced data whose high frequency content is as accurate as possible.

C. Long period removal of various types, dependent on the nature of integrated velocity and displacement, and on the shape of the Fourier spectra. This ensures the remaining long period content is as accurate as possible.

Each of these processing groups has received attention recently in our efforts to upgrade the quality of the corrected data, making use of the most recent research results. A more detailed description of some of the components follows.

A1. Digitization of the original 70 mm film record, or a film copy specially prepared for automatic trace following, is performed commercially by IOM-TOWILL of Santa Clara, California. They provide digitized nonequispaced versions of all data and reference traces at an approximate density of 600 samples per second (sps). Higher density digitization is performed automatically around sharp peaks, while less dense performance results when operator intervention is required at trace intersections or severe trace lighting.

A2. Records are digitized in sections, or "frames", of 10 cm length, corresponding to 10 sec durations. Records from this aftershock are mostly two frames long. These have been reassembled by making use of ink lines previously inserted perpendicular to the film transport direction, and digitized in each of the two adjacent frames.

A3. The one-half sec time marks are operator-digitized and used to define the time coordinates of the traces. The instrument's sensitivity is used to scale the amplitudes to accelerations. These are nominal accelerations, particularly at frequencies greater than about 15 Hz, prior to any instrument correction.

A4. The data are interpolated to equispaced 600 sps, in preparation for subsequent processing which, although designed to alter the frequency content, is none-the-less carried out in the time domain.

B. Steps B5, B6, and B7 are carried out simultaneously with a combination convolution operator, acting sequentially on the 600 sps time series.

B5. Any anti-aliasing low-pass filter at a frequency of 100 Hz ensures the removal of any noise in the digital data between 100 Hz and 300 Hz, including that which could have been aliased into this

range by the earlier interpolation to 600 sps. This step guarantees that there is negligible energy transferred to the 0 to 100 Hz range by the subsequent decimation (in B7) to 200 sps.

B6. In the frequency range between 0 and 50 Hz an instrument correction is applied, using the natural period and damping of the accelerometer. We have replaced the centered difference scheme for the first and second derivatives with a contribution to the combined convolution operator. This time domain convolution has 61 weights spanning 0.1 sec, and reduces the errors in instrument correction at high frequencies to negligible proportions. Figure 3 shows the ideal instrument correction to 30 Hz compared with the centered difference correction; the amplitude response of the convolution operator is almost indistinguishable from the ideal curve. Figure 4 shows the complete operator response to 300 Hz. A cosine taper is fitted between the instrument correction, applied to the range 0-50 Hz, and the anti-aliasing filter, applied to the range 100-300 Hz. For the specfic input parameters for this filter, it is noted that amplification of almost five items will occur if frequencies between 60 and 70 Hz are present.

B7. A data density of 200 sps, providing a convenient representation of the original analog record, is produced by decimation.

The presence of long period noise in a record that has been processed through the instrument correction stage becomes evident on calculating the velocity and displacement. Displacements magnify long-period content while making high frequency content less visible. The decision on whether to make a long period correction or not, and of what form the correction should be, is based on previous experience (Basili and Brady, 1978), the results of statistical noise investigation (Trifunac and Lee, 1978) and the actual appearance of velocity, displacement, and Fourier spectra. Among the options currently available in the USGS processing scheme are the following.

C8. The removal of a linear trend in velocity, or the removal from the complete velocity trace a linear trend calculated from a specific section of it, is a suitable procedure if it proves to be the only correction required.

C9. Long period removal can be accomplished by an Ormsby filter (Basili and Brady, 1978) suitably adapted to the record, or a Butterworth bidirectional filter (Fletcher and others, 1980).

C10. Records which commence with high-amplitude P-wave arrivals will need a cosine taper fitted to the beginning of the record prior to the calculation of the Fourier spectrum.

SELECTION OF FILTER

Most of the original film records from the aftershock under investigation clearly showed the presence of a 4 sec component which had commenced during the main shock 2-1/2 min earlier. Our regular procedure for selecting a long period limit for these records would have resulted in leaving

this 4 sec component untouched. In order to study the detailed arrivals of P (where possible) and S waves we have removed all long period content greater than 2 sec, with the 0.5 Hz Butterworth filter whose effect is shown in figure 5. The 4 sec component displacement is shown also, by substituting a 0.2 Hz filter, which removes all periods longer than 5 sec. For comparison purposes, the displacement when no filtering is applied is also shown.

In order to provide an overall view of the quality of the long period processing, figures 6 and 7 have been prepared showing the calculated displacements from stations on the El Centro array with radio time, arranged on a common time scale. The 0.5 Hz filtered data has been used, so as not to be contaminated with the 4 sec signal. Figure 6 shows the displacements in the 230° direction, that is, perpendicular to the fault in the southwest direction, approximately. Stations 1 through 6 lie to one side of the fault, while station 11 lies 13 km from the fault on the other side. The figure lists the fault distance and epicentral distance for the stations. The time scale indicates seconds, after 23 hr 19 min, October 15, 1979, UTC. The arrows on the displacement plots indicate the peak values, which are enumerated on the vertical axes. The arrival of the transverse shear wave, a pulse in the 230° direction, is reasonably clear on all records, although preceded by a preparatory movement in the opposite direction, at stations 2 and 11. The simultaneous arrival at stations 4, 5, and 6, between 10 and 11 km from the epicenter, define a shear wave velocity of 2.2 km/sec.

Figure 7 shows the displacements in the 140° direction (parallel to the fault, approximately southeast). For stations 1 through 5 a very clear pulse in the southeast direction is visible, while stations 6 and 11 show a clear pulse in the opposite direction. Given the clarity of these displacement pulses, this implies that the initial rupture for this aftershock occurred on a plane that passes to the northeast of station 6, whereas the Imperial Fault passes to the southwest.

CONCLUSIONS

The improvements made to the USGS processing scheme for strong-motion accelerograms have concentrated on improved high frequency content, an improved instrument correction, maximum use of densely digitized data and freedom to choose interactively from a variety of long period filtering schemes. The clarity and coherence of the displacements integrated from the corrected accelerograms from the M 5.0 aftershock 2-1/2 min after the Imperial Valley Earthquake main shock provide confidence in the overall quality of the improvements, insofar as they apply to short duration recordings.

REFERENCES

[1] Matthiesen, R. B. and R. L. Porcella, 1980, "Strong Motion Data Summary Imperial Valley Earthquake of October 15, 1979 and Aftershocks," in Seismic Engineering Program Report September-December 1979, USGS Circular 818C.

[2] Basili, M. and A. G. Brady 1978, "Low-Frequency Filtering and the Selection of Limits For Accelerogram Corrections," Proceedings 6th European Conference on Earthquake Engineering, Dubrovnik, Yugoslavia.

[3] Trifunac, M. D. and V. W. Lee, 1978, "Uniformly Processed Strong Earthquake Ground Accelerations in the Western USA for the Period from 1933 to 1971," Report No., CE 78-01, University of Southern California, Los Angeles, California.

[4] Fletcher, J. B., A. G. Brady, and T. C. Hanks, 1980, "Strong-Motion Accelerograms of the Oroville, California, Aftershocks: Data Processing and the Aftershock of 0350 August 6, 1975," BSSA, 70, 1, pp. 243-267.

Table 1. USGS Aftershock Accelerographs
First 2-1/2 Minutes

Event 288/23 hr UTC	M_L	Strong Motion Station																						
		SM	13	12	PT	11	CX	10	9	DA	8	7	6	5	BR	4	BC	HV	3	2	CP	1	SS	N
17:28														x	x									
17:37											x		x	x	x	(x)			(x)					
17:41									x	x	x	x	x	x	(x)	(x)			(x)	(x)				6
17:47															x					(x)				
18:03							x						x	(x)	x		(x)	(x)						
18:21									x	x	x	x	x	x		(x)			(x)	(x)				6
18:42									x	x	x	x	x	x			x	x						7
18:57													x											
19:01													x											
19:20													x											
19:35	5.0					x	x	x	x	x	x	x	x	x	x	x	x	x	x	x		x		16
289 0549	5.3					x	x				x			x		x	x			x	x	(x)		9
0619	5.1					x					x			x		x	x			x	x	x	x	9
0658	5.8	(x)	(x)			x	x				(x)			x		x				x	x	x	x	11
2317	5.2																			x		x	x	3
Fault distance km:		26	22	18	15	13	10	9	6	5	4	1	1	4	6	7	7	8	13	16	21	22	28	

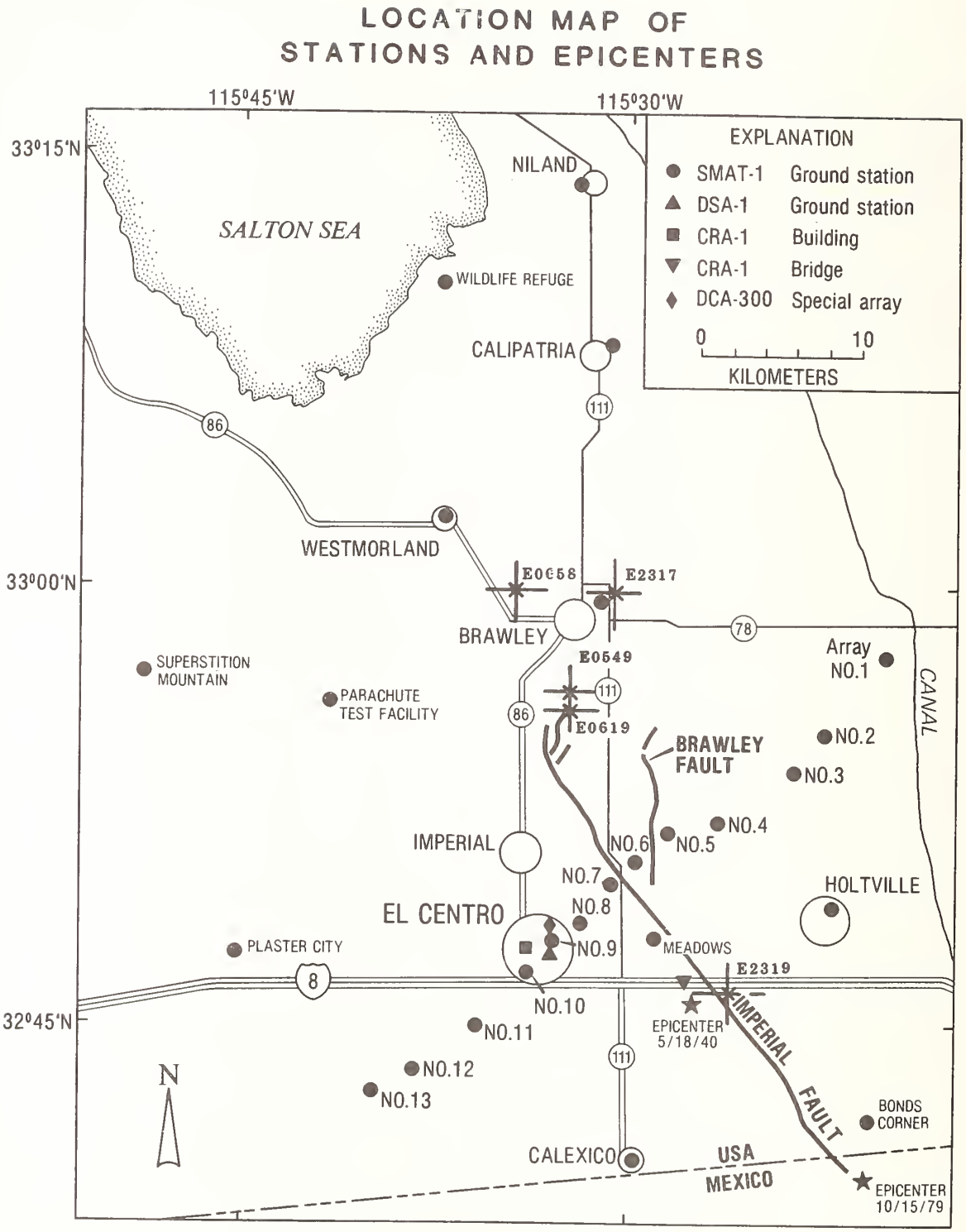

Figure 1. Location map of stations and epicenters

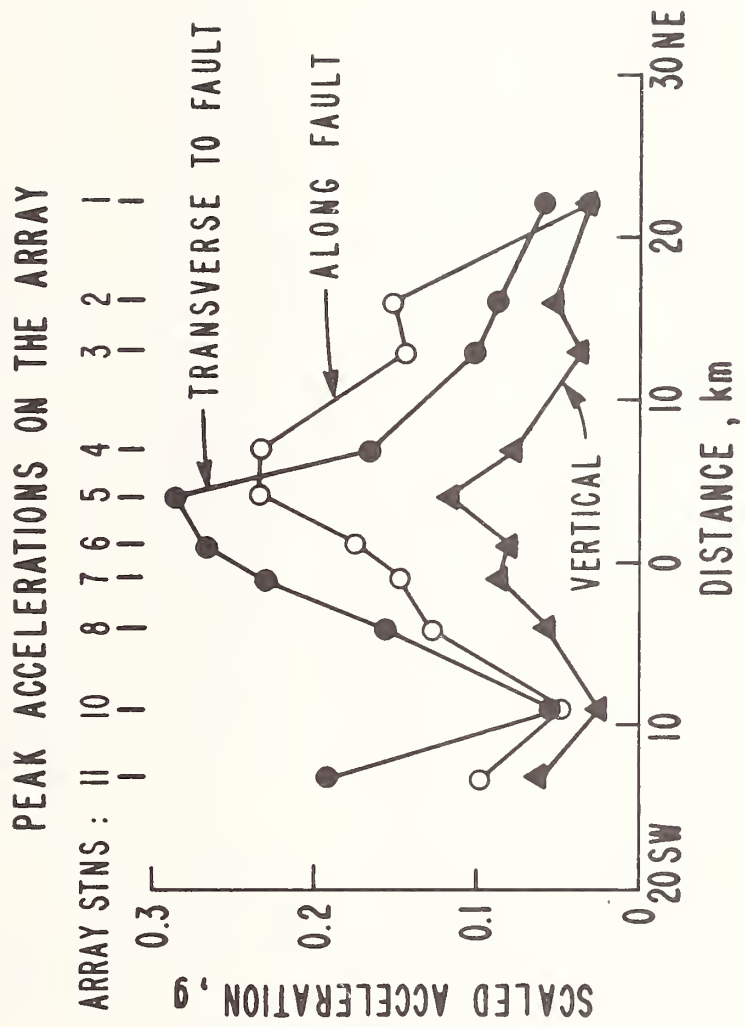

Figure 2. Peak scaled accelerations at the stations on the El Centro Array. These accelerographs are aligned transverse and parallel to the Imperial Fault.

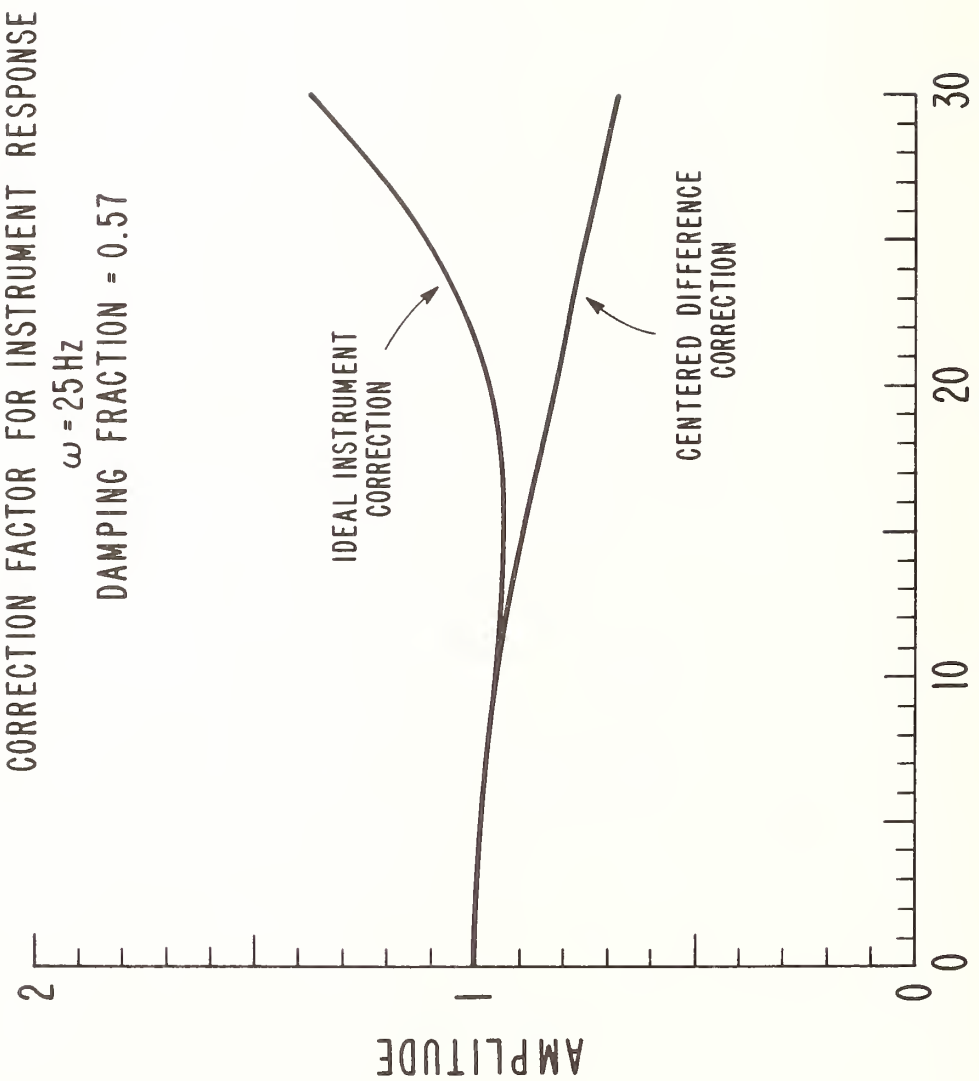

Figure 3

Figure 3. Correction factor applied in the time domain for instrument response. The number of weights in convolution operator has been chosen to insure that its amplitude response is indistinguishable from the ideal instrument correction shown.

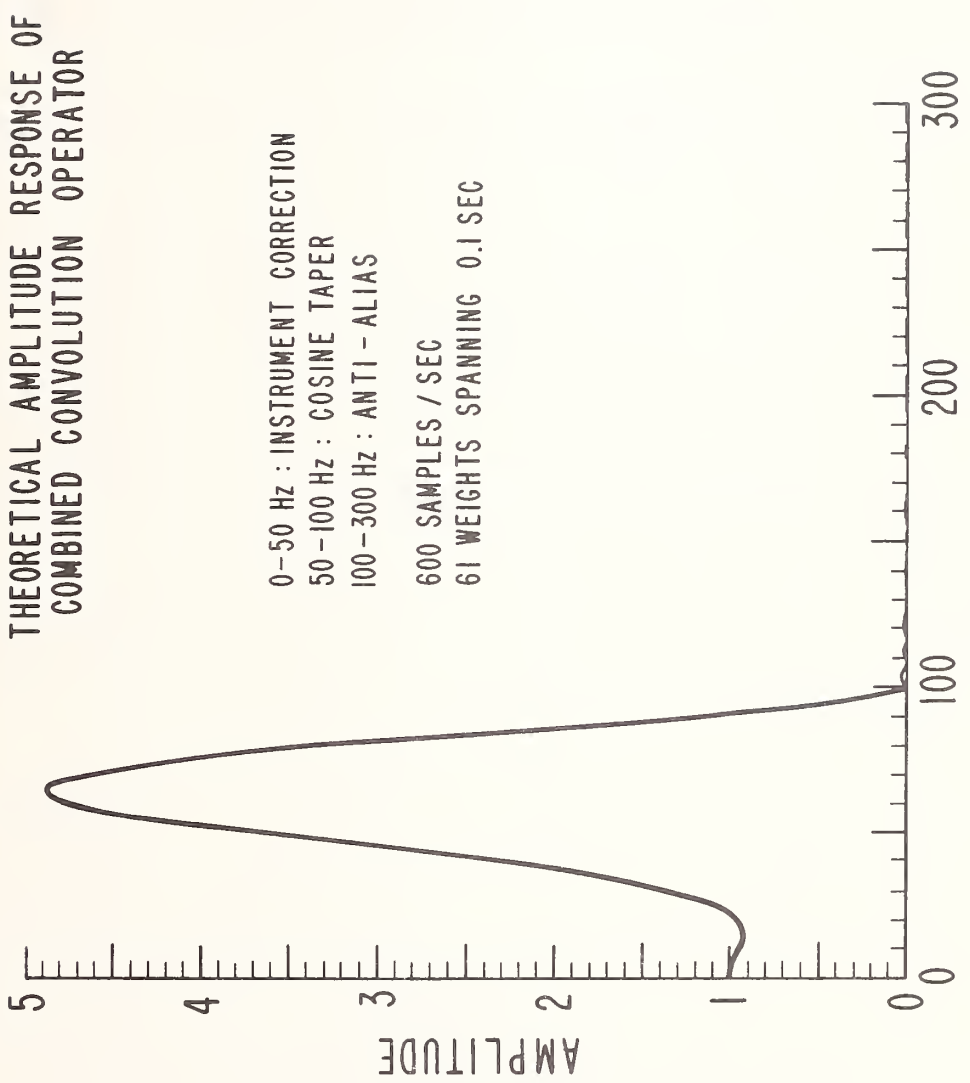

Figure 4

Figure 4. Theoretical amplitude response of the combination convolution operator. Actual operator response is almost indistinguishable from this curve.

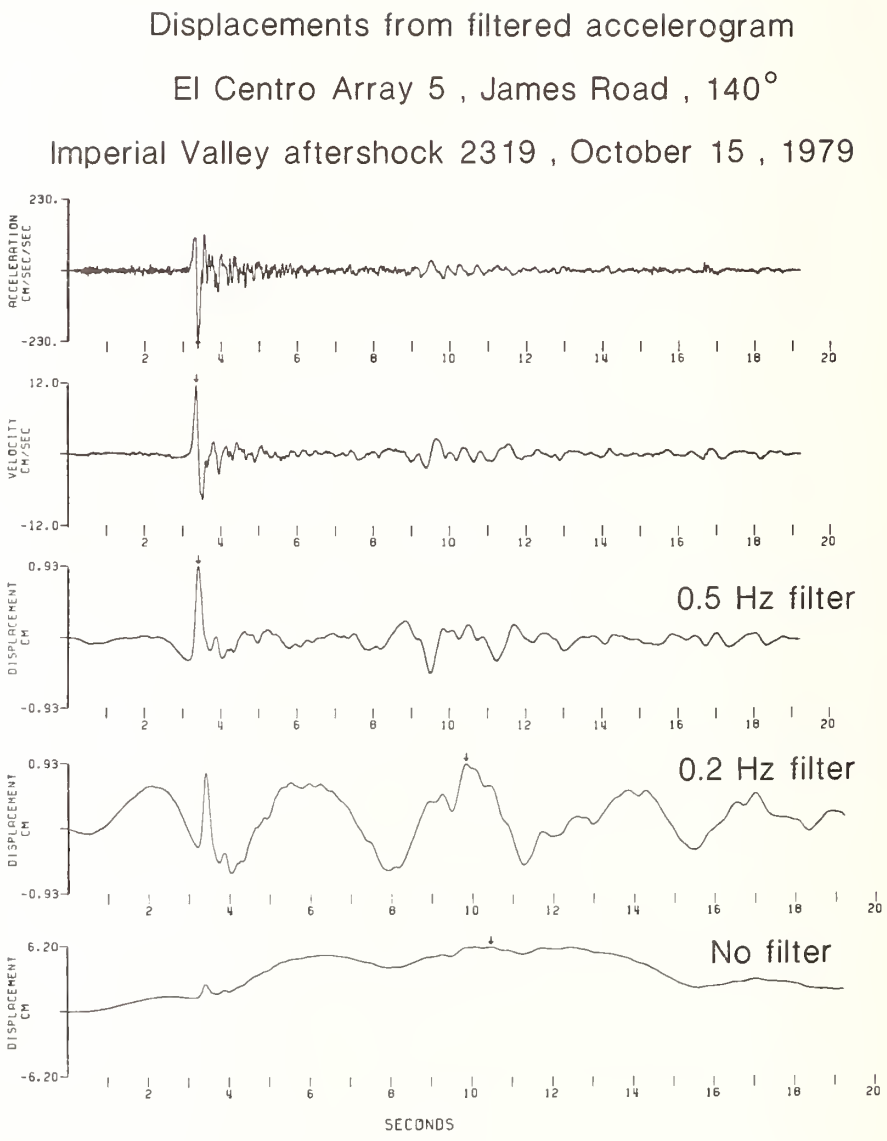

Figure 5

Figure 5. Acceleration, velocity and displacement of sample record with 0.5 Hz high-pass Butterworth filter. Additional displacement curves are result of substituting a 0.2 Hz filter, and no filter.

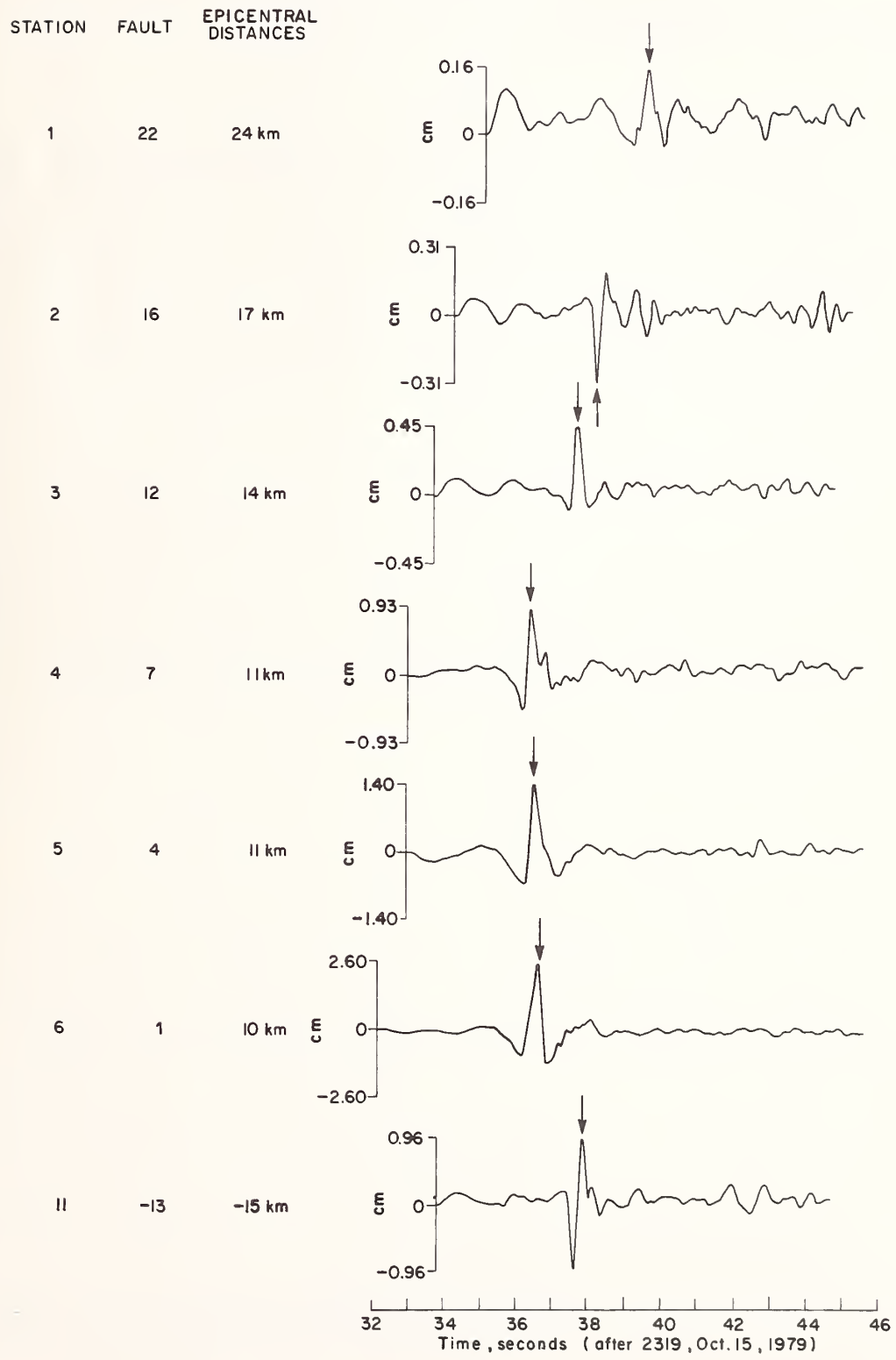

Figure 6. Displacements in 230° direction for seven stations with radio time on the El Centro Array.

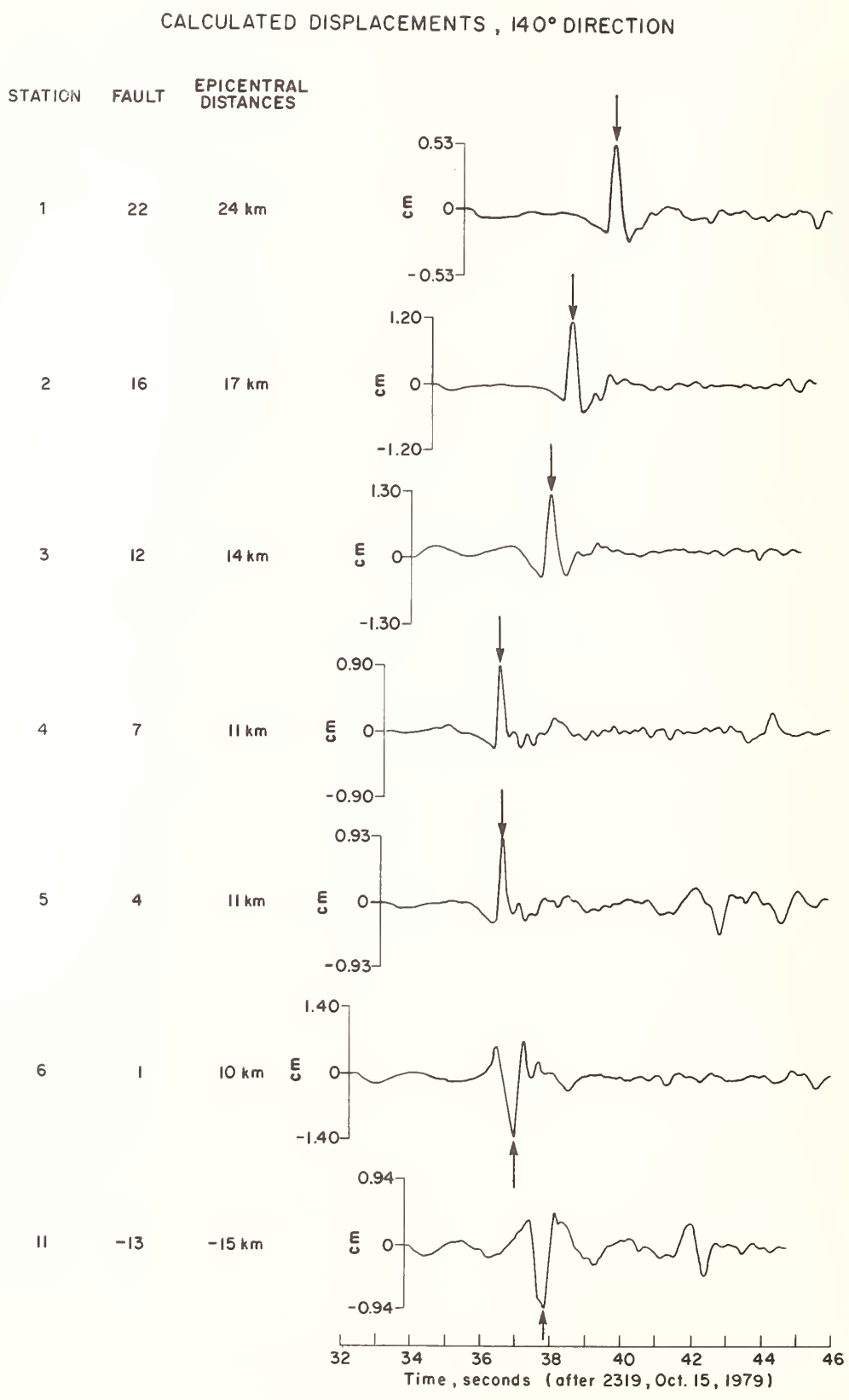

Figure 7. Displacements in 140° direction for seven stations with radio time on the El Centro Array.

DENSE INSTRUMENT ARRAY OBSERVATION BY THE PUBLIC WORKS RESEARCH INSTITUTE AND ANALYSES OF SOME RECORDS

Tadayoshi Okubo
Tadashi Arakawa
Kazuhiko Kawashima

Public Works Research Institute
Ministry of Construction

ABSTRACT

It is important for large structures such as bridges and lifeline facilities to consider differential motions between points of the ground in estimating the design ground motions. It is well recognized that such motions are significantly dependent on local geological and topological conditions. In order to investigate such effects on earthquake ground motions, the normal type of strong motion observation performed at each individual site is not enough, and installation of a dense instrument array is indispensible.

Besides the laboratory observation array at its campus, the Public Research Institute is now on the way to deploy four local laboratory arrays around the Suruga Bay-Izu area in Shizuoka Prefecture, Japan, within 4 years, starting in the 1981 fiscal year.

This report presents one of the four local laboratory arrays in the Sagara area, at which instrumentation has been completed and observations were initiated in 1981 fiscal year, and shows some analyses of array data obtained at the PWRI campus. Analyses for finite strains induced in ground during earthquakes, effects of differential motion on structural response in terms of multi-support response spectrum, and wave propagation characteristics in vertical and horizontal directions are studied.

OUTLINE OF THE DENSE INSTRUMENT ARRAY PROGRAM OF THE PUBLIC WORKS RESEARCH INSTITUTE [3, 4, 5, 6]

Based upon the knowledge accumulated through past strong motion observations, it is widely recognized that characteristics of ground motions, especially ground motions in the short period range which is important for engineering structures, are strongly dependent on source characteristics, path conditions between the source and the observation site, and local geological and topological conditions. Realizing that the damage of large structures, such as bridges and lifeline facilities, in past earthquakes is significantly related to relative motions of points from 10 m to several hundred meters apart in distance, it is very important to investigate effects of local geological and topological conditions on strong ground motions. For such a purpose, present single, isolated observations performed widely are insufficient, and installation of a dense instrument array in indispensable [1, 2, 3].

Recognizing the importance of investigating the effects of local geological and topological conditions on earthquake ground motions, the Public Works Research Institute had requested research funds to promote a dense instrument array program at 10 locations in Japan. This program consists of the deployment of at least 10 strong motion accelerographs for each location. As the first stage of such a program, 4 of the 10 locations, i.e., Sagara, Yaizu, Numazu, and Matsuzaki, which are located around Suruga Bay-Izu region designated as one of the six high priority sites by the International Workshop on Strong Motion Earthquake Instrument Arrays [1, 2], have been planned to be deployed within 4 years starting in fiscal year 1981. A total budget of approximately 211 million Yen (approximately 1 million U.S. dollars) is to be invested for the deployment at these four sites. Figure 1 shows the location of the four sites as well as the location of local laboratory array at PWRI, which will be described later. The first array station at Sagara area has been already deployed and in operation. The second array station is to be deployed at the Yaizu area in fiscal year 1982.

DENSE INSTRUMENT ARRAY AT SAGARA AREA

LOCATION AND SITE SELECTION

The Sagara area is located near Omaezaki in Shizuoka Prefecture facing Suruga-Bay, approximately 170 km southwest of Tokyo as shown in figure 1. Figure 2 shows the geological features around the site as well as the array instrumentation. The ground surface material of Sagara consists of soft alluvium clay deposits. Baserock of this area is the Sagara Group, tertiary layers consisting of alternate layers of sandy and clayey rock, which appears very widely around the site with shear wave velocity of 500 ~ 1000 m/sec. The thickness of the Sagara Group is considered to be approximately 1000 meters.

The ground condition was precisely investigated at 5 points within the site. Figure 3 shows the soil profiles with the standard penetration test N-values and distribution of the shear wave velocity. In addition to figure 3, data from 29 borings conducted in the past were collected, and based on these data, the geological structure at the site was formulated as shown in figure 4.

Ten 3-component strong motion accelerographs were installed on the surface at points from no. 1 to no. 10 (refer to figure 2) along an approximate L-shaped configuration. The direction of two legs of the L-shaped configuration is selected such that the subsurface ground condition varies along the legs. Four 3-component down-hole accelerometers were also installed at four points (nos. 4, 5, 8, and 10, refer to figure 2) as deep as 36 m so that the baserock (Sagara Group) motion can be obtained. The signals of each down-hole accelerometer are transmitted via cable to the strong motion accelerographs, which have the same specifications with those installed on the surface. The distance

between two adjacent strong motion accelerographs on the surface varies from 100 to 350 meters, and the length of two legs of L-shaped configuration is approximately 300 meters.

The deployment of strong motion accelerographs was completed in mid-Febraury and operation was initiated on February 24, 1982.

INSTRUMENTS

The array consists of 14 strong motion accelerographs (refer to figure 5) with independent triggering and recording systems. Time code generators are equipped for each instrument so that exact triggering time can be recorded at each site.

The main specifications of the strong motion accelerographs are summarized in table 1. Velocity feedback servo accelerometers are adopted and a maximum acceleration of $\pm$ 1G can be recorded within the frequency range of 0.1 ~ 30 Hz. The acceleration signals are digitized by a 16 bit A to D converter to have a dynamic range of 96 dB. Gain ranging was not adopted to avoid zero shift of acceleration. Sampling time of the A to D converter is 1/200 sec and the digital data are stored on a digital cartridge tape.

Self-triggering with pre-event memory of 5 sec and auto resetting after the earthquake are provided. The maximum acceleration recorded can be checked by digital display immediately after the earthquake. Thus, ground acceleration for 40 min in length can be recorded totally.

It is very important in independent triggering and recording systems to have a common base time between strong motion accelerographs. For such a purpose, accurate crystals with nominal accuracy of 10^{-7} (0.3 sec per month) are employed in the time code, and auto resetting of the crystals is performed in each hour with use of a NHK time signal. It is estimated that the differences of time between an arbitrary pair of strong motion accelerographs to be less than one-half of the sampling time, i.e., 1/400 sec.

Floating battery chargers are provided to supply electricity for no shorter than 25 hr in case of suspension of commercial electricity. A water tight die casting aluminum case encloses the system and is pressure rated at two times the atmospheric pressure.

Before installation at the site, a performance test of the strong motion accelerographs was conducted with use of shaking table as shown in figure 6.

ANALYSES OF LOCAL LABORATORY ARRAY DATA AT PWRI

GROUND STRAINS FROM STRONG MOTION ARRAY DATA

Array observation has been performed at the PWRI campus since July 1979 with the use of a local laboratory array as shown in figure 7 [4, 5, 6], and 21 records as shown in table 2 have been

obtained up to the present time. Figure 8 shows epicenter locations of earthquakes triggered by the array. Most of them are small earthquakes which occurred around the observing site, but three of them have a magnitude of six or greater on the Richter scale (JMA). Because the records induced by small magnitude earthquakes do not produce meaningful results, only records by earthquakes with a magnitude 4 or greater were used in the following analysis.

Ground strains were calculated based on the array data in table 2. Data processing, double integration of accelerations records and mathematical expression of finite ground strains were presented in previous reports [4, 8], and are not presented herein. Eight tetrahedrons were formulated based upon 10 observing points of the local laboratory array at A-field as shown in figure 9, i.e., 4 tetrahedrons for calculating lower level ground strains and 4 for calculating the upper level ground strains. In each tetrahedron, displacements of ground in x, y, and z directions are assumed to be linear [10]. Thus, six component strains ε_x, ε_y, ε_z, γ_{xy}, γ_{yz}, and γ_{zx}, which are constant within the tetrahedron, can be obtained. Table 3 shows averaged ground strains determined by averaging strains within four tetrahedrons at upper and lower levels. It is noted from table 3 that the upper level strains are generally larger than the lower level strains by a factor of 2 to 5.

With respect to ε_x, ε_y, and γ_{xy}, relations between maximum strains and maximum velocities (velocity at A2CO and A46CO for the upper and lower level strains, respectively) were obtained as shown in figure 10. Disregarding the data with maximum velocity less than 0.15 cm/sec, one obtains the correlation between strains and velocities in the form

$$\left.\begin{aligned} \varepsilon &= 20.4 \times v^{0.428} \times 10^{-6} \\ \gamma_{xy} &= 27.5 \times v^{0.810} \times 10^{-6} \end{aligned}\right\} \text{ for upper level}$$

$$\left.\begin{aligned} \varepsilon &= 12.6 \times v^{0.552} \times 10^{-6} \\ \varepsilon_y &= 13.2 \times v^{0.518} \times 10^{-6} \end{aligned}\right\} \text{ for lower level} \qquad (1)$$

which may be important as basic data in determining design earthquake ground motions of underground lifeline facilities. More large ground motion data is required to have accurate relations of equation (1) which can be applicable for large ground strains.

EFFECTS OF SPACIAL VARIATIONS OF GROUND MOTION ON STRUCTURAL RESPONSE IN TERMS OF MULTI-SUPPORT RESPONSE SPECTRUM

In order to investigate effects of differential motions between points of the ground on response characteristics of extended structures, multi-support earthquake response spectrum may be defined. As a most simple case, when a rigid mass m supported by two springs with stiffnesses k_A and k_B is excited by seismic forces $\ddot{u}_{gA}(t)$ and as shown in figure 13, the equation of motion may be written as:

$$m\ddot{u}_t + c\dot{u}_t + (k_A + k_B)\, u_t - k_A\, u_{gA} - k_B\, u_{gB} = 0 \tag{2}$$

in which $\ddot{u}_t$, $\dot{u}_t$, and u_t represent absolute acceleration, velocity, and displacement, respectively, of the mass, and c represents a viscous damping coefficient. According to the general dynamic response theory of multi-support structures [11], the absolute displacement can be conveniently decomposed into a quasi-static displacement, u_s, and a dynamic displacement, u, i.e.,

$$u_t = u_s + u \tag{3}$$

From the definition of a quasi-static displacement, u_s can be obtained as

$$u_s = \frac{1}{k_A + k_B}\,(k_A u_{gA} + k_B u_{gB}) \tag{4}$$

and substituting equations (3) and (4) into equation (2), one obtains

$$m\ddot{u} + c\dot{u} + (k_A + k_B)u = -\frac{m}{k_A + k_B}\,(k_A \ddot{u}_{gA} + k_B \ddot{u}_{gB}) \tag{5}$$

When the mass is excited by either $\ddot{u}_{gA}$ or $\ddot{u}_{gB}$ at both supports, it is easy to show the equation of motion given by equation (5) can be written as:

$$\begin{aligned} m\ddot{u} + c\dot{u} + (k_A + k_B)\, u &= -m\ddot{u}_{gA} \\ m\ddot{u} + c\dot{u} + (k_A + k_B)\, u &= -m\ddot{u}_{gB} \end{aligned} \tag{6}$$

Introducing a coefficient γ as:

$$\gamma = \frac{k_B}{k_A} \tag{7}$$

and $\omega_0 = \sqrt{(k_A + k_\gamma)/m}$, equations (5) and (6) can be written in the form

$$\ddot{u} + 2h\omega_0 u + \omega_0^2 u = -\ddot{u}_g \tag{8}$$

where

$$u_g = \begin{cases} \dfrac{\ddot{u}_{gA} = \gamma \ddot{u}_{gB}}{1 + \gamma} & \text{..... multi excitation by } \ddot{u}_{gA} \text{ and } \ddot{u}_{gB} \\ \ddot{u}_{gA} & \text{..... excitation by } \ddot{u}_{gA} \\ \ddot{u}_{gB} & \text{..... excitation by } \ddot{u}_{gB} \end{cases}$$

Solving equation (8), one can define absolute acceleration response spectra S^A, S^B, and S^{AB} as

$$S^A = | \ddot{u} + \ddot{u}_{gA} | \max$$

$$S^B = | \ddot{u} + \ddot{u}_{gB} | \max \tag{9}$$

$$S^{AB} = \left| \ddot{u} = \frac{\ddot{u}_{gA} + \gamma \ddot{u}_{gB}}{1 + \gamma} \right| \max$$

Then the spectral ratio between multi-support excitation and rigid support excitation may be defined as

$$\eta_A = \frac{S^{AB}}{S^A}$$

$$\eta_B = \frac{S^{AB}}{S^B} \tag{10}$$

The base-shear at supports A and B can be obtained from equation (2) as

$$F_A = k_A(u_t - u_{gA}) = k_A \left\{ u - \frac{\gamma(u_{gA} - u_{gB})}{1 + \gamma} \right\}$$

$$F_B = k_B(u_t - u_{gB}) = k_B \left\{ u - \frac{\gamma(u_{gA} - u_{gB})}{1 + \gamma} \right\} \tag{11}$$

When the mass is excited by either u_{gA} or u_{gB} at both supports, the base shear F_A and F_B can be obtained from equation (11) as

$$F_A = k_A u$$

$$F_B = k_B u \tag{12}$$

Defining the maximum base shear of F_A and F_B given by equation (11) as F_A^{AB} and F_B^{AB}, respectively, F_A and F_B given by equation (12) when the mass is excited is by $\ddot{u}_{gA}$ as F_A^A and F_B^A, respectively, and F_A and F_B by equation (12) when the mass is excited by $\ddot{u}_{gB}$ as F_B^B and F_B^B, respectively, the base shear ratio between multi-support excitation and rigid support excitation may be defined as

$$\xi_A^A = \frac{F_A^{AB}}{F_A^A}, \qquad \xi_B^A = \frac{F_B^{AB}}{F_B^A}$$

$$\xi_A^B = \frac{F_A^{AB}}{F_A^B}, \qquad \xi_B^B = \frac{F_B^{AB}}{F_B^B} \tag{13}$$

In an attempt to investigate effects of horizontal gradients in ground motions according to equations (9), (10) and (13), selected were six pairs of free-field accelerations records triggered

simulataneously at the two points 100 m apart in distance at PWRI as shown in table 4. In the computation, the critical damping ratio, h, in equation (8) and the coefficient γ in equation (7) were assumed as 0.05 and 1.0, respectively.

Figures 12, 13, and 14 show the absolute acceleration response spectra, response spectrum ratios and base shear ratios, respectively. It should be noted here that the geological conditions at A-field of PWRI is almost uniform [4]. Therefore, the points selected for the computation have essentially the same ground conditions. From these analyses, the following can be pointed out:

1. The response spectrum ratios S^{AB}/S^{A} and S^{AB}/S^{B} are generally less than unity although they depend on the ground motions and natural period T. It implies that the acceleration response of mass is significantly reduced in amplitude in the multi-support excitations as compared with the accelerations response of mass in rigid support excitations.
2. The base shear ratio becomes a significantly large value at short natural periods, T, and decreases to almost unity with an increasing of the natural period, T. The reason for the large value of the base shear ratio at short natural periods T, may be considered that the dynamic displacement u, which depends on the natural period T, is generally small at short natural periods, T while the maximum value of the quasi-static displacements, u_s is independent on T for a specific pair of ground motions. Thus, at short natural periods the base shear associated with quasi-static displacement, u_s is predominantly larger than that associated with the dynamic displacement u, and this makes the base shear ratio very large at short natural periods. It should be mentioned that from equation (12) the base shear associated with quasi-static displacment, u_s is zero in the rigid support excitation. The natural period at which the base shear ratio approaches unit is approximately 1 sec for the ground motions considered herein.

WAVE PROPAGATION CHARACTERISTICS

The ground acceleration induced by a specific earthquake may be characterized by a function of space coordinates x, y, and z, as defined in figure 7 and time t in the form of $a = a(x, y, z, t)$. Let $a_m(t) = a(x_m, y_m, z_m, t)$ and $a_n(t) = a(x_n, y_n, z_n, t)$ represent accelerations at point $m(x_m, y_m, z_m)$ and $n(x_n, y_n, z_n)$, respectively. Then the cross spectrum $S_{mn}(f)$ may be obtained from a cross correlation function $R_{mn}(\tau)$ as [9]

$$S_{mn}(f) = \int_{-\infty}^{\infty} R_{mn}(\tau) e^{-i2\pi f\tau} d\tau = C_{mn}(f) - i\, Q_{mn}(f) \tag{14}$$

in which $C_{mn}(f)$ and $Q_{mn}(f)$ represent cospectrum and quadspectrum, respectively [9].

The amplitude and phase of equation (14) can be expressed as

$$\begin{aligned} |\, S_{mn}(f)\,| &= \sqrt{C_{mn}^2(f)+Q^2_{mn}(f)} \\ \theta_{mn}(f) &= \tan^{-1}[Q_{mn}(f)/C_{mn}(f)] \end{aligned} \tag{15}$$

Assuming that certain time delay between $a_m(t)$ and $a_n(t)$ exists, the delay time τ_{mn} may be obtained as

$$\tau_{mn}(f) = \frac{\theta_{mn}(f)}{2\pi f} \tag{16}$$

Then, expressing $L = \sqrt{(x_m - x_n)^2 + (y_m - y_n)^2 + (z_m - z_n)^2}$ as a distance between point m and n, the apparent wave velocity associated with propagation of seismic waves $V_{mn}(f)$ may be expressed as

$$V_{mn}(f) = \frac{L}{\tau_{mn}(f)} = \frac{2\pi f L}{\theta_{mn}(f)} \tag{17}$$

Based on array data obtained at PWRI campus, it was attempted to get apparent wave propagation velocity between two measuring points in vertical and horizontal directions. Selected were the records at A-field triggered by EQ-10, EQ-11, and EQ-12, as shown in table 5.

ANALYSIS OF VERTICAL PROPAGATION

Taking point m and n as A46CO and A2CO (refer to figure 7), respectively, power spectra $S_{mn}(f)$ and $S_{nn}(f)$, cross spectrum $S_{mn}(f)$, phase $\theta_{mn}(f)$ and apparent velocity $V_{mn}(f)$ were determined as shown in figure 15. Figure 16 shows frequency response function (amplitude) $|H| = \sqrt{S_{nn}/S_{mm}}$ between the point m and n [4], which have clear peaks at the frequency of 1.4 Hz, 4.0 Hz, and 9.5 Hz. From comparisons between figures 15 and 16, systematic change of phase depending on peak frequencies of frequency response function can be observed.

For the explanation of phase between two points apart in the vertical direction, a simple analytical model, which assumes vertical propagation of shear waves in a one-dimensional column, was considered. Assuming the ground consists of two layers with perfectly elastic material as shown in figure 17, the equations of motion can be written in the form [12]

$$\rho_n \frac{\partial^2 u_n}{\partial t^2} = \left(\mu_n + \xi_n \frac{\partial}{\partial t}\right) \frac{\partial^2 u_n}{\partial z^2} \qquad (n = 1, 2) \tag{18}$$

in which ρ_n, μ_n, and ξ_n represent mass, shear rigidity and damping coefficient, of n-th layer, respectively, and u_n represents displacement of n-th layer. General solution of equation (18) can be given as

$$\begin{aligned} u_2(z, t) &= a \exp(i\omega t + f_2 z) + A \exp(i\omega t - f_2 z) \\ u_1(z, t) &= B \exp(i\omega t + f_1 z) + C \exp(i\omega t - f_1 z) \end{aligned} \tag{19}$$

where

$$f_n = \frac{\rho_n \omega^2}{\mu_n + i\xi_n\omega} \qquad (n = 1, 2) \tag{20}$$

Substituting boundary conditions at z = 0 and z = H as given by

$$z = 0 \; ; \; (\mu_1+\xi_1)\frac{\partial}{\partial t})\frac{\partial u_1}{\partial z} = 0$$

$$z = H \; ; \; (u_1 + \xi_1\frac{\partial}{\partial t})\frac{\partial u_1}{\partial z} = (u_2 + \xi_2\frac{\partial}{\partial t})\frac{\partial u_2}{\partial z} \tag{21}$$

into equation (19), the unknown constants A, B, and C can be determined, and u_1 and u_2 are obtained as

$$u_1(z, t) = \frac{2}{\Phi_1 + i\Phi_2}\cos(f_1 z)\exp(if_2 H)\, a\exp(i\omega t)$$

$$u_2(z, t) = [\exp(if_2 z) + \frac{\Phi_3 + i\Phi_4}{\Phi_1 + \Phi_2}\exp\{if_2(2H - z)]\, a\exp(i\omega t) \tag{22}$$

where

$$\Phi_1 = \cos P_1 \cosh Q_1+\alpha\{\cos(N_2-N_1)\cos P_1\sinh Q_1+\sin(N_2-N_1)\sin P_1\cosh Q_1\}$$

$$\Phi_2 = \sin P_1 \sinh Q_1+\alpha\{\cos(N_2-N_1)\sin P_1\cosh Q_1-\sin(N_2-N_1)\cos P_1\sinh Q_1\}$$

$$\Phi_3 = \cos P_1 \cosh Q_1-\alpha\{\cos(N_2-N_1)\cos P_1\sinh Q_1+\sin(N_2-N_1)\sin P_1\cosh Q_1\}$$

$$\Phi_4 = \sin P_1 \sinh Q_1-\alpha\{\cos(N_2-N_1)\sin P_1\cosh Q_1-\sin(N_2-N_1)\cos P_1\sinh Q_1\}$$

$$\alpha = P_1V_1M_1/P_2V_2M_2$$

$$M_n = \sqrt[4]{1 + (\frac{\xi np}{\mu_n})^2} \quad , \; N_n = \frac{1}{2}\tan^{-1}(\frac{\xi_n p}{\mu_n})$$

$$P_1 = \frac{pH}{v_1}\frac{\cos N_1}{M_1} \quad , \; Q_1 \frac{pH}{v_1}\frac{\sin N_1}{M_1} \tag{23}$$

Then, the frequency response function between z = H and z = 0 can be written as

$$H = \frac{u_1(0, t)}{u_1(H, t)} = \frac{1}{\cos f_1 H} \tag{24}$$

Assuming that the damping is small for simplicity, i.e., $\xi_1 = 0$, equation (24) gives

$$H = \frac{1}{\cos\frac{pH}{v_1}} \tag{25}$$

Figure 18 shows amplitude and phase predicted by equation (25). Taking L and v_1 as 44 mm (46 - 2 m) and 267 m/sec (averaged shear wave velocity at A-field), respectively, the predicted first and second peak frequency of amplitude is equal to 1.5 Hz and 4.5 Hz, respectively, which is very close

to the observed results presented in figure 16. The phase predicted by equation (18) is also close to the observed results for the frequency from 0 to 6 Hz. It may be concluded from these results that the apparent wave velocity presented in figure 15 can be explained by the propagation of shear waves in the vertical direction.

ANALYSIS OF HORIZONTAL PROPAGATION

Taking point m and n as A50S and A50N respectively, for EQ-10, and as A50W and A50E, respectively, for EQ-11 and EQ-12, power spectra $S_{mm}(f)$ and $S_{nn}(f)$, cross spectrum $S_{mn}(f)$, phase $\theta_{mn}(f)$ and apparent velocity $V_{mn}(f)$ were determined as shown in figure 19. It is noted that the apparent velocity $V_{mn}(f)$ in the horizontal direction takes on a significantly large value for all three earthquakes.

CONCLUDING REMARKS

The dense instrument array at the Sagara area was introduced, which was installed as the first of the four arrays at Suruga Bay-Izu region following the dense instrument array program of the Public Works Research Institute. Observation of the array was initiated on February 24, 1982.

Some results of analyses used to investigate ground strains induced during earthquakes, effects of differential motions on structural response, and wave propagation characteristics were also presented. In order to investigate the effect of local topological and geological conditions, further developments of analytical procedure are expected.

ACKNOWLEDGMENTS

The authors express their sincere thanks and appreciation for cooperation of the many organizations concerned, expecially Chubu Regional Construction Bureau of Ministry of Construction, Shizuoku Prefecture and Sagara Town.

REFERENCES

[1] International Association for Earthquake Engineering: Strong-Motion Earthquake Instrument Arrays, Proc. of the International Workshop on Strong-Motion Earthquake Instrument Arrays, edited by W. D. Iwan, 1978, Honolulu, Hawaii, U.S.A.

[2] Iwan, W. D., "The Deployment of Strong Motion Earthquake Instrument Arrays," Earthquake Engineering and Structural Dynamics, Vol. 7, 1979.

[3] Okubo, T., "Dense Instrument Array Program," Civil Engineering Journal, Vol 22, No. 4, 1980 (in Japanese).

[4] Okubo, T., T. Iwasaki, and K. Kawashima, "Dense Instrument Array Program of the Public Works Research Institute and Preliminary Analyses of Some Records," 13th Joint Meeting, UJNR, Tsukuba, 1981.

[5] Okubo, T., T. Iwasaki, and K. Kawashima, "Dense Instrument Array Program of the Public Works Research Insittute and Preliminary Analysis of the Records," 7th European Conference on Earthquake Engineering, Athens, Greece, 1982.

[6] Okubo, T., T. Iwasaki, and K. Kawashima, "Dense Intrument Array Program in Public Works Research Institute for Observing Strong Earthquake Motion, Some Recent Earthquake Engineering Research and Practice in Japan," The Japanese National Committee on the International Association for Earthquake Engineering, 1980.

[7] Iwasaki, T., "Free-field and Design Motions During Earthquakes," International Conference on Recent Advances in Geotechnical Earthquake Engineering and Soil Dynamics, St. Louis, MO, 1981.

[8] Wang, L. R. L., K. Kawashima, Y. H. Yeh, and K. Aizawa, "Study of Ground Strains from Strong Motion Array Data for Lifeline Application," Technical Note of Public Works Research Institute, Vol. 39, 1981.

[9] Hino, M., "Spectrum Analysis," Asakura Printing, 1976.

[10] Zienkiewicz, O. C., "The Finite Element Method in Engineering Sciences," McGraw-Hill, 1971.

[11] Tseng, W. S. and J. Penzien, "Analytical Investigations of the Seismic Response of Long Multiple Span Highway Bridges, Report No. EERC 73-12, Earthquake Engineering Research Center, University of California, Berkeley, 1973.

[12] Kanai, K., "Relation Between the Nature of Surface Layer and the Amplitude of Earthquake Motions, II," Bulletin of Earthquake Research Institute, University of Tokyo, 1953.

Table 1. Main Specifications of Accelerographs Used for Local Laboratory Array at Sagara Area

	Type	Triaxial, velocity feedback with calibration coil
Accelerometer	Full Scale Range	+ 1G
	Natural Frequency	5 Hz
	Damping Ratio	>30
Trigger System	Sensitive Direction	Vertical
	Acceleration Set Point	0.005G (changeable)
	Operation Cycle	Self-actuating for duration of earthquake, with automatic reset 5 seconds after averaged acceleration in horizontal direction becomes less than 5 gals
Recording System	Type	Digital
	Number of Track	4
	Magnetic Tape	Digital cartridge; 60 in/sec
	Number of Bits	16 bits
	Dynamic Range	$\pm$ 92 dB
	Sampling Rate	200 Samples/sec/channel
	Max. Recording Time	Approximately 40 minutes
	Pre-event Memory	5 seconds for each channel
Time Code Generator	Accuracy of Crystal	$\pm 10^{-7}$
	Auto Adjustment of Time of Crystal	Each 1 hour by NHK time signal
Power Requirement	Voltage	12 VDC
	Battery Charger	Float charger supplied; approved for less than 25 hours after suspension of commercial electricity
Case		Water tight case for proof of twice of atmospheric pressure

Table 2. Earthquake Ground Records Triggered by Local Laboratory Array at PWRI (A-field)

Eq. No.	Date	Epicenter			Epicentral Distance (km)	JMA Magnitude	Depth (km)
		Region	Longitude	Latitude			
EQ-1	1979.10.9	Off Ibaraki	139°50'	36°09'	27	4.1	50
EQ-2	1979.11.25	Off Ibaraki	140°01'	36°41'	122	5.4	90
EQ-3	1979.12.14	SW Ibaraki Pref.	141°20'	36°45'	156	3.9	40
EQ-4	1979.12.16	E Tochigi Pref.	138°57'	35°31'	142	3.0	20
EQ-5	1980.2.1	---	---	---	---	---	--
EQ-6	1980.4.21	Off Ibaraki	141°51'	36°02'	198	4.0	60
EQ-7	1980.5.6	---	---	---	---	---	--
EQ-8	1980.5.11	---	---	---	---	---	--
EQ-9	1980.6.18	Central Chiba Pref.	140°01'	35°38'	55	4.6	80
EQ-10	1980.6.29	Off E of Izu Pen.	139°14'	34°55'	163	6.7	10
EQ-11	1980.9.24	Northern Tokyo Met.	139°42'	36°06'	42	6.0	60
EQ-12	1980.9.25	Central Chiba Pref.	140°12'	35°30'	71	6.1	70
EQ-13	Same with EQ-12						
EQ-14	1981.1.28	SW Ibaraki Pref.	139°48'	36°12'	32	Very Small	60
EQ-15	1981.3.12	SW Ibaraki Pref.	140°06'	36°00'	14	About 4	60
EQ-16	1981.9.2	Off Ibaraki Pref.	141°06'	35°48'	99	6.0	40
EQ-17	19.81.9.3	SW Ibaraki Pref.	139°48'	36°06'	25	Very Small	60
EQ-18	1981.9.14	SW Ibaraki Pref.	140°06'	36°06'	3	4.8	70
EQ-19	1981.10.14	SW Ibaraki Pref.	140°00'	36°06'	7	Very Small	50
EQ-20	1981.11.30	SW Ibaraki Pref.	139°54'	36°06'	16	4.2	60
EQ-21	1982.3.7	Kashima-Nada	140°40'	36°28'		5.6	60

Notes: (1) Records of EQ-1 ~ EQ-12 were obtained by temporal recording system with 37 channel analog data recorder.

(2) Records of EQ-12 ~ EQ-21 were obtained by digital data acquisitions.

(3) EQ-12 is the same earthquake as EQ-13.

Table 3. Upper and Lower Strains at A-Field

Eq. No.	Strains at Lower Level ($x10^{-6}$)						Strains at Upper Level ($x10^{-6}$)						Strain Ratio (Upper/Lower)					
	ϵ_x	ϵ_y	ϵ_z	γ_{xy}	γ_{yz}	γ_{zx}	ϵ_x	ϵ_y	ϵ_z	γ_{xy}	γ_{yz}	γ_{zx}	ϵ_x	ϵ_y	ϵ_z	γ_{xy}	γ_{yz}	γ_{zx}
EQ-1	10.4	4.9	5.2	11.3	10.4	8.7												
EQ-2	7.55	5.9	6.9	10.7	13.6	14.7												
EQ-6	9.55	8.8	7.2	7.55	15.2	13.4												
EQ-9	5.7	5.4	4.2	6.35	11.4	8.0												
EQ-10	12.4	29.6	9.4	11.1	27.7	25.2												
EQ-11	29.9	--	15.9	--	32.1	37.6												
EQ-13	10.8	14.4	12.4	14.6	--	60.1	39.8	15.4	12.4	56.4	54.2	57.7	3.69	1.07	1.0	3.86	--	0.96
EQ-16	9.0	12.2	14.3	13.0	44.1	31.6	49.4	29.0	14.3	76.7	42.0	37.2	5.49	2.38	1.0	5.90	0.95	1.18
EQ-18	5.0	4.3	4.5	6.15	7.5	13.1	13.7	9.1	4.5	12.0	6.0	13.4	2.74	2.12	1.0	1.95	0.8	1.02
EQ-20	5.8	3.2	3.2	4.9	17.2	7.85	16.6	--	3.2	18.4	17.8	17.7	2.34	--	1.0	3.76	10.3	2.25
EQ-21	10.8	10.9	--	16.7	10.4	78.2	47.5	26.5	--	61.8	79.5	66.4	4.40	2.43	---	3.70	0.76	0.85

Table 4. Ground Motions Used for Multi-support Response Spectra

Case	Eq. No.	Date	u_{gA}				u_{gB}			
			Point No.	Component	Max. Acc. [gal]	Max. Disp. [cm]	Point No.	Component	Max. Acc. [gal]	Max. Disp. [cm]
1	EQ-10	1980.6.29	A50N	NS	7.81	0.46	A50S	NS	4.84	0.23
2	EQ-10	1980.6.29	A50N	EW	3.71	0.29	A50S	EW	3.96	0.32
3	EQ-11	1980.9.24	A50E	NS	14.81	0.17	A50W	NS	28.13	0.16
4	EQ-11	1980.9.24	A50E	EW	24.61	0.20	A50W	EW	20.30	0.16
5	EQ-12	1980.9.25	A50E	NS	12.81	0.21	A50W	NS	13.65	0.27
6	EQ-12	1980.925	A50E	EW	14.96	0.23	A50W	EW	14.03	0.27

Note (1) Refer to figure 7 for point number.

(2) u_{gA} and u_{gB} are ground motions defined by equation (2).

Table 5. Ground Motions Used for Wave Propagation Analysis

Case	EQ. NO.	Date	Vertical Propagation				Horizontal Propagation			
			Point-m		Point-n		Point-m		Point-n	
1	EQ-10	1980.6.29	A46CO	EW	A2CO	EW				
2							A50S	NS	A50N	NS
3							A50S	EW	A50N	EW
4	EQ-11	1980.9.29	A46CO	EW	A2CO	EW				
5							A50W	NS	A50E	NS
6							A50W	EW	A50E	EW
7	EQ-12	1980.9.25	A46CO	EW	A2CO	EW				
8							A50W	NS	A50E	NS
9							A50W	EW	A50E	EW

Note: (1) Refer to figure 7 for point number.

(2) Points m and n are defined in equation (14).

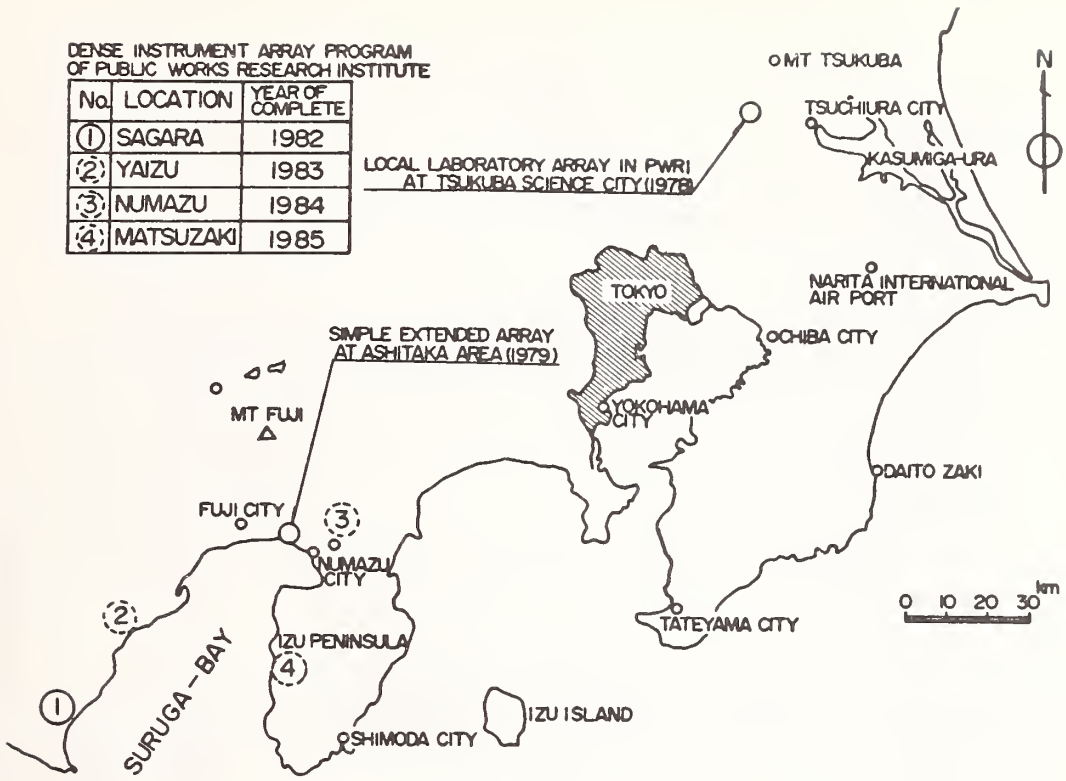

Fig. 1 Locations of Dense Strong-Motion Array by PWRI

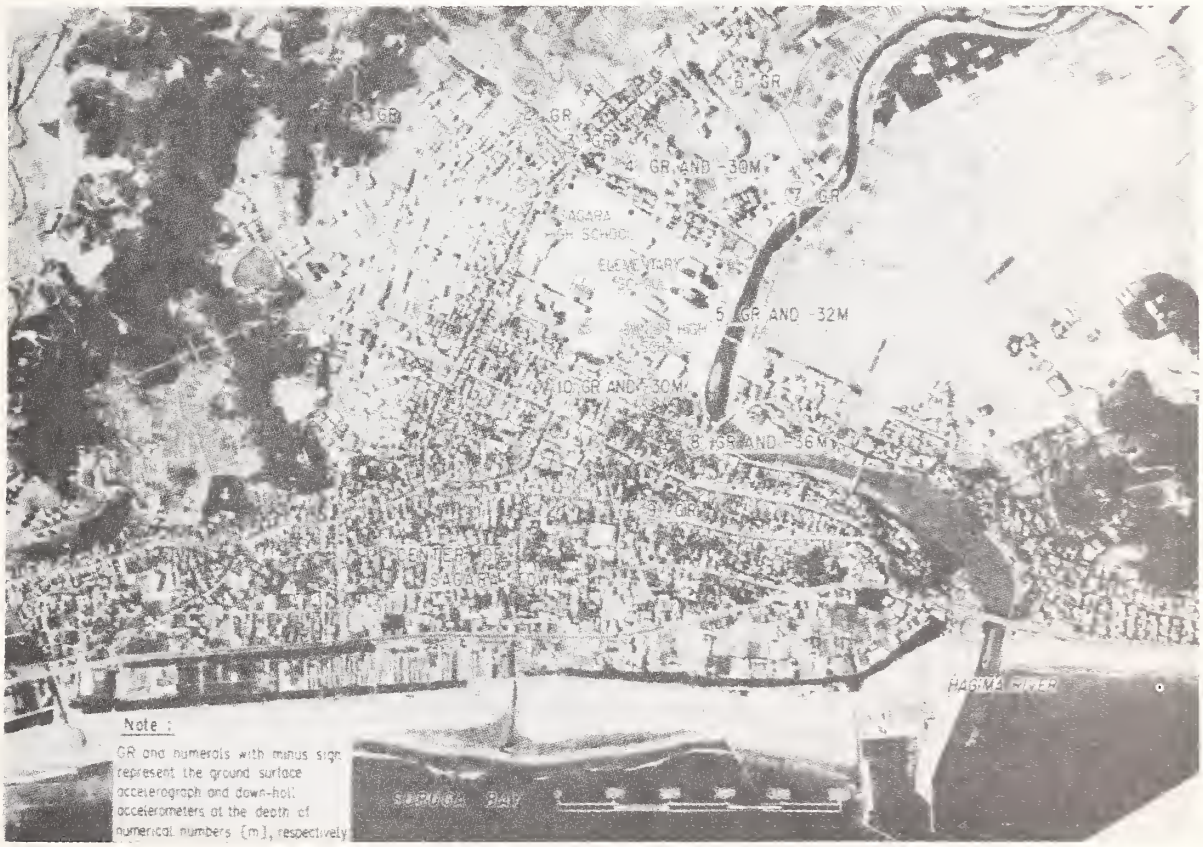

Fig. 2 Accelerograph Stations at Local Laboratory Array at Sagara Area, Shizuoka Prefecture

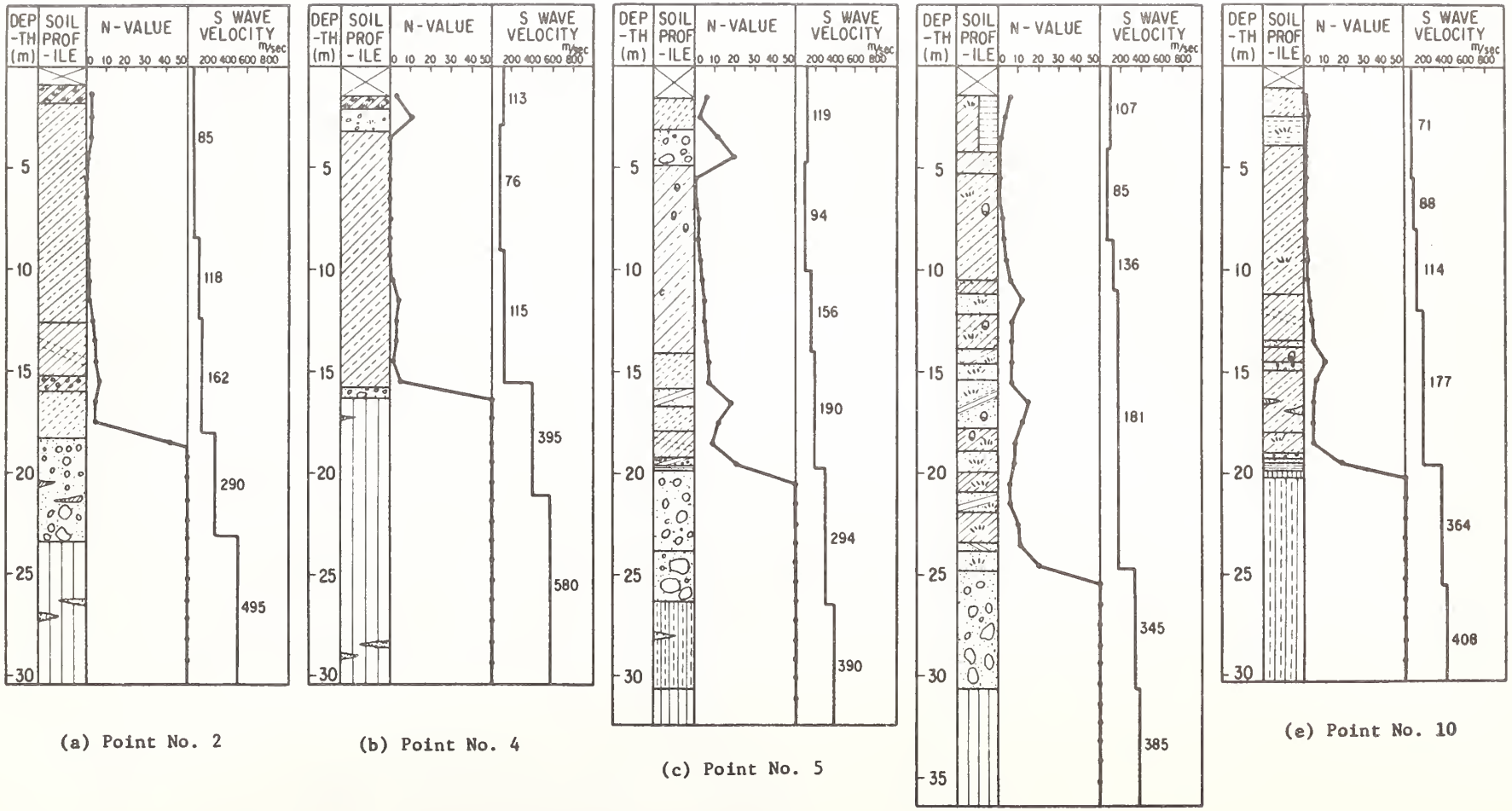

(a) Point No. 2

(b) Point No. 4

(c) Point No. 5

(d) Point No. 8

(e) Point No. 10

Fig. 3 Typical Soil Profile at Sagara Area

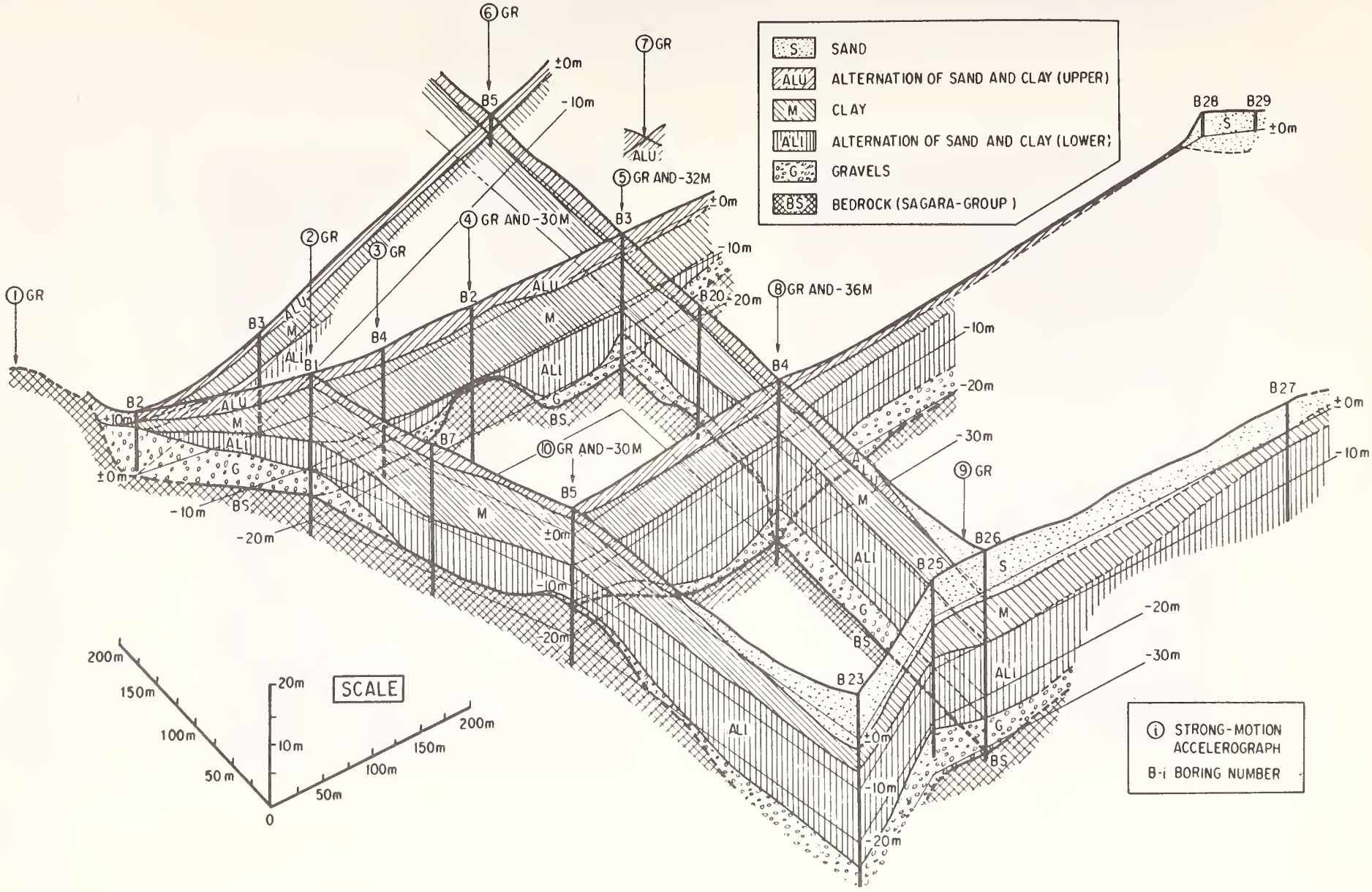

Fig. 4 Ground Conditions at Array Region of Sagara Area

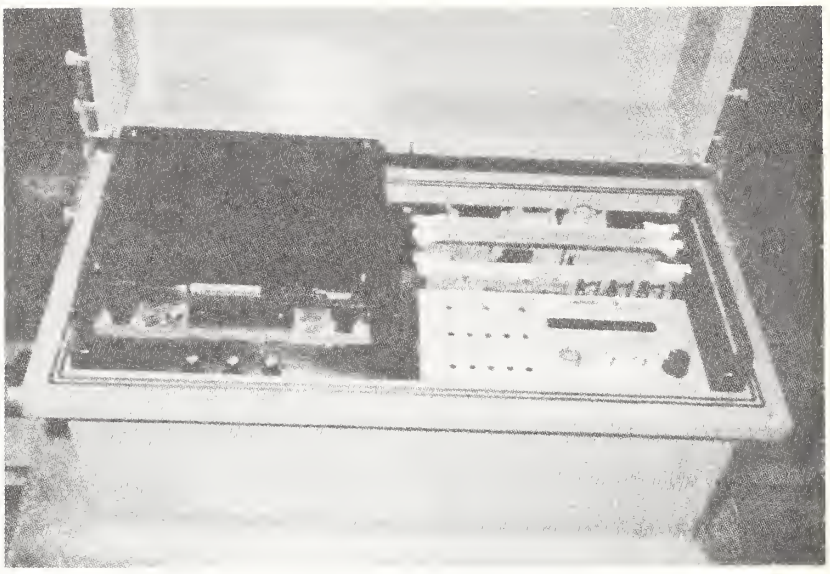

Fig. 5 Strong Motion Accelerograph Used for Local Laboratory Array at Sagara Area

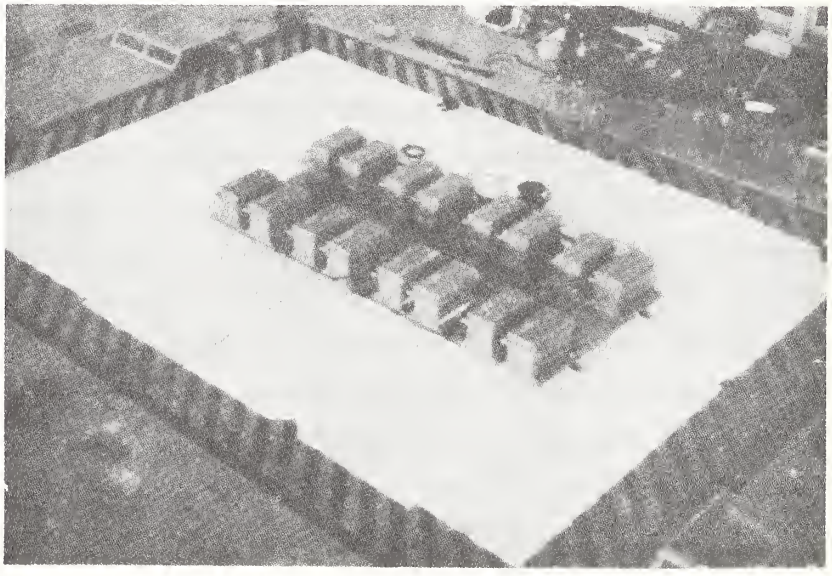

Fig. 6 Shaking Table Test of Strong Motion Accelerographs

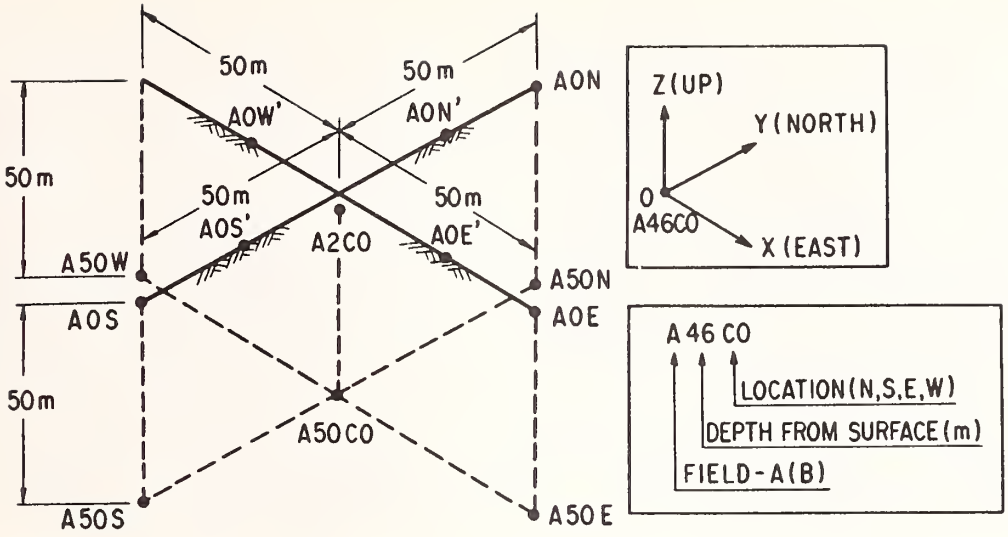

Fig. 7 Notation of Measuring Point of Local Laboratory Array at PWRI (A-Field)

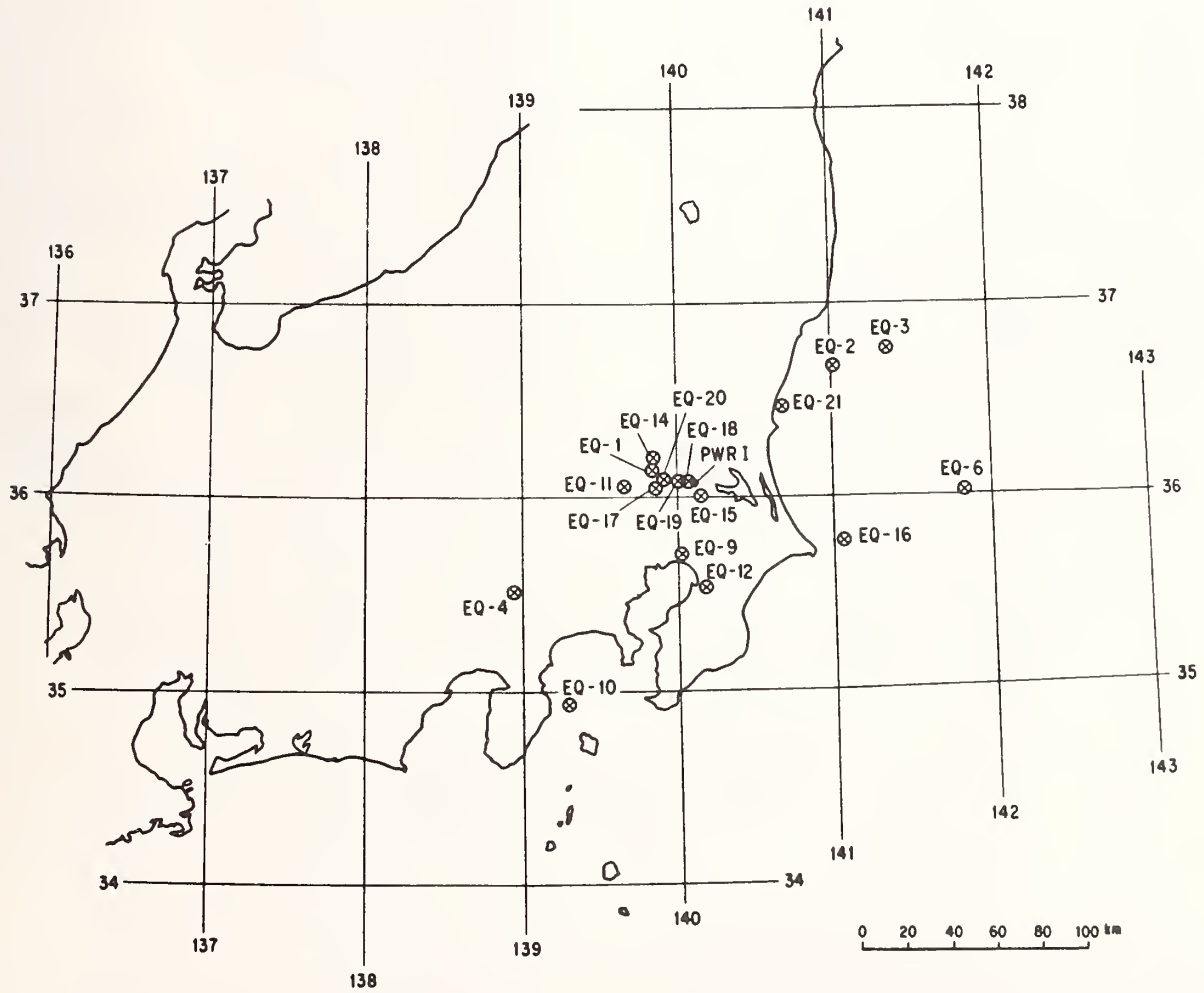

Fig. 8 Epicenters of Earthquake Triggered by Local Laboratory Array at PWRI

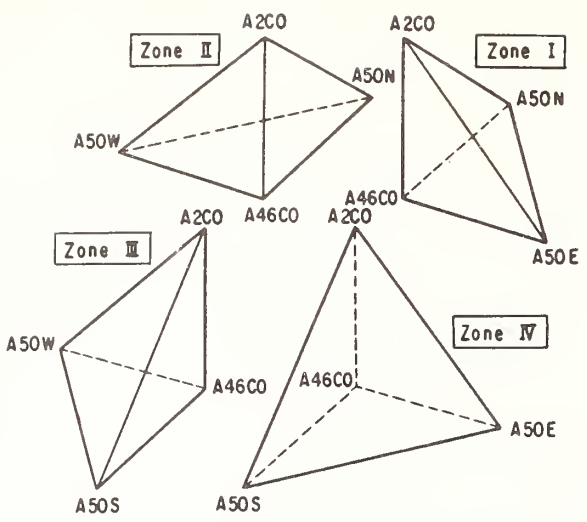

(a) Tetrahedrons for Calculating Lower Level Strains

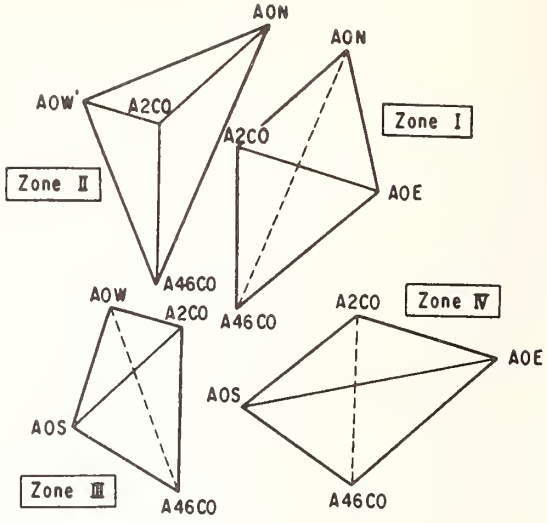

(b) Tetrahedrons for Calculating Upper Level Strains

Fig. 9 Tetrahedrons Formulated to Calculate Ground Strains

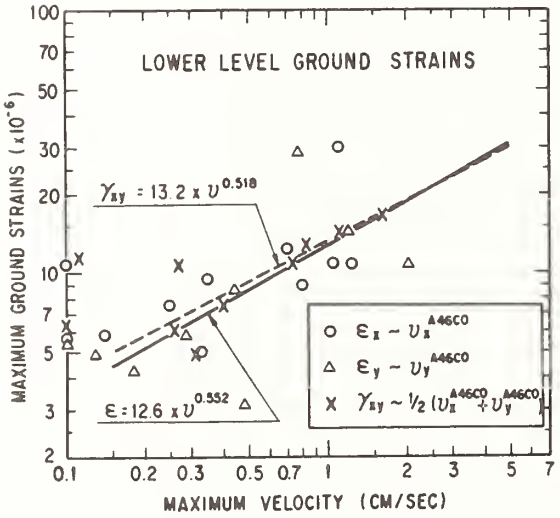

(a) Lower Level Ground Strains

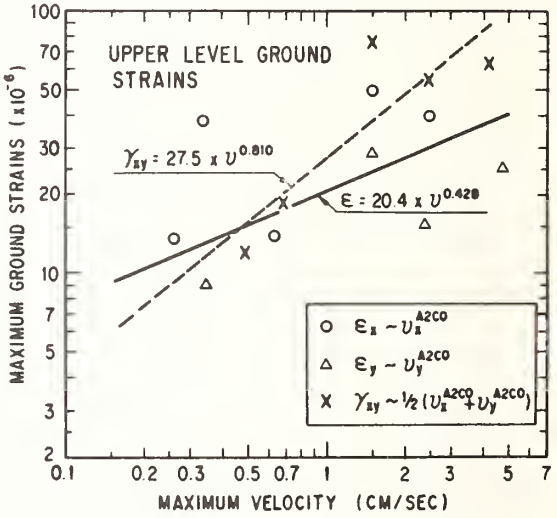

(b) Upper Level Ground Strains

Fig. 10 Relation between Ground Strain and Particle Velocity

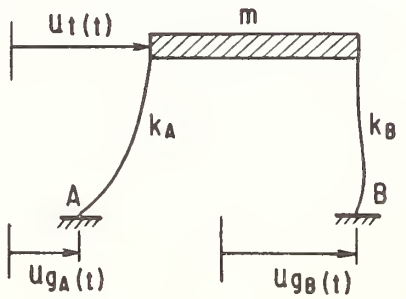

Fig. 11 Multi-supported Excitation of One Degree of Freedom

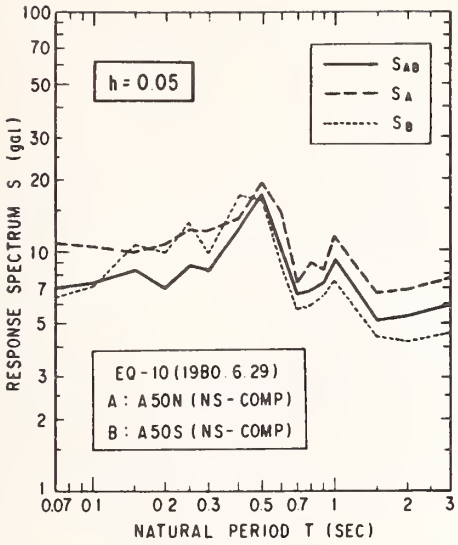

(a) Case-1

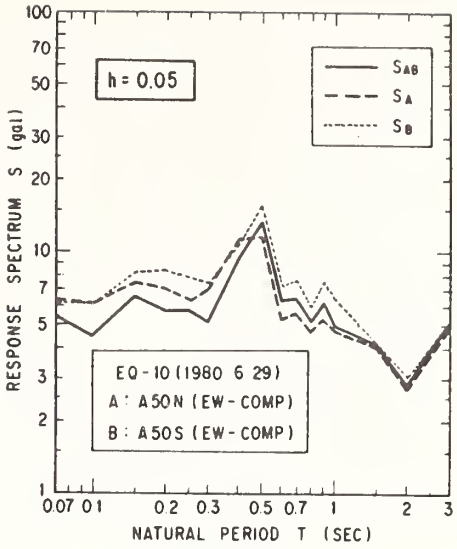

(b) Case-2

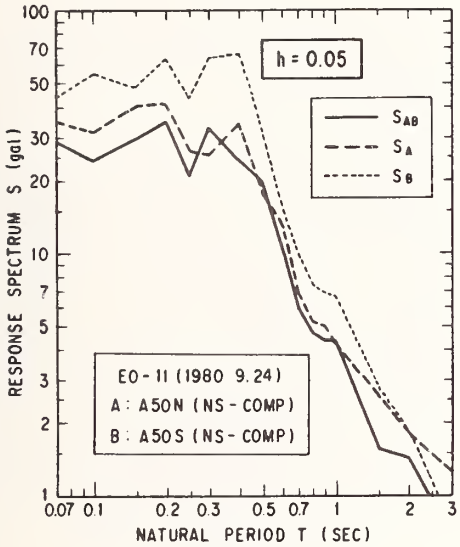

(c) Case-3

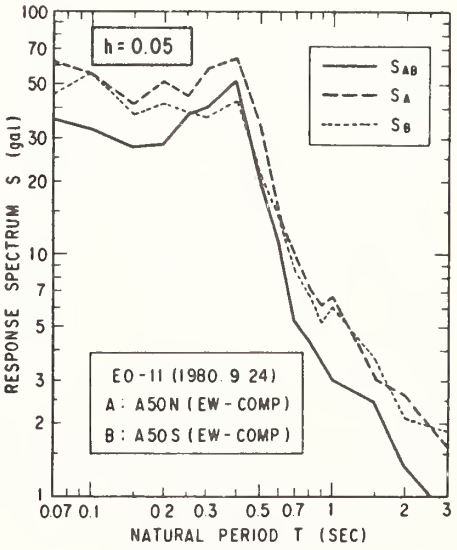

(d) Case-4

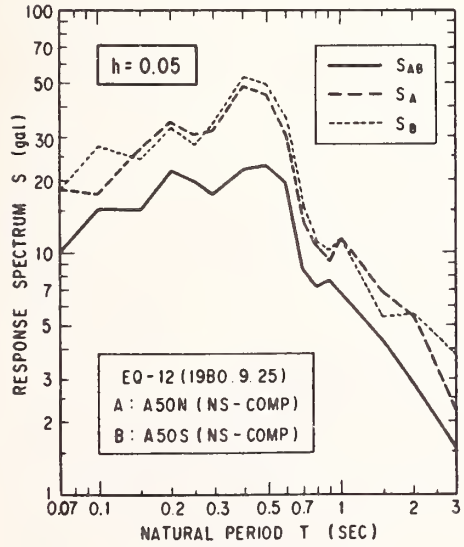

(e) Case-5

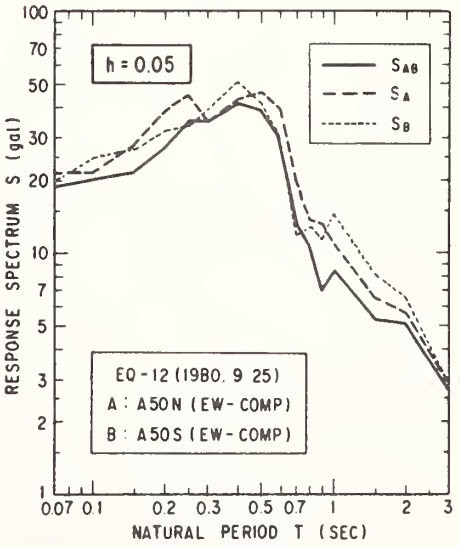

(f) Case-6

Fig. 12 Absolute Acceleration Response Spectra S^{AB}, S^{A} and S^{B}

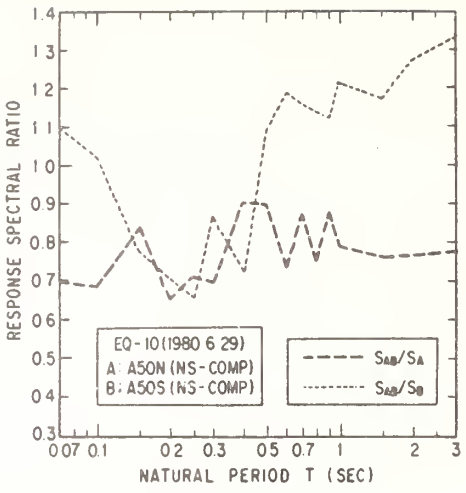

(a) Case-1

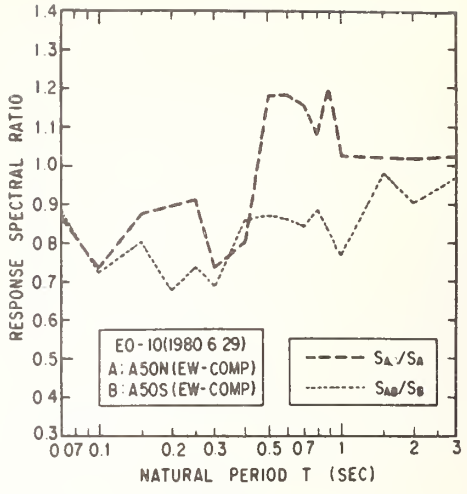

(b) Case-2

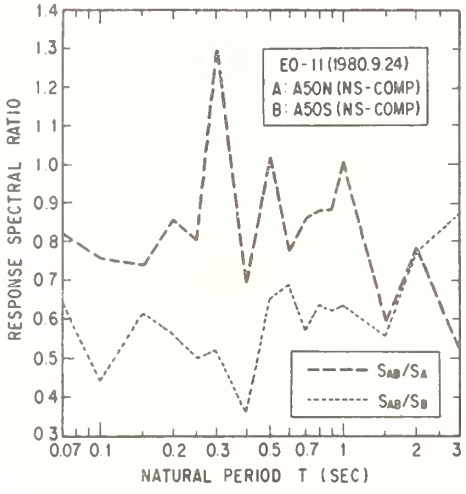

(c) Case-3

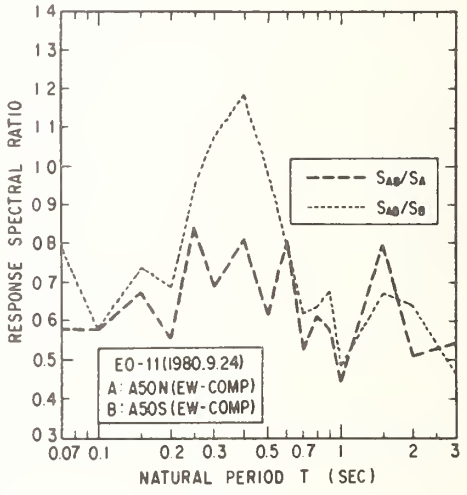

(d) Case-4

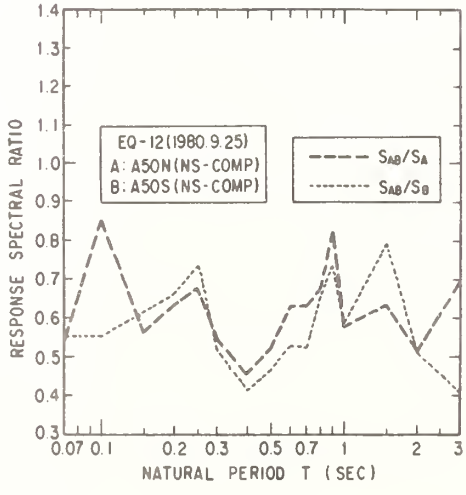

(e) Case-5

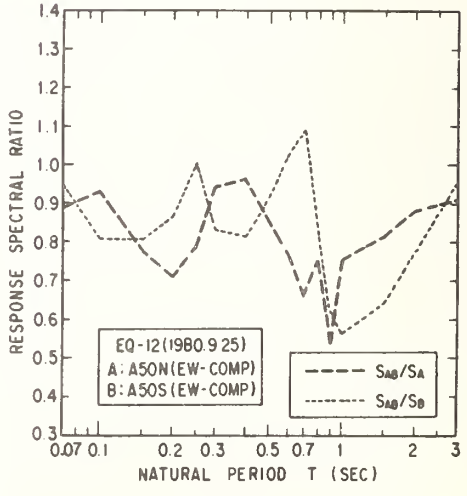

(f) Case-6

Fig. 13 Absolute Acceleration Response Ratio S^{AB}/S^{A} and S^{AB}/S^{B}

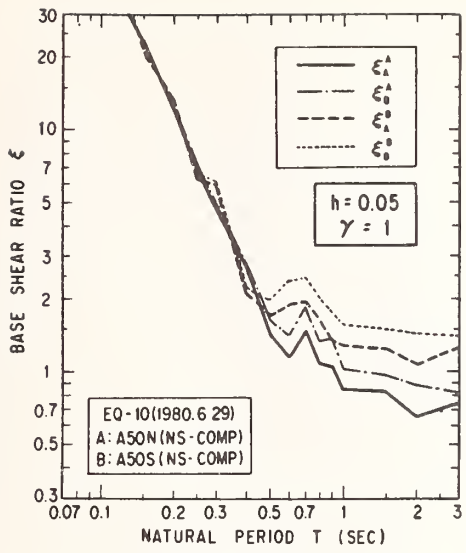

(a) Case-1

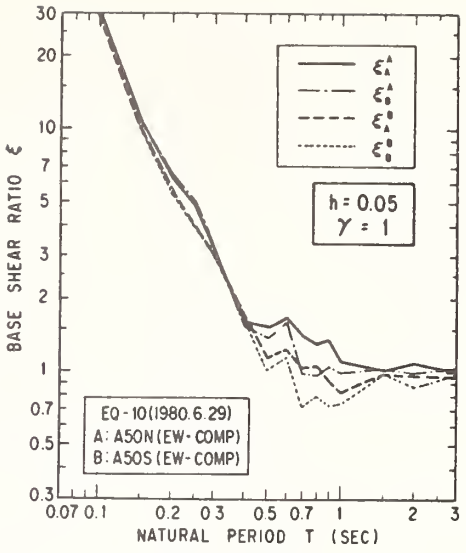

(b) Case-2

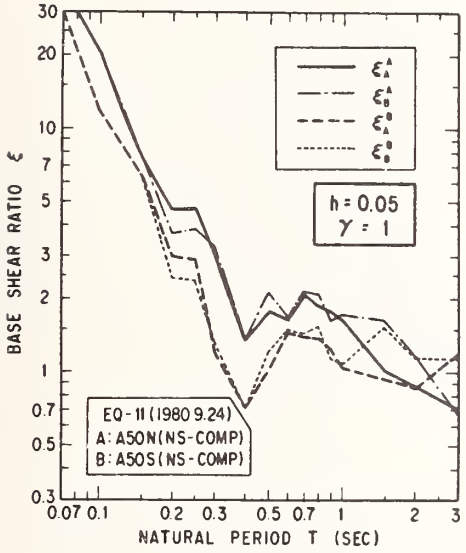

(c) Case-3

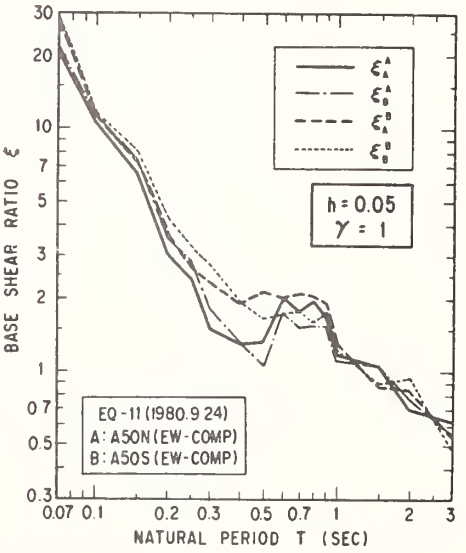

(d) Case-4

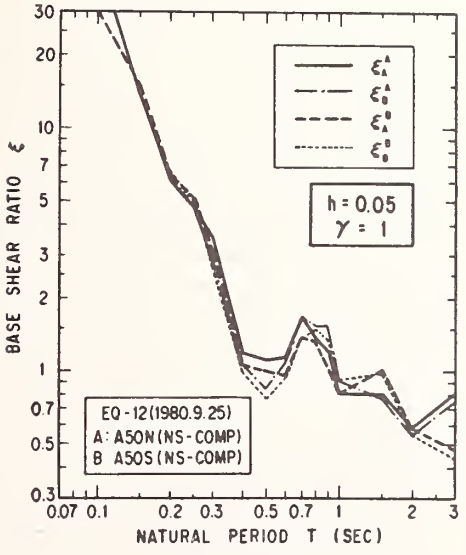

(e) Case-5

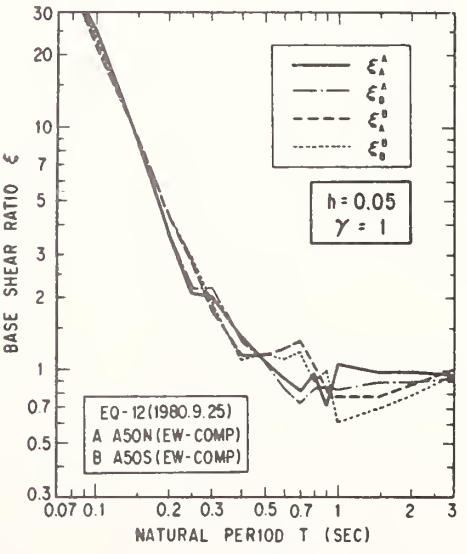

(f) Case-6

Fig. 14 Base Shear Ratio

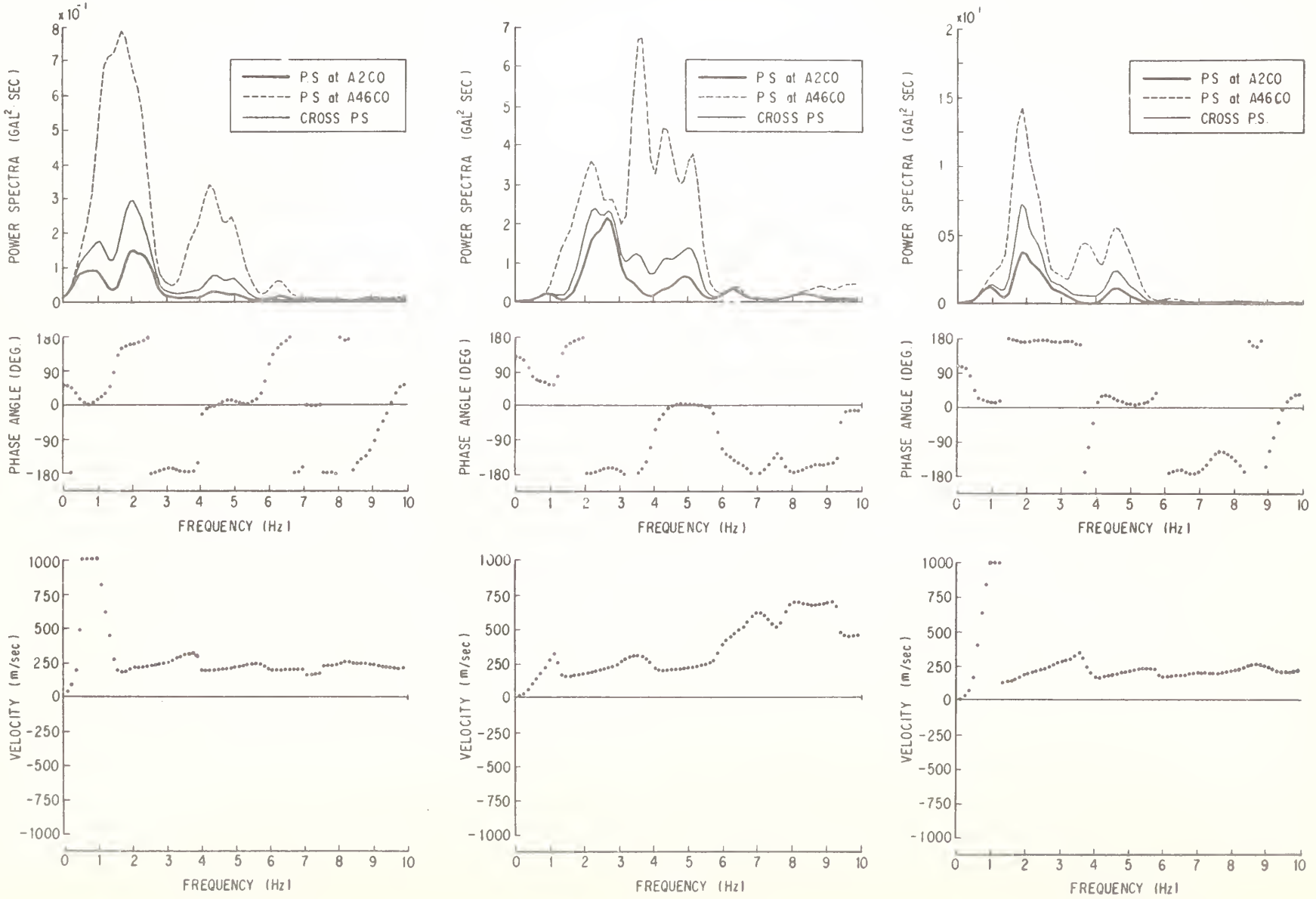

(a) Case-1 (EQ-10)

(b) Case-4 (EQ-11)

(c) Case-7 (EQ-12)

Fig. 15 Power Spectra S_{mm}, S_{nn} and S_{mn}, Phase Angle θ_{mn} and Apparent Velocity V_{mn} in Vertical Direction between A20C0 and A46C0 at A-Field of Local Laboratory Array of PWRI Compus

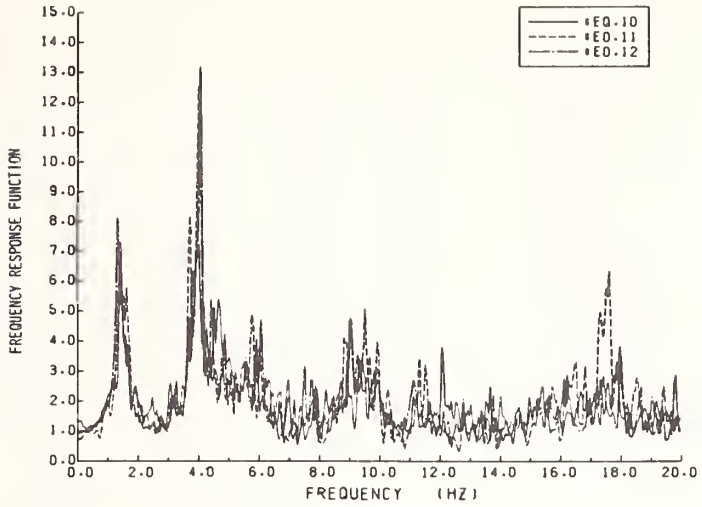

(i) NS-COMPONENT

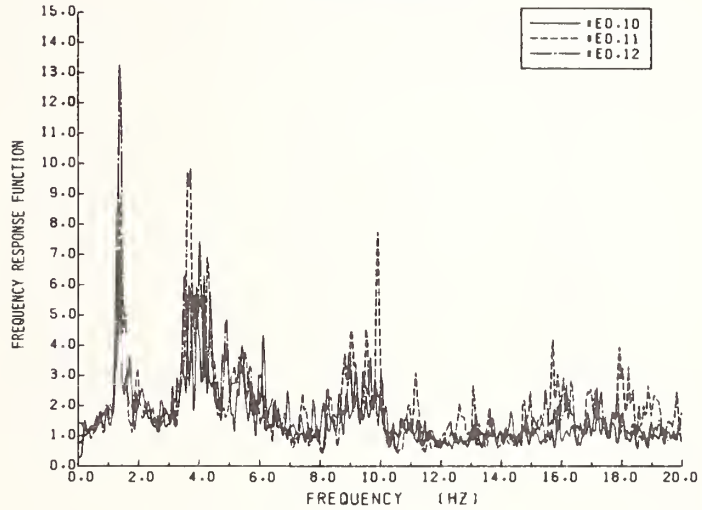

(ii) EW-COMPONENT

Fig. 16 Frequency Response Function (Amplitude) between A2C0 and A46C0 at Local Laboratory Array of PWRI Campus

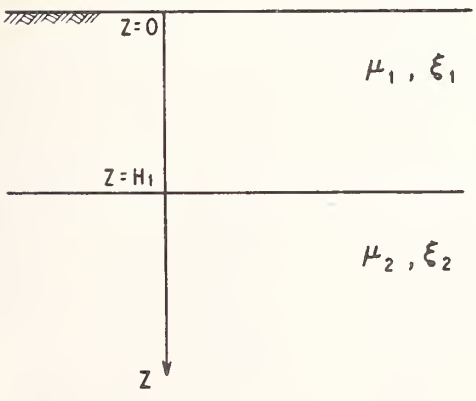

Fig. 17 Analytical Model of Vertical Propagation of Shear Wave

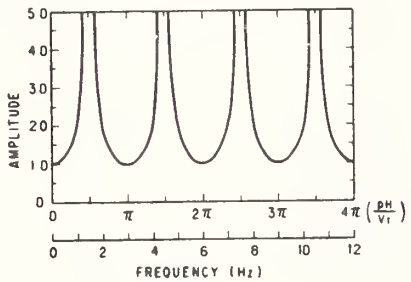

(a) AMPLITUDE

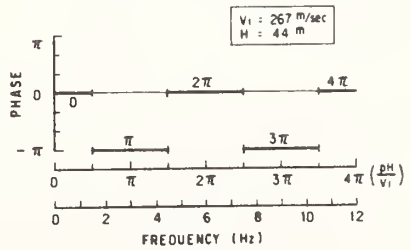

(b) PHASE

Fig. 18 Predicted Amplitude and Phase between A46C0 and A2C0 at A-Field

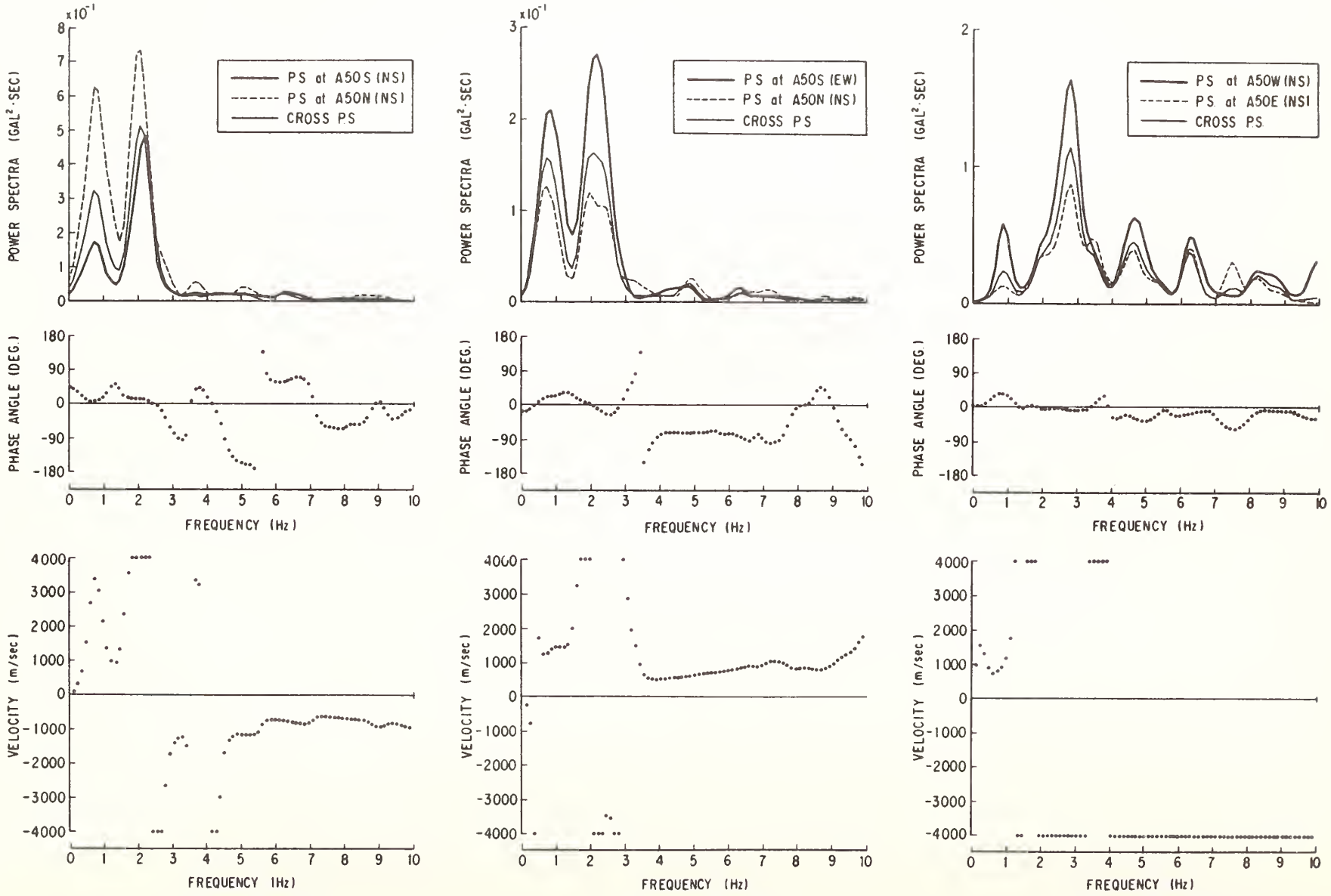

(a) Case-2 (EQ-10)

(b) Case-3 (EQ-10)

(c) Case-5 (EQ-11)

Fig. 19 (1) Power Spectra S_{mm}, S_{nn} and S_{mn}, Phase Angle θ_{mn}, and Apparent Velocity V_{mn} in Horizontal Direction between A50S and A50N (Cases 2 and 3), and, between A50W and A50E (Case 5) at A-Field of Local Laboratory Array at PWRI Campus

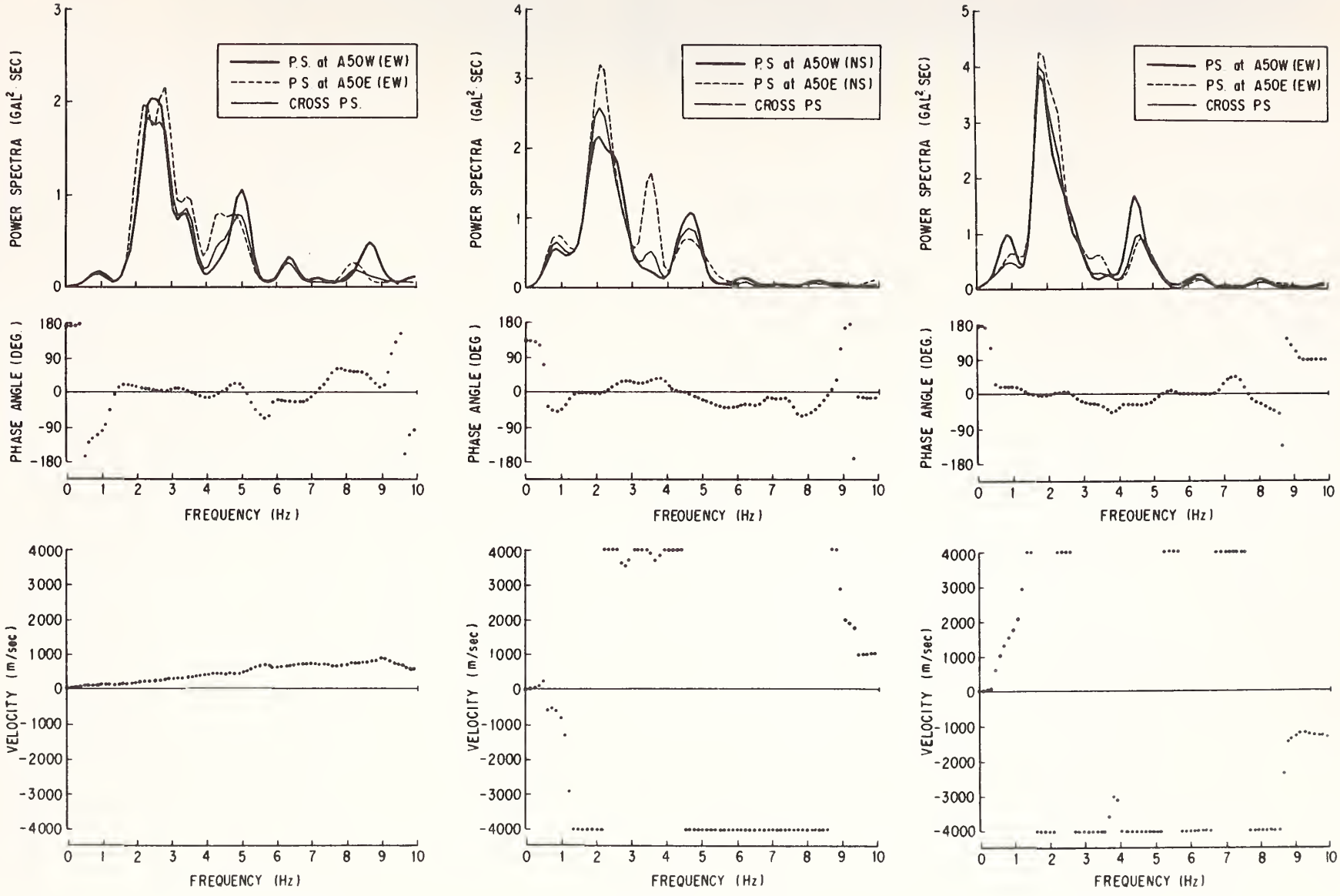

Fig. 19 (2) Power Spectra S_{mm}, S_{nn} and S_{mn}, Phase Angle Θ_{mn}, and Apparent Velocity V_{mn} in Horizontal Direction between A50W and A50E at A-Field of Local Laboratory Array at PWRI Campus

GRAVEL DRAINS AS A COUNTERMEASURE TO LIQUEFACTION OF THE GROUND

Yasushi Sasaki and Eiichi Taniguchi

Public Works Research Institute
Ministry of Construction

ABSTRACT

This paper presents the effectiveness of gravel drains installed to minimize damage of a "half buried type road" caused by liquefaction of the surrounding sand deposit. Large-scale shaking table tests and finite element analyses were used in the study.

INTRODUCTION

Many engineering structures have been damaged by liquefaction of sand deposits during earthquakes. There are several methods that can be used to reduce damage of structures caused by liquefaction such as: (a) to increase the ground resistance by compacting soils; (b) to support structures by piles; and (c) to dissipate pore water pressure developed during shaking by installing drains. On the gravel drain method, which is one of the drainage methods, Seed et al. [1] have studied it analytically, Tokimatsu et al. [2] have performed small size model tests, and Ishihara et al. [3] have conducted some in situ tests. However, it appears to the writers that not enough knowledge has been accumulated on the effectiveness of gravel drains as a countermeasure to liquefaction.

This paper presents the effectiveness of gravel drains installed to minimize damage of a "half buried type road" caused by liquefaction of the surrounding sand deposit. It is a follow up report. The first report was presented to the 13th Joint Meeting of the UJNR in May 1981.

LARGE-SCALE SHAKING TABLE TESTS

TEST PROCEDURE

The same shaking table (12 m x 12 m) which was used in the tests of 1980, was used in the tests of 1981. The shaking table belongs to the National Research Center for Disaster Prevention of Science and Technology Agency in Japan.

A steel box of 12 m in length, 3.5 m in height and 2 m in width was installed on the shaking table and a model ground of 3 m in height was constructed in the box.

The same sand for model ground, same gravel for gravel drains,and same half buried type road model used in the tests of 1980 were used again in this study. Table 1 shows the physical properties of the sand and gravel.

Figure 1 shows the models used in the tests. Models 1 through 6 were used in the shaking tests of 1980 and models 7 through 11 were used in the shaking tests of 1981.

Sand was compacted at lifts of 30 cm for the models of 1981, while it was compacted at lifts of 50 cm for the models constructed in 1980. The sand was compacted in an air-dried condition followed by infiltration of water from the bottom of the box to saturate the sand deposit.

In the tests of 1981, sampling was performed by using a sand sampler shown in figure 2 to determine the degree of saturation. Shear wave velocity was also measured to obtain the shear modulus of sand. Table 2 shows the characteristics of the model ground for all the models tests.

The gravel drains are composed of a layer of no. 5 gravel, 20 cm in width, and a filter of no. 7 gravel, 10 cm in width. The drains are positioned on both sides of the half buried type road model.

The model grounds were shaked in a longitudinal direction by sinusoidal loading. Resonant tests were performed at an acceleration of 20 gal, and then liquefaction tests were carried out at 150 gal in acceleration, 2 Hz in frequency and 30 sec in duration (conditions for 1980 tests are 200 gal in acceleration, 5 Hz in frequency and a duration of 60 sec). Acceleration and pore water pressure were measured by 17 accelerometers and 40 pore water pressure transducers installed in the model ground and vertical displacement of the half buried type road model was also measured.

TEST RESULTS

Figure 3 shows an example of the acceleration records measured in model 11 during excitation. The figure shows that the acceleration began to decrease at 2 sec after excitation. The acceleration in the shallower part of the ground at 2 seconds or longer after excitation became smaller, as shown in figures 4(b), (c), and (e) for models 8, 9, and 11. However, this observation was found to be affected by pore water pressure developed in the model ground. In models 7 and 10, such a tendency was not as clearly identified as was seen in models 8, 9 and 11.

Figure 5 illustrates the change of pore water pressure with time measured at a depth of 1.5 m. In the region away from the gravel drains and the half buried type road model, the pore water pressure started increasing at the beginning of the excitation and became constant at 4 to 6 seconds after the excitation. This constant value was equal to 80 - 90 percent of the initial effective overburden pressure indicating that the model ground was almost fully liquefied.

In the region near the gravel drain, the pore water pressure began to increase at the beginning of the excitation but it began to decrease at 5 to 6 sec after the excitation in model 11 due to the dissipation of pore water pressure by gravel drains.

The pore water pressure in the gravel drains was noticed to increase to about 30 percent of the initial effective overburden pressure.

If sand deposit surrounding the half buried type road mode l was liquefied due to the development of large pore water pressure, large uplift pressure would act on the half buried structure, to push the structure up. On the other hand, if gravel drains were installed under and near the half buried type road model to reduce the buildup of pore water pressure, the uplift pressure would be decreased.

Figure 6 shows the maximum values of pore water pressure directly under the half buried type road model and at points away from it. The maximum values shown in this figure are the weighted mean values of the maximum pore water pressures measured at the same depth. In models 10 and 11, wall type gravel drains were installed under the half buried type road model. In these two cases, the mean value of the pore water pressure in the gravel drain and in the sand deposit, which was slightly higher, was taken as the representative value.

Figure 6 indicates that the maximum pore water pressures in the sand deposit away from the half buried type road model increased to 75 percent to 90 percent of the initial effective overburden pressure, and that the maximum pore water pressures directly under the half buried type road model with gravel drains were smaller. The initial effective overburden pressure under the half buried type road model was smaller than that away from the half buried type road model because the unit weight of the half buried type road model is less than that of the surrounding sand deposit. The ratio of the pore water pressure to the initial effective overburden pressure was 40 to 75 percent at a depth of 10 cm from the bottom of the gravel layer under the half buried type road model.

Figure 7 shows the upward displacement of the half buried type road model during excitation. Figure 8 shows the relationship between the final upward displacement of the half buried type road model and the location of gravel drains. The figure indicates that the upward displacement of the half buried type road model without any countermeasure to liquefaction was over 24 cm. The magnitude of displacement was reduced to 3 to 7 cm by installing gravel drains around the structure.

FINITE ELEMENT ANALYSIS

MODELS USED IN ANALYSIS

The analysis took into account the buildup of pore water pressure in model grounds, and the dissipation of pore water pressure through gravel drains and through the surface of the model ground.

A computer program "SADAP-II", which modified from a two-dimensional finite element computer program "SADAP" [5] developed in Soil Dynamics Division of PWRI, was used in this analysis. The modification includes the addition of functions to analyze pore water pressure buildup and dissipation.

The fundamental equation of the pore water pressure buildup and dissipation is expressed by

$$\frac{\partial}{\partial x}\left(\frac{k_x}{\rho_w g}\frac{\partial u}{\partial x}\right) + \frac{\partial}{\partial y}\left(\frac{k_y}{\rho_w g}\frac{\partial u}{\partial y}\right) = m_v\left(\frac{\partial u}{\partial t} - \frac{\partial u_g}{\partial t}\right) \tag{1}$$

where u : pore water pressure in the ground

p_w : desity of pore water

g : acceleration of gravity

k_x : coefficient of permeability in x direction

k_y : coefficient of permeability in y direction

m_v : coefficient of volumetric compressibility

u_g : pore water pressure generated in the ground by cyclic shear stress

It is assumed that flow of the pore water is governed by Darcy's law.

There are several methods available in predicting pore water pressure, u_g, developed in the ground: (a) a method which traces the effective stress path during liquefaction; (b) a method which expresses the volume change as a function of shear strain or shear stress using stress or strain history; and (c) an approach using plastic theory. In this analysis, Ishihara and Tohata's [7] model was used to predict the pore water pressure, u_g. Their model is based on the effective stress path and is referred to as the Ishihara model in this paper.

In the Ishihara model, the stress path for the virgin loading can be assumed to be a parabola governed by

$$\sigma_v' = m - \frac{B_\rho'}{m}\tau^2 \tag{2}$$

where

σ_v' : effective vertical stress

B_ρ' : soil constant representing the characteristics of the pore water pressure buildup

m : parameter for locating a current parabolic stress path at each time step of computation

The increase of pore water pressure occurs during unloading and reloading and its result in the decrease of the effective stress is given by

$$\Delta\sigma_v' = -B_u'\left(\frac{\tau}{\sigma_{v0}'} - \frac{\tau_m}{\sigma_{v0}'}\right)\left(\frac{\sigma_v'}{\sigma_{v0}'} - \kappa\right)\Delta\tau \quad \text{for } \sigma_v' \geq \kappa\sigma_{v0}'$$

$$\Delta\sigma_v' = 0 \quad \text{for } \sigma_v' < \kappa\sigma_{v0}' \tag{3}$$

where

τ_m : maximum shear stress applied to the soil in the most recent cycle

B_u' : soil constant representing the pore water pressure buildup during unloading and reloading

σ'_{vo} : initial effective vertical stress

κ : parameter representing the point that the pore water pressure ceases to build up when the vertical effective stress decreases to a certain value

After the stress path crosses the phase transformation line, the stress path during the increase in shear stress is assumed to trace a hyperbolic curve given by

$$\left(\frac{\sigma'_v}{a}\right)^2 - \left(\frac{\tau}{a \tan\phi_1}\right)^2 = 1 \qquad (4)$$

where

ϕ_i : the angle of shear resistance in the low confining pressure

a : parameter for locating a current hyperbola

In unloading, the stress path is assumed to follow a straight line which is tangent to the hyperbolic curve.

The computer program, SADAP-II, also employs the Hardin-Drnevich model to express the nonlinearity of the stress-strain relationship of soil. The equation of motion is solved by direct integral method.

The pore water pressure in the ground is determined by calculating the pore water pressure, u_g, developed during a time increment, from shear stress, τ , in the same time increment and equations (2) to (4), and also by calculating the dissipation of pore water pressure from equation (1).

Soil constants used in the equations were determined by cyclic triaxial and torsional tests, as given in tables 3 and 4.

In another paper [8], the authors compared the pore water pressure buildup calculated by the Ishihara model and Seed model. The results indicated that the pore water pressure calculated by Ishihara model agreed better with the experimental results than by Seed model.

RESULTS OF ANALYSIS

Figure 9 shows a finite element model used to analyze model 7. Figure 10 compares the calculated accelerations with the experimental values at a depth of 1.5 m. Figure 11 shows the amplification of acceleration by calculation and experiment, and figure 12 shows an example of hystersis loop of the stress-strain relationship.

These figures indicate that the calculated accelerations agree well with the test results and the analysis reasonably duplicates the behavior of model ground during excitation.

Figure 13 compares the pore water pressure buildup by calculation and experiment at a depth of 1.5 m in model 7. The calculated pore water pressure begins to increase immediately after excitation, while the measured pore water pressure started to increase at 5 to 6 sec after excitation.

This is probably due to the fact that this model ground has been shaken twice at an acceleration of 90 gal before the excitation from which the results were shown in this figure. The resistance of the model ground to liquefaction must have been increased due to previous cyclic shearing. Such a phenomenon didn't occur for other models without pre-shaking. In model 10 (figure 14), the measured pore water pressure increased immediately after excitation begins.

Figures 13 and 14 indicate that the behavior of pore water pressure in the ground can be reasonably modeled by the finite element analysis, taking into account the buildup and dissipation of pore water pressure.

As shown in figure 15, the pore water pressure calculated by this analysis qualitatively duplicates well the measured pore water pressure buildup. Nevertheless, the calculated values are smaller than the measured ones. In particular, the calculated pore water pressure near the gravel drains under the half buried type road model is much smaller than the measured value and it certainly needs further investigation.

CONCLUSIONS

This paper described the large-scale shaking table tests and the finite element analyses performed to demonstrate the effectiveness of gravel drains used as a countermeasure to liquefaction of sand deposit. The following conclusions were obtained:

1. Pore water pressure buildup can be reduced near the gravel drains.
2. The influence region of gravel drains was about 50 cm [4] from the center of the gravel drains in models used in this series of tests.
3. The dissipation of pore water pressure after the end of excitation is accelerated by gravel drains.
4. A large uplift pressure would act on the half buried type road model due to the pore water pressure developed in the ground unless any countermeasure to liquefaction is installed.
5. The uplift can be reduced by installing gravel drains under the half buried type road model and the upward displacement of the half buried type road model can be substantially decreased.
6. The finite element model which considers the buildup and dissipation of pore water pressure duplicates very well the liquefaction characteristics of the model ground.
7. The calculated pore water pressures near gravel drains using the finite element model is consistently smaller than the measured values, thus it needs further investigation.

ACKNOWLEDGMENTS

The authors would like to express their appreciation to the staff of the National Research Center of the Ministry of Construction also helped in preparation of the large-scale models used in the tests. Their cooperation is greatly acknowledged.

REFERENCES

[1] Seed, H. B., and J. R. Booker, (1977) "Stabilization of Potentially Liquefiable Sand Deposits Using Gravel Drains," Journal of the Geotechnical Engineering Division, ASCE 103, GT7.

[2] Tokimatsu, K. and Y. Yoshimi, (1980) "Effects of Vertical Drains on the Bearing Capacity of Saturated Sand During Earthquakes," Proceeding of International Conference of Engineering for Protection from Natural Disaster, Bangkok.

[3] Ishihara, K., A. Saito, and H. Arima, (1980) "Application of Crushed Stone Piles as a Solution to Liquefaction Problem of Revetment," Tsuchi To Kiso, Vol. 28, No. 4 (in Japanese).

[4] Sasaki, Y. and E. Taniguchi, (1981) "Investigations of Gravel Drains as a Countermeasure to Liquefaction," 13th Joint Meeting of UJNR.

[5] Koga, Y., S. Tateyama, and Y. Karasawa, (1981) "SADAP-1, A Computer Program for the Static and Dynamic Analyses of Earth Structures Considering Non Linear Stress-strain Relationship of Soils," Memorandum of the Public Works Research Institute No. 1688 (in Japanese).

[6] Ishihara, K. (1981) "Response Analysis of the Ground Considering Liquefaction," Tsuchi To Kiso Vol. 29, No. 11 (in Japanese).

[7] Ishihara, K. and I. Towhata, (1981) "One-Dimensional Soil Response Analyses During Earthquakes Based on Effective Stress Method," Journal of the Faculty of Engineering, the University of Tokyo Ser. (B).

[8] Sasaki, Y., and E. Taniguchi, (1982) "Large Scale Shaking Table Tests on the Effectiveness of Gravel Drains for Liquefiable Sand Deposits," Proceeding of the International Conference on Soil Dynamics and Earthquake Engineering, at Southampton University, England (in print).

Table 1. Properties of Sand and Gravel

	Sand	Gravel		
		No. 5	No. 6	No. 7
Specific Gravity	2.73	2.69	2.52	2.69
Maximum Grain Size (mm)	4.76	39	20	9.5
Mean Grain Size D_{50} (mm)	0.28	22	9.5	3.3
Uniformity Coefficient	2.91	--	--	--
Permeability Coefficient (cm/s)	1.18	6.1	1.31	5.79

Table 2. Properties of Model Ground

Model No.[1]	ρ_d (g/cm^3)	ρ_t (g/cm^3)	e	Dr (%)	k_V (cm/sec)	k_H (cm/sec)	S_r[2] (%)	V_s[3] (m/s)
7	1.47	1.93	0.855	45.9	7.60×10^{-3}	10.87×10^{-3}	92.5	89
8	1.45	1.92	0.874	41.1	11.97×10^{-3}	9.54×10^{-3}	--	95
9	1.45	1.92	0.874	41.1	13.59×10^{-3}	11.88×10^{-3}	92.8	86
10	1.44	1.91	0.884	38.6	9.62×10^{-3}	11.10×10^{-3}	--	91
11	1.44	1.91	0.890	37.1	12.34×10^{-3}	10.30×10^{-3}	--	83
1	1.46	1.92	0.868	42.6	--	--		
2	1.44	1.91	0.888	39.6	15.74×10^{-3}	9.92×10^{-3}		
3	1.45	1.92	0.875	40.9	--	--		
4	1.49	1.94	0.821	54.6	7.9×10^{-3}	--		
5	1.47	1.93	0.850	47.2	--	--		
6	1.48	1.93	0.841	49.5	--	--		

[1] No. 1-6 1980 tests
No. 7-11 1981 tests

[2] S_r is the mean value of measurement by sand sampling.

[3] V_s is the measured value by wooden bloc hitting method.
(performed after resonant test)

Table 3. Constants Used for Simulation of Model Ground

Material / Constants		Sand	Concrete	Gravel	Sponge
Initial Shear Modulus G_o(kgf/cm^2)		2400.	2400.	2400.	2400.
Density ρ_t (t/m)		1.93	2.66	1.90	1.10
Cohesion c (tf/m^2)		0.0	450.0	0.0	0.0
Friction Angle ϕ (deg)		36.6	0.0	45.0	36.6
Earth Pressure Coefficient at Rest K_o		0.5	0.5	0.5	0.5
Poisson's Ratio	Static ν_s	0.3	0.167	0.3	0.3
	Dynamic ν_d	0.49	0.167	0.49	0.49
$G_o=K\sigma_o'^n$	K(tf/m^2)	2400.	1150000.	2400.	2400.
	n	0.5	0.0	0.5	0.0
Parameters for Hardin-Drnevich Model α		0.9	0.0	0.9	0.0
Permerbility Coefficient (cm/sec)	K_v	1.05×10^{-2}	1.0×10^{-7}	11.0	1.05×10^{-1}
	K_H	1.05×10^{-2}	1.0×10^{-7}	11.0	1.05×10^{-1}
Coefficient of Volume Compressibility Mv(cm^2/kg)		0.015	0.015	7.5×10^{-3}	0.15
Linearity		nonlinear	linear	nonlinear	linear

Table 4. Constants Used for Calculation of Pore Water Pressure Buildup

$B\acute{p}$	$B\acute{u}$	$\theta\acute{s}$
0.0058	0.2233	33.0

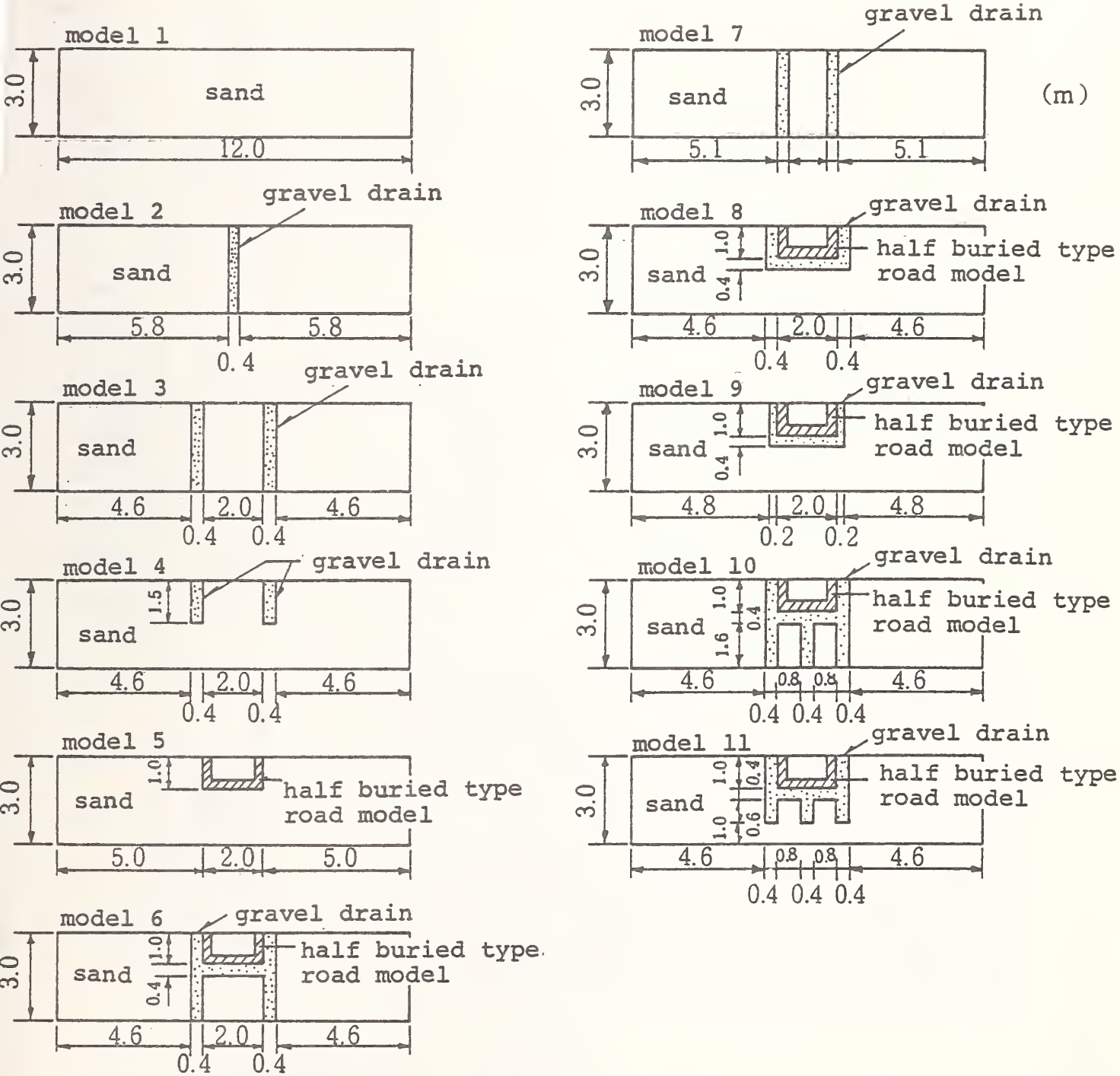

Figure 1 Model ground

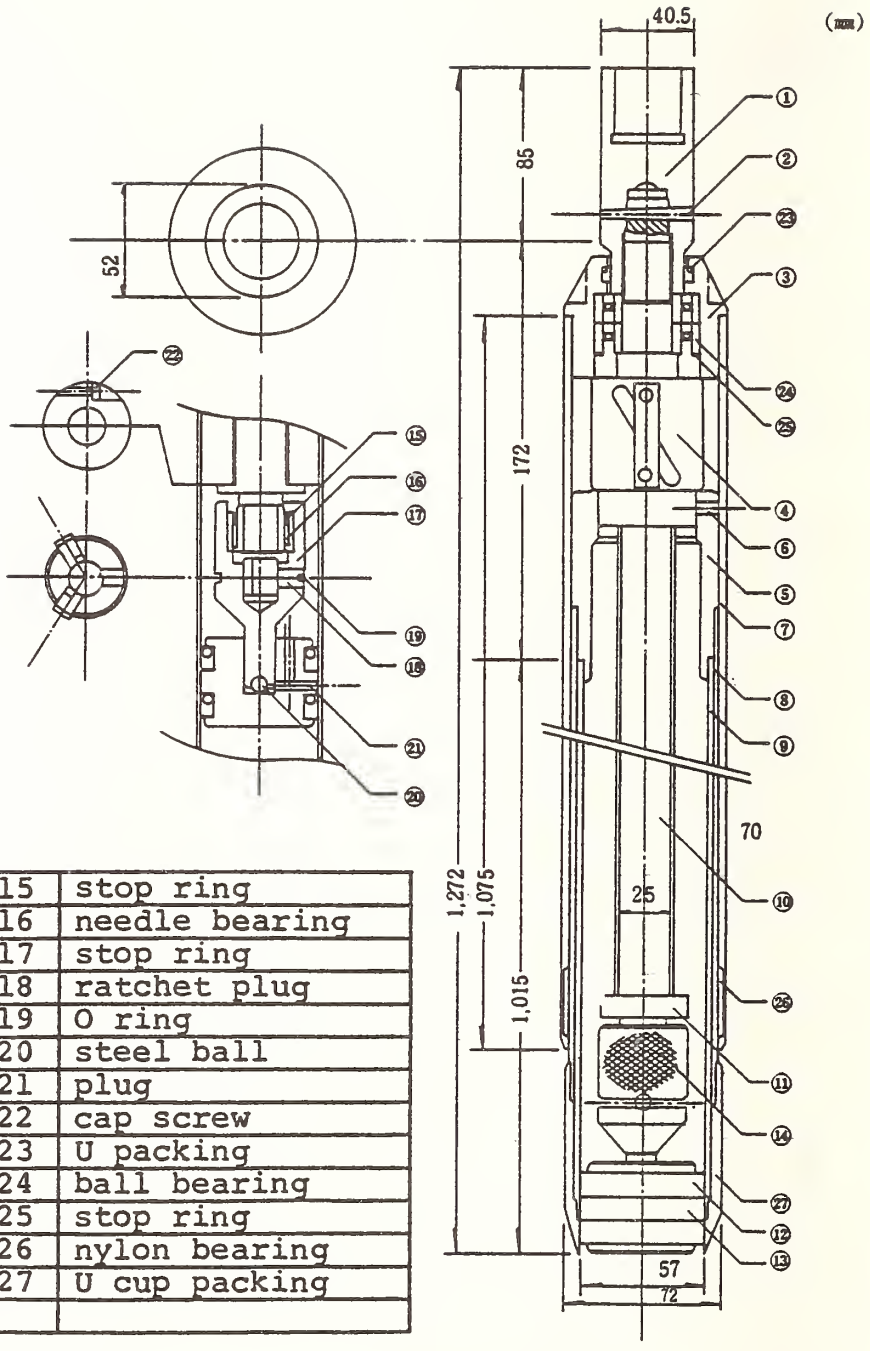

1	lod coupling	15	stop ring
2	taper pin	16	needle bearing
3	head	17	stop ring
4	ball screw nut	18	ratchet plug
5	inner head	19	O ring
6	hollow set	20	steel ball
7	outer tube	21	plug
8	inner tube	22	cap screw
9	lining tube	23	U packing
10	ball screw shaft	24	ball bearing
11	stopper	25	stop ring
12	piston	26	nylon bearing
13	shoe	27	U cup packing
14	one way crutch		

Figure 2 Sand sampler

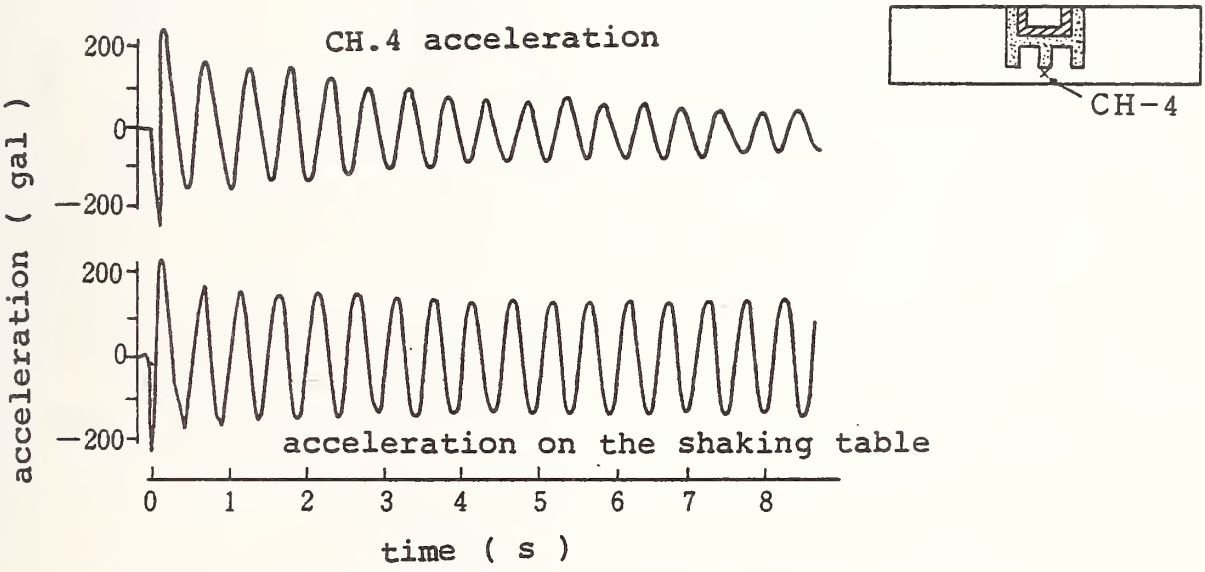

Figure 3 Example of acceleration record (model 11)

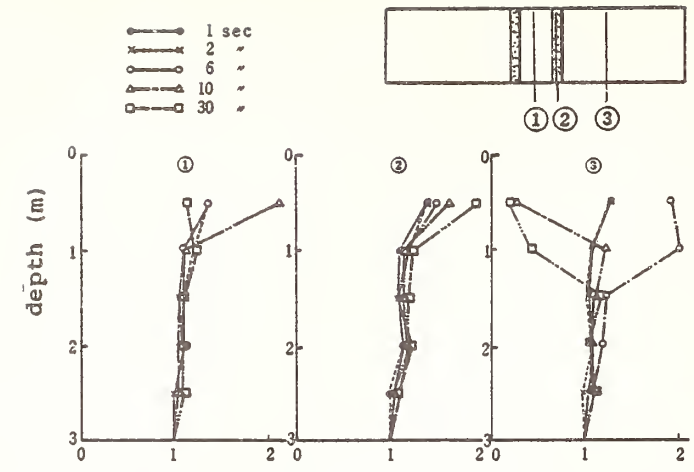

(acceleration on the shaking table = 148 gal)

(a) model 7

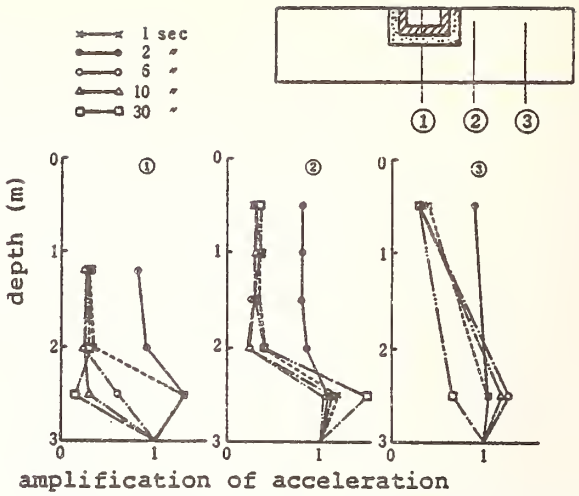

(acceleration on the shaking table = 140 gal)

(b) model 8

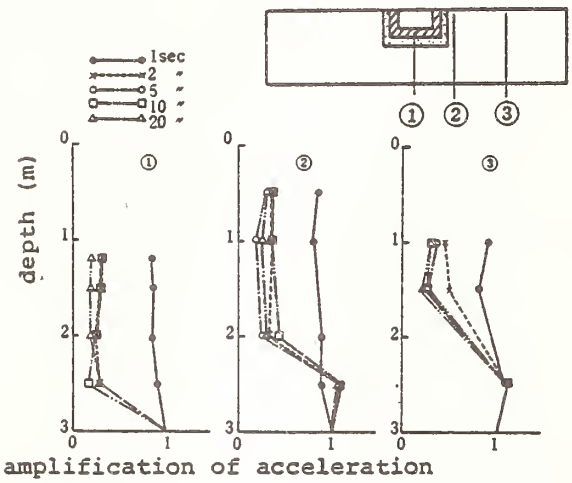

(acceleration on the shaking table = 144 gal)

(c) model 9

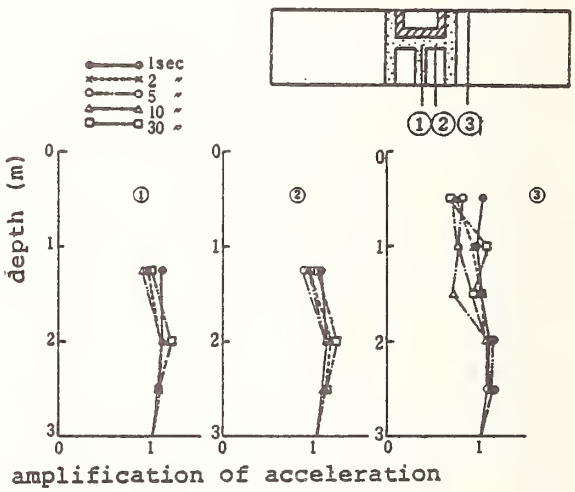

(acceleration on the shaking table = 140 gal)

(d) model 10

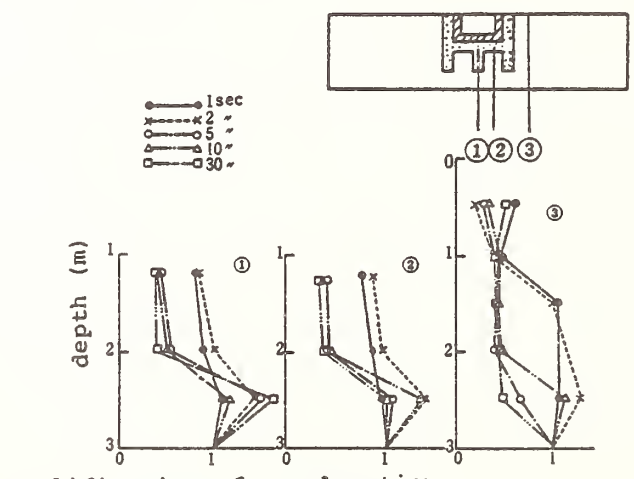

(acceleration on the shaking table = 136 gal)

(e) model 11

Figure 4 Amplification of acceleration along vertical direction

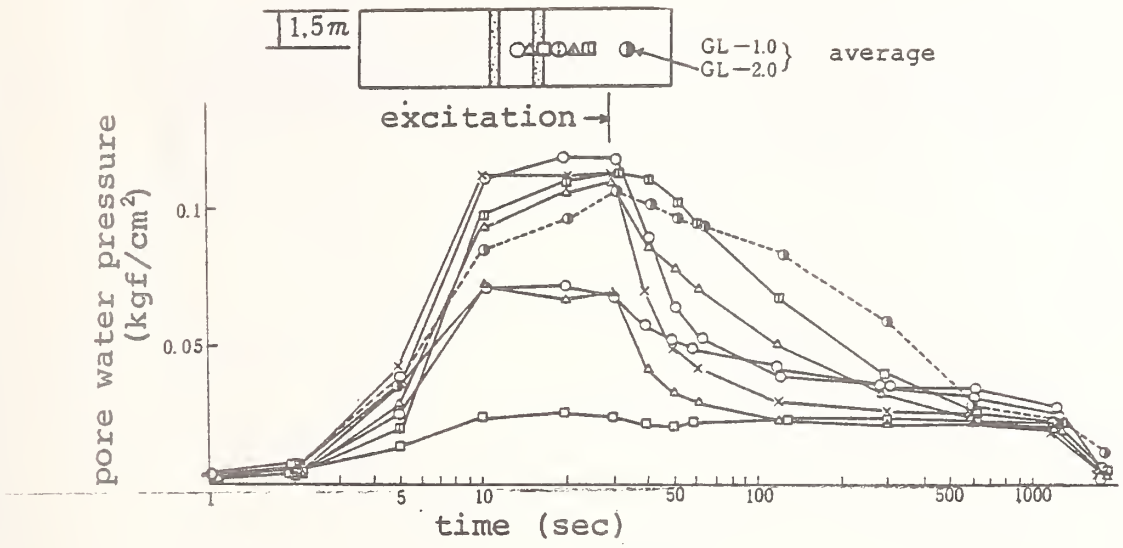

(a) model 7

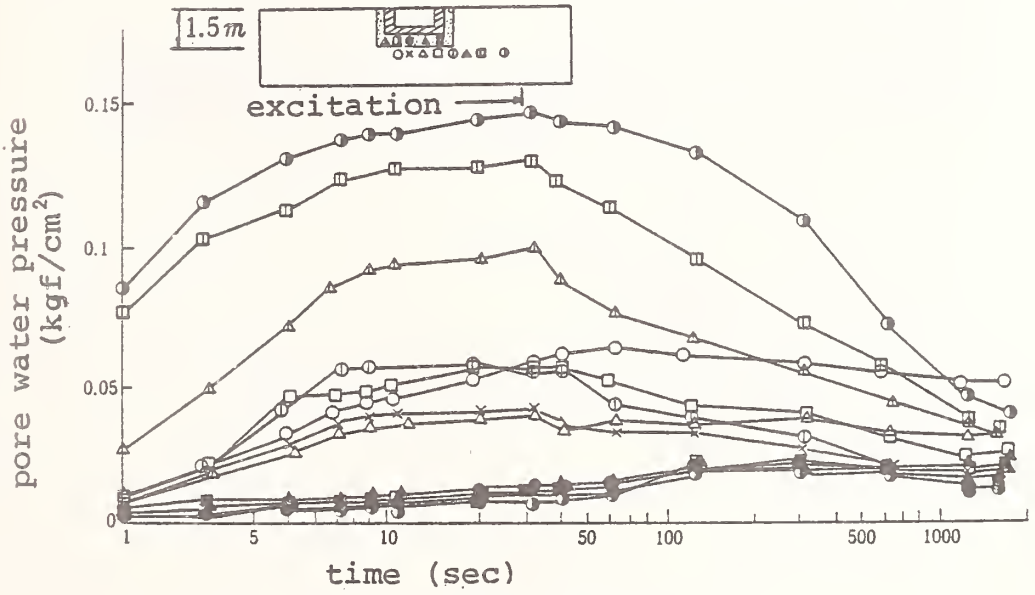

(b) model 8

Figure 5 Change of pore water pressure with time

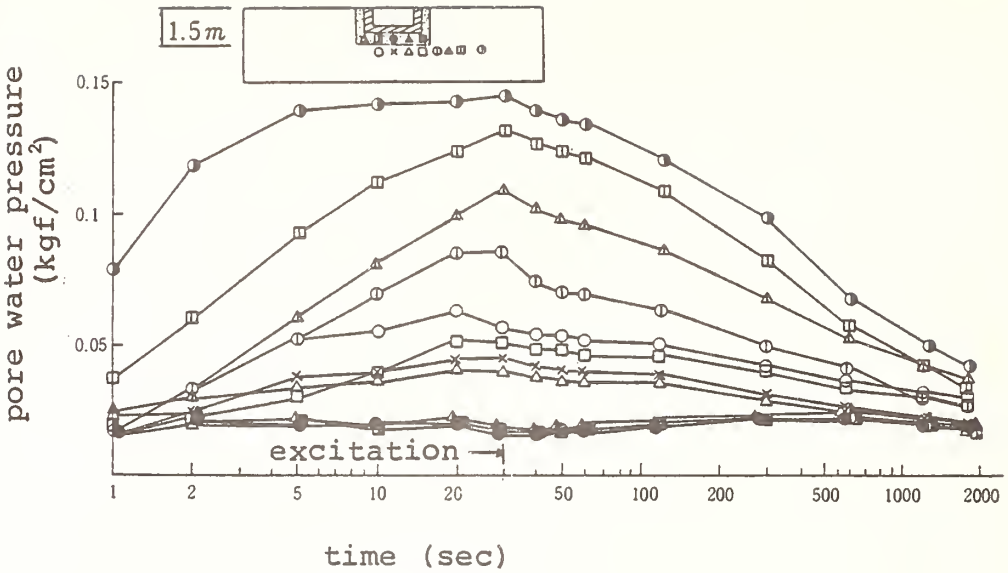

(c) model 9

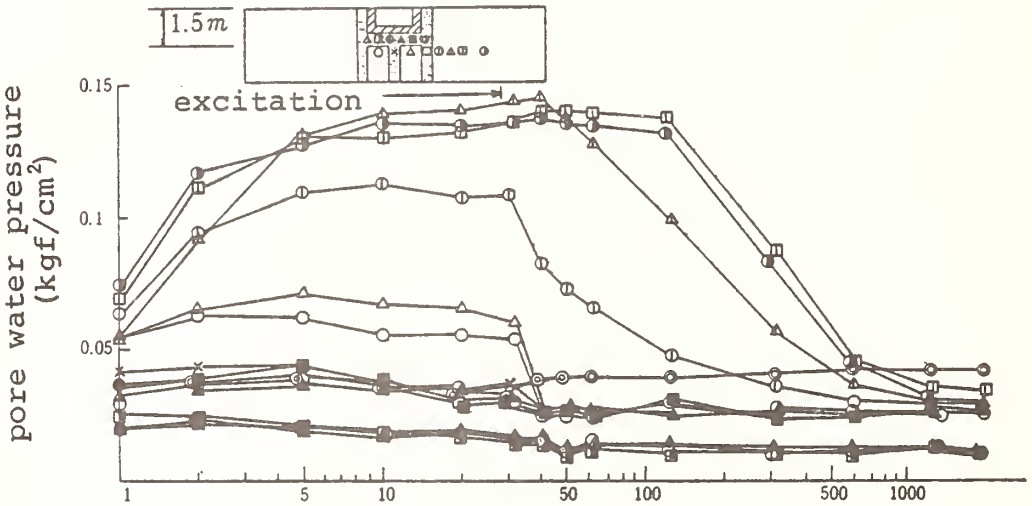

(d) model 10

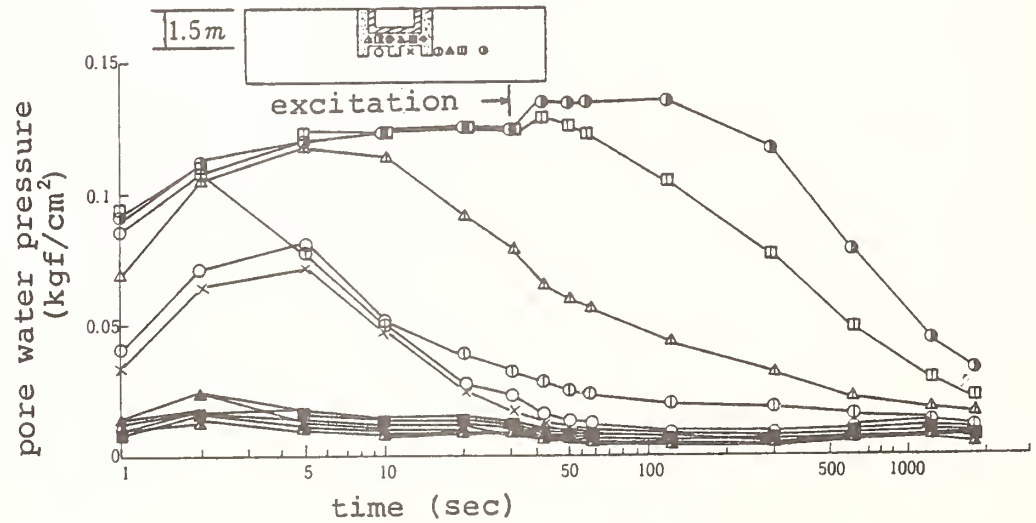

(e) model 11

Figure 5 Change of pore water pressure with time, (Continued)

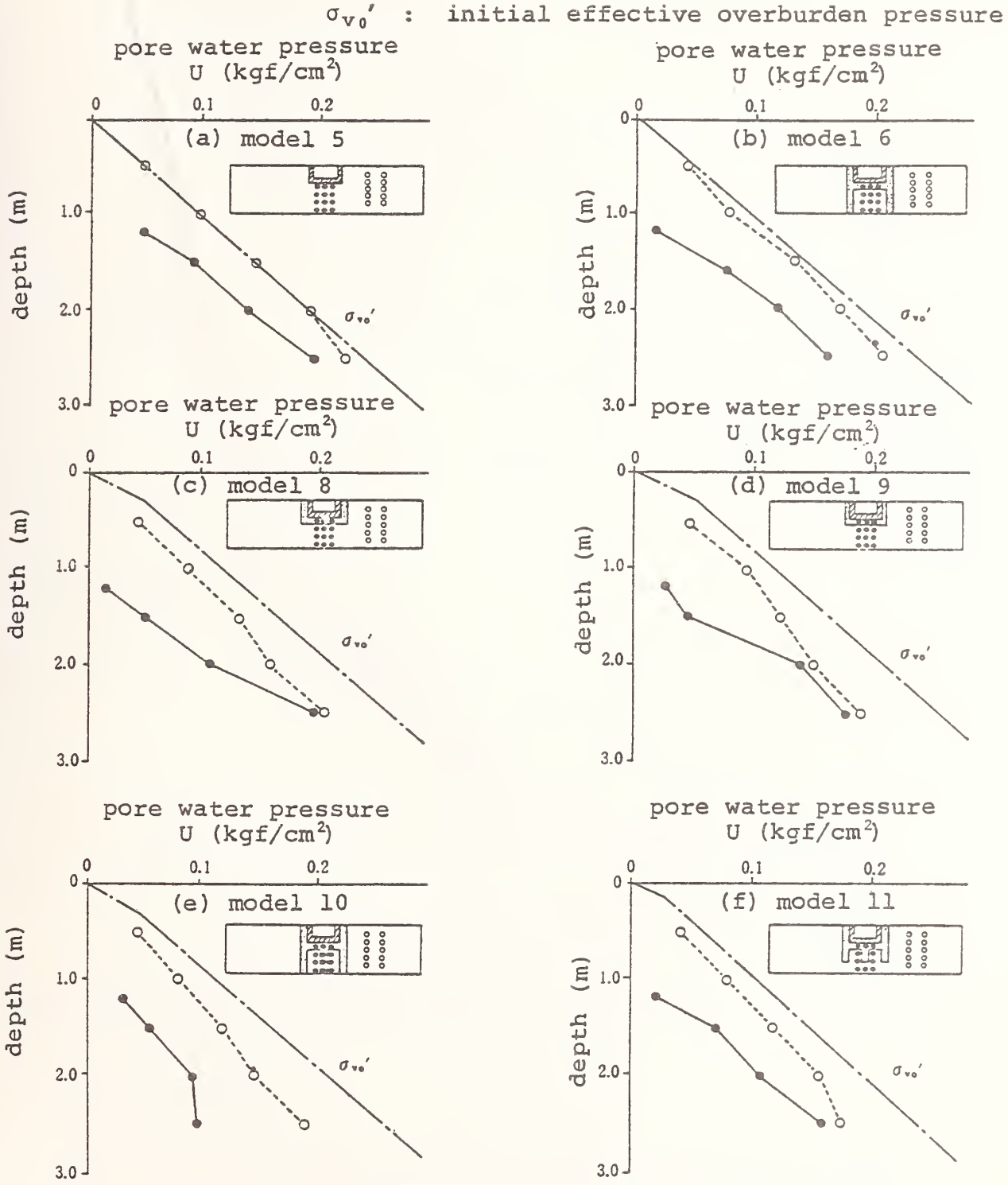

Figure 6 Maximum pore water pressure just under the half buried type road model

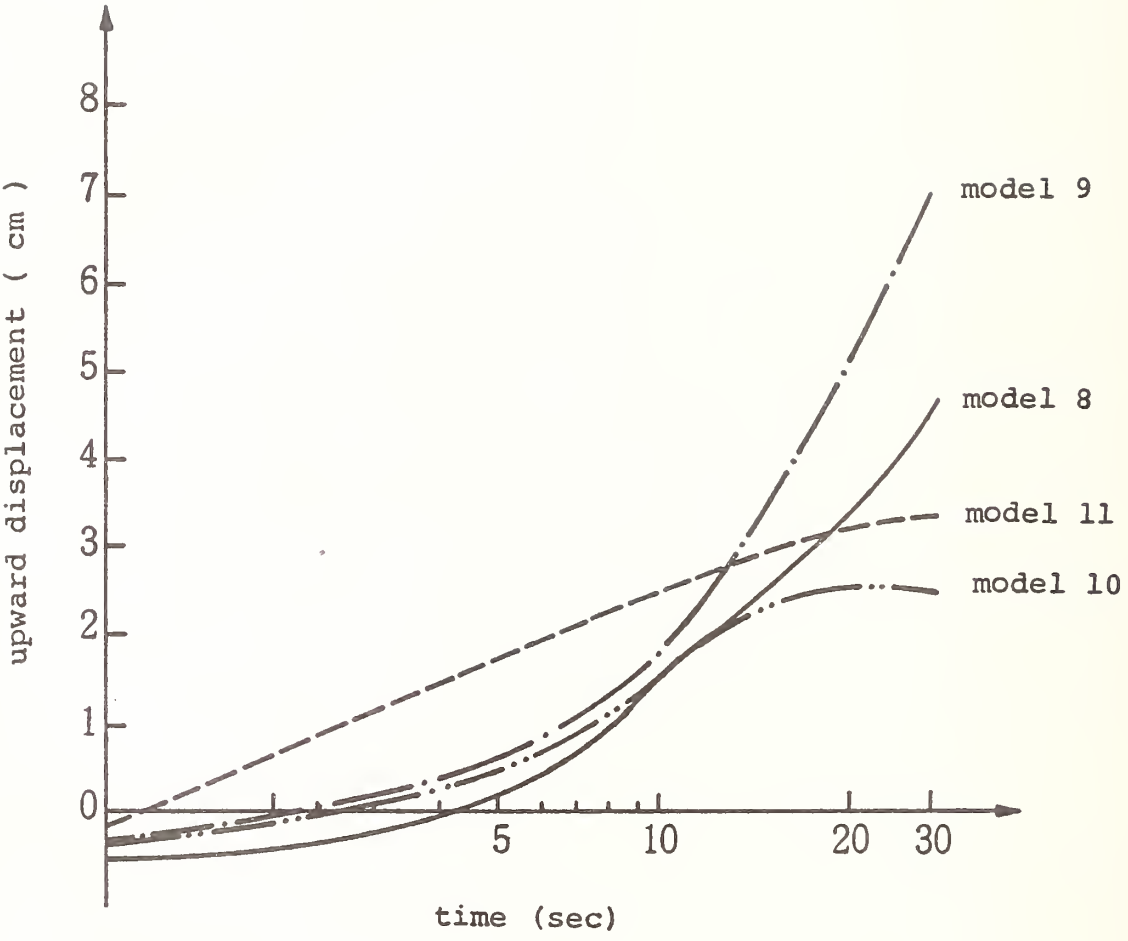

Figure 7 Upward displacement of half buried type road model

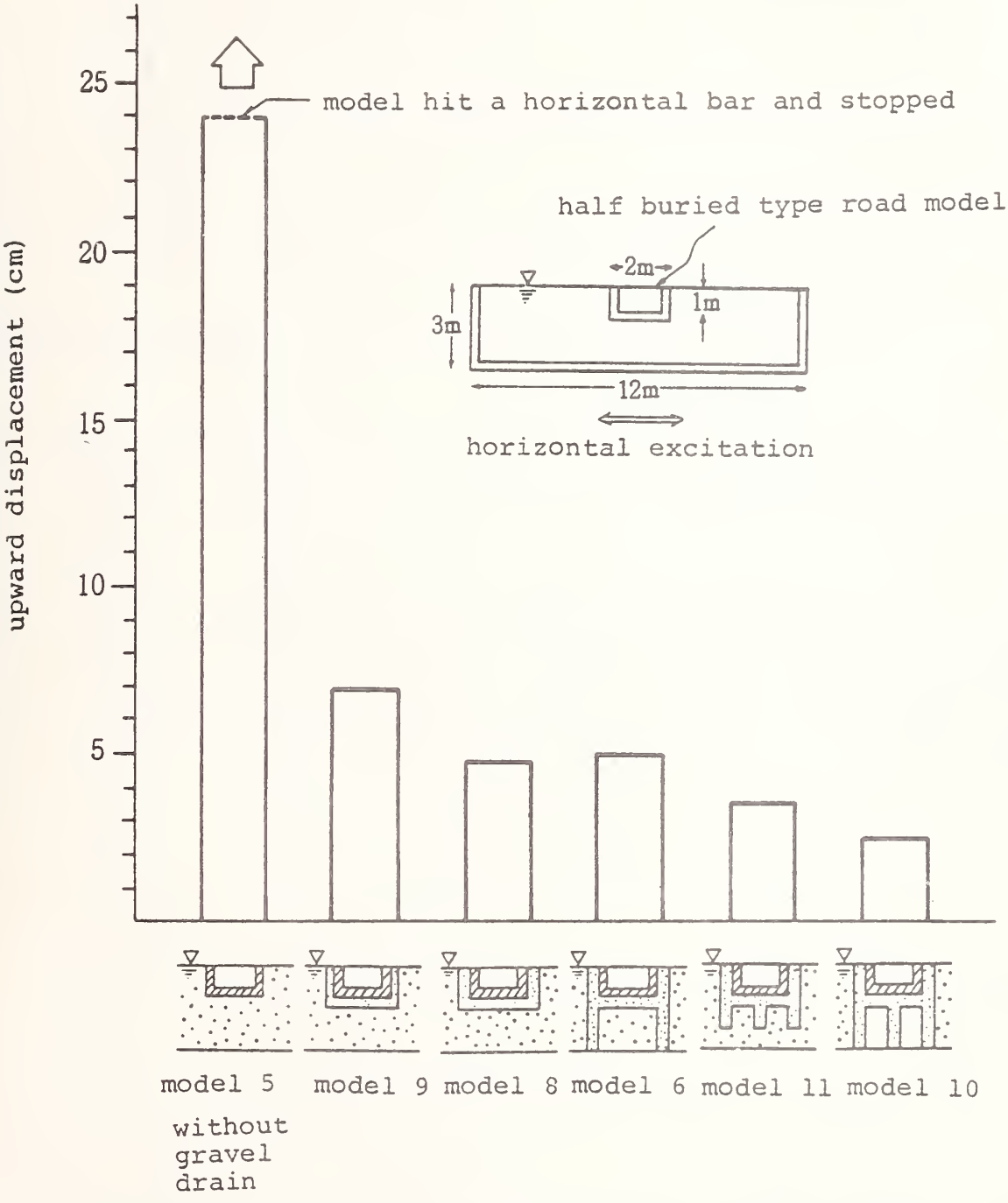

Figure 8 Effect of gravel drain to restrain upward displacement of half buried type road model

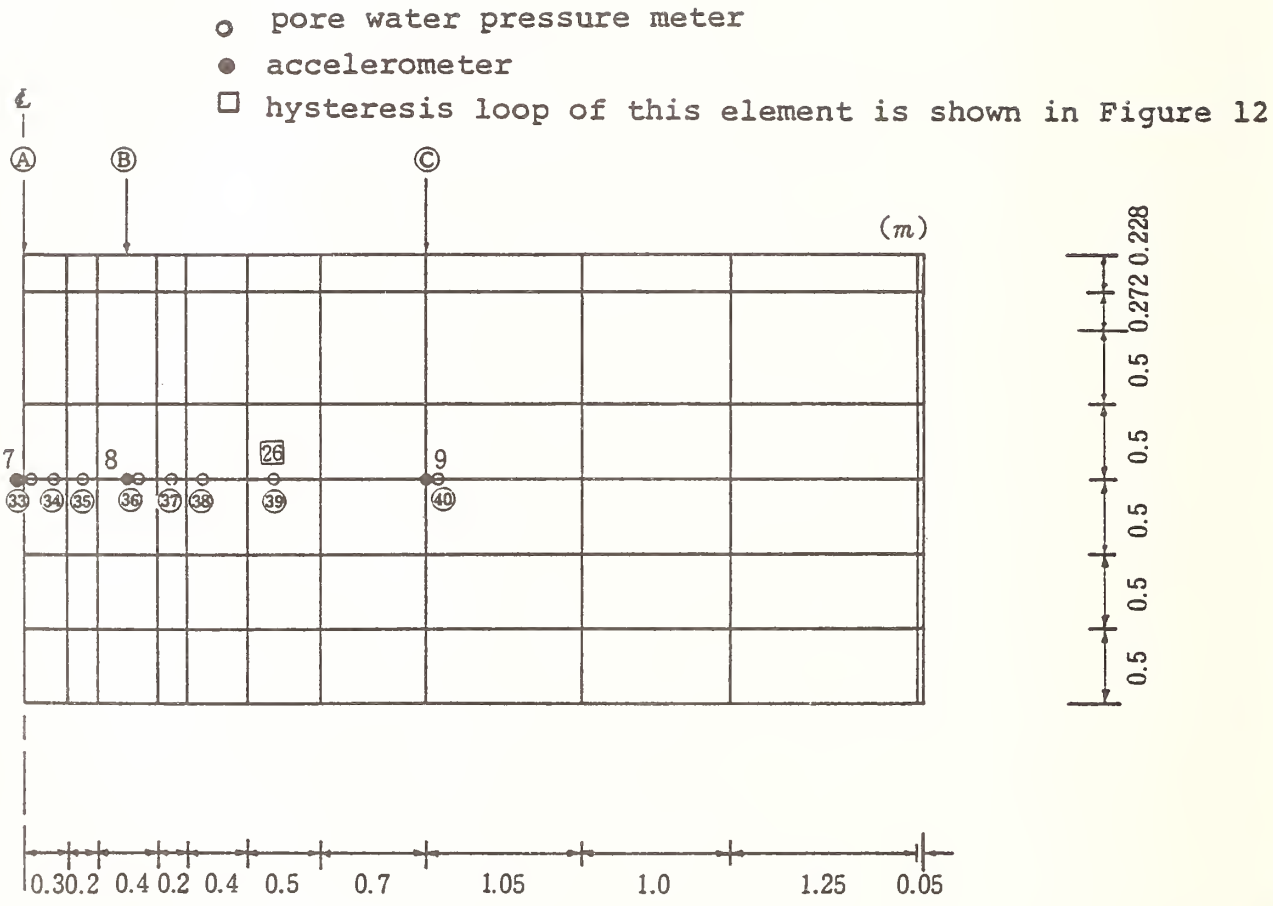

Figure 9 Finite element model (model 7)

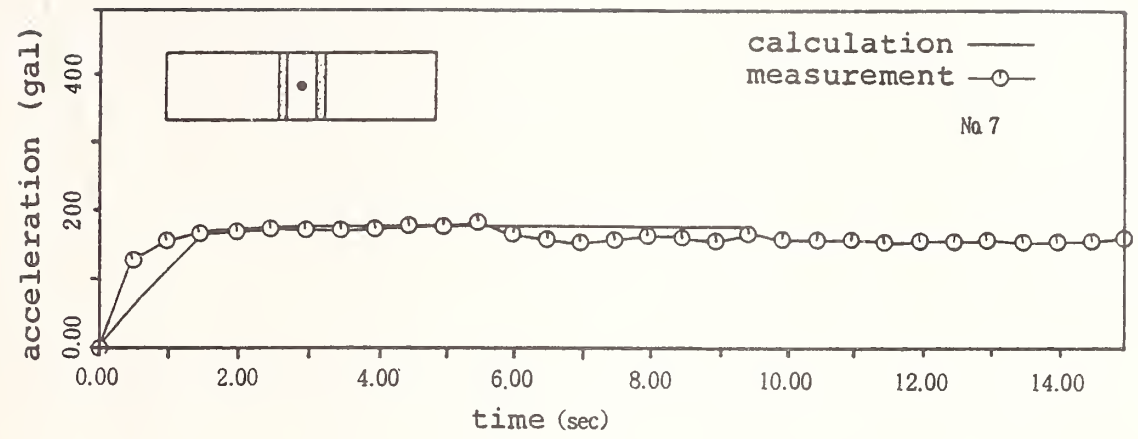

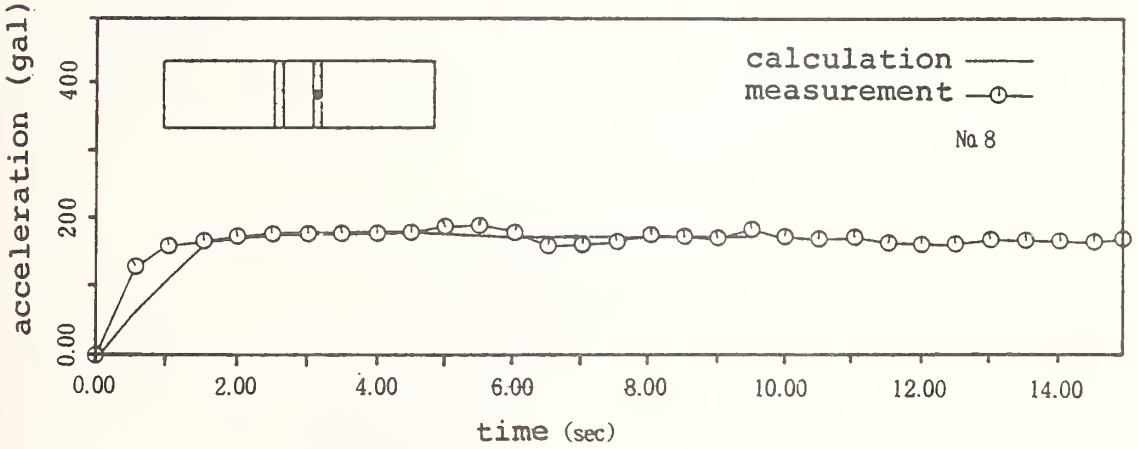

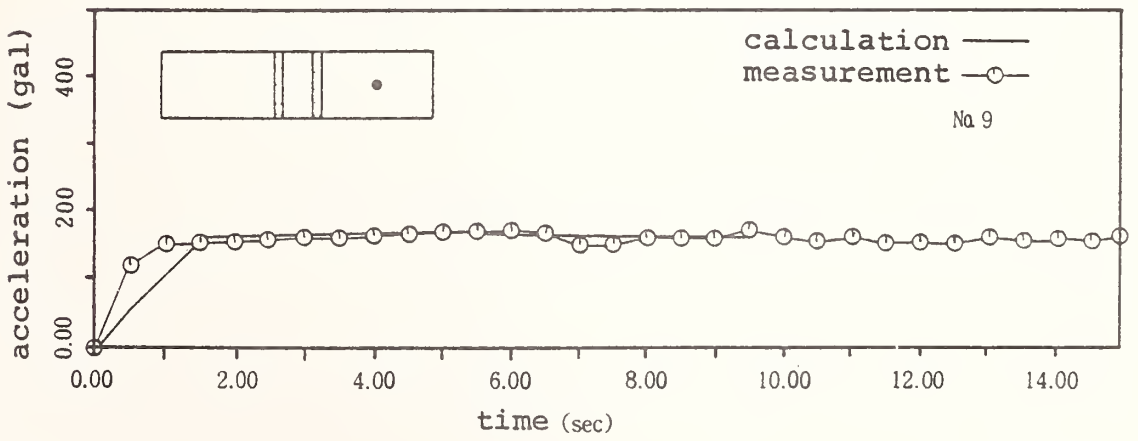

Figure 10 Conparison of acceleration of calculation and measurement

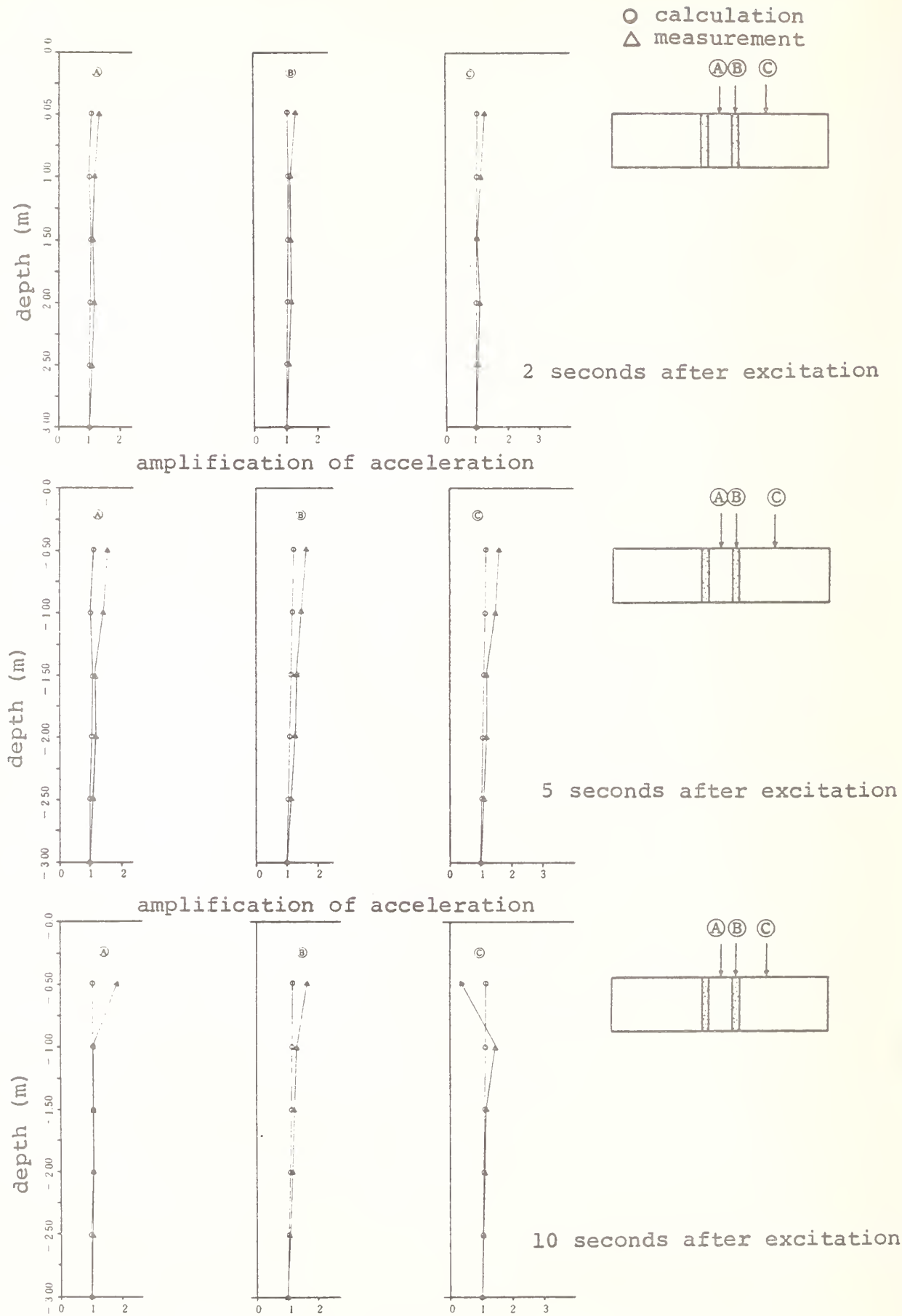

Figure 11 Amplification of acceleration

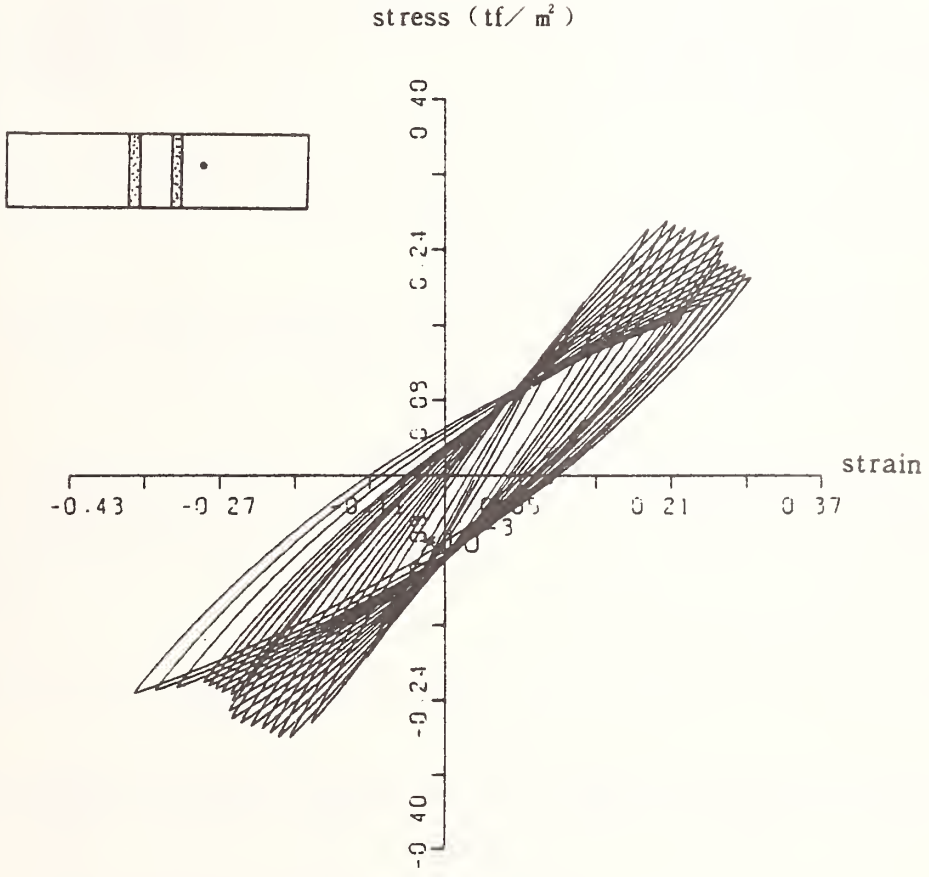

Figure 12 Hysteresis loop of stress - strain relationship

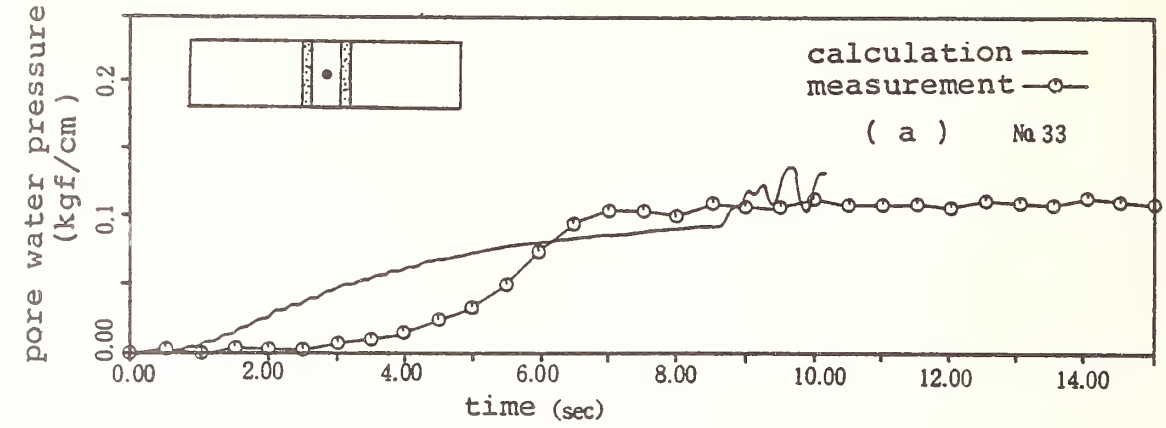

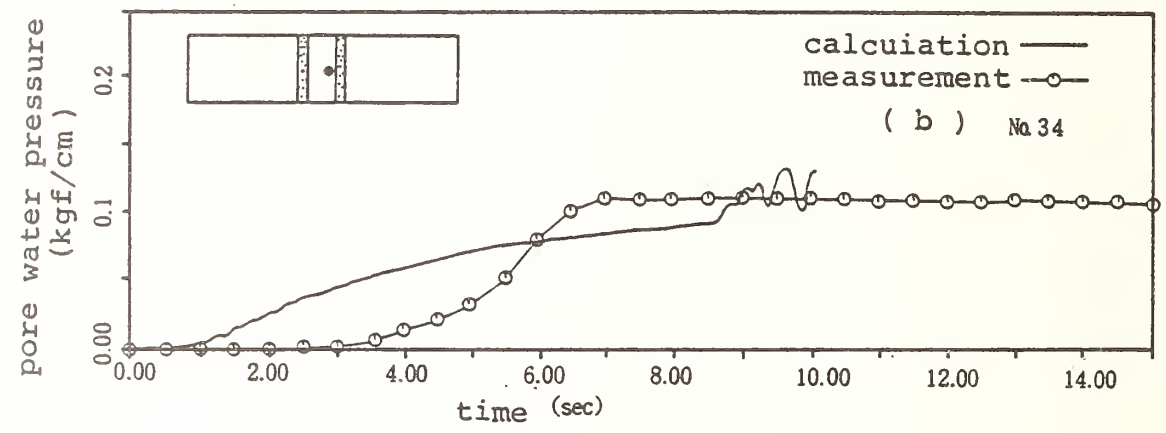

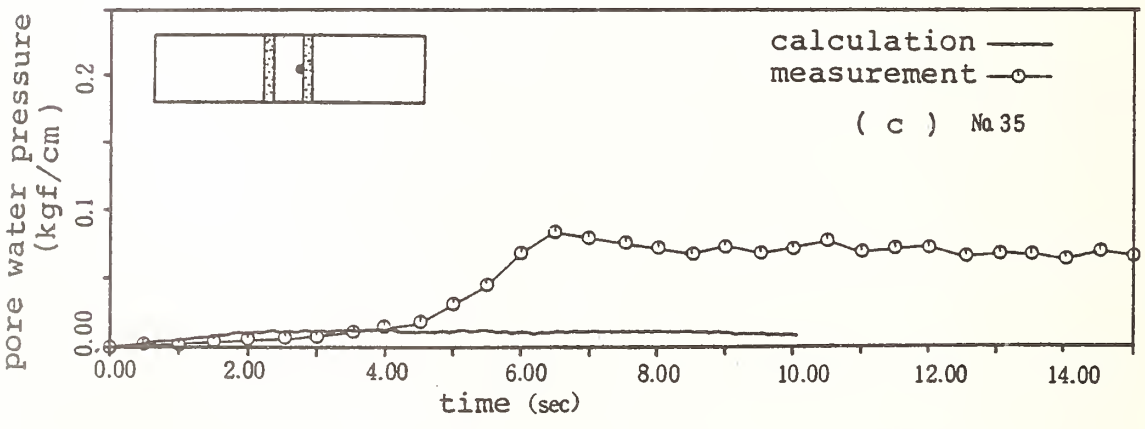

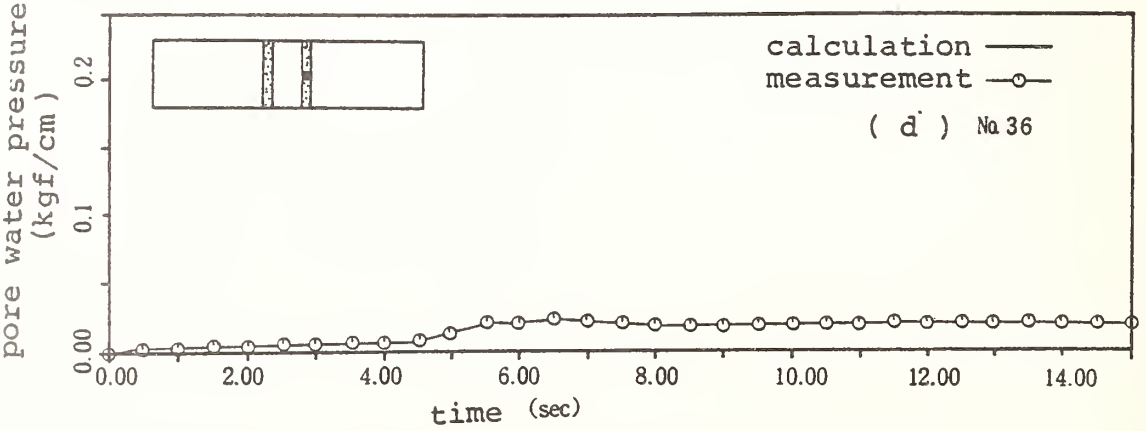

Figure 13 Comparison of pore water pressure (model 7)

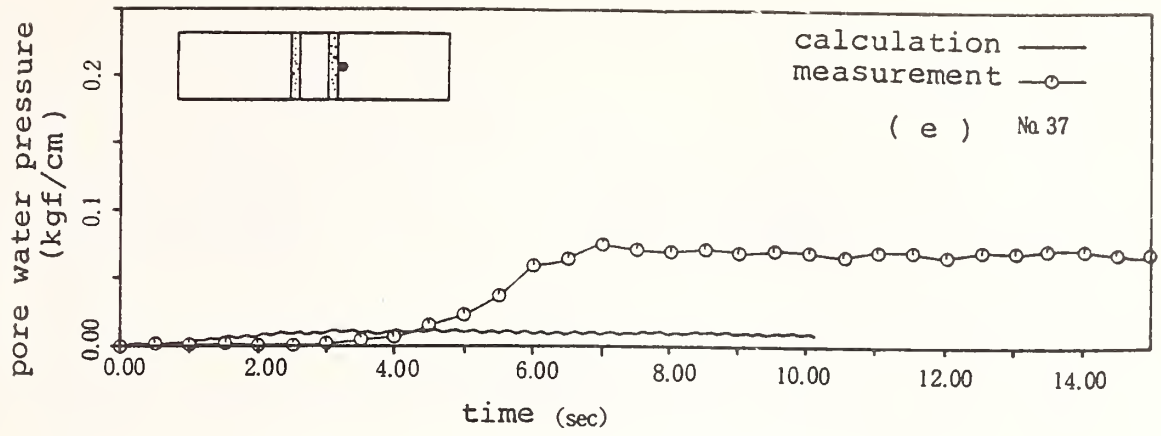

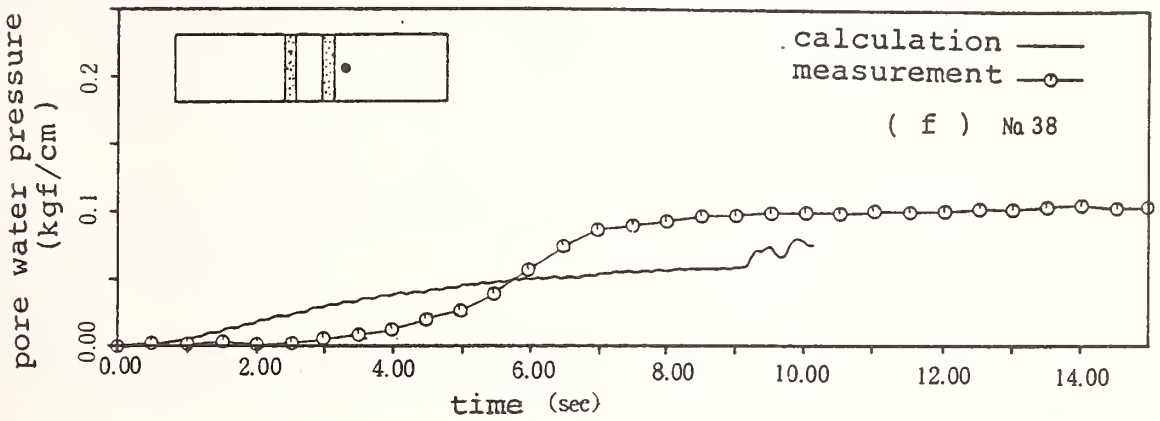

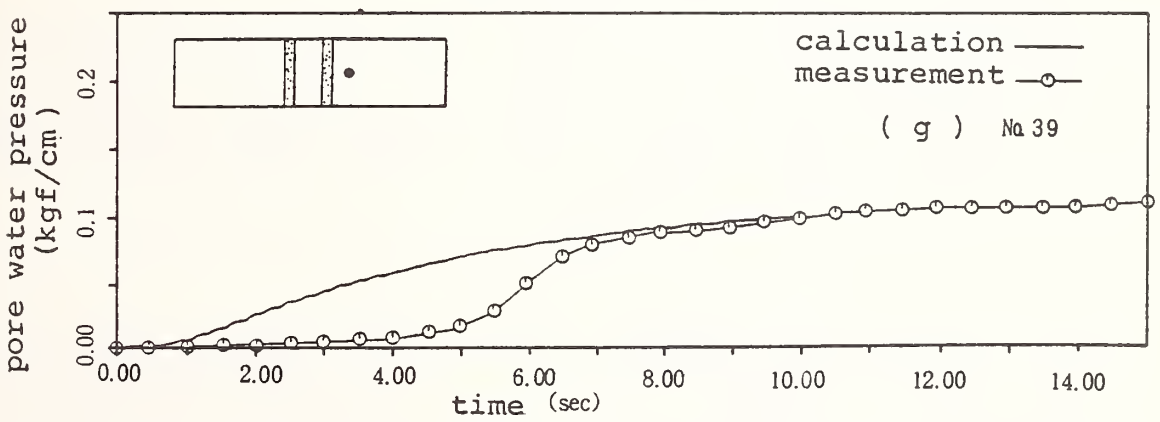

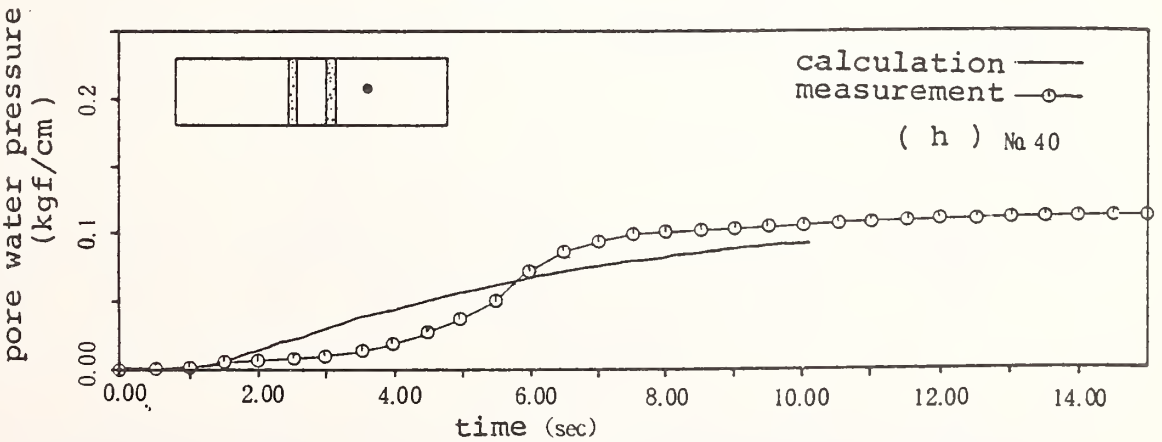

Figure 13 Comparison of pore water pressure (model 7)

(Continued)

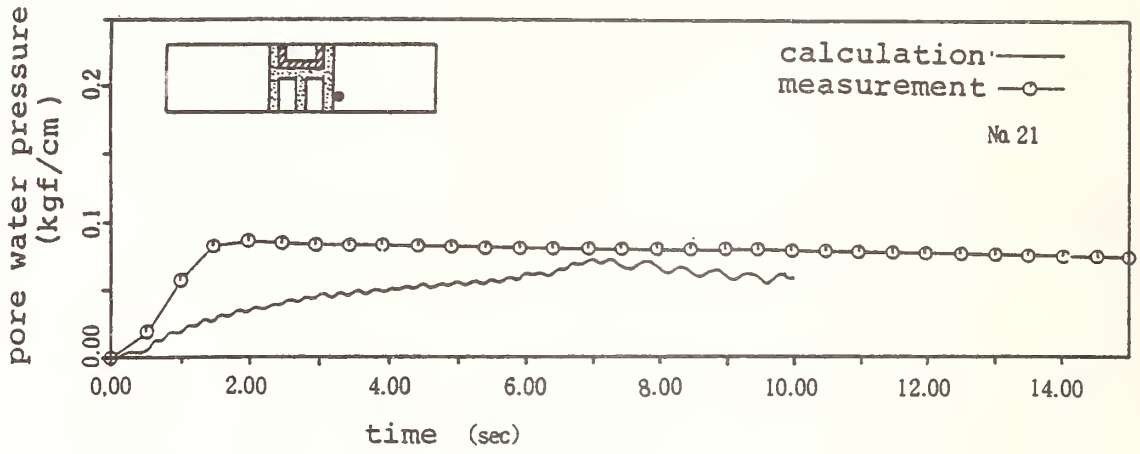

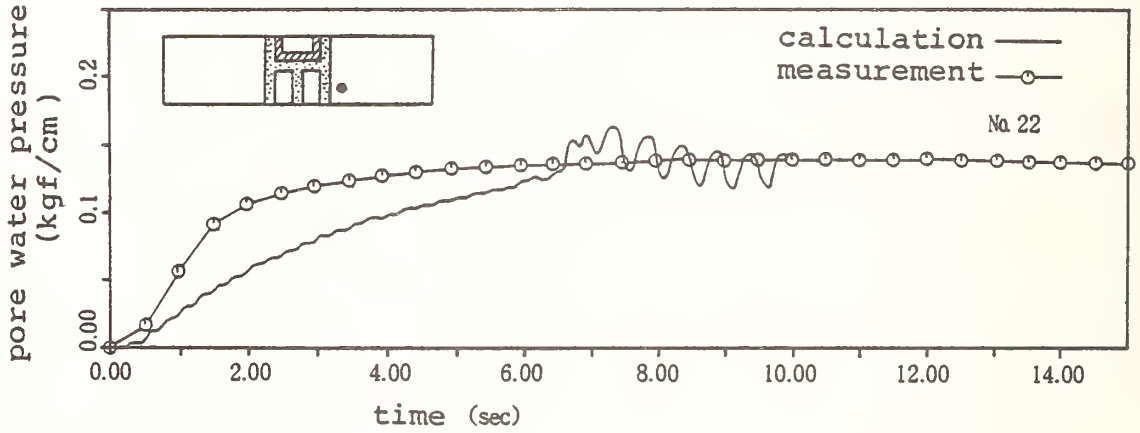

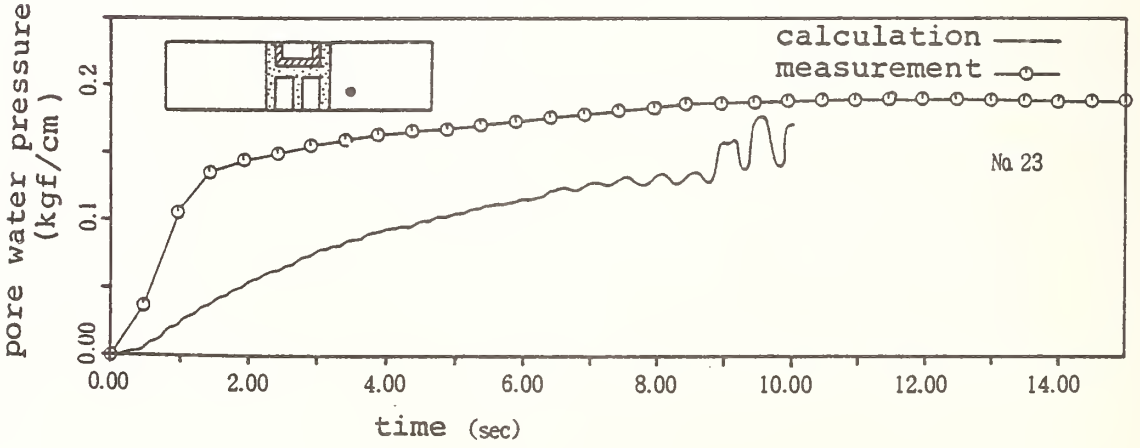

Figur 14 Comparison of pore water pressure (model 10)

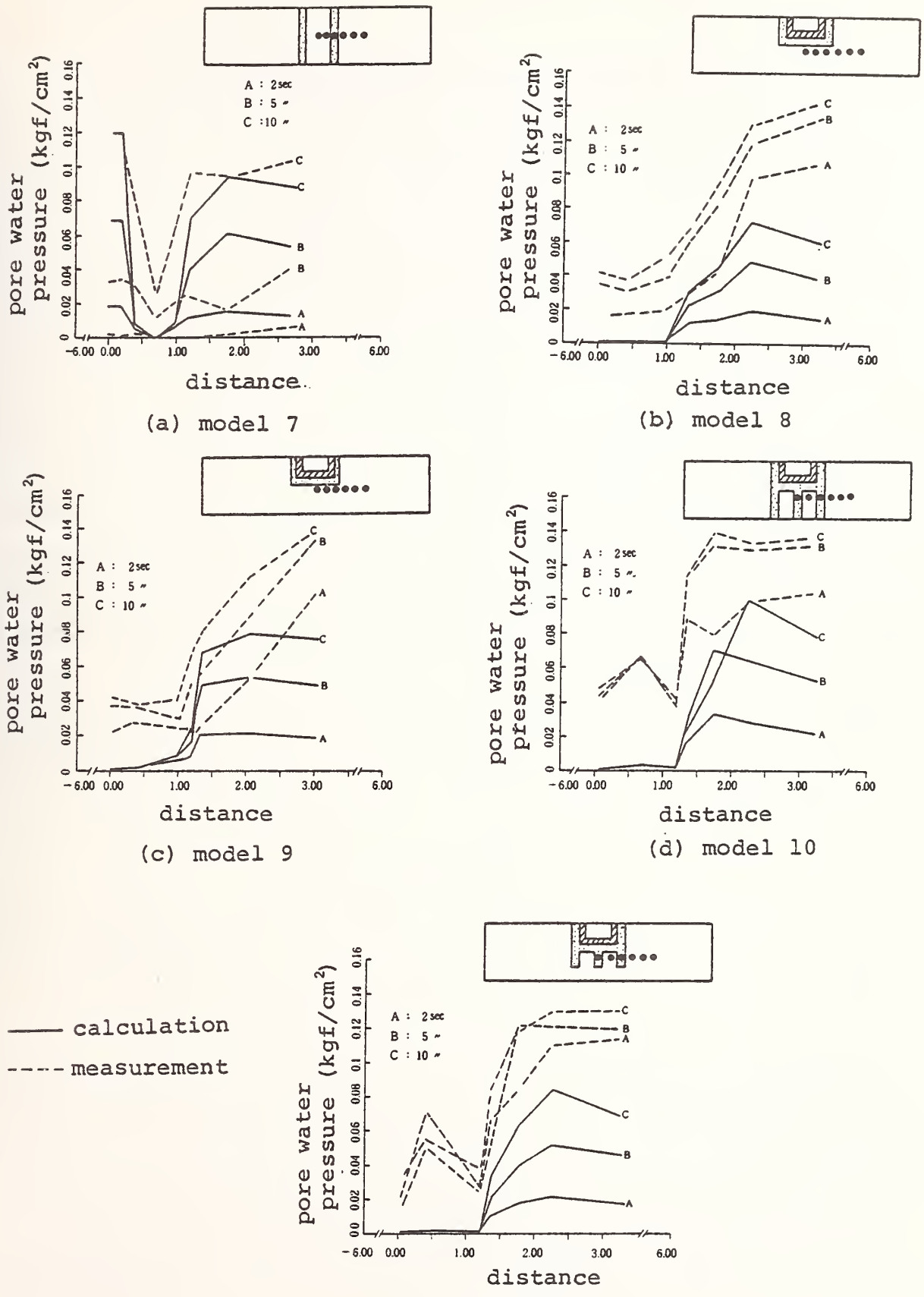

Figure 15 Comparison of pore water pressure at a depth of 1.5 m

VOLUME CHANGE AND EXCESS PORE WATER PRESSURE BUILDUP AS A FUNCTION OF DEGREE OF SATURATION OF SANDS DURING RESONANT COLUMN TESTING

Riley M. Chung
Felix Y. Yokel
Erik D. Anderson

Geotechnical Engineering Group
Structures Division
Center for Building Technology
National Engineering Laboratory
National Bureau of Standards
Washington, DC 20234

ABSTRACT

Torsional resonant column tests were conducted on saturated and partially saturated hollow cylindrical Monterey No. 0 sand specimens to study the characteristics of pore water pressure buildup and volume change of the specimen as a function of degree of saturation.

Results of the tests indicated that there exists a threshold shear strain value of about 2×10^{-3} percent for fully saturated sand specimens, below which three is no buildup of excess pore water pressure. The threshold value was observed at about 5×10^{-3} percent when the volume change during testing was used as the criterion.

The degree of saturation was found to have a considerable effect on the threshold strain and the pore water pressure buildup, but it had not detectable effect on the volume change as measured by the displaced pore water.

INTRODUCTION

Transient as well as steady-state ground vibrations can cause significant settlements in sandy soils. Sources of ground vibration associated with such settlement are earthquakes [11, 13, 14, 17, 23], traffic loads [4], pile driving, forge hammers [3], and machines.

Volume changes of dry sands subjected to cyclic loading were studied by Silver and Seed [20], who presented test results on the volume decrease resulting from cyclic strains and discussed factors affecting soil compaction. Most investigators who have been involved in testing saturated sands studied the liquefaction phenomenon. Generally, measurement of volume change during the cyclic loading has been of secondary interest in the course of most liquefaction studies.

When attempting to saturate soil specimens, the degree of saturation is evaluated by measurement of the B-parameter [22], which is defined as $\Delta u/\Delta\sigma_3$, where Δu is the change in excess pore water pressure and $\Delta\sigma_3$ is the change in effective confining pressure. Normally, the specimen is considered fully saturated when the B-values exceeds 0.95. A slightly lower value of 0.92 may

be considered satisfactory for cohesionless material testing [21]. In 1977, Sherif, et al. [18] pointed out that the phenomenon of initial soil liquefaction is not limited to fully saturated soils. They established a general relationship between the B-value and the initial degree of saturation. Using this relationship, they found that soils with a low degree of saturation (a B-value of 0.25) can liquify, and the pore water pressure buildup pattern is similar to the one developed in fully saturated loose sands.

This study deals with the characteristics of both pore water pressure buildup and volume change of sand specimens at various degrees of saturation prior to the application of cyclic loading.

TEST EQUIPMENT AND SETUP

Tests were conducted with a resonant column device of the Drnevich type [8] with the specimen fixed at the base and excitation forces applied to the top of the specimen. The apparatus has the capability of applying both longitudinal and torsional vibration excitations; however, only the torsional mode was used in the tests. The test setup is shown in figure 1. Figure 2 shows the panel for pressure control and volume change measurements.

Hollow cylindrical specimens were used. They were chosen in preference to solid specimens in order to reduce the variation of shear strains. The specimens were constructed using a mandrel covered by a membrane to form a nominal inner diameter of 35 mm and a split mold also covered by a membrane to form a nominal outer diameter of 71 mm. Nominal height of the specimen was 76 mm. Actual specimen dimensions varied slightly from the nominal values and were measured individually for each specimen constructed as will be described later. Figure 3 shows the top view of a specimen after it was constructed inside the molds and before the placement of the top platen.

TEST MATERIAL

Monterey No. 0 sand was used. A particle size distribution curve and the selected index properties of this sand, obtained by Mulilis, et al. [12], are shown in figure 4 and table 1, respectively. The sand is a commercially available washed uniform fine to medium beach sand having a group symbol of SP in accordance with the Unified Soil Classification System [2], composed of quartz and feldspar particles. The maximum and minimum dry unit weight determinations were performed in accordance with ASTM D2049-69 [1] and Kolbuszewski's method [9], respectively.

TEST PROCEDURES

Oven-dried materials were used in the preparation of the specimens and all of the specimen were prepared to a relative density of approximately 60 percent using a moist tamping method with the exception of specimen M-7, where a dry tapping method was used instead. The method of "under-compaction" described by Ladd [10] was adopted for preparing the specimens. In the moist tamping, a moisture content of 6 percent was used. The amount of material required to fill a known volume was divided into five equal parts. The first part of the material was spooned into a space confined at the inner boundary by the inner mandrel, and a split mold at the outer boundary to form the first layer. The membrane inside the split mold was tightly backed up against the split mold by vacuum. Tamping on the layer surface was required to reach the desired layer thickness which was calculated using the Ladd method. Subsequent parts of the weighed material were placed into the annular space in the same manner. In dry tapping, the first part of the material was poured into a funnel which was resting on the bottom platen, and then the funnel was raised slowly to allow the material to flow into the annular space. Only slight tapping on the wall of the split mold was required to reach the required layer thickness. Subsequent parts of the weighed material were poured into the same funnel with its bottom resting on top of the layer being constructed. By dividing the total weight of the specimen into five parts and constructing the specimen in a sequence of five layers, an approximately uniform density distribution throughout the height of the specimen can be achieved [10]. Special care should be given to the top layer to make sure that the loss of material due to placement be kept to a minimum and the top surface be compacted so that it is even with the top of the split mold. A white apron was placed around the split mold so that any loss of material would be detected and recovered. In addition, a small tin can containing 1 g of sand was placed next to the area of specimen preparation and was used as the reference base to check qualitatively against the amount of material lost during the specimen preparation. In all cases, the amount of material loss was much less than 1 g.

The test apparatus does not have the capability to circulate water through the specimen once the specimen is set up in the testing chamber. Therefore, to achieve saturation, the specimen was flushed before the top platen was placed on the specimen. After many trials, it was found that saturation can be accomplished by first flushing CO_2 upward through the specimen under a very low pressure (less than 10 kPa) to displace the air within the specimen and subsequently dissolving and expelling the CO_2 by deaired distilled water flowing also upward through the specimen. The flow of water was stopped when visual observation indicated that the top of the specimen was saturated. The top platen was then put into place and the rubber membranes adjusted around the top platen.

The vacuum was then removed from the split mold and a suction of 20 kPa was applied through the bottom platen to hold the specimen in place. It should be noted that the application of a relatively low magnitude of suction is essential to achieve a high degree of saturation of the specimen later through backpressure application. Higher magnitudes of suction (up to 80 kPa) resulted in a lower degree of saturation within the specimen. Because this is the high suction applied at this stage would tend to withdraw more water from the specimen thus resulting in a less saturated condition prior the application of back pressure. The split mold and the inner mandrel were then removed while the suction in the specimen was maintained.

Actual dimensions of the prepared specimens were measured with suction maintained in the specimen. The length of the specimen was determined by arranging the measurements at two diametrically opposite positions. The outer diameters were measured at two elevations and at 90° displacement between the directions of measurement and averaged. The actual outer diameter of the specimen is the above measured average value minus twice the average membrane thickness. The inner diameter of the specimen was measured earlier when the inner membrane had been placed over the inner mandrel. The dry unit weight of the specimen was then calculated using its measured dimensions. After complete assembly of the apparatus around the top platen, a plexiglass cylinder was placed around the assembly and was enclosed by a top plate which housed all the transducers for input driving force, output acceleration, and displacement. The response of pore water pressure was measured by a pore pressure transducer mounted to the bottom platen. Deaired water was allowed to flow into the chamber and to fill the chamber to the level just below the driving magnets. A pressure of 20 kPa was then applied in the chamber and the suction within the specimen was slowly released so that the specimen was completely supported by a positive (confining) chamber pressure of 20 kPa. While the specimen was under this confining pressure in the test chamber, and also earlier when the specimen was held by a suction of 20 kPa within the specimen, a small-amplitude torsional shakedown test was conducted with an average shear strain amplitude of about 5×10^{-4} percent to determine the system response. By observing the LVDT readings which measured the change in specimen height, the tests were also used to detect any specimen disturbance due to the assembling operation of the test setup.

A backpressuring technique was used to enhance the degree of saturation of the specimen. The magnitudes of the confining pressure and backpressure were increased simultaneously in increments of 20 to 50 kPa to bring the final magnitude of backpressure to about 400 to 500 kPa. The B-values were checked at each increment and showed a steady increase toward unity with increasing backpressure. Confining pressure was then brought to the desired magnitude for specimen consolidation. An effective consolidation pressure of 96 kPa was used for all specimens.

The resonant column testing was initiated with the application of a very small torsional excitation force to the top of the specimen so that the average shear strain amplitude of the specimen was on the order of 10^{-3} percent or less. The frequency of the torsional excitations was rapidly changed until resonant frequency was observed. The frequency was then kept constant and no attempt was made to maintain resonance for a period of about 2 min. At that point, the resonant frequency, acceleration, longitudinal displacement, and any buildup of the excess pore water pressure were recorded. The applied force was then removed from the top of the specimen and the pore water pressure readout was continuously monitored for any tendency to return to its original value, which was equal to the magnitude of the backpressure.

If there was a residual excess pore water pressure after removal of the cyclic load, the drainage valve was opened to allow the release of this residual excess pore water pressure. The amount of water flowing out of the specimen to return the pore water pressure to the magnitude of the backpressure was read from the burette and was recorded.

The torsional excitation force was then increased to a higher level, normally to double the magnitude of the previous level, and the test procedures described above was repeated. A maximum average shear strain amplitude of about 5×10^{-2} percent was obtained using this resonant column testing procedure.

TEST RESULTS

A summary of specimen characteristics for the six tests are given in table 2. The average dry density of the specimens was 1575.3 kg/m^3 with a range of 1573 to 1577 kg/m^2 and a standard deviation of 1.37 kg/m^3. This average unit weight is equivalent to a void ratio of 0.678 and a relative density of 59.3 percent.

The average shear strain amplitude was computed by the following equation:

$$\gamma = (RCF)(RTO)\frac{d_o^3 - d_i^3}{d_o^2 - d_i^2}\quad\frac{1}{3H_c}\,100\ \% \tag{1}$$

where RCF = rotational transducer calibration factor for the transducer used in establishing resonance, radians/volt$_{rms}$.

RTO = rotational transducer output for transducer used in establishing resonance, volts$_{rms}$.

d_o = outer diameter of the spcimen, m.

d_i = inner diameter of the specimen, m.

H_c = specimen height after consolidation, m.

No adjustment for volume change due to the application of the torsional excitation force was used in the computation since the total volume change of the specimen during cyclic torsional loading did not exceed 0.5 percent.

Figure 5 shows a plot of the stabilized excess pore water pressure versus average cyclic shear strain at the end of the approximate 2 min loading interval of each amplitude of the torsional excitation force. For each value of shear strain above the threshold strain, the excess pore water pressure increased as the test proceeded and stabilized at the value shown in the plot, even after the excitation force was removed. While the excess pore water pressure increased it was possible to achieve resonance for a short time period, as evidence by the elliptical trace on the oscilloscope screen. At the point where the excess pore water pressure stabilized at its maximum value, the excitation was no longer at resonant frequency as evidenced by the distortion of the elliptical trace. Consequently, accelerometer readings tended to decrease as the elliptical trace began to tilt.

The effect of the degree of saturation is readily seen in figure 5. Specimen M-3, which had the lowest B-value of 0.30, exhibited the slowest excess pore water pressure buildup. The threshold strain for excess pore water pressure buildup decreased with an increase in the B-values, which are tabulated in figure 5. For specimens M-2 and M-7, which have B-values of 0.99 and 0.96 respectively, the excess pore water pressure started to build up at an average shear strain of about 2×10^{-3} percent.

The threshold shear strain, γ_t, below which there is no buildup of excess pore water pressure was obtained from figure 5 for each specimen and is shown as a function of the B-parameter in figure 6. For the range of B-values obtained in this study (0.99 to 0.30), γ_t varied from 2×10^{-3} percent to 7×10^{-3} percent. For the B-values greater than 0.92, which can be considered as satisfactory for saturated sand specimen testing, the range of γ_t is from 2 to 4×10^{-3} percent. It is also noted that the magnitude of γ_t is relatively insensitive to the degree of saturation for B-values below 0.90. A decrease of B-value from 0.90 to 0.50 shifted the threshold shear strain from 4×10^{-3} percent to 6×10^{-3} percent. Additional testing will be required to substantiate these findings for other granular materials.

The concept of the existence of a threshold shear strain when a saturated loose to medium density cohesionless deposit is subjected to earthquake loading has been studied by Dobry et al. [5] in a cooperative project between the National Bureau of Standards, Rensselaer Polytechnic Institute, and Woodward-Clyde Consultants. In the study, strain-controlled dynamic triaxial tests were conducted by applying a number of uniform cycles of strain to saturated Monterey No. 0 sand specimens,

and the characteristics of the excess pore water pressure buildup were evaluated as a function of the shear strain amplitude. The results for 100 strain cycles are shown as curve A in figure 5 for comparison. Curve A shows a threshold shear strain value at about 10^{-2} percent which is higher than the values obtained by resonant column testing. This difference may in part, be attributable to the different loading conditions. In the torsional resonant column tests, the direction of the shear strain is reversed. This was not the case in the cyclic triaxial tests represented by curve A.

The volume of water expelled from the specimens to release the excess pore water pressure at different magnitudes of average shear strain is given in figure 7. No volume change measurements were made on specimen M-2. The volume change is expressed as a percent of the total volume of the specimen after consolidation, $\Delta V/V_c$. Note that the volume change is not very sensitive to the B-parameter. This contrasts with the high sensitivity of the excess pore water pressure buildup to the B-parameter (figures 5 and 6), and is an indication that a relatively minor change in the volume of water can cause a large change in the B-parameter. The correlation between volume change and the average shear strain is closely approximated by the single curve shown in figure 8. Below shear strain of about 5×10^{-3} percent, no volume change was observed. Figure 8 also shows the vertical strain due to the compaction in ten cycles during cyclic simple shear testing conducted on Crystal Silica No. 20 sand specimens by Silver and Seed [20]. The Crystal Silica No. 20 sand is a uniform angular quartz sand with a mean grain size, D_{50}, of 0.65 mm and a specific gravity of 2.65. The maximum and minimum void ratios determined by Silver and Seed [19] are 0.973 and 0.636, respectively. Dry sand specimens were used in their testing and the curve shown in figure 8 was obtained from the testing of specimens prepared to a relative density of 60 percent (void ratio of 0.777) and subjected to confining pressures of 24, 96, and 192 kPa. Note that both curves in figure 8 exhibit similar trends; however, the threshold strain in the simple shear test was higher, and the volume change for a given strain lower.

In figure 9, the buildup of the excess pore water pressure is plotted as a function of volume change for different B-parameters. Again it can be seen that the excess pore water pressure buildup is very sensitive to B-value, and thus even a minor volume of air in the voids would have a considerable effect.

The magnitude of excess pore water pressure buildup during resonant column testing can be compared with the relationship proposed by Drnevich in 1972 [7] on the basis of results from cyclic torsional shear tests on hollow cylindrical specimens.

$$\frac{\sigma'_{3t}}{\sigma'_3} = \frac{1}{(1 + b_c N^{0.75})} \tag{2}$$

$$b_c = \exp \frac{-7.50}{\left(\frac{\gamma}{\gamma_r}\right)^{0.2}} \tag{3}$$

$$\sigma'_{3t} = \sigma'_3 - \Delta u_t \tag{4}$$

$$\gamma_r = \frac{\tau_{max}}{G_{max}} \tag{5}$$

$$\tau_{max} = \sigma'_3 \sin \phi' \tag{6}$$

where σ'_3 = initial effective confining pressure

σ'_{3t} = effective confining pressure at any time, t

Δu_t = excess pore water pressure at any time, t

γ_r = reference shear strain

γ = shear strain at any time, t

τ_{max} = shear stress at failure

G_{max} = shear modulus at very small shear strain amplitude

ϕ' = effective angle of shear resistance

N = number of strain cycles in testing, a 2 min duration was used herein to calculate the N value.

The equation below, which was revised by changing the exponent of N in equation (2) from 0.75 to 1.10, was found to provide a good fit of the experimental results for the tests with high B-parameters:

$$\frac{\Delta u}{\sigma'_3} = 1 - \frac{1}{(1 + b_c N^{1.10})} \tag{7}$$

The comparison between the measured and calculated excess pore water pressures using equation 7 is shown in figure 10. Note that the agreement is very good for specimens M-2 and M-7 which have high B-values of 0.99 and 0.96, respectively. Agreement for the other two specimens, M-4 and M-5, which have B-values of 0.90 and 0.93, respectively, is poor. Drnevich [7] noted that because the reference strain concept has been used to normalize shear strain, the same framework could be applied to other saturated sands but the coefficients may differ slightly. This is the case in this instance. Equation 7 was derived for the possible maximum excess pore water pressures associated with a given average shear strain for the duration of cyclic shear application. After the possible maximum excess pore water pressure is reached, it will not increase even when a large number of additional cycles are applied. The equation, therefore, no longer applies.

SUMMARY AND CONCLUSION

(1) Threshold Strain: Based on the cyclic loading test results on dry sands, Drnevich and Richard [6], Youd [24], and Pyke [16] all concluded that there is a threshold cyclic shear strain, γ_t, of the order of 10^{-2} percent, below which no densification occurs. A value of γ_t of about 10^{-2} percent also correlates rather well with the experimental results for dry sands reported by Silver and Seed [20] as shown in figure 5 and with strain-controlled test results on saturated sands reported by Dobry et al. [5] and Park and Silver [15]. However, figure 5 indicates that the threshold shear strain value for fully saturated sand specimens in this study is about 2×10^{-3} percent when the threshold is determined by the onset of the buildup of the excess pore water pressure in the torsional resonant column test. When the volume change during testing is used to determine the threshold shear strain, γ_t was estimated at about 5×10^{-3} percent as shown in figure 8. In either case, the threshold strain observed in the tests reported herein was smaller than the threshold strains reported in the literature.

Several reasons for the discrepancy are suggested:

(a) Detection of the threshold strain requires sensitive measurements. The measurement of pore water pressure increase in saturated specimens is considered the most sensitive measurement, since large increases in excess pore water pressure are associated with minor volume changes. Measurement of the water volume expelled from a saturated sample, measured to the next 0.1 ml, is a less sensitive measurement than the excess pore water pressure increase, but it is probably still more sensitive than the detection of volume change by the vertical LVDT measurement in a dry sample which was used by Drnevich and Richart [6]. It is reasonable to assume that the more sensitive the measurement, the lower the threshold strain it will detect. This would account for the fact that γ_t measured by the onset of excess pore water pressure development was 2×10^{-3} percent, γ_t associated with the displacement of a measureable volume of water was 5×10^{-3} percent, and γ_t associated with a measurable change in the height of the specimen was 1×10^{-2} percent.

(b) The above reasoning would not explain the threshold strain of 10^{-2} percent measured by Dobry et al. [5], which was determined by very sensitive measurements of excess pore water pressure buildup. However, there is a difference between the loading condition in the torsional resonant column test and that in the triaxial test. The resonant column test involves a reversal of the direction of the shear stress which does not occur in the triaxial test. In addition, Dobry et al. [5] used a limited number of stress cycles (up to 300), while the number of cycles in the resonant column is very high (about 15,000) for a 2 min time period.

(2) Saturation: The B-parameter had a considerable effect on the threshold strain and the pore water pressure buildup, but it had no detectable effect on the volume change as measured by the expelled pore water. This is an indication that even a minor amount of air will have a considerable effect on the excess pore water pressure buildup. Thus, the B-parameter in liquefaction studies should be equal to or higher than 0.95.

(3) The Effect of Magnitudes of Applied Cyclic Stress on the Pore Water Pressure Buildup: As the test data in figure 5 indicate, an application of a large number of torsional stress cycles, which causes an initial shear strain above the threshold strain, does not necessarily lead to liquefaction ($\Delta u \rightarrow \sigma_3$). Rather, the excess pore water pressure will stabilize at a certain level. While there is no satisfactory explanation for this phenomenon at the present time, there are indications that this response is probably attributable to a cyclic strain hardening effect, i.e., after a sufficiently large number of cycles, no volume change occurs. This effect is attributed to particle rearrangement or soil fabric change. Whether this phenomenon can be extrapolated from the test specimen to a field condition is not known at the present time.

REFERENCES

[1] ASTM D2049-69, "Relative Density of Cohesionless Soils," Annual Book of ASTM Standards, Part 19, Soil and Rock; Building Stones.

[2] ASTM D2487-69, "Classification of Soils for Engineering Purposes," Annual Book of ASTM Standards, Part 19, Soil and Rock; Building Stones.

[3] Barkan, D. D. (1962), Dynamics of Bases and Foundations, McGraw-Hill Book Company, Inc., New York.

[4] Crockett, J. H. A. (1966), "Some Practical Aspects of Vibration in Civil Engineering," Symposium on Vibration in Civil Engineering, Butterworths, London, pp. 253-271.

[5] Dobry, R., R. S. Ladd, F. Y. Yokel, R. M. Chung, and D. Powell, (1982), "Prediction of Pore Water Pressures Buildup and Liquefaction of Sands During Earthquakes by the Cyclic Strain Method," National Bureau of Standards, Building Science Series 138, March, 150 p.

[6] Drnevich, V. P. and F. E. Richart, Jr. (1970), "Dynamic Prestraining of Dry Sand," Journal of the SMFD, ASCE, Vol. 96, No. SM2, March, pp. 453-469.

[7] Drnevich, V. P. (1972), "Undrained Cyclic Shear of Saturated Sand," Journal of the SMFD, ASCE, Vol. 98, No. SM8, August, pp. 807-825.

[8] Drnevich, V. P., B. O. Hardin, and D. J. Shippy, (1978), "Modulus and Damping of Soils by Resonant Column Method," ASTM STP 654, Dynamic Geotechnical Testing, pp. 91-125.

[9] Kolbuszewski (1948), "General Investigtaion of the Fundamental Factors Controlling Loose Packing of Sands," Proc. Second Int. Conf. SMFE, Rotterdam, Vol. 7, pp. 47-49.

[10] Ladd, R. S. (1978), "Preparing Test Specimens Using Under Compaction," Geotechnical Testing Journal, ASTM, Vol. 1, No. 1, March, pp. 16-23.

[11] Maslov, N. N. (1957), "Questions of Seismic Stability of Submerged Sandy Foundations and Structures," Proc. Fourth Int. Conf. SMFE, London, England, Vol. 1, pp. 368-372.

[12] Mulilis, J. P., C. K. Chan, and H. B. Seed, (1975), "The Effects of Method of Sample Preparation on the Cyclic Stress-Strain Behavior of Sands," Report No. EERC 75-18, EERC, University of California, Berkeley, July.

[13] Ohsaki, Y. (1966), "Niigata Earthquake, 1964, Bulding Damage and Soil Conditions," Soil and Foundation, Vol. VI, No. 2, pp. 15-37.

[14] Ohsaki, Y. (1969), "The Effect of Local Soil Conditions Upon Earthquake Damage," Proc. Seventh Int. Conf. SMFE, Specialty Session 2, Mexico, pp. 3-32.

[15] Park, T. and M. L. Silver, (1975), "Dynamic Soil Properties Required to Predict the Dynamic Behavior of Elevated Transportation Structures," U.S. DOT Report DOT-TST-75-44, May.

[16] Pyke, R. M. (1973) "Settlement and Liquefaction of Sands Under Multi-Directional Loading," Ph.D. Dissertation, University of California, Berkeley, California.

[17] Ratamal, E. and E. Kausel, (1969) "Vibratory Compaction of the Soil and Tectonic Subsidence During the 1960 Earthquake in Valdevia, Chile," Proc. Fourth World Conf. Earthquake Engineering, Santiago, Chile, Feburary.

[18] Sherif, M. A., I. Ishibashi, and C. Tsuchiya, (1977) "Saturation Effects on Initial Soil Liquefaction," Technical Note, Journal of the GED, ASCE, Vol. 103, No. GT 8, pp. 914-917.

[19] Silver, M. L. and H. B. Seed, (1971) "Deformation Characteristics of Sands Under Cyclic Loading," Journal of the SMFD, ASCE, Vol. 97, No. SM8, pp. 1081-1098.

[20] Silver, M. L. and H. B. Seed, (1971) "Volume Change in Sands During Cyclic Loading," Journal of the SMFD, ASCE, Vol. 97, No. SM9, pp. 1171-1182.

[21] Silver, M. L. (1977), "Laboratory Triaxial Testing Procedures to Determine the Cyclic Strength of Soils," NUREG-0031, NRC-6.

[22] Skempton, A. W. (1954), "The Pore Pressure Coefficients A and B," Geotechnique, Vol. 4, pp. 143-147.

[23] Yoshimi, Y and K. Tokimatsu, (1977), "Settlement of Buildings on Saturated Sand During Earthquakes," Soils and Foundations, Vol. 17, No. 1, March, pp. 23-38.

[24] Youd, T. L., (1972) "Compaction of Sands by Repeated Shear Straining," Journal of the SMFD, ASCE, Vol. 98, No. SM7, July, pp. 709-725.

Table 1. Index Properties for Monterey No. 0 Sand, Mulilis, et al. (1975) [12]

Unified Soil Classification System Group Symbol	SP
Mean Specific Gravity	2.65
Particle Size Distribution Data	
D_{50}[1/], mm	0.36
C_c[2/]	0.90
C_u[3/]	1.50
Dry Density Data	
Maximum, kg/m^3	1693.15
Minimum, kg/m^3	1430.45

Notes:

1. D_{50}, mean grain size
2. $C_c = (D_{30})^2/(D_{60} \times D_{10})$, coefficient of curvature
3. $C_u = D_{60}/D_{10}$, coefficient of uniformity

Table 2. Summary of Resonant Column Tests With Pore Water Pressure Measurement

Specimen	Dry Unit Weight	Relative Density	Voil Ratio	B-Value
	kg/m^3	%	e	
M - 2	1577	60.0	0.676	
M - 3	1575	59.3	0.678	0.30
M - 4	1573	58.5	0.680	0.93
M - 5	1576	59.6	0.677	0.90
M - 6	1576	59.6	0.677	0.82
M - 7	1575	59.3	0.678	0.96

Notes:

(1) All specimens are hollow cylindrical in shape

(2) All specimens were prepared using a moist tamping method except specimen M-7, which was prepared by dry tapping method

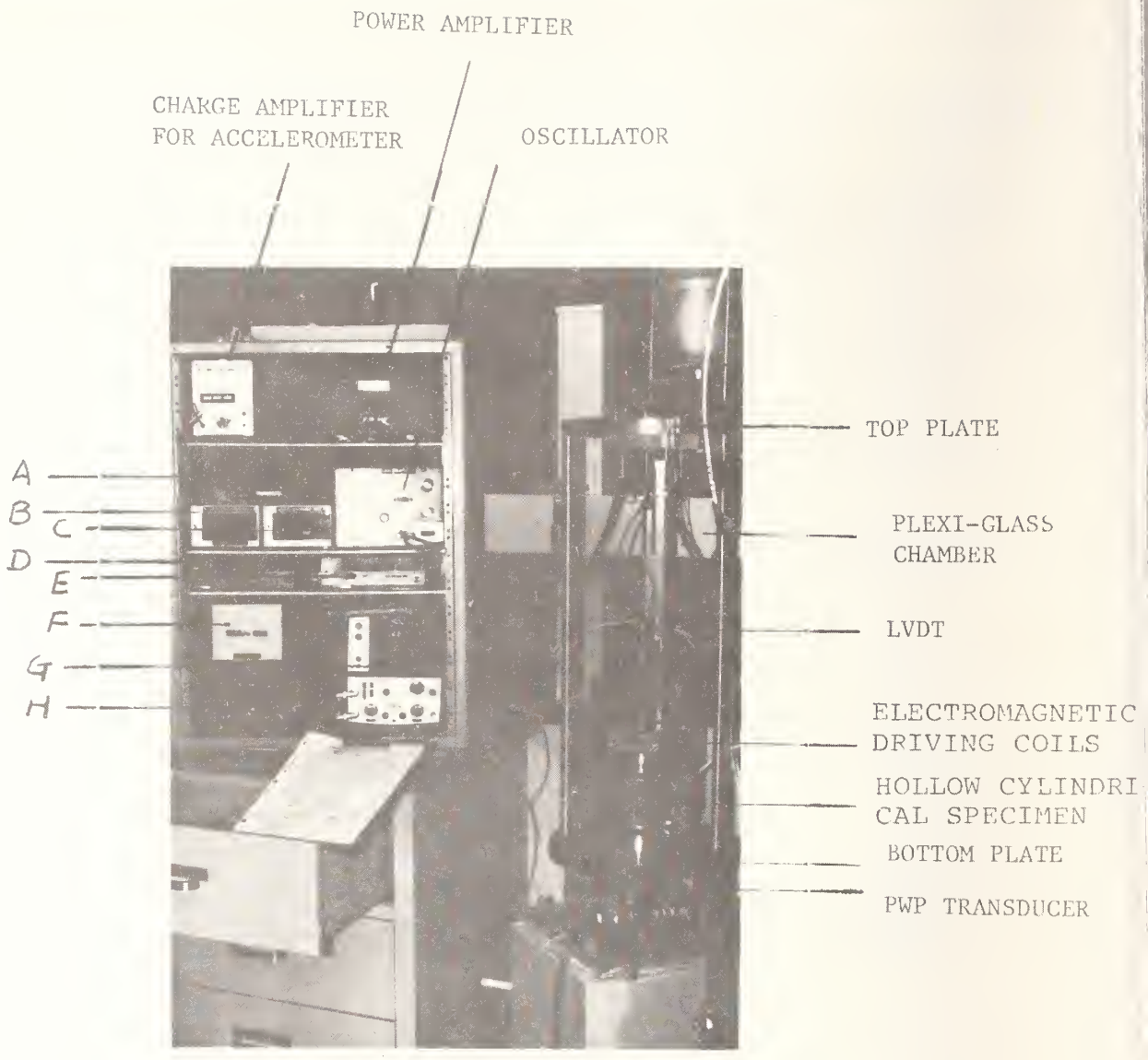

A. CLOCK

B. DIGITAL READOUT FOR LVDT

C. DIGITAL READOUT FOR PORE WATER PRESSURE

D. DIGITAL READOUT FOR TORSIONAL EXCITATION FORCE AND ROTATIONAL TRANSDUCER OUTPUT

E DIGITAL FREQUENCY METER

F. MAIN SWITCH

G OSCILLOSCOPE

H. CONTROL BOX

Figure 1. Resonant column test set-up

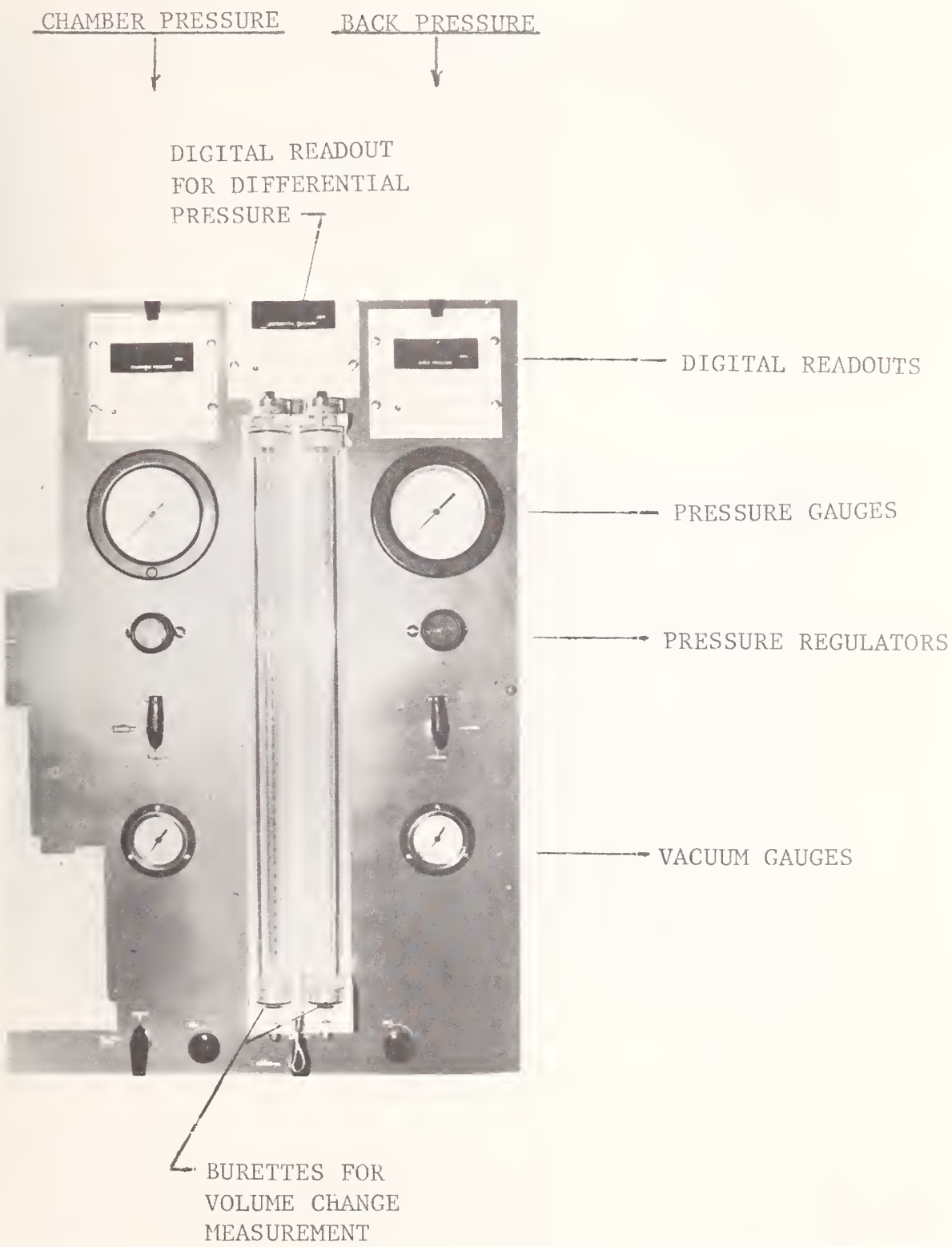

Figure 2. Panel for pressure control and volume change measurement

Figure 3. Top view of a hollow cylindrical specimen constructed between the inner and outer molds

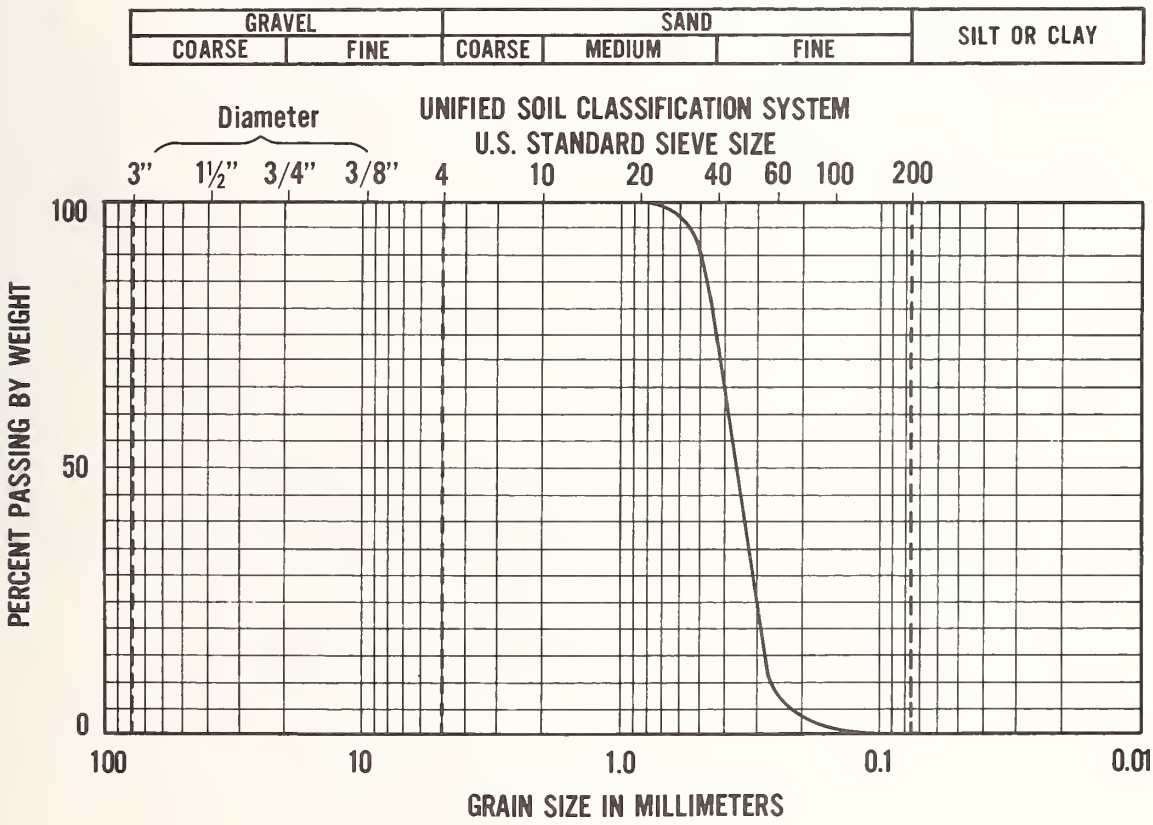

Figure 4. Grain size distribution of Monterey No. 0 sand [12]

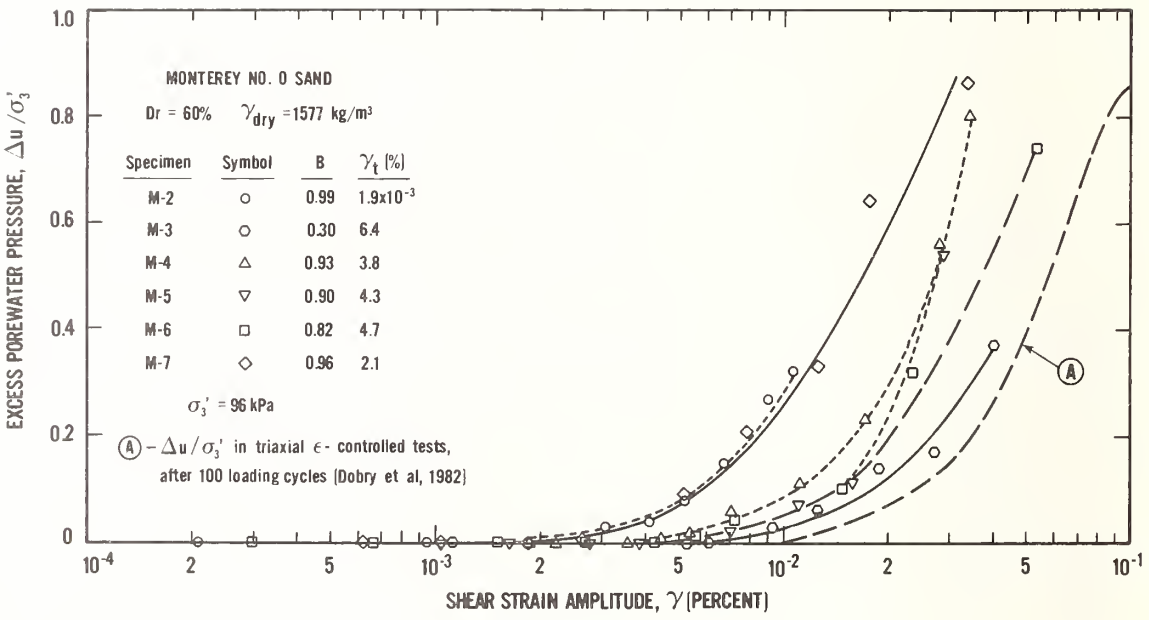

Figure 5. Excess pore water pressure as a function of shear strain amplitude

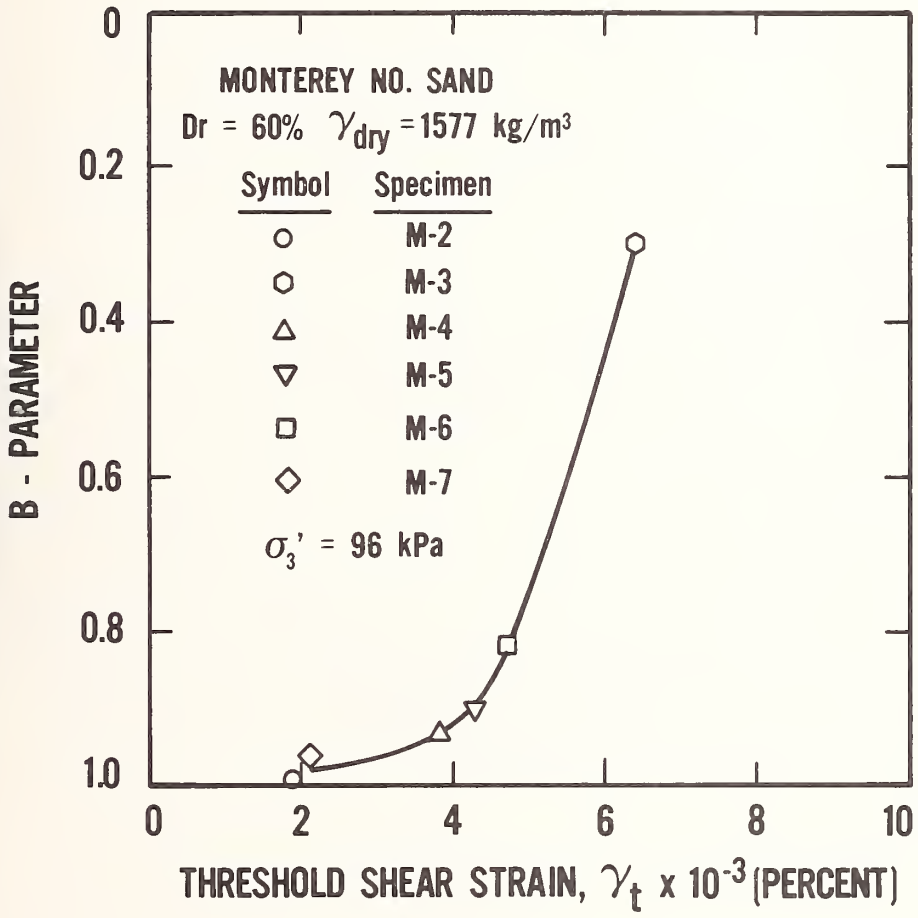

Figure 6. Threshold shear strain as a function of B-parameter

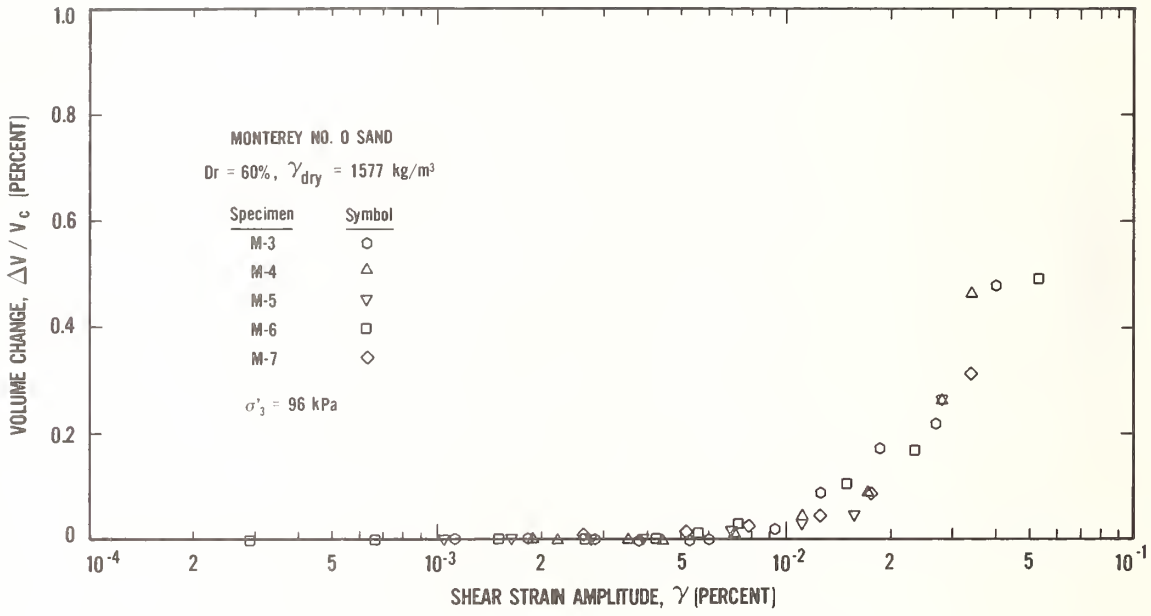

Figure 7. Volume change as a function of shear strain amplitude

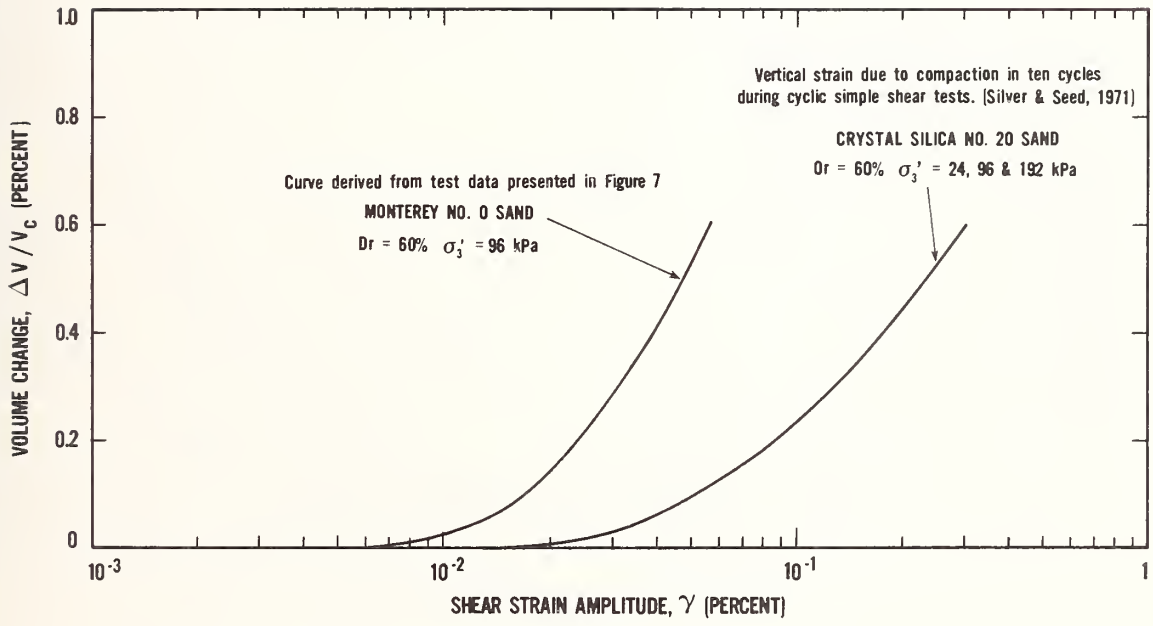

Figure 8. Comparison of volume change between dry and saturated sand specimen testing

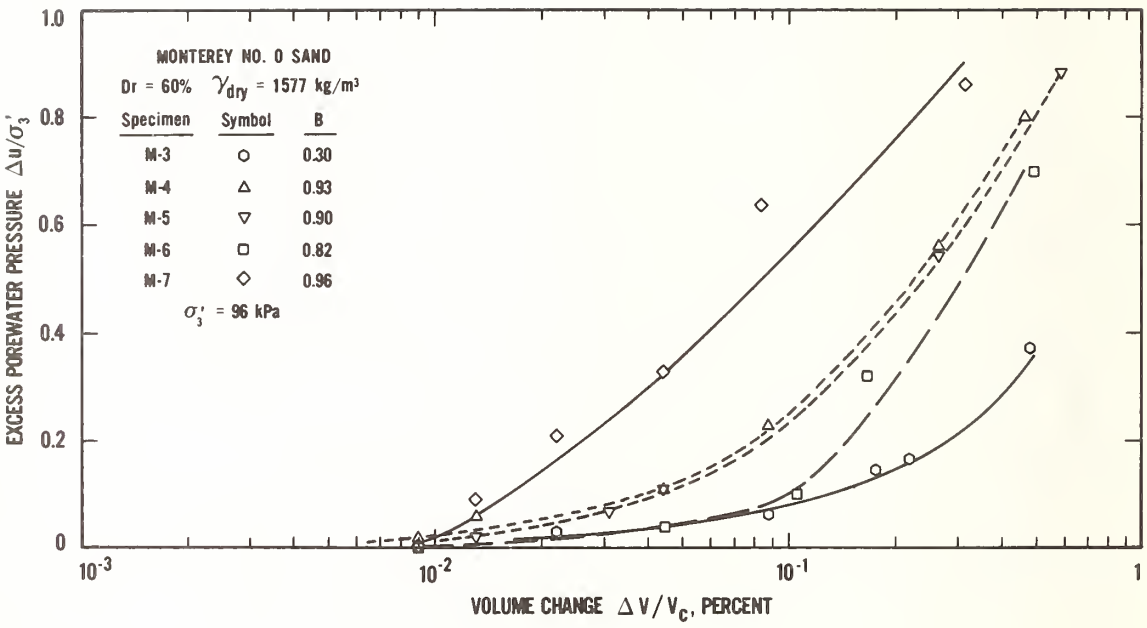

Figure 9. Volume change as a function of excess pore water pressure

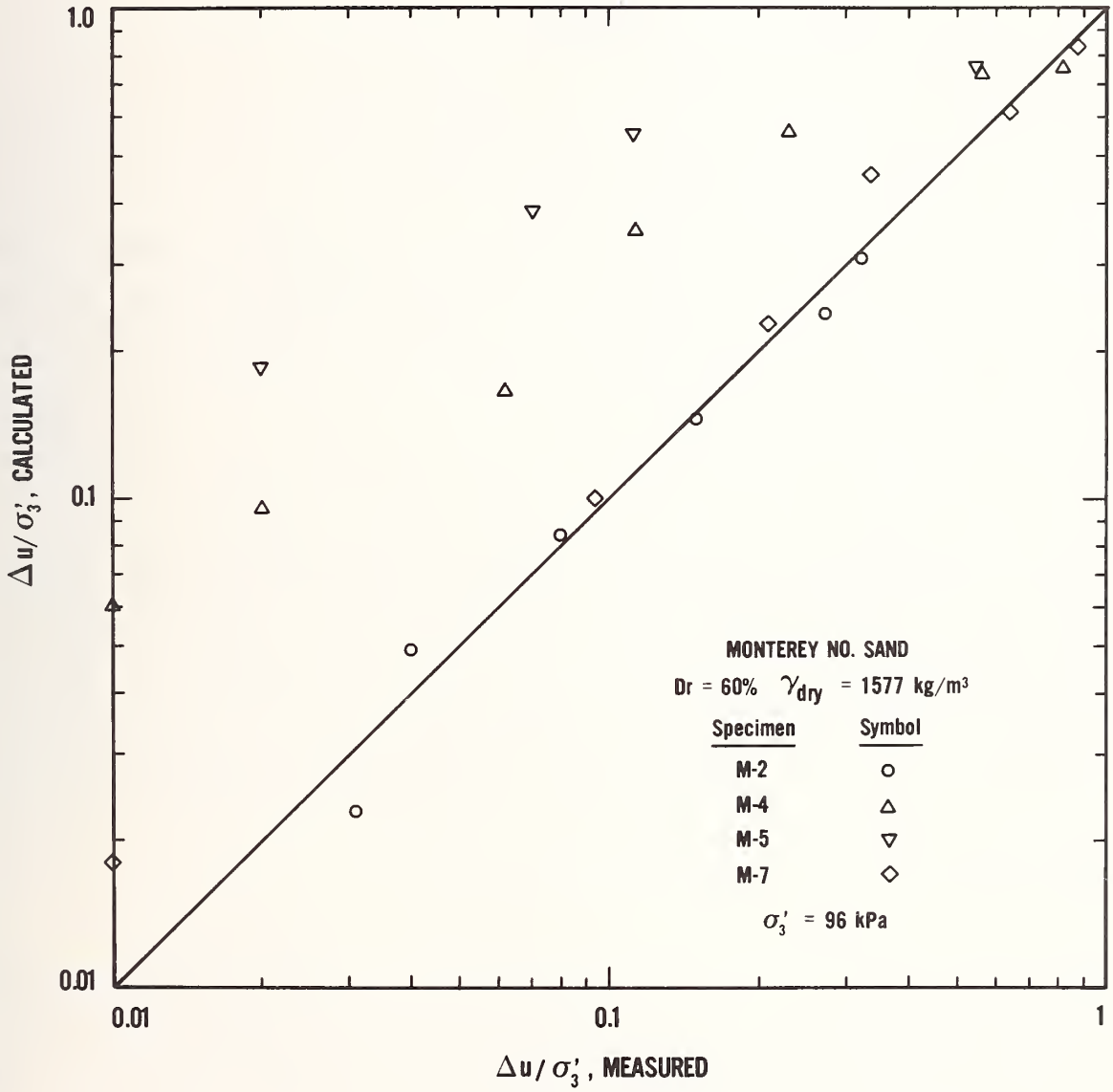

Figure 10. Calculated excess pore water pressure ratio versus measured excess pore water pressure ratio

ESTIMATION PROCEDURES OF LIQUEFACTION POTENTIAL AND ITS APPLICATION TO EARTHQUAKE RESISTANT DESIGN

Toshio Iwasaki
Tadashi Arakawa
Ken-ichi Tokida
Toshio Kimata

Earthquake Disaster Prevention Department
Public Works Research Institute
Ministry of Construction

INTRODUCTION

Simplified methods to evaluate the effects of saturated sandy, soils are needed for the reasonable earthquake resistant design of structures considering soil liquefaction. Iwasaki et al., (1978), proposed two simplified methods which use a liquefaction resistance factor F_L and a liquefaction potential index I_L to evaluate the liquefaction potential of saturated sandy soils. Based on these proposed methods, the liquefaction potential can be estimated simply by using the fundamental properties of soils, i.e., N-values from the Standard Penetration Test, unit weights, mean particle diameters, and the maximum acceleration at the ground surface.

In this paper, the two simplified methods are first introduced, and to prove the effectiveness of the proposed methods, the values of both F_L and I_L at 64 liquefied sites and 23 non-liquefied sites during past six earthquakes are calculated according to these simplified methods. Also, shaking table tests on soil liquefaction are carried out for the saturated sandy model ground. Furthermore, several application methods using the factor F_L, the excess pore water pressure induced in the saturated sandy soils and the effects of soil liquefaction on the resistance properties of the soils surrounding structures are described. Finally, some case studies on earthquake resistant properties of civil engineering structures considering soil liquefaction are carried out according to the proposed procedures on soil liquefaction properties.

SIMPLIFIED METHODS

LIQUEFACTION RESISTANCE FACTOR (F_L)

The ability of a soil element at an arbitrary depth to resist the liquefaction may be expressed by the liquefaction resistance factor (F_L) identified by Eq. (1).

$$F_L = \frac{R}{L} \tag{1}$$

When the factor F_L of a certain soil is less than 1.0, the soil is judged to liquefy during an earthquake.

R in Eq. (1) is the in-situ resistance or undrained cyclic strength of a soil element to dynamic loads during the earthquake, and can be simply evaluated according to numerous undrained cyclic shear test results using undistributed specimens as follows,

for $0.04 \text{ mm} \leq D_{50} \leq 0.6 \text{ mm}$

$$R = 0.0882 \sqrt{\frac{N}{\sigma_v' + 0.7}} + 0.225 \log_{10} \frac{0.35}{D_{50}} \tag{2a}$$

for $0.6 \text{ mm} < D_{50} \leq 1.5 \text{ mm}$

$$R = 0.882 \sqrt{\frac{N}{\sigma_v' + 0.7}} - 0.05 \tag{2b}$$

where N is the number of blows from the Standard Penetration Test, σ_v' is the effective overburden pressure (in kg/cm^2), and D_{50} is the mean particle diameter (in mm).

L in Eq. (1) is the dynamic load induced in the soil element by a seismic motion, and can be simply estimated by

$$L = \frac{\tau_{max}}{\sigma_v'} = \frac{\alpha_{s\,max}}{g} \cdot \frac{\sigma_v}{\sigma_v'} \cdot r_d \tag{3}$$

where τ_{max} is the maximum shear stress (in kg/cm^2), $\alpha_{s\,max}$ is the maximum acceleration at the ground surface (in gals), g is the acceleration of gravity (=980 gals), σ_v is the total overburden pressure in (kgf/cm^2), and r_d is the reduction factor of dynamic shear stress to account for the deformation of the ground. From a number of seismic response analyses for soils, Iwasaki et al., (1978) proposed the following relation for the factor r_d.

$$r_d = 1.0 - 0.15Z \tag{4}$$

where Z is the depth in meters.

LIQUEFACTION POTENTIAL INDEX (I_L)

The ability to resist liquefaction at a given depth of soil can be evaluated by the factor F_L. However, the damage to structures due to soil liquefaction is affected considerably by the size of the earthquake and the extent of the liquefaction. In view of this fact, Iwasaki et al., (1978) also proposed the liquefaction potential index (I_L) defined by Eq. (5) to estimate the severity of liquefaction at a given site.

$$I_L = \int_0^{20} F \cdot W(Z) dz \tag{5}$$

where $F=1-F_L$ for $F_L \leq 1.0$ and $F=0$ for $F_L \geq 1.0$, and $W(Z)=10-0.5Z$ (Z in meters) as shown in figure 1. W(Z) accounts for the degree of soil liquefaction according to the depth, and the triangular shape of W(Z) and the depth of 20 meters are used based on observations in liquefaction phenomena during past earthquakes. For the case of $F_L=0$ for the entire depth, I_L becomes 100, being the highest, and for the case of $F \geq 1.0$ for the entire depth, I_L becomes 0 being the lowest.

CASE STUDIES ON F_L AND I_L FOR PAST EARTHQUAKES

Both the liquefaction resistance factor F_L and the liquefaction potential index I_L were calculated using the proposed methods for 64 liquefied sites and 23 non-liquefied sites where geotechnical information was available during six earthquakes. These earthquakes were: the Nobi Earthquake of 1891 (Magnitude=8.0), the Tonankai Earthquake of 1944 (M=8.0), the Fukui Earthquake of 1948 (M=7.8), the Niigata Earthquake of 1964 (M=7.5), the Tokachi-oki Earthquake of 1968 (M=7.9), and the Miyagi-ken-oki Earthquake of 1978 (M=7.4). According to these results, the properties of both F_L and I_L were investigated. The liquefied sites and the non-liquefied sites for the case studies are summarized in table 1(A) and (B), respectively.

CHARACTERISTICS OF THE FACTOR F_L

Figures 2(A) and 2(B) show typical calculation results of F_L with depth at a liquefied site and a non-liquefied site, respectively. It can be seen that F_L is mostly less than 1.0 for the liquefied layers, and greater than 1.0 for the non-liquefied layers.

F_L-values with depth at all liquefied and non-liquefied sites in the Niigata Earthquake (see table 1) are summarized in figure 3. In this figure the liquefied layers are estimated based on damage to structures (see figure 2(A)). It can be also seen that F_L is mostly less than 1.0 for the liquefied layers and the liquefied layers are likely to be situated at the depth of about 10 meters or shallower.

Figure 4 shows the frequency and the accumulative incidences of F_L-values calculated for both liquefied and non-liquefied layers at all sites in table 1. According to figure 4, it is found that the distribution of F_L at the liquefied layers is very different from that at the non-liquefied layers. At the liquefied layers most (about 87 percent) of F_L-values distribute in the range less than 1.0, while at the non-liquefied layers most (about 85 percent) of F_L-values distribute in the range more than 1.0. However, it must also be noticed that about 13 percent of the F_L-values exceed 1.0 at the liquefied layers and about 15 percent of the F_L-values are less than 1.0 at the non-liquefied layers.

APPLICATION OF THE SIMPLIFIED METHOD TO AN IN-SITU SITE

In this paper one example is introduced of the application of the simplified method based on the factor F_L for an in-situ liquefied site during a past earthquake. The Yuriage-kami Dyke along the Natori River was damaged by the Miyagi-ken-oki Earthquake of 1978 and sand boils were observed at numerous points near the Dyke shown in figure 5. After the earthquake, detail investigations on soil liquefaction were carried out at both the liquefied and the non-liquefied points, i.e., the liquefied points Y-1 and Y-2, and non-liquefied points Y-3 and Y-4, are shown in figure 5.

Figure 6 illustrates the soil profiles, N-values, D_{50} and F_L-values at the liquefied points (Y-1, Y-2) and the non-liquefied point (Y-3). At this site, both the simplified analyses and the detailed analyses are carried out to calculate the F_L-values with depth. In the simplified analyses, three levels of maximum ground surface accelerations i.e., 180, 240 and 300 (gals) are supposed, in view of the measured strong-motion records nearby. In the detailed analyses, the ground acceleration recorded on the rocky layer during this earthquake is used as input at the estimated base. A maximum acceleration of 150 gals is assumed. From figure 6, it is found that the soil liquefaction occurred at the points which had F_L-values almost less than 1.0. In this way it is shown from the in-situ investigations that the liquefaction resistance factor F_L is effective to evaluate the liquefaction potential of saturated, sandy soils.

CHARACTERISTICS OF THE INDEX I_L

Figure 7 summarizes both the relation between the number of cases and I_L, and the relation between the accumulative percentages and I_L, at all liquefied and non-liquefied sites in table 1. Figure 7 shows that I_L for liquefied sites seems to be higher than those at non-liquefied sites, i.e., for non-liquefied sites I_L is generally less than 15 and the percentage that I_L is less than 5 is about 70 percent. On the other hand, for liquefied sites, the percentage that I_L is less than 5 is only about 20 percent and at about 50 of the sites, I_L is more than 15. From these results, the following simplified procedure for assessing soil liquefaction based on the index I_L may be proposed as a preliminary guideline:

$I_L = 0$: Liquefaction risk is very low,

$0 < I_L \leq 5$: Liquefaction risk is low,

$5 < I_L \leq 15$: Liquefaction risk is high,

$15 < I_L$: Liquefaction risk is very high.

From the above, it is shown that the index I_L, may be used reasonably to assess the liquefaction potential at a given site.

SHAKING TABLE TESTS ON SOIL LIQUEFACTION

Shaking table tests were carried out to clarify: a) the properties of soil liquefaction, b) the effects of soil liquefaction on structural foundations, and c) the effectiveness of the proposed liquefaction resistance factor, F_L. A loose saturated sand ground model 0.95 m deep, 6 m long and 3m wide was prepared on a shaking table, and four kinds of pile foundation models were set up in the sand, as shown in figure 8. In the tests, the table was excited with sinusoidal motion at a constant frequency of 7 Hz, and the input table accelerations ranged from 30 gals to 250 gals, as listed in table 2. Accelerations and pore water pressures were measured in the sand. Accelerations, displacements and earth pressures of the pile models were also observed.

Figure 9 is an example of test results, i.e., the distribution of a degree of soil liquefaction and the time history for test 2. The degree of soil liquefaction is defined by the factor L_u,

$$L_u = \Delta u/\sigma'_v \tag{6}$$

where Δu is the excess pore water pressure. Sands with L_u of 1.0 are assumed to completely liquefy. From figure 9 it appears that soil liquefaction spreads from the surface to the bottom of the ground gradually.

Figure 10 shows the relationship between the top displacement of the pile model (Model-2) and the degree of soil liquefaction with depth as defined by H_L/H_0 (where H_L is proportional to the area completely liquefied, and H_0 is proportional to the thickness of the ground model). When the ratio H_L/H_0 becomes 1.0, the entire ground is liquefied. It is seen that the displacement of the pile tends to increase as H_L/H_0 increases.

Figures 11 and 12 show the typical relationships between accelerations, pore water pressures and F_L-values for non-liquefied cases and liquefied cases, respectively. In these figures, F_L-values are estimated by Eqs. (2) and (3). It is found that F_L-values decrease according to the increase of pore water pressures, and that F_L-values are less than 1.0 for the liquefied layers and are higher than 1.0 for the non-liquefied layers.

Figure 13 summarizes the relation between F_L and L_u for the liquefied layers. From this figure, it is seen that F_L decreases as L_u increases and that F_L is less than 1.0 for L_u of 0.5 or higher and is more than 1.0 for L_u of 0.5 or lower. Furthermore, figure 13 illustrates that the sand layers are likely to completely liquefy when F_L decreases to less than 0.6

From these shaking table tests, it is shown that the proposed factor F_L may be used adequately to estimate soil liquefaction potential of saturated sand layers.

METHODS FOR EVALUATING EFFECTS OF LIQUEFACTION

The effects of soil liquefaction on structures are required to be clarified quantitatively for establishing the earthquake resistant design of concrete structures. In this section, several methods using the factor F_L are introduced to evaluate the effects of soil liquefaction quantitatively.

PROBABILITY OF SOIL LIQUEFACTION

It is shown in figure 4 that for a certain value of F_L both possibilities of liquefaction and non-liquefaction may be expected. Therefore, an estimate is needed to determine the probability of soil liquefaction for a certain F_L-value. Figure 14 shows the relation between the probability of liquefaction or non-liquefaction and F_L, estimated from the results in figure 4. In figure 4, 500 cases for both liquefied and non-liquefied layers have been collected. From this figure, the probability of liquefaction or non-liquefaction can be estimated using the F_L-value. For example, the probability of liquefaction for F_L-value of 1.0 is about 50 percent and that for a F_L-value less than about 0.6 is almost 100 percent.

PORE WATER PRESSURE

Excess pore water pressures generated in sand layers are very important in soil liquefaction studies. In this paragraph, the simplified procedures for evaluating excess pore water pressure using a F_L-value are introduced.

Dynamic Soil Tests

From dynamic triaxial tests on the cyclic strength for soil liquefaction, a typical relation between the shear stress ratio τ/σ_v' (τ:shear stress) and the number of cycles N_1 to generate liquefaction is shown in figure 15, and the relation is approximately given by Eq. (7),

$$(\tau/\sigma_v') = aN_1^b \tag{7}$$

where constant values, a and b are decided based on the dynamic triaxial tests as shown in figure 15. If liquefaction is assumed to occur for the cyclic strength R with the number of cycles N_R and for the dynamic load L with the number of cycles N_L, the relations on both R and L may be obtained from equations (8a) and (8b), respectively,

$$R = (\tau_R/\sigma_v') = aN_R^b \tag{8a}$$

$$L = (\tau_L/\sigma_v') = aN_L^b \tag{8b}$$

where τ_R and τ_L are the shear strength and the shear load, respectively. From Eqs. (1), (8a) and (8b), the following relation is obtained.

$$F_L = (N_R/N_L)^b \tag{9}$$

On the other hand, the relationships between $\Delta u/\sigma_v'$ and N/N_1 (N, N_1: number of cycles before liquefaction and that at complete liquefaction, respectively) are obtained, for example, as shown in figure 16. Because N_R and N_L are regarded as N and N_1, respectively, the following relation can be assumed.

$$(N_R/N_L) = (N/N_1) \tag{10}$$

Combining Eqs. (9) and (10), we obtain

$$(N/N_1) = (F_L)^{1/b} \tag{11}$$

Therefore, the pore water pressure can be estimated by the factor F_L as follows, according to the test results shown in figure 16.

$$(\Delta u/\sigma_v') \simeq (N/N_1) = (F_L)^{1/b} \tag{12}$$

Shaking Table Tests

Pore water pressures can be estimated by the factor F_L based on shaking table tests, i.e., by using the relation shown in figure 13.

Relation Between Pore Water Pressure and F_L

Figure 17 summarizes the relationship between pore water pressure and F_L according to the proposed methods, i.e., dynamic soil tests and shaking table tests. From this figure, pore water pressure can be simply evaluated from the F_L-values.

PROPERTIES OF LIQUEFIED SAND LAYER

For establishing a reasonable method of earthquake resistant design of structures considering soil liquefaction, it is important to clarify the properties of liquefied sand layers. For the purpose of estimating the lateral bearing properties of liquefied sand layers quantitatively, simple static loading tests are carried out.

Figure 18 shows the outline of the test apparatus. The saturated sand specimens are consolidated by the air pressure through the rolling diaphgram seal. In the center of the rolling diaphgram seal, a loading plate (6 cm in diameter) is connected. The specimens are consolidated by two values of confining pressure (σ_v'), i.e., 0.5 and 1.0 (kgf/cm^2), and after three-hours of consolidation the excess pore water pressures (Δu) are induced into the specimen. The ratio of the pore water pressure to the confining pressure is changed from 0 to 0.95 continuously. Under a certain induced ratio the static loading test is carried out, and the static load and the displacement of the loading plate are measured.

Figure 19 shows a typical test result, i.e., the relation between the static load P (in kgf) and the displacement δ (in mm), according to the different ratios of pore water pressure. From this figure it is found that the bearing capacity of the soil specimen is affected by the increase of pore water pressure.

Figure 20 summarizes the results of the overall tests. In this figure the bearing coefficient (coefficient of subgrade reaction, Ed.) of the soil is defined by

$$K = P/(A \cdot \delta) \tag{13}$$

where K is a bearing coefficient (in $kgf/cm^2/mm$) and A is the an area of the loading plate (in cm^2). From this figure it is found that the bearing coefficient of the soil decreases with an increase of the pore water pressure.

Figure 21 shows the relation between K/K_0 and L_u based on the results in figure 20. K_0 is the bearing coefficient when pore water pressure equals zero. From this figure the degree of decrease of the bearing coefficient of the soil induced by liquefaction can be quantitatively evaluated from a degree of soil liquefaction.

From the test results in figure 13, the relation between the value of F_L and L_u can be assumed as follows:

$$\left\{\begin{array}{llll} & F_L \leqq 0.6, & & L_u < 1.0 \\ 0.6 < & F_L \leqq 0.8, & 0.9 \leqq & L_u < 1.0 \\ 0.8 < & F_L \leqq 1.0, & 0.5 \leqq & L_u < 0.9 \\ 1.0 < & F_L \quad , & & L_u < 0.5 \end{array}\right\} \tag{14}$$

Thus, the average relation between K/K_0 and L_u may be proposed as the four stages shown in figure 21 after considering the test results and the relation in Eq. (14). The relation between F_L and K/K_0 can be approximately estimated as

$$\left\{\begin{array}{lll} & F_L \leqq 0.6, & K/K_0 = 0 \\ 0.6 < & F_L \leqq 0.8, & K/K_0 = 1/3 \\ 0.8 < & F_L \leqq 1.0, & K/K_0 = 2/3 \\ 1.0 < & F_L \quad , & K/K_0 = 1 \end{array}\right\} \tag{15}$$

The results of the above-mentioned approach on the resistance of liquefied sand layers were already applied to the actual design of a highway bridge (Japan Road Assocation) as shown in table 3. In this table the reduction factor D_E is equivalent to K/K_0.

CASE STUDIES ON EARTHQUAKE RESISTANT PROPERTIES FOR STRUCTURES CONSIDERING LIQUEFACTION

Earthquake resistant designs of structures considering soil liquefaction are very important. In this section the results of case studies on earthquake resistant properties for typical structures, i.e., Showa Bridge and Yuriage-kami River Dyke using the simplified procedures on soil liquefaction introduced in previous sections are introduced to investigate the effects of soil liquefaction during earthquakes.

SHOWA BRIDGE

The Showa Bridge was damaged during the Niigata Earthquake in 1964, i.e., the five simple girders fell into the water as shown in figure 22. One of the causes of the damage is presumed to be the surrounding ground liquefaction. The effects of soil liquefaction to the earthquake response properties of the bridge are investigated during the results shown in table 3.

The investigation is carried out for one of the piers of the bridge, i.e., Pier 5 (see figure 22). Figure 23 shows the outline of the substructure for both before and after the earthquake and the results of assessing soil liquefaction using F_L-values. After the earthquake, all substructures were reinforced as shown in figure 23. According to the F_L-values with depth, the ground surrounding Pier 5 is estimated to have been liquefied at a depth of about 10 meters or shallower.

The earthquake response properties of Pier 5 under the conditions for both before and after the earthquake are calculated by using the Seismic Coefficient Method. The input design horizontal seismic coefficients K_h are 0.15, 0.20 and 0.25. In the calculation, the lateral bearing coefficients of ground, i.e., k (kgf/cm^3) at the depth of $1/\beta$ (in meter) [$\beta = \sqrt[4]{kD/4EI}$, k: Lateral Bearing Coefficient (in tf/m^3), D: Diameter of Pile (in meter), E: Elastic Modulus (in t/m^2), I: Moment of Inertia of Pile (in m^4)] are changed according to the degree of soil liquefaction. The degree of soil liquefaction is presumed to be equivalent to the reduction factor D_E identified in table 3 and the input reduction factors are 1, 2/3, 1/3 and 0.

Figure 24 summarizes the relationships between the calculated maximum displacement of the top of Pier 5, i.e., (cm) and the reduction factor or the lateral bearing coefficient of the ground. From this figure, it is found that the displacements of the substructure increase according to the decrease of the D_E-value or k-value, i.e., the increase of the degree of soil liquefaction, and increase remarkably when the bearing capacities decrease almost to zero. It can also be seen that the displacement of the substructure decreases by adding reinforcement.

From the above discussion, it is obvious that effects of soil liquefaction are very important in the earthquake resistant design of bridges.

YURIAGE-KAMI RIVER DYKE

The Yuriage-kami River Dyke was damaged during the Miyagi-ken-oki Earthquake in 1978 as shown in figure 5. The river dyke near the point Y-1 was damaged severely and yet at the points Y-3 and Y-4, the river dyke was not damaged. In this paragraph the analytical results on the stability for both the damaged river dyke and the non-damaged river dyke considering the excess pore water pressure induced by the earthquake are introduced.

The excess pore water pressure is estimated simply by using equation (12). The distribution of F_L-values must be estimated in order to use equation (12). In this example, the F_L-values are calculated in detail, i.e., the in-situ resistance R and dynamic load L in equation (1) are estimated from the dynamic triaxial tests and from the finite element analyses, respectively.

Figure 25 shows the distribution of F_L-values in the sandy soils calculated at both the damaged river dyke and the non-damaged portion. Comparing the results for both sites, it can be seen that the area whose F_L-values are less than 1.0 is larger at the damaged river dyke than that at the non-damaged one.

Figure 26 shows the distribution of the excess pore water pressure (Δu) which is calculated based on the results in figure 25 at both the damaged river dyke and the non-damaged one. From this figure, the magnitude of the excess pore water pressure at the damaged river dyke seems to be larger than that at the non-damaged one.

The stability analyses of the river dykes are conducted using the Friction Circle Method to obtain the minimum safety factor F_S. The horizontal seismic coefficients (K_h) used are 0.0 (i.e., before earthquake), 0.15 and 0.2. Furthermore, the effects of soil liquefaction, i.e., the excess pore water pressure calculated in figure 26, to the stability of river dykes are also investigated. Figure 27 summarizes the relationship between the minimum safety factor F_S and the horizontal seismic coefficient considering the excess pore water pressure, Δu. It is found that the factor F_S considering the occurrence of excess pore water pressure decreases and the factors F_S at the damaged river dyke, i.e., the point Y-1 are less than the ones at the non-damaged river dyke, i.e., the points Y-3 and Y-4 with respect to the excess pore water pressure.

From the above, it is also obvious that the excess pore water pressure induced during earthquakes is also a very important factor in the stability of soil structures.

CONCLUSIONS

Two simplified methods based on the liquefaction resistance factor F_L and the liquefaction potential index I_L are proposed to assess the liquefaction potential. From these studies, it is found that the F_L-value is mostly less than 1.0 for liquefied layers and greater than 1.0 for non-

liquefied layers. The F_L-value is a very useful factor to estimate the soil liquefaction for a given layer. It is also found that the I_L-value at liquefied sites differs noticeably from those at non-liquefied sites and seems to be a useful index to assess the liquefaction potential at a given site.

From the experimental tests, it is also shown that the effects of liquefaction can be reasonably assessed by F_L-values.

The importance of the effects of soil liquefaction during earthquakes to the earthquake response properties of structures is also clarified.

ACKNOWLEDGMENTS

The studies described above were greatly assisted by Dr. Toshio Iwasaki at the Earthquake Engineering Division of Public Works Research Institute, Professor Fumio Tatsuoka at the Institute of Industrial Science, the University of Tokyo, Dr. Susumu Yasuda at Kiso-jiban Consultants Co., Ltd., and Mr. Seiichi Yoshida, Former Assistant Researcher at the Public Works Research Institute. The authors wish to express sincere thanks to these four individuals.

REFERENCES

1. Iwasaki, T., Tatsuoka, F., Tokida, K., and Yasuda, S. (1978), "A Practical Method for Assessing Soil Liquefaction Potential Based on Case Studies at Various Sites in Japan," 2nd International Conference on Microzonation for Safer Construction Research and Application.
2. Iwasaki, T. and Tokida, K. (1980), "Studies on Soil Liquefaction Observed During the Miyagi-ken-oki Earthquake of June 12, 1978," Proc., 7th World Conference on Earthquake Engineering.
3. Iwasaki, I. and Tokida, K. (1981), "Soil Liquefaction Potential Evaluation with Use of the Simplified Procedures," Proc., International Conference on Recent Advances in Geotechnical Earthquake Engineering and Soil Dynamics.
4. Iwasaki, T., Arakawa, T., and Tokida, K. (1982), "Simplified Procedures for Assessing Soil Liquefaction During Earthquakes," Proc., International Conference on Soil Dynamics and Earthquake Engineering.
5. Japan Road Association (1980), "Specifications for Highway Bridges, Part V, Earthquake Resistant Design," (in Japanese).
6. Kuribayashi, E. and Tatsuoka, F. (1975), "Brief Review of Liquefaction During Earthquakes in Japan," Soils and Foundations, Vol. 15, No. 4.
7. Tatsuoka, F., Iwasaki, T., Tokida, K., Yasuda, S., Hirose, M., Imai, T., and Kon-no, M. (1980), "Standard Penetration Tests and Soil Liquefaction Potential Evaluation," Soils and Foundations, Vol. 20, No. 4.

Table 1 Sites for Analysis of Soil Liquefaction Evaluation

(A) Liquefied Sitea

No.	Site			Earthquake	Ref.
1	Shinano River	1	Niigata City	Niigata, 1964, M=7.5	
2	Railroad Bridge	2			
3	Higashi-Kosen Bridge	Br. 1			(3)
4		Be. 2			
5		Br. 4			
6	Bandai Bridge	Br. 6			
7	Yachiyo Bridge	Br. 1			
8		Br. 5			
9		Br. 7			
10	Shin-Matauhama Bri.	Br. 2			
11	Taihei Bridge	Br. 1			
12		Br. 2			
13	Showa Bridge	Br. 1			
14		Br. 2			
15		Br. 3			
16		Br. 2			
17		Br. 3			
18	Niigata Airport				(4)
19	Sekiya				
20	Niigata Railroad Hospital	Br. 1			(1)
21		Br. 2			
22		Br. 1			
23		Br. 2			
24	Kawagishi-Cho	Br. 1			(5)
25		Br. 2			
26		Br. 3			
27		Br. 4			
28	Kawagishi-Cho	BC21-2			(1)
29		BC21-3			
30		BC104			
31		BC14			
32	Nanae Beach	Br. 1	Hakodate City	Tokach-Oki, 1968, M=7.9	(6)
33		Br. 2			
34		Br. 3			
35	Hachinohe City				(7)
36	Gifu City		Gifu Pref.	Nobi, 1891, M=8.0	(2)
37	Unuma	Kagamigahara			
38	Ogaaeike				
39	Mangoku, Ohgaki				
40	Meikodori		Nagoya City	Tonankai, 1944, M=8.0	
41	Kohmei				
42	Inaei				
43	Takaya 45		Fukui Pref.	Fukui, 1948, M=7.3	
44	Maruoka No. 2				
45	Takaya 2-168				
46	Abukuma Bridge	Br. 4	Miyagi Pref.	Miyagi-ken-Oki, 1978, M=7.4	(8)
47	Mouth of Abukuma River				
48	Yuriage-Kami	Y - 1			
49	"	Y - 2			
50	Yuriage Bridge	No. 1			
51	"	No. 2			
52	"	No. 3			
53	Yamazaki				
54	Oiri (1)				
55	"	No. 2			
56	Uomachi	B - 1			
57	"	B - 2			
58	Rifu	No. 12			
59	Shiomi	No. 1			
60	"	No. 2			
61	"	No. 3			
62	Nakamura	N - 4			
63	"	N - 5			
64	Wabuchi	W - 2			

(B) Non-Liquefied Sites

No.	Site			Earthquake	Ref.
1	Jindoji		Niigata City	Niigata, 1964, M=7.5	(3)
2	Kogane-cho				
3	Higaahi Koaen	Br. 5			
4	Shin Matauhama Bri.	Br. 1			
5	Omiya 266K 712M				
6	Showa Bridge	Br. 4			
7	Niahi Oh-Hats-Cho				
8	Gotsnda Bridge	Br. 1			
9	"	Br. 2			
10	Maruoka		Fukui Pref.	Fukui, 1948, M=7.3	(2)
11	Nakamura	N - 1	Miyagi Pref.	Miyagi-ken-Oki, 1978, M=7.4	(8)
12	"	N - 2			
13	Yuiage-kami	Y - 3			
14	Kitakami River	No. 10			
15	Natori River, 3.2 Km				
16	Kinnou Bridge	P_8			
17	Abukuma Bridge	Br. 1			
18	"	Br. 2			
19	Eai Bridge	No. 1			
20	Minami Sendai	No. 2			
21	Uomachi	A - 1			
22	"	A - 2			
23	Wabuchi	W - 3			

Reference

(1) BRI (1965)
(2) BRI (1969)
(3) Japaneae Society of Civil Engineera
(4) Ishihara (1976)
(5) J.S.S.M.F.E. (1976)
(6) Kiahida (1970)
(7) Ohashi et al. (1977)
(8) Yasuda et al. (1980)

Table 2 Input Motion

Test No.	Input Motion	Input Acceleration (gals)
1	Sinuaoidal 7 HZ	30
2		80
3		80
4		50
5		80
6		150
7		150
8		250

Table 3 F_L-D_E Relation

F_L	Depth, Z (m)	Reduction Factor, D_E
$F_L \leq 0.6$	$Z \leq 10$	0
	$10 < Z \leq 20$	1/3
$0.6 < F_L \leq 0.8$	$Z \leq 10$	1/3
	$10 < Z \leq 20$	2/3
$0.8 < F_L \leq 1.0$	$Z \leq 10$	2/3
	$10 < Z \leq 20$	1

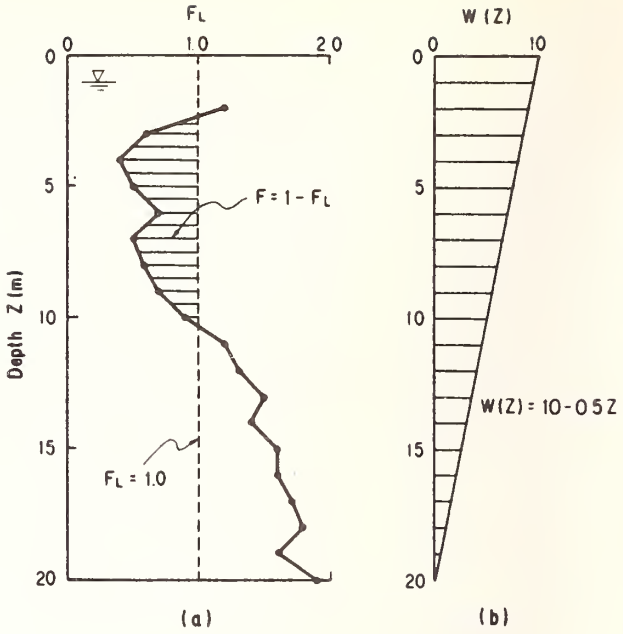

Fig. 1 Integration of F_L

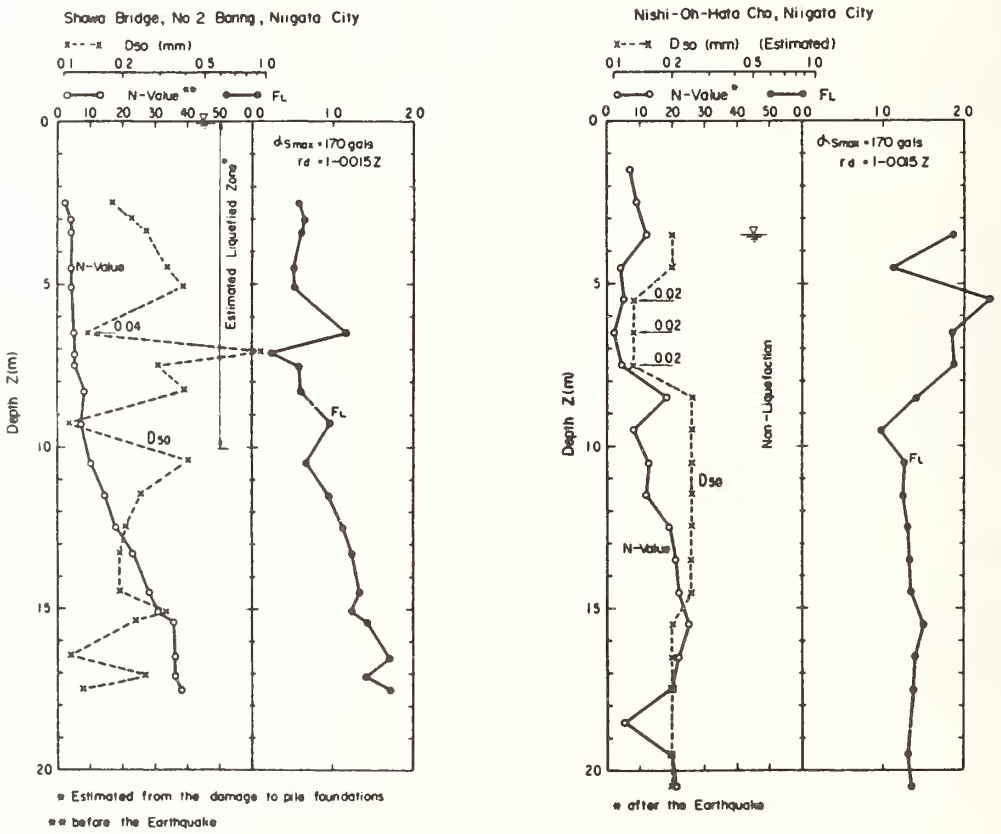

Fig. 2 Relationships between F_L and Depth

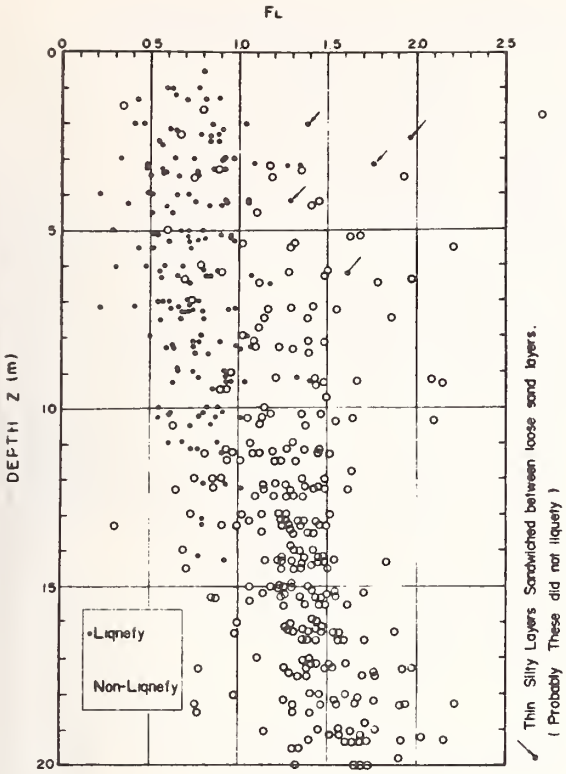

Fig. 3
Relationship between F_L and Depth at the Liquefied and Non-Liquefied Sites during the Niigata Earthquake

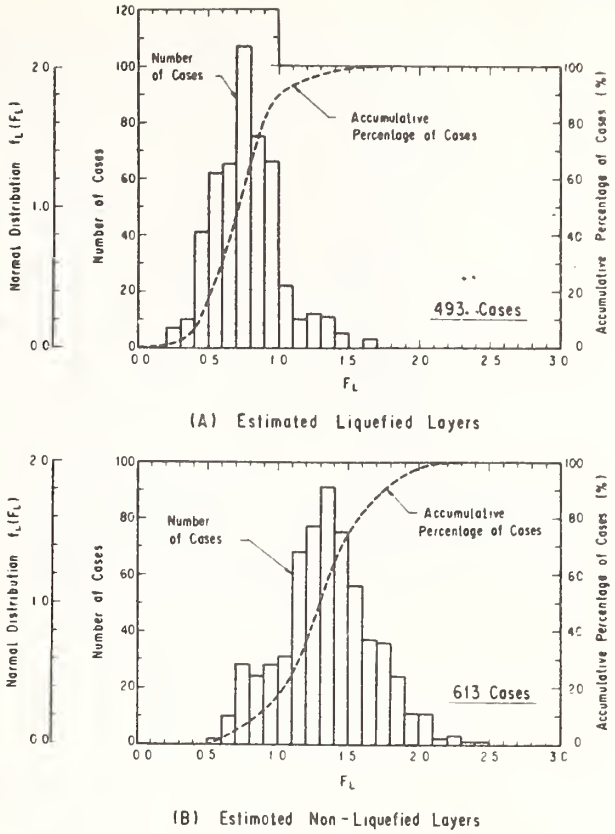

Fig. 4
Distribution of F_L Values and Their Accumulative Incidences, in Percentage, Comparing Liquefied Sites with Non-Liquefied Sites in Table 1

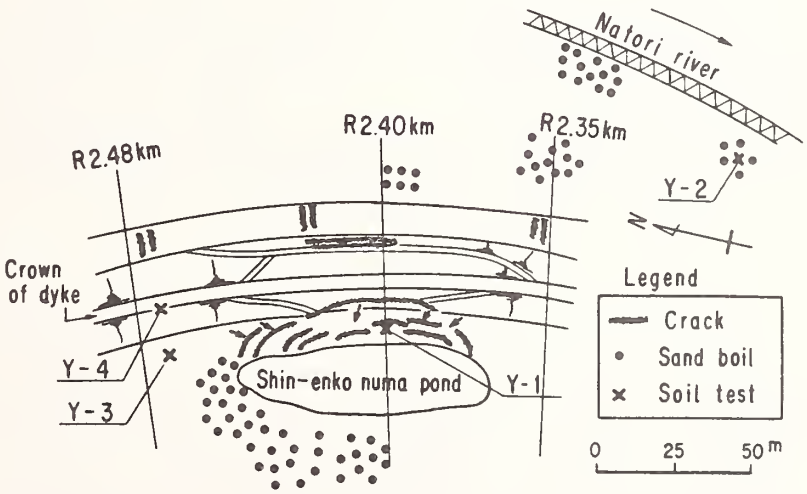

Fig. 5
Plan of Yuriage-kami Dyke and Points of Soil Tests

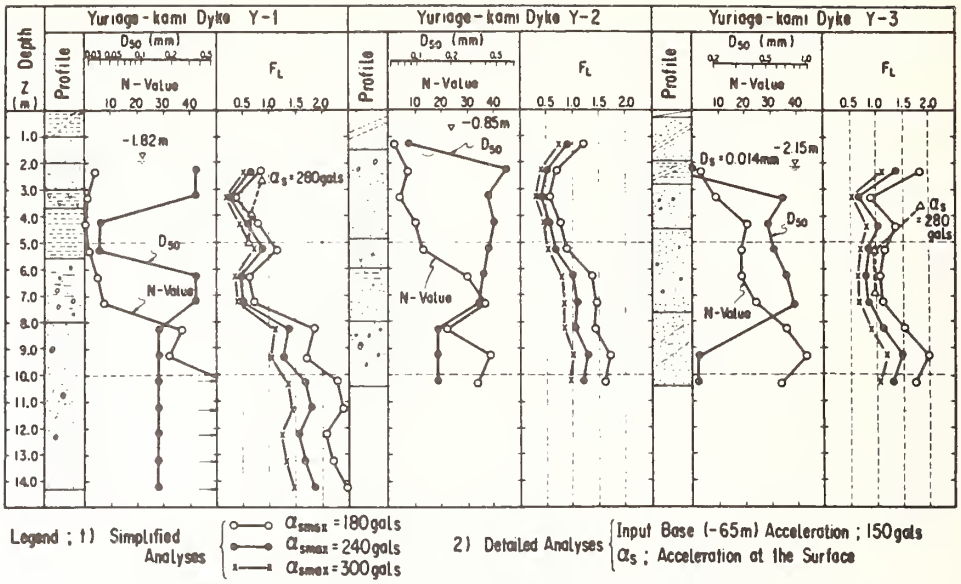

Fig. 6 F_L-values at Yuriage-kami Dyke (Y-1, Y-2; liquefied, Y-3; non-liquefied)

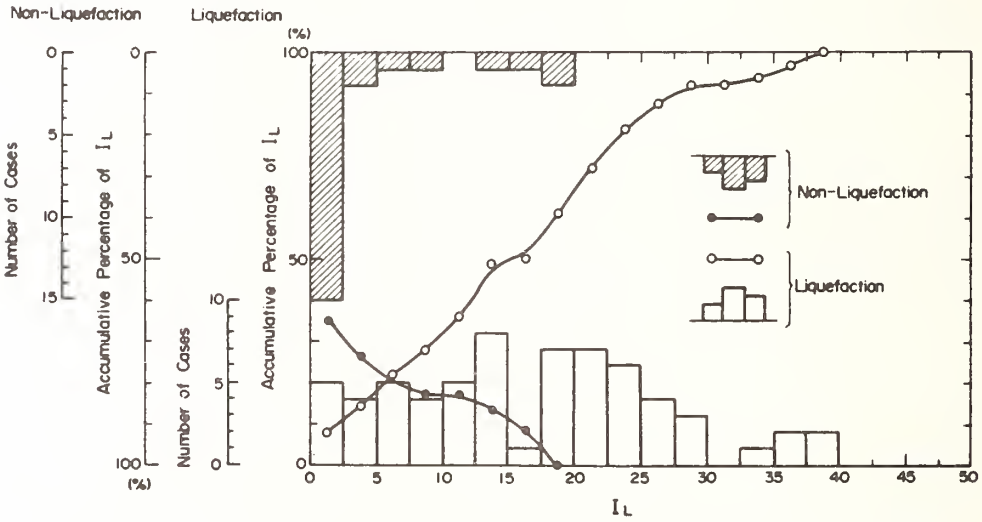

Fig. 7 Distribution of I_L Values and Their Accumulative Incidences, in Percentage, Comparing Liquefied Sites with Non-Liquefied Sites in Table 1

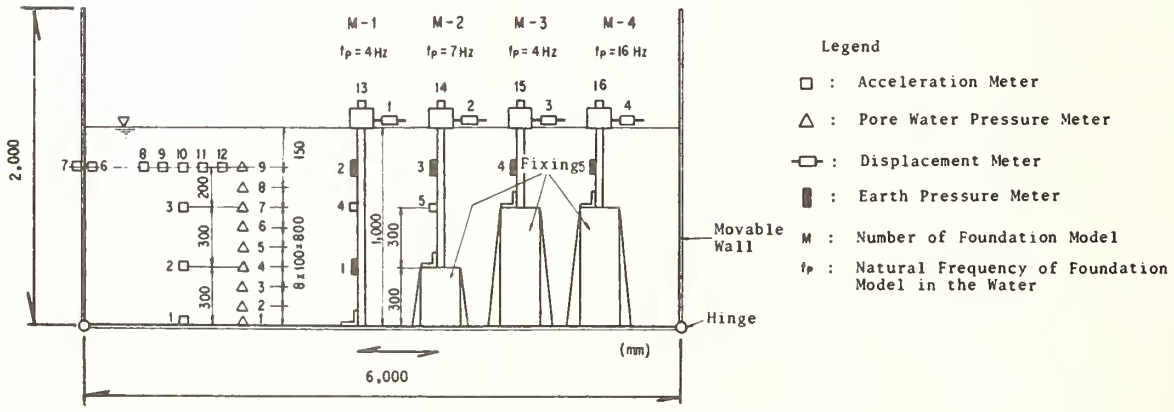

Fig. 8 Outline of Test Models and Measurement

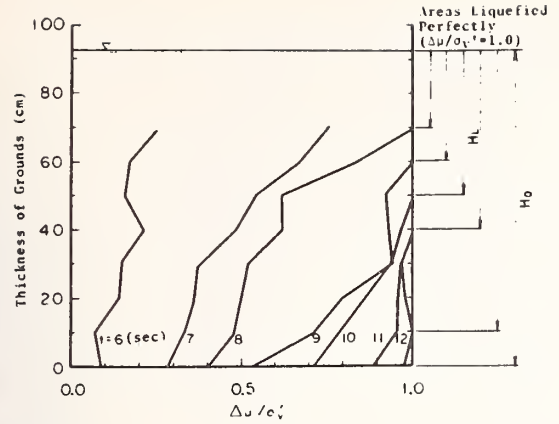

Fig. 9
Time History of the Rate of Ground Liquefaction $\Delta u/\sigma\acute{v}$ (Test 2)

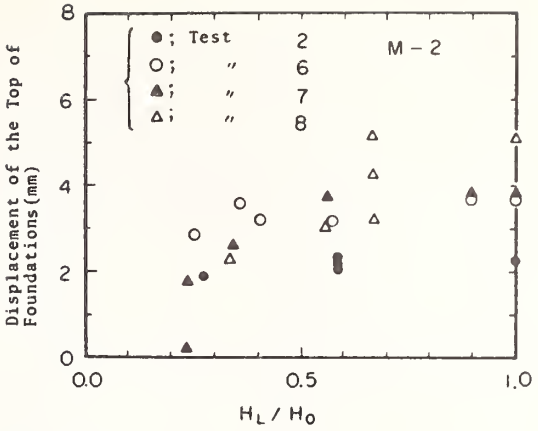

Fig. 10
Relationship between the Displacement of the Top of the Foundation Model and the Degree of Soil Liquefaction H_L/H_0

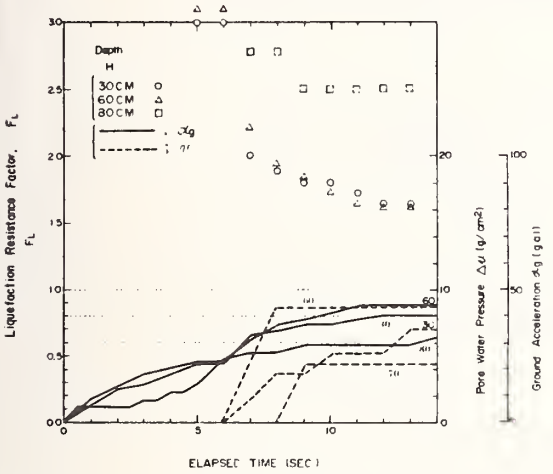

Fig. 11
Relationships between Pore Water Pressure and Acceleration of Non-Liquefied Sand Layers and F_L Values in Shaking Table Tests

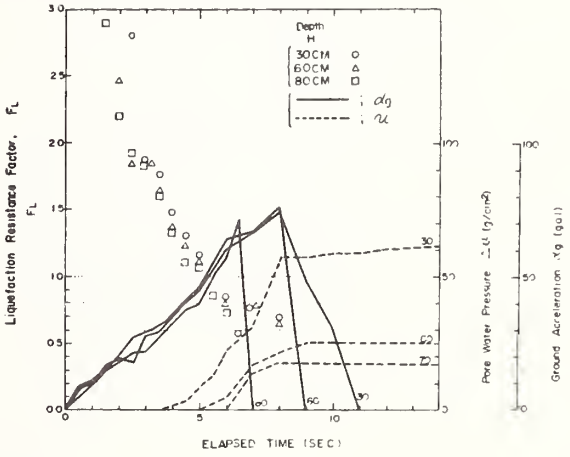

Fig. 12
Relationships between Pore Water Pressure and Acceleration of Liquefied Sand Layers and F_L Values in Shaking Table Tests

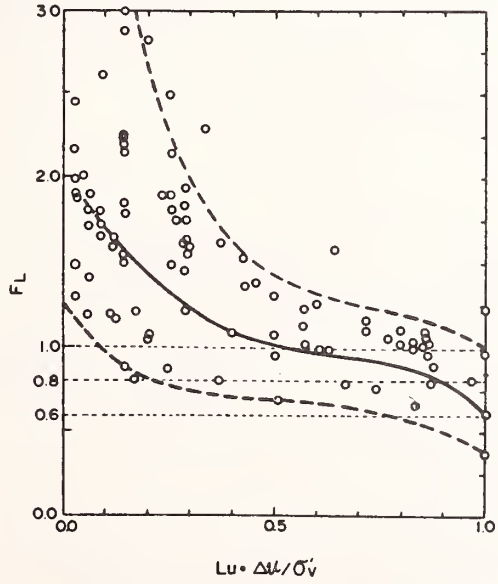

Fig. 13
Relationships between F_L Values and the Rate of Ground Liquefaction $\Delta u/\sigma\acute{v}$ in Shaking Table Tests

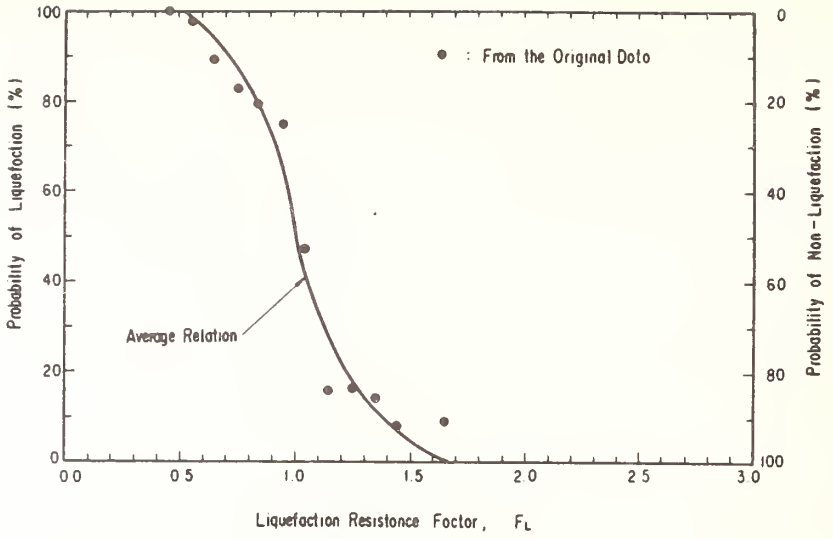

Fig. 14
Relationship between Probability of Liquefaction or Non-Liquefaction and F_L

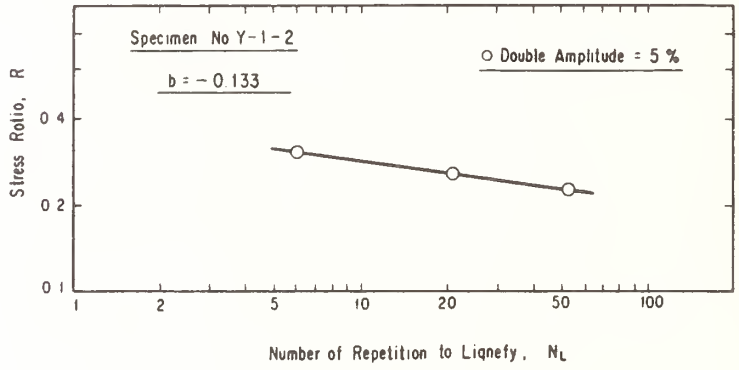

Fig. 15
An Example of Relationship between R and N_L (Dynamic Triaxial Test)

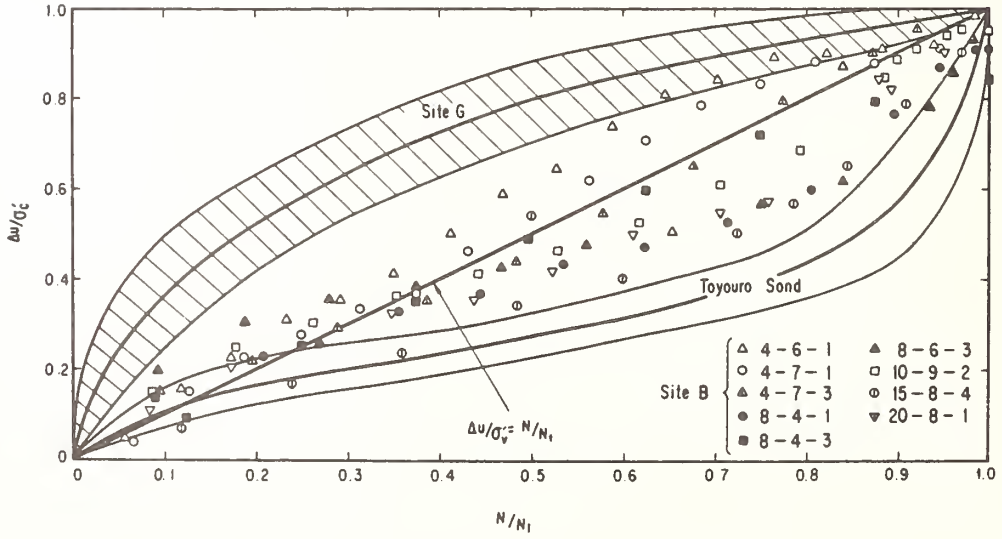

Fig. 16 Relationships between $\Delta u/\sigma_v'$ and N/N_L

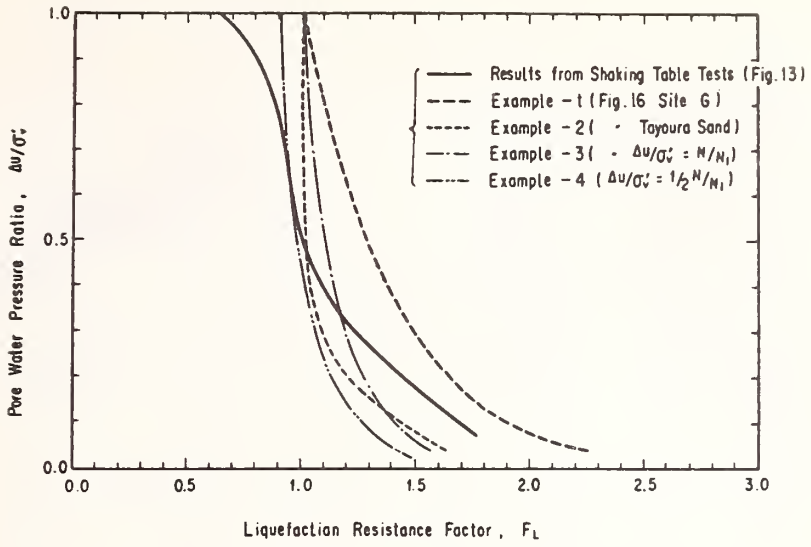

Fig. 17 Relationships between $\Delta u/\sigma'_v$ and F_L

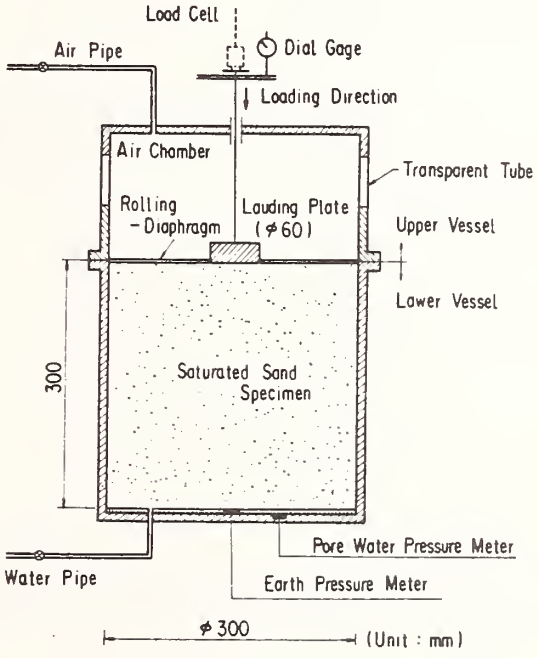

Fig. 18 Test Apparatus

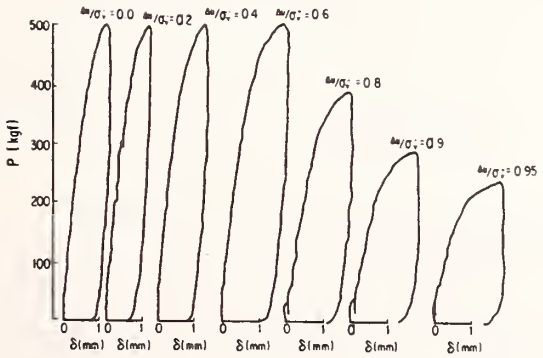

Fig. 19
An Example of Static Loading Test Results

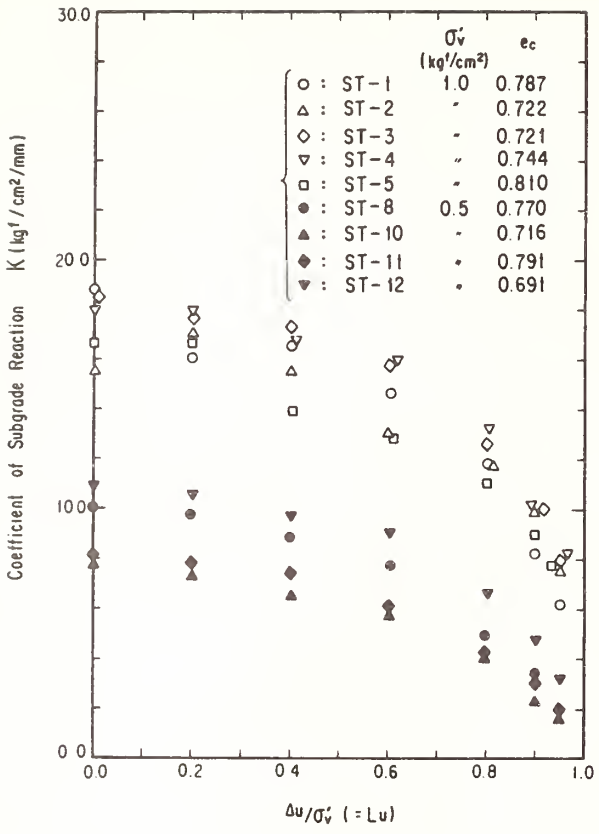

Fig. 20
Relationships between K and $\Delta u/\sigma'_v$

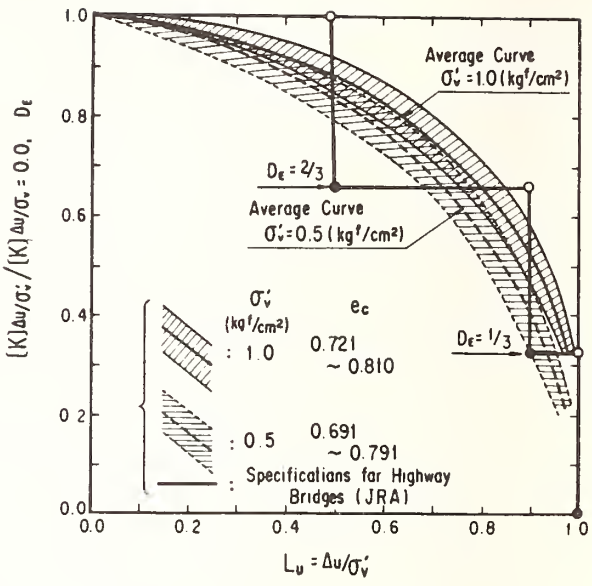

Fig. 21
Relationships between K/K_0, D_E and Lu ($=\Delta u/\sigma'_v$)

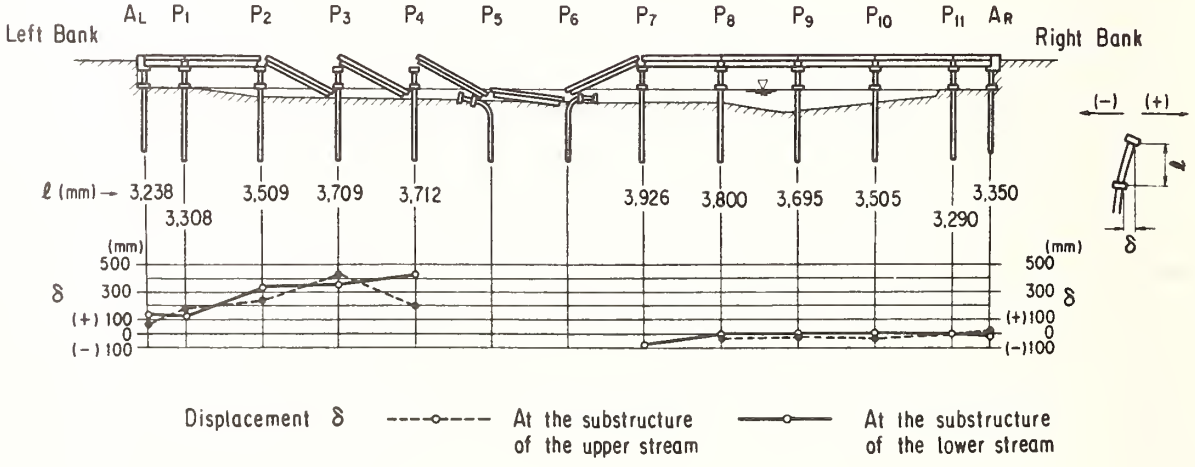

Fig. 22
The Circumstances of Showa Bridge Damaged during the Niigata Earthquake

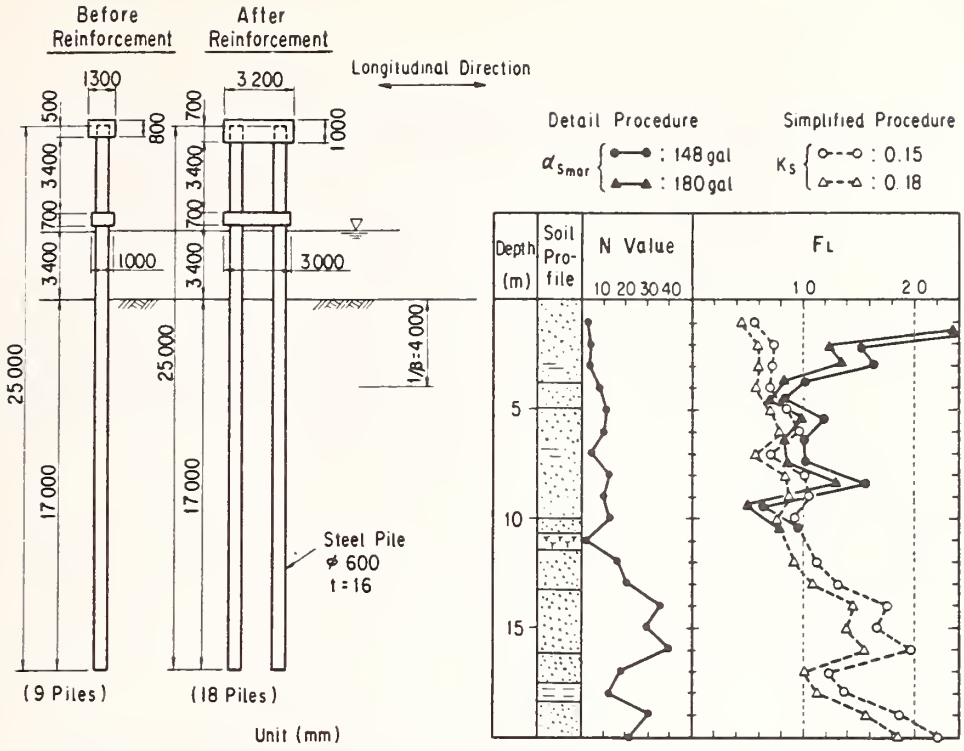

Fig. 23
The Substructure (P5) of the Showa Bridge and the Results of Assessment of Soil liquefaction Using F_L-values

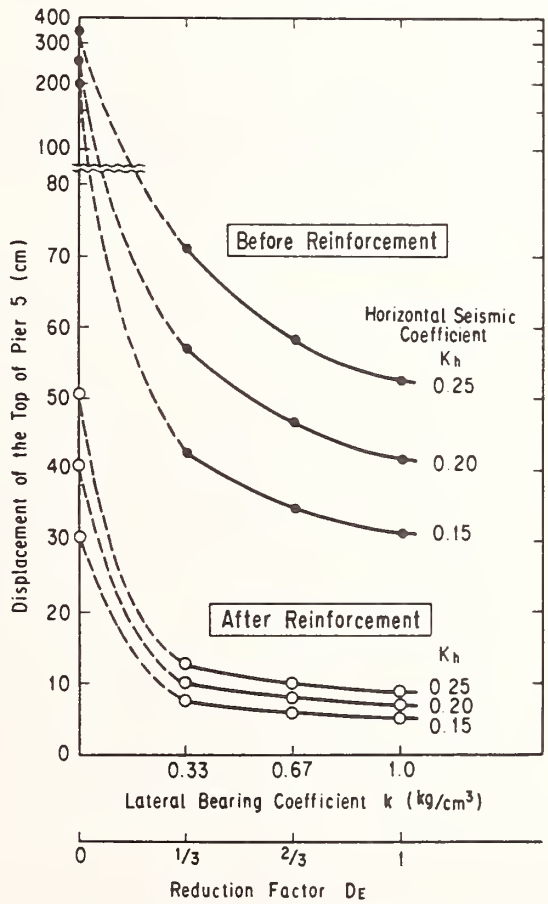

Fig. 24
Relationships between the Maximum Displacement of the Top of Pier 5 and the Reduction Factor D_E or the Lateral Bearing Coefficient of Grounds k

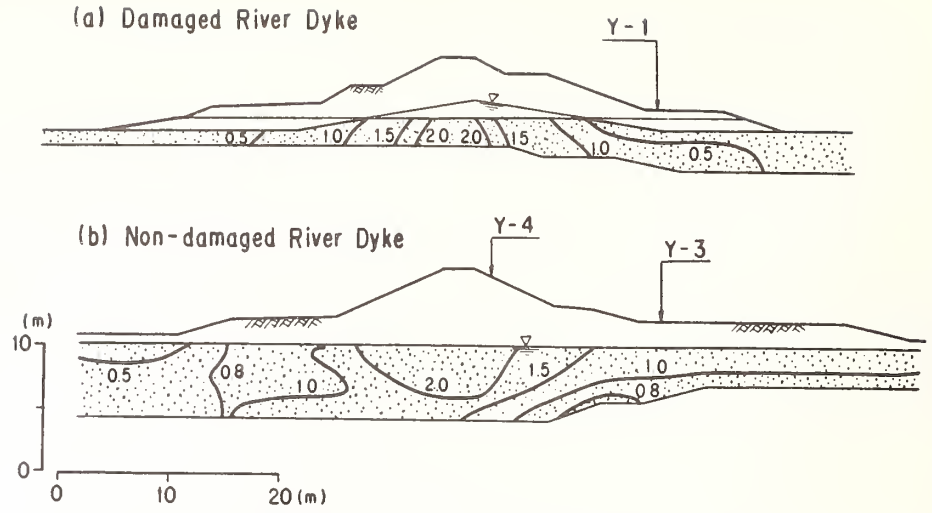

Fig. 25 Distribution of F_L-values Comparing Liquefied River Dyke with Non-liquefied River Dyke

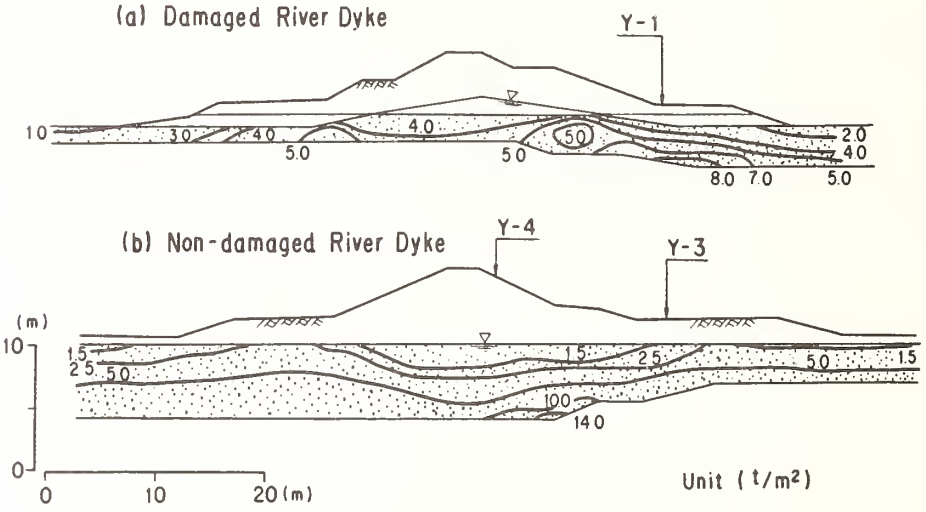

Fig. 26 Distribution of Excessive Pore Water Pressure Comparing Liquefied River Dyke with Non-Liquefied River Dyke

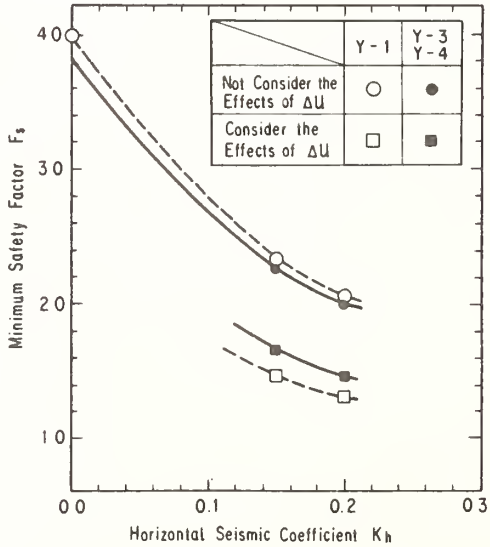

Fig. 27 Stability of River Dykes Considering Excessive Pore Water Pressure Occurred During Earthquakes

COUPLED HYDRODYNAMIC RESPONSE CHARACTERISTICS AND WATER PRESSURES OF LARGE COMPOSITE BREAKWATERS

Tatsuo Uwabe
Setsuo Noda
Hajime Tsuchida

Port and Harbour Research Institute
Ministry of Transport

ABSTRACT

In order to prevent damage by tsunami, a large composite breakwater is planned in deep sea at a depth of 60 m at the bay mouth of Kamaishi in the Tohoku district. For the purpose of examining the seismic behavior of the breakwater, an analysis of coupled hydrodynamic response characteristics and water pressures of the breakwater was carried out by means of a shaking table model test and an earthquake response calculation using the Finite Element Method.

In case the caisson of the composite type breakwater does not resonate, the model tests show that the hydrodynamic pressures acting on a caisson is calculated by the Westergaard formula using the water depth and the seismic coefficient at the top of the mound. (Mound means earth and/or rockfill).

In order to use earthquake response calculation for practical application, it is essential to investigate whether the modeling and material property values simulate the acutal field condition or not. It is concluded that the method for analyzing structure-water systems using the Finite Element Method is appropriate for simulating the dynamic response and hydrodynamic pressures of the fill type breakwater.

INTRODUCTION

A large composite type breakwater which protects against tsunamis and serves as an expansion of port functions is planned for construction in deep sea at the depth of 60 m at the bay mouth of Kamaishi in Tohoku district. The sectional form which is now under design is a composite type structure made up of a rubblestone mound and a caisson. The rubblestone mound and the caisson become massive because of the deep sea of 60 m. With no past record of construction in a deep sea of 60 m, it is necessary to investigate technical problems related to this magnitude of construction. The dynamic response analysis in the water is especially important to prevent the breakwater structure from being damaged by a tsunami.

The coupled hydrodynamic response of the large composite breakwater made up of rubblestone mound and caisson has many uncertain points. Therefore, model vibration tests in the water were carried out as a first analysis of the dynamic behavior of the breakwater. It is difficult to satisfy the

law of similitude for the vibration model test in all aspects. Therefore, the coupled hydrodynamic response calculation was also carried out. The dynamic response calculations of structures and the ground were easily performed on a computer. However, it is very important to investigate the correctness of the calculation method, modeling, and property values for practical use. The calculation method was judged adequate by comparing the predicted calculation with the results of vibration tests.

In this report, the aims of the vibration test analysis were the coupled hydrodynamic responses, the dynamic water pressures, and comparison of the earthquake response calculation.

VIBRATION MODEL TESTS

The coupled hydrodynamic response of the breakwater comprising of a rubblestone mound and caisson is very complicated. Therefore, the first vibration test was carried out for the caisson model, the breakwater model was used in the next vibration test. Figure 1 shows the caisson model and figure 2 shows the breakwater model. The prototype of the breakwater was selected from several design sections whose seismic coefficient is 0.2. The models were made trying to satisfy the law of similitude [1]. Table 1 shows the results of similitude analysis, prototype values, and model values. The Takahagi sand is used for the model fill. The soil test results of this sand are given as follows: the specific gravity is 2.66; the maximum and minimum void ratio are 0.90 and 0.65, respectively; the effective grain size is 0.90 cm; and the uniformity coefficient is 1.5.

Two shaking tables of the Port and Harbour Research Institute were used for tests. Both shaking tables are of the electromagnetic type. The maximum driving force of one shaking table is 12 t.G. and the frequency range varies from 0.5 to 100 Hz. The inside dimensions of the box are 1.5 x 5 x 1.5 m. Another shaking table is almost the same as the above mentioned table except the box has inside dimensions of 3 x 3 x 1.2 m.

The input wave forms of the tests are a sine wave and random earthquake motions. The frequency ranges for the sine wave excitation tests varied from 5 Hz to 50 Hz at 1 Hz intervals. The earthquake accleration time histories with a similitude requirement were generated in the computer from strong motion earthquake records. The similitude ratio of time is $1:\sqrt{75}$. Original strong motion earthquake records consist of the incident wave computed from the ground surface record (S-252 N-S) of the 1968 Tokachi-oki Earthquake [2] at Hachinohe and the record (S-1210 E41N) of Ofunato in the 1978 Miyagi-ken-oki Earthquake [3].

Vibration tests consisted of dry model tests and submerged model tests. The sequence of vibration tests are given below. Test 1 is a sine wave excitation at 10 gal. Test 2 is at 50 gal. The others are earthquake wave excitations.

RESULTS OF TESTS

DYNAMIC RESPONSE OF THE BREAKWATER

Figure 3 shows the recorded waves of the sine wave tests. These waves were recorded at 1 Hz steps from 5 Hz to 50 Hz. An amplitude ratio of the response wave to the input wave gives the acceleration response ratio. Figures 4 and 5 show wave forms of input earthquake motions and Fourier spectra. Figure 6 shows recorded earthquake waves at each measuring point of the model.

Figure 7 shows the acceleration response curves of the caisson top and the mound (fill) top. When the input acceleration is 10 gal, two peaks of the acceleration response curve occur for the caisson top at 18 Hz and 35 Hz. These frequencies are considered to be the first and the second mode, respectively. When the input acceleration is 50 gal, the frequency of the first mode decreases and response ratio at the resonant frequency decreases. The acceleration response curve of the mound top gives a peak at 38 Hz, when the input acceleration is 10 gal. In the case of 50 gal, the acceleration response ratio of the mound top is a maximum at 31 Hz. The decrease of the acceleration response ratio and the resonant frequency is due to the nonlinear characteristics of the Takahagi sand fill material.

Figure 8 shows a maximum acceleration ratio (a ratio of the maximum response acceleration to the maximum input acceleration of the earthquake wave) versus height. When the input acceleration is more than 100 gal, the maximum acceleration ratio is greater than 1. The maximum acceleration ratio of the caisson top is large, especially in the case of 10 gal. The maximum acceleration ratio decreases as the input acceleration increases. In the case of around 200 gal, the maximum acceleration ratio is nearly equal to 1. Figures 9 and 10 show the relation of the maximum response ratio versus the maximum input acceleration for the caisson top and the mound top. In the case of the sine wave, the maximum acceleration is a maximum value of the acceleration response ratio. The maximum acceleration ratio of the sine wave is greater than that of the earthquake wave, as the maximum acceleration ratio of the sine wave is the ratio at the resonant frequency. An effect of the differences of the input waves to the maximum acceleration ratio is great in the case of 10 gal. The simple linear regression analysis for the data whose maximum input acceleration was more than 40 gal gave the following relations of the maximum acceleration ratio and the maximum input acceleration.

For the caisson top

$$\log_{10} R_c = 1.860 - 0.728 \log_{10} \alpha$$

For the mound top

$$\log_{10} R_m = 1.229 - 0.522 \log_{10} \alpha$$

where

R_c : Maximum acceleration ratio of the caisson top

R_m : Maximum acceleration ratio of themound top

α : Maximum input acceleration (gal) ($\alpha \geq 40$ gal)

The double circles in figure 9 show the results of the strong motion observation for the Ofunato tsunami breakwater which is the same type as the Kamaishi breakwater and whose water depth is 35 m.

Figure 11 shows the test results of the caisson model on the vibration table. The acceleration response curve of the caisson top in figure 11 is the case of 50 gal. A dotted line and a solid line will be referred to in the next chapter. This figure shows that the resonant frequency decreases with water and that the acceleration response ratio of the resonant frequency has no change with water. Figure 12 shows the effects of water on the acceleration response ratio. This figure shows that the acceleration response ratio of a dry model is almost the same as that of a submerged model.

Figure 13 shows the effects of water depth on the response characteristics of the breakwater model. The acceleration response curves of the caisson top with 0, 50, and 80 cm water depth for input acceleration of 10 gal are shown. This figure shows that the resonant frequency decreases with water depth.

DYNAMIC WATER PRESSURES ON BREAKWATERS

According to the current design standard of Port and Harbour Facilities, the dynamic water pressures on the caisson of the breakwater are given by the Westergaard formula [4]. This well known formula computes the dynamic water pressure on a vertical face. Dynamic water pressures against an inclined face are given by Zanger [5].

The formulas of Westergaard and Zangar give the dynamic water pressures against a rigid vertical and inclined face, respectively. In these formulas it is assumed that the structure and foundation vibrate as one. Therefore, these formulas are not applied to resonant structures which give different response acceleration at each height. On the other hand, these formulas assume that the input motion is a sine wave. It is, therefore, necessary to investigate for the earthquake ground motion. When the dynamic water pressures on the caisson of the breakwater are calculated using Westergaard's formula, it is assumed in the current design standard that the water depth in the formula is the depth of the mound bottom. It is also assumed that the water depth is the depth of the caisson bottom. Since the dynamic water pressures on the caisson depend on the water depth for the structures in the deep sea, it is very important to investigate the water depth in Westergaard's formula. In this report, the above problems were analyzed according to the results of the vibration tests.

Figures 14 and 15 show the dynamic water pressures versus depth for a sine wave of 5 Hz. The maximum acceleration input motion was 50 gal. Figure 14 shows the dynamic water pressures on the caisson and the mound slope with 80 cm water depth. Figure 15 shows the dynamic water pressures on the mound slope with a water depth of 55 cm. The acceleration response ratio of the 5 Hz sine wave is almost equal to 1 according to the response curve of figure 7. It is assumed that the breakwater model vibrates as a rigid body; therefore, the dynamic water pressures calculated by the Westergaard and Zangar formulas whose assumption is a rigid body can be compared to the test results of figures 14 and 15. Figure 14 shows that the dynamic water pressures calculated with the water depth of the caisson's bottom is almost the same as the results of the tests. Figure 15 shows that the dynamic water pressures of Zangar's formula is equal to the test results. In figure 14, the test results is slightly larger than that computed using Zangar's formula.

Figure 16 shows the dynamic water pressures on the breakwater versus depth for the earthquake motion. In this figure, the vertical axis is the water depth and the abscissa is the ratio of the dynamic water pressures to the seismic coefficient (maximum acceleration/acceleration of gravity). The solid lines show the Westergaard's formula using a water depth equal to the caisson's bottom (25 cm) and Zangar's formula. A dashed line shows Westergaard's formula using a water depth equal to the mound's bottom (80 cm). The maximum acceleration of the input earthquake motion was from 45 to 207 gal. The dynamic water pressures on the slope were divided by the seismic coefficient given by the maximum acceleration at each point of the slope. The maximum acceleration ratio of the earthquake motion is less than 3 for the input maximum acceleration of more than 50 gal according to figure 8. When the maximum acceleration of the input earthquake motion is about 200 gal, the maximum acceleration ratio becomes equal to 1. This is due to the strain dependence of the shear modulus and damping of the mound. According to figure 16, the dynamic water pressure of the test results on the caisson is smaller than that of the Westergaard formula with the water depth at the caisson's bottom. Therefore, we use the dynamic water pressure on the caisson of the breakwater as given by the Westergaard formula with the water depth at the caisson's bottom. But this is only correct when the breakwater does not resonate, or when the maximum acceleration of the input earthquake motion is more than 50 gal. Figure 16 also shows that the dynamic water pressure on the slope of the test results is larger than that using Zangar's formula. This is due to the dynamic characteristics of the slope surface.

COUPLED HYDRODYNAMIC RESPONSE ANALYSIS OF BREAKWATERS

In this chapter, the adequacy of a coupled hydrodynamic response calculation method was investigated by means of a comparison of calculations and vibration test results.

The resonant frequency of the breakwater model decreases with an increase of input maximum acceleration as shown in figure 7. This is due to the strain dependence of the shear modulus and damping of the mound. In order to calculate the dynamic response of the breakwater, it is necessary to consider the nonlinear characteristics of the mound material. The nonlinear earthquake response analysis in which the shear modulus and damping of the material change every moment is not now a practical calculation method because of the complexity of the calculation and large computer time required. The equivalent linear method in which the strain dependence of the shear modulus and damping are considered is not a real nonlinear earthquake response analysis. Nevertheless, it is a very practical method and has been used frequently.

Because the coupled hydrodynamic response FEM program discussed here is a linear method, the shear modulus and damping are given by another FEM program which is the equivalent linear model. Therefore, the coupled hydrodynamic response calculation is discussed in this chapter after the equivalent linear response calculation is examined.

EARTHQUAKE RESPONSE ANALYSIS OF BREAKWATER BY EQUIVALENT LINEAR FEM

The computer program FLUSH coded by Lysmer et al. [6] was used in this analysis. As the material of the mound is Takahagi sand, it is necessary to know the stress-strain relation of this sand to calculate earthquake response. Since there was no data from dynamic triaxial tests for the Takahagi sand, the stress-strain relation of Takahagi sand was then obtained from vibration table tests. It is assumed that the vibration table test results, whose confining pressure is not large, are reasonable to estimate the stress-strain relation of Takahagi sand because the confining pressure of the mound model is small. The vibration table test results of Arai et al. [7, 8] were used in this investigation. The data discussed here are the test results of the sand layer whose height is 0.6 m and length is 5 m. Table 2 shows the resonant frequency and response ratio of the sand layer. The response calculations were conducted by the program FLUSH modeling the sand layer. The stress-strain relation of Takahagi sand was chosen so that resonant frequency from the FEM model and those from the test results agreed. Table 2 shows the calculated values and Figure 17 shows the stress-strain relation of the Takahagi sand. The shear modulus, at very small strains (10^{-4} percent) is given by the following equation.

$$G_o = 621 \quad \frac{(2.17-e)^2}{1+e} \quad (\sigma'_m)^{0.14} \quad (kgf/cm^2)$$

where

G_o : shear modulus at very small strains,
e : void ratio, and
σ'_m : effective confining pressure.

The dashed line in figure 17 shows the results from Iwasaki, Tatsuoka, and Takagi [9] considering the effect of confining presures on the stress-strain relation of the sand. The damping factor is different, but the shear modulus is almost the same.

Figure 18 shows the FEM model of the breakwater. Figure 19 shows the property values used in the calculations. The element at the bottom of the caisson was made to indicate the dynamic characteristics of the caisson. The stress-strain relation of this element is shown in figure 20. It is assumed that the added mass due to the water represents the coupled hydrodynamic effects. The added mass which corresponds to the dynamic water pressures was used for the response calculations. The specific weights of the caisson and mound are 2.86 and 2.50 tf/m^3 which include the added mass.

Figures 21 and 22 show the calculated and observed acceleration response curves. Figure 23 shows the earthquake response wave forms. The above two earthquake waves are the calculated and observed response acceleration of the caisson top. The next two are those of the mound top. The bottom wave is the input earthquake motion whose maximum acceleration is 11 gal. The calculated waves appear almost the same as the observed ones which leads one to assume that this earthquake response calculation using the equivalent linear method is reasonable.

COUPLED HYDRODYNAMIC RESPONSE CALCULATION BY THE FEM

Westergaard's research is well known for the calculation of dynamic water pressure, and in Japan, the investigations of Hatano [10] and Kotsubo [11] were reported. Recently, the coupled hydrodynamic response calculation method using the FEM were proposed [12, 13].

In this report, the coupled hydrodynamic response calculation program was developed. This computer program was called BEAD (Bank Earthquake Analysis with Dynamic Water Pressures). The comparison of calculation and test was carried out using the computer program BEAD in order to verify the adequacy of this calculation method. The caisson model on the vibration table was investigated before the breakwater model. The acceleration response curves of the caisson top were shown previously in figure 11. Constant values of the element of the caisson bottom were used to give the same resonant frequency between calculation and test. The calculated acceleration response ratio is shown by the solid line in figure 11. The coupled hydrodynamic response calculation was then carried out. The results of the coupled hydrodynamic response calculation is shown as the dashed line in figure 11. This dashed line is almost the same as the test results. Therefore, it is concluded that the effects of the water on the dynamic response of the submerged structure is represented by the added mass.

Figure 24 shows a comparison of dynamic water pressures from calculations and from tests. The frequencies of the input sine wave are 5 Hz and 18 Hz. The dynamic water pressure of the input

frequency of 18 Hz at a point W2 was different between calculations and tests. But the other computed dynamic water pressures are almost the same as those of tests.

Figure 25 shows the FEM model of the breakwater for the computer program BEAD. Because the computer program BEAD is a linear calculation method, it is necessary to assign constant values considering strain dependence of the shear modulus and damping. The constant values given by the FLUSH computation were used for the BEAD computation. The damping factors were given for each mode because the response analysis of BEAD is a modal analysis. These damping factors were chosen to give similar acceleration between the calculations and tests. The specific weight of the mound was 2.4 tf/m^3 considering the dynamic pore water pressures of the mound. This value is betwen 2.36 tf/m^3 for the computation of the sand layer and 2.50 tf/m^3 for the calculation of the breakwater. Figure 26 shows the comparison of the calculations and tests for the sine wave input motion. The maximum acceleration of the input motion was 49 gal. The frequencies of the input motion are 5 Hz and 14 Hz. The 14 Hz is the resonant frequency of the breakwater. The dynamic pressures on the caisson show good agreement between the calculations of BEAD and the test results, as shown in figure 26. The dynamic water pressures under the mound top in figure 26 are those on the slope of the mound. The calculated dynamic water pressures on the slope are smaller than the observed values. The damping factor in figure 26 was 0.215.

Figures 27, 28, and 29 show the calculated and observed wave forms for the earthquake input motion. The Hachinohe wave form was used for the input motion. The maximum accleration of the input motion was 40 gal. Figure 27 shows the acceleration wave forms. The mode number considered for the calculation was less than the 5th. The resonant frequencies of each mode were 20.2, 36.6, 48.4, 63.8, and 64.1 Hz respectively. The damping factor of the 1st mode was 0.09 and the damping factor for the 2nd to 5th mode was 0.15. Figure 27 shows good agreement between the calculated and observed acceleration wave forms. Figures 28 and 29 show the wave forms of the dynamic water pressures. Calculated dynamic water pressures on the caisson are almost the same as the observed values as shown in figure 28. However, the calculated dynamic water pressures on the slope of the mound are smaller than the test results. Comparing the response acceleration at W6 point on the slope, the calculated value of 91 gal is smaller than the observed value of 146 gal. Hasegawa and Kikuzawa [14] reported that the reason why the acceleration response ratio of the slope surface is larger than that of the center of the mound is the strong nonlinear characteristics of the slope surface material. Therefore, the constant value of the slope surface material should be taken into account. In this report, the dynamic behavior of the slope surface is not discussed further but will be discussed in the future.

CONCLUSIONS

1. In the case of the earthquake input motion, the maximum acceleration ratios of the caisson top and the mound top decreased with an increase of the input maximum acceleration. The relations between the maximum acceleration ratio and the maximum input acceleration were obtained in the following equations.

Caisson Top

$$\log_{10} R_c = 1.860 - 0.728 \log_{10} \alpha$$

Mound Top

$$\log_{10} R_m = 1.229 - 0.522 \log_{10} \alpha$$

where

R_c : maximum acceleration ratio of caisson top,

R_m : maximum acceleration ratio of mound top, and

α : maximum input acceleration (gal) ($\alpha \geq 40$ gal).

Good agreement was obtained between the above relations of the caisson top and strong motion observation results of the Ofunato Tsunami breakwater.

2. When a breakwater does not show large response because of nonresonance and nonlinear characteristics induced by a large input acceleration, the dynamic water pressure on the caisson for the input earthquake motion is calculated by the Westergaard formula with the water depth at the caisson's bottom.

3. In the case of the uncoupled hydrodynamic response analysis, the dynamic behavior is estimated by incorporating an added mass for a dynamic response calculation.

4. From the practical point of view, for the strain range discussed here, the nonlinear behavior of the fill under seismic forces can be estimated by an equivalent linear analysis if analytical modeling is done with appropriate constants.

5. If the selection of a model with a constant value is used, it is concluded that the dynamic water pressure on the structure under water is given by, the coupled hydrodynamic response calculation (program BEAD).

REFERENCES

[1] Uwabe, T., S. Noda, S. Chiba, and S. Higaki, "Coupled Hydrodynamic Response Characteristics and Water Pressures of Large Composite Breakwaters," Report of the Port and Harbour Research Institute, Vol. 20, No. 4, December 1981 (in Japanese).

[2] Tsuchida, H., E. Kurata, and K. Sudo, "Strong-motion Earthquake Records on the 1968 Tokachi-oki Earthquake and Its After Shocks," Technical Note of PHRI, No. 80, June 1969.

[3] Kurata, E. S. Iai, Y. Yokoyama, and H. Tsuchida, "Strong-motion Earthquake Records on the 1978 Miyagi-ken-oki Earthquake in Port Areas," Technical Note of PHRI, No. 319, June 1979.

[4] Westergaard, H. M.. "Water Pressures on Dams during Earthquakes," Trans. ASCE 98, 1933, pp. 418-434.

[5] Zangar, C. N., "Hydrodynamic Pressures on Dams Due to Horizontal Earthquake," Proc. Exper. Stress Analysis, Vol. 10, No. 2, 1953.

[6] Lysmer, J., T. Udaka, C. F. Tsai, and H. B. Seed, "FLUSH-A Computer Program for Approximate 3-D Analysis of Soil Structure Interaction Problems," EERC 75-30, 1975.

[7] Arai, H. and Y. Umehara, "Vibration of Saturated Sand Layers," Report of PHRI, Vol. 13, No. 2, June 1974 (in Japanese).

[8] Arai, H., M. Iwabuchi, S. Nakazawa, and S. Kitajima, "Vibrational Properties of Sand Layers," Report of PHRI, Vol. 13, No. 2, June 1974 (in Japanese).

[9] Iwasaki, T., F. Tatsuoka, and Y. Takagi, "The Strain Dependence of the Shear-modulus and Damping of the Sand, the 12th Japan National Conference on S.M.F.E., May 1977, pp. 417-420 (in Japanese).

[10] Hatano, T., "Seismic Force Effects on a Gravity Dam (No. 3)," Proceedings JSCE, No. 5, November 1950, pp. 83-90 (in Japanese).

[11] Kotsubo, S., "Dynamic Water Pressures on Dams Due to Irregular Earthquakes," Proceedings JSCE, No. 47, August 1957, pp. 38-45 (in Japanese).

[12] Chakrabarti, P. and A. K. Chopra, "Earthquake Response of Gravity Dams Including Reservoir Interaction Effects," Report No. EERC 72-6, University of California, Berkeley, December 1972.

[13] Saini, S. S., P. Bettess, and O. C. Zienkiewicz, "Coupled Hydrodynamic Response of Concrete Gravity Dams Using Finite and Infinite Elements," Earthquake Engineering and Structural Dynamics, Vol. 6, 1978, pp. 363-374.

[14] Hasegawa, T. and M. Kikuzawa, "The Identification of Dynamic Properties of a Fill-type Dam," The 16th Joint National Conference on S.M.F.E., 1981, pp. 1273-1276 (in Japanese).

Table 1. Similitude

		Required Ratio	Prototype Value	Required Model Value	Actual Model Value						
					Test 1			Test 2			Test 3
					Case 1, 2	Case 3	Case 4	Case 1, 2	Case 3	Case 4	Case 2
	Height (cm)	1:75	40×10^2	53	55	55	55	55	55	55	55
	Width (cm)	1:75	600×10^2	800	150	150	150	300	300	300	150
	Slope	1:1	1:2	1:2	1:2	1:1.6	1:2	1:2	1:2	1:2.5	1:2
	Unit Ory Weight (gf/cm^3)	1:1	1.8	1.8	1.6	1.6	1.4	1.53	1.56	1.52	1.54
M	Unit Weight Liquid (gf/cm^3)	1:1	1.0	1.0	0.99	0.99	0.84	0.99	0.99	0.84	0.96
U	Effective Grain Size (D_{10}, cm)	1:75	20	2.7×10^{-1}	1.4×10^{-1}	1.4×10^{-1}	1.4×10^{-1}	1.4×10^{-1}	1.4×10^{-1}	1.4×10^{-1}	1.4×10^{-1}
N	Coefficient of Permeability (cm/s)	$1:\sqrt{75}$	7	8.1×10^{-1}	6.4×10^{-1}	6.4×10^{-1}	8.4×10^{-1}	7.1×10^{-1}	6.8×10^{-1}	7.2×10^{-1}	7.0×10^{-1}
O	Angle of Internal Friction	1:1	35	35	32	32	29	31	31	31	31
	Water Depth (cm)	1:75	60×10^2	80	80	80	80	80	80	80	80
C											
A	Height (cm)	1:75	21×10^2	28	28	28	28	28	28	28	28
I	Width (cm)	1:75	17×10^2	23	23	23	23	23	23	23	23
S	Unit Ory Weight (gf/cm^3)	1:1	2.1	2.1	2.1	2.1	2.1	2.1	2.1	2.1	2.1
S											
O											
N											

Table 2. Comparison of Resonant Frequency and Acceleration Response Ratio by Vibration Tests and FLUSH Calculations

Takahagi Sand (Dry)

Maximum Input Acceleration (gal)	Resonant Frequency (Hz)		Acceleration Response Ratio	
	Tests	Calculations	Tests	Calculations
12	42	41.8	18.9-13.1	15.09
65	34	34.0	(7.7)	6.2
120	29	29.0	4.4	4.4
205	25	25.2	(2.7)	3.5

( ) Different test result.

Takahagi Sand (Saturated)

Maximum Input Acceleration (gal)	Resonant Frequency (Hz)		Acceleration Response Ratio	
	Tests	Calculations	Tests	Calculations
13	28	29	8.1	9.9
79	20	21	---	4.2
133	18	18	3.6	3.5

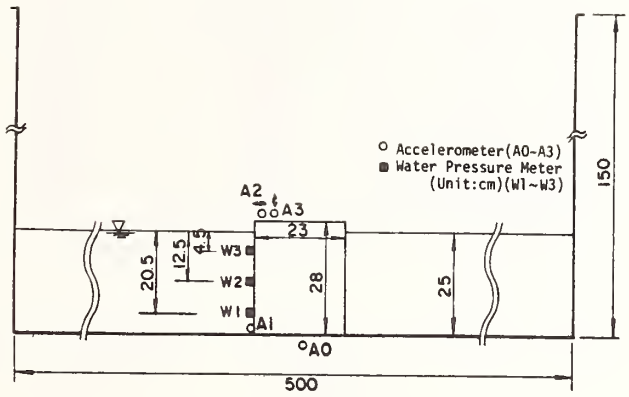

Fig. 1 Section of Caisson Model

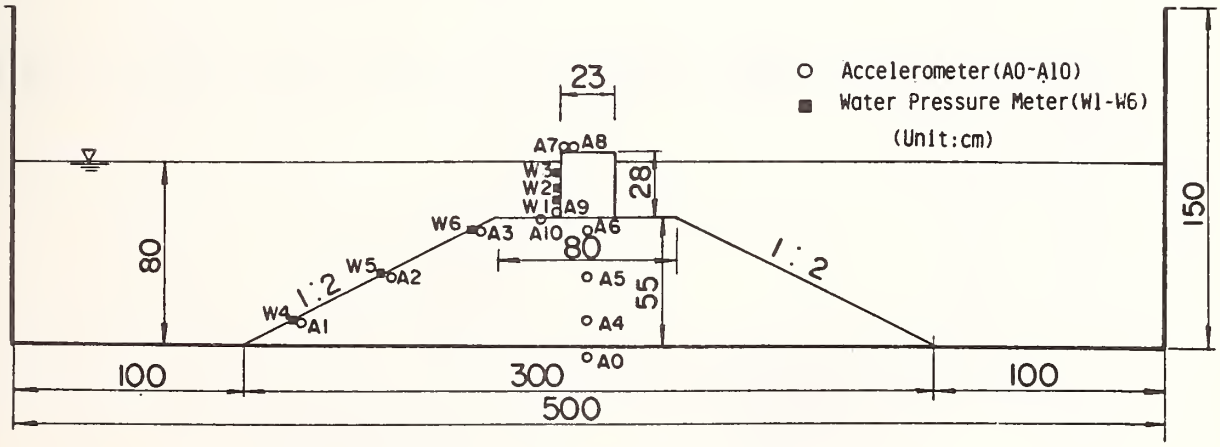

Fig. 2 Section of Breakwater Model

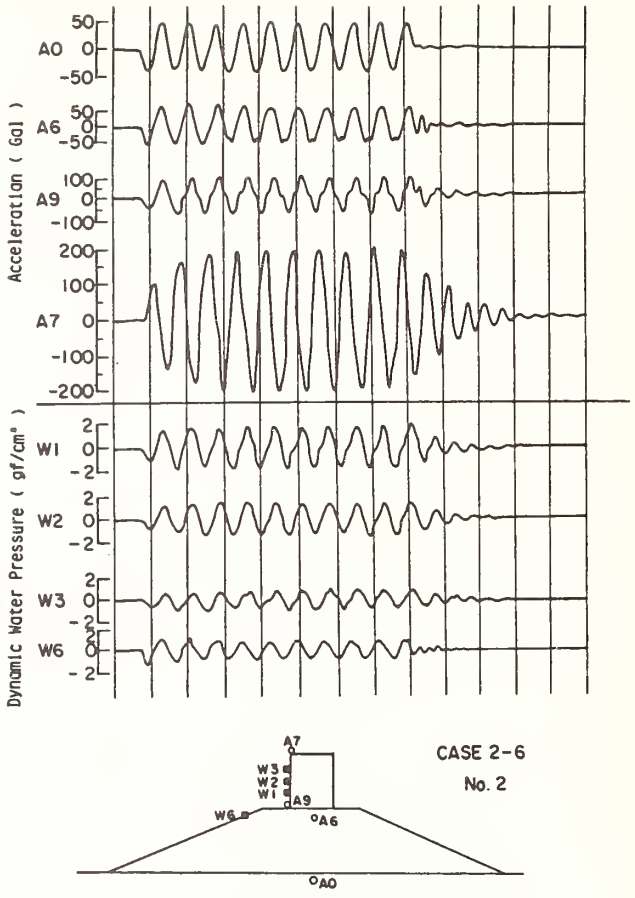

Fig. 3 Recorded Wave Forms

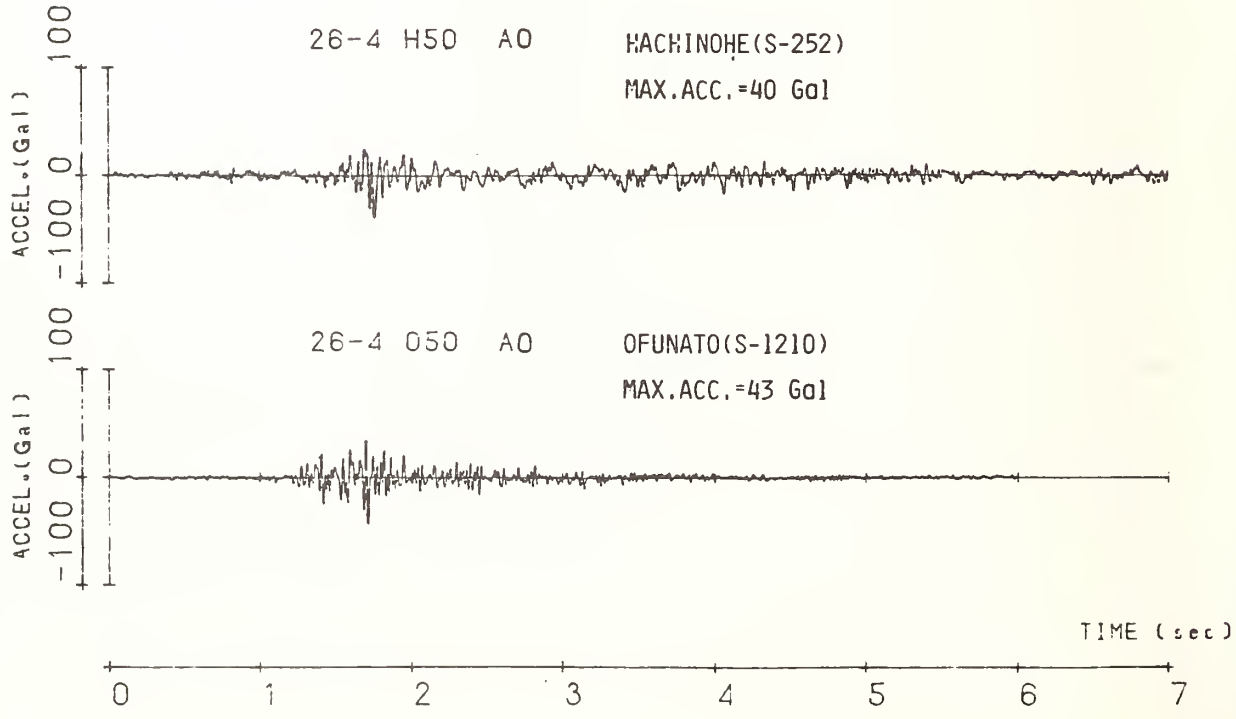

Fig. 4 Earthquake Acceleration Input

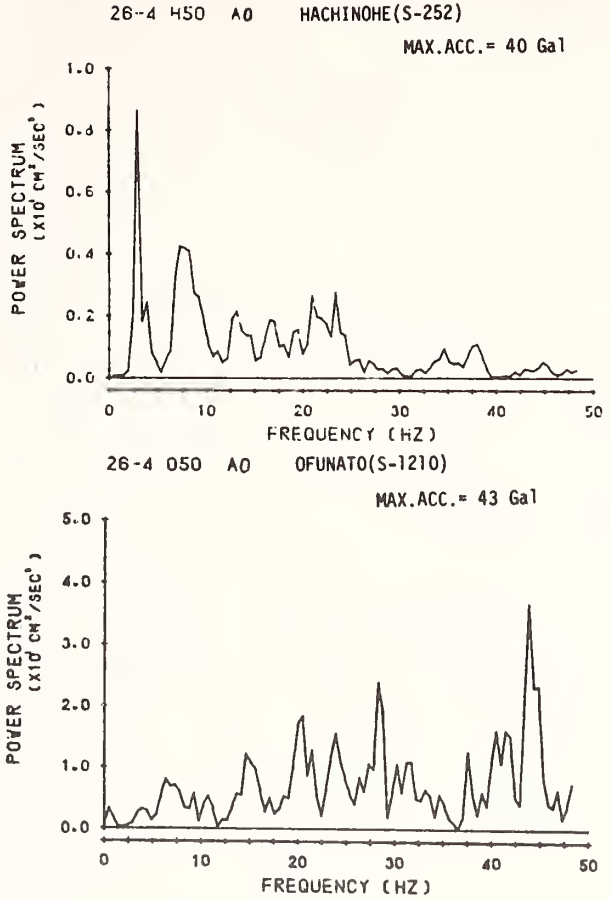

Fig. 5 Power Spectra of Earthquake Acceleration Input

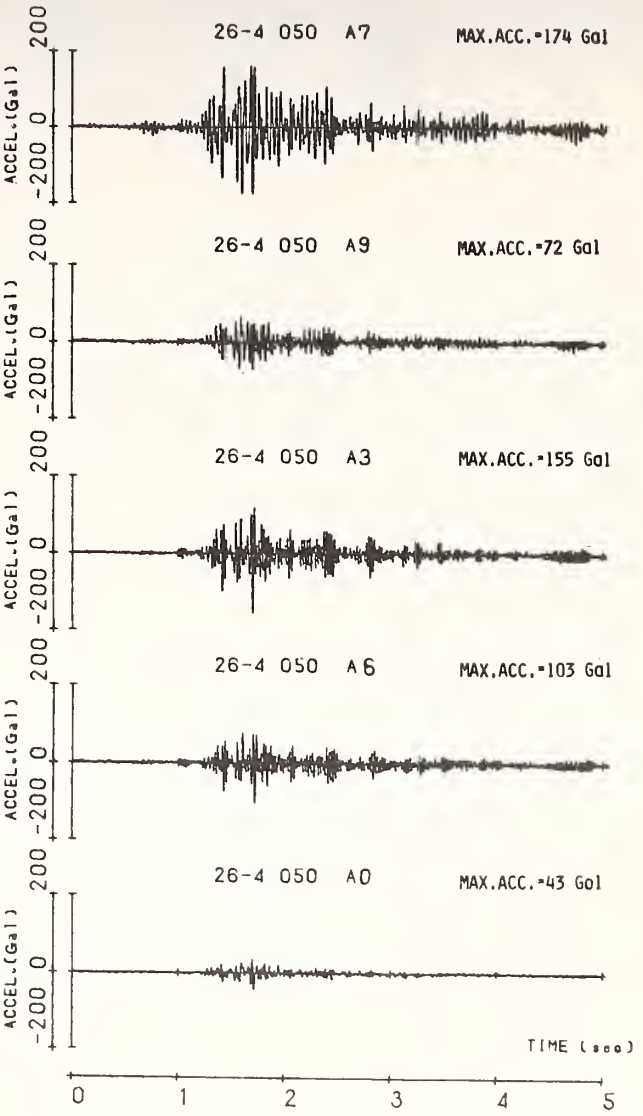

Fig. 6 Response Acceleration

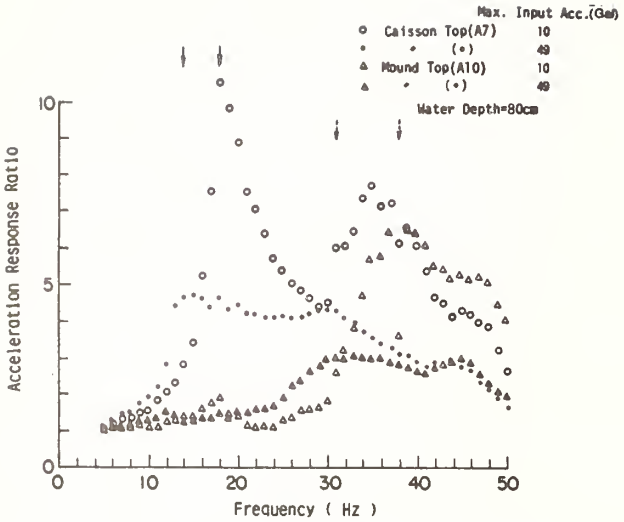

Fig. 7 Effects of Maximum Input Acceleration on Acceleration Response Curve

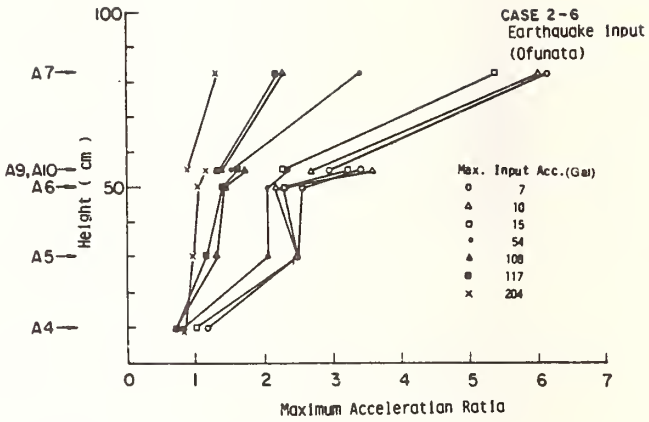

Fig. 8 Maximum Acceleration Ratio versus Height

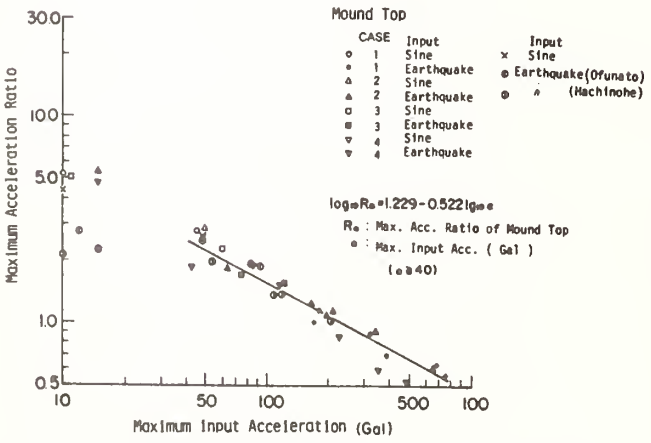

Fig. 9 Maximum Acceleration Ratio of Mound Top versus Maximum Input Acceleration

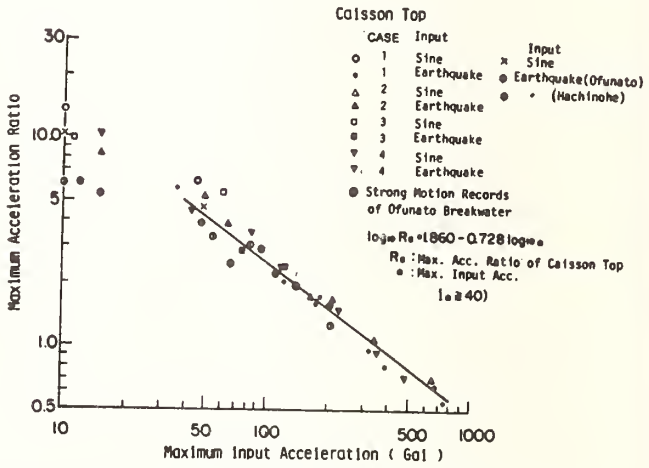

Fig. 10 Maximum Acceleration Ratio of Caisson Top versus Maximum Input Acceleration

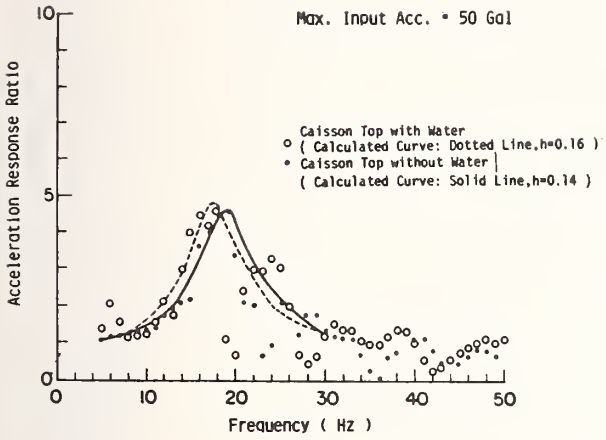

Fig. 11 Acceleration Response Curve of Caisson Top on Vibration Table

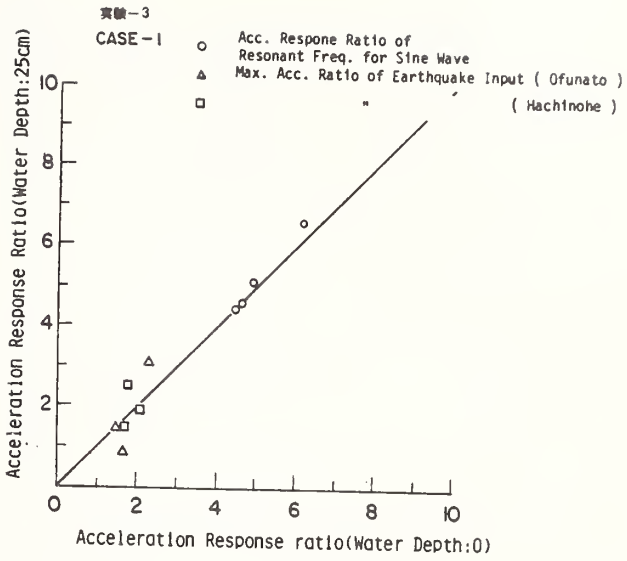

Fig. 12 Effects of Water on Acceleration Response Curve

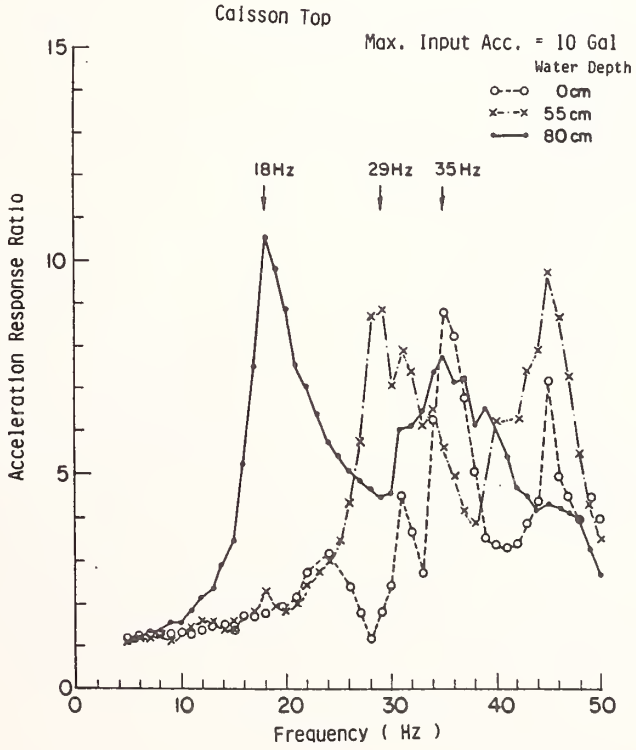

Fig. 13 Effects of Water on Maximum Acceleration Ratio of Caisson Top

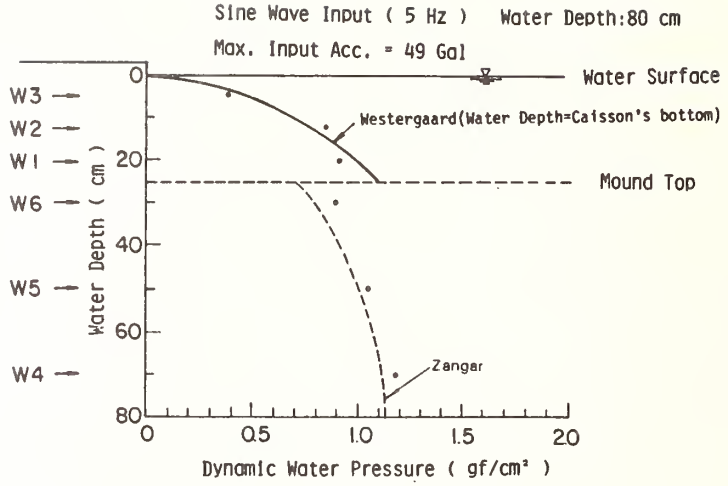

Fig. 14 Dynamic Water Pressures versus Water Depth (80cm) for Sine Wave Input (5 Hz)

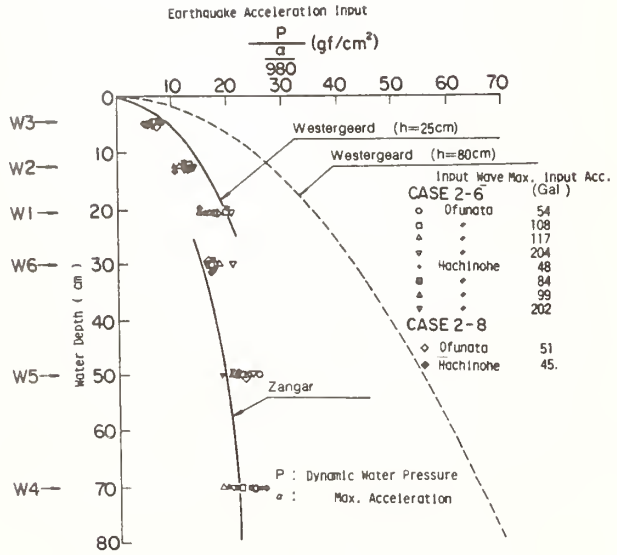

Fig. 16 Dynamic Water Pressures versus Water Depth for Earthquake Acceleration Input

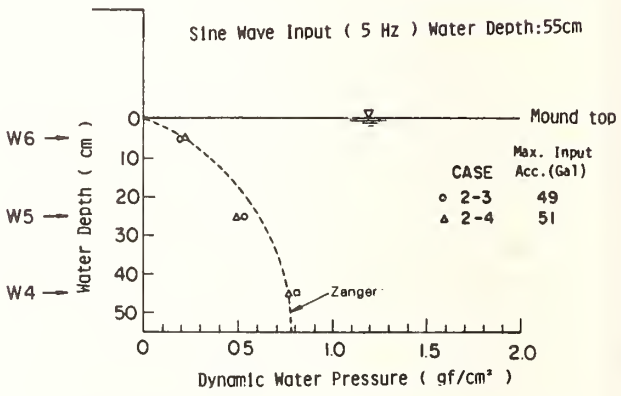

Fig. 15 Dynamic Water Pressures versus Water Depth (55cm) for Sine Wave Input (5 Hz)

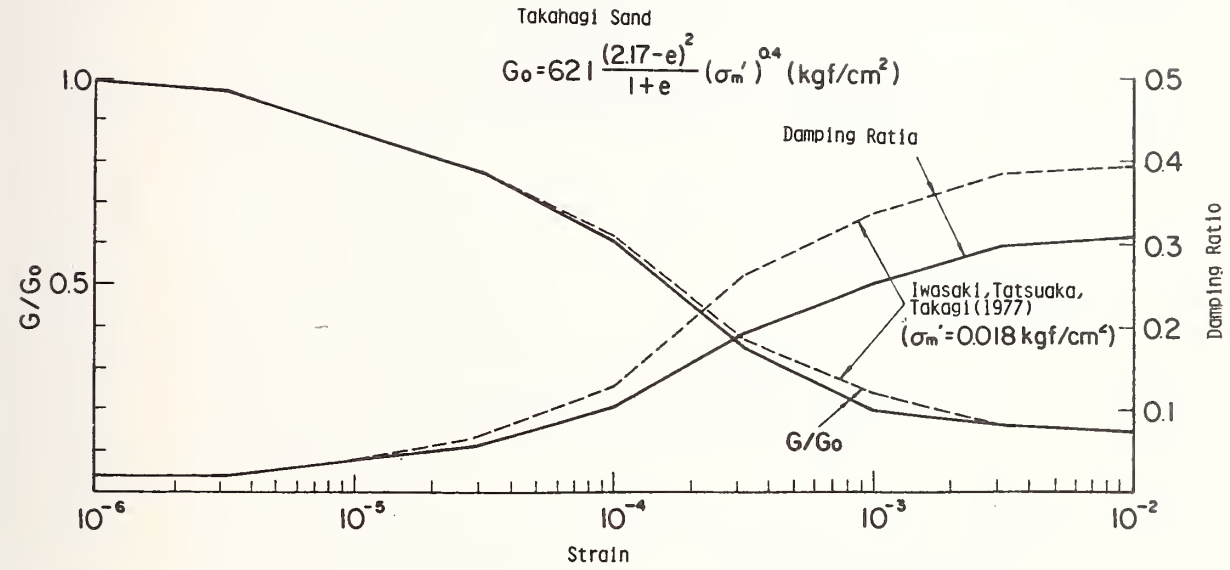

Fig. 17 Shear Modulus and Damping Ratio for Takahagi Sand

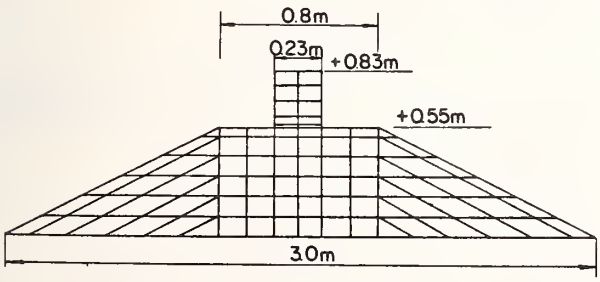

Fig. 18 FEM Model for Breakwater (FLUSH)

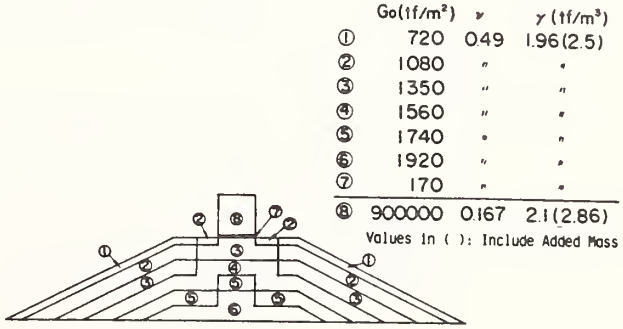

Fig. 19 Properties of Breakwater Model

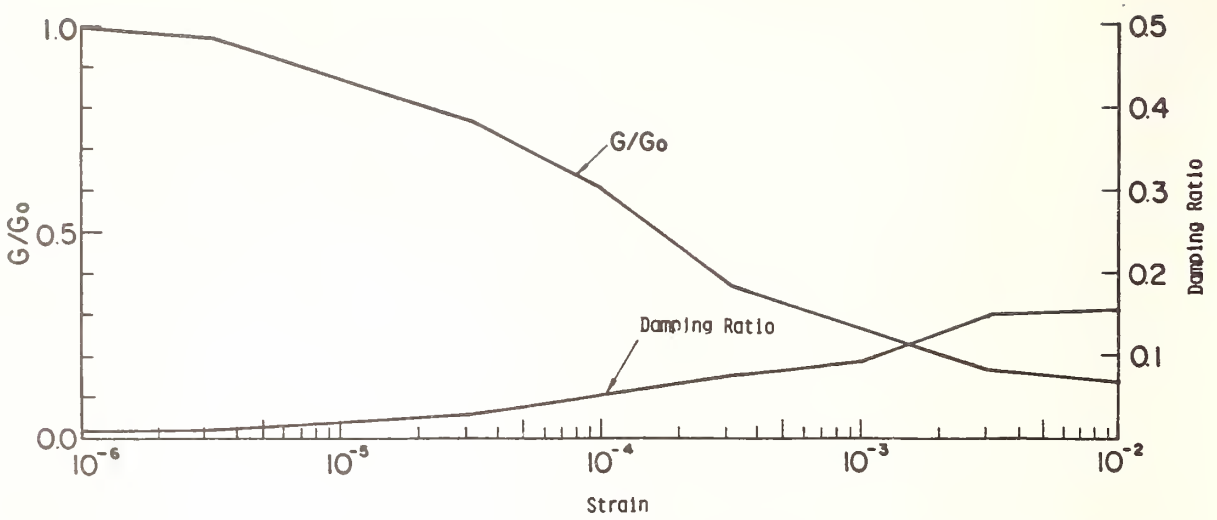

Fig. 20 Shear Modulus and Damping Ratio for Bottom Element of Caisson

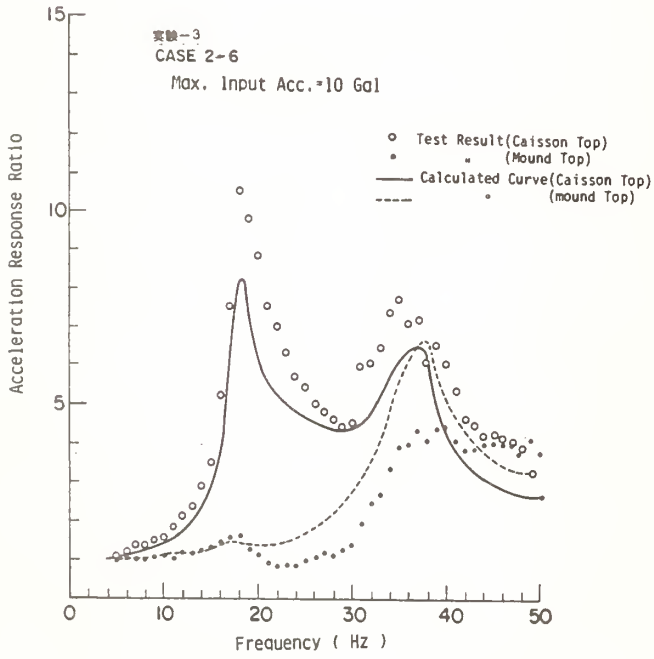

Fig. 21 Comparison of Acceleration Response Curve by Vibration Tests and FLUSH Calculations for 10 Gal Input

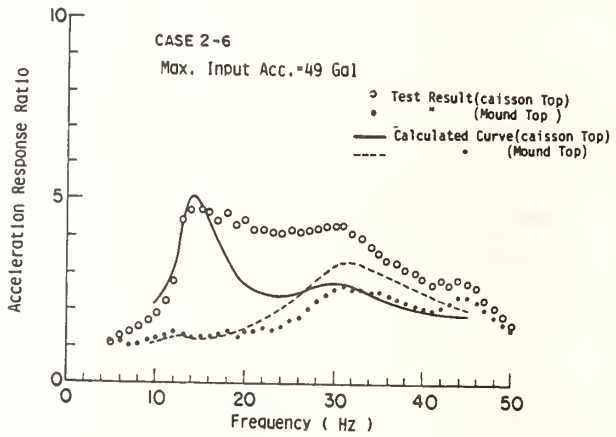

Fig. 22 Comparison of Acceleration Response Curve by Vibration Tests and FLUSH Calculations for 50 Gal Input

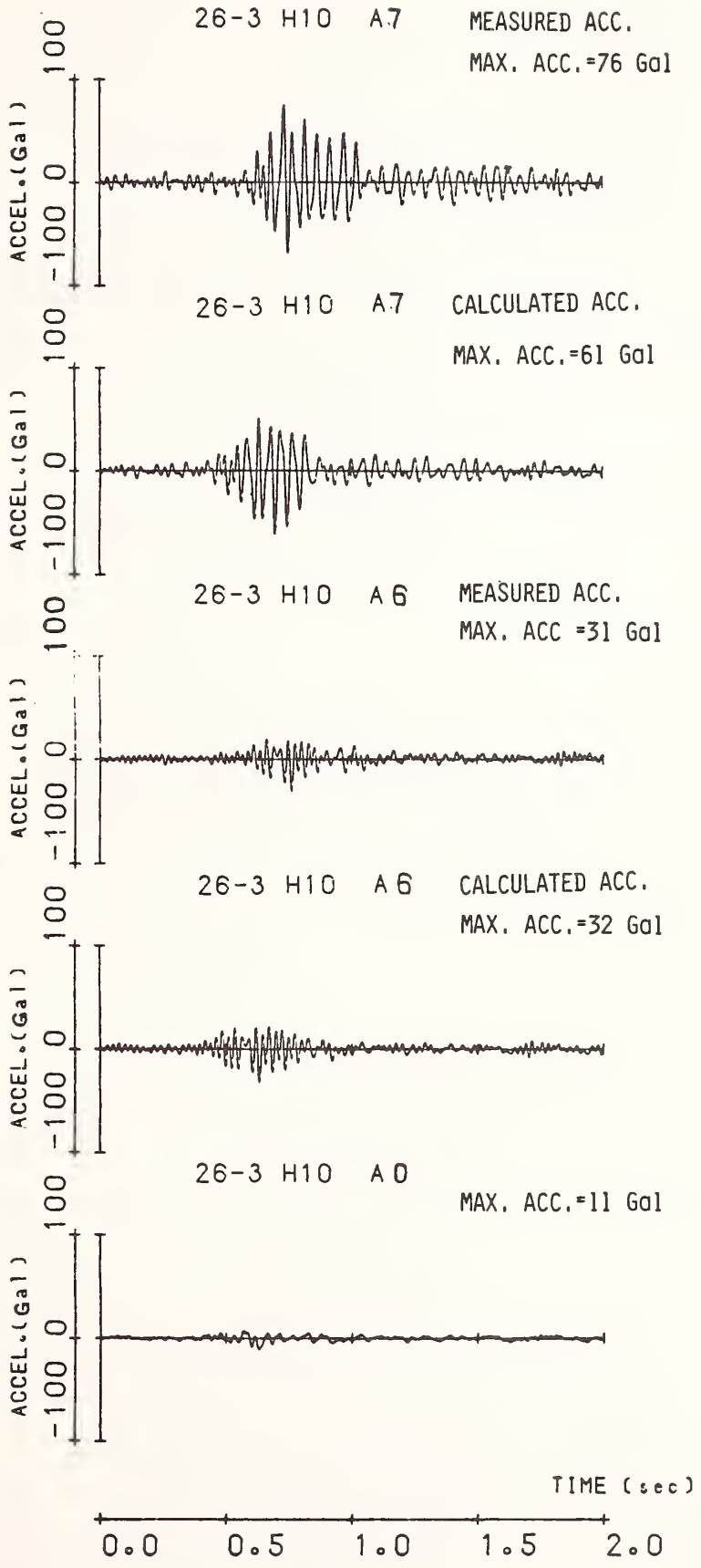

Fig. 23 Comparison of Acceleration Wave Forms by Vibration Tests and FLUSH Calculations

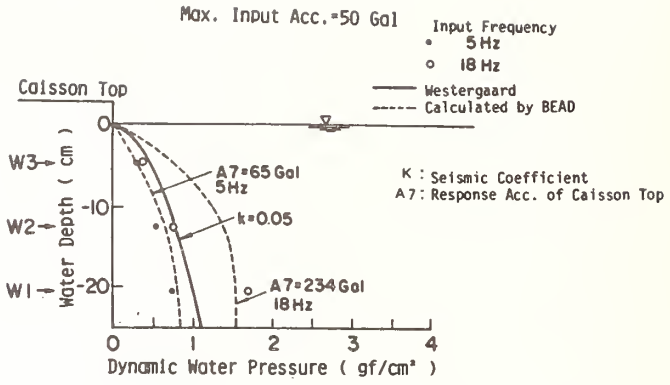

Fig. 24 Comparison of Dynamic Water Pressures by Vibration Tests and BEAD Calculations

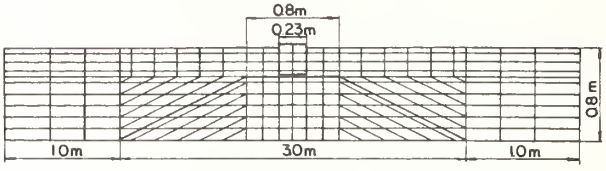

Fig. 25 FEM Model of Breakwater (BEAD)

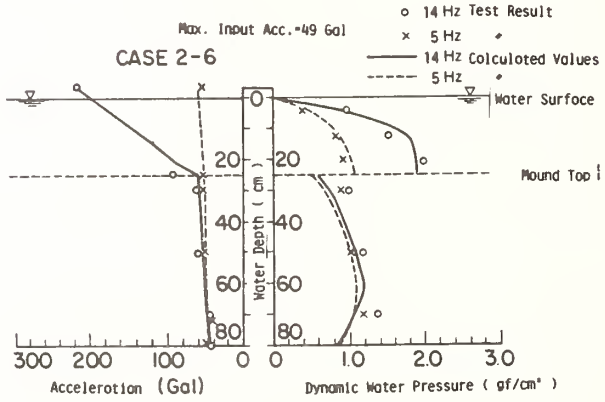

Fig. 26 Comparison of Dynamic Water Pressures and Maximum Acceleation by Vibration Tests and BEAD Calculations

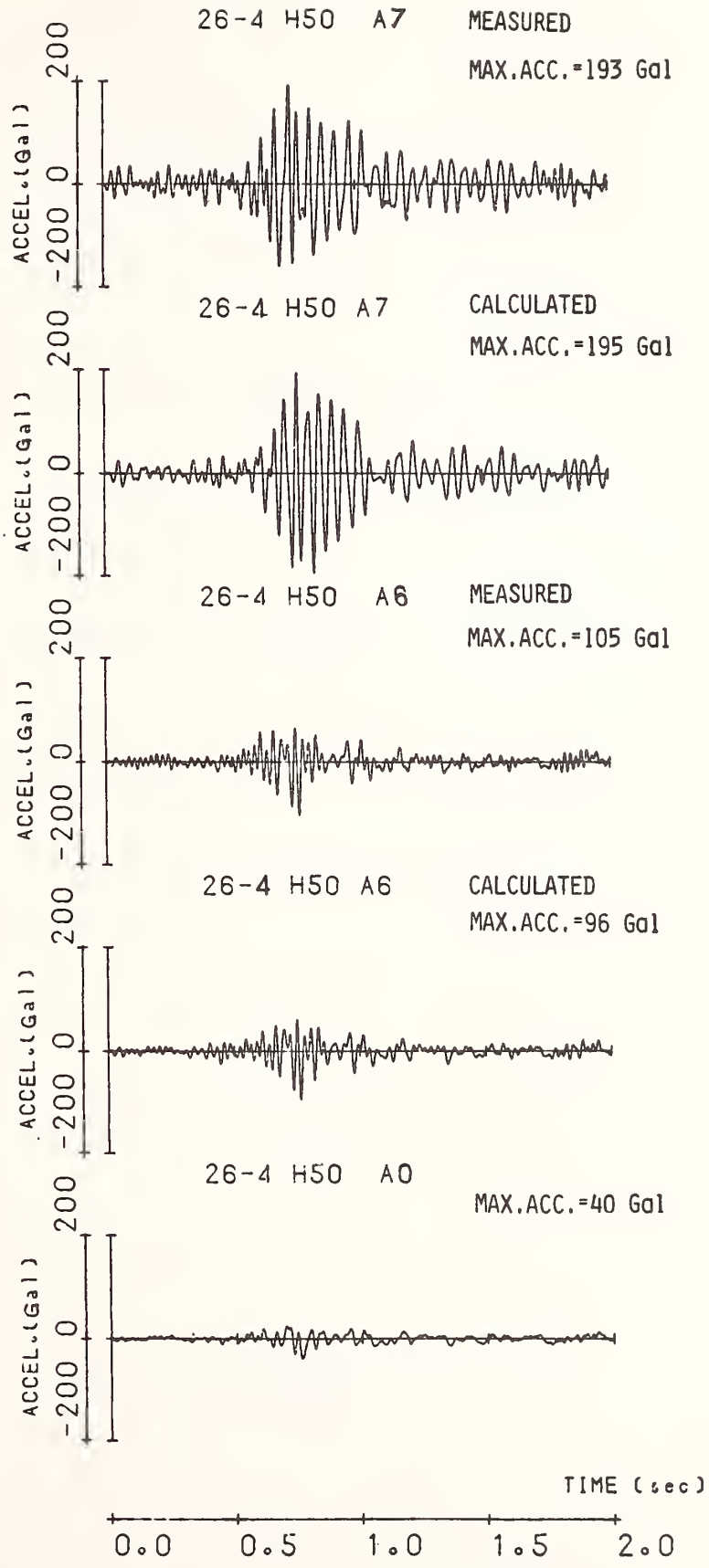

Fig. 27 Comparison of Acceleration Wave Forms by Vibration Tests and BEAD Calculations

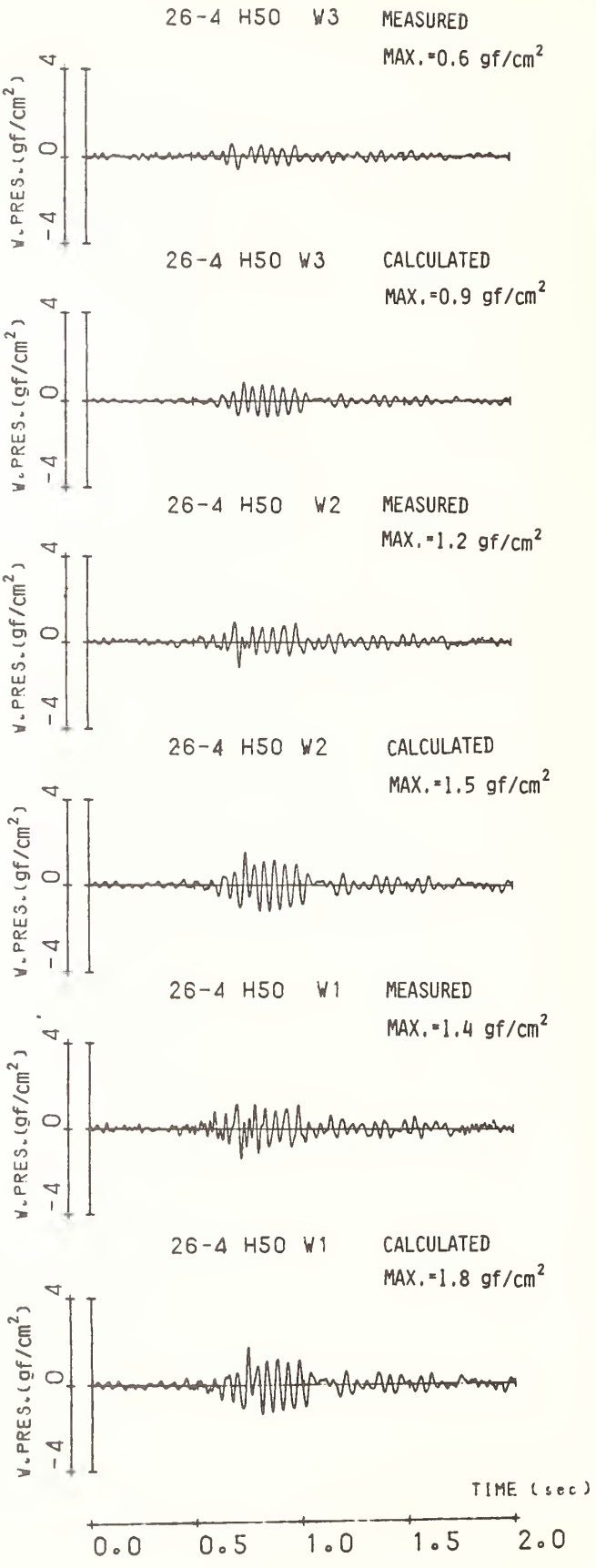

Fig. 28 Comparison of Dynamic Water Pressures on Caisson by Vibration Tests and BEAD Calculations

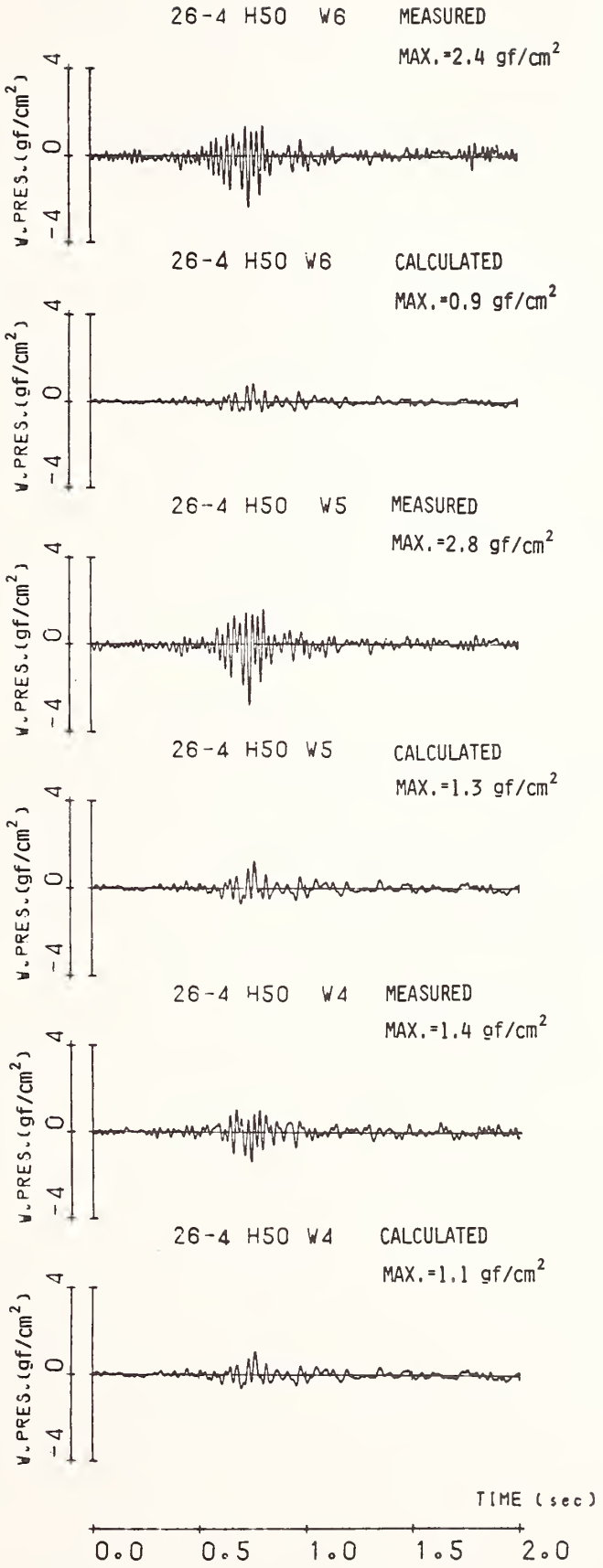

Fig. 29 Comparison of Dynamic Water Pressures on Slope of Mound by Vibration Tests and BEAD Calculations

DYNAMIC ANALYSIS OF EMBANKMENT SECTIONS, RICHARD B. RUSSELL DAM

Arley G. Franklin
Mary Ellen Hynes-Griffin

Research Civil Engineers
U.S. Army Engineer Waterways Experiment Station
Vicksburg, Mississippi

ABSTRACT

Seismic safety of the Russell Dam embankments was evaluated with a permanent displacement analysis, judged appropriate after laboratory cyclic testing verified the nonsusceptibility of embankment and foundation materials to liquefaction. The analysis included determination of critical or yield accelerations by means of conventional limit analysis, estimation of amplification of ground accelerations in the embankment through a visco-elastic shear-beam analysis, and estimation of deformations by means of a Newmark sliding block model. The results indicate that if the dam is subjected to the maximum possible earthquake for the site, superficial displacements would not exceed 3 ft and displacements on deep-seated surfaces would not exceed 1.5 ft.

INTRODUCTION

The Richard B. Russell Dam is presently (1981) under construction on the Savannah River between Hartwell and Clark Hill Dams at river mile 275.1 (U.S. Army Engineer District, Savannah, 1978). The dam will consist of a gravity-type concrete structure in the original river channel, flanked by rolled-fill, zoned earth embankments (figure 1). The crest elevation of both the concrete and earth sections is 495 ft. The right, or west, embankment section, which is in the state of Georgia, is 2180 ft long and has a maximum height of 162 ft. The east embankment section, in South Carolina, is 480 ft long and has a maximum height of approximately 45 ft. The maximum power pool is at elevation 475 ft. The policy of the Corps of Engineers (CE) on seismic design and analysis of dams is set forth in Engineer Regulation (ER) 1110-2-1806 (U.S. Army, 1977), which mandates geological and seismological review for all new CE dams, and dynamic analyses under certain conditions. Richard B. Russell Dam is in an area classified as of "moderate" seismic probability, bordering the highly seismic region centered in Charleston, South Carolina. In accordance with ER 1110-2-1806, a geological and seismological study was done to evaluate the possibility that a potentially damaging earthquake might occur at the site and to select a design earthquake (U.S. Army Engineer District, Savannah, 1977). This was followed by a dynamic analysis using the Newmark sliding block approach [Hynes-Griffin, 1979].

EMBANKMENT ZONING

There are four major material types in the dam and its foundation: (a) dredged river sand, a poorly graded micaceous sand (SP) obtained from the river and used as shell material; (b) impervious core material consisting of residual soil and weathered rock that classifies variously as CH and MH to ML; (c) intensely weathered rock obtained from the natural overburden, a material which is similar to the core material but coarser and with a wider gradation band, and is used as transition zones between shell and impervious core; and (d) foundation zones of natural overburden, highly variable residual soil weathered rock materials that often reflect the original structure of the parent rock. The foundation materials have been left in place under the embankment sections except in the diversion channel and "terminal cones," or wraparound sections at the ends of the concrete dam. Typical ranges of gradation, plasticity, and maximum density are shown in table 1.

Zone geometry and material types vary along the dam axis, some typical sections are shown in figure 2. The embankment has a section with an upstream shell of intensely weathered rock, an impervious core, and a downstream shell of river sand from the right (Georgia) abutment to Sta 14+00 (figure 2a). From Sta 14+00, the intensely weathered rock zone tapers into a transition zone between the core and an upstream shell of river sand (figure 2b). These zones taper eastward so that there is a homogeneous impervious section at Sta 23+00. Upstream slopes have riprap faces (not shown in figure 2). A compacted rock-fill shell covers the impervious material that wraps around the end of the concrete gravity section. The South Carolina terminal cone is similarly designed. The remainder of the South Carolina embankment is primarily impervious material with an upstream riprap face, a sand drain downstream, and a downstream shell of intensely weathered rock (figure 2c). A reservoir water level at el. 475, the maximum power pool elevation, was assumed for the analysis.

DESIGN EARTHQUAKE

From the geological and seismological studies (U.S. Army Engineer District, Savannah, 1977) it was concluded that the greatest earthquake that could occur at the site would be one of two types. The first is a nearby earthquake of magnitude 5.5, possibly reservoir-induced, of short duration (5 sec), with a peak bedrock acceleration of 0.4 to 0.5 g and peak bedrock velocity of 30 to 45 cm/sec at the site. The second represents a distant earthquake of magnitude 7.5, a peak acceleration of 0.2 g, and duration of approximately 20 sec. Nine records were chosen for this analysis. Bedrock motions for the nearby earthquake were obtained from records of Oroville, California, earthquake of August 1, 1975; the Parkfield, California, earthquake of June 27, 1966; the Helena, Montana, earthquake of October 31, 1935; and the Koyna, India, earthquake of December 10, 1967. For the distant earthquake five records obtained at various locations during the San Fernando, California, earthquake

of February 9, 1971, were used. The earthquake accelerograms were scaled to obtain motions consistent with those specified. Of the nine records used, the two that the analysis showed to be the most severe were the S 25 W component of the Temblor no 2 record, Parkfield earthquake, and the east-west component of the Carroll College record, Helena earthquake. The scaled records had peak accelerations of 0.46 g and 0.40 g, respectively, and peak velocities of 30 cm/sec and 36.6 cm/sec, respectively. (For the Parkfield record, the peak velocity determined the scale factor, while for the Helena record, it was the peak acceleration.)

ANALYSIS

The analytical approach used for the Richard B. Russell Dam is based on the concept outlined by Newmark (1965), in which the displaced part of an embankment is modeled as a rigid block on an inclined plane, subjected to earthquake motions which cause the block to slide on the plane. Additional contributions to a coherent procedure using this approach have been made by Ambraseys and Sarma (1967), Sarma (1975, 1979), Goodman and Seed (1965), and Makdisi and Seed (1977).

This method of analysis does not predict changes in strength due to shaking, and so is generally not appropriate where a question of failure through liquefaction must be addressed. On the other hand, if limited loss of shear strength due to shaking or to shear displacement is anticipated, it can be accommodated in the analysis by use of suitable reduced strengths.

In this case, a review of field and laboratory test data and the design of the cross sections indicate that significant potential for liquefaction does not exist. The saturated materials in the Georgia embankments, typified by Sta 20+00, figure 2, are the river sand, an upstream transition zone, and the core. The micaceous river sand is easily compacted to a high relative density and strength. Data from the test fills indicate that relative density of the sand will be in the range of 95 to 100 percent. The other materials of the embankment, the impervious core material and intensely weathered rock, while variable, have good compaction characteristics and static strengths. Typically, they have a wide gradation and are somewhat plastic, as shown in table 1. Materials of this nature have not been known to liquefy during earthquakes. The same is true of the residual soil and weathered rock foundation. A program of laboratory cyclic triaxial tests verified that in all foundation and embankment materials degradation of strength due to shaking is negligible.

The major components of a permanent displacement analysis of the Newmark type, as applied by the Waterways Experiment Station, are shown in figure 3. The primary component is the analysis of motions of a system consisting of a rigid block on an inclined plane, chosen to represent a potential sliding mass in an embankment, as described by Newmark. A conventional limit analysis, or slope stability analysis, with slight modifications, provides the shearing resistance between the block

and the plane. Because base motions may be amplified upon being propagated upward through an embankment, a rigid-body model is likely to yield unconservative estimates of displacements, and an analysis of the amplification response of the embankment is incorporated to accourt for that aspect of the embankment behavior.

CRITICAL ACCELERATION STABILITY ANALYSIS

The shearing resistance between the potential sliding mass and the underlying base is evaluated in terms of a critical acceleration, N, defined as the level of base acceleration (that is, of the ground or embankment below the sliding surface) that will reduce the factor of safety against sliding to unity. In other words, it is the base acceleration that will make sliding imminent. The value of N, which is expressed as a fraction of g, the gravitational acceleration, is obtained through a stability analysis which is similar to conventional pseudostatic stability analyses, but which includes two special features. One is that the stability is evaluated in terms of a critical acceleration rather than a factor of safety, and the other is that, because the amplified accelerations vary over the height of the embankment, critical accelerations must be determined for possible sliding masses whose bases lie at various elevations in the section. The analysis may be performed using conventional stability analysis methods such as those of Bishop (1955) or Morgenstern and Price (1965) with strength values appropriate for earthquake loading. Trial values of acceleration may be used to find the value that reduces the factor of safety to unity. The Sarma method [Sarma, 1975], which employs a slip surface of arbitrary shape, determines the value of N directly.

In principle, the analysis can be performed on either a total or an effective stress basis, but the problems of estimating pore pressures induced by cyclic shearing are avoided by using a total stress analysis, which was done for Russell Dam. Following usual CE practice for static stability analyses, this analysis used a composite shear strength envelope based on the S test (consolidated-drained) at low confining pressures and the R test (consolidated-undrained) at high confining pressures. That is, at any confining pressure, the lower of the R and S strengths was used. This strength envelope conservatively takes into account possible dissipation of shear-induced negative pore pressures that might occur in the field but cannot occur in an undrained test in the laboratory. Strength parameters used for analysis are shown in table 2. The simplified Bishop [Bishop, 1955; McDonnell-Douglas Automation Company, 1973) and the Sarma method [Sarma, 1973, 1975; Hynes, 1978] were used to determine critical accelerations. The analysis assumes that steady-state seepage exists when the earthquake occurs.

For a fairly symmetrical section, upstream failure surfaces usually have lower critical accelerations than downstream surfaces at the same elevation. This is because in a submerged slope,

the buoyant unit weight of the soil determines the normal stress on the failure surface which in turn determines the shear strength from the S-R envelope. In a nonsubmerged slope, the total unit weight determines the available strength. On the other hand, the horizontal acceleration involves the total unit weight acting in a horizontal direction, and the horizontal inertia force is thus determined by the total unit weight in either case. For this reason, while a total of eight sections were analyzed, only one, that at Sta 45+50, was a downstream slope. This section has a long, steeply sloping foundation layer overlying the bedrock. For this slope, the moist unit weight was used throughout because the phreatic surface was at or below the sliding surfaces of interest. The sections analyzed are identified in figure 1, except for Sta 23+00, which is near the Georgia terminal cone.

Results of the critical acceleration analysis are exemplified by figure 4. Figure 4a shows critical slip circles at various elevations in the embankment at Sta 20+00 and the associated values of the critical acceleration N, as a fraction of gravity. Figure 4b shows the critical acceleration values plotted against elevation of the base of the failure surface.

SLIDING BLOCK ANALYSIS

The elements of the sliding block analysis are shown in figure 5 [Franklin and Chang, 1977]. The potential sliding mass shown in figure 5a is in a condition of impending failure, so that the factor of safety equals unity. This is caused by the circumstance that both the base and the mass are accelerating toward the left of the sketch with an acceleration of Ng. The acceleration of the mass is limited to this value by the limit of the shear stresses that can be exerted across the contact, so that if the base acceleration were to increase, the result would be that the mass would move downhill relative to the base. By D'Alembert's principle, the limiting acceleration is represented by an inertia force NW applied pseudostatically to the mass in a direction opposite to the acceleration.

The force polygon for this situation is shown in figure 5b. The angle of inclination of the inertia force, θ, may be found as the angle that is most critical; that is, the angle that minimizes, N. Its value is usually within a few degrees of zero, and the results of the analysis were not sensitive to it, so it can generally be ignored. The angle β is the direction of the resultant S of the shear stresses on the interface and is determined in the course of the stability analysis. The same force polygon applies to the model shown in figure 5c: a sliding block on a plane inclined at an angle β to the horizontal. Hence, the use of the sliding block model to represent the sliding mass in an embankment.

The force-displacement relation that is assumed to apply to this system is shown in figure 5d. The force in this diagram is the inertia force corresponding to the instantaneous acceleration of the

block and the displacement is the sliding displacement of the block relative to the base. It is usually assumed that resistance to uphill sliding is large enough that all displacements are downhill. This assumption, in addition to simplifying the calculations, is both realistic and conservative.

If the base (i.e., the inclined plane) is subjected to some sequence of acceleration pulses (the design earthquake) large enough to induce sliding of the block, the result will be that, after the earthquake motion has abated, the block will come to rest at some displaced position down the slope. The amount of that permanent displacement, which will be called u, can be computed by using Newton's second law of motion (F = ma) to write the equation of motion for the sliding block relative to the base, and then numerically or graphically integrating (twice) to obtain the resultant displacement. During the time intervals when relative motion is occurring, the acceleration of the block relative to the base is given by:

$$\ddot{u} = a_{rel} = (a_{base} - N) \cdot \frac{\cos(\beta-\theta-\phi)}{\cos \phi} = (a_{base} - N) \cdot \alpha \qquad (1)$$

where

a_{rel} = relative acceleration between the block and the inclined plane,

a_{base} = acceleration of the inclined plane, a function of time,

N = critical acceleration level at which sliding begins,

β = direction of the resultant shear force and displacement, and the inclination of the plane,

θ = direction of the acceleration, measured from the horizontal, that makes N a minimum,

ϕ = friction angle between the block and the plane.

The acceleration a_{base} is the earthquake acceleration acting at the level of the sliding mass in the embankment. It is assumed to be equal to the bedrock acceleration multiplied by an amplification factor κ which accounts for the quasielastic response of the embankment.

The permanent displacement is determined by twice integrating the relative accelerations over the total duration of the earthquake record. It is assumed that ϕ, β, and θ do not change with time; thus, the coefficient α is a constant and is not involved in the integration. In the final stage of the analysis, the result of the integration is multiplied by the coefficient α, the determination of which requires knowledge of the embankment properties and the results of the pseudostatic analyses. For most practical problems, the coefficient α does not differ from unity by more than about 20 percent (figure 6), and so is of minor importance. For the present analysis, the acceleration was assumed to act in the horizontal direction, so that θ = 0. Sensitivity analyses by Sarma (1975) of

this simplifying assumption show that the critical value of θ is not large and the resulting error in N is insignificant.

The integration can be readily visualized on a plot of base velocity versus time, which is obtained by a single integration of the acceleration record (figure 5e). Since the slope of the velocity curve is the acceleration, the limiting acceleration Ng of the block defines the velocity curve for the block by straight lines in those parts of the plot where the critical acceleration has been exceeded in the base. Point A in figure 5e represents the point at which the base acceleration first exceeds the critical acceleration, and thus is the point in time at which relative motion begins. Point B is the point at which the velocities of the base and the block become equal, and so is the end of relative motion until the critical acceleration is again exceeded. The area between the curves gives the relative displacement.

In this analysis, the characteristics of the potential sliding mass in the embankment are represented only by the critical acceleration, N, the base acceleration required to make sliding imminent, the coefficient α, and the amplification factor κ; the latter two of which are simply constant multiplying factors. Thus, the permanent displacement, u, for a particular earthquake record can be determined as a function of N/A, where Ag is the peak value of the earthquake acceleration, and the u versus N/A curve for $\alpha = 1$ and $\kappa = 1$ can be determined from the earthquake record without reference to a particular embankment. Figure 7 shows these curves for the Parkfield and Helena records, scaled, as described earlier to peak accelerations of 0.46 g and 0.40 g, respectively.

EMBANKMENT RESPONSE ANALYSIS

Amplification of ground motions in the embankment may be examined by analysis of a shear-beam model of the embankment-foundation system. A closed-form solution has been obtained by Sarma (1979) for the problem illustrated by figure 8. The model considered is an untruncated triangular wedge of height h_1, with a shear wave velocity S_1, and density ρ_1, underlain by a foundation layer with thickness h_2, shear wave velocity S_2, and density ρ_2. Both the wedge and foundation are linearly viscoelastic and have the same damping ratio D. The earthquake motions are considered to be rigid-body motions in the rock underlying the foundation layer, and it is assumed that all motions are horizontal (hence, a shear-beam model). Shear wave velocities and damping values are chosen so as to be consistent with expected strain levels. The computation of accelerations is carried out in the time domain.

The amplification analysis requires an estimate of a single average shear wave velocity for the embankment and a second shear wave velocity for the foundation, or the ratio of the two velocities.

At the Russell Dam site, velocity measurements were obtained from field surveys on test fills and foundation soils and from laboratory resonant column tests on representative borrow and foundation materials. On the basis of these data, and considering degradation of shear wave velocity with shear strain, an average shear wave velocity of 400 ft/sec was adopted as representative of the embankment and 800 ft/sec was adopted for the foundation. A damping value of 20 percent was adopted for both embankment and foundation.

The fundamental period T_o of the embankment-foundation system can be estimated from the chart by Sarma (1979) shown in figure 9, in which geometry and material parameters are described in terms of the dimensionless parameters m and q, which are defined as

$$m = \frac{\rho_1 S_1}{\rho_2 S_2} \text{ and } q = \frac{S_1 h_2}{S_2 h_1} \tag{2}$$

Table 3 shows how these values vary over the length of the embankment.

For use with the sliding block analysis, accelerations are averaged over a wedge that is selected to be approximately equivalent in volume and location to a potential sliding mass with its base at some chosen elevation, as shown in figure 10. The average acceleration acting on the wedge at any instant is taken as:

$$a_{av} = \frac{\int_A a(y)\,dA}{A} \tag{3}$$

where a(y) is the acceleration of the area element dA, at elevation y, and A is the total area of the wedge.

The largest average acceleration that acts on the wedge at any time during the earthquake shaking is produced as the output of the computer program, and the ratio of that acceleration value to the peak bedrock acceleration is taken as the amplification factor κ for the wedge. Values of κ for the Helena earthquake record are plotted against the embankment fundamental period T_o in figure 11. Curves are shown for wedges with their bases at various distances y_b/h_1 (defined in figure 10) from the crest, for a single combination of m and q values (m = 0.5, q = 0.185). Similar plots were generated for the combinations (m = 0, q = 0) and (m = 0.5, q = 0.5), which permitted amplification factors for the sections that were analyzed to be obtained by interpolation or by modest extrapolation.

COMPUTATION OF POTENTIAL DISPLACEMENT

The potential displacement for sliding surface with its base at a particular level in the embankment is calculated using the following elements: (a) the value of critical acceleration N for

a particular elevation, as determined from the stability analysis; (b) the peak average acceleration value for the sliding mass with its base at that elevation, determined as the product of the peak bedrock acceleration A and the amplification factor κ, from the dynamic response analysis; and (c) the u versus N/A curve for the design earthquake, determined from the sliding block analysis. The curve of displacement u versus N/A (which gives displacements for an amplification factor of unity) is entered at the appropriate value of $N/\kappa \cdot A$ to obtain a value of displacement u which is then multiplied by κ and α to obtain the final displacement estimate, u_m. Figure 12 shows a plot of potential displacements for slip surfaces with their bases at various elevations at Sta 20+00. Potential displacements shown are computed from the Helena record; other earthquake records yielded smaller values.

The displacement versus elevation plot does not represent the expected deformed shape of the embankment. Rather, an individual point on the curve represents the permanent displacement that a single sliding mass with its base at that elevation would undergo, under the assumption that there is only one sliding surface. Only one of these surfaces is likely to develop, because the more intense components of accelerations propagating upward from the bedrock cannot be transmitted above a sliding surface. For this reason, the choice of the largest of the potential permanent displacements determined from the curve is considered to be conservative. The direction of the displacement vector is given by the angle β, the direction of the resultant shearing resistance, obtained from the stability analysis.

The results are summarized in table 4, which shows the largest potential displacements computed for all of the sections analyzed. The displacements are categorized as occurring on shallow surfaces, deep surfaces within the embankment (embankment surfaces), and deep surfaces through the foundation (foundation surfaces). It can be observed from the table that the largest displacements generally are for shallow slip surfaces at the shorter sections. These sections have fundamental periods closer to the peaks in the amplification charts. Also, the conservative choice of the S strength envelope for low confining pressures leads to low critical acceleration values for shallow sliding surfaces and possibly to overestimation of permanent displacements.

All of the computed displacements are less than 3 ft, and, except for Sta 5+00 and 42+50, the displacements for these shallow surfaces are on the order of 1.5 ft, and the displacements on deeper surfaces in the embankment are on the order of 1/2 ft or less. For those sections underlain by a foundation layer, the largest displacement occurs at Sta 45+50 and has an estimated value of 1.5 ft. Although this amount of displacement in no way threatens loss of the reservoir or the integrity of the filters and drains, the downstream slope was subsequently changed from 1:2.5 to 1:4. Since the

18 in. displacement estimate did not indicate a dangerous situation, an additional analysis of the 1:4 slope was not deemed necessary. The calculated displacement along a deep surface of Sta 5+00 is on the order of 1 ft and at all other sections with a foundation layer, the displacements are on the order of 1/2 ft or less.

CONCLUSION

In evaluating the seismic safety of the Richard B. Russell Dam, two primary modes of failure were considered: (a) failure due to liquefaction or seismically induced loss of strength in the embankment or foundation materials; and (b) failure by sliding due to horizontal earthquake accelerations. Consideration of the characteristics of the foundation and embankment materials led to the conclusion that they were not susceptible to liquefaction; this conclusion was verified by a program of cyclic triaxial tests. Evaluation of safety against failure by sliding was done by means of an analysis using Newmark's sliding block model. Amplification of base motions through quasielastic embankment response was estimated by means of a linear viscoelastic shear-beam analysis due to Sarma (1979). The permanent displacements obtained from the analysis probably represent an upper bound, because the general approach that was adopted was to use conservative choices of parameters describing earthquake motions and material properties. Such an approach is believed to be appropriate in an analysis with the sole purpose of verifying the safety of a structure, because: (a) it reduces the effort required if the margin of safety is high; (b) the quantities obtained are not intended for comparison with observational data, since the probability of occurrence of the design earthquake is very low; and (c) existing observational data to compare with values obtained by this method of analysis are limited. Because of this conservatism, and because the descriptions of physical behavior used in the analysis are considerably simplified and idealized, a high degree of precision is not to be looked for in the results. The numerical values should be regarded as approximations only.

The largest permanent displacements calculated were less than 3 ft, for shallow sliding surfaces high in the embankment. Such deformations represent predictions of superficial damage. The largest value computed for a deep sliding surface was 1.5 ft, on the South Carolina embankment; most calculated displacements for deep sliding surfaces were 0.5 ft or less. Considering the 20 ft of freeboard that will exist with the water level at maximum power pool, such deformations would not threaten the overall stability of the embankment or the integrity of the reservoir.

ACKNOWLEDGMENT

The work described in this paper was performed for the U.S. Army Engineer District, Savannah. The authors are indebted to the U.S. Army Engineer Waterways Experiment Station and the Corps of Engineers for permission to present this paper.

REFERENCES

[1] Ambraseys, N. N. and S. K. Sarma, 1967, "The Response of Earth Dams to Strong Earthquakes," Geotechnique, Vol. 17, No. 2, pp. 181-213.

[2] Bishop, A. W., 1955, "The Use of the Slip Circle in the Stability Analysis of Slopes " Geotechnique, Vol. 5, No. 1, pp. 7-17.

[3] Franklin, A. G. and F. K. Chang, 1977, "Earthquake Resistance of Earth and Rock-Fill Dams: Permanent Displacements of Earth Embankments by Newmark Sliding Block Analysis," Miscellaneous Paper S-71-17, Report 5, U.S. Army Engineer Waterways Experiment Station, CE, Vicksburg, MS.

[4] Goodman, R. E. and H. Bolton Seed, 1966, "Earthquake-Induced Displacements in Sand Embankments," Journal of the Soil Mechanics and Foundations Division, American Society of Civil Engineers, Vol. 92, No. SM2, Proceedings Paper 4736.

[5] Hynes, M. E., 1978, "EQS Users Manual: A Computer Program for the Static and Dynamic Analysis of Earth Slopes by the Sarma Method," Miscellaneous Paper No. S-78-13, U.S. Army Engineer Waterways Experiment Station, CE, Vicksburg, MS.

[6] Hynes-Griffin, M. E., 1979, "Dynamic Analysis of Earth Embankments for the Richard B. Russell Dam and Lake Project," Report to U.S. Army Engineer District, Savannah, U.S. Army Engineer Waterways Experiment Station, CE, Vicksburg, MS.

[7] Makdisi, F. I. and H. Bolton Seed, 1977, "Simplified Procedure for Estimating Dam and Embankment Earthquake-Induced Deformations," Journal of the Geotechnical Engineering Division, Vol. 104, No. GT7, Proceedings Paper No. 13898, pp. 849-867.

[8] McDonnell-Douglas Automation Company, 1973, "ICES Slope Stability Analysis System Users Manual," McDonnell-Douglas Corporation, St. Louis, MO.

[9] Morgenstern, N. R. and V. E. Price, 1965, "The Analysis of the Stability of General Slip Surfaces," Geotechnique, Vol. 15, No. 1, pp. 79-93.

[10] Newmark, N. M., 1965, "Effects of Earthquakes on Dams and Embankments," Geotechnique, Vol 15, No. 2, pp. 139-160.

[11] Sarma, S. K., 1973, "Stability Analysis of Embankments and Slopes," Geotechnique, Vol. 23, No. 4, pp. 423-433.

[12] Sarma, S. K., 1975, "Seismic Stability of Earth Dams and Embankments," Geotechnique, Vol. 25, No. 4, pp. 743-761.

[13] Sarma, S. K., 1979, "Response and Stability of Earth Dams During Strong Earthquakes," Miscellaneous Paper GL-79-13, U.S. Army Engineer Waterways Experiment Station, CE, Vicksburg, MS.

[14] U.S. Army, 1977, Engineer Regulation No. 1110-2-1806, Office of the Chief of Engineers, Washington, DC, April 30, 1977.

[15] U.S. Army Engineer District, Savannah, 1977, "Geological and Seismological Evaluation of Earthquake Hazards at the Richard B. Russell Project, Design Earthquake Report.

[16] U.S. Army Engineer District, Savannah, 1978, "Earthquake Embankments, Design Memorandum 17, Richard B. Russell Dam and Lake, Savannah River, Georgia and South Carolina," Vol. I.

Table 1. Properties of Embankment Materials

Material Type	Percent Passing No. 4 Sieve	Percent Passing No. 200 Sieve	Plasticity Index	Maximum Dry Density (pcf)
Dredged river sand	98 to 100	0 to 13	--	94.2 to 113.7
Intensely weathered rock	70 to 100	17 to 48	2 to 21	114.2 to 130.5
Impervious core material	100	52 to 98	5 to 44	78.4 to 116.2
Foundation overburden	100	42 to 70	3 to 34	77.7 to 110.6 (in situ)

Table 2. Strength Parameters Used for Analysis

Material Type	R		S	
	ϕ(o)	C(tsf)	ϕ(o)	C(tsf)
Dredged river sand	25	0.4	34	0
Intensely weathered rock	14	0.4	38	0
Impervious core material	14	0.3	26	0
Foundation overburden	14 16	0.2* 0.4	30	0

* Two values used because of high variability.

Table 3. Geometry and Fundamental Period for Sections Analyzed

Section	Dam Height (ft)	Foundation Thickness (ft)	m	q	$\bar{a}_1$	T_o (sec)
Station 5+00	45	30	0.5	0.33	2.00	0.35
Station 10+00	65	30	0.5	0.23	2.13	0.48
Station 16+25 diversion channel	162	0	0.0	0.00	2.41	1.06
Station 20+00	100	20	0.5	0.10	2.29	0.69
Station 23+00	110	10	0.5	0.05	2.40	0.72
Georgia terminal cone	155	0	0.0	0.00	2.41	1.01
Station 42+50 (upstream)	45	10	0.5	0.11	2.28	0.31
Station 45+50 (downstream)	45	10	0.5	0.11	2.28	0.31

Table 4. Summary of Potential Displacements

Section	Shallow Surfaces		Embankment Surfaces		Foundation Surfaces	
	u_m (in)	β(°)	u_m (in)	β(°)	u_m (in)	β(°)
5+00	30*	18	5**	6	10**	14
10+00	6**	17	6**	9	6**	12
16+25	6*	18	2*	13	--	--
20+00	12*	18	2*	11	4*	16
23+00	10*	18	2*	12	4*	16
Georgia terminal cone	5*	18	1*	10	--	--
42+50	24*	18	4**	9	3**	6
45+50	6*	14	3**	9	18**	18

* Helena
** Parkfield

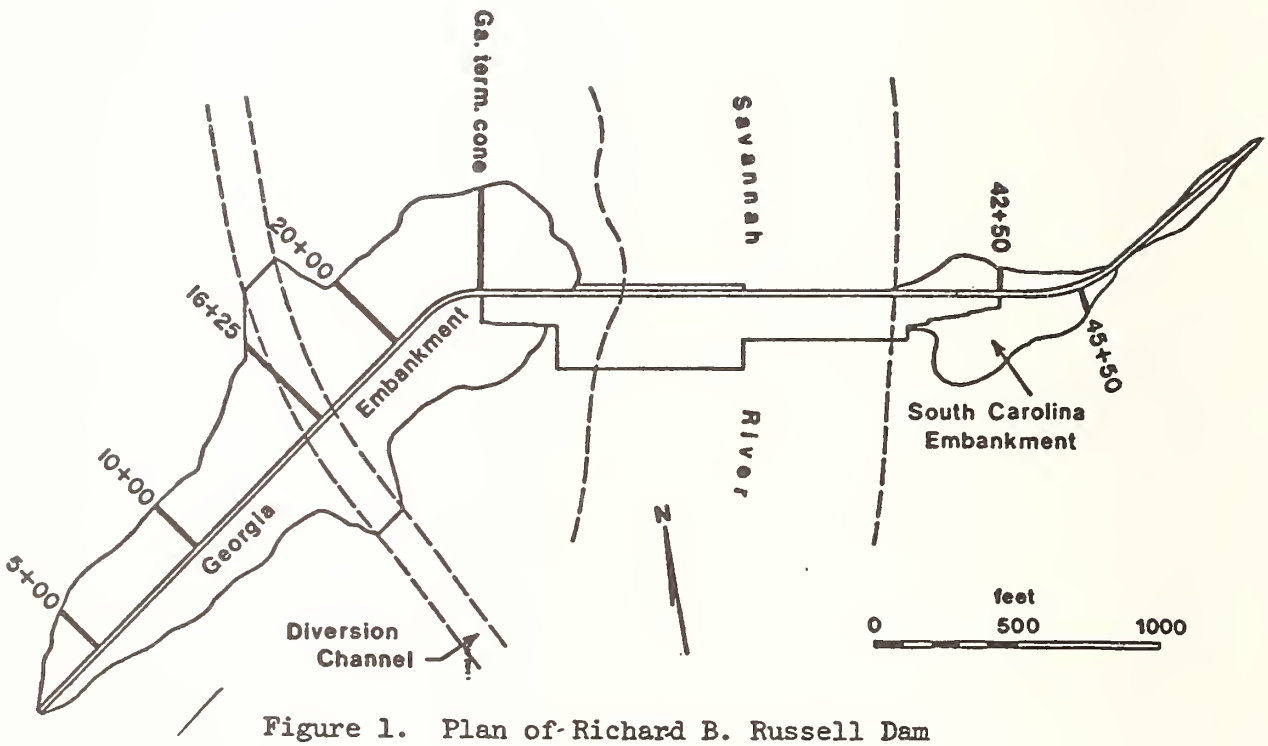

Figure 1. Plan of Richard B. Russell Dam

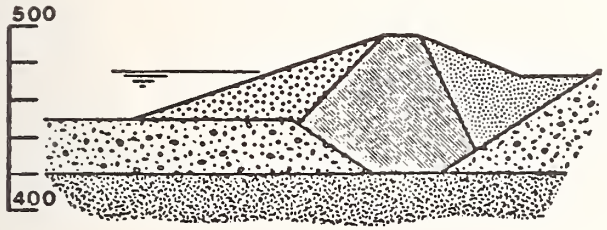

a. Sta. 5+00

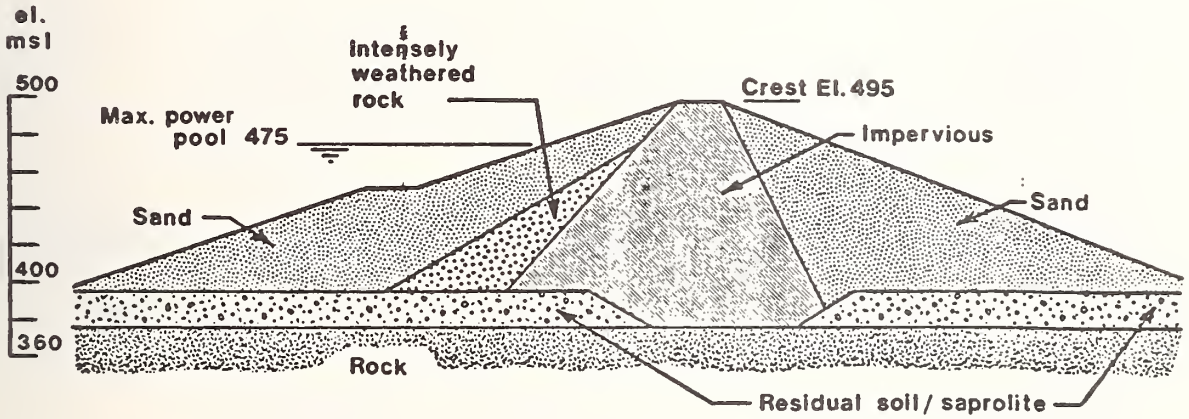

b. Sta. 20+00

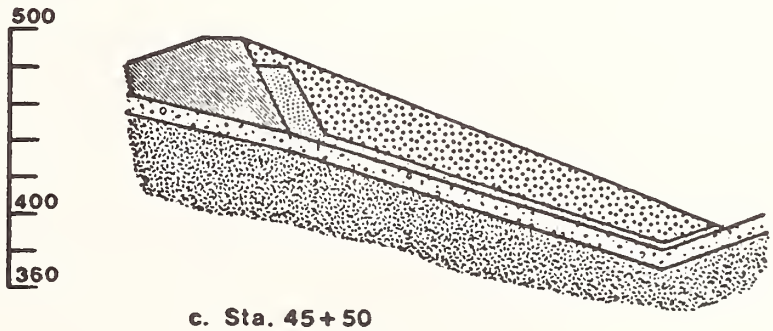

c. Sta. 45+50

Figure 2. Typical embankment sections

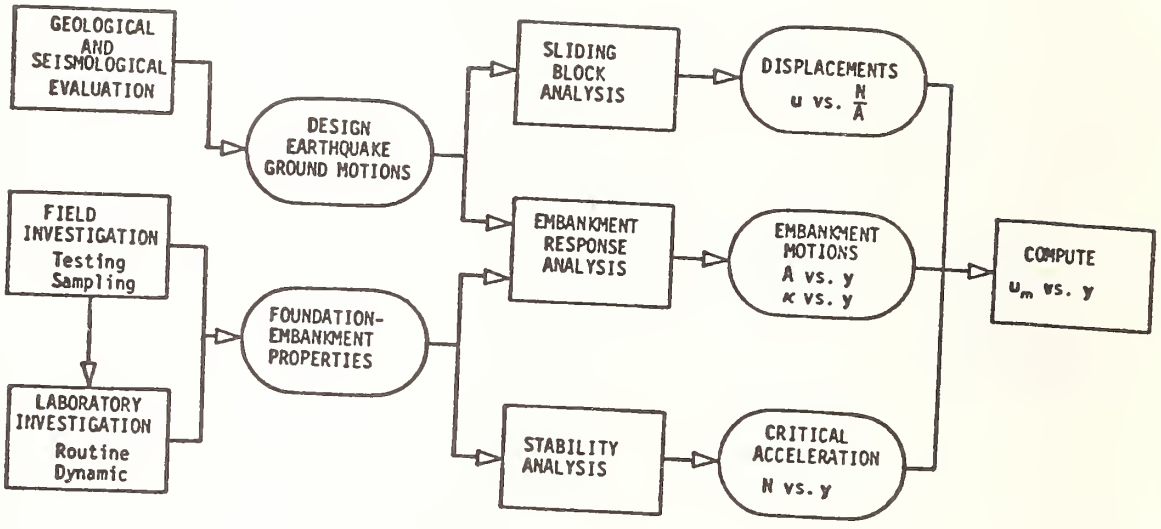

Figure 3. Permanent displacement analysis

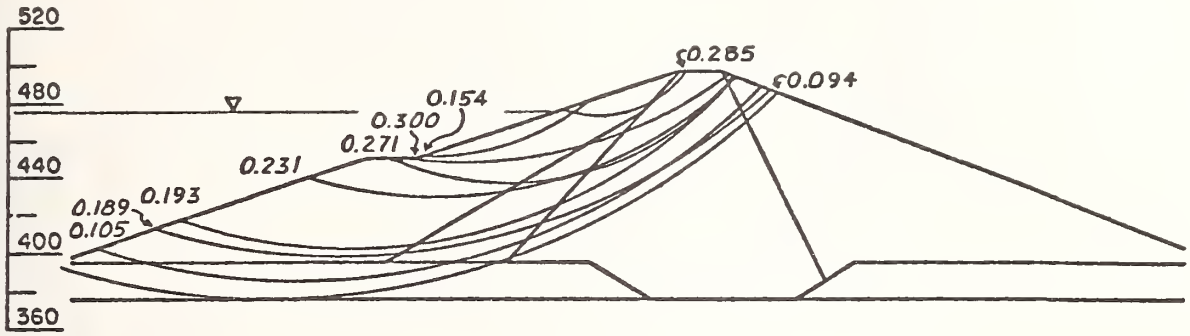

a. Critical slip surfaces

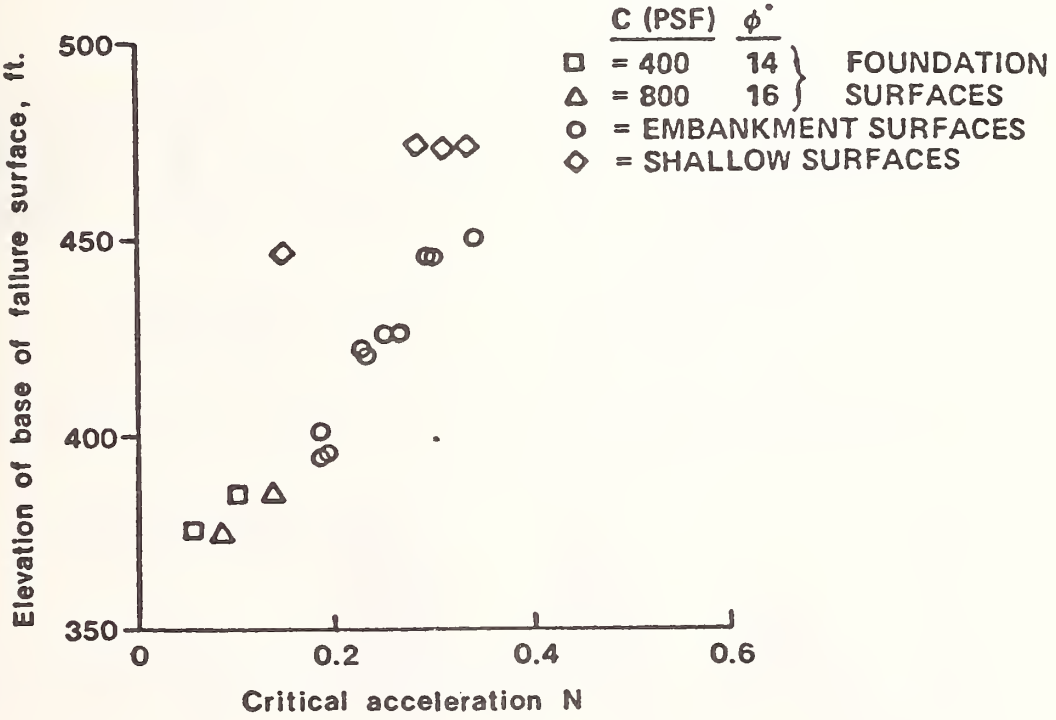

b. Critical acceleration vs. elevation

Figure 4. Results of stability analysis for Sta 20+00

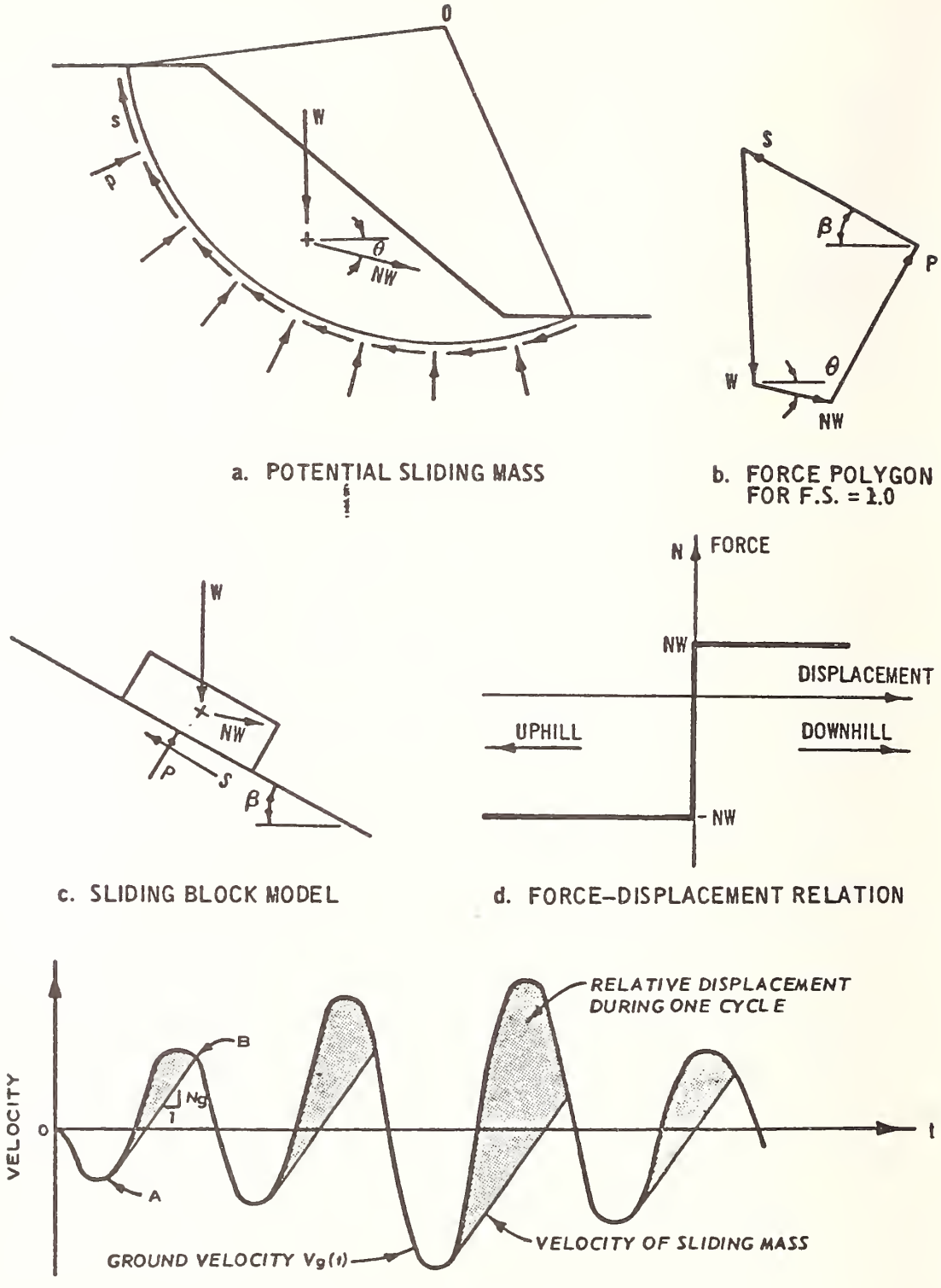

Figure 5. Elements of the Newmark sliding block analysis

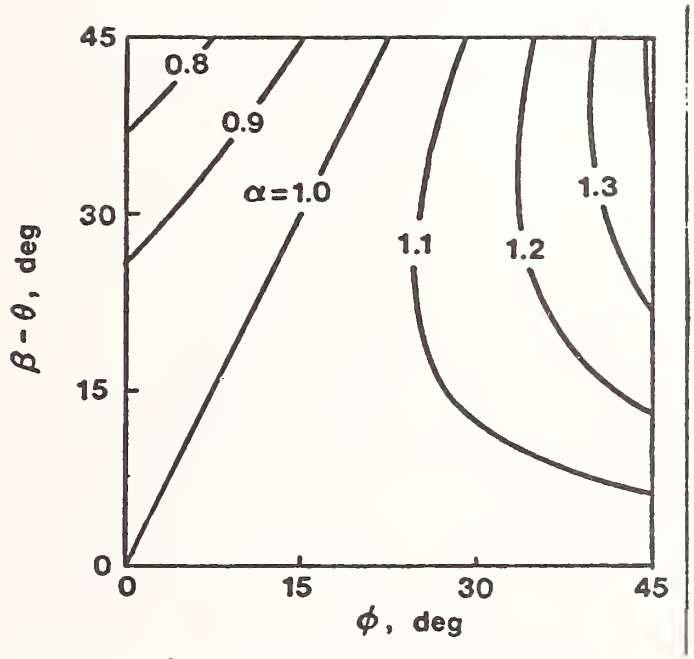

Figure 6. Values of the coefficient α

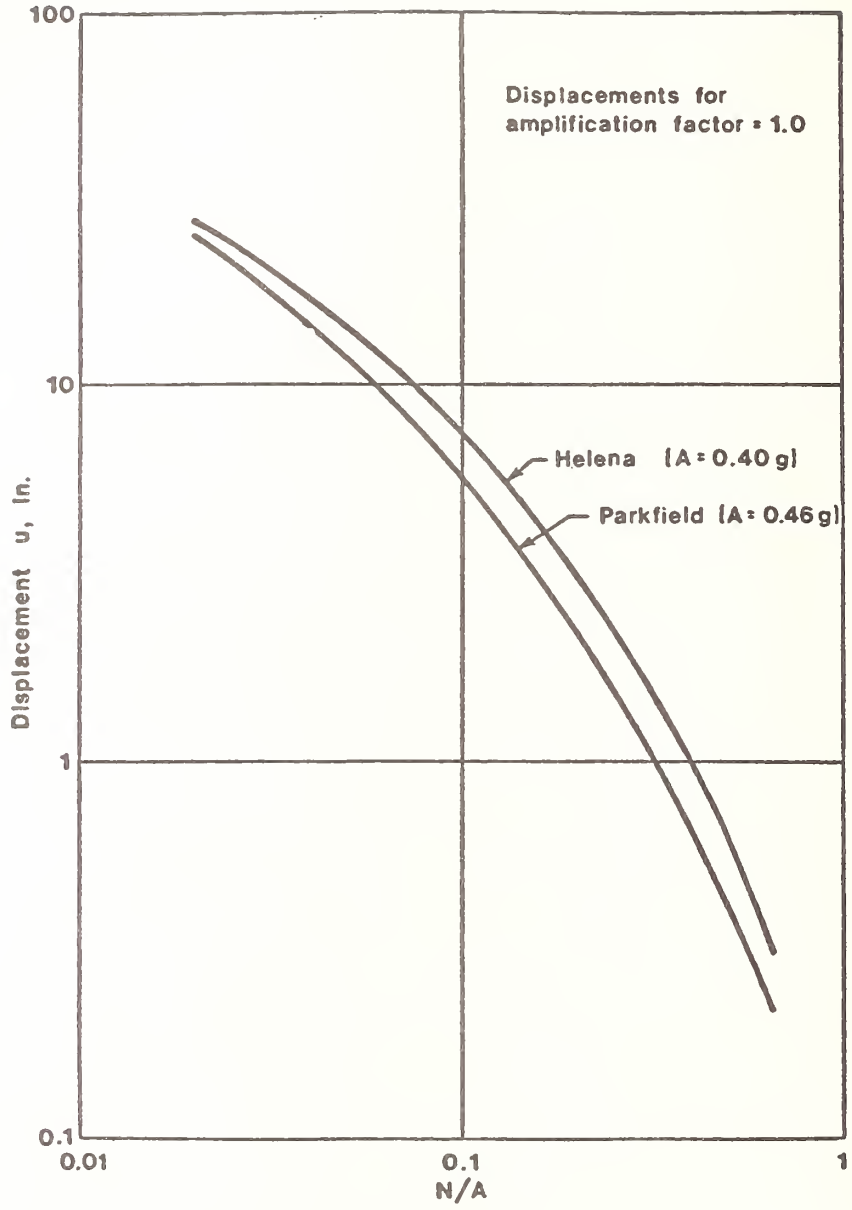

Figure 7. Displacement vs. N/A for Helena and Parkfield records scaled to peak accelerations of 0.40 and 0.46 g

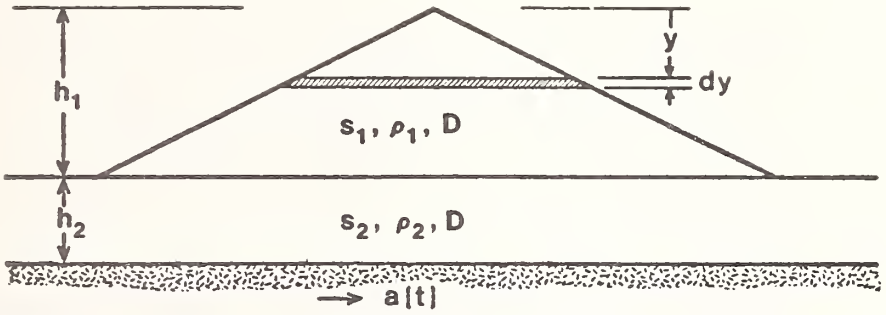

Figure 8. Mathematical model for viscoelastic shear-beam analysis of embankment and foundation response by the Sarma method

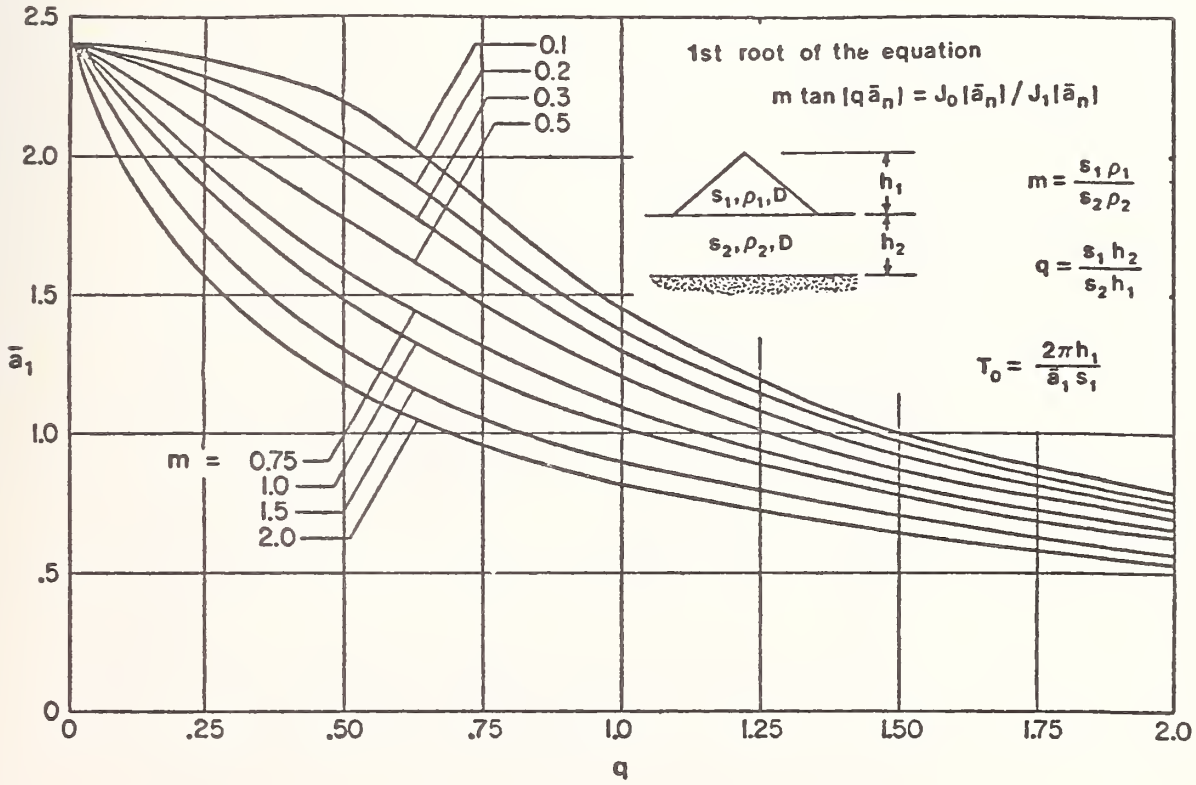

Figure 9. Fundamental period T_0 of embankment-foundation system (after Sarma, 1979)

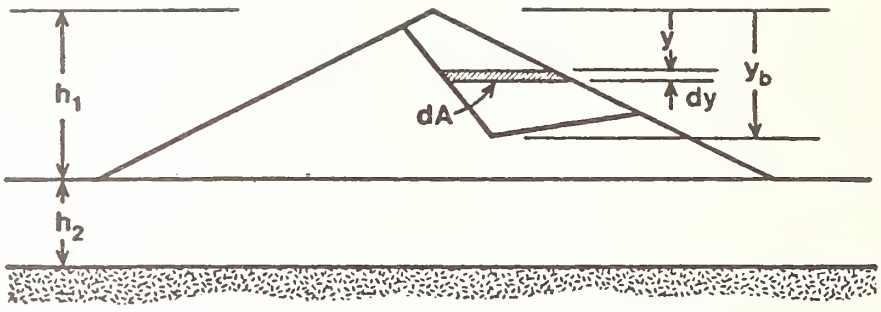

Figure 10. Computation of average acceleration on the sliding mass

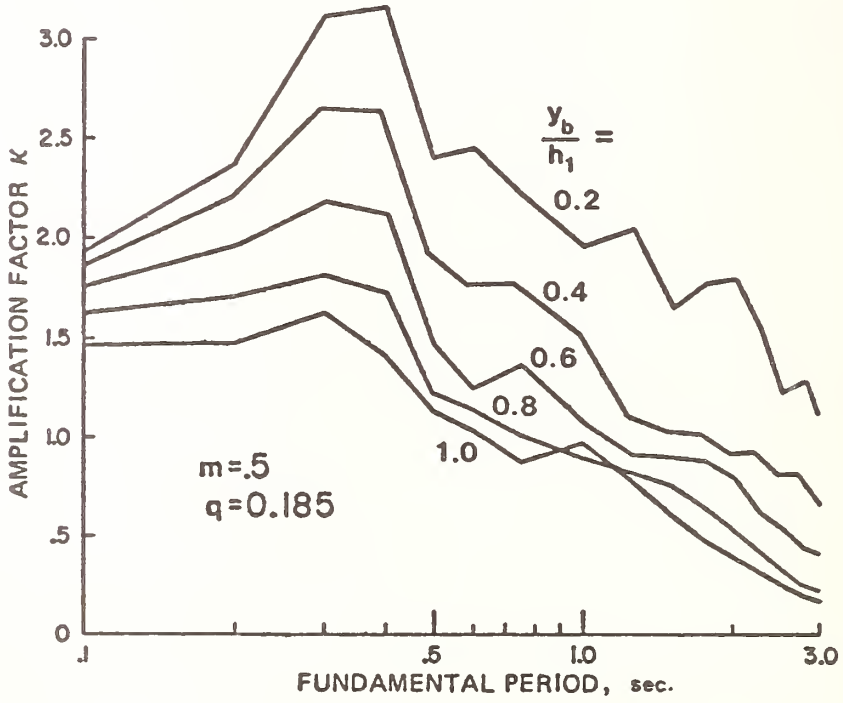

Figure 11. Amplification factors for the Helena, Montana, record; m = 0.5 , q = 0.185 , Damping = 20%

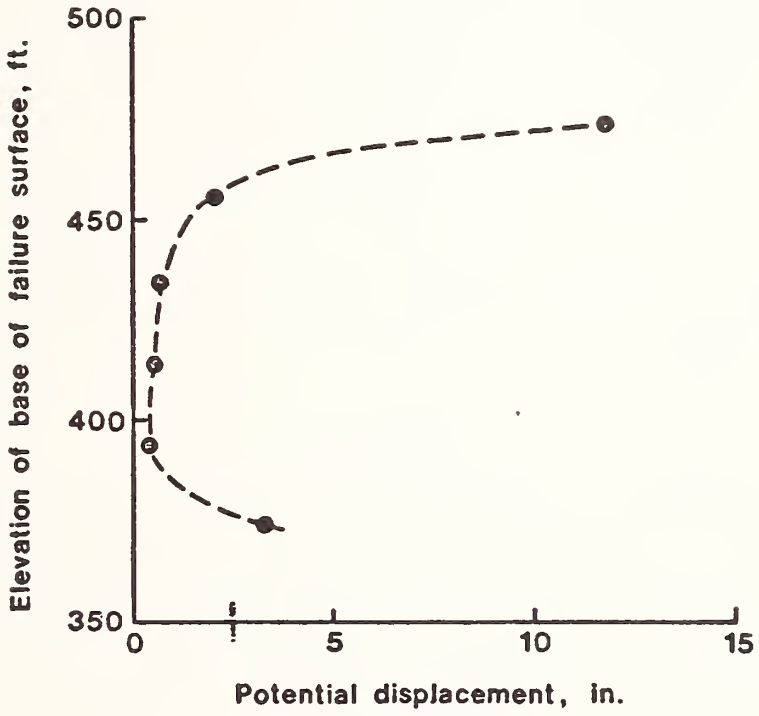

Figure 12. Potential permanent displacements for Sta 20+00, from the Helena record

PIPE STRESSES DURING EARTHQUAKES BASED ON A TWO-DIMENSIONAL SEISMOMETER ARRAY OBSERVATION

Hajime Tsuchida
Ken-ichiro Minami
Osamu Kiyomiya
Setsuo Noda

Structures Division
Port and Harbour Research Institute
Ministry of Transport

ABSTRACT

Pipe stresses developed during earthquakes are influenced by the relative displacement of an ambient ground. The strains caused by the relative displacement of the ground are closely related to the magnitude of the earthquakes, the epicentral distances, the subsoil conditions, and the properties of the wave propagation in surface layers. Analyses of records obtained by a two-dimensional seismometer array observation at the Tokyo International Airport were carried out to evaluate the behavior of the pipelines during earthquakes. Pipe stresses are calculated from the ground deformation by the observation. The stresses calculated by the deformation method, which has been used for earthquake resistant design in Japan, and by the dynamic response analysis are compared with those from the observation.

INTRODUCTION

The apparent unit weight of a buried pipe including a liquid such as petroleum is about the same as that of an ambient soil. If the rigidity of a buried pipe is almost the same as that of its surrounding soil, the existence of the pipe should hardly have any influence on the behavior of the ground motion during earthquakes. The deformation characteristics of a pipe and its ambient ground may be viewed from another angle. If the rigidity of the pipe is much greater than that of the ambient ground or sliding occurs between the pipe and the ground, the deformation of the pipe should be considerably smaller than the ground. This leads to say that the pipe stresses are also smaller and thus yields to the safety side in the design work.

Pipe stresses can be calculated once the behavior of the ground is known since the behavior of a pipe during earthquakes is influenced by the ground deformation. The deformation characteristics of a ground during earthquakes is influenced by several factors such as wave propagation and variations in subsurface conditions, to name just a couple. These factors should be thoroughly evaluated in order to understand the behavior of the pipe subjected to earthquake loadings. Simulation models should also be taken into consideration in the above factors when the pipe stresses are calculated using these models. The dynamic response method of a mass-spring system is selected in this paper in addition to the traditional seismic deformation method to compute the stresses developed in the

buried pipes. The paper also makes comparisons of the results of the pipe stresses obtained from different methods.

SEISMOMETER ARRAY OBSERVATION

LAYOUT

An array has been established in a part of the Tokyo International Airport [1, 2]. The total length of the array is 2500 meters. Six ground surface accelerometers were installed at equal intervals along the observation line as shown in figure 1. The locations where the accelerometers were positioned are designated by alphabets from A through F. Each accelerometer has two horizontal components which are parallel and perpendicular to the observation line. Four downhole accelerometers were also installed in holes at points A and F. The downhole accelerometers at point A were installed at -1.0 m and -67.2 m in depth in the hole, and those at point E were at -1.0 m and -49.6 m in depth. The downhole accelerometers have three components.

SUBSURFACE CONDITIONS

Subsurface conditions at the seismometer array site is shown in figure 2. The subsurface conditions were determined based on the results of 69 borings carried out at the airport. Onsite pulse tests were also conducted at points A and E. Results of this investigation are given in figures 3 and 4 for points A and E, respectively. At point A, the material from the ground surface to -65 m in depth is classified as silty clay having N values of about 10. A dense diluvial deposit with $N > 50$ was encountered below the silty clay layer to the bottom of the boring. The sand stratum where N values are greater than 50 and the velocity of the S wave is more than 300 m/s is assumed to be the baserock for the analysis conducted in this paper. The surface of the baserock is almost horizontal between points A and D since the soil conditions between these two points seem to be uniform. The dense diluvial deposit was encountered at -47 m in depth at point E and the surface of the baserock at point E is therefore assumed to be sloped upward from point D.

OBSERVATION SYSTEM

The observation system is shown in figure 5. Natural frequency of the accelerometers installed at the ground surface is 2 Hz and their damping factor is more than 17. Range of the system sensitivity including recorders varies from 0.1 Hz to 30 Hz. Natural frequency of the downhole accelerometers is 5 Hz and their damping factor is more than 10. Overall sensitivity on the recording paper in the electromagnetic oscillographs is about 1 mm per gal. This sensitivity can be decreased by changing resistors of the circuit when large values of amplitude are input to the recorders.

DATA REDUCTION

Analyses of the recorded data include integration of the acceleration records and calculation of the phase shift among the displacement records. The filter used in the integration procedure [3, 4] has been developed at the Port and Harbour Research Institute which was called "variable filter." According to this procedure, low frequency components of the acceleration records are cutoff and the cutoff frequency (f_c) of the filter varies according to the properties of the frequency components in order to keep the error for every frequency component to be constant. The phase shifts among the displacement records are calculated from cross-correlation coefficient. The phase shifts provide the information of the phase velocities and propagation directions of the earthquake waves along the observataion line.

OBSERVATION RECORDS

Eighty-five records have been accumulated since the observation system was installed. Records of 8 out of these 85 earthquakes listed in table 1 were selected for the analysis. The records indicated that the maximum horizontal component of the acceleration at the ground surface is less than 50 gal. These eight selected earthquakes may be divided into three groups according to the epicentral distance and depth of the hypocenter from the observation sites (figure 6). Those of short epicentral distance and shallow depth of the hypocenter (TIA-9 and 41); (2) intermediate epicentral distance and deep depth of the hypocenter (TIA-3, 6, 10, and 17); and those of long epicentral distance and deep depth of the hypocenter (TIA-20 and 50). Typical examples of the acceleration records and the velocity time histories and displacement time histories calculated by the integration procedure are given in figure 7.

PIPE STRESSES DERIVED FROM THE OBSERVATION RECORD

The deformation curves (y) at a certain time can be determined from the calculated displacement time histories [5] for both longitudinal (y_L) and transverse (y_T) directions. These curves are approximated using Fourier series given below:

$$y = \frac{a_0}{2} + \sum_{i=1}^{2} \left\{ a_i \cos \frac{i\pi}{3} \left(\frac{x}{d}\right) + b_i \sin \frac{i\pi}{3} \left(\frac{x}{d}\right) \right\} + \frac{a_3}{2} \cos \pi \left(\frac{x}{d}\right)$$

where

d = distance between two adjacent points,

a_i, b_i = coefficients of Fourier series.

Assuming that the pipe strain is equal to the ground strain, the axial strain (ε_L) of the pipe can be computed by the formula $\varepsilon_L = dy_L/dx$ and the axial stress by $\sigma_L = \varepsilon_L E$. The bending strain ($\varepsilon_b$)

is given by $\varepsilon_b = \frac{D}{2} \frac{dy_b}{dx^2}$, and the bending stress is expressed by $\sigma_b = \varepsilon_b E$ (where E = modulus of elasticity and D = pipe diameter). An example of the deformation and strain curves obtained from the above procedures is given in figure 8.

The maximum axial and bending stresses calculated between points A and C where the subsurface conditions are considered uniform along the observation line are listed in table 2. The stresses between points C and F, where the subsurface conditions vary, are listed in table 3. Both tables indicate that the calculated bending stresses are very small in comparison with the calculated axial stresses in all cases. The ratio of the maximum axial strain to the maximum surface acceleration is defined as γ and the relationship among γ, the epicentral distance and the magnitude of the earthquake is presented in figure 9. Figure 9 shows that the value of γ is in proportion to the epicentral distance and the magnitude of the earthquake is small for groups (1) and (3) earthquakes mentioned before for the reason that the relative displacement between two adjacent points is small because the waves were propagated upward from the baserock to the observation line. On the other hand, the waves in group (2) earthquakes were propagated mainly through the subsoil layer, thus resulting in larger values of the pipe stresses. Angles from the observation line to the azimuths of the earthquakes are shown in figure 10. The waves in group (2) earthquakes have reached the observation line from nearly an angle of 45 degrees causing a larger ratio of Σ Lmax/αmax.

The results just presented suggest that the relative displacement of the ground is related to the path and direction of the wave propagation. The time shift (τ) along the observation line can be calculated by the cross-correlation coefficent and the phase velocities and the directions of the earthquake waves can be obtained from the time shifts. The result of the computation is given in figure 11. This figure shows that the direction of the wave propagation was not along the observation line only. The directions were not fixed and in some cases were even reversed. This phenomena can be explained by the reasons that the paths of the wave propagation with respect to the observation line are related to the depth between the ground surface and the baserock, the azimuths of the earthquakes, and so on.

Since the seismometers were installed at the interval of 500 m, it is impossible to catch earthquakes with apparent wave lengths less than 500 m. Therefore, the wave lengths should be confirmed. Apparent wave velocities (c) along the observation line were calculated to be 1.2 to 10.1 km/s as shown in figure 12. The wave lengths were then calculated from the equation of L = c T (where T = dominant period of the displacement time-history) and were varied from 1.4 to 11.1 km. This result shows that the earthquake waves with wave lengths less than 500 m were at least not dominant.

PIPE STRESS DERIVED FROM SEISMIC DEFORMATION METHOD

The seismic deformation method, which is another method used to compute the pipe stress, is specified in the Ordinance of Technical Code for Petroleum Pipeline. The mathematical model of the pipeline in this code is taken as a rod or a beam on an elastic foundation to analyze the deformation and stress of the model. The input earthquake waves are assumed to be sinusoidal. The axial stress (σ_L) and the bending stress (σ_b) are computed using the following equations:

$$\sigma_L = \lambda_1 \frac{\pi U_g E}{L}$$

$$\sigma_b = \lambda_2 \frac{2\pi^2 D U_g E}{L^2}$$

where

U_g = amplitude of horizontal ground displacement at the ground surface,

L = wave length of earthquake waves in the subsoil layer,

λ_1, λ_2 = coefficients determined by the rigidities of the pipe and the ground and the wave length ($\lambda_1 = \lambda_2 = 1.0$ used in this analysis).

Pipe stresses derived from the seismic deformation method are listed in tables 4 and 5. The bending stresses are not included in the tabulation since their values are very small (less than 1 kgf/cm^2). The calculated stresses are considerably larger than the stresses from the observation records (tables 2 and 3). Ratios (R) of the calculated stresses to the stresses from the observation records are shown in figure 13. In all cases, the seismic deformation method results in much larger values of the axial stresses than those obtained from the observation records. The value of R is less than 0.67 under the uniform subsoil condition. In the case of group (1) earthquakes, R is less than 0.1. In the design procedure, the earthquake waves are assumed to reach the pipeline from five directions and therefore the total stress should be multiplied by 1.77 which would even lower the values of the ratio given in figure 13. The reasons that there are a large difference in R values may be explained as follows: (1) the wave lengths used in the seismic deformation method are considerably shorter than the apparent wave lengths calculated from the observed records; and (2) the horizontal displacement amplitudes used in the seismic deformation method are larger than those obtained from the observed records.

DYNAMIC RESPONSE ANALYSIS

The model used in the dynamic response analysis is shown in figure 14. The surface layer is cut into slices along the pipeline axis and each slice is 420 m wide, 50 m thick, and 40 to 60 m high. Each slice is represented by an equivalent mass-spring system and the masses are connected to each other along the pipeline axis by springs representing the rigidity of the ground. The springs of the

model are assumed to be linear and a damping coefficient of 0.05 is assigned because the maximum acceleration in the records is comparably small.

The acceleration records obtained at the downhole accelerometers are used as input data. These input acceleration waves (f(t)) are assumed to travel in the baserock parallel to the pipe axis, i.e., the input record is expressed as f(t-d/c) for each slice, where d is the distance from the end of pipeline to a certain mass and c is the velocity of the wave propagation.

Results of the dynamic response analysis are shown in figures 15 and 16. The subsurface conditions from point A to point B was modeled using digitized acceleration time history of TIA-17 as input data. Figure 15 indicates that the velocity of the input acceleration time-history was varied from a range of 250 m/s to almost infinity. The infinite velocity means that the input acceleration time-histories are entirely the same for every mass with respect to times. Dispersion of the velocity of the wave propagation with respect to the frequency was not considered in the model. Figure 15 also shows that the value of the response displacement along the observation line at the ground surface increases with the increase of the velocity and becomes almost constant when the velocities are above 1.5 km/s. An apparent wave velocity of TIA-17 along the observation line was about 1.2 km/s. The corresponding response displacement at the ground surface for this velocity was 0.36 cm in the observation records and 0.23 cm in the dynamic response analysis (figure 15). Figure 16 indicates that the maximum pipe stress of 7.5 kgf/cm^2 was calculated at the velocity of 1.5 km/s, which agrees rather well with the maximum axial stress from the observation records at about 9.8 kgf/cm^2.

CONCLUSIONS

Conclusions obtained from the study presented herein can be summarized as follows:

1. The pipe stresses developed under earthquake loading are closely related to the properties of the earthquakes (magnitude, distance of epicenter, depth, etc.) and the paths and the directions of the wave propagation. The ratio of the maximum stress to the maximum acceleration at the ground surface is in direct proportion to the magnitude as well as the distance of the epicenters of the earthquakes used in the analysis.
2. The apparent velocities at the ground surface along the observation line vary from 1.2 to 10.1 km/s. The dominant wave lengths of the displacement waves are in the range of 1.4 to 11.1 km.
3. The axial stresses calculated by the seismic deformation method are larger than the axial stresses obtained from the observation records. The bending stresses evaluated using both methods are very small.

4. The dynamic response analysis which uses a mass-spring and considers the wave propagation in the baserock provides a good method to correlate the characteristics of the ground surface response and the pipe stresses from the observation records.

REFERENCES

[1] Tsuchida, H., E. Kurata, and S. Hayashi, "Observation of Earthquake Response of Ground With Horizontal and Vertical Seismometer Arrays," Proc. of the Sixth World Conference on Earthquake Engineering, Vol. 1, Janaury 1977, pp. 509-514.

[2] Hayashi, S., H. Tsuchida, and E. Kurata, "Observation of Earthquake Response of Ground With Horizontal and Vertical Seismometer Arrays," Wind and Seismic Effect, Proc. of the Eighth Joint UJNR Panel Conference, NBS Special Publication 477, May 1977, pp. III-16-III-25.

[3] Iai, S., E. Kurata, and H. Tsuchida, "Digitization and Corrections of Strong-Motion Accelerograms," Technical Note of the Port and Harbour Research Institute, No. 286, March 1978, 56 p.

[4] Iai, S., E. Kurata, H. Tsuchida, and S. Hayashi, "Integration of Strong-Motion Accelerograms," Wind and Seismic Effect Proc. of the Tenth Joint UJNR Panel Conference, NBS Special Publication 560, October 1980, pp. 7.1-7.16.

[5] Tsuchida, H., K. Minami, O. Kiyomiya, E. Kurata, and H. Nishizawa, "Stress of Buried Pipe During Earthquakes Based on Two Dimensional Seismometer Array Observation," Report of the Port and Harbour Research Institute, Vol. 20, No. 4, December 1981, 40 p.

[6] Ministerial Ordinance on Engineering Requirements for Facilities for Oil Pipeline Enterprise, Ordinance No. 2 of Ministry of International Trade and Industry, Ministry of Transport, Ministry of Construction, and Ministry of Autonomy, 1972.

[7] Ministerial Notification on Details of Engineering Requirements for Oil Pipeline Enterprise, Notification No. 1 of Ministry of International Trade and Industry, Ministry of Transport, Ministry of Construction and Ministry of Autonomy, 1973.

[8] Kiyomiya, O., "On Earthquake Resistant Design Method of Submarine Pipelines," Technical Note of the Port and Harbour Research Institute, No. 307, December 1978, 71 p.

Table 1. Earthquake Data

No.	Date	Epicenter	Latitude of the Epicenter	Longitude of the Epicenter	Magnitude	Depth of the Hypocenter	Epicentral Distance
TIA-3	1974. 5. 9	Off Izu Pen.	34°34' N	138°48' E	6.9	10	140
TIA-6	1974. 7. 8	Off Ibaragi Prefecture	36°25' N	141°12' E	6.3	40	161
TIA-9	1974. 8. 4	The Tone River	36°01' N	139°55' E	5.8	50	54
TIA-10	1974. 9.27	Off Boso Pen.	33°43' N	141°31' E	6.4	60	259
TIA-17	1974. 11.16	Around Choshi	35°45' N	141°15' E	6.1	40	125
TIA-20	1974 11.30	Near Torishima Island	30°36' N	138°46' E	7.5	320	558
TIA-41	1977. 6. 4	North of Tokyo Bay	35°31' N	140°03' E	4.6	60	26
TIA-50	1978 3. 7	Off Tohkaido	32°08' N	137°44' E	-	440	424

Table 2. Pipe Stresses from the Observation (Points A-C)

No.	Points	Axial Stress		Bending Stress	
		σ_b (kgf/cm^2)	T (s)	σ_b (kgf/cm^2)	T (s)
TIA-3	A - B	13.4	37.97	0.0082	33.14
	B - C	-15.1	26.91		
TIA-6	A - B	7.1	93.54	0.0032	96.60
	B - C	6.7	34.44		
TIA-9	A - B	8.0	9.71	0.0044	11.64
	B - C	7.6	10.62		
TIA-10	A - B	5.0	97.23	0.0034	87.89
	B - C	- 6.7	16.75		
TIA-17	A - B	-11.3	46.26	0.0054	99.09
	B - C	- 9.2	70.85		
TIA-20	A - B	15.1	97.20	0.0075	82.33
	B - C	15.1	100.02		
TIA-41	A - B	$\pm$ 0.4	3.46	0.0002	2.70
	B - C	$\pm$ 0.8	3.48		
TIA-50	A - B	5.0	55.53	0.0004	54.80
	B - C	6.3	53.00		

T : time

Table 3. Pipe Stresses from the Observation (Points C-F)

No.	Axial Stress			Bending Stress		
	σ_b (kgf/cm^2)	X (m)	T (s)	σ_b (kgf/cm^2)	X (m)	T (s)
TIA-3	-36.1	1700	26.73	0.019	1000	49.20
TIA-6	-13.6	2300	26.23	0.010	1500	34.32
TIA-9	21.4	2300	12.12	0.013	1475	21.80
TIA-10	10.2	2250	66.37	0.007	50	72.54
TIA-17	28.8	1725	27.50	-0.021	1500	50.44
TIA-20	34.4	1800	102.73	-0.019	1475	79.81
TIA-41	- 1.9	2250	2.80	0.001	2500	2.67
TIA-50	-14.5	1650	57.87	0.010	2000	55.79

X : distance from point A

Table 4. Pipe Stresses (Points A-C)

No.	Axial Stress		Bending Stress	
	Observation	Seismic Deformation Method	Observation	Seismic Deformation Method
TIA-3	15	41	0.0082	0.29
TIA-6	7	32	0.0032	0.22
TIA-9	8	118	0.0044	0.82
TIA-10	7	23	0.0034	0.16
TIA-17	11	37	0.0054	0.26
TIA-20	15	44	0.0075	0.31
TIA-41	1	86	0.0002	0.60
TIA-50	6	55	0.0004	0.38

Table 5. Pipe Stresses (Points C-F)

No.	Axial Stress		Bending Stress	
	Observation	Seismic Deformation Method	Observation	Seismic Deformation Method
TIA-3	-36	59	0.019	0.54
TIA-6	-14	38	0.010	0.34
TIA-9	21	133	0.013	1.21
TIA-10	10	33	0.007	0.30
TIA-17	29	43	0.021	0.39
TIA-20	34	56	0.019	0.51
TIA-41	- 2	112	0.001	1.02
TIA-50	-14	90	0.011	0.82

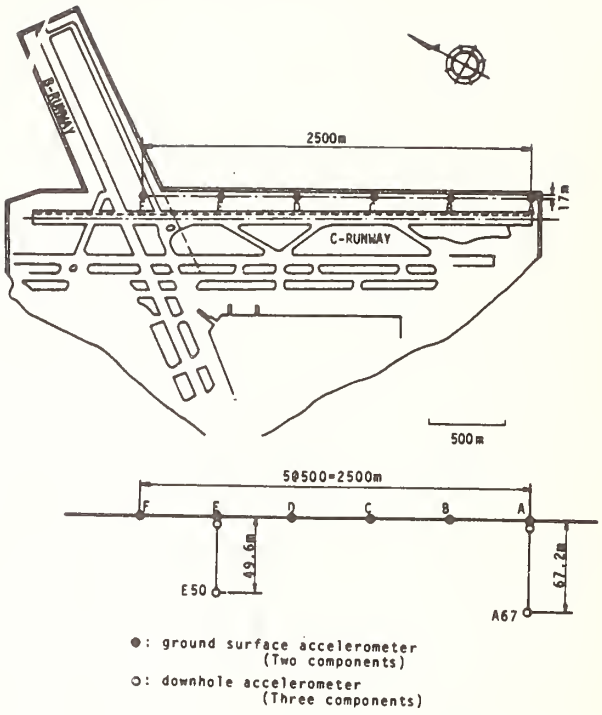

Fig. 1 Deployment of Accelerometers

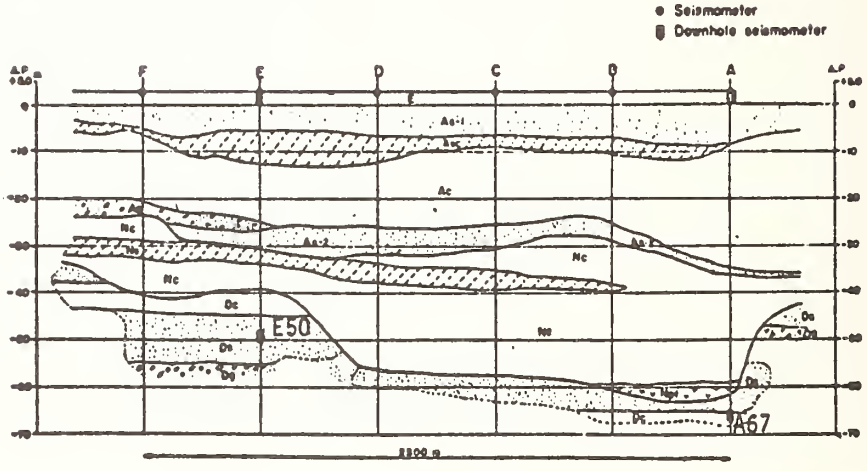

Key (Fill) E : Fill, (Alluvial deposit) A_{s-1} : Sand, A_{sc} : Silty sand, A_c : Silty clay, A_{s-2} : Sand, A_g : Sandy gravel, (Diluvial deposit) N_c : Silty clay, N_s : Silty sand, N_{pt} : Peat, D_s : Sand, D_g : Sandy gravel, D_c : Silt.

Fig. 2 Soil Conditions

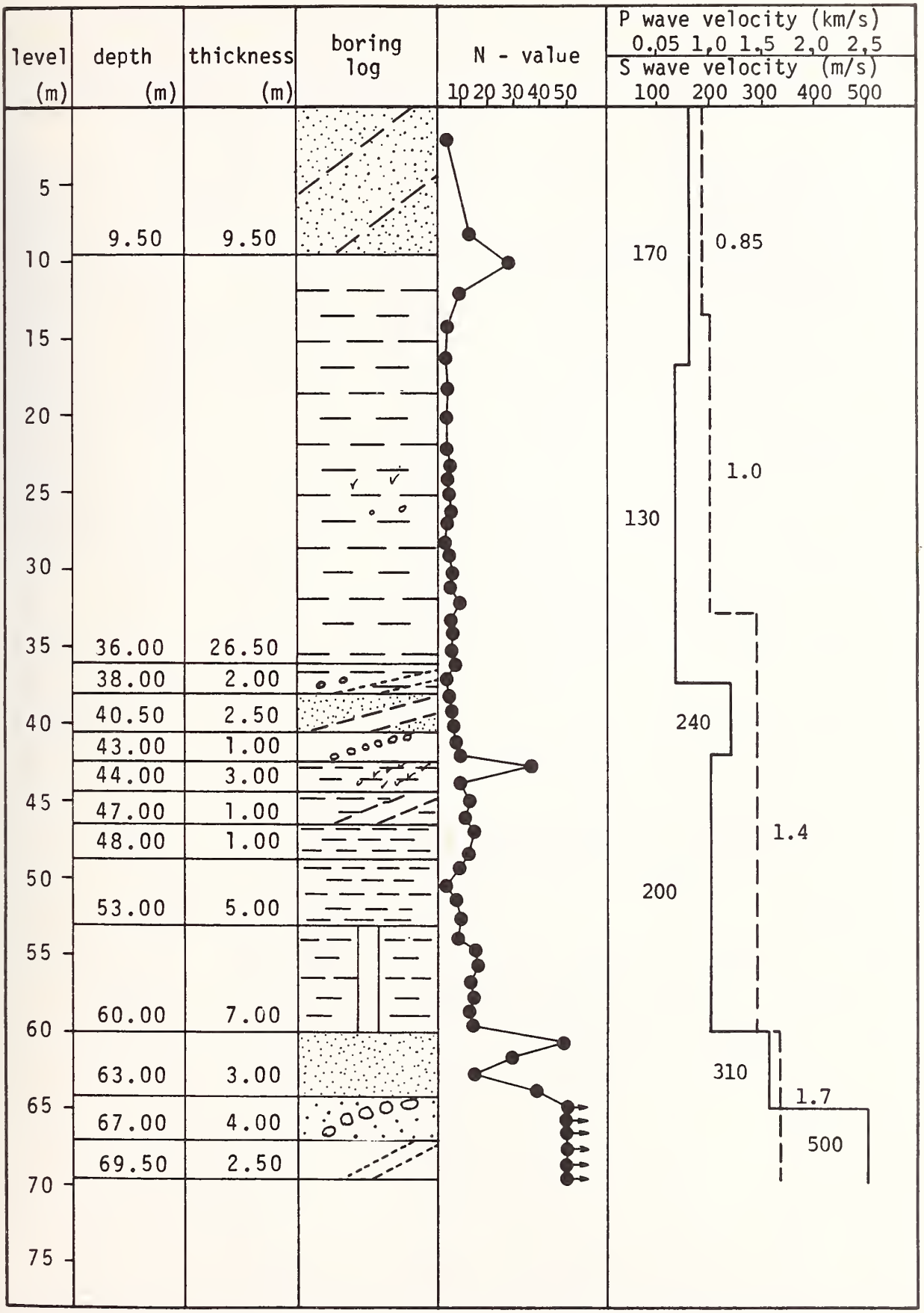

Fig. 3 Soil Condition at A Point

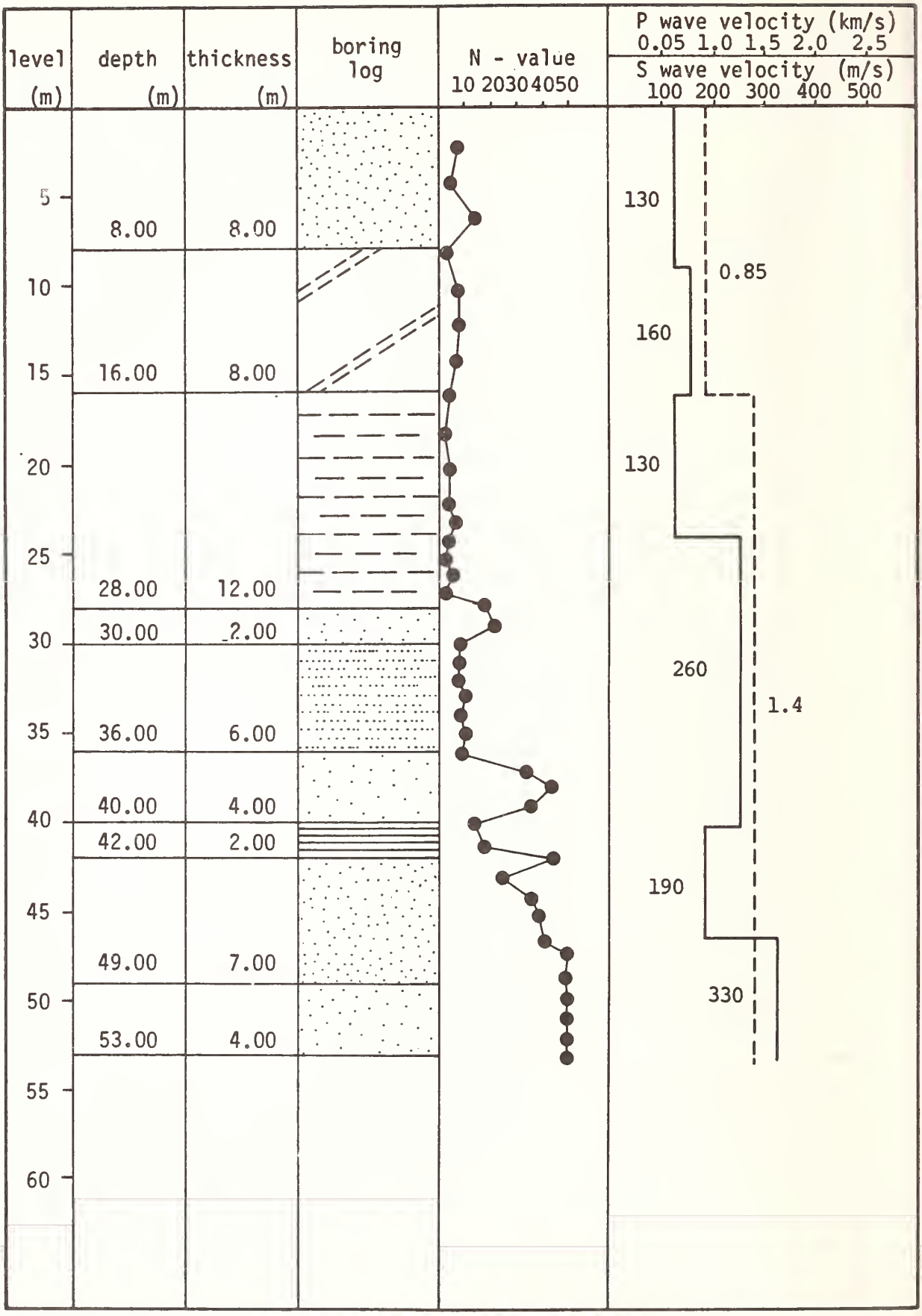

Fig. 4 Soil Condition at E Point

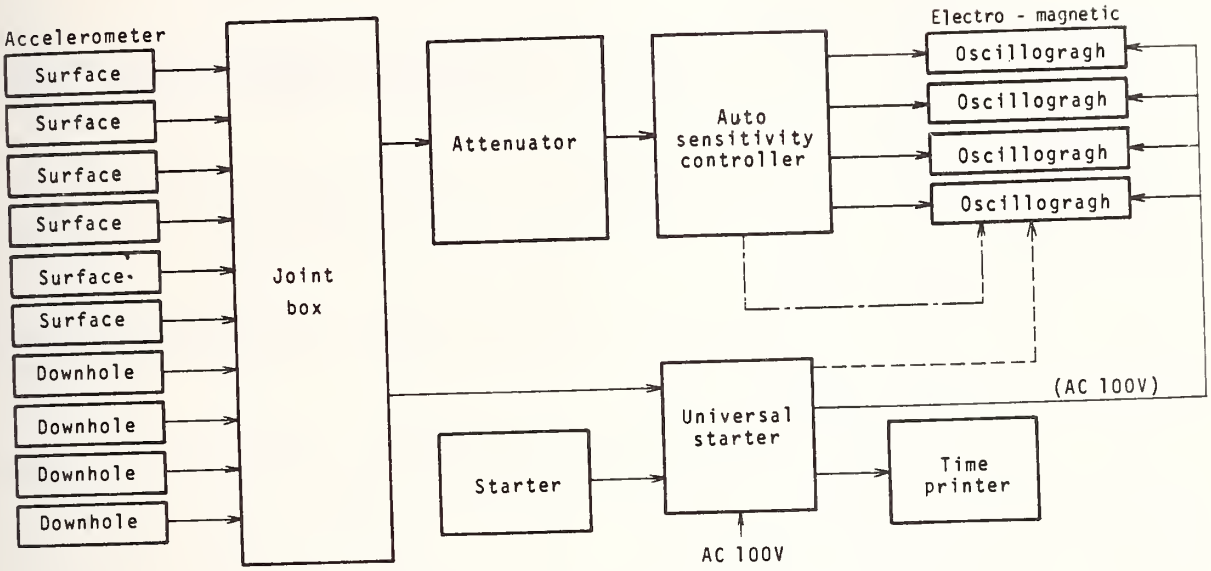

Fig. 5 Observation System

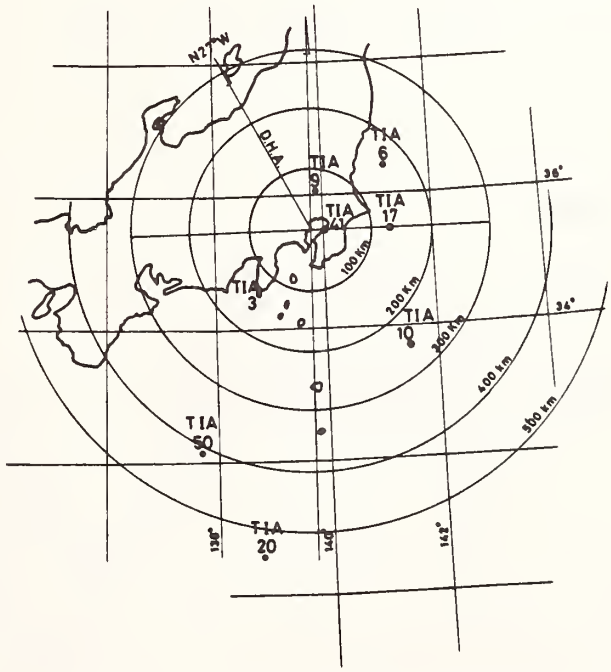

Fig. 6 Locations of Epicenter

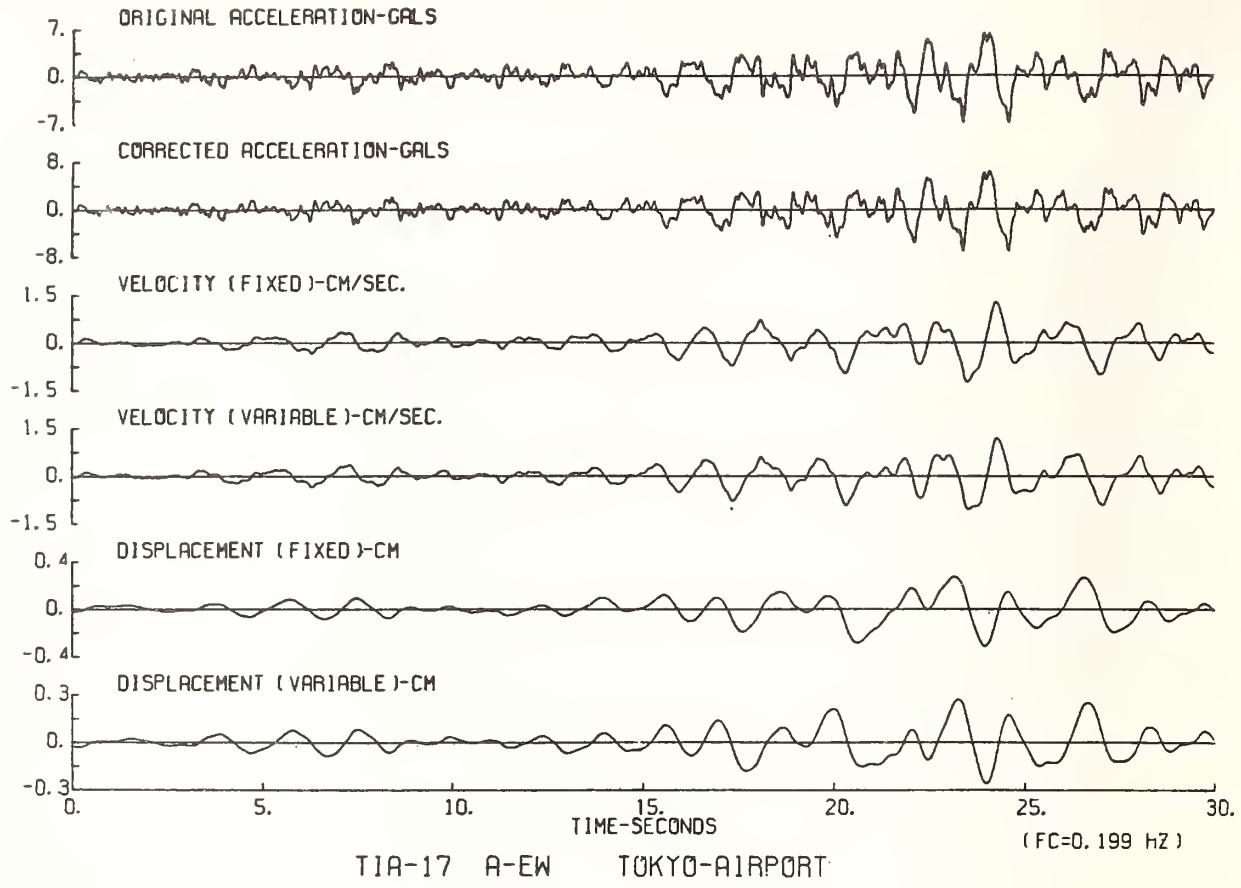

Fig. 7 Examples of Records

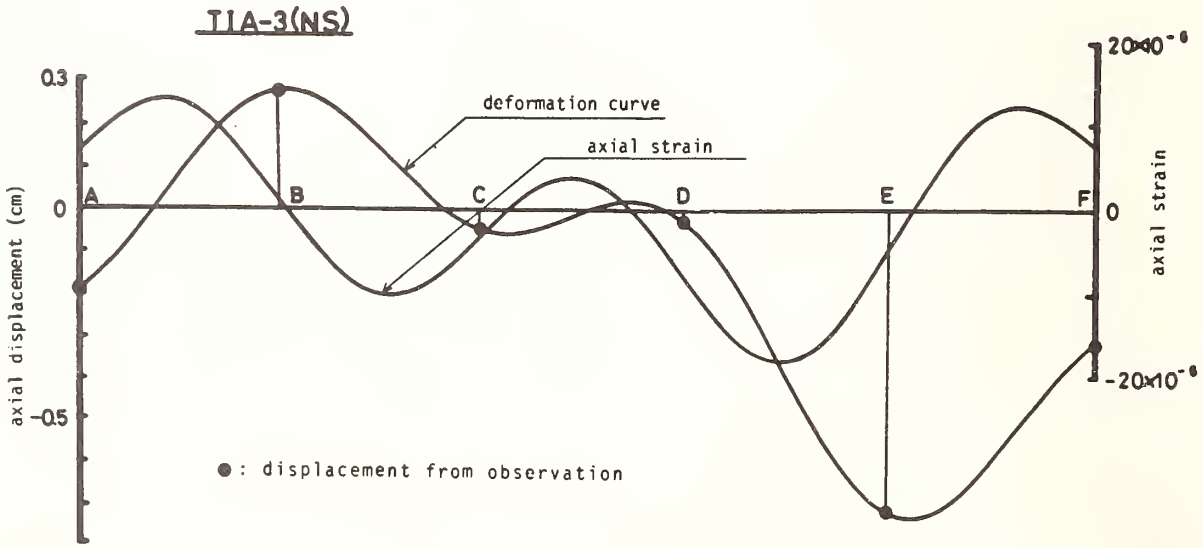

Fig. 8 Deformation Curve and Axial Strain

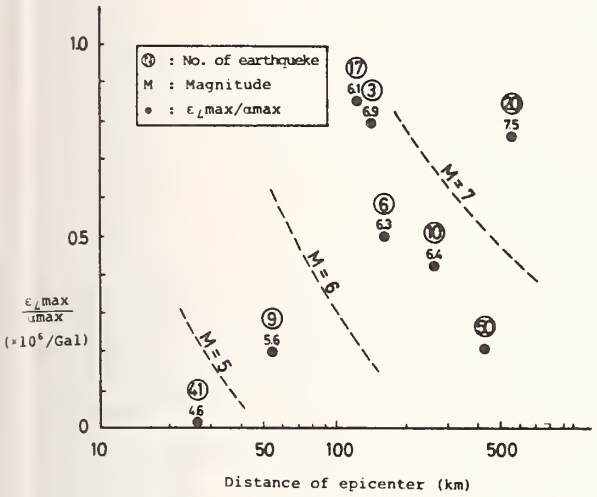

Fig. 9 Strains and Distance of Epicenter

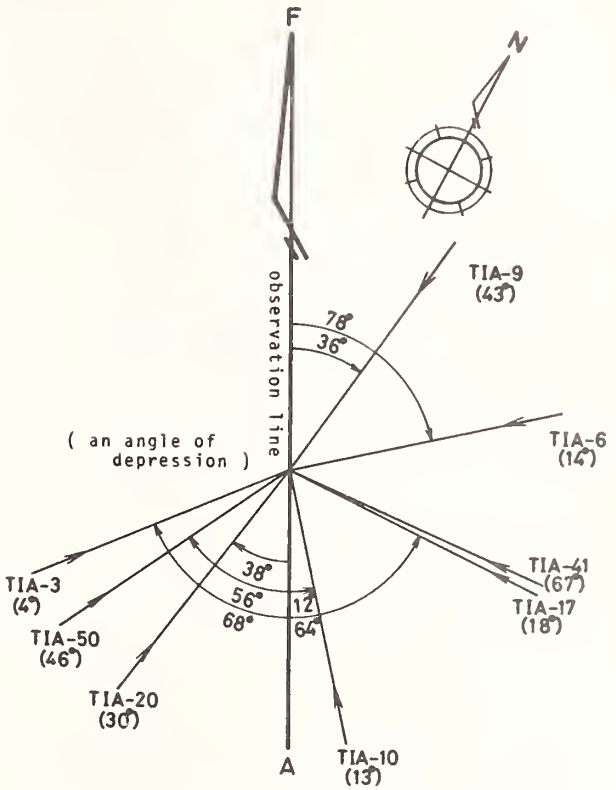

Fig. 10 An Angle of the Azimuth to the Observation Line

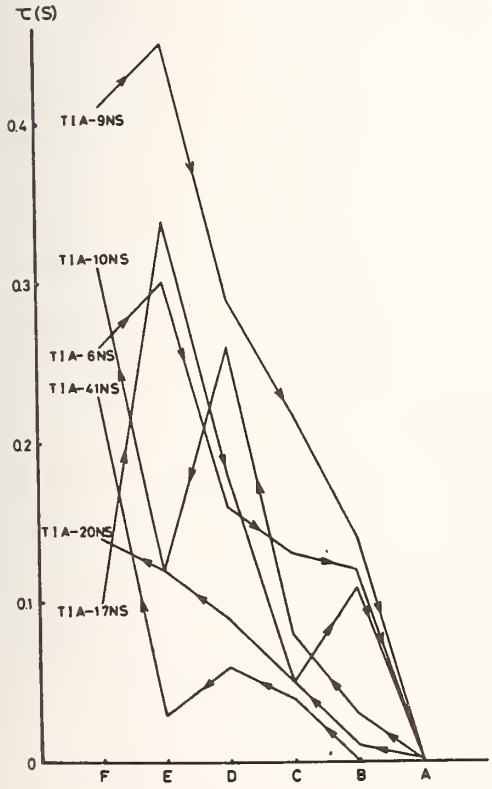

Fig. 11 Phase Delays

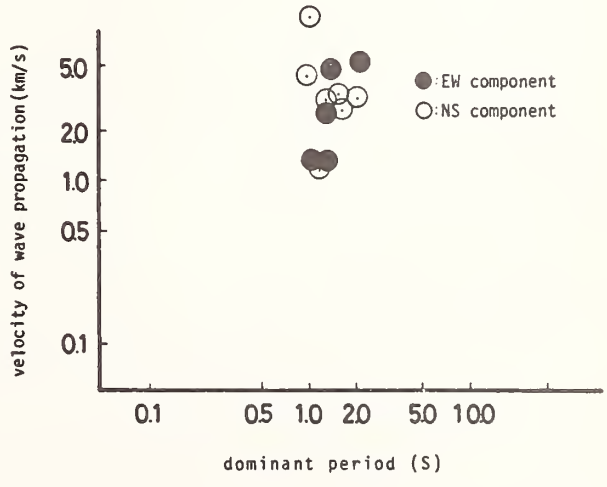

Fig. 12 Velocity of Wave Propagation

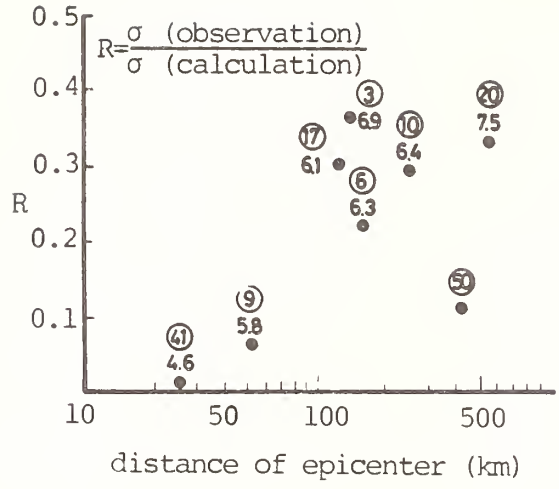

Fig. 13 Ratio of the Observation to the Calculation

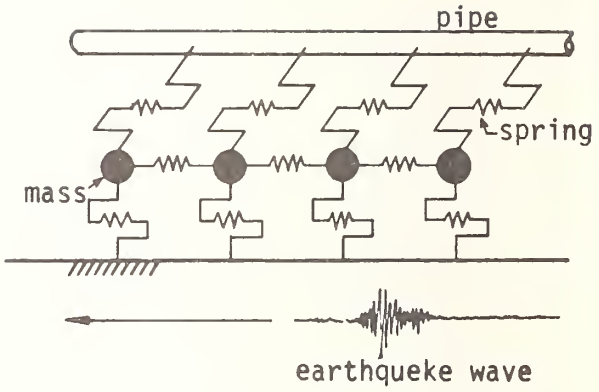

Fig. 14 Calculation Model

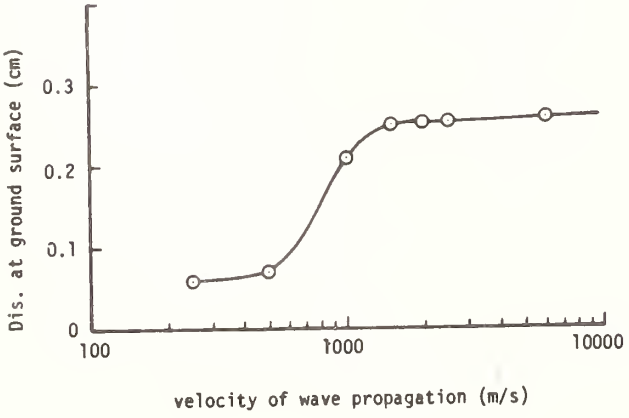

Fig. 15 Displacement at Ground Surface

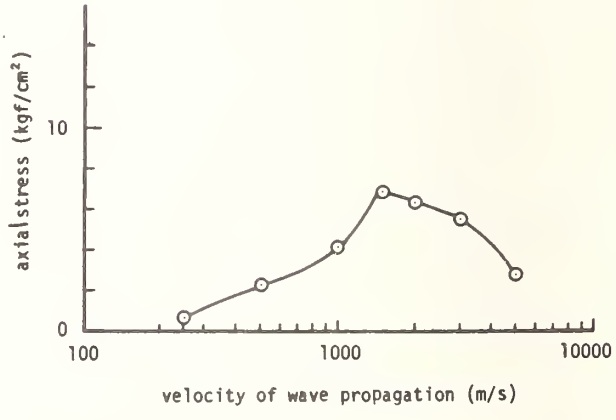

Fig. 16 Axial Stress in Pipe

BUCKLING AND RUPTURE FAILURE IN PIPELINES DUE TO LARGE GROUND DEFORMATIONS

Dr. Teoman Ariman

Associate Dean for Graduate Studies and Research
Director of Petroleum and Energy Research Institute
College of Engineering and Physical Sciences
University of Tulsa
Tulsa, Oklahoma 74104

ABSTRACT

A concise and up-to-date review of buckling and rupture failure in pipelines due to ground deformations is presented. It is shown that, in comparison to surface structures, pipeline systems are particularly vulnerable to local differential movements of ground. It is noted that permanent differential movements may be caused by any earthquake and that the movements can assume a variety of patterns depending on local soil conditions and the presence of faults. Therefore, the response of buried pipelines to permanent ground movement is an important part of lifeline earthquake engineering.

INTRODUCTION

During an earthquake, permanent differential movements of ground can be caused by faulting, soil liquefaction, slope instability and local compaction of the ground [1,2]. Buried pipelines can be damaged either by permanent movements of this type and/or by seismic ground waves. For instance surface faults, landslides, and local compaction of the ground in the 1971 San Fernando Earthquake caused the rupture and/or buckling failures in water, gas, and sewage lines [3,4,5] with high concentrations of pipeline damage along the Sylmar segment of the San Fernando fault [6-8]. Similarly, the 1972 Managua Earthquake caused surficial displacement along four prominent strike-slip faults through the downtown area of the city and nearly all water mains crossing the faults ruptured. Although relatively old and/or corroded pipelines have been damaged by wave propagation [9], seismic ground shaking alone generally cannot be expected to cause any major rupture and/or buckling failure in properly designed, manufactured and laid out welded steel pipelines [10-13]. This outcome is in complete agreement with the investigation of Youd [16]. After examining the 1971 San Fernando Earthquake effects in detail, he concluded that strong and ductile steel pipelines withstood ground shaking but were unable to resist the large permanent ground deformations generated by faulting and ground failures.

Furthermore, it is important to recognize that permanent differential movements may be caused by any earthquake and that the movements can assume a variety of patterns depending on local soil conditions and the presence of faults. Therefore, the response of buried pipelines to permanent

ground movement is an important part of lifeline earthquake engineering and its investigation is in line with the recommendations of a number of committees and individual researchers. For instance, Iwan [4] listed the investigation of effects of large soil movement on piping systems as a high priority subject. The ASCE Technical Council on Lifeline Earthquake Engineering [15] stated several research topics that deserve immediate attention in the engineering community. Among them are differential ground movements and fault crossing pipelines.

PIPELINE RESPONSE TO GROUND FAILURE

Pipeline damage is directly related to the patterns of ground movements. For example, reverse oblique faulting along the Sylmar segment of the San Fernando Fault Zone caused widespread compression and tension failures of buried pipelines [5,6,34,40]. The pattern of pipeline damage was consistent with the patterns of tensile and compressive ground strains by Slemmons [33] and Friedman et al. [41] as characteristic of reverse-slip faulting. In addition, significant features of the damage pattern also were related to the effects of left lateral slip, which contributed to either extension or compression as a function of pipeline orientation [2,7,34].

In a similar fashion, concurrent tensile and compressive distortions are associated with secondary earthquake effects. For example, lateral spreading caused by liquefaction will impose tension and pullout distortion near the boundaries between sliding and stable ground. At the same time, severe compressive strains and buckling may be imposed in the central position of the mobile ground as soil movements tend to converge into erosional basins or tongue-like patterns of mass translation. Patterns of this type were observed near Juvenile Hall during the 1971 San Fernando Earthquake [34,42,43], where substantial damage to gas transmission lines was reported [26]. Furthermore, lateral spreading during the 1964 Alaska Earthquake caused severe buckling of bridges [44] and underscores a potential siting and design problem for pipelines at river crossings [34].

A survey of damage caused by the 1971 San Fernando Earthquake indicates that, in comparison to surface structures, pipeline systems are particularly vulnerable to local differential movement. The area of surface fault displacement caused by the earthquake was approximately one-half of one percent of the area affected by strong ground shaking [2,24]. Nevertheless, approximately 25 percent of all pipeline breaks in the area of strong ground shaking occurred at or near fault crossings [1,2]. In addition, the earthquake triggered over 1,000 landslides [5]. Block movements of soil along the northwest rim of the Upper Van Norman Reservoir and an extensive, tongue-like spreading of soil along the reservoir's eastern shore caused severe damage to water and gas transmission lines [25-27].

The surface faulting associated with the 1971 San Fernando Earthquake occurred mainly on a left lateral thrust fault, which has been designated by the U.S. Geological Survey (USGS) as the San

Fernando Fault Zone which consists of four individual segments of the fault [1,7,28]. Among them, the Sylmar segment intercepted the largest part of the water and gas transmission and distribution systems.

Figures 1a and 1b represent a schematic view of the Sylmar segment of the San Fernando Fault Zone including damage to the water and gas mains [1,2]. Although the Sylmar segment was roughly 1.8 miles long in the east-west direction, the figures show only about 1 mile of the segment which was located in the City of Los Angeles along its eastern end. The ground displacements on the Sylmar segment occurred within a zone ranging from 150 to 350 ft in width [7]. The broad boundaries of this zone are shown by the dashed lines in each figure. Note that most of the lateral movement and approximately one-half of the vertical displacements occurred within a zone 150 ft wide along the southern edge of the fault [1,6,7,24]. This zone is represented by the ruled area in each figure.

The ground north of the Sylmar segment was thrust upward and left laterally (to the west) along ruptures dipping 70° to the north [1,24]. The general sense of this displacement is indicated in figure 2 [1,2], which represents an oblique view of the block movement. The maximum strike and reverse dip slip components of fault movement were 6.2 and 4.9 ft, respectively [24]. As shown in the figure, the strike-slip component of movement caused a net compression of the northeast-trending lines and a net extension of the northwest-trending lines.

The distribution of movement within the fault zone was complex. Frequently, large displacements were concentrated along individual scarps. At Comenta Avenue, a 30 ft wide shear zone showed a total of 1.5 ft vertical offset and 6 ft left lateral offset [1,7]. However, the maximum displacement across individual breaks in the fault zone were often much less than these. Horizontal shortening across the zone was consistently between 1.8 and 2.5 ft [1,7]. As shown in figure 3 [1,2], the nature of the ground movements within the actual fault zone differ substantially from that outside the zone. Within the zone, both northwest- and northeast-trending lines were compressed, as indicated by the buckling of pipelines at all orientations and by the offsets of pavement slabs [1,7,25, 27]. Some northwest-trending lines that failed by compression within this zone also failed by tension immediately north of the zone [1,7].

The mechanics of the ground deformation within the zone are as yet unknown, but it is significant for the analysis of pipeline behavior to recognize that high angle thrust faults can generate permanent ground compressive movements in all directions, even though the faulting may show a significant component of strike-slip movement [1,2].

Most pipelines in the San Fernando area were buried primarily in alluvial sand and gravel at depths between 2.5 and 5.0 ft. The operating pressures for the gas and water distribution lines were

approximately 60 to 150 psi, respectively. A detailed study of the damage to pipelines was reported in a number of references [2,19,25-27]. A brief reference will be made here regarding the damage to gas pipelines.

As shown in figure 1b, the gas distribution system in the area under consideration was composed of welded steel pipelines. Individual pipe lengths were approximately 40 ft service lines, typically 3/4 to 1 in. in diameter, connected to the distribution lines through welded service ties.

Damage occurred at similar levels of intensity on both northeast- and northwest-trending lines. Ruptures occurred mostly by buckling and twisting of the steel distribution lines, although in many locations service ties were sheared at their connections with the mains. Damage was extensive in the western part of the fault segment where differential ground movements were largest. Severe damage was sustained by a 16 in. steel transmission line on Foothill and Glenoaks Boulevards [9,25]. There were 52 separate breaks in, approximately a 6 mile length of this transmission line. In a number of sections it is observed that the 16 in. steel pipe buckled under the compressive forces, as shown in figure 4 [25]. Failures due to the buckling phenomenon were particularly dominant in transmission lines crossing the Sylmar segment of the fault.

Table 1 summarizes the various causes of permanent differential ground movement [34]. Faults, for example, may include strike-slip and dip-slip components. This type of faulting is particularly important with respect to the pattern of ground deformation and potential level of damage [32-35]. Liquefaction distortions have been classified according to three types of failure: lateral spread, flow failure, and loss of bearing capacity [34,36]. Landslides can assume a variety of different forms. Many landslides caused by earthquakes are characterized by gradual changes in elevation punctuated by scarps with modest offsets ranging from several inches to 1 or 2 ft [34]. Maximum distortions generally are concentrated along the slide margins where movements tend to replicate strike and normal slip faulting and thus, are subject to many of the same modeling techniques that apply for surface faults.

In recent years, a few investigations have been devoted to the behavior of oil pipelines subject to strike-slip faulting [37-29]. These studies have shown the close relationship between pipeline performance and key variables such as the angle of pipeline/fault intersection and the frictional resistance along the longitudinal axis of the pipe. It is important to note that these investigations have dealt only with the tension case. Furthermore, as indicated by O'Rourke and Trautmann [1,2], they do not address the pipelines typical of the gas and water distribution systems.

This review indicates the need and the importance of a research program to analyze the buckling and rupture failures of buried pipelines due to permanent, large and earthquake induced ground

deformations. At present, a research program supported by a grant[1] from the National Science Foundation to the University of Tulsa has been conducted under the direction of the author.

REFERENCES

[1] O'Rourke, T. D., and C. H. Trautmann, "Analytical Modeling of Buried Pipeline Response to Permanent Earthquake Displacements," Geotechnical Engineering Report 80-4, July 1980.

[2] O'Rourke, T. D., and C. H. Trautmann, "Buried Pipeline Response to Permanent Earthquake Ground Movements," ASME Paper 80-C2/PVP-78, 1980.

[3] Bolt, B. A., "Earthquake Risk in Relation to Earthquake Characteristics," Bull. 196, California Div. of Mines and Geology, 314-322, 1975.

[4] King, P. V. and J. M. Betz, "Earthquake Damage to a Sewer System," Journal of Water Pollution Control Federation, Vol. 44, No. 5, 859-867, 1972.

[5] Steinbrugge, K. V., et al., "San Fernando Earthquake February 9, 1971," Pacific Fire Rating Bureau, 465 California St., San Francisco, CA., 1971.

[6] Kamb, B., et al., "Pattern of Faulting and Nature of Fault Movement in the San Fernando Earthquake," U.S. Geological Survey, Professional Paper 733, 41-54, 1971.

[7] U.S. Geological Survey Staff, "Surface Faulting," The San Fernando, California, Earthquake February 9, 1971, U.S. Geological Survey, Professional Paper 733, 55-76, 1971.

[8] Youd, T. L., R. F. Yerkes, and M. M. Clark, "San Fernando Faulting Damage Its Effect on Land Use," Proc. Conf. Earthquake Engineering and Soil Dynamics, ASCE, Vol. 11, 1111-1125, 1978.

[9] Steinbrugge, K. V., W. K. Cloud, and N. H. Scott, "The Santa Rosa, California, Earthquakes of October 1, 1969," U.S. Dept. of Commerce, Rockville, MD, 1970.

[10] Muleski, G. E., T. Ariman, and C. P. Aumen, "A Shell Model of a Buried Pipe in a Seismic Environment," J. Pressure Vessel Technology, ASME, 101, 44-50, 1979.

[11] Chen, C. C., T. Ariman, and L. H. N. Lee, "Elastic Buckling Analysis of Buried Pipelines Under Seismic Loads," ASME Paper 80-C2/PVP-76, 1980.

[12] Lee, L. H. N., T. Ariman, and C. C. Chen, "On Buckling of Buried Pipelines by Seismic Excitation," ASME Paper 80-C2/PVP-75, 1980.

[13] Muleski, G., and T. Ariman, "On Fracture of Buried Pipelines Under Seismic Excitations," manuscript under preparation for the NSF Grant ENV-77-23236.

---

[1] National Science Foundation Research Grant "Buckling and Rupture of Pipelines Due to Large Ground Deformations" Grant No. CEE-8121674 to the University of Tulsa under the direction of T. Ariman.

[14] Iwan, W. D., "Earthquake Resistance of Public Utility Systems - A Report of the Findings of the California Governor's Interagency Earthquake Committee," Proceedings of the U.S. National Conference on Earthquake Engineering, EERI, 378-395, 1975.

[15] Task Committee on Research Needs of the Committee on Research of the Technical Council on Life line Earthquake Engineering, "Research Needs in Lifeline Earthquake Engineering," Journal of Technical Councils of ASCE Vol. 105, NOTC2, 343-362, 1979.

[16] Youd, T. L., "Ground Movements in the Norman Lake Vicinity During San Fernando, California, Earthquake of February 9, 1971," U.S. Dept. of Commerce, Vol. III, 197-206, 1973.

[17] Ariman, T., and G. E. Muleski, "A Review of the Response of Buried Pipelines Under Seismic Excitations," Earthquake Engineering and Structural Dynamics, Vol. 9, 133-151, 1981.

[18] Chen, C. C., T. Ariman, and M. Katona, "A Finite Element Analysis of Buried Pipelines Under Seismic Excitations," Lifeline Earthquake Engineering-Buried Pipelines, Seismic Risk and Instrumentation, Edited by Ariman, T., S. C. Liu, and R. E. Nickell, PVP-43, ASME, 133-142, 1979.

[19] Shinozuka, M., and H. Kawakami, "Underground Pipe Damages and Ground Characteristics," The Current State of Knowledge of Lifeline Earthquake Engineering, ASCE, 282, 1977.

[20] Isenberg, J., and J. P. Wright, "Survey of Existing Underground Water Pipelines with Emphasis on Their Seismic Resistance," Interim Grant Report IR-1, prepared for the National Science Foundation, Grant No. ENV-P-76-9838, 1976.

[21] Kratky, R. C., and M. G. Salvadori, "Strength and Dynamic Characteristics of Mechanically Jointed Cast-Iron Water Pipelines," Grant Report No. 3a, prepared for the National Science Foundation, Grant No. PFR-78-10549, 1978.

[22] Wang, L. R., M. J. O'Rourke, and R. R. Pikul, "Seismic Vulnerability, Behavior and Design of Buried Pipelines," Final Technical Report, sponsored by the National Science Foundation, Grant No. PFR-76-14884, 1979.

[23] Ariman, T., and G. E. Muleski, "Recent Developments in Seismic Analysis of Buried Pipelines," Proceedings of the 2nd U.S. National Conference on Earthquake Engineering, EERI, 643-652, 1979.

[24] Housner, G. W., and P. C. Jennings, "The San Fernando California Earthquake," Int'l. Journal on Earthquake Engineering and Structural Dynamics, Vol. 1, 5-31, 1972.

[25] Subcommitte on Water and Sewerage Systems "Earthquake Damage to Water and Sewerage Facilities," San Fernando, California, Earthquake of Feb. 9, 1971, U.S. Dept. of Commerce, Vol. II, 75-193, 1973.

[26] Southern California Gas Company "Earthquake Effects on Southern California Gas Company Facilities," San Fernando, California Earthquake of February 9, 1971, U.S. Dept. of Commerce, Vol. II, 59-64, 1973.

[27] McNorgan, J. D., "Gas Line Response to Earthquakes," Journal of Transportation Engineering, ASCE, TE4, 821-826, 1973.

[28] Durham, H. W. "Managua - Its Construction and Utilities," Engr. News Record, 696-700, April 23, 1931.

[29] Sulton, D. I., "The Managua Earthquake," Military Engineer, Vol. 23, 354-361, 1931.

[30] Brown, R. D., P. L. Ward, and G. Plafker, "Geologic and Seismologic Aspects of the Managua, Nicaragua, Earthquakes of December 23, 1972," U.S. Geological Survey Professional Paper 838, 1973.

[31] Youd, T. L. and S. N. Hoose, "Historic Ground Failures in Northern California Triggered by Earthquakes," U.S. Geological Survey Professional Paper 993, 1-176, 1978.

[32] Taylor, C. L. and L. S. Cluff, "Fault Displacement and Ground Deformation Associated with Surface Faulting," Proc. Conf. on Current State of Knowledge of Lifeline Earthquake Engineering, ASCE, 338-353, 1977.

[33] Slemmons, D. B., "State-of-the-Art for Assessing Earthquake Hazards in the United States: Faults and Earthquake Magnitude," Miscellaneous Papers S-73-P, Report 6, U.S. Army Engineer Waterways Experiment Stations, 1977.

[34] O'Rourke, T. D., "Buried Pipeline Response to Earthquake-Induced Ground Failure," Research proposal submitted to and funded by the National Science Foundation (courtesy of the principal investigator), 1981.

[35] Meyers, W. D., and W. Hamilton, "Deformation Accompanying the Hebgen Lake Earthquake of August 17, 1959," U.S. Geological Survey Professional Paper 435-I, 155-198, 1964.

[36] Youd, T. L., "Major Cause of Earthquake Damage is Ground Failure," Civil Engineering, ASCE, 47-51, April 1978.

[37] Newmark, N. M., and W. J. Hall, "Pipeline Design to Resist Large Fault Displacement," Proc. U.S. Nat'l. Conf. on Earthquake Engr., Ann Arbor, Mich., 416-425, 1975.

[38] Kennedy, R. P., A. W. Chow and R. A. Williamson, "Fault Movement Effects on Buried Oil Pipeline," Journal of Transp. Engr., ASCE, TE5, 617-633, 1977.

[39] Kennedy, R. P., A. C. Darrow, and S. A. Short, "Seismic Design of Oil Pipeline Systems," Journ. of Tech. Councils, ASCE, TC1, 119-134, 1979.

[40] Youd, T. L., R. F. Yerkes, and M. M. Clark, "San Fernando Faulting Damage and Its Effect on La Use," Proc. Conf. Earthquake Engineering and Soil Dynamics, ASCE, Vol. II, 1111-1125, 1978.

[41] Friedman, M., J. Handin, J. M. Logan, K. D. Min, and A. W. Stearns, "Experimental Folding of Rocks Under Confining Pressure: Part III Faulted Drape Folds in Multilithologic Layered Specimens," Bull. Seismological Society of America, Vol. 87, 1047-1066, 1977.

[42] Smith, J. L., and R. B. Fallgren, "Ground Displacement at San Fernando Juvenile Hall and the Sylmar Convertor Station," Bull. 196, California Div. of Mines and Geology, 157-163, 1975.

[43] Youd, T. L., "Ground Movements in the Van Norman Lake Vicinity During San Fernando Earthquake," San Fernando California, Earthquake of Feb. 9, 1971, U.S. Dept. of Commerce, Vol. III, 197-206, 1973.

[44] McCulloch, D. S., and M. G. Bonilla, "Effects of the Earthquake of March 27, 1964 on the Alaska Railroad," U.S. Geological Survey Professional Paper 545-D, D1-D159, 1970.

ACKNOWLEDGMENT

This work presented in this paper is part of a research program supported by the National Science Foundation Grant No. CEE-8121674 to the University of Tulsa. The grant is from the Siting Research Program of the Division of Civil and Environmental Engineering, National Science Foundation. The author acknowledges the encouragement and advice of Dr. S. C. Liu, Program Director, during the course of the research program.

Table 1. Summary of Earthquake-Induced Permanent Ground Movements [34]

Form of Permanent Ground Movement	Specific Modes of Failure	Earthquakes During Which Specific Failure Modes Caused Pipeline Damage
Faulting	Strike-slip	1906 San Francisco, 1931 Managua, 1940 Imperial Valley, 1968 Borrego Mountain, 1972 Managua
	Reverse-slip	1952 Kern County, 1971 San Fernando
	Normal-slip	1959 Hebgen Lake
Liquefaction	Lateral Spreads	1906 San Francisco, 1964 Alaska, 1971 San Fernando
	Flow Failure	1957 San Francisco, 1964 Alaska
	Bearing Capacity Loss	1906 San Francisco, 1952 Kern County, 1959 Hebgen Lake
Landslides	Rock Falls	1906 San Francisco, 1952 Kern County, 1959 Hebgen Lake, 1964 Alaska, 1971 San Fernando, 1972 Managua
	Relatively Shallow Slumping and Sliding of Soil	1906 San Francisco, 1952 Kern County, 1959 Hebgen Lake, 1964 Alaska, 1971 San Fernando, 1972 Managua
	Relatively Deep Rotational and Translational Soil Movement	1952 Kern County, 1959 Hebgen Lake, 1964 Alaska
Seismic Compaction		1957 San Francisco 1968 Borrego Mountain

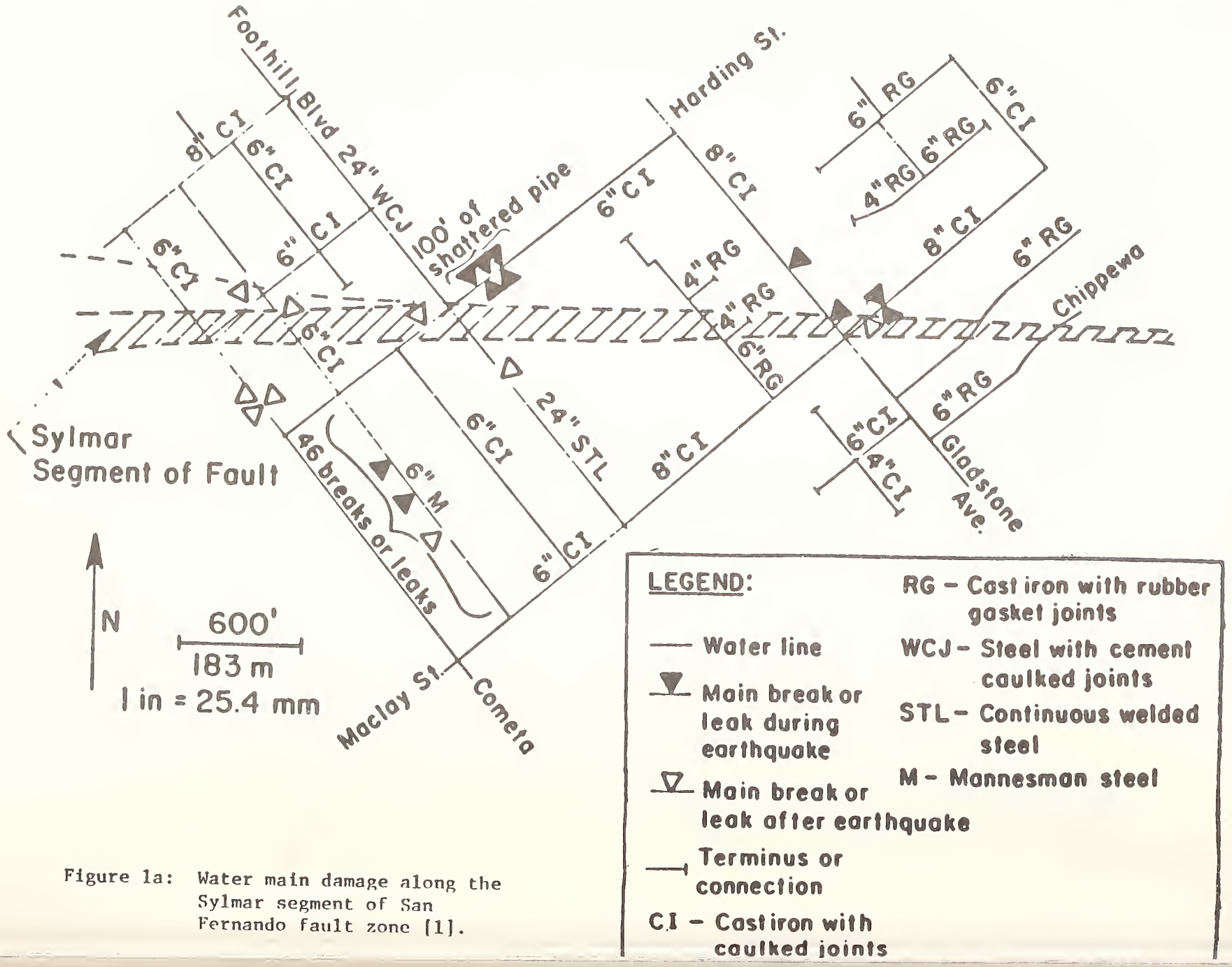

Figure 1a: Water main damage along the Sylmar segment of San Fernando fault zone [1].

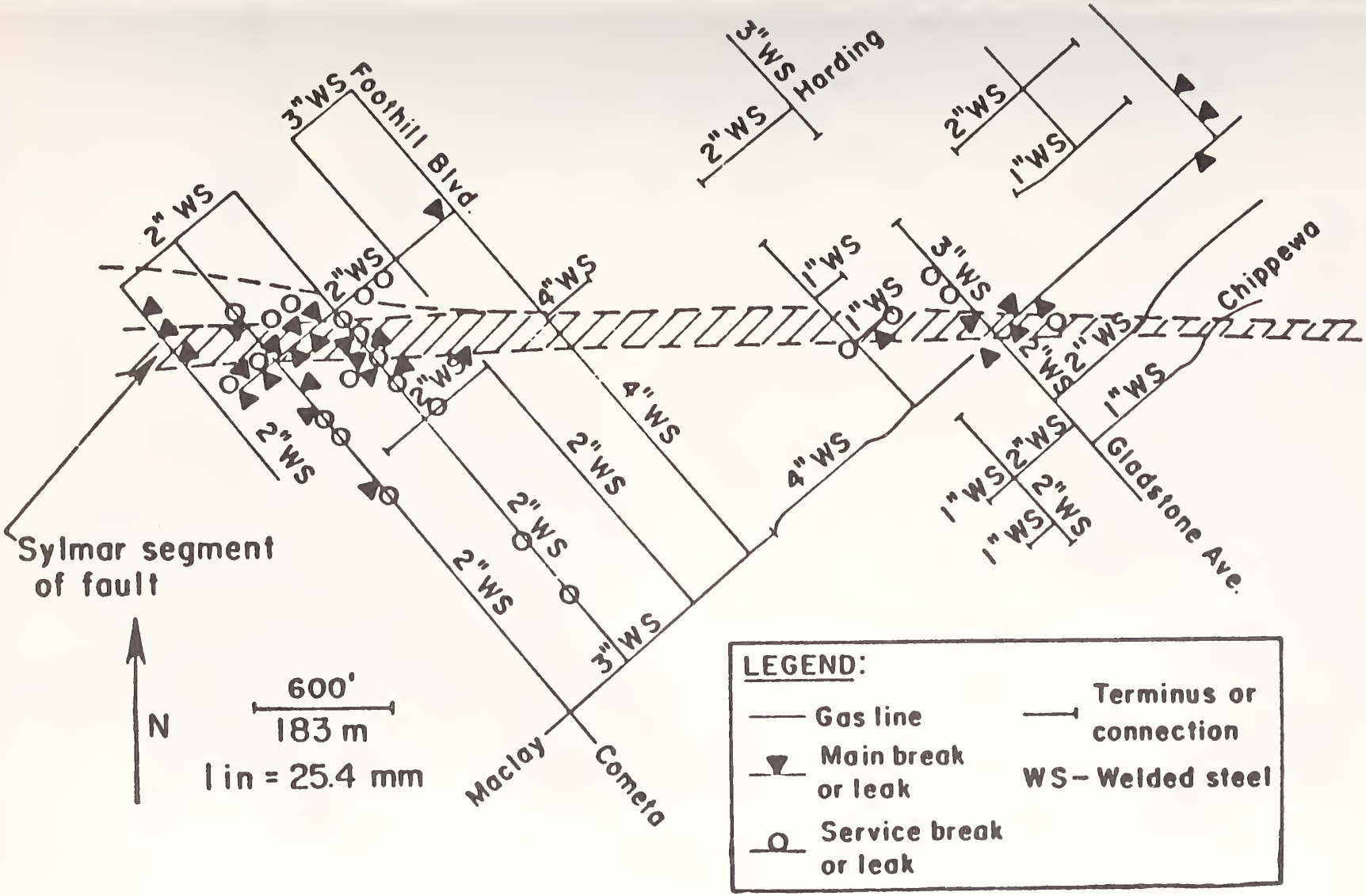

Figure 1b: Gas main damage along the Sylmar segment of San Fernando fault zone [1].

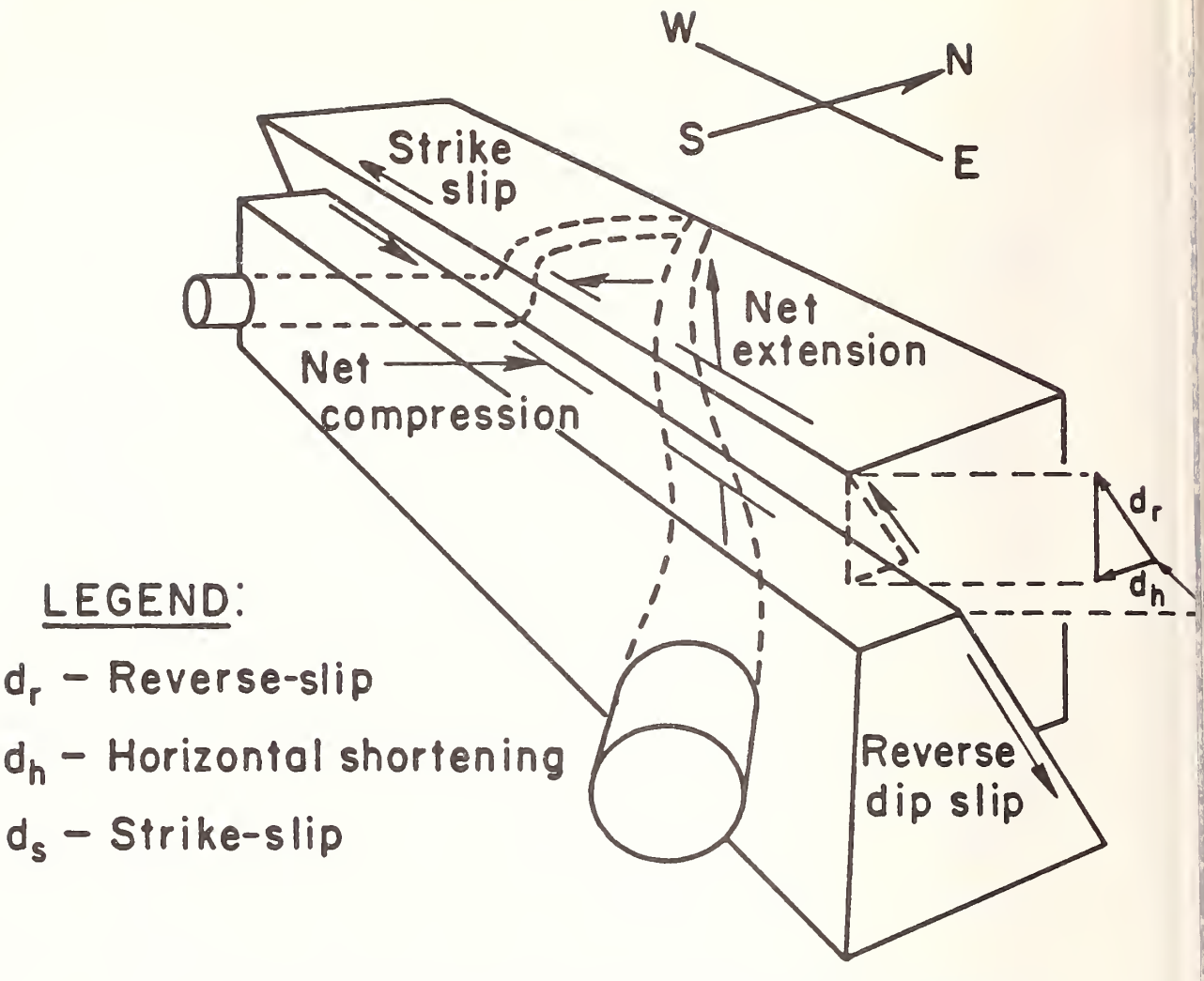

Figure 2: Block diagram of San Fernando fault motion [1].

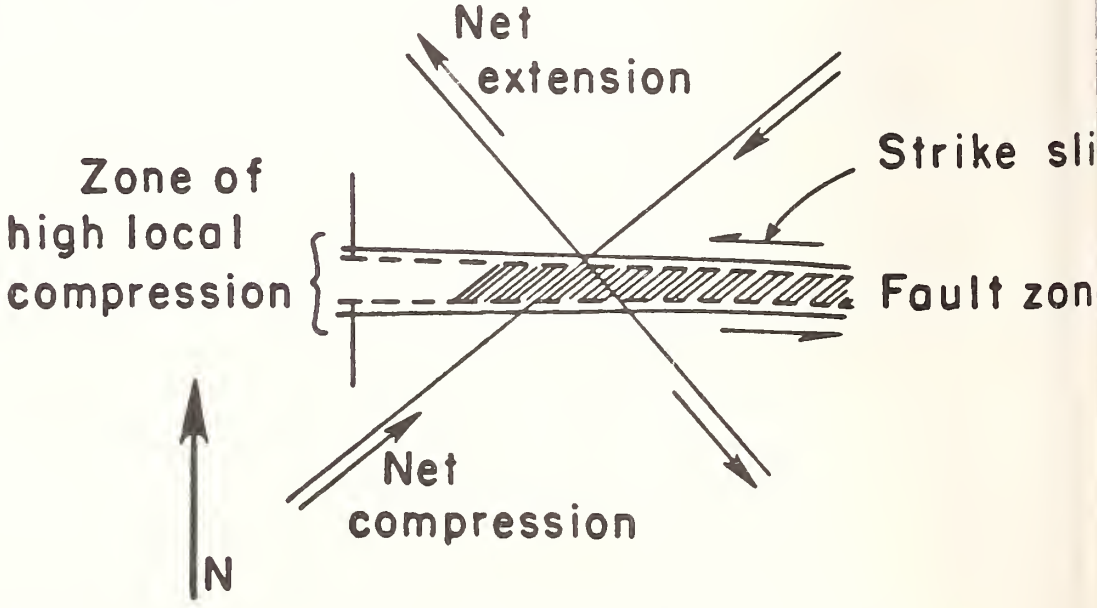

Figure 3: Relative ground displacements associated with San Fernando faulting [1].

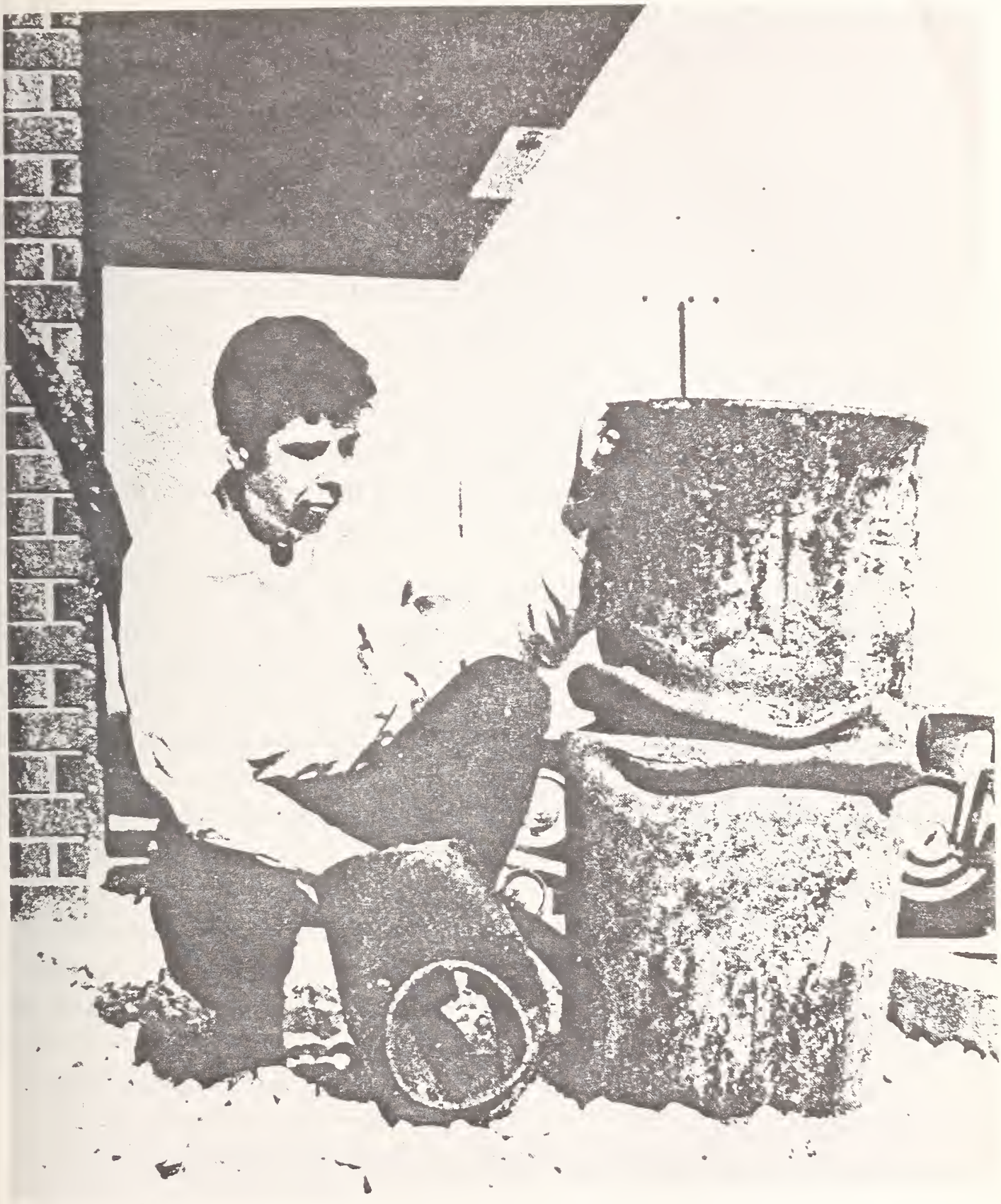

Figure 4 Compression Forces Buckled 16 inch Steel Pipe and 10 inch T.

EXPERIMENTAL STUDIES ON SEISMIC BEHAVIOR OF STRUCTURAL MEMBERS USING A DYNAMIC STRUCTURAL TESTING FACILITY AT PWRI

by

Eiichi Kuribayashi
Toshio Iwasaki
Ryoji Hagiwara

Public Works Research Institute

Takayuki Hadate

Prime Minister's Office

ABSTRACT

Dynamic structural testing facilities of an earthquake engineering laboratory were recently completed in March 1980 at Tsukuba by the Public Works Research Institute, Ministry of Construction. Four experiments as shown in table 1 were conducted so far using the facilities. Outlines of the facilities and two experiments conducted in the fiscal year of 1980 using the facilities are described.

OUTLINES OF THE DYNAMIC STRUCTURAL TESTING FACILITIES

The recently completed dynamic structural testing facilities were developed to study dynamic behavior of structural members and soils during earthquakes. Loading tests are conducted in a test pit (20 m x 15 m x 5 m) using actuators with performance specifications shown in table 2 and figure 1. The actuator can make excitations up to 125 tons with displacement amplitude up to 125 mm and frequency range of 0 to 30 Hz of arbitrary waves. With the actuators, static and dynamic loading tests of large-scale specimens can be performed. The details of the facilities are mentioned below.

(1) Buildings (figures 2, 3, 7)

The testing building (main building) has a test pit (L.20 m x W.15 m x H.5 m) embedded below the ground level. The actuators can be set on any part of the walls of the pit. It also has an operation room, data recording room, data processing room, data communication terminal, instrument storeroom, exhibition room, storeroom, utility room, and workshop.

The hydraulic power generation annex has a hydraulic power supply and electric power supply.

(2) Actuator (table 2, figures 1, 4)

Two actuators are installed in the pit. Each actuator is capable of ±125 t of maximum excitation, ±125 mm of maximum stroke and ±1 m/sec of maximum velocity with the frequency range of DC~30 Hz. An actuator is 3 m long and weighs 4 t.

The hydraulic power is provided by the hydraulic power supply in the annex. The excitation is controlled independently for two actuators by the control system. It is excited by an analog or digital control system.

(3) Hydraulic Power Supply (figure 8)

The hydraulic power supply is installed in the hydraulic power generation annex. The accumulators (6 x 200) are used for a high velocity test (maximum excitation time is 10 sec.). The accumulators are released for the long-time durability and fatigue test in which only the oil pumps (2 x 300 /min) are used. The capacity of the hydraulic power supply was determined to make the large velocity test possible. It is operated by remote control from the operation room.

(4) Control System (figures 5, 9)

The actuators are controlled by the analog or digital control system. The excitation can accomodate sinusoidal, triangular, rectangular ramp waves and earthquake motions. Sweep excitation and the excitation with a designated power spectrum density are also possible. The drive is corrected, if necessary, by comparing the excitation with the expected input motion.

(5) Data Aquisition (figures 6, 9)

The data aquisition system has 32 channels for dynamic data and 128 channels for static data. The data are stored in the disk system through the A/D converter and the digital computer. The data are compiled and analyzed later to get the dynamic characteristics of the specimens.

DYNAMIC LOADING TEST FOR ESTIMATION OF JOINT STIFFNESS OF SUBMERGED TUNNEL SEGMENTS

PREFACE

For the further and efficient development of Tokyo and Osaka Bay areas, the feasibility studies of the arterial highway networks are being carried out by the Ministry of Construction.

In these studies, the submerged tunnel method is considered to be the most feasible one in order to cross shipping routes. The geological survey shows that the evaluation of the earthquake resistance of the tunnel, especially, that of the joints of tunnel elements is critical for the application of the method. The axial force, bending moment, and shear force of the elements greatly depend on the dynamic stiffness characteristic of the joints. Therefore, the modeling of the joints is critical for the successful application of the computer simulation analysis.

The joint consists of the rubber gasket, PC cables, and the shear key, etc. The experiment was performed by static and dynamic loading tests to investigate the nonlinear dynamic response characteristics of the rubber gasket.

EXAMPLES OF SUBMERGED TUNNEL WITH RUBBER GASKET TYPE JOINT

Some of the tunnels which have the joints of this kind are the Daiba Tunnel on the Keiyo Line (1973-1980, Tokyo), the Tokyo Harbor Tunnel (1971-1976, Tokyo), the Elbe Tunnel (1968-1973, Hamburg), the Rotterdam Metro Tunnel (1960-1968, Amsterdam), etc.

EXCITATION TESTS FOR ESTIMATION OF JOINT STIFFNESS OF SUBMERGED TUNNEL SEGMENT

(1) Model

A typical cross section and a flexible joint of the submerged tunnel planned in the Tokyo Bay area are shown in figure 12. The basic shape of the rubber gasket used in the test was the Gina type (figure 13). The model of the rubber gasket was determined through the preceeding tests to have the length and the width of 30 cm and the height of 21 cm, which was a full scale model. The hardness of the body was 60 degrees, and the gasket had a small projection on the top and the bottom.

(2) Test Apparatus

An actuator was attached to the movable wall as shown in figure 10. Moreover, in order to keep the axis of the piston rod of the actuator, it was fixed horizontally and vertically by the supporter as shown in figure 11.

(3) Excitation and Measurement

The excitation test was performed by compressing the gasket by the sinusoidal and triangular exciting patterns after compressing the gasket to the predetermined height, 100 to 57.5 percent of the original height, in 20 seconds.

The static test was performed by loading the gasket by compressing to the same height as the exciting test in 30 seconds. An unloading test was also performed for the same duration.

The load and the deformation of the gasket were measured by a load cell and a transducer in the actuator and recorded in magnetic discs in a mini-computer via an A/D converter. The dynamic and static loading and unloading curves were made by the use of a graphic display. Figure 14 shows some examples of the excitation patterns.

(4) Test Results

The dynamic hardening ratio is defined by equation 1.

$$Rk = \frac{Kd}{Ks} \tag{1}$$

where, Kd is the dynamic spring constant (t/mm), and Ks is the static spring constant (t/mm) as defined in figure 15.

Figure 16 shows the static loading and unloading curves. As shown in this figure, the first loop was a little different from the following loops which seemed to be indifferent to the repetition

of loading and unloading. Therefore, we used the loops after the second loading in the calculation of Ks.

Figure 17 shows Ks for the compression (height decrease) of 25, 30, 35, 40 percent, etc. It is noted that the static spring constant increased as the compression increased. Figure 18 shows the hysteresis curves and figure 19 shows the dynamic spring constant, Kd. Table 3 shows the spring constants and the dynamic hardening ratio, Rk. It is noted from these results that in the cases of displacement control tests, the dynamic spring constants were somewhat different between sinusoidal and the triangular exciting patterns and ranged from 1.62 to 6.27. Effects of frequency of excitation showed a small effect on the dynamic spring constant and the dynamic hardening ratio, a little higher for 1.0 Hz than for 0.5 Hz.

In the case of the load control tests, the results showed the same tendency as the displacement control tests, however, the difference of compression ratio gave a little higher value than those of the displacement control test.

The changes of the dynamic spring control were shown in figure 19 and the corresponding dynamic hardening ratios were shown in figure 20.

The principal parameters which determine the dynamic spring constant were the compression ratio, the amplitude of dynamic displacement and load, etc. The larger the compression or the smaller the amplitude of dynamic load and displacement with the same compression, the greater the spring constant. The dynamic hardening ratio had the same tendency as the spring constant.

The frequency had little effect on the dynamic spring constant and the dynamic hardening ratio.

The secant of the unloading curve for the static loading test gave approximately the same value of the dynamic spring constant. [1,2]

Several possible evaluation methods for obtaining the dynamic spring constant could be obtained from the test results as follows:

A: A method in which the constant is estimated from the expected compression ratio and the amplitude of dynamic load and displacement.

B: A method in which the constant is estimated from the dynamic spring constant and the dynamic hardening ratio.

C: A method in which the constant is estimated by taking the secant on the unloading curve obtained by the static test corresponding to the expected amplitude of load and displacement.

Method A gave the best fit and methods B and C were almost as good. In the case of methods B and C, the static loading and unloading curves were approximated as

$$P = \alpha \cdot \delta^{\beta},$$

where, P is load (tons), δ is displacement (mm), and α, β are coefficients of the approximation curve. α and β were obtained as values of $0.97 \sim 5.47 \times 10^{-6}$ and 3.71~4.19 as shown in figure 21. The values of the dynamic spring constants evaluated by methods A, B, and C are shown in table 4. It is considered that the method B is the most effective.

REFERENCES

[1] Earthquake Engineering, "Report on Experiment Using Large Scale Model of Joint Member of Submerged Tunnel Segment", January 1980.

[2] Eiichi Kuribayashi et al., "Evaluation Method of Joint Stiffness Property of Submerged Tunnel Segment", January 1978.

REVERSED CYCLIC LOADING TEST OF REINFORCED CONCRETE BRIDGE PIER MODELS

It is desirable to consider the non-linear characteristics and ductility of a reinforced concrete bridge pier in its earthquake-resistant design.

The following describes the results of model loading tests of a reinforced concrete bridge pier to investigate its seismic behavior to the ultimate state.

OUTLINE OF THE EXPERIMENT

Reversed cyclic loading tests of the models of a Ban-no-su Bridge pier in Kojima-Saka-ide Route of Honshu-Shikoku Bridge were conducted. Ban-no-su Bridge is a double deck bridge for a highway and a railway, and its pier columns are divided into upper and lower columns as shown in figure 22. For this kind of a structure, detailed studies on seismic behavior of the upper column subjected to earthquake excitations in the transverse direction are needed in the earthquake-resistant design. For this reason, model loading tests of the upper column of the reinforced concrete pier were conducted.

Scales of the models used in the experiment were $1/(4\sqrt{2})$ for six specimens and 1/4 for one specimen. Conditions of the models were determined as shown in table 5 and figures 23~30 to investigate seismic behavior of the actual bridge column and effects of the assumed structural conditions on aseismic performances of the column.

A lateral load was applied to the column models at the center of gravity of the superstructure. The input was controlled by load up to the reinforcement yield point and by the displacement after that. In the case of load-controlled input, load was increased step by step, and load was returned to zero for each step. In the case of displacement-controlled input, the input displacement was N δ_0 (δ_0: calculated yield displacement of the basic model, N = 1,2,3,4,5), and the repeat of the same displacement input was three times for No. 1 model (one-directional loading) and ten times for other models (reversed loading). Figure 31 are the photos of the experiment.

RESULTS OF THE EXPERIMENT

Yield load, ultimate load, yield displacement, ultimate displacement, and potential energy of the column models obtained by the loading tests are shown in table 6. Load-displacement curves obtained by the one-directional (No. 1) and reversed (No. 3) loading tests are shown in figures 32 and 33. In the load-displacement curve of the basic model (No. 3), load increased even after longitudinal reinforcements had yielded, and it became maximum (ultimate load) when input displacement was 2~3 δ_0. The ultimate load of the basic model was 20~30 percent larger than the yield load. After that, load decreased to the level of yield load when input displacement was 4~5 δ_0 (ultimate

displacement). When loading was repeated with the same displacement, load decreased remarkably by the first loading cycle and did gradually by subsequent loading cycles. The stiffness at the yield point decreased to 1/3~1/4 of the initial stiffness. The shape of the hysteresis loop was spindle-shape at the initial stage and shifted to an inverse-S shape as the input displacement became large and the cycle of loading increased.

Final destruction modes of each model are shown in figure 34. In the case of one-directional loading (No. 1 model), cracks occurred at the base of the column at first, but the specimen finally failed in shear by the crack which developed diagonally from the hunch. The specimen with large-diameter longitudinal reinforcement and without side reinforcement (No. 4 model) also failed in shear. Other models failed in bending at the base of the column.

Load-displacement envelope curves of the first loading cycle (n = 1) are shown in figure 35. Comparisons of aseismic performance of the column models are shown in figures 36~40.

The yield load and the ultimate load of the one-directional loading model (No. 1 model) and the reversed-loading basic model (No. 3 model) were about the same. But the ultimate displacement of No. 3 model was 40 percent of that of the No. 1 model. By reversed loading, displacement ductility ratio (ultimate displacement δ_u/yield displacement δ_y) decreased to 1/2~1/3 of that by one-directional loading (figure 36).

As for the effects of the hunch at the base of the upper column, the yield load and the ultimate load of the model with a hunch (No. 3 model) were 20~30 percent larger than those of the model without a hunch (No. 2 model). The ultimate displacement of both models were about the same. The displacement ductility ratio of both the models in the hunch-comparison direction were about the same, too. But the displacement ductility ratio of the model with a hunch was 10~20 percent smaller than that of the model without a hunch in the hunch-tension direction because of larger yield displacement of the former model than the latter model (figure 37).

Comparing the test results of the model with large-diameter longitudinal reinforcements and without reinforcement (No. 4 model) and those of the basic model (No. 3 model), the former failed in shear at the upper part of the column, while the latter failed in bending at the base of the column. No. 4 model was about 10 percent smaller in yield load, about 20 percent smaller in ultimate load, and about 40 percent smaller in displacement ductility ratio than the No. 3 model.

As for the effects of an axial load, the model with an axial load corresponding to the dead load of the superstructure (No. 7 model) was about 20 percent larger in yield load, about 10 percent larger in ultimate load, but 10~20 percent smaller in displacement ductility ratio than the model without an axial load (No. 3 model) (figure 38).

Comparing the test results of the SRC model (No. 6 model) and the RC model (No. 3 model), the ~20 percent larger in yield and ultimate loads than the latter. This is because the actual strength of the steel frame was larger than the nominal strength, while the SRC model was designed based on the nominal strength. The SRC model and the RC model can be said to have had similar aseismic performances after all (figure 39).

In the case of SRC models, the model with studs on steel frames below the base of the column (No. 6 model) and the model without studs (No. 5 model) had similar aseismic performances (figure 40). This is because of small influence of the pulled-out of steel frames.

Equivalent damping factors (h) obtained from the hysteresis loops were h = 0.02~0.04 at the displacement amplitude of δ_0, h = 0.06~0.10 at $2\delta_0$, and h = 0.10~0.13 at amplitude larger than $3\delta_0$.

ANALYTICAL INVESTIGATIONS

Calculated and measured load-displacement envelope curves of n = 1 for the one-directional loading model (No. 1 model) and the basic model (No. 3 model) were compared as mentioned below. The following is the calculation procedure of a load-displacement curve.

Divide the upper column into m-elements in the axial direction. Calculate bending moment M_c, M_y, M_u and curvature ϕ_c, ϕ_y, ϕ_u of each element at the cracking, yield, and ultimate states to obtain M-ϕ relationships as shown in figure 41. M_c and ϕ_c can be calculated by equation (2).

$$M_c = W(\sigma_{bt} + \frac{N}{A_g})$$
$$\phi_c = \frac{M_c}{E_c I_g} \qquad (2)$$

where,

σ_{bt}: bending tensile strength of concrete

N: axial load to the element

A_g, I_g: equivalent sectional area and equivalent moment of inertia of area

W: section modulus

E_c: Young's modulus of concrete

For the calculation of M_y, ϕ_y, M_u, and ϕ_u, divide each element into n-small elements and obtain the strain of each small element assuming the stress and strain to be constant within the small element. Using the obtained strain, obtain the corresponding stress by stress-strain curves as assumed in figure 42 and the neutral axis satisfying equations (3) and (4)

$$N = \sum_{i=1}^{n} \sigma_{ci} \cdot \Delta A_{ci} + \sum_{i=1}^{n} \sigma_{si} \cdot \Delta A_{si} \qquad (3)$$

$$M = \sum_{i=1}^{n} \sigma_{ci} \cdot X_i \cdot \Delta A_{ci} + \sum_{i=1}^{n} \sigma_{si} \cdot X_i \cdot \Delta A_{si} \quad (4)$$

where,

N, M: axial load and bending moment to the element

σ_{ci}, σ_{si}: stress of concrete and reinforcements in the small element

ΔA_{ci}, ΔA_{si}: sectional areas of concrete and reinforcements in the small element

X_i: distance from concrete or reinforcements of the small element to the neutral axis

Calculate bending moment by equation (4) and curvature by equation (5)

$$\phi = \frac{\varepsilon_{c0}}{X_0} \quad (5)$$

where,

ε_{c0}: extreme fiber strain

X_0: distance from the compressive edge of concrete to the neutral axis

Obtain M_y, ϕ_y assuming the yield strain of reinforcements as $\varepsilon_s = \sigma_{sy}/E_s$ (σ_{sy}: yield strength of a reinforcement, E_s: Young's modulus of a reinforcement) and M_u, ϕ_u assuming the ultimate strain of concrete as $\varepsilon_c = 0.0035$.

Calculate lateral displacement caused by the bending deformation of the upper column by equation (6).

$$\delta_i = \int_0^{y_i} \theta dy \approx \sum_{j=2}^{i} \frac{\theta_j + \theta_{j-1}}{2} \cdot \Delta y_{j-1}$$
$$\theta_j = \int_0^{y_j} \phi dy \approx \sum_{k=2}^{i} \frac{\phi_k + \phi_{k-1}}{2} \cdot \Delta y_{k-1} \quad (6)$$

where,

δ_i: deflection of section-i of y_i-distant from the base of the upper column

θ_j, θ_{j-1}: rotation angles of jth and j-1th sections from the base of the upper column

Δy_{j-1}: distance between j-1th and jth sections from the base of the upper column

Rotation at the base of the upper column was measured in the experiment. Analytic models as shown in table 7 were used for the calculation of a P-δ curve to take the rotation into consideration.

Estimated load-displacement curves at the loaded point of the column by the analytic models above mentioned are shown in figures 43~46 where measured ones are also represented.

In Case A in which the upper column was fixed at the base, the estimated yield displacement was 45 percent of the measured one in the hunch-compression direction and 40 percent of that in the hunch-tension direction. Displacement caused by the rotation at the base of the upper column was 35 percent

of the measured total displacement in the hunch-compression direction and 30 percent of that in the hunch-tension direction in the experiment. This indicates the importance of taking the rotation into consideration in the estimation of the displacement. When the estimated displacement was corrected by the measured rotation, it became 80 percent of the measured total displacement in the hunch-compression direction and 70 percent of that in the hunch-tension direction. Estimated load-displacement curves after the yield point differed from the measured ones. The estimated ultimate displacement of the basic model (No. 3 model) is about a half of the measured one (figure 43).

In Case B in which the hunched column was extended to the footing, the estimated yield displacement was small in the hunch-compression direction and large in the hunch-tension direction as compared with the measured yield displacement. In this model, members below the base of the upper column yielded before those at the base of the column did by the hunch-tension load (figure 44). In

Case C and Case D, the estimated rotation angle θ subjected to the one-directional load and 2θ considering the effect of reversed loading were used to estimate the displacement. As for a load-displacement curve, Case D ($+\theta$) in the hunch-compression direction and Case D (-2θ) in the hunch-tension direction gave good agreement with the measured curve (figures 45, 46).

For a more precise estimation, it is necessary to consider shear deformation and the effect of the concentration of cracking in the calculation of displacement. Moreover, it is necessary to investigate the stress-strain relationship of concrete and reinforcement, bending moment-curvature relationship, and effects of side reinforcement and confining reinforcement to estimate a load-displacement curve after the yield point more precisely.

CONCLUSIONS

The following results were obtained by the model loading tests of an upper column of the Ban-no-su Bridge pier of Honshu-Shikoku Bridge.

(1) Stiffness of the reinforced concrete column decreases by the cracking. Stiffness at the yield stage is 1/3~1/4 of the initial stiffness.

(2) Maximum strength of the column is 10~30 percent larger than the yield strength.

(3) Displacement ductility ratio (ultimate displacement/yield displacement) of the column is 10 when subjected to one-directional (hunch-compression direction) loads and 4 when subjected to reversed loads. Reversed loading makes the ductility ratio decrease to 1/2~1/3 of that by one-directional loading.

(4) In the case of reversed cyclic loading with the same displacement, load decreases remarkably by the first cycle of loading and decreases gradually by the following cycle of loading.

(5) The shape of the hysteresis loop is spindle-shaped at the initial stage and shifts to an inverse-S shape as the input displacement becomes large and the cycle of loading increases. The equivalent damping factor of hysteresis damping of the column is h = 0.02~0.05 at the yield stage and h = 0.10~0.13 after the yield of reinforcement.

(6) The load-displacement envelope curves until the maximum load in the case of one-directional loading and reversed loading are almost the same. After the maximum load, the load decreases more remarkedly in the case of reversed loading than in the case of one-directional loading as the input displacement increases.

(7) A hunch at the base of the upper column makes the yield load and the ultimate load 20~30 percent larger than those of the column without a hunch. The hunched column was destroyed by bending-failure in the experiment, but it should be noted that the possibility of shear-failure becomes large by the hunch.

(8) The column with large-diameter longitudinal reinforcements and without side reinforcements failed in shear at the upper part, and its strength and ductility were rather small.

(9) When an axial load corresponding to the dead load of the superstructure is applied, yield load and ultimate load increase 20 percent and 10 percent respectively, and ductility becomes 10~20 percent less than those without an axial load.

(10) Aseismic performance of RC and SRC columns are almost the same.

(11) Effect of studs at the base of the upper column to prevent pull out of steel frames was small in the experiment.

(12) Rotation of the upper column by the pullout of longitudinal reinforcement at the base of the column was observed. This rotation caused 35 percent of the displacement at the top of the column in the hunch-compression direction and 30 percent of that in the hunch-tension direction in the experiment.

(13) Difference between estimated and measured values of the yield load and the ultimate load was within 15 percent of the measured values for the first cycle of loading. Further investigations are needed to consider the effects of reversed loading and an axial load.

(14) A load-displacement envelope curve up to the yield point can be estimated by the method described under Analytical Investigations with the assumption of rotation at the base of the column. But a load-displacement envelope curve after the yield point can not be estimated precisely by the method. Further investigations are needed on stress-strain relationship of concrete and reinforcement, effects of confining reinforcements, axial loads, and reversed cyclic loading, etc.

ACKNOWLEDGEMENTS

The authors express their deep thanks for the cooperation of Honshu-Shikoku Bridge Authority in the experiment.

REFERENCES

[1] Public Works Research Institute, Ministry of Construction, "Reversed Cyclic Loading Test of Bridge Pier Models," Technical Memorandum of PWRI No. 1730, October 1981.

[2] Public Works Research Institute, Ministry of Construction, ":tudies on the Earthquake-resistant Design Method for Simple Reinforced Concrete Bridge Piers," Technical Memorandum of PWRI No. 1513, July 1979.

[3] Ministry of Construction, "New Earthquake-Resistant Design Methods," (proposal), Technical Memorandum of PWRI No. 1185, March 1977.

[4] Japan Road Association, "Design Regulations for Highway Bridges V Earthquake-Resistant Design," May 1980.

[5] Japan Civil Engineering Society, "An Investigation Report on Aseismicity and Site Ground Conditions of Honshu-Shikoku Bridge," March 1981.

[6] Yoshimaro Matsuzaki, Eiichi Kuribayashi, Ryoji Hagiwara, "An Experimental Study on Strength and Ductility of a L-shaped Reinforced Concrete Member Subjected to Reversed Cyclic Loads," 16th Meeting on Earthquake Engineering, July 1981.

[7] Yoshimaro Matsuzaki, Eiichi Kuribayashi, Ryoji Hagiwara, "An Experimental Study on Strength and Ductility of a Reinforced Concrete Member Subjected to Reversed Cyclic Loads," 36th Annual Meeting of Japan Civil Engineering Society, October 1981.

Table 1. Experiments Using the Dynamic Structural Testing Facility

Fiscal Year	Experiment
1980	(1) Dynamic Loading Test for Estimation of Joint Stiffness of Submerged Tunnel Segments Scale of the Model : 1/1 Input : Sinusoidal waves
	(2) Reversed Cyclic Loading Test of Reinforced Concrete Bridge Pier Models Scale of the Model : $1/(4\sqrt{2})$, 1/4 Input : Statically-reversed cyclic loading
1981	(3) Dynamic Loading Test on Seismic Behavior of Water Supply Pipes Scale of the Model : 1/1 Input : Sinusoidal waves
	(4) Dynamic Loading Test of Reinforced Concrete Bridge Pier Models Scale of the Model : 1/4~1/6 Input : Sinusoidal waves

Table 2. Main Specifications of the Actuator

Item	Performances
(1) Maximum Excitation	± 125 t/1 Actuator
(2) Maximum Stroke	± 125 mm
(3) Maximum Speed	± 1 m/sec
(4) Frequency Range	DC 30 Hz
(5) Excitation Motions	Sinusoidal Waves Triangular Waves Rectangular Waves Ramp Waves Earthquake Motions
(6) Maximum Excitation Time	10 sec (At Maximum Velocity)
(7) Control of Input Motions	Analog Control and Digital Control
(8) Control Item	Acceleration, Velocity or Displacement
(9) Exciter	Electro-hydraulic Servo System
(10) Hydraulic Power Supply	Main Pump 300 /min x 2 with 200 /10 sec x 6 Accumulators (3 Accumulators/1 Actuator) x 2

Table 3. Dynamic Spring Constant and Dynamic Hardening Ratio

Displacement Control							
Input Motion	Compression Ratio (%)	Dynamic Displacement Amplitude (mm)	K_d		R_k		Note
			0.5 Hz	1.0 Hz	0.5 Hz	1.0 Hz	
Sinusoidal Wave	30.0	±2	(ton/mm) 1.970	(ton/mm) 2.103	1.79	1.91	K_d: Dynamic Spring Constant R_k: Dynamic Hardening Ratio
		8	1.621	1.659	1.47	1.51	
	32.5	2	1.960	2.000	1.50	1.54	
		8	1.742	1.821	1.34	1.40	
	35.0	2	3.140	3.240	1.74	1.80	
		8	2.627	2.663	1.46	1.48	
	37.5	2	4.085	4.306	1.41	1.48	
		8	2.866	2.863	0.99	0.99	
	40.0	2	5.995	6.445	1.87	2.01	
Triangular Wave	30.0	2	2.004	2.065	1.82	2.02	
		8	1.619	1.630	1.47	1.48	
	32.5	2	2.004	2.154	1.52	1.66	
		8	1.810	1.872	1.40	1.44	
	35.0	2	3.215	3.405	1.79	1.89	
		8	2.149	2.320	1.19	1.29	
	37.5	2	4.313	4.453	1.49	1.54	
		8	2.799	2.858	0.97	0.99	
	40.0	2	5.874	6.269	1.84	1.96	
Load Control							
Input Motion	Compression Ratio (%)	Dynamic Load Amplitude (ton)	K_d		R_k		
			0.5 Hz	1.0 Hz	0.5 Hz	1.0 Hz	
Sinusoidal Wave	30.0	±8	(ton/mm) 1.579	(ton/mm) 1.626	1.44	1.49	
	35.0	8	2.986	2.984	1.66	1.66	
		16	2.455	2.576	1.36	1.43	
	40.0	8	8.497	8.303	2.66	2.59	
		16	7.219	7.442	2.26	2.33	
Triangular Wave	30.0	8	1.601	1.696	1.46	1.54	
	35.0	8	2.992	3.167	1.66	1.76	
	40.0	8	8.260	8.648	2.58	2.70	

Table 4. Dynamic Spring Constant Estimated by Each Evaluation Method

Compression Ratio (%)	Dynamic Spring Constant			Note
	Evaluation Method A	Evaluation Method B	Evaluation Method C	
30	1.6	1.8	1.4	
32.5	1.7	2.3	1.7	
35	2.6	2.9	2.4	
37.5	3.9	3.6	3.0	

Table 5. Test Cases

Model	Test Conditions
No. 1 $1/(4\sqrt{2})$ one-directional loading model	One-directional loading, other conditions are the same as basic model
No. 2 $1/(4\sqrt{2})$ without hunch model	Without hunch, other conditions are the same as basic model
No. 3 $1/(4\sqrt{2})$ basic model	Same structural conditions as the actual bridge (main reinforcement - D13, reversed cyclic loading)
No. 4 $1/(4\sqrt{2})$ large-diameter reinforcement, without side reinforcement	Large-diameter reinforcement and without side reinforcement (main reinforcement - D29, reversed cyclic loading)
No. 5 $1/(4\sqrt{2})$ SRC - without stud model	SRC without stud (CT shape steel + D13 reinforcement, reversed cyclic loading)
No. 6 $1/(4\sqrt{2})$ SRC - with stud model	SRC with stud (CT shape steel + D13 reinforcement, reversed cyclic loading)
No. 7 1/4 model	Same structural conditions as the actual bridge (main reinforcement - D13, reversed cyclic loading)

Note: Axial load of 118 t corresponding to the dead load of the superstructure was applied to 1/4 model, but no axial load was applied to $1/(4\sqrt{2})$ models.

Table 6. Results of the Experiment (n = 1 P-δ Envelope Curve)

Loading Direction	Hunch-tension							Hunch-compression						
	No. 1 One-directional loading	No. 2 Without hunch	No. 3 Basic model	No. 4 Large-diameter reinforcement, without side reinforcement	No. 5 SRC without stud	No. 6 SRC with stud	No. 7 1/4 model	No. 1 One-directional loading	No. 2 Without hunch	No. 3 Basic model	No. 4 Large-diameter reinforcement, without side reinforcement	No. 5 SRC without stud	No. 6 SRC with stud	No. 7 1/4 model
Yield Load P_y(t)	-	-55	-75	-69	-72	-79	-175	75	61	72	66	80	85	177
Ultimate Load P_u (t)	-	-69	-89	-73	-94	-96	-187	92	73	89	68	100	101	200
P_u/P_y	-	1.25	1.19	1.06	1.31	1.22	1.07	1.23	1.20	1.24	1.03	1.25	1.19	1.13
Yield Oisplacement δ_y (cm)	-	-2.3	-2.6	-2.6	-2.2	-2.3	-4.1	2.0	2.1	2.1	2.3	1.9	2.2	3.2
Ultimate Oisplacement δ_u (cm)	-	-7.8	-7.5	-4.5	-8.5	-8.3	-9.6	19.6	7.6	7.9	4.9	8.5	7.6	10.9
δ_u/δ_y	-	3.4	2.9	1.7	3.9	3.6	2.3	9.8	3.6	3.8	2.1	4.5	3.5	3.4
Potential energy E_u (t·cm)	-	354	442	201	529	540	1,190	1,610	366	407	210	579	505	1,430
δ_0/δ_y	-	0.78	0.69	0.69	0.82	0.78	0.63	0.9D	0.86	0.86	0.78	0.95	D.82	0.81

Notes: P_y: Load applied at the top of the column at the time of yield of outer reinforcements.

P_u: Maximum load in n = 1 P-δ envelope curve

δ_y: Displacement at the top of the column corresponding to P_y

δ_u: Displacement corresponding to P_y after δ_y in n = 1 P-δ envelope curve

E_u: Integration of P-δ envelope curve up to the ultimate displacement.

Table 7 Analitic Model for the Estimation of a P—δ Curve

Case	Case A	Case B	Case C		Case D	
Model	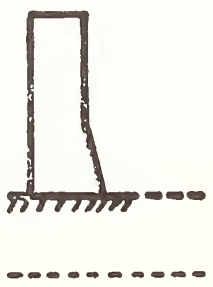	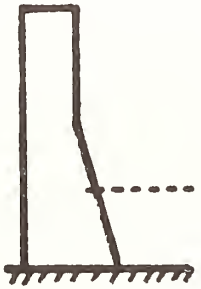	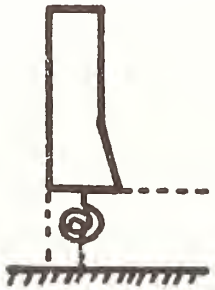			
Loading Direction	Hunch-compression, Hunch-tension	Hunch-compression, Hunch-tension	Hunch-compression	Hunch-tension	Hunch-compression	Hunch-tension
Consideration of Rotation		Rotation is considered by the deformation of the extended part of the column.	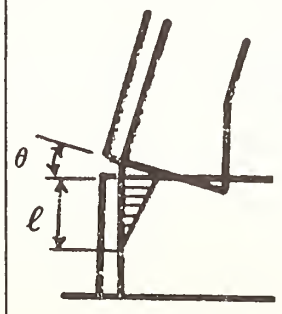 θ and 2θ	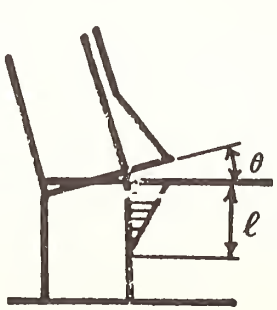 θ and 2θ	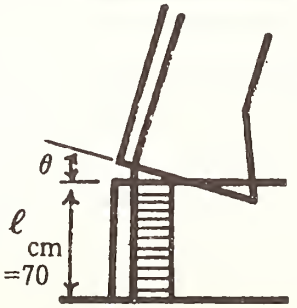	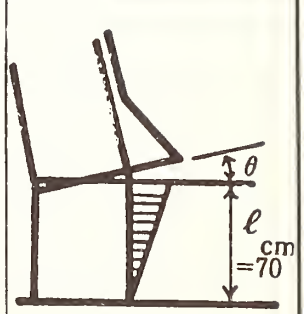 θ and 2θ
Remark	Column is fixed at the base.	Hunched column is extended to the footing.	Rotation is considered by the pulled-out of reinforcements. $\ell = \frac{A_s \cdot \sigma_s}{U \cdot \tau_{bs}}$		Rotation is considered by the extension of reinforcements below the base of the column to the footing.	Rotation is considered by the pulled-out of reinforcements.

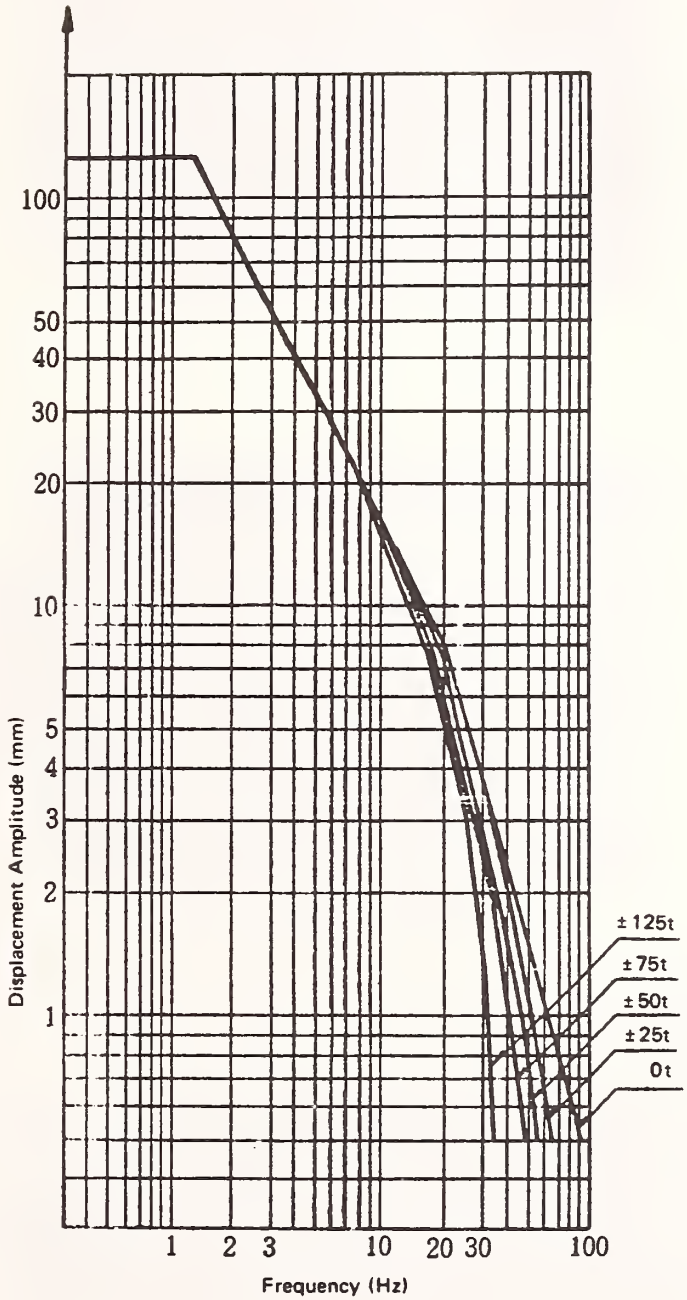

Fig. 1 Performance Curve of the Actuator

Fig. 2 Earthquake Engineering Laboratory

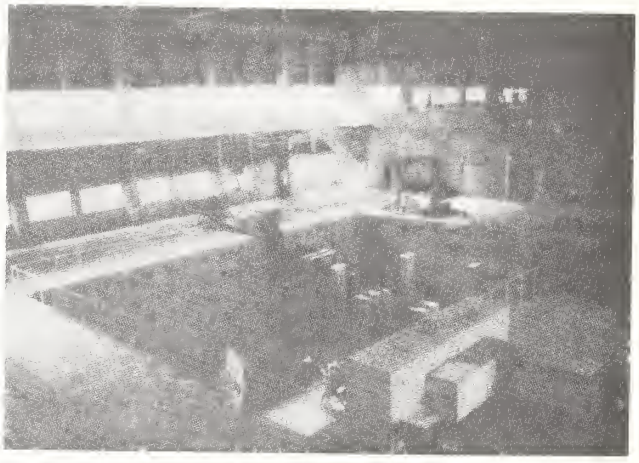

Fig. 3 Inside of the Earthquake Engineering Laboratory (Test Pit)

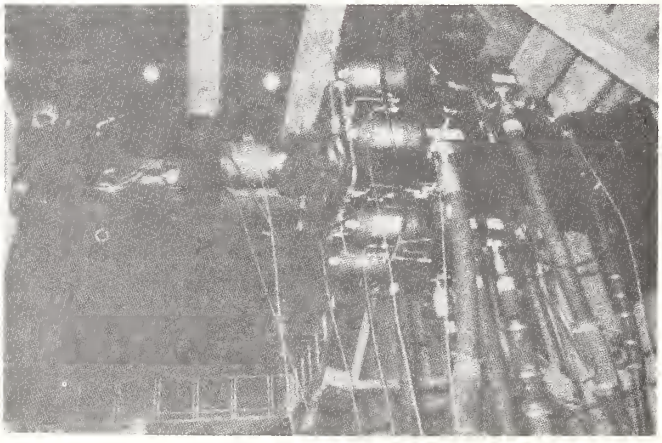

Fig. 4 Actuator

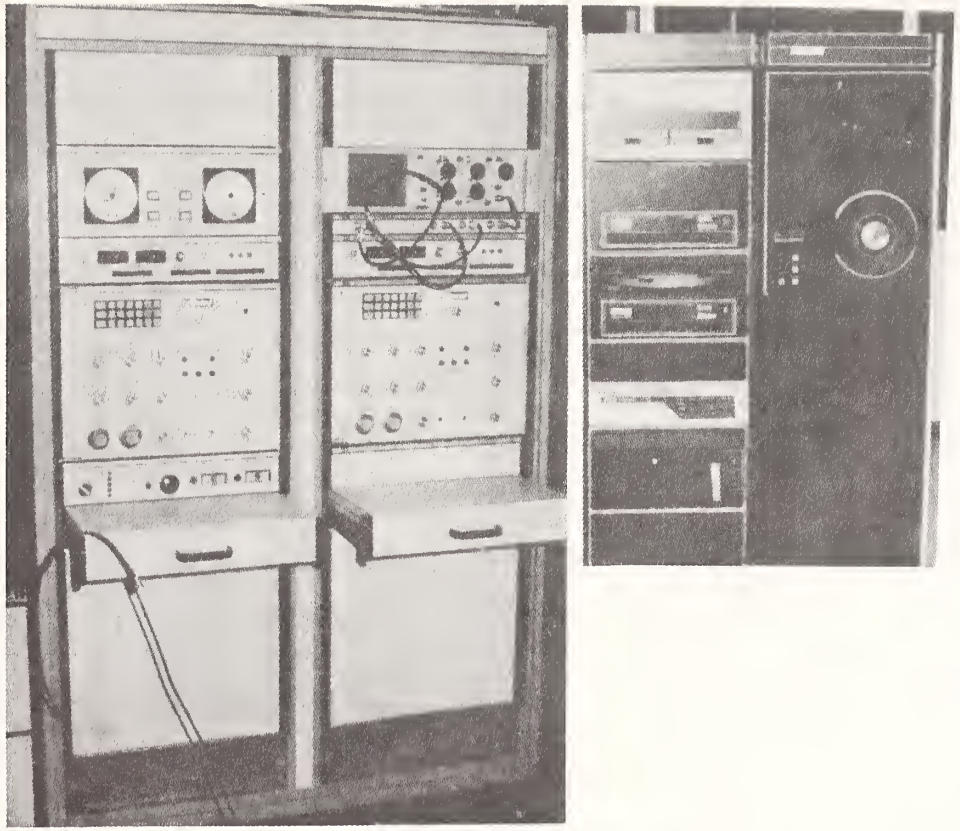

Fig. 5 Controller

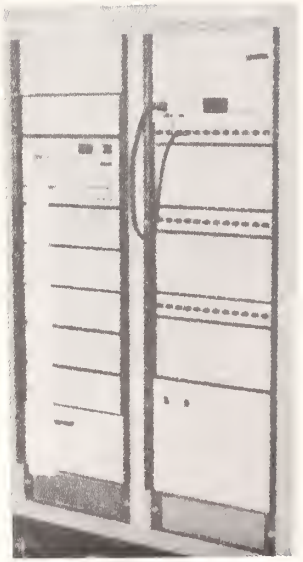

Fig. 6 Data Acquisition Device

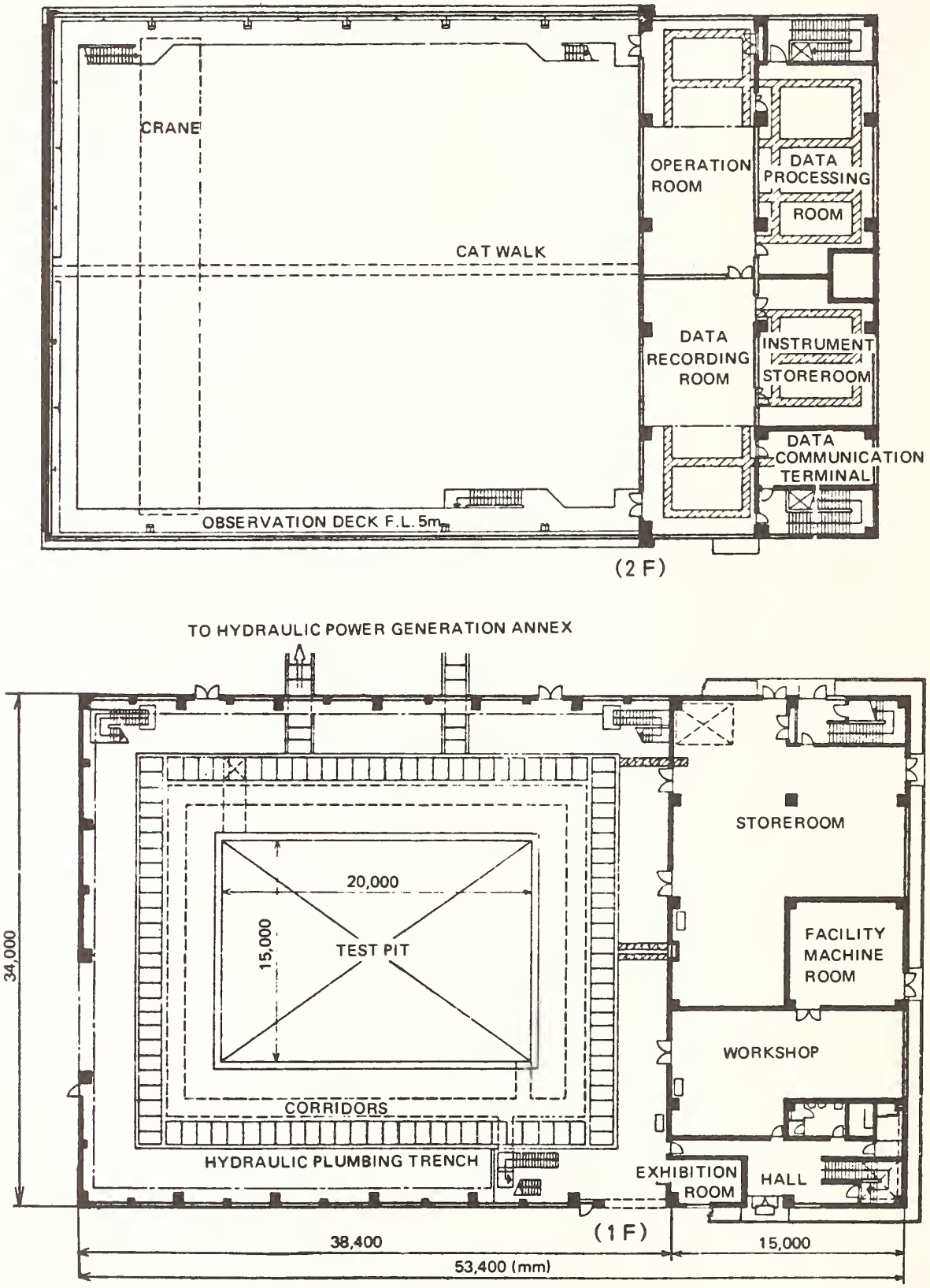

Fig. 7 Outlines of the Earthquake Engineering Laboratory

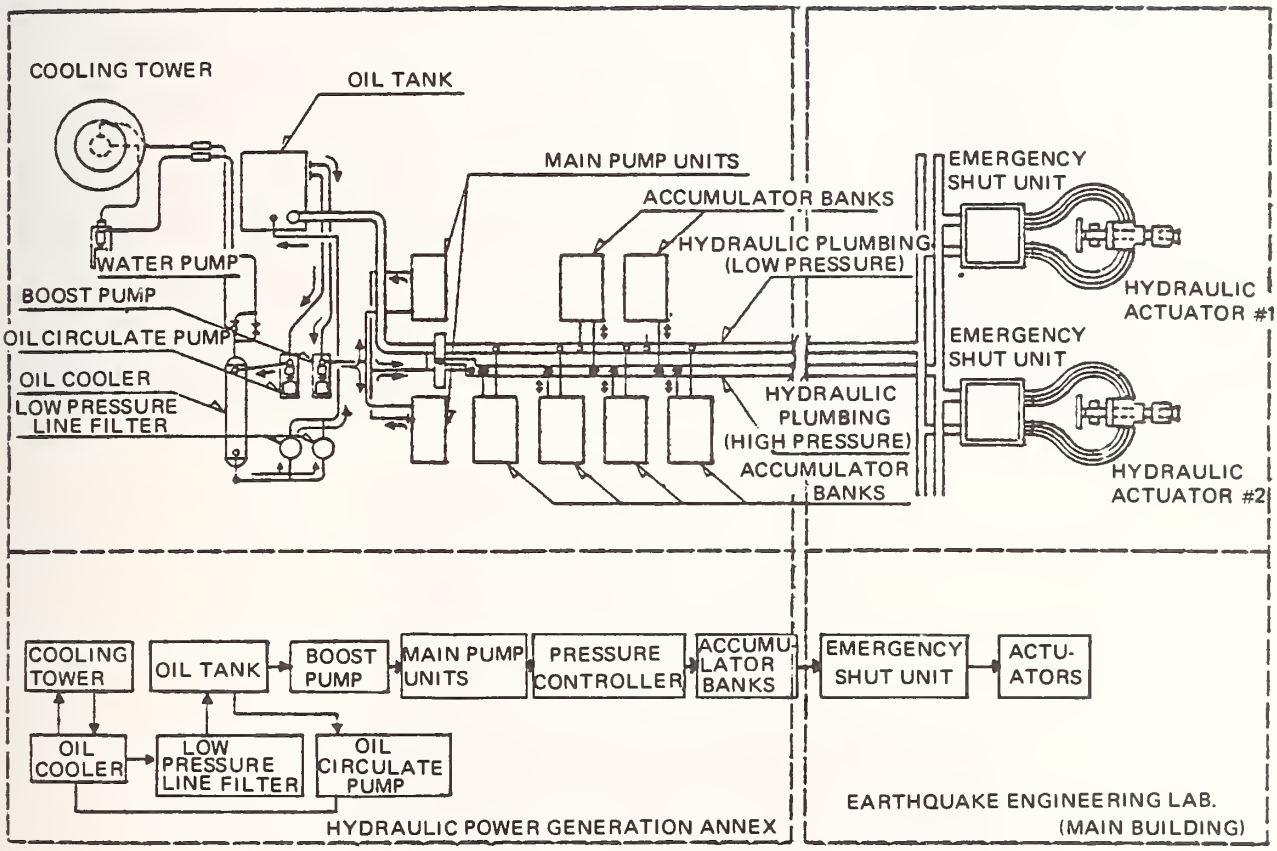

Fig. 8 Hydraulic Power Supply System

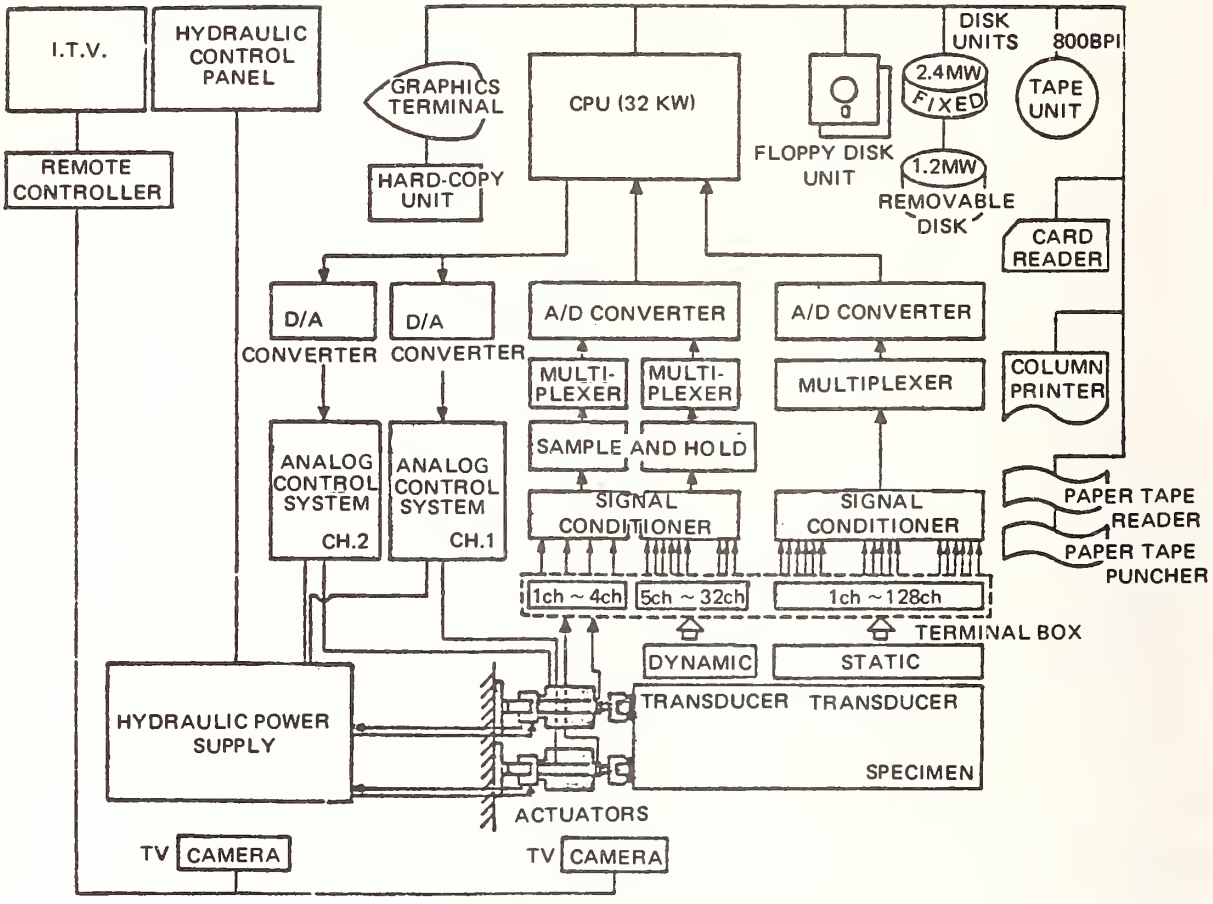

Fig. 9 Control System Diagram

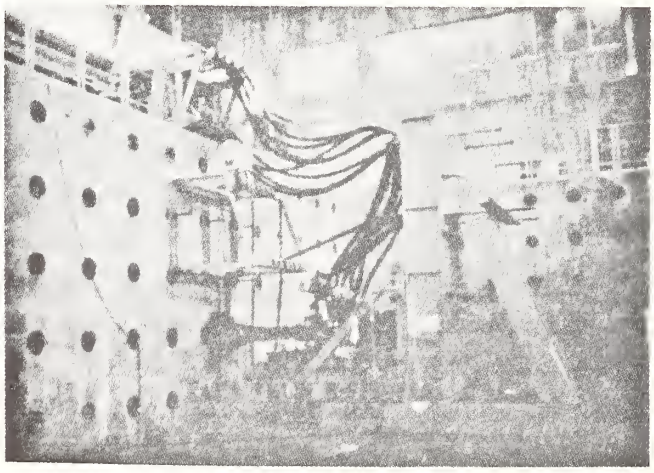

Fig. 10 Movable Wall

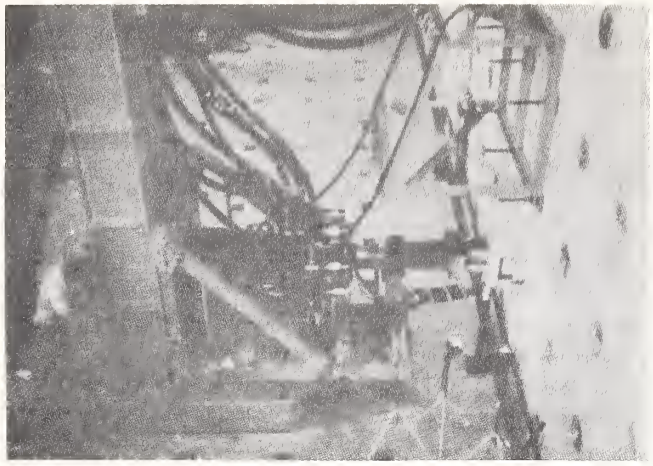

Installed Actuator

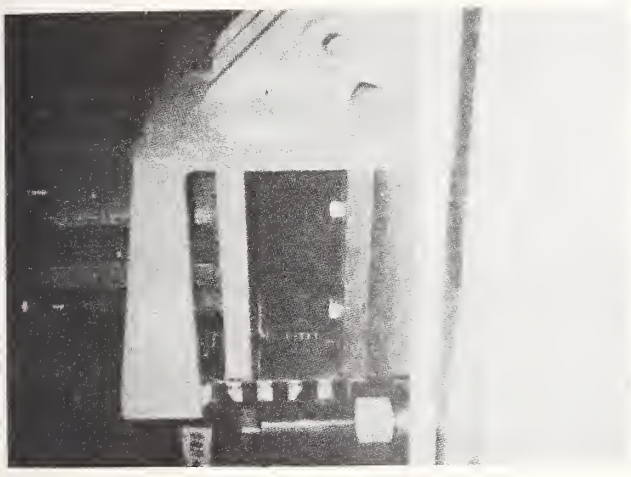

State of 0 ton Loading

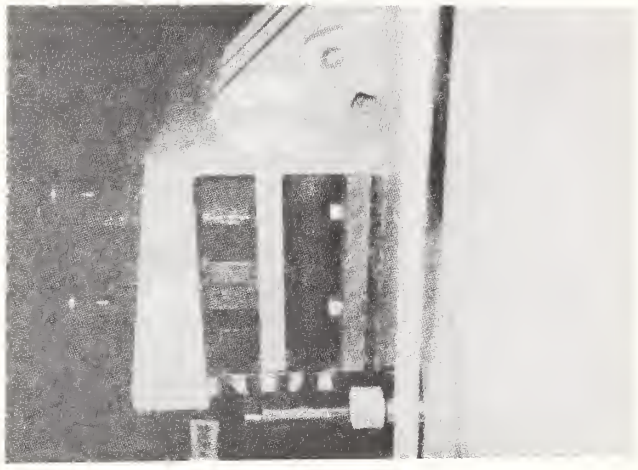

State of 50 ton Loading

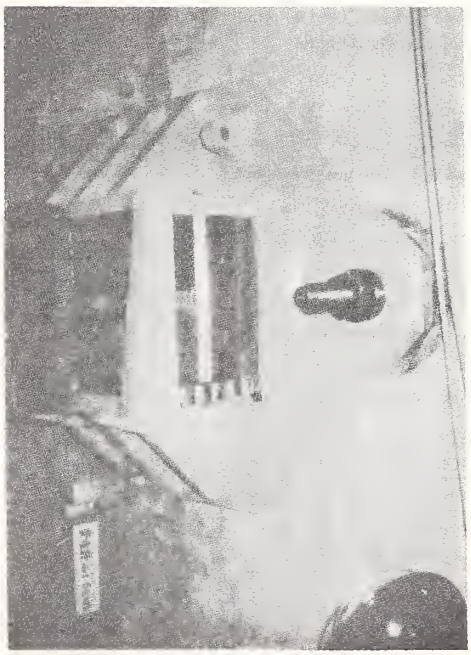

State of 70 ton Loading

Fig. 11 Loading State

[Unit: mm]

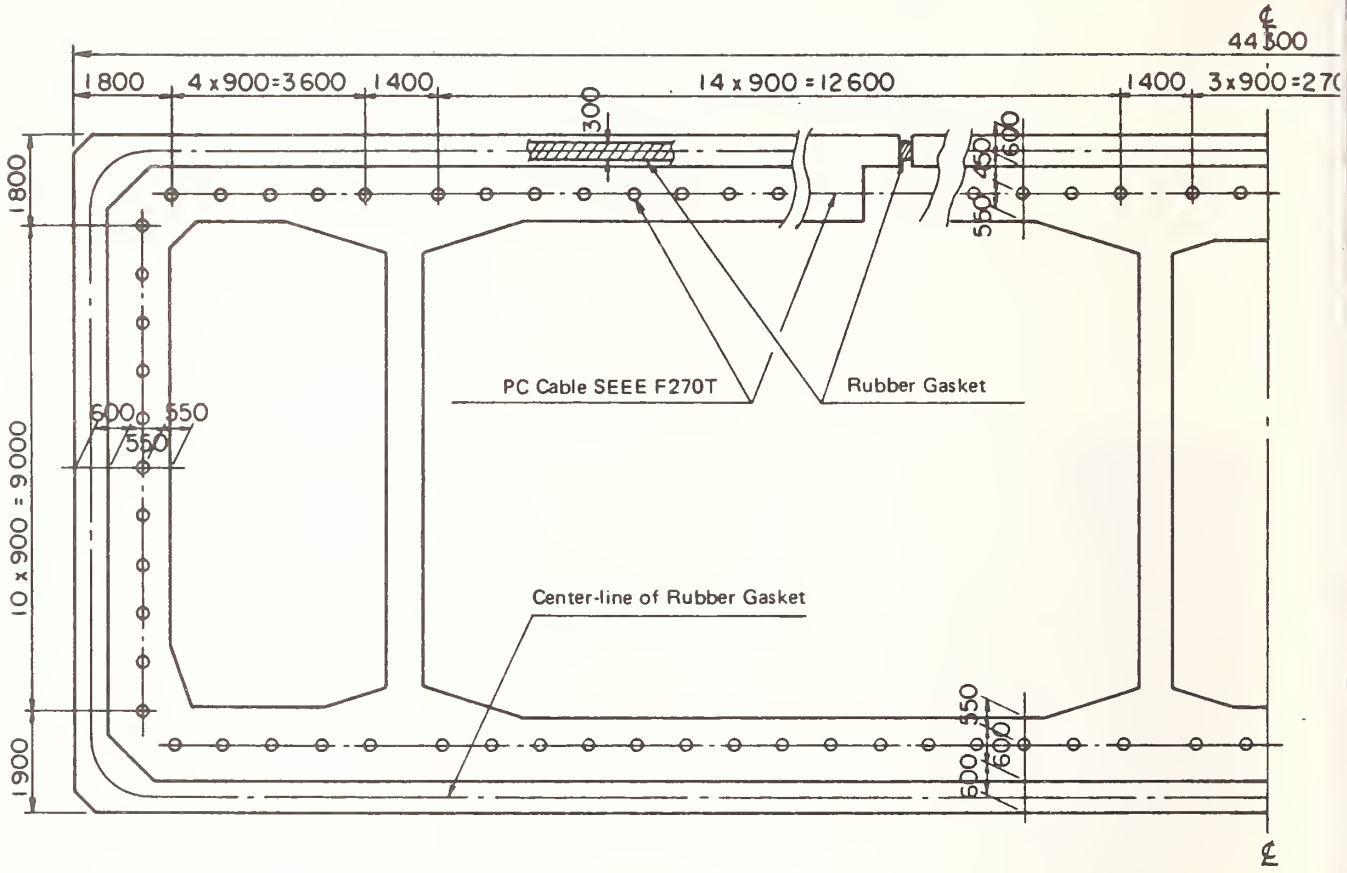

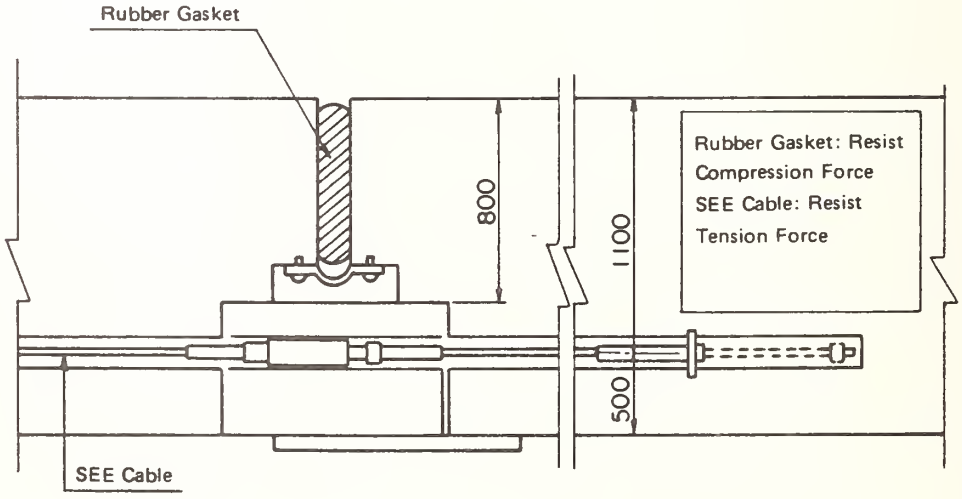

Fig. 12 Example of Standard Cross Section and Joint Structure of A Submerged Tunnel

[Unit: mm]

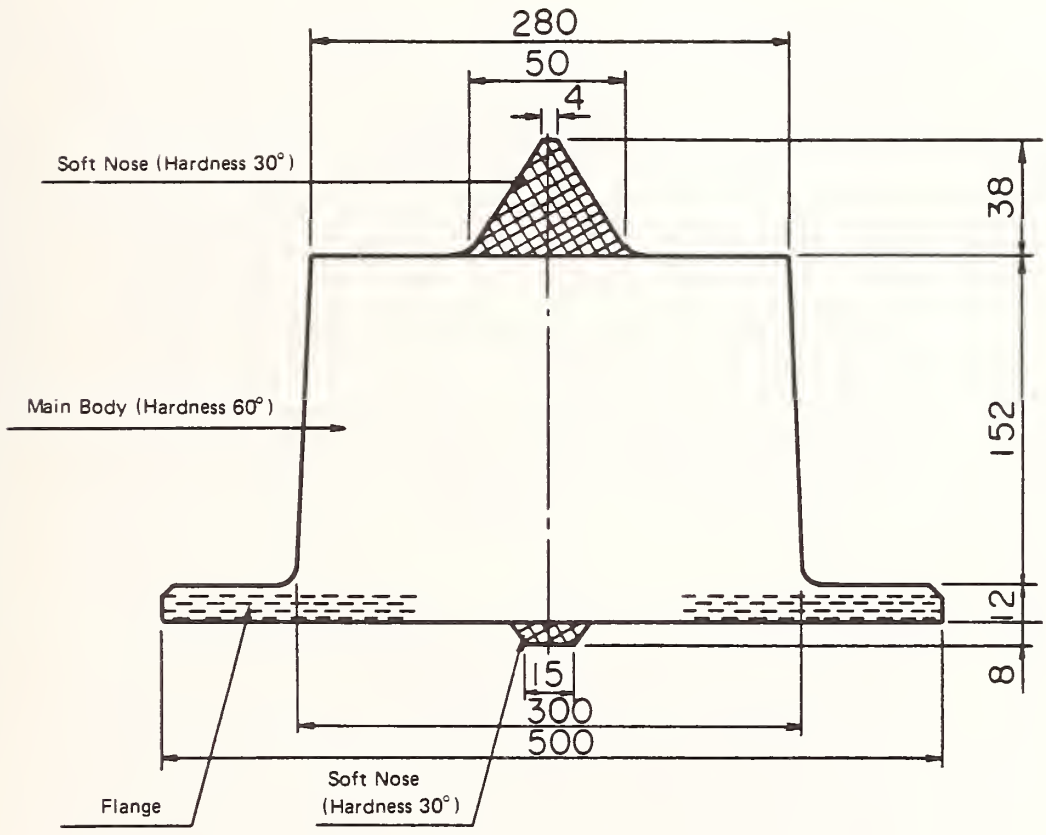

Fig. 13 Basic Shape of the Rubber Gasket

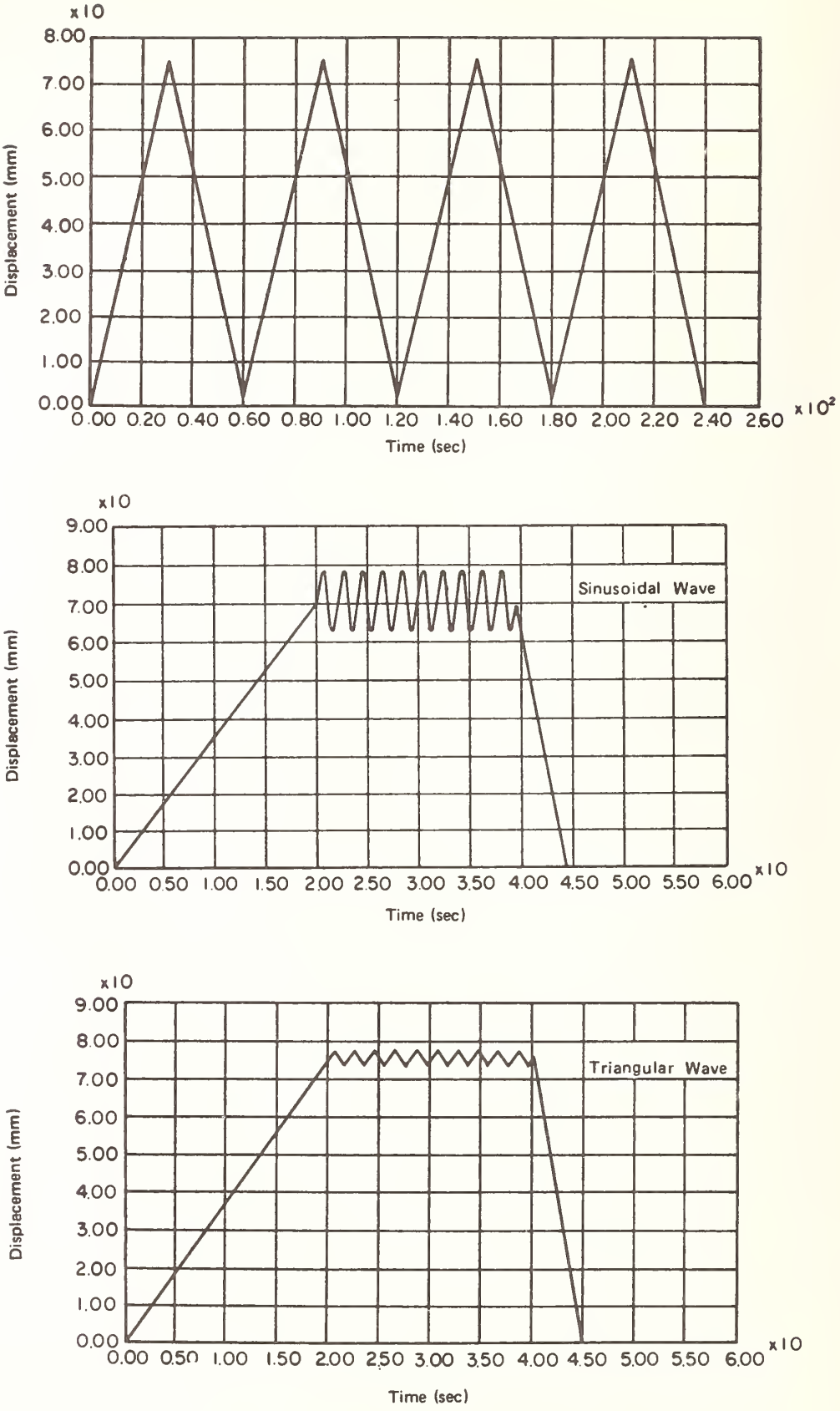

Fig. 14 Examples of Input Motions of Static and Dynamic Loading

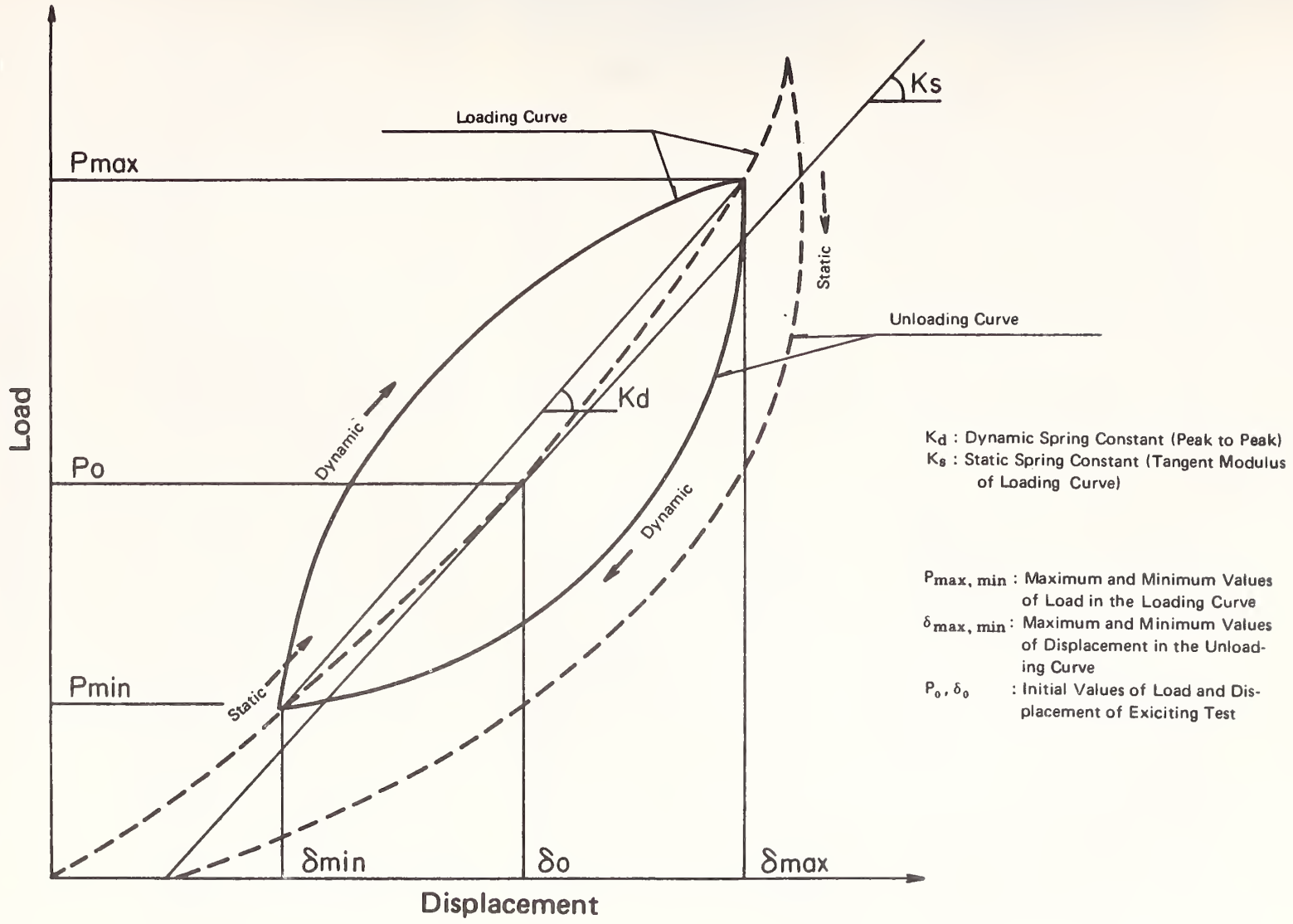

Fig. 15 Dynamic Spring Constant and Static Spring Constant

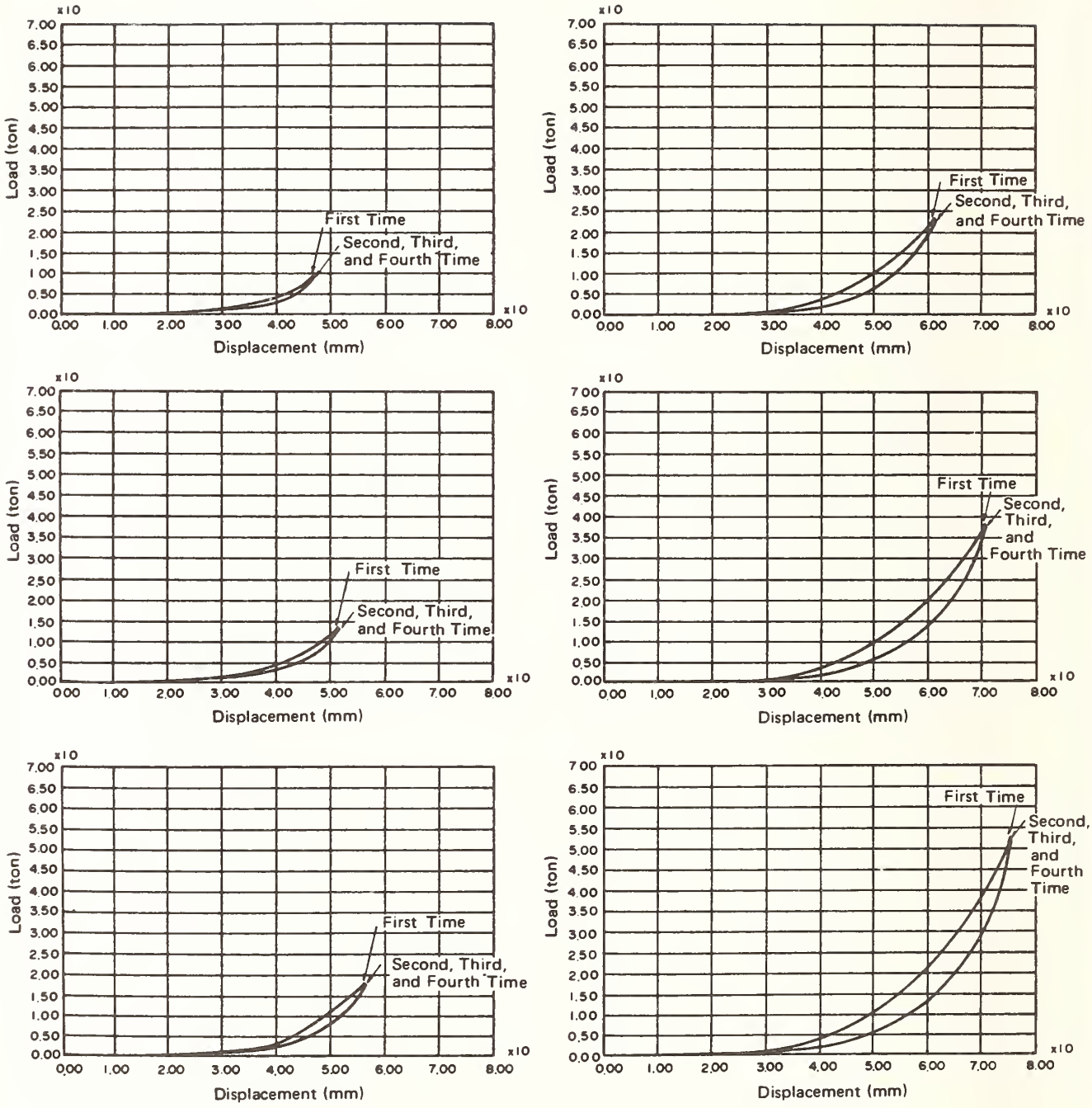

Fig. 16 Static Loading and Unloading Curve

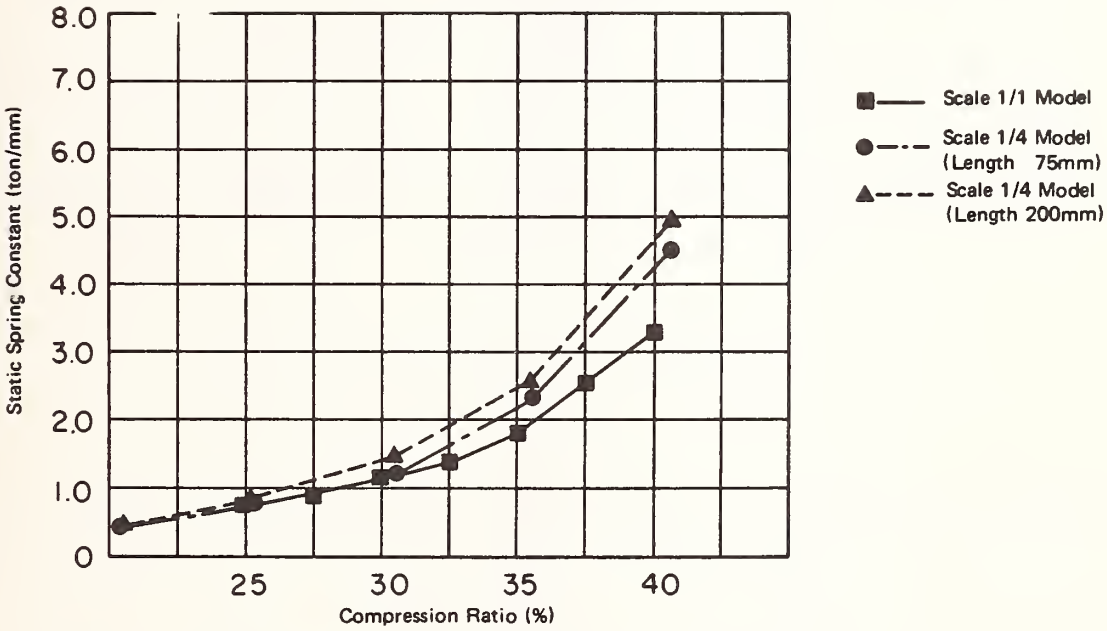

Fig. 17 Static Spring Constant

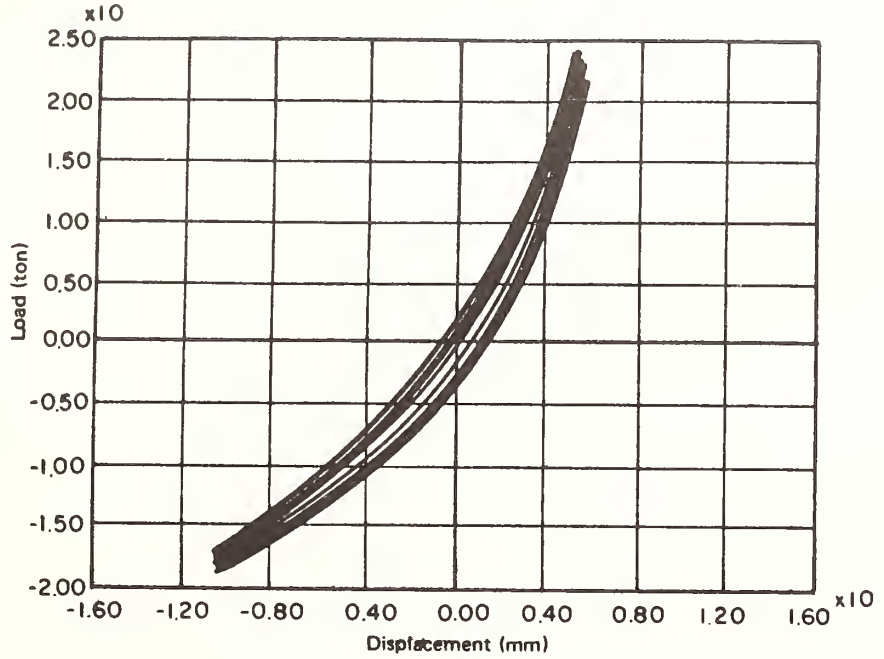

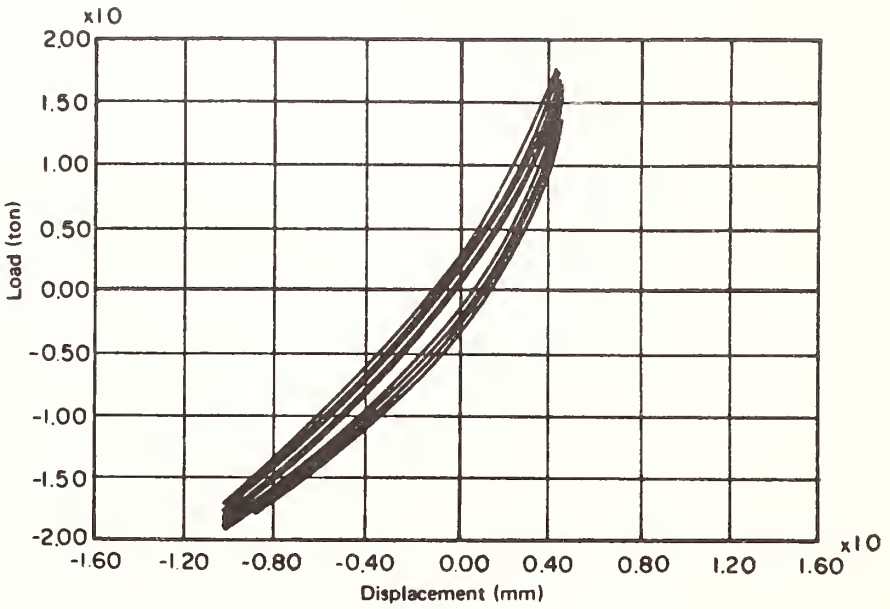

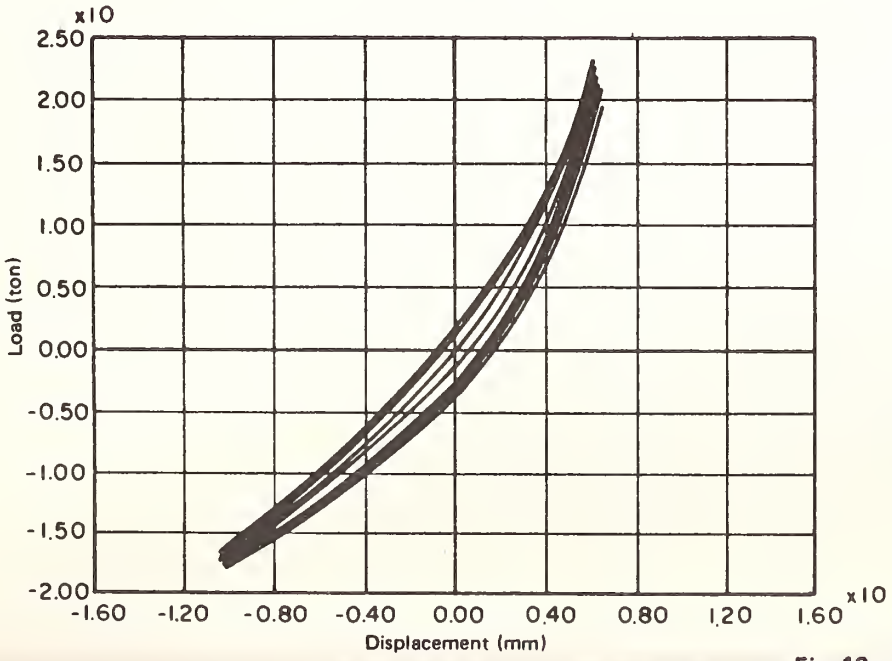

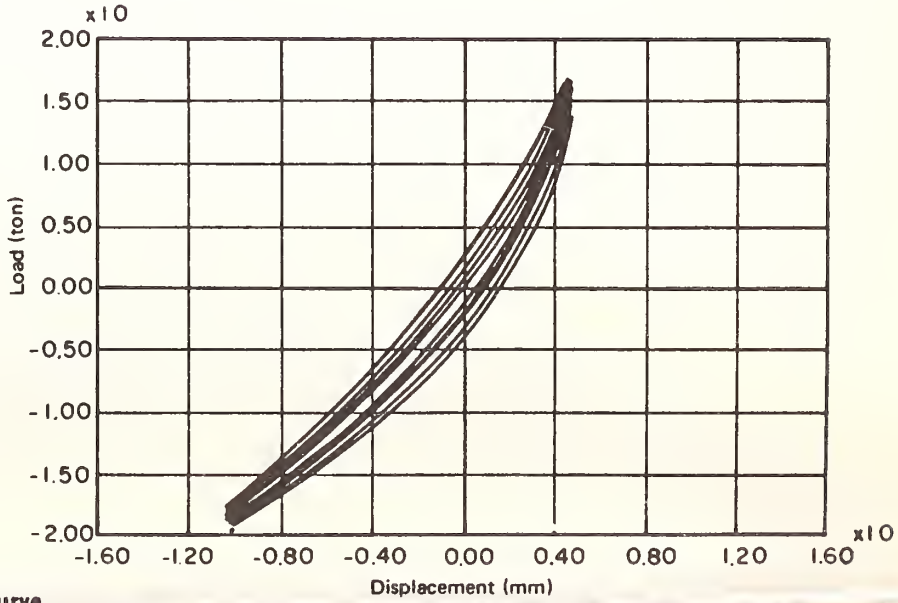

Fig. 18 Hysteretic Curve

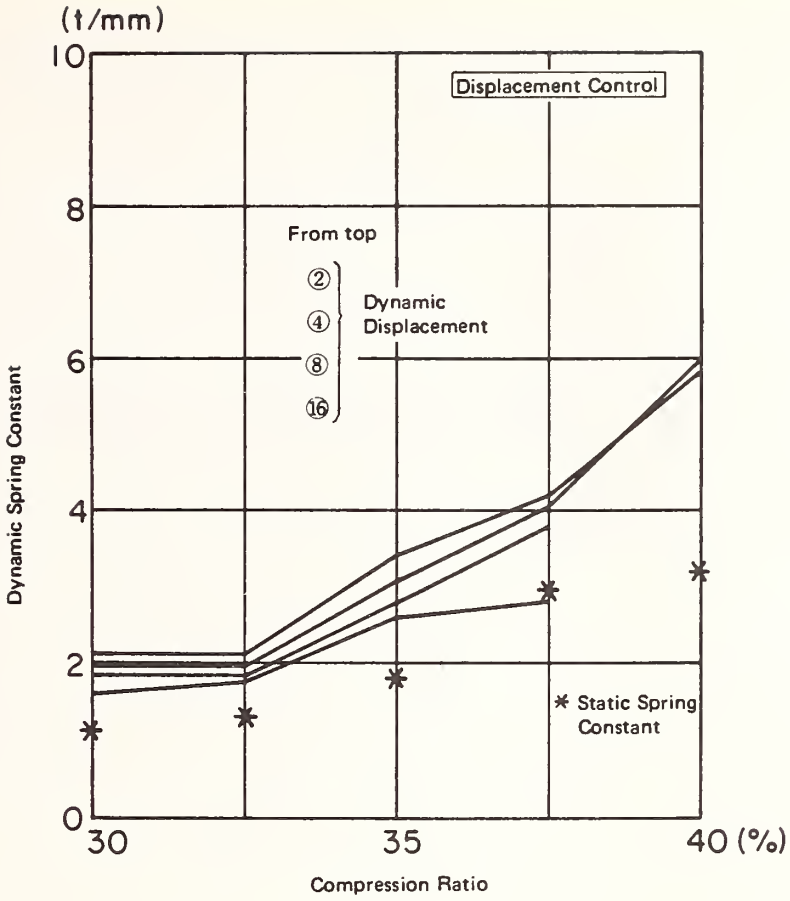

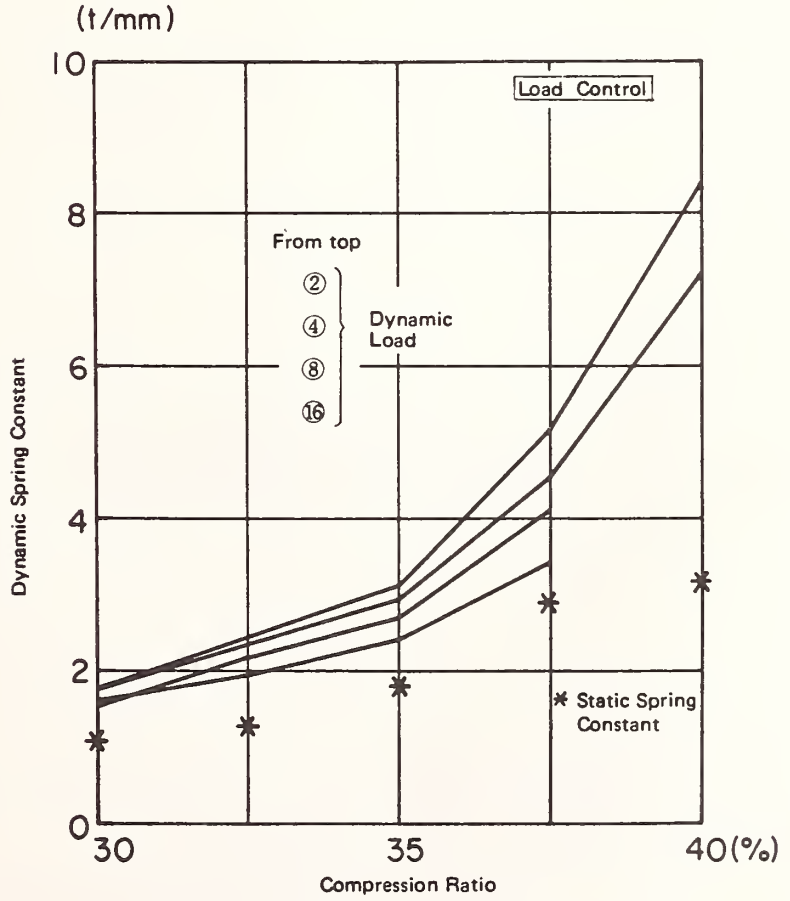

Note: Figures in O show dynamic displacement amplitude (mm)

Fig. 19 Variation of Dynamic Spring Constant due to Compression Ratio

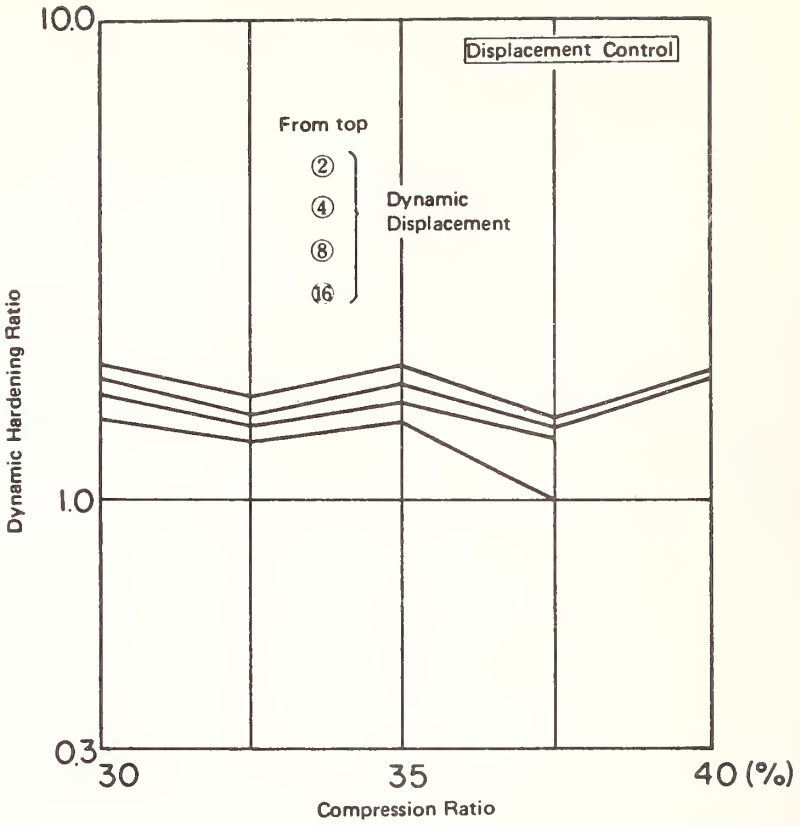

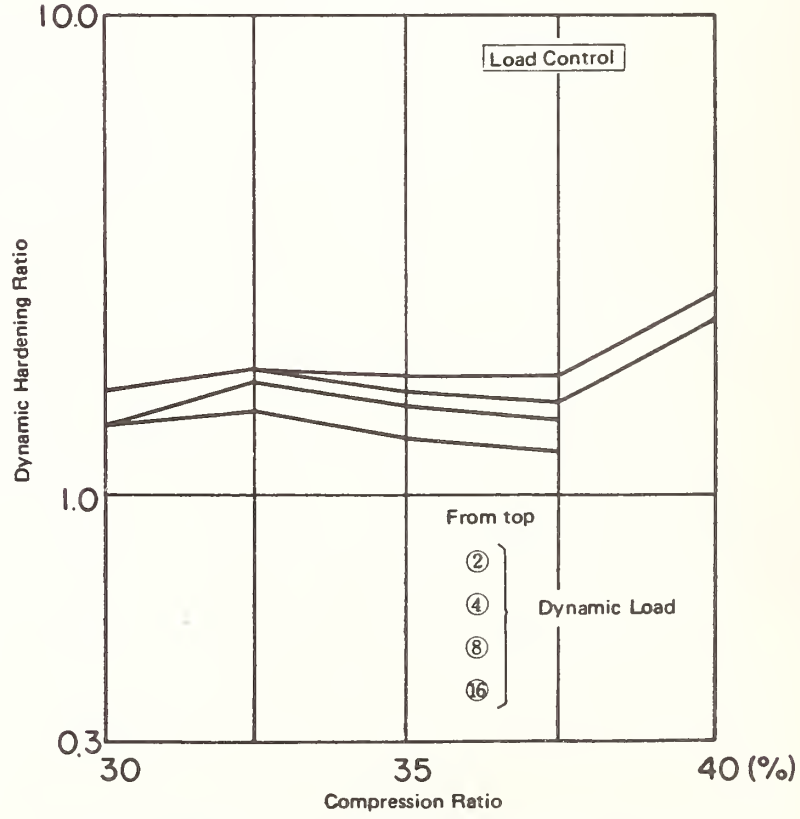

Note: Figures in O show dynamic displacement amplitude (mm)

Fig. 20 Dynamic Hardening Ratio

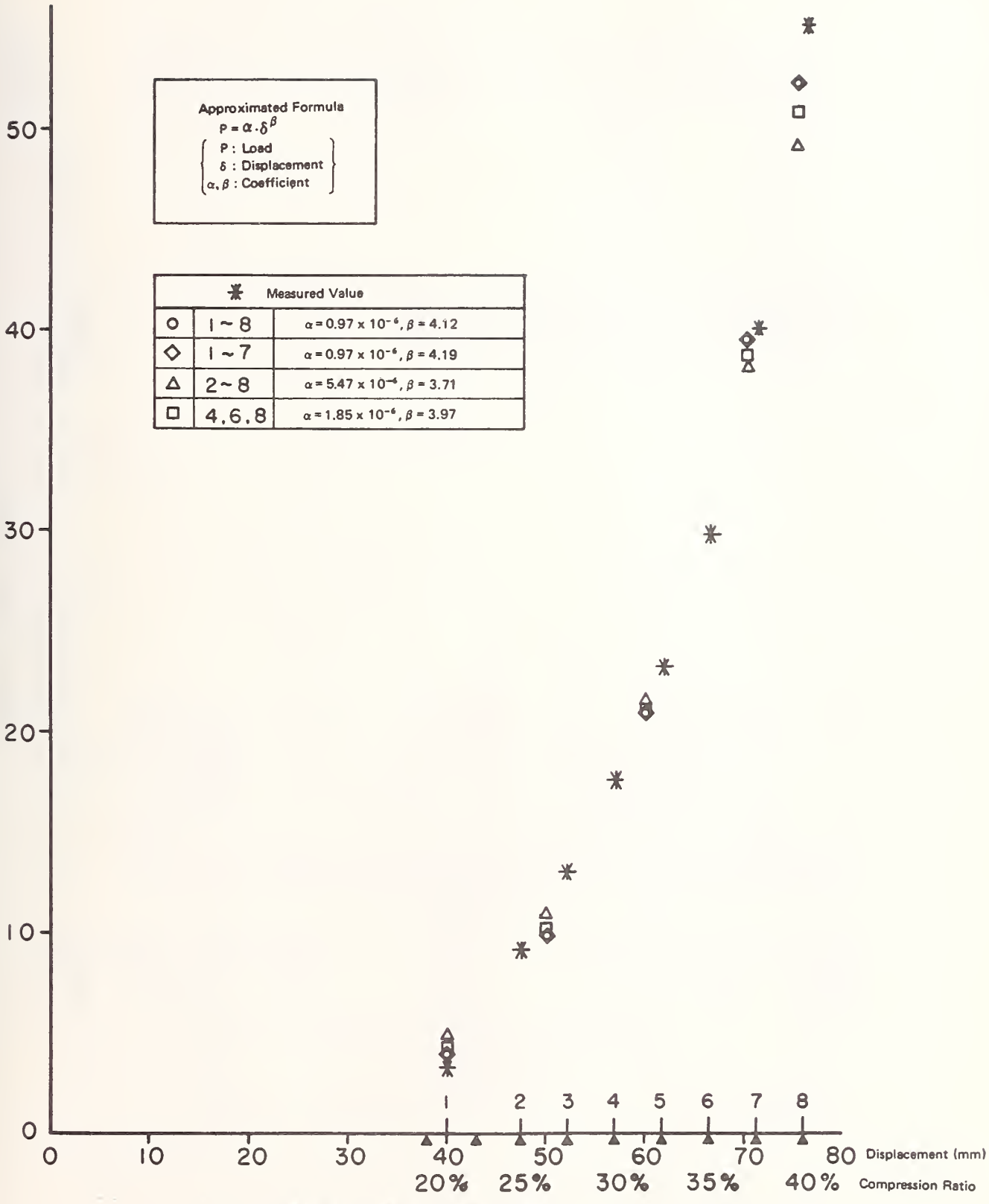

Fig. 21 α, β Obtained by Method of Least Square

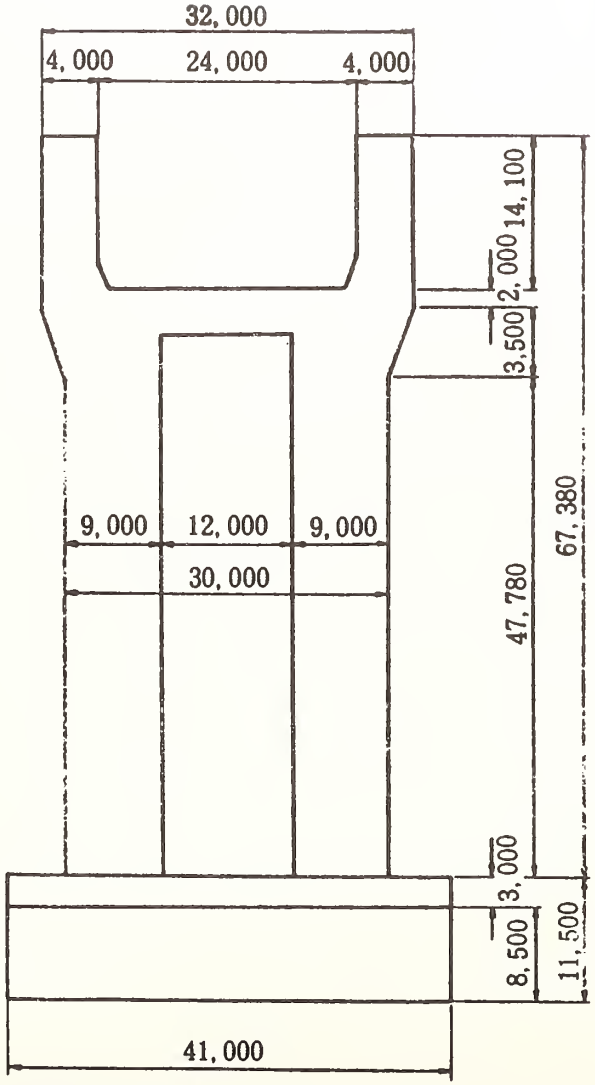

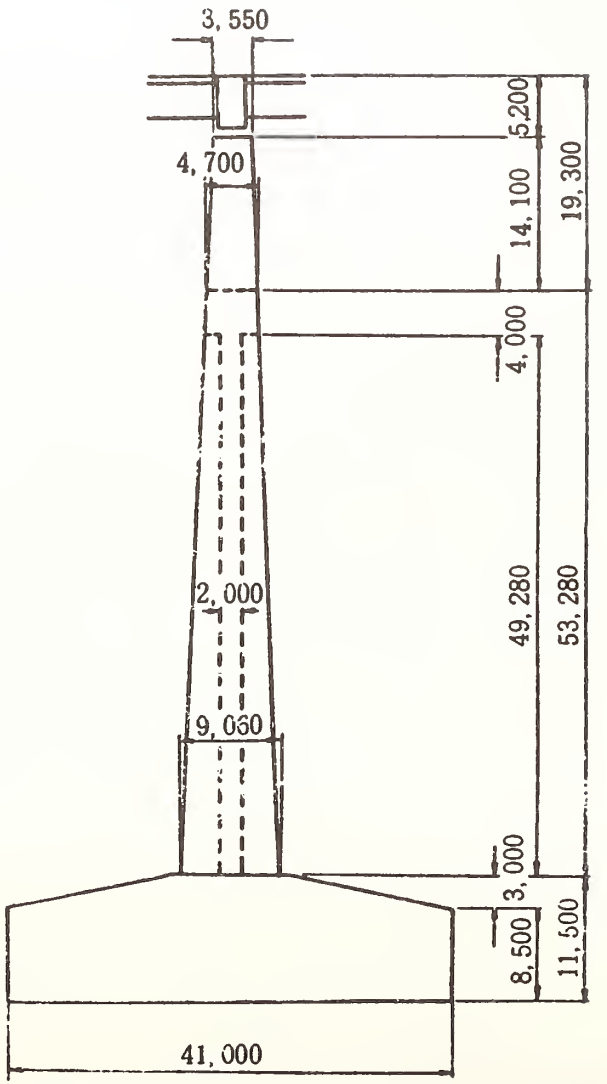

Unit: mm

Fig. 22 Pier of Ban-no-su Bridge

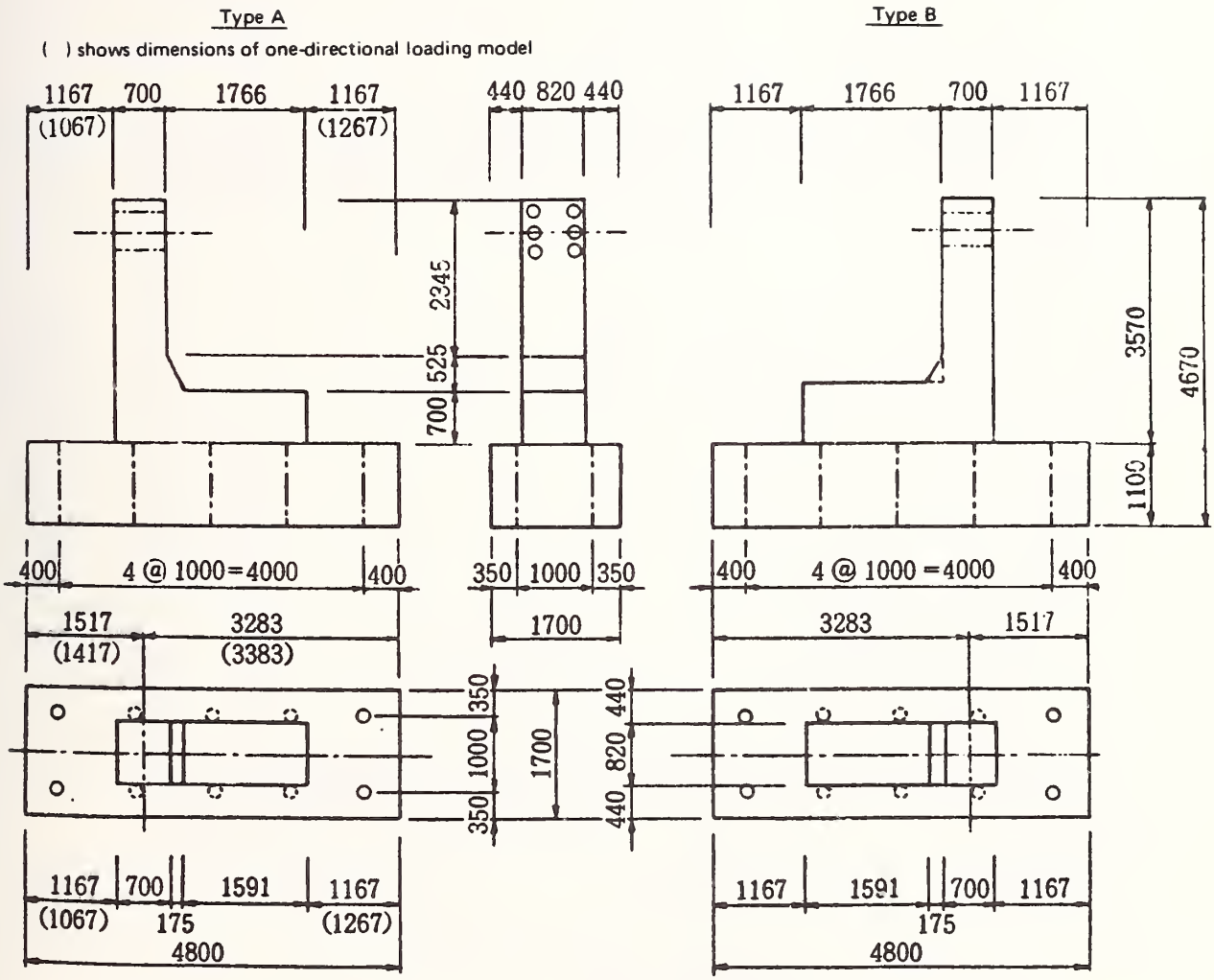

Fig. 23 Dimensions of $1/(4\sqrt{2})$ Model

Unit: mm

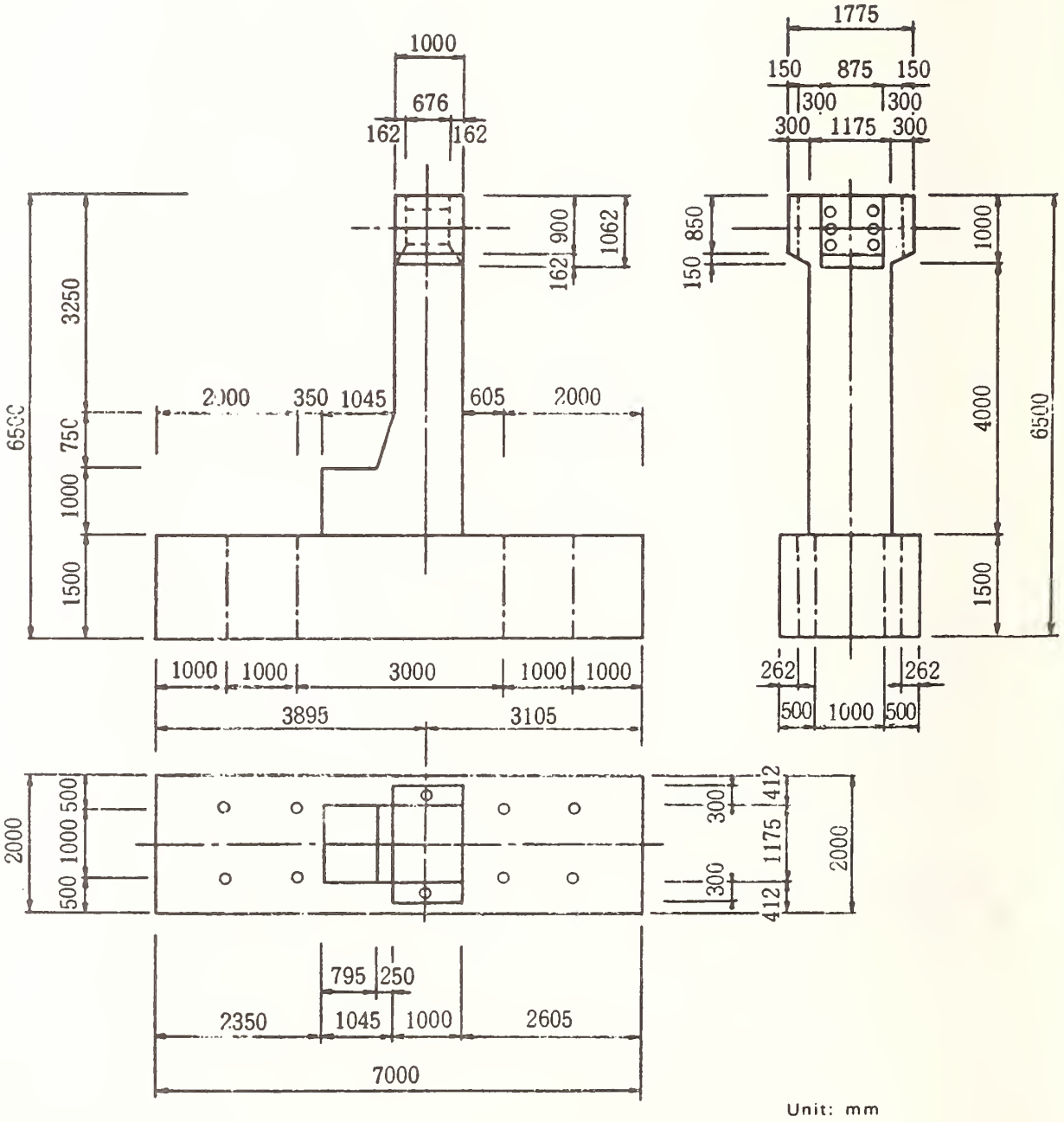

Fig. 24 Dimensions of 1/4 Model

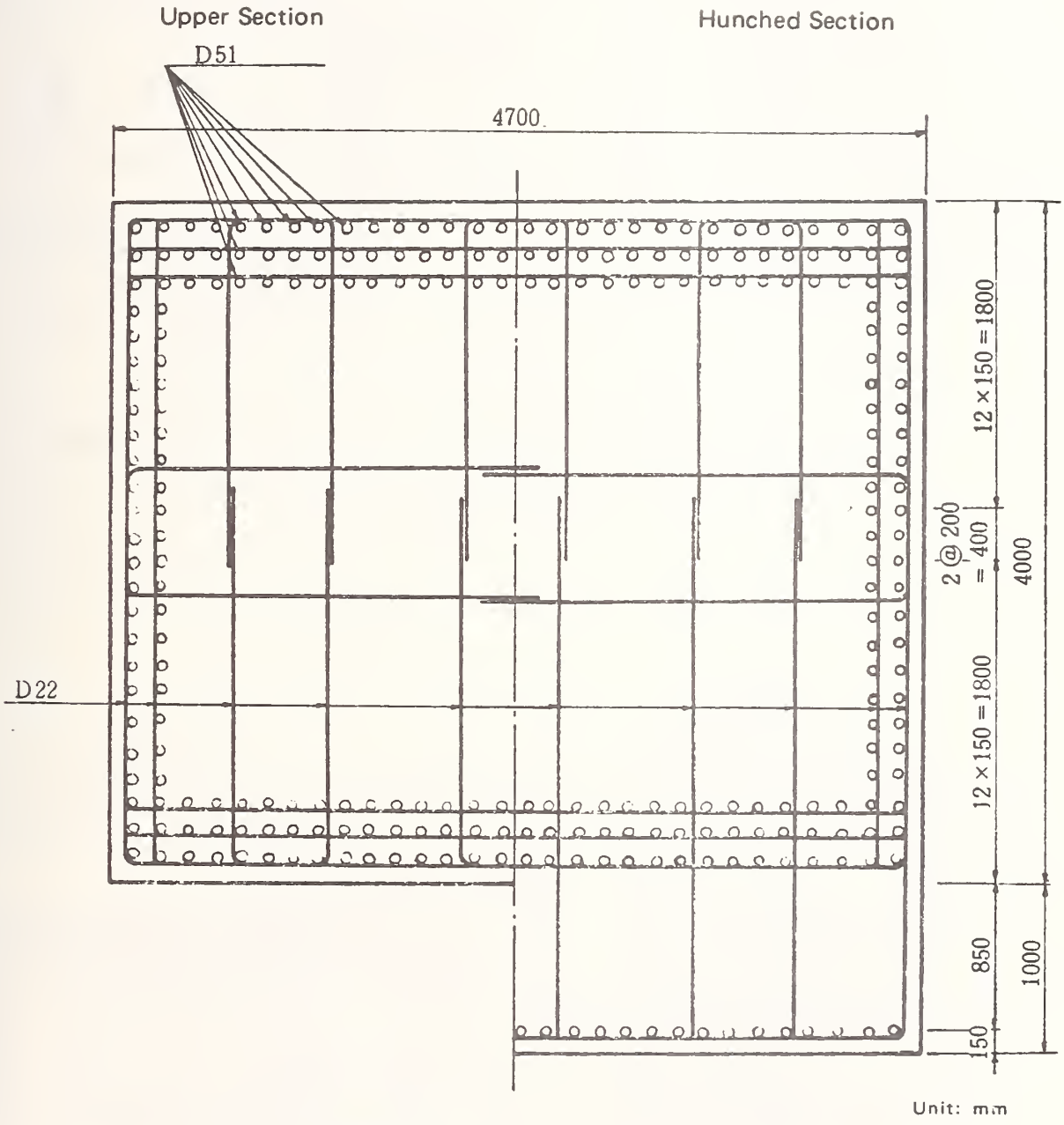

Fig. 25 Section of the Upper Column of Ban-no-su Bridge Pier

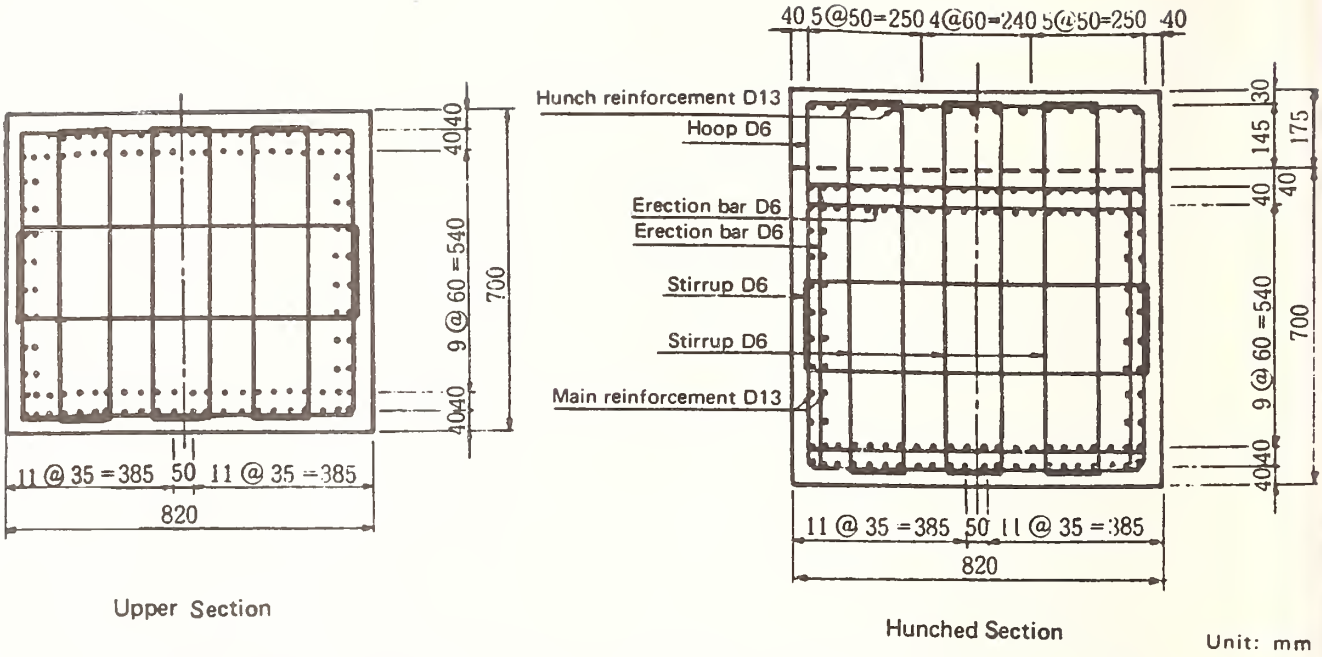

Fig. 26 Section of the Columns of No. 1 (One-directional Loading) and No. 3 (Basic) Models

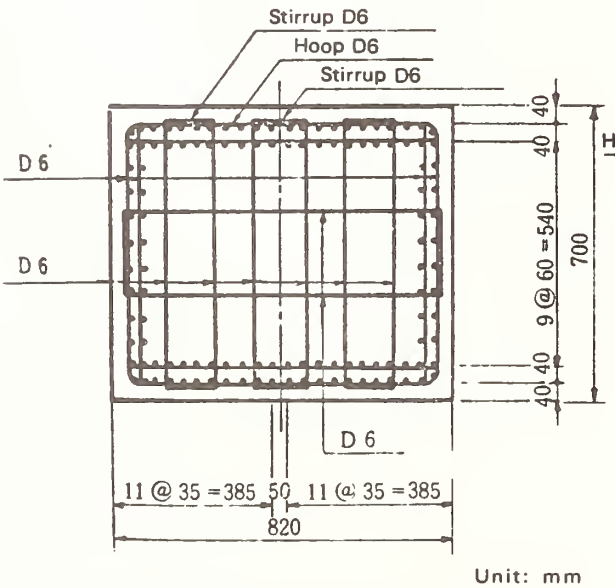

Fig. 27 Section of the Column of No. 2 (Without Hunch) Model

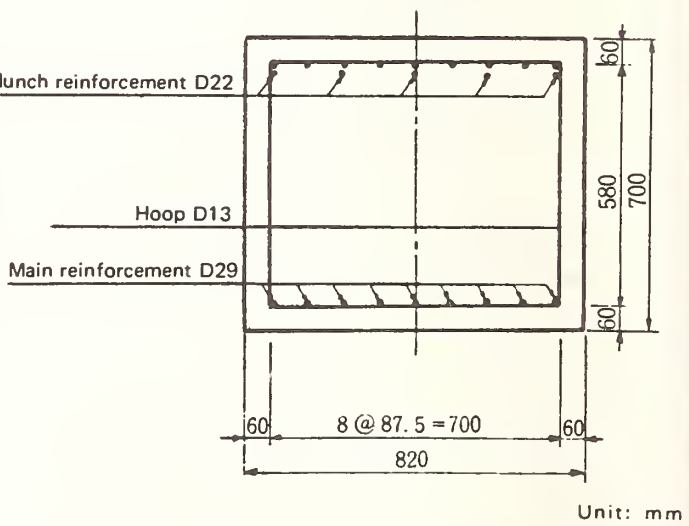

Fig. 28 Section of the Column of No. 4 (Large-diameter Reinforcement and Without Side Reinforcement) Model

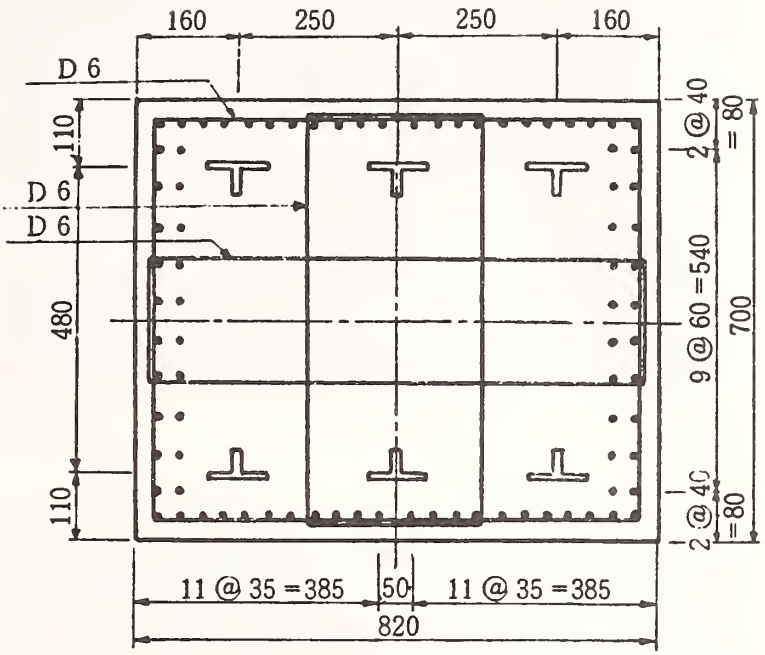

Fig. 29 Section of the Columns of No. 5 (SRC-Without Stud) and No. 6 (SRC-With Stud) Models

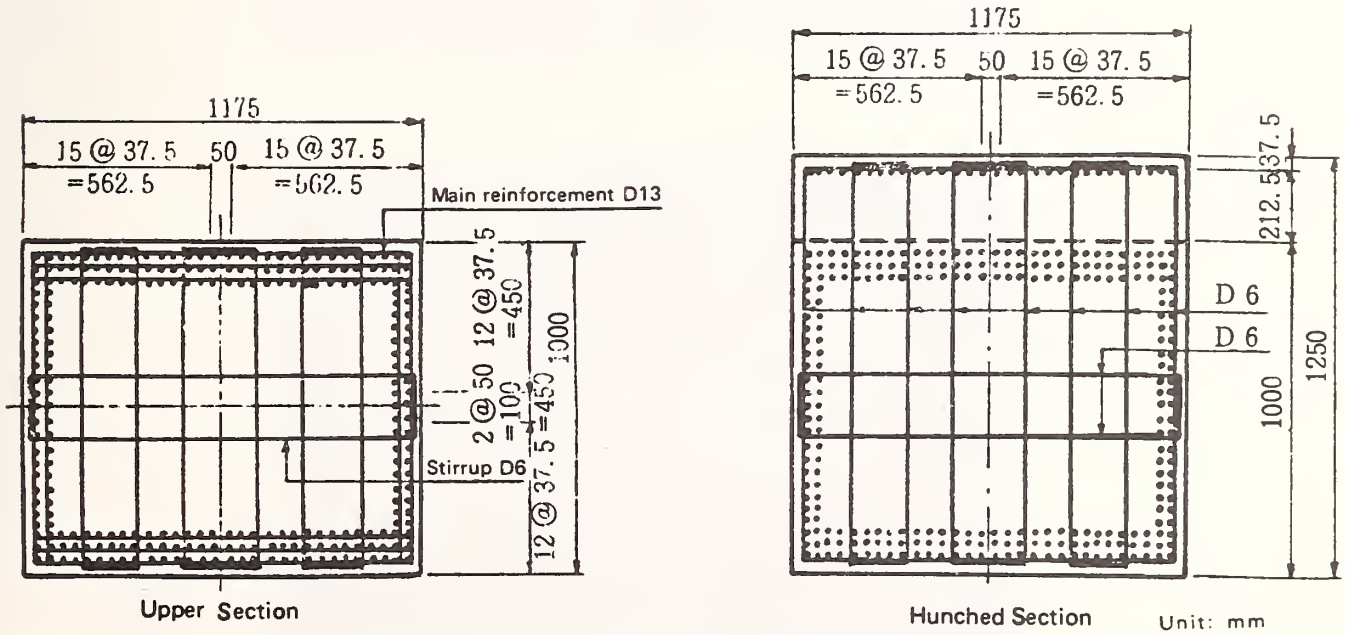

Fig. 30 Section of the Column of No. 7 (1/4) Model

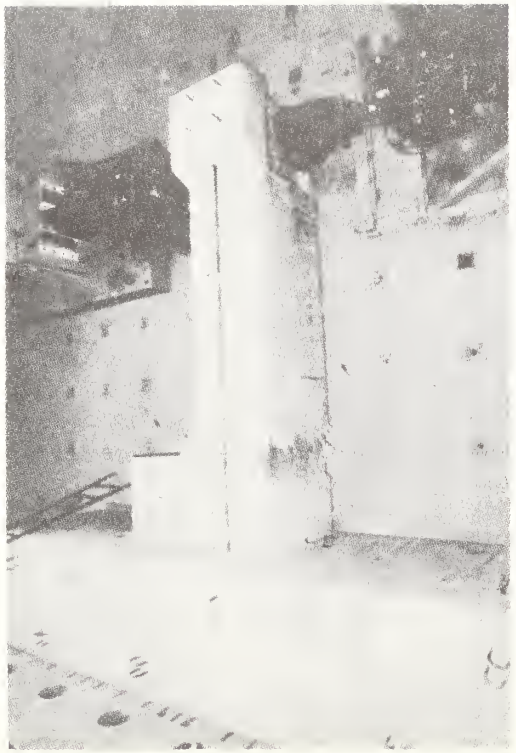

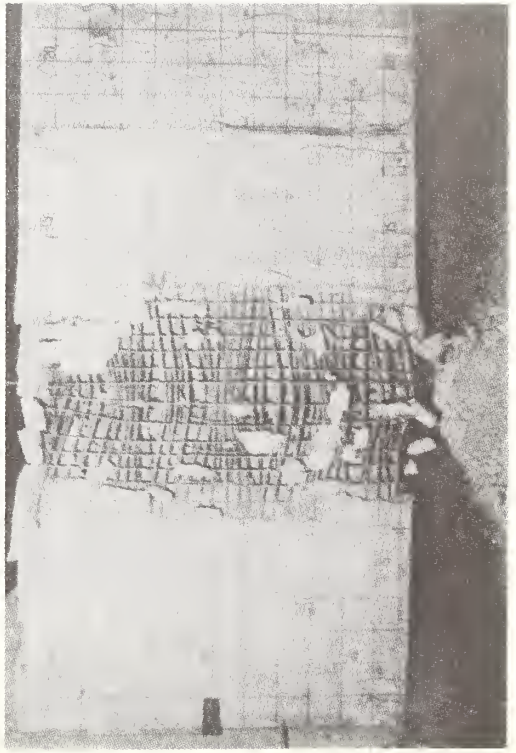

Fig. 31 Photos of the Experiment

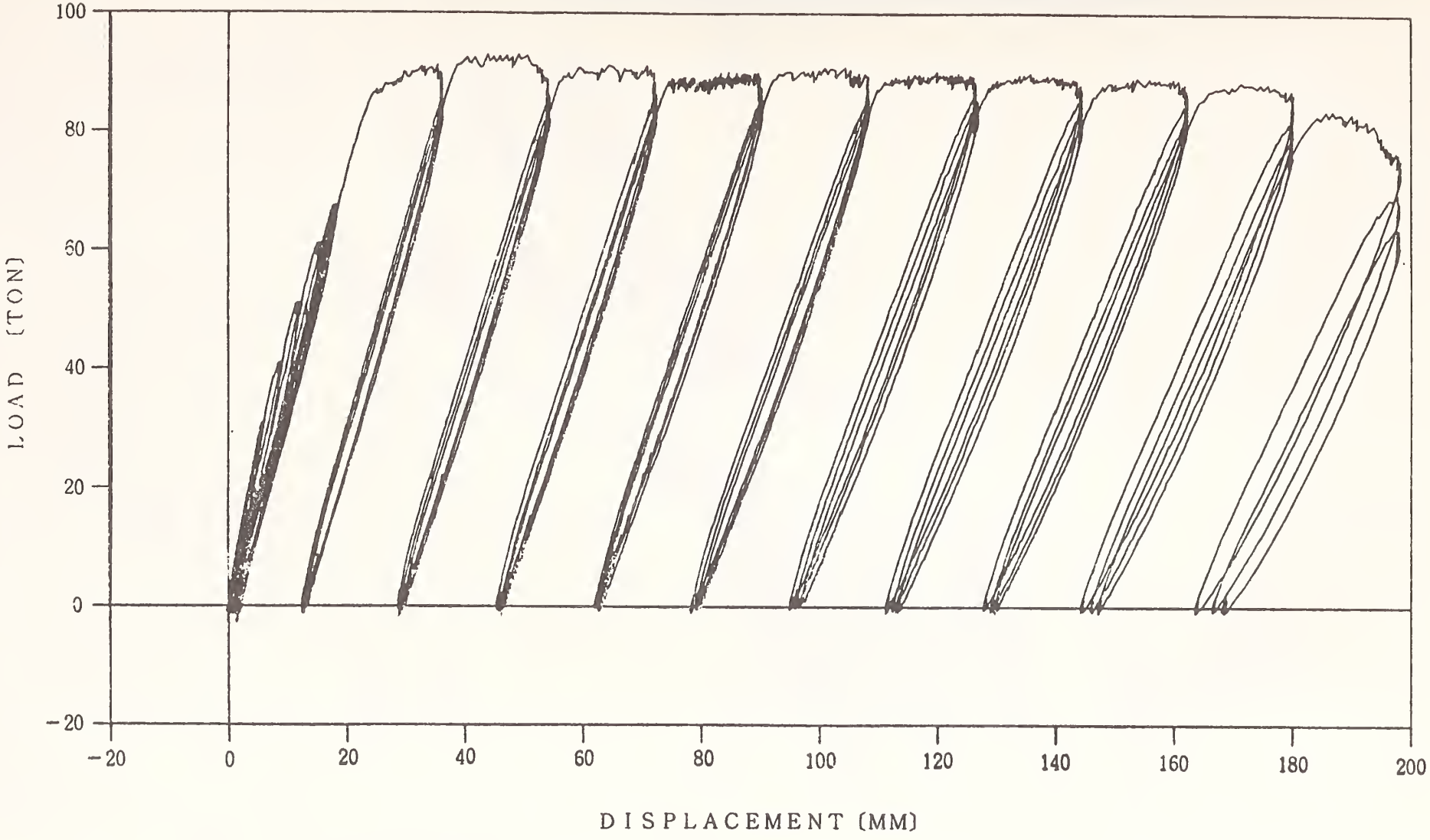

Fig. 32 Load-displacement Curve of No. 1 (One-directional Loading) Model

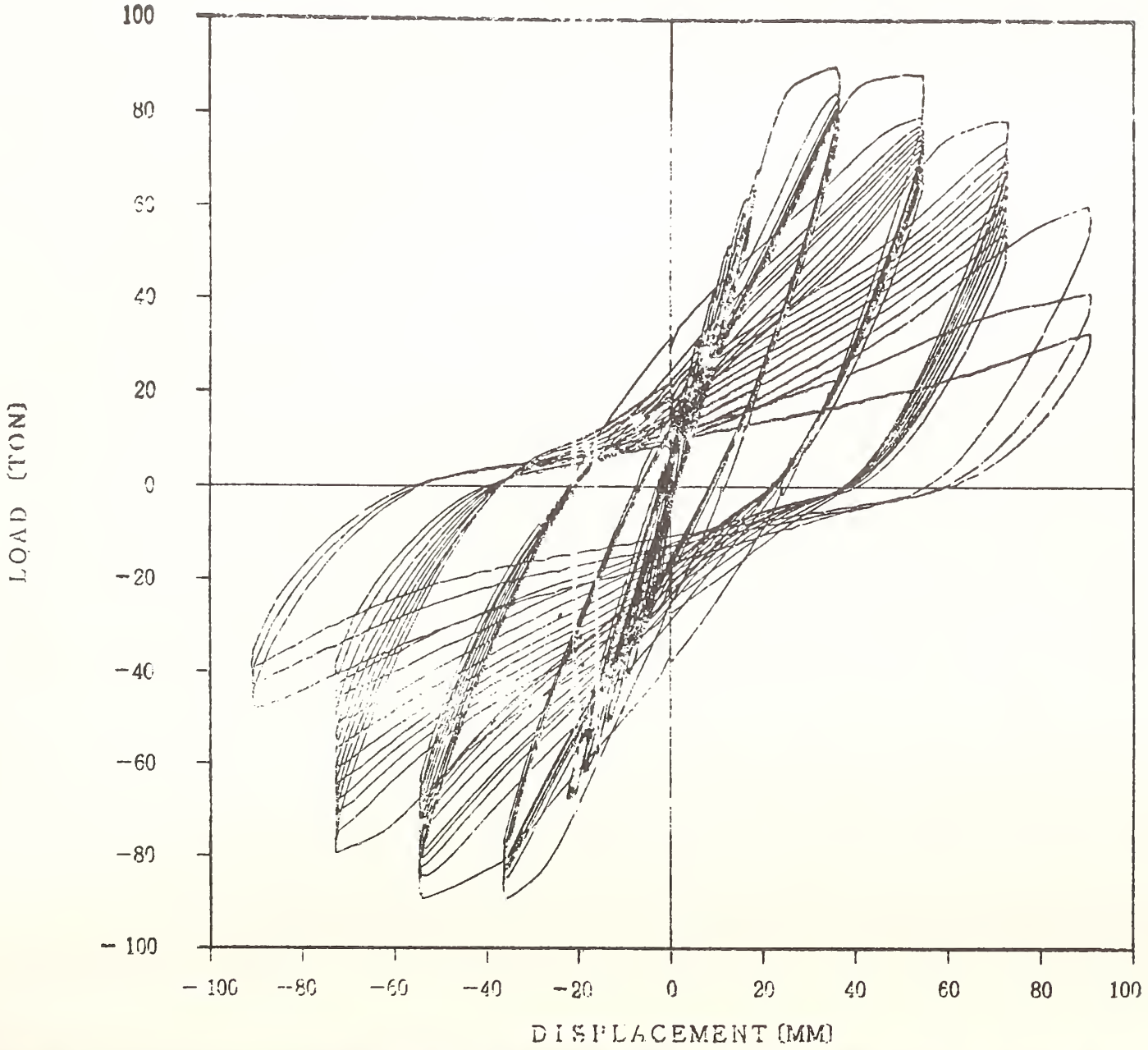

Fig. 33 Load-displacement Curve of No. 3 (Basic) Model

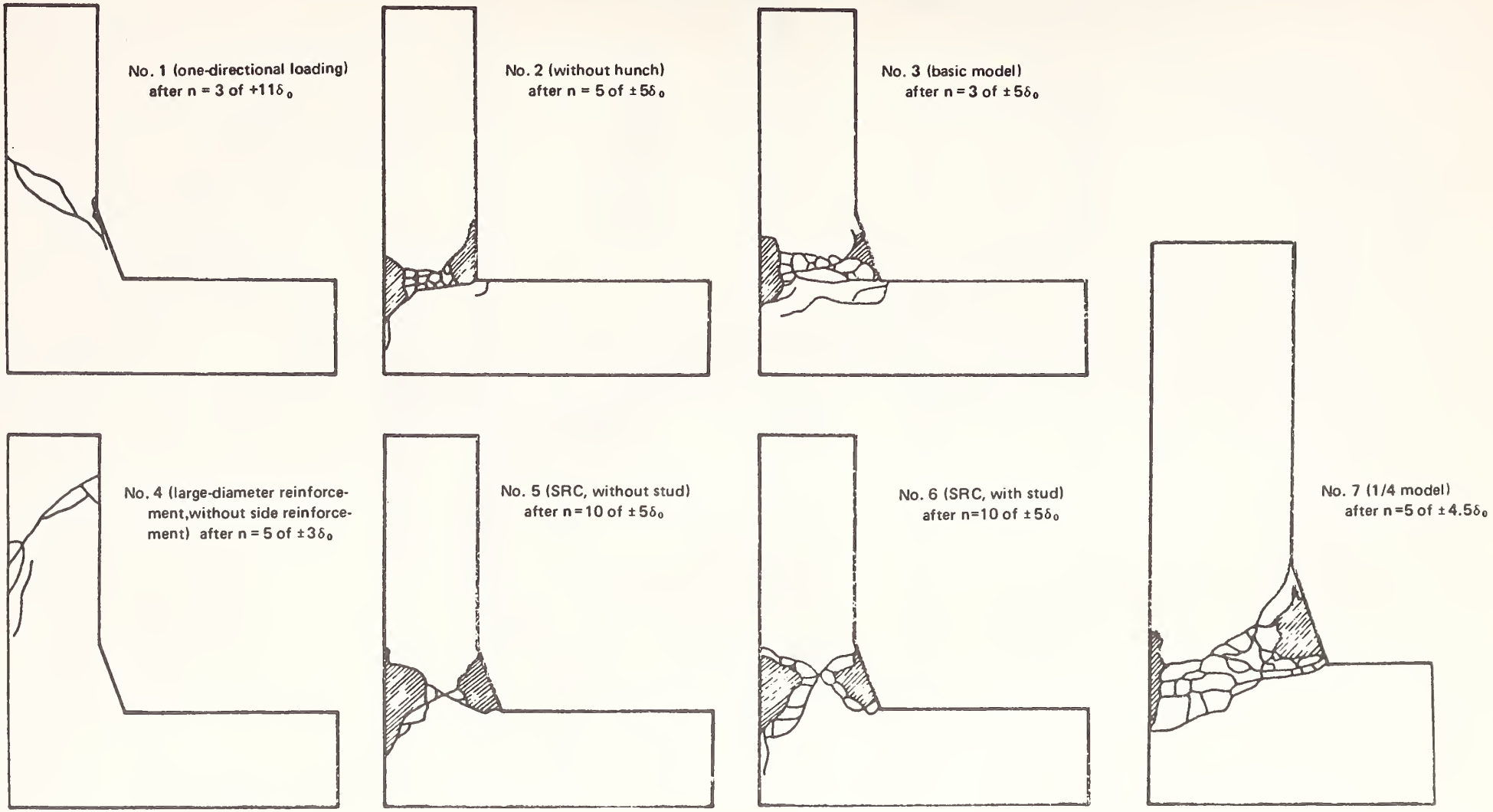

Fig. 34 Final Destruction Modes of Specimens

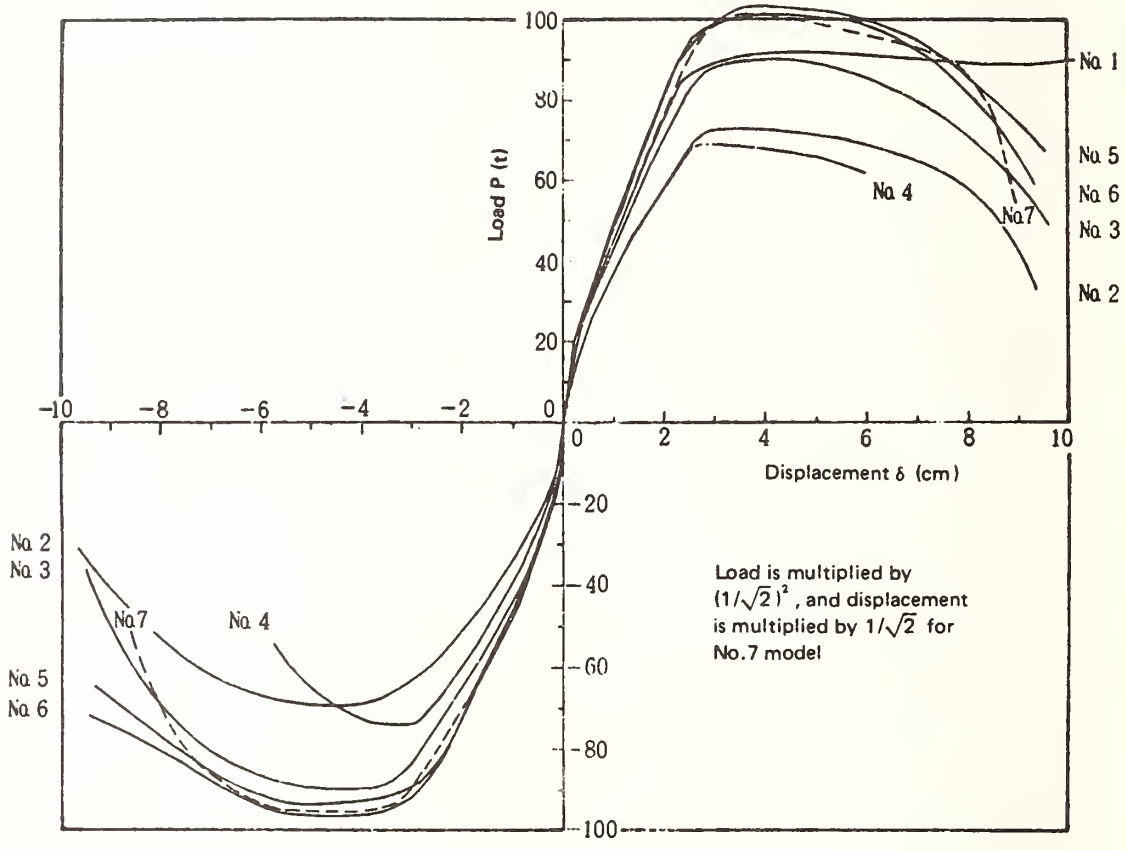

Fig. 35 Load-displacement Envelope Curve (n = 1)

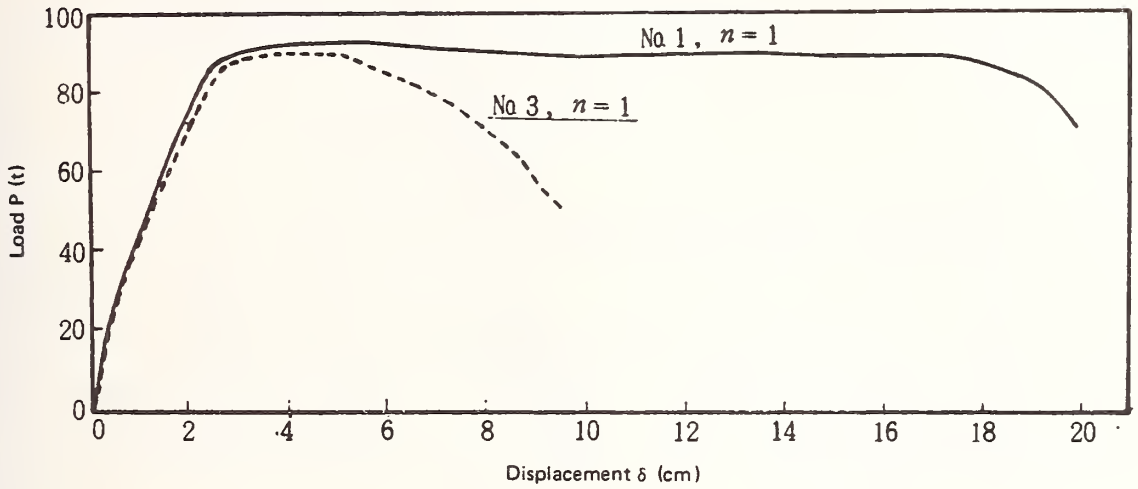

Fig. 36 Effect of Reversed Loading (Comparison of No. 1 and No. 3 Models)

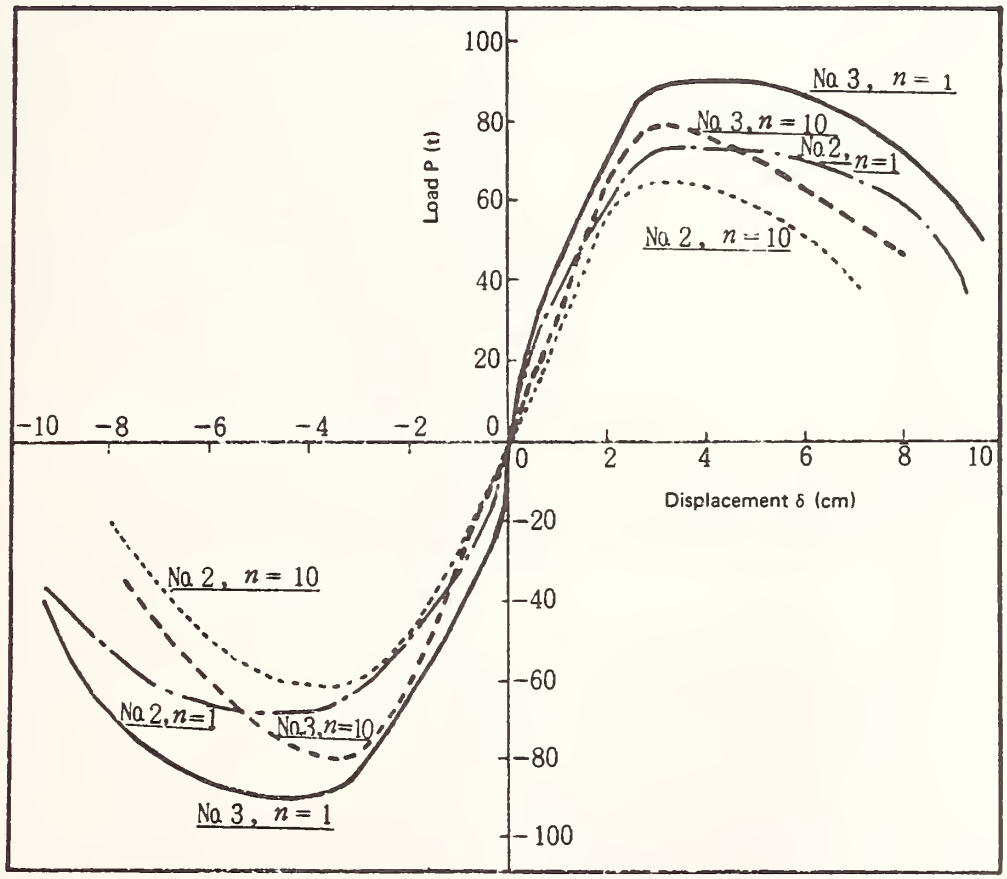

Fig. 37 Effect of the Hunch (Comparison of No. 2 and No. 3 Models)

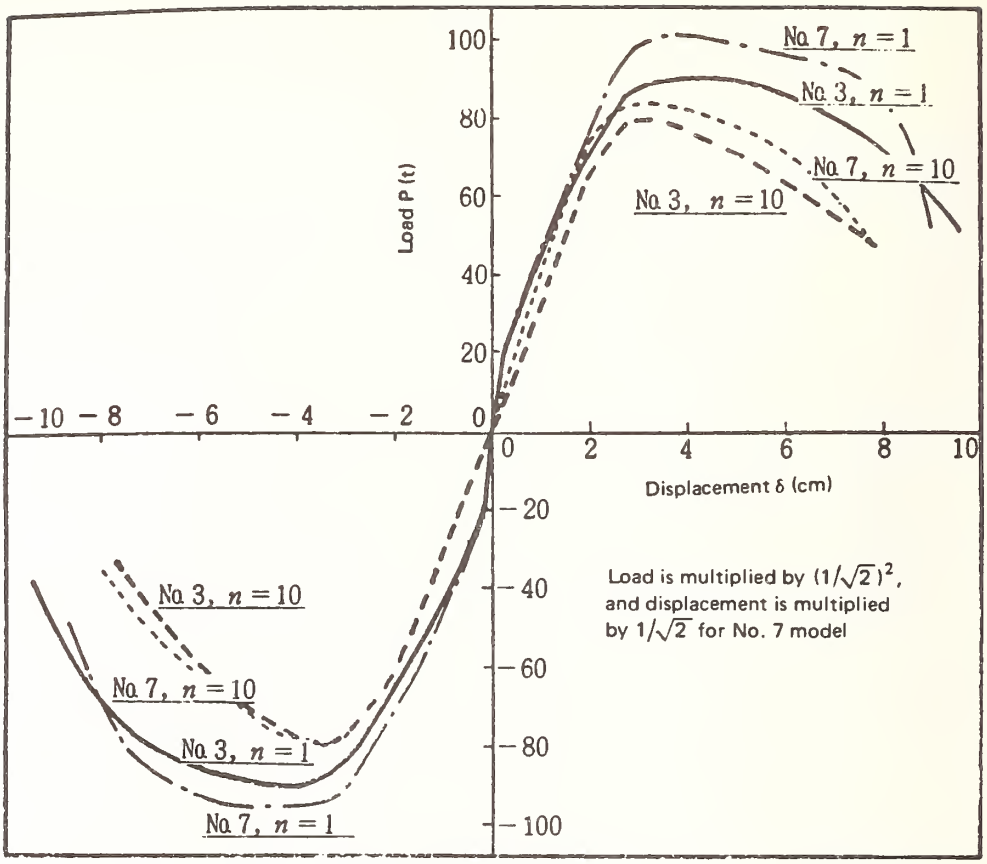

Fig. 38 Effect of an Axial Load (Comparison of No. 3 and No. 7 Models)

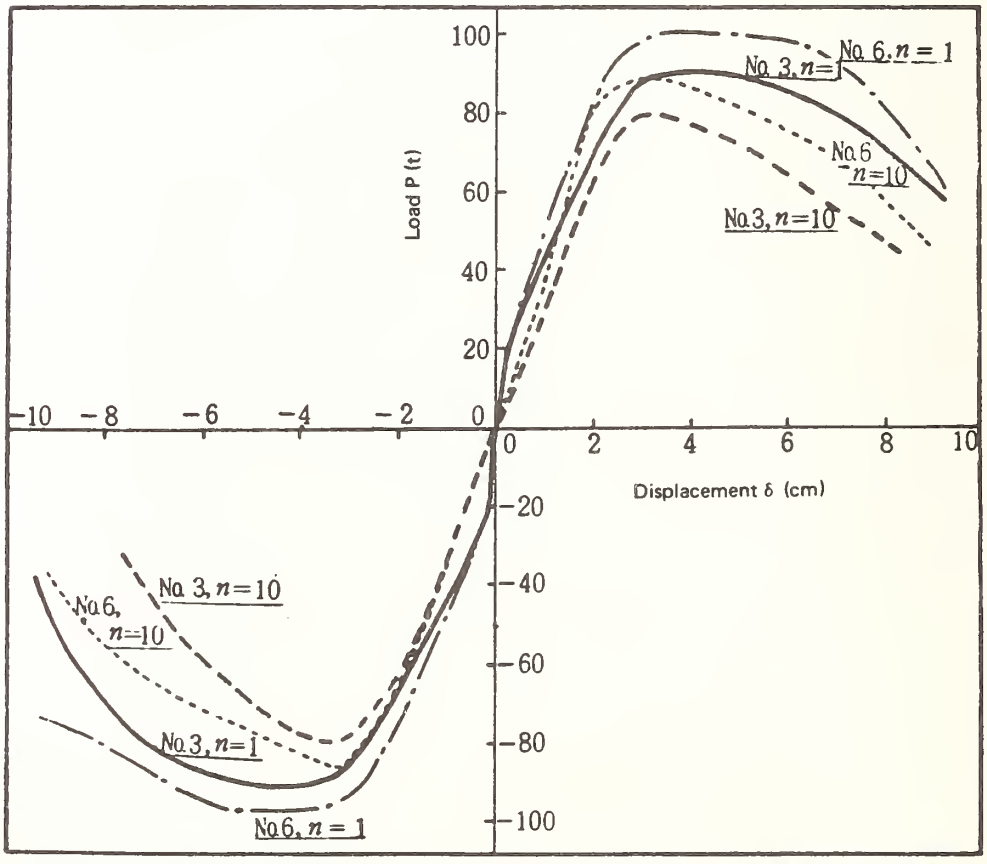

Fig. 39 Comparison of RC and SRC Structures (Comparison of No. 3 and No. 6 Models)

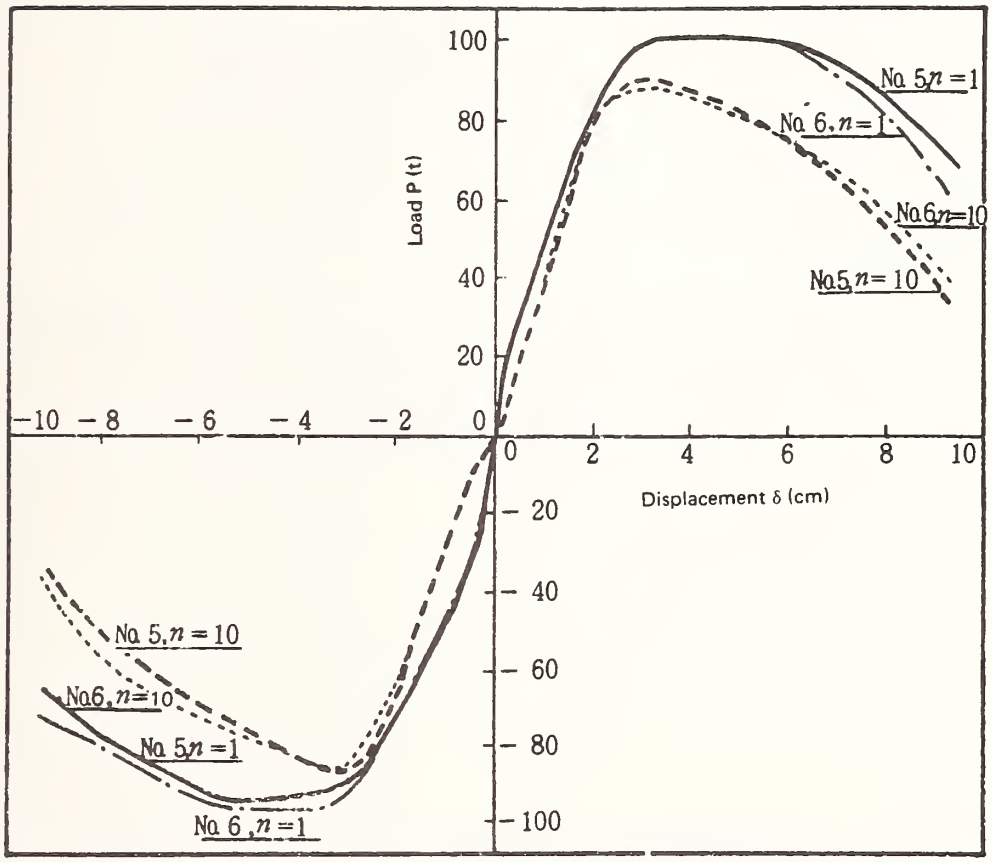

Fig. 40 Effect of Studs (Comparison of No. 5 and No. 6 Models)

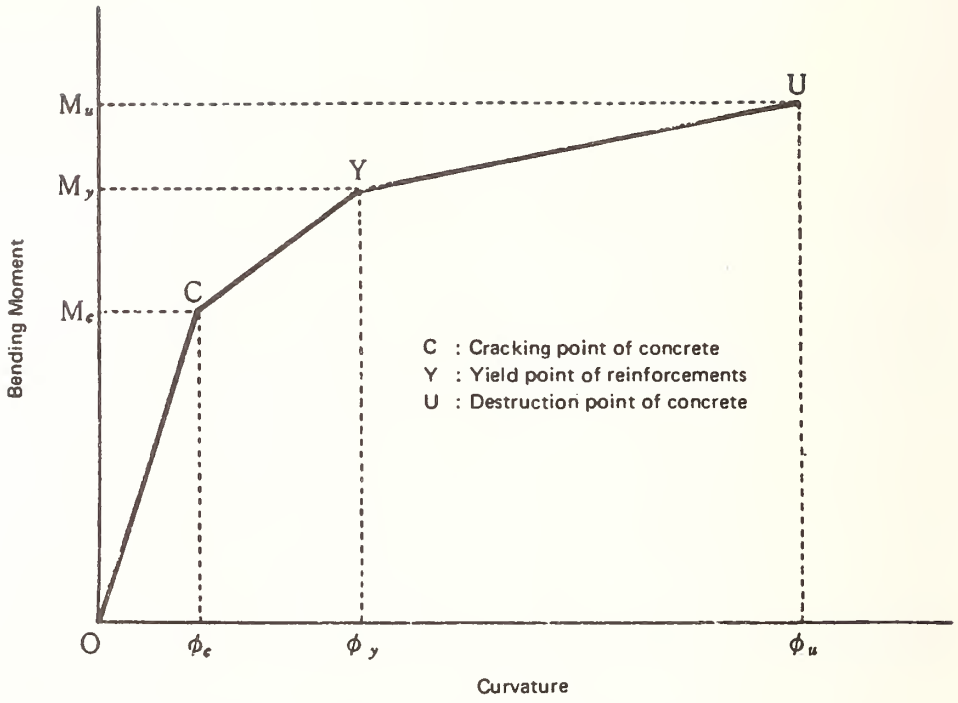

Fig. 41 Assumption of the M-ϕ Relationship

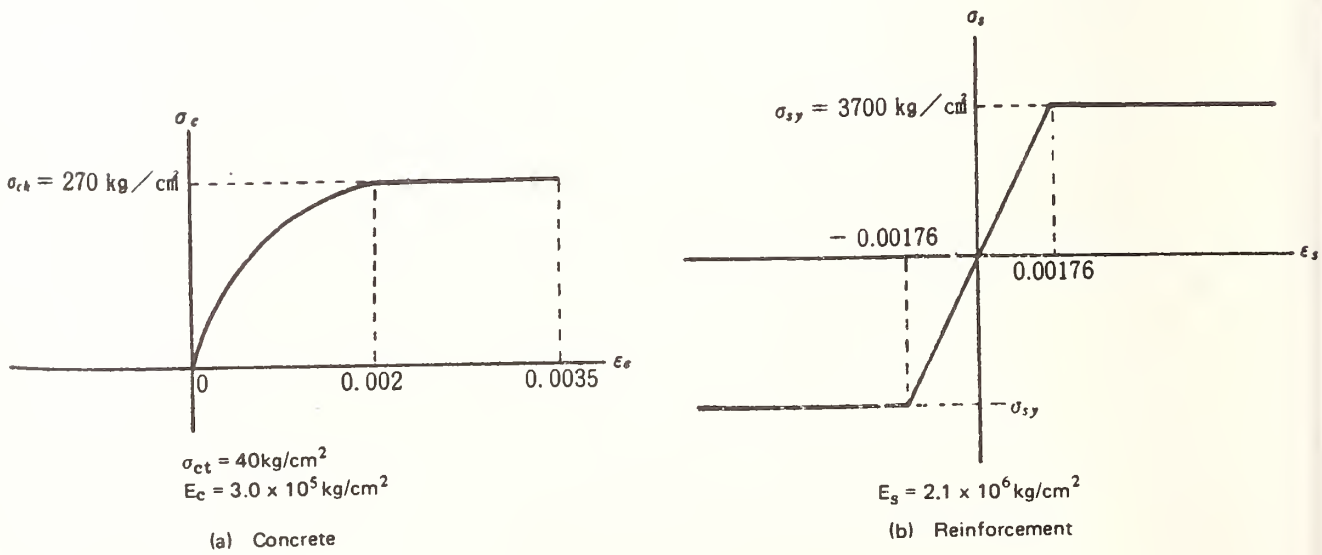

Fig. 42 Assumption of the Stress-strain Relationship of Materials

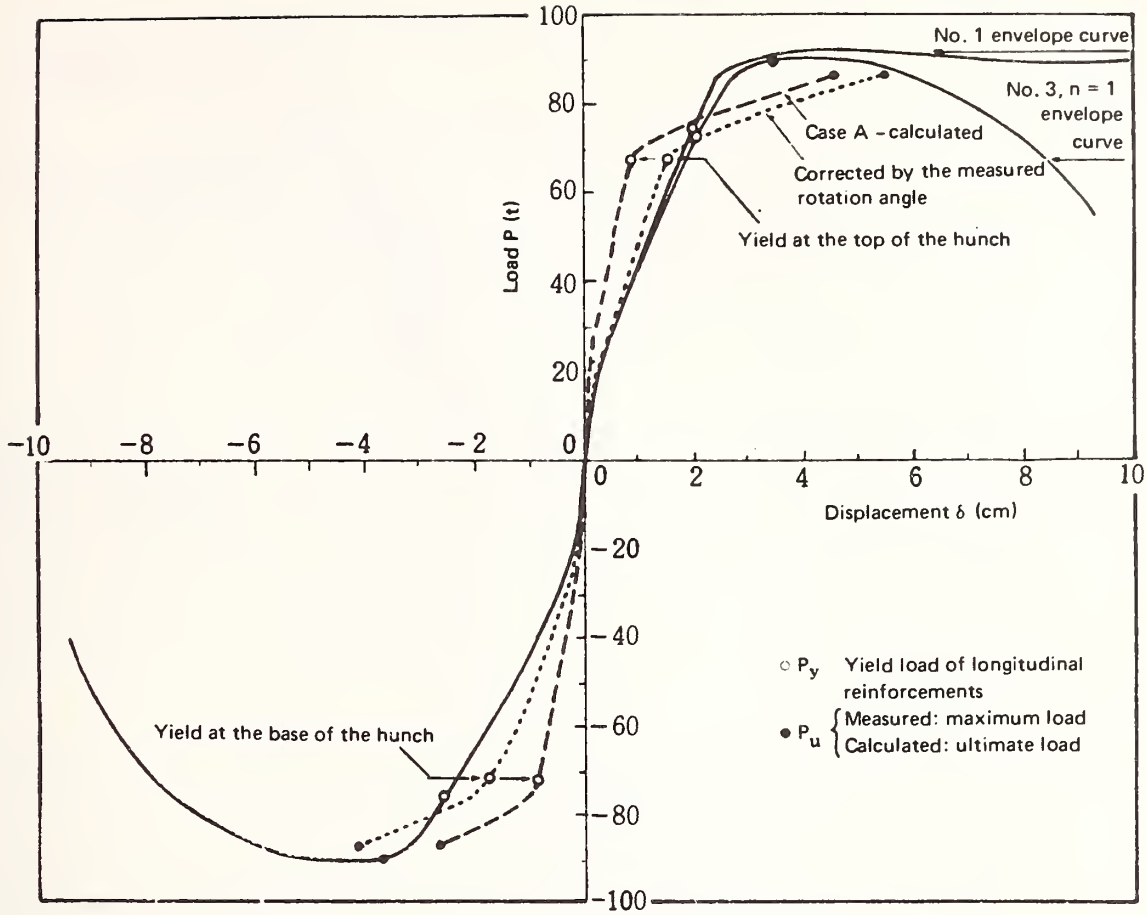

Fig. 43 Comparison of Case A - calculated and Measured P-δ Curves

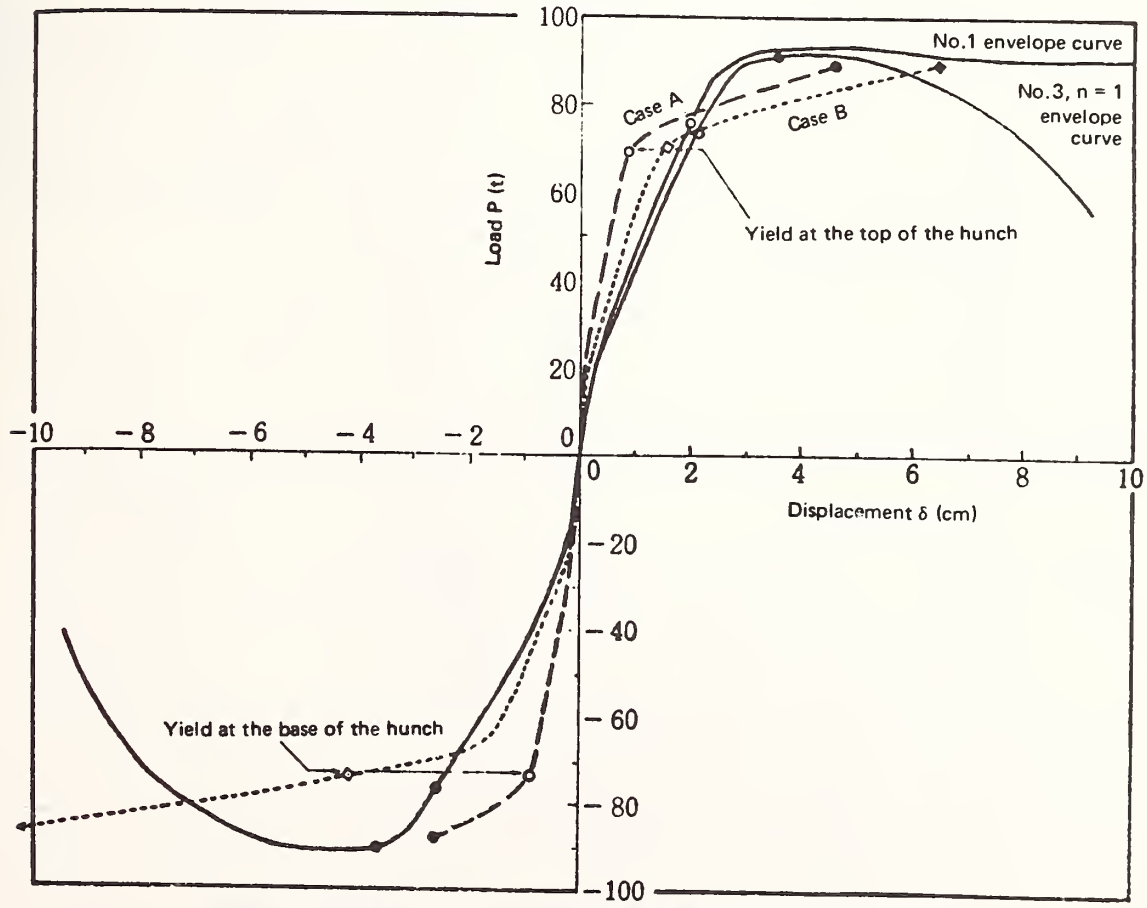

Fig. 44 Comparison of Case B - calculated and Measured P-δ Curves

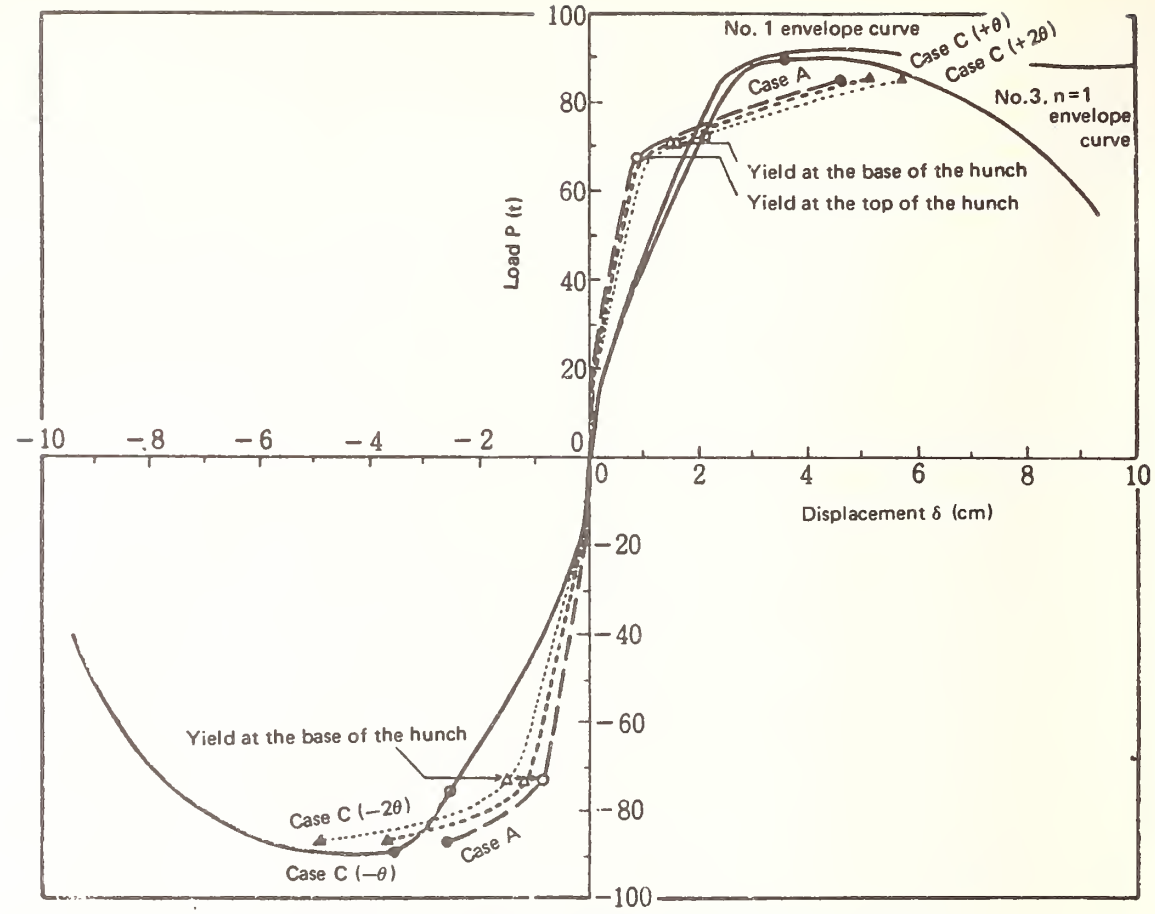

Fig. 45 Comparison of Case C - calculated and Measured P-δ Curves

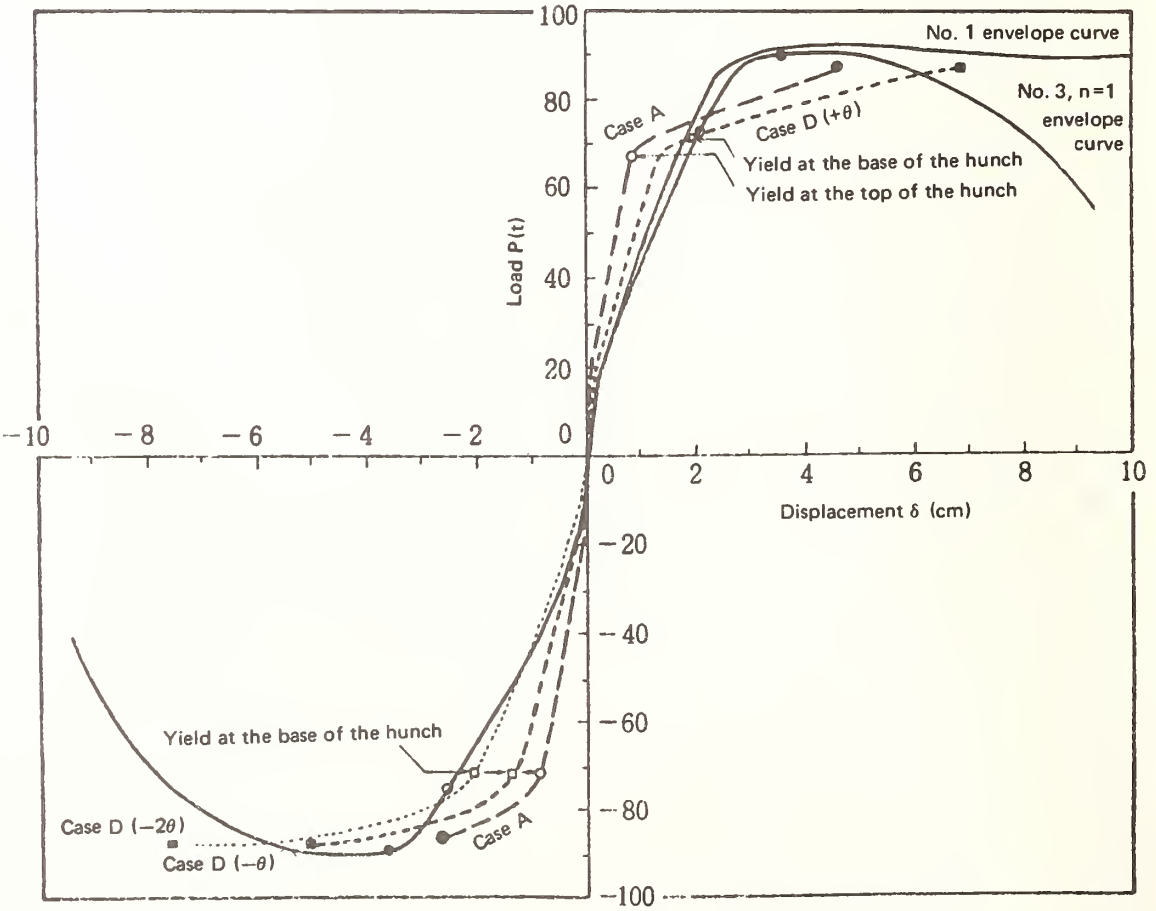

Fig. 46 Comparison of Case D - calculated and Measured P-δ Curves

REPORT OF THE URAKAWA-OKI EARTHQUAKE OF MARCH 21, 1982

Tomomitsu Yasue, Toshio Iwasaki, Yasushi Sasaki,
Hideya Asanuma and Takeo Nakajima

Public Works Research Institute
Ministry of Construction

ABSTRACT

On Sunday morning, March 21, 1982, a severe earthquake of magnitude 7.3 on the Richter Scale hit Urakawa-oki, off Urakawa, the southern part of Hokkaido Island in Japan. This report briefly describes an outline of the earthquake and damage to civil engineering structures due to the Urakawa-oki Earthquake of March 21, 1982.

OUTLINE OF EARTHQUAKE

From the report of the Japan Meteorological Agency (JMA)[1], the outline of the earthquake is summarized as follows:

1) Date and Time: 11:32 a.m., Sunday, March 21, 1982

2) Magnitude (Richter Scale): 7.3

3) Epicenter: 20 km off Urakawa, 150 km south-east from Sapporo, 42.1°N, 142.6°E

4) Depth: 10 km

5) JMA Intensities: 6 - Urakawa

4 - Tomakomai, Sapporo, Otaru, Iwamizawa, Hiroo, Kuchan, and Obihiro

3 - Kushiro, Asahikawa, Muroran Hakodate, Aomori, and Morioka

Figure 1 illustrates the epicenter and JMA intensities at various locations reported by the JMA. Figure 2 is a detailed map showing epicenters of aftershocks, as well as the main shock epicenter, obtained from a densely instrumented network of the Science Department of Hokkaido University [2]. From figure 2 it is seen that the epicenter is located off Mitsuishi about 15 km west from Urakawa, and the depth is about 30 km.

Strong-motion accelerographs recorded accelerations at several locations. Table 1 tabulates typical values of peak accelerations on grounds and structures. The locations and peak accelerations are also shown in figures 3 and 4. Unfortunately, no record was available near the epicenter. The largest acceleration (about 300 gals) was triggered at Hiroo, about 60 km east from the epicenter. At Horoman Bridge located about 40 km east from the epicenter, the peak value was only about 80 gals (uncorrected value obtained from SMAC-B2 type accelerograph). Peak accelerations at Sapporo City were also about 70 gals.

DAMAGE STATISTICS

Table 2 indicates the general damage statistics to persons and various facilities. It is seen from this table that no one was killed, 21 were seriously injured, and 146 were slightly injured. Most injuries were caused by the overturning of furniture and scalds due to the overturning of kettles containing boiling water. As for public facilities, damage to highways, bridges, ports, and water supply systems were comparatively severe.

DAMAGE TO HIGHWAYS

The National Highway Route 235 connecting between Tomakomai and Erimo sustained rather heavy damage. Landslides of mountain sides on highways took place at five locations between Shizunai and Higashi (east) - Shizunai, Shizunai town, shown in photos 1-3. Retaining walls of sea sides of the highway overturned and failed at Koshiumi Area, Mitsuishi town, as shown in photo 4. Settlements of highway embankments were observed at a number of locations. Photo 5 shows an example of the embankment settlements. All of those damages were quickly repaired by temporary repair works, and all portions (except Shizunai Bridge described in the next section) were open to public traffic in 3 days after the occurrence of the earthquake. It will take a few months, however, to completely finish the repair work.

HIGHWAY BRIDGES

The Shizunai Bridge, spanning the Shizunai River in Shizunai town, was severely damaged. The bridge is located in the north end of the focal area as seen in figure 2. The general drawings of the bridge are illustrated in figure 5. This bridge has 9-span steel plate girders, 2 abutments and 8 piers. Foundations of most of the piers (P1 to P7) are open caissons with a diameter of 6 m and a depth of 16 m. The foundation of P8 is a footing foundation. Soils are rather soft near the surface in the right-bank and the central part, as shown in figure 5. Each pier has a circular reinforced concrete column with a diameter of 2.2 m. The superstructure has 9 spans (3 of 3-spans continuous steel plate girders). Three pier columns of P2, P3, and P6 sustained heavy cracks. Column P3 was especially seriously cracked, as shown by photos 6 to 8. Photos 9 and 10 show the damage to P2 and P6, respectively. Three other pier columns of P4, P5 and P7 sustained light cracks, as shown in photos 11, 12, and 13, respectively.

Temporary repair work to P2, P3 and P6 were finished by the middle of April, and this bridge was reopened to light traffic (less than 5 tons) on April 15.

The Ministry of Construction and the Hokkaido Development Agency are now investigating the causes of the damage to the bridge columns and the procedures for permanent repair.

Several bridges sustained minor damage, such as small cracking of reinforced concrete pier columns and reinforced concrete girders. Settlements of back fills of abutments were observed at many bridge sites, as usually seen in past, strong earthquakes.

RIVERS, COASTS, DAMS, AND SLOPES

Dyke protection made of concrete block were damaged. A water gate located shortly down from the right-abutment of the Shizunai Bridge had differential settlements of about 30 cm at its back fills. The water gate and piers did not sustain any damage.

Dykes suffered from cracking (5 cm wide, 50 cm deep or more, and 5 m long) at the downstream from the right-abutment of the Shizunai Bridge.

Coastal retaining walls slid, inclined, and even overturned at the Koshiumi area of Mitsuishi town, as shown in photo 4.

Although one dam (Niicappu Dam) recorded peak acceleration of 136 gal at the crown, no damage to the dam was observed.

A few steep slopes slide in Shinzunai and Urakawa towns. In Urakawa town, one steep slope which was reinforced by slope protection facilities did not sustain any damage.

WATER SUPPLY SYSTEMS

Water supply systems sustained rather severe damage, an interruption of water supply was reported at 14,088 houses in 11 towns. In Urakawa town, 165 locations had pipeline damage. It took about ten days to repair and reopen the system at the town. Damage to the water supply systems affected people's daily lives most seriously. The water pipeline systems in Urakawa town have one valve at every 200 m length. This facilitated the discovery of damaged portions and repair work.

OTHER FACILTIES

Telephone lines were broken at 590 locations, and electricity was shut off at 10,400 homes. These interruptions were repaired very quickly, and within 24 hr at the most.

Japanese national railways also sustained heavy damage to railway bridges, slopes, and embankments at a total of 156 locations. The railways reopened early in April to Urakawa, and on April 14 to Samani, the east terminal.

No fires were reported.

LESSONS LEARNED FROM THE URAKAWA-OKI EARTHQUAKE

1. Earthquake resistant design methods of reinforced concrete pier columns should be examined, in view of the damage to pier columns of the Shizunai Bridge. Also, quick repair methods should be prepared in advance.

2. Back fills should be strengthened (well compacted) as settlements of back fills approaching bridges and water gates were frequently observed.
3. Important portions of slopes should be strengthened as natural soil slopes are vulnerable to earthquake shaking.
4. It took a long time to assess the extent of damage to underground water pipelines. Technology to judge the extent of damage to pipelines should be developed.
5. Although bridge substructures sustained heavier damage, bridge superstructures did not have any serious damage, as seen in past earthquakes.
6. Water supply pipeline systems which have many valves are very efficient in finding damaged portions and in repairing.
7. Assessment of the degree of damage to various civil engineering structures was rather difficult. Simple procedures of damage assessment should be prepared for practical purposes.
8. Fires can be avoided during and after an earthquake, if precautions are taken. Daily earthquake drills were not realistic in anticipation to large earthquake shaking.

REFERENCES

[1] Sapporo Regional Meteorological Station, Japan Meteorological Agency, "Report of the Urakawa-oki Earthquake and Tsunami of March 21, 1982," March 27, 1982.

[2] Hokkaido University (Science Department), "Report of the Urakawa-oki Earthquake," March 31, 1982.

Table 1. Peak Accelerations from Strong-Motion Measurements

Station	Location Direction Δ(km)	Ground Acceleration (gal) H-A	H-B	Vert.	(Structural Acceleration (gal) H-A	H-B	Vert.	Instrument
1. Horoman Br.	40	53	76	25	80	73	35	SMAC-B2
2. Hiroo Br.	62	247	207	69	175	170	63	SMAC-Q
3. Tokachi Port	62	151	263	78	--	--	--	ERS
4. Hiroo JMA,BRI	62	206	297	69	--	--	--	SMAC-B
5. Tomakomai Port	86	63	64	21	--	--	--	SMAC-B2
6. Nishikioka Br.	95	77	58	25	107	67	40	SMAC-B2
7. Shimamatsu-zawa Br.	105	115	95	38	--	--	--	SMAC-Q
8. Chiyoda Br.	112	48	53	10	(P) 53 (A) 43	95 46	15 15	SMAC-B2
9. Sapporo I.C. Br.	130	(274)	(318)	(51)	(299)	(377)	(92)	SMAC-Q
10. Sapporo Hokkaido U.	130	72.5	66	30	--	--	--	SMAC-M
11. Muroran Port	130	138	169	44	--	--	--	SMAC-B2
12. Ishikari Estuary Br.	151	35	43	15	83	48	15	SMAC-B2
13. Otaru Port	168	15	18	4	--	--	--	SMAC-B2
14. Otanoshike Br.	170	18	14	3	--	--	--	SMAC-B2

Notes: (1) Δ denotes an epicentral distance equal to the distance between an observation station and the epicenter, the center of the octagon of the main shock is shown in figure 2.

(2) Records are taken by Hokkaido Development Bureau, Port and Harbour Research Institute, and Building Research Institute.

(3) Accuracy of Sapporo I.C. Br. Instruments is under study.

Table 2. Damage Statistics (Hokkaido)

As of April 2, 1982

Damages To		Damage Quantity	Damage Cost (Million Yen)	Remarks
Inhabitants	Fatality	0	--	
	Serious Injury	21		
	Slight Injury	146		
Residential Houses	Collapse	13	95	
	Half Collapse	30	123	
	Partial Failure	670	185	
Non-residential Houses	Collapse	14	68	
	Half Collapse	8	10	
Agriculture Facilities and Cattle		113	482	
Public Works and Facilities	River	49	470	
	Highway	33	726	
	Bridge	5	358	
	Coast	10	155	
	Port	24	1,015	
	Slope	2	1,118	
	City	2	13	
Fishery		33	23	
Forestry		73	121	
Sanitary, Facilities		29	85	Including Water Supply
Commercial, Industrial Facilities		1,483	1,437	
School		127	141	
Social Welfare		18	14	
Telephone		9	100	
Railroad (JNR)		156	850	
Electricity		142	33	
Others		37	140	
Grand Total		3,102	7,762	

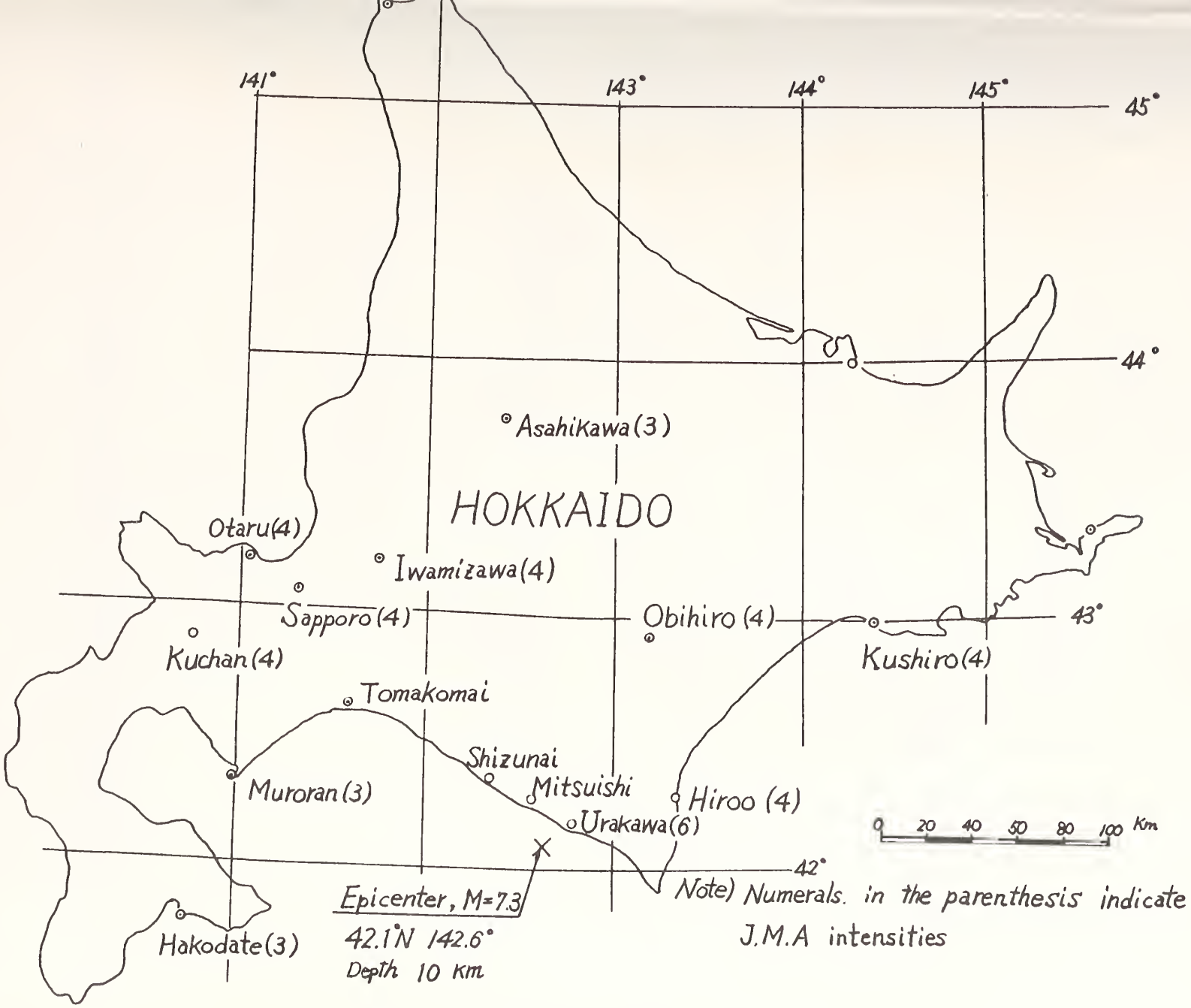

Figure 1. Epicenter and J.M.A. Intensities,
(Urakawa-oki Earthquake of March 21, 1982)

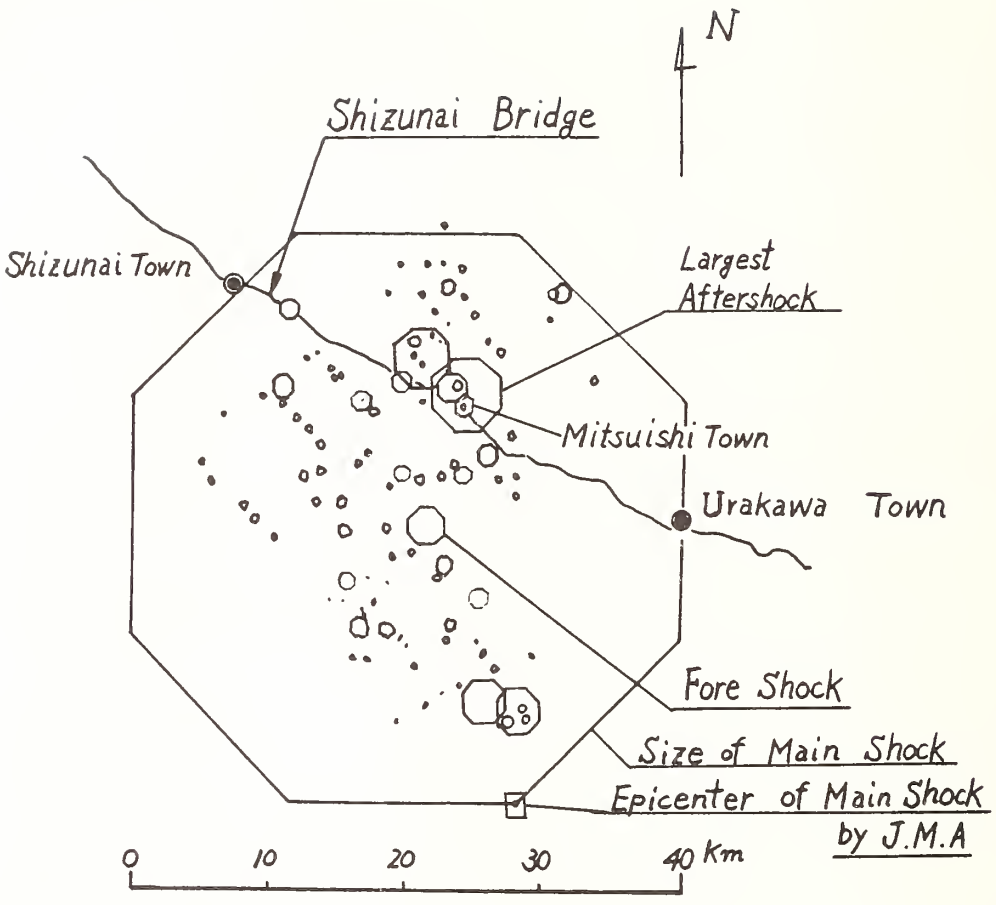

Figure 2. Epicenters of fore shock, main shock, and numerous aftershocks (after Science Department, Hokkaido University)

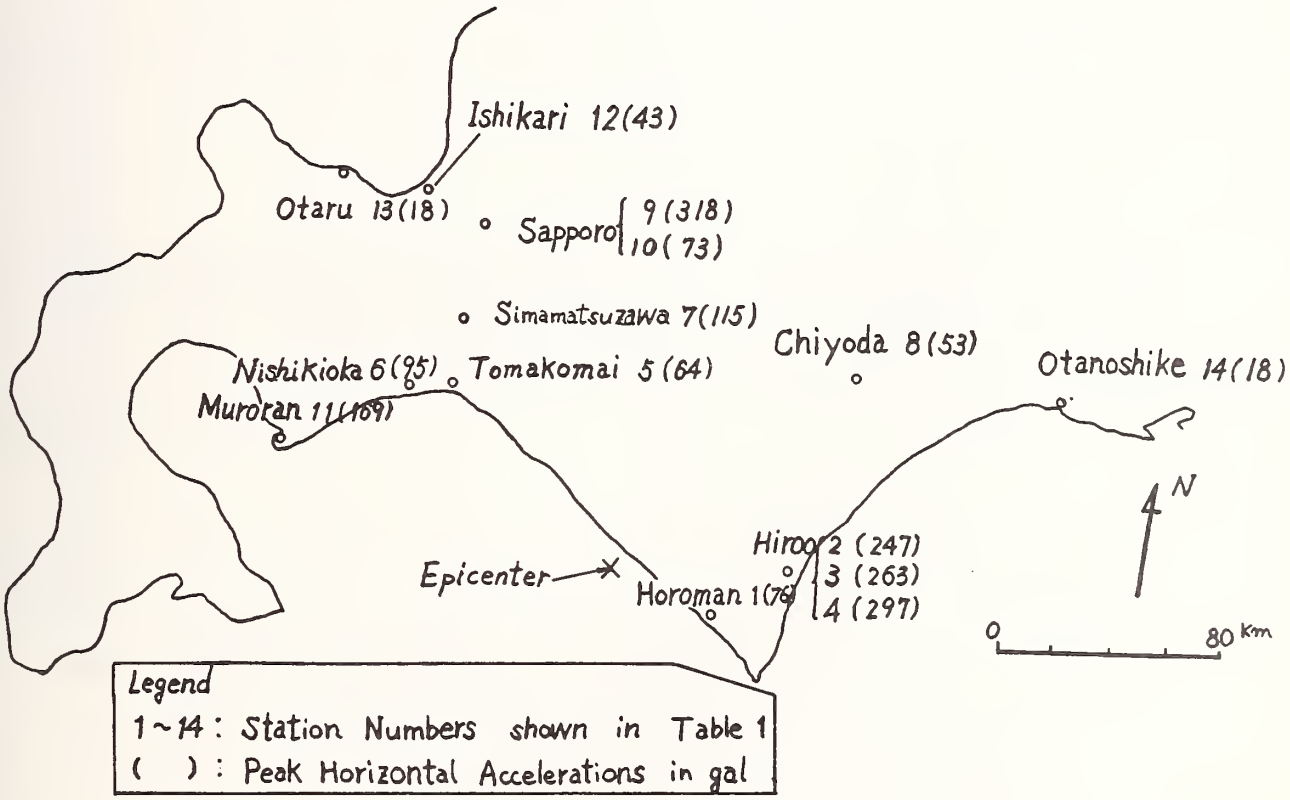

Figure 3. Strong motion stations recorded and peak horizontal accelerations on ground

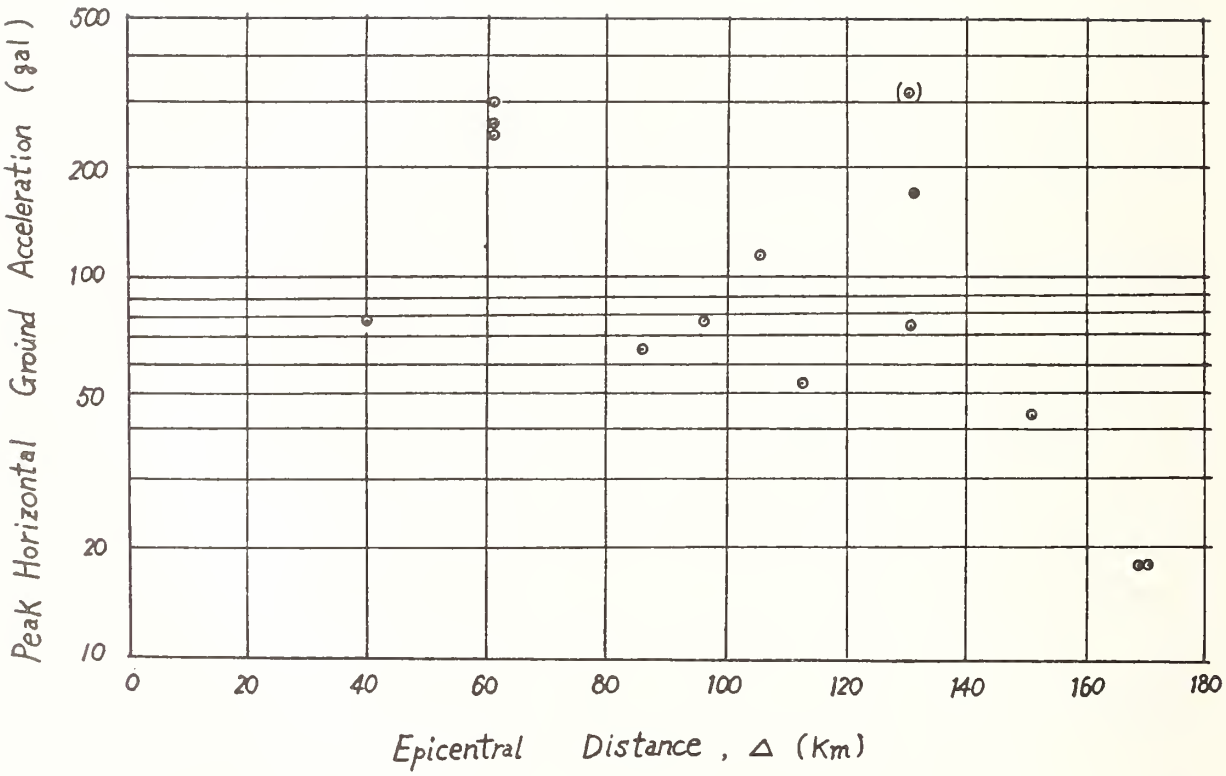

Figure 4. Epicentral distance versus peak horizontal ground acceleration
(Δ is measured from the center of octagon of figure 2)

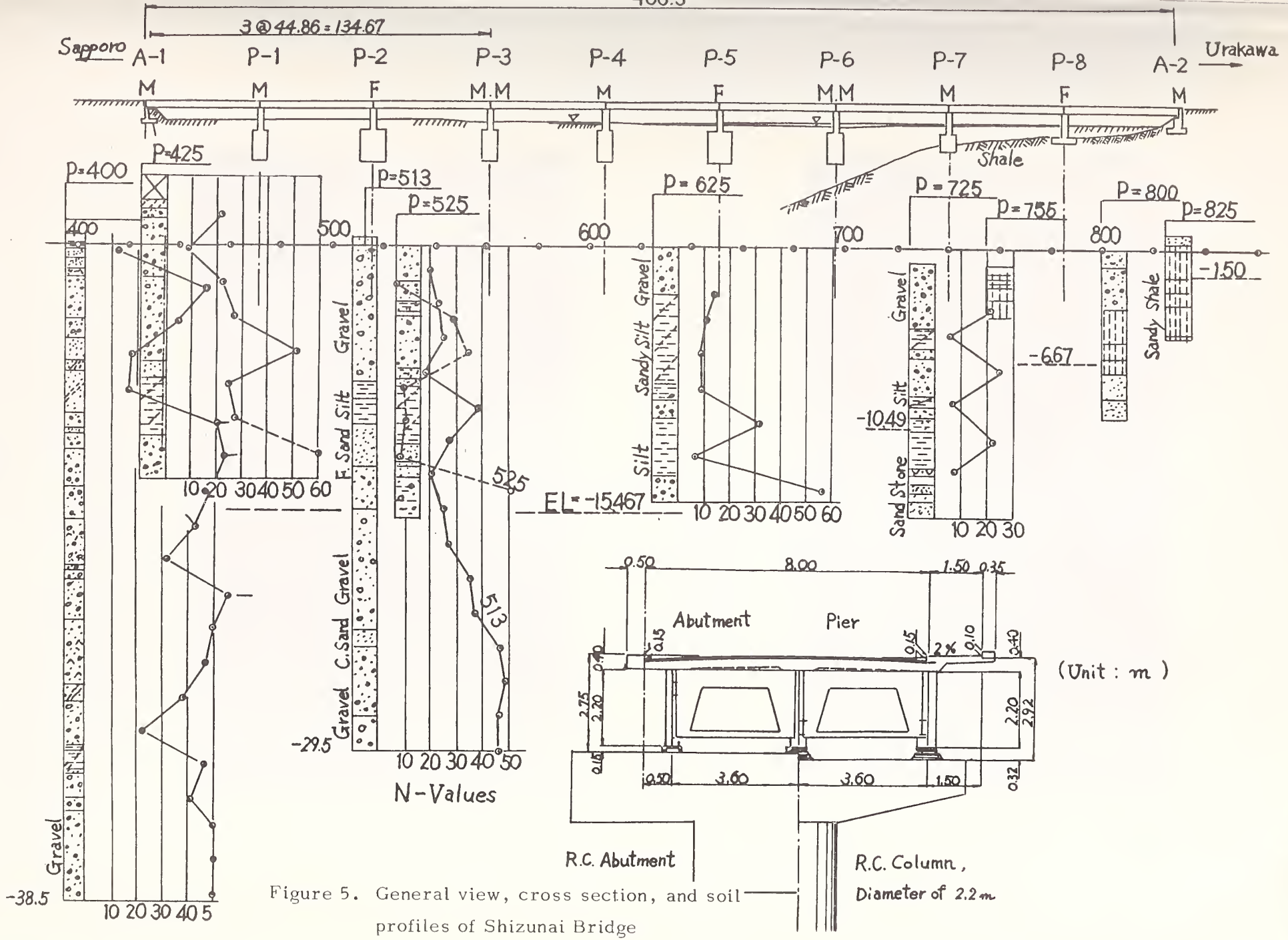

Figure 5. General view, cross section, and soil profiles of Shizunai Bridge

Photo. 1 Damage to Slope along National Highway Route 235, at Irifune Area, Shizunai Town. An electric post was overturned.

Photo. 2 Damage to Slope along National Highway Route 235, at Irifune Area, Shizunai Town, A Wagon was Buried under Soils.

Photo. 3 Light Damage to Slope along National Highway Route 235, at Irifune Area, Shizunai Town. Retaining Walls Protected from a Large Failure.

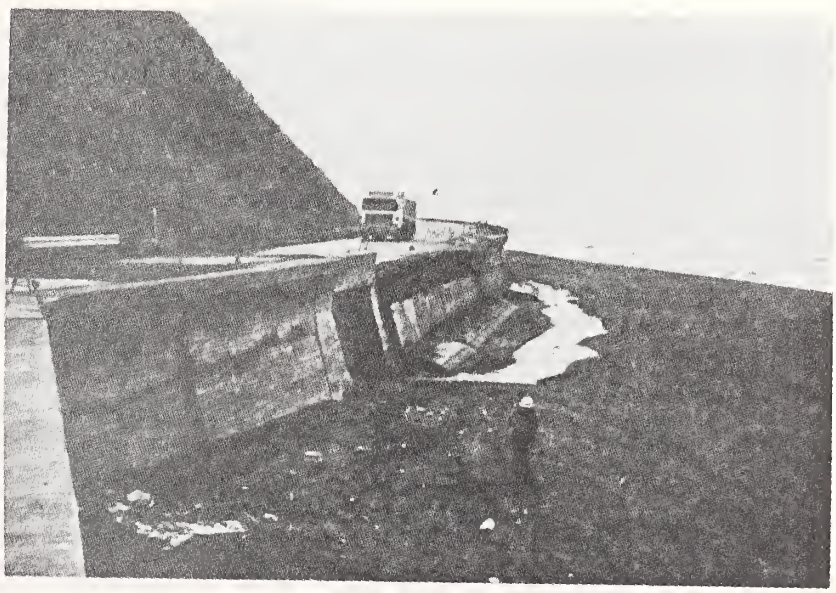

Photo. 4 Overturning of Coastal Retaining Walls along National Highway Route 235, at Koshiumi Area, Mitsuishi Town.

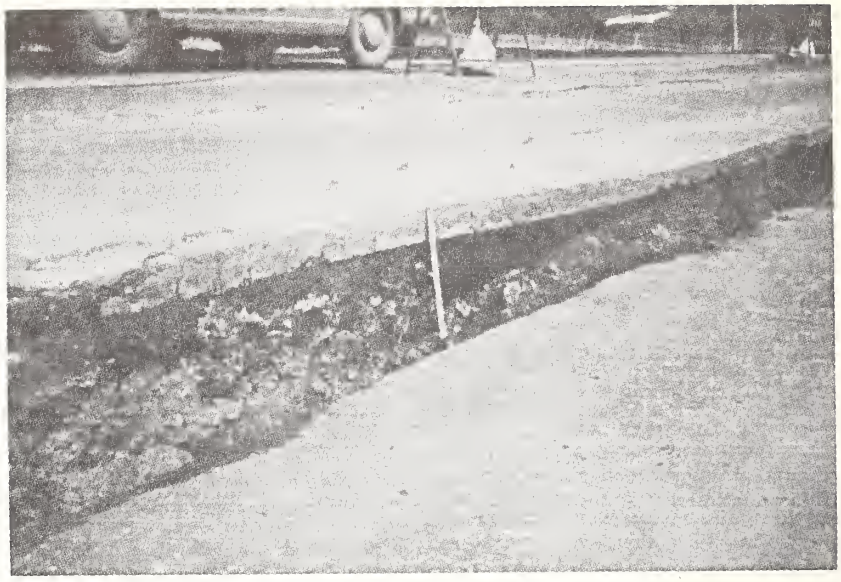

Photo. 5 Settlement of Embankment of National Highway Route 235 Near Ura Bridge, Shizunai Town.

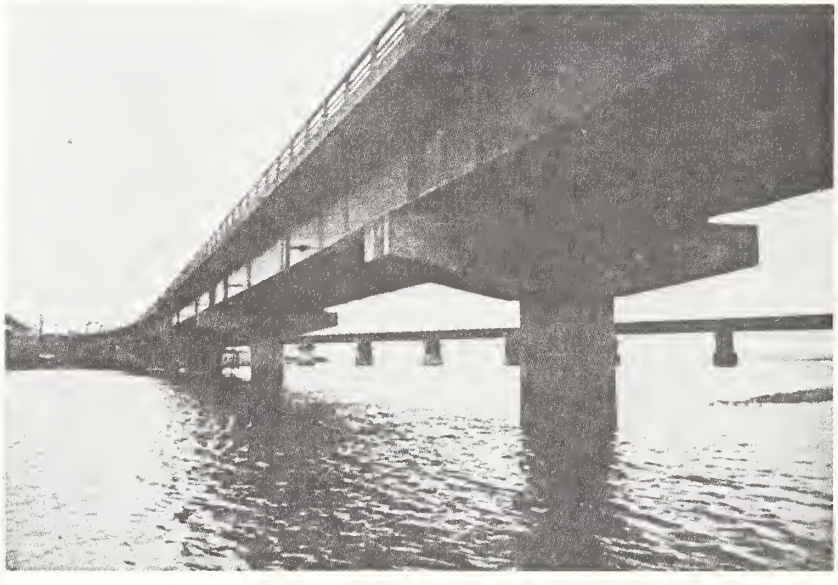

Photo. 6 A View of Shizunai Bridge from Right-Bank to Left-Bank and Down-Stream, Closest Pier is Pier 4.

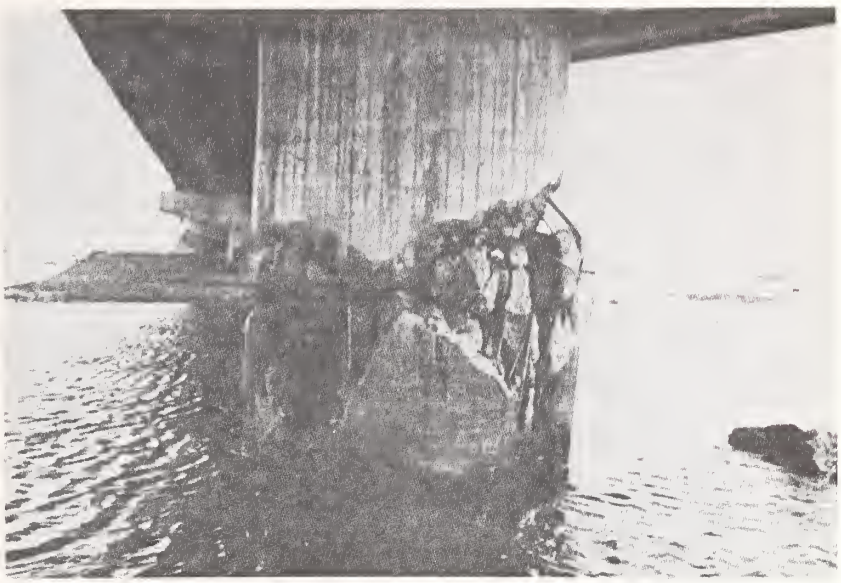

Photo. 7 Damage to Pier 3 of Shizunai Bridge, seen from Pier 2.

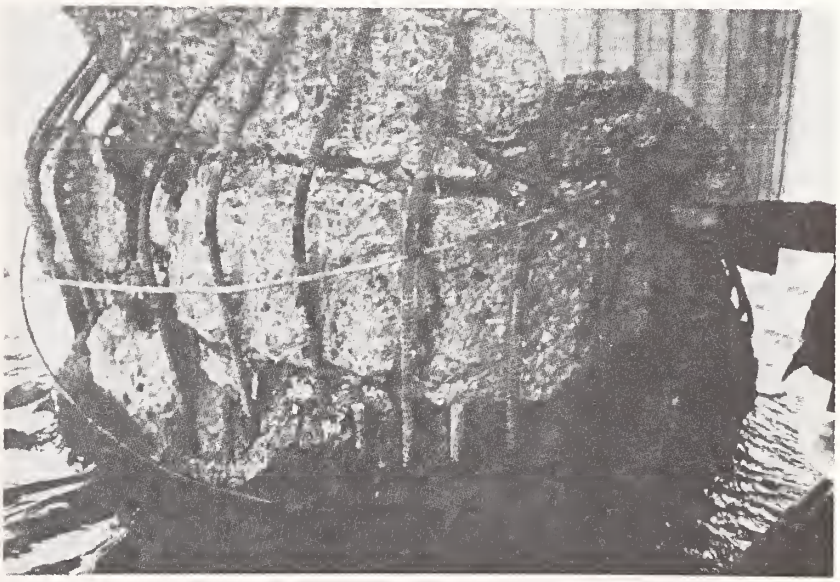

Photo. 8 Closer View of Failed Section of Pier 3 of Shizunai Bridge, seen from Down-Stream. Cut-off of Bars is seen.

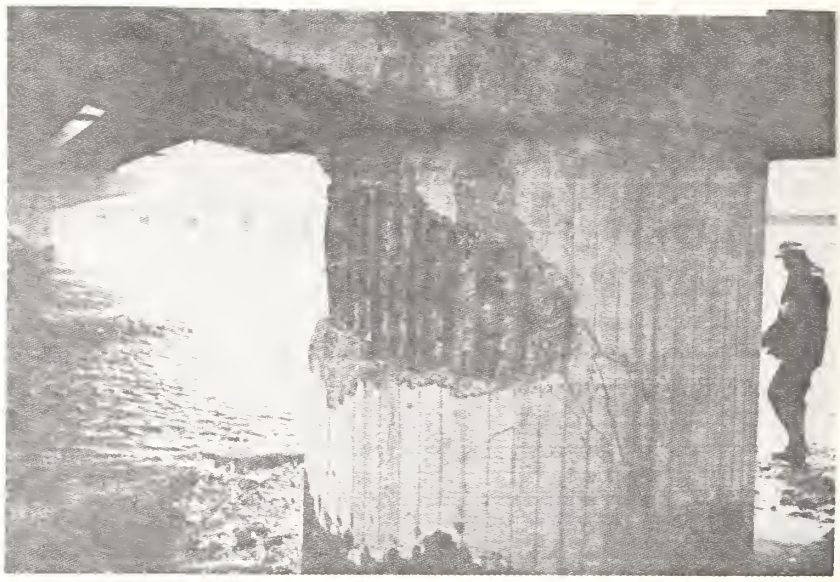

Photo. 9 Damage to Pier 2 of Shizunai Bridge, seen from Up-stream of Pier 1 side.

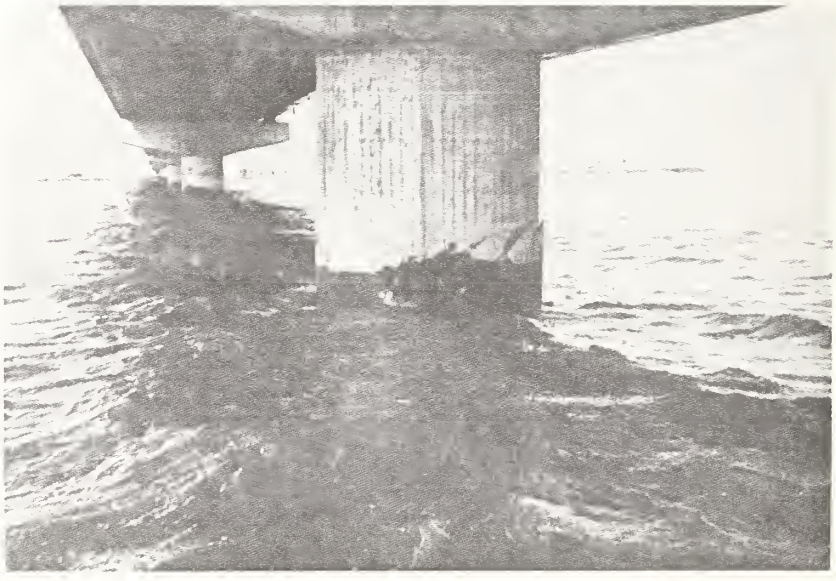

Photo. 10 Damage to Pier 6 of Shizunai Bridge, seen from Pier 7.

Photo. 11
Damage to Pier 4 of
Shizunai Bridge.

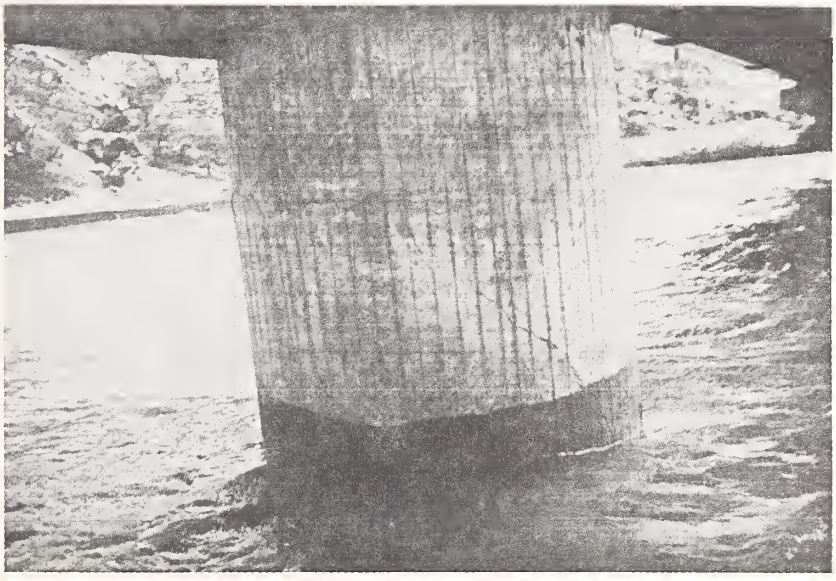

Photo. 12
Damage to Pier 5 of
Shizunai Bridge
Diagonal Cracking is
Seen Down-stream Side.

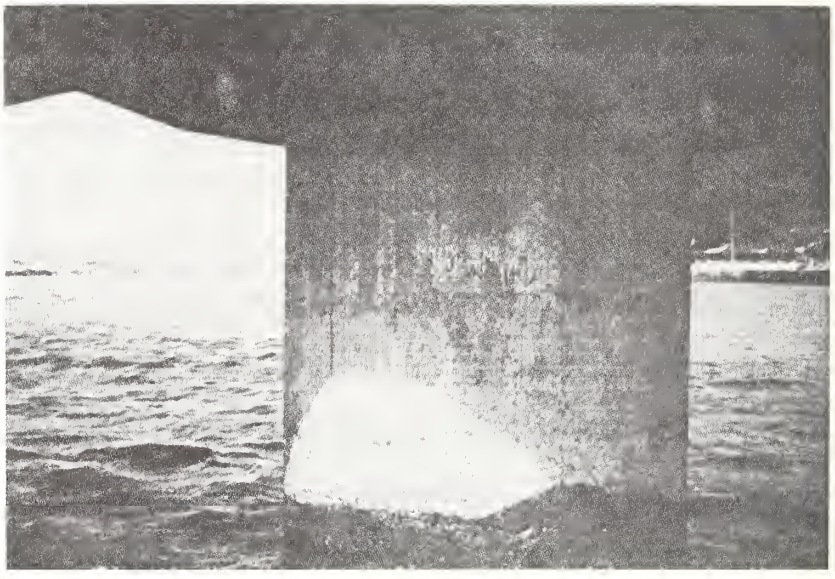

Photo. 13
Damage to Pier 7 of
Shizunai Bridge,
Light Horizontal
Cracking is Seen.

LINEAR VERSUS NONLINEAR BEHAVIOR OF CABLE STAYED BRIDGES

John F. Fleming

Associate Professor of Civil Engineering
University of Pittsburgh
Pittsburgh, PA

ABSTRACT

The first modern cable stayed bridge was constructed in Sweden in 1955. Since that time over 100 major bridges of this type have been built throughout the world. One of the major difficulties which many designers must face, when confronted with the task of designing a structure of this type, is a lack of knowledge of how they behave under static and dynamic design loads. It is well known that cables exhibit a nonlinear force-elongation relationship due to the change in sag with axial load. The purpose of this paper is to describe the results to date of an ongoing investigation into the effect of nonlinear behavior upon the overall static and dynamic response of cable stayed bridges. Mathematical models representing several actual or proposed bridges, under a variety of static and dynamic loads, were considered in the study.

NONLINEAR STATIC ANALYSIS

The static displacements for a linear structural system can be easily computed by solving the set of linear simultaneous stiffness equations:

$$[K]\{D\} = \{W\} \tag{1}$$

in which [K] is a matrix containing the stiffness influence coefficients for the structure, {D} are the joint displacements and {W} are the static joint loads. The terms in the matrix [K] can be computed by summing the stiffnesses of the individual members at each joint in the structure. The terms in [K] are constants which do not change as the linear structure deforms.

For a nonlinear structural system the stiffness of the structure changes as the structure deforms, therefore, the terms in the matrix [K] change as the load is applied. This greatly complicates the analysis of the structure since it is usually not feasible to algebraically solve the set of nonlinear simultaneous stiffness equations corresponding to equation (1). For most structures it is necessary to resort to some sort of numerical solution to determine the displacements.

Several approaches may be used to obtain a numerical solution for the static displacements and stresses in a general nonlinear structural system. Two procedures which are well suited for application to complex multi-degree of freedom systems are an Incremental Approach and an Iterative Approach.

In an Incremental Approach the total load is applied in small increments, assuming that the stiffness of the structure remains constant during the application of each load increment. The stiffness of the structure is recomputed corresponding to its deformed shape at the end of each load increment. The total displacements are obtained by adding the values which occur during a load increment to the values at the beginning of the load increment. If the total load is applied in a large number of increments, so that the change in stiffness over any load increment is relatively small, this approach can give an acceptable engineering solution. A graphical representation of this procedure is shown in figure 1. It can be seen that the error accumulates for each step. If the total number of increments is sufficiently large, however, the accumulated error can be well within the limits of acceptable engineering accuracy.

In an Iterative Approach the total load is applied in one increment. The displacements are initially computed using the tangent stiffness of the undeformed structure, however, the stiffness is then recomputed corresponding to this deformed shape before the member end loads are computed. Since the final stiffness used to compute the member end loads differs from the initial stiffness used to compute the joint displacements, equilibrium will not be satisfied and unbalanced loads will exist at the joints. These unbalanced loads must next be applied as a new set of joint loads, with the corresponding change in displacements being computed using the stiffness corresponding to the new deformed position of the structure. The final solution can be obtained by iterating until the unbalanced forces at the end of a load cycle are smaller than an acceptable tolerance limit. A graphical representation of this procedure is shown in figure 2. This approach is very similar to the classical Newton-Raphson Method for solving nonlinear equations.

In the static analysis procedure used in this investigation, a Combined Approach was used, in which the unbalanced loads were applied incrementally during each iteration cycle. This results in faster convergence.

SOURCES OF NONLINEAR BEHAVIOR

Under normal static design loads the material in a cable stayed bridge can be considered to remain elastic, however, the overall load-deformation relationship may be nonlinear. Three sources of nonlinear behavior have been proposed by previous investigators. These are: the nonlinear sag tension relationship for the inclined cables; the interaction of the bending deformations and high axial forces in the towers and longitudinal deck members; and the overall changes in geometry which occur in the structure under normal design loads.

It has been shown in an investigation at the University of Pittsburgh [1, 2, 3], using mathematical models representing actual or proposed bridges, that under normal static design loads

the effects of both the change in geometry of the structure and the axial-bending interaction in the towers and deck members is negligible. The primary source of nonlinear behavior is the sag in the cables, therefore, only this effect will be considered in the remainder of this discussion.

COMPUTATION OF STRUCTURAL STIFFNESS

In order to use the Combined Approach to compute the displacements and member end loads, it is necessary to compute the structure stiffness matrix, [K], corresponding to the deformed shape of the structure after each load increment is applied. Since [K], for any structural system, is obtained by adding the individual member stiffnesses at the joints, it is therefore necessary to express the stiffness of the individual members in terms of the deformed shape of structure.

STIFFNESS OF CABLES

When an axial tension force is applied to the ends of a cable, the ends will move relative to each other along the axis of the cable. For other types of tension members this relative movement is usually due entirely to the elongation of the member resulting from the strain in the material. For a cable, the relative end movement is the result of three distinct actions in the cable. First, there is a change in strain in the cable material. This change in strain can be considered to vary linearly with stress, under normal static design loads, and is governed by the modulus of elasticity of the material. Second, there is a change in the sag of the cable, exclusive of material strain. This change in sag is strictly a geometric effect and is governed by the length of the cable, the weight of the cable, and the tension force in the cable. The sagged shape of the cable is a catenary, for which equations are given in many elementary mechanics textbooks. This change in sag varies nonlinearly with the change in the tension force in the cable. Third, there is a rearrangement of the individual wires in the cable cross section under changing load. This deformation is known as constructional stretch. Part of this deformation is permanent, and is usually eliminated by the cable manufacturer by prestretching the cable to a load greater than the working load during the manufacturing process. The nonpermanent part of this deformation, which results from untwisting of the helically wound wires under applied load, can be compensated for by using a reduced effective modulus of elasticity of the cable material. For example, ASTM Specification A536 states that the effective modulus of elasticity for prestretched helical strand should be taken as 23 to 24 million pounds per square inch, depending upon the diameter of the strand. The actual material modulus is approximately 29 million pounds per square inch. This effective modulus is assumed to be independent of the tension in the cable.

The total apparent change in length of a cable is a result of the sum of the three previously described effects. Therefore, since the sag varies nonlinearly with the axial tension force in the cable, the axial stiffness of the cable will also vary in a nonlinear manner. A convenient method for considering the nonlinearity in the inclined cables is to consider an equivalent straight chord member, as shown in figure 3, with an equivalent modulus of elasticity which combines both of the effects of material and geometric deformations. An expression for this equivalent modulus, as derived by Ernst [4] is:

$$Eeq = Eef/[1+[(wH)^2AEef/12T^3]] \tag{2}$$

where Eeq is the equivalent modulus, Eef is the effective modulus of the cable including stranding effects as described previously, w is the weight of the cable per unit length, H is the horizontal projected length of the cable, A is the cross section area, and T is the tension force. This equivalent modulus can be used to express the stiffness of any cable member, [Km]c, in the local member coordinate system shown in figure 4 in the form:

$$[Km]c = \begin{bmatrix} AEeq/Lc & -AEeq/Lc \\ -AEeq/Lc & AEeq/Lc \end{bmatrix} \tag{3}$$

where Lc is the chord length of the cable member.

Stiffness of Bending Members

The stiffness of a typical three-dimensional frame bending member, [Km]b, can be expressed as a 12 by 12 member stiffness matrix, in the local member coordinate system shown in figure 5 in the form:

$$[Km]b = \begin{bmatrix} k(1,1) & k(1,2) & \cdots & k(1,12) \\ k(2,1) & k(2,2) & \cdots & k(2,12) \\ \vdots & \vdots & & \vdots \\ k(12,1) & k(12,2) & \cdots & k(12,12) \end{bmatrix} \tag{4}$$

in which

$$k(1,1) = k(7,7) = -k(1,7) = -k(7,1) = AE/L \tag{5a}$$

$$k(2,2) = k(8,8) = -k(2,8) = -k(8,2) = 12EIz/L^3 \tag{5b}$$

$$k(3,3) = k(9,9) = -k(3,9) = -k(9,3) = 12EIy/L^3 \tag{5c}$$

$$k(2,6) = k(6,2) = k(2,12) = k(12,2) = -k(6,8) = -k(8,6) = -k(8,12) = -k(12,8) = 6EIz/L^2 \tag{5d}$$

$$k(3,5) = k(5,3) = k(3,11) = k(11,3) = -k(5,9) = -k(9,5) = -k(9,11) = -k(11,9) = 6EIy/L^2 \tag{5e}$$

$$k(4,4) = k(10,10) = -k(4,10) = -k(10,4) = GKt/L \tag{5f}$$

$$k(5,5) = k(11,11) = 4EIy/L \quad (5g)$$

$$k(6,6) = k(12,12) = 4EIz/L \quad (5h)$$

$$k(5,11) = k(11,5) = 2EIy/L \quad (5i)$$

$$k(6,12) = k(12,6) = 2Ez/L \quad (5j)$$

where E is the material modulus of elasticity, L is the member length, A is the cross section area, Iy and Iz are the moments of inertia of the cross section about the local principal y and z axes, respectively, and Kt is the torsional constant for the cross section. The bending stiffness is assumed to be independent of the load on the members, as described previously.

STATIC ANALYSIS COMPUTER PROGRAM

A computer program which uses the analysis procedure just described has been developed on the University of Pittsburgh DEC PDP-10 Computer System for analyzing three-dimensional cable stayed bridge structures under static dead and live load and user specified initial cable tensions. The Combined Approach is used to reduce the unbalanced loads in the system to an acceptable user specified level. The overall stiffness matrix for the system is recomputed at the beginning of each load increment in order to account for the nonlinear behavior of the system. Extensive studies, using mathematical models representing several actual or proposed bridges, have shown that it is usually sufficient to divide the unbalanced load into three increments during the first iteration cycle and then to apply the remaining unbalanced load in one increment for each succeeding cycle. The program has been developed so that the user can specify the number of load increments to be used.

NONLINEAR DYNAMIC ANALYSIS

The equations of motion for a lumped mass system subjected to a set of concentrated dynamic loads can be written in the form:

$$[M]\{A\} + [C]\{V\} + [K]\{D\} = \{W(t)\} \quad (6)$$

where [M], [C], and [K] are the mass matrix, the viscous damping matrix, and the stiffness matrix of the system; {D}, {V}, and {A} are the displacements, the velocities, and the accelerations corresponding to each dynamic degree of freedom at the mass points; and {W(t)} are the externally applied dynamic loads. If the variation of the loads is known with time, the displacements can be computed by solving the set of differential equations represented by equation (6). It will be found, however, that for most dynamic loads which are considered in the design of bridge structures, such as wind or seismic ground motion, it is not feasible to obtain an exact algebraic solution for the displacements. In a cable stayed bridge the solution procedure is further complicated by the changing stiffness of the cables, as described previously, thus, resulting in a variation of the

stiffness matrix [K] as the structure deforms. The only practical approach is to use some type of numerical procedure to solve the equations of motion.

Many different numerical procedures have been presented in the literature. Several popular methods, which have been shown to give acceptable results for the solution of structural dynamics problems are: the Average Acceleration Method [5]; the Newmark Beta Method [6]; and the Wilson Theta Method [7]. Each of these is a single step forward procedure, therefore, the change in stiffness of the structure can be easily considered by recomputing the stiffness matrix [K] corresponding to the deformed shape of the system at the beginning of each time step during the solution process. The change in the stiffness of the cables can be considered by using the equivalent modulus given previously in equation (2). This process has been used in the investigation reported here.

BEHAVIOR OF CABLE STAYED BRIDGE STRUCTURES

In order to investigate the behavior of cable stayed bridges, under static and dynamic loads, a number of analyses have been performed for several mathematical models with properties similar to actual or proposed bridges.

STATIC BEHAVIOR

The first results which will be presented correspond to a set of analyses designed to investigate the static behavior of cable stayed bridges under normal design loads. Figures 6 and 7 show the variation of the normalized vertical deflection at center span, with the static uniform deck load, for the mathematical models shown in figures 8 and 9, respectively. The mathematical model shown in figure 8 has the cables acting in two planes on either side of the roadway and has properties similar to the Luling Bridge located in Louisiana. The bridge represented by the mathematical model shown in figure 9 has a single cable plane in the center of the roadway and has properties similar to the proposed Weirton-Steubenville Bridge across the Ohio River. The individual curves in figures 6 and 7 correspond to different values of the initial cable tensions, ranging from 0.25 to 2.0 times the full design values for each cable.

These curves show that the load-displacement relationship is nonlinear for low values of the uniform deck load, however, as the load is increased up to a maximum of five times the full dead load, the relationship becomes more linear. For loads equal to the full dead load, or greater, the relationship is essentially linear for all initial cable tensions considered. For long span bridges the majority of the static design load is usually the dead load of the structure, therefore, the maximum loads considered in these analyses are much larger than any loading which might be expected under normal operating conditions. The nonlinear effect also decreases as the initial cable tension

is increased. Similar results were obtained for the other mathematical models which were considered in the investigation for other computed quantities, such as: the horizontal displacement at the top of the towers; the moments in the deck or the towers; and the final cable tensions [2].

The results of these analyses lead to the conclusion that a cable stayed bridge structure does behave in a nonlinear manner for low loads, however, after the full dead load deformed position has been reached, the structure can be considered to behave linearly. The tension in the cables apparently reaches a value such that the equivalent modulus, given in equation (2), can be considered to remain constant. This indicates that the stiffness of the structure, which is represented by the slope of the curves shown in figures 6 and 7, can be considered to be constant for static or dynamic live loads. This means that linear analysis techniques, such as influence lines for static loads and the Response Spectrum Method for dynamic loads, are applicable to this type of structure, starting at the dead load deformed position. However, if an accurate solution is to be achieved, the nonlinear behavior of the structure under the initial dead load should be considered to arrive at the correct stiffness to be used in the linear analysis.

DYNAMIC BEHAVIOR

In order to investigate the dynamic behavior of cable stayed bridges, several time history analyses were performed, for a mathematical model representing an actual bridge, for several different dynamic loadings [8, 9]. One of the loadings which was considered was the ground motion due to the vertical component of the May 18, 1940, El Centro, California Earthquake. The purpose of the time history analyses was not to investigate the level of stress produced in the structure, but rather to investigate the degree of nonlinear behavior. It was assumed that the material in the bridge remained elastic during the dynamic response. The only source of nonlinear behavior which was considered was the cable sag.

The mathematical model considered for the time history analyses was a single load bearing plane of the Norbruke Bridge in Dusseldorf, Germany as shown in figure 10. The mathematical model consisted of 22 nodes and 31 members. The mass was assumed to be lumped at the nodes and only the translational degrees of freedom were considered.

In order to perform a dynamic time history analysis, the stiffness of the structure must be known for any deformed position of the structure during the response. It was assumed in the analyses reported here that the structure started at rest in the dead load deformed position. Therefore, before a dynamic analysis could be performed it was necessary to perform a static analysis to compute the stiffness of the structure under the static dead load. The static analysis procedure described previously was used.

Three distinct types of analyses were performed consisting of the following combinations of static and dynamic analysis; linear static analysis to compute the structure stiffness in the static dead load deformed position and linear dynamic analysis, in which the stiffness is assumed to remain constant, hereafter denoted as Linear-Linear; nonlinear static analysis and linear dynamic analysis, hereafter denoted as Nonlinear-Linear; and nonlinear static analysis and nonlinear dynamic analysis, in which the stiffness is recomputed corresponding to the deformed shape of the structure at the beginning of each dynamic time step, hereafter denoted as Nonlinear-Nonlinear. The combination of linear static analysis and nonlinear dynamic analysis was not considered.

Figure 11 shows the variation of the undamped vertical displacement of the deck at center span, for the three types of analyses just described, for the El Centro ground motion. It can be seen that the Nonlinear-Linear and Nonlinear-Nonlinear analyses gives almost identical results, which vary considerably from the Linear-Linear analysis. Similar results were obtained for the variation of the tension in one of the cables as shown in figure 12. Again, the plotted points for the Nonlinear-Linear and Nonlinear-Nonlinear analyses fall almost on top of each other and are distinctly different than the Linear-Linear analysis. The results of these analyses, and several other analyses which were performed for both a simulated dynamic wind loading and a moving traffic load [8], indicate that although a nonlinear static analysis is required to obtain the stiffness of the structure in the dead load deformed position, a linear dynamic analysis will suffice starting at this position. This is an important conclusion since a linear time history dynamic analysis is much simpler and more economical to perform than a nonlinear analysis. Also, this permits the use of strictly linear analysis techniques, such as the Response Spectrum Method. The application of this procedure to the dynamic analysis of cable stayed bridges is presently being investigated in the research program being performed at the University of Pittsburgh.

SUMMARY AND CONCLUSIONS

It has been shown that even though a cable stayed bridge does behave in a nonlinear manner under applied load, it can be considered to be a linear system for static or dynamic live loads. The stiffness of the system increases as the load is increased until it reaches essentially a constant value under the action of the full dead load. Starting at the dead load deformed position linear analysis procedure can be used to determine the response of the bridge under static or dynamic live loads.

ACKNOWLEDGMENTS

The investigation reported here was sponsored in part by National Science Foundation Grant PFR-7923023 to the University of Pittsburgh with John F. Fleming as principal investigator.

REFERENCES

1] Kokoski, D. L., "Three Dimensional Nonlinear Analysis of Cable Stayed Bridge Structures," M.S. Thesis, Department of Civil Engineering, University of Pittsburgh, 1979.

2] Fabian, R. A., "Behavior of Cable Stayed Bridges and Techniques for Their Analysis," M.S. Thesis, Department of Civil Engineering, University of Pittsburgh, 1980.

3] Zenk, J. D., "Static and Dynamic Analysis of Cable Stayed Bridges," M.S. Thesis, Department of Civil Engineering, University of Pittsburgh, 1982.

4] Ernst, J. H., "Der E-Modul von Seilen unter Berucksichtigung des Durchanges," Der Bauingenieur, February 1965.

5] Fleming, J. F. and J. P. Romualdi, "A General Procedure for Calculating Dynamic Response Due to Impulsive Loads," Journal of the Franklin Institute, Vol. 275, No. 2, February 1963.

6] Newmark, N. M., "A Method of Computation for Structural Dynamics," Proceedings of the American Society of Civil Engineers, Vol. 85, No. EM3, July 1959.

7] Wilson, E. H., "A Computer Program for the Analysis of Underground Structures," SESM Report 68-1, Department of Civil Engineering, University of California, Berkeley, 1968.

8] Egeseli, E. A., "The Nonlinear Dynamic Response of a Cable Stayed Girder Bridge to Various Loadings," Ph.D. Dissertation, Department of Civil Engineering, University of Pittsburgh, 1975.

9] Fleming, J. F. and E. A. Egeseli, "Dynamic Behavior of a Cable Stayed Bridge," Journal of Earthquake Engineering and Structural Dynamics, Vol. 8, No. 1, 1980.

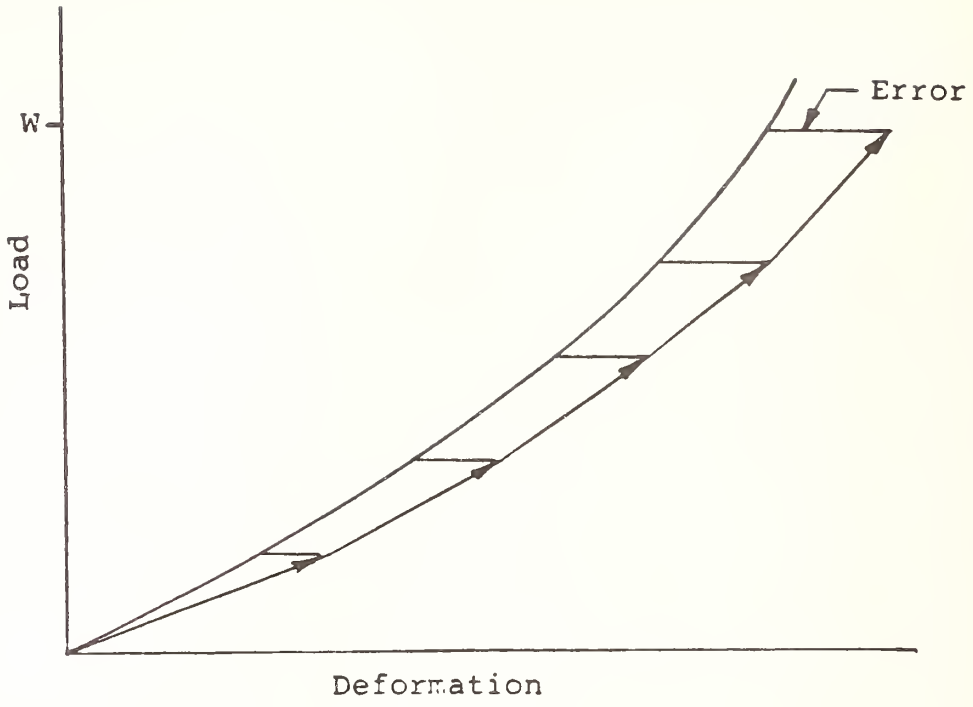

Figure 1. Incremental approach

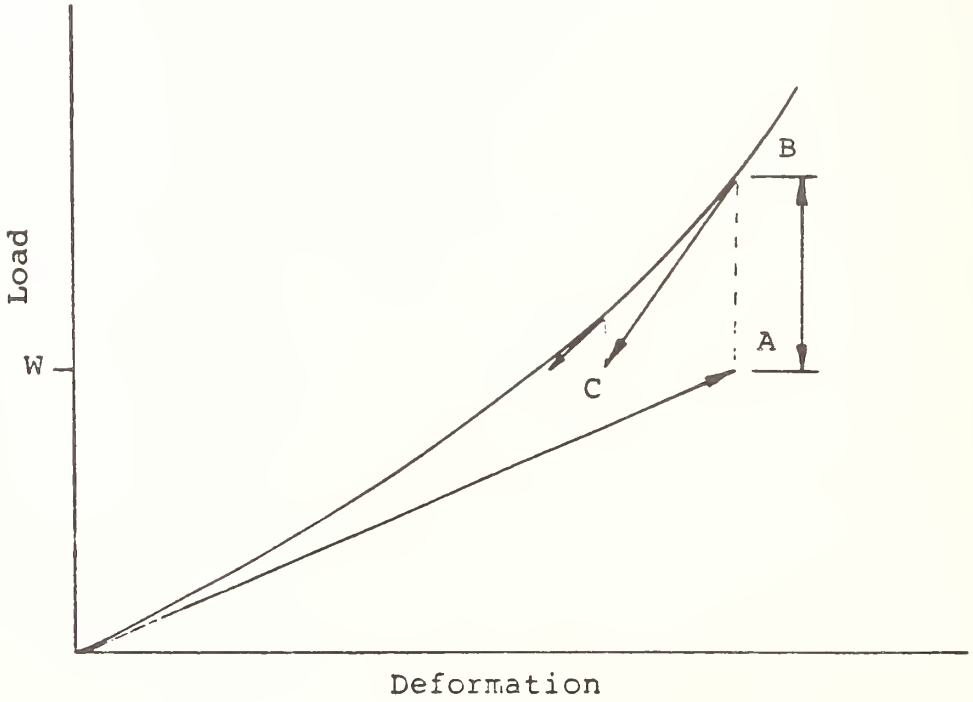

Figure 2. Iterative approach

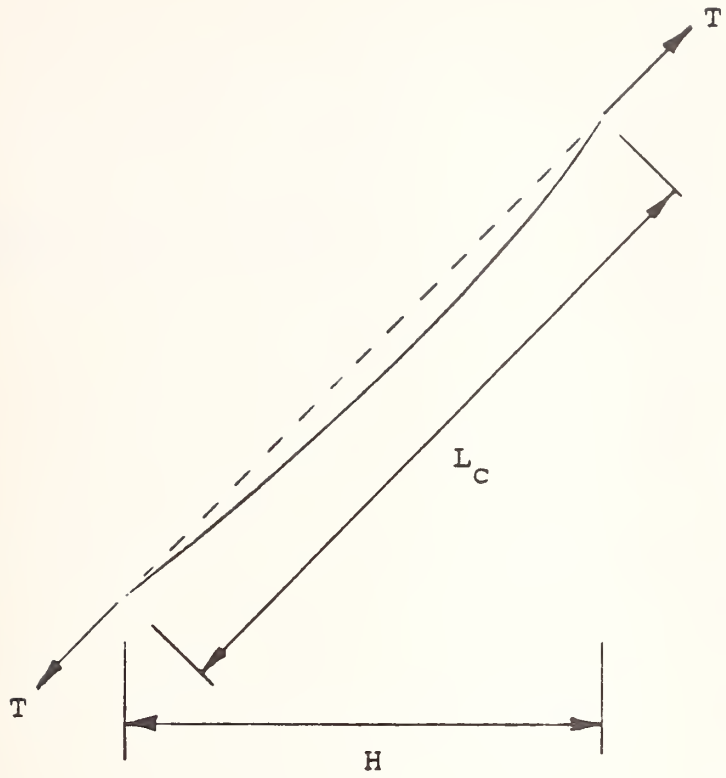

Figure 3. Inclined cable member

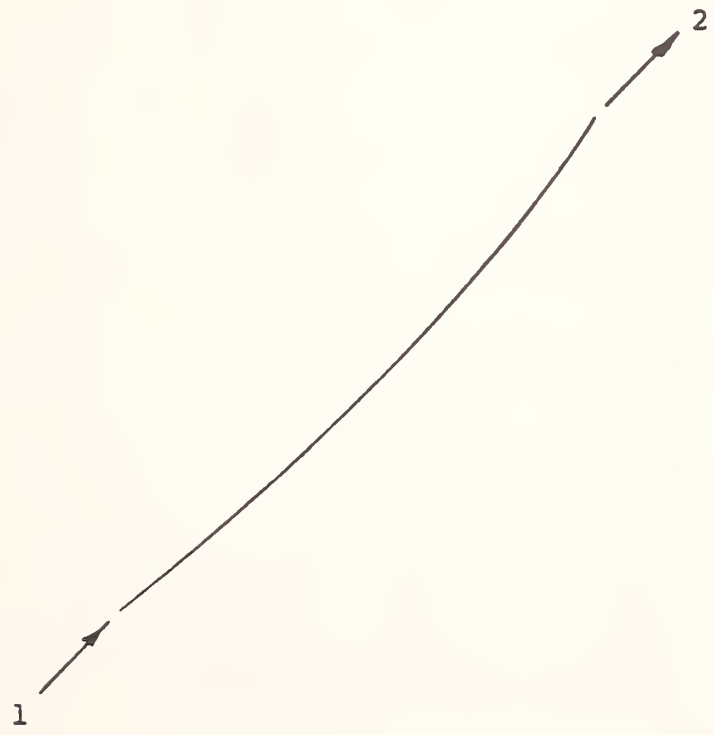

Figure 4. Local cable member coordinate system

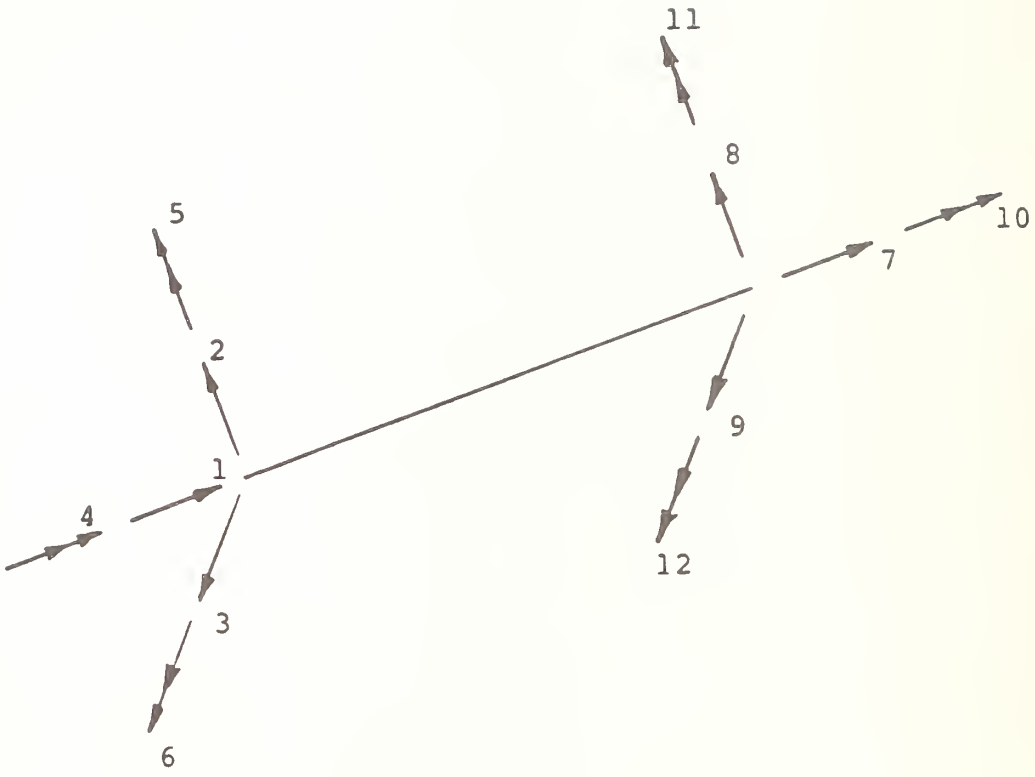

Figure 5. Local bending member coordinate system

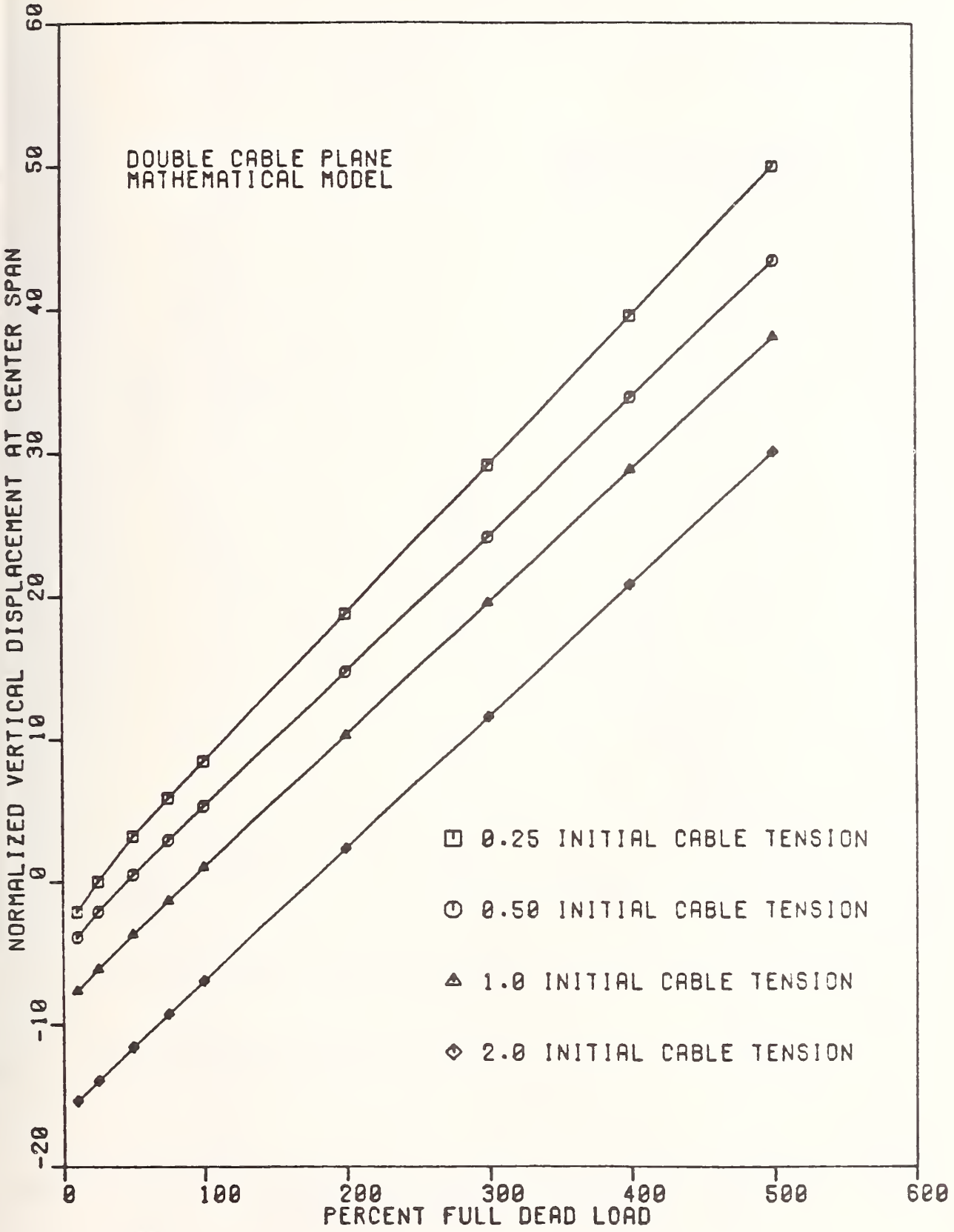

Figure 6. Effect of cable non-linearity

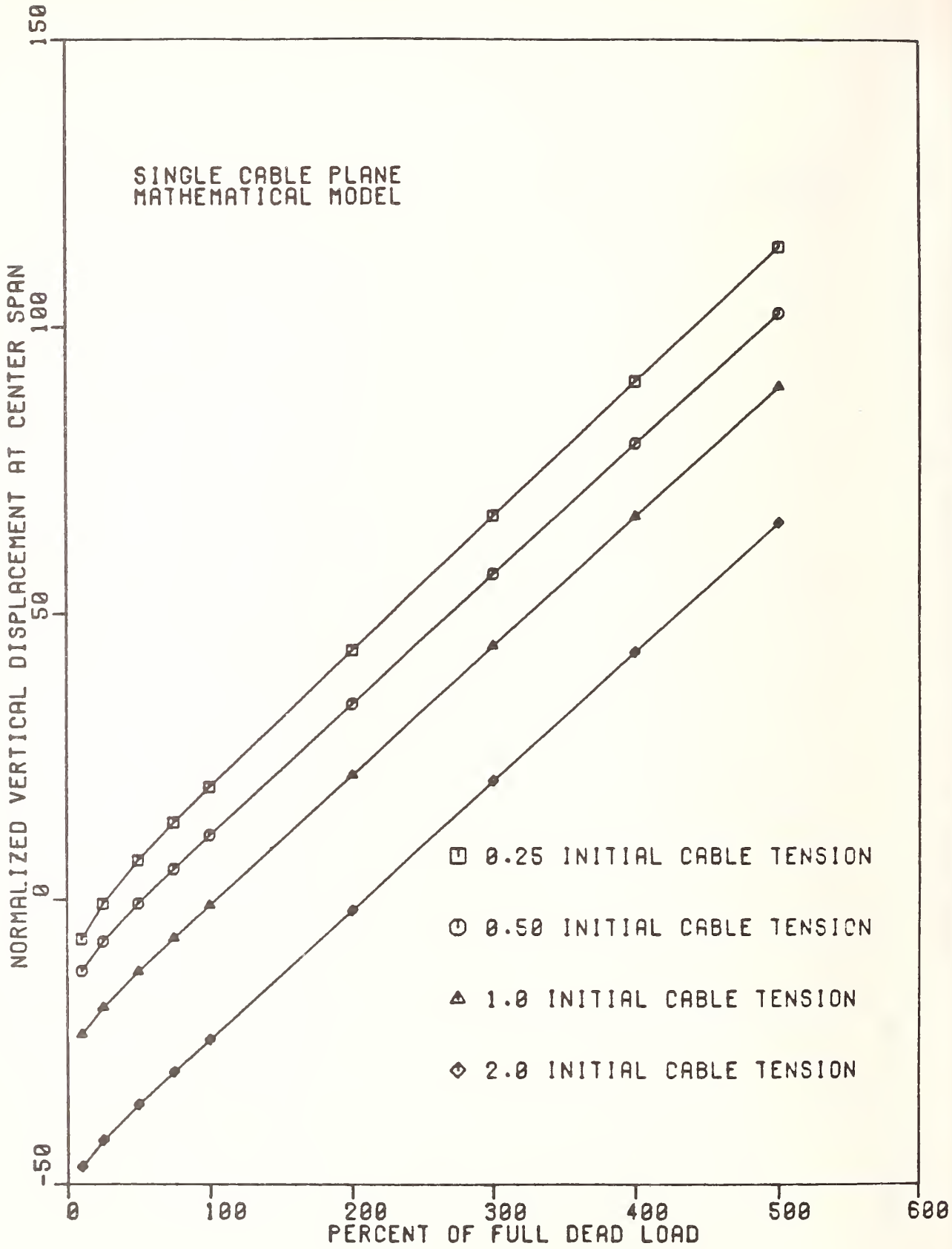

Figure 7. Effect of cable non-linearity

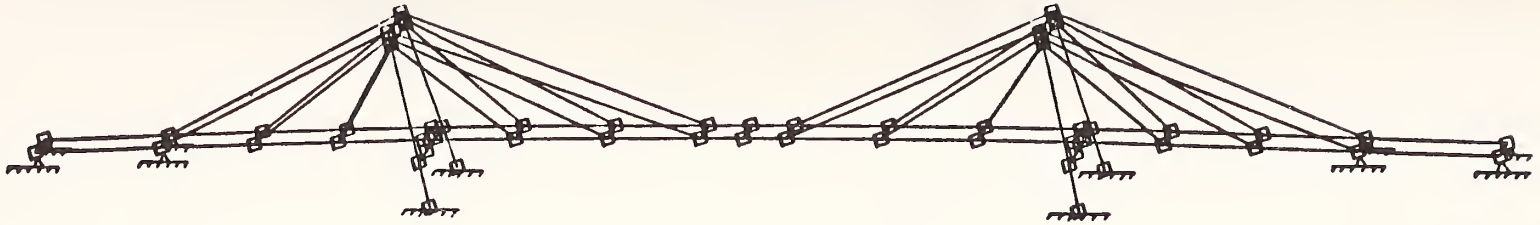

Figure 8. Double cable plane mathematical model

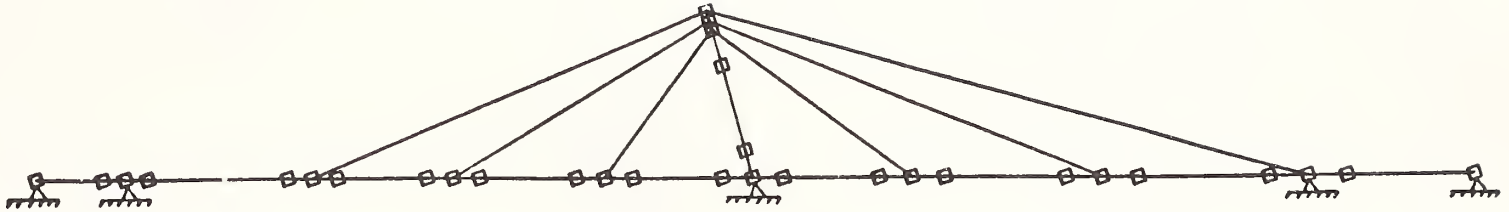

Figure 9. Cable plane mathematical model

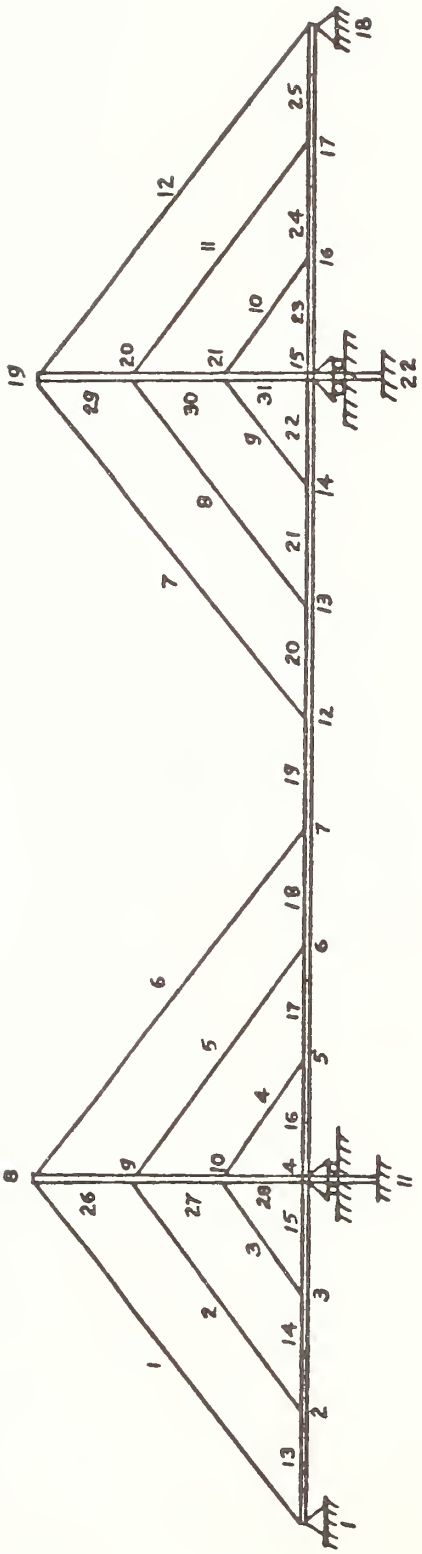
1
2
3
4
5
6
7
8
9
10
11
12
13
14
15
16
17
18
19
20
21
22
23
24
25
26
27
28
29
30
31

Figure 10.

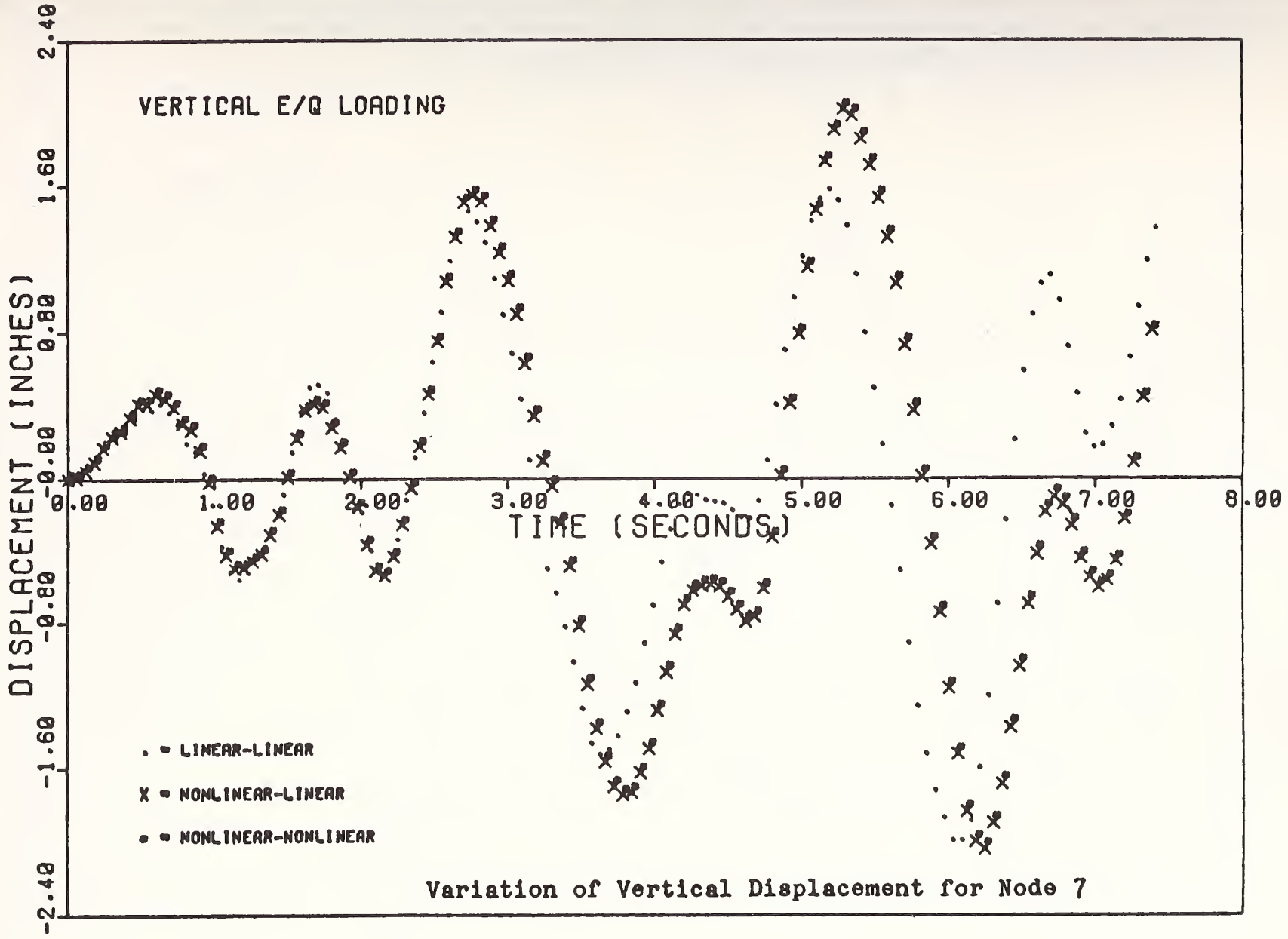

Figure 11. Variation of vertical displacement for Node 7

Variation of Tension in Cable 1
VERTICAL E/Q LOADING
CHANGE IN TENSION (K)
TIME (SECONDS)
. = LINEAR-LINEAR
X = NONLINEAR-LINEAR
• = NONLINEAR-NONLINEAR
-120.00
-80.00
-40.00
0.00
40.00
80.00
120.00
0.00
1.00
2.00
3.00
4.00
5.00
6.00
7.00
8.00

BEHAVIOR OF CONCRETE-FILLED STEEL TUBES

Nobuyuki Narita
Shoichi Saeki
Michio Kanai
Toshio Ohshio

Ministry of Construction
Public Works Research Institute

ABSTRACT

In our country, bridge piers are subjected to strong motions due to earthquake. Furthermore, size of bridge piers are strictly limited in metropolitan highways and in monorails. High ductility and high resistance is, therefore, required for bridge piers in Japan. In this regard, use of concrete-filled steel tubes is examined.

Steel tubes have very high resistance; however, steel tubes are liable to yield by local buckling and to lose ductility after yielding. Concrete piers with adequate reinforcing have good ductility; however, they are large-sized. Concrete-filled steel tubes are thin steel tubes with concrete and shear connectors in the tubes. When they are subjected to a strong motion, the concrete prevents the local buckling of thin steel tubes and the steel tubes give adequate reinforcing to the concrete. Therefore, even small-sized concrete-filled steel tubes have excellent ductility and resistance.

Sometimes, concrete-filled steel tubes have been used for bridge piers or building members. However, they were used just to increase the rigidity of the members or to stiffen the steel tubes, and were not designed as composite structures. In our report, the concrete-filled steel tubes are regarded as composite structures to expect higher resistance and ductibility. At present, many problems are not resolved to design concrete-filled steel tubes as composite structures, such as provisions for shear connectors, plate thickness and so on. These problems are examined in detail in this paper. Based on the results of full-size tests, design recommendations are presented.

The following reports are coming in series.

Part I Compression Members

Part II Long Columns

Part III Bending Members

Part IV Beam Columns

INTRODUCTION

Bridge piers should be designed to resist earthquakes which are expected during the lifetime of the structures. However, we may state that it is a waste of the national budget to construct bridge

piers which can resist the severest earthquake. In this regard, the concept of "minimum total cost" should be introduced.

Brittle structures which may cause disasters due to the collapse of the structures should be avoided as much as possible. On the other hand, ductile structures may have some local failures, but they will not lose resistance even in the region of large deformations. This approach is, therefore, desirable for bridge piers. Examples of both types of structures are given in figure 1. For example, figure 1(a) shows a ductile structure and figure 1(b) shows the brittle structures.

Steel tubes are ductile or brittle depending on the Diameter/thickness ratio (D/t). Thin steel tubes are economical in elastic design, but they are usually brittle. Thick steel tubes are usually ductile, but they are not economical in elastic design. Therefore, it is very difficult to determine the adequate D/t value for bridge pier design.

In this regard, the behavior of composite concrete-filled steel tubes is excellent. Concrete prevents the local buckling of thin steel tubes, while the steel tubes give adequate reinforcing to the concrete. Therefore, concrete-filled steel tubes have excellent resistance and ductility. However, we do not have good specifications to design the concrete-filled steel tubes as composite structures. In the following chapters, the behavior of the concrete-filled steel tube is examined in detail based on the full-size tests with a 3000 ton testing machine at the P.W.R.I. The test results of the short compression members are described.

DESIGN PROBLEMS OF CONCRETE-FILLED STEEL TUBES

Concrete-filled steel tubes are sometimes used for bridge piers and building members; however, they are used to provide rigidity to the members or to stiffen the local buckling resistance of the steel tubes. Higher economy can be expected by designing the concrete-filled steel tubes as steel-concrete composite structures. In this regard, the following problems should be addressed.

1) When the steel and concrete are both elastic, Poisson's ratio of the concrete (about 1/6) is much smaller than that of the steel (about 0.3). Therefore, under axial compression, concrete and steel will separate from each other in a cross section (figure 2). When steel and concrete are connected by studs or other means, steel will be subjected to compression in the hoop direction. On the other hand, when steel and concrete are not connected, they both will behave independently, and they will not be a composite structure. Therefore, how to provide adequate bond between steel and concrete is a important problem. Natural bond may not be enough and studs may be required.

2) When steel and concrete become plastic, Poisson's ratio of the concrete increases to about 0.5 which is much larger than that of the steel. Therefore, steel tubes will be subjected to tension

in the hoop direction. At this time, steel and concrete will behave together without the bond, and high resistance and ductility are expected. These effects should be examined.

3) The behavior described above is affected by many factors such as plate thickness, concrete strength, steel strength, arrangement of studs and many others. These interrelations should be investigated and design specifications should be provided.

In this report, the above problems are examined. Meanwhile, the following problems should be further studied to give complete design specifications. These will be described in the coming reports in this series.

4) Under bending, concrete will be subjected to tension, and may result in cracking. Resistance and rigidity of concrete-filled steel tubes under bending should be, therefore, examined. At the same time, arrangement of shear connectors should be examined.

5) Under repeated loading the resistance of concrete-filled steel tubes may decrease, due to the extension of cracking, the accumulation of plastic strain, the stress concentrations around studs and so on. Furthermore, the bond between concrete and steel may be lost. The aspects should be examined in detail.

6) The resistance of long columns composed of concrete-filled steel tubes should be examined. The evaluation of slenderness ratio is very complicated in composite structures.

OUTLINE OF THE TESTS

In the compression tests, ten full-scale specimens were fabricated. A full-size specimen is needed to provide studs inside the steel tubes, and to examine the bond problem in detail. The configuration of the specimens are shown in figure 4, and the specifications shown in table 1.

Steel plate materials is SM 50Y, which has nominal yield strength of 3600 kg/m^2. Tensile strength of the material was tested by test pieces taken from bent up steel tubes. The results are shown in table 2.

The steel tubes are bent up as shown in Photo 1, and welded from inside and outside as shown in Photo 2 and Photo 3. The welding was carried out as shown in figure 5 and table 3. The studs were welded by a stud-gun, as shown in Photo 4.

The specifications for the concrete and the concrete strength are shown in table 4. After casting the concrete, the concrete will shrink to some extent which will prevent uniform loading of the specimen. Therefore, non-shrinkage mortar was cast at the top and bottom of the specimen three weeks after casting the corner, and then top and bottom plates were welded to the specimen. Both top and bottom plates were machined in order to obtain uniform loading (Photo 5 - Photo 7).

Specimens A-1 to A-4 are steel tube specimens without concrete in them. A-3 is same as A-2, but it is for cyclic loading.

Specimens B-1 to B-6 are concrete-filled steel tubes. B-1 to B-4 are the same ones as A-1 to A-4 respectively, except for the concrete and the studs in them. B-5 is the same as B-2, but it is not provided with studs. B-6 is also the same as B-2, but it has high strength concrete in it.

In the tests, total deformation, strain of the steel tubes (128 points) and out-of-plane deflection of the steel tubes (52 points) were measured by a computer system. Figure 6 shows the strain gauges. Figure 7 shows the measurement of out-of-plane deflection. Photo 8 shows the testin machine and the measurement system.

TEST RESULTS AND ANALYSIS

RESISTANCE OF CONCRETE-FILLED STEEL TUBES

The theoretical values and the test results of the resistance of the specimens are listed in table 5. Effects of residual stresses and initial deflections are considered in the following Donnell-Wan equations:

$$\sigma_{cr} = \sigma_y \left(N - \sqrt{N^2 - \sigma_{c\ell}/\sigma_y}\right) \qquad (1)$$

in which

σ_{cr} = local buckling strength, where effects of initial imperfections are considered,

σ_y = yield strength of the steel

$\sigma_{c\ell}$ = elastic local buckling strength of the steel tube, which is obtained from

$$\sigma_{c\ell} = \frac{E}{\sqrt{3\ (1 - \nu^2)}} \frac{t}{R}$$

E, ν = modulus of elasticity and Poisson's ratio of the steel, respectively

R, t = radius and plate thickness of the steel tube, respectively

N = constant obtained from

$$N = \frac{1}{2}\left(1 + \frac{\sigma_{cl}}{\sigma_y} + \frac{U.E}{2\sigma_y}\right)$$

U = measure of initial imperfections

$U = 0.001$ is recommended on the Highway Bridge Specifications in Japan

S_y = resistance of the steel tube, obtained from the yield strength of the steel.

In table 5, the resistance of the specimens A-1 to A-4 is sometimes lower than the theoretical values (S_b), because of the effects of initial imperfections which is significant in the thin plate steel tubes.

The following three cases can be considered in regard to the theoretical resistance of the specimens B-1 to B-6.

Case 1: When the steel tube and the concrete behave independently, the resistance will be $S_c + S_b$.

Case 2: When they are connected together, the concrete will prevent local buckling of the steel tube when the resistance will be $S_c + S_y$.

Case 3: When the concrete is confined by the hoop tension of the steel tube in the plaste region, the concrete strength will be higher than the cylinder strength; then, the resistance will be higher than $S_c + S_y$.

Table 5 shows that the resistance of the specimens B-1 to B-3 is about the same as $S_c + S_y$, because even in these thin-plate specimens, local buckling is prevented by the concrete. The resistance of the specimen B-4 is higher than $S_c + S_y$, because the thin steel tube confines the concrete and the concrete strength is higher than the cylinder strength. Therefore, the resistance (or axial capacity) of case 2 is expected in the thin plate concrete-filled steel tubes and the resistance (or axial capacity) of case 3 is expected in the thin plate cases.

On the other hand, the resistance of B-5 is smaller than that of B-2, and it is nearly the same as the resistance of case 1 where the steel tube and the concrete behave independently. Studs may be, therefore, needed to obtain the resistance of case 2.

Finally, the resistance of the specimen B-6 is much higher than $S_c + S_y$, that is, the resistance of case 3 is obtained. The steel tube of B-6 is the same as that of B-2, i.e., it is a rather thin plate. Actually, the resistance of B-2 was that of case 2.

Therefore, the status of the concrete is another important factor in estimating the total resistance. In the B-2 specimen, the concrete was broken into small blocks in the plastic region, but the higher strength concrete of B-6 specimen was not broken even in plastic region. This is why high resistance was obtained in the B-6 specimen. Therefore, high-strength or high-quality concrete is needed to expect the resistance of case 3.

DUCTILITY OF CONCRETE-FILLED STEEL TUBES

The ductility of the specimens can be examined by load-deformation curves, which are shown in figures 8 through 17.

Figures 8 through 10 shows that the thin plate steel tubes have small ductility, and lose strength after attaining the maximum strength. Photo 9 shows the local buckling of specimen A-2 which caused the loss of ductility. Figure 11 shows that the thick plate steel tube had good ductility. The thick plate steel tube will not undergo local buckling as shown in Photo 10.

Figures 12 through 17 show that even thin plate concrete-filled steel tubes have good ductility.

Furthermore, the ductility is not lost in repeated loadings. Therefore, concrete-filled steel tubes are good for bridge piers as far as compression members are concerned. Even specimen B-5 without studs showed good ductility.

Photo 11 shows specimen B-2 after loading. Concrete-filled steel tubes are also subject to local buckling as shown in the photo. However, even in the plastic region, the local buckling did not spread out, and the specimen did not lose its capacity. Photo 12 shows the specimen B-3 which was loaded to the large-deformation region. At that time, the pipe diameter was increased significantly at the center due to hoop tension. However, it did not lose its axial capacity. Therefore, as far as hoop tension action is concerned, concrete-filled steel tubes will keep their ductility.

In the previous section, it was mentioned that high strength concrete was required to provide the resistance of case 3. It really depends on whether the concrete is broken or not. Photo 13 shows the concrete after loading, where no local buckling of the steel tube is observed. Photo 14 shows the concrete where local buckling is observed. In the Photo 14, the concrete is broken in small blocks. It is reasonable to conclude that, if the concrete is strong enough, the concrete will not be broken even in the plastic region. Therefore, the capacity of case 3 can be expected. If the concrete is not strong enough, the concrete will be broken into small blocks in the plastic region. At that time, the resistance of case 3 cannot be expected, as the hoop tension is not great enough. Actually, specimen B-6 did not show any local buckling, thus showed the resistance of case 3 (Photo 15).

In the load-deformation curves shown in figures 12 through 17, the rigidity of the specimens are somewhat lower than the theoretical value. The stress-strain relationship concrete given in equation (2) is used for theoretical relationship.

$$\sigma = \sigma_{ck} \frac{\varepsilon}{0.002} \left(2 - \frac{\varepsilon}{0.002}\right) \quad 0 < \varepsilon < 0.002 \tag{2}$$

In the equation, the ratio of the modulus of elasticity is 8.5 at $\varepsilon = 0$, which is reasonable for concrete.

The following comments are given to explain the above.

1) The residual stresses due to the studs may bring about lower rigidity. Actually, specimen B-5 which has no stud, shows relatively high rigidity.

2) It is reported that the quality of the cast concrete and its curing in the airtight condition in a pipe is not preferred. Therefore, the rigidity of the concrete itself might have been lower than expected.

BEHAVIOR OF LONGITUDINAL STRAIN

Figures 18 through 27 show the behavior of the longitudinal strains of the specimens. All the strains were measured at the surface of the steel tubes. The figure shows the strains where local buckling was observed. Therefore, local buckling behavior can be observed from the figures.

Figures 18 through 20 show that local buckling of the specimens is essentially elastic, because they are thin plate steel tubes. Figure 21 shows that specimen A-4 did not attain local buckling and showed only elasto-plastic behavior.

Figures 22 through 27 show some disturbance of the strains which may be caused by residual stresses due to the studs. They also show that the rigidity of the specimens is somewhat lower than the theoretical values, which was described in the previous section. But besides these, no special problem can be observed. The residual stresses due to studs may cause fatigue problems if subjected to large cyclic loadings. For bridge piers, this problem can be neglected.

Behavior of Hoop Strain

As described in chapter 2, the concrete and the steel tube of a concrete-filled steel tube will separate from each other in elastic region. Regarding the problem, the following theoretical solution may be obtained.

First, when the steel and the concrete behave independently, the hoop strains of the steel tube and the concrete is expressed by the following formulas.

$$\varepsilon_{hs} = -\nu_s \cdot \varepsilon_x \tag{3}$$

$$\varepsilon_{hc} = -\nu_c \cdot \varepsilon_x \tag{4}$$

where, ε_x equals the londitudinal strain, and ν_s and ν_c are the Poisson's ratios of the steel and concrete, respectively.

When the steel and concrete are connected together by the bond stress, σ_{co}, the hoop strain of the steel is expressed by the following (figure 28).

$$\varepsilon_{hs} = -\left(\nu_s \varepsilon_x + \frac{\sigma_{co} \cdot R}{Es \cdot t}\right) \tag{5}$$

where R and t are the radius and the thickness of the steel tube. The hoop strain of the concrete is

$$\varepsilon_{hc} = -\left(\nu_c \cdot \varepsilon_x - \frac{(1 - \nu_c)\ \sigma_{co}}{Ec}\right) \tag{6}$$

If the concrete and the steel behave together, ε_{hs} must be equal to ε_{hc}. Therefore, σ_{co} can be expressed as follows.

$$\sigma_{co} = \frac{\nu_c \cdot \nu_c}{[(R/t)/Es + (1 - \nu_c)/Ec]} \varepsilon_x \tag{7}$$

and ε_{hs} can be expressed as

$$\varepsilon_{hs} = - \varepsilon_x \quad \nu_s - \frac{\nu_x - \nu_c}{[1 + (1 - \nu_c)\frac{t.Es}{R.Ec}]} \tag{8}$$

Now, to examine the behavior of the concrete-filled steel tubes, where the maximum capacity is attained, let's assume that Es/Ec = 15.0. Assuming that σ_y = 4000 kg/cm^2, the required bond stress is expressed as follows:

$$\sigma_{co} = \frac{533}{R/t + 12.5} \text{ (kg/cm}^2\text{)} \tag{9}$$

and the hoop strain is expressed as follows, assuming that Es/Ec = 7.0 in this case

$$\varepsilon_{hs} = 0.3 - \frac{2}{15[1 + 5.83(t/R)]} \varepsilon_x \tag{10}$$

If the concrete and the steel behave independently, the hoop strain will be expressed by equation (3). If they behave together, the hoop strain will be expressed by equation (10), the required bond stress is expressed by equation (9).

When the bond is maintained, the Poisson's ratio of the specimen is not 0.3, but

$$0.3 - \frac{2}{15\ [1 + 5.83\ (R/t)]} ,$$

the modified Poisson's ratio. In table 6, the bond stress σ_{co} and the modified Poisson's ratio are listed.

Figures 29 through 38 show the behavior of hoop strains. In the figures, the theoretical curves obtained from equation (3) and equation (10) are also shown. The hoop strains of the specimens A-1 to A-4 are the same as the theoretical curves. The hoop strains of specimen B-1 to B-4 and B-6 are the same as the theoretical values, obtained from the modified Poisson's ratio. However, the hoop strains of specimen B-5 is closer to the theoretical values, obtained from a Poisson's ratio of 0.3. Therefore, it is concluded that the natural bond between concrete and steel is not enough to connect them together, and without studs, the concrete and the steel will behave independently. They will behave together with adequate studs. Therefore, studs may be required in the design of concrete-filled steel tubes to be used as composite structures.

CONCLUSIONS

The following conclusions about the behavior of concrete-filled steel tubes under compression are warranted.

1) When studs are provided, the sum of the steel yield strength and the concrete cylinder strength can be expected regardless of the steel plate thickness and the concrete strength. When a thicker plate is used, or high strength concrete is used, higher capacity can be expected because of the hoop tension action of the steel tubes.

On the other hand, when studs are not provided, the resistance of concrete-filled steel tubes will be the sum of the buckling strength of the steel tubes and the concrete cylinder strength, because they behave independently.

2) Concrete-filled steel tubes have good ductility, while steel tubes themselves usually have small ductility. Concrete-filled steel tubes will exhibit local buckling. Also, the concrete inside will be broken if: 1) the plate is not thick, 2) if the concrete is not of adequate strength, but it will not reduce the capacity nor the ductility significantly. In this case, the effect of hoop tension cannot be expected.

3) Judging from the hoop strain behavior, concrete-filled steel tubes without studs cannot be designed as composite structures. Adequate studs may be required for composite concrete-filled steel tubes.

REFERENCES

[1] Tomie, M. et a., "Design Problems of Concrete-Filled Steel Tubes," Column No. 73, 1979.7.

[2] Tomie, M. et al., "State-of-the-Art of Concrete-Filled Steel Tubes," Concrete Engineer, Vol. 13, No. 2, 3, 1975.

[3] Kishida, H. et al., "Bending Strength of Concrete-Filled Steel Tubes," JSSC, Vol. 15, No. 164.

[4] Oki, T. et al., "Concrete-Filled Steel Tubes in Compression," Journal of the Japan Socity for Architectural Engineers, Vol. 69, 1961.

[5] Saito, J. et al., "Concrete-Filled Steel Tubes with Low Strength Mortar," Report of Ohbayashigumi, Vol. 9, 1974.

[6] "Specification for Concrete-Filled Steel Tubes," Japan Society for Architectural Engineers, 1980.2.

[7] Donnell, L.H. and Wan, C.C., "Effect of Imperfections on Buckling of Thin Cylinders and Columns Under Axial Compression," Journal of Applied Mechanics, 1950.3.

[8] Gardner, N.J. and Jacobson, E.R., "Structural Behavior of Concrete-Filled Steel Tubes," ACI Journal, 1967.7.

[9] Neogi, P.K., Sen, H.K., and Chapman, J.C., "Concrete-Filled Tubular Steel Columns under Eccentric Loading," The Structural Engineer, No. 5, Vol. 47, 1969.5.

[10] Schilling, C.G., Buckling Strength of Circular Tubes, ASCE, Vol. 91, No. ST.5, 1965.

[11] Yamada, M., "Experimental Study on the Concrete-Filled Steel Tubes," Journal of the Japan Society for Architectural Engineers, Vol. 103, 1964.10.

[12] Oki, T., "Concrete-Filled Steel Tubes Under Eccentric Loading," Journal of the Japan Society for Architectural Engineers, 1965.9.

Table 1. Specifications for the Test Specimens

No.	Diameter x Plate Thickness	Concrete	Stud	Yield Strength of Steel	Concrete Strength	Remarks
A-1	700 x 6	without	without	4600	254	
A-2	700 x 8	without	without	4720	254	
A-3	700 x 8	without	without	4720	254	for cyclic loading
A-4	700 x 12	without	without	4000	254	
B-1	700 x 6	with	with	4600	224	
B-2	700 x 8	with	with	4720	254	for cyclic loading
B-3	700 x 8	with	with	4720	254	
B-4	700 x 12	with	with	4000		
B-5	700 x 8	with	without	4720	254	
B-6	700 x 8	with	with	4720	410	

Table 2. Yield Strength of Steel

Size	Yield Strength (kg/cm^2)	Breaking Strength (kg/cm^2)	Elongation (%)
ø 700 x 6	4570	5700	23.4
	4620	5750	23.0
	4630	5670	22.1
average	4600	5700	22.8
ø 700 x 8	4720	5650	25.8
	4720	5660	26.8
	4720	5620	25.7
average	4720	5640	25.8
ø 700 x 12	4000	5710	22.4
	4030	5770	22.1
	3970	5770	21.6
average	4000	5750	22.0
nominal	3700 up	5000 ~ 6200	15 up

Table 3. Specifications for Welding

Plate Thickness	Place	I	V	Velocity
12 (mm)	Inside	560A	38V	37cm/mm
	Outside	580	36	30
8	Inside	430	35	50
	Outside	580	38	45
6	Inside	370	32	85
	Outside	580	36	60

Table 4. Specifications for Concrete

Nominal	Unit	Water	Cement	Fine Aggregate	Coarse Aggregate
σ = 210 kg/cm^2	1 m^3	152 kg	249 kg	826 kg	1110 kg
σ = 400 kg/cm^2	1 m^3	151 kg	357 kg	650 kg	1179 kg

Concrete Strength

Nominal	(1)	(2)	(3)	Average
210	241	247	247	245
400	438	436	429	434

Table 5. Theoretical and Experimental Resistance

No.	Experimental Resistance	Theoretical Resistance					Experimental	Experimental
		Sc(t)	Sb(t)	Sy(t)	SC+Sb(t)	Sc+Sy(t)	Sc+Sb	Sc+Sy
A-1	540	---	567	602	567	602	0.95	0.90
A-2	753	---	786	821	786	821	0.96	0.92
A-3	760	---	786	821	786	821	0.97	0.93
A-4	1087	---	1010	1037	1010	1037	1.07	1.05
B-1	1509	911	567	602	1478	1513	1.02	1.00
B-2	1730	900	786	821	1686	1721	1.03	1.01
B-3	1722	900	786	821	1686	1721	1.02	1.00
B-4	2230	879	1010	1037	1889	1916	1.18	1.16
B-5	1694	900	786	821	1686	1721	1.00	1.10
B-6	2663	1595	786	821	2381	2416	1.12	1.10

Sc is the resistance of the concrete, obtained from concrete cylinder test result

Sb is the resistance of the steel tube, obtained from the local buckling strength of the steel tube.

Table 6. Modified Poisson's Ratio of the Specimens

Specimen	B-1	B-2 B-3 B-5 B-6	B-4
R/t	58.3	43.8	29.4
σ_{co} (kg/cm^2)	7.5	9.5	12.8
Modified Poisson Ratio	0.179	0.182	0.189

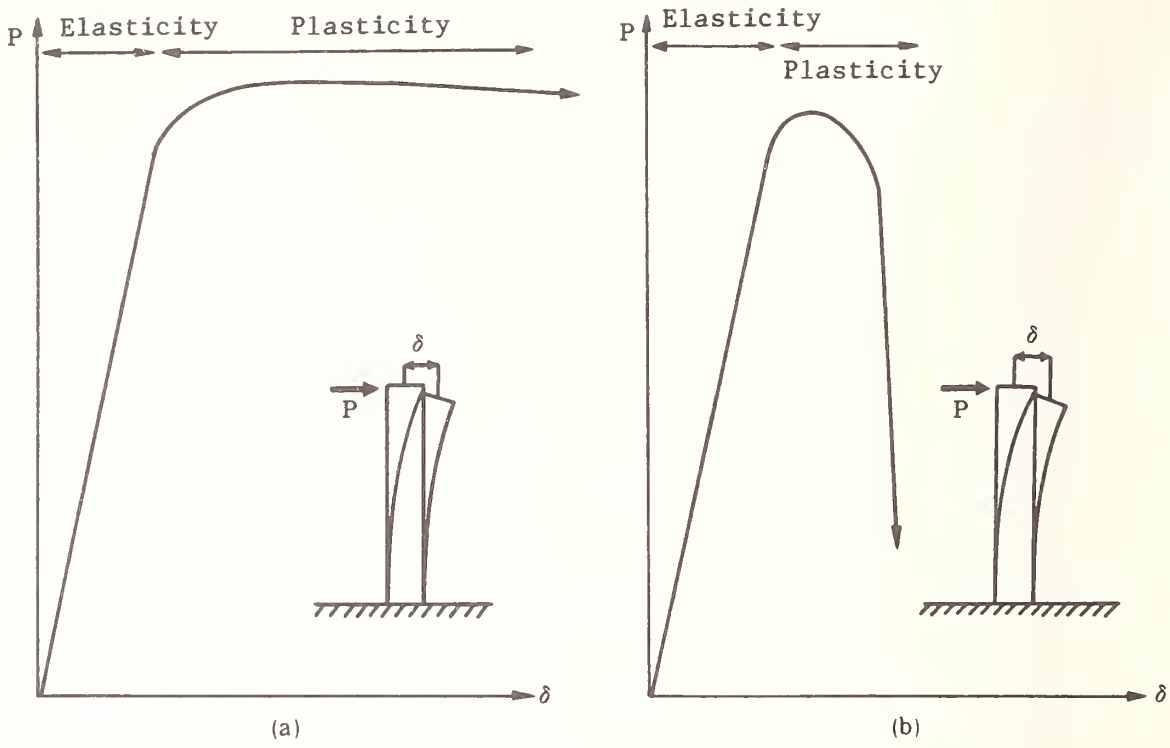

Fig. 1 Ductile and Brittle Structures

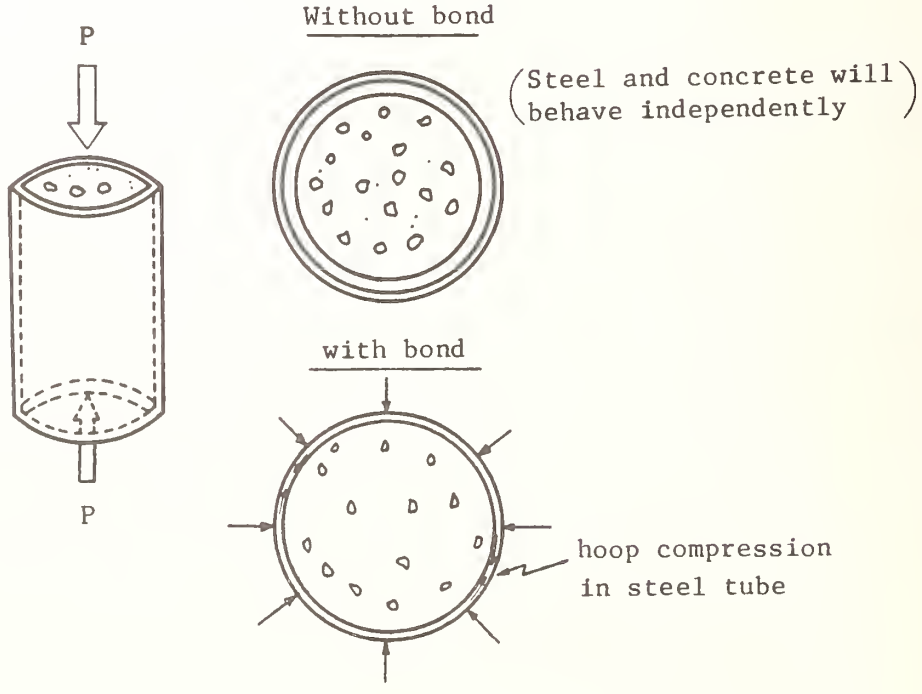

Fig. 2 Behavior in Elasticity

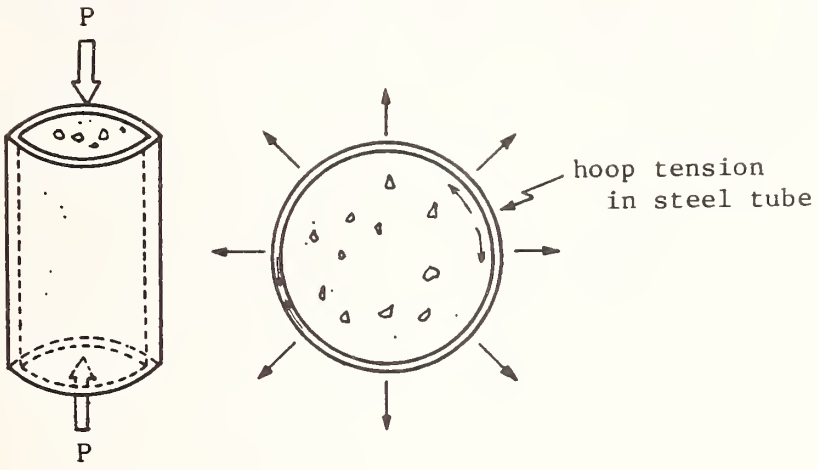

Fig. 3 Behavior in Plasticity

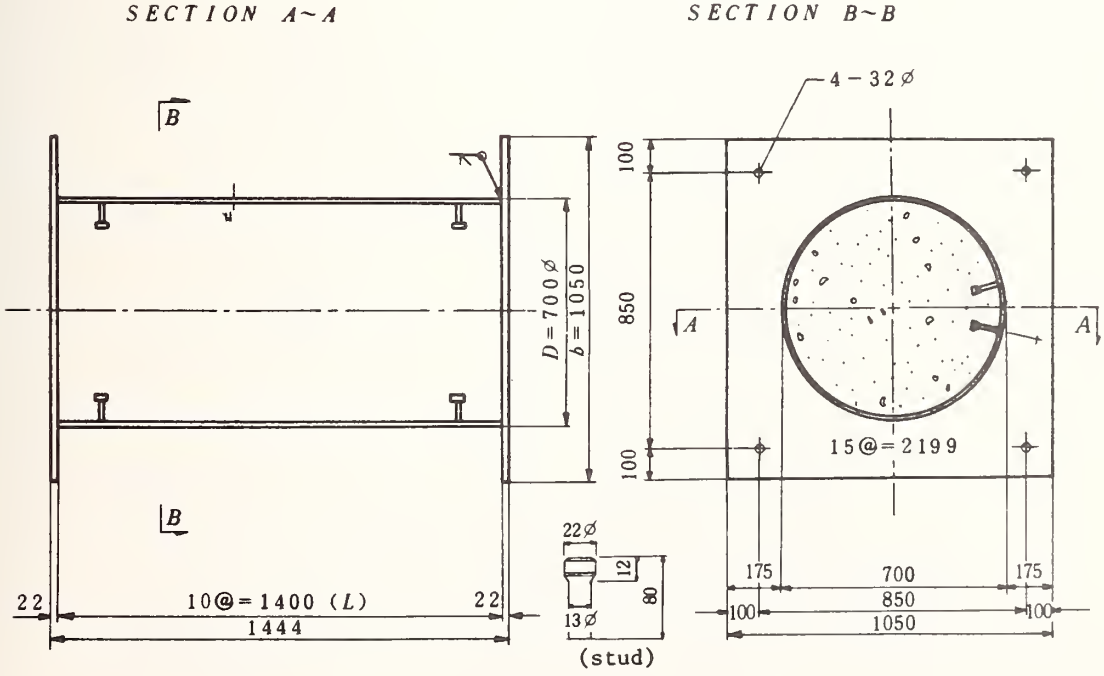

Fig. 4 Configuration of Test Specimen

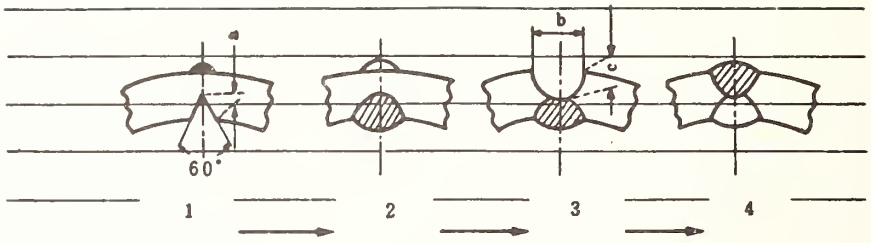

Dimensions

Plate thickness	a	b	c
12	3	10	5
8	2	8	3
6	2	-	-

Fig. 5 Welding Process

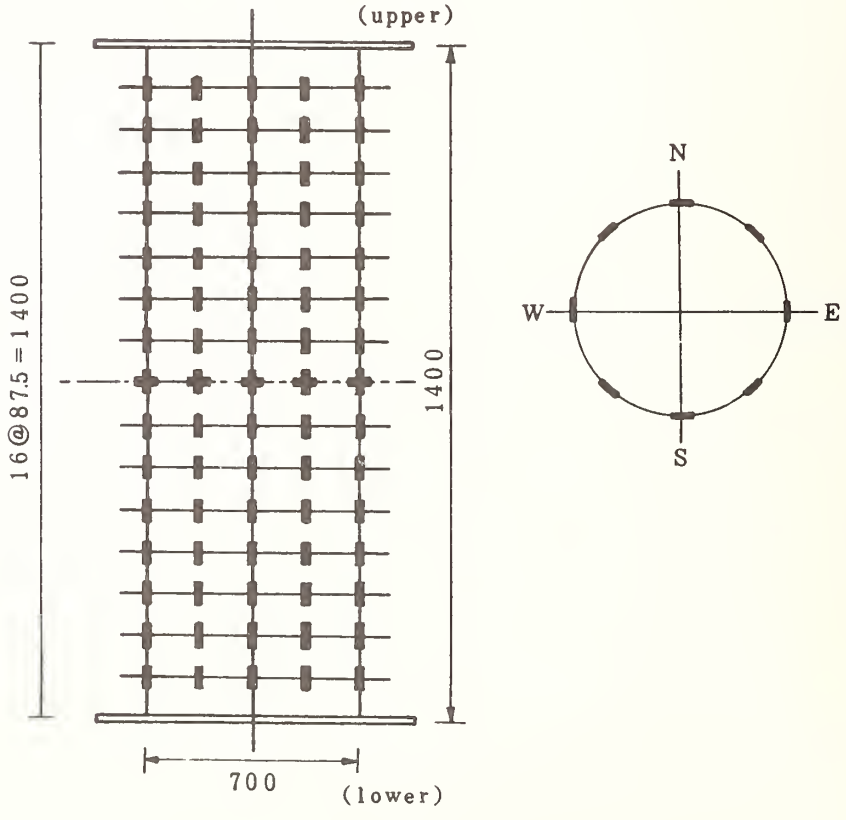

Fig. 6 Measurement of Strain

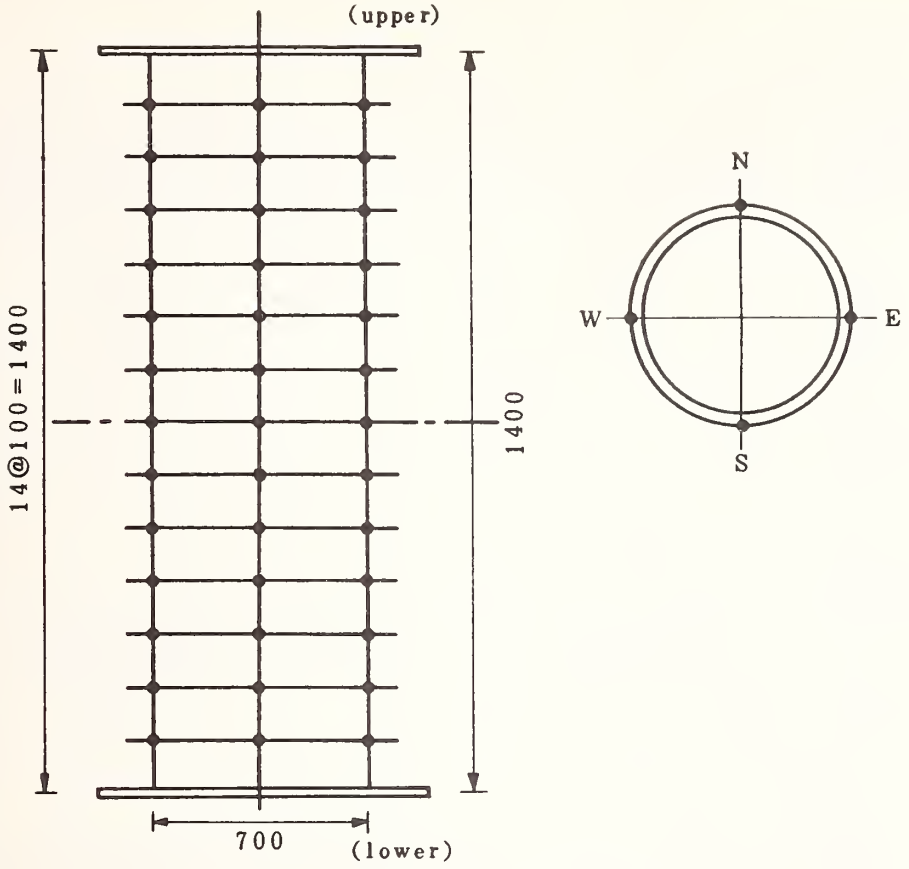

Fig. 7 Measurement of Out-of-Plane Deflection

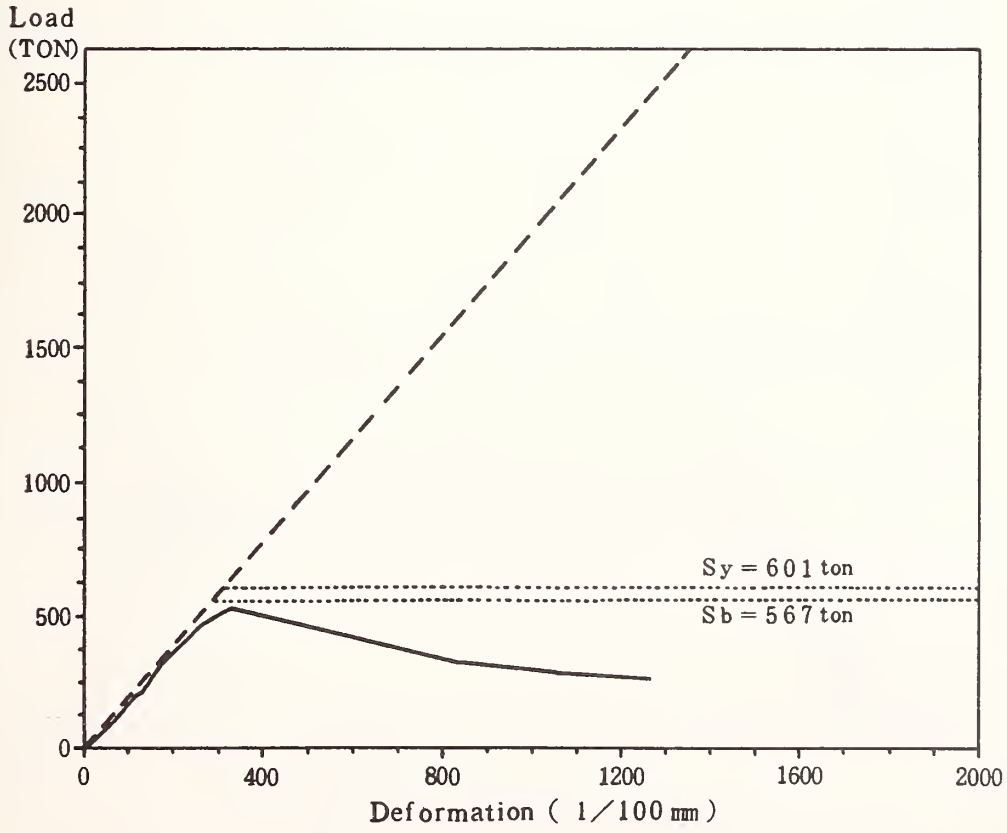

Fig. 8 Load - Deformation Curve (A - 1)

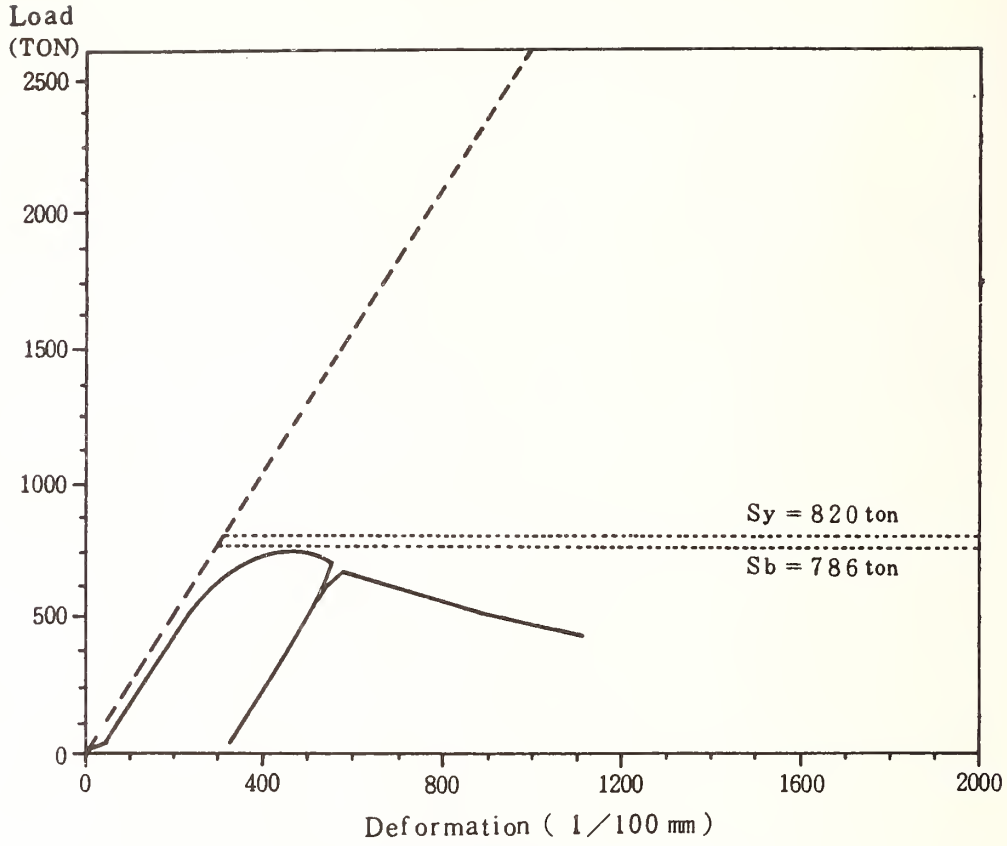

Fig. 9 Load - Deformation Curve (A - 2)

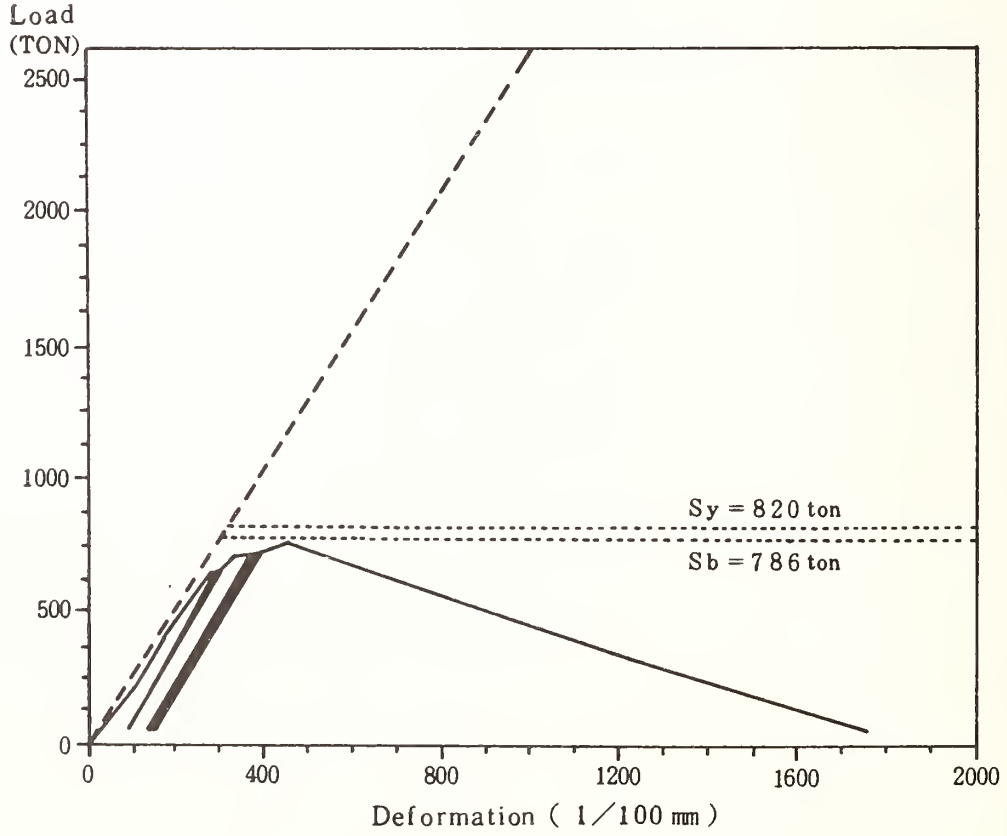

Fig. 10 Load - Deformation Curve (A - 3)

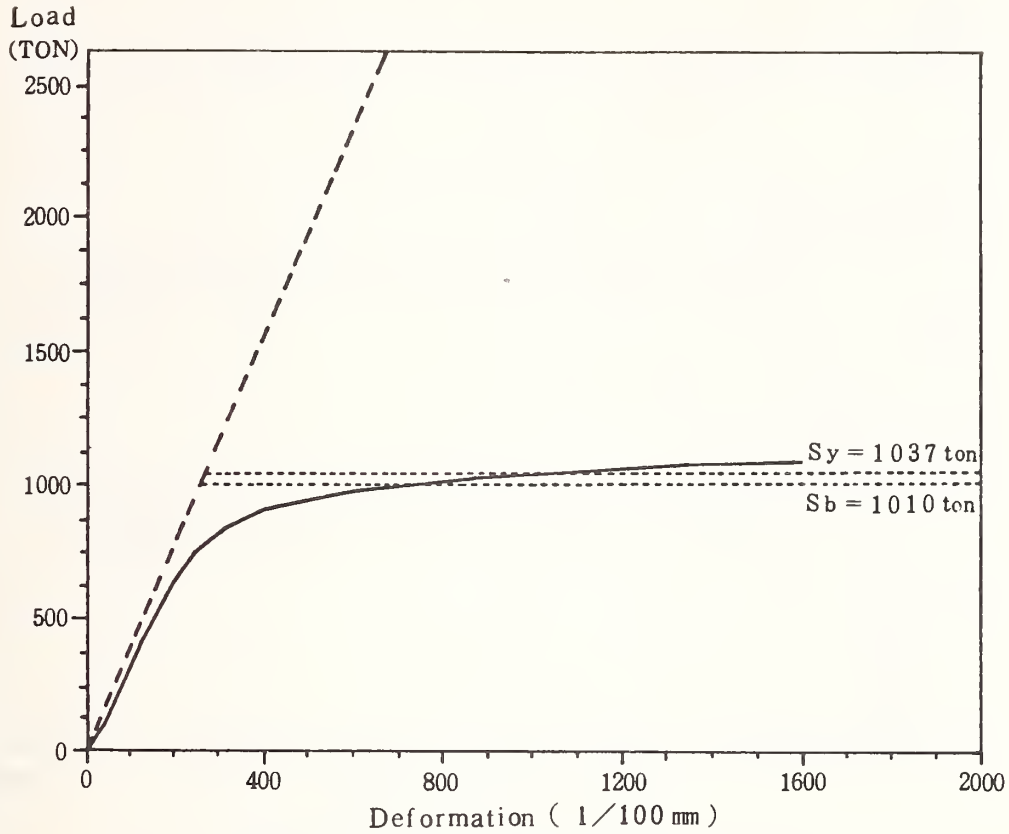

Fig. 11 Load - Deformation Curve (A - 4)

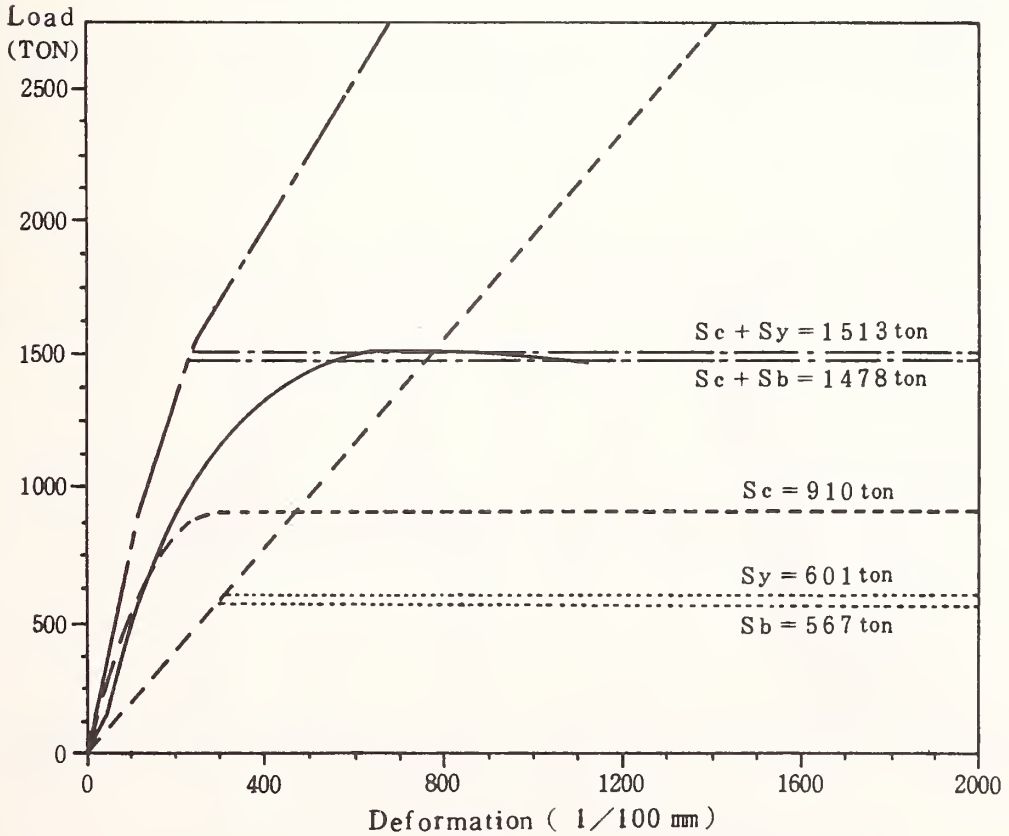

Fig. 12 Load - Deformation Curve (B - 1)

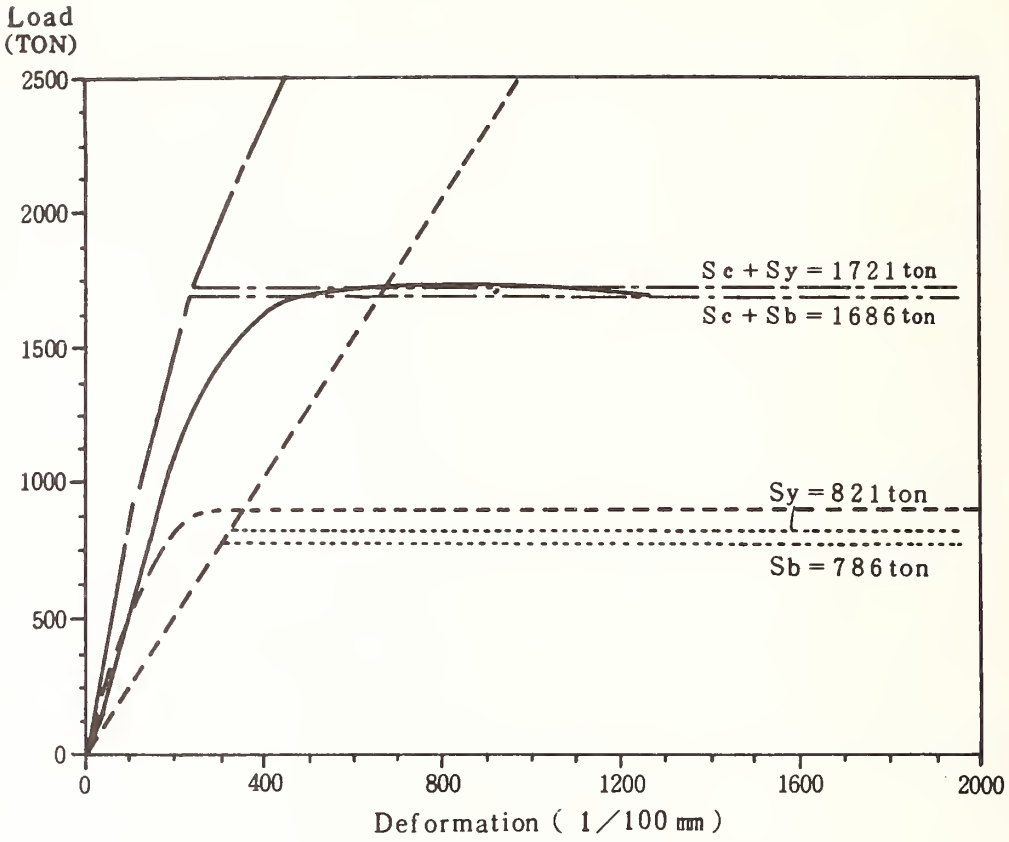

Fig. 13 Load - Deformation Curve (B - 2)

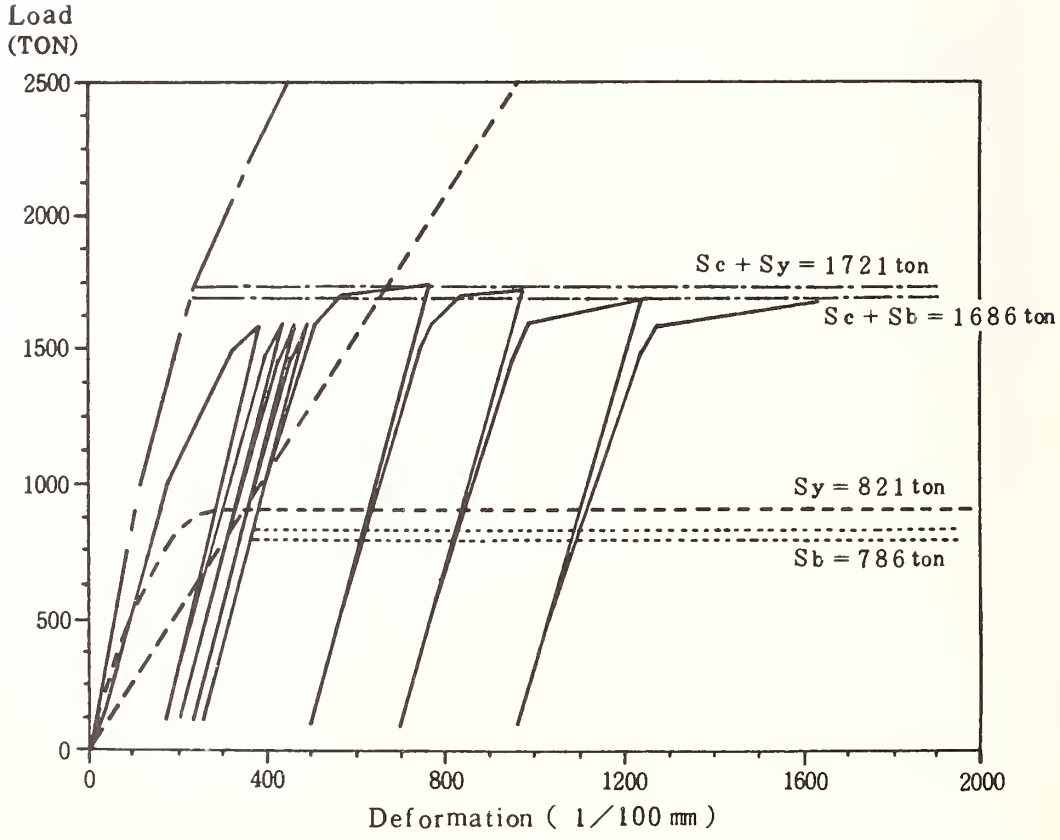

Fig. 14 Load - Deformation Curve (B - 3)

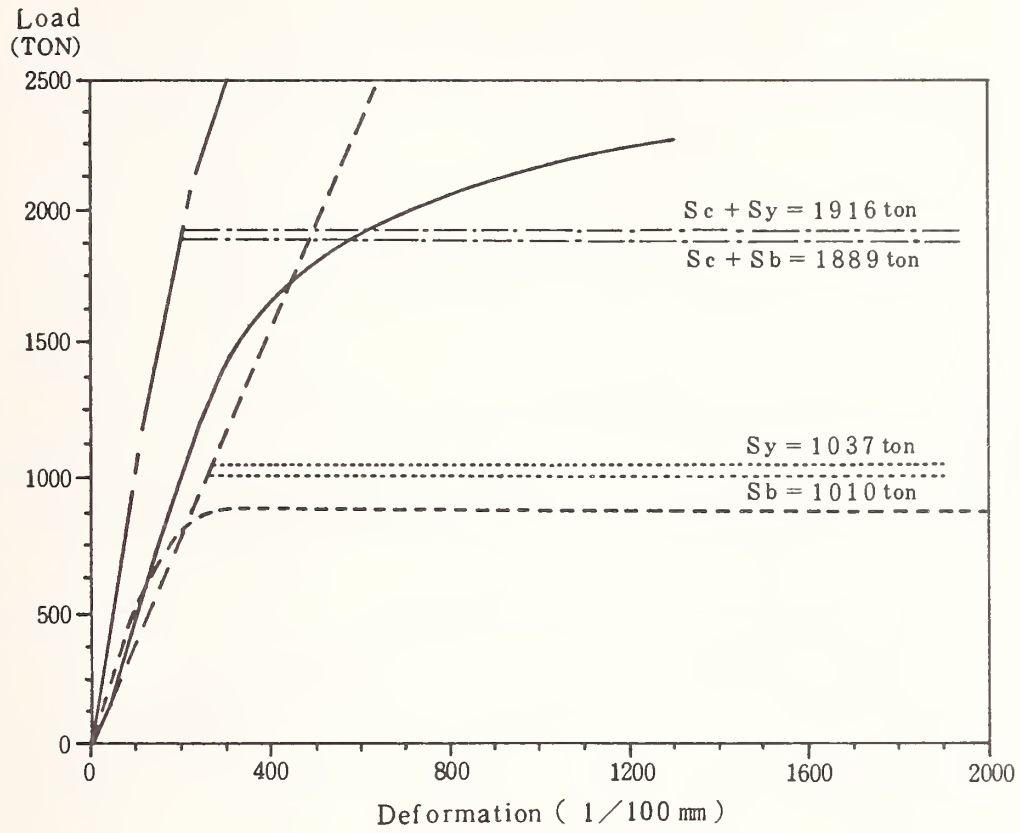

Fig. 15 Load - Deformation Curve (B - 4)

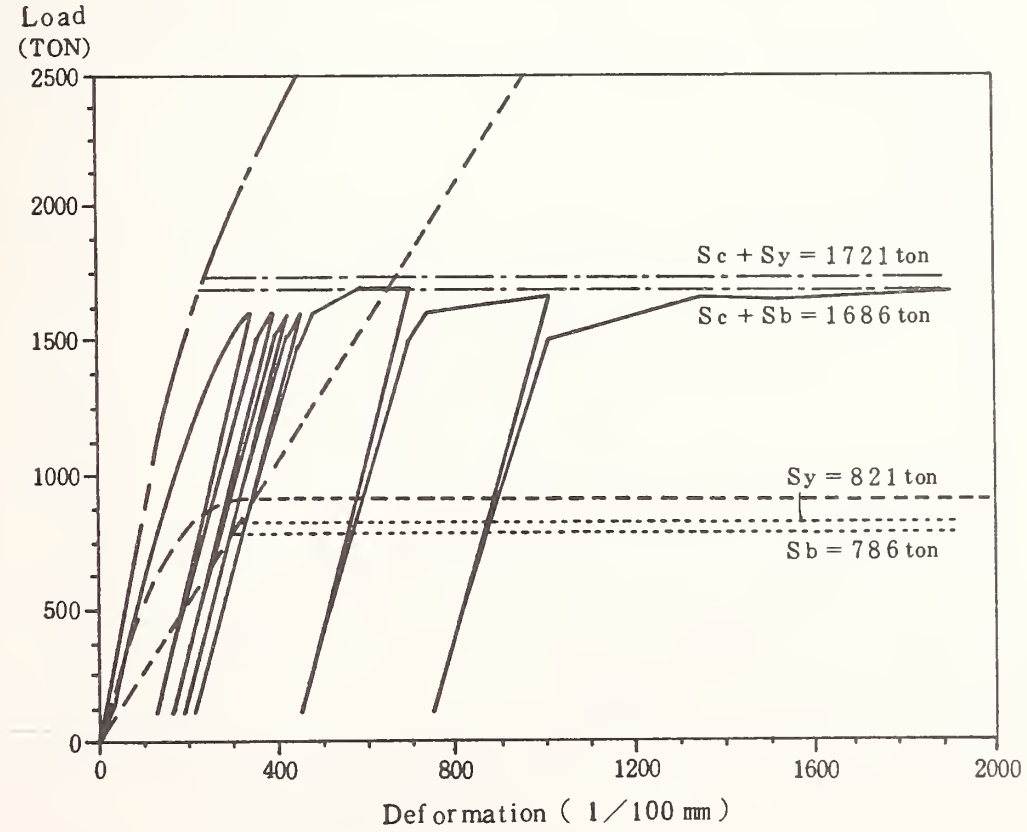

Fig. 16 Load - Deformation Curve (B - 5)

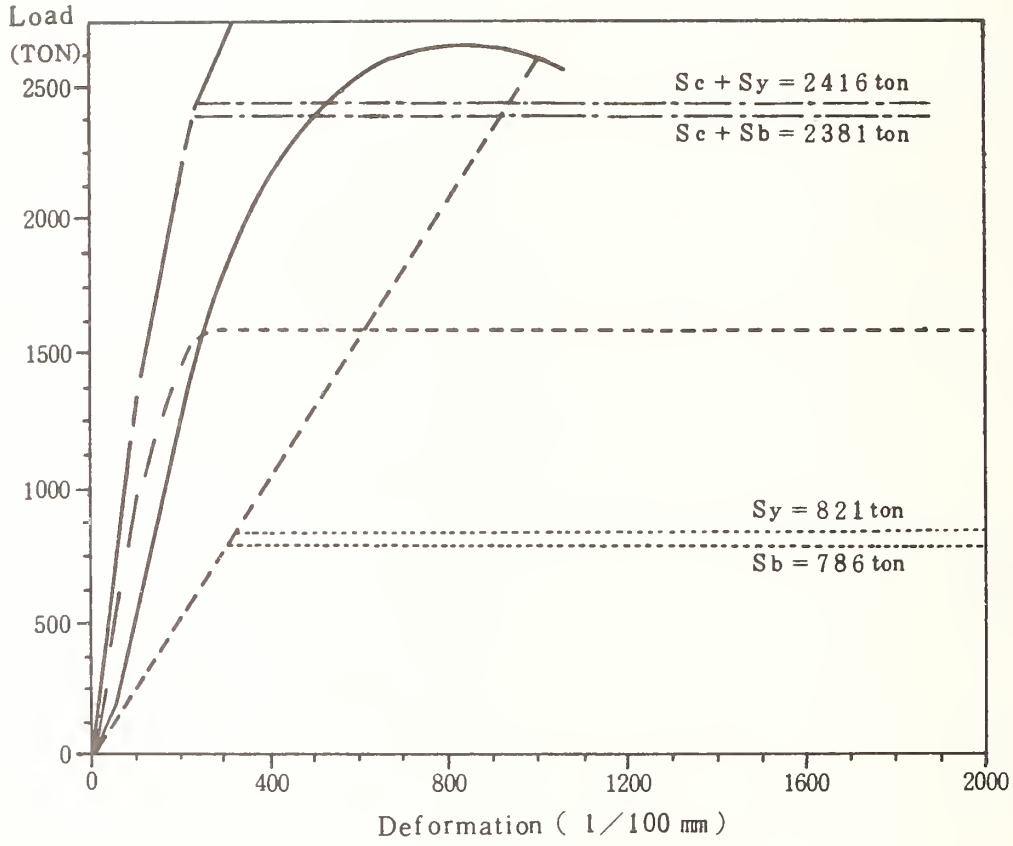

Fig. 17 Load - Deformation Curve (B - 6)

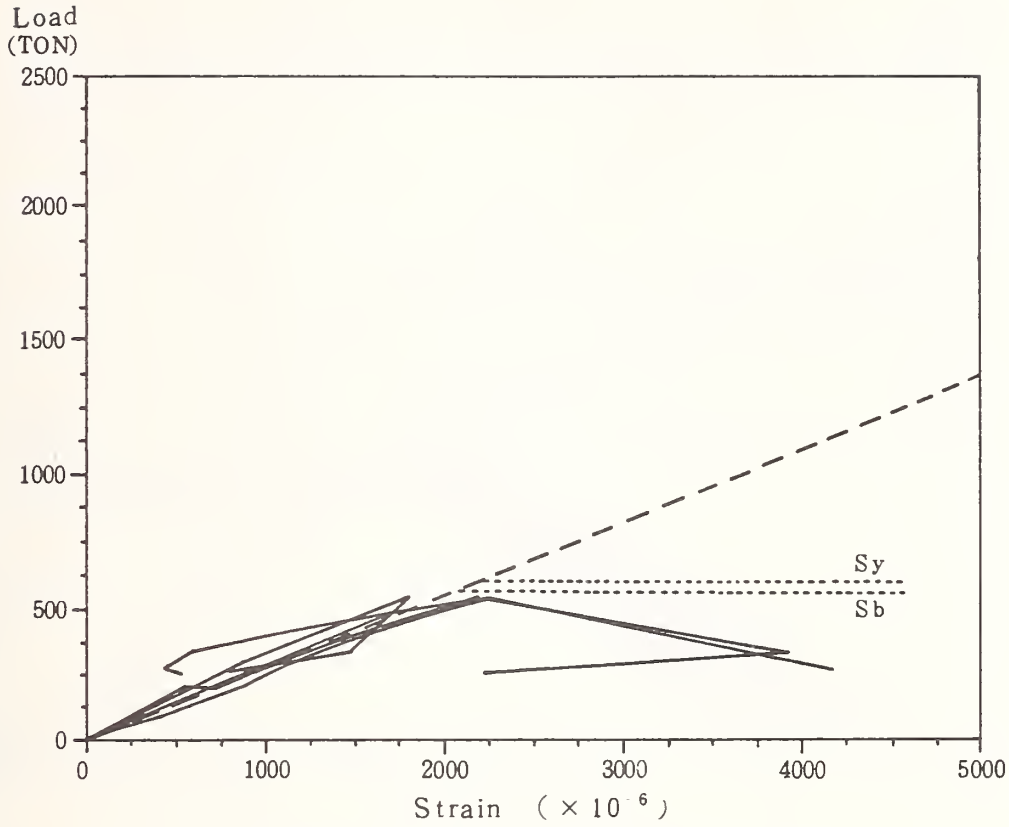

Fig. 18 Load - Strain Curve (A - 1)

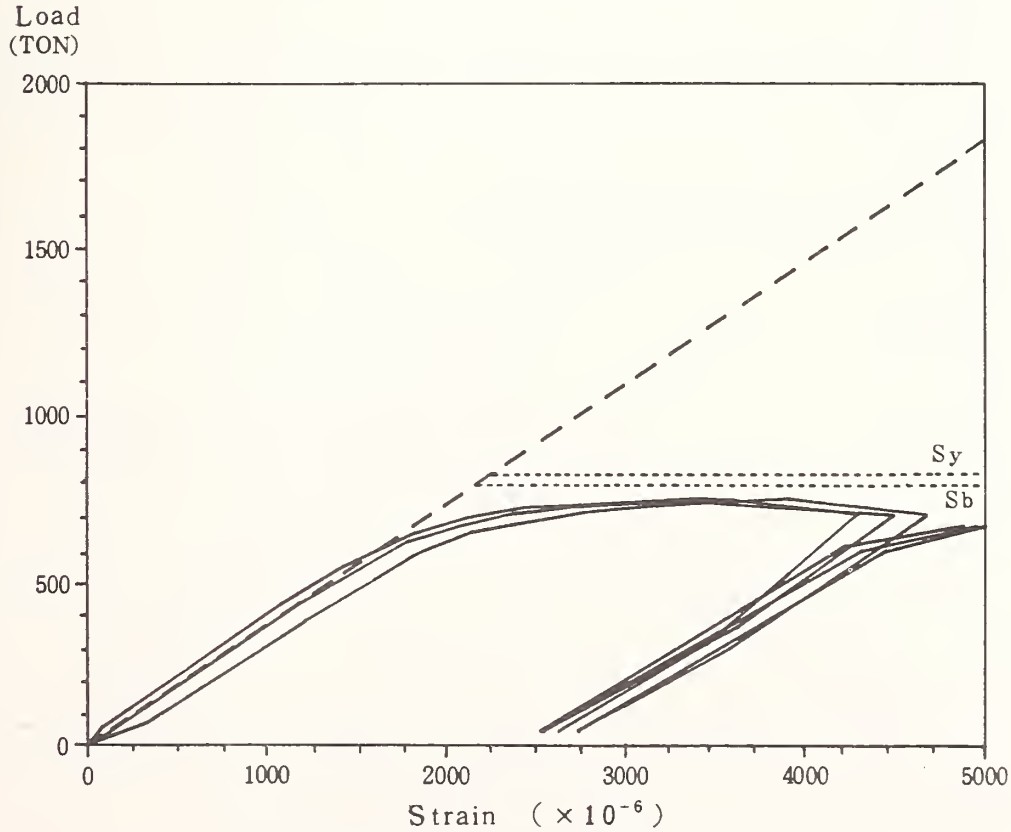

Fig. 19 Load - Strain Curve (A - 2)

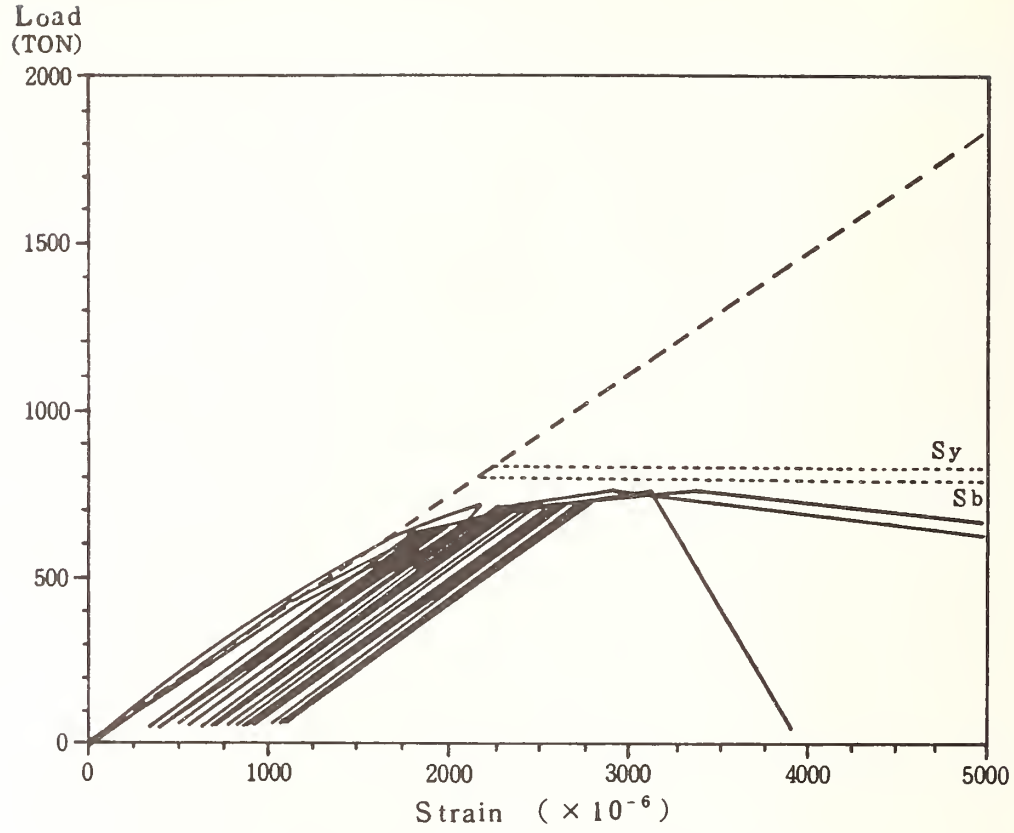

Fig. 20 Load - Strain Curve (A - 3)

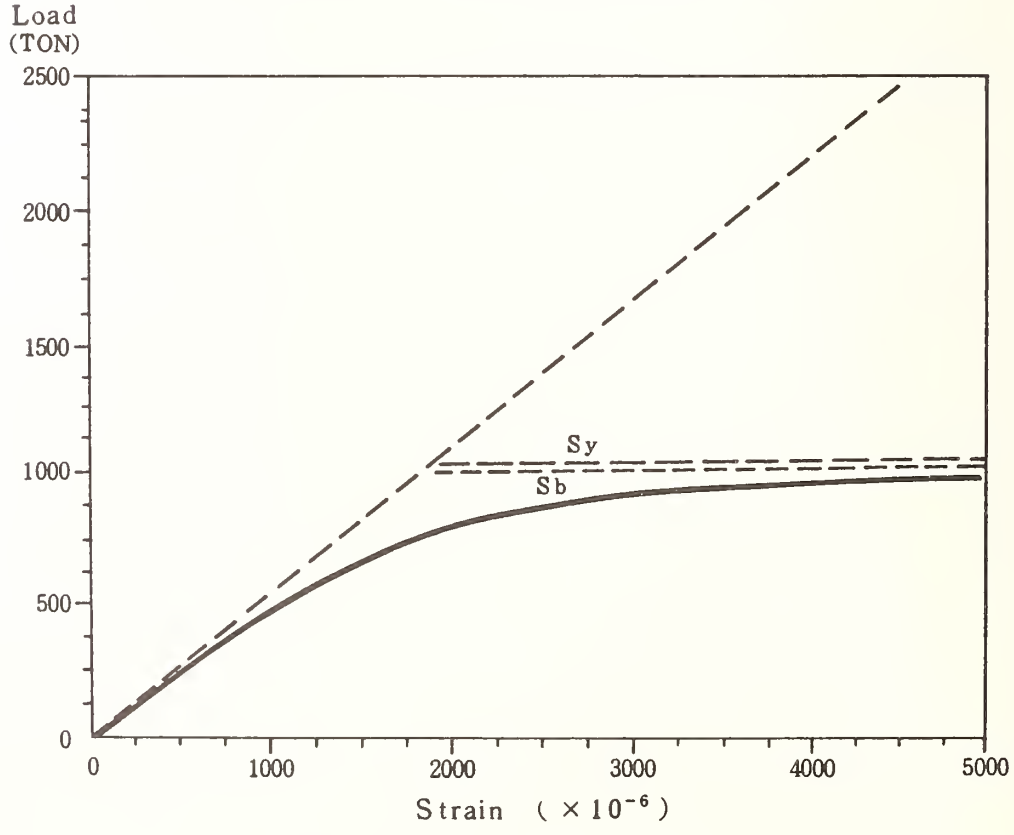

Fig. 21 Load - Strain Curve (A - 4)

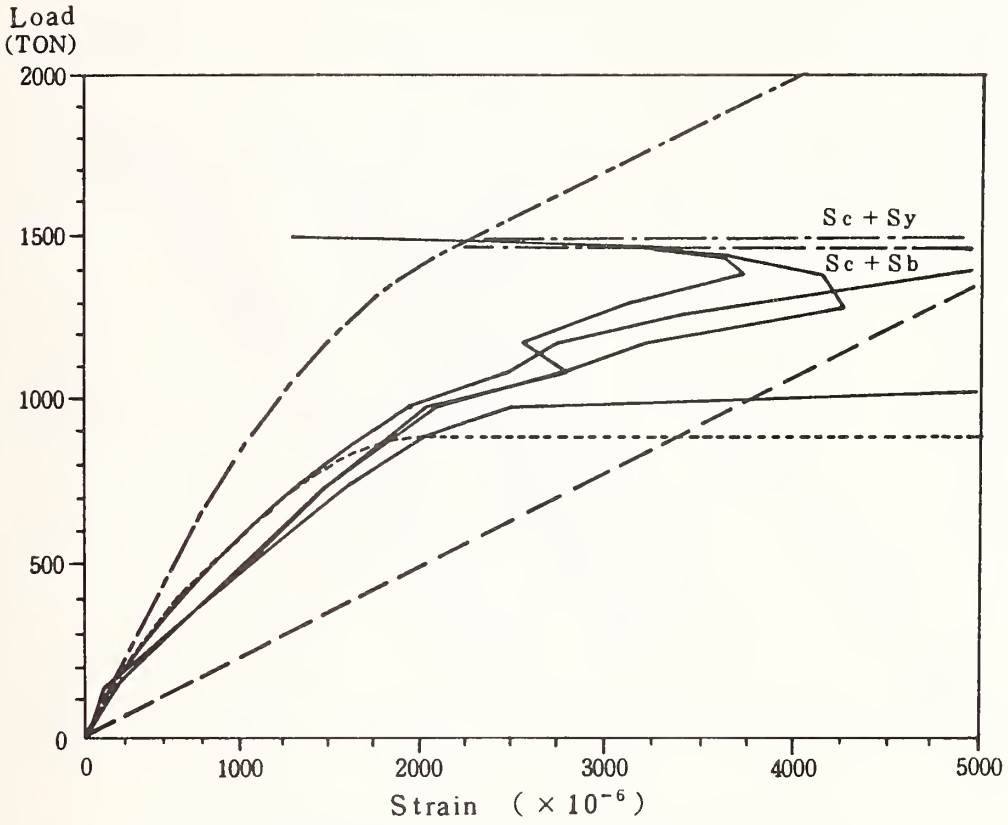

Fig. 22 Load - Strain Curve (B - 1)

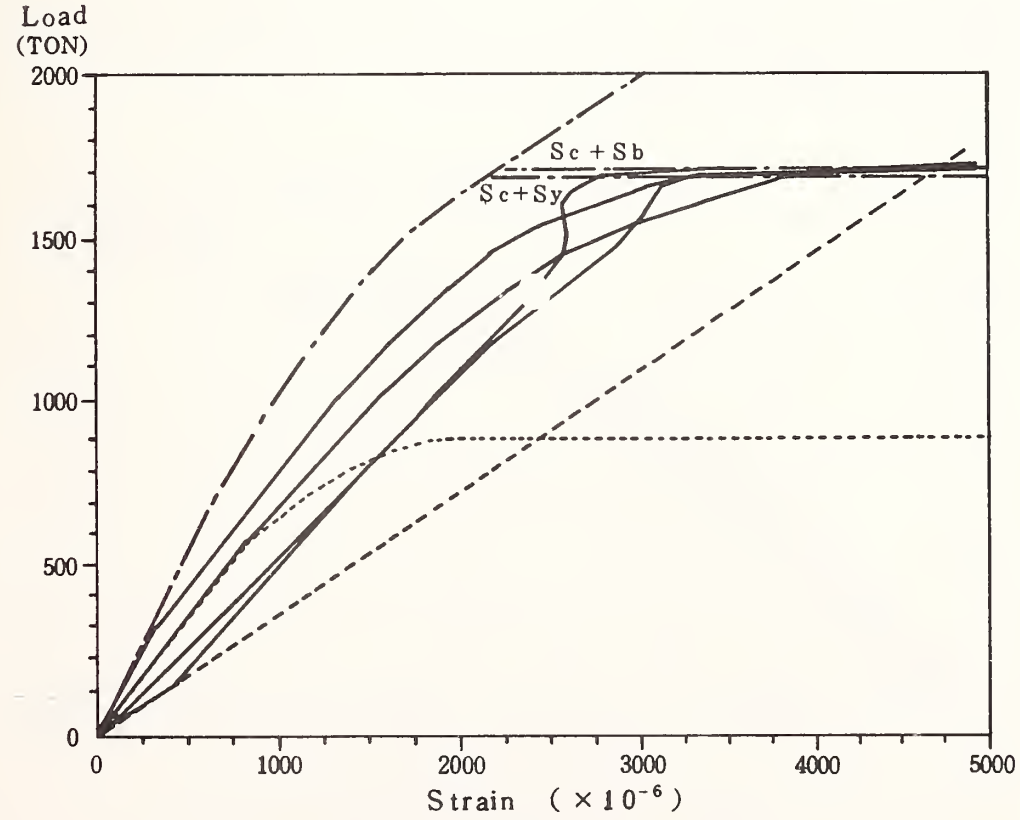

Fig. 23 Load - Strain Curve (B - 2)

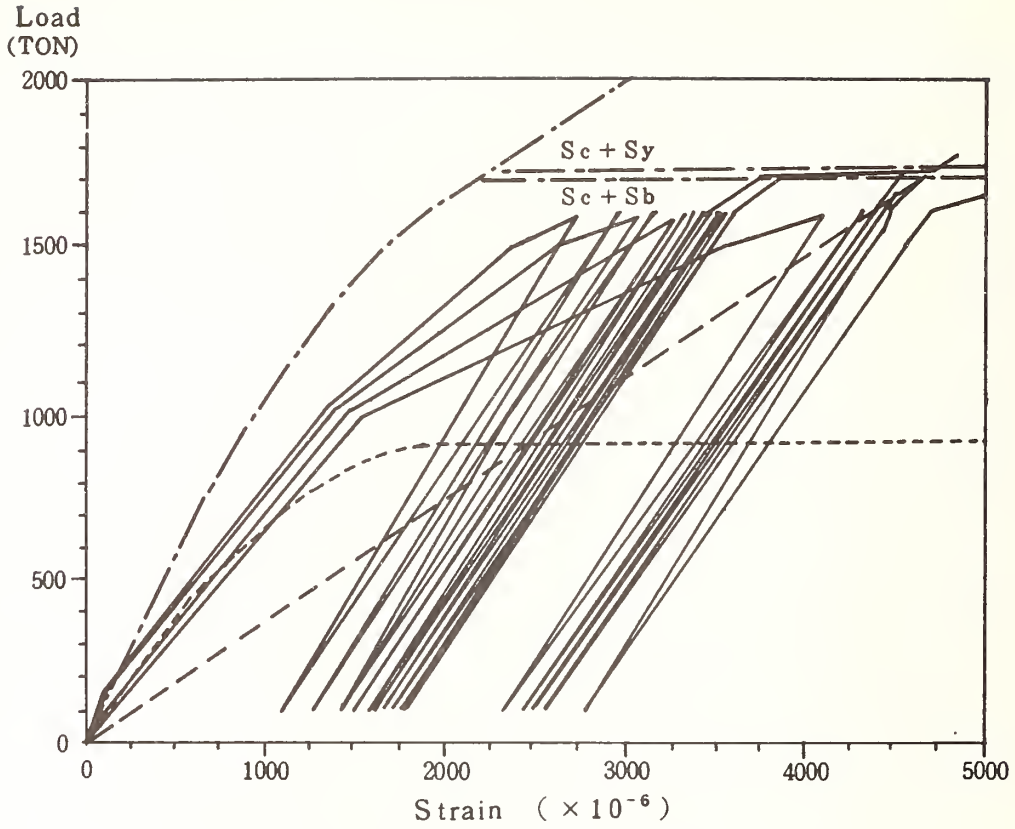

Fig. 24 Load - Strain Curve (B - 3)

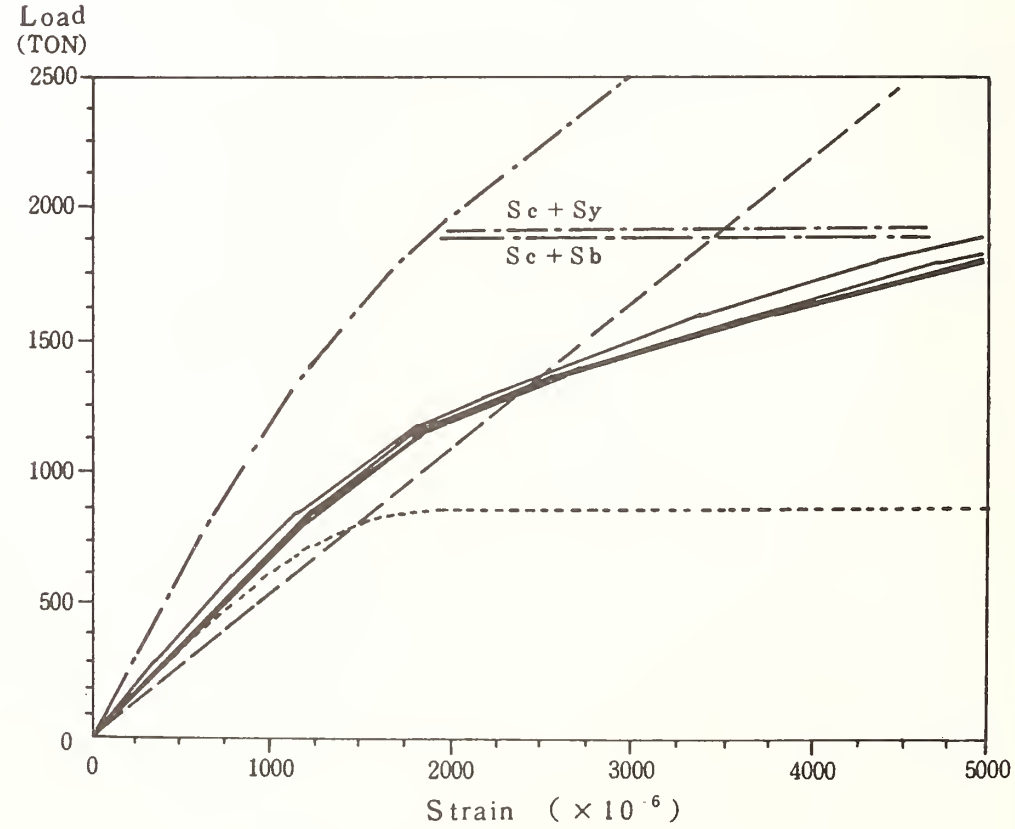

Fig. 25 Load - Strain Curve (B - 4)

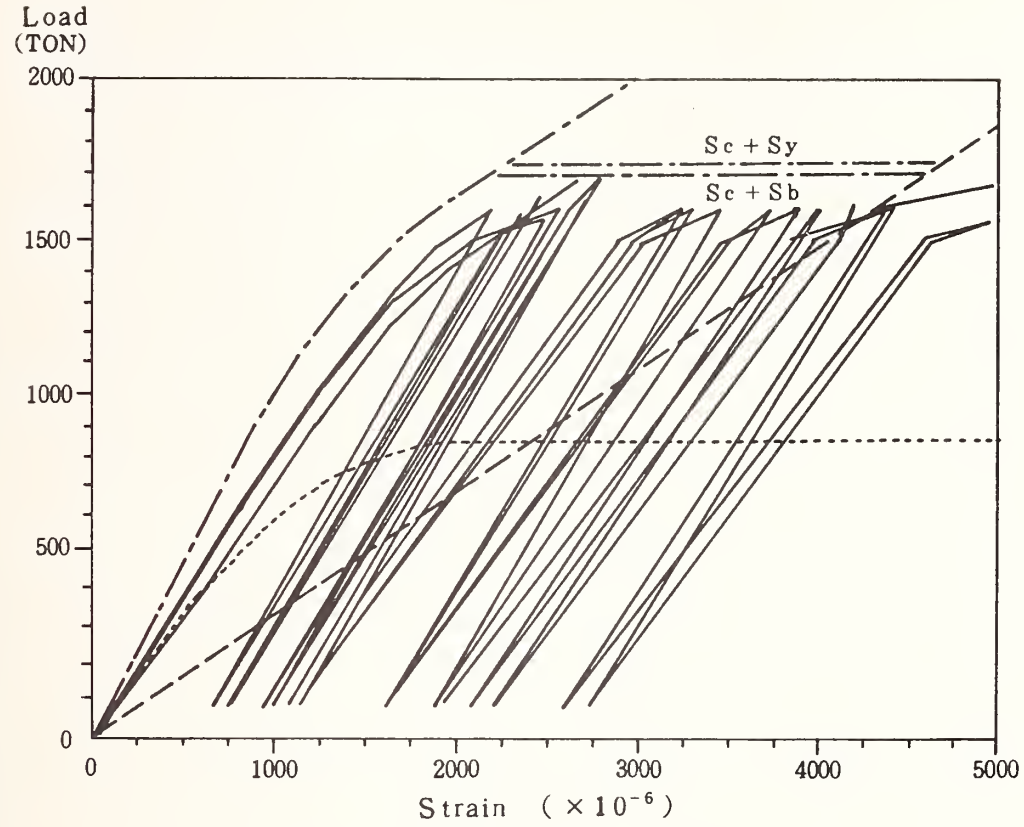

Fig. 26 Load - Strain Curve (B - 5)

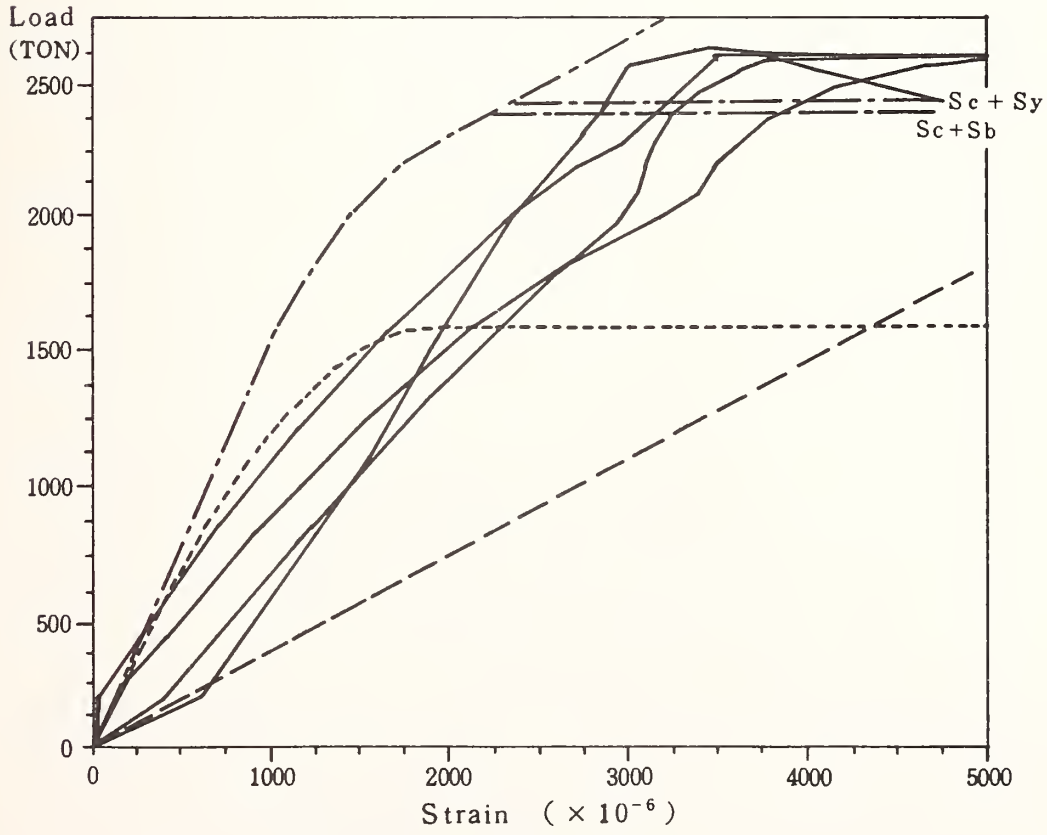

Fig. 27 Load - Strain Curve (B - 6)

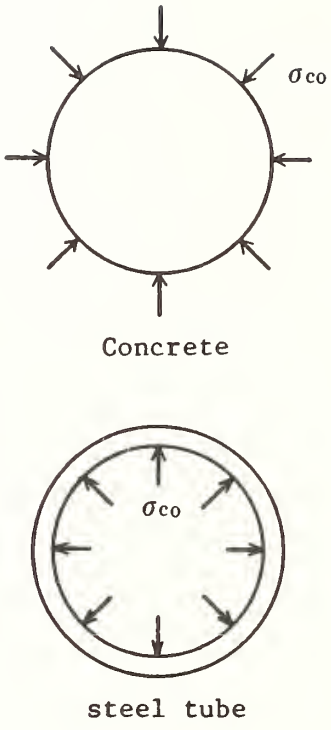

Figure 28. Bond Stress

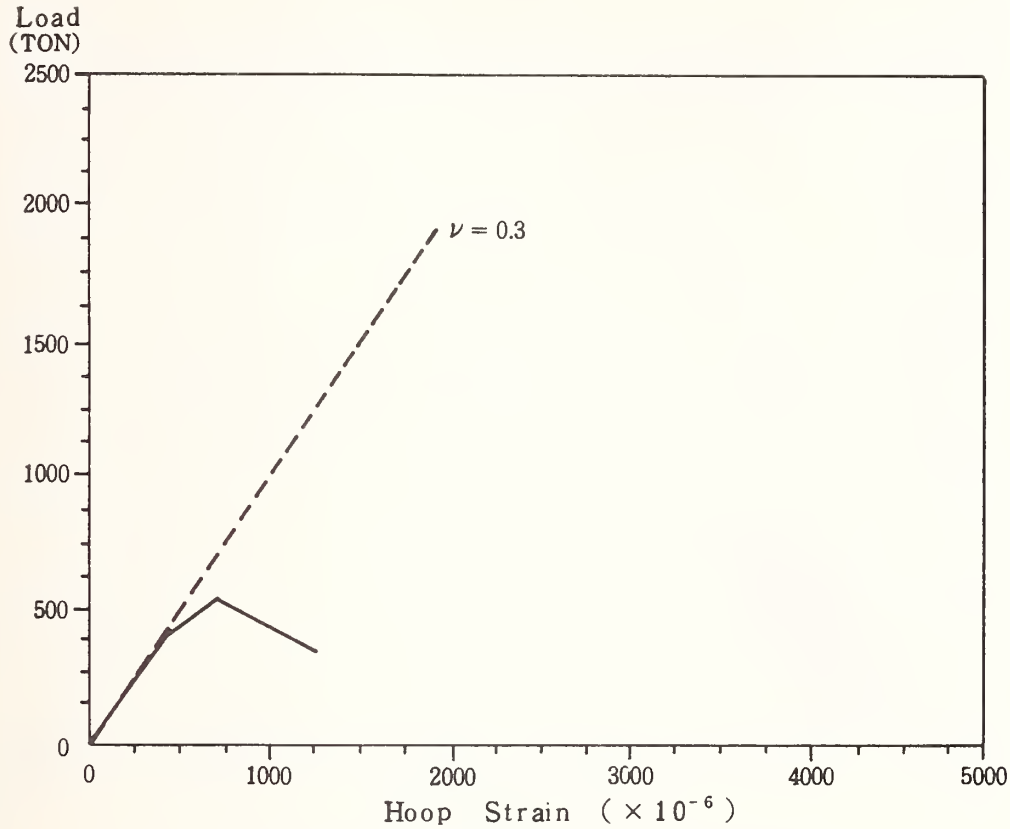

Fig. 29 Load - Hoop Strain Curve (A - 1)

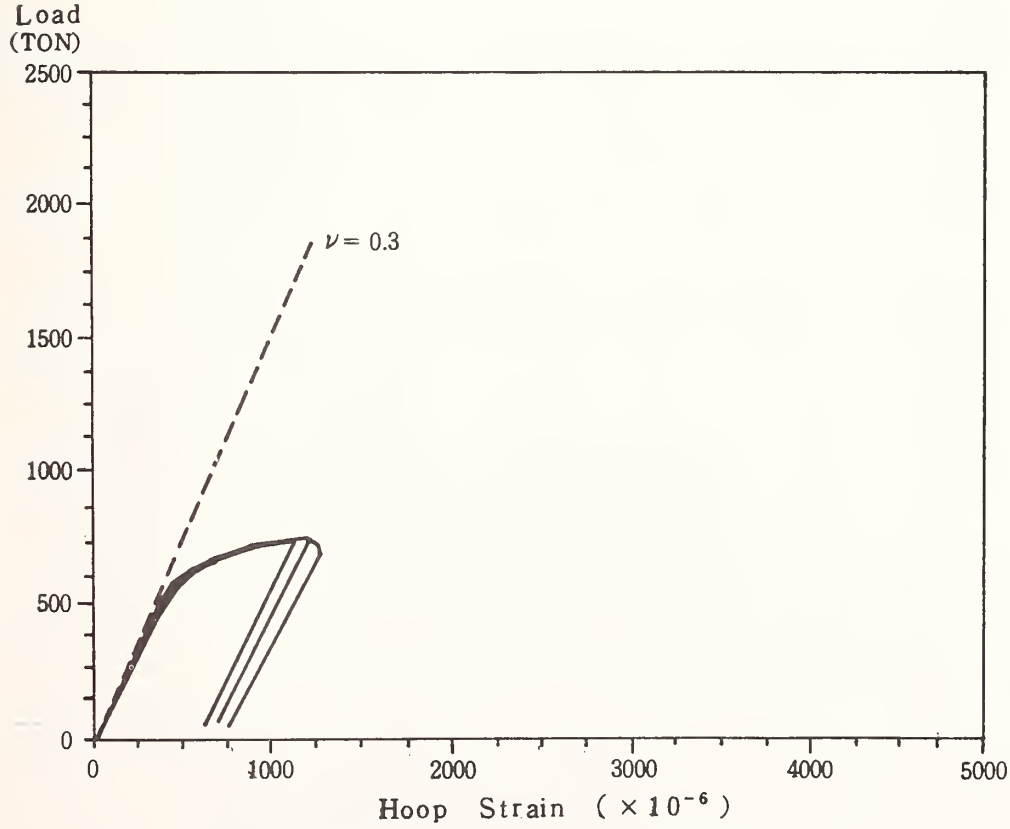

Fig. 30 Load - Hoop Strain Curve (A - 2)

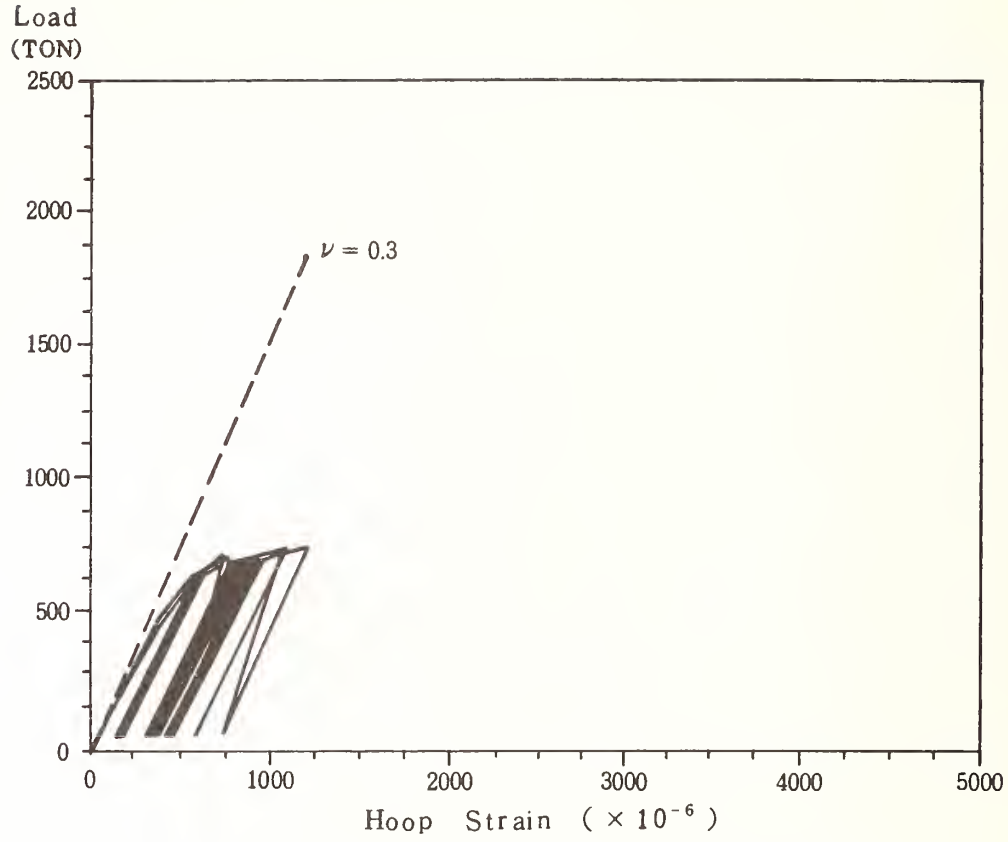

Fig. 31 Load - Hoop Strain Curve (A - 3)

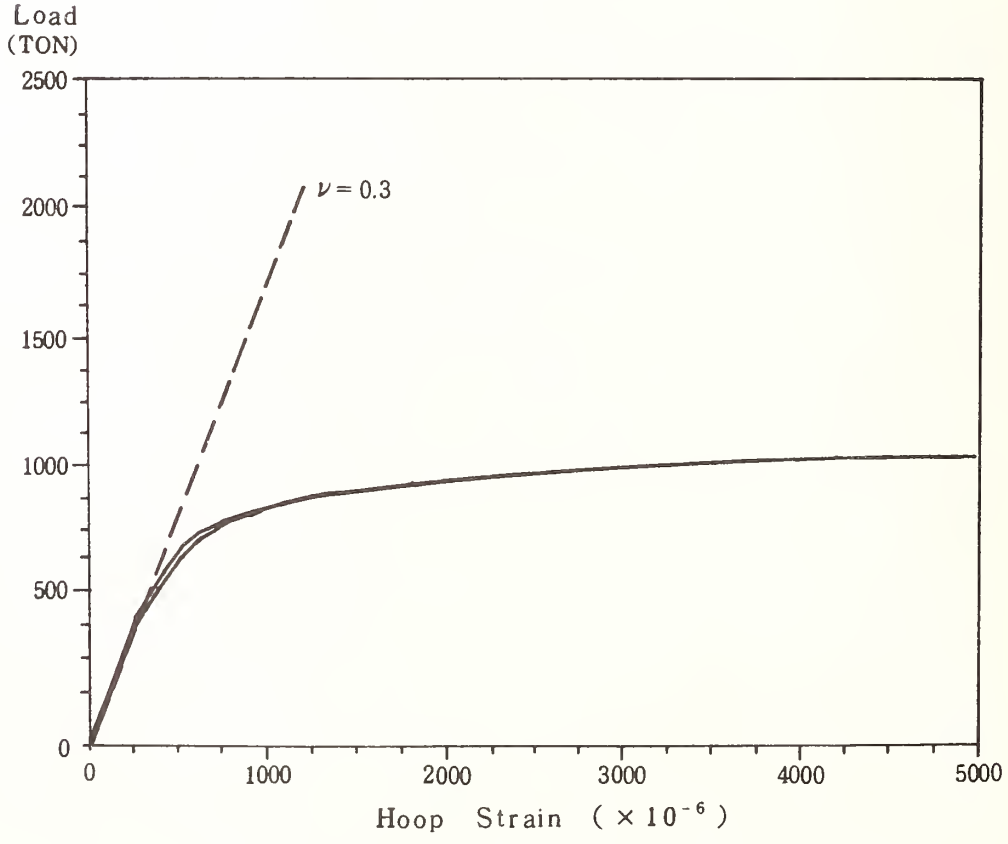

Fig. 32 Load - Hoop Strain Curve (A - 4)

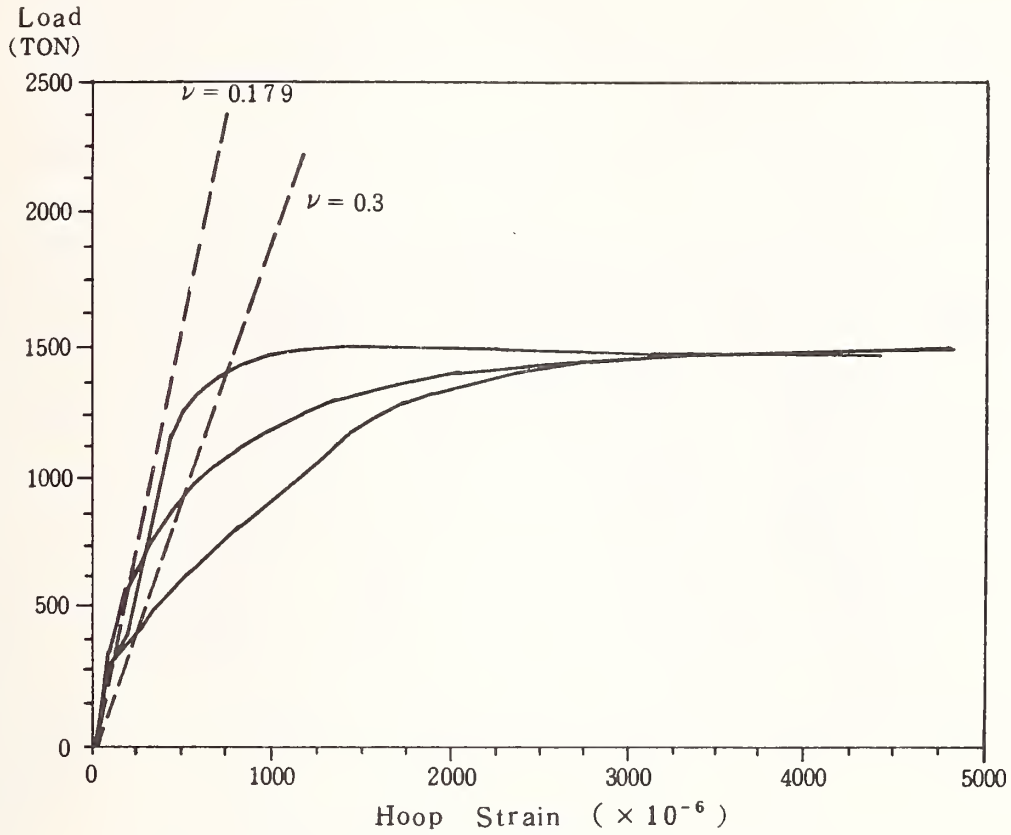

Fig. 33 Load - Hoop Strain Curve (B - 1)

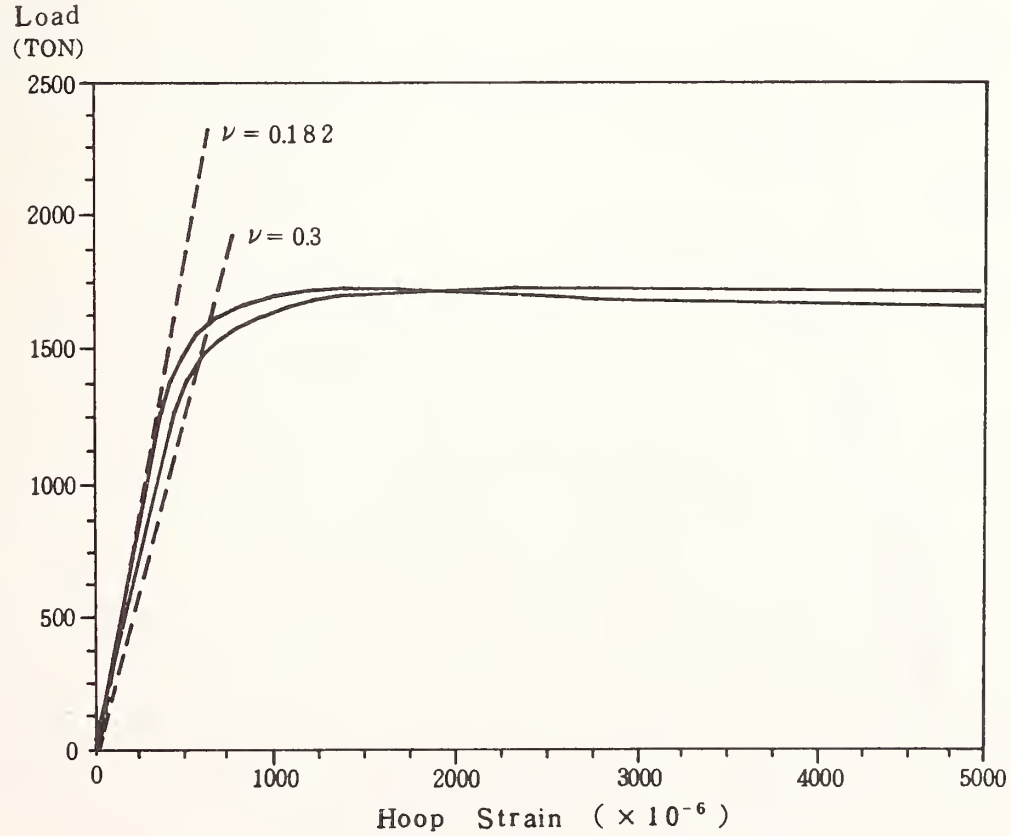

Fig. 34 Load - Hoop Strain Curve (B - 2)

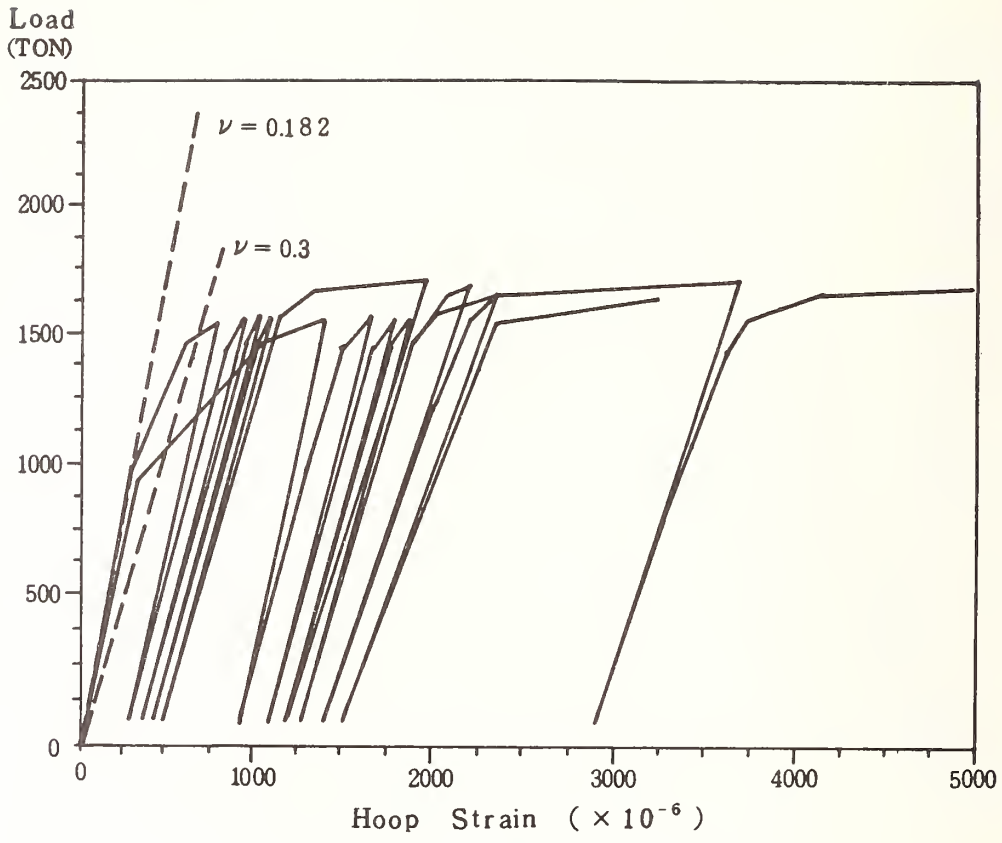

Fig. 35 Load - Hoop Strain Curve (B - 3)

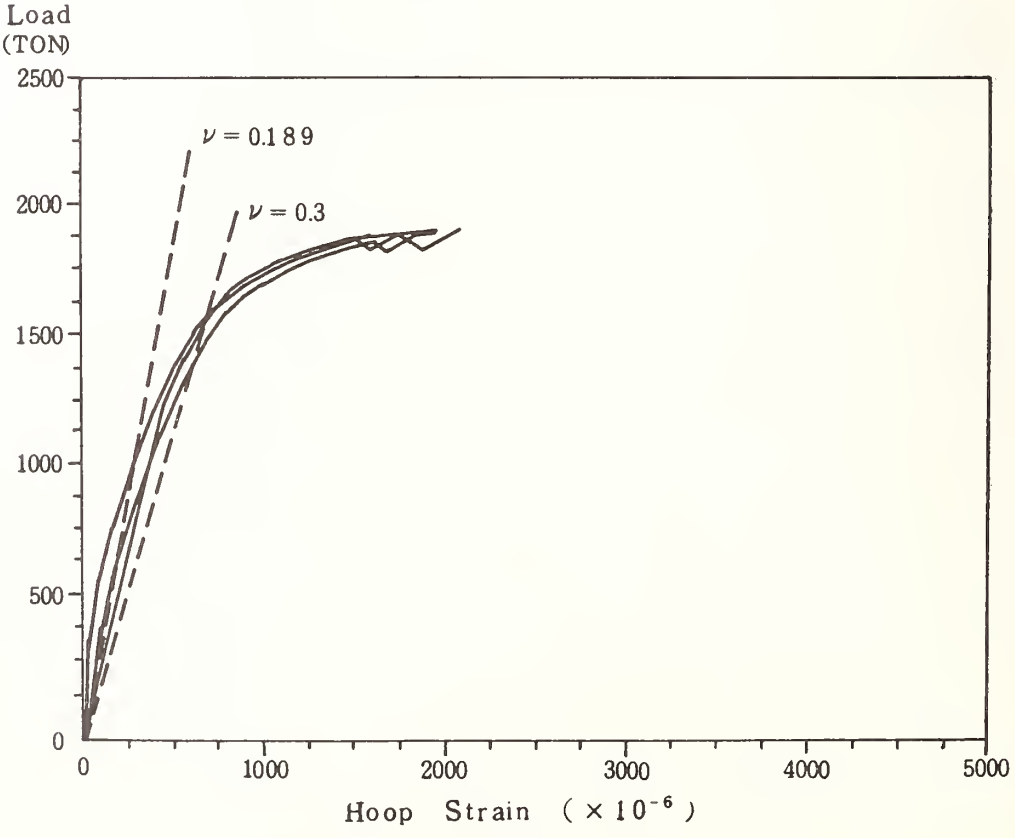

Fig. 36 Load - Hoop Strain Curve (B - 4)

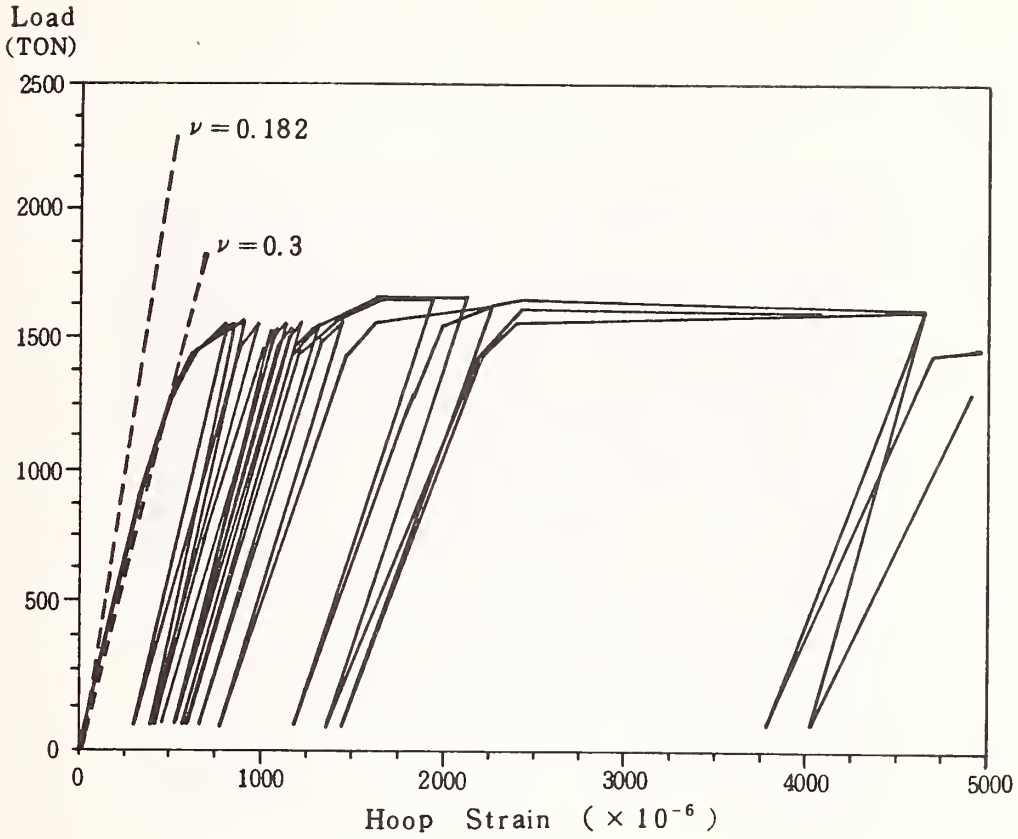

Fig. 37 Load - Hoop Strain Curve (B - 5)

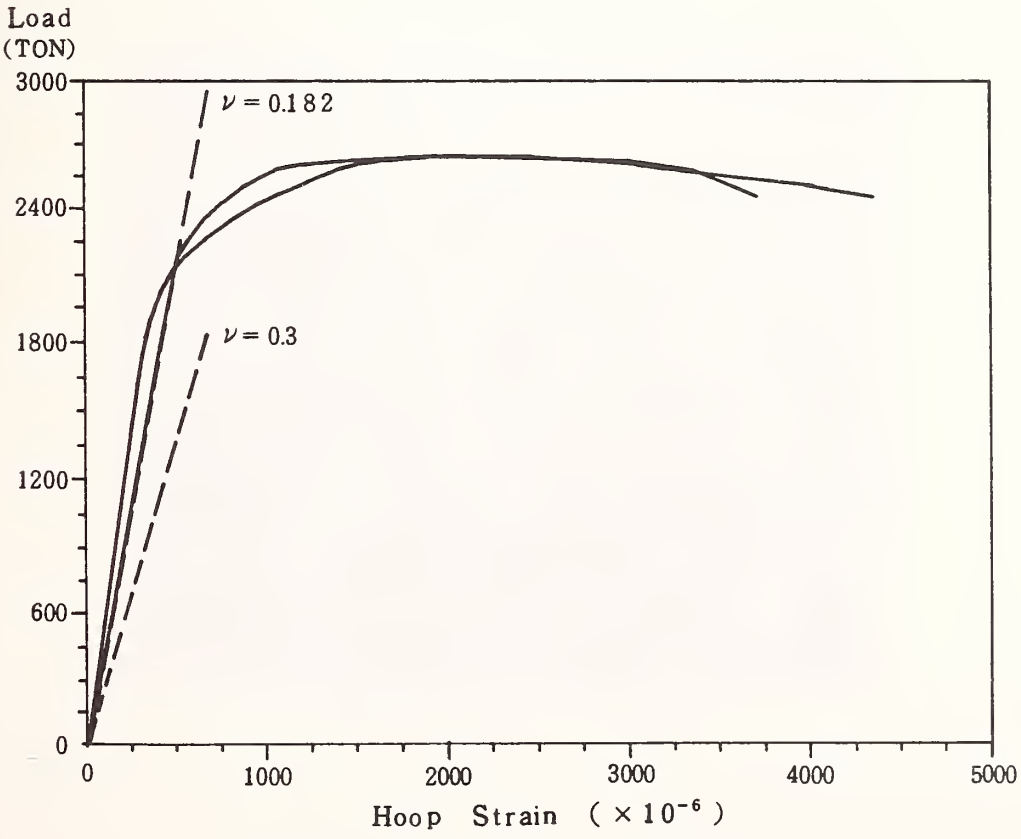

Fig. 38 Load - Hoop Strain Curve (B - 6)

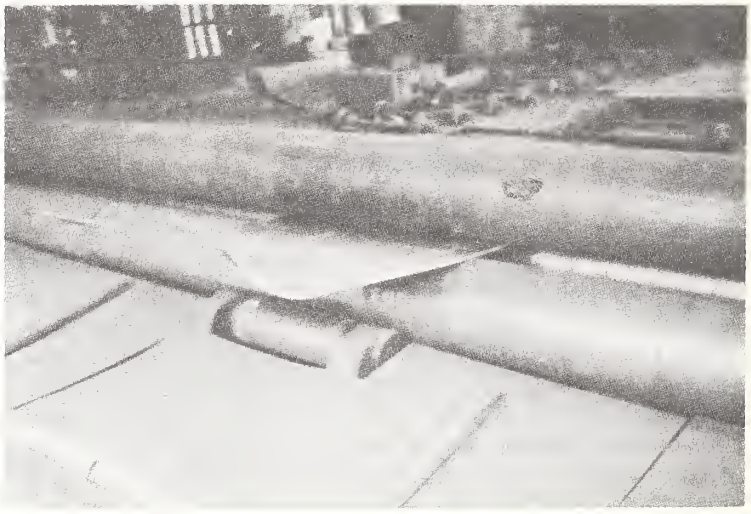

Photo-1. Bending Process of Steel Tubes

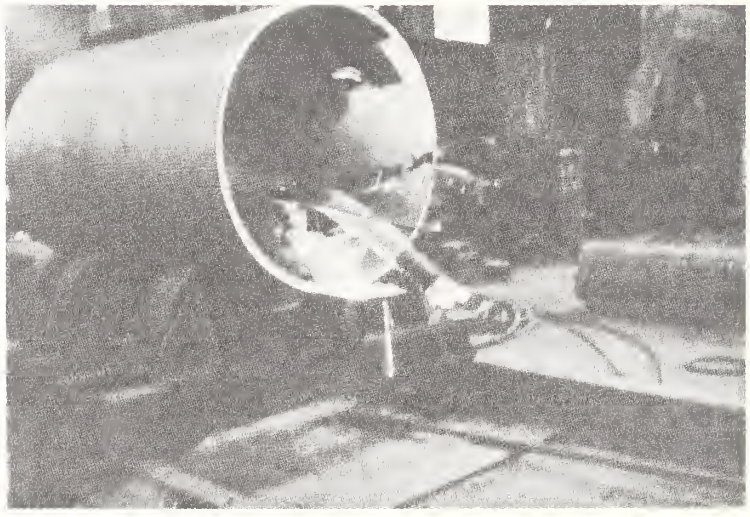

Photo-2. Welding (Inside)

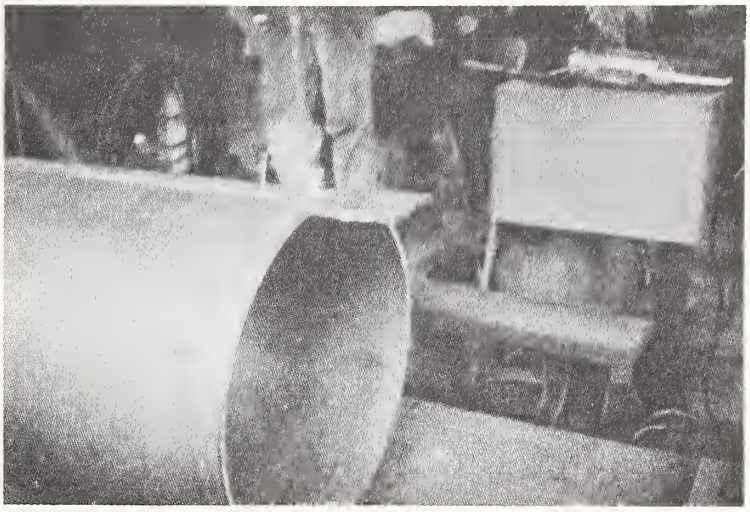

Photo-3. Welding (Outside)

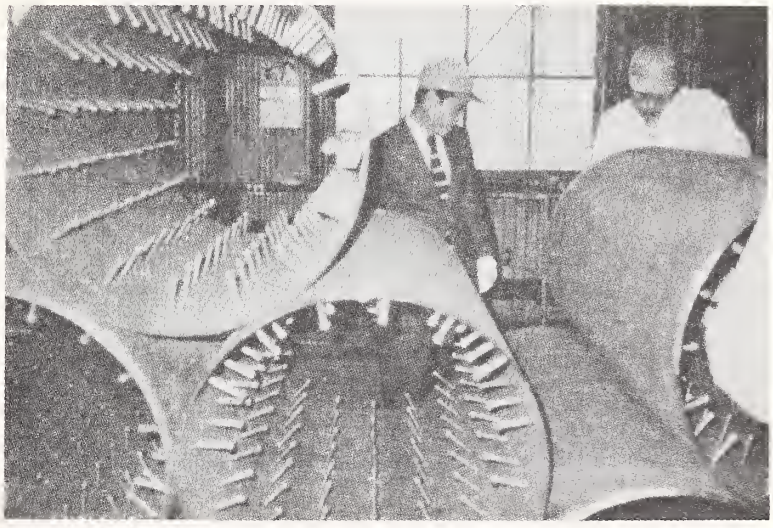

Photo-4. Stud Welding

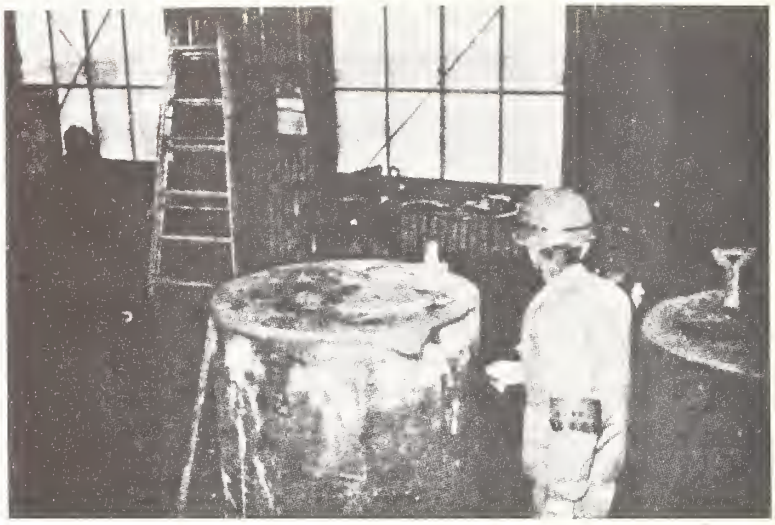

Photo-5. Mortar Casting

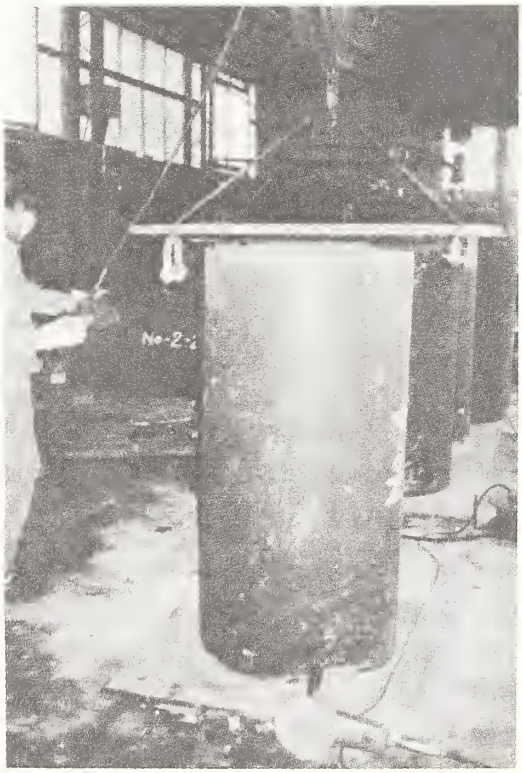

Photo-6. Bottom and Top Plate

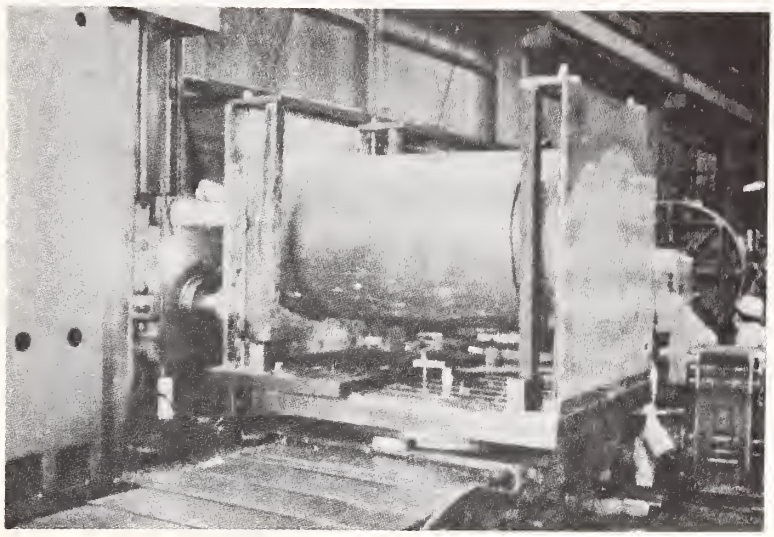

Photo-7. Grinding of Top and Bottom Plate

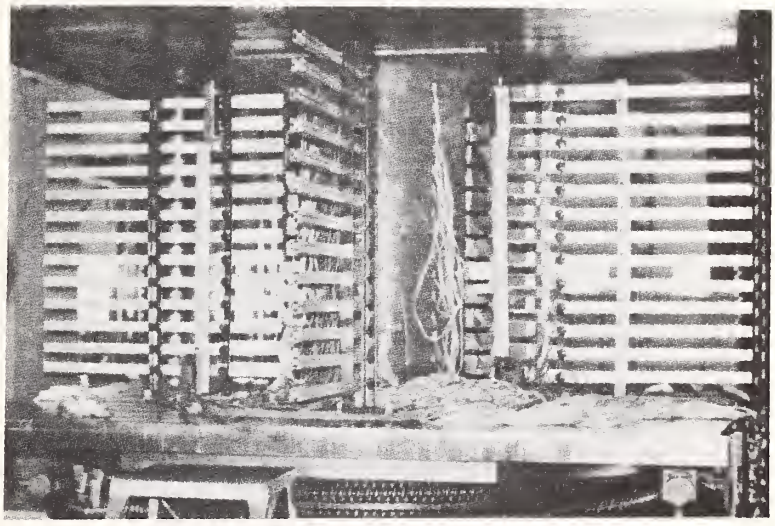

Photo-8. Measurement of Out-of-Plane Deflection

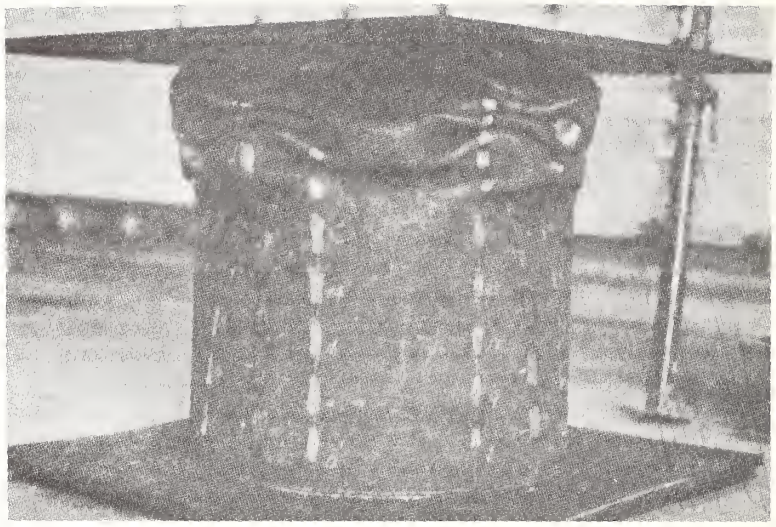

Photo-9. Specimen A - 2 After Loading

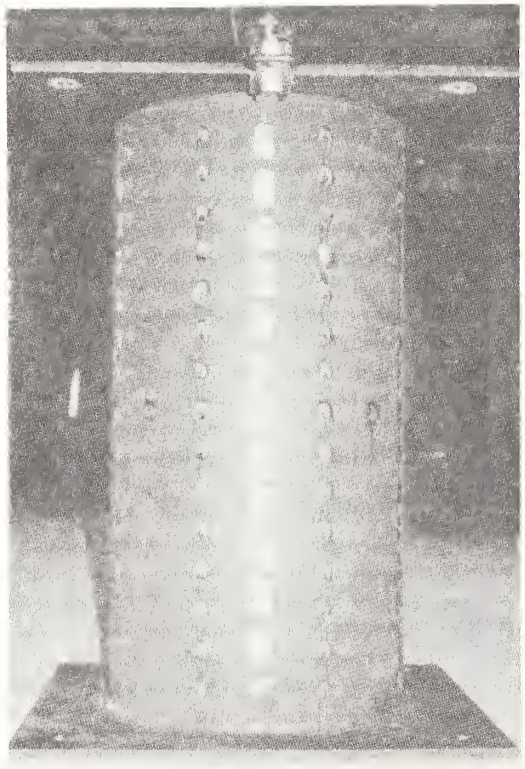

Photo-10. Specimen A - 4 After Loading

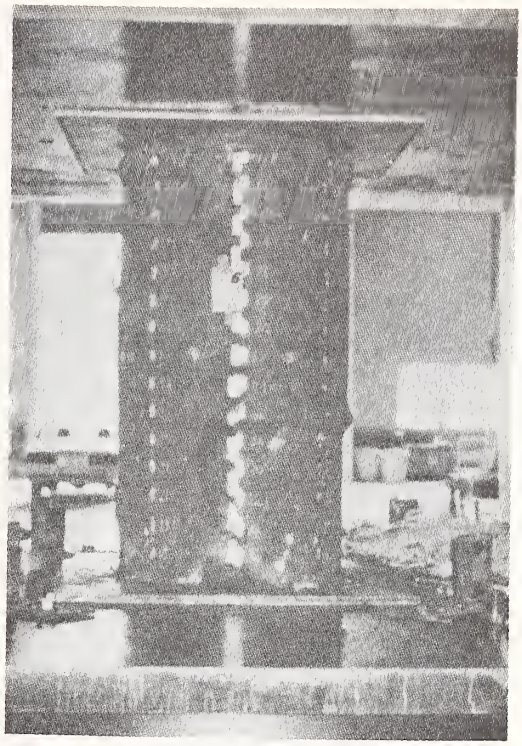

Photo-11.
Specimen B - 2 After Loading

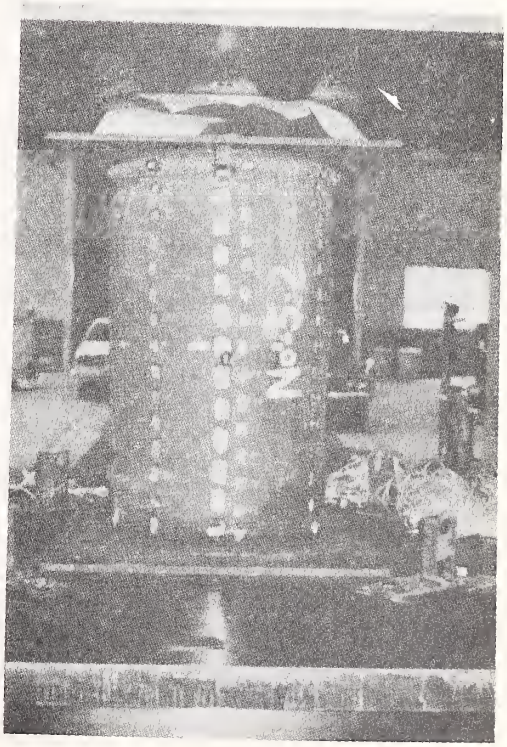

Photo-12.
Specimen B - 3 After Loading

Photo-13.
Concrete After Loading

Photo-14.
Concrete After Loading

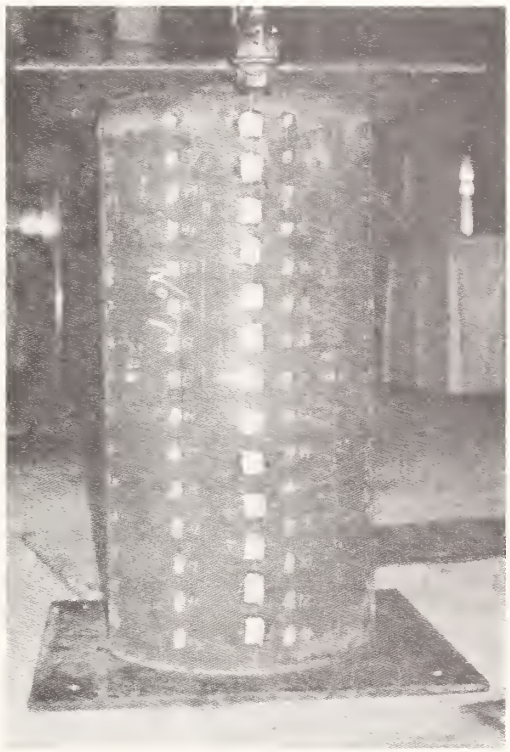

Photo-15. Speimen B - 6 After Loading

MICROCOMPUTER FOR EARTHQUAKE STUDIES

S. K. Takahashi

Naval Civil Engineering Laboratory
Port Hueneme, CA 93043

J. V. Tyrrell
Naval Facilities Engineering Command
Washington, DC 22332

ABSTRACT

The use of microcomputers is now a practical reality for the small engineering office. The reasons for the immediate popularity are the low initial cost of the system ($4K to $8K), the large number of software programs available and its versatility.

The cost of a typical microcomputer (MC) system, one that is operational at the Naval Civil Engineering Laboratory, with a 64K RAM (Random Access Memory), dual 8 in. disk drives, and letter quality printer, is about $8K (figure 1). Presently, it has an 8-bit processor (figure 2), but it can be upgraded to a 16-bit processor at any time. Similarly, the memory can be upgraded from 64K to 128K as the need arises. One standard parallel port and two RS-232C serial ports allows the addition of printers, plotters, digitizers, and communications with data bases and other computers. Presently, two drives provide 932,000 characters of storage; the addition of two more drives (figure 3) will bring the total capacity to about two million characters. If a hard disk drive system is utilized, it can access 8.4 million characters. The Daisy Wheel letter quality printer (figure 4) was selected so that drafts and final manuscripts could be written and stored on the diskette for instant retrieval and modifications of the text. Additional information and specifications of the MC can be found in reference 1.

This MC adapts easily to the choice of languages such as BASIC, COBOL, FORTRAN, etc., because the system has no primary language stored in Read Only Memory (ROM). Transfer of information, from one installation that uses a microcomputer which utilizes the CP/M system to another Navy agency also utilizing a microcomputer that uses 8 in. single-sided, single-density diskette, can be made easily on the 8 in. diskette with 128 byte record size because this is the standard international interchange format.

DATA BASE STORAGE AND RETRIEVAL

SEISMICALLY DEFICIENT BUILDINGS DATA

The Naval Facilities Engineering Command (NAVFACENGCOM) began their Earthquake Vulnerability Program in 1974 and have coordinated the rapid seismic analysis survey of most of the major Navy

installations located in the high seismic zones. Recently, the major responsibility of executing this task has been delegated to the Western Division of NAVFACENGCOM. The Rapid Seismic Analysis Procedure (RSAP, reference 2), has been used by the Navy and its consultants to analyze over 800 buildings at Naval installations located in the United States and overseas.

Initially, the RSAP structural and cost data were stored on the IBM System 6 Word Processor. These data were the structural properties, replacement cost, damage cost, estimate, etc. The more recent data, which contain information on the detailed structural seismic analysis, are being stored on the MC diskette utilizing the readily available word processing, filing, and planning programs.

The software program utilized for this purpose is the Profile II (reference 3) which can be very easily mastered. Once the data (figure 5) is recorded on the diskette (figure 6) only the specific information desired may be extracted in table form. For instance, if it is desired to select only the buildings on which detailed seismic analyses were performed, the data can be searched and the required information would be printed as shown in figure 7. Furthermore, if it were desired to separate the information according to the type of building (concrete, steel, wood, masonry), this can be done and the results are shown in figure 8. Many other options are available.

STRONG MOTION INSTRUMENTATION DATA

NAVFACENGCOM has also established a program to install strong motion instrumentation on Navy-unique structures, hospitals, and selected buildings at Navy installations where no instrumentation has been installed. Presently, strong motion accelerographs have been installed at North Island Naval Air Station (plane hangar); Long Beach Naval Shipyard (near drydock 2); Alameda Naval Air Station (plane hangar); Mare Island Naval Shipyard (near drydocks); Puget Sound Naval Shipyard (near drydocks); Naval Regional Medical Center, Bremerton; Public Works Center, Guam; and Naval Regional Medical Center, Guam. Installation of additional seismographs is planned.

The Profile II software is also utilized to store information on the strong motion accelerographs as shown in figure 9. The instrumentation in the field needs to be maintained periodically. This consists of checking the battery voltages and photographic paper and making periodic calibration traces. The Navy installations personnel in the field usually provide assistance in performing some of the maintenance. Remainders to perform maintenance are sent to the appropriate Navy installations by merging a base letter utilizing the SCRIPSIT 2.0 (reference 4) software (word processor) with the data stored on the Profile II software. The base letter and the merged letter are shown in figures 10a and 10b, respectively. The names and addresses of the Navy field installations are also stored on the Profile II diskette for the printing of mailing labels.

STRUCTURAL ANALYSIS

There are several general purpose structural analysis programs available for the 64K MC. One of the most popular programs is the MICRO-ETABS (reference 5) which can be used to analyze a multistory frame building with infill walls and diagonal bracing under static and earthquake loads. For this program, the floors are assumed to be rigid. The static loads may be combined with a lateral earthquake input which is specified as a time-history ground acceleration or as an acceleration spectrum response; three-dimensional mode shapes and frequencies may also be evaluated. The complete program can be run on the MC, thus, saving dial-up computer terminal and run time charges. However, it will take a much longer time than a mainframe computer to complete the analysis, depending on the complexity of the structure being analyzed. As long as time is available, different cases may be run on the same structure to check out all options. Since the MC is in the immediate vicinity, the engineer can be doing other work while the computer is performing the analysis. The program capacity for a 64K system is as follows:

$(NS) \times (NC) < 140$

where (NS) is the number of stories in a frame

and (NC) is the number of column lines in a frame

The use of the MICRO-ETABS requires the use of a CP/M (control program for microprocessors) operating system. CP/M (reference 6) has become a standard operating system for microcomputers and is used for most engineering programs. A recommended reading on basic CP/M is by Zaks (reference 7). The post-processors available for MICRO-ETABS are the MICRO-AISC (reference 8) and the MICRO-ACI (reference 9). An editor, which is a highly interactive program, allows the user to prepare input data files and to examine, modify, and selectively print output files. One of the more easily used editors is called "EDDIE" (reference 10).

Another general purpose structural program is called SAP81 (reference 11), which was specially written for the microcomputer. This static analysis program utilizes a free-field type of input and has a printer plot program. This program utilizes three-dimensional prismatic members with bending, shearing, and axial deformations and plane, axisymmetric and membrane finite elements. With the proper software, frequencies and mode shapes may be determined. The program can accommodate about 800 joints and 1000 elements on a 64K CP/M system. One-half of a symmetrical drydock model (figure 11) with 238 nodal points and 192 plane elements was run for gravity load and equivalent soil pressure on the sidewall and under the floor slab. The actual run time was 66 min and the output to line printer run time was 41 min.

OTHER CAPABILITIES

With the purchase of a direct-connect modem II (see reference 1 for further description) and specially written software, the MC can act like a remote job entry (RJE) terminal connected to a mainframe computer. The advantage of this system can be utilized when a very large structural computer model needs to be analyzed, one that is too large for the MC. The data can be entered into the MC and debugged at no computer cost. The data can then be transmitted via the modem to the mainframe computer for execution.

Using the FORTRAN (FORmula TRANslator) language supplied on the diskette, engineering programs can be written on the MC. The software has five modules consisting of the Editor, Compiler, Linking Modules, Subroutine Library, and a Source and Listing File Print Utility.

CONCLUSION

The present day 64K microcomputer with dual 8 in. diskette drives is very versatile. It can store a vast amount of data, which can be rearranged when putout. It can also: merge a base letter with the data file; analyze complex three-dimensional structures subjected to static and dynamic loads; write engineering programs; and act as a terminal to a mainframe computer.

REFERENCES

[1] Radio Shack 1982 TRS-80 Microcomputer Catalog No. RSC-7, A Division of Tandy Corporation, Fort Worth, TX.

[2] Civil Engineering Laboratory, TM-M51-78-02: Rapid Seismic Analysis Procedure, by T. K. Lew and S. K. Takahashi, Port Hueneme, CA, April 1978.

[3] Profile II, Radio Shack, TRS-80, Software Library (electronic filing system that can search through records to find the files desired and keep track of names and addresses), TRSDOS Operating System, Tandy Corporation, 1981.

[4] SCRIPSIT 2.0, Model II Reference Manual (word processing system which can be used to merge names, addresses, and information from Profile II programs for fast, automatic printout of form letters), TRSDOS Operating System, Tandy Corporation, 1981.

[5] Engineering Solutions, MICRO-ETABS, Extended Three-Dimensional Analysis of Building Systems for Microcomputers, 1930 Shattuck Ave., Berkeley, CA 94704, January 1982.

[6] Bove, Tony, Approaching CP/M, Data Cast 001, pp. 29-51.

[7] Zaks, Rodnay, The CP/M Handbook with mp/m, SYBEX, Inc., 1980.

[8] Engineering Solutions, MICRO-AISC, A Postprocessor for the Stress Check of Three-Dimensional Moment Resisting Steel Frames, 1930 Shattuck Ave., Berkeley, CA 94704, Janaury 1982.

[9] Engineering Solutions, MICRO-ACI, Design of Ductile Concrete Space Frames, 1930 Shattuck Ave., Berkeley, CA 94704, January 1982.

[10] Wilson, E. L., Structural Engineering Work Station for CP/M - Microcomputers, SAP, Inc., July 1981.

[11] Wilson, E. L., SAP-81, Structural Analysis Programs for Small or Large Computer Systems, SAP, Inc., January 1981.

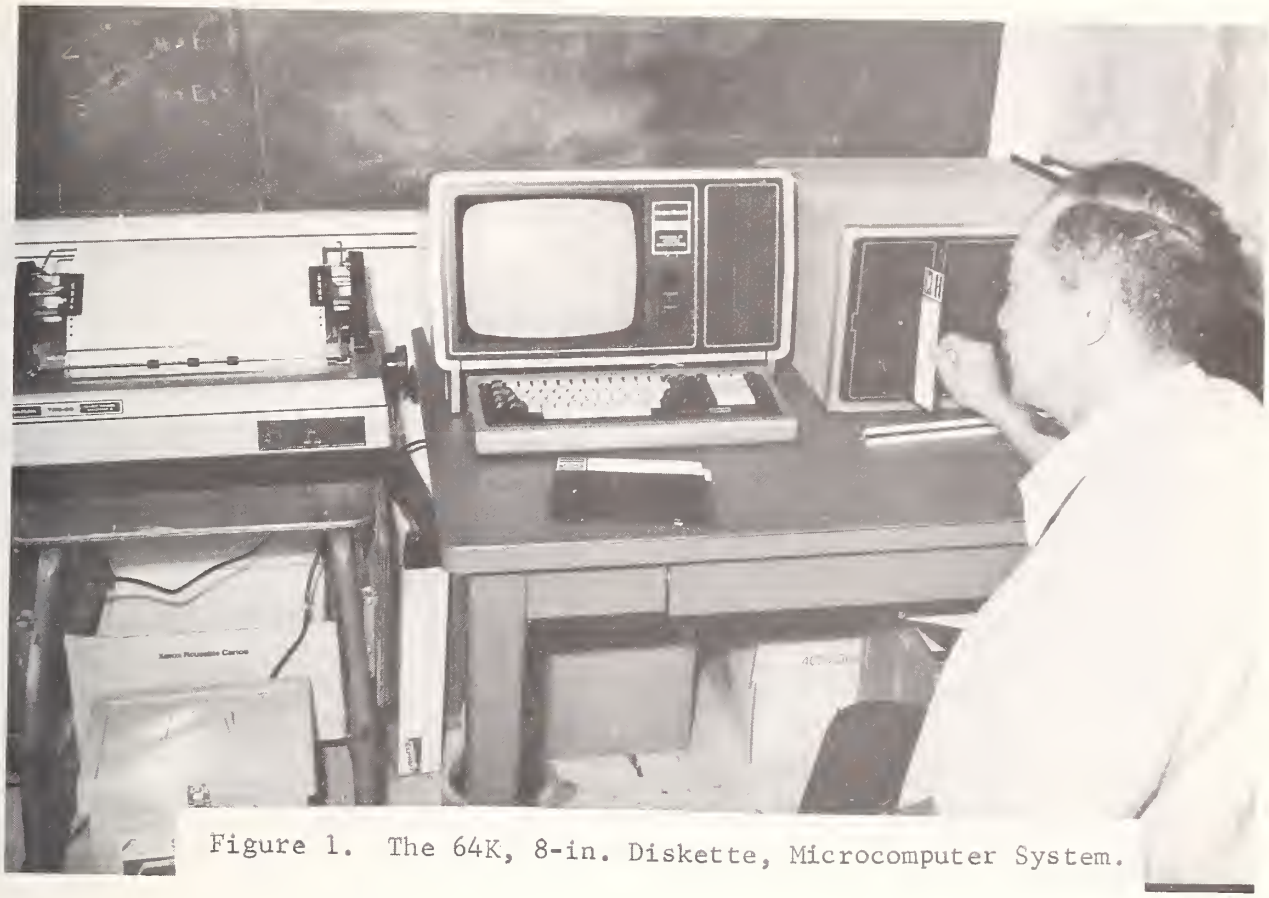

Figure 1. The 64K, 8-in. Diskette, Microcomputer System.

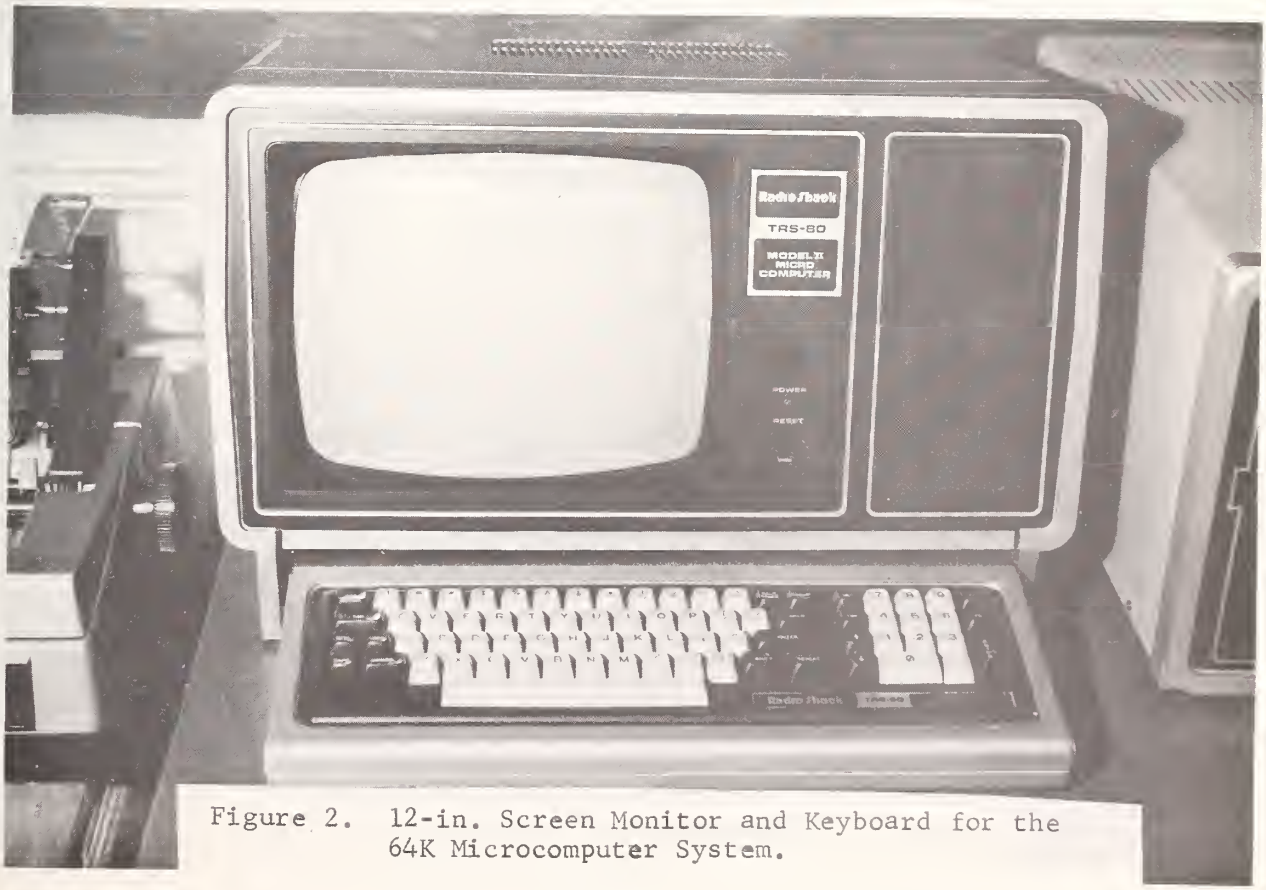

Figure 2. 12-in. Screen Monitor and Keyboard for the 64K Microcomputer System.

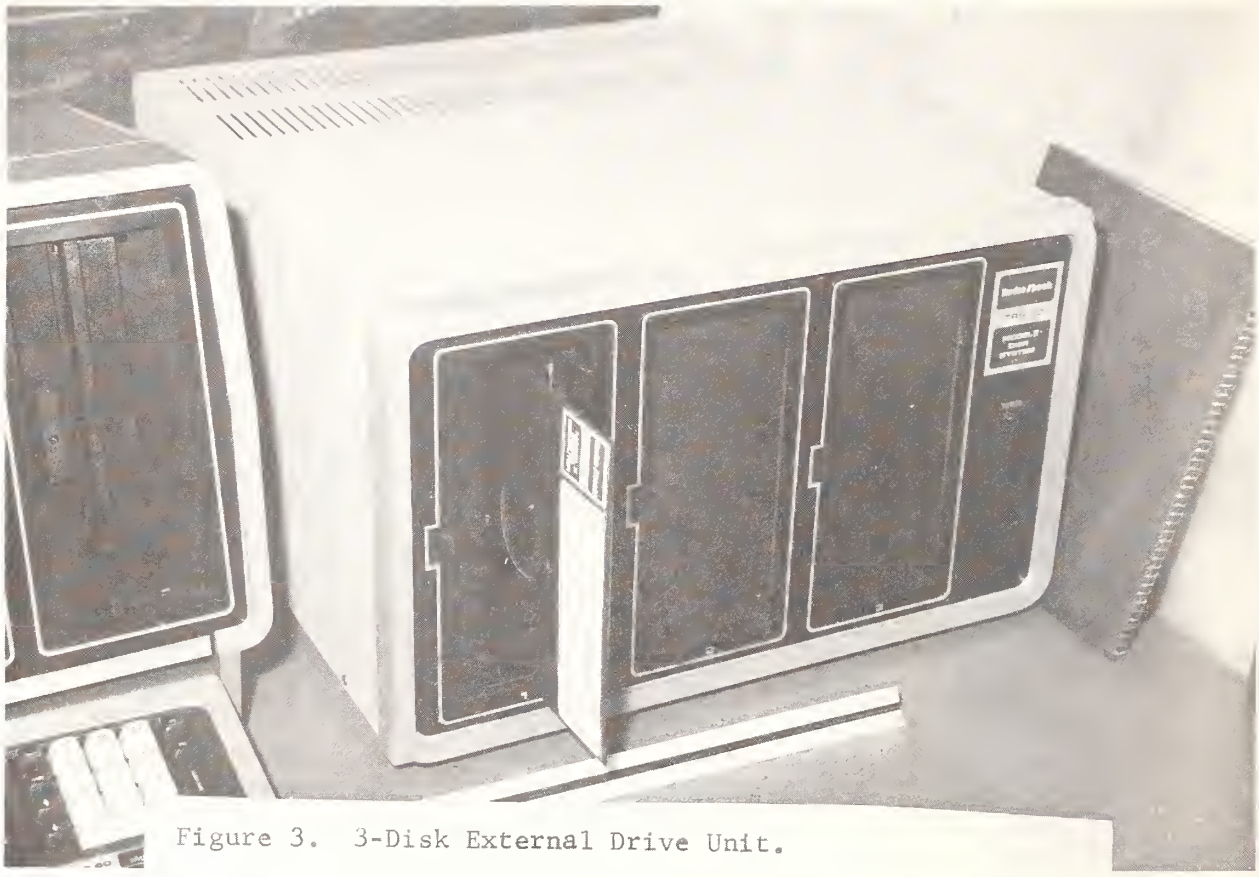

Figure 3. 3-Disk External Drive Unit.

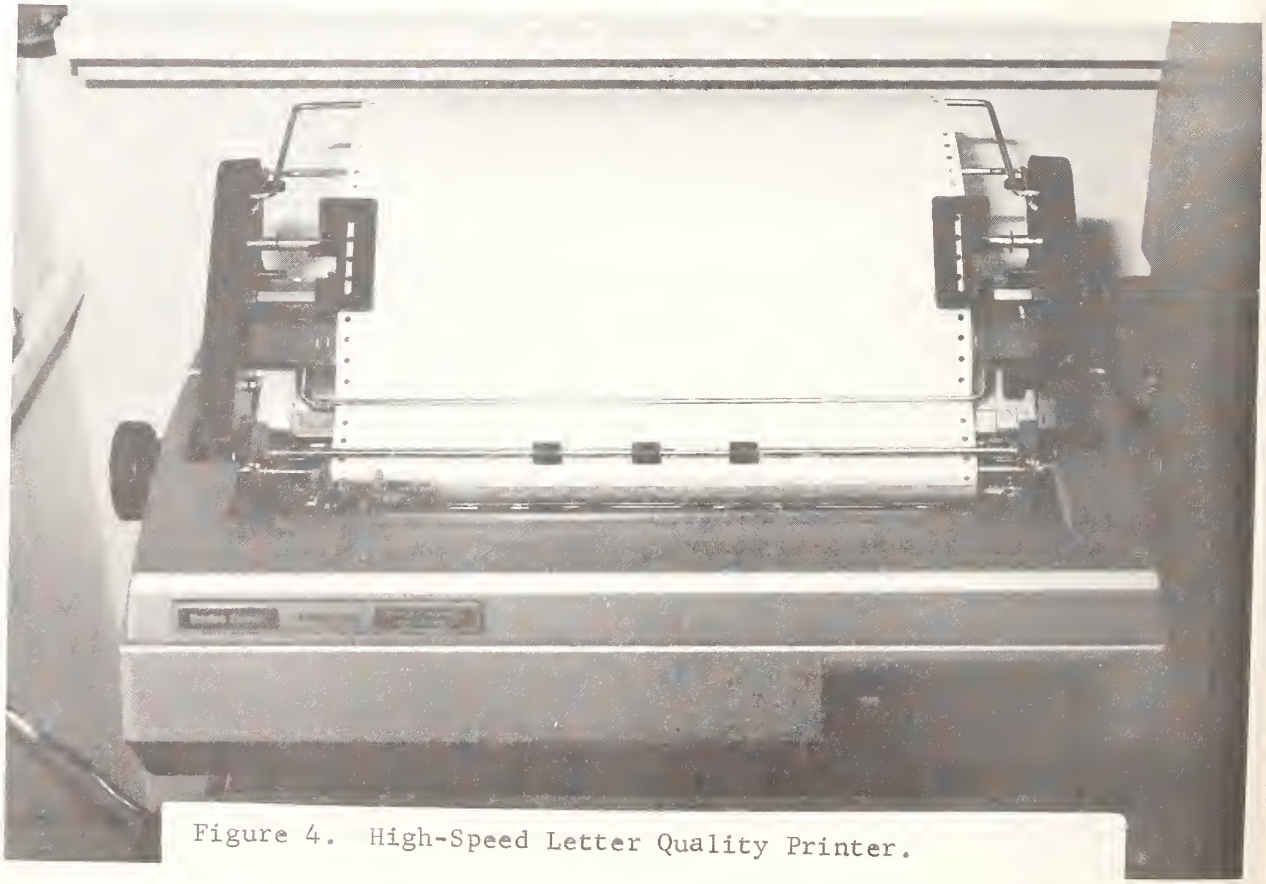

Figure 4. High-Speed Letter Quality Printer.

EARTHQUAKE SAFETY INVESTIGATION SUMMARY OF NAVAL INSTALLATIONS
Installation NCBC PORT HUENEM ; Use FIRE STA ; Type of Const WOOD
Bldg No 430 Year Built 1946 ; No of Stories 1 ; Avg Unit Wt 2.15 PCF
Length 122 ; Width 87 ; Area 7290 ; Vol 118700 ; (FT-LB Units)
Story Ht 16 ; Total Ht 51 ; Repl Cost(RPC)/Date 201 ($K)/9-29-76
Const: Roof COMP OVER RAFTERS & TRUSS ; Col
Ext Walls TYP WOOD CONST. AND PLASTER ; Int Walls TYP WOOD & PLASTER
Floors CONCRETE ; Foundations 4" SLAB & CONT. FTGS
Lat Force Res Syst: Horiz ; Vert SHEAR WALL/TRUSS ACT
Des Base Shear Coef ; Max Ground Site Acc 0.20 (G)
Base Shear (G) Duc Fac (MU): Long ; Trans
Capacity: Yield Long 0.260 ; Trans 0.200 ; Ult Long 0.340 ; Trans 0.260
Demand: Yield Long 0.482 ; Trans 0.474 ; Ult Long 0.378 ; Trans 0.378
Nat Per(sec) Yield Long 0.240 ; Trans 0.230 ; Ult Long 0.360 ; Trans 0.360
Damping(%) Yield Long ; Trans ; Ult Long ; Trans
Damage Est(%)Yield Long 100.0 ; Trans 100.0 ; Combined 100
RSA Eval by CEL ; Damage Est 201 ($K)
Det Str Anal by H.J. DEGENKOLB ASSOC. ; Criteria(P355,UBC,etc) P355
Rehab Cost(RHC)/Date 68 ($K)/ 11-23-81 ; Unit Cost 7.00 ($/SQ FT)
RHC/RPC = 2.940 ; Notes: ID#219. 00004

EARTHQUAKE SAFETY INVESTIGATION SUMMARY OF NAVAL INSTALLATIONS
Installation NCBC PORT HUENEM ; Use HUMID WHSE ; Type of Const CONCRETE
Bldg No 810 Year Built 1955 ; No of Stories 1 ; Avg Unit Wt 1.75 PCF
Length 608 ; Width 200 ; Area 121600 ; Vol 3131200 ; (FT-LB Units)
Story Ht 25.8 ; Total Ht 25.8 ; Repl Cost(RPC)/Date 1948 ($K)/9-29-76
Const: Roof BUILD-UP/PRECST ROOF PANL ; Col STEEL FRAMES
Ext Walls CONCRETE ; Int Walls CONCRETE
Floors 7.5" CONCR. SLAB ; Foundations FOOTINGS WITH SLAB
Lat Force Res Syst: Horiz ; Vert SHEAR WALS/FRAME ACT
Des Base Shear Coef ; Max Ground Site Acc 0.20 (G)
Base Shear (G) Duc Fac (MU): Long ; Trans
Capacity: Yield Long 0.210 ; Trans 0.230 ; Ult Long 0.360 ; Trans 0.270
Demand: Yield Long 0.328 ; Trans 0.405 ; Ult Long 0.364 ; Trans 0.179
Nat Per(sec) Yield Long 0.090 ; Trans 0.850 ; Ult Long 0.140 ; Trans 1.450
Damping(%) Yield Long ; Trans ; Ult Long ; Trans
Damage Est(%)Yield Long 100.0 ; Trans 65.7 ; Combined 89
RSA Eval by CEL ; Damage Est 1725 ($K)
Det Str Anal by H.J. DEGENKOLB ASSOC. ; Criteria(P355,UBC,etc) P355
Rehab Cost(RHC)/Date 1380 ($K)/ 11-24-81 ; Unit Cost 11.40 ($/SQ FT)
RHC/RPC = 0.708 ; Notes: ID#225. 00005

Figure 5. Earthquake Safety Investigation Summary of Naval Installations, Record Nos 00004 & 00005.

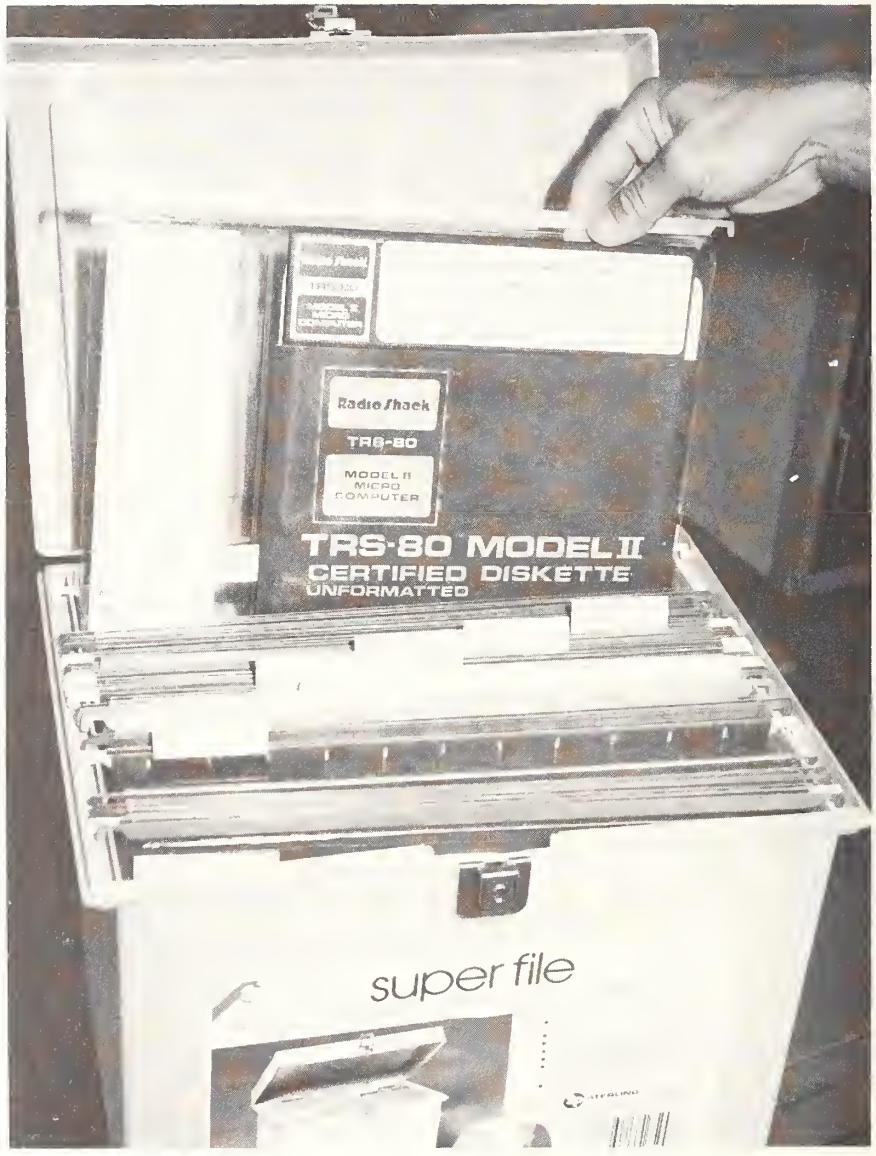

Figure 6. 8-in. Single-Sided, Double Density Diskette and Hanging File Storage Box.

SUMMARY OF RSAP AND DETAILED SEISMIC ANALYSIS
(sectionalized buildings are indicated by ( ))
(rehabilitation cost is given for the whole building)

NAVAL INSTALLATION	BLDG NO.	CONST.TYPE	REPL. COST (RPC, $K)	DAMAGE (%)	ESTIM. ($K)	REHABILITATION COST (RHC, $K)	($/PSF)	RHC/RPC	DETAIL ANALYSIS BY	REC. NO.
NCBC PORT HUENEM	14(1)	WOOD	135	100	135	908	12.15	0.371	H.J. DEGENKOLB ASSOC.	00002
NCBC PORT HUENEM	14(2-4	WOOD	2315	100	2315	908	12.15	0.371	H.J. DEGENKOLB ASSOC.	00003
NCBC PORT HUENEM	430	WOOD	201	100	201	68	7.00	2.940	H.J. DEGENKOLB ASSOC.	00004
NCBC PORT HUENEM	810	CONCRETE	1948	89	1725	1380	11.40	0.708	H.J. DEGENKOLB ASSOC.	00005
NCBC PORT HUENEM	813	STEEL	1665	100	1511	920	17.60	0.553	H.J. DEGENKOLB ASSOC.	00006
NSY LONG BEACH	132	STEEL	17260	79	13680	320	0.46	0.019	H.J.DEGENKOLB ASSOC.	00007
NSY LONG BEACH	210	CONCRETE	15914	49	7834	1612	7.00	0.101	H.J. DEGENKOLB ASSOC.	00008
NSY LONG BEACH	303	MASONRY	11926	100	11926	163		0.014	H.J. DEGENKOLB ASSOC.	00009
NAS ALAMEDA	10	CONCRETE	3241	67	2161	510	28.00	0.157	H.J. DEGENKOLB ASSOC.	00010
NSC OAKLAND	533	STEEL	709	59	418	941	15.00	1.327	H.J. DEGENKOLB ASSOC.	00011
PWC GUAM	372(1)	CONCRETE	1054	49	521	2000	33.00	0.531	H.J. DEGENKOLB ASSOC.	00012
PWC GUAM	372(2)	CONCRETE	468	43	203	2000	33.00	0.531	H.J. DEGENKOLB ASSOC.	00013
PWC GUAM	372(3)	CONCRETE	322	40	130	2000	33.00	0.531	H.J. DEGENKOLB ASSOC.	00014
PWC GUAM	372(4)	CONCRETE	146	0	0	2000	33.00	0.531	H.J. DEGENKOLB ASSOC.	00015
PWC GUAM	372(5)	CONCRETE	177	44	78	2000	33.00	0.531	H.J. DEGENKOLB ASSOC.	00016
PWC GUAM	372(6)	CONCRETE	145	57	83	2000	33.00	0.531	H.J. DEGENKOLB ASSOC.	00017
PWC GUAM	372(7)	CONCRETE	667	9	61	2000	33.00	0.531	H.J. DEGENKOLB ASSOC.	00018
PWC GUAM	372(8)	CONCRETE	790	53	416	2000	33.00	0.531	H.J. DEGENKOLB ASSOC.	00019
PWC GUAM	4910(A	CONCRETE	36219	94	33900	2500	60.00	0.049	H.J. DEGENKOLB ASSOC.	00020
PWC GUAM	4910(B	CONCRETE	14729	56	8234	2500	60.00	0.049	H.J. DEGENKOLB ASSOC.	00021
NSY PUGET SOUND	147	STEEL	4690	60	2800	5664		1.208	CYGNA CONSUL. ENGR., INC	00022
NSY PUGET SOUND	290	CONCRETE	2540	43	1090	5660		2.228	CYGNA CONSUL. ENGR., INC	00023
NSY PUGET SOUND	371	WOOD				861			CYGNA CONSUL. ENGR., INC	00024
NSY PUGET SOUND	434	CONCRETE		50	200	922			CYGNA CONSUL. ENGR., INC	00025
NSY PUGET SOUND	448	MASONRY	1320	100	1320	1822		1.380	CYGNA CONSUL. ENGR., INC	00026
NSY PUGET SOUND	455	MASONRY	2570	63	1620	3780		1.471	CYGNA CONSUL. ENGR., INC	00027
NSY PUGET SOUND	466	CONCRETE	1160	50	580	1374		1.184	CYGNA CONSUL. ENGR., INC	00028
NSY PUGET SOUND	469	STEEL	2130	23	490	503		0.236	CYGNA CONSUL. ENGR., INC	00029
NSY PUGET SOUND	491	MASONRY	1240	67	830	1301		1.049	CYGNA CONSUL. ENGR., INC	00030
NSY PUGET SOUND	497	CONCRETE	290	67	190	563		1.941	CYGNA CONSUL. ENGR., INC	00031
NSY PUGET SOUND	506	CONCRETE	1050	77	810	303		0.289	CYGNA CONSUL. ENGR., INC	00032
NSY PUGET SOUND	513	WOOD	1900	20	380	2716		1.430	CYGNA CONSUL. ENGR., INC	00033

Figure 7. Summary of the RSAP and Detailed Seismic Analysis Data Obtained by Searching the Profile II electronic File.

SUMMARY OF RSAP AND DETAILED SEISMIC ANALYSIS
(sectionalized buildings are indicated by ( ))
(rehabilitation cost is given for the whole building)

NAVAL INSTALLATION	BLDG NO.	CONST.TYPE	REPL. COST (RPC, $K)	DAMAGE (%)	ESTIM. ($K)	REHABILITATION COST (RHC, $K)	($/PSF)	RHC/RPC	DETAIL ANALYSIS BY	REC. NO.
PWC GUAM	372(7)	CONCRETE	667	9	61	2000	33.00	0.531	H.J. DEGENKOLB ASSOC.	00018
PWC GUAM	372(8)	CONCRETE	790	53	416	2000	33.00	0.531	H.J. DEGENKOLB ASSOC.	00019
PWC GUAM	4910(A	CONCRETE	36219	94	33900	2500	60.00	0.049	H.J. DEGENKOLB ASSOC.	00020
NCBC PORT HUENEM	810	CONCRETE	1948	89	1725	1380	11.40	0.708	H.J. DEGENKOLB ASSOC.	00005
PWC GUAM	372(3)	CONCRETE	322	40	130	2000	33.00	0.531	H.J. DEGENKOLB ASSOC.	00014
NSY PUGET SOUND	290	CONCRETE	2540	43	1090	5660		2.228	CYGNA CONSUL.ENGR.,INC	00023
NSY LONG BEACH	210	CONCRETE	15914	49	7834	1612	7.00	0.101	H.J. DEGENKOLB ASSOC.	00008
NSY PUGET SOUND	434	CONCRETE		50	200	922			CYGNA CONSUL.ENGR.,INC	00025
NAS ALAMEDA	10	CONCRETE	3241	67	2161	510	28.00	0.157	H.J. DEGENKOLB ASSOC.	00010
PWC GUAM	372(4)	CONCRETE	146	0	0	2000	33.00	0.531	H.J. DEGENKOLB ASSOC.	00015
PWC GUAM	372(1)	CONCRETE	1054	49	521	2000	33.00	0.531	H.J. DEGENKOLB ASSOC.	00012
PWC GUAM	372(2)	CONCRETE	468	43	203	2000	33.00	0.531	H.J. DEGENKOLB ASSOC.	00013
PWC GUAM	372(5)	CONCRETE	177	44	78	2000	33.00	0.531	H.J. DEGENKOLB ASSOC.	00016
NSY PUGET SOUND	497	CONCRETE	290	67	190	563		1.941	CYGNA CONSUL.ENGR.,INC	00031
NSY PUGET SOUND	466	CONCRETE	1160	50	580	1374		1.184	CYGNA CONSUL.ENGR.,INC	00028
PWC GUAM	372(6)	CONCRETE	145	57	83	2000	33.00	0.531	H.J. DEGENKOLB ASSOC.	00017
NSY PUGET SOUND	506	CONCRETE	1050	77	810	303		0.289	CYGNA CONSUL.ENGR.,INC	00032
PWC GUAM	4910(B	CONCRETE	14729	56	8234	2500	60.00	0.049	H.J. DEGENKOLB ASSOC.	00021

Figure 8. Summary of the RSAP and Detailed Seismic Analysis Data for Only the Concrete Buildings by Searching the Profile II Electronic File.

STRONG MOTION ACCELEROGRAPH STATION DATA BY NCEL, PORT HUENEME, CA

INST STATION NAME GUAM1 NAVAL INSTALLATION PWC GUAM
NAVAL ACTIVITY PLANNIN LOCATION GUAM MI
ADDRESS & ZIP FPO SAN FRAN 96630
LATITUDE 13 24 52N LONGITUDE 144 39 24E INSTAL DATE 6/01/79
ACCELEROGRAPH SMA1 SER NO 3329 RECORDER SMA1 SER NO 3329
BUILDING NO 372 FLOOR LEVEL 1 ROOM NO CONF

INSTALLED BY NCEL PERSONNEL NAME TAKAHASHI AV PHONE1 360 4684

MAINTAINED BY PWCGUAM CONTACT TABIANDO AV PHONE2 339 9176

MAINTENANCE SCHEDULE:
BATTERY CHECK (NEXT DATE) 3/30/82
PAPER CHANGE NEEDED (NEXT DATE) 12/10/83
TEST CALIBRATION TRACE 8/10/82

COMMENTS 2/22/82 HAVE NOT BEEN IN CONTACT WITH THEM. 00001

STRONG MOTION ACCELEROGRAPH STATION DATA BY NCEL, PORT HUENEME, CA

INST STATION NAME GUAM2 NAVAL INSTALLATION PWC GUAM
NAVAL ACTIVITY NRMC LOCATION GUAM MI
ADDRESS & ZIP FPO SAN FRAN 96630
LATITUDE 13 28 24N LONGITUDE 144 44 08E INSTAL DATE
ACCELEROGRAPH SMA1 SER NO 3330 RECORDER SMA1 SER NO 3330
BUILDING NO SG B FLOOR LEVEL 1 ROOM NO 1

INSTALLED BY NCEL PERSONNEL NAME TAKAHASHI AV PHONE1 360 4684

MAINTAINED BY PWCGUAM CONTACT TABIANDO AV PHONE2 339 9176

MAINTENANCE SCHEDULE:
BATTERY CHECK (NEXT DATE) 3/30/82
PAPER CHANGE NEEDED (NEXT DATE) 12/10/83
TEST CALIBRATION TRACE 8/16/81

COMMENTS 2/22/82 NEED TO CONTACT THEM FOR MAINTENANCE 00002

Figure 9. Strong Motion Instrumentation Installation Information, Record Nos. 00001 and 00002.

April 21, 1982

From: S. K.Takahashi, NCEL
To: {NAME}, {INSTALLATION}

Subject: Strong Motion Instrumentation Maintenance

1. It would be appreciated if subject maintenance be provided as indicated below:

Station Name {STATION NAME}
Building Name {BUILDING NO}
Type of instrumentation {INSTRUMENT}

Instrument	Last Date	Next Date
SMAorCRA(battery)	{SLAST DATE}	{SNEXT DATE}
FILM (change paper)	{FLAST DATE}	{FNEXT DATE}
CALIBRATION TRACE	{CLAST DATE}	{CNEXT DATE}

(send magazine with calibration trace to NCEL)

2. Please acknowledge the maintenance performed by circling one of the categories above, fill in the actual date of maintenance (/ /) on this sheet, and mail a copy of this sheet to NCEL, Port Hueneme, CA 93043.

3. If you have any questions or need additional supplies related to the accelerograph, please contact Stan Takahashi at AV360-4684 or Dave Corrente at AV360-5782.

a. Base Letter

April 21, 1982

From: S. K.Takahashi, NCEL
To: W. TABIANDO, PWCGUAM

Subject: Strong Motion Instrumentation Maintenance

1. It would be appreciated if subject maintenance be provided as indicated below:

Station Name GUAM1
Building Name 372
Type of instrumentation SMA1

Instrument	Last Date	Next Date
SMAorCRA(battery)	01/01/81	03/30/82
FILM (change paper)	01/01/81	12/10/83
CALIBRATION TRACE	01/01/81	08/10/82

(send magazine with calibration trace to NCEL)

2. Please acknowledge the maintenance performed by circling one of the categories above, fill in the actual date of maintenance (/ /) on this sheet, and mail a copy of this sheet to NCEL, Port Hueneme, CA 93043.

3. If you have any questions or need additional supplies related to the accelerograph, please contact Stan Takahashi at AV360-4684 or Dave Corrente at AV360-5782.

b. Merged Letter

Figure 10. Strong Motion Instrumentation Maintenance Letter to be Forwarded to Naval Installations

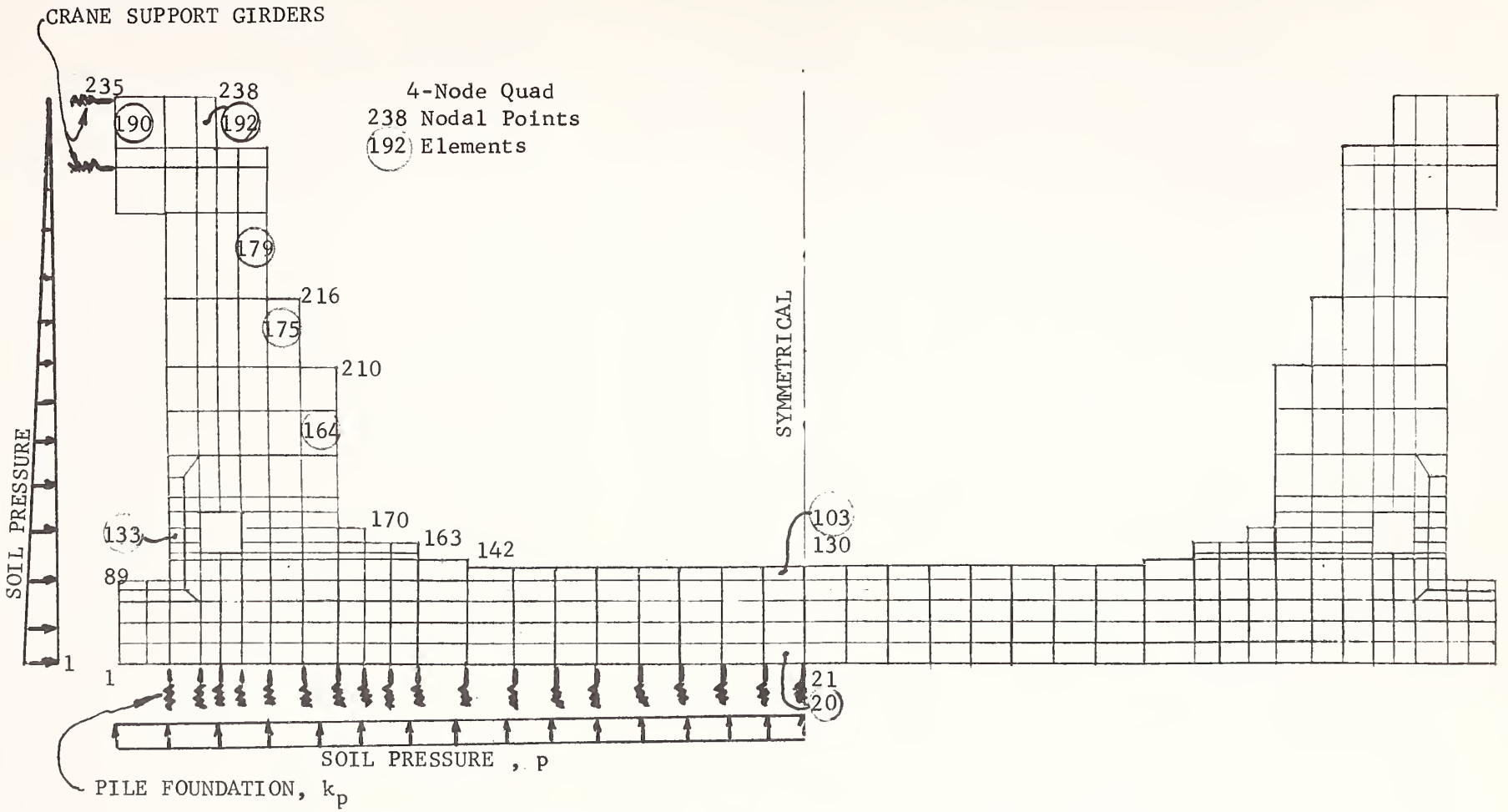

Figure 11. Computer model of one-half of a graving drydock

A TSUNAMI RESEARCH PLAN FOR THE UNITED STATES

Eddie Bernard

Pacific Marine Environmental Laboratory
Nataional Oceanic and Atmospheric Administration
Seattle, WA 98105

ABSTRACT

In response to the identification of deficiencies in tsunami research, a group of scientists and government representatives developed a coherent research plan to address these problems. The plan is designed to foster a course of action that will focus research on forecasting tsunami dangers and evaluating coastal hazards. A brief review of the status of tsunami research is presented and needs for priority research are identified. The three highest need areas are: 1) tsunami observational program, 2) modeling and design related to terminal effects, and 3) tsunamigenic earthquake identification. Two moderate need areas include the creation of a tsunami data set and the development of emergency preparedness programs.

INTRODUCTION

Tsunami are forceful oceanic waves that result from the displacement of seawater during an earthquake or a tectonic shift under the sea. Tsunami are also caused by volcanic eruptions, landslides, rockfalls, and submarine slumps.

Flooding, erosion, and sheer impact associated with tsunami cause hazard to life and damage to property. When strong tsunami currents flood the land, they erode foundations of homes and businesses, weaken the understructures of bridges and railway tracks, wash away seawalls and roads. The force of some tsunami have even damaged structural steel and reinforced concrete buildings. Floating debris -- boats, cars, and pieces of buildings and trees -- causes additional damage as it collides with other structures. Fires result when oil spills from wrecked ships or damaged storage and refinery facilities and sewage and chemical pollution are caused when pipes and tanks are ripped apart by the force of these waves. Of increasing concern is the potential effect of tsunami drawdown when receding waters uncover cooling water intakes associated with nuclear power plants.

The continental United States has not been seriously affected by a tsunami since 1964. During these past 18 years, interest in tsunami research in the United States has declined sharply. The report from the 1979 workshop sponsored by the National Science Foundation (NSF) to review the status of tsunami research states that input from tsunami research estimating the impact of tsunami has been inadequate for warnings, risk analysis, or engineering design.

Present techniques of tsunami prediction are severely limited. The only way to determine, with certainty, if an earthquake is accompanied by a tsunami is to note the occurrence and epicenter of the earthquake and then to track the arrival of the tsunami at a network of Pacific tide stations. Although it is possible to predict when tsunami will arrive at coastal locations, it is not yet possible to predict the wave height, number of waves, duration of the hazard, or the forces to be expected from such waves at specific locations. Without reliable quantitative estimates of force, it is not possible to recommend appropriate measures to protect people and property.

The present warning system reflects this critical problem; it is a reactive system conducive to overreaction, underreaction, or panic and will remain so until we create a valid and responsible system to forecast the severity of tsunamis.

In response to these deficiencies, scientists and government representatives (see appendix I) have developed a coherent plan for tsunami research in the United States. The plan is designed to foster a course of action that will focus research on forecasting tsunami dangers and evaluating coastal hazards. The reliable forecasting of tsunami dangers can provide a basis for recommending the evacuation of people, removal of boats and ships, and specification of firefighting and police procedures. The evaluation of a coastal tsunami hazards potential for coastal areas can lead to guidelines for appropriate land-use and to criteria for engineering design in potentially threatened areas. Achieving these goals should reduce the destruction of lives and loss of property from future tsunamis.

COMPREHENSIVE TSUNAMI RESEARCH PLAN

To achieve the goals of forecasting tsunami dangers and evaluating coastal tsunami hazards to reduce loss of life and destruction of property from future tsunami, we must carefully define these goals, evaluate the present state of knowledge, formulate appropriate objectives, and take steps to achieve them.

Forecasting the severity of tsunami for selected coastal locations means being able to predict the following within 1 hr of tsunami generation:

1. Arrival time of tsunami.
2. Maximum wave heights.
3. Duration of hazardous conditions.
4. Maximum currents in harbors.

For tsunami that impact the United States coastlines in less than 1 hr after generation, special mitigation measures should be taken on the basis of the identification of a specified hazard zone.

Such predictions provide a basis for evacuating people, moving boats and ships, outlining firefighting and police procedures, and allowing people to return to evacuated areas when danger has passed.

Evaluating coastal tsunami hazards means:

1. Determining the probability of occurrence within the limits of available historical data.
2. Delineating the maximum limits of inundation for zoning and evacuation purposes.
3. Determining maximum forces exerted on stationary and moveable objects within inundation zones for land-use regulation and structural standards.

Such information provides land-use guidelines and criteria for engineering design for potentially threatened areas and establishes a basis for reducing life and property loss from tsunami.

The use of forecasted dangers, coupled with determination of the hazard zone, enables communities to react to save lives and protect property with minimal disruption to essential services. The Tsunami Research Plan is directed toward this effort.

EVALUATING PRESENT KNOWLEDGE OF TSUNAMI

The current state of tsunami research can be described in seven areas that range from understanding of the geophysical aspects of the phenomenon to use of this information in an emergency situation. These divisions illustrate the interdependencies of science, engineering, and policy-making. For the purpose of this report, we will define the seven areas as follows:

Tsunamigenic Earthquakes: Large-magnitude, shallow focus submarine earthquakes that involve vertical deformation of the sea floor are the principal generators of tsunami. Because seismic waves propogate 30 times faster than the speed of a tsunami, identification of earthquake waves associated with tsunamis is essential to forecasting the genesis of a given tsunami.

Tsunami Generation: The transfer of energy from the earthquake to the ocean in the form of tsunami is poorly understood because of lack of adequate measurements at the source. Understanding generation processes is important to determining the hazard zone and forecasting tsunami wave heights for locally generated tsunami.

Tsunami Propagation: Once the ocean surface is displaced by the earthquake, that point in the ocean acts as a radiator of waves that traverse the entire ocean basin. Modeling techniques have the benefit of only one direct observation of these waves in the open ocean environment from a small tsunami. Since these waves ultimately encounter populated shoreline, understanding the propagation processes that take place as the tsunami approach the shoreline is imperative to provide accurate forecasting.

Terminal Effects: Tsunami cause damage to structures by: 1) strong currents produced by waves overtopping structures; 2) direct force of the surge produced by the wave; 3) hydrostatic pressure created by flooding behind a structure; and 4) erosion at the base of the structure. Additional damage may be caused by debris propelled by the tsunami into other objects. Tsunami engineers believe increased understanding of wave runup and drawdown harbor and bay response, surge or drybed and forces on structures will contribute most toward the mitigation of the hazard.

Instrumentation: Improved instrumentation is essential to obtaining measurements necessary for investigation and prediction of tsunami. Real time sensors, oceanographic measurement devices, and efficient telecommunications are the basic tools for this purpose.

Warning: Tsunami generated at great distances from the affected area are termed teleseismic. Improvements in forecasting and modeling wave impacts will enable the warning centers to improve services.

Tsunami generated at the earthquake source are termed local. Since warning centers are not capable of responding to tsunami in less than 15 min, public education programs must prepare inhabitants and visitors for proper response.

Most tsunami are both local and teleseismic in potential danger.

Social Response/Risk Analysis: Any mitigation measures taken must balance the cost of these changes with the benefits to society. Integration of the public needs with the development of warning strategies is critical for balanced utilization of resources. To achieve this balance, investigation and improvements in the existing historical data sets are required.

Table 1 presents an assessment summary of the current status of research for each of these areas. An evaluation of the state-of-the-art of each research area is given in the second column of table 1. This evaluation describes the status as either low (know almost nothing of value to mitigate tsunami hazards) or moderate (know enough to assess next step necessary to mitigate tsunami hazards).

The State-of-the-Art column is divided into modeling (analytical or physical representation of tsunami) and observations (measurements of tsunami). As one examines the state-of-the-art, note that moderate modeling with low observations means that measurements are necessary to verify modeling efforts. Modeling will advance forecasting abilities or hazard zone determinations only with proper verification. Likewise, moderate observations with low modeling illustrate a need for data analysis and interpretation to ensure mitigation of tsunami hazards.

The next column in table 1 lists recommendations to mitigate tsunami hazards for each area of research. These recommendations emerged from a thorough review of our present capabilities as well

as policy concerns. Agencies that are candidates for conducting or funding the research are listed in the final column.

IDENTIFYING NEEDS

The workshop participants translated the recommendations listed in table 1 into priorities based on relative needs as shown in table 2. Two need levels emerged. High need means that the effort is essential to mitigating the hazards of tsunami, and moderate need means that the effort is significant in reducing tsunami hazards. In view of these needs, we are prepared to present plans for achieving our goals.

FORMULATING PLANS

In this section we will elaborate on the needs presented in table 2 to explore the rationale for these recommendations.

TSUNAMI OBSERVATION PROGRAM

For every proposed effort in table 2, the need for measurement of tsunami is specified. At present, no instruments in use are capable of recording any single phase of tsunami activity with both precision and accuracy. The highest need, therefore, is to design and install instruments that will accurately measure tsunami and tsunami force. Requirements for the observational program include the following:

A. For tsunami along the coastline:

   1. For measurements in shallow water:

      Installation of standard tsunami gages with fixed, calibrated frequency band at key locations.

   2. For wave force measurements during tsunami flooding:

      Creation of a highly specialized group to design and activate an observation plan. The U.S. Army Corps of Engineers has established a hurricane response team to deploy instruments to measure flooding forces in potentially affected areas. Perhaps a tsunami group could be a subset of this larger effort. Also, the Earthquake Engineering Research Institute surveys the impacts of major earthquakes throughout the world. The tsunami group could complement the earthquake survey for tsunami events.

B. For tsunami in the open ocean:

   An array of instruments to measure open ocean tsunami should be deployed to obtain data adequate for model verification.

MODELING AND DESIGN RELATED TO TERMINAL EFFECTS

a) Establishment of Theoretical and Laboratory Program for Fluid/Structure Interactions

Both theoretical and laboratory programs are needed to analyze and understand the fluid/structure interactions responsible for tsunami damages. Such programs should lead to a classification of the modes and extent of structural damages according to type of structure and means of damage. Observed damages should be documented and quantified as rapidly as possible following a tsunami and before relief operations begin. Followup studies should be planned to determine cost of replacement and repairs.

b) Determination of Structural Design Criteria

Better criteria for engineering design for structures located in areas where tsunami inundation is possible can be developed through an observation program to collect data on damages that have occurred in previous tsunami. Theoretical and experimental programs would link investigations of wave/structure interactions to relevant tsunami characteristics and, with proper interpretation, would provide useful criteria for engineering design that offers protection from tsunami.

TSUNAMIGENIC EARTHQUAKE IDENTIFICATION

We recommend instrumentation, telemetry, and data processing to permit real-time inference of sea floor displacement to identify tsunamigenic earthquakes/seismic data. This is a costly activity, and it should be conducted in coordination with other seismological research and monitoring activities. Coordination of seismological research to examine the seismic characteristics of tsunamigenic earthquakes may be a cost-effective way to explore an insufficiently understood area of research. A coordinating group should be established to define tsunami seismological research requirements earthquakes to accomplish the goal of seismically differentiating between tsunamigenic and other earthquakes as they occur.

TSUNAMI DATA SET CREATION

Increase and scrutinize the tsunami historical datasets at World Data Centers in Boulder, CO, and Moscow, USSR, and the International Tsunami Information Center. These data can be used to determine the risks from tsunami flooding which, in turn, can be utilized for policy planning.

Tsunami risk analysis should be undertaken as an integral part of studies related to social response, using the criterion of balancing the impact of tsunami with the cost of mitigating impacts. Risk analysis, as performed for other hazards of nature such as flooding, severe storms, and earthquakes, should be used for similar analysis of tsunami risk problems.

EMERGENCY PREPAREDNESS PROGRAM DEVELOPMENT

An educational plan should be undertaken to prepare the public for tsunami in potentially threatened communities as identified by historical data. The program should include local authoritie who establish standard operating procedures, enforcing officials who implement these procedures, and the people living in the area.

A model available for study is the State of Hawaii, County of Hawaii, plan. Because of the efforts of dedicated Hawaiian county authorities, the public is well educated and responded well to a locally generated tsunami in 1975. During this 1975 tsunami, which led to the death of two people, more deaths and other losses were averted because people had been advised about safety procedures through the effort of the continuing program of public education.

Emergency preparedness has a priority below that of measurements, observations, and earthquake signal analysis in terms of the research plan, but should have top priority within other emergency preparedness agencies.

CONCLUSION

The plan we have presented here addresses research needs to mitigate tsunami hazards. It incorporates the scientific, social, and economic needs to provide a road map for resource allocations in future planning exercises. We are conviced that emphasis on tsunami measurements, modeling and design in the shoreline area, and identification of tsunamigenic earthquakes will mitigate the hazards from tsunami in the United States.

Table 1. Status of Tsunami Research

Research Area	State-of-the-Art Modeling/Observations		Recommendations to Mitigate Tsunamic Hazard	Agencies*
Tsunamigenic Earthquakes	Low	Moderate	Instrumentation, telemetry, and data processing to permit real-time inference of sea floor displacement.	USGS/NSF/FEMA
Tsunami Generation	Moderate	Low	Field surveys of tsunamigenic earthquakes to determine surface deformations for modeling purposes.	USGS/COE/NSF/HI
Tsunami Propagation	Moderate	Low	Measurements of tsunami in oceanic and coastal areas.	NOAA/NSF/HI
Terminal Effects	Moderate	Low	Measurements of surge velocity, pressure, and other fields to advance modeling of runups, drawdown, bore formation, and forces on structures.	NSF/COE
Instrumentation	Moderate		a) Real-time seismic and tsunami measurements b) Coastal tsunami measurements.	NOAA/COE/HI
Warning: Teleseismic			Ability to predict tsunamigenesis from seismic data and runup.	NOAA/FEMA
Local			Emergency preparedness to prepare public.	
Social Response/ Risk Analysis	Low	Low	Increase and verify existing data sets in World Centers A** and B*** and the International Tsunami Information Center for application to risk analysis.	NOAA/FEMA NRC/NSF

* USGS, ...NSF (see appendix II for identification).
** A: Boulder, CO
*** B: Moscow, USSR

Table 2. Tsunami Research Plan Priorities

Need	Proposed Efforts	Priority	Research Areas
High	Tsunami Observation Program Design and install instruments to measure: a) tsunami along the coastline b) tsunami in the open ocean	I	All areas
High	Modeling and Design Related to Terminal Effects a) establish theoretical and laboratory program for fluid/structure interactions b) determine structural design criteria	II	Terminal effects
High	Tsunamigenic Earthquake Identification Establish a coordinating body of Federal agencies to examine seismic characteristics of tsunamigenic earthquakes	II	Instrumentation/ tsunamigenic earthquakes
Moderate	Tsunami Data Set Creation Increase and verify existing data sets and utilize in risk analysis	III	Social response/ risk analysis
Moderate	Emergency Preparedness Program Development Create public awareness program of potential dangers of tsunami	III	Warning

Appendix I

Workshop Participants

Study Group Leader:

Richard Goulet
National Science Foundation

George Carrier
Harvard University

Jerry Harbor
U.S. Nuclear Regulatory Commission

Phil Hseu
National Science Foundation

James Houston
U.S. Army Corps of Engineers

Li-San Hwang
Tetra Tech, Inc.

Hiroo Kanamora
California Institute of Technology

George Lea
National Science Foundation

Keen Lee
Tetra Tech, Inc.

Bernard LeMehaute
Rosenstiel School of Marine &
Atmospheric Sciences
University of Miami

Chi Liu
National Science Foundation

Coordinator:

Eddie Bernard
National Oceanic and Atmospheric
Administration

Harold Loomis
Joint Institute for Marine and
Atmospheric Research
University of Hawaii

Dennis Moore
Joint Research for Marine and
Atmospheric Research
University of Hawaii

Frederic Raichlen
California Institute of
Technology

Roger Stewart
U.S. Geological Survey

Charles Theil
Federal Emergency Management
Agency

David Tung
North Carolina State
University

William Van Dorn
Scripps Institute of
Oceanography

Andrew Vastano
Texas A&M University

Ted Wu
California Institute of
Technology

Appendix II. List of Acronyms

COE	U.S. Army Corps of Engineers
FEMA	Federal Emergency Management Agency
HI	State of Hawaii
NOAA	National Oceanic and Atmospheric Administration
NRC	Nuclear Regulatory Commission
NSF	National Science Foundation
USGS	U.S. Geological Survey

DIGITAL DATA SERVICES FOR TSUNAMIS AND ENGINEERING SEISMOLOGY

James F. Lander

National Geophysical and Solar-Terrestrial Data Center

ABSTRACT

The consolidation of NOAA's environmental data banks in one system, the development of digital data directories, dictionaries, and inventories, the use of data base management systems and mass store, and accessibility of the whole system remotely offer new opportunities for users to directly get data shaped to their needs from multiple discipline files. A National Environmental Data Referral Service can help users find data in the system and elsewhere worldwide. Possibilities of networking with bibliographic and other data bases are also promising.

INTRODUCTION

There are significant developments in the system for managing data in NOAA which are revolutionizing data services. The first of these, the Data Archive Management and User Services I - DAMUS I - is just beginning its operational phase in Asheville, NC. It will provide mainframe computing for all of EDIS' computing. It will have a mass store system, a data base management system, COM and other peripheral devices, and will serve the National Climatic Center locally and the National Geophysical Data Center in Boulder and the National Oceanographic Data Center and other centers in Washington via communication links. By next year the system will allow users to access the facility remotely, peruse the directory, dictionary, and inventories, access and process data and output to list, microfilm, or tape or the the user's terminal or computer. The successor system, DAMUS II, is in final specification stage and should be in place by 1984. This will provide substantially larger computing power and accessibility. Improvements in global communications can make these data bases accessible to users anywhere. A second system being developed is the National Environmental Data Referral Service NEDRES - which will give users access to digitally searchable information on the existence of environmental data bases held elsewhere. Among the advantages of the new system for users of tsunami and engineering data in digital form including digital inventories of analog data are accessibility under a generalized data base management system. Thus, data of any specified characteristics can be located. For example, it can locate tsunamigenic earthquakes of this century originating in the Aleutian Islands which produced waves of at least 1 m anywhere in Hawaii for which there are available marigrams. It is possible to digitize and store all tsunami marigrams. Similarly, strong motion records could be compared with epicenters, intensity, and seismographic data.

SYSTEMS

Until November 1981, each of the EDIS data centers maintained their data bases and had separate arrangements for computing. All of the EDIS data bases and servicing software have been converted to operate on two Univac 1100/10 mainframe computers located in Asheville, NC (see figure 1). The centers in Boulder and Washington communicate via 9600 baud lines. Presently, data requests come into the centers and are entered into the system. Simple requests for lists, tape copies, cards, and COM are sent directly to the user by the Asheville facility. Others may be returned to the originating center for plotting, editing, or other individual handling. The present system has 5.2 megabytes of disk capacity. An IBM 3850 mass store system is on the premise and should be operational by this summer. It has a 35 billion byte capacity and can expand to 256 billion. Offline storage of the canisters makes an almost unlimited capacity quickly available. Users will be able to request data from the centers in the usual way by letter or telephone or later by establishing an account they can call in directly and be guided through the system by a hierarchy of directories, dictionaries, and inventories. They will be able to see what data exist in the system including analog data holdings. They will be able to inspect the data, perform computations on it, and get the results as tape, cards, lists, plots, or COM mailed to them or the results could be dropped to their terminal or computer for further processing.

The Data Base Management System, System 2000, allows for large data bases to be stored in a generalized way. Data satisfying any set of criteria can be recovered quickly.

The National Environmental Data Referral Service (NEDRES) recognizes the need to help users find data which may not be held by EDIS. It acts similar to a digital bibliographic data base in letting users search the descriptions on a word or combination of words such as "storm (adjacent to) surge." The present file consists of about 14,000 data base descriptions and is being tested by EDIS. If it is developed as planned, it could be available for public access with the then-available data base descriptions by October 1983. It will eventually include national and international listings. It will include data files broadly in meteorology, oceanography, geophysics, including environmental pollution. It is a vast undertaking and will necessarily be incomplete. It will employ input from the existing data centers which have staff knowledgeable of related data bases held elsewhere, and from a network of state contributors for the U.S. It will probably be associated with international groups such as ICSU's CODATA Directory Project (see table 1).

DATA BASES

One of the first data bases to be put on the system under the data base management system is the Tsunamis of the Pacific History. Over the last decade, K. Iiada of Japan, S. L. Soloviev of the

USSR, and G. Pararas-Carayannis and D. Cox of the U.S., have been compiling and verifying a definitive catalog of Pacific tsunamis. The file now has information on over 1000 tsunami events since earliest reports. Because of their long history many of the reports are of Japanese origin. The catalog contains information on the universal date and time, effects reported from all sites, the references to the event, tsunami intensity and magnitude, tsunami source region, local dates, and a validity code. The latter based on a five step scheme from 0 (did not occur) to 4 (definite) is necessary since earlier accounts may be somewhat difficult to evaluate as to what actually occurred. Zero validity events are often duplicates with slightly different date or mistakes in conversion from historical calendars to universal dates. They are carried in the file to prevent their being rediscovered and added to the file. The catalog will be published but will also exist in digital form under System 2000. In its digital form it will be searchable on any combination of parameters and will access information on related files. These latter include the inventory of marigrams, inventory of tsunami photographs, earthquake hypocenter, and intensity data, inventories of available analog seismograms or direct access to digital seismograms, bathymetric data, and, perhaps later, tsunami travel time curves and digitized marigrams (see figure 2).

For Engineering Seismology the approach will be similar. Our Hypocenter Data File which includes basic information on 360,000 earthquakes from most of the known catalogs including several from Japan, is already operating under System 2000. The digital inventories of our analog holdings are mostly prepared. Digital seismographic data from the SRO and WWSSN stations will soon go on the mass store. The digital wave form of strong motion data will likewise be stored. This includes the recently acquired collection of 177 components of Japanese data for the 1956-1978 period compiled and corrected by EXXON and issued as a printed catalog, "Strong Motion Data from Japanese Earthquakes," WDC-A Report SE-29.

Each earthquake intensity report for all U.S. earthquakes from 1925 to the present and some larger older earthquake intensity reports are in digital form. This file of 110,000 observatories will also be accessible under System 2000 so that searches could be made about any area, intensity range, date, and/or town names.

CONCLUSION

The application of data base management to large multidiciplinary files will open up the possibility of user controlled data services that are rapidly and remotely available. While costs have not been addressed, the system, particularly when upgraded to DAMUS II in 1984, will provide abundant computing power and storage for huge amounts of data. The application is limited by the

availability of digital data or digital inventories. It could be networked to other computing systems, including bibliographic files, NEDRES, or socioeconomic data.

Table 1. National Environmental Data Referral Service (NEDRES)

Purpose

To improve access to worldwide environmental data needed for government and private decisionmaking by providing a publicly available, computer searchable environmental data index and referral service.

Goals

Identify for users the existance, location, and characteristics of environmental data files relevant to their needs.

Meet statutory and national program requirements for a data referral service.

Serves as a resourcce for U.S. participation and exchange with international data referral systems, such as those of WMO, IOC, CODATA, and UNEP.

Types of Environmental Data Referenced by NEDRES

Climatological and meteorological

- standard surface and upper atmosphere
- atmospheric radiation, physics, and chemistry
- air quality

Oceanographic

- physical, chemical, biological
- ocean mineral and energy resources
- ocean pollution

Geophysical

- geomagnetic and seismological
  - marine geological and geophysical
  - solar-terrestrial physics
- geodetic and cartographic
- glaciological
- aquatic ecological and limological

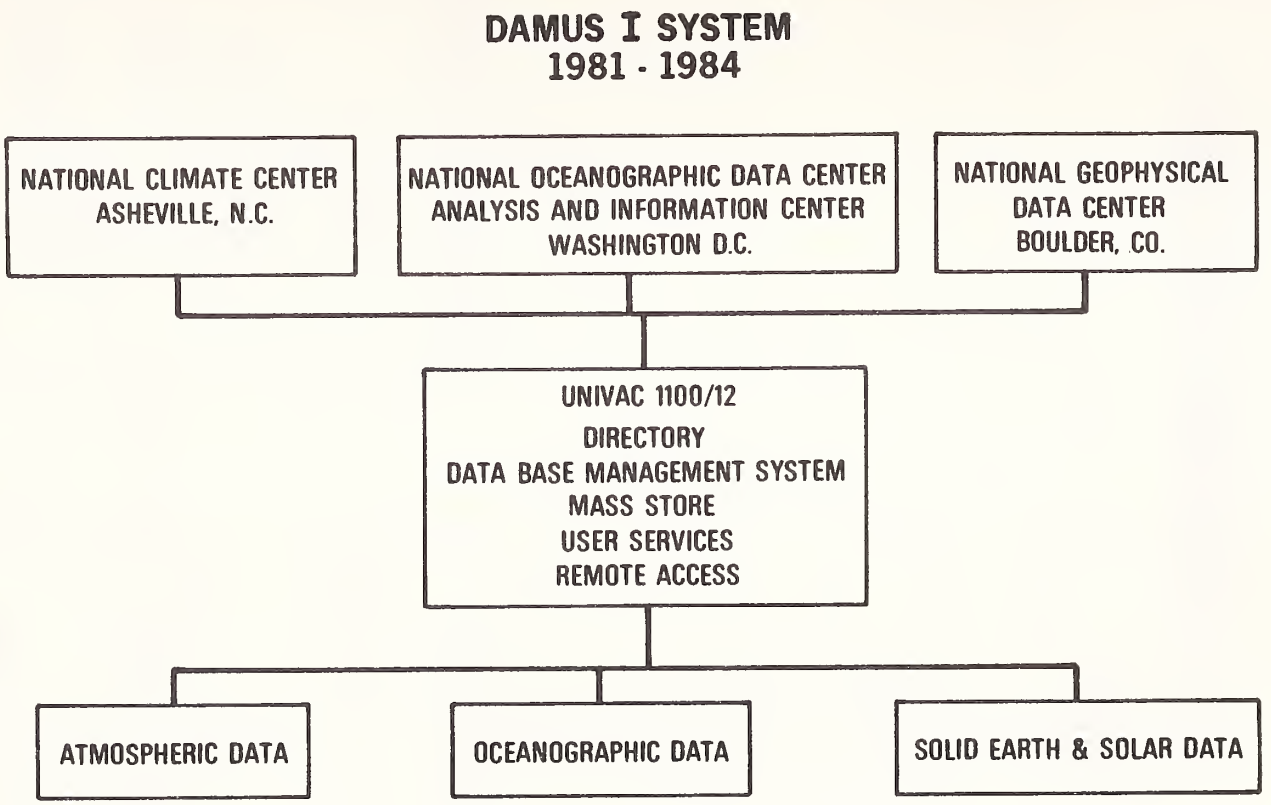
DAMUS I SYSTEM
1981 - 1984
NATIONAL CLIMATE CENTER
ASHEVILLE, N.C.
NATIONAL OCEANOGRAPHIC DATA CENTER
ANALYSIS AND INFORMATION CENTER
WASHINGTON D.C.
NATIONAL GEOPHYSICAL
DATA CENTER
BOULDER, CO.
UNIVAC 1100/12
DIRECTORY
DATA BASE MANAGEMENT SYSTEM
MASS STORE
USER SERVICES
REMOTE ACCESS
ATMOSPHERIC DATA
OCEANOGRAPHIC DATA
SOLID EARTH & SOLAR DATA

Figure 1.

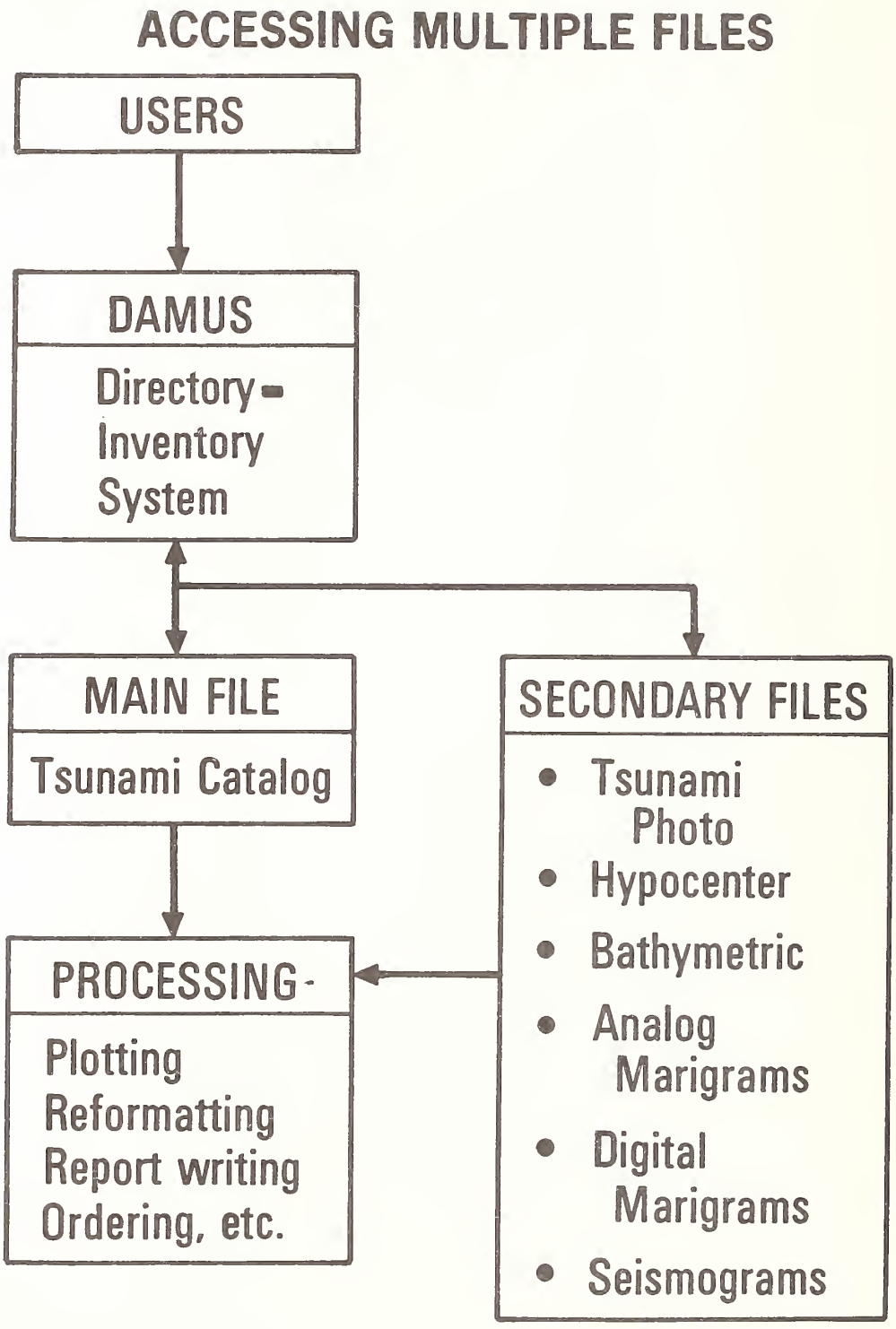
ACCESSING MULTIPLE FILES
USERS
DAMUS
Directory -
Inventory
System
MAIN FILE
Tsunami Catalog
PROCESSING -
Plotting
Reformatting
Report writing
Ordering, etc.
SECONDARY FILES
• Tsunami Photo
• Hypocenter
• Bathymetric
• Analog Marigrams
• Digital Marigrams
• Seismograms

Figure 2.

CONSTRUCTION OF THE FULL-SCALE REINFORCED CONCRETE TEST SPECIMEN

J. K. Wright

Associate Professor
Department of Civil Engineering
The University of Michigan
Ann Arbor, Michigan

ABSTRACT

A short summary of the construction of the full-scale seven-story reinforced concrete building is presented. Differences between Japanese and U.S. construction practices are discussed. Cross section dimensions and reinforcement details for important portions of the structure are also presented.

INTRODUCTION

The full size seven-story reinforced concrete structure, scheduled to be tested as part of the U.S.-Japan Cooperative Earthquake Program [1], was constructed in the Large Size Structural Laboratory of the Building Research Institute, Ministry of Construction, Tsukuba, Japan. Construction started on September 17, 1980, and the last concrete was cast on January 12, 1981.

The general layout of the building is shown in figures 1 through 3. Figure 1 is a general plan view and shows nominal span lengths. The location of the reaction wall is also shown in figure 1. The test structure consisted of three frames (A,B,C) parallel to the loading direction and four frames (1,2,3,4) perpendicular to the loading direction.

A general elevation of frame B is given in figure 2. Spans 1-2 and 3-4 are open frames, but span 2-3 is a shear wall with a nominal thickness of 20 cm (8 in). The girders of spans 1-2 and 3-4 and the longitudinal reinforcement for those girders are not continued through the shear walls.

Figure 2 also shows the floor level notation used in this report, starting from level Z0 at the laboratory floor to level ZR at the roof. This notation is not the same as is typically used in U.S. Research reports, which would commonly label floor level Z2 as the first floor, etc. Story designations used in this report are standard, that is, the first-story runs from level Z1 to Z2, etc. Frames A and C are pure open frames and have dimensions identical to those given in figure 2.

A general elevation of frame 4 is given in figure 3. Both spans A-B and B-C have 15 cm (6 in) thick shear walls, but the walls do not frame into the columns. A 1 m gap was provided between the face of the columns and the edge of the wall to permit easy passage of instrumentation beams. In frame 4, pairs of openings (440 mm by 500 mm) were provided at each floor level to permit the passage of instrumentation beams. Frame 1 is identical to frame 4 except the openings for the loading beams

were not required. The walls in frames 1 and 4 are expected to increase the torsional stiffness of the structure and thus ensure the structure will move only in the NS direction when loaded. Frames 2 and 3 are pure open frames and have dimension identical to those given in figure 3.

CONSTRUCTION TECHNIQUE

The seven-story test structure was constructed by Japanese construction workers employed by Kajima Corporation. Some of the differences between Japanese and the U.S. construction techniques are presented here.

In Japan the main longitudinal reinforcing bars of beams and columns are usually spliced by gas pressure welding instead of by lapping the bars. The gas pressure welding technique essentially butt fuses successive bars.

At the start of the gas pressure welding method the ends of the reinforcing bars are cleaned and sanded and then a hydraulic cylinder is used to align the bars. The gap between the bars is to be less than or equal to 3 mm. No misalignment or warp is permitted. An acetylene torch, which has a twin semicircular head, is then used to heat the butt zone. The butt zone is defined as a length of bar extending one bar diameter above and below the gap. When the butt zone reaches a red hot condition, the soil pressure in the hydraulic cylinder is increased so the ends of the reinforcing bars are clamped together with pressure of 300 kg/cm^2. Heat is applied during the clamping process until a bulge of at least 1.4 times the bar diameter is developed. Heating is then stopped and after the bar had lost its "fire color", the clamping device is removed.

The final quality of the weld depends on the chemical composition of the reinforcing steel, the skill of the welder, and the environmental conditions. Specifications [2] for the gas pressure welding process have been developed by the Japanese Pressure Welding Society. A report [3] of tests on gas pressure welding of reinforcing bars is available from Nippon Steel Corporation.

For the seven-story test structure, an agreement was reached which allowed the gas pressure welding technique to be used for splices of main reinforcement in the foundation and all the columns. Standard U.S. lap joints were used in all beams, slabs, and walls.

A second construction difference in Japan is that all of the concrete for the columns and walls in a certain story level, and for the beams and slabs at the next higher floor level, is cast at the same time. In typical U.S. practice the columns and walls are cast first and then, at a later date, the floor slab and beams are cast. The Japanese casting practice was used in the seven-story test structure.

CONCRETE DIMENSIONS

In general, the as built dimensions were very close to the nominal dimensions. Several dimensional checks were made and no significant deviations from the nominal dimensions were found.

Nominal dimensions for the beams in frames A, B, and C were 300 mm (12 in) width and 500 mm (20 in) total depth. Nominal column dimensions were 500 mm by 500 mm (20 in by 20 in). The nominal thickness of the shear wall in frame B was 200 mm (8 in).

REINFORCEMENT DETAILS

Nominal reinforcement details for the major structure members were as follows:

Beams of frames A, B, and C: All D19 bars (approximately no. 6 bar); end sections had three top bars and two bottom bars; midspan sections had two top bars and three bottom bars.

Columns: Eight D22 bars (approximately no. 7 bar) uniformly distributed around the cross section.

Wall in frame B: D10 bars (approximately no. 3 bar) were used in both faces at a 200 mm (8 in) spacing both vertically and horizontally.

Important reinforcement details for frames A and C are noted here:

1. Within a region extending one-quarter of the clear span from the face of the column, all of the floor beams were to have stirrups provided at a spacing approximately equal to one-forth of the effective beam depth. The spacing was to be increased to approximately one-half of the effect beam depth in the center region of the beam span.
2. Perimeter hoops were to be provided at a 100 mm (4 in) spacing over the total height of the columns, including the beam to column joint regions.
3. Cross ties were to be provided at a 100 mm (4 in) spacing over the first 0.6 m (24 in) of the columns above the foundation (level Z1). For the remaining portion of the total column height, except at the beam to column joints, cross ties were to be provided at a 0.6 m (24 in) spacing. No cross ties were to be used in the beam to column joints.
4. All of the beam bars terminating at an exterior column were to be anchored with a 90 degree hook. The portion of the beam bar extension beyond the hook was to pass through the midheight of the beam to column joint and was to be in the same vertical plane as the external edge of the column confined region.
5. All of the column bars were to be terminated at the roof level with a 180 degree hook which extended toward the column centroid.

Important differences in reinforcement details between frame B and frames A and C are noted here:

1. For the columns which bounded the shear wall, columns B2 and B3, cross ties were to be provided at a 100 mm (4 in) spacing over the full height of the first three-stories. They were not to be provided in the beam to column joints. For the fourth- through the seventh-stories, cross ties were to be provided at a 0.6 m (24 in) spacing.
2. All of the beam reinforcement terminated with 90 degree hooks in the wall boundary columns. The anchorage was to be the same as that described item 4 for frames A and C.
3. The horizontal wall reinforcement was to be anchored by extending the bar straight to the exterior edge of the confined region of the wall boundary columns.
4. The vertical wall reinforcement was to be anchored into the foundation with a straight extension of 0.4 m (16 in) below the top of the foundation.

MATERIAL PROPERTIES

The nominal yield stress of all the reinforcement used in the test structure was 3500 kgf/cm^2 (50 ksi). The average measured yield stress was 3870 kgf/cm^2 (55 ksi) for the wall reinforcement, 3650 kgf/cm^2 (52 ksi) for the beam longitudinal reinforcement, and 3530 kgf/cm^2 (50 ksi) for the column longitudinal reinforcement.

Two different concrete strengths were used in the test structure. Concrete with a nominal strength of 255 kgf/cm^2 (3600 psi) was used in the first four-stories and concrete with a nominal strength of 270 kgf/cm^2 (3800 psi) was used in the upper three-stories. The change to a higher strength concrete was made because of the cooler temperatures inside the laboratory during the casting of the upper stories.

REFERENCES

[1] "U.S.-Japan Cooperative Earthquake Research Program," Program Announcement, National Science Foundation, Washington, D.C., December 1979.

[2] "Standard Specification for Gas Pressure Welding of Reinforcing Bars," The Japanese Pressure Welding Society, Tokyo, Japan, February 1979.

[3] Takano, S., Yokokawa, T., and Ikeno, T., "Automatic Gas Pressure Welding for Concrete Reinforcing Bars," Products Research and Development Laboratories, Nippon Steel Corporation, Sagamihara, Japan, August 1976.

[4] "Recommendations for a U.S.-Japan Cooperative Research Program Utilizing Large-Scale Testing Facilities," Report to the National Science Foundation, Earthquake Engineering Research Center Report No. UCB/EERC-79/26, University of California, Berkeley, September 1979.

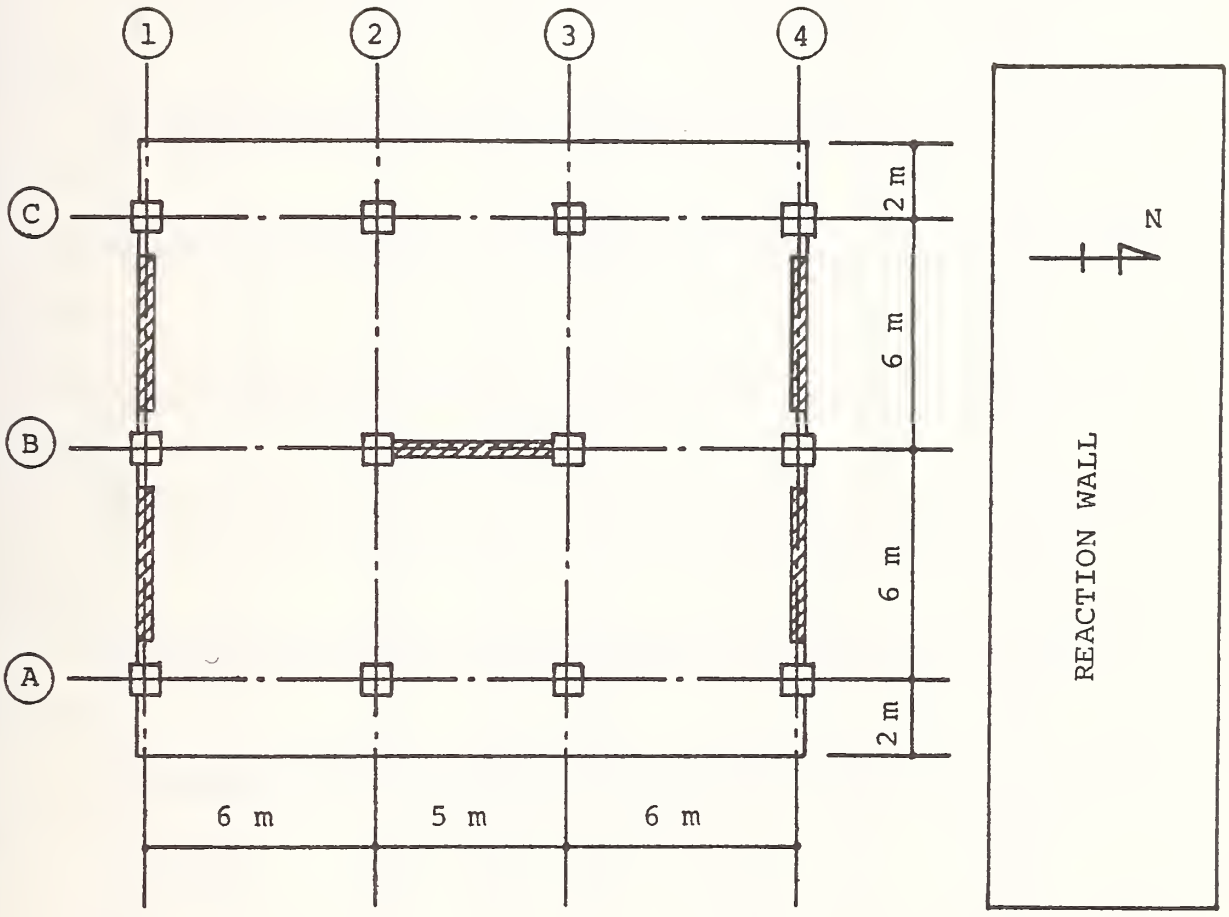

Fig. 1. General Plan View

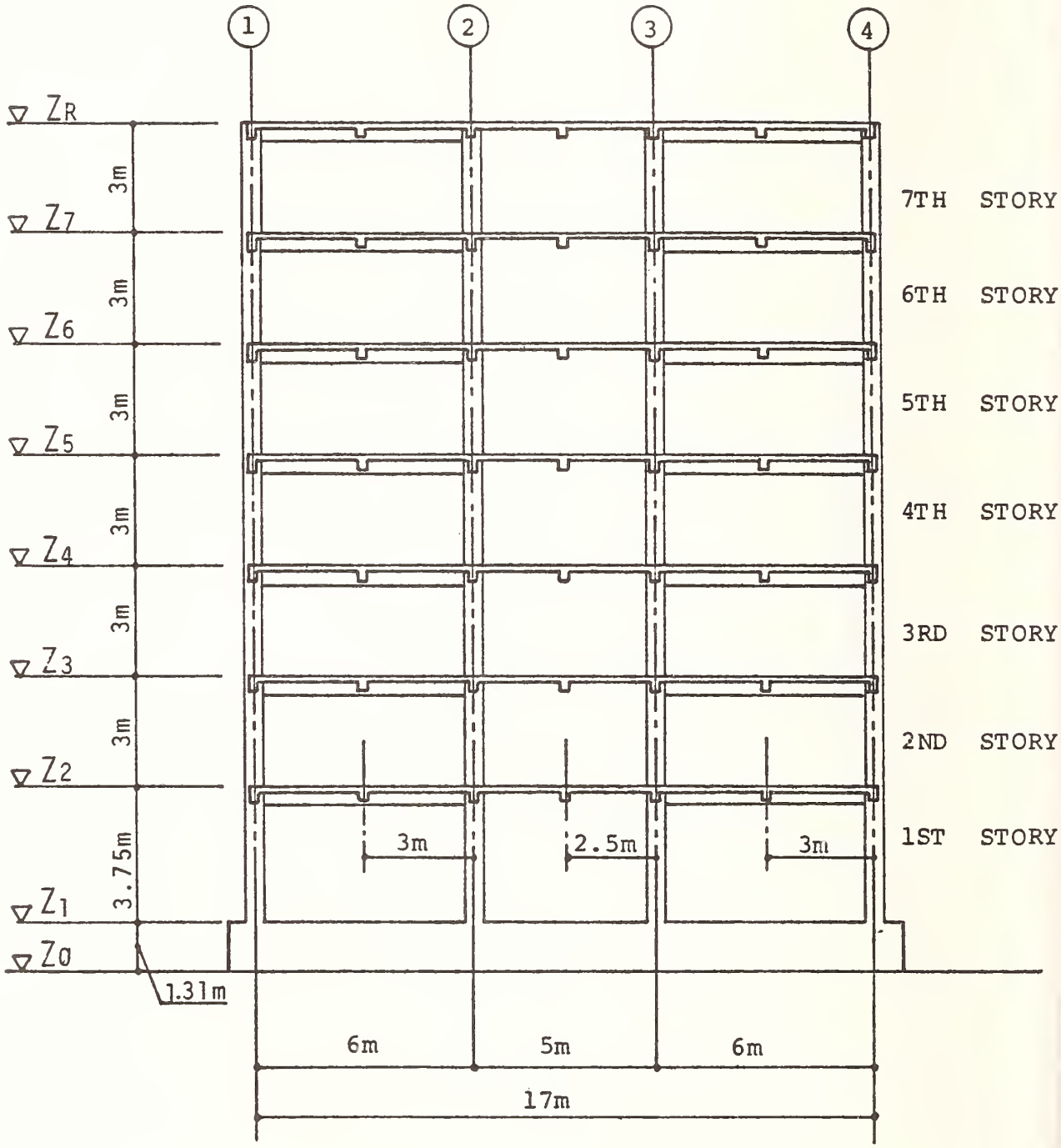

Fig. 2. Elevation, Frame B

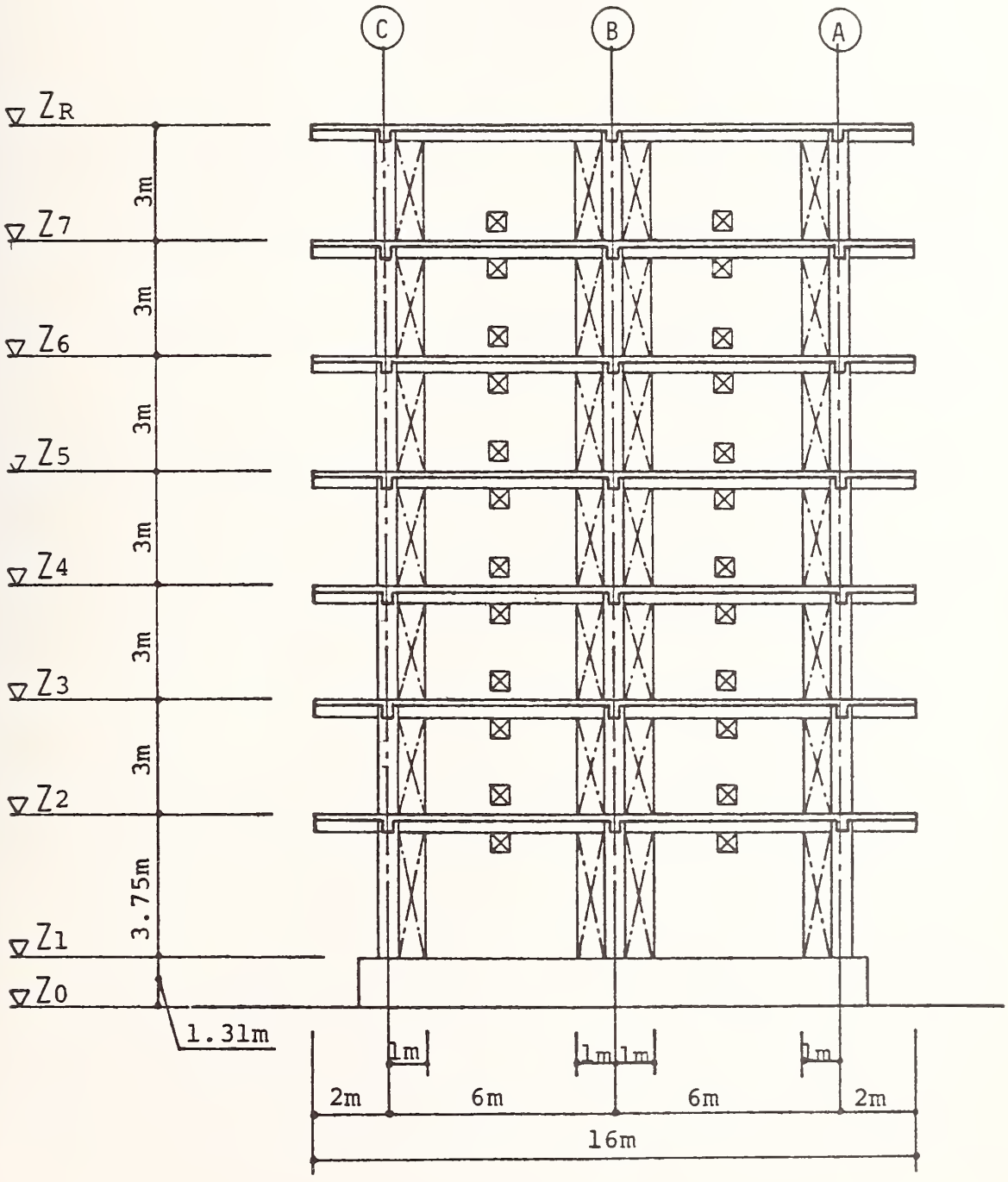

Fig. 3. Elevation, Frame 4

PROGRESS REPORT ON THE FULL-SCALE SEISMIC EXPERIMENT OF A SEVEN-STORY REINFORCED CONCRETE BUILDING -- PART 1 PSEUDO-DYNAMIC TEST BEFORE REPAIR --

Shin Okamoto, Shinsuke Nakata, Yoshikazu Kitagawa,
Manabu Yoshimura, and Takashi Kaminosono

Building Research Institute
Ministry of Construction

ABSTRACT

The appropriate evaluation of strength and deflection characteristics of building structures is a fundamental requirement for the proper estimation of structural safety in the event of major earthquake disturbances. Various unsolved problems yet remain for this evaluation due to complexity of the combination of randomness in earthquake ground motions with nonlinear behavior of structural systems. Effects of scale and construction quality make the precise evaluation more complicated and difficult.

In order to predict the behavior of structures subjected to seven earthquake ground motions, many analytical models of materials, members, and systems were developed, and numerical analyses have been made. Nevertheless, it is uncertain whether or not the results of these studies represent the true behavior of the structures because of various approximations, assumptions, and simplifications in the course of modeling and analysis. Static loading tests of full-scale models provide useful information on strength and deformation characteristics of structures, but the true margin of safety of those structures cannot be estimated.

To simulate the earthquake response of a structural model, the pseudo-dynamic test procedure is considered to be one of the most effective testing techniques if the model is beyond the capacity of a shaking table. In the Building Research Institute (BRI), Ministry of Construction, a computer-actuator on-line system was developed in 1980, and subsequently a series of pseudo-dynamic tests of a full-scale model of a seven-story reinforced concrete building with the cooperation of the Joint Technical Coordination Committee members have been performed. The primary objectives of the test were: (1) to calibrate the accuracy of techniques developed for analyzing structures under static or dynamic loading, and (2) to estimate the true margin of safety of the structure. The test was also expected to provide fundamental data for current seismic design.

TEST SPECIMEN

Figure 1 illustrates the test model set on the test floor of the BRI Large Structure Laboratory. The model is a seven-story reinforced concrete building, which is 21.75 m in total height and 272 m^2

in floor area. The story height is 3.75 m for the first-story and 3.0 m for the second- through seventh-stories. The cross section of the columns and beams is 500 mm x 500 mm and 300 mm x 500 mm respectively. The load was applied in the X direction (figure 1). The model has a shear wall of 200 mm in thickness in the middle plane parallel to the loading (X) direction (plane B in figure 1). The wall was considered to be the primary lateral load resisting element. Shear walls of 150 mm in thickness were also arrayed in the exterior planes perpendicular to the loading (X) direction (planes 1 and 4 in figure 1). The walls, isolated from the surrounding columns, were expected to restrain out-of-plane deformation of the model during loading.

Members of the model were designed based upon the present building specifications of both the U.S. (figure 2) and Japan, as well as preliminary response analysis. A comparison between design shear force in the U.S. and Japan is shown in tables 1 and 2.* The details of the reinforcement are shown in figure 3. Since the study intended to achieve an economical design, the sections were considerably less reinforced than those conforming with U.S. and Japanese practices. In accordance with the U.S. practice, boundary columns attached to the shear wall were heavily reinforced in the first- and second-stories in order to ensure sufficient ductility of the wall. Each of the closed hoops and cross ties, therefore, were arranged with a pitch of 100 mm. The shear wall did not have any beam in its own plane. To validate the design, a numerical frame analysis was made by using the Degrading Trilinear model. The Miyagiken-oki Earthquake of 1978 was employed for the analysis, and the resultant story rotation was 1/50 and 1/100 for the maximum acclerations of 500 and 300 gal, respectively.

Concrete was mixed so that the compressive strength would be 270 kg/cm^2 after 28 days. Reinforcing bars of SD35, equivalent to grade 50, were used. The material properties of the concrete and steel are tabulated in table 5.

OUTLINE OF THE PSEUDO-DYNAMIC TESTING

The ultimate purpose of the test is to investigate the seismic resistance of buildings designed according to the present building specifications in the U.S. and Japan. In this respect, performing a Pseudo-Dynamic Test of a multi-degree-of-freedom (MDOF) system is not suitable for obtaining data most effectively for immediate use. In the MDOF system, external force distribution is not only complex but also varies randomly with time. Considering this uncertainty, the members in the first JTCC meeting reached the following agreement in carrying out the Pseudo-Dynamic Test:

---

* The differences of reinforcement and calculated shear capacity between U.S. and Japan are tabulated in tables 3 and 4.

1. The test should be carried out by using a modified ground motion so that the first vibrational mode of the model would dominate in the response.
2. Shear reversal should not occur over the height of the specimen for the tests in which the angle of rotation is beyond 1/1000. Here, the angle of rotation is defined as the lateral displacement at the roof level divided by the total height.
3. The model must experience three complete cycles of load reversal with 1/400 of angle of rotation.
4. The model must experience nine complete cycles of load reversal in the entire test program.

To meet the terms of the agreements various modified ground motions were generated, and numerical analyses were made. In addition, preliminary tests were repeated to assure the capability of the online system. Finally it was decided to test the model as a single-degree-of-freedom (SDOF) system with external forces distributed in an inverted triangular mode in order to satisfy the first and second conditions.

A MDOF system can be reduced to an equivalent SDOF system if the mode of deflection is assumed. Suppose that lateral deflection at floor levels and its mode of deflection are represented by vectors {Xr} and {Ur} in a MDOF structural system, then:

$$\{Xr\} = \{Ur\} \cdot x \tag{1}$$

where: $x = f(t)$ is a function varying with time

Applying the virtual work theorum to equations of motion of the MDOF system with no viscous damping gives an expression:

$$\Sigma Mr\ (\ddot{X}r + \ddot{x}o)\ dXr + \Sigma Prdxr = 0 \tag{2}$$

where:

Mr = mass at the rth floor level

Pr = external lateral force at the rth floor level

$\ddot{X}r$ = acceleration at the rth floor level

$\ddot{x}o$ = ground acceleration

Substituting equation 2 into equation 1 leads to:

$$(\Sigma MrUr^2) \cdot \ddot{x} + \Sigma PrUr = -(\Sigma MrUr)\ \ddot{x}o \tag{3}$$

This equation represents the equation of motion of the equivalent SDOF system and can be rewritten as:

$$\tilde{\tilde{m}}\ddot{x} + \tilde{p} = \tilde{\tilde{m}}\ddot{x}o \tag{4}$$

where: $\tilde{m} = \Sigma MrUr$ (equivalent mass)

$\beta = \Sigma MrUr / \Sigma MrUr^2$ (model participation factor)

$\tilde{x} = (1/\beta)\, x$ (equivalent displacement)

$\tilde{p} = \Sigma PrUr$ (equivalent external shear)

Static frame analysis of the test model was carried out to find an appropriate mode of deflection for the equivalent SDOF system. An inverted triangular lateral force distribution was used for the analysis. By using the average mode, the displacement at the roof level X_7 is related to the equivalent displacement $\tilde{X}$ as:

$$X_7 = 1.422\tilde{x} \tag{5}$$

Analogously, the base shear Q_1 is related to the equivalent external shear $\tilde{P}$ as:

$$Q_1 = 1.457\tilde{P} \tag{6}$$

Equation 4 can be written in a different form as:

$$\tilde{m} \cdot n\ddot{\tilde{x}} + n\tilde{P} = -\tilde{m} \cdot n\ddot{x}_o \tag{7}$$

where subscript n denotes that the equation belongs to time $t = n\Delta t$, with Δt as time increment. According to the central difference method,

$$n\dot{\tilde{x}} = (n+1\ \tilde{x} - n-1\tilde{x}) / 2\Delta t \tag{8}$$

$$n\ddot{\tilde{x}} = (n+1\ \tilde{x} - 2n\tilde{x} + n-1\tilde{x}) / \Delta t^2 \tag{9}$$

Substituting equations 8 and 9 into equation 7,

$$n+1\tilde{x} = 2 \cdot n\tilde{x} - n-1\tilde{x} - \frac{n\tilde{P}}{\tilde{m}}(\Delta t)^2 - n\ddot{x}o\ (\Delta t)^2 \tag{10}$$

TEST RESULTS

VIBRATION TEST

Table 6 shows the sequence of the entire test program. Vibration and static tests were executed twice: before and after the pseudo-dynamic test. Vibrational and stiffness characteristics of the specimen were investigated in both the intact and damaged stages of the specimen.

For the pseudo-dynamic test, a total of 541 wire strain gages were glued at strategic locations to the concrete and reinforcing bars. In addition, vertical and horizontal displacements of the

than the corresponding elements of the stiffness matrix gained in the intact stage. The difference demonstrates the degradation of stiffness after the psuedo-dynamic test. From the stiffness matrix, natural periods of the specimen at the damaged stage are computed as 0.887, 0.171 and 0.885 sec for the first, second, and third modes, respectively.

INVERTED TRIANGULAR LOAD TEST

Figure 5 shows the shear force resisted by each lateral load resisting component of the fifth-story. The shear was computed from the reading of triaxial concrete gages glued on the components. The shear wall resisted 52 percent of the total shear while according to the analysis, the wall was predicted to take 58 percent of the total shear resistance.

PSEUDO-DYNAMIC TEST

a) PSD1

Test PSD1 was programmed in order to evaluate the accuracy of the equivalent SDOF pseudo-dynamic testing. In the analysis, the envelope of hysteresis curves was taken to be trilinear, and Takeda's model was used for representing the hysteretic characteristics. The initial stiffness was computed on the basis of the stiffness matrix and the fundamental period obtained from the static and vibration tests. The natural period of the SDOF system is found to be 0.43 sec, which coincides with the fundamental natural period predicted by the vibration test. No cracks were observed after the test.

b) PSD2

In test PSD2, the ground motion used in PSD1 was input a second time with the maximum ground acceleration of 105 gal. Correlation between the test and the numerical analysis is excellent during the first 2 sec of ground motion. Comparison between two hysteretic characteristics, one used in the analysis and the other derived from the test, has revealed that the cracking load was significantly lower in the analysis than in the test. The analytical cracking load, therefore, was shifted from 91 tons to 153 tons, and the specimen was reanalyzed. The time history curve computed in the analysis reasonably duplicates the experimental curve. Therefore, the cracking load of 153 tons was adopted in the subsequent numerical analysis.

The test was executed with the specified ground motion for the first 3.8 sec and extended for another 0.7 sec in a free vibration mode. The fundamental natural period was found to be 0.55 sec, which is 1.28 times longer than the elastic natural period (0.43 sec). In the test cracks developed in the lower part of the shear wall, boundary beams, and slabs.

c) PSD3

By using the modified hysteretic characteristics, numerical analysis was performed many times to find a ground motion which would satisfy the JTCC requirements. Eventually the artificial wave based on the Taft earthquake of 1952 was selected, and the maximum ground acceleration was set at 320 gal so that the maximum angle of rotation would be limited to 3/400.

Figure 6 indicates that the experimental and analytical time-history curves stand very close to each other for the first 4 sec of ground motion. At about 4.5 sec, the maximum displacement of 240 mm at the roof level (an angle of rotation of 1/91) was attained. In the succeeding time period, the experimental curve constantly surpassed the analytical curve by about 24 percent. The discrepancy between two curves seems to be attributable to the overestimate of the area of the hysteresis loops in Takeda's model. The overestimated hysteresis loops in the analysis, therefore, caused more hysteretic damping, which resulted in less deformation. After 10 sec of ground motion, the test was continued in a free vibration mode; the natural period was increased to 1.16 sec in this stage.

During the test, many shear and flexural cracks developed in the lower part of the shear wall. Concrete fragments were chipped off at shear wall-to-boundary beam junctions, and concrete started crushing at the base of boundary columns.

d) PSD4

The E-W component of the Hachinohe Earthquake of 1968 was selected in test PSD4. The maximum ground acceleration was taken as 350 gal to aim at the maximum angle of rotation of 1/75. As shown in figure 7, experimental and analytical time history curves are nearly identical for the entire time period. Based upon the finding in the previous test (PSD3) that the analytical hysteretic characteristics had overestimated hysteretic damping, some parameters of Takeda's model were modified for this analysis. During the test, the maximum angle of rotation reached 1/64 and 1/68 in the positive and negative directions respectively (figure 8).

No new cracks were observed during the test, but a substantially wider crack width had developed (figure 9). At the maximum displacement level, a flexural crack of 4 mm width developed at the base of the boundary column, where shear cracks extended in the shear wall were more than 1 mm wide. Boundary beams sustained severe damage in the test. Concrete pieces fell off at their junctions with the shear wall, and one of the reinforcing bars in the beam of the sixth-story buckled.

During the pseudo-dynamic test in a free vibration mode, which was executed in the last stage of the test, the natural period was 1.48 sec. This natural period was three times as long as the natural period in the intact stage.

Table 1. Oesign Shear Force

	New Code (Japan 1981)	U.B.C (1979)
Calculation of Shear Force	$Q_i=C_iW_i$ $C_i= ZR_tA_iC_o$ (2nd Step) $Q_{DS}F_{ES}CW$	$V_u=ZIKCSW$ V_u=Base Shear
Standard Shear Force Ratio	C_o (1st ; $C_o \geq 0.2$) (2nd ; $C_o \geq 1.0$)	C $C = \frac{1}{15\sqrt{T}} \leq 0.12$ *
Zone Factor	Z Z=0.7-1.0	Z Z=0.0-1.0
Vibration Factor	R_t $T<Tc$ $R_t=1.0$ $T_c \leq T<2T_c$ $R_t=1.0-0.2(T/T_c-1)^2$ $2T_c \leq T$ $R_t=1.6\ T_c/T$	S $T/T_s \leq 1.0$ $S=1.0+T/T_s-0.5(T/T_s)^2$ $T/T_s>1.0$ $S=1.2+0.6\ T/T_s$ $-0.3(T/T_s)^2$ T ; Natural Period of Structure T_c, T_s ; Natural Period of Soil
Structure Factor	D_s D_s=0.25-0.55	K K=0.67-2.50
Occupance Importance Factor	----------	I = 1.0 - 1.5
Vertical Load	W ; O.L+L.L	W ; O.L (incl. Partition)
Distribution of Seismic Load	Q_i $Q_i=C_iW_i$	F_x $F_x = (Vn-Ft)\frac{w_xh_x}{w_ih_i}$ F_t ; Additional force at the top $F_t=0.07TV \leq 0.25V$, $T \leq 0.7 > F_t=0.0$
Natural Period of Structure	T=h(0.02+0.01)	$T = 0.0906\ \frac{h_n}{\sqrt{D}}$ 0; Width

Table 2. Comparison of Oesign Shear Force

Japan (1981)	U.B.C. (1979)
Z = 1.0	Z = 1.0
R_t = 1.0	I = 1.0
A_1 = 1.0	K = 0.8
C_0 = 0.2	C = 0.096
	S = 1.5
Q_{CB} = 0.2 W	V_u = 0.115 W (Q_B = 0.179 W)

Table 3 List of Column & Beam

		$_1C_1$	$_1C_2$	$_1C_3$	$_1C_4$	$_2G_1$	$_2G_2$	$_2G_3$
A.C.I. (1977)		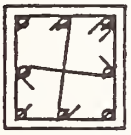	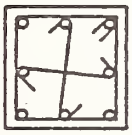	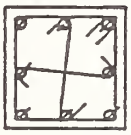	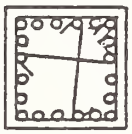	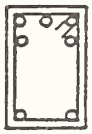		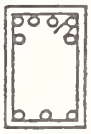
Bars	T	8-D22	8-D25	8-D22	20-D25	5-D25	5-D22	6-D25
	B					2-D25	2-D22	3-D25
Hoop ST.	E	2-D13@200	2-D13@200	2-D13@200	3-D13@100	2-D10@150	2-D10@200	2-D10@100
	C	3-D13@100	3-D13@100	3-D13@100		2-D10@100	2-D10@100	
JAPAN		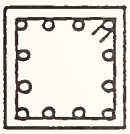	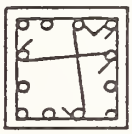	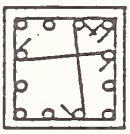	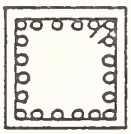	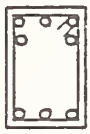	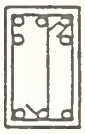	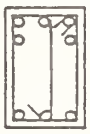
主筋	T	12-D25	12-D25	12-D25	20-D25	5-D25	5-D25	5-D25
	B					3-D25	3-D25	3-D25
Hoop ST.		2-D13@100	3-D13@100	3-D13@100	2-D13@100	2-D13@100	3-D13@100	3-D13@100

Table 4. Comparison of Shear Capacity

	Japan	A.C.I.	
		U.S. Calc	Japan Calc
Shear Capacity	700	340	565

Table 5. Material Properties of Concrete and Steel

(a) Mechanical properties of Concrete

Before Test (PSD 1)

	F_c (kg/cm^2)	ε_c (%)	E_o ($x10^5 kg/cm^2$)	E 1/3 ($x10^5 kg/cm^2$)	F_{sp} (kg/cm^2)
1st Story	289.4	0.218	2.72	2.37	24.2
5th Story	294.5	0.210	3.08	2.54	23.6

After Test (PSD 4)

	F_c (kg/cm^2)	ε_c (%)	E_o ($x10^5 kg/cm^2$)	E 1/3 ($x10^5 kg/cm^2$)	Fsp (kg/cm^2)
1st Story	283.3	0.222	2.22	2.13	23.8
5th Story	291.5	0.219	2.29	2.14	24.6

F_c : Compressive strength of field cured $10^{\emptyset}$ x 20 cylinder
ε_c : Strain at compressive strength
E_o : Initial tangent modulus
E1/3 : Secant modulus at one-third of compressive strength
F_{sp} : Splitting strength

(b) Mechanical properties of reinforcing bars

	σ_y (t/cm^2)	σ_u (t/cm^2)	ε_y (%)	ε_{st} (%)	ε_u (%)	E_s ($x10^6 kg/cm^2$)
D 10	3.87	5.67	0.210	1.80	16.55	1.84
D 13	3.93	5.65	0.211	--	19.31	1.86
D 16	3.85	5.72	0.221	1.94	17.46	1.74
D 19	3.65	5.73	0.214	1.68	19.84	1.71
D 22	3.53	5.75	0.191	1.23	21.42	1.85
D 25	3.78	5.66	0.201	2.18	19.70	1.88

σ_y : Yield stress
σ_u : Maximum stress
ε_y : Yield strain
ε_{st} : Strain hardening strain
ε_u : Elongation
E_s : Elastic modulus

Table 6. Test Sequence and Description of Program

Test No.	Contents
VT 1	Free and forced vibration tests
FLL 1	Single load application tests
SL 1	Static tests under inverted triangular load distribution
PSD 1	δ max = ±3 mm (Rmax = 1/7000) MIYAGIKENOKI TOHOKU U. NS Gmax = 23.5 gal
PSD 2	δ max = ±55 mm (Rmax = 1/400) MIYAGIKENOKI TOHOKU U. NS Gmax = 105 gal
PSD 3	δ max = ±163 mm (Rmax = 3/400) 1952 TAFT EW Gmax = 320 gal
PSD 4	δ max = ±290 mm (Rmax = 1/75) TOKACHIOKI HACHINOHE EW Gmax = 350 gal
FLL 2	Single load application tests
VT 2	Free and forced vibration tests
	Repairs by epoxy injection
VT 3	Free and forced vibration tests
	Arrangement of nonstructural tests
VT 3	Vibration tests
FLL 3	Single load application tests
SL 2	Static tests under inverted triangular load distribution
PSD 5-7	Pseudo-dynamic tests as SDOF sytem (1/7000 - 3/400)
SL 3	Static tests under uniform load distribution (Rmax = 1/50)

δmax : The target maximum displacement at roof floor
Rmax : The target maximum angle of rotation (δmax/H
(H : Total height of the specimen)
Gmax : The maximum acceleration of input ground motion

Table 7. Results of Vibration Tests

(Before P.D. Test)

	Type of Test	Unbalanced Moment (force)	Fundamental Period (sec)°1	Maximum Displacement Acceleration	Damping Coefficient	Remarks
VT 1	E	-	0.42 (0.11)	(59.5 gal)	2.6% (--)	Period in EW Direction: 0.30, 0.089 sec
	M	-	0.42 (0.11)	5μ	--	Torsional Period: 0.23 sec
	F	(2.4 ~ 3.8 ton)	0.43	0.5 ~ 0.7 mm	2.1%	Static Test: 0.448, 0.125 sec Frame Analysis 0.468, 0.123 sec
	D	20 kg.m	0.43 0.11	1.1 m	1.9% (1.2%)	

(After P.D. Test)

VT 2	M	-	0.76 (----)	5μ	--	Period in EW Direction: 0.44, 0.14 sec
	F	(0.5 ~ 3.5 ton)	0.8 ~ 0.87	0.1 ~ 1.0 mm	2.0% ~ 3.2%	Torsional Period: 0.30 sec
	D	5 ~ 20 kg.m	0.83 ~ 0.91 (0.17 ~ 0.20)	0.3 ~ 0.9 mm	0.9% ~ 1.9% (1.2%)	

E : Earthquake observation, M : Micrometer measurement.
F : Free vibration test, D: Forced vibration test.
°1 ( ) indicates second period (sec).

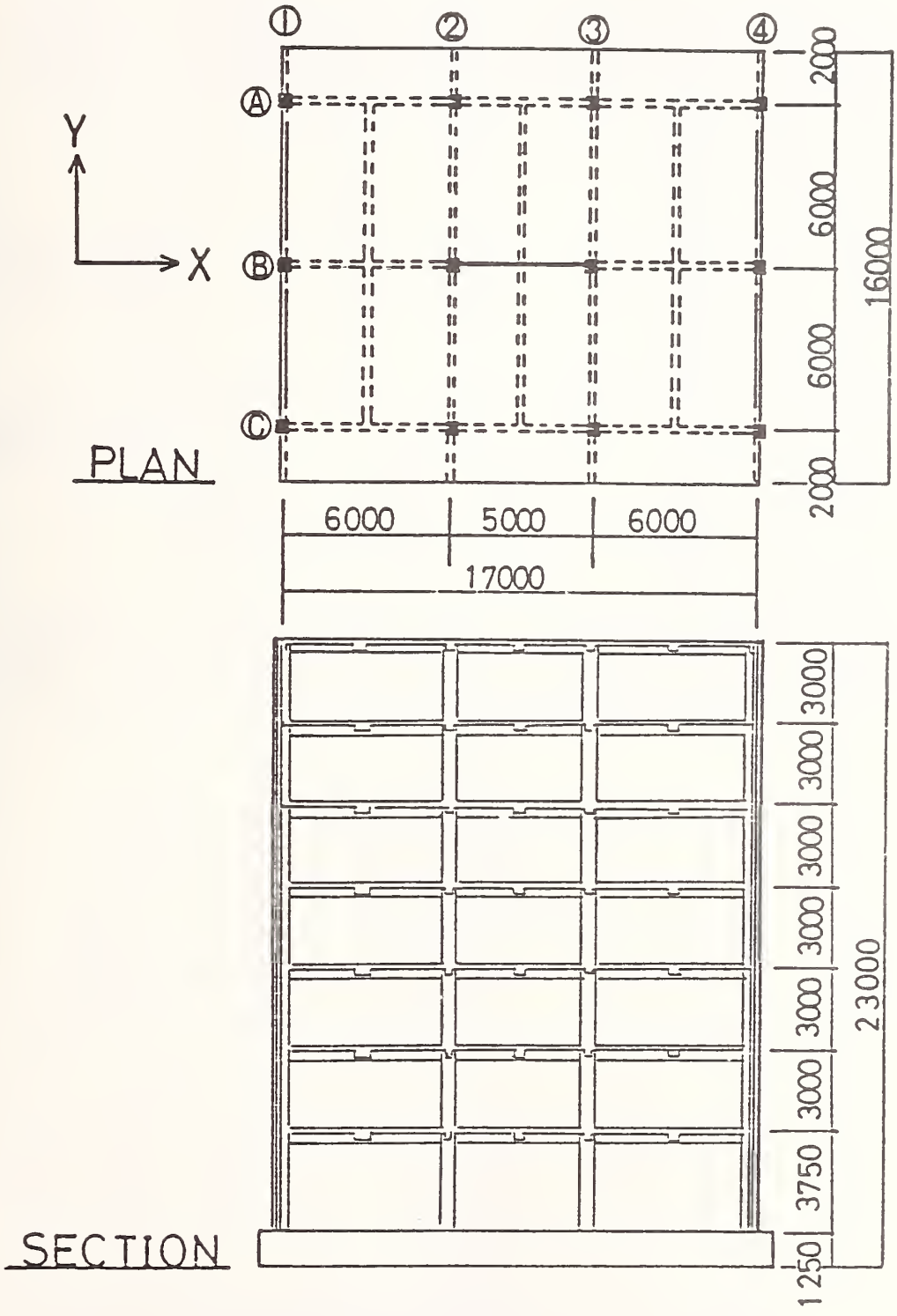

Fig. 1 Plan,Elevation,and Dimension of the Specimen

$$\begin{cases} l_1 = 1.4 \cdot l_d \ (\times 2/3) \\ l_2 = 1.0 \cdot l_d \ (\times 2/3) \end{cases} \quad \leq \#11 \quad l_d \geq \begin{cases} 0.0594 A_b f_y / \sqrt{f_c} \\ 0.00569 d_b f_y \end{cases}$$

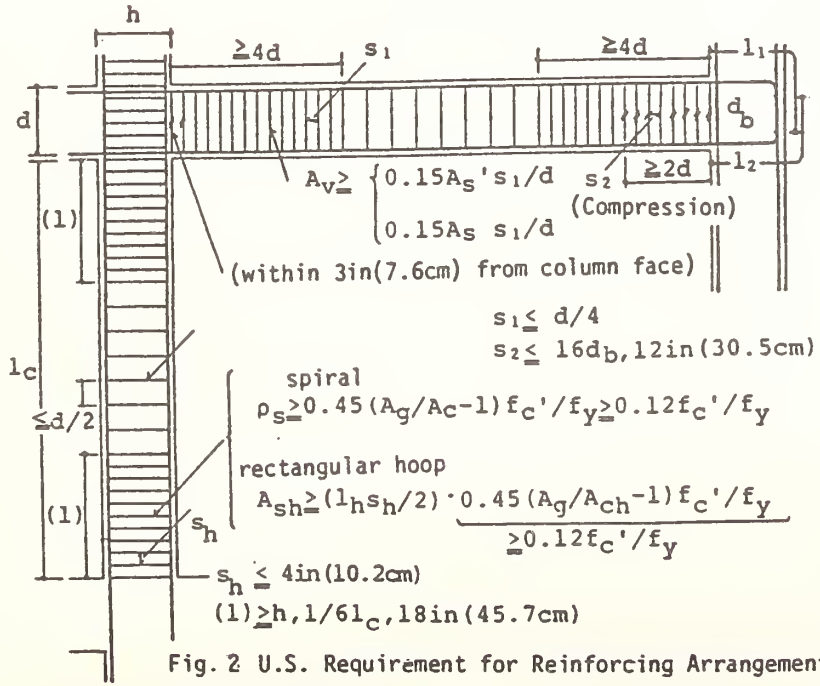

Fig. 2 U.S. Requirement for Reinforcing Arrangement
(A.C.I. Apendix A5,A6)

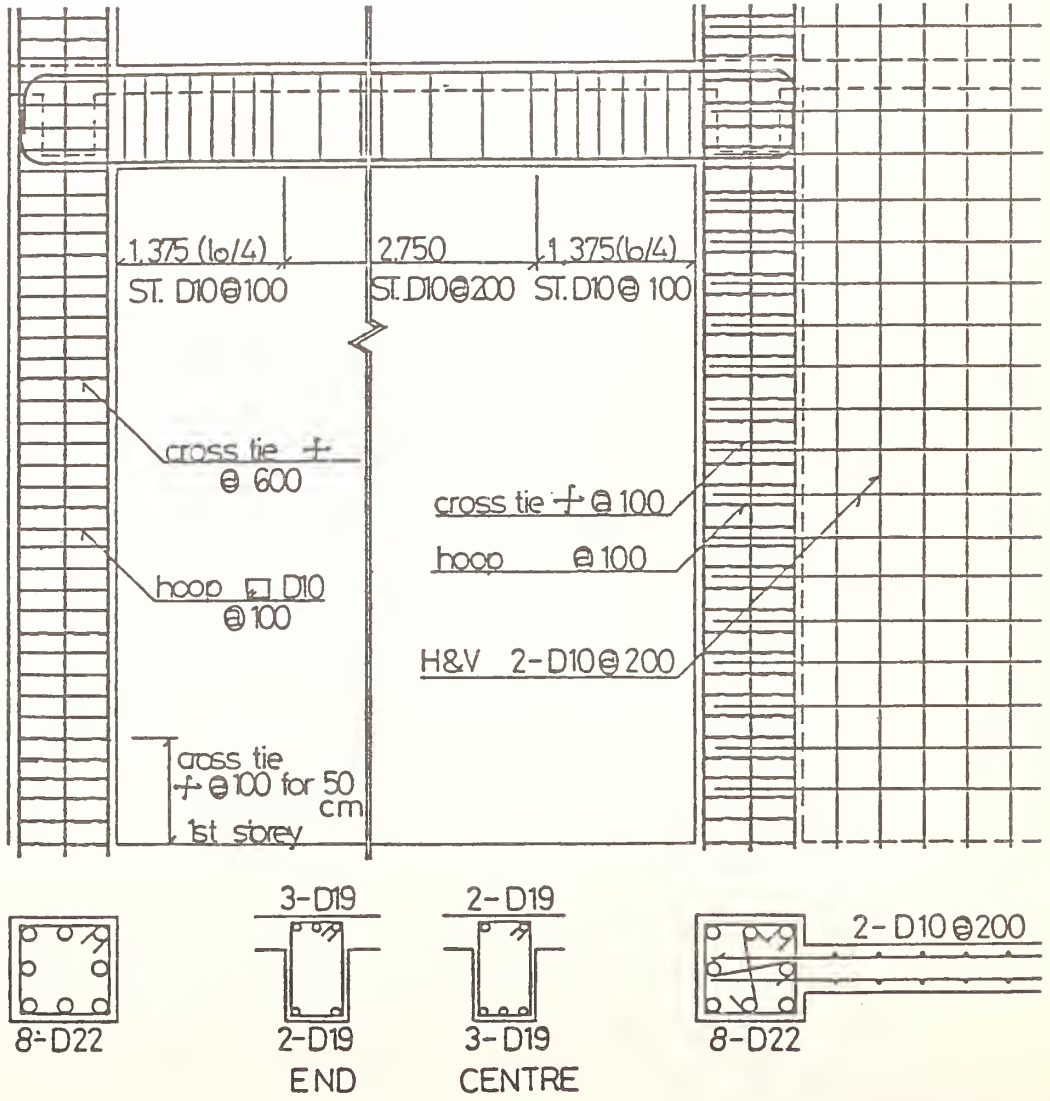

Fig.3 Details of Reinforcing First Floor

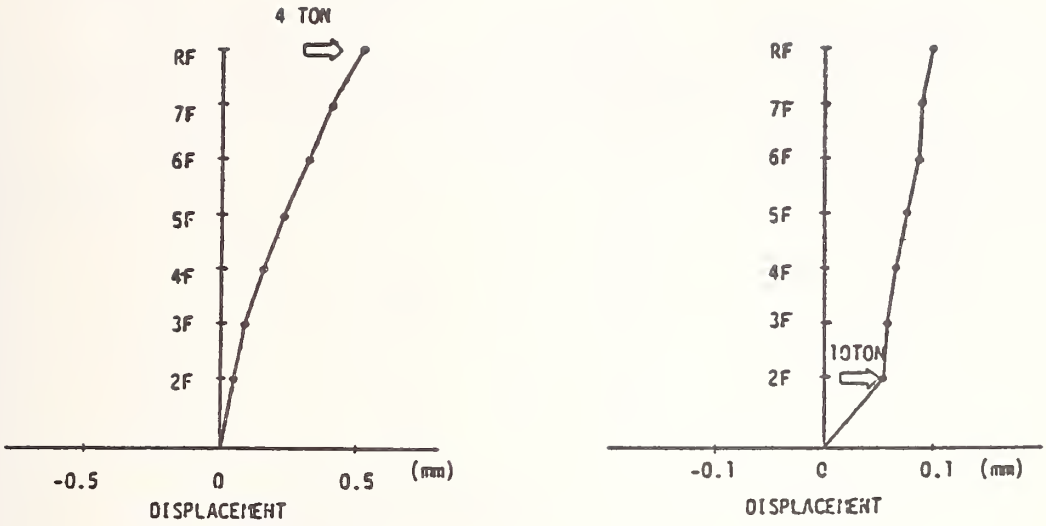

Fig.4 Distribution of Story Displacement Under Static Load

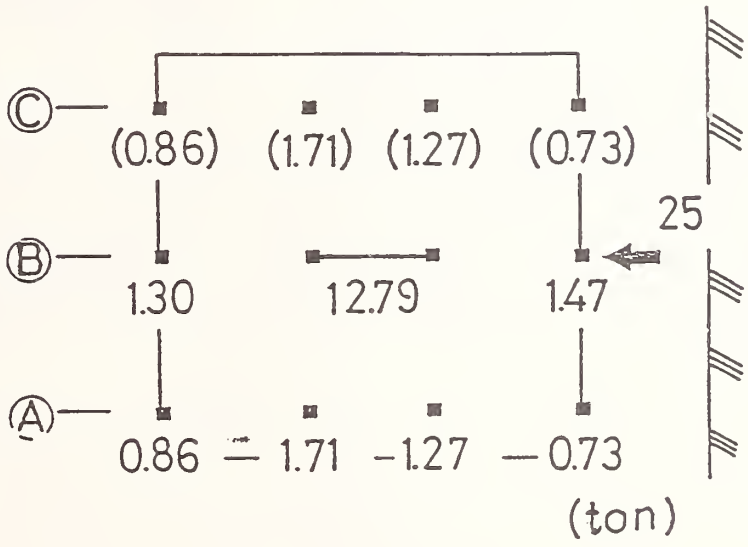

Fig.5 Measured Shear Force Distribution (5th Story)

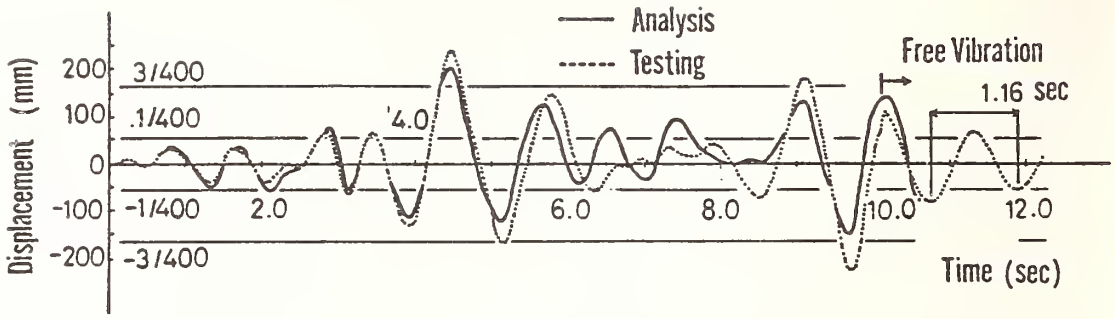

TEST 3

Fig.6 Time History of RF Displacement
(320.0 gal)

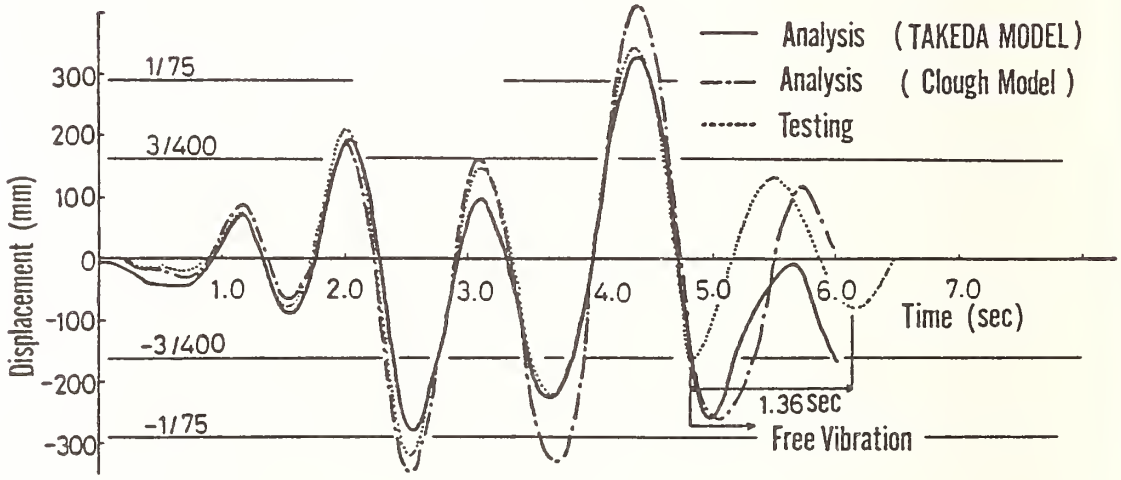

TEST 4

Fig.7
Time History of RF Displacement
(350.0 gal)

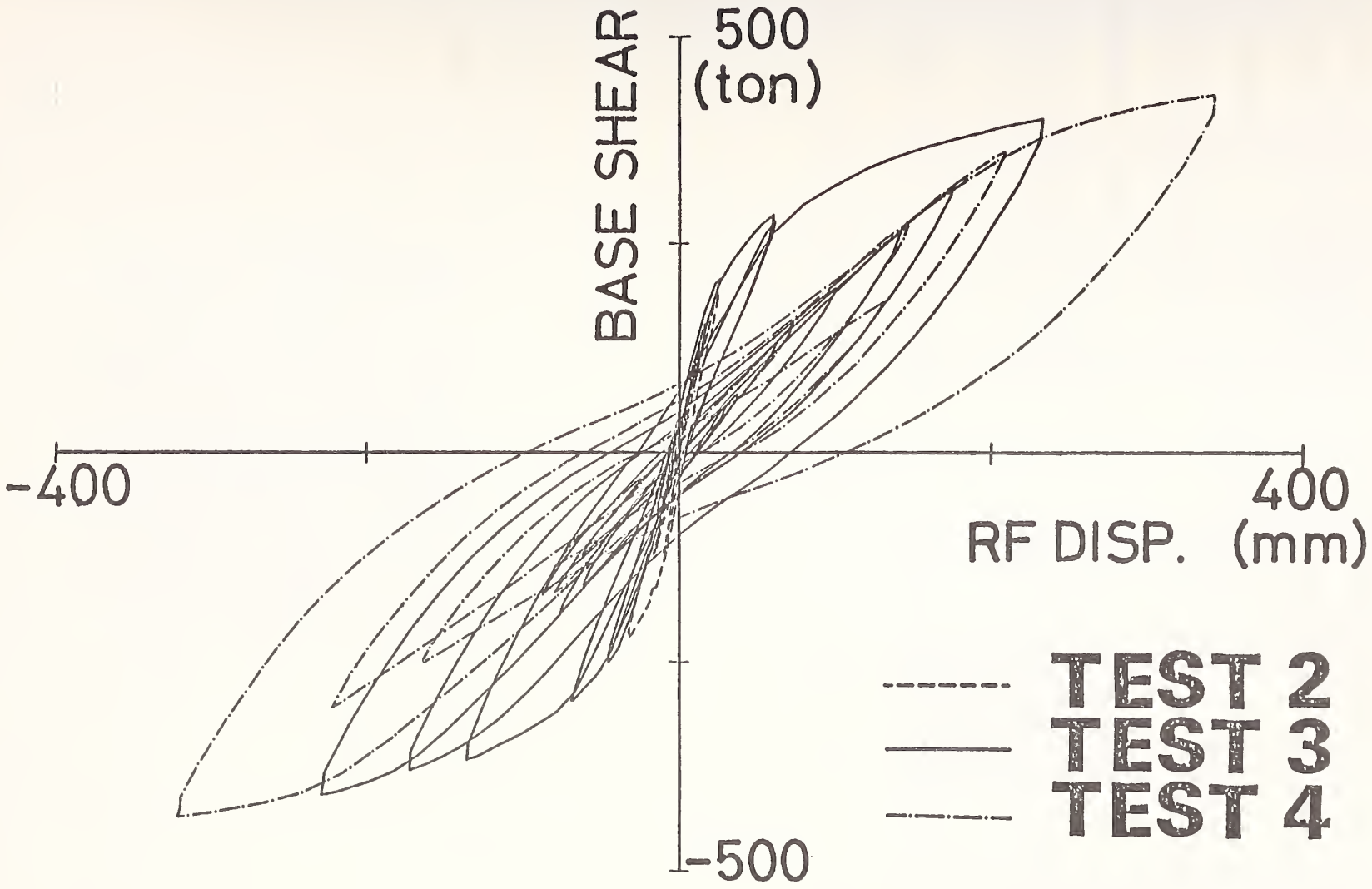

Fig.8 Hysteresis Loops of Roof Floor Displacement

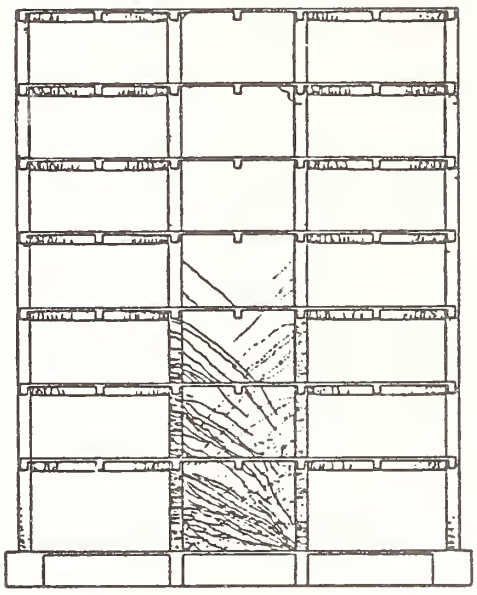

FRAME-B (after TEST-4)

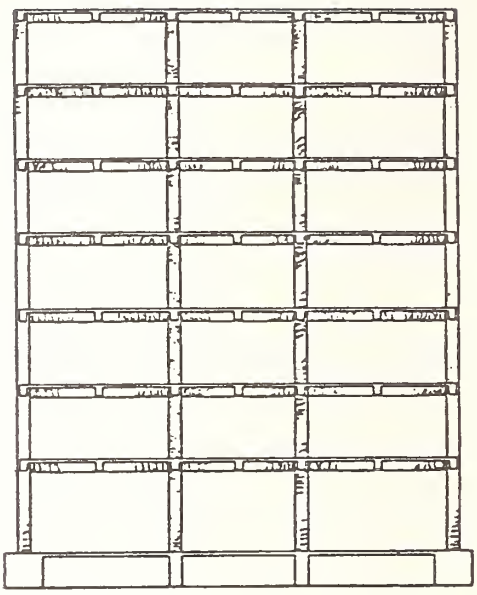

FRAME-C (after TEST-4)

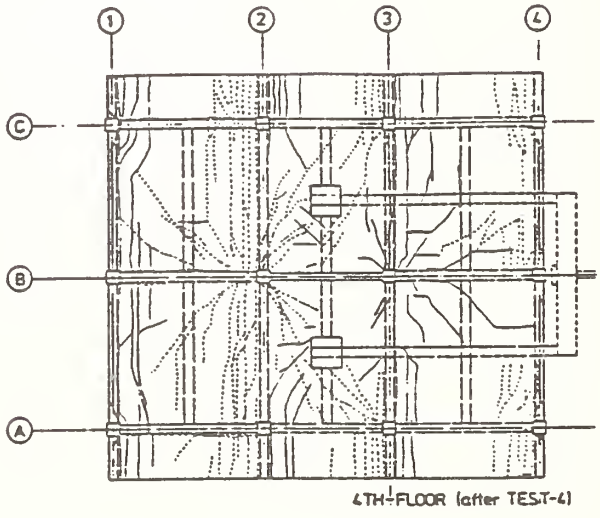

4TH FLOOR (after TEST-4)

Fig.9 Crack Pattern of the Specimen

A PROGRESS REPORT ON THE FULL-SCALE SEISMIC EXPERIMENT OF A SEVEN-STORY REINFORCED CONCRETE BUILDING
-- PART 2 PSEUDO-DYNAMIC TEST AFTER REPAIR --

Shin Okamoto, Shinsuke Nakata, Yoshikazu Kitagawa,
Manabu Yoshimura, and Takashi Kaminosono

Building Research Institute
Ministry of Construction

ABSTRACT

After the psuedo-dynamic test of the full-scale reinforced concrete structure, repair works and the installation of nonstructural elements to the damaged structure were carried out. The hinge zone of the beams and the shear wall of the structure were repaired by using epoxy resin. The repair works proved to be economically effective for the reuse of the damaged structure after earthquake damage from the viewpoint of recovering the stiffness and the strength of the structure. The aseismic arrangements of nonstructural elements such as partition walls, spandrel walls, window glasses, etc. were verified through a series of pseudo-dynamic tests.

REPAIR OF THE SHEAR WALL AND HINGE ZONES

In the final test (PSD4(TEST4)) before repair, crack patterns of a full-scale structure were observed as shown in figure 9 in part 1. The location of the cracks in the beams were concentrated in the hinge zone.

In the shear wall, cracks were observed in the lower three-stories, and crushing of concrete did not occur. For the crack repairing, epoxy resin was used. In figure 1a), b), and c), only the hatched portions of the cracks were injected by epoxy resin because of a limited budget. Only the column assemblies of the top of the seventh-floor and the bottom of the first-floor were repaired.

The physical properties of the epoxy resin are shown in table 1. Young's modulus of epoxy resin is far smaller than that of concrete. However, the tensile strength of epoxy resin is about ten times higher than that of concrete. Table 2 shows the damage of beam ends connecting to the shear wall. Compression failure and concrete exfoliation were observed for almost all the beams. These exfoliated portions were repaired by using epoxy mortar after being cleaned up. The physical properties of the epoxy mortar are shown in table 3. The bottom longitudinal reinforcing bars buckled at four of the fourteen beam ends adjacent to the shear wall. In order to reinstall these bars to the original slab, three kinds of repair procedures were applied as shown in figure 2 according to the type of buckling.

One of these procedures was to repair the buckled bars by a special steel plate (6 mm thickness and 50 mm width) which was fixed by an inserted anchor bolt (figure 2b). At the place which was most severely buckled on the top floor level, a U-shaped stirrup bar was installed and welded to a steel plate at the floor level for its anchor, by removing a part of the concrete floor slab. At the buckled bars, additional bars of the same size were installed by welding them to these buckled bars (figure 2c).

WORKS OF NONSTRUCTURAL MEMBERS

SPANDREL WALL WORKS

In conjunction with the repair work, the reinforced concrete spandrel walls were set at one span of A and C frames from the second-floor to the top floor level as shown in figure 3. On the second- and third-floors, the reinforcing bars of the walls were anchored to the columns and floor slab by inserting anchor bolts. At other stories, those anchors had been set in advance. As shown in the lower left corner of figure 3, connecting parts of the spandrel wall with the column of frame B is different from those parts of frame A which had a narrow width (60 mm). The brick masonry spandrel walls are installed in the left hand span of frames A and C of the fifth-floor level as shown in the same figure. Frame A has a 1 cm clearance between the column and the brick masonry spandrel.

PARTITION WALLS

Details of partitions wall settings are shown in table 4. These walls were installed only in the third- and fifth-floors. The wall types used were gypsum board framed by light gage steels (GBM-1, 2), gypsum lath mortar or plaster board framed by timber, cement mortar and artificial light-weight concrete board framed by light gage steel, and concrete brick masonry.

Glass windows and their frames were set on the spandrel wall in the third- and fifth-floors as shown in figure 3. These frames are composed of three glass windows, of which the central one can slide and the others are fixed. The glass of 5 mm thick, and some windows were covered with polyester films or installed wire fabric in order to prevent glass scattering caused by story drift. Two kinds of putty were used to fix the glass frames. One type is hardening putty and the other type is flexible, which is considered as aseismically effective. Pipe lines for the water supply were also installed through all stories. However, these test results are not yet available.

TEST RESULTS AFTER REPAIRING

BEHAVIOUR OF THE STRUCTURE

The sequence of psuedo-dynamic tests for the full-scale test building after repairing was planned to be quite the same as those before repairing. They included four steps: modified Miyagi-

other hand in the case of frames fixed by flexible putty, the destruction of glasses occurred in a later stage (story drift angle of 1/100).

RESULTS OF VIBRATION TESTS

The vibration tests were carried out in the same way as those before repair. The observed date of the natural period of the test structure through these tests is shown in figure 15. Note that the values of the natural period from the free vibration test and the forced vibration test are almost the same. The natural period was reduced to about 0.6 sec after the repair works. This shows that the stiffness of the structure was recovered by repair works.

The natural period became 0.5 sec by the installation of nonstructural elements. The natural period from the pseudo dynamic free vibration test was larger than that from other vibration tests. This indicates that the natural period of the structure depends on the displacement amplitude in vibration.

CONCLUDING REMARKS

This paper reports the test of a full-scale reinforced concrete building conducted at the Building Research Institute, Ministry of Construction. Various test programs were carried out in order to investigate the seismic characteristics of the building. These programs included a vibration test, a static test, and a pseudo-dynamic test. Major findings and areas of further research are summarized as follows:

1) The fundamental natural period of the specimen, 0.43 sec in the intact stage, increased in proportion to the level of damage that the specimen sustained. At the end of test PSD4, by which time the specimen had undergone severe damage, the natural period was 1.48 sec, more than three times as high as the initial natural period.

2) The frame analysis was found to adequately simulate the static behavior of the specimen. According to the test and its analysis, the shear wall resisted in its elastic range about 55 percent of the total shear force applied to the fifth-floor.

3) The maximum base shear carried by the specimen was 440 tons. On the other hand, the maximum base shear computed by means of the plastic hinge method was 429 tons, which is 98 percent of the experimental maximum base shear. The analytical prediction has proven appropriate if all of the slab reinforcement is considered effective to the flexural resistance of the beams, when the restraint caused by a frame perpendicular to the shear wall is taken into account.

4) The maximum angle of rotation obtained during test PSD4 was 1/64, at which point the specimen showed ductile behavior since the shearwall, the major lateral load resisting component, was damaged in a flexural mode.

5) Dynamic analysis of a one-mass system succeeded in simulating the behavior of the specimen under the pseudo-dynamic test. We are continuing the effort to correlate the response of the equivalent SDOF system with the true response of the specimen.

6) After repair work and the installation of nonstructural elements for the test specimen, the repair work, at a reasonable expense for earthquake damage were found to be economically feasible. The test results have shown that when damage is confined to small areas it can be repaired effectively using materials such as epoxy to restore the capacity. The applications of such material in damage rehabilitation technology will be one of the new areas needing further attention.

Table 1. Physical Properties of Epoxy Resin

Items	Unit	Test Value		
Specific Gravity		118	JIS K 5911	
Visocity	c.p.s	340	BH	(20°C)
Pot Life	minute	19		(20°C-500g)
Hardness	shore D	D-87	ASTM D 2240	(20°C-7)
Tensile Strength	kg/cm	527	JIS K 6911	(20°C-7)
Compressive Strength	kg/cm	922	JIS K 6911	(20°C-7)
Tensile Shear Strength	kg/cm	144	JIS K 6850	(20°C-7)
Impact Strength	kg.cm/cm	107	JIS K 6911	(20°C-7)
Bond Strength for Cement Mortar	kg/cm	36		(20°C-7)

Base Resin : Epoxy Resin
Curing Agent : Poly-amide Amin

Table 2. Detailed Damage of Beam Ends

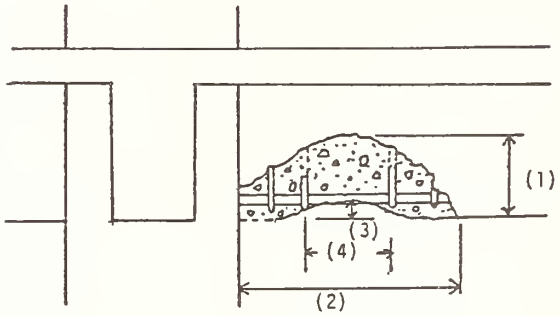

Location		Spalled Region					
Story ----	N,S	(1) max Height	(2) Max Length	(3) Max Depth	(4) Max. Stirrup Spacing	Buckling	Repair Procedure
7TH	N	17 (cm)	45	4	19	Slight	2
7TH	S	12	30	3	?	No	1
6TH	N	20	50	7	25	Severe	3
6TH	S	22	50	3	12	No	1
5TH	N	14	50	3	8	No	1
5TH	S	13	40	3	12	No	1
4TH	N	17	50	3	10	No	1
4TH	S	13	40	3	15	No	1
3RD	N	15	60	4	21	Slight	2
3RD	S	16	40	3	13	No	1
2ND	N	17	40	3	14	No	1
2ND	S	17	40	3	15	Slight	2
1ST	N	5	15	3	?	No	1
1ST	S	10	20	3	12	No	1

Table 3. Physical Properties of Epoxi Mortar

Items	Test	Unit	101	
Specific Gravity	JIS K 7112	-	1.70±0.10	(1.72)
Flexural Strength	JIS K 7203	kg/cm	400	(425)
Compressive Strength	JIS K 7208	kg/cm	600	(837)
Young's Modulus	JIS K 7208	kg/cm	(4.0-8.0) x 10	(6.73)
Tensile Strength	JIS K 7113	kg/cm	200	(257)
Impact Strength	JIS K 7111	kg.cm/cm	1.5	(1.88)
Hardness	JIS K 7215	HoD	85	
Tensile Shear Strength	JIS K 6850	kg/cm	110	(145)

Table 4 Details of Non Structural Elements

Material	Symbol	Detail
Concrete Brick Masonry	CB	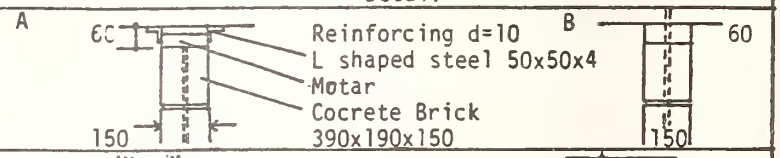
Plaster Board Framed by Light Steel (Floor Slab ≒ Ceiling)	GBM-1	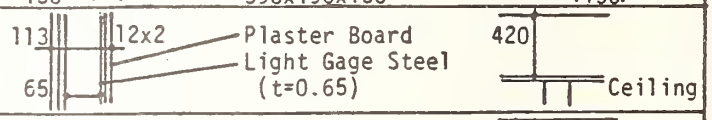
Plaster Board Framed by Light Steel (Slab ≒ Slab)	GBM-2	
Window Sash	AL-1 AL-2	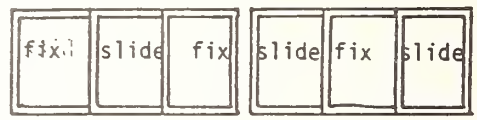 Flexible Putty Hardening Putty AL-1; Float Glass t=5mm Vinyl Tape Stick AL-2; Float Glass t=5mm Polyester Film Stick
Artificial Light Weight Concrete Board	ALC	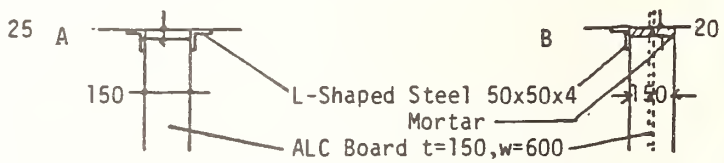
Lath Board Plaster Finishing Framed Timber	GBW	
Metal Lath Mortar Finishing Framed Light Gage Steel	MSM	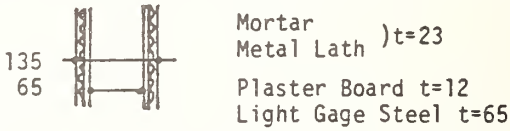
Window Sash	AL-3 AL-4	Flexible Putty Haddening Putty AL-3; Float Glass t=5mm Vinyl Tape Stick AL-4; Wire Mesh Glass t=6.3mm

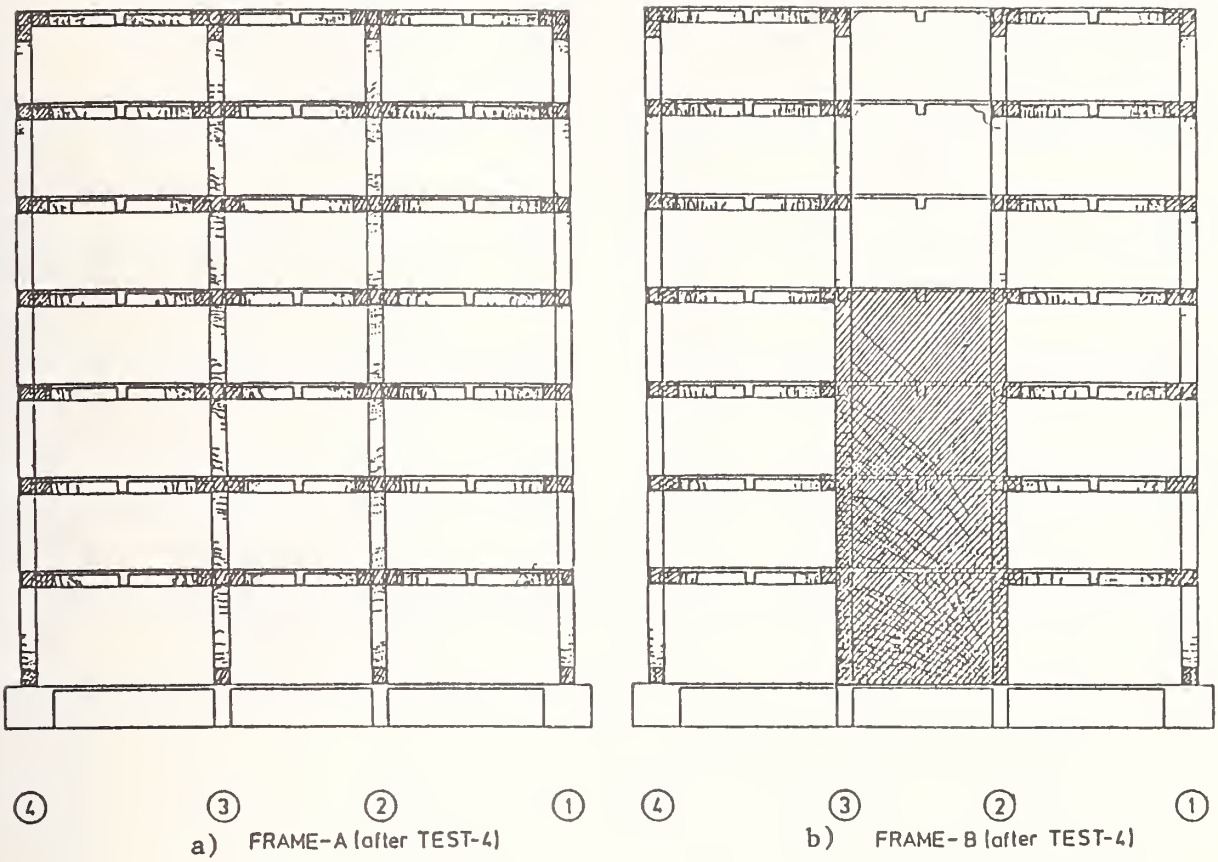

Fig.1 Repaired Portions by Epoxy Resin

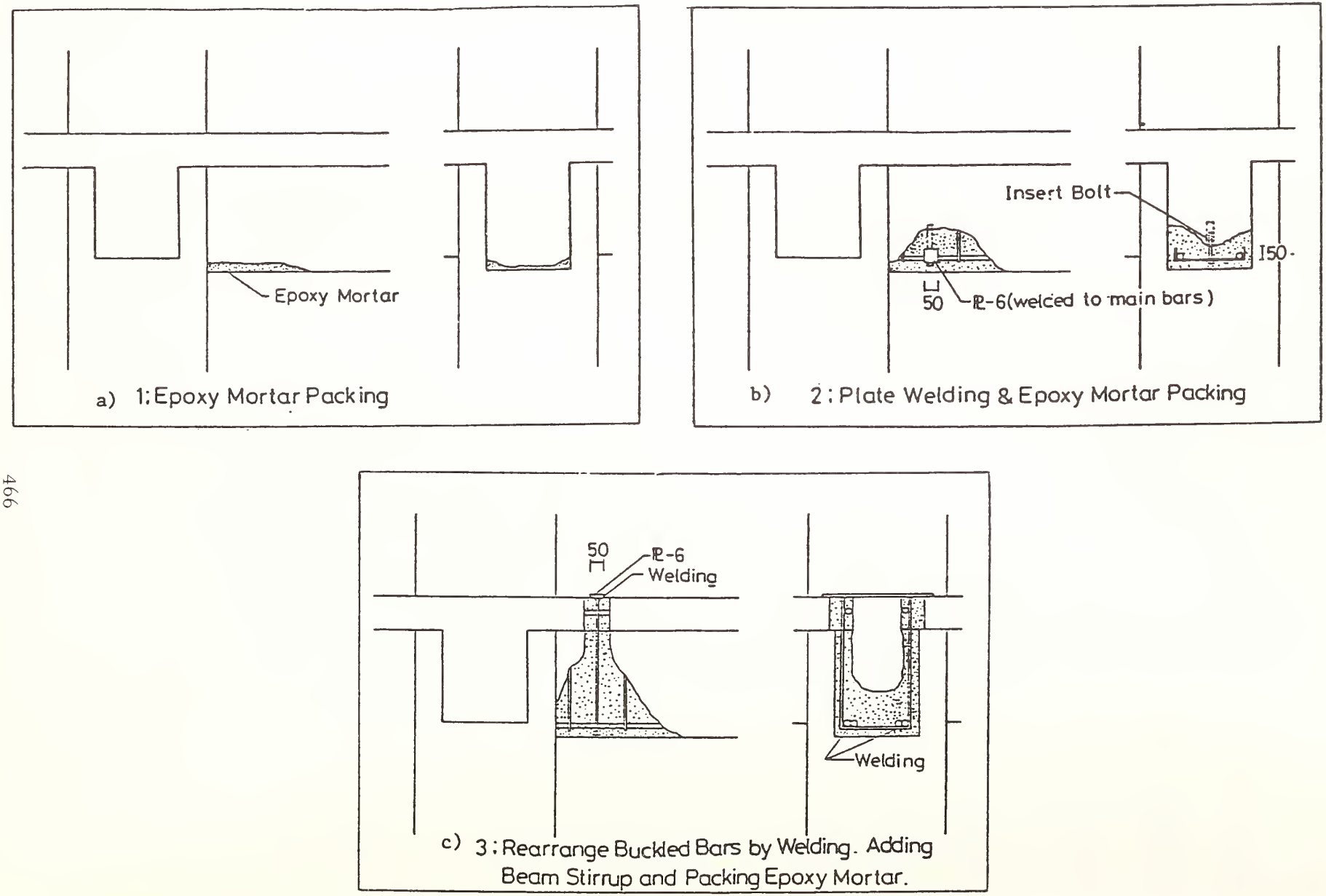

Fig. 2 Details of Repair Works at Beam End

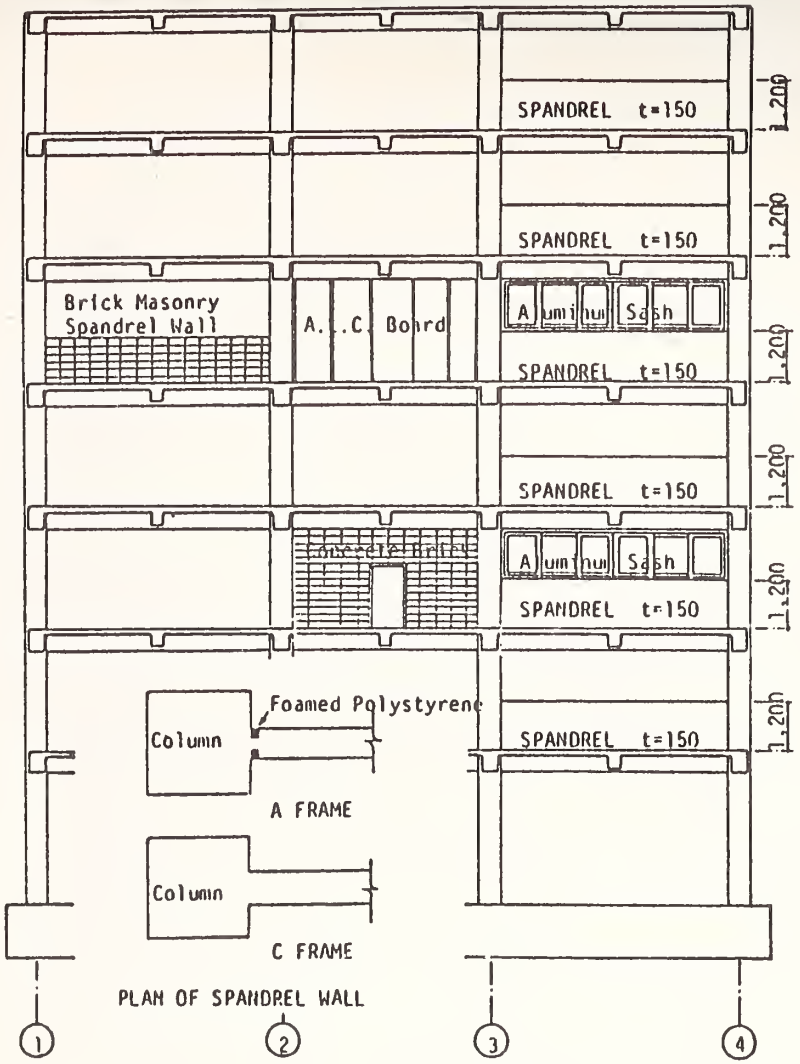

Figure 3. Installation of spadrel walls.

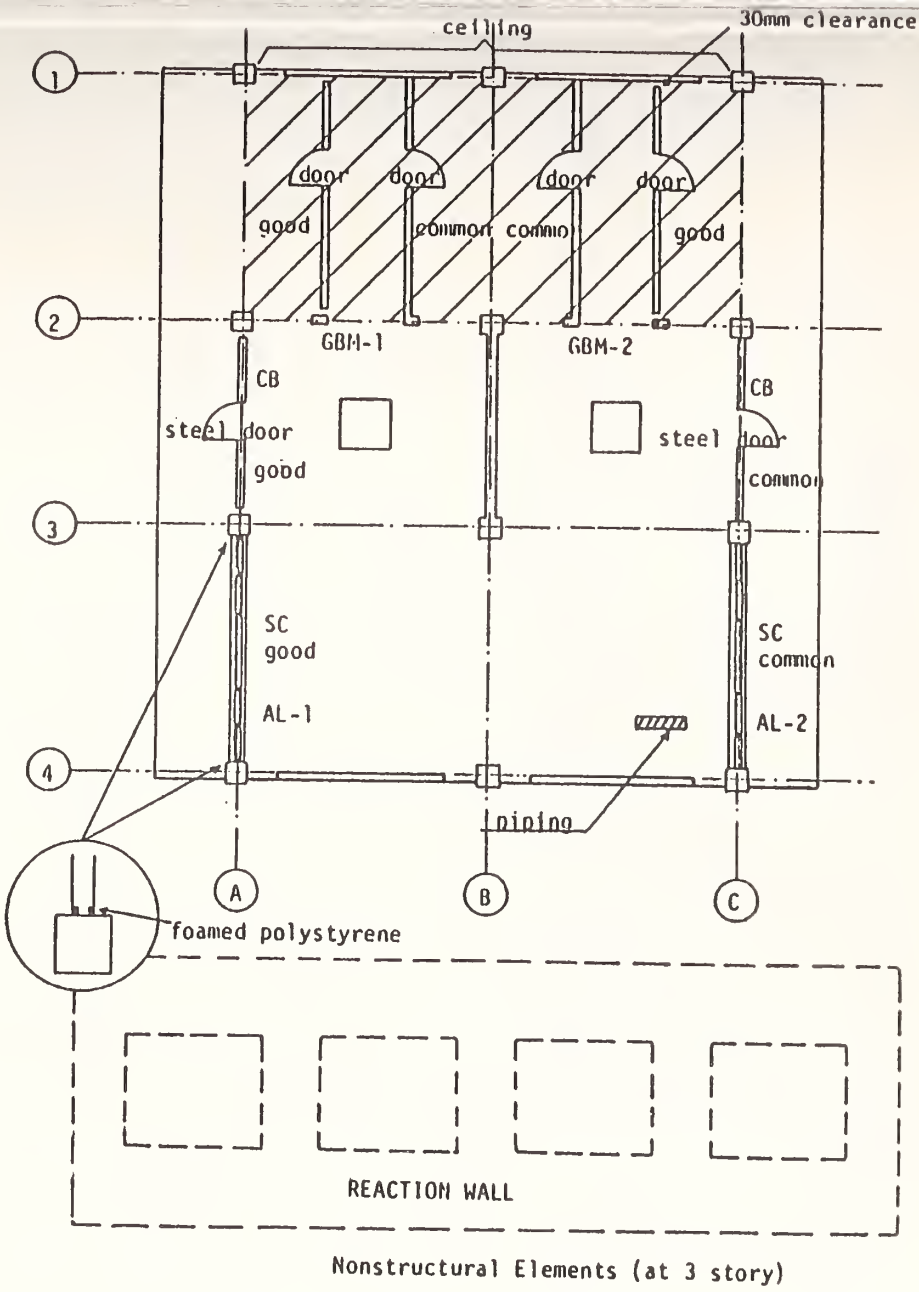

Nonstructural Elements (at 3 story)

Figure 4. Installation of partition walls

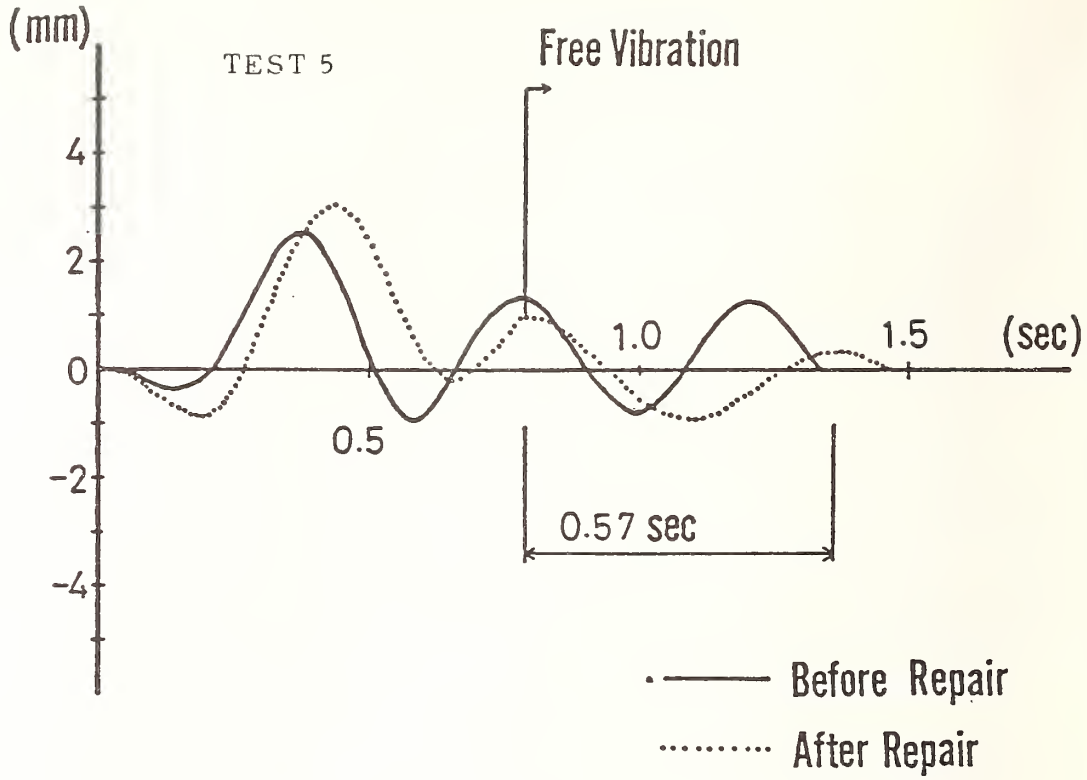

Fig. 5 Response Time Hystory

TEST 5

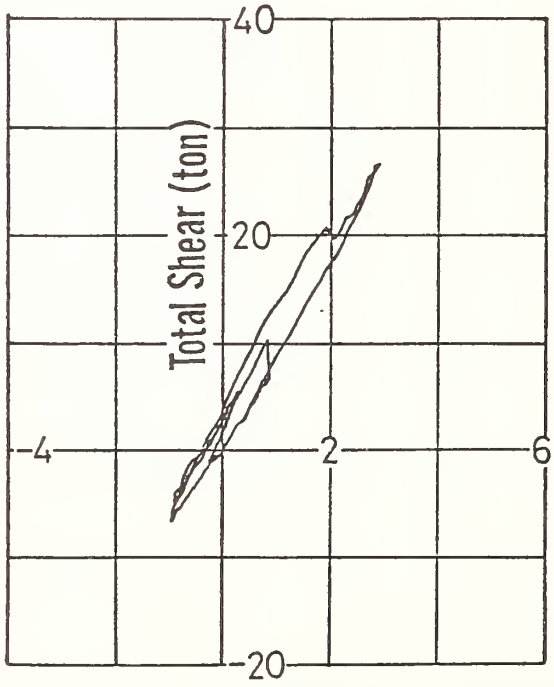

Total Shear Force vs. RF Displacement Relationship

Fig. 6 Hysteresis Loops

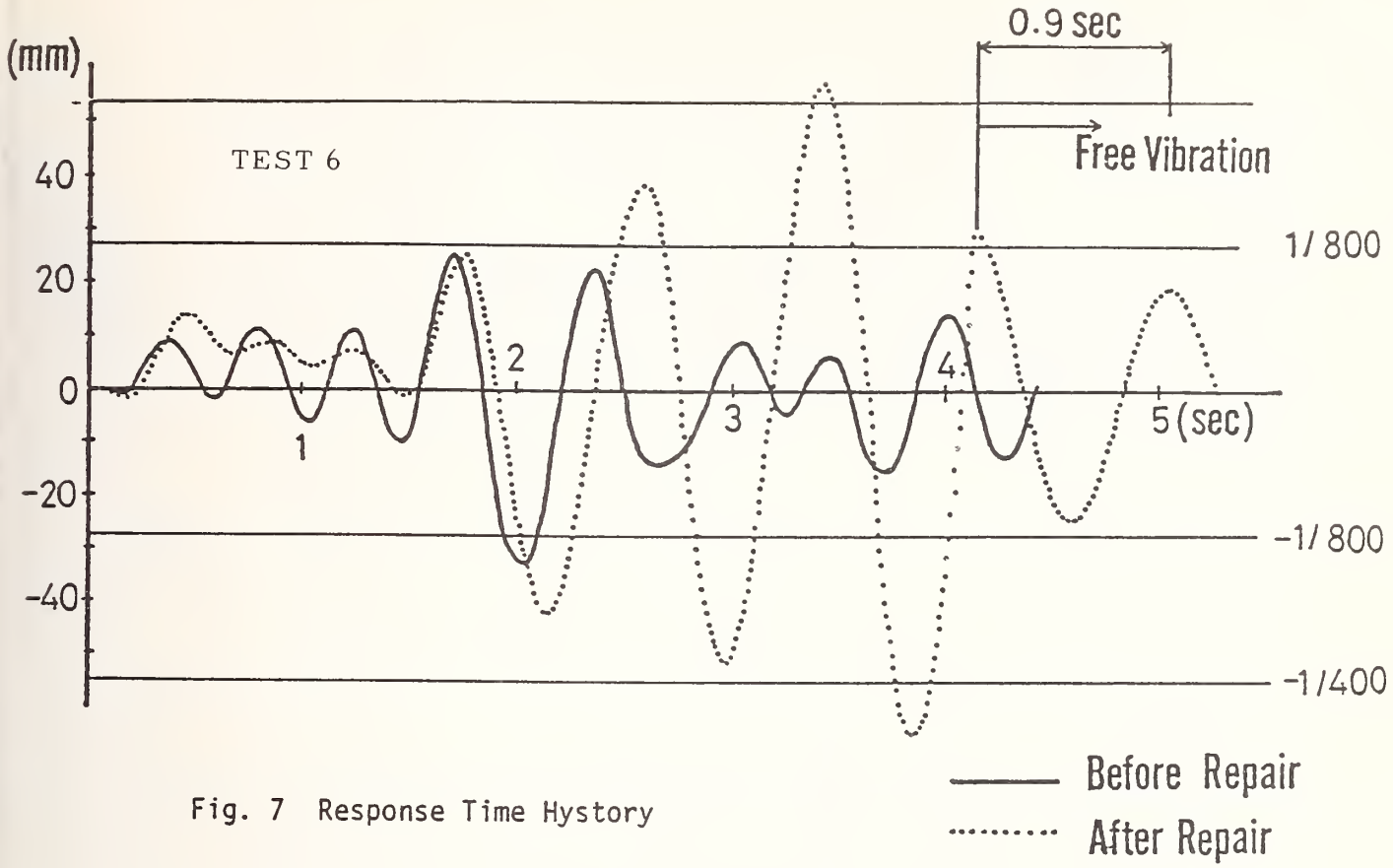

Fig. 7 Response Time Hystory

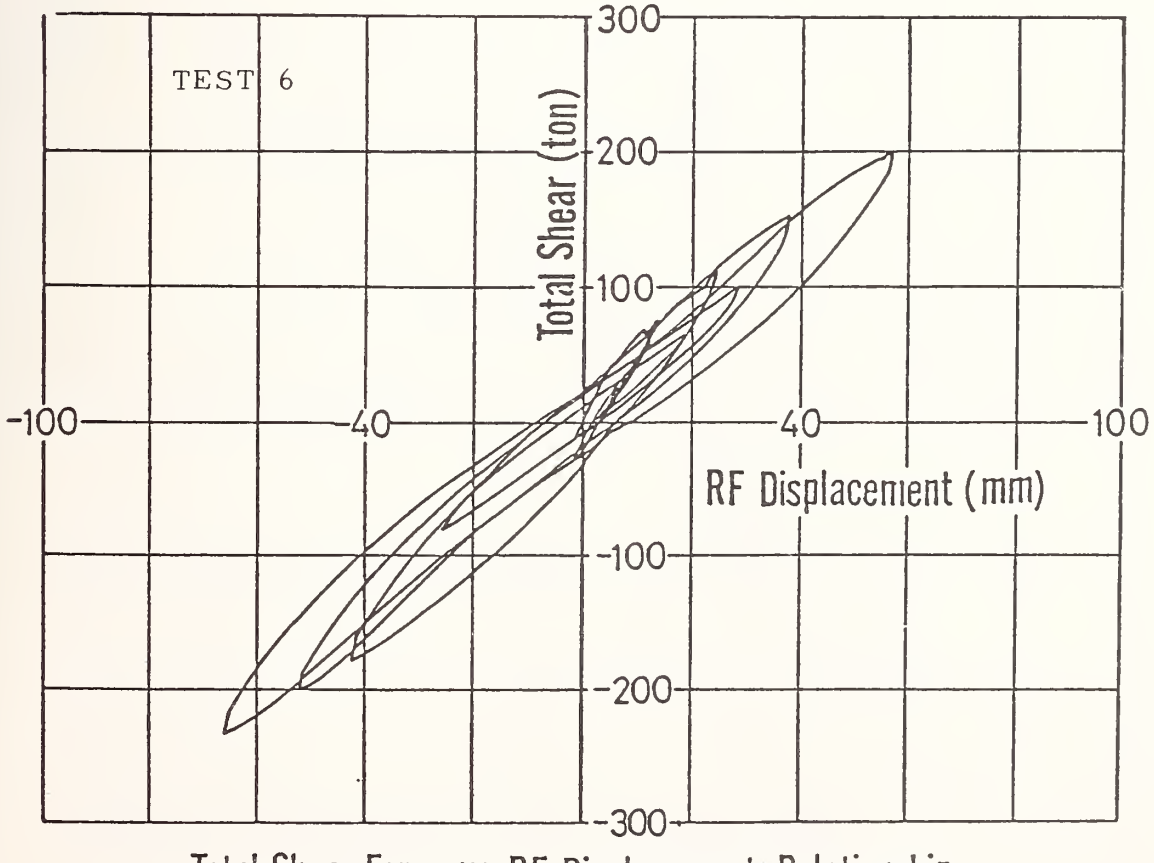

Total Shear Force vs. RF Displacement Relationship

Fig. 8 Hysteresis Loops

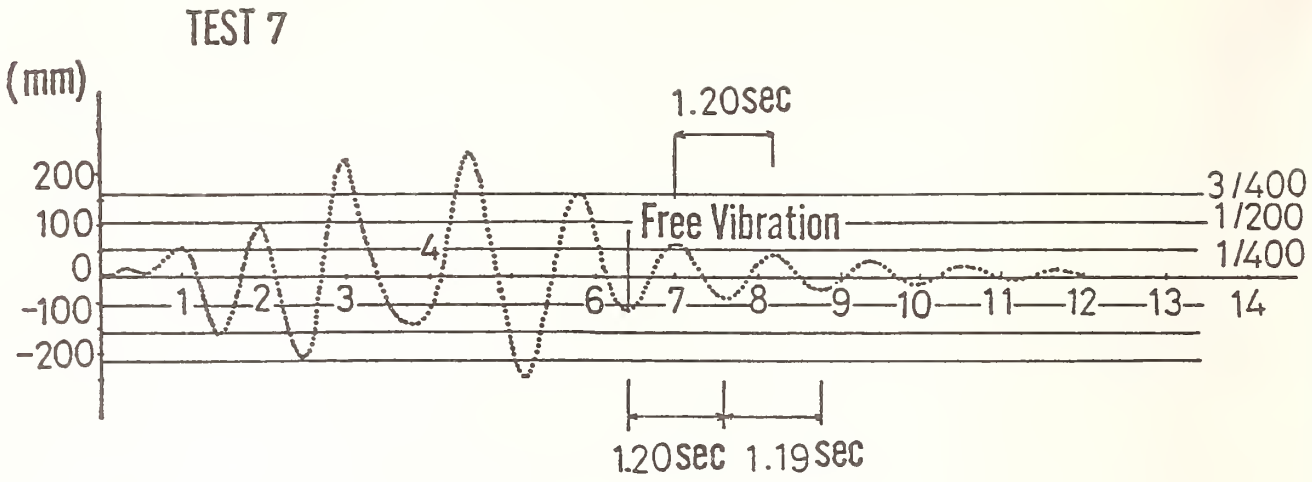

Fig. 9 Response Time Hystory

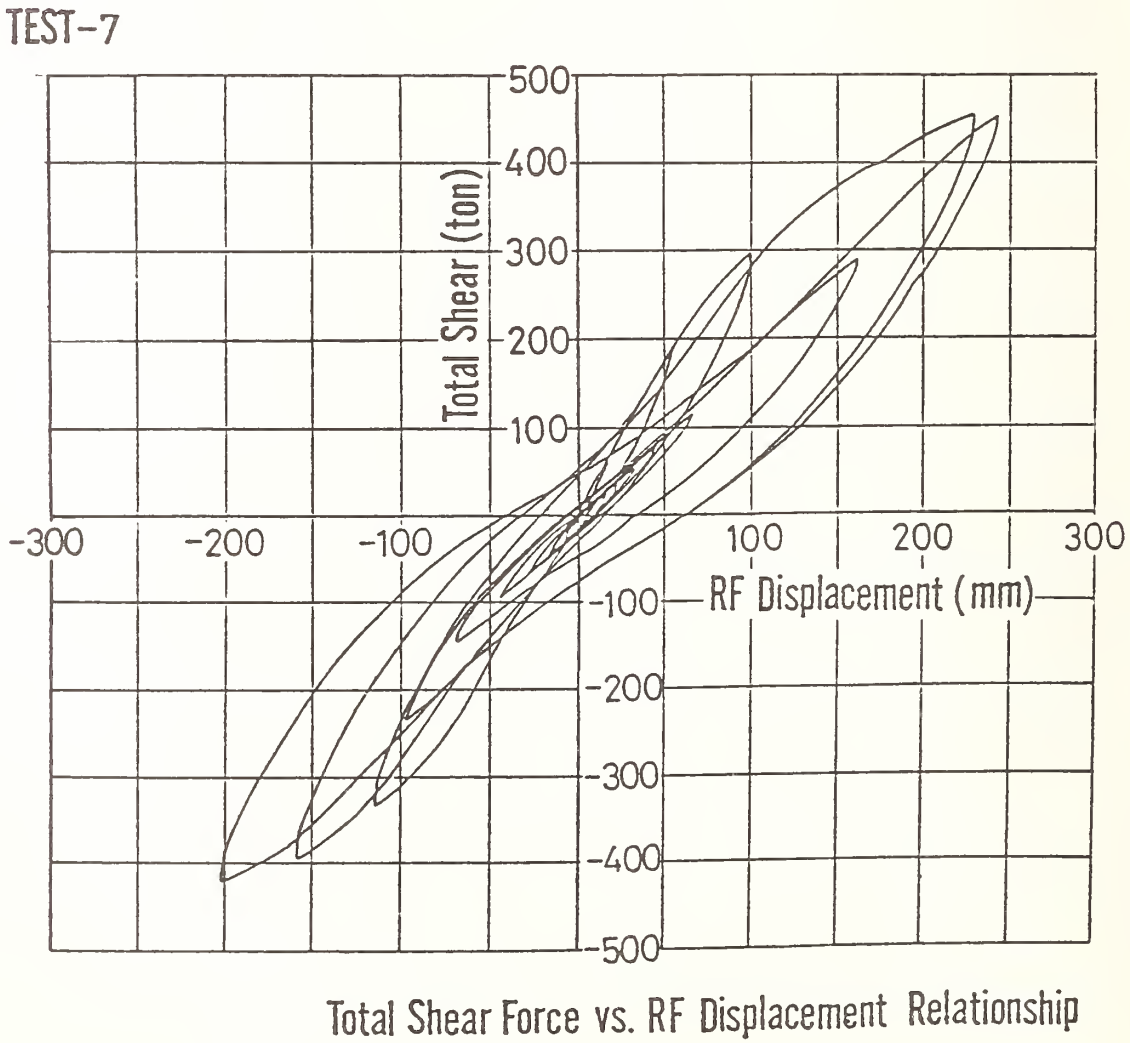

Fig. 10 Hystersis loops

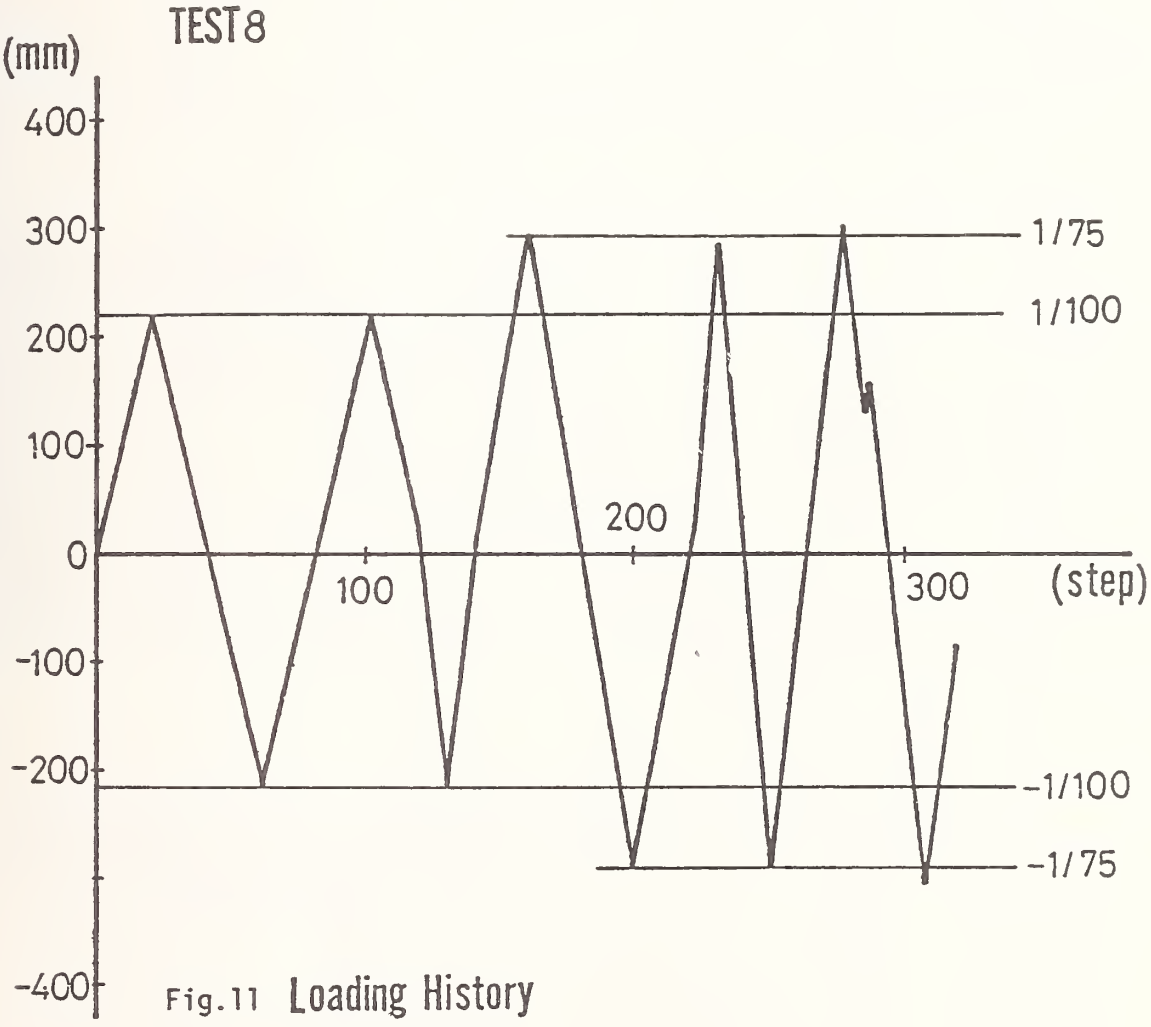

Fig.11 Loading History

TEST-8

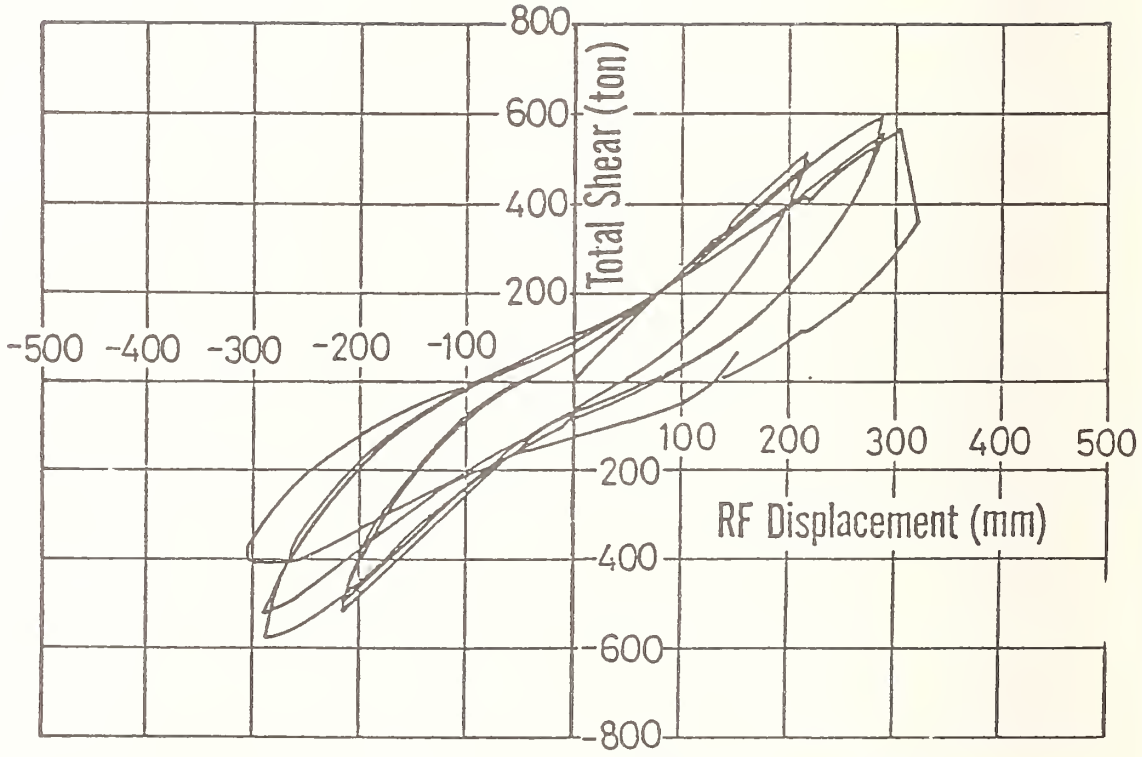

Fig. 12 Total Shear Force vs. RF Displacement Relationship

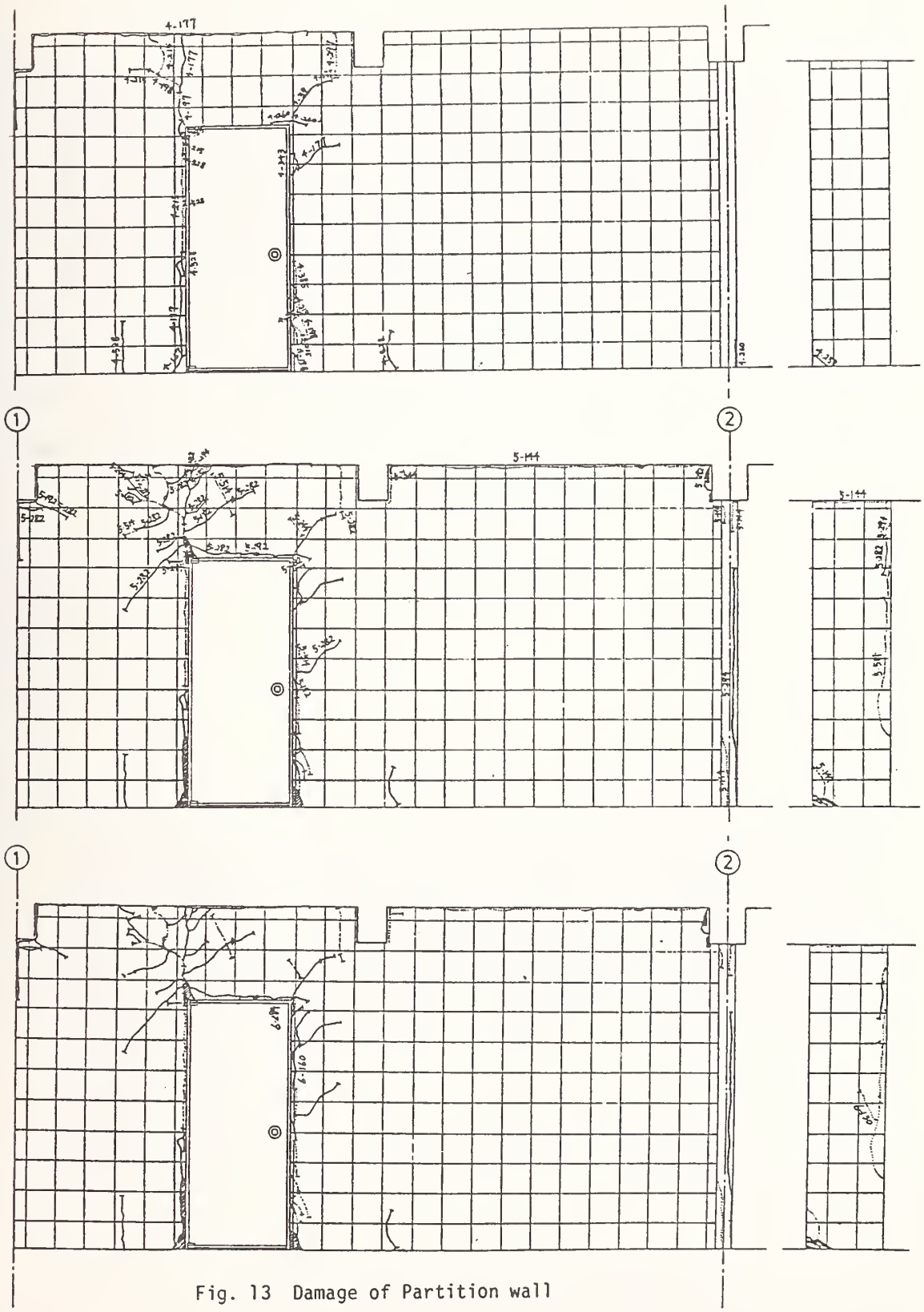

Fig. 13 Damage of Partition wall

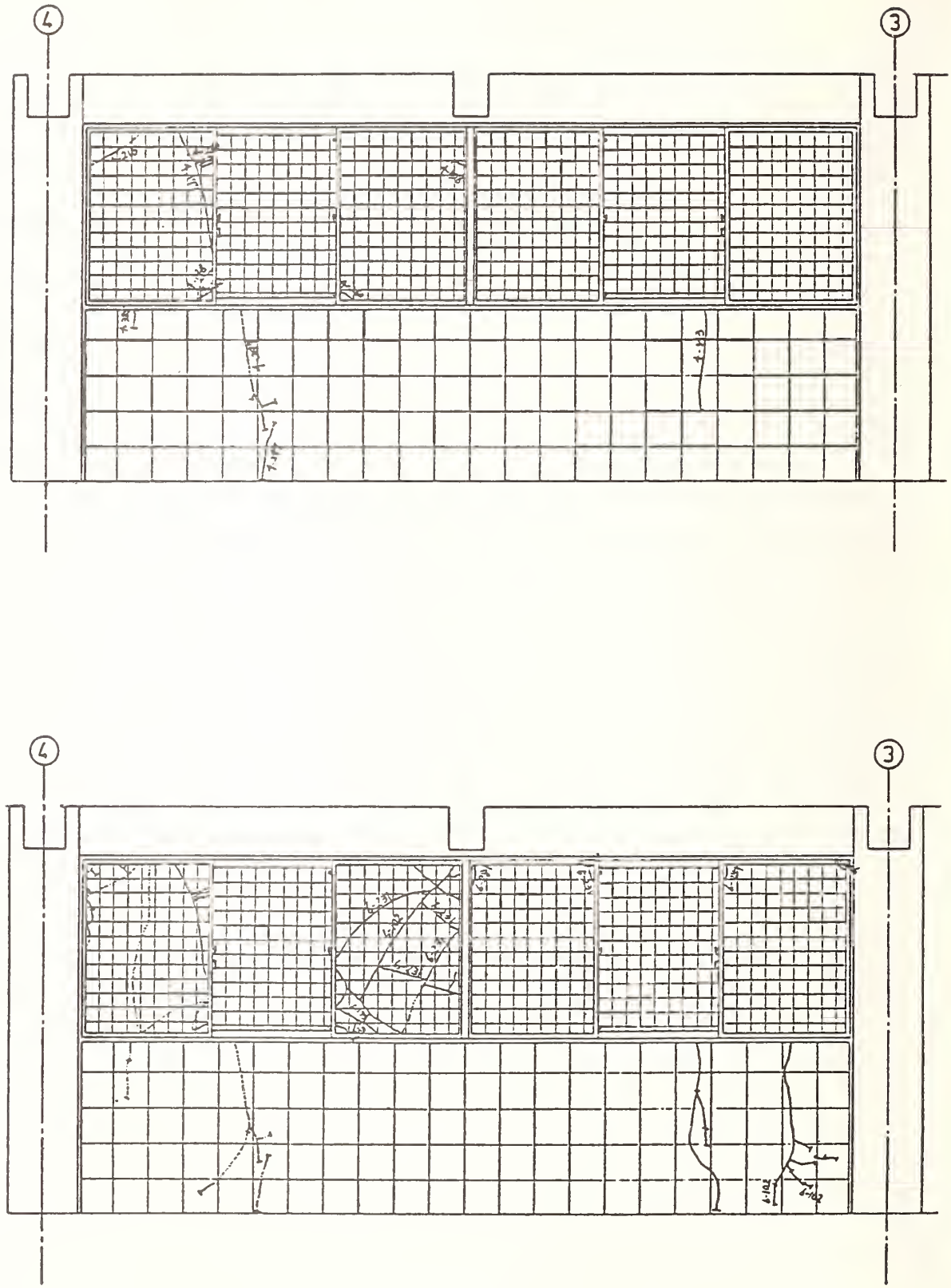

Fig.14 Damage of Glasses & Spandrel Wall

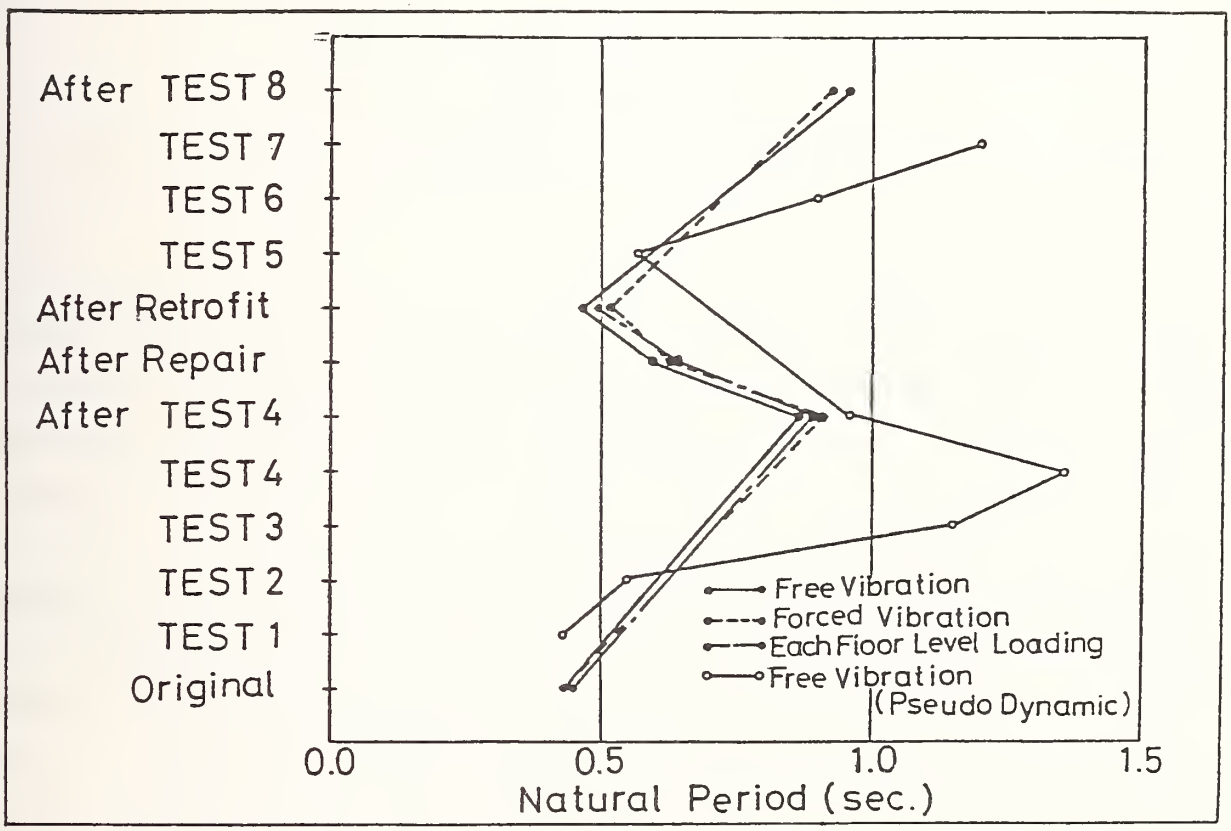

Fig.15 Transition of Measured Natural Period by Vibration Test

TESTS OF PLANAR WALL ASSEMBLIES UNDER IN-PLANE STATIC REVERSING LOADS

B. J. Morgan

Senior Structural Engineer
Analytical Design Section
Construction Technology Laboratories
Portland Cement Association
Skokie Illinois

H. Hiraishi

Research Engineer
Building Research Institute
Japan

W. G. Corley

Divisional Director
Engineering Development Division
Construction Technology Laboratories
Portland Cement Association
Skokie, Illinois

ABSTRACT

During the 1968 Tokachi-Oki Earthquake in Japan, numerous reinforced concrete school buildings of modern design suffered heavy damage. Following that earthquake, a joint seminar under the sponsorship of the U.S.-Japan Cooperative Science Program was held in Sendai, Japan in 1970. One purpose of the seminar was to identify and define programs of research that could be conducted effectively on a cooperative basis between the United States and Japan.

Prompted by discussions held at Sendai, a U.S.-Japan Cooperative Research Program on Earthquake Engineering was established under the U.S.-Japan Cooperative Science Program. The period of this program was initially 1973 to 1975. A program review meeting was held in Hawaii in 1975. Several formal recommendations grew out of the presentations and discussions at this meeting. One of these recommendations was that a cooperative research program should be established with emphasis on large-scale testing of structural systems. During the period of 1974 to 1978, government delegates on a separate U.S.-Japan Panel on Wind and Seismic Effects arrived at the same conclusions.

Based on conclusions and recommendations of both university and government groups, a planning group was established to define specific details of research to be carried out. After four meetings during 1977 to 1979, the planning group recommended that research should focus on "studies to determine the relationship among full-scale tests, small-scale tests, component tests, and analytical studies." [1] With regards to the testing effect associated wth concrete structures, the following were selected to do the research:

a. Building Research Institute, Japan - Full-Scale Tests of Building

b. Construction Technology Laboratories of the Portland Cement Assoc., U.S.A. - Medium-Scale Tests of Structural Wall Assemblies

c. University of Texas, U.S.A. - Full-Scale Tests of Beam/Column Connections

d. University of Illinois, Urbana, Illinois, U.S.A. - Small-Scale Shake Table Tests

e. University of California, Berkeley, California, U.S.A. - Medium-Scale Shake Table Tests

This paper presents a brief review of tests conducted by Construction Technology Laboratories (CTL). Also, preliminary findings of comparisons with the full-scale tests conducted in Japan are given.

TEST SPECIMENS

Two planar specimens were tested at the Construction Technology Laboratories. These were a wall-frame assembly and an isolated wall.

WALL-FRAME

Figure 1 shows the wall-frame assembly just prior to the start of testing. The test specimen represented the wall-frame center section of the full-scale structure tested in Japan. It consisted of a structural wall with a single bay of beams and columns to each side. The CTL specimen was seven-stories high.

In addition to the wall-frame located at its center, the full-scale structure had two beam-column frames located one to each side of, and parallel with, the wall-frame section. In plan, the fullscale structure was 12 m (39 ft) by 17 m (56 ft) measured to the centerlines of the corner columns as shown in figure 2.

Dimensions of the CTL specimen were scaled from the full-scale structure in the ratio of one to three-and-one-half. This scaling provided a structure approximately 6.2 m (20-1/2 ft) high and 4.9 m (16 ft) wide from column to column. The column section was 143 mm (5-5/8 in) square. The web of the structural wall was 57 mm (2-1/4 in) thick. Stubs cast integrally with the wall and beams simulated a floor slab at each level.

To ensure proper consolidation in such small sections, a fine aggregate concrete was used. The design strength of the concrete in the full-scale specimen was 270 kg/cm^2 (3840 psi).

To achieve this moderate strength, a fine aggregate to cement ratio of 4.9 to 1 was utilized with a water/cement ratio of 0.65 to 0.75. Also, cold water was used in the mix to keep the slump at this high water/cement ratio in the range of 38 mm (1-1/2 in) to 51 mm (2 in).

The primary reinforcement in the beams and columns was no. 3 bars conforming to ASTM Designation: A615 Grade 60. Deformed 6 mm hot rolled bars with properties similar to grade 60 were used as primary reinforcement in the boundary elements of the structural wall. Deformed wire was used for wall reinforcement, hoops, ties and stirrups. This wire was heat-treated to obtain stress-strain characteristics similar to those of grade 60 bars.

ISOLATED WALL

The isolated wall test specimen is shown in figure 3. This specimen duplicated the wall portion of the wall-frame structure except that it did not have slab stubs. The isolated wall also was shorter than the wall-frame specimen. It represented the first five levels of the seven level wall-frame specimen.

LOADING

WALL-FRAME

As shown in figure 1, the wall-frame test specimen was positioned between reaction walls. It was loaded laterally with an inverted triangular distribution. This distribution closely simulated the earthquake-like lateral load used in the test of the full-scale structure. The inverted triangular distribution was achieved by using a seven element whiffletree on each side of the specimen. The whiffletree distributed load from a single hydraulic ram anchored to the reaction wall to seven load rods attached to the sides of the slabs at the center of the wall. The specimen was loaded alternately in each lateral direction.

The columns and boundary elements were loaded vertically. A single hydraulic ram acting through a four element whiffletree was used. Part of the vertical whiffletree is visible in figure 1 at the top of the structure.

ISOLATED WALL

The isolated wall was loaded laterally with a single load applied at the top of the fifth-story level of the specimen. This was at the same level as the centroid of the inverted triangular load system used for the wall-frame specimen. The externally applied bending moment and shear at the first story of both specimens was thus the same.

LOAD HISTORY

At the start of the test, each specimen was first loaded vertically. Lateral load was then applied in groups of three full reversing cycles. The lateral displacement was increased for each

three cycle group until the specimen reached the point where it could no longer adequately maintain a load level for a given imposed displacement.

INSTRUMENTATION

For the wall-frame specimen, a total of 389 measurements were recorded at 233 test stages including data from 330 strain gages. Eighty-three measurements were recorded at 135 test stages during the test of the isolated wall.

TEST RESULTS

BEHAVIOR

The mechanism that developed within the wall-frame specimen consisted of hinging in the columns and wall at the base of the structure with all other hinging taking place in the beams. The mechanism was fully developed at a drift ratio of 1.5 percent measured at the top of the specimen. This drift occurred at maximum lateral load. Drift is defined as the ratio of the absolute lateral deflection of a point to the height of that point above the baseblock. The drift ratio measured at the top of the first-story was 1.6 percent. Drifts measured at other stories were approximately 1.5 percent. The load-deflection relationships obtained during the test are given in figure 4.

Yield strain in the reinforcement was first exceeded in the boundary element of the structural wall at the base. This first yield occurred at 65 percent of the maximum lateral load. Nearly all the tensile reinforcement at the base of the wall had yielded at 69 percent of the maximum lateral load.

The isolated wall reached its maximum lateral load capacity at a drift of approximately 1 percent. Drifts measured at the other stories of the specimen were approximately the same. The load-deflection relationships obtained during the test are given in figure 5.

First yield occurred in the reinforcement at the base of the boundary element at 83 percent of maximum lateral load. Essentially all tensile reinforcement at the base of the wall had yielded at 93 percent of maximum load.

During both tests, the wall boundary element that was in tension elongated considerably when compared to the shortening of the boundary element in compression. Moreover, most of this vertical elongation was concentrated in the first-story. After yield was well developed, the wall rotated essentially as a rigid body about a pivot point located at the base of the boundary element in compression. The boundary element in tension elongated more or less uniformly from the baseblock to the top of the first-story.

ANALYSIS

A structural analysis was made of both specimens utilizing the measured mechanical properties of the materials. Maximum moment capacities of the wall, beams and columns were determined from a moment/curvature analysis assuming plane sections remain plane during bending. Strain hardening of the reinforcement was considered. Imposed axial load effects were included in the analysis. Maximum load capacity of the wall frame as determined by the test was 1.1 times the analytically predicted maximum load. Maximum test load for the isolated-wall was 1.04 times the analysis value. Table 1 summarizes the results of the structural analysis and identifies the force and moment distribution within the elements of the wall-frame system.

As would be expected, the wall and beams were the primary moment resisting elements, while the wall and columns were the shear resisting elements. For the configuration tested, however, the beams contributed more to the moment capacity of the overall system than the columns contributed to the shear capacity. Therefore, the applied shear to moment ratio in the wall of the wall-frame specimen was different from that of the isolated wall specimen where only the wall resisted all the applied shear and moment.

STRAIN GAGE RESULTS

Reinforcement in the slab was instrumented at one of the upper levels in the wall-frame specimen. The measured strain indicated that the slab reinforcement was acting effectively with beam reinforcement in negative bending out to a distance of four to six times the slab thickness from the beam. This substantiates the design recommendation discussed in reference 2 that slab reinforcement may be considered effective in negative bending to a distance of four times the slab thickness from the beam. This result also is consistant with tests made of box girders [3] where reinforcement was found to be effective, as much as six times the wall thickness of the horizontal element in tension.

Results from strain gages on the boundary element hoops indicated that they are subjected to significant strain only over the lower portions of the first-story. Strains in all other boundary element hoops monitored were relatively small. These data further substantiate a conclusion made by other researchers [4] that special confinement reinforcement is required only for the lower portions of the boundary elements of a structural wall. Present U.S. codes [5,6] call for special confinement for the full height of boundary elements.

It is noted that none of the instrumented column hoops or beam stirrups experienced strain in excess of yield, even though several instrumented stirrups were located in beam hinging regions.

COMPARISON WITH FULL-SCALE TEST

It appears, from a preliminary review of some of the test results of the full-scale structure, that the cracking patterns and overall behavior of the wall-frame test specimen were very similar to that of the full-scale structure.

The detailed analysis of the full-scale test results is still in progress in Japan. It is evident, however, that strength of the full-scale structure is greater than would be predicted from an analysis based on the isolated wall and wall-frame test results where the wall-frame and two beam-column frames of the full-scale structure are considered as two-dimensional structural systems. It is presently reasoned that the increased strength is due in large measure to three-dimensional effects. The two factors which appear to be the major contributors are the transverse beams and the floor slabs.

As discussed previously, the boundary element of the structural wall in tension elongated considerably when compared to the shortening of the compression boundary element. Most of this elongation was concentrated in the first-story. As a consequence, beams running transverse to the tension boundary element in the full-scale structure experienced relative vertical movement of their ends. This came about because they were connected on one end to the boundary element which was displacing vertically, and on the other end to a conventional frame which experienced little vertical deformation. Since transverse beams framed into both sides of the wall of the full-scale structure. Their contribution to overall strength could have been significant.

In the planar wall-frame structure, the slab stubs deformed in one plane only as they contributed to the bending strength of the beams. In the full-scale structure, the slab in the vicinity of the tension boundary element deformed in two planes. The slab worked with the beams both in the plane of, and transverse to, the structural wall. Therefore, the full-scale structure with slabs deforming in two planes could very well have been stronger than would be predicted from the test of a wall-frame specimen with slab stubs deforming in only one plane.

CONCLUSIONS

Results have indicated that the calculated capacities of the isolated wall and wall-frame specimen agreed reasonably with measured results. This further strengthens confidence in the analytical procedure currently used in design. Also, it appears that the behavior of the medium-scale wall-frame assembly was very similar to the behavior of the wall-frame of the full-scale test specimen.

The results demonstrate how all structural elements in a system are interrelated and influence each others behavior. This is particularly true in real three-dimensional structures where the

analysis is often performed on typical two-dimensional frames or sections where out-of-plane behavior is conservatively neglected. It is noted that the analysis of the test results indicate that a lower bound on the strength of full-scale structure was arrived at by conservatively neglecting out-of-plane effects.

REFERENCES

[1] U.S.-Japan Planning Group, Cooperative Research Program Utilizing Large-Scale Testing Facilities, "Recommendations for a U.S.-Japan Cooperative Research Program Utilizing Large-Scale Testing Facilities," Report No. UCB/EERC-79/26, Earthquake Engineering Research Center, University of California, Berkeley, California, September 1979.

[2] Park, R. and T. Paulay, "Reinforced Concrete Structures," John Wiley and Sons, 1975.

[3] Carpenter, J. E., et al., "Design of Bent Caps for Concrete Box-Girder Bridges," Research and Development Bulletin RD032.01E, Portland Cement Association, Skokie, Illinois.

[4] Oesterle, R. G., A. E. Fiorato, and W. G. Corley, "Reinforcement Details for Earthquake-Resistant Structural Walls," Concrete International, American Concrete Institute, Vol. 2, No. 12, December 1980.

[5] "Building Code Requirements for Reinforced Concrete," (ACI 318-77), American Concrete Institute, Detroit, Michigan.

[6] International Conference of Building Officials, Uniform Building Code, 1979 Edition, Whittier, California.

Table 1. Specimen Load Capacities

Specimen	Moment		Lateral Force	
	in.-kips	Percent of Total	kips	Percent of Total
Wall-frame				
Calculated				
Wall	4179	51	31.7	70
Beam	3759	45	-	-
Columns	327	4	13.6	30
Total	8265	100	45.3	100
Measured				
Total	9091		50.0	
Measured / Calculated	1.10		1.10	
Isolated Wall				
Calculated	4019		22.8	
Measured	4195		23.8	
Measured / Calculated	1.04		1.04	

Fig. 1 Wall-Frame Test Specimen

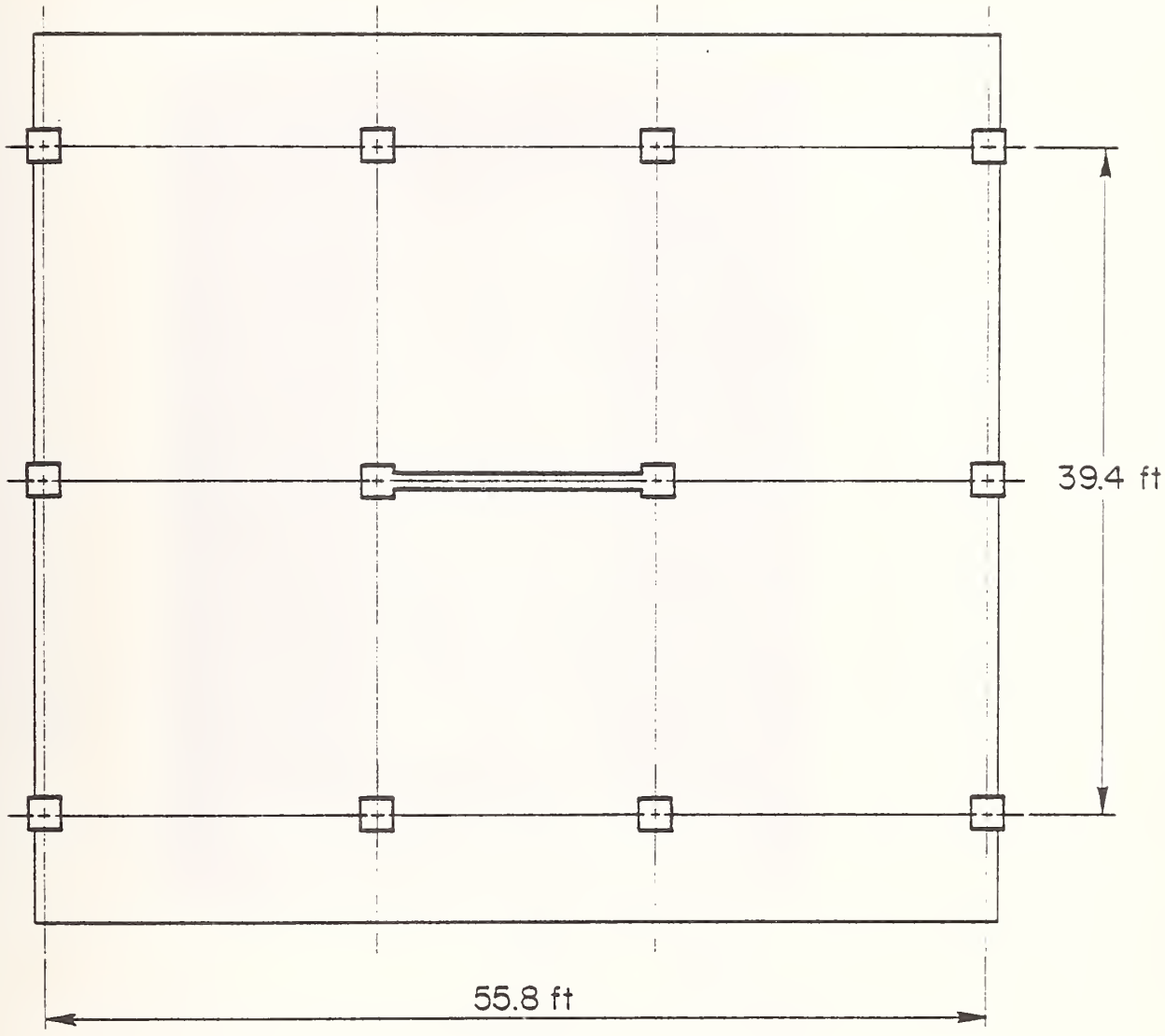

Fig. 2 Full-Scale Test Structure - Plan View

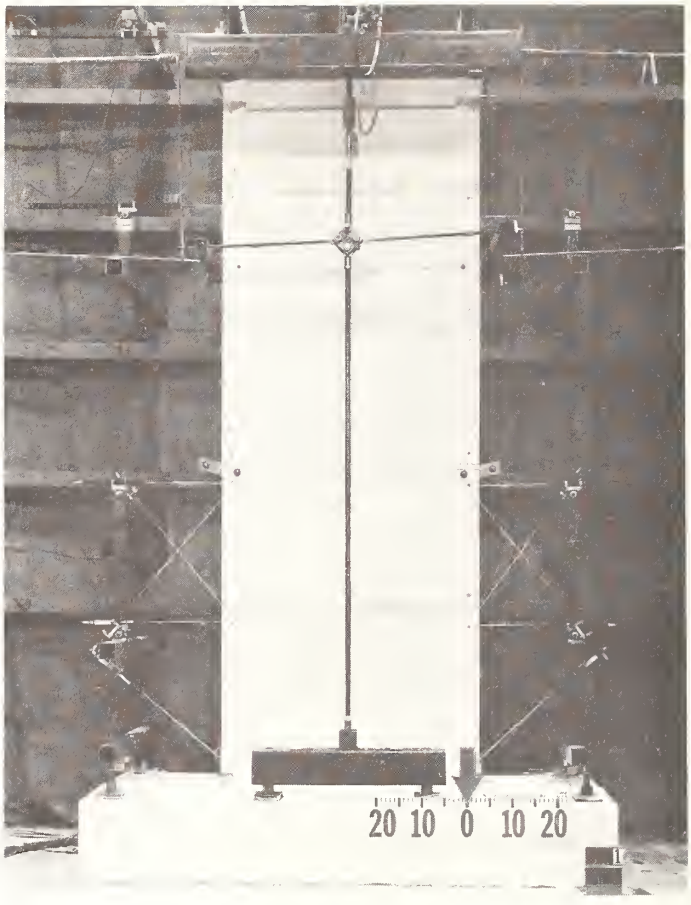

Fig. 3 Isolated Wall Test Specimen

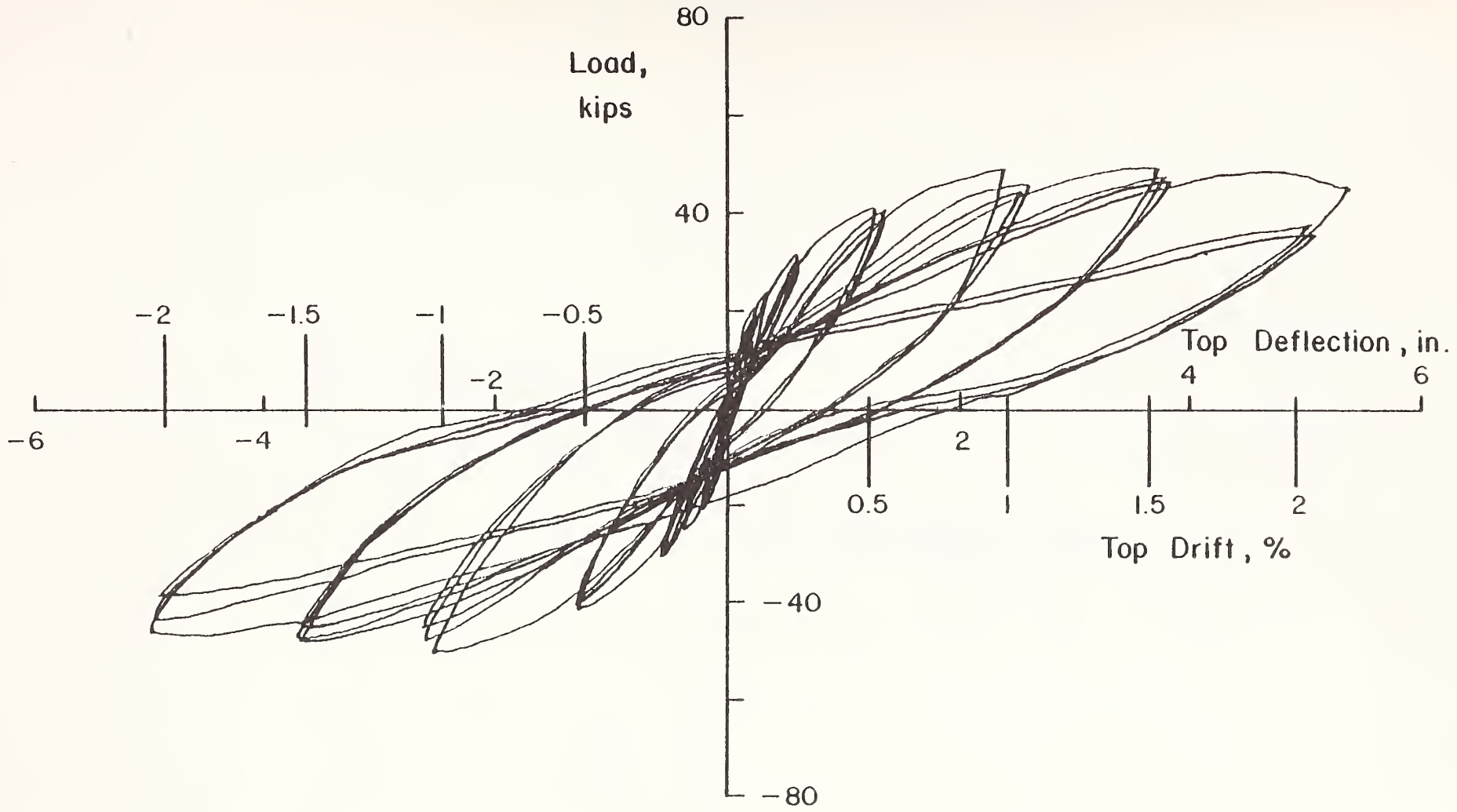

Fig. 4 Load versus Top Deflection, Wall-Frame Specimen

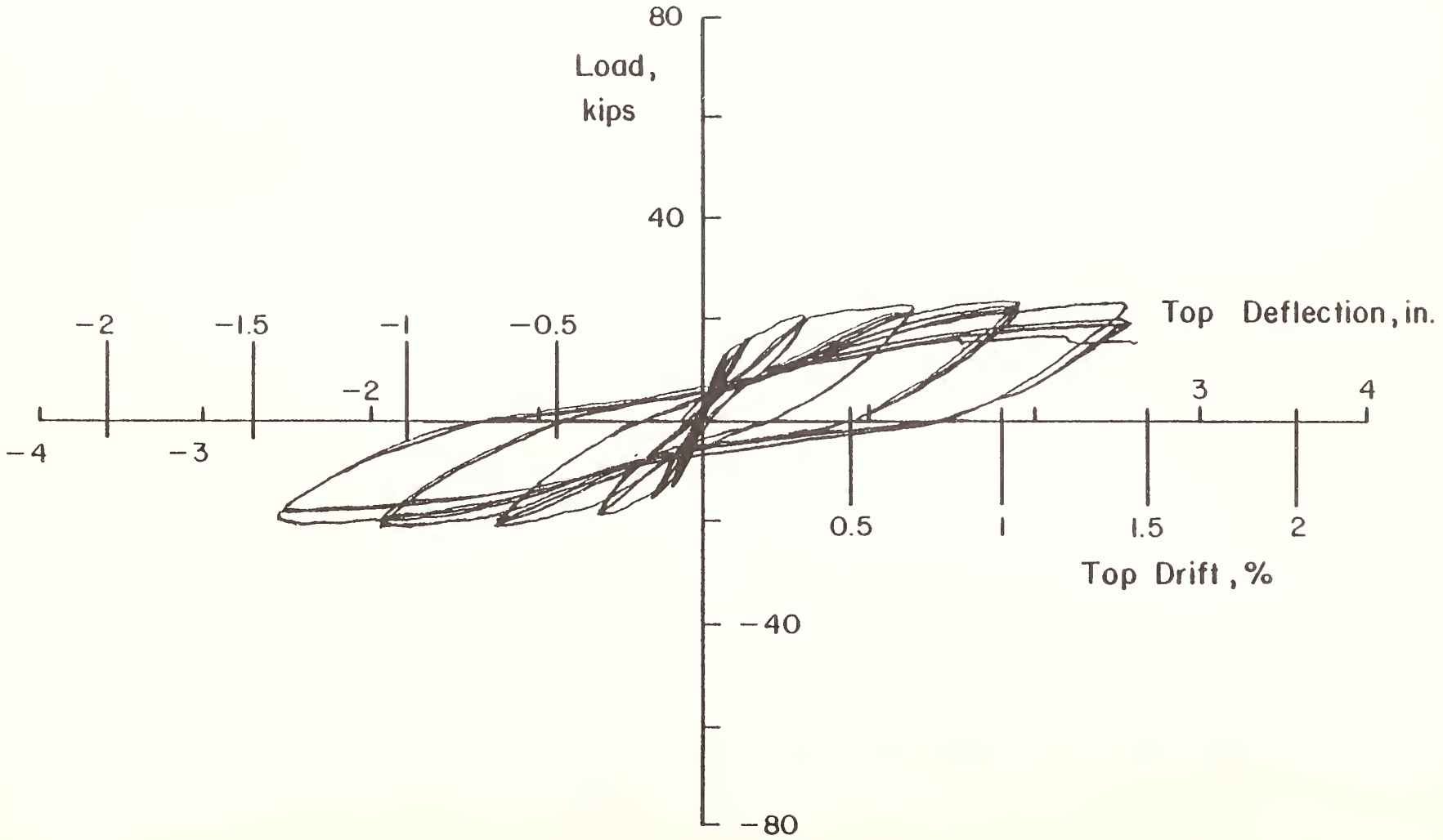

Fig. 5 Load versus Top Deflection, Isolated Wall Specimen

RESEARCH PROGRAM ON THE FULL-SCALE SEISMIC EXPERIMENTS OF STEEL BUILDINGS

Makoto Watabe
Hiroyuki Yamanouchi
Mitsumasa Midorikawa
Toshifumi Fukuta
Takashi Kaminosono

Building Research Institute
Ministry of Construction

ABSTRACT

This research program is conducted in accordance with recommendations prepared by the U.S-Japan planning group established in 1977 under the auspices of the U.S.-Japan Panel on Wind and Seismic Effects, United States-Japan Natural Resources (UJNR) Program. Research activities from these recommendations have been conducted under the Joint Technical Coordinating Committee (JTCC), which consists of researchers from both countries.

In its first year, the Structural Steel Phase was begun by experiments on structural members and subassemblages. These results would support analyses on a full-scale test building. The support tests consist of four experimental programs. They are: (1) static tests on three-story steel planar frames, (2) dynamic and pseudo-dynamic tests on steel frames (designated as a Correlation test), (3) static tests on composite girders, and (4) static tests on column-to-footing connections. The second year's main program is to conduct tests on the full-scale six-story steel building using the pseudo-dynamic testing method. The test building consists of two unbraced moment-resisting frames and a braced frame with K-braces. This structure would represent a portion of an overall building. Two types of K-bracing systems, the concentric K and the eccentric K, should be used in different stages of testing. It should be tested in several stages using a loading procedure simulating realistic seismic conditions. At the final stage of testing, nonstructural elements such as curtain walls and partitions should be added to the structural system and the entire structure should be loaded to failure. In the third year, analyses and estimation on the full-scale test will be done, associated with supplementary tests on subassemblages. Comprehensive consideration will be directed to seismic safety of steel buildings.

INTRODUCTION

As a part of the U.S.-Japan Cooperative Research Program Utilizing Large-scale Testing Facilities, research on steel building structures has started from the fiscal year 1981 for 3 years, following the 2 year project on reinforced concrete building structures.

This research program is conducted in accordance with recommendations prepared by the U.S.-Japan planning group established in 1977 under the auspices of the U.S.-Japan Panel on Wind and Seismic Effects, United States-Japan Natural Resources (UJNR) Program. Research activities by these recommendations have been conducted under the Joint Technical Coordinating Committee (JTCC), which consists of researchers from both countries. A full account of the history and progress of this large project is described in references 1 and 2.

In its first year, the Structural Steel Phase was begun with experiments on structural members and subassemblages. These results would support analyses on a full-scale test building. The second year's main program is to conduct tests on the full-scale six-story steel building using the pseudo-dynamic testing method. In the third year, analyses and estimation on the full-scale test will be done, associated with supplementary tests on subassemblies. Comprehensive consideration will be directed to seismic safety of steel buildings. Table 1 shows the overall schedule of this project.

To develop this program in the research and financial phases, the Japan National Cooperative Research Committee has been organized among the Building Research Institute, Ministry of Construction the Building Contractors Society (a corporation of construction companies), and the Kozai Club (a corporation of steel companies and steel fabricators).

SUPPORT TESTS

OUTLINE OF SUPPORT TESTS

The support tests consist of four experimental programs. They are: (1) static tests on three-story steel planar frames, (2) dynamic and pseudo-dynamic tests on steel frames (designated as a Correlation test), (3) static tests on composite girders, and (4) static tests on column-to-footing connections. The outline of these programs can be described as follows:

STATIC TEST ON THREE-STORY STEEL PLANAR FRAMES

One-half scaled models of the lower three-stories on the full-scale structure will be tested to examine their hysteretic characteristics. Particular attention will be directed to investigating the interaction between K-braces and frames and the effect of member deformability on the overall behavior.

COPRELATION TEST BETWEEN DYNAMIC AND PSEUDO-DYNAMIC TESTS

This test is planned to investigate the capacity of the pseudo-dynamic testing technique which would simulate the real behavior of steel structures subjected to ground motions. For this purpose, both shaking table and pseudo-dynamic tests will be carried out by using identical specimens.

STATIC TEST ON COMPOSITE GIRDERS

Typical composite girders used in the full-scale structure will be tested for their hysteretic behavior, and the restoring force characteristics of the composite girders will be identified.

STATIC TEST ON COLUMN-TO-FOOTING CONNECTION

Elastic-plastic behavior of the footing used in the full-scale structure can be examined in this test. One of the major topics under observation is the connection details of a column with a brace. The results will be useful to evaluate the effectiveness of the footing design adopted for the full-scale structure.

STATIC TEST ON THREE-STORY STEEL PLANAR FRAMES

Six specimens, approximately one-half scale model of the lower three-stories of the full-scale specimen, are prepared for this test. Two of them are K-braced frames with composite girders. The other four specimens have some different composition of members from these two prototype specimens, as described later.

Each specimen is composed of two identical planar frames having three-stories as shown in figure 2.1. The lower two-stories would be a target for this supporting test, because the boundary conditions are not so realistic at the upper levels as the prototype structure will be.

At the top floor prepared mainly for loading, lateral and vertical forces will be applied so as to simulate stresses in the members of the lower stories of the full-scale structure.

The braces, girders, and columns are selected to have compact cross sections in the sense of local buckling. Their connections are designed to be strong enough to cover the full-plastic state of the members. Therefore, the structure should be ductile even after the buckling of the braces or the yielding of the girders and columns. Rectangular tubes are adopted for the braces to ensure in-plane buckling of these braces.

The test specimens have the following characteristics associated with specific quantities listed in table 2.1. These specimens are expected to support a prediction on the hysteretic behavior of the full-scale structure.

Specimen 1 and 2:

The restoring force characteristics for concentric K-braced frames will be identified, considering the composite actions of the girders. For this purpose, two different loading programs will be adopted, with each specimen receiving one program.

Specimen 3:

This is an unbraced frame without slabs. The girders and columns have the same sizes as those of specimens 1 and 2, to investigate the inelastic behavior of the moment frame in comparison with the concentric K-braced frames.

Specimen 4:

This specimen is a concentric K-braced frame without slabs. Dimensions of the members are identical with those in specimens 1 and 2, to evaluate the effects of reinforced concrete slabs on the inelastic behavior of the braced frame in comparison with specimens 1 and 2.

Specimen 5:

This specimen has also a concentric K-braced frame without slabs. However, the slenderness ratios of the braces are approximately 1.5 times larger than those of specimens 1 and 2. Dimensions of beams and columns are the same as those of specimens 1 and 2. This specimen will be tested to estimate the effect of slenderness of braces on the post-buckling behavior of braced frames.

Specimen 6:

This is also a braced frame without slabs, having a different collapse mechanism from other specimens; that is, the columns are relatively smaller in strength than the girders. The difference in contributions of failure modes to the overall behavior of these assemblages will be evaluated by this additional specimen.

CORRELATION TEST BETWEEN DYNAMIC AND PSEUDO-DYNAMIC TESTS

The primary purpose of this test is to examine the correlation between the results obtained from shaking table tests and pseudo-dynamic tests. This correlation study is believed to best calibrate the effectiveness of the pseudo-dynamic testing technique. The flow of this test is as follows:

First, a shaking table test is performed. Then, an identical specimen as that used in the shaking table test is tested by the pseudo-dynamic testing technique. The acceleration history recorded on the surface of the shaking table is used as an input ground motion for this pseudo-dynamic test.

A total of eight specimens, every two of which are identical, will be prepared in this test as shown in figure 2.2. These specimens are considered to be 1/3 scaled models of the full-scale prototype. To properly take the scale effect into account, additional weight, with which the total weight of the specimen is to be 1/9 of its prototype, will be loaded on the specimen. Further, input acceleration times scale will be contracted to $1/\sqrt{3}$. The four types of test specimens have the following characteristics.

Type 1: One-story Unbraced Frame

Girders in the specimen are significantly greater in strength and stiffness than columns. The specimen, therefore, is considered as a single degree of freedom system.

Type 2: Two-story Unbraced Frame

Analogously to type 1 specimen, the specimen is designed to exhibit column failure.

Type 3: Two-story Braced Frame

This specimen has diagonal braces in both stories, whereas, the dimensions of beams and columns are identical with those in type 2 specimen. The braces are designed to carry about 70 percent of the total lateral force at the failure stage. Types 2 and 3 specimens can be treated as two degrees of freedom systems.

Type 4: Five-story Braced Frame

Girder and column flexural stiffness are identical in this specimen. Yield hinges then are expected to occur in the girders. The braces are designed so that they would yield simultaneously under a base shear of about 0.2 in base shear coefficient. In the design calculation, the external lateral forces are distributed along the height in accordance with the distribution profile in Japan New Seismic Code.

STATIC TEST OF COMPOSITE GIRDERS

The girder of the specimen is approximately the same size as that of the sixth-floor of the full-scale specimen as shown in figure 2.3. Columns and braces that are one-half in length of these of the full-scale structure are erected from the composite girder so that this assemblage could also simulate the composite girder behavior of other floors. In this assemblage, the girder is extended on one side by one-half of the span length to take the effect of an adjacent girder into account. Cirder-to-column and brace-to-column connections are securely welded to ensure sufficient deformation and strength capacities of the specimen.

Specimen 1:

This is a model of the braced planar frame of the full-scale prototype structure to evaluate the effects of bracings on the structure of the composite girder. Stud connectors are used to transmit shear forces from the steel girders to the reinforced concrete slabs, especially after the braces buckle.

Specimen 2:

This specimen consists of columns and composite girders. Columns in the specimen are greater in strength and stiffness than composite girders. This specimen will be tested to identify the restoring force characteristics of the composite girders. Stud bolts are used to securely tighten the steel with the reinforced concrete slabs even in the failure state of the structure.

STATIC TEST ON COLUMN-TO-FOOTING CONNECTIONS

The specimen is an approximate full-scale model of a column base-to-footing assemblage of the full-scale structure. The assemblage of the interior column in the braced bay will be tested because this column receives a brace at its base and, therefore, the hysteretic behavior of this assemblage is most complex. Primary variables in this test are: (1) the intensity of the bending moment and horizontal shear force applied to the column base, and (2) the bearing mechanism of the footing against punching shear. For this purpose, three specimens will be prepared, with the characteristics of each specimen being summarized below.

SUMMARY OF SPECIMEN

Specimen 1:

The footing concrete is designed to resist bending moment and shear force transferred from the column base by direct bearing. The allowable punching shear stress is limited to $1.48\sqrt{F_c}$ in designing this specimen, where F_c means the standard strength of concrete for design.

Specimen 2:

The bending moment and shear force are resisted by a combination of footing concrete and steel hoops surrounding the column. The design punching shear stress is taken as $3.49\sqrt{F_c}$ in this specimen.

Specimen 3:

Three mechanisms: the bearing of the footing concrete, the steel hoops around the column, and the dowel action of studs welded on the column flanges, are combined to resist the bending moment and shear force. The design punching shear used for this specimen is $7.03\sqrt{F_c}$.

After this test, a feasible design of a column base-to-footing will be finalized for the full-scale test building.

RESEARCH PROGRAM ON THE FULL-SCALE SEISMIC TESTS OF A STEEL BUILDING

SUMMARY

A six-story steel framed office building has been recommended for purposes of comparing actual full-scale building behavior with model behavior and computer simulation and for assessing the damage

and safety levels of the buildings designed using current design practices. Figure 3.1 shows the floor plan of the test building and the elevation view of the braced frame. The exterior frames are unbraced moment-resisting frames, whereas, the interior frame is braced by K-braces. The floor system suggested for this building consists of metal decking and cast-in-place lightweight structural concrete. To develop composite action, it should be connected to the girders and floor beams by means of headed shear connectors. All structural members should be made of ASTM A36 steel. Two types of K-bracing systems, the concentric K and the eccentric K, should be used in different stages of testing. The test building should be essentially of welded construction which is the most common construction method for highrise buildings in both countries.

DESIGN OF FULL-SCALE SIX-STORY STEEL BUILDING

The prototype structure should be designed to satisfy the requirements of both the 1976 Uniform Building Code (USA) and the 1980 Japanese Aseismic Design Code. In some respects the design requirements in the two codes are significantly different. However, it is possible to achieve a compromise design which inherently incorporates the basic design philosophies in these codes. The primary difference is the magnitude of equivalent seismic forces used in the static design procedure. In order to arrive at a structural steel building that will satisfy the code requirements of each country, gravity loads should be considered in the basic design. Some of these loads may not be precisely the current practice in either country, but they are very similar to the values at the present time.

DESIGN CRITERIA AND DETAILS

1. The design base shear coefficient should be 0.197.
2. In calculating the design earthquake lateral forces, live load and exterior wall weight should not be included.
3. Columns and girders should be designed using wide flange shapes in inch size. Material with the characteristics of ASTM A36 steel is used.
4. Braces should be designed using structural tubing with square section. Material with the characteristics of ASTM A500 grade B steel is used.
5. Girders and floor beams should be designed to act compositely with the floor using headed shear connectors.
6. Braces are designed to resist both tension and compression. It is desirable to proportion the braces so that buckling would be confined to the plane of the frame.

7. Girders in braced frame are to be designed without considering the supporting effect provided by the braces.
8. Girder-to-column connections are designed to be moment connections in loading direction and shear connections in transverse direction.
9. Column bases should be designed to be fixed so that they would never be damaged before plastic hinges will be formed at the lower ends of the columns.

DESIGNED FULL-SCALE BUILDING

A designed six-story steel office building is shown in figure 3.1 and table 3.1, representing a real building and considering the capacity of the testing facilities available. This structure would represent a portion of an overall building.

TEST PROGRAM

The test should be conducted in several stages using a loading procedure simulating seismic conditions. The multi-degree pseudo-dynamic procedure should be considered for this application. At the final stage of testing, nonstructural elements such as curtain walls and partitions should be added to the structural system and the entire structure should be loaded to failure.

It is recommended that the test program for the full-scale steel building include free vibration tests and floor slab repairs as judged necessary and appropriate. Three levels of loading should be considered in the pseudo-dynamic testing: (a) working stress level, (b) post-buckling of braces level, and (c) post moment-frame yielding level. In order to maximize the amount of knowledge that may be gained from the program, the test sequence as shown in table 3.2 is proposed. Concentric K-braces should be used for the first phase full-scale test. The second phase test should be eccentric braces.

FUTURE SCHEDULE

Support test in Japan will start in April 1982. The final design of the full-scale test building will be revised, especially in connection details, by helpful results from the support tests. During this progress, the third JTCC meeting will be held in July of 1982 in Tsukuba, Japan. One of the purposes of this meeting is to finalize the design of the full-scale building structure and to discuss the test sequence including input earthquake motions and nonstructural members. For budgetary reasons, of the Japanese side, the full-scale test specimen must be completed by the end of February 1983 at the latest, and then tests should be started immediately.

Obviously, many troubles between both countries during planning and executing this project will occur. However, it is also one objective of this cooperative program to gain experience by overcoming such difficulties.

REFERENCES

[1] U.S.-Japan Planning Group, "Recommendations for a U.S.-Japan Cooperative Research Program Utilizing Large-Scale Testing Facilities," Report No. UCB/EERC-79/26, Earthquake Engineering Research Center, University of California, Berkeley, CA, September 1979.

[2] Kamimura, K., M. Watabe, O. Sakaguchi, M. Hirosawa et al., "Progress Report on U.S.-Japan Large-Scale Aseismic Experiments for Building Structures," 13th Joint Meeting, U.S.-Japan Panel on Wind and Seismic Effects, UJNR, Tsukuba, Japan, May 1981.

Table 1-1 The Schedule of Full-Scale Six-Story Steel Building Test

Contents \ Year and Month		1982												1983												1984			
		1	2	3	4	5	6	7	8	9	10	11	12	1	2	3	4	5	6	7	8	9	10	11	12	1	2	3	4
Support Test	Tests on Braced and Unbraced Three-Story Frames		Manufacturing			Tests on Braced and Unbraced Three-Story Frames																							
	Correlation Study between Pseudo-Dynamic Test and Shaking Table Test		Manufacturing			Pseudo-Dynamic Test and Shaking Table Test																							
	Tests on Continuous Composite Beam-to-Column Assemblages and Effect of Strain Rate		Manufacturing			Test								by the Building Contractors Society and the Kozai Club															
	Tests on Column-to-Footing Connections		Manufacturing				Test							by the Building Contractors Society and the Kozai Club															
	Supplement Test I																												
	Supplement Test II																												
• Full-Scale Six-Story Building Test		Design						Order						Preparation for Loading and Measurement												Tests on Fire Prevention			
			Preliminary Analysis							Manufacturing					Full-Scale Test-I						Full-Scale Test-II								
						Detail Design Measurement			Plan			Fabrication Construction						Repair, Braces		Replace and Nonstructural			Demolishment Elements						

Table 2.1 Characteristics of the Second Floor in Each Specimen

Static Test of Three-Story Steel Planar Frames

	Specimens No. 1 & 2	Specimen No. 3	Specimen No. 4	Specimen No. 5	Specimen No. 6
Slenderness Ratio of Bracings (K factor = 0.5)	51.7	-	51.7	77.5	51.7
Qu	61.7(t)	10.1(t)	55.6(t)	46.4(t)	56.7(t)
bQu/Qu	0.74		0.82	0.78	0.80

Qu : the ultimate lateral shear strength of the specimen.
bQu : the ultimate lateral shear strength of braces.

Table 3.1. Member Sizes

Size of Girders

Floor	G_1	G_2	G_3	G_4	G_5
R	16W31	16W31	16W31	18W35	21W50
6	16W31	16W31	16W31	18W35	21W50
5	16W31	18W35	18W35	18W35	21W50
4	18W35	18W35	18W35	18W35	21W50
3	18W35	18W40	18W40	18W35	21W50
2	18W40	18W40	18W40	18W35	21W50

Size of Columns

Story	C_1	C_2	C_3	C_4	C_5	C_6
6-5	10W49	10W33	10W33	10W33	12W40	10W33
4-3	12W65	12W53	10W39	10W60	12W72	10W60
2	12W79	12W65	12W50	12W79	12W106	12W79
1	12W87	12W87	12W65	12W106	12W136	12W106

Size of Braces

Story	BR_1	
6	Tube	4x4x1/5.56
5	Tube	5x5x1/5.56
4	Tube	5x5x1/4
3	Tube	6x6x1/4
2	Tube	6x6x1/4
1	Tube	6x6x1/2

Table 3-2 Proposed Loading Sequence

Exp. Step

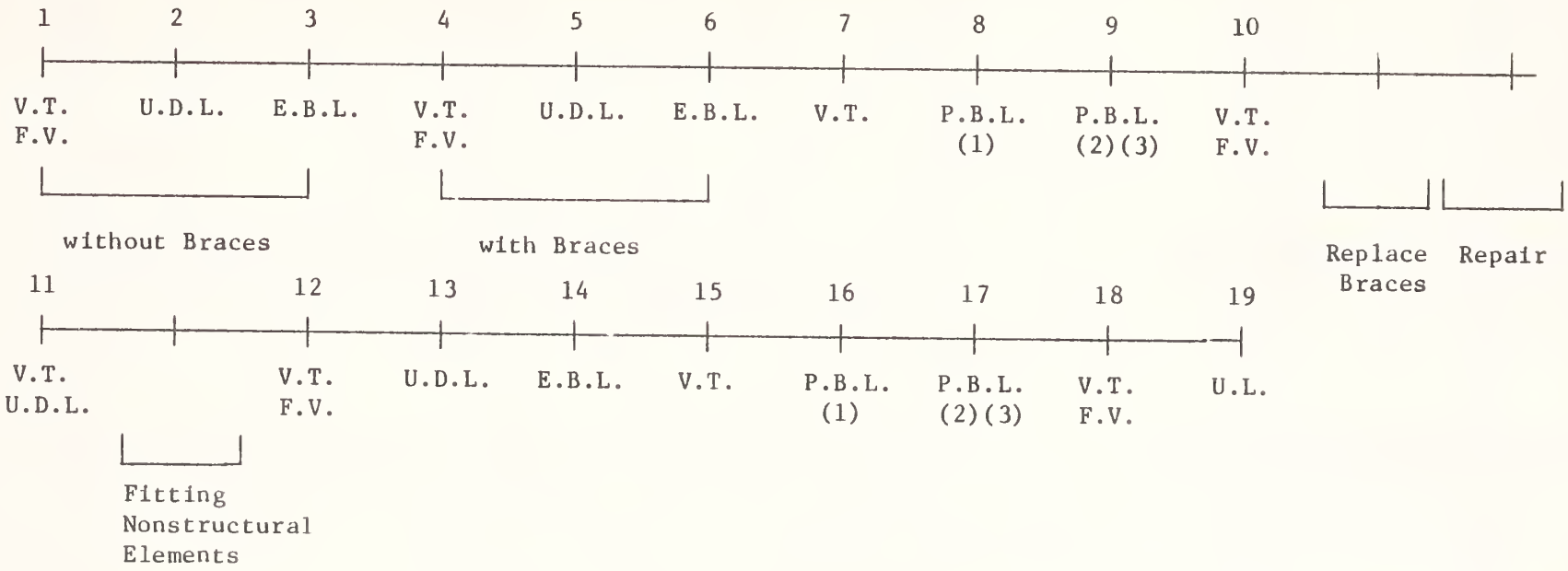

Notes: V.T. ; vibration test less than 2mm amplitude including microtremor measurement

F.V. ; free vibration test less than 2mm amplitude

U.D. ; unit deformation loading less than 1/1000 story deformation angle

E.B.L. ; elastic behavior loading (about 50 gal, within working stress level)

P.B.L. ; plastic behavior loading (about 300 gal, detailed discussion should be done in future)

U.L. ; ultimate loading (———— detailed discussion should be done in future)

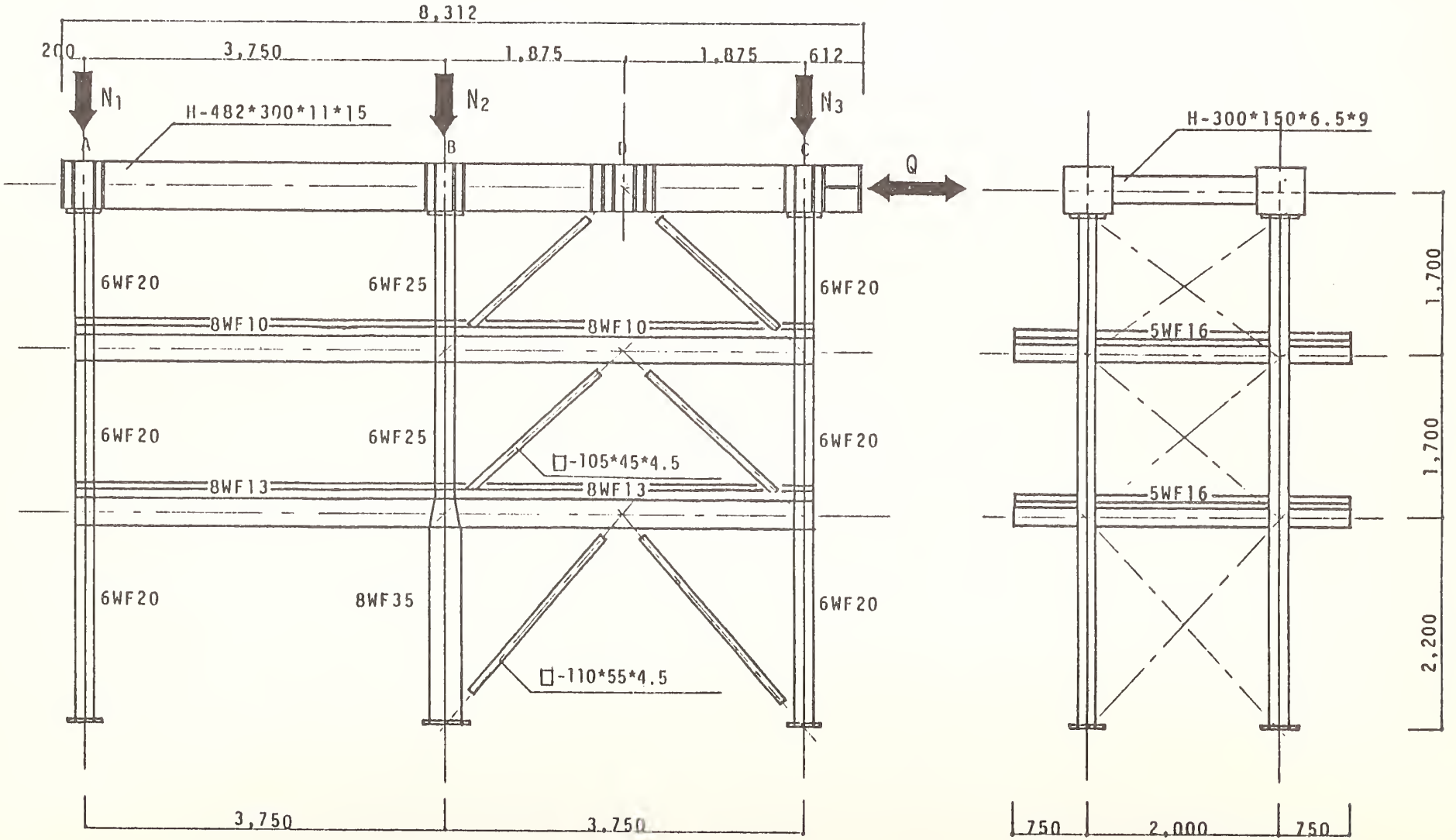

Fig.2-1 Test Specimen No.1 ,Static Test of Three Story Steel Planar Frames

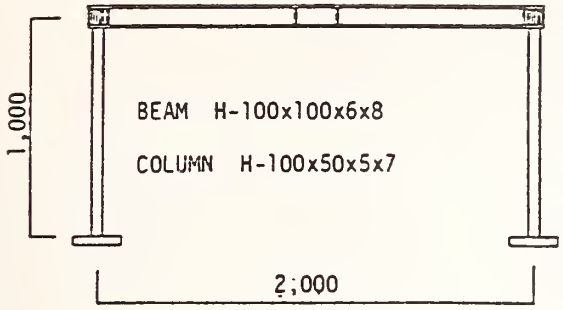

1 Story Unbraced Frame

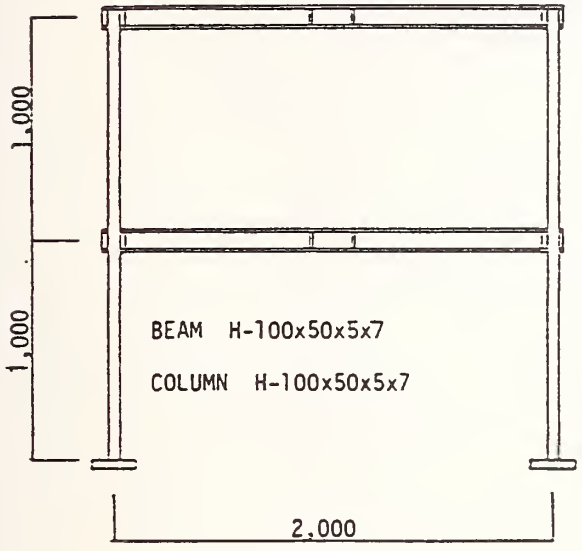

2 Story Unbraced Frame

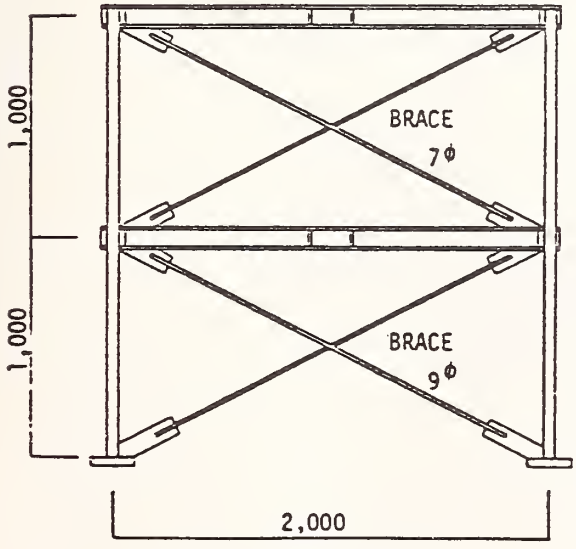

BEAM H-100x50x5x7

COLUMN H-100x50x5x7

2 Story Braced Frame

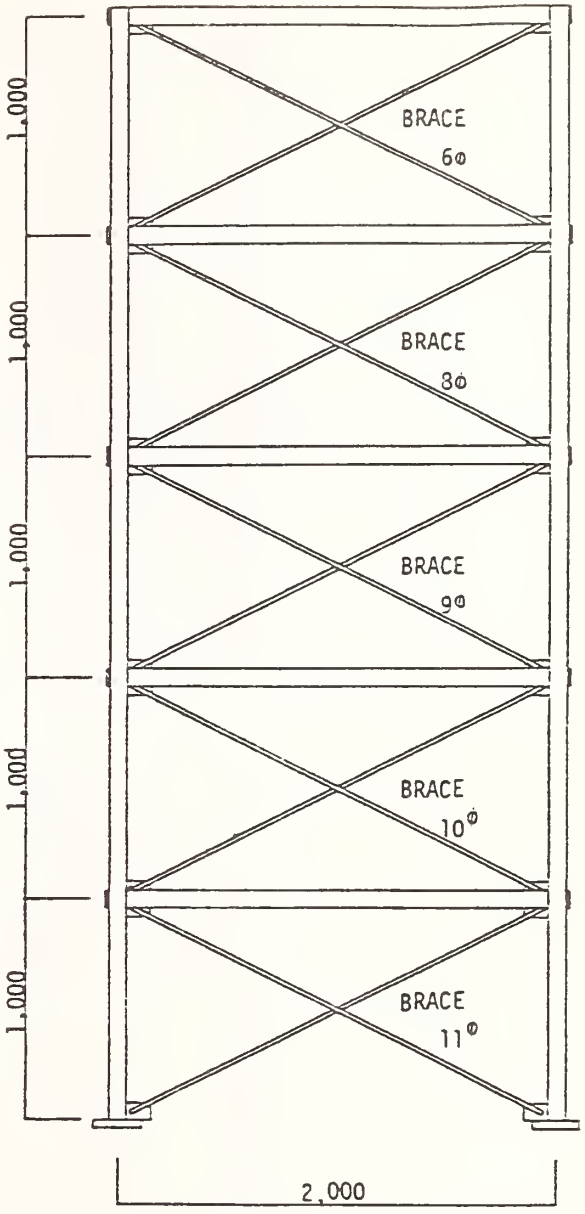

5 Story Braced Frame

BEAM H-150x75x5x7

COLUMN H-150x75x5x7

Fig.2-2 Test Specimens of Corelation Test

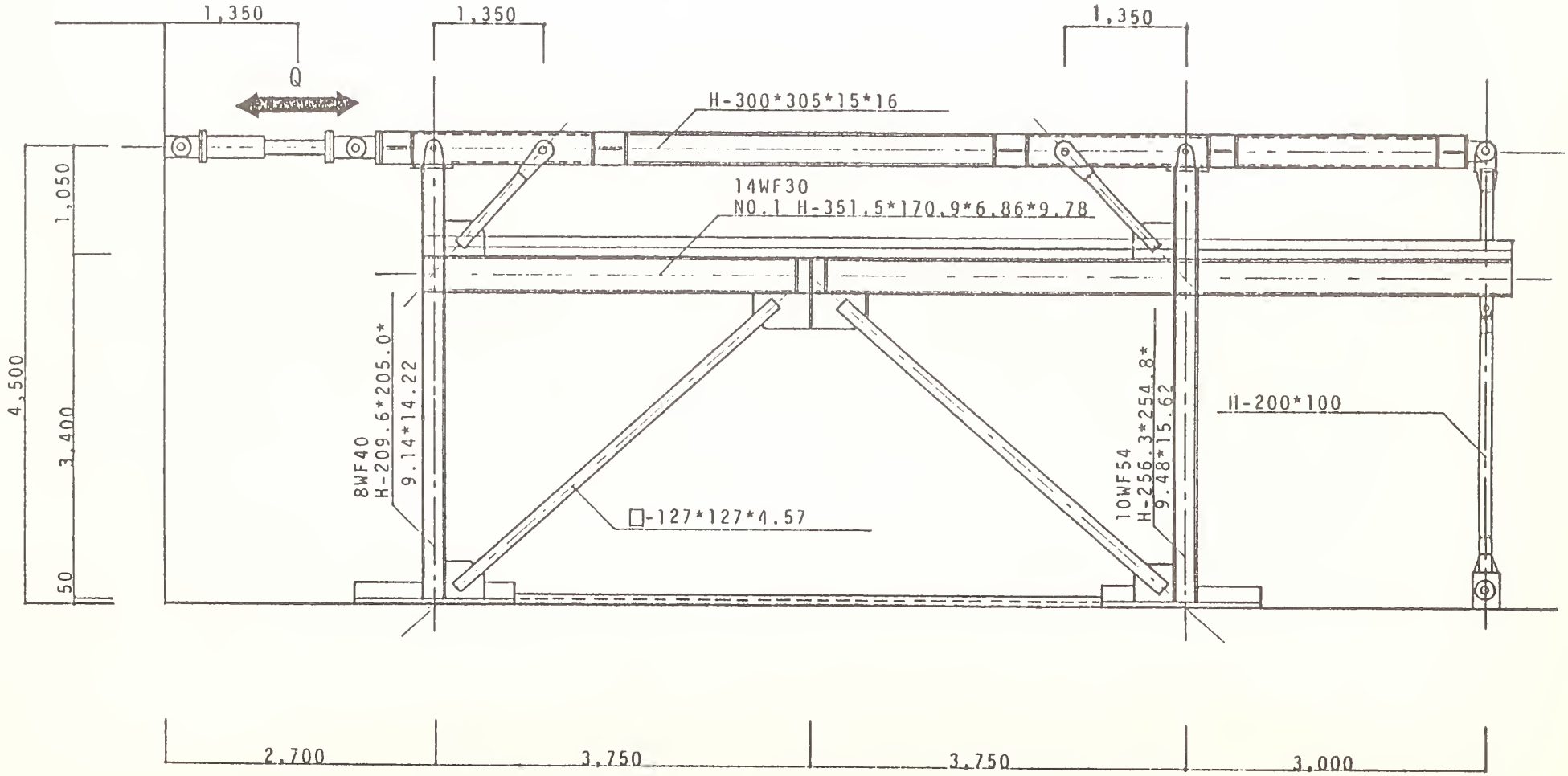

Fig.2-3 Test Specimen No.1 ,Static Test of Composite Beams

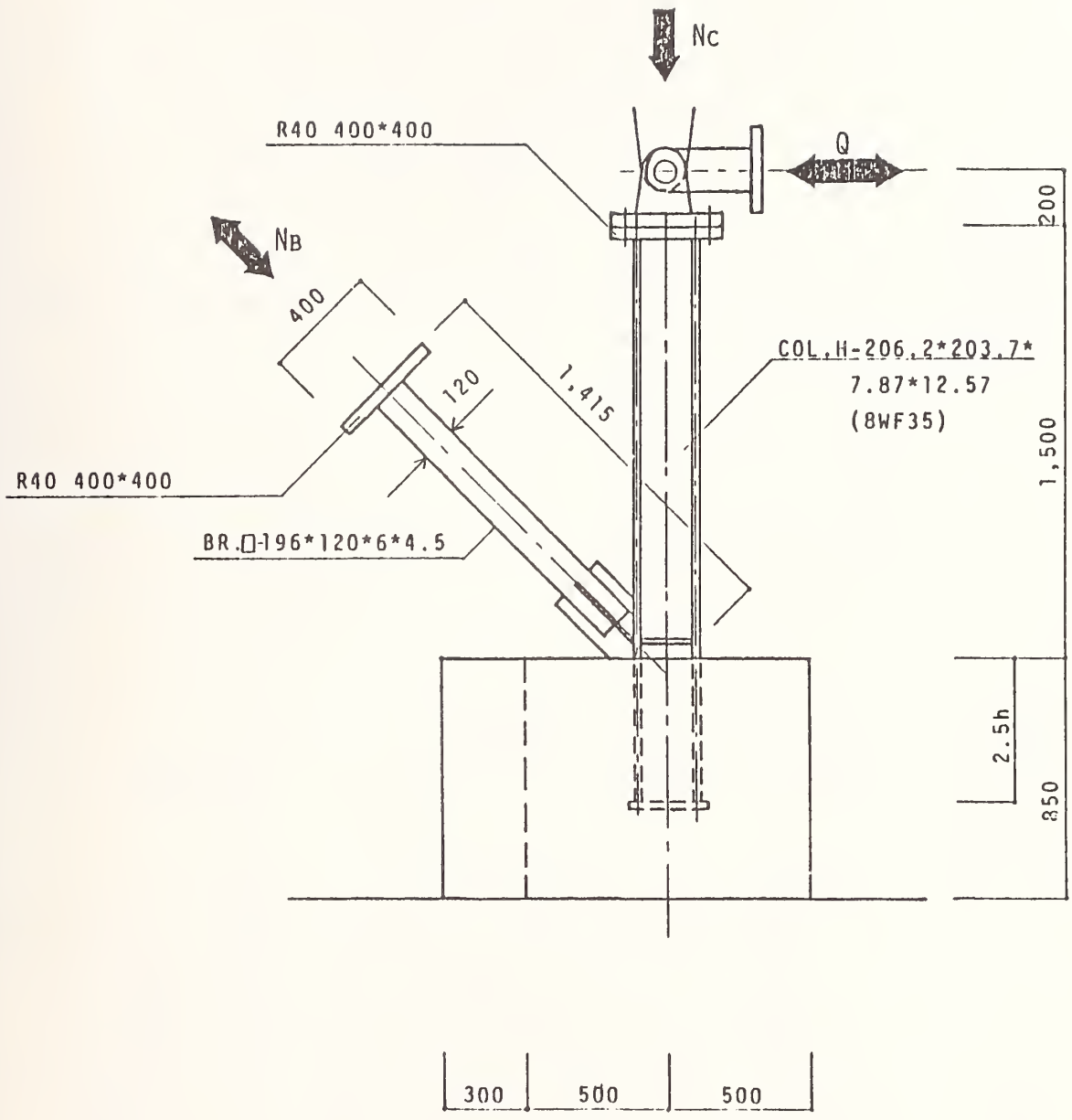

Fig.2-4 Test Specimen of Footings

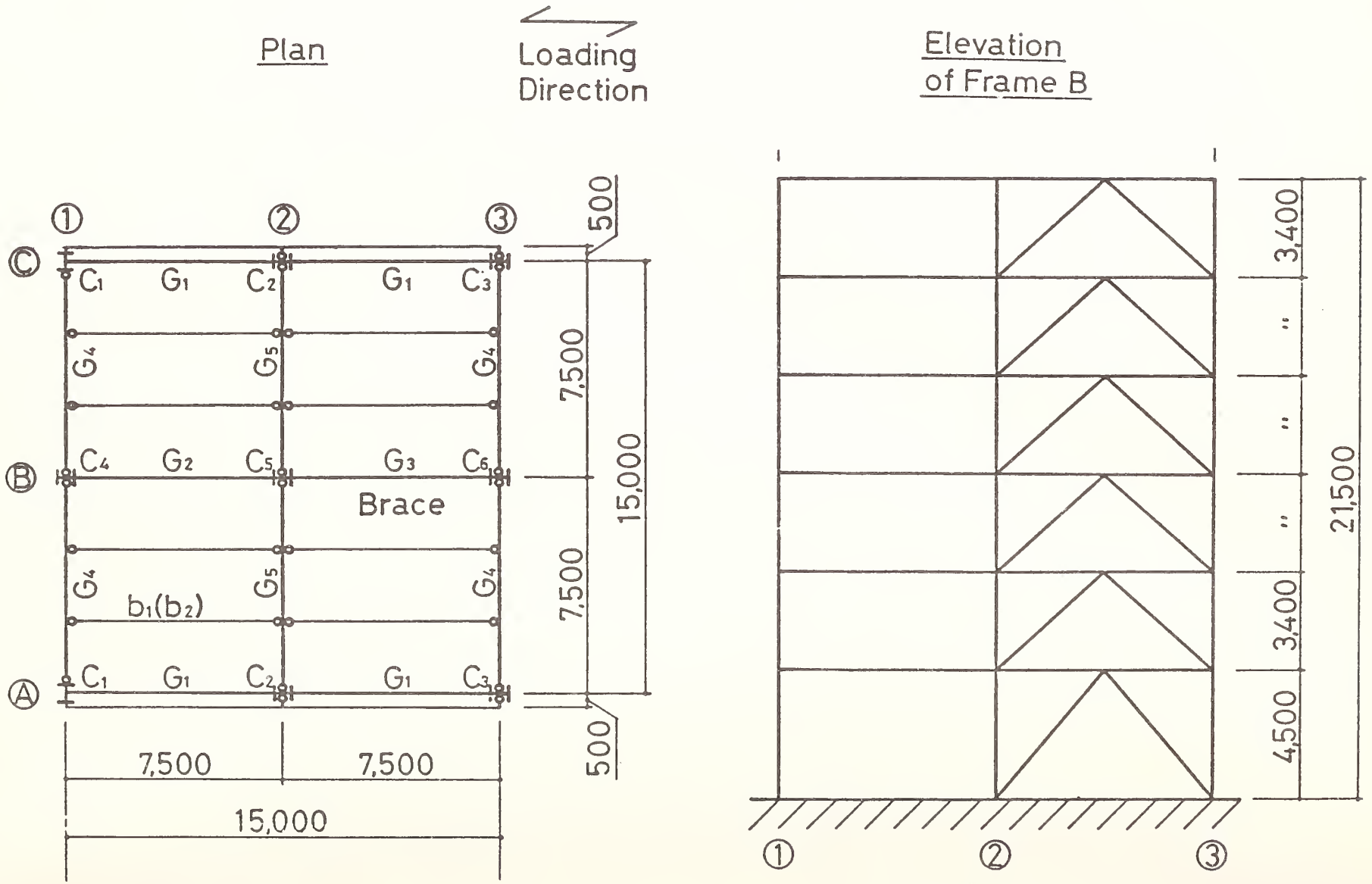

Fig. 3-1 Plan and Elevation of a
Full-Scale Six-Story Steel Building

UNITED STATES FOREIGN ASSISTANCE PROGRAM ON TSUNAMI HAZARD

Gerald T. Hebenstreit

Technology and Ocean Science Department
Science Applications, Inc.
McLean VA 22102

Paul F. Krumpe

Office of Foreign Disaster Assistance
U.S. Agency for International Development
Washington, DC 20523

ABSTRACT

The Office of Foreign Disaster Assistance, U.S. AID, and Science Applications, Inc., are developing a program to make the results of current tsunami research techniques available to disaster control officials in developing nations which are subject to potentially severe tsunami hazards. This program uses a combination of historical study of past tsunamis and computer modeling of possible future tsunamis to assess the threat to specific areas. The first applicaton of the program has been to the potential threat arising from tsunamis generated in the Peru-Chile Trench.

This paper outlines the techniques used in the computer modeling, the choice of specific earthquake sources, and the results of early studies. Research is currently underway to examine in more detail tsunami behavior in areas which appear strongly threatened. We discuss briefly our approach to this phase of the problem and our plans for transferring the results of the program to officials in developing nations.

INTRODUCTION

Tsunamis have historically been an infrequent but very real threat to the lives and property of people living along the shores of the Pacific Ocean. The threat is two-fold. The more heavily studied, at least in the United States, is the far-field threat, which arises when a major earthquake produces destructive ocean waves which strike coastlines thousands of kilometers from the epicenter. Tsunamis which cause such far-reaching effects are mercifully rare. For example, since 1946, only five tsunamis in the Pacific Ocean have been that destructive.

The second threat, which is somewhat more frequent, can be termed the near-source threat. The waves generated by a tsunamigenic earthquake in a shallow coastal area not only spread out into the open Pacific but also up and down the coast in the vicinity of the source. Tsunamis always produce a near-source threat, but not always a far-field threat. For example, Berninghausen (1962) lists 49 tsunamis which produced, at the very least, measurable waves on the coasts of South America between

1562 and 1960. All but four of these were generated inside South American coastal waters suggesting the importance of near-source threat.

Tsunamis, of course, threatens both the well-developed and the lesser-developed countries (LDC's) of the Pacific community. Several of the well-developed countries, notably Japan, Canada, and the United States, have applied their technical expertise to the scientific, technical, logistical, and social problems attendant on the tsunami threat. Many of the lesser developed countries do not have the means, either technical or economic, to undertake similar courses of study. The question then arises: can existing scientific techniques be brought to bear on tsunami-related problems specific to developing nations in an attempt to help these nations reduce their susceptibility to tsunami hazards?

In response to this question, disaster assistance personnel of the Office of Foreign Disaster Assistance, U.S. AID, have combined with scientists from Science Applications, Inc., to develop a tsunami hazard assistance program designed to make the results of current tsunami research available to disaster control officials of developing nations. The overall program has four specific goals:

- Research and Development

  Assemble and put into use a tool for the systematic study of the Pacific wide tsunami threat

- Education

  Use these results to sensitize inhabitants of threatened areas (in LDC's) and their leaders to the nature of their hazard.

- Planning

  Present these results in a fashion suitable for use by national officials in planning evacuation and disaster relief programs, coastal zoning requirements, facility location, and construction criteria, etc.

- Warning

  Provide additional background information to civil authorities faced with the need for making real-time hazard response decisions.

The ultimate goal of the program, of course, is to assist developing nations in the task of tsunami hazard reduction.

CURRENT STATUS OF THE PROGRAM

A pilot study of the research and development phase of the tsunami hazard assistance program began in October 1980. This phase requires the completion of six tasks listed in table 1. To date,

tasks 1 through 4 have been completed, for one source area, [Hebenstreit, 1981 and Hebenstreit and Whitaker, 1981] and tasks 5 and 6 are in process.

ORIENTATION OF THE STUDY

An examination of the distribution of tsunamigenic earthquake epicenters (figure 1) shows that tsunamis can originate in almost any portion of the Pacific margins (specifically along active plate boundaries). An examination of available tsunami listings [Berninghausen, 1962; Iiada et al., 1967, Pararas-Carayannis and Calebaugh, 1977] shows that the areas most likely to produce tsunamis which threaten the entire basin are, in not particular order, South America, Alaska-Aleutian Islands, and Kamchatka-Kurile Islands.

The number of source areas to be considered is large, as is the number of potential targets. In order to reduce the problem to a manageable size, we chose to examine one source region and the effect on the entire basin due to tsunamis originating in that region. This is in contrast to studies, such as that of Brandsma et al. (1979), which focused on the threat to one target region due to tsunamis arising from all possible sources. Either approach is equally valid; we feel that ours allows us to test the entire program, from R&D to warning phase, in the most efficient manner.

Because of the considerable interest generated in recent years by predictions of major earthquakes in the Peru-Chile Trench, we chose the South American coastline as our first tsunami source region for study.

MODELING APPROACH

A major obstacle to the analysis of tsunami hazard in specific areas is the scarcity of historical data. This is partly due to the infrequent occurrence of tsunamis; it is compounded by the difficulties of obtaining accurate wave height measurements, inundation levels, and damage reports, especially in LDC's. A study of tsunami threat cannot rest solely on the historical record, except in a few widely scattered locations. Thus, we chose to supplement the existing historical record with computer simulations of events that could possibly occur in the foreseeable future.

We must be careful at this point to establish the thrust of this study clearly. We do not intend to predict the future and tell local governments what <u>will</u> happen. Instead, we will present them with a summary of what <u>has</u> happened in the past in their regions and scientifically reasonable estimates of what <u>could</u> happen in the future if all of our assumptions are valid. The key concept to bear in mind is that we are not seeking absolute accuracy but a reasonable estimate of the potential threat.

A number of computer codes have been developed to simulate the generation and propagation of tsunamis in a variable-depth ocean (e.g., Brandsma et al., 1975 and Houston et al., 1975). Most of these models are based on some form of the classical linearized equations for long waves in a homogeneous, incompressible fluid:

$$\frac{\partial u}{\partial t} - fv + g\frac{\partial \eta}{\partial x} = 0 \tag{1}$$

$$\frac{\partial v}{\partial t} + fu + g\frac{\partial \eta}{\partial y} = 0 \tag{2}$$

$$\frac{\partial}{\partial t}(h+\eta) + (h+\eta)\left[\frac{\partial u}{\partial x} + \frac{\partial v}{\partial y}\right] = 0 \ , \tag{3}$$

where u,v are water velocity components in x,y directions, h is depth of the ocean floor below mean sea level, η is the free surface elevation relative to MSL, f is the coriolis parameter, and g is local gravitational acceleration. The various codes differ mainly in their algorithms for obtaining solutions to equations (1) through (3) and their choice of boundary conditions. Rather than develop our own code, we chose to use two existing ones: SEAWAVE, developed by Brandsma et al. (1975) for long distance propagation of tsunamis, and SSURGE, developed by R. O. Reid at Texas A&M University for propagation of long waves on the continental shelf.

The procedure used in the simulations is quite straightforward. Once a potential tsunami source is identified (see section on "Seismic Sources"), the expected sea floor displacement is imposed on the sea surface (under the assumption that all bottom motion is transmitted to the surface more or less instantaneously) and the waves allowed to radiate out of the source area. The simulation continues until the tsunami has entered the shallow waters near the shores of the Pacific basin. At points offshore of the various coasts, and in suitably deep water, wave heights are recorded. The trend of maximum calculated offshore wave heights along a coastal area is used as a measure of the threat to that area and serves to identify threatened areas requiring subsequent study.

SEAWAVE was used to simulate tsunami propagation to the far-field. It is a very efficient code suitable for such large-scale problems. On the other hand, SSURGE was used for near-source propagation. This model, originally developed to simulate storm surge propagation onto the continental shelf, is more complicated and expensive, but retains its accuracy and stability over long propagation distances in relatively shallow water.

SEISMIC SOURCES

In order to specify the sea surface displacement which forms the basis of the tsunami we must specify the location of the source and the parameters of the earthquake. We know several pieces of information which simplify the task of intelligently choosing potential source locations. We know that most tsunamigenic earthquakes are shallow focus events occurring along active tectonic plate

boundaries, especially in the vicinity of submarine trenches where an oceanic plate is being subducted under a continental plate. We know that tsunamigenic earthquakes tend to be large magnitude ($\geq$ 7.0 as a rule) thrust faults. We also know that within subduction zones with a history of large magnitude thrust faulting (and possibly of tsunami production) it may be possible to identify sections in which seismic stresses are building and in which stress relief will likely take the form of a major earthquake. Such sections are, of course, referred to as seismic gaps. By using the seismic gap investigations of Kelleher (1972) and McCann et al. (1978) we were able to identify four regions of the Peru-Chile Trench with high potential for major earthquakes in the future. These are indicated schematically in figure 2. The fifth zone (E in the figure) is the area predicted by Brian Brady (U.S. Bureau of Mines, Denver) to be the site of a major earthquake in 1981. In all of these locations we assumed that an earthquake would fill the gap.

Once the source areas were depicted we used examinations of the historical patterns of earthquakes in these regions (Stauder, 1973, 1975 and Kelleher et al., 1974) to establish reasonable parameters (fault length and width, focal depth, dip angle, slip displacement) for the types of earthquakes experienced in these areas. This information was then used to develop bottom displacement scenarios which could be used to drive the propagation model.

Two types of displacement patterns were used. One, a very simple "brute force" event, assumed uniform uplift of the fault block and resulted in uniform vertical displacement of the sea surface in the source area. This pattern pumps a good deal of potential energy into the water column in a broad range of wavelengths.

The second pattern, more seismically sophisticated, used the source dislocation model of Mansinha and Smylie (1971) to produce spatially varying patterns of uplift. This type of approach, which produces potential energy over a narrower wavelength range, was used with success by Aida (1978) to simulate tsunamis occurring near Japan.

SAMPLE RESULTS

The results from the near-field and far-field propagation studies are too extensive to present here. Two large reports (Hebenstreit, 1981 and Hebenstreit and Whitaker, 1981) provide all of the details. We will examine the results of one case in order to convey a sense of the modeling process.

Source zone A (see figure 2) is a large region (550 km long by 100 km wide) located northwest of Lima, Peru, oriented so that the fault axis parallels the trench. The hypothesized earthquake would have a magnitude of 8.7 on Kanamori's (1977) magnitude scale. The surface wave pattern resulting from the variable displacement pattern for this event is shown in figure 3. The highest portion of the leading wave is propagating toward the southwest, although wave energy spreads in all directions.

Figures 4a, 4b, and 4c show the coastlines of three specific geographical areas which the tsunami strikes. Areas of possible threat are indicated on each plot. The wave heights indicated are the maximum values calculated by the models at points offshore. Heights of 1.0 m (near-source) and 0.25 m (far-field) may or may not be threatening. But in each case they represent heights well above the average height calculated on each coast.

On the basis of our results, thus far, we have identified three geographical areas which we feel should be looked at more closely. These are the west coast of South America, especially around Lima and Arica, the eastern coasts of Luzon and Mindanao in the Philippines, and the northeastern coast of New Guinea. These areas seem to be subjected to focusing of high wave energy levels no matter where the source is located. The South American Coast, of course, is likely to be threatened by any large tsunami generated in the Peru-Chile Trench. The distant areas seem to be threatened because of refraction by Pacific topography and the directionality of wave fronts leaving the South American coast.

Not all of the postulated earthquakes produce tsunamis which appear capable of basin wide destruction. The case cited in this section, for example, may not constitute much of a far-field threat. The fact that energy seems to be consistently concentrated in certain locations, however, does seem to indicate that further study is needed. And, of course, every tsunami produces a potential near-field threat.

CURRENT RESEARCH

We are currently examining tsunami propagation onto the shore in the threatened areas. To do this, we have adapted another storm surge model, SURGE-II (Reid et al., 1977), which has the capability for modeling the propagation of long waves onto dry land and the resulting inundation. We plan to use this model to demonstrate both the capabilities of current technology and the potential tsunami hazard facing each location.

To our knowledge, this modeling technique, developed originally for storm surge problems, has never been applied to tsunamis. We are in the process of verifying its applicability by modeling the localized earthquake/tsunami which occurred along the coasts of Ecuador and Colombia in December 1979 (Herd et al., 1980).

FUTURE PLANS

The completion of the current research will mark the end of the R&D phase of the pilot study and the beginning of the process of technology transfer to LDC's. The first step will be the publication of two final project reports. The first will be the traditional technical report, which addresses in

detail the scientific issues faced in the course of the study. This will be suitable for publication in the scientific literature.

The second report will be of a less technical nature and will concentrate on the results of the study and the potential magnitude of the tsunami threat demonstrated. This report will be geared to the level of local, nontechnical, disaster control officials who are required to formulate plans for coping with the hazards faced by their populace. We feel strongly that this second type of report is equally as important as the technical documentation. The goals of this program were formulated with the idea of transferring tsunami technology to the level at which it must actually be used in order to reduce the hazard. The aim is to close the sometimes awesome gap between the scientist who carries out the study and the persons who must have the information for their decisionmaking process. We hope that these reports, if properly presented, will form the basis for the technology transfer which must occur if this study is to prove useful.

ACKNOWLEDGMENTS

Dr. Herbenstreit's participation in this study was made possible under research contracts AID/SOD/PDC-C-0404 and PDC-009-C-00-2041-00. We would like to acknowledge Dr. Martin Howell, Director, OFDA, U.S. AID, who has encouraged this study and made Mr. Krumpe's participation possible.

REFERENCES

[1] Aida, I., 1978, Reliability of a Tsunami Source Model Derived from Fault Parameters, J. Phys. Earth, 26, pp. 57-73.

[2] Berninghausen, W. H., 1962, Tsunamis Reported from the West Coast of South America, Bull. Seismological Society of America, 52, pp. 915-921.

[3] Brandsma, M., D. Divoky, and L. -S. Hwang, 1975, "SEAWAVE - A Revised Model for Tsunami Applications," Tetra Tech., Inc., Pasadena, CA, NTIS Number: PB-252-705.

[4] Brandsma, M., D. Divoky, and L. -S. Hwang, 1979, "Tsunami Atlas for the Coasts of the United States," Tetra Tech., Inc., Pasadena, CA, Report NUREG/CR-1106/TC-486, NTIS Number: NUREG/CR-1106.

[5] Herbenstreit, G. T., 1981, "Assessment of Tsunami Hazard Presented by Possible Seismic Events: Far-field Effects," Science Applications, Inc., McLean, VA, Tech. Report SAI-82-599-WA.

[6] Herbenstreit, G. T. and R. E. Whitaker, 1981, "Assessment of Tsunami Hazard Presented by Possible Seismic Events: Near-source Effects," Science Applications, Inc., McLean, VA, Tech. Report SAI-82-651-WA.

[7] Herd, D. G., T. L. Youd, H. Meyer, J. L. Arango, W. J. Person, and C. Mendoza, 1980, The Great Tumaco, Colombia Earthquake of 12 December 1979, Science, 211, pp. 441-445.

[8] Houston, J. R., R. W. Whalin, A. W. Garcia, and H. L. Butler, 1975, "Effect of Source Orientation and Location in the Aleutian Trench on Tsunami Amplitude Along the Pacific Coast of the Continental United States," U.S. Army Engineer Waterways Experiment Station, Report H-75-4, NTIS Number: AD-A014145.

[9] Iiada, K., D. C. Cox, and G. Pararas-Carayannis, 1967, "Preliminary Catalog of Tsunamis Occurring in the Pacific Ocean," Hawaii Institute of Geophysics, University of Hawaii, Honolulu, Repot HIG-67-10.

[10] Kanamori, H. 1977, The Energy Release in Great Earthquakes, J. Geophys. Res., 82, pp. 2981-2987.

[11] Kelleher, J. A., 1972, Rupture Zones of Large South American Earthquakes and Some Predictions, J. Geophys. Res., 77, pp. 2087-2103.

[12] Kelleher, J. A., J. Savino, H. Rowlett, and W. McCann, 1979, What and Where Great Thrust Earthquakes Occur Along Island Arcs, J. Geophys. Res., 79, pp. 4889-4899.

[13] Mansinha, L. and D. E. Smylie, 1971, The Displacement Fields of Inclined Faults, Bull. Seismological Society of America, 61, pp. 1433-1440.

[14] McCann, W. R., S. P. Nischenko, L. R. Sykes, and J. Krause, 1978, Seismic Gaps and Plate Tectonics: Seismic Potential for Major Plate Boundaries, Proceedings of Conference VI: Methodology for Identifying Seismic Gaps and Soon-to-Break Gaps, U.S. Geological Survey Open-File Report 78-949, pp. 441-584.

[15] Pararas-Carayannis, G. and J. Calebaugh, 1977, "Catalog of Tsunamis in Hawaii," World Data Center A for Solid Earth Geophysics, NOAA/EDIS, Boulder, CO, Report SE-4.

[16] Reid, R. O., A. C. Vastano, and T. J. Reid, 1977, "Development of SURGE II Program with Application to the Sabine-Calcasieu Area for Hurricane Carla and Design Hurricanes," Coastal Studies, Inc., College Station, TX, Report TP-77-13.

[17] Stauder, W., 1973, Mechanism and Spatial Distribution of Chilean Earthquakes with Relation to the Subduction of the Oceanic Plate, J. Geophys. Res., 78, pp. 5033-5061.

[18] Stauder, W., 1975, Subduction of the Nazca Plate Under Peru as Evidenced by Focal Mechanisms and by Seismicity, J. Geophys. Res., 80, pp. 1053-1064.

Table 1. Research and Development Tasks

1. Identify Tsunamigenic Earthquake Zone
   - o Seismic Gap Theory
   - o Historical Seismicity Patterns
2. Simulate Tsunami Generation
   - o Near-source Propagation
   - o Far-field Propagation
3. Identify Threatened Coastal Areas
4. Prioritize Threatened Areas
   - o High Waves
   - o Population Density
   - o Economic Factors
5. Simulate Tsunami Assault on Most Potentially Threatened Areas
6. Detailed Hazard Assessment
   - o Flooding Zones
   - o Maximum Wave Heights
   - o Runup

Figure 1. Epicenters of tsunamicgenic earthquakes in the Pacific Ocean during the period 1900-1969. (courtesy EDIS/NGSDC/NOAA, Boulder, CO)

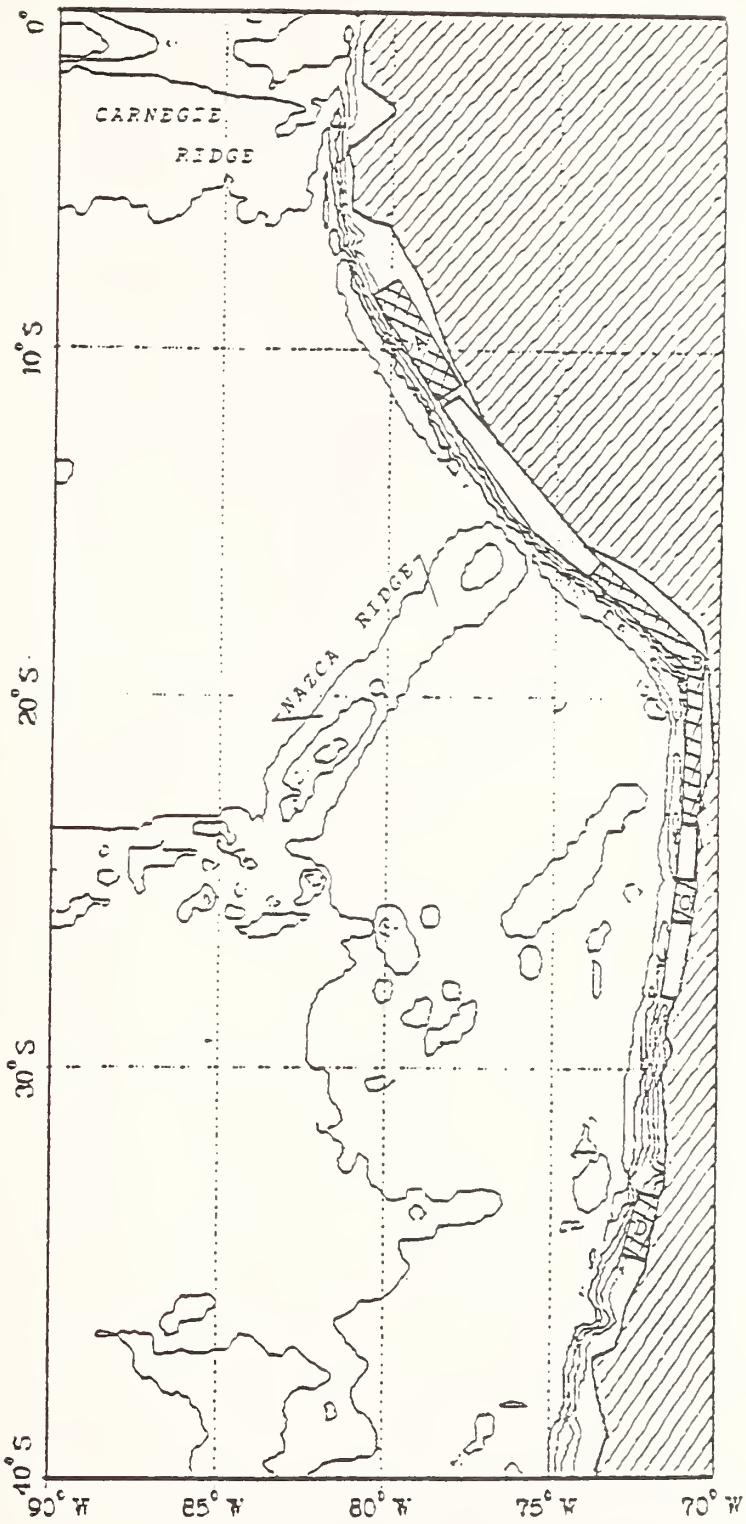

Figure 2. Approximate zones of possible major earthquakes used as tsunami sources. Zones A, B, C, and D are represented by cross-hatched areas. The open area beginning 12°S and continuing through zones B and C to end at 28°S is zone E.

Figure 3. Surface elevation (positive only) one hour after a uniform uplift in source zone A. Contours correspond to 0.1, 0.2, 0.5, 1.0, and 2.0 m.

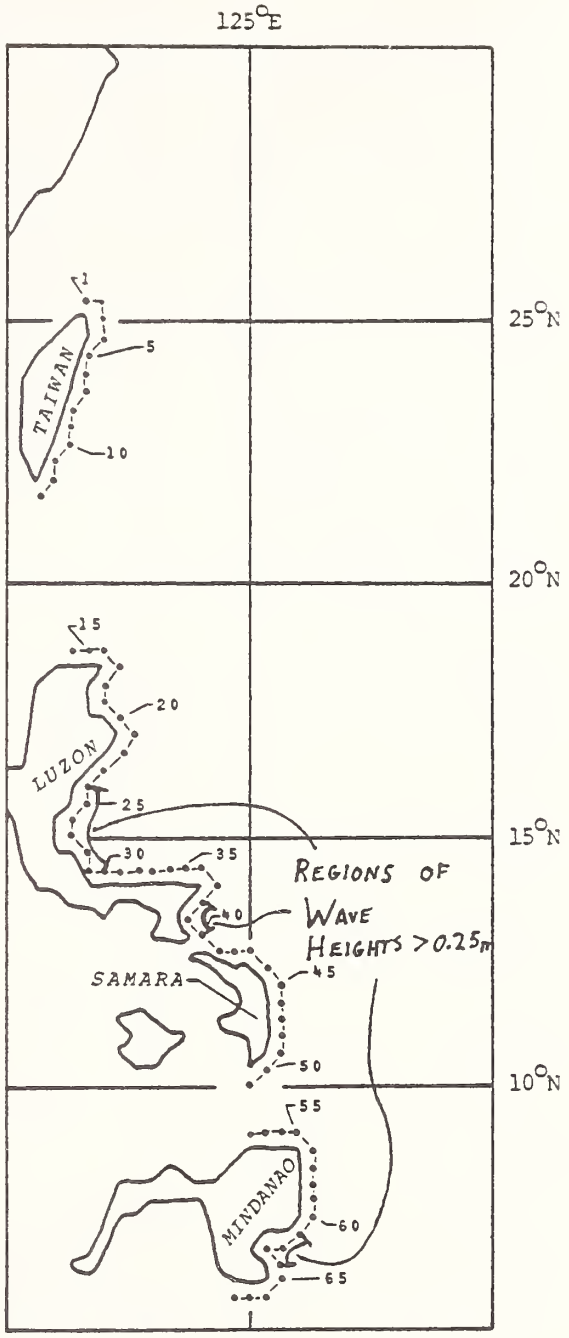

(a)

Figure 4a. Schematic representation of Taiwan and Philippine coastlines. Numbers refer to indexing scheme used in the computations. Sections of coast threatened by above average waves are noted.

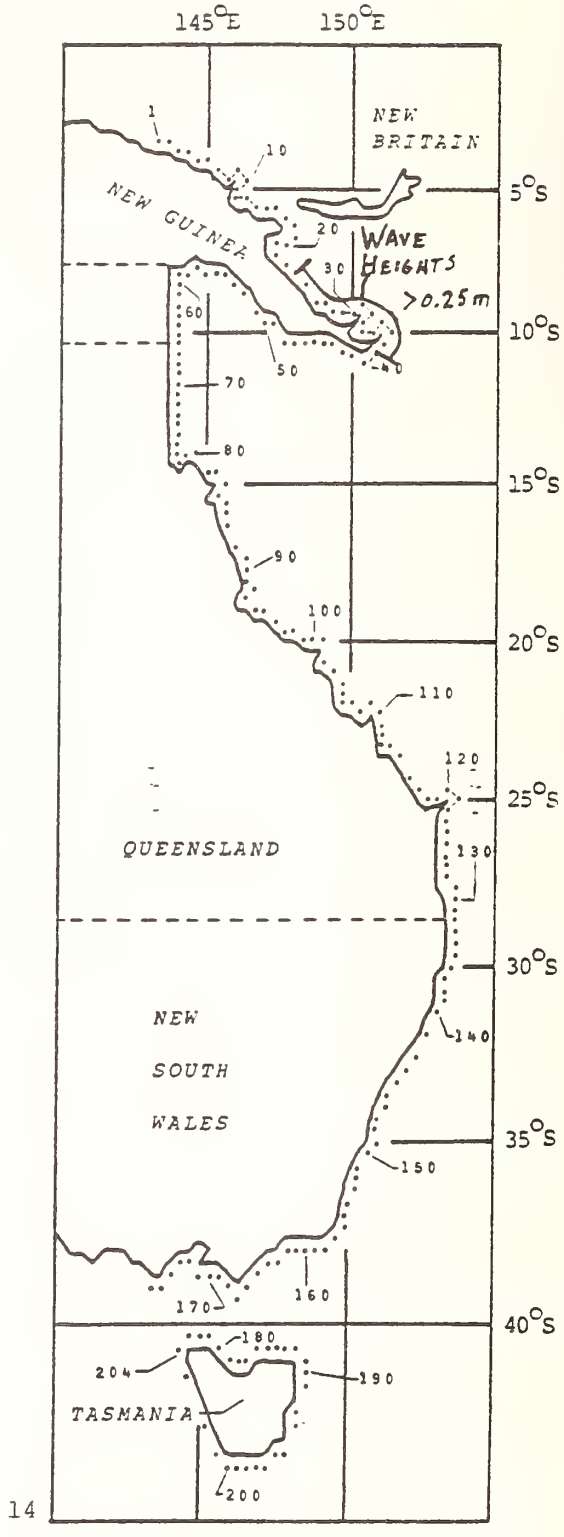

(a)

Figure 4b. Same as 4a, except for New Guinea and Australia. Only threatened points on New Guinea are noted.

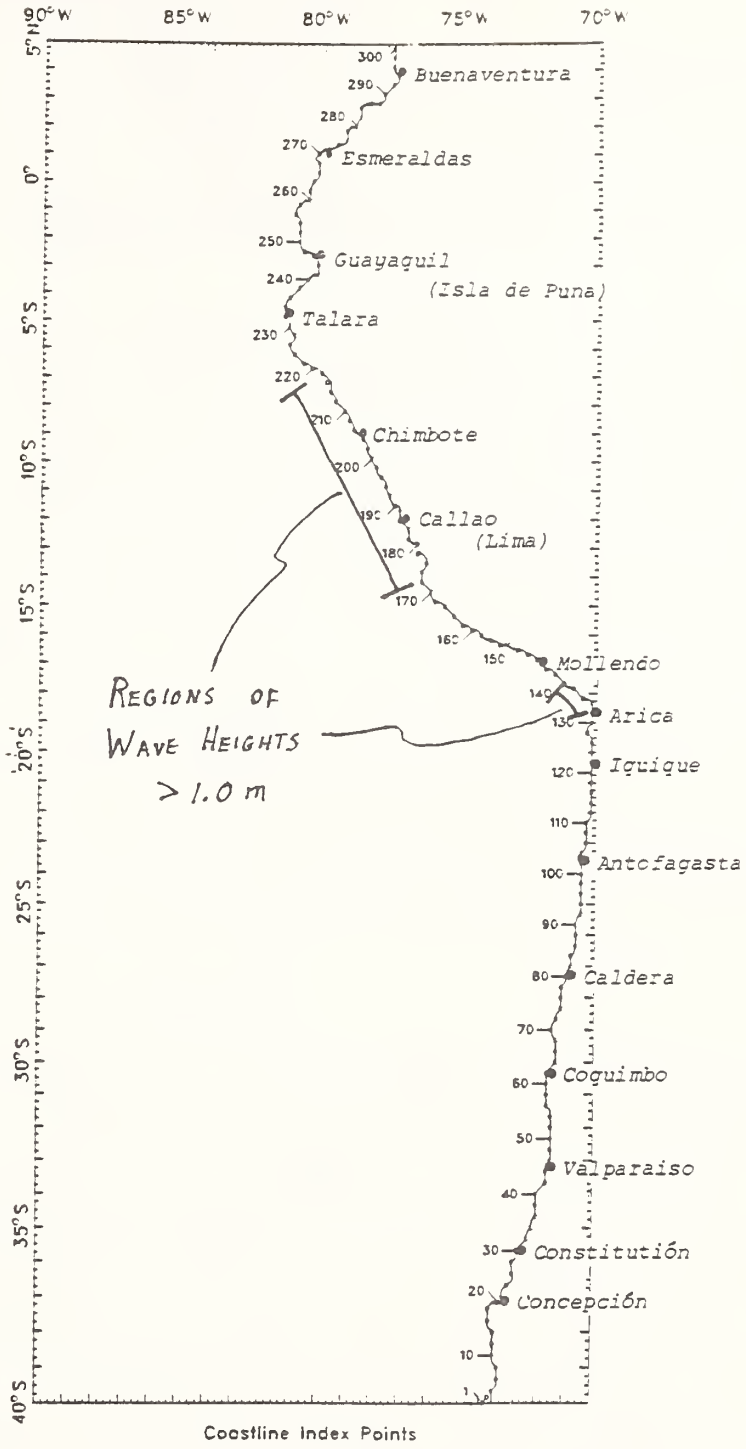

Figure 4c. Same as 4a, except for South America.

TECHNICAL COOPERATION IN DEVELOPING COUNTRIES ON EARTHQUAKE ENGINEERING

Katsuro Kamimura
Makoto Watabe
Yuji Ishiyama
and
Yutaka Yamazaki

Building Research Institute
Ministry of Construction

ABSTRACT

In order to improve earthquake engineering techniques in developing countries, it is necessary, apart from direct technical cooperation, to raise the standards of research and techniques in the country concerned from a long-term point of view. The International Institute of Seismology and Earthquake Engineering, the Building Research Institute, has been conducting training programs in seismology and earthquake engineering since 1962 for the purpose of training researchers and engineers from developing countries. These training programs have played an immeasurable role in raising the standards of research and techniques in developing countries.

This report is intended to outline the surveys on earthquake disasters conducted overseas in connection with the Institute and to introduce the training programs. In addition, the report will also briefly touch upon the cooperation programs for Indonesia and Peru under the Bilateral Earthquake Engineering Cooperation Program with which the Institute is closely associated.

INTRODUCTION

With advanced aseismatic building techniques in Japan, the ratio of damage by earthquake has shown a significant decline in recent years in spite of the fact that the country is one of the major earthquake countries in the world. In comparison, in the countries of the Middle and Near East and of Central and South Americas, earthquakes continue to leave many victims, sometimes in tens of thousands by one earthquake. These countries continue to suffer heavy damage to life because insufficient consideration has been given to not only private houses but also to commerical buildings.

Houses are made of domestic materials available in abundance and at low prices. In the case of Japan, it means wooden structures. However, in the countries of the Middle and Near East and of Central and South Americas, the most common form of structure is made of mud bricks dried in the sun called "adobe." The adobe structure is most effective in blocking the strong sunlight; but its resistance to earthquakes is practically nil. However, even this defect can be overcome with the latest earthquake engineering techniques. These countries are placing great expectations on technical cooperation provided by advanced countries for research on aseismatic building techniques.

To make adobe structures earthquake proof is a major problem and there are many other problems to be solved concerning the prevention of disasters due to earthquakes.

Even in the case of Japan, it is a generalization to say that aseismatic structures have made advances. There are many buildings to which no aseismatic consideration has been given and such buildings continue to be constructed. Since these buildings have not, fortunately, encountered a major earthquake, the danger has not been properly recognized by the architects themselves, not to speak of the general public.

The damage which may be inflicted upon these buildings, which has low resistance to earthquakes, may be ascertained through the study of surveys conducted on earthquake disasters in various countries. It is useful not only for the country stricken by an earthquake but also for Japan to survey and analyze earthquake disasters in various countries in order to prevent similar disasters in the future. These surveys will provide valuable data not only for devising aseismatic structures but for formulating wide-ranging earthquake countermeasures, e.g., evacuation measures and first-aid activity, in all earthquake countries.

In order to improve earthquake engineering techniques in developing countries, it is necessary, apart from direct technical cooperation, to raise the standards of research and techniques in these countries from a long-term point of view. Since 1962 the International Institute of Seismology and Earthquake Engineering, the Building Research Institute, has been conducting training programs in seismology and earthquake engineering for the purpose of training researchers and engineers from developing countries, totalling 500 persons from 50 countries.

These programs are playing an immeasurable role in raising the standards of research and techniques in developing countries. This report is intended to outline the surveys on earthquake disasters conducted overseas in connections with the Institute and to introduce the training programs. In addition, the report will also briefly touch upon the cooperation programs for Indonesia and Peru under the Bilateral Earthquake Engineering Cooperation Program.

OUTLINE OF OVERSEAS SURVEYS ON EARTHQUAKE DISASTERS

Surveys of earthquake disasters overseas which the Building Research Institute was involved in during the past ten years or so include: December 23, 1972, "The Managua Earthquake", which occurred directly under Managua, the capital city of the Central American country of Nicaragua (Ms=6.2, depth of hypocenter 5 km, about 10,000 persons died); March 4, 1977, "The Romania Earthquake," which occurred in the Socialist Republic of Romania, about 160 km north-northeast of the capital city of Bucharest (M=7.2, depth of hypocenter about 110 km, about 1,500 persons died); October 10, 1980, "The Algeria Earthquake," which struck El Asnam in northwestern Algeria (Ms=7.3, depth of hypocenter 10

km, about 3,000 persons died); and, right after that, on Nov. 23, "The Southern Italy Earthquake," which occurred in the south of Italy (M=6.8, depth of hypocenter 40 km, more than 3,000 persons died). In this report is an outline of the field surveys and technological cooperation involved in the two earthquakes which occurred at around the end of 1980, "The Algeria Earthquake" and "The Southern Italy Earthquake."

THE SURVEY IN ALGERIA

The shallow earthquake in the inland area of northern Algeria caused much damage to the region, mostly in the city of El Asnam (Pop. 125,000). Out of all the structures in the city (about 10,000), 20% could be used, 40% couldn't be used and 40% needed to be examined in detail in the future. No major damage was seen in rivers, dams, floodgates, or roads, but the lifeline facilities such as sewers, telephones, and city gas received so much damage that they had to be abandoned. The causes of this extensive damage were:

- Since it was supposedly a shallow earthquake hitting right under the city, the earthquake ground motion locally was large.
- Many old low-rise houses were made of brick or stone and had insufficient structural ductility.
- In the case of reinforced concrete structures, it was generally the case they were soft-first-story structures with slender columns or structures with short columns, or one with few walls, or structures in which walls were irregularly distributed, resulting in heavy damage. In addition, there were many cases of inadequate arrangement of reinforcing bars at column-beam joints.

THE SURVEY IN ITALY

This too was an earthquake occurring inland, but the damage from it extended across a wide area, about 160 km from east to west and 70 km north to south. In the small cities in the mountains, buildings were made in the traditional construction method using stones, without earthquake-proofing, and hence many collapsed. Also, in the city of Avellino (Pop. about 80,000), located about 230 km southwest of Rome, there are two clearly defined sections, the old and the new. The old section is comprised of stone buildings built in this same traditional way, while the new section is made of of 5-7 story reinforced concrete structures. The damage in the old section was remarkable, and there were deaths and injuries only in the old section.

LESSONS FOR COUNTERMEASURES AGAINST EARTHQUAKES IN JAPAN

Both of these earthquakes occurred directly below the cities, but there was no evidence of the phenomenon of severe damage resulting from vertical ground motions. And it seems that almost all of the buildings damaged were damaged because they had poor earthquake resistance. Examples of necessary relief activities during and after the Algeria and Italy earthquakes suggest the importance of the following countermeasures, which are needed even in Japan.

(1) Investigations of earthquake resistance and promotion of strengthening of existing buildings

Since there are existing buildings which are not sufficiently earthquake-proof, it is necessary to promote extensive investigations of earthquake resistance and strengthening of buildings used by an unspecified large number of people.

Furthermore, it is necessary to further promote the earthquake-proofing of roads, government facilities and public utilities, so that they will be sufficiently aseismatic to provide relief and recovery services after the quake.

(2) Expansion of measures for relief, recovery and reconstruction

It is necessary, for quick and effective relief, recovery and reconstruction, to further develop the reconstruction skills of cities and strengthen the post-quake organization, by first securing relief bases and emergency transport routes and construction of temporary emergency shelters.

In particular, since heavy equipment is needed for securing thoroughfare of the main roads required in relief activities, as well as for securing transport routes, it is necessary to plan each policy with the cooperation of businesses owning cranes, tractors, and mechanical shovels.

(3) Judging the extent of earthquake damage of buildings and repairs

If buildings which have become less resistant to earthquakes after being damaged are mistakenly used, they will be damaged greatly in an aftershock or in the next medium-sized earthquake. Therefore, it is necessary to develop technical skills for retaining the remaining resistance of buildings hit by an earthquake, for appropriately judging whether they can still be used, and for promoting repairs.

(4) Strengthening measures against fires in crowded urban areas

In Algeria and Italy, small fires broke out here and there after the earthquakes, but because the buildings are made of brick and stone, the fires were not able to spread. In the case of Japan which has wooden structures, there is the danger, in dense urban areas, of fires spreading extensively and turning into a big city fire.

For this reason, it is necessary to further provide safety areas and evacuation routes, as well as to make safety zones with road and aseismatic structures to prevent large fires.

(5) Development of technology for prevention of earthquake damage

In order to strengthen and expand the countermeasures for prevention of earthquake damage listed in (1)-(4) above, the following technology, which is the basis of these countermeasures, must be further developed.

a. Methods of predicting earthquakes striking directly under a city, though it's not easy to pick up signs from the earthquakes.

b. Techniques of microzoning of ground that is closely related to earthquake damage.

c. Techniques for estimating remaining earthquake resistance in damaged buildings and judging possibilities whether they can still be used, and techniques for rebuilding and repair of damaged buildings. Also, construction technology corresponding to the extent of damages of the buildings.

d. Research through joint U.S.-Japan large-scale experiments on improving construction technology and aseismatic design, including effective repairs and reinforcement.

e. Urban fire prevention technology, such as techniques to prevent large fires in cities, and countermeasures for lifeline systems in cities (transportation, communication and supply lines).

RESEARCH AND TRAINING IN SEISMOLOGY AND EARTHQUAKE ENGINEERING AT THE BUILDING RESEARCH INSTITUTE

With the Building Research Institute, there is the International Institute of Seismology and Earthquake Engineering (IISEE). This research and training institute was inaugurated on January 1, 1962. This year is exactly its 20th year. As was mentioned earlier, this institute was founded with the purpose of training researchers and technicians from developing countries in seismology and earthquake engineering. Its graduates come from about 50 countries and number as many as 500. Figure 1 shows the distribution of institute graduates over a map of the distribution of earthquakes in the world. It can be seen that institute trainees have come from nearly all of the countries in the intense seismic zones of Eastern Europe, the Middle and Near East, India, Southeast Asia, and Central and South America. Figure 2 shows how many lives were lost in past earthquakes for these zones (compiled from data from the Seismological Division of the Meteorological Agency). Figure 2 groups the world's major earthquake zones into four regions: a) the Middle and Near East, and the Mediterranean coast, b) Central and South America (including Mexico), c) China, India and Southeast Asia, and d) Japan.

This grouping was not decided from a seismological point of view. Nor is there any reason to view them too carefully in terms of numbers of deaths, in view of the fact, though figures are

relatively accurate for deaths below 1,000, there are many cases where the data on deaths over 1,000 are estimates. Figure 2 simply shows that since the Fukui Earthquake in 1946, so far Japan has not experienced any earthquake killing more than 1,000 people, though there have of course, been many earthquakes since then. These earthquakes include the Niigata Earthquake, the Tokachi-Oki Earthquake and the Miyagi-ken-Oki Earthquake. It should not be assumed that since there are no earthquakes there is no damage. In contrast to Japan, it is clear from the figure that even recently other areas have lost from thousands to tens of thousands of lives in one earthquake.

The countries in these regions won't be able to eradicate earthquake disasters with just this institute's training. But, when each country takes positive steps against earthquake disasters, talented people who are knowledgeable in seismology and earthquake engineering will be needed. It is obvious that even if there is direct technical cooperation such as that mentioned below, unless these countries have the potential for responding direct technical aid, prevention of earthquake disasters will not become a reality. During the course of technical cooperation, these countries must make that technology their own, otherwise, at the end of the technical cooperation program the countries will be right back where they started from. The importance of this training in IISEE should be recognized in this sense too.

Since fiscal year 1979, the Institute has, as a rule, held a refresher seminar on earthquake engineering for its exparticipants every other year. Through this, exparticipants acquire the most up-to-date knowledge on earthquake engineering, and it is expected that they will be further enthused about the subject. In addition, a separate seminar was held in March of this year in Indonesia for Indonesia and neighboring countries called the "Third Countries' Training."

The above-mentioned training has been undertaken at the International Institute of Seismology and Earthquake Engineering, the Building Research Institute. In order to give satisfactory lectures, various university professors and businessmen have enthusiastically given their assistance. Furthermore, the trainees' lodging expenses and everything involved in entering the program have been paid for by the Japan International Cooperation Agency (JICA).

EARTHQUAKE DISASTER PREVENTION TECHNICAL COOPERATION PROGRAMS FOR INDONESIA AND PERU

In 1972 the Government of Indonesia requested technical assistance related to housing policies and development of construction technology. Since then, a survey group was sent to investigate the course of technical cooperation, and teams of experts based on the survey group's recommendations were then sent to Indonesia.

Three teams of experts have been sent so far in connection with residences, the first from 1974 to 1977, the second from 1977 to 1979, and the third from 1979 to the present. When the first and

second teams were sent, there were areas in which a consensus was not always reached, concerning preparations to the technical cooperation program, ranking of the experts, and how to move forward with the actual work. As a result, the teams had to face numerous difficulties.

In sending the third team, with the accumulation of personal exchanges from the first and second teams and the sincerity of the Japanese technical cooperation, effective cooperation could take place. During the third team's stay, concrete projects were put into action (the KTA-20 project, etc.) and through action related to these projects, effective technical cooperation has developed.

Besides the above technical cooperation on residences, Indonesia has requested technical cooperation for an aseismatic experimental research program (Project KTA-38), and at present experts are being sent from the Building Research Institute for long-term work.

In other quarters, a request came from the Government of Peru for Japanese technical cooperation on plans for earthquake disaster prevention in the capital city of Lima. The survey group dispatched proposed that technical cooperation include sending teams of experts to Peru for 3 month periods each year for 3 years and providing the equipment necessary for the program, as well as training counterparts from Peru in Japan.

Based on this course of action, from fiscal 1979, the first year, the first and second teams of experts were sent (their work was reported on at the 12th and 13th Joint Meetings), and this year, the last of the program, the third team was also sent.

Peru is pressing for further long-term technical cooperation after this program ends. At present, a proposal for a Latin American Earthquake Engineering Research Center (tentative name), put forth by the first and second teams, is being looked into, including long-term technical cooperation in the founding and operations of this center.

CONCLUSIONS

The surveys of earthquake damage, training at the Building Research Institute and technical cooperation programs in Indonesia and Peru have all been mentioned. These three things may not seem to be related, but they are all important in the technical cooperation for developing countries, and none of them should be omitted. Surveys of earthquake damage and training, as was shown, are useful, both directly and indirectly, for effective earthquake disaster prevention in developing countries. However, as was the problem in the early stage of technical cooperation in Indonesia, there are also times when the technical cooperation does not always proceed as smoothly as expected.

Even if the latest technology and most advanced equipments are brought to these countries, if there isn't a sufficient foundation for them, they will never develop. The countries must have the skills to repair equipment if they are broken and the technology to produce imitations themselves.

In this sense, simple and effective technology and equipment corresponding to these countries' level of science and technology and industrial standards are most useful. It is necessary to be sufficiently aware of the developing countries' circumstances and to give prudent consideration to technical cooperation that will take root and grow in these countries.

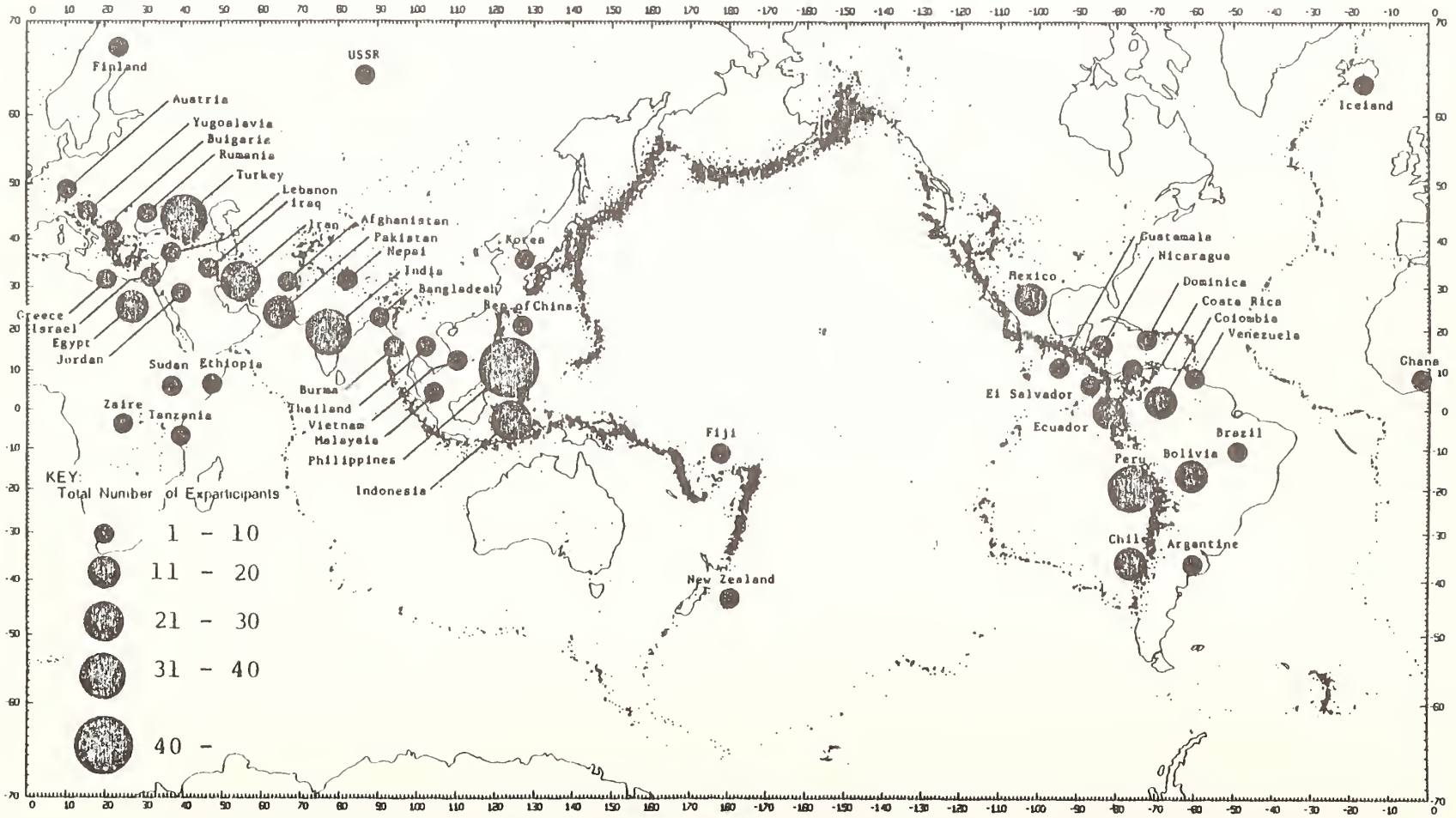

Figure 1. Distribution of IISEE exparticipants on the Seismicity Map of the World (July 1981)

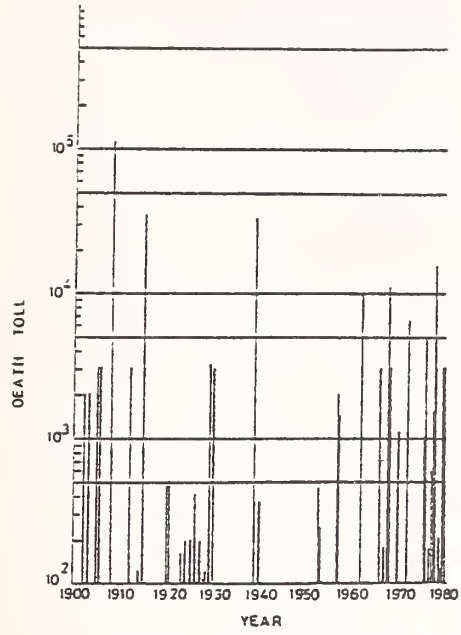

a. The Middle and Near East, and The Mediterranean Coast

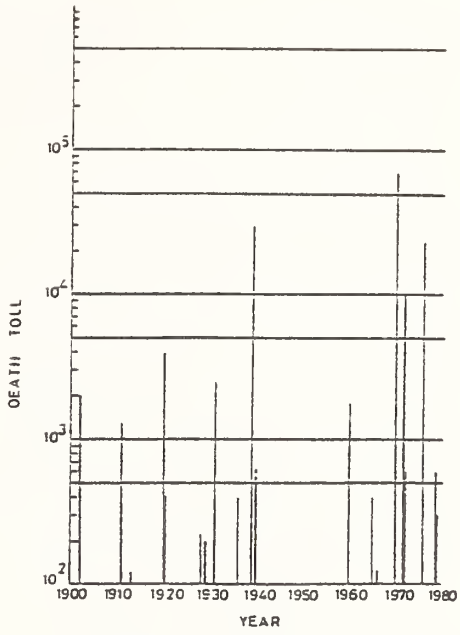

b. Central and South America

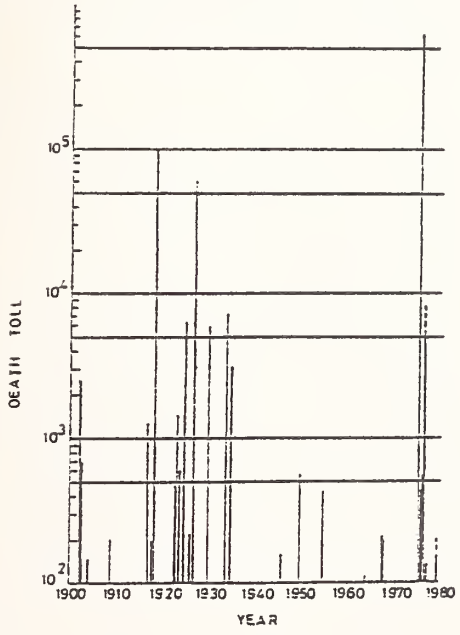

c. China, India and Southeast Asia

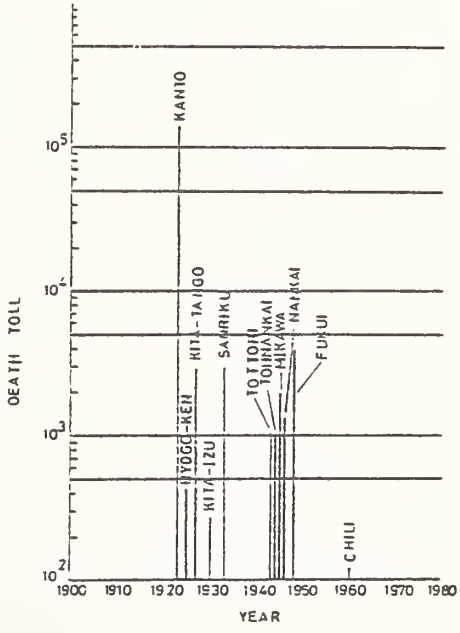

d. Japan

Figure 2. Loss of lives due to past earthquakes

INCREMENTAL EXPANSION AND ASEISMIC DESIGN OF LOW-COST HOUSING IN SITES AND SERVICES PROJECTS

Emil Simiu

Center for Building Technology
National Bureau of Standards
Washington, DC 20234

INTRODUCTION

In recent years, sites and services projects have evolved into one of the more effective components of urban strategies dealing with the enormous shelter problems faced by developing countries. In sites and services projects the responsibility for building the shelter itself rests to a large extent with the beneficiary.

For reasons of hygiene and fire safety and to facilitate immediate occupancy, sites and services plots are in many instances provided initially with sanitary cores, fire walls, and a rudimentary partial shelter. Depending upon his evolving needs and ability to pay for the requisite materials and labor, the beneficiary then completes the dwelling in incremental stages. His direct involvement in the building effort -- usually referred to as self-help -- can be expected to yield a product more suitable to his needs and, to the extent that financing costs and overhead are reduced, more economical than would be the case for conventional construction.

The advantages of incremental expansion by self-help should not obscure some potential technical pitfalls, particularly with regard to construction in earthquake and typhoon (cyclone) prone regions. This is true even where the level of conventional technical skills available to the sites and services beneficiaries can be assumed to be reasonably adequate.

It will be shown in this paper that incremental expansion schemes pose special and delicate structural design problems that arise from the evolutionary nature of the building process in sites and services projects. A first type of problems arises if an initial but incomplete shelter core is provided on the site. In that case efficient ways must be found to ensure the structural integrity of the initial construction. A second type of problems is due to the difficulty of tying successive incremental portions of the dwelling both to the initial construction and among themselves in such a manner as to create systems that are structurally sound at all times. Without due attention to such problems the resulting construction can be unnecessarily uneconomical as well as constituting a serious hazard to life and property in case of earthquake or tropical cyclone. These two types of problems will be illustrated by using examples of shelter construction in actual sites and services projects.

CASE STUDIES

An example will first be shown pertaining to the question of ensuring efficiently the structural integrity of the initial construction (figure 1). In this example the initial construction consists of masonry walls with reinforced concrete columns, and of a sanitary core built integrally with the central wall. The outer walls are connected to the central wall by roof joists.

In conventional construction only minimal, if any, provision would be made to ensure the independent resistance to horizontal loads of walls such of those of figure 1. Indeed, it would be expected that transverse walls or other bracing elements would provide the requisite resistance, since such elements would be built at the same time as or shortly after the walls in question. However, in the case of sites and services projects the construction of a complete, inherently aseismic or wind-resistant structural assembly could take months or even years. Indeed, the beneficiary could first add to the initial construction temporary elements with no seismic or wind resistance capacity whatsoever, as shown in figures 2 and 3. For this reason the initial construction should be capable of resisting earthquake or wind loads independently. In the case shown in figure 1, the solution adopted to achieve this end was to reinforce heavily the concrete columns provided at the ends of the walls. The columns thus function as vertical cantilever beams supporting the tributary earthquake and wind loads specified by the local building code. This solution, if carried out consistently, imposes a penalty not only in terms of scarce materials and skilled labor for the columns themselves, but for their foundations as well. It would therefore appear that in this instance a structural configuration would be advisable that would take advantage of the box-like shape of the sanitary core by transmitting horizontal loads to the latter via inexpensive diagonal bracing in the plane of the roof.

The second type of problems previously mentioned is concerned with tying the successive shelter increments effectively both to the initial construction and among themselves. This type of problems is illustrated in figures 4 and 5. In this case the initial construction consists of the fire wall seen on the left of figure 4, a sanitary core (hidden in figure 4 behind the fire wall), and a roof with its structure resting partially on wood posts. It is seen in figure 4 that there is no functional connection -- indeed, there is a cleavage -- between the fire wall provided initially and the masonry wall built by self-help. Moreover, the system is designed in such a manner that the continuity of the masonry is broken by the wood posts provided as part of the initial core unit (figure 5). Since, owing to imperfect detailing of the connection between the masonry wall and the roof (figure 6), walls may be inadequately supported at the top, the disjointed masonry wall parts built by self-help will perform poorly when subject to earthquake or wind loads.

The illustrations presented here suggest that structural problems inherent in the incremental expansion scheme should not be the concern of the structural engineer alone. Indeed, the structural design on the project from which these case studies were taken can be rated as excellent, given the limited experience available and the lack of systematic studies in the area of design for incremental expansion on the one hand, and the architectural constraints imposed in this case at the structural design stage on the other hand. It is the writer's opinion that an increased awareness of the structural problems illustrated here must inform the total design process, i.e., that architectural and structural constraints should be considered in a coordinated manner, rather than sequentially and independently.

To conclude, first, initial core configurations and details should be developed that allow efficient lateral force paths, thereby eliminating unnecessary structural costs. Second, design schemes should be devised that do not force the adoption of poor structural details for the connections among the incrementally added portions of the shelter. The first conclusion concerns primarily construction costs. The second conclusion concerns primarily structural safety. Poor structural detailing has been in the past and can be in the future the cause of loss of life and property on a massive scale in case of earthquake or tropical cyclone. For this reason the importance of this second conclusion cannot be overemphasized.

ACKNOWLEDGMENTS

The work reported in this note was conducted while the writer served as a consultant to the Urban Development Department of the World Bank under the terms of the U.S. Department of Commerce Science and Technology Fellowship. This work would not have been possible without the effective cooperation of Messrs. John M. Courtney, who served as project monitor, David B. Cook, Michael A. Cohen, David Williams, and Charles Smith, Jr. all of the World Bank.

Figure 1

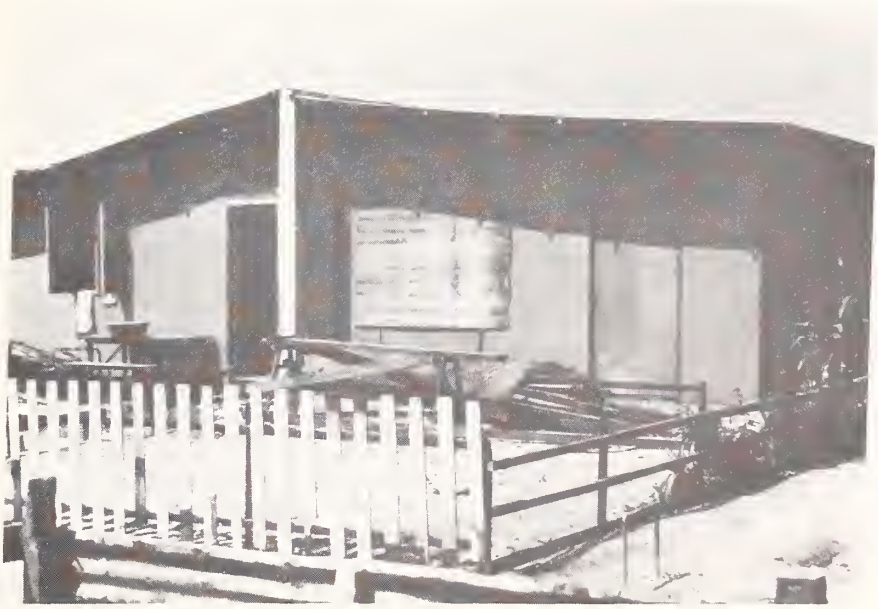

Figure 2

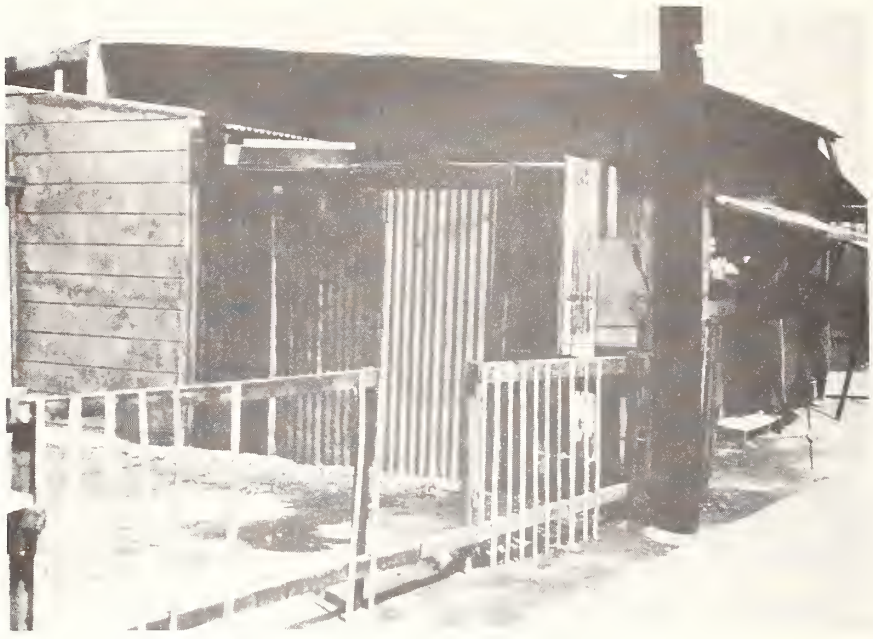

Figure 3

Figure 4

Figure 5

Figure 6

STORM SURGE FORECASTING

Celso S. Barrientos

Center for Environmental Assessment Services
Environmental Data and Information Service
National Oceanic and Atmospheric Administration

ABSTRACT

The National Weather Service of the National Oceanic and Atmospheric Administration (NOAA) has the responsibility to provide forecasting and warning of impending storm surges. This presentation will summarize the storm surge forecast models now in use by NOAA and briefly discuss certain other storm surge models.

INTRODUCTION

Storm surge is abnormal water level above or below the normal tide level. Although the most common storm surge is the positive deviation, negative storm surges can also cause problems in many locations, i.e., Baltimore Harbor in Chesapeake Bay and Toledo Harbor in Lake Erie.

Storm surge is a significant phenomenon. Nine out of ten deaths and 90 percent of the damages in hurricanes are due to storm surge. Hundreds of millions of dollars are lost on the East Coast of the U.S. due to storm surges caused by winter storms. If we can only alleviate 10 percent of the damage due to storm surge, on the average we can save about a hundred million dollars a year on property damage. Of course, the primary aim of forecasting is to prevent loss of life.

The National Weather Service (NWS), NOAA has the responsibility to provide forecast and warning for impending storm surge. Hurricane storm surge can affect 3500 miles of coast in the Gulf and East Coasts of the United States. In winter time, the east coast cyclones can produce storm surges for almost the entire East Coast - from Georgia to Maine. During the recent storm, "The Ash Wednesday" storm (March 1962) produced a 3.6 m storm surge in Southern Long Island, NY and Hurricane Camille 1969 produced 8 m storm surge in Biloxi, MS. In 1906, 6000 inhabitants perished during a hurricane that struck Galveston, TX. Because of these destructions, we must develop methods for forecasting and warning for potential storm surges.

This is the fifth year of my involvement in this Panel of the UJNR. In my previous presentations, I described different forecast models for storm surge forecasting. Today, I will present a summary of the storm surge forecast models in NOAA and touch briefly on the other models in other government agencies, universities, and private companies.

FACTORS IN STORM SURGE GENERATION

Basically, there are two meteorological forces that generate storm surge - direct wind effect and low atmospheric pressure (inverted barometer effect). The low pressure and the wind acting on the ocean surface produce a rotating mound of water. When this mound of water reaches the coastal area, it will feel the bottom of the continental shelf and the storm surge is the result. In deep water, the mound of water is only a few centimeters high and hardly discernible. It is only in reaching the shallow coastal area, that storm surge is of a destructive level because of the conversion of the small amount of kinetic energy into potential energy.

After the surge is generated by meteorological forces, there are three broad categories of physical factors influencing the surge. These are:

a) Meteorology
   - driving forces
   - storm track: direction and speed
   - intensity of storm
   - size of storm

b) Geography and bathymetry
   - coastal configuration, orientation, features
   - depth field, 2-D slope of bottom
   - presence of bays and estuaries

c) Oceanography
   - tides
   - waves
   - phasing of tide with surge.

All of the above factors can affect the surge to increase or decrease. When most of the factors are contributing on the positive side, then the surge can be very devastating. A large hurricane, moving toward the Mississippi Delta at just the right speed (resonant), can produce a very high surge.

Since storm surge is atmospherically driven, a successful forecast method is dependent on a good storm model. A good oceanic model will not result in a good storm surge model unless coupled with a good storm model. This point is generally overlooked by oceanographers and engineers.

DEVELOPMENT OF FORECAST TECHNIQUES

In the old U.S. Weather Bureau, storm surge forecast was needed as part of the warning services provided to the public. Therefore, there is a strong incentive to develop the techniques. The earliest approach used was simple regression. The observed surge heights were related to the

pressure depression of the storm. An equation is derived, and used for future storms to forecast storm surge.

Later regression scheme includes spatial values of pressure and wind. Equations derived have higher accuracy, thus better forecast. Statistical forecast equations are still used in NOAA particularly for extratropical storms. This method has been fairly successful.

The dynamic models have undergone various degrees of complexities. The development is closely related to the advances in computing systems. Earlier models are simple 1-D, bathystrophic, and steady-state. Present models are 3-D, multi-layer, and time dependent.

Pioneering works in U.S. universities were done in Chicago and Texas A&M. At NOAA, Dr. Harris and later Dr. Jelesnianski made significant contributions in surge dynamic modeling. Two dynamic models are in use in NOAA for predicting hurricane surge: SPLASH - a model to forecast surges at the coast and SLOSH - for forecasting surges over land, bays, and/or estuaries. For extratropical cyclones, statistical equations are used for individual locations in the East Coast of the United States.

The U.S. Army Corps of Engineers have a continuing need for storm surge models. They have been involved in both development and application. The Corps of Engineers use the model for design and construction in the coastal areas. The enactment of the Flood Insurance Act has contributed strongly to expand the work on storm surge. Many private companies and universities are doing work to estimate storm surge potentials in coastal communities for flood insurance purposes. The flood insurance program is probably the strongest incentive for progress in storm surge modeling during the last decade. The Nuclear Regulatory Commission (NRC) also has interest on storm surge forecast models. The models are used by NRC to make an estimate of surge frequency in the design of nuclear power plants.

VIBRATORY CONE PENETROMETER TO ASSESS THE LIQUEFACTION POTENTIAL OF THE GROUND

Yasushi Sasaki
Yasuyuki Koga

Pubic Work Research Institute
Ministry of Construction

ABSTRACT

This paper describes a vibratory cone penetrometer that aims to investigate the liquefaction potential of sand deposit in a direct and simple manner in the field, and also the test results in the laboratory using the vibratory cone penetrometer. This cone penetrometer was developed on the basis that the point resistance of the static penetration with vibration or the difference of the point resistance between the above penetration and the static penetration reflects the liquefaction potential of the ground. Such a presumed characteristic was found in the laboratory tests, which were performed on model sand deposits of various relative density and overburden pressure. As a result, the applicability of this new vibratory cone penetrometer was validated.

INTRODUCTION

It is well known that the liquefaction phenomenon of loose sand deposit during an earthquake can cause tremendous damage to various engineering structures. Estimation of the possibility and degree of liquefaction is done based on the comparison of the liquefaction potential of the ground and the expected magnitude of the ground vibration. The methods to estimate the liquefaction potential can be classified into two: one is to conduct laboratory tests of samples obtained from the ground, and the other is to conduct field exploration such as soundings including standard penetration tests (SPT) and in-situ tests by means of artificial vibration and impact loadings on the ground. The second author reported a method to use the explosives in a borehole in the 6th Joint Meeting (1974) [1] to estimate the liquefaction potential.

Among these field test methods, the N-value obtained from SPT is the most frequently used index to estimate the liquefaction potential. SPT has been widely used as a general investigation method because of its high penetration capability and its ability of obtaining disturbed soil samples. However, the N-value is affected by not only the density and overburden pressure but also the lateral pressure and the soil gradation of the ground. It is also affected by the falling method of the hammer, the diameter of the rod, and so on.

Considering such a present state, the authors have developed a simple field investigation apparatus to estimate the liquefaction characteristics of the ground in a direct manner and the results of the tests conducted so far using this method are presented herein.

OBJECTIVES

The specific purposes of the development are as follows:

1) The N-value of the sandy ground which is likely to liquefy is less than 10 to 15. In fact, the generally lowest N-value of the sand deposit is 5 to 6. It has been accepted that the most accurate N-value should have a scatter of about 2 to 3 from such a value. The scatter of 2 to 3 of N-value in this range has significant effect on the estimated liquefaction strength. Therefore, it is desirable to develop a more precise investigation method to at least supplement the SPT method.

2) The N-value is affected by the soil gradation, i.e., N-value gets smaller as fine content of the soil increases. Furthermore, the characteristics of excess pore water pressure buildup due to vibration and the strength characteristics of the soil with large fine content are different from those of soils with small fine content. A method to explore such characteristics is required.

3) It is sometimes necessary to obtain undisturbed samples to perform laboratory tests by means of large scale or special sampling methods. But it is still questionable if we can evaluate accurately the disturbance effect during sampling, transportation, and preparation of a specimen. In order to avoid such effect, in situ test methods are preferrable.

PENETRATION TEST APPARATUS

(1) Outline of the Apparatus

The same penetration apparatus as that of a Dutch cone penetrometer is modified for the newly developed penetration test apparatus. The penetrometer is used to measure the point resistance when the cone at the bottom of the rod is penetrated with a constant rate (1 cm/sec as a standard). An electric bar-type vibrator, which is used to compact fresh concrete, is installed inside the penetration cone to enable the cone to penetrate downward with the addition of vibration. The effect that such vibration gives to the ground is not the same as that during earthquake. The extent of its effectiveness is limited to a rather small region around the penetration cone, nevertheless the magnitude of vibration can be strong enough to collapse the soil structure around the cone to develop excess pore water pressure. Consequently lower point resistance than that by penetration without vibration is obtained due to the strength reduction of the ground. This indicates that the decreased point resistance during vibratory penetration (i.e., static penetration with vibration) or the rate of decrease from that of static penetration (without vibration) may be used as an index to estimate the liquefaction potential of the ground.

A similar method, but in a large scale, to investigate the liquefaction potential is the use of pile driving vibration [2]. In this method, vertical acceleration and pore water pressure in the ground are measured while actual pile of 250 to 400 mm in diameter are driven into the ground by a vibro-hammer. It has been shown that pore water pressure builds up by the vibration during penetration of a bar-type object. Moreover, the amount of buildup of the pore water pressure is large against the same acceleration when the ground is loose. Ishihara [2] showed that the correlation between acceleration and N-value to generate a 10 percent pore water pressure of the effective overburden pressure is a good index of liquefaction potential reflecting the geological history of the ground. Acceleration and pore water pressure are usually measured at a point of 1 m from the center of the pile. The magnitude of acceleration and pore water pressure adjacent to the pile should be greater than that measured.

Estimation of the liquefaction potential by the newly developed vibratory cone penetrometer is based on the point resistance which is mainly governed by the ground behavior next to the cone, therefore vibration source can be smaller than that used in pile driving method. Moreover, the pile driving method follows load control in load application, therefore the penetration rate is likely to vary depending on the ground strength. The result is nevertheless not directly used but the correlation between acceleration and pore water pressure is used for the estimation as stated above. On the other hand, the vibration cone penetration method developed by the authors follows displacement control, and the point resistance when varies to penetrate the ground is used for the estimation. The acceleration and pore water pressure are treated as hidden factors.

(2) Penetration Apparatus and Cone

The penetration apparatus of this new test equipment is the same as the Dutch cone penetration test apparatus (2 tf type). By converting rotation of the handle into vertical penetration by means of a chain and rack gear as shown in Photo 1, it penetrates the rod with the cone on its bottom. The amount of penetration at top of the rod is measured by a potentiometer. The height of the apparatus is 2.4 m and its weight of 100 kgf. The penetration cone is shown in figure 1. A new feature of this cone is that an electric rotor and an unbalanced mass vibrator connected with it are installed inside the cone. Since the vibrator applies an outward centrifugal force toward the radial direction, the cone does an eccentric rotation around the axis. The size and shape of the new vibratory cone and the standard cone are summarized in table 1. The apex angle is 60° in both cones. The diameter of the vibrator of the new cone is 41 mm whereas that of the standard cone is 35.7 mm. The revision was made to accommodate the diameter of the vibrator. According to the theory of cone penetration, point resistance qc, the penetration force per unit cross sectional area of the cone, is not affected by

the cross sectional area itself. Therefore the difference of the cross section should not affect the comparison. The vibratory cone in which a rotor and a vibrator are installed is about 79 cm in length while that of the standard one is about 25 cm long. Weight of the vibratory cone is 6.3 kgf (including the 4.3 kgf vibrator) while that of the standard one is 1.1 kgf. Specifications of the vibrator and the generator are given in table 2. The centrifugal force of the standard vibrator which is used for the compaction of fresh concrete is reduced to 1/5 of the standard one (160 kgf) for this new cone. This is because the centrifugal force of the standard vibrator is so large that it reduces the point resistance of a sand deposit of relative density of about 50 percent to almost zero, thus suggests that less centrifugal force is required for adequate use. Strain gage type transducers are installed at tip of the cone to measure the point force, surface friction, and excess pore water pressure buildup during penetration. The characteristics of the transducers are shown in table 3. Rods used to penetrate the cone into ground are the conventional hollow ones used for the standard Dutch cone penetrometer. They are 28 mm in outer diameter, 16 mm in inner diameter and 1 m in length.

TESTING METHOD IN A MODEL SAND DEPOSIT

(1) Testing Sand Container

A small sand container was used to conduct a series of tests to evaluate the ability and performance of the new cone penetrometer. The container is 1.6 m in length, 1.0 m in width and 1.5 m in depth made of steel (figure 2). Overburden pressure can be applied on the model ground through a loading plate using four hydraulic jacks. Each hydraulic jack can apply 3.5 tf at the maximum which results in a maximum pressure of 0.9 kgf/cm^2. The loading plate has nine holes for penetration testing.

(2) Preparation of the Test Ground

The sand of the test ground was Sengenyama sand whose properties are shown in table 4.

The test ground was made in a following way: (1) scattering wet sand in 10-20 cm thickness, (2) compacting by human foot or wooden tamper, (3) piling up the sand deposit into 1 m in total thickness, (4) putting the loading plate on the ground, (5) applying overburden pressure by hydraulic jacks, and (6) supplying water from the bottom of the container. Several different densities were prepared by changing the compaction methods. The density was measured by using a mould to collect samples when the test ground was piling up.

(3) Testing Method

Although many different penetration methods have been considered, four methods shown in figure 3 have been used. Method A is to measure static point resistance continuously downward to obtain the point resistance (q_c^S). Method B is to measure vibratory point resistance continously downward (q_c^V). Methods C1 and C2 are to measure q_c^S and q_c^V downward alternately. This is intended to measure both resistances at a close locations as possible since the scatter of point resistance was easily expected at each location within the test ground. Consequently, the comparison of resistance of q_c^S and q_c^V for the same soil condition was expected. Penetration was done continuously at a constant rate of 1 cm/sec. In methods C1 and C2, starting and stopping of the vibrator was repeated at intervals of 10 cm or 20 cm. Among nine penetration tests in one test ground, six tests were performed on normally consolidated state and three tests on overconsolidated state by unloading a part of the overburden pressure. Standard combination of the penetration methods was shown in table 5. Figure 3 shows these penetration methods in a schematic way and it also shows the locations where the electrically and continously measured data were read.

PENETRATION TEST RESULT AND ITS CONSIDERATION

(1) Test Ground Condition

Penetration method and density of each test ground are summarized in tables 5 and 6. The relative density of each test ground has almost always a 20 percent scatter, indicating the range of scatter in such test grounds made by the methods described above.

(2) Penetration Test Results

Figures 4 and 5 give the examples of the measured results of the point resistance. Figures 4 and 5 show the result of test ground no. 1 and 2 having average relative densities of 31 percent and 58 percent, respectively. The overburden pressure was 0.8 kgf/cm^2 in both cases. Solid line shows the static point resistance, q_c^S, and dotted line shows the vibratory point resistance, q_c^V. In test ground no. 1 in figure 4, the maximum of q_c^S was 17 -20 kgf/cm^2 at a depth of 0.2 m. q_c^S gradually decreased with depth and also indicated periodic variation below the depth of 0.2 m. The reason why q_c^S decreased with depth is not known at present, but it may be attributed to the nonuniformity in compaction of the test ground, or the fact that overburden pressure did not act completely downward due to the side friction of the container. The downward periodic variation was probably the result of how the test ground was piled up and compacted. Such a tendency was remarkable when the test ground was made by human foot compaction which resulted in a low density (figure 4). In this test ground, g_c^V showed rapid reduction when the penetration method was switched from static penetration to

vibratory penetration. Such a tendency was clearly observed in the case of method C1 where static and vibratory penetrations were performed alternately. Moreover, in the case of method B the periodical variation in q_c^v was also observed as in q_c^s, in addition to that q_c^v was consistently smaller than q_c^s. In method C1, q_c^s was less than that by method A, which suggests that the static penetration behavior is influenced by the preceding vibratory penetration right above that location. Pore water pressure was generated where the penetration method was switched from static to vibratory. As a result of this pore pressure buildup, the reduction of q_c^v from q_c^s can be considered as the result of reduction of the effective stress around penetration cone. In figure 5, no significant differences between q_c^s in method A and q_c^v in methods B and C1 can be observed, and both q_c^s and q_c^v were around 60 kgf/cm^2 below 0.3 m depth. In this case no periodical variation of q_c^s and q_c^v, as was seen in figure 4, could be detected either. This indicates that the test ground, which was compacted by wooden tamper, was made fairly uniform. The magnitude of the excess pore water pressure buildup during vibratory penetration was also small in this case. Though the figures are not shown, similar results to figure 4 were obtained in test ground No. 3, 4, 6, 7, 8, 9 (D_r = 24 - 55 percent) and no difference between q_c^v and q_c^s was observed in test ground no. 5 (D_r = 67 percent).

Figure 6 shows static and vibratory point resistances of each test ground, for normal and overconsolidation states. In this figure, q_c^s and q_c^v are average values of all readings shown in figure 3. From figure 6, it can be said that q_c^v is small when q_c^s is small. Although this does not necessarily suggest that q_c^v is a better index than q_c^s for the liquefaction potential evaluation, q_c^v can be considered as a more direct index since it reflects the pore water pressure characteristics due to vibration, as was seen in figures 4 and 5. Such a fact shall be further supported by test results on different kind of sands in future researches.

Considering figure 6 to give the difference between q_c^s and q_c^v, the following can be said. While there is little difference between q_c^s and q_c^v when q_c^s is greater than 50 kgf/cm^2, q_c^v is remarkably smaller when q_c^s was less than 35 kgf/cm^2. Furthermore, when q_c^s is less than 15 kgf/cm^2, the decreased amount of q_c^v from q_c^s is smaller than when q_c^s was over 15 kgf/cm^2. Since there is a correlation between q_c^s, the relative density, D_r, and the overburden pressure within a certain range for this test ground, the tendency observed for measured q_c^s stated above can be considered to hold for other D_r values. Let us define a new index to represent the degree of decrease of point resistance q_c^v from q_c^s normalized by q_c^s, as follows:

$$D = 1 - \frac{q_c^v}{q_c^s}$$

This implies that the degree of decrease of q_c^v by vibratory penetration is small as D approaches 0. Figure 7 shows the correlation between D defined above and D_r. According to figure 7(a) (normal consolidation), D does not depend much on D_r below $D_r \cong 50$ percent for $\sigma_v = 0.5$ kgf/cm^2, but decreases remarkably for the range of $D_r = 50 - 70$ percent. Moreover, in the case of $\sigma_v = 0.8$ kgf/cm^2, D shows a gentle decrease above $D_r = 40$ percent, and decrease remarkably for the range of $D_r = 50 - 60$ percent. Therefore in the range of $D_r = 40 - 70$ percent, D is smaller for the same value of D_r if the overburden pressure is large, and the decreasing tendency of D against the increase of D_r was remarkable. For overconsolidated condition, the more obvious tendency that D is dependent on D_r is clearly shown in figure 7(b) in the range of $D_r = 30 - 60$ percent. For the same overconsolidation ratio (OCR $\cong$ 1.6), D is smaller when the initial overburden pressure is 0.8 kgf/cm^2 than when it is 0.5 kfg/cm^2.

CONCLUSIONS

The mechanism of a newly developed vibratory penetration apparatus to assess the liquefaction potential of sand ground and its test results in a sand container were presented. As a result of a series of tests, it was found that the penetration resistance of this vibratary penetrometer reflects the excess pore water pressure characteristics generated by the vibratory penetration which leads to the possibility to assess the liquefaction potential by this penetrometer. Further investigation on the proposed index to correlate the decreased vibratory point resistance and relative density is required. Morever, the relation between such an index and conventional liquefaction strength must be established based on experiments in future researches.

REFERENCES

[1] Yamamura, K. and Koga, Y., "Estimation of Liquefaction Potential by Means of Explosion Test," 6th Joint Meeting of US-Japan Panel on the Wind Seismic Effect, 1974.

[2] Ishihara, K. et al., "Field Measurements of Dynamic Pore Pressure During Pile Driving," Proc. Int. Conf. on Microzonation, 1972.

[3] Ishihara, K. et al., "Investigation of Liquefaction of the Ground by Pile Driving (in Japanese)," Proc. 10th Conf. of JSSMFE, 1975.

Table 1. Comparison of Vibratory Cone and Standard Cone

	Vibratory Cone	Standard Cone
Diameter	41 mm	35.7 mm
Length	790 mm	205 mm
Apex Angle	60°	60°
Weight	6.3 kgf	1.1 kgf

Table 2. Vibrator and Power Source

Item	Size, etc.
Diameter	41 mm
Length	576 mm
Frequency	200 c/s
Power Source	High Frequency Generator: 1.5 KVA, 48 V
Centrifugal Force	32 kgf

Table 3. Specification of Transducers

Symbol	Item	Type	Capacity	Remarks
q_c	Load transducer of point resistance	Strain gauge	1 tf	Cross sectional area 13.2 cm^2
f_c	Load transducer of side friction	Strain gauge	1 tf	Measurement area 100 cm^2
P	Pore pressure transducer	Strain gauge	2 kgf/cm^2	
D	Displacement transducer of penetration	Potentiometer	106 cm	

Table 4. Property of Test Sand

D_{60} (mm)	0.31
D_{10} (mm)	0.15
D_{50} (mm)	0.28
Uniformity Coefficient U_c	2.07
Specific Gravity G_s	2.721
Max. Void Ratio e_{max}	1.039
Min. Void Ratio e_{min}	0.615
Max. Density ρ_d (g/cm^3)*	1.65
Optimum Water Content Wopt(%)*	17.9

* By Compaction Test

Table 5. Cases of Penetration Test Method

Penetration Method	Loading Condition	
	Normal Consolidation	Over Consolidation
A	2	1
B	2	1
C1, C2	2	1

Table 6. Test Ground Condition

Test Ground No.	Compaction Method	Number of Layers	Water Content W(%)	Dry Density ρ_d(g/cm^3)	Relative Density Dr(%)		Overburden Pressure σ_v(kgf/cm^2)
					Average	Range	
1	Human Root Compaction, 20 times	6	7.3	1.43	30.5	19.3~39.4	0.8→0.5
2	Wood Tamper Compaction, 5 times	9	8.9	1.52	58.2	51.7~66.3	0.8→0.5
3	Human Foot Compaction, 5 times	5	8.7	1.48	46.2	32.3~58.7	0.5→0.3
4	Wood Tamper Compaction, 2 times	5	12.2	1.41	24.4	13.2~33.7	0.5→0.3
5	Wood Tamper Compaction, 5 times	8	13.4	1.55	67.1	58.7~77.4	0.5→0.3
6	Wood Tamper Compaction, 2 times	8	14.2	1.49	50.7	39.6~57.6	0.5→0.3
7	Wood Tamper Compaction, 4 times	6	13.2	1.51	54.5	44.3~65.6	0.5→0.3
8	Wood Tamper Compaction, 3 times	8	11.8	1.44	34.4	21.9~41.7	0.8→0.5
9	Wood Tamper Compaction, 3 times	7	14.7	1.48	46.5	34.4~61.6	0.8→0.5

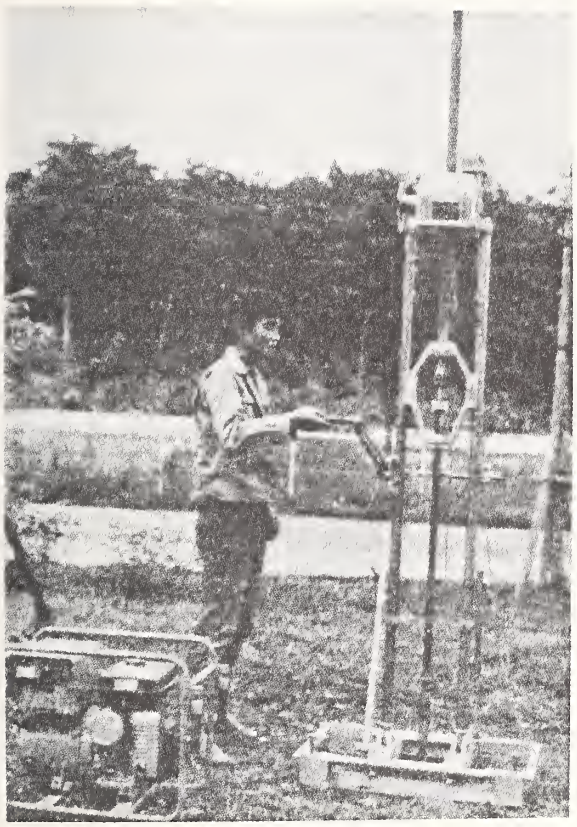

Photo. 1

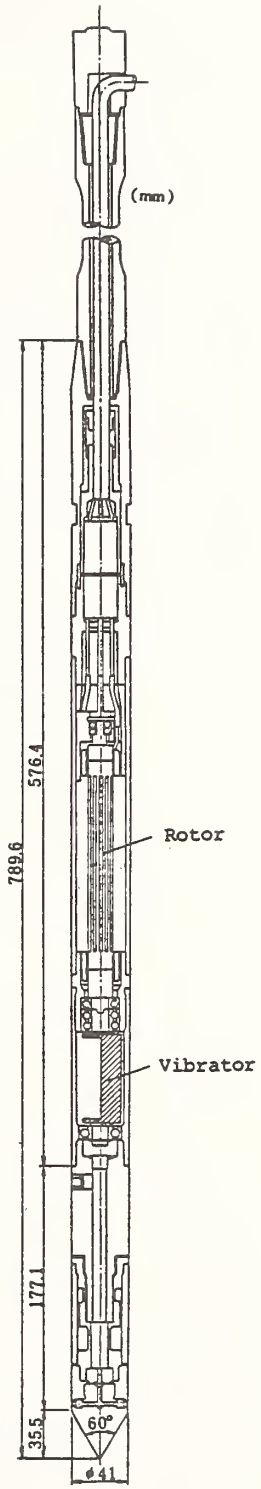

Fig. 1 Diagram of Vibratory Cone

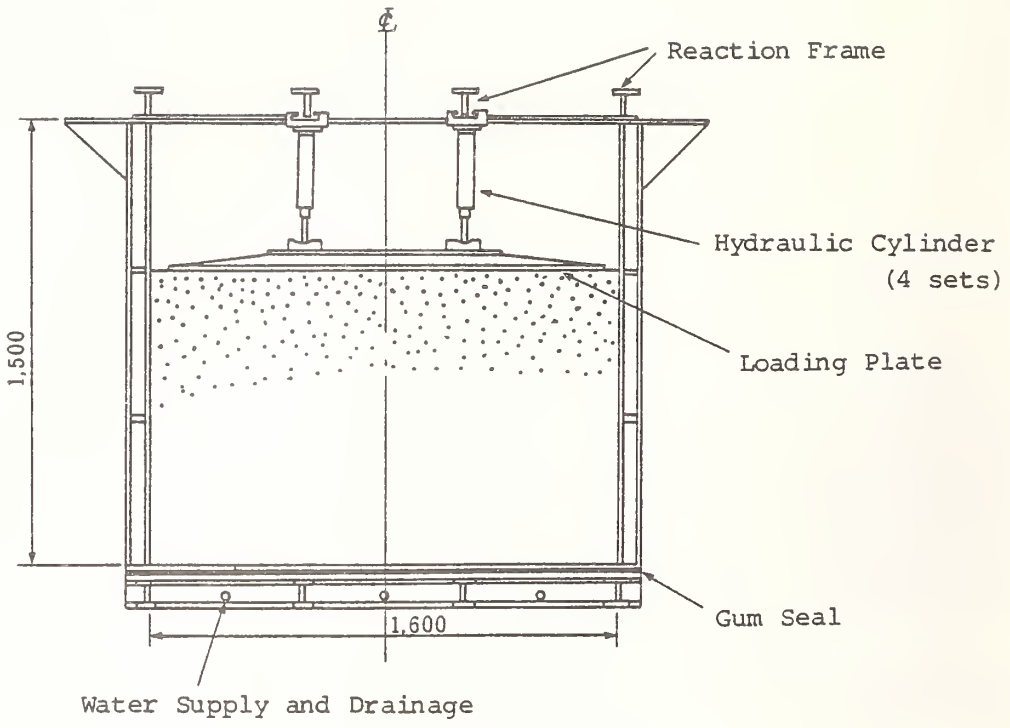

Fig. 2 Test Sand Box

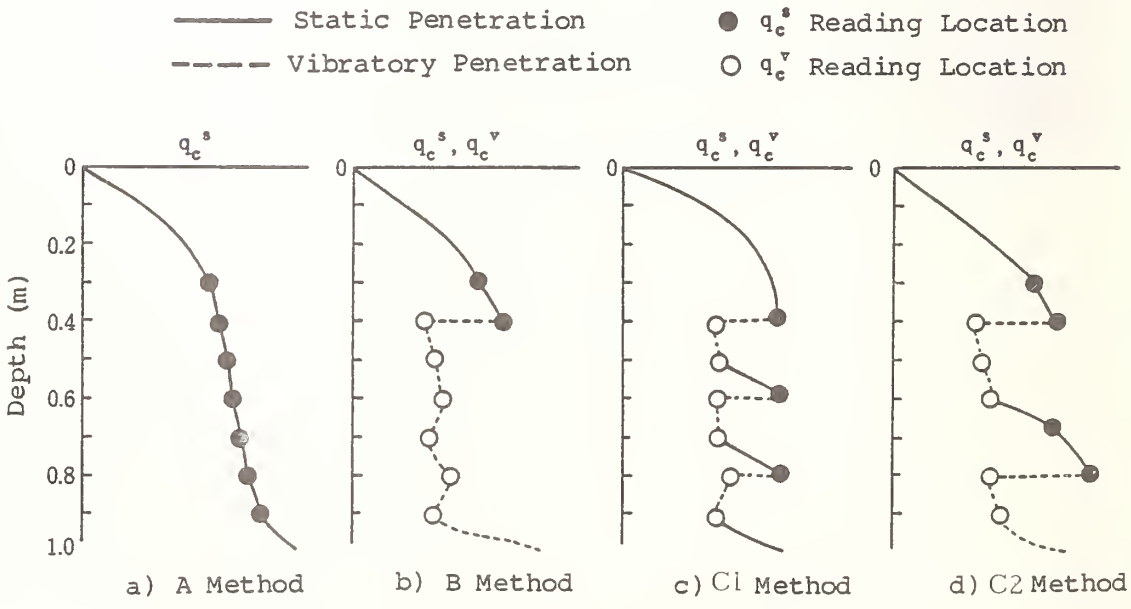

Fig. 3 Penetration Test Method

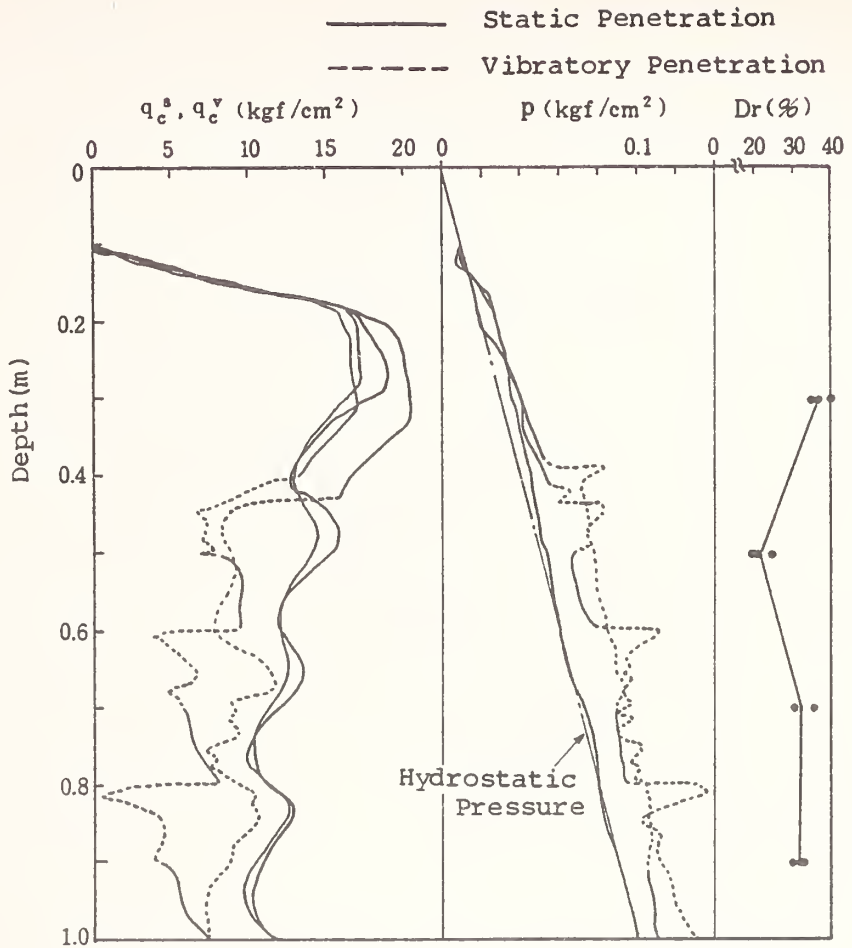

Fig. 4 Example of Penetration Test Result (Loose Condition)

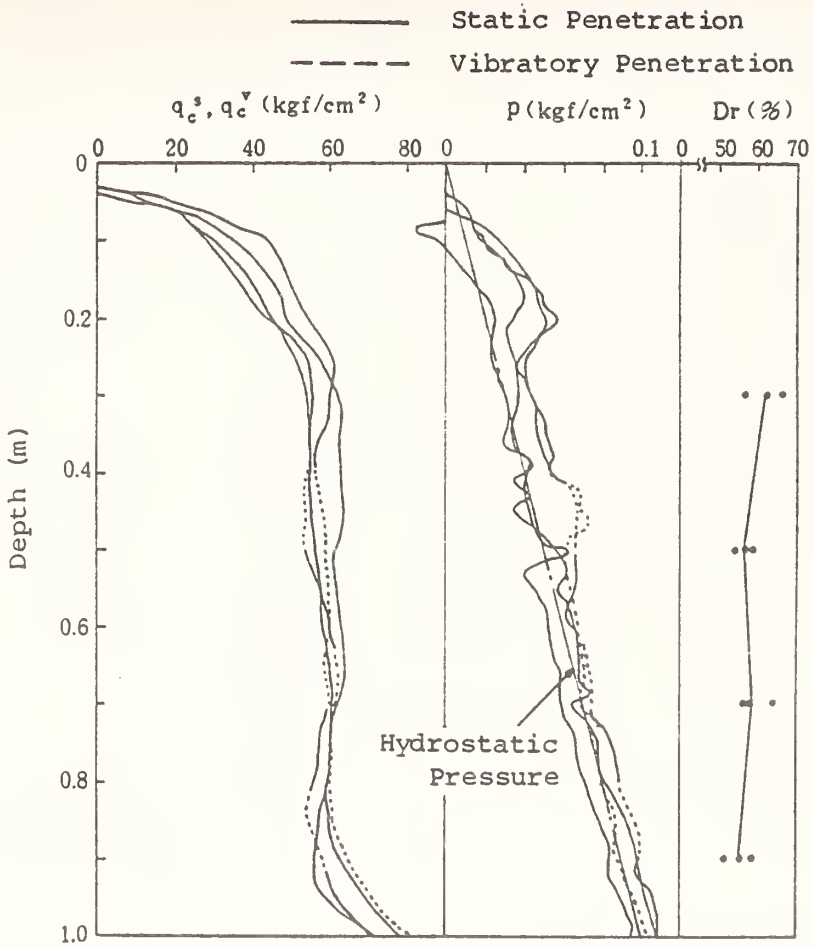

Fig. 5 Example of Penetration Test Result (Dense Condition)

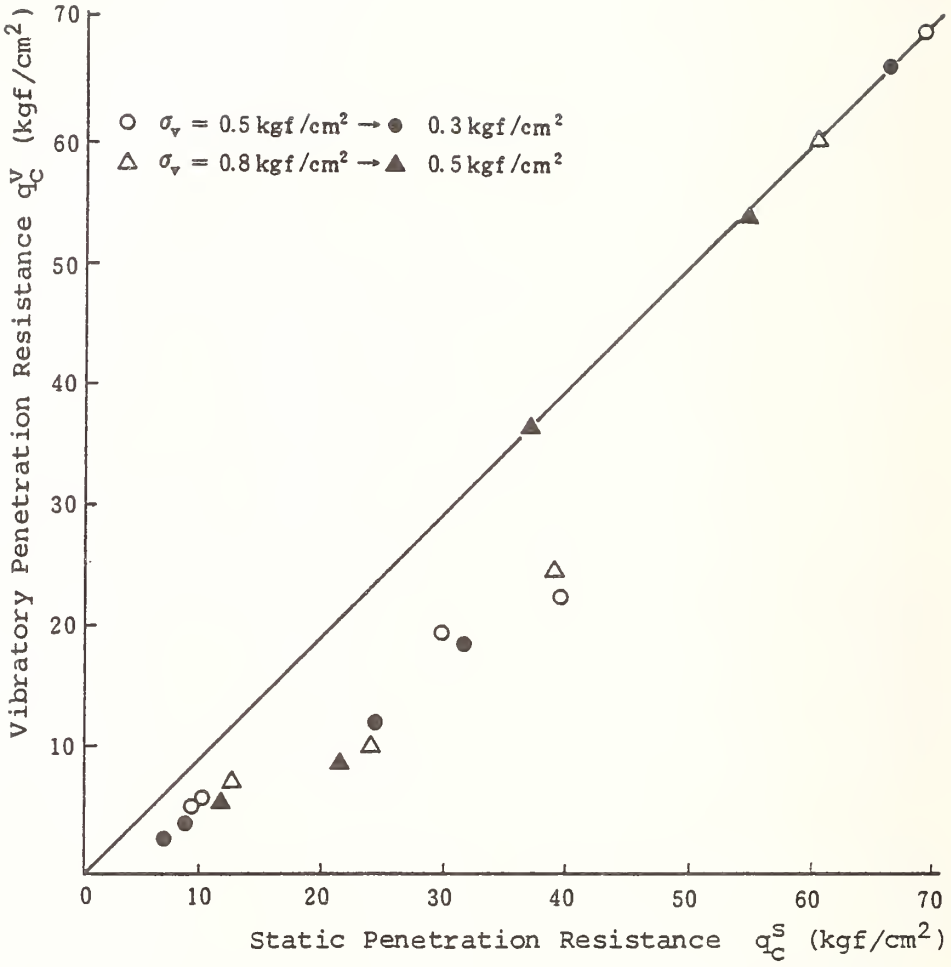

Fig. 6 Relationship of Static and Vibratory Penetration Resistance

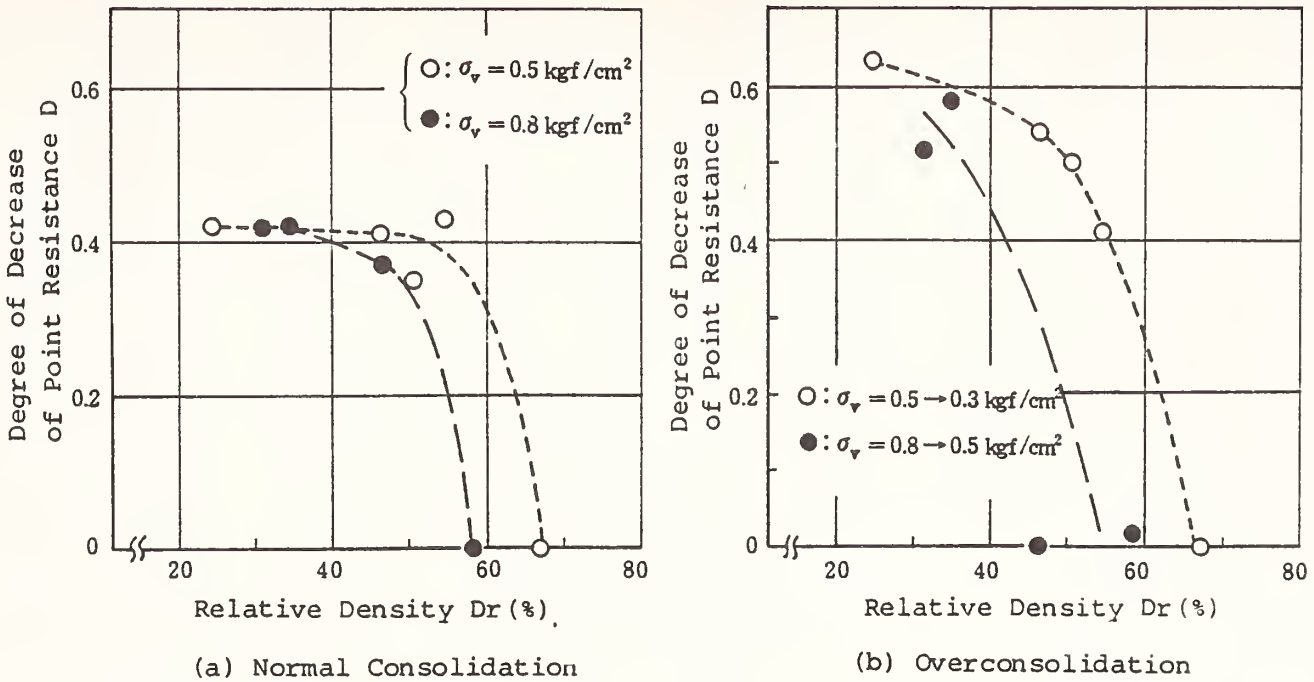

(a) Normal Consolidation

(b) Overconsolidation

Fig. 7 Effect of Relative Density or Degree of Decrease of Point Resistance

DIRECT EVALUATION METHOD FOR FLOOR RESPONSE SPECTRA

Makoto Watabe

Building Research Institute
Ministry of Construction

ABSTRACT

Floor response spectra are generally obtained by response analyses when the results by response analyses in time history of structures are employed as input excitations. It is possible to apply the random vibration theory to evaluate the maximum responses of structures and their floor response spectra without response analyses in time history.

In this paper, the calculation procedure of maximum responses of structures and their floor response spectra subjected to nonstationary random earthquake ground motions are proposed. The method herein proposed is verified to be valid and very useful when its results are compared with the results obtained by the general method.

INTRODUCTION

The response spectra provide one of the most important factors of earthquake ground motions for seismic design of structures. Various design response spectra have been proposed based on the spectral analyses of a number of observed accelerograms. In the response analyses of very important structures such as nuclear power plants, the simulated earthquake ground motions are generated so as to fit the design response spectra given. The responses of structures subjected to input earthquake ground motions described above are applied as excitation for floor response spectra used in seismic design of equipment and piping systems. Another approach for evaluating the maximum responses of structures and their floor responses is to apply the random vibration theory.

In this paper, the author proposes the direct evaluation method of floor response by the random vibration theory, where the characteristics of the input ground motions are represented by spectral density, duration and nonstationarity.

MAXIMUM RESPONSE PREDICTION OF A SINGLE-DEGREE OF FREEDOM SYSTEM

The maximum response of a single-degree of freedom system subjected to a nonstationary random ground motion $\ddot{y}(t)$ is predicted as follows:

$$E\{|J(t)|max\} = M \checkmark E\, J^2(t)\} \tag{1}$$

where E denotes ensemble average, J(t) are response values in terms of time, t, and $J^2(t)$ and M are the mean square of J(t) and the peak factor of $E\{J(t)|max\}$ to $\checkmark E\{J^2(t)\}$, respectively.

If $\ddot{y}(t)$ is a nonstationary random process given by the product of a deterministic intensity the function I(t) which varies slowly in terms of t and a stationary random process $\ddot{y}_s(t)$ having zero mean value, $\ddot{y}(t)$ can be expressed by equation (2).

$$\ddot{y}(t) = I(t) \cdot \ddot{y}_s(t) \tag{2}$$

The ensemble average of the mean square of response J(t) in the duration time, Td, is obtained approximately as follows:

$$E\{\overline{J^2(t)}\} \doteq \overline{I^2(t)} \cdot E\{\overline{J_s^2(t)}\} \tag{3}$$

where $J_s(t)$ is the responses subjected only to the stationary ground motion $\ddot{y}_s(t)$.

The stationary random process $\ddot{y}_s(t)$ is assumed to be represented by the following discrete expression;

$$\ddot{y}_s(t) = \sum_{j=1}^{N} Aj \cdot \cos(\omega j + \phi j) \tag{4}$$

where N is the number of harmonic waves superposed, Aj is the amplitude at frequency ωj, and ϕj is the random phase angle with a uniform distribution probability between 0 and 2π. Through the integration of the square values of responses Js(t) in a system having a critical damping ratio ξ, and an undamped natural circular frequency λ, $E\{\overline{J_s^2(t)}\}$ can be obtained as follows;

$$E\{J_s^2(t)\} = \sum_{j=1}^{N} \frac{1}{2} A^2 j \cdot |H_J(i\cdot\omega j)|^2 \cdot \gamma \tag{5}$$

in which $H_J(i\cdot\omega j)$ is the complex frequency response function of J(t) and can be expressed by equation (6) with regard to a relative displacement x(t).

$$Hx(i\cdot\omega) = \frac{1}{\lambda^2 - \omega^2 + i2\xi\lambda\omega}, \quad i = \sqrt{-1} \tag{6}$$

The coefficient γ in equation (5) represents the effect of transient state of response, γ is 1.0 for $\omega j \neq \lambda$ and is given as follows for $\omega j = \lambda$;

$$\gamma(\omega j = \lambda) = 1 - \{-\exp(-\xi\lambda Td)\} \cdot \{3 - \exp(-\xi\lambda Td)\}/2\xi\lambda Td \tag{7}$$

Based on the result of past researches, the peak factor, M, in equation (1) is expressed as follows:

$$\log M = f_1 + f_2 / f_3 \{(\log Neq) f_3 - 1\} \tag{8}$$

where,

$$\begin{aligned} f_1 &= 0.2 + 0.55 \log R + 0.22R - 0.86\xi 0.076R - 1.3 \\ f_2 &= 0.12R - 0.96\{1 - \exp(-100\xi)\} \\ f_3 &= R^{11}\xi\{0.28 + 0.84\exp(-13\xi)\} \end{aligned} \tag{9}$$

The coefficient Neq in equation (8) indicates the equivalent number of waves crossing zero baseline to either positive or negative direction over the entire duration. It can be estimated by taking the spectral moment of response $J_s(t)$, i.e.,

$$Neq = Td/2\pi \cdot \sqrt{\overline{E[J_s^2(t)]}/E[\overline{J_s^2(t)}]} \tag{10}$$

The constant R in equation (9) represents the nonstationarity of input ground motions, $\ddot{y}(t)$, and is expressed as follows:

$$R = \int_0^{Td} E[\ddot{y}^2(t)]dt / \int^{Td} | I^2(t) |_{max} \cdot E[\ddot{y}_s(t)]d \tag{11}$$

$$= \overline{I^2(t)}/|I^2(t)|_{max}$$

MAXIMUM RESPONSE OF MULTI-DEGREES OF FREEDOM SYSTEM

The solutions of equations of motion in multi-degrees of freedom system can be obtained by using the mode-superposition method and expressed;

$$Jr(t) = \sum_m \beta_m Urm\, Jm(t) \tag{12}$$

in which Jr(t) is the response value at rth freedom, βm and Urm are the participation factor and the mode shape of the mth mode, respectively. Jm(t) is the solution of the equation of motion for mth mode having the modal frequency λm and the modal damping ξm. The modal damping can be evaluated by energy consideration, even if the damping matrix of the system can not be uncoupled by the normal-coordinate transformation using the undamped eigen-vectors.

When the input process is represented by equations (2) and (4), the ensemble average of mean square of responses Jr(t) can be written by the following relations;

$$E[\, J_r^2(t)\,] = I^2(t) \cdot E[\, J_{rs}^2(t)\,] \tag{13}$$

$$E[\, J_{rs}^2(t)\,] = \sum_m \sum_\ell \sum_m \beta\, U_{rm}\, \beta\, U_{r\ell} \sum_j \frac{1}{2} A_j^2 Re\{H_{Jm}(i\cdot\omega j) \cdot H_{J\ell}(-i\cdot\omega j)\} \cdot \gamma \tag{14}$$

where $H_{Jm}(i\cdot\omega)$ is the complex frequency response function of Jm(t), and γ is given by equation (7) in the case of m=ℓ and ωj=λm and the other cases, γ is 1. The peak factor for the maximum response $E[|J_r(t)|_{max}]$ is estimated by equation (8). An equivalent damping value ξ in equation (9) may be weighed in proportion to the contribution ratio of each modal power to the total one.

For the prediction of floor response at the rth freedom, it is assumed that the absolute acceleration responses $^a r(t)$ at the rth freedom can be expressed by the form of equations (2) and (4). The amplitude Arj at a frequency of stationary part of input process becomes as follows;

$$Arj = Aj\left[\sum_m \sum_\ell \sum_m \beta\, U_{rm}\, \beta_\ell\, U_{r\ell} Re\{Ham(i\cdot\omega j)\cdot Ha\ell(-i\cdot\omega j)\}\cdot\gamma\right]^{1/2} \tag{15}$$

$$Ham(i\cdot\omega) = \frac{\lambda_m^2 + i2\xi_m\lambda_m\omega}{\lambda_m^2 - \omega^2 + i\ 2\xi_m\lambda_m\omega} \tag{16}$$

Therefore, the floor response spectrum can be estimated by the similar process for a single-degree of freedom system described above.

To demonstrate this stochastic procedure to evaluate the responses of a multi-degrees of freedom system and floor responses, the lumped mass model including the effect of soil-structure interaction as shown in figure 1 is employed as an example of a nuclear power plant. The members of this model have both flexure and shear deformations. The damping matrix is composed of Rayleigh damping with 5 percent of the critical damping value in both the first and the second modes of the structure, and 10 percent viscous damping for the foundation soil. The natural periods of the lst, 2nd, and 3rd modes are 0.32, 0.15, and 0.12 seconds, respectively, and the modal dampings, 4.4, 8.3, and 6.4 percent, respectively. The eigen-vectors are shown in figure 2.

The input process is represented in the form of equations (2) and (4), and the properties are given by equations (17) and (18) to simulate Taft 1952-EW component.

$$I(t) = C(\tau+t)\cdot\exp\{1-C(\tau+t)\} \tag{17}$$

$$C = 0.16,\ \tau = 0.25 \text{ sec.}$$

$$A(\omega) = \sqrt{4G(\omega)\Delta\omega}$$

$$G(\omega) = \frac{\omega^4}{(\omega^2-1)^2+2\omega^2} \sum_{k=1}^{2} \frac{p_k^4+4h_k^2\ P_k^2\ \omega^2}{(p_k^2-\omega^2)2+4h_k^2\ P_k^2\ \omega^2} \cdot Gok \tag{18}$$

$$P_1 = 2\pi/0.35 \quad \text{rad/sec}, \quad h_1=0.15, \quad Go1=20\ Gal^2\cdot\text{sec}$$

$$P_2 = 2\pi/0.68 \quad \text{rad/sec}, \quad h_2=0.25, \quad Go2=80\ Gal^2\cdot\text{sec}$$

The nonstationarity R of input process in a duration of 30 sec, defined by equation (11), is 0.383. The 14 samples of simulated group motions are generated and the mean maximum value of these accelerations is 265 gals. A sample of the simulated ground motions and the responses are shown in figure 3.

The comparison of response spectra of input process, calculated by both simulated ground motions and the stochastic procedure is presented in figure 4. The results of the maximum values of the responses of the model structure and the floor response spectra by the analysis based on the step-by-step calculation and the theoretical analysis are shown in figures 5 through 7.

DIRECT EVALUATION OF FLOOR RESPONSE SPECTRA FROM DESIGN RESPONSE SPECTRA

When the design response spectra of input ground motion are given, the floor response spectra can be evaluated directly by the stochastic method introduced above. In this case the maximum responses and floor response spectra can be estimated by the process shown in figure 8.

Examples of the floor response spectra of a nulcear power plant modeled into a lumped mass system as shown in figure 9 are presented herein. In these examples, the supporting soils with either 500 and 1000 m/sec as shear wave velocity are assumed and the fundamental periods of soil-structure interaction systems in the two kinds of soils are 0.49 and 0.29 sec, respectively. The mode shapes are shown in figure 10. The design response spectra proposed by Ohsaki et al., with magnitude 7.0 and epicentral distance 20 km, or magnitude 8.4 and epicentral distance 90 km are employed in these analyses. These response spectra with 5 percent dampings are shown in figure 11. In the stochastic analysis, it is assumed that the input ground motions are stationary and have the duration time, Td, defined as follows;

$$\log Td = 0.31M - 1.2 \quad \text{in sec.} \tag{19}$$

in which M is the magnitude of the earthquake.

Results of the floor response spectra are presented in figures 12 through 15. In these figures, the results by the stochastic method proposed by Vanmarcke and the step-by-step calculation are also shown. The input ground motions for the later analysis are generated to fit the design response spectra. Time histories of the simulated ground design motion and the fitting status to the design response spectra for an earthquake of magnitude 8.4 are given in figures 16 and 17.

CONCLUSIONS

In this paper, the relation between the maximum response and the factors of an input process was established and the method proposed was verified by computer simulations. On the basis of these numerical experiments, it is concluded that the maximum responses of a structure and its floor response spectra can be estimated using this proposed method with a reasonable accuracy, once the arbitrary design response spectra are given.

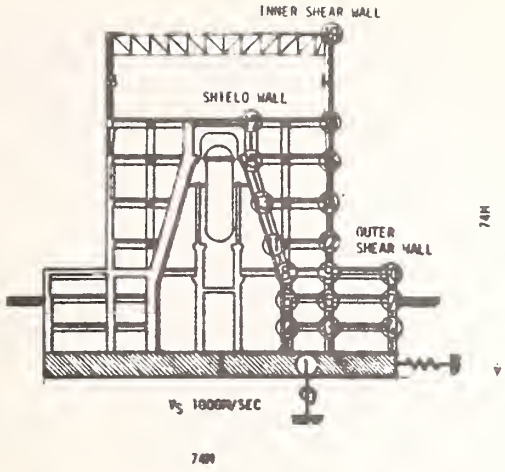

Fig.1 An Example of A Nuclear Power Plant and Its Lumped Mass Model

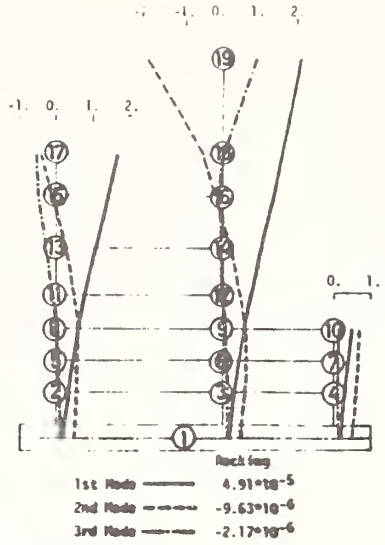

Fig.2 , Eigen Vectors multiplied by Participating Factor

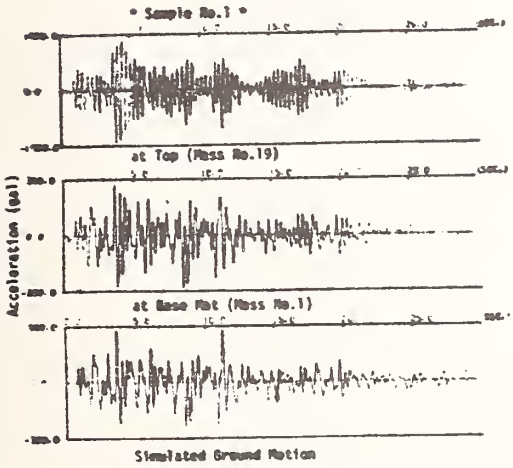

Fig.3 A Simulated Ground Motion and Responses

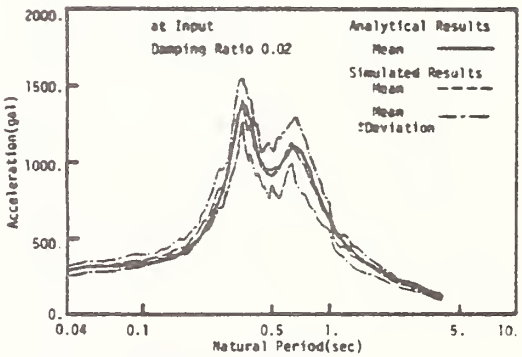

Fig.4 Response Spectra of Input Ground Motion

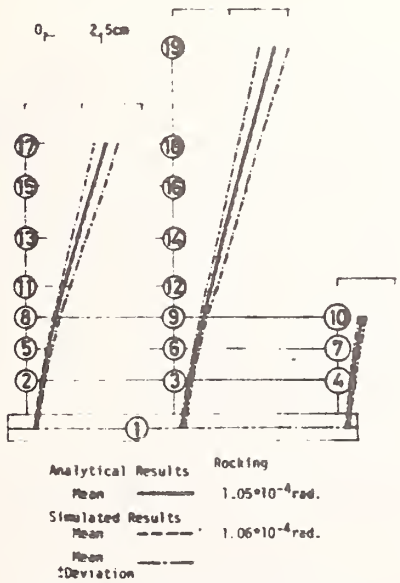

Fig.5 Maximum Responses of Relative Displacements

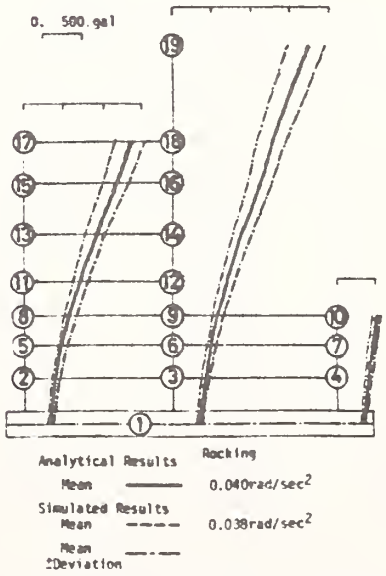

Fig.6 Maximum Responses of Accelerations

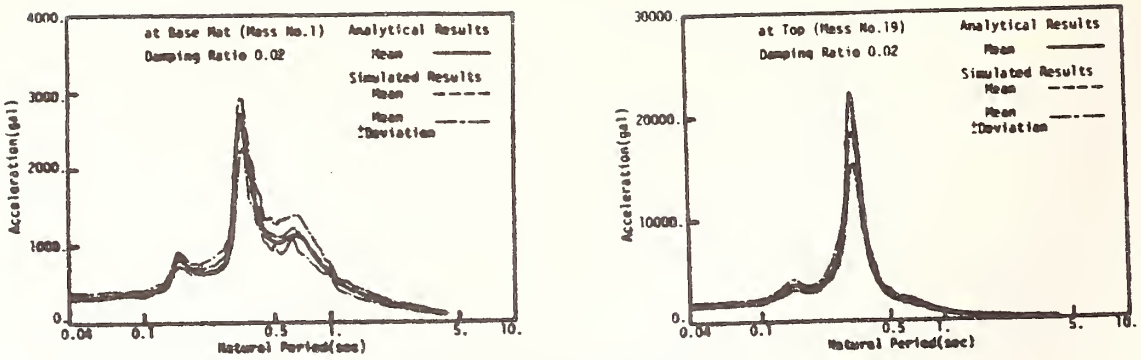

Fig.7 Floor Response Spectra

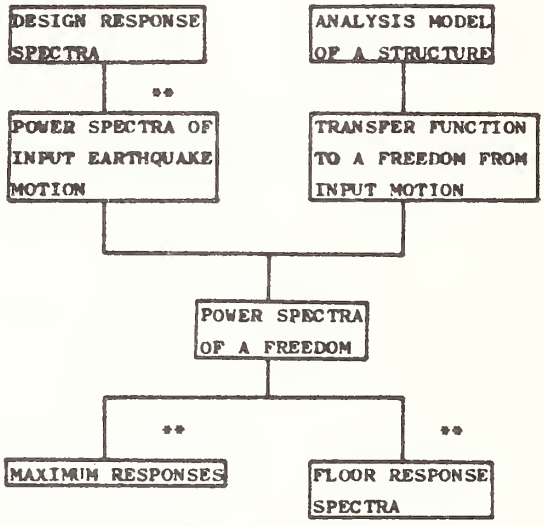

** Random vibration theory

Fig.8 Process of Direct Estimation for Maximum Responses and Floor Response Spectra with Design Response Spectra

Fig.9 Lumped Mass Model

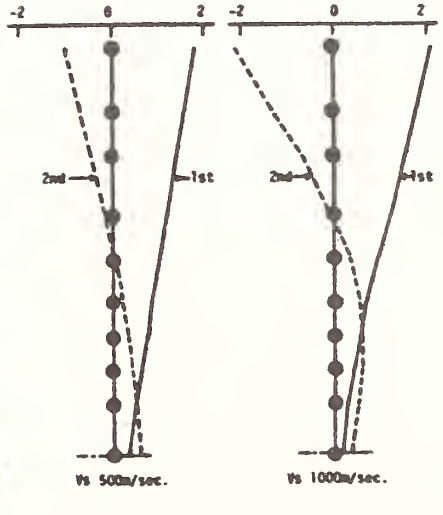

Fig.10 Eigen Vectors multiplied by Participation Factor

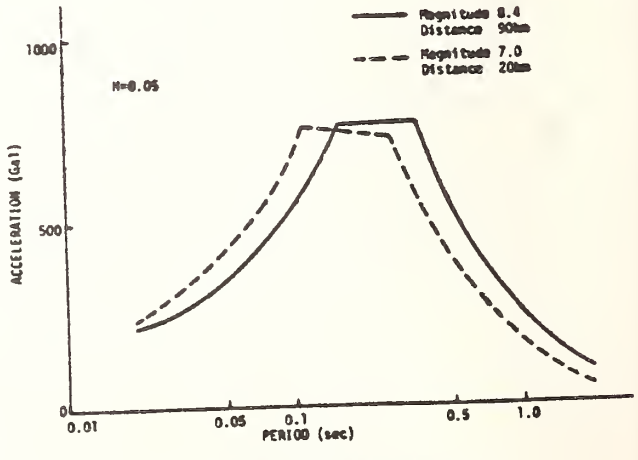

Fig.11 Design Response Spectra

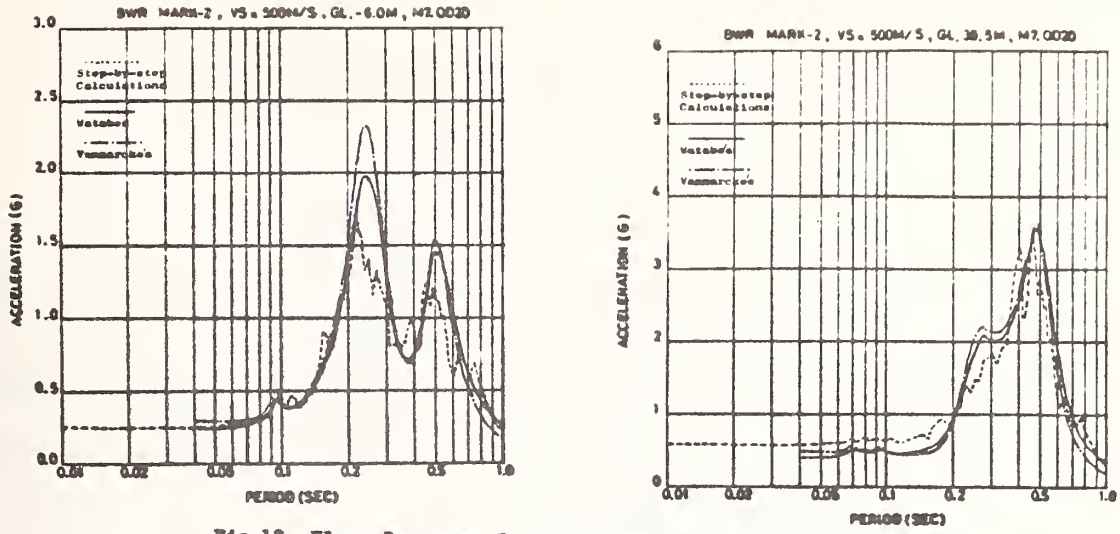

Fig.12 Floor Response Spectra (Damping Ratio 1%); Vs=500m/sec, Magnitude 7.0 and Epicentral Distance 20km

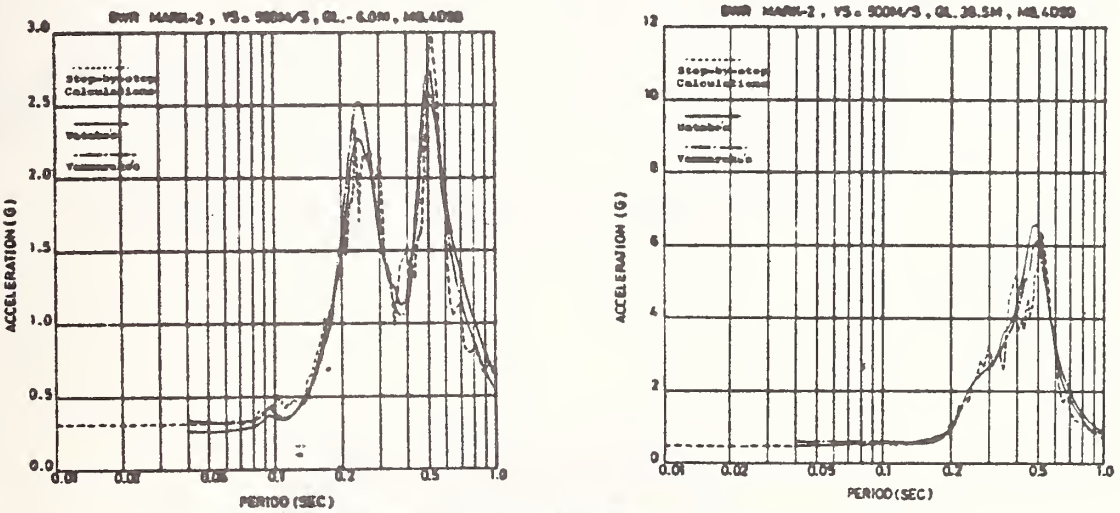

Fig.13 Floor Response Spectra (Damping Ratio 1%); Vs=500m/sec, Magnitude 8.4 and Epicentral Distance 90km

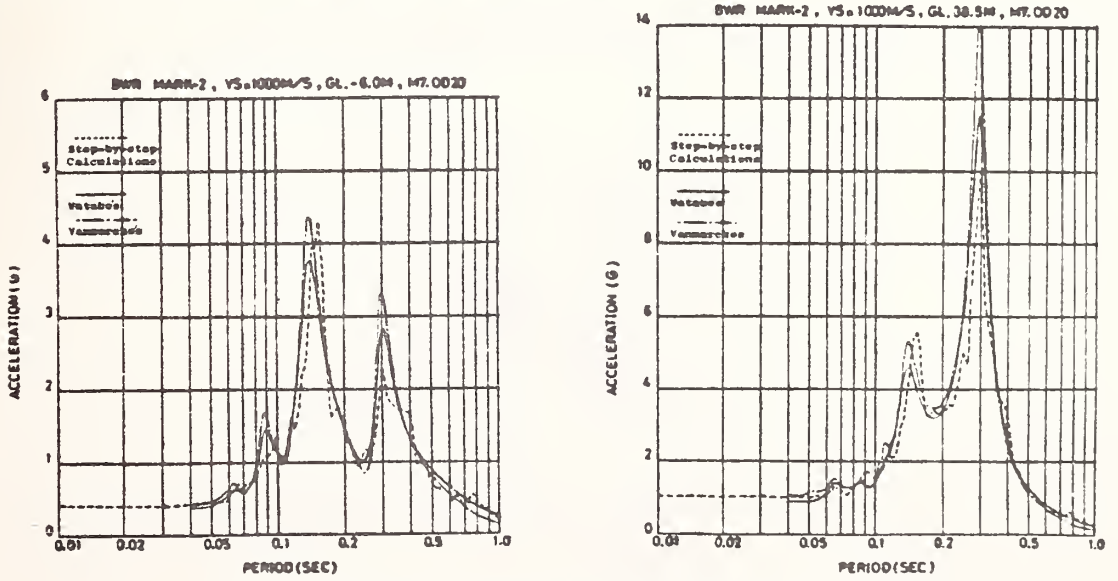

Fig.14 Floor Response Spectra (Damping Ratio 1%); Vs=1000m/sec, Magnitude 7.0 and Epicentral Distance 20km

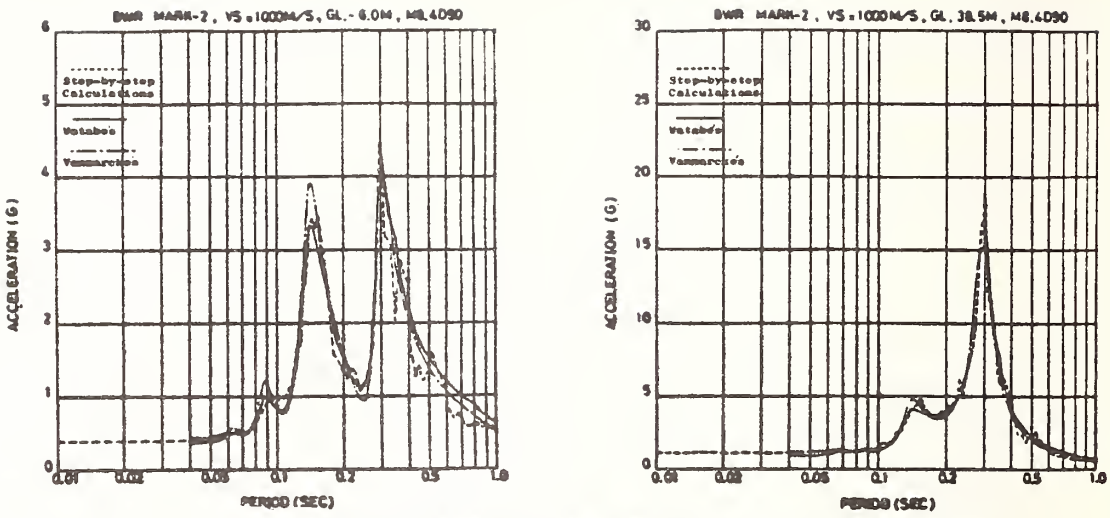

Fig.15 Floor Response Spectra (Damping Ratio 1%); Vs=1000m/sec, Magnitude 8.4 and Epicentral Distance 90km

Fig.16 Simulated Ground Motion generated so as to bit the Design Response Spectra

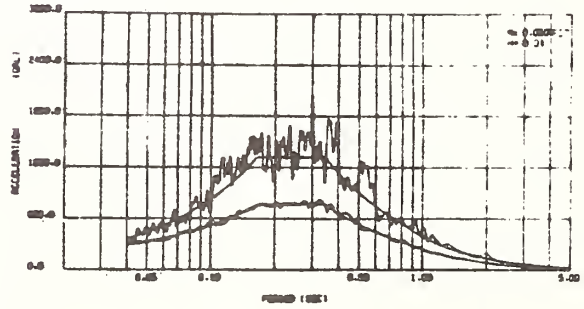

Fig.17 Fitting Status to Design Response Spectra with 5% Dampings and Calculated Response Spectra with 1% Dampings

A PROCEDURE FOR ESTIMATING INDIRECT EFFECTS OF EARTHQUAKES ON ECONOMY

Eiichi Kuribayashi
Toshio Iwasaki
Takeo Nakajima

Public Works Research Institute
Ministry of Construction

ABSTRACT

This paper discusses the economic damage caused by the Miyagi-ken-oki Earthquake of 1978. The earthquake has brought about extensive structural damage and the amount of direct losses has reached 269 billion yen. In consequence of the physical damage, the aftermath of the earthquake lasted about four months and one of the severest effects came out in the reduction of value-added in the local economy. This paper studies the reduction of value-added in Miyagi Prefecture after the Miyagi-ken-oki Earthquake of 1978.

INTRODUCTION

Disaster caused by earthquakes can be classified into two categories, i.e., direct damage and indirect effects. The former represents physical damage to engineering structures and facilities and the latter does social and economic damages which are consequently caused by the former.

For example, in the Kanto Earthquake of 1923, with the Richter magnitude of 7.9, much aftermath was observed in Japanese economy as shown in figures 1 and 2, and table 1. It is seen from these figures that income and tax revenue decreased clearly in 1923 except Osaka. Also in the Izu-Ohshima-Kinkai Earthquake of 1978, economic losses of tourist industry in a certain area were noticed for about six months due to the damage to transportation systems in spite of little structural damage to hotel facilities. Figure 3 and table 2 indicate the decrease in customers to Shimoda City lasted from the outbreak of the earthquake to June 1978.

From these examples it is understood that the economic damage should be taken into account, as well as the physical damage, in planning earthquake disaster mitigation programs.

This paper discusses the economic damage estimated for the Miyagi-ken-oki Earthquake of 1978.

INDIRECT EFFECTS OF EARTHQUAKES

Indirect effects of earthquakes can be classified into economic damage and social damage. Stagnation of industrial activities, decreases in industrial products, individual income, purchasing power, and tax revenue, and expenditure are considered as typical economic damages. Interruption of transportation, electric power, water supply, telephone and telegraph, etc., decreases in civil

services and information services, and unfavorable reputation of damaged areas are considered as typical social damage.

Since economic damage can be evaluated quantitatively, it may be evaluated analytically. On the contrary, it is rather difficult to quantitatively estimate social damage because it is affected qualitatively by social environments. For the reason this paper discusses only the economic damage.

There are two phases in the effects of earthquake disaster on economic damage. One is the negative effects such as the damage to the material and machinery of industry, and decrease in productivity. The other is the positive effects (or economic resistances) such as the increases in demand for materials, equipment and labors for repairing.

The negative effects can be regarded as the economic damage. In the actual economic statistics, however, economic damage is not always conspicuous, because these negative and positive effects interact each other, thus the apparent economic index sometimes recovers quicker than the real index does, as shown in figure 4. Accordingly, the definition of economic damage is important when discussing indirect effects of earthquakes.

In this paper the economic damage is defined as the damage resulted from functional disorder due to physical damage to structures and facilities. It is mainly formed by the reduction of value-added due to stagnation of the industrial activities.

The economic damage can be divided into the following three:

1. Reduction in value-added resulted from the decrease in production caused by the damage to facilities (primary damage).
2. Reduction in value-added resulted from the decrease in production caused by the lack of raw materials and energy supply (secondary damage).
3. Other losses which are affected by the primary and secondary damages (higher order damage).

A flow chart of these processes may be expressed as follows:

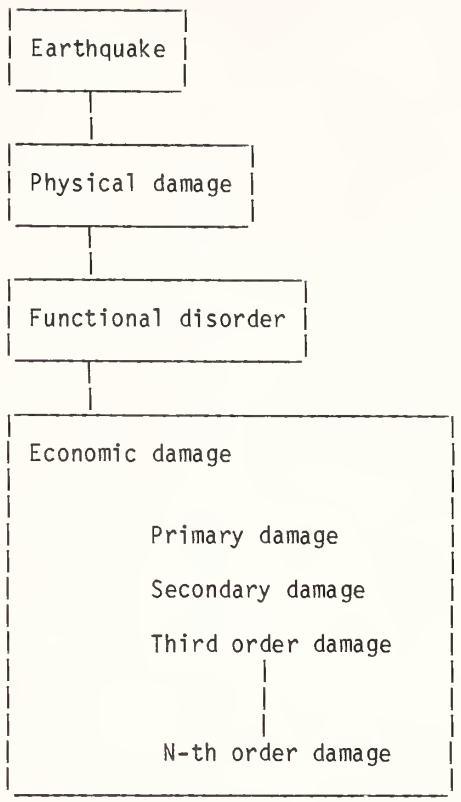

Higher order damages may arise theoretically. For actual cases, however, it may reduce gradually as the order goes up, and will be approximately replaced by other factors. It seems that the higher order damages may be generally negligible. So the effects of the higher order damages are ignored in this paper.

Under the assumption above, the economic damage is considered as the extra expenditure from government sectors (excluding physical damage - such as reconstruction work), plus extra expenditure from the primary and secondary damages to private sectors.

The extra expenditure from the government sectors are as follows:

1. Temporary extra expenditure:
   1) Disaster relief money (based on the disaster relief law);
   2) Condolence money (based on the law of payment of condolence money and loan of disaster aid fund).
2. Grants for supplying loan interest:
   1) Supply of interest of disaster loan.
3. Decrease in revenue:
   1) Tax reduction (based on the law of tax reduction, exemption and grace for damaged people);
   2) Rental fee reduction;

3) Exemption from national health insurance due;

4) Decrease in tax revenue due to decrease in income.

Among the above, the decrease in income tax does not always stand out clearly. Although decreases in income following earthquakes are serious problems, income of some sectors (such as the construction sector) will go up. As a result decrease and increase in income tax may sometimes be cancelled out.

The structure of economic damage can be illustrated as:

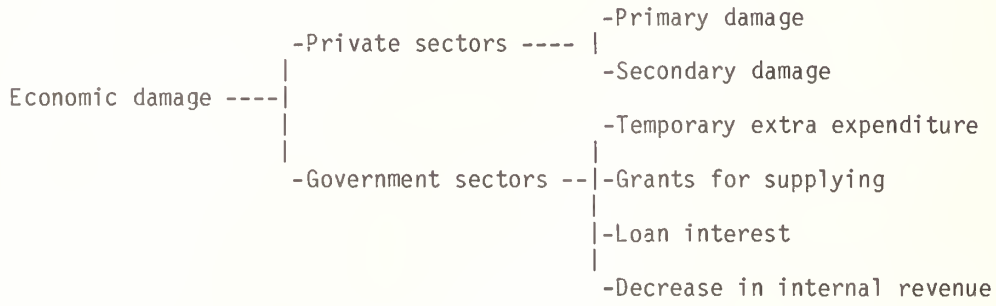

RELATION BETWEEN PHYSICAL DAMAGE AND ECONOMIC DAMAGE

Since economic damage is caused by physical damage, it is the first question whether or not the economic damage can be estimated by the loss of physical damage. If this relation is clear, it will be easier to estimate the overall earthquake disaster including physical and economic damages. However, between them only qualitative relation can be found. As the qualitative relation depends on complicated social phenomena, it is hard to directly estimate the economic damage from the loss of physical damage.

For instance, the breakage of only a small part of a certain facility may cause the stagnation of production in the long-term, the relative functional trouble such as traffic obstruction may reduce the production activity, and the influences of shutdown of computer systems may spread widely to various fields. No consistent rule can be found between them.

As a matter of fact, it is almost impossible to establish mathematical relationships between physical damage and economic damage, thus methods to estimate economic damage may have to be developed independently.

ECONOMIC DAMAGE IN THE MIYAGI-KEN-OKI EARTHQUAKE OF 1978

According to the final report of the Miyagi-ken-oki Earthquake of 1978, the loss of physical damage in Miyagi Prefecture amounts to 268, 760 million yen. It was equivalent to 9.8 percent of the net prefectural product of Miyagi Prefecture in 1978 (2,738,600 million yen), and was nearly equal to the rate of yearly increase in net prefectural product, as shown in figure 5.

The loss of physical damage to various fields are given in table 3. The economic damage follows these damages. Especially, fields related to production activities such as commercial and industrial facilities, public assets (roads, bridges, river conservation, etc.), and public utilities (electric power, gas, water supply, telecommunication, etc.) affect the economic damage significantly. The loss of these three fields consists of about one-half of the total loss, so that a large part of economic damage is supposed to be these three fields. However, the effects of the earthquake on the rate of economic growth in the Miyagi Prefecture that might be reflected by the economic damage was hardly seen in the economic statistics. There is no obvious difference between the rate of the national economic growth and that of the prefectural economic growth, as shown in figure 6.

According to the Miyagi Prefectural economic statistics, the reason why the obvious decrease in economic growth cannot be seen, is explained as follows. The rates of economic growth in some fields are fairly larger than that of net prefectural product (9.8 percent). The rate in banking, insurance, and real estate sectors is 17/6 percent, and that of the construction sector is 15.9 percent. It seems that the construction sector is affected by the demand for reconstruction of dwellings, repair of public assets, buildings, and industrial facilities.

Furthermore, the tax revenue was not affected by the earthquake damage conspicuously. The reason might be that prosperity sectors (such as the construction field) and depression sectors (such as the manufacturing field) interacted, and as a result the tax revenue did not change.

Although the effect of the Miyagi-ken-oki Earthquake is not seen in the annual statistics, the prefectural industrial production indices in monthly data reduced markedly for 3 to 4 months after the outbreak of the earthquake. The comparison of the industrial production indices of the Miyagi Prefecture with that of the Nation is shown in figure 7. This clearly indicates the indices of Miyagi went down for several months. On the contrary, the effect of the Kanto Earthquake of 1923 can be seen in the national economic statistics as shown in figures 1 and 2, and table 1. The decrease in the corporate income in Tokyo caused decreases in the national income and in the tax revenue of the central government.

The Miyagi-ken-oki Earthquake is not a large earthquake as it causes a large economic damage because the economic resistance compensates for the consequential economic damage effectively. The effect of the economic resistance depends widely on years, regions and characteristics of the damage. Therefore, if a larger earthquake attacks the metropolitan area, the economic resistance could not compensate for the economic damage. The case of the Kanto Earthquake is clearly one such example.

In the case of the Miyagi-ken-oki Earthquake, a sudden increase in demand was seen as an aftermath, and the symptoms of inflation rose. If the earthquake damage overwhelmed the economic resistance, the risk of inflation would be predicted.

ESTIMATION OF COST OF ECONOMIC DAMAGE TO LIFELINE FACILITIES

It is found from the previous section that economic damage of an earthquake can be hardly estimated from the economic statistics. One of the keys to grasp the total economic damage is to appropriately sum up economic losses of all companies concerned. An economic loss can be grasped by the difference between a hyopothetical income estimated by ignoring the outbreak of the earthquake and the real income reduced by the earthquake.

The following are examples of calculation of economic losses in typical lifeline utilities for the case of the Miyagi-ken-oki Earthquake of 1978.

GAS SUPPLY UTILITIES

The loss of the gas utilities estimated by Gas Bureau of Sendai City is shown in table 4 [1].

From the table it is found that the loss excluding the removal expense amounts to about 1,037 million yen.

The total loss of the gas utilities caused by the earthquake is estimated by the authors to be 1,092 million yen, as shown in table 5. Out of this amount, the loss due to the indirect damage will be the decreased in gas rate and profits which amount to 131 million yen. The indirect loss is about 12 percent of the total loss. The decrease in gate rate is a reduction and exemption of gas rate for damaged people immediately after the earthquake. The decrease in profit was calculated by summing up the decrease in the gas supply for present customers for 2 months succeeding the earthquake and the decrese in supply for potential new customers to whom the Bureau could not supply gas due to the delay of opening services until December 1978.

Decrease in gas supply for present customers in June and July 1978	3,723,000m^3
Decrease in gas supply for potential new customers	583,000m^3
Unit price	54.15 yen/m^3
Profit ratio	50%

Decrease in Profit = (3,723,000 + 583,000) x 54.15 x 0.5 = 116,585 thousand yen

ELECTRIC POWER UTILITIES

The loss of electric power utilities estimated by the Tohoku Electric Power Company is given in table 6 [2]. This table shows that the total loss amounts to about 3,200 million yen. The loss of the damage to facilities is calculated from repairing expenses. This excludes the decrease in electric rate due to the shutdown of electricity.

The total loss of the electric power utilities caused by the earthquake is estimated by the authors to be 2,100 million yen, as shown in table 7. Among this the decrease in electric rate is regarded as the loss due to the indirect effects. It amounts to 547 million yen and is 26 percent of the total loss. In this table, the loss of the facility damage is not the restoration expense but the loss of residual value.

In this case, the decrease in generated output followed by the power plant damage did not affect the decrease in power supply because another power company (Tokyo Electric Power Company) gave stop-gap aids. The technical assistance from other companies was not much, thus the payment to the assistance was not accounted.

WATER SUPPLY UTILITIES

An estimate of the loss of water supply utilities by the Water Supply Bureau of Sendai City amounts to about 255 million yen as shown in table 8 [3]. The total loss of the water supply utilities caused by the earthquake is estimated by the authors as shown in table 9. The total loss amounts to 307 million yen. Among this the expense for checking water leakage and the expense for temporary water supply services are regarded as losses due to the indirect effects. The sum amounts to 58 million yen, and is equal to 19 percent of the total loss. In this table, the decrease in income is that in water rate from the damaged customers.

In this paper the total loss excludes the loss of leakage. More attention should be given to the loss of leakage water in estimating the total loss. The reason why this is excluded in the total loss estimate is that the volume of leakage water was not available.

ECONOMIC DAMAGE TO LOCAL GOVERNMENT

It is also difficult to grasp the economic damage to the local public bodies. The authors attempted to calculate the loss due to the indirect effects of the earthquake on Sendai City.

According to the Sendai Municipal Government, the total loss in Sendia City amounts to 193,964 million yen as of March 1979. This is the sum of the direct loss due to the physical damage to private and government sectors, as shown in table 10.

The authors calculated the loss due to the indirect effects of the earthquake on the city. The loss amounts to 407 million yen, as shown in table 11. This is only 0.2 percent of the direct loss. Among the indirect loss, the reduction and exemption of taxes, and the decrease in municipal tax revenue followed by the decrease in the individual income are primary factors. The sum of these two is 319 million yen and is 78 percent of the total indirect loss. On the other hand, the settlement revenue of the general account of Sendai City of the fiscal year of 1978 is 312,765 million yen. The total losses of the direct and indirect effects are approximately 62 percent and 0.13 percent, respectively, of the settlement revenue of 1978.

CONCLUSIONS

From the studies shown in this paper the following conclusions can be made:

(1) The economic damage caused by a large earthquake is considered mainly as the reduction of value added. They are as follows:

   a) Reduction of value-added followed by the decrease in production due to facility damage.

   b) Reduction of value-added followed by the decrease in production due to the lack of raw materials and energy supply.

   c) Extra expenditure and revenue decrease in government sectors related to earthquake disaster.

2) For grasping the effects of the economic damage it seems useful to make use of national income statistics. However, the increase in demand followed by the physical damage also arises. This phenomenon can be defined as the economic resistance against the damage, and the resistance sometimes overcomes the stagnation of economic activities, as shown in figure 4. Because of this, the effects of the economic damage might not be seen in macro-scale, when the economic resistance is extensive.

3) The time when the Kanto Earthquake occurred in 1923 was a transition period from the prosperity after World War I to the great depression. The decrease in the real national expenditure was clearly seen, as shown in figure 2. On the other hand, in the Miyagi-ken-oki Earthquake the net prefectural product was independent of the earthquake disaster. The economic resistance depends on the year, earthquake scale, regional characteristics, and the socio-economic background. More investigations should be done in the future.

4) Judging from observations of the relation between the physical damage and the economic damage caused by earthquakes, only qualitative relation rather than quantitative one can be found between them. Therefore, it is almost impossible to make mathematical expressions between them.

5) When estimating the economic damage precisely, it will be necessary to integrate the loss due to the indirect effects on each body in both private and government sectors. In this paper, the loss of gas, electric power and water supply utilities, and Sendai municipal office in the Miyagi-ken-oki Earthquake were calculated. Although it is considered difficult to thoroughly grasp amounts of losses due to indirect damage of private and government sectors, it became rather clear that the losses due to indirect effects can be approximately estimated.

(6) It is almost impossible to grasp and estimate the effects of the economic damage on the long-term economic fluctuations precisely, especially it is hard to estimate how long and how far the effects extend. Seeing from the cases of the Kanto Earthquake of 1923, the Izu-Ohshima-Kinkai Earthquake of 1978 and Miyagi-ken-oki Earthquake of 1978, the indirect effects remain for 4 months to 2 years after the outbreaks of earthquakes. Therefore, it is necessary to further advance the studies on the structure of the economic damage from the viewpoint of both macro-economics and micro-economics.

(7) It will be very important to analyze the following points in the future, through studies on the structure of the economic damage:

Effects of the countermeasure

Economic role of public works after earthquakes

Efficiency of stimulating the private demand after earthquakes

Finance and the monetary policy after earthquakes

ACKNOWLEDGMENTS

The assistance of the Miyagi Prefectural Government, Sendai Municipal Office and Tohoku Electric Power Company for collecting extensive information for this paper are greatly appreciated. The authors also express their appreciation to the helpful advice of Messrs. O. Ueda, T. Tazaki, and M. Shibata given in formulating this paper.

REFERENCES

[1] Gas Bureau of Sendai City, "Records of the Miyagi-ken-oki Earthquake and Repair of Gas Facilities," December 1978.

[2] Tohoku Electric Power Company, "Report on Disasters due to the Miyagi-ken-oki Earthquake of 1978," December 1978.

[3] Water Supply Bureau of Sendai City, "Records of Damage from the Miyagi-ken-oki Earthquake of 1978 and its Countermeasures," October 1978.

Table 1. Economic Fluctuation in the Kanto Earthquake of September 1, 1923

(Thousand Yen)

Item	F.Y.	1920	1921	1922	1923	1924	1925
Income	Japan	3,830,110	4,269,871	4,604,706	4,512,262	4,677,116	4,884,517
	Tokyo	1,040,227	1,027,665	*1,027,665	965,697	1,127,957	1,241,291
	Osaka	553,862	492,452	519,279	545,367	580,760	572,148
Tax	Revenue	696,257	785,852	896,404	787,203	887,238	894,809

After Year Book of Japanese Statistics, Bureau of Statistics

* Note - Since the data of Tokyo in 1922 is lacking, the figure of 1921 is taken as an approximate.

Table 2. Transition of the Number of Guests in Shimoda, Shizuoka Prefecture

Persons

	Jan	Feb	Mar	Apr	May	Jun	July	Aug	Sep	Oct	Nov	Dec	Total
Amended Average (1) 1973-1977	64,883	72,853	96,060	73,335	81,787	60,260	74,346	143,885	64,501	86,642	81,225	41,128	940,905
(2) 1978	37,759	14,689	48,161	46,648	51,030	43,846	77,602	132,863	52,220	67,055	70,409	42,693	684,975
(3) = (2)/(1)	0.582	0.202	0.501	0.636	0.624	0.727	1.044	0.923	0.810	0.774	0.867	1.038	0.728

Table 3. The Losses Due to the Physical Damage Caused by the Miyagi-ken-oki Earthquake of 1978

Field	Million Yen	Percent
I. Dwellings	78,890	29.35
II. Medical and Sanitary Facilities	5,260	1.96
III. Commercial and Industrial Facilities	95,750	35.63
IV. Agricultural, Forestry, and Fishery Facilities	17,220	6.41
V. Educational Facilities	7,590	2.82
VI. Roads, Bridges, and River Conservation	29,160	10.48
VII. Others (Public utilities among others)	35,880 (12,740)	13.35 (4.47)
Total	268,760	100.00

After Miyagi Prefectural Government

Table 4. Rough Estimates of Losses of Gas Utilities Caused by the Miyagi-ken-oki Earthquake of 1978

After Miyagi-ken-oki Earthquake and the restoration of gas utilities, Gas Bureau, Sendai Municipal Office, December 1978

	(Thousand Yen)
(1) Restoration expenses	819,933
(i) Factories	72,348
(ii) Buried pipes	633,425
(iii) Miscellaneous expenses (for mobilization and public relation)	91,160
(iv) Other	23,000
(2) Facilities removal	770,880
(3) Decrease in profit	216,783
Total	1,807,596

Table 5. Losses of Gas Utilities Caused by the Miyagi-ken-oki Earthquake of 1978

	(Thousand Yen)
(1) Restoration expenses	743,657
(i) Factories	71,796
Minato factory	17,954
Haranomachi factory	53,942
(ii) Buried Pipes	629,671
Aids from other companies (excluding personnel payment)	420,312
Materials	56,068
Restoration of roads	69,698
Inspection and repair	56,586
Tools	27,007
(iii) Miscellaneous Expenses	42,190
Traffic expenses	7,224
Pubic relations	7,402
Expendables	12,513
Communication	2,424
Fuel	2,655
Other	9,972
(2) Repair of Supply Facilities to Customers 2,488 cases x @5,000 yen	12,440
(3) Personnel Expenses for Aids	49,638
Staff members 3,524 man-dayx@12,000 yen	42,288
Contractors 490 man-dayx@15,000 yen	7,350
(4) Demolishing of Gas Holder	67,000
(5) Drainage of Gas Pipes	23,000
(6) Overwork Payment in June and July	65,000
Losses due to physical damage (sum of (1) to (6))	960,735
(7) Gas rate Reduction (for Supplied Gas)	14,800
(8) Decrease in Profit (for Unsupplied Gas)	116,585
Losses due to indirect effects (sum of (7) and (8))	131,385
Total	1,093,120

Table 6. Rough Estimates of Losses of Electric Power Utilities Caused by the Miyagi-ken-oki Earthquake of 1978

(After report of damage due to the Miyagi-ken-oki Earthquake of 1978, Tohoku Electric Power Co.)

	(Million Yen)
Hydrogenerating station	1
Thermal generating station	770
Transmission line	220
Substation	1030
Service wire	130
Communication	40
Other	1000
Total	3200

Table 7. Losses of Electric Power Utilities Caused by the Miyagi-ken-oki Earthquake of 1978

	(Thousand Yen)
(1) Losses of the Facility damage	1,552,892
Repair of buildings	264,356
Repair of machinery	789,583
Repair of others	245,356
Miscellaneous expenses	45,314
Removal of fixed assets	41,133
Loss of disposal of fixed assets	167,150
(2) Power Rate Reduction	547,000
Decrease in supply	367,000
Loss due to power stoppage	180,000
(3) Total (sum of (1) and (2))	2,099,892

Table 8. Rough Estimate of Losses of Water Supply Utilities Caused by the Miyagi-ken-oki Earthquake of 1978

(After report on damages caused by the Miyagi-ken-oki Earthquake of 1978 and countermeausres, Water Works Bureau, Sendai Municipal Office)

	(Thousand Yen)
Intake and reservoir facilities	1,800
Clear water facilities	12,400
Water distribution facilities	33,400
Distributing pipes	111,400
Service pipes	13,600
Buildings	5,300
Other	77,100
Total	255,000

Table 9. Losses of Water Supply Utilities Caused by the Miyagi-ken-oki Earthquake of 1978

	(Thousand Yen)
(1) Restoration expenses	
Resorvoir and conduit facilities	510
Clean water facilities	25,846
Distribution and service facilities	203,420
Buildings	7,945
Restoration of roads	4,099
Other	6,796
(2) Leakage checking	56,000
(3) Extraordinary water supply service	2,104
(4) Water rate reduction	716
Sum of losses due to indirect effects (2) to (4)	58,820
Total	307,436

Table 10. Damages Statistics in Sendai City Caused by the Miyagi-ken-oki Earthquake of 1978 (After Sendai City)

(As of March 31, 1979)

Item	Quantity	Loss (Thousand Yen)	Item	Quantity	Loss (Thousand of Yen)
Casualties			Educational Facilities		
Fatalities	13		Elementary schools	64	202,517
Severely injured	170		Junior high schools	28	128,480
Slightly injured	9,130		Senior high schools	26	1,003,785
			Nonregular schools	101	265,534
Subtotal	9,313		Cultural assets	2	6,440
			Subtotal		1,611,756
Dwelling					
Ruined	769	8,181,160			
Half ruined	3,481	1,972,080	Welfare		
Partly damaged	74,487	47,816,030	Nurseries	30	12,000
Furniture	112,874	33,688,260	Social welfare institutions	30	202,234
Gates, fences	42,631	17,395,510			
Public rented houses	2,048	206,208	Subtotal	60	214,234
Subtotal		126,960,248			
			Public Assets		
Medical Facilities			Roads	165	402,627
Hospitals	418	559,200	Bridges	20	92,817
Sanitary facilities	13	116,206	River conservation	84	1,001,322
Refuse disposal facilities	16	200,572	Parks	19	70,744
			Erosion control	1	97,993
Subtotal	447	875,978	Subtotal	290	1,665,503
Commercial and Industry			Urban facilities		
Large business	272	19,578,670	Transportation	23	52,000
Small business	21,934	37,195,510	Water supply	23	265,000
			Sewage	41	37,000
Subtotal	22,206	56,774,180	Gas	370	728,773
			Electric power		2,033,000
			Communication	2,660	850,000
			Public buildings	89	1,110,759
			Subtotal	3,206	5,066,532
Agriculture					
Agriculture production (ha)	100	20,000			
Agriculture facilities	3,935	745,804	TOTAL		193,964,754
Livestock facilities	1	30,454			
Forestry facilities	7	65			
Subtotal		796,323			

Table 11. Losses Due to Indirect Effects in Sendai City Caused by the Miyagi-ken-oki Earthquake of 1978

	(Thousand Yen)
Condolence money	4,250
Tax reduction	153,525
Reduction of taxation charges	128
Reduction of welfare charges	416
Reduction of nursery fees	213
Exemption of national health insurance dues	73,584
Refuse disposal expenses	8,965
Decrease in tax revenue	166,100
Total	407,181

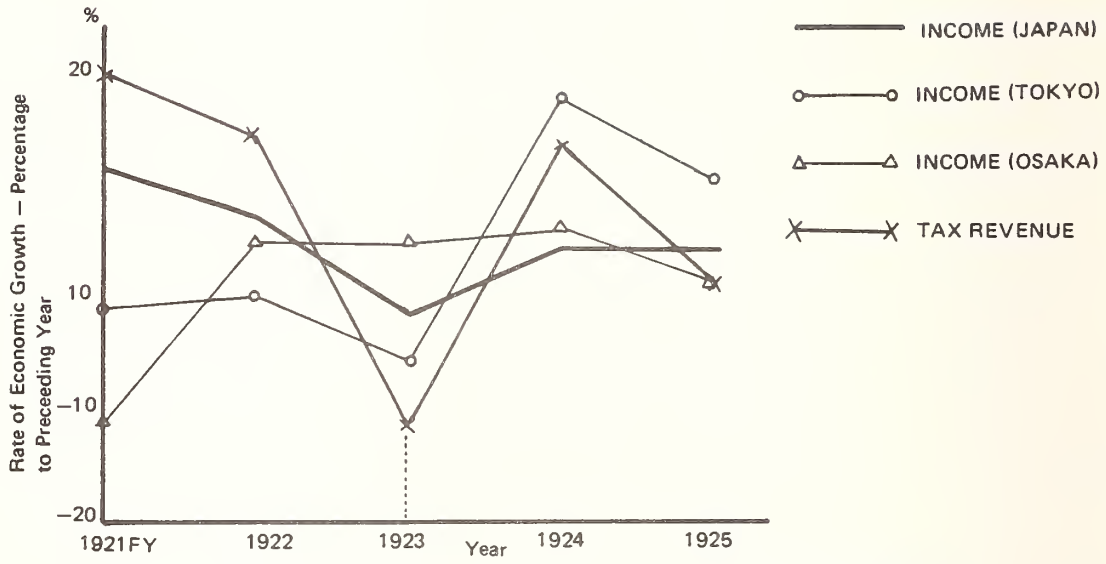

Fig. 1 Economic fluctuation in the Kanto Earthquake of 1923

The decrease of income in Japan and Tokyo and that of tax revenue are seen in 1923, but income in Osaka does not change.

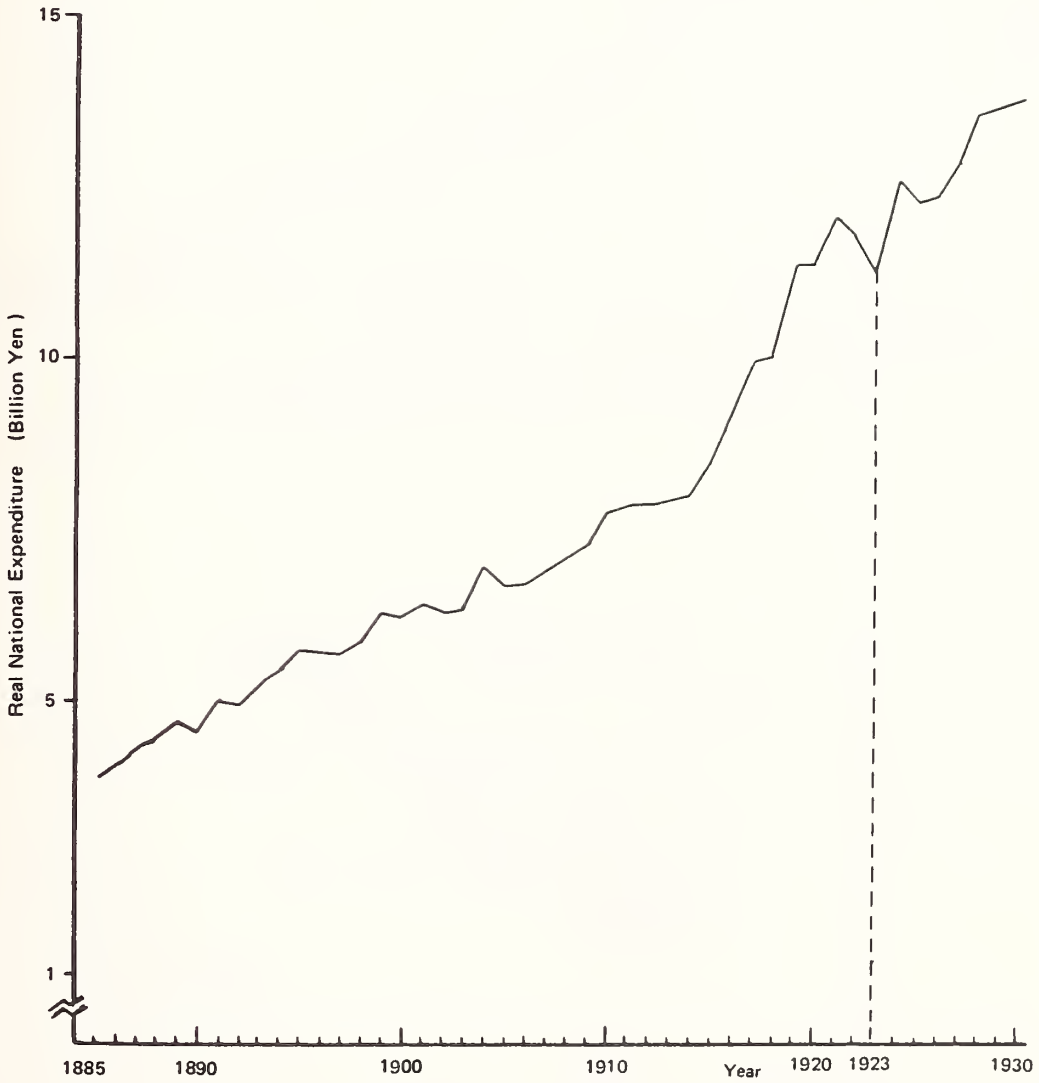

Fig. 2 Fluctuation of real national expenditure in Japan

Source: National Income handbook, Economic Planning agency

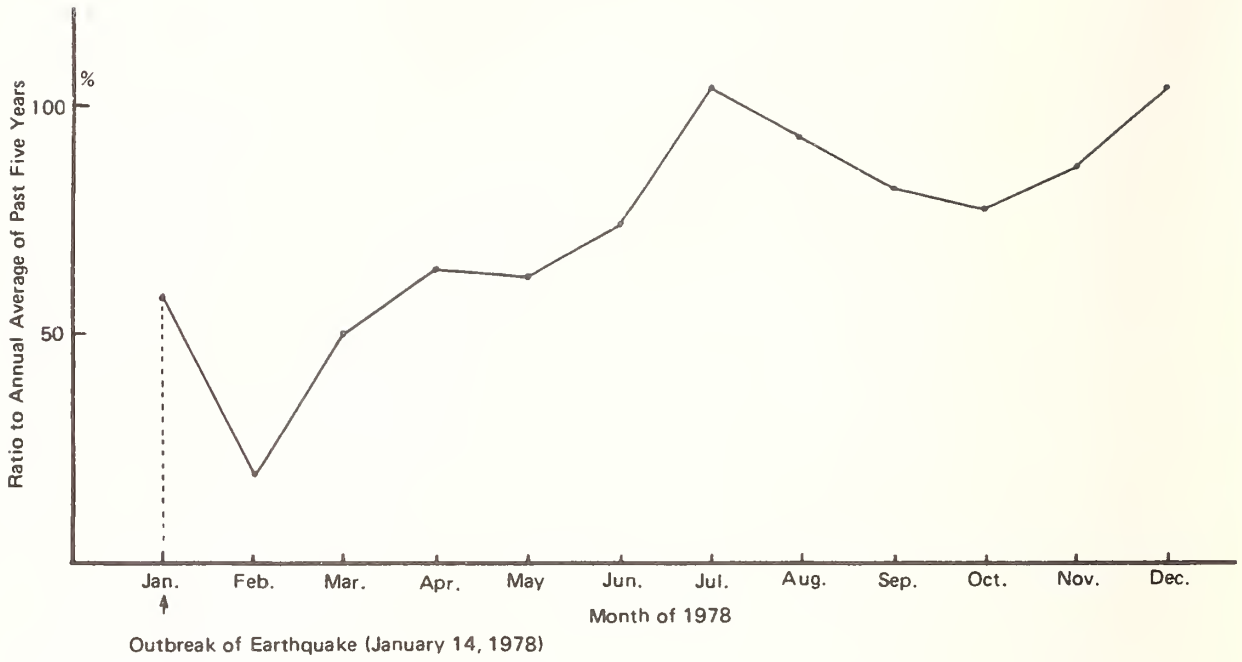

Fig. 3 Transition of the number of guests in Shimoda, Shizuoka Prefecture

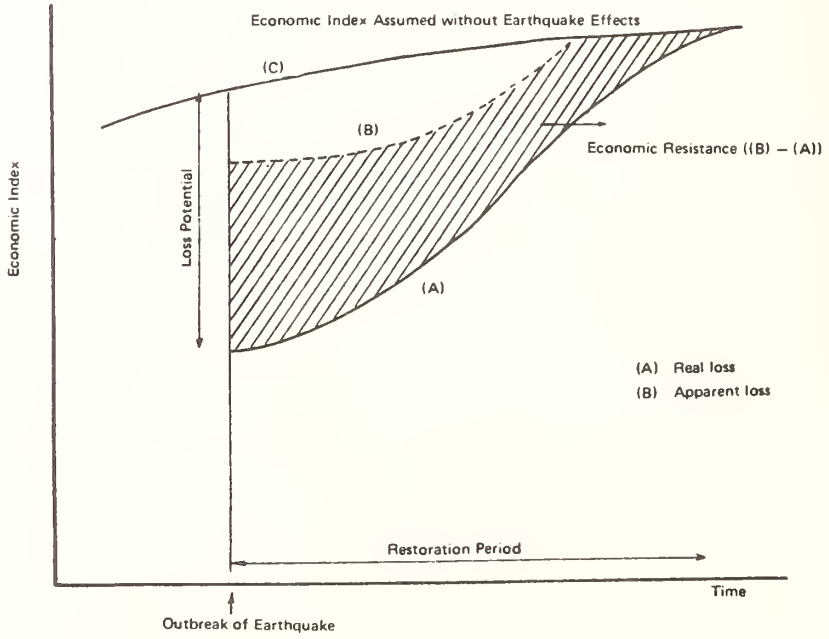

Fig. 4 Economic Resistance in Economic Loss due to Earthquake

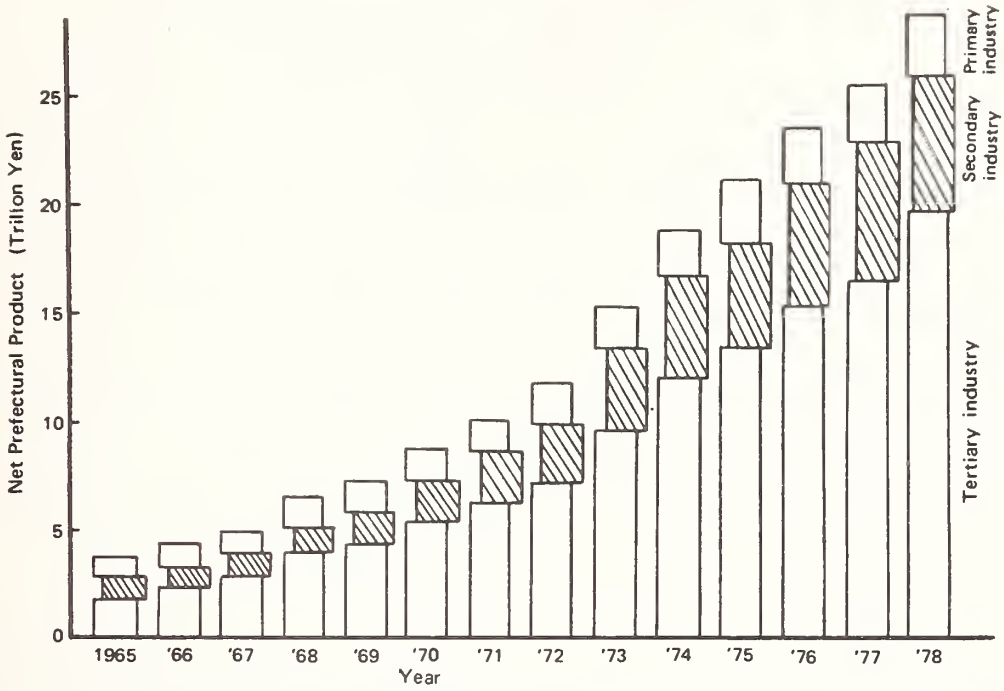

Fig. 5 Transition of industrial origin of net prefectural product in Miyagi Prefecture

(After Prefectural Income Statistics, Economic Planning Agency)

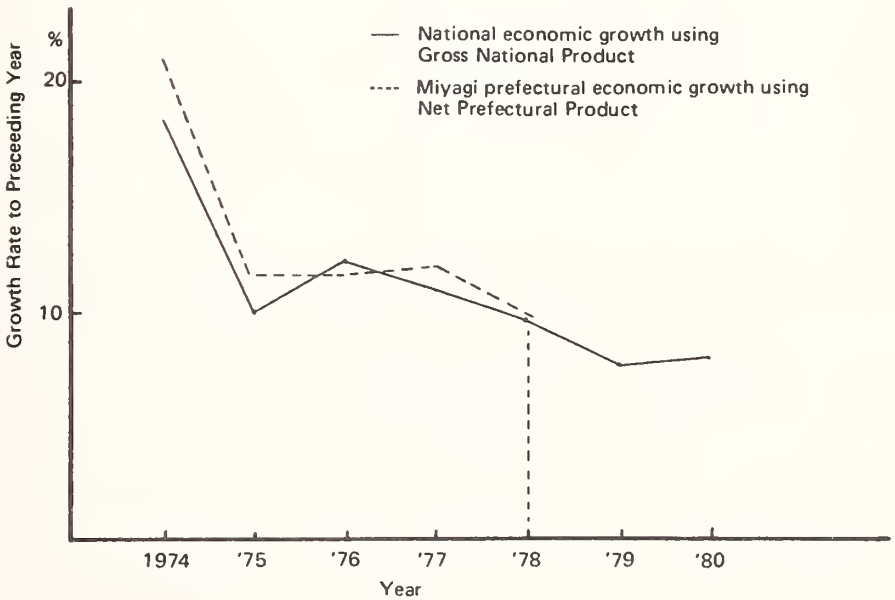

Fig. 6 Transition of the rate of economic growth in the Miyagi-ken-oki Earthquake of 1978

(After Annual Books of National Econimic Accounting and Prefectural Income Statistics, Economic Planning Agency)

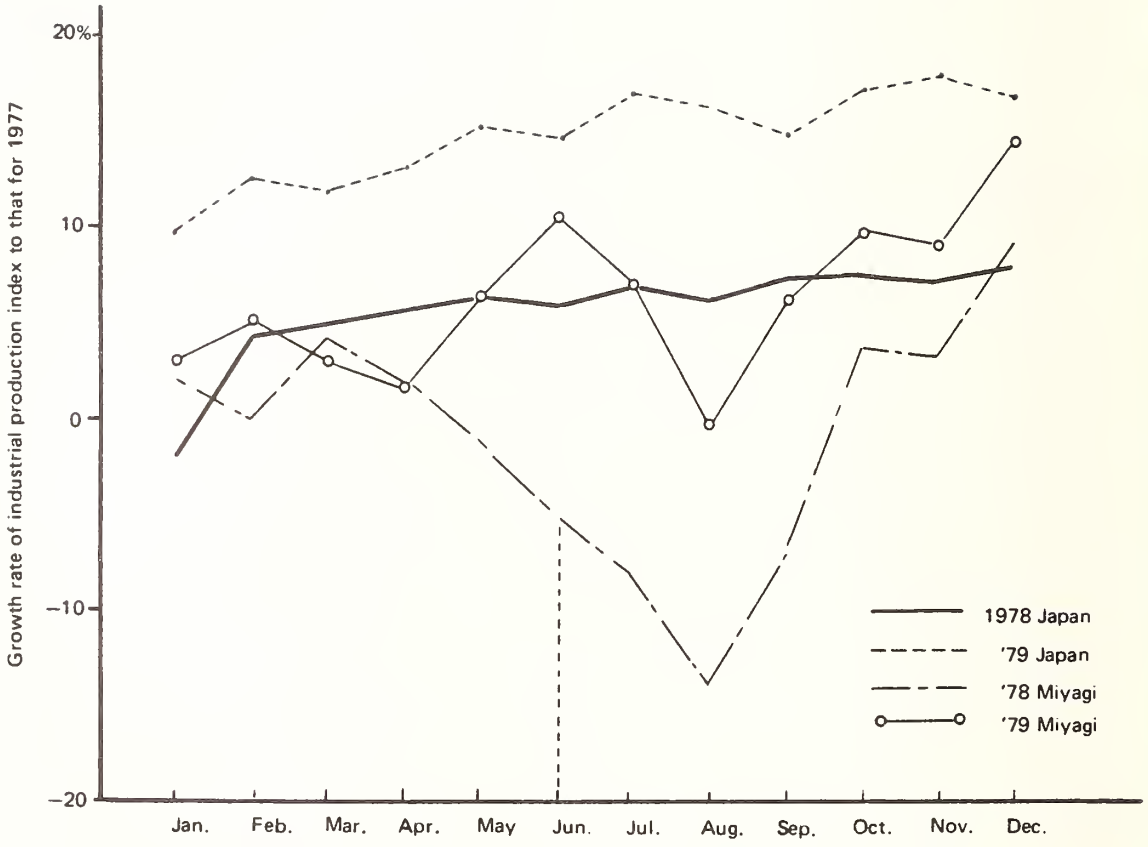

The decrease of the indices caused by Miyagi-ken-oki Earthquake of Jun. 13, 1978 can be seen between June and September.

Fig. 7 Transition of industrial production index

(After Miyagi Statistics, Miyagi Prefectural Office)

DYNAMIC TESTS OF ROCKFILL DAM MODELS

Norihisa Matsumoto, Mitsuo Totoda and Minori Shiga

Public Works Research Institute
Ministry of Construction

ABSTRACT

Dynamic tests of two-dimensional rockfill dam models with a central impervious core were conducted using a shaking table. Heights of the models were 74 cm and 84 cm respectively. Models were excited with horizontal sinusoidal motion and the frequency response functions of the models were obtained.

The response characteristics of the models were compared between full and empty reservoir conditions. The models were also subjected to scaled earthquake motions and the nature of the failure during earthquake motions were compared with the case of the sinusoidal motion input.

INTRODUCTION

Behavior of rockfill dam during earthquake is usually investigated by means of, firstly, numerical computation using material properties obtained from laboratory testing; secondly, analyses of earthquake records observed at prototype dams; and thirdly, dynamic model tests. To design dams to resist earthquakes, the general computational method of analysis is considered to be most effective. However, it is preferable that validity of the computational procedures can be confirmed by comparing with the earthquake records in prototype dams. One of the authors presented the comparison between computational results and observed behavior at the 13th Joint Meeting of the UJNR in Tsukuba. Although the efforts to install strong motion seismographs at prototype dams is continuing, it is still not easy to obtain earthquake records in a short period which can be useful to verify the computational methods. Therefore, model dynamic tests were carried out to verify the computational methods by confirming that the models did reproduce the dynamic response characteristics predicted by the analytical procedure and results of these tests are presented in this paper.

Rockfill dam models made of prototype materials were constructed on a shaking table and they were subjected to both sinusoidal motions and scaled earthquake motions. The frequency response functions of the models were obtained from the accelerations at the dam and the base. The frequency response functions showed nonlinear characteristics, i.e., the natural frequency of the model and the amplification ratio decreases with the increase in input motion of the shaking table, which is consistent with the analytical results. The effects of reservoir and slope of the upstream surface were discussed.

ROCKFILL DAM MODELS

Two-dimensional models were made in the steel rectangular box with the height of 1.5 m, the length of 8.0 m and the width of 2.8 m. Cross sections of the models are shown in figure 1. Materials for models were crushed rock and soils. Of the 6 models tested, 2 were 74 cm high and 4 were 84 cm high, as given in table 1.

Model materials were compacted with hand-vibrator in four layers. Materals for filter and rock zones were placed at their dry conditions and the core was constructed with soils at their optimum water content. Density and water content of the models are summarized in table 2. 29 accelerographs were installed in models No. 1 and 2 and 17 in models No. 3 through 6.

EARTHQUAKE SIMULATOR FACILITY

Dynamic tests were performed using the earthquake simulator facility for dams at the Public Works Research Institute, Ministry of Construction. This facility includes a 4 m by 4 m "shaking table" or earthquake simulator, the dynamic triaxial compression testing equipment for embankment dam materials and the dynamic uniaxial testing equipment for concrete. Main features of the shaking table are shown in table 3. The 12.0 m high, 16.5 wide and 34.6 m long building which houses this equipment is serviced by two 20 and 5 ton bridge cranes.

NONLINEAR CHARACTERISTICS OF THE MODELS

Model No. 1 was subjected to sinusoidal motion with the frequency ranging from 5 Hz to 70 Hz while the acceleration amplitude was maintained constant. Figure 3 shows the frequency response function of the crest of the model to the base i.e., the ratio of the peak acceleration between the dam crest and the base as a function of the frequency of the input motion. Figure 3 indicates that the first natural frequency, which was 31 Hz for the input excitation of 10 gal, decreased with the increase of input motion, and it reduced 12 Hz for the input excitation of 200 gal. Assuming that the first natural frequency of the model is proportional to $\sqrt{\frac{G}{\rho}}$, where G is the shear modulus of elasticity and ρ is the density, G for 200 gal input motion is 15 percent of G for 10 gal input motion. The amplification ratio also decreased from 15 to 6, thus indicating that the damping increases with the increase of input acceleration.

Figure 4 shows the distribution of maximum response acceleration in the model at the resonant frequency. It is known that vibration of the model was in shear motion and the amplification ratio of the dam decreased with the increase of input motion.

RESERVOIR EFFECTS

Model No. 2 was constructed with the same material and the same dimension as model No. 1. However, water was stored on the upstream side of this model. The frequency response function of model No. 2 is shown in figure 5 in comparison with that of model No. 1. In figure 5, it is shown that the natural frequency and the amplification ratio of the model decreased when the reservoir was filled with water. This indicates that the shear modulus of the model materials became smaller and the damping became larger by saturation.

Denoting the average damping ratio of the rockfill dam to be h, the amplification ratio of the crest to the base is approximately 1/h according to the results of several examples of dynamic analyses of rockfill dams. The damping ratios shown in figure 6 are estimated using this relationship. Figure 6 indicates that the damping ratio ranges from 5 to 12 percent when the reservoir is empty and 10 to 25 percent when the reservoir is filled.

EFFECTS OF UPSTREAM SLOPING

Models No. 3 through 6 were constructed using the same material. These models also had the same cross-section except that models No. 3 and 4 had an upstream slope of 2.5H: 1V and models No. 5 and 6 had a slope of 3.0H: 1V. The effect of upstream sloping is shown in figure 7 which suggests that flattening the upstream slope from 2.5H to 3.0H to 1V results in a slight decrease in first natural frequency of the model and the amplification ratio. At the second natural frequency, the amplification ratio decreases considerably.

EXCITATION BY EARTHQUAKE MOTION

The earthquake simulator facility is capable of excitating the shaking table by a prescribed earthquake motion. Models No. 3 through 6 were subjected to two kinds of earthquake motion recorded at two damsites, i.e., Tarumizu Dam and Naruko Dam. Since natural frequency of the model is about 20 Hz, the recorded accelerograms were scaled to cover the frequency range of the significant modes of the model. Time history of the acceleration at the base and crest, are shown in figures 8 through 11.

COLLAPSE OF MODELS

Tests presented above were under relatively small amplitude excitation. Each model was subjected to an excitation up to 400 gal at the shaking table. During sinusoidal excitation, with the increase of input motion unstable cobbles on the slope surface fell at the natural frequency excitation. With further increase of the input motion, the shallow surface at the downstream slope slipped and the core and shell zones were separated at the crest. If the collapse of the model is defined as the separation of the core and shell zones, both models No. 1 and 2 collapsed when the acceleration of

separation of the core and shell zones, both models No. 1 and 2 collapsed when the acceleration of the shaking table was about 125 gal r ırdless of the reservoir condition. In this case, the peak acceleration at the top of the dam was 600 gal for the empty reservoir and 400 gal for the full reservoir. Models No. 3 through 6 which were excited by earthquake motion did not collapse up to a peak acceleration of 400 gal. Duration of the shaking at the resonant frequency was necessary to damage the rockfill dam model.

CONCLUSIONS

Conclusions obtained from the tests presented herein are given below:

1. Nonlinear response characteristics of the model were obtained from the sinusoidal excitation tests. With the increase of the input motion from 10 gal to 200 gal, the natural frequency of the model decreased to 40 percent of the initial value, and the shear modulus of the model materials was estimated to decrease to 15 percent of the initial value. Average damping ratio of the model increased from 5 percent to 12 percent when the reservoir was empty, to 10 percent to 25 percent where the reservoir is filled.
2. Models No. 1 and 2 subjected to sinusoidal motion collapsed at the level of base motion of 125 gal. Models No. 3 through 6 subjected to scaled earthquake motions did not collapse up to a peak acceleration of 400 gal. It is thus concluded that duration and frequency of the base motion are influential to the collapse of the model.

Table 1. Dimensions of Rockfill Dam Models

Model No.	Height (cm)	Slope		Reservoir	Excitation
		Upstream	Downstream		
1	74	2.8 : 1	2.0 : 1	Empty	Sinusoidal motion
2	74	2.8 : 1	2.0 : 1	Full	Sinusoidal motion
3	84	2.5 : 1	2.1 : 1	Full	Tarumizu record*
4	84	2.5 : 1	2.1 : 1	Full	Naruko record**
5	84	3.0 : 1	2.1 : 1	Full	Tarumizu record
6	84	3.0 : 1	2.1 : 1	Full	Naruko record

* Earthquake motion recorded at Tarumizu Dam in 1978.
** Earthquake motion recorded at Naruko Dam in 1978.

Table 2. Density and Water Content of Materials

Model No.	Wet Density (g/cm)		Dry Density (g/cm)		Water Content	
	Core	Rock	Core	Rock	Core	Rock
1	1.593	1.710	1.262	1.675	26.2	2.1
2	1.607	1.710	1.305	1.675	23.1	2.1
3	1.188	1.999	0.961	1.987	23.6	0.6
4	1.193	1.959	0.989	1.947	20.6	0.6
5	1.200	1.921	0.979	1.910	22.6	0.6
6	1.193	1.984	0.978	1.970	22.0	0.7

Table 3. Main Features of Performances

Table	Steel deck structure Size : 4.0 m x 4.0 m Weight : 13.5 ton
Maximum loading capacity	40 ton
Maximum stroke	+ 100 mm in the horizontal direction $\mp$ 50 mm in the vertical direction
Maximum acceleration	+ 1.0 g in the horizontal direction $\mp$ 1.0 g in the vertical direction
Exciter	Horizontal : two 29.5 ton actuators Vertical : four 27.3 ton actuators
Direction of excitation	Biaxial of one horizontal and vertical
Input motions	Sinusoidal and arbitrary motions

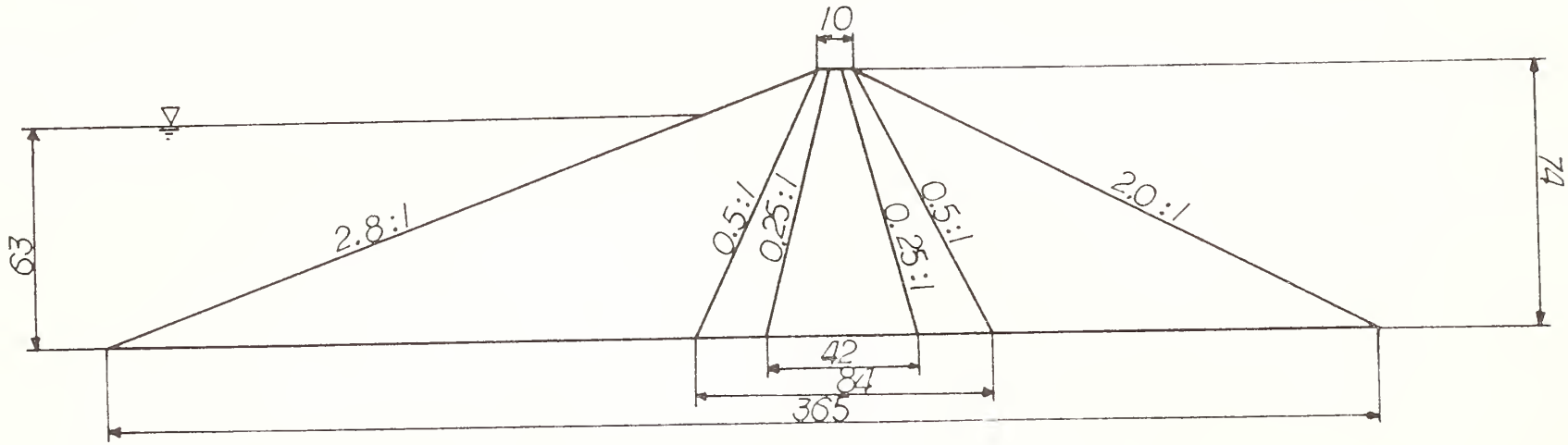

(a) MODEL NO. 1 TO 2

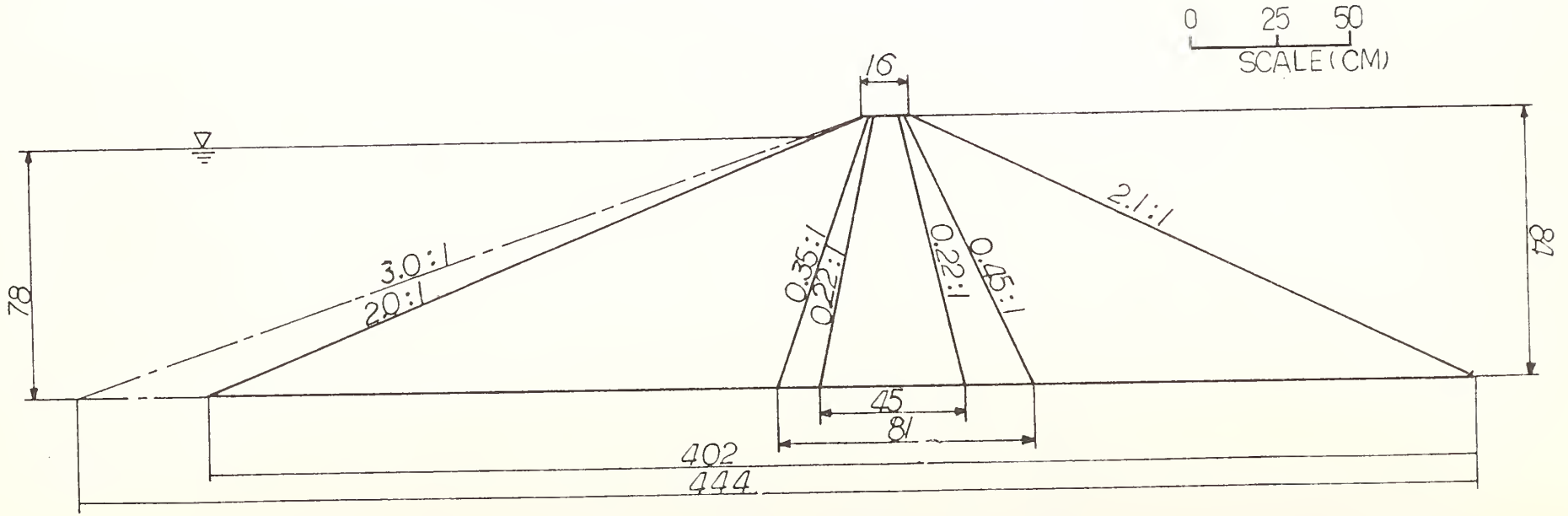

(b) MODEL NO.3 TO 6

Figure 1. Cross section of models

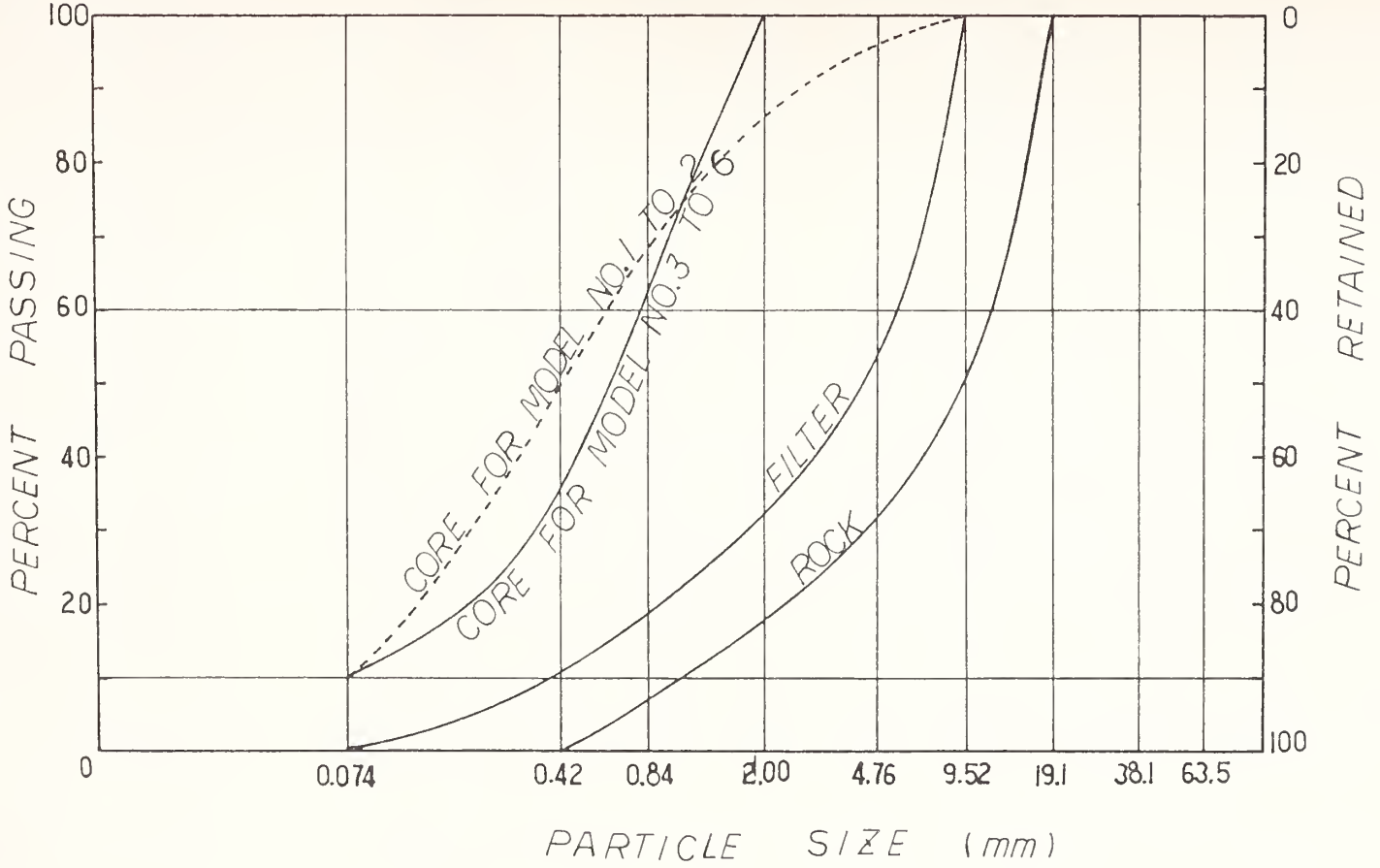

Figure 2. Gradation of materials

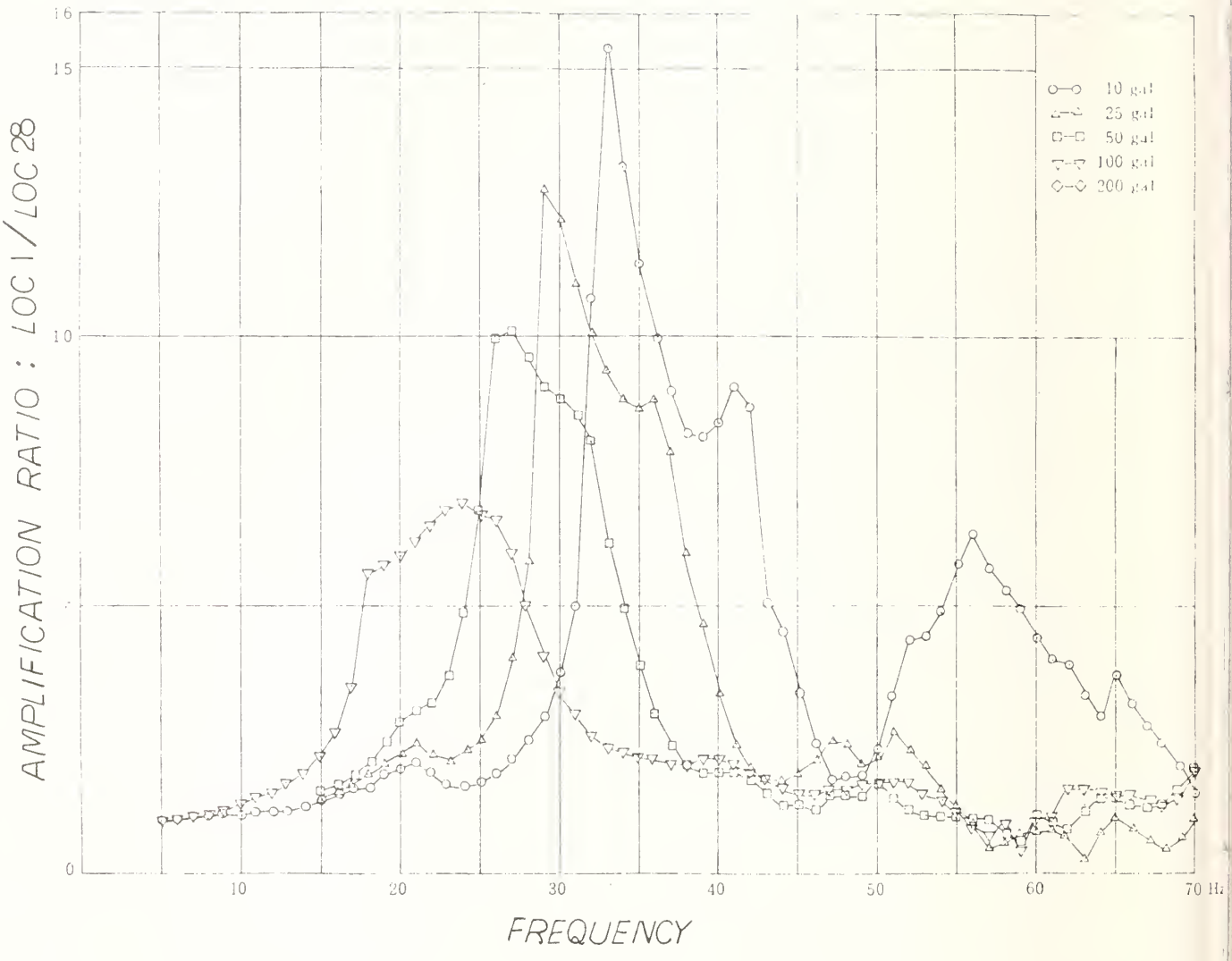

Figure 3. Frequency response function of model no. 1

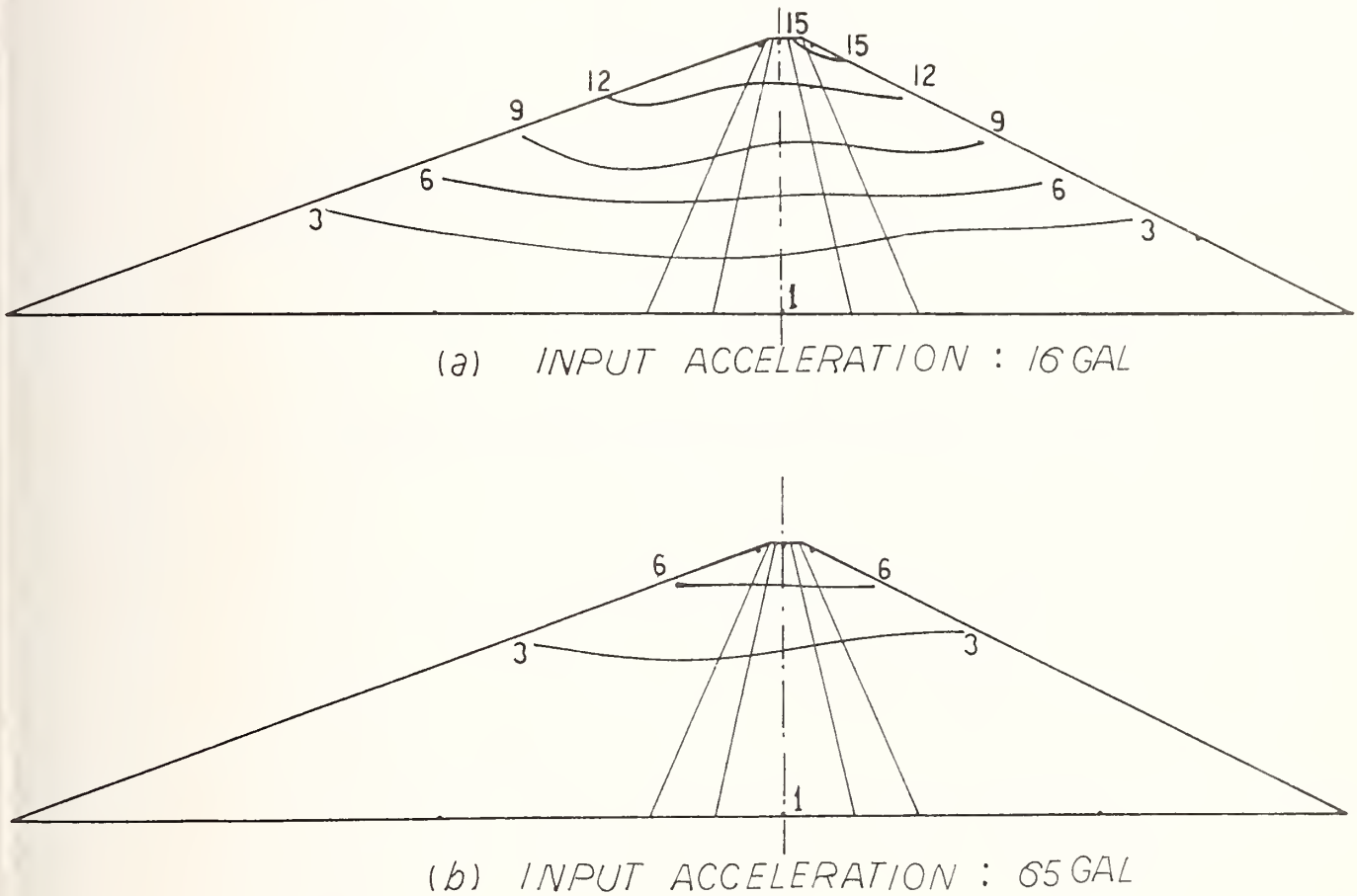

Figure 4. Distribution of maximum response acceleration ratio

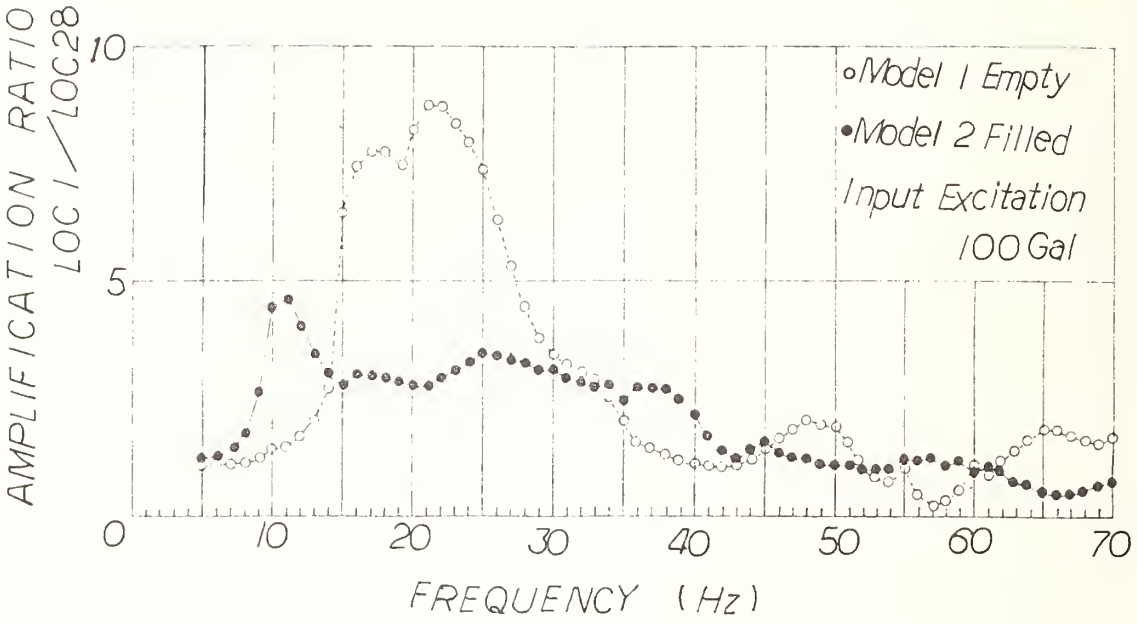

Figure 5. Frequency response function of model nos. 1 and 2

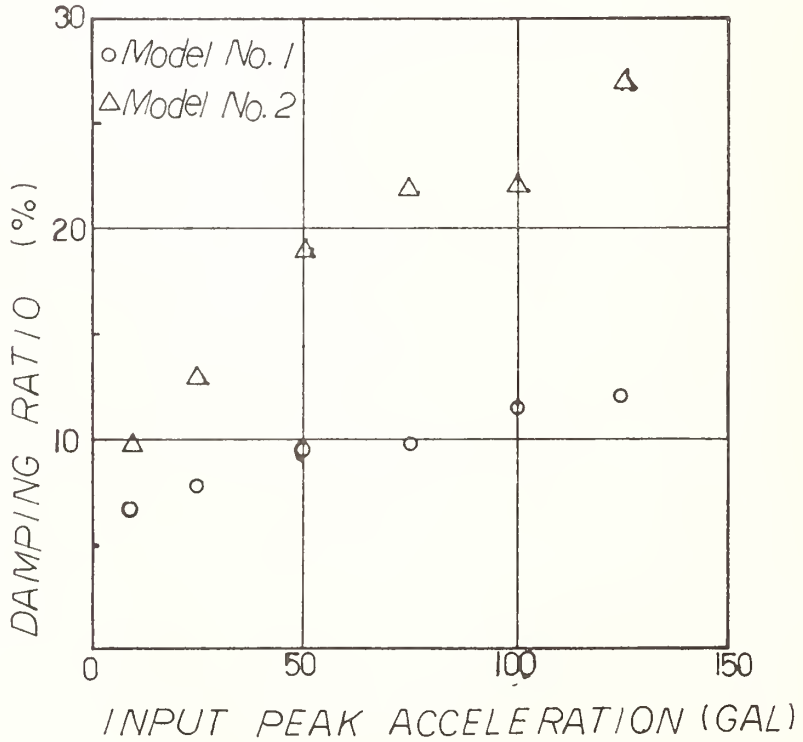

Figure 6. Average damping ratio

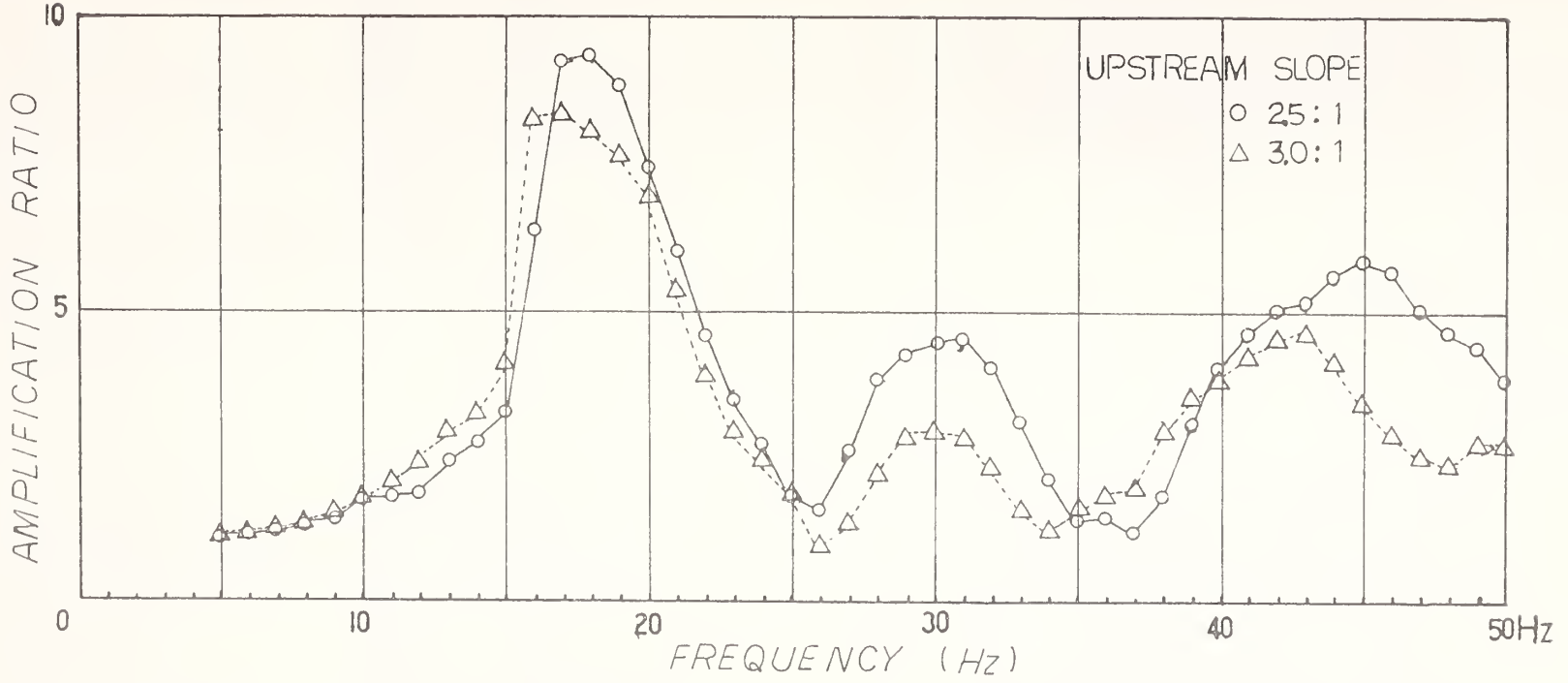

Figure 7. Effects of upstream sloping

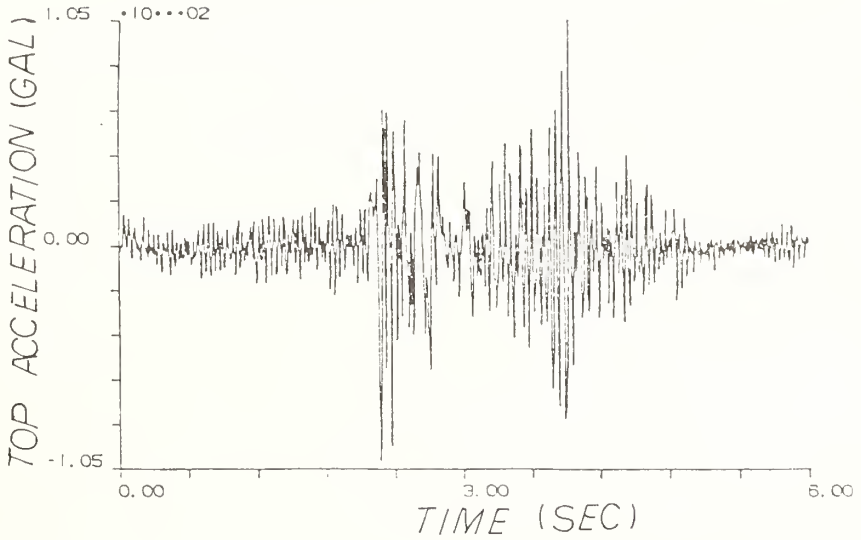

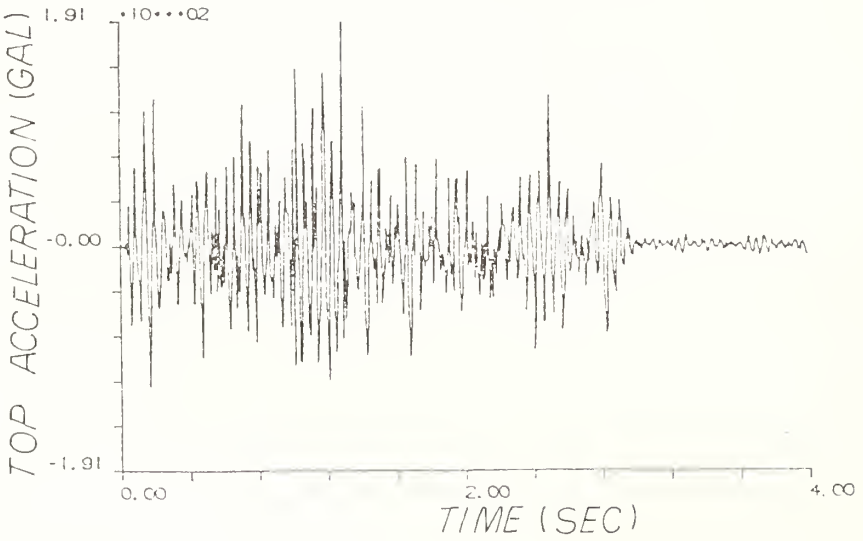

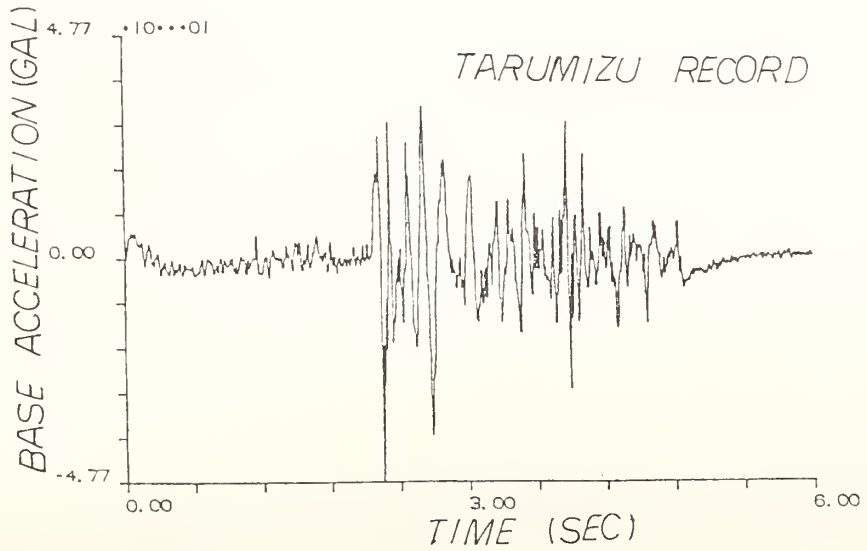

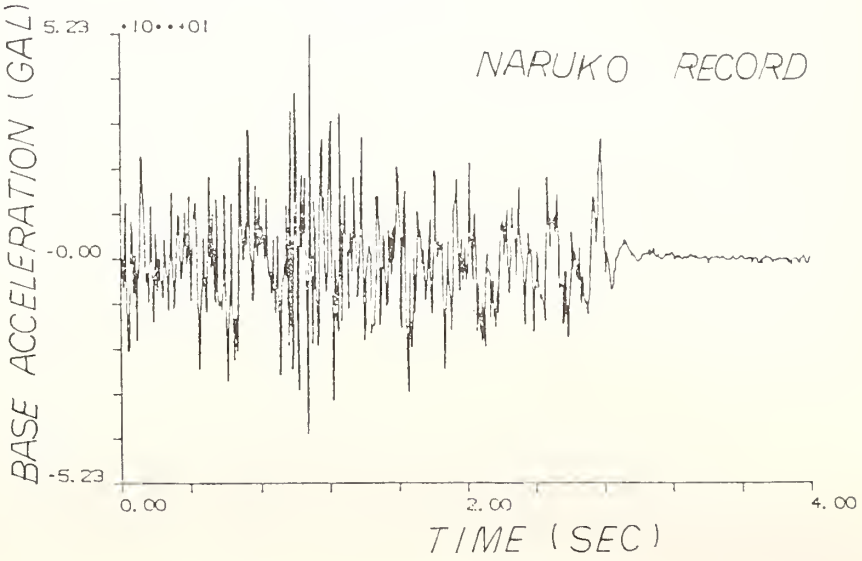

Figure 8. Time history of model no. 3

Figure 9. Time history of model no. 4

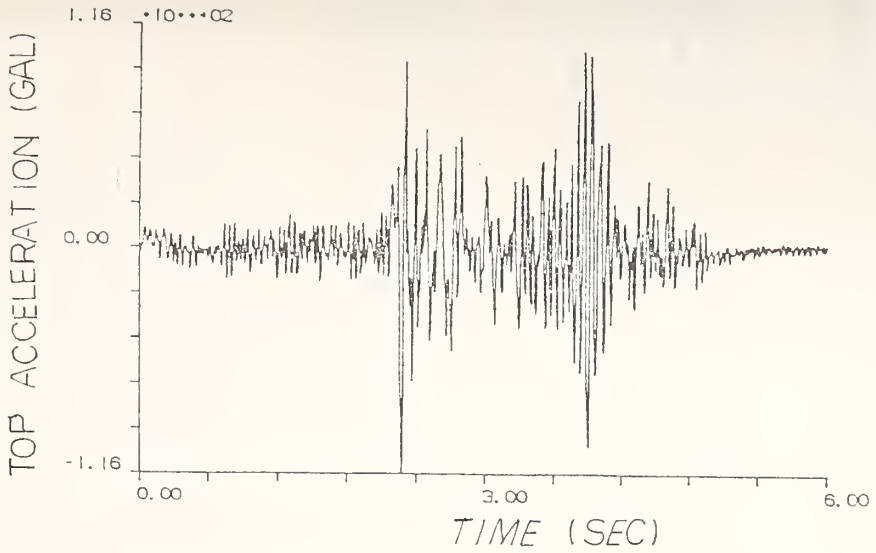

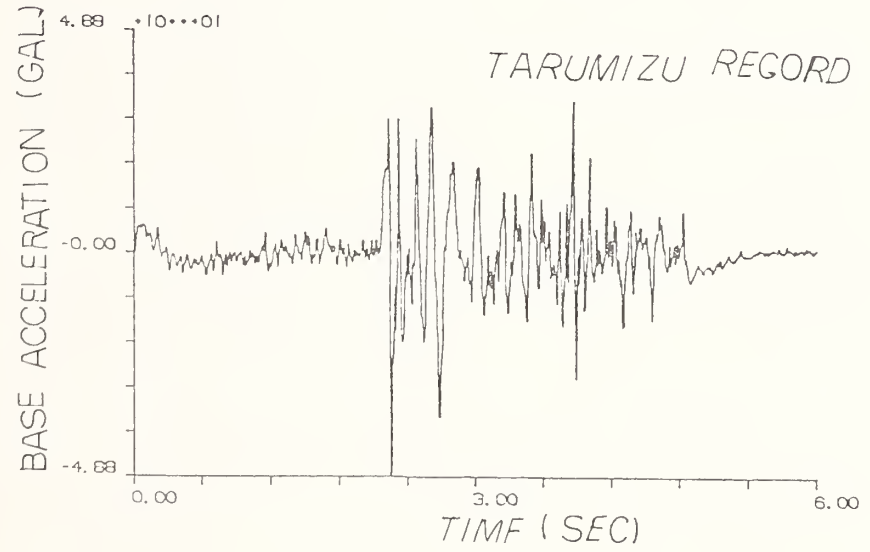

Figure 10. Time history of model no. 5

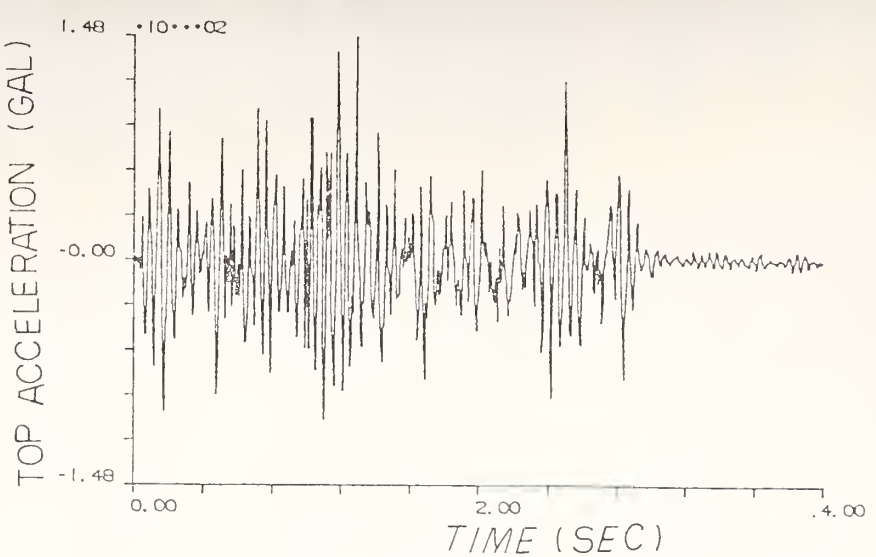

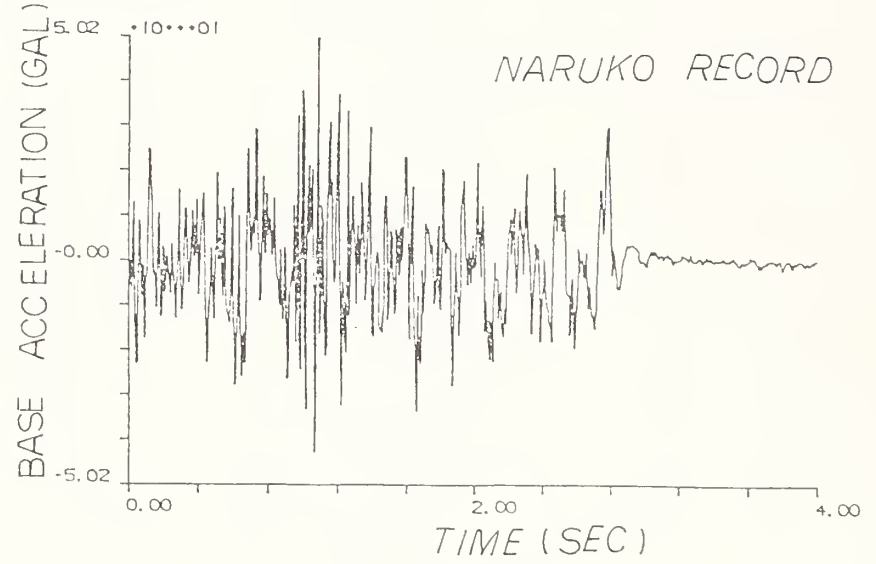

Figure 11. Time history of model no. 6

THE CONNECTING METHOD FOR PILE HEAD AND FOOTING OF PILE FOUNDATIONS SUBJECTED TO A HORIZONTAL LOAD

Nobuyuki Narita
Hideya Asanuma
Jiro Fukui
Yoji Yamamoto

Public Works Research Institute
Ministry of Construction

ABSTRACT

It is necessary for the foundation of a bridge structure to efficiently transmit the load from the superstructure to the ground. In the case of a pile foundation, in particular, it is necessary to give sufficient consideration to the safety of the connection of pile head and footing because of sudden changes in cross section and rigidity. Various connecting methods have been developed. However, there remain many points which need to be clarified with regard to the ultimate strength, load-deformation characteristics, etc. of the connection.

INTRODUCTION

In the case of a pile foundation, the connection of the pile head and footing tends to form a weak point in the structure because of the sudden change in cross sectional area and resulting stress concentration. Various connecting methods have therefore been devised. The current Specifications for Highway Bridge Part IV: Substructure, provides that the connection be based on a rigid connection as a rule, and prescribes two types of connecting methods.

In Method A, the piles are embedded into the footing to the depth of their diameter. In Method B, the piles are embedded 10 cm into the footing and reinforced by steel bars. Though these methods have proved to be safe, the ultimate strength or the dominant parameter which determines it, are not fully understood. Moreover, the development of a simpler connecting method from the viewpoint of construction is needed.

The tests described herein are intended to obtain basic data for simplifing the connecting method of a steel pipe pile and a footing. This will be accomplished by ascertaining the ultimate strength and the stress transfer mechanism of the connection subjected to a horizontal and bending load for different connecting methods and by comparing the results.

CONNECTING METHODS PRESCRIBED BY THE SPECIFICATIONS FOR HIGHWAY BRIDGES

The connecting and design method prescribed by the current Specifications for Highway Bridges are outlined below.

(1) Connecting Method

The piles and footing shall be connected by either of the following two methods.

Method A: The piles are embedded to a definite length into the footing so as to resist the pile head restraining moment by the embedded parts of the piles.

Method B: The piles are not so deeply embedded in the footing and reinforced mainly by steel bars, thereby resisting the pile head restraining moment.

(2) Design Method

1) Designing by Method A

a) The piles and footing are rigidly connected together and so designed to be able to resist all forces acting on the pile head such as driving and pull-out forces, horizontal force and moment.

b) The pile heads are embedded at least as much as the pile diameter into the footing.

c) Vertical bearing stress of footing concrete

$$\sigma_{cv} = \frac{P}{\frac{\pi}{4}D^2} \leqq \sigma_{ca}$$

d) Horizontal bearing stress of footing concrete

$$\sigma_{ch1} + \sigma_{ch2} \leqq \sigma_{ca}$$

$$\sigma_{ch1} = \frac{H}{D\ell}$$

$$\sigma_{ch2} = \frac{6M}{D\ell^2}$$

e) Punching shear stress of footing concrete

$$\tau = \frac{P}{\pi(D+h_1)h_1} \leqq \tau_a$$

f) Cover plate and cross reinforcing plate

$\tau_1 = \tau_2 = 2$ mm, $h_2 = 30$ cm

g) With regard to the piles at the edge of the footing, the horizontal punching shear stress is considered to be in compliance with Article 120 of the Specifications for Reinforced Concrete.

where,

σ_{cv}: vertical bearing stress (kg/cm^2)

σ_{ch1}: horizontal bearing stress caused by horizontal force (kg/cm^2)

σ_{ch2}: horizontal bearing stress caused by moment (kg/cm^2)

τ: punching shear stress (kg/cm^2)

σ_{ca}: allowable bearing stress of concrete (kg/cm^2)

τ_a: allowable shear stress of concrete (kg/cm^2)

P: driving force (kg)

H: horizontal force (kg)

M: moment (kg•cm)

D: pile diameter (cm)

ℓ: embedded length of pile (cm)

t_1: thickness of cover plate (mm)

h_1: distance from pile head to the top surface of footing (cm)

t_2: thickness of cross reinforcing plate (mm)

h_2: height of cross reinforcing plate (cm)

2) Designing by Method B

a) The piles and footing are rigidly connected together and designed to resist all forces acting on the pile heads, such as the driving and pull-out forces, horizontal force, and moment.

b) The pile heads are embedded 10 cm into the footing.

c) A study shall be made in accordance with the design of steel pipe piles by methods A; c), e), f), and g).

d) Horizontal bearing stress of footing concrete.

$$\sigma_{ch} = \frac{H}{D\ell} < \sigma_{ca}$$

e) Stress of virtual reinforced concrete section.

When driving force P and moment M or pull-out force P_t and moment M act, the reinforced concrete section is assumed to consider the stresses of concrete and reinforcing bars.

f) Anchorage of reinforcing bars

1) Shear stress of weldments

$$\tau_s = \frac{\sigma_{sa} A_{st}}{1.4\lambda\ell_0} \leq \tau_{sa}$$

2) Anchorage length of reinforcing bar

$$L_0 = \frac{\sigma_{sa} A_{st}}{\tau_{0a} \cdot u}$$

In general, $L_0 = 35\ d$

OUTLINE OF THE TEST

Testing was conducted in 14 cases shown in table 1 by means of changing the parameter which seemed to exercise influence on the ultimate strength of the connection subjected to horizontal and bending load. In series A, specimens were constructed according to method A, and series B to

Method B. Figure 4 shows a general plan of the standard specimen and figure 5 shows the details of the connection of each specimen.

Figure 6 shows the loading method whereby the specimen was turned over with line bearing support at four points of the footing and static horizontal load was applied to the pile section 60 cm from the footing face. Displacement and strain were measured for each loading stage and the distribution of cracks in footing was observed. Details of the positions of the displacement gauge and of the strain gauge will be omitted.

TEST RESULTS

Figures 7, 8, and 9 show the relationship between the load and horizontal displacement at the loading point. Figure 7 is based on the specimens in series A, figure 8 on the specimens in series B with a different number, angle, and installation of steel bars, and figure 9 on the specimens in series B with a different composition of pile heads. The following points merge from the above figures.

1) In both series, all specimens showed roughly the same initial slope, showing no effect on the parameter.

2) In series A, the curve began to bend around the crushing point of the footing concrete on the backside of the loading point with both specimens, showing that the strength of the footing concrete is closely related to the ultimate strength.

3) There was some difference in the behavior after yielding and the ultimate strength between tests A-1 and A-2. However, the difference was small. It may therefore be concluded that the cover plate has little effect on the ultimate strength.

4) With all specimens in series B, the curve began to bend around the yielding point of the steel bars on the tension side, showing a close relationship between the strength of steel bars and the ultimate strength of the connection.

5) The ultimate strength of test specimens for which the number of steel bars was the only variable changed (when B-2 was 1, B-3 was 0.39 and B-4 0.69), shows that the number of steel bars greatly affected the ultimate strength.

6) Since the ultimate strength of test specimen B-5 with steel bars extended outward at 45° is smaller than that of B-2 by about 20 percent, it is recommended that steel bars be embedded straight into the footing.

7) B-10 with steel bar baskets embedded in the steel pipe showed a similar behavior to that of B-4 with the same number of steel bars welded onto the steel pipe, also showing roughly the same ultimate strength.

8) B-11 with steel bars put into holes in the steel pipe has about 15 percent less ultimate strength than B-2.

9) With those specimens with a different composition of pile heads, the ultimate strength of B-9 with circular steel bars was rather large. However, it was not a significant difference and it may be concluded that the composition of pile heads does not affect the ultimate strength.

There is a difference in the depth of the steel pipe in the footings between methods A and B. Consequently, they have different support mechanisms for the connection against horizontal and bending loads. Figure 10 shows the distribution of stress on the footing surface in the case of a 5 ton load for A-2 and B-2. In the case of A-2, compressive stress occurred on the backside of the loading point in the direction of the loading axis; but there was hardly any on the front side of the loading point. It shows that the load was resisted mainly by the bearing strength of footing concrete of the backside of the loading point. In the case of B-2, the distribution of stress on the backside of the loading point was similar to that of A-2; but a large tensile stress occurred on the front side of the loading point at a right angle to the loading direction. This is because the depth of the steel pipe is small in method B, and the bearing stress of the footing concrete is not sufficient for the bending load; the tension of the steel bars works to resist it.

The cover plate used in the connecting method prescribed in the Specifications for Highway Bridges is primarily intended to disperse the vertical load. However, it is expected to be a weak point when the horizontal and bending load are acting. Figure 11 shows the distribution of bending stress on the steel pipe under a 15 ton load. In the case of A-1 with cover plate, large bending stress occurred near the surface of the footing because there was no concrete in that section of the steel pipe embedded in footing. No buckling occurred in the present test, because a thick steel pipe (t/d = 3.5 percent), was used. However, it seems necessary to consider fully this possibility with an actual structure.

Figure 12 shows the relationships between the load and the strain of steel bars on the tension side for B-2 and B-11. B-11 showed a steeper initial slope than B-2; so the strain was smaller than B-2 for the same load. However, the strain suddenly increased from about 11.5 tons, reaching the final stage at about 12 tons. This is probably because the load was not sufficiently transmitted initially due to a gap between the hole in the steel pipe and steel bars but was transmitted sufficiently with the gap disappearing halfway, concentrating on the steel bars.

CONCLUSIONS

The results of the horizontal load tests on the connection between a steel pipe pile and concrete footing may be summarized as below.

1) The dominant parameter for the ultimate strength in method A is the bearing strength of footing concrete.

2) When the cover plate is used, stress is concentrated at the steel pipe near the surface of the footing. It is thus necessary to consider the possibility of buckling. It did not seem to affect the ultimate strength.

3) The dominant parameter for the ultimate strength in method B is the strength and the number of steel bars. Other parameters had no effect.

4) It is advisable to embed steel bars straight into the footing.

5) The steel pipe with steel bar baskets embedded in it has the same ultimate strength as that with steel bars welded onto it.

REFERENCES

1. "Specifications for Highway Bridge: Part IV: Substructure," Japan Highway Association, May 1980.
2. Yoshio Adachi, "Rigidity of the Connection of Pile and Footing," Civil Engineering Journal, Vol. 16, No. 10, October 1974.
3. Seiji Kuromasa and Masaya Hirosawa, "Ultimate Strength of the Embedded Section of the Pile Head," Steel Pile, Edited by the Soil Engineering Association, September 1960.

Table 1. Types of Specimens

Connecting Method		Method A			Method B										
Specimen No.		A-1	A-2	A-3	B-1	B-2	B-3	B-4	B-5	B-6	B-7	B-8	B-9	B-10	B-11
Numbers of bars	0 pc.	-	-	-			o								
	4 pcs.	-						o						o	
	8 pcs.				-	-			-	-	-	-	-		-
Angle of bars ψ	0°				-	-		-		-	-	-	-	-	-
	45°								o						
Vertical load	No	-	-	-	-	-	-	-	-		-	-			
	Compression V = 5 tons									o					
Filling concrete	Footing underside	-	-	-	-	-	-	-	-	-		-	-		
	ID										o			o	o
Circular steel bars	0 pc.	-	-	-	-	-	-	-	-	-	-	-		-	-
	2 pcs.												o		
Cover plate	Yes	o			o										
	No		-	-		-	-	-	-	-	-	-	-	-	-
Circumferential bond of piles	Yes	-	-		-	-	-	-	-	-	-		-	-	-
	No			o								o			
Remarks		o: Variable parameter													

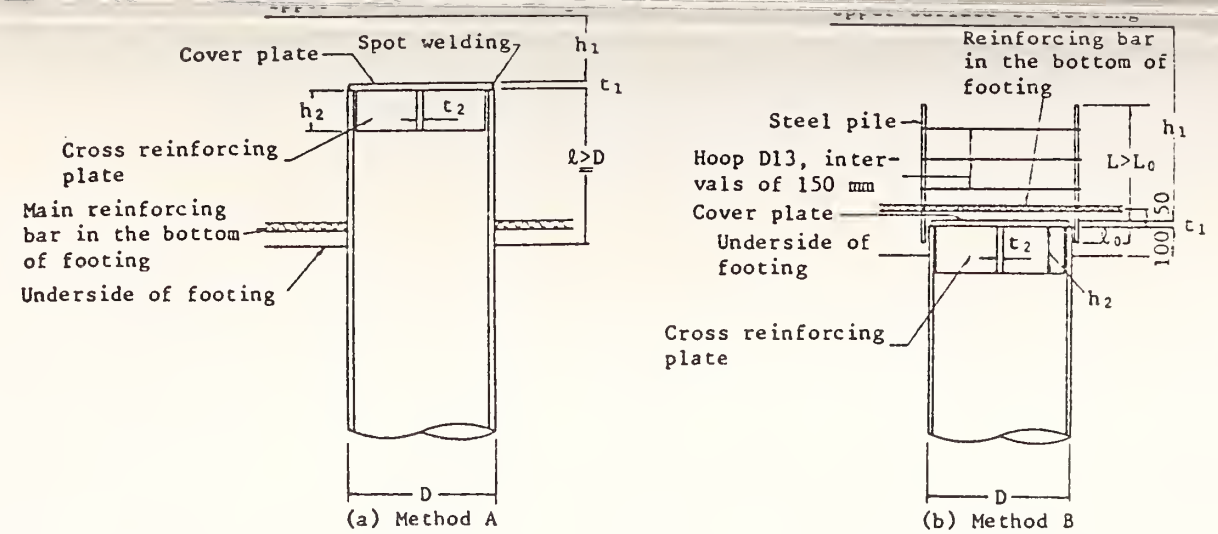

Fig. 1 Connecting Methods

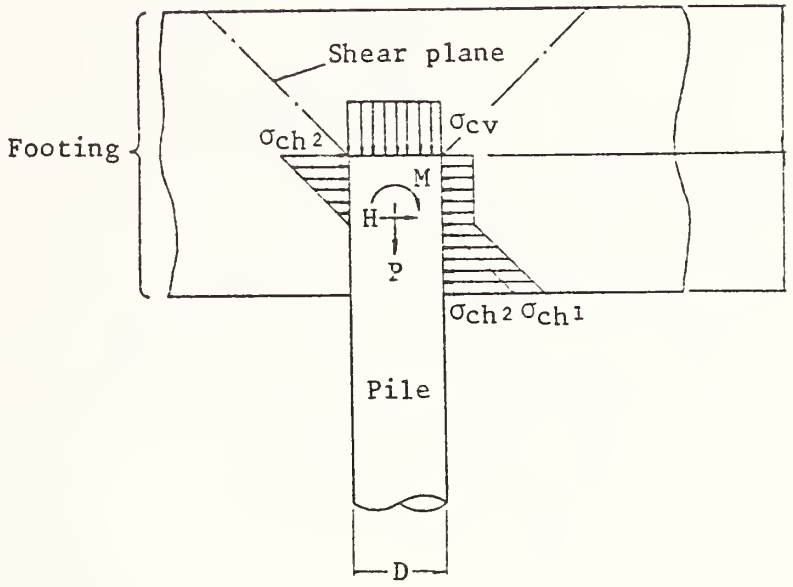

Fig. 2 Connection by Method A

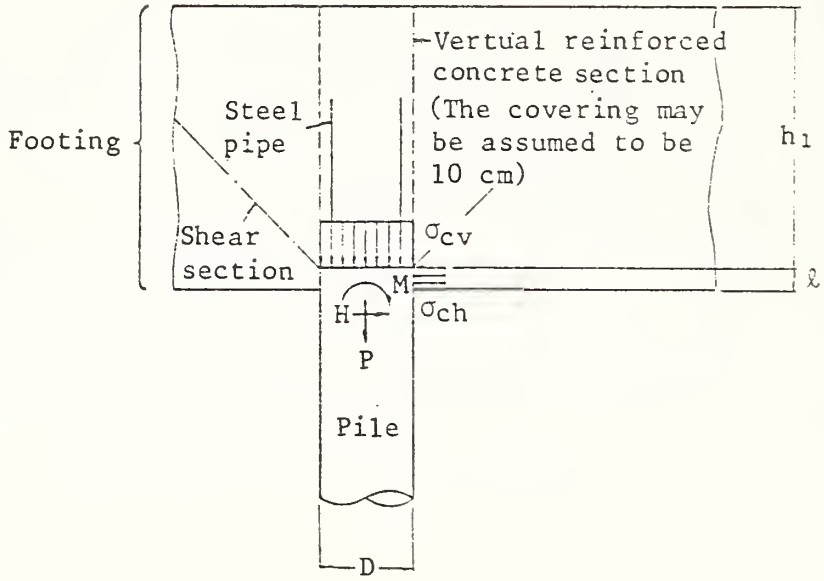

Fig. 3 Connection by Method B

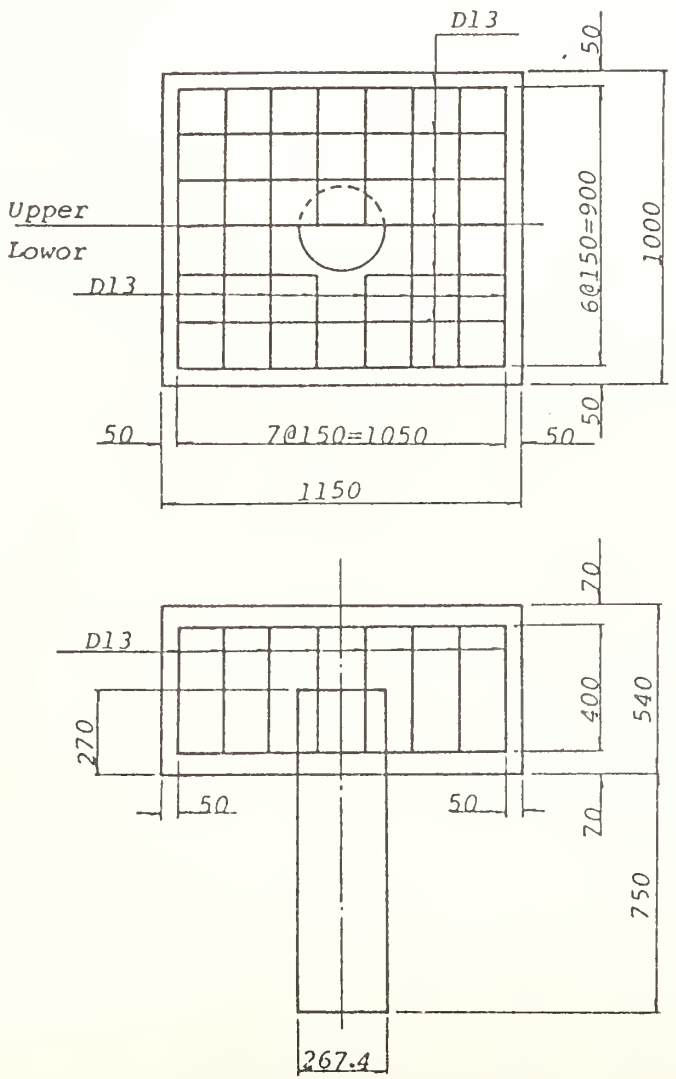

Method A

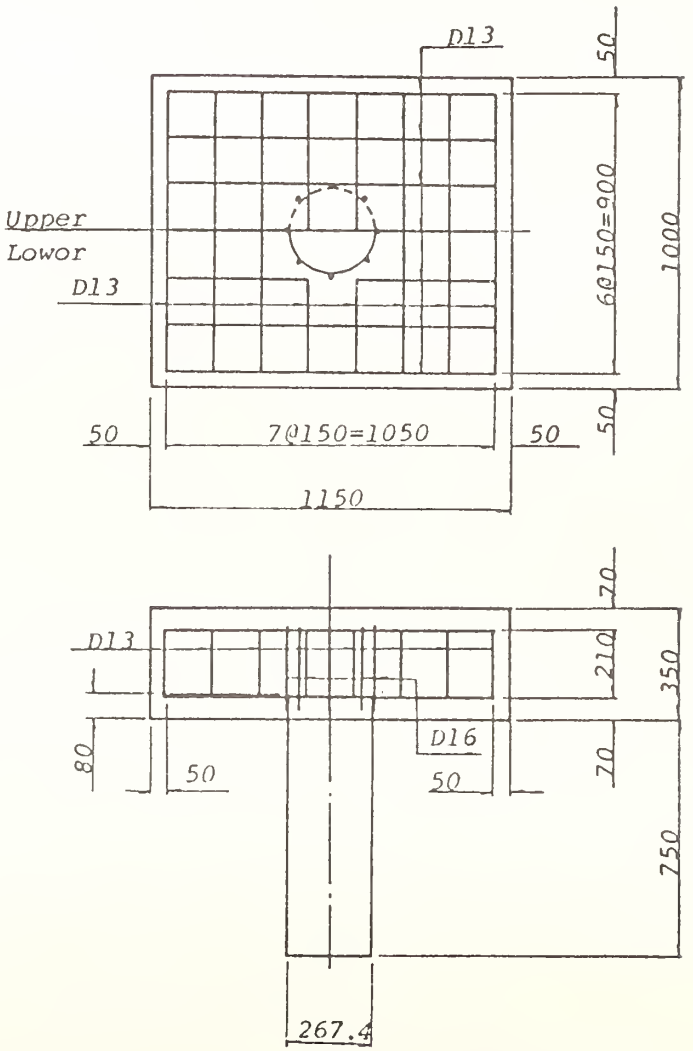

Method B

Fig. 4 General Plan of Series A and B

Specimen No.	A-1	A-2	A-3	B-1	B-2	B-3	B-4
Composition	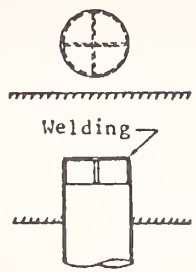	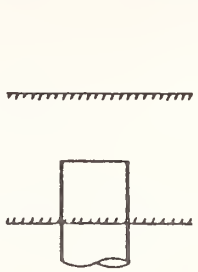	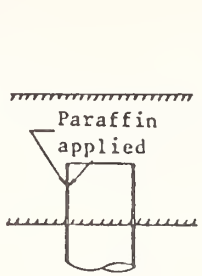	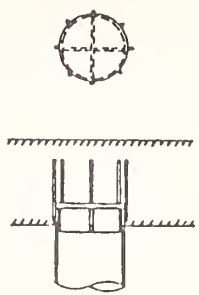	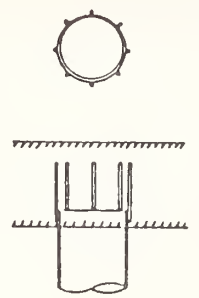	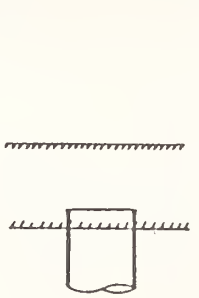	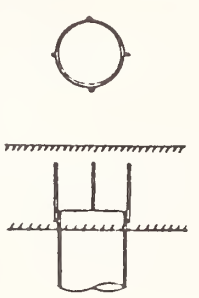
Remarks	With cover plate	Standard	No circumferential bond	With cover plate	Standard (8 steel bars)	No steel bars	4 steel bars
Specimen No.	B-1	B-6	B-7	B-8	B-9	B-10	B-11
Composition	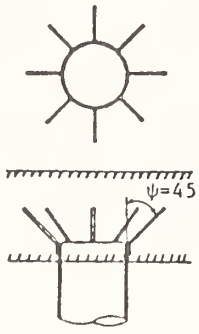	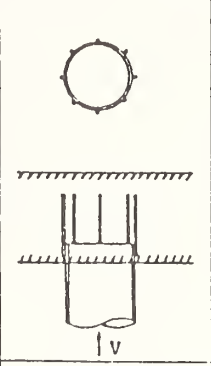	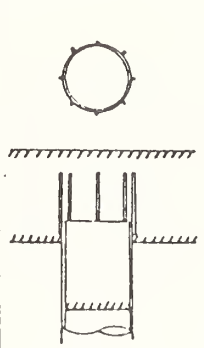	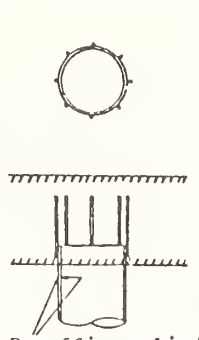	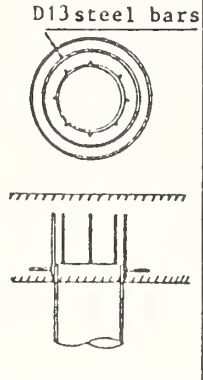	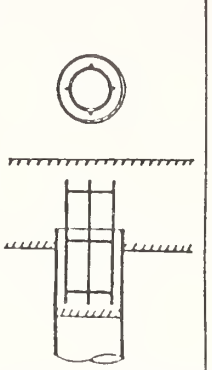	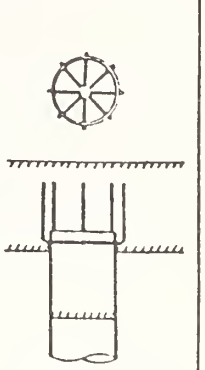
Remarks	ψ=45°	V=5 ton	Filled	No circumferential bond	With circular steel bars	Non-welding type(steel bar basket embedded)	Non-welding type (steel bars)

Fig. 5 Detail of the Connection

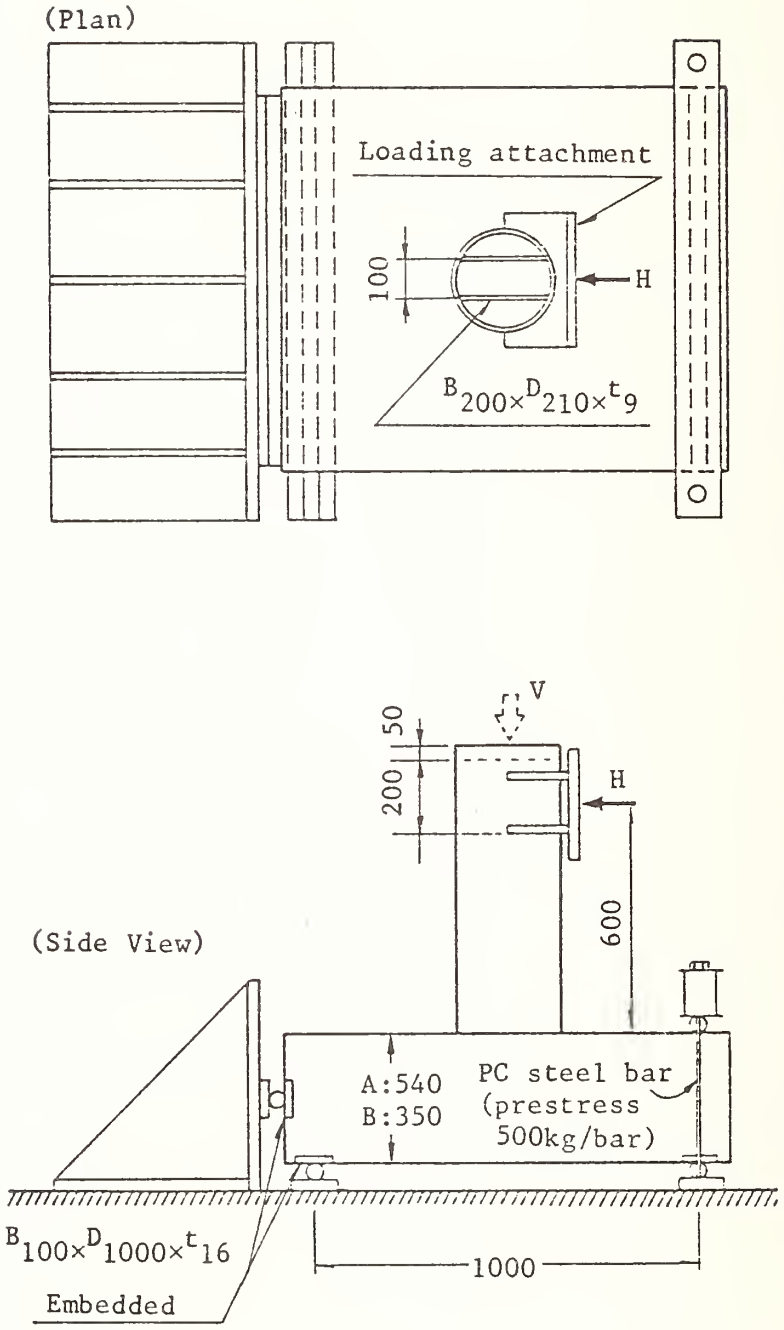

Fig. 6 Loading Method

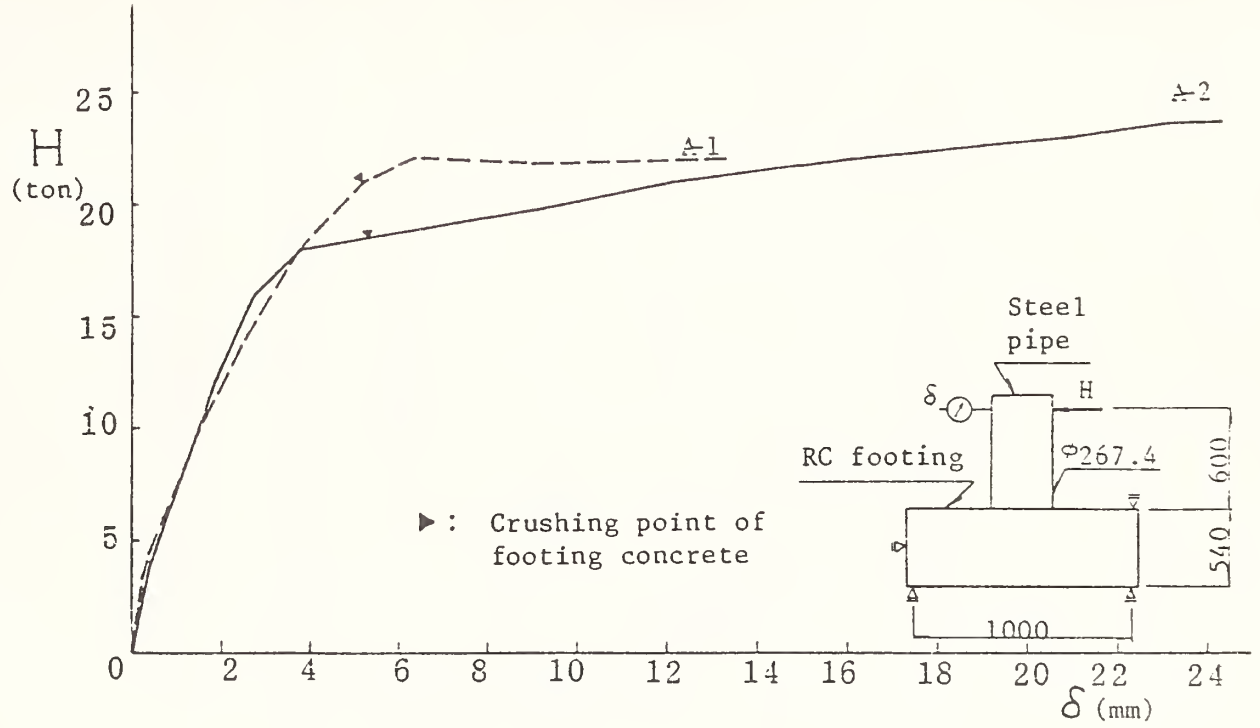

Fig. 7 Load-Deflection at Loading Point

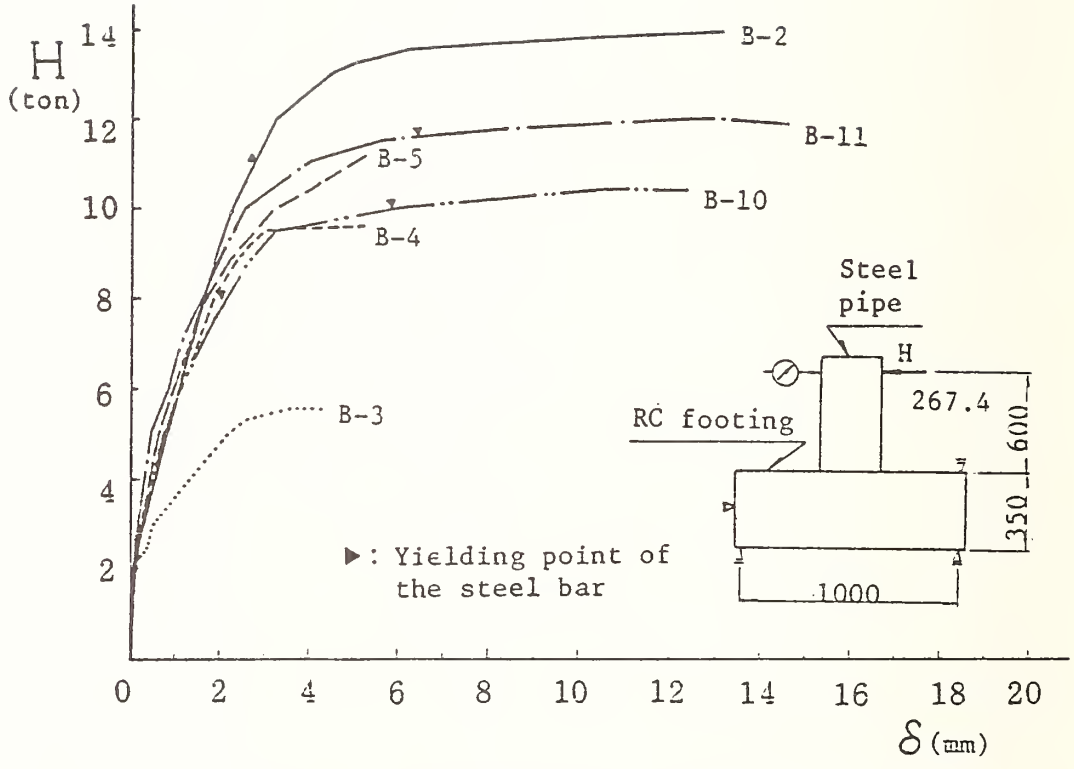

Fig. 8 Load-Deflection at Loading Point

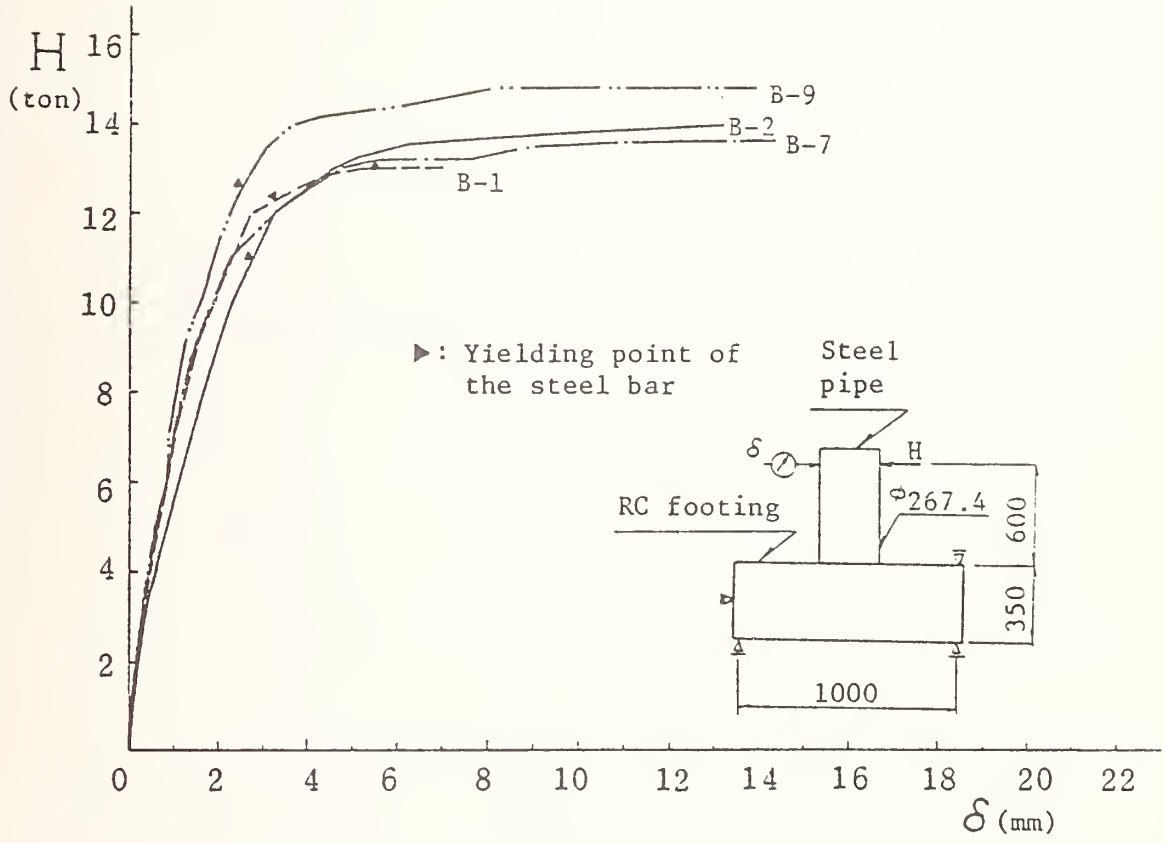

Fig. 9 Load-Deflection at Loading Point

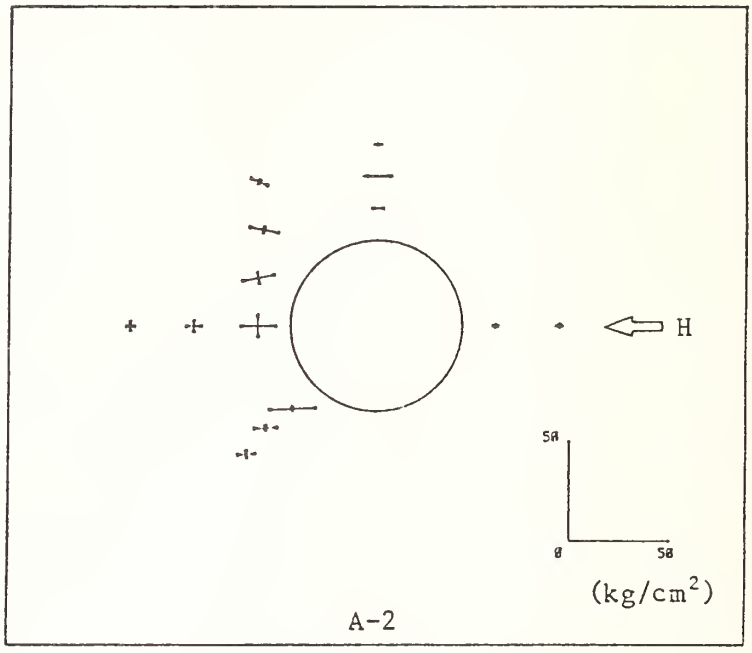

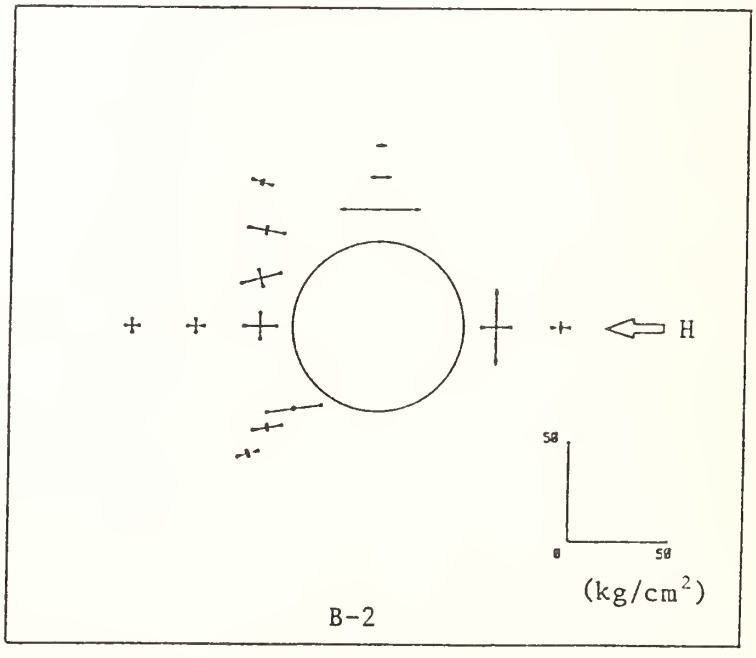

Fig. 10 Distribution of Stress on Footing Surface

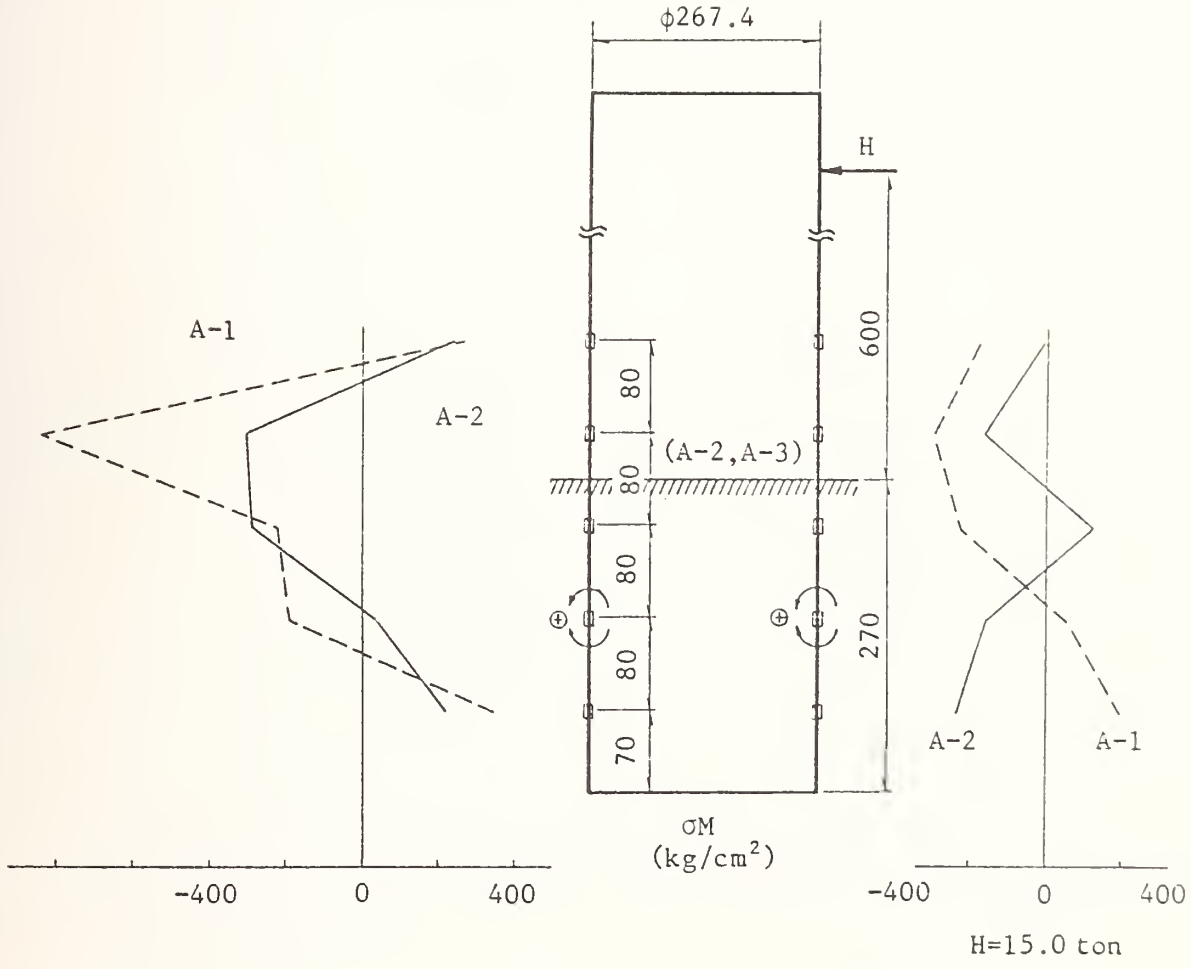

Fig. 11 Distribution of Bending Stress on Steel Pipe

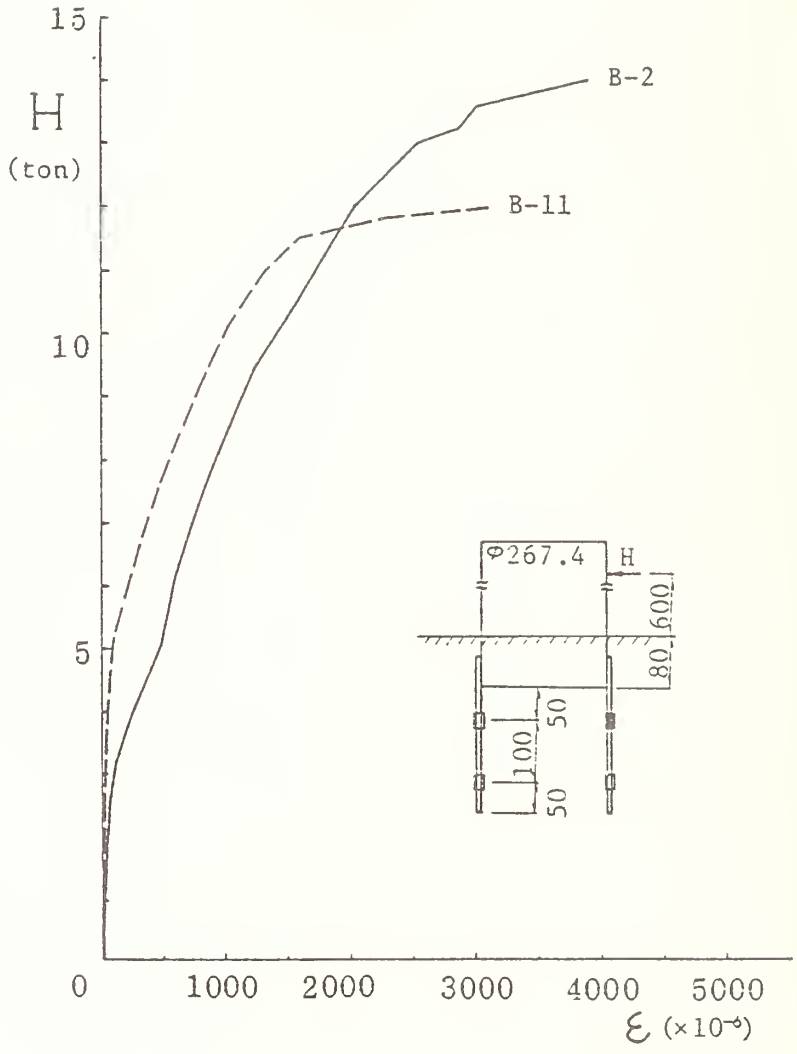

Fig. 12 Load-Strain of Steel Bars

ON THE STATUS OF IN SITU STRONG GROUND MOTION AND STRUCTURAL RESPONSE INVESTIGATIONS

C. Rojahn

Applied Technology Council
Berkeley, California

R. D. Borcherdt

U.S. Geological Survey

ABSTRACT

Strong-motion data from large earthquakes provide the basis for the design of buildings, bridges, dams, and other critical structures as well as the basis for research on fundamental problems related to earthquake hazard evaluation, earthquake processes, and internal structure of the earth. Review of existing strong-motion data acquisition programs in the United States shows significant progress in instrument deployment since 1933, but that significant improvements in data acquisition capabilities are needed for scientific and engineering research studies. The need for installation of several additional well-designed strong-motion arrays (free field, structures) in areas of high seismic potential worldwide is readily apparent as well as the need to develop instrumentation to reduce maintenance costs. Review of existing analog and digital strong-motion recording systems indicates that proven reliability and level of technical maintenance expertise still recommend analog systems for applications involving small amounts of data and long-term deployment. Those applications involving highly trained technicians, improved quality data, and large amount of data are facilitated by using digital instrumentation. Recent applications of digital technology in other fields suggests that numerous improvements in digital recorders are feasible and warranted.

Review of recently collected strong-motion data sets shows a significant increase in the strong-motion data base for moderate-sized earthquakes with that from the earthquakc in Imperial Valley, California (October 15, 1979) being most complete. Compilations of these data show a critical scarcity of in situ information on near field ground motions and damaging structural response levels for earthquakes larger than magnitude 7.

INTRODUCTION

Safeguarding life and property from the destructive effects of earthquakes is a major national as well as worldwide problem. Since the most widespread destructive effects of earthquakes are due to strong shaking, either directly through shaking-induced structural damage, or indirectly through shaking-induced ground failures, effective programs to measure, analyze, and predict strong shaking-induced ground failures, effective programs to measure, analyze, and predict strong

earthquake-generated ground motions and structural response to such motions are vital to national and international earthquake hazard reduction efforts. Earthquake strong-motion data provide the basis for the design of engineered buildings, bridges, dams, and other critical structures as well as the basis for research on fundamental problems related to earthquake engineering, earthquake processes, and internal structure of the earth.

Since the previous Microzonation Conference in 1978, there has been a significant increase in the number of strong-motion records obtained from moderate-size earthquakes and a slight increase in the number of structural-response data sets from instrumented structures. In addition, there has been significant progress in the area of instrument development, data processing, and data dissemination. These subjects are discussed in subsequent sections of this report, which is limited to a discussion of the status of U.S. strong-motion programs, current instrumentation, recent data sets, and current processing, dissemination, and analysis capabilities.

Even though there has been a substantial increase in the strong-motion data base in recent years and in spite of the fact that several large (greater than magnitude 7) damaging earthquakes occur each year in different parts of the world, there is still a scarcity of ground-motion data for large earthquakes at distances less than 40 kilometers. The lack of data on the response of instrumented structures, particularly damaged structures, to strong earthquake motions is even more critical. The scarcity of data is due to inadequate amounts of instrumentation and defines an urgent need for expanding both the U.S. and international programs to collect and disseminate near-fault strong ground motion and structural response data.

U.S. STRONG-MOTION PROGRAMS

Strong-motion instrumentation programs in the United States are operated by a number of Federal, state, and local agencies and several universities with varying degrees of coordination provided by a national program operated by the United States Geological Survey (USGS). The national strong-motion program began in 1932 with the installation of nine accelerographs at ground sites and in buildings in California. Less than 8 months later, the instruments installed at Long Beach, Vernon, and Los Angeles recorded the ground motions from the 1933 Long Beach Earthquake (Matthiesen, 1980). These first useful records of damaging earthquake ground motions indicated amplitudes as large as 0.25 g and provided an impetus for rapid development of the program. Since that time the number of strong-motion instrument locations in the United States has increased substantially with a number of Federal and state agencies initiating programs as a result of the 1964 Alaska and 1971 San Fernando, California Earthquakes.

Currently there are over 2,000 accelerograph installations located in 38 states as indicated in figure 1. Most of these accelerographs are located at, in, or near buildings or other structures, and most are located in California (figure 2). The two largest networks are operated by the California Division of Mines and Geology (CDMG), which manages the California Strong-Motion Instrumentation Program, and the USGS, which operates a national strong-motion program. In addition to its own instruments, the USGS also operates on a reimbursable basis the instruments owned by the California Department of Water Resources (CDWR), the Federal Highway Administration (FHWA), the Metropolitan Water District (MWD) of Los Angeles, the Veterans Administration (VA), and several other agencies. Other large networks are operated by the Army Corps of Engineers and the University of Southern California (USC), and smaller networks are operated by the California Institute of Technology, the University of California at Los Angeles (UCLA), Lamont-Doherty Geophysical Observatory, and others.

The various agencies and institutions that operate these networks have had different objectives and are subjected to different constraints. Some desire research programs directed toward the understanding of basic problems in engineering seismology, whereas other are concerned with a regulatory function so as to provide a basis for the decision regarding the continued operation of the facility. In general, the existing strong-motion networks are designed to obtain data for one of the following purposes: (1) ground-motion studies; (2) structural-response studies; and/or (3) facility-evaluation studies. Following is a brief summary of the networks operated for these various purposes.

GROUND-MOTION ARRAYS

Currently there are approximately 629 installations designed for the express purposes of obtaining ground-motion data (table 1). One hundred and eighty eight of these are operated by the USGS, 244 by the CDMG, 74 by the USC, 51 by the VA, and 72 by other institutions (Switzer and others, 1980). In addition, there are numerous instruments nationwide located at instrumented structure sites that may provide additional ground-motion data (see sections following on Structural-Response Arrays and FacilityEvaluation Arrays). Seventy-two percent of the existing ground-motion sites are located in California, 19 percent in other parts of the West, 4 percent in the Central U.S., and 5 percent in the East (table 1). Approximately 25 percent of the instruments are installed in instrument shelters, and the remainder are installed in buildings one-story and higher at ground level or in the basement. Sites in the latter category are not considered to be ideal "free-field" sites and may yield strongmotion recordings that include structure-induced motions.

The national program operated by the USGS, which is currently funded in part by the National Science Foundation, includes ground-motion instruments installed in regional arrays and at isolated

sites nationwide, and in three closely-spaced-instrument arrays in California. The regional arrays are located in Alaska (51 instruments, including those of cooperating agencies, figure 3), along the San Jacinto and San Andreas faults in Southern California (37 instruments), Hawaii (19 instruments, figure 4), the New Madrid region of the Mississippi Valley (16 instruments, plus those of cooperating agencies, figure 5), and the Pacific Northwest (16 instruments). The isolated sites nationwide are located at VA hospital facilities in seismic zones 2 and 3, as defined in the Uniform Building Code (ICBO, 1973), and at a few facilities located in zone 1. The closely-spaced-instrument arrays are located in Bear Valley (1 array, 9 stations) and the Imperial Valley (2 arrays, 19 instruments). The largest of the arrays in the Imperial Valley is the El Centro Array, which was designed to obtain data on ground-motion attenuation and consists of 13 stations in a 45 km long array that crosses the Imperial Fault near El Centro (figure 6). The El Centro Differential Array, also located in the Imperial Valley, is a 6 instrument 300 m long array in El Centro (special array, figure 6) that is designated specifically to record differential ground-motions at closely spaced intervals (Bycroft, 1980).

The California strong-motion program, established in 1972 and operated by the CDMG, is funded by a tax on building permits and has as its objective the instrumentation of representative geologic sites and structures statewide. The CDMG ground-motion stations are located at numerous isolated sites statewide and in several closely-spaced-instrument arrays including: the APEEL Array operated cooperatively with the USGS in the San Francisco Bay Region (9 stations in a linear array crossing the San Andreas and Hayward Faults), the Chalome-Shandon Array (5 stations in a linear array crossing the San Andreas Fault near Chalome), and the Gilroy Array (5 stations in a linear array crossing the Calaveras Fault established in conjunction with the USGS near Gilroy). The CDMG also operates a 3 instrument down-hole stations in San Benito.

The other extensive U.S. ground-motion network is that of the University of Southern California. This network is located in the Los Angeles region and is intended to provide data for the study of the influence of subsurface geology and local site conditions. Smaller ground-motion networks and isolated stations are also operated by other universities and agencies; these include Lamont-Doherty Geological Observatory, the California Institute of Technology, and the University of California at Berkeley, which operates a 3 instrument down-hole array in Richmond, California.

STRUCTURAL RESPONSE ARRAYS

Currently there are approximately 109 structures nationwide instrumented to obtain data for structural response studies (table 2). Seventy six buildings, 14 bridges, and 19 dams. Many of these structures have been extensively instrumented to obtain information on the important aspects

of structural response. In the case of buildings, for example, the instrumentation is located so as to provide information on the overall deflected shape of the structure and to differentiate torsional and translational response. Other structures contain less instrumentation but are of interest because of the importance and location of the structure. In either case the general intent is to obtain data that can be used to improve engineering design practice.

The structures instrumentation program of the USGS consists of 9 buildings and 9 bridges (table 2), 11 of which are maintained with funds provided by other agencies that own the instruments. Most of the structures in this program have been extensively instrumented in accordance with instrumentation techniques developed at the USGS (Rojahn and Matthiesen, 1977; Rojahn and Ragget, 1981), approximately one-half of the structures are located in California, several in Alaska and Washington, and one each in New York and Missouri. During the late 1960s and early 1970s, instruments in numerous code-instrumented buildings in California were also maintained under this program, then operated by the Seismological Field Survey of the Coast and Geodetic Survey (later known as the Environmental Science Services Administration and still later as the National Oceanic and Atmospheric Administration). Since 1973, however, the maintenance of code-instrumented buildings in California has been phased out out of the national program due to changes in funding and objectives of the program.

The structures instrumentation program of the CDMG, which currently contains 51 buildings, 4 bridges, and 19 dams, may eventually contain more than 400 instrumented structures, if projections made several years ago prove to be accurate. The objective of this program is to instrument representative buildings, bridges, dams, and other structures statewide to obtain data to improve engineering design practice. Because the program is funded through a tax on new building construction in California, the CDMG program naturally emphasizes the instrumentation of buildings. Most of the structures instrumented under the program have been instrumented in accordance with techniques developed at the USGS (Rojahn and Matthiesen, 1977; Rojahn and Raggett, 1981), and the vast majority are located at sites where damaging levels of ground motion can be expected to occur within the expected useable life of the instrumentation (20 to 40 years). The structures are selected on the basis of advice provided by an advisory panel (the Strong-Motion Instrumentation Committee of the California Seismic Safety Commission), which acts on recommendations provided by organizations such as the Structural Engineers Association of California, the California Department of Transportation, and other state and local agencies that operate structures that could be adversely affected by earthquakes.

The remaining instrumented structures (table 2) have been instrumented by the faculty of several universities interested in the solution of earthquake engineering problems. The California Institute

of Technology has instrumented 2 buildings, UCLA operates instruments in 14 buildings (11 of which are originally LA code-instrumented buildings), and the University of Nevada operates instruments on 1 bridge. Most if not all, of these programs have been funded by the National Science Foundation.

FACILITY-EVALUATION ARRAYS

Currently there are more than 460 structures instrumented nationwide to obtain data to evaluate the safety of the instrumented structure following earthquake-induced strong-ground shaking (tables 3a, 3b, and 3c): 133 dams, 12 pumping, power, and filter plants, and more than 315 buildings. What differentiates these arrays from those designed to obtain structural response information are the amount and location of strong-motion instrumentation. Structures instrumented to provide safety-evaluation data generally contain less instrumentation than would be required to provide data adequate for rigorous three-dimensional structural response studies. More specifically, structures instrumented for facility evaluation normally contain only that instrumentation required to provide information on ground motion input, peak structural response, and changes in model properties, particularly natural period changes.

Most of the instrumented buildings that fall under this category (table 3b) are ten-stories or higher and most are located in California, primarily in Los Angeles. Those buildings instrumented because of building code requirements contain three accelerographs: one in the basement, one near midheight, and one near the top. The other buildings normally contain two or three accelerographs: one in the basement, one near the top, and one near midheight if there is a third. In the near future the City of Los Angeles may reduce the number of instruments required per building to one near the top because it is believed that data from such instrumentation will provide data sufficient for safety evaluation. At present most of the instruments installed for safety evaluation in buildings are not regularly maintained.

Dams instrumented for facility-evaluation purposes are located nationwide (table 3a) and most are instrumented by the Army Corps of Engineers (ACOE). In most cases the accelerographs are located on the abutment, toe, and/or crest of the dam. ACOE maintains its network in coordination with the USGS maintenance program, whereas instruments on the other dams are maintained on a reimburseable basis by the USGS.

All 12 pumping, power, and filter plants are located in California and all are maintained on a reimburseable basis by the USGS. Most plants contain two instruments at different levels, one of which is normally the basement or lowest level.

U.S. STRONG-MOTION INSTRUMENTATION

ANALOG SYSTEMS

Most of the current strong-motion programs in the U.S., as well as in Mexico, Central America, South America, and many European countries, use a self-triggering three-component 1 g analog accelerograph to record strong ground shaking. The most extensively utilized instrument of this type is the SMA-1 (Kinemetrics). This system records on 70 mm photographic film, has a dynamic range of about 55 dB at a sensitivity of 1.8 cm/g, a useable bandwidth of about 0.06-35 Hz, accelerometers with a natural frequency of 20-25 Hz and critical damping of 60 to 70 percent, and can be equipped to record an external time standard.

Although the triaxial analog systems are also utilized extensively in code-instrumented buildings and on many dams nationwide, recent experience has shown that a multi-channel remote-accelerometer central-recording analog system is more useful for recording strong-motion response of buildings, bridges, dams, and other structures. The system most widely used is the CRA-1 (Kinemetrics) accelerograph and consists of a 13-channel CR-1 analog recorder, which records on 178 mm (7 in) photographic film, and uniaxial, biaxial, and/or triaxial FBA force-balance accelerometers. The FBA accelerometers, which have a natural frequency of approximately 50 Hz, are connected by low-voltage data cable to the central-recording unit. Like the SMA-1, the CR-1 recording unit is battery powered, is triggered by horizontal or vertical motion that equals or exceeds 0.01 g, and can be equipped to record an external time standard. The system is also designed to record acceleration with frequency components nominally within the range 0-50 Hz and with maximum amplitudes of 1 g.

A high degree of field reliability has been established for the analog systems and for many applications the systems are superior to other currently available commercial systems. The systems are especially appropriate for those applications involving a minimal level of technical expertise, long-time intervals between strong events, and extreme temperature or otherwise harsh operating environments. When compared to the more recently developed digital systems, some disadvantages of the analog system are the lack of information on initial p-wave onset times, requirements for digitization capabilities, and decreased dynamic range. These disadvantages for many applications, however, are less important than the increased amount of reliability that exists for the analog systems.

DIGITAL SYSTEMS

Within the last decade several digital recording systems have been developed. The systems available in the United States are of two basic types: (1) systems that are strictly hardwired such as the DCA-301 (Terra-Technology), the DCS-302 (Terra-Technology), the DR-100 (Sprengnether), DSA-1

(Kinemetrics), and the PDR-1 (Kinemetrics); and (2) systems more recent in design that utilize microprocessors and are in varying degrees software controlled, such as the GEOS (USGS), the PDR-2 (Kinemetrics), and the MCR-600 (Teledyne). In principal the software-based systems are more versatile in that instrumentation functions can be readily changed simply by modifying computer programs as opposed to modification of hardware components. Ease in making such changes has advantages in modifying systems to incorporate improvements offered by a rapidly changing state-of-the-art and in utilizing the systems for a wide variety of applications.

Some of the more significant differences between the various digital systems are evident in terms of signal conditioning characteristics, analog to digital (A/D) conversion characteristics, trigger algorithms for event detection, clock characteristics for signal timing, recording media for data storage, power requirements, physical dimensions, design concepts, and reliability. A tabulation of characteristics for six digital systems is reproduced in table 4 (Fletcher, personal communication). The specifications indicated in the table are meant to be only representative, as the systems are being continuously improved.

A major difference in the signal conditioning characteristics of the various systems (table 4) involves the number of input channels and types of sensors. Those systems capable of recording 6 channels (GEOS, PDR-2, DCS-302) can be used to simultaneously record the output from geophones (velocity transducers) as well as force-balance accelerometers, thereby substantially increasing the range of signals that can be recorded on scale, resulting in a capability to record small events as well as very large earthquakes without changing instrument settings. In addition, the 6-channel systems are useful for a wide variety of applications such as seismic-refraction measurements, microearthquake studies, and ambient-vibration studies in buildings.

Some major differences in the A/D characteristics of the various systems involve (table 4) number of bits, gain ranging, and sample rate. The 16-bit system provides for a linear dynamic range of 96 dB and the 12-bit systems provide 72 dB linear dynamic range. Gain ranging increases the dynamic range of the 12-bit systems and increases the range of events that can be recorded on scale but limits system resolution and the accuracy of spectral analyses. Gain ranging can usually be added to most systems at little additional cost. The maximum sampling rates control the high frequency cutoff of the systems. In the case of DR-100, PDR-2, and GEOS these maximum rates vary for each channel depending on the number of channels selected for recording.

Software-based trigger algorithms (table 4) (MCR-600, PDR-2, GEOS) provide versatility in the trigger algorithms can be easily modified as the technology improves as opposed to analog triggers which require replacement of hardware to incorporate changes. Clock stability characteristics

(table 4) are important for applications requiring long-term deployment. In such situations it is important to have automatic clock correction capabilities in the instrument (PDR-2, GEOS) or to have maintenance personnel frequently visit the instrument to check clock drift. Power consumption (table 4) is also an important factor for long-term deployment of the instruments; in this case it is not only the power consumed by the recording system that is important but also that consumed by the sensor if forced-balance accelerometers are used.

The recording media (table 4) determines the recording time, the type of playback capability required, and the reformatting procedure needed to interpret the data. Individualized cassette recording requires corresponding cassette readers in order to transfer the data to a computer compatible format. Standardized cartridge recorders in general utilize more standardized readers and require less specialized equipment to transfer the data to a computer-compatible format.

The design concepts on which the instruments are based influence instrument reliability, operator errors, and long-term flexibility (table 4). Alphanumeric character displays (GEOS) permit establishment of interactive English language set up procedures that minimize operator error during instrument set up and maintenance. A principal difference in design concepts among the software based systems is indicated by the number of microprocessors utilized in the systems. Some systems (MCR-600) utilize microprocessors to perform dedicated tasks with the system structure being similar to hardwired systems; other systems (PDR-2) permit more control of system operation by the microprocessor while still requiring performance of dedicated tasks; and other systems (GEOS) are designed in modules with each module controlled by the single central microprocessor. The latter type of system can be treated somewhat as a small computer in the field and easily modified by changing hardware modules and associated software.

The authors' experience suggests for many applications of strong-motion instruments, especially those in which instruments are expected to be on location for several years and record only a few events, that analog instruments are probably preferable at this time primarily because of proven reliability and the level of technical expertise required for maintenance. For the applications involving highly trained technicians and large amounts of recorded data, digital instruments are preferable not only because they provide improved quality data but because of the ease with which large amounts of data can be analyzed. In the future, as the reliability of digital systems is established, they will no doubt gradually replace analog systems.

Digital technology is currently highly advanced, but only recently has been applied to the problem of acquiring strong-motion data. Applications in other fields suggest that, if appropriate

development resources are utilized to stimulate commercial interest, small, compact, and inexpensive digital strong-motion recorders could be developed. Development of an inexpensive but reliable instrument could greatly accelerate the rate at which recorders are being deployed on a worldwide basis and significantly improve the present data base for the design of earthquake-resistant structures.

U.S. DATA PROCESSING AND DISSEMINATION

Centers in the U.S. established to process strong-motion data are located at the USGS in Menlo Park, California, the CDMG in Sacramento, California, and the University of Southern California in Los Angeles. These centers are intended primarily to process data from digital and analog instruments from permanent and temporary stations and to analyze data for engineering and seismological applications. The centers utilize lazer-scan and automatic digitization procedures to process the analog film records and dedicate hardware to process the digital records. A major objective for these centers is development of data processing capabilities so that data can be rapidly processed according to standard techniques and made available on cards, magnetic tape, and possibly telephone computer terminals to users within a few weeks of receipt of the records. Substantial effort has also be underway (Basili and Brady, 1978; Trifunac and Lee, 1978; Fletcher and others, 1979; Raugh, 1981; Sunder and Conner, 1982) to improve processing procedures based on earlier work done at the California Institute of Technology (Trifunac and Lee, 1973).

Current information about strong-motion data available in the western hemisphere can be easily accessed via the Strong-Motion Information Retrieval System developed at the USGS (Converse, 1978). The system provides users with information on data characteristics, recording environment, and archive location via computer terminal and telephone (415-329-8600). Digital and analog copies of the more significant strong-motion records collected in the United States are available from the National Geophysical and Solar Terrestrial Data Center (D62) in Boulder, Colorado 80302, and the National Information Service for Earthquake Engineering, California Institute of Technology, Pasadena, California 91125. Analog copies are available on 35 mm or 70 mm film, and on paper; digital copies are available on punched cards and magnetic tape.

RECENT U.S. STRONG-MOTION DATA OF ENGINEERING AND SEISMOLOGICAL SIGNIFICANCE

Several sets of strong-motion data have been recorded in the near field of moderate earthquakes since the Microzonation Conference in 1978. Even though the most significant of these is clearly the data recovered from the October 15, 1979 Imperial Valley Earthquake, several additional data sets have been recorded that provide useful information on various questions significant for earthquake engineering and strong-motion seismology. A list of the more significant strong-motion data sets

collected since the last conference is given in table 5. The list and subsequent discussion are provided as a reference guide for the recent data sets.

In addition to the data collected from the moderate-sized main events, rather extensive sets of strong-motion data generated by aftershocks have been obtained for the Coyote Lake, Imperial Valley, Livermore, Mammoth Lakes, Mexicali, and New Brunswick events. A description of some of the more noteable aspects of these data sets are also summarized below.

COYOTE LAKE EARTHQUAKE

Noteable aspects of the August 6, 1979 magnitude -5.9 (M_L) Coyote Lake, California Earthquake strong-motion data set include: an accelerograph record from a station located very near the end of the fault rupture zone (1.2 km) as well as records from a 5-station array perpendicular to the zone of surface rupture. The linear array extended from a bedrock location on the eastern side of the surface rupture across an alluvial valley to bedrock 8 km west of the zone of surface rupture (figure 7). In addition, the event produced more than 47 free-field accelerograph records and 22 recordings in structures mostly at distances greater than 40 km. More than 50 aftershocks with magnitudes less than 4.0 were recorded on 9 digital recorders. These data, useful for interpreting the main shock records and for describing characteristics of the fault rupture zone at depth (Spudich, personal communication), are available on request from the USGS.

IMPERIAL VALLEY EARTHQUAKE

The October 15, 1979 magnitude -6.6 (M_L) Imperial Valley, California Earthquake generated the most comprehensive set of strong-motion accelerograph data yet recorded from a damaging earthquake in the United States. These data are of special significance because they include the first set of closely-spaced ground-motion records obtained close to fault traces activated by a moderate earthquake as well as the first set of records from extensive arrays in a severely damaged building and on a highway overpass bridge. In addition, numerous aftershocks were recorded on some of the stations in the permanent array and on 12 digital (Boore and others, 1980) and 9 analog accelerographs (Anderson and Heaton, 1982) temporarily installed after the main shock.

Of particular importance to engineering seismology are the data obtained from the 45 km long 13-station El Centro ground-motion array and from the 300 m long 6-accelerograph El Centro differential array (figure 6). Strong-motion data from the 45 km long array (figure 8) provide information on the nature of shaking close to and at increasing distance from the fault rupture, whereas those from the differential array are particularly applicable to the study of earthquake-induced stresses in such extended structures as bridges, dams, pipelines, and large mat foundations for nuclear power

stations. These data also include the largest ground accelerations yet recorded anywhere in the world.

From a structural-engineering point of view, the strong-motion data from the severely damaged six-story Imperial County Services Building in El Centro are undoubtedly the most significant of this earthquake. Data from the building's 13-channel accelerograph system (figure 9), designed specifically for acquiring information that could lead to improvements in engineering design practice, provide a complete description of building response before, during, and after the occurrence of severe structural damage (Rojahn and Mork, 1981; Pauschke and others, 1981). These data (figure 10) are exceptional because the time and mechanism of structural failure can be inferred directly from the recorded data. In addition, the record from the base of the building is significantly different than that obtained at a free-field site approximately 100 m east of the building (figure 11); these data clearly indicate that soil-foundation-structure interaction occurred at the site.

Data from the 26-channel accelerograph system on the two-span Meloland Road-Interstate Route 8 overcrossing, located approximately 0.5 km from the fault rupture zone, are also significant. Although the film transport in one of the two 13-channel recorders malfunctioned during the earthquake, these data provide important information on the three-dimensional model response of the bridge during and after strong ground shaking and show the effect of soil-foundation-structure interaction at the site (Rojahn and others, 1980). The bridge did not sustain any significant structural damage during the earthquake.

MAMMOTH LAKES EARTHQUAKES

The May 1980, Mammoth Lakes, California Earthquakes (magnitude 6.0, 6.1 and 6.2 (M_L)) yielded 26 accelerograph recordings over a distance of 1.5 to 46.8 km (Turpen, 1980) as well as several recordings at more distant stations. Of special note were the recordings obtained at three of the stations within 20 km of the epicenters. One of these stations is a CDMG-instrumented earth-fill dam (Long Valley Dam) with accelerometers located on an abutment, at several locations on the crest and downstream face of the dam, and downstream on bedrock; another is a one-story gymnasium (Mammoth Lakes High School Gymnasium) with an extensive array of accelerometers located on the roof diaphragm and at the base of the building. In addition, an unusually large number of aftershocks followed these events with 38 of the aftershocks within 72 hr after the first shock being of magnitude 4 to 5. Twelve digital event recorders were deployed in the epicentral region (figure 12). More than 1500 events were recorded on the digital array. Of these events approximately 150 were of interest for aftershock studies (Spudich and others, 1981), and 50 were of interest for source parameter studies (Archuleta and others, 1982).

EASTERN U.S. RECORDS

The noteable strong-motion data sets recently recorded in the eastern U.S. are from Monticello, South Carolina; Franklin Falls, New Hampshire; and New Brunswick, Canada. The main-event records that were collected at Monticello and Franklin Falls are of special interest because they were generated by magnitude -2.8 and magnitude -4.7 sources, respectively, at distances less than 10 km. The New Brunswick main event was not recorded on any strong-motion instruments; however, at the request of the Canadian Department of Energy, Mines, and Resources, 7 digital recorders were deployed by the USGS at 4 stations with the result that 12 aftershocks were recorded at 3 or more stations within a 10 km radius of the sources. The largest aftershock was of magnitude 3.5 with a peak recorded acceleration of 80 cm/sec^2. Considering the scarcity of strong-motion data collected in the Eastern U.S., these data are significant for engineering design and various source-mechanisms and attenuation studies.

OTHER RECORDS

Other recently recorded strong-motion data sets that provide important information on structural response are these recorded in two buildings within 15 km of the August 13, 1978 magnitude -5.1 (M_L) Santa Barbara, California Earthquake (Porter, 1978) and those recorded in two buildings located 17 km and 24 km, respectively, from the epicenter of the magnitude -5.5 (M_L) Livermore, California Earthquake of January 24, 1980 (Porcella and Switzer, 1982). The 4-story steel-frame Freitas building in Santa Barbara, the three-story reinforced-concrete shear-wall North Hall at the University of California at Santa Barbara, and the one-story Eastman Kodak warehouse in San Ramon, in which the Livermore earthquake data were recorded, contained extensive multi-channel remote-recording accelerograph systems installed under the CDMG program; the Livermore VA Hospital contained only two triaxial accelerographs, one in the basement and one at the roof level. Data from North Hall and the Livermore VA Hospital are particularly significant because both buildings were structurally damaged during the earthquake (Miller and Felszeghy, 1978; Matthiesen, 1980).

DISCUSSION

The strong-motion data collected from events prior to an including the Imperial Valley event have provided significant increases in the available strong-motion data base for moderate-sized earthquakes as well as several important data sets from instrumented structures. Compiliations of the ground-motion data such as those of Joyner and Boore (1981) and Campbell (1982), however, emphasize the critical scarcity of near-field ground-motion data for events larger than magnitude 7 and suggest the need to increase cooperative international efforts to collect such data. In spite of

the fact that recent events have provided significant information on the response of three buildings damaged by moderate-sized earthquakes, there is also an acute scarcity of structural-response data from damaged structures. In total, there now exists only six sets of strong-motion data from buildings damaged in the U.S.; the other three sets were recorded during the 1971 San Fernando, California Earthquake in buildings instrumented as a result of municipal-code requirements.

Recent studies of the available near-field ground-motion data suggest that the character of high-frequency strong ground motions as recorded near the ruptures associated with moderate earthquakes are influenced significantly by the dynamics of the rupture process on the fault surface. By way of example, Hanks and McGuire (1982) have developed a far-field model for estimating rms acceleration and peak accelerations as a function of moment, stress drop, and characteristic source size on the basis of considering acceleration time histories as band limited, finite duration white Gaussian noise. Madariaga (1982) has utilized an anti-plane crack model to estimate the far-field spectrum of acceleration time histories. The model predicts a flat acceleration spectrum consistent with the Hanks and McGuire (1982) model and an W^{-2} fall off for high frequencies. As other examples, Boatwright (1981) and Das and Aki (1979) have developed models and used free-field recordings to interpret near-field high-frequency strong-motion recordings in terms of irregularities of the slip velocity on the fault surface. Such irregularities can be interpreted to be associated with barriers or asperities encountered by the rupture front and strongly influence the character of near-field high-frequency ground motions. A comprehensive examination of the influence of rupture dynamics on the nature of acceleration time histories was undertaken at a recent workshop (Boatwright, 1982). Results of this workshop again emphasized the need for broad-band, wide-dynamic range recordings of strong earthquake ground motions from well-designed arrays, not only to improve the data base for engineering design, but also to improve descriptions of fault rupture dynamics pertinent to descriptions of strong shaking in generating structural damage and ground failure.

There have been substantially fewer studies of structural-response data in recent years than studies of ground-motion data, primarily because of the scarcity of structural-response data from damaged structures. The attention received by the severely-damaged Imperial County Services Building and the strong-motion data generated therein emphasizes the importance of such data and suggests that the current data set from six damaged structures is critically deficient.

ACKNOWLEDGMENT

The efforts of Joe Fletcher in compiling the data for table 4 are gratefully acknowledged.

REFERENCES

[1] Anderson, J. G. and T. H. Heaton, 1982, "Aftershock Accelerograms Recorded on a Temporary Array in the Imperial Valley, California Earthquake of October 15, 1979," U.S. Geological Survey Professional Paper 1254 (in press).

[2] Archuletta, R. J. and P. Spudich, 1982, "Analysis of Near-source Static and Dynamic Measurements from the 1979 Imperial Valley Earthquake," in Boatwright, J., ed., Conference Proceedings XVI, U.S. Geological Survey Open-File Report (in press).

[3] Archuletta, R. J., E. Cranswick, C. Mueller, and P. Spudich, 1982, "Source Parameters of the 1980 Mammoth Lakes, California Earthquake Sequence," Journal of Geophysical Research, (in press).

[4] Basili, M. and A. G. Brady, 1978, "Low-frequency Filtering and the Selection of Limits for Accelerogram Corrections," Proceedings, 6th European Conference on Earthquake Engineering, Dubrovnik, Yugoslavia, v. 1, p. 251-258.

[5] Boatwright, J., 1981, "Quasi-dynamic Models of Simple Earthquakes; Application to an Aftershock of the 1975 Oroville, California, Earthquake," Bulletin of the Seismological Society of America, v. 71, p. 69-94.

[6] Boatwright, J., 1982, "The Dynamic Characteristics of Faulting Inferred From Recordings of Strong-ground Motion," Conference Proceedings XVI, U.S. Geological Survey Open-File Report (in press).

[7] Boore, D. M., J. B. Fletcher, E. D. Sembera, and R. J. Archuletta, 1980, "A Preliminary Study of Selected Aftershocks of the 1979 Imperial Valley, California Earthquake from Digital Acceleration and Velocity Recordings [abs.]," Earthquake Notes (Seismological Society of America), v. 50, p. 49.

[8] Bycroft, G. N., 1980, "El Centro, California Differential Ground Motion Array," U.S. Geological Survey Open-File Report 80-919, 15 p.

[9] Campbell, K. W., 1981, "Near-source Attenuation of Peak Horizontal Acceleration," Bulletin of the Seismological Society of America, v. 71, p. 2039-2070.

[10] Converse, A. M., 1978, "Strong-motion Information Retrieval System Users Manual," U.S. Geological Survey Open-File Report 79-289, 51 p.

[11] Das, S. and K. Aki, 1979, "Fault Plane with Barriers, A Versitile Earthquake Model," Journal of Geophysical Research, v. 82, p. 5658-5670.

[12] Fletcher, J. B., A. G. Brady, and T. C. Hanks, 1980, "Strong-motion Accelerograms of the Oroville Aftershocks: Data Processing and the Aftershock of 0350 August 6, 1975," Bulletin of the Seismological Society of America, v. 70, p. 243-267.

[13] Hanks, T. C. and R. K. McGuire, 1982, "The Character of High-frequency Strong Ground Motion," Bulletin of the Seismological Society of America, v. 71, p. 2071-2095.

[14] International Conference of Building Officials (ICBO), Uniform Building Code. Whittier, California, p. 131.

[15] Joyner, W. B. and D. M. Boore, 1981, "Peak Horizontal Acceleration and Velocity from Strong-motion Records Including Records from the 1979 Imperial Valley, California Earthquake," Bulletin of the Seismological Society of America, v. 71, p. 2011-2038.

[16] Madariaga, R., 1982, "A String Model for the High Frequency Radiation from Earthquake Faulting," in Boatwright, J., ed., Conference Proceedings XVI, U.S. Geological Survey Open-File Report (in press).

[17] Matthiesen, R. B., 1980, "Building Instrumentation Programs," in Proceedings, Workshop on Interpolation of Strong-Motion Earthquake Records Obtained In and/or Near Buildings. UCLA Report No. 8015, Los Angeles, p. 5-21.

[18] Miller, R. K. and S. F. Felszeghy, 1978, "Engineering Features of the Santa Barbara Earthquake of August 13, 1978," University of California at Santa Barbara Report UCSB-ME-78-2, 140 p.

[19] Pauschke, J. M., C. S. Oliveira, H. C. Shah, and T. C. Zsutty, 1981, "A Preliminary Investigation of the Dynamic Response of the Imperial County Services Building During the October 15, 1979 Imperial Valley Earthquake," Stanford University Dapartment of Civil Engineering Report 49, 100 p.

[20] Porcella, R. L., 1978, "Strong-motion Instrumentation in the Central and Eastern United States," Earthquake Notes (Seismological Society of America), v. 49, no. 2, p. 3-14.

[21] Porcella, R. L., 1979, "Recent Strong-motion Records," Seismic Engineering Program Report, January-April 1979, U.S. Geological Survey Circular 818-A, p. 2.

[22] Porcella, R. L., 1980, "Recent Strong-motion Records," Seismic Engineering Program Report, May-August 1979, U.S. Geological Survey Circular 818-B, p. 2.

[23] Porcella, R. L. and R. B. Matthiesen, 1979, "Strong-motion Instrumentation in the Imperial Valley," California, Seismic Engineering Program Report, January-April 1979, U.S. Geological Survey Circular 818-A, p. 7.

[24] Porcella, R. L., R. B. Matthiesen, R. D. McJunkin, and J. T. Ragsdale, 1979, "Compiliation of Strong-motion records from the August 6, 1979 Coyote Lake Earthquake," U.S. Geological Survey Open-File Report 79-385 and California Division of Mines and Geology Preliminary Report 25, 71 p.

[25] Porcella, R. L. and J. C. Switzer, 1982, "Recent Strong-motion Records," California, Seismic Engineering Program Report, January-April 1980, U.S. Geological Survey Circular 854-A, p. 4

[26] Porter, L. D., 1978, "Compiliation of Strong-motion Records Recovered from the Santa Barbara Earthquake of August 13, 1978," California Division of Mines and Geology Preliminary Report 22, 43 p.

[27] Raugh, M. R., 1981, "Procedures for Analysis of Strong-motion Records [abs]," Earthquake Notes (Seismological Society of America), v. 52, no. 1, p. 17.

[28] Rojahn, C. and R. B. Matthiesen, 1977, "Earthquake Response and Instrumentation of Buildings," Journal of the Technical Councils of ASCE, v. 103, no. TC1, p. 1-12.

[29] Rojahn, C. and J. T. Ragsdale, 1980, "Strong-motion Records from the Imperial County Services Building, El Centro," in Leeds, D. J. ed., Imperial County, California, Earthquake, October 15, 1979. Berkeley, California, Earthquake Engineering Research Institute Reconnassance Report, p. 173-184.

[30] Rojahn, C., J. T. Ragsdale, J. D. Raggett, and J. H. Gates, 1980, "October 1980, October 15, 1979 Main-shock Strong-motion Records from the Meloland Road-Interstate Route 8 Overcrossing, Imperial County, California," U.S. Geological Survey Open-File Report 80-1054.

[31] Rojahn, C. and P. N. Mork, 1981, "An Analysis of Strong-motion Data from a Severely Damaged Structure, the Imperial County Services Building, El Centro, California," U.S. Geological Survey Open-File Report 81-194, 48 p.

[32] Rojahn, C. and J. D. Raggett, 1981, "Guidelines for Strong-motion Instrumentation of Highway Bridges," U.S. Department of Transportation Federal Highway Administration Report FHWA/RD-82/016, 116 p.

[33] Spudich, P., E. Cranswick, J. Fletcher, E. Harp, C. Mueller, R. Navarro, J. Sarmiento, J. Vinton, and R. Warrick, 1981, "Acquisition of Digital Seismograms During the Mammoth Lakes, California, Earthquake Sequence of May-June 1980," U.S. Geological Survey Open-File Report 81-381.

[34] Sunder, S. S. and J. J. Conner, 1982, "A New Procedure for Processing Strong-motion Earthquake Signals," Bulletin of the Seismological Society of America, v. 72, p. 643-661.

[35] Switzer, J., D. Johnson, R. Maley, and R. Matthiesen, 1981, "Western Hemisphere Strong-motion Accelerograph Station List - 1980," U.S. Geological Survey Open-File Report 81-664, p. I-1 - I-87.

[35] Trifunac, M. D. and V. Lee, 1973, "Routine Computer Processing of Strong-motion Accelerograms," California Institute of Technology Earthquake Engineering Research Laboratory Report EERL 73-03, 360 p.

[36] Trifunac, M. D. and V. Lee, 1978, "Uniformly Processed Strong-motion Earthquake Ground Acceleration in the Western United States of America for the Period of 1933 to 1971," University of Southern California Report CE78-01.

[37] Turpen, C. D., 1980, "Strong-motion Records from the Mammoth Lakes Earthquakes of May 1980," California Division of Mines and Geology Preliminary Report 27, 41 p.

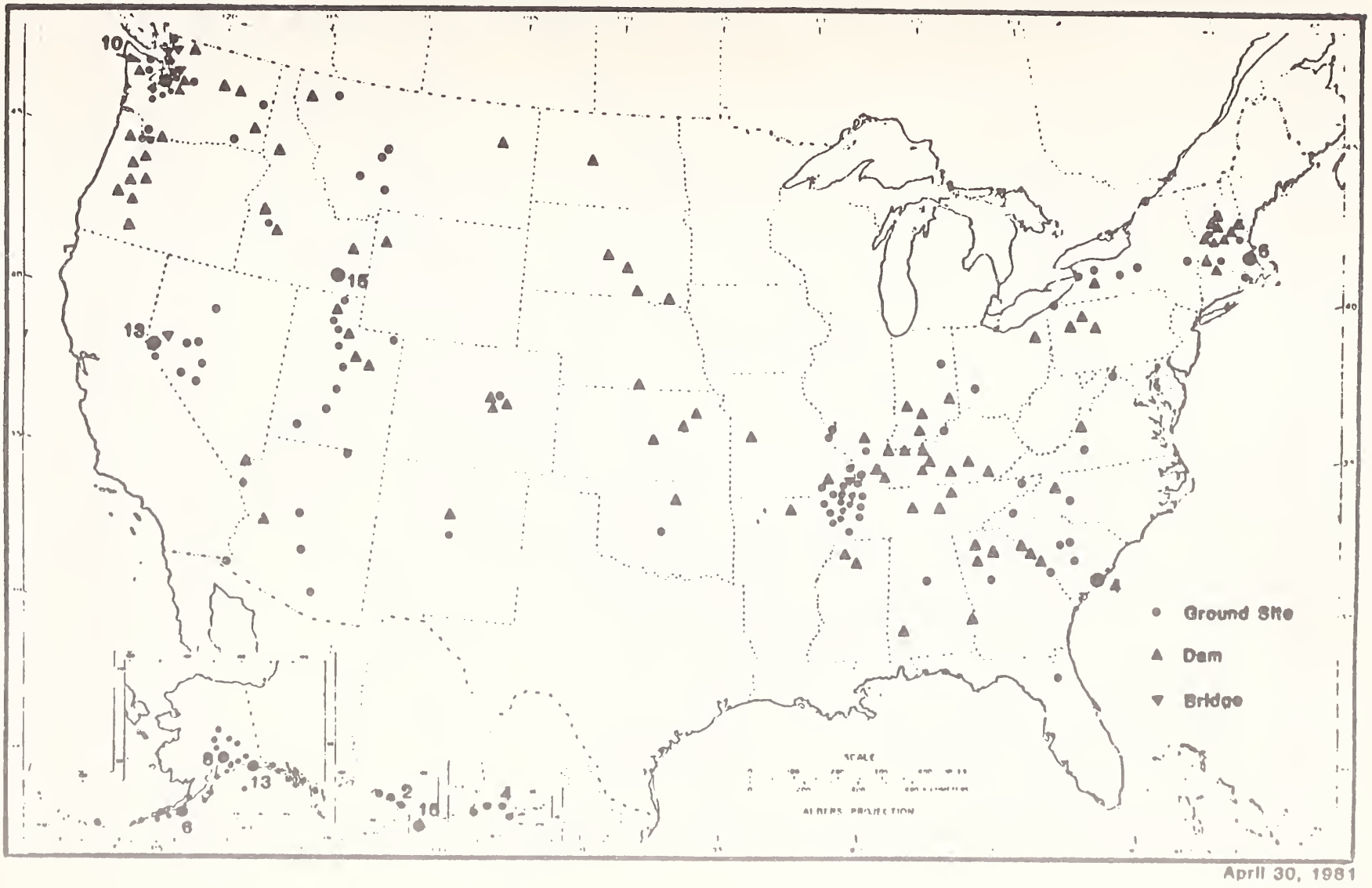

Figure 1.- Known accelerographs in the United States outside of California. Excludes commercial nuclear-powered electrical generating plants. April 30, 1981.

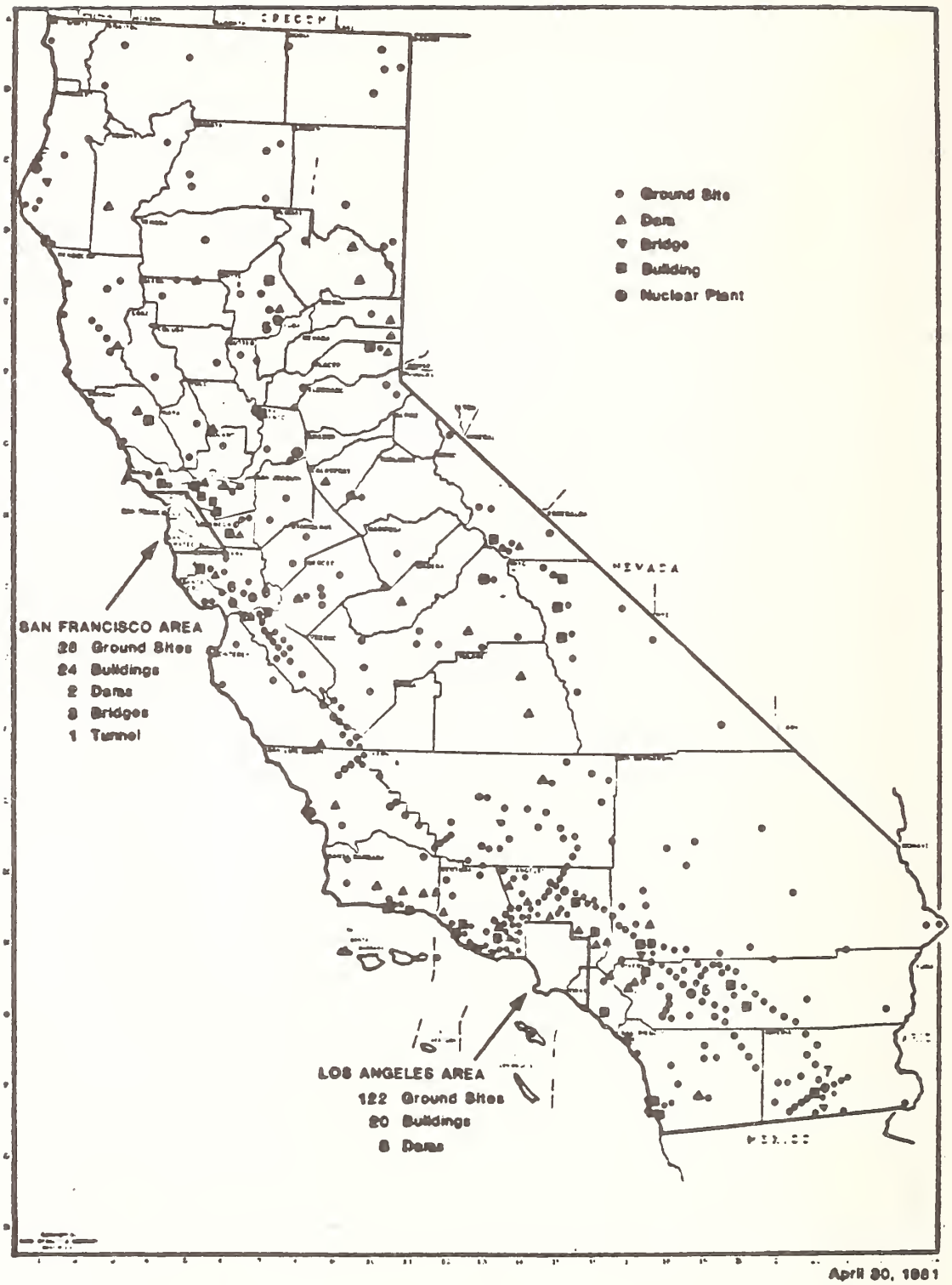

Figure 2.- Known accelerographs in California. Excludes instruments required by building codes. April 30, 1981.

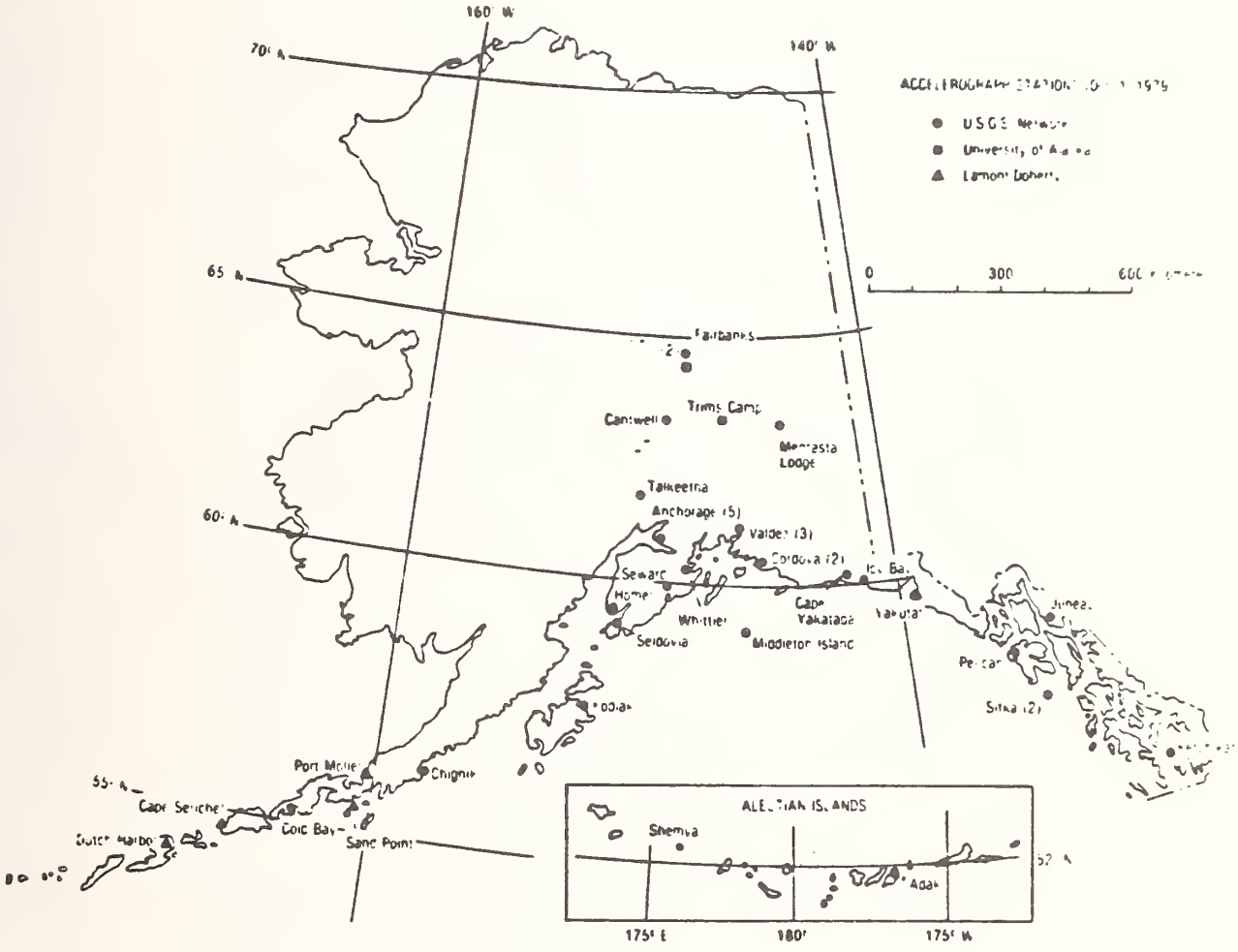

Figure 3.- Accelerograph stations in Alaska. Numbers in parenthesis are the total accelerograph stations at the indicated locality (from Porcella, 1979).

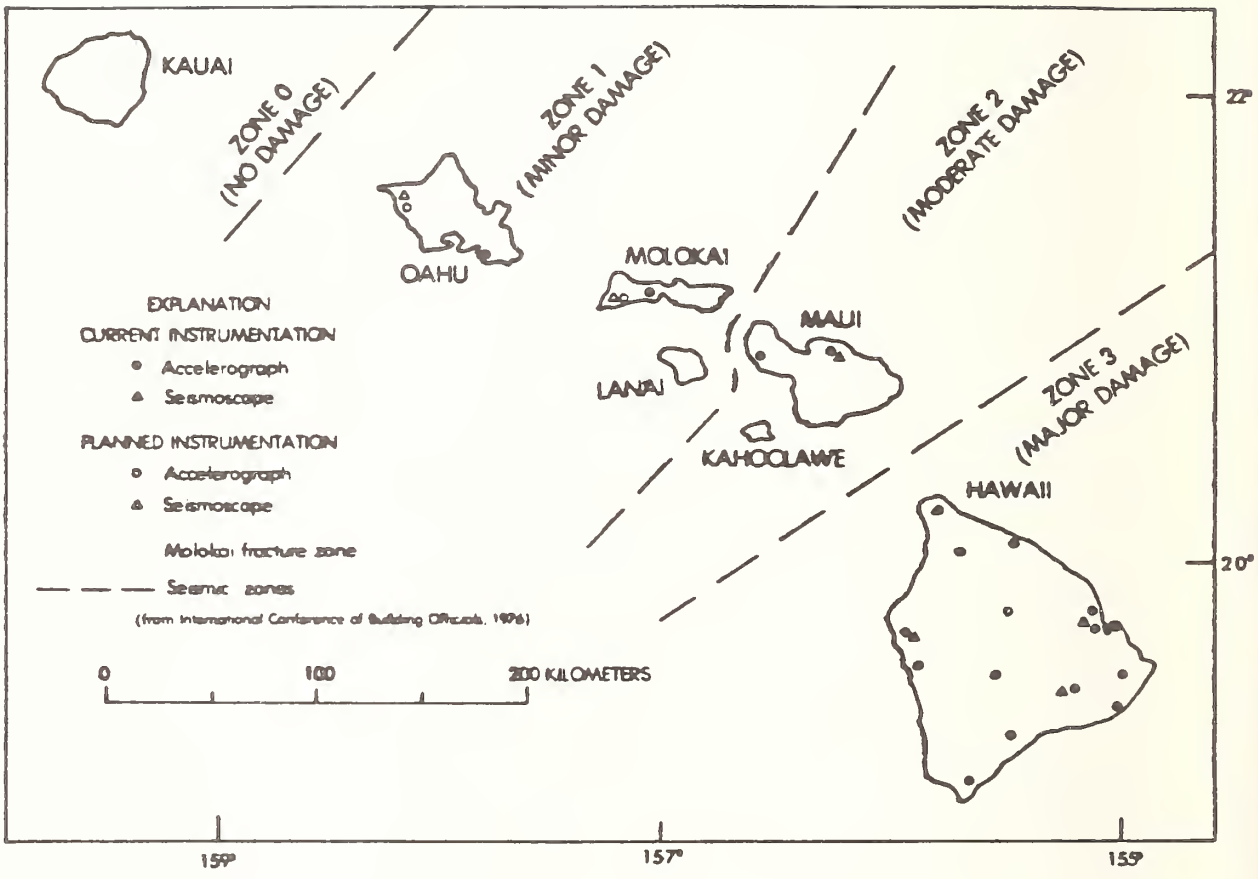

Figure 4.- U.S. Geological Survey strong-motion network in Hawaii (from Porcella, 1980).

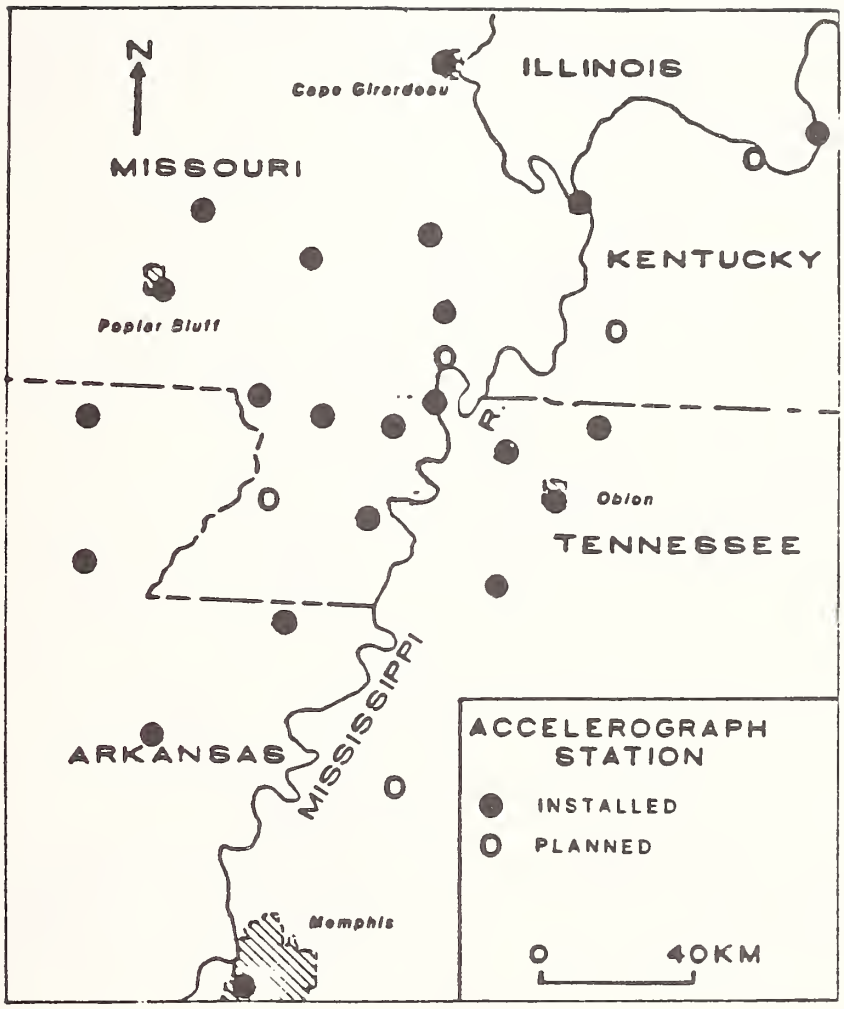

Figure 5.- Strong-motion network for the New Madrid seismic zone (after Porcella, 1978).

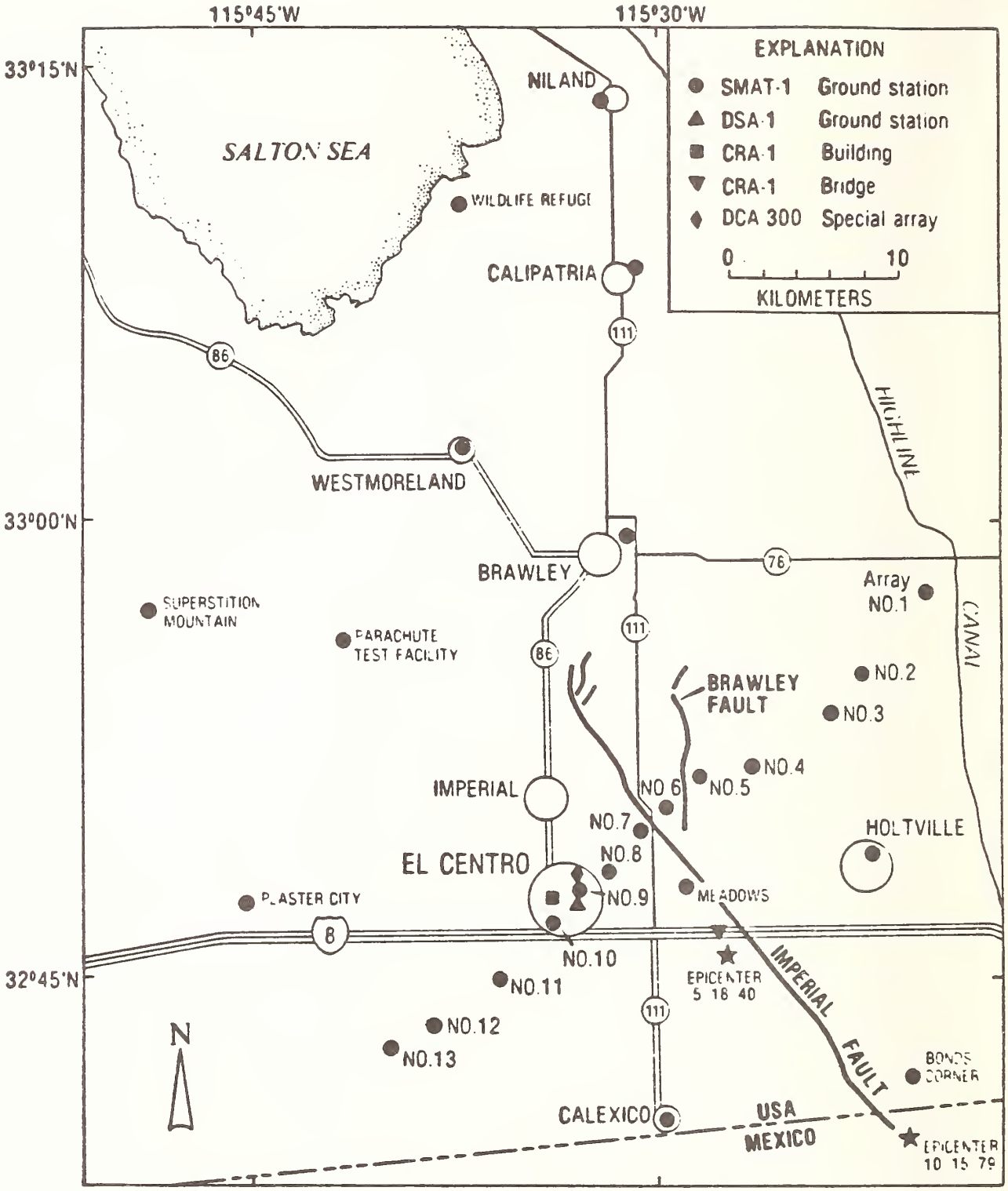

Figure 6.- Strong-motion stations in the Imperial Valley (from Porcella and Matthiesen, 1979).

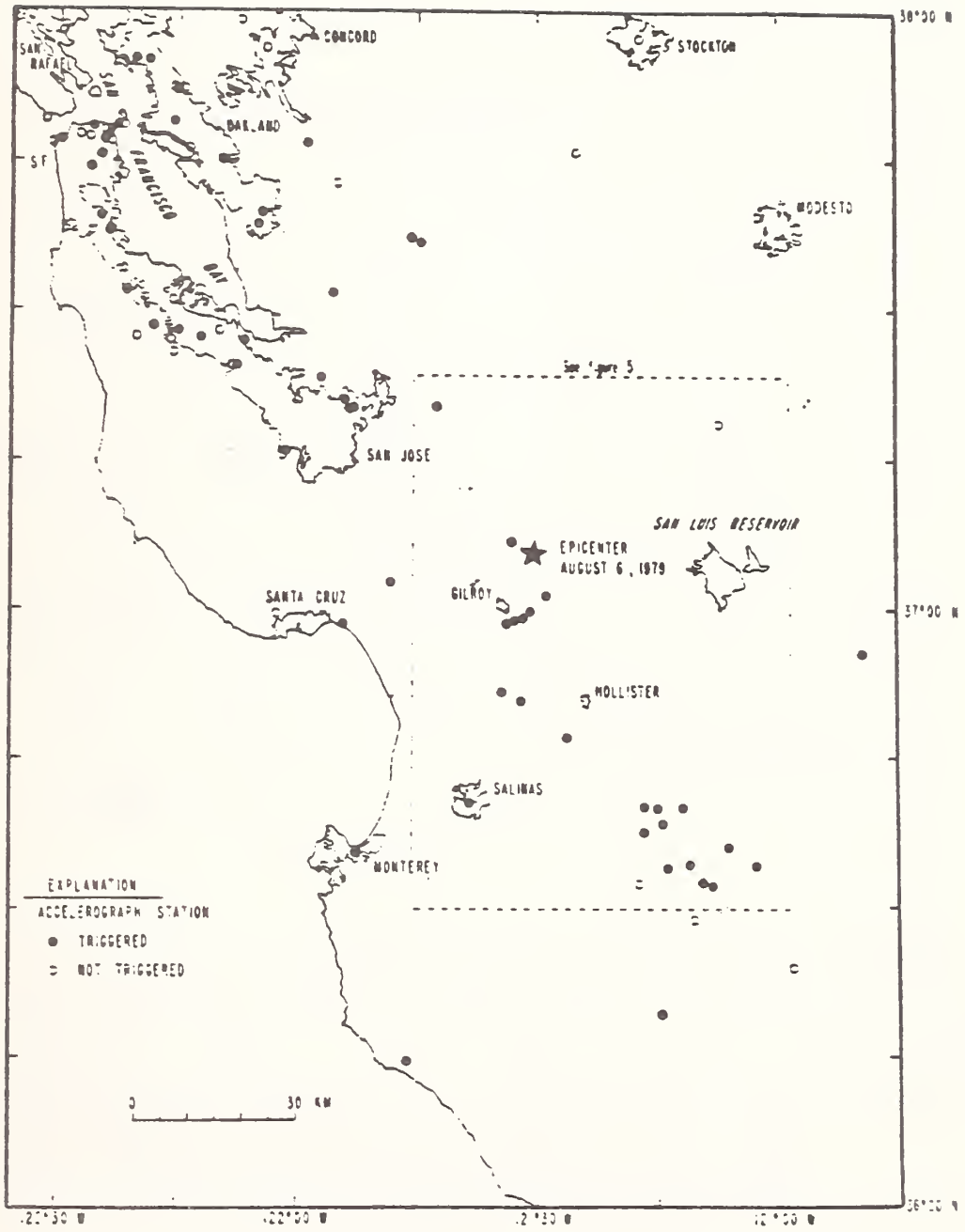

Figure 7.- Location of strong-motion stations in the region of the August 6, 1979 Coyote Lake, California earthquake (from Porcella and others 1979).

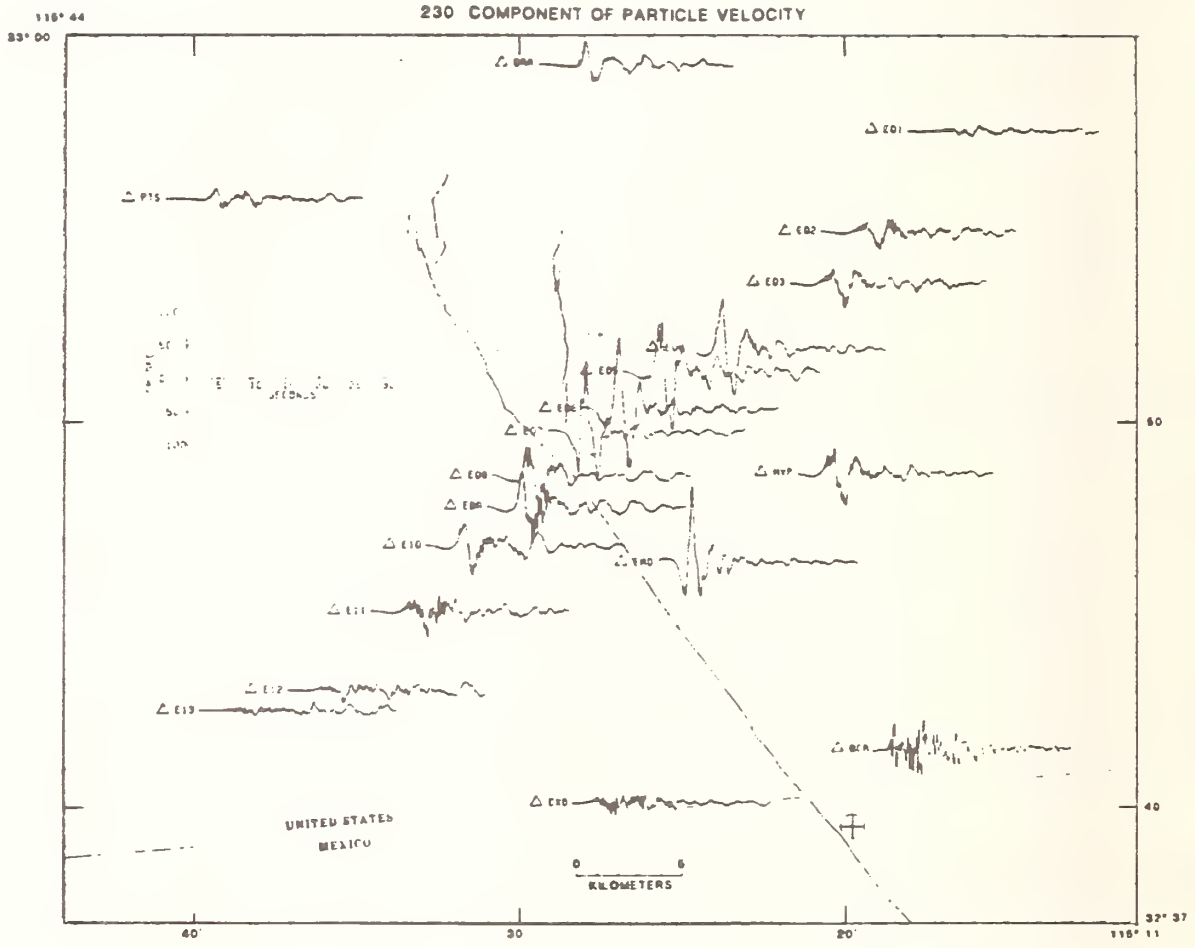

Figure 8.- Horizontal ground velocity at the USGS El Centro ground motion array (sites V01-V13) and four other strong-motion accelerograph sites in the Imperial Valley (sites BAR, HVL, BCR, and CXO). Location of October 15, 1979 earthquake epicenter shown by cross hairs. (from Archuletta and Spudich, 1982).

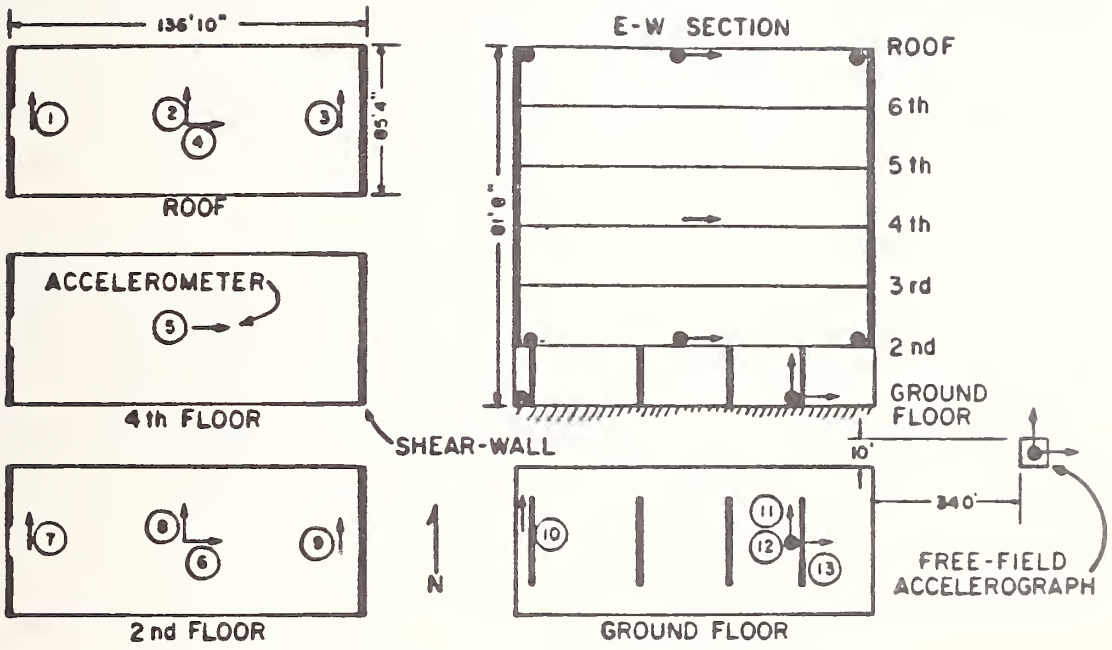

Figure 9.- Locations of FBA accelerometers (arrows with numbers) and SMA-1 accelerograph at Imperial County Service Building and adjacent free-field site, El Centro, California (after Rojahn and Ragsdale, 1980). Arrows denote direction of positive acceleration (on trace).

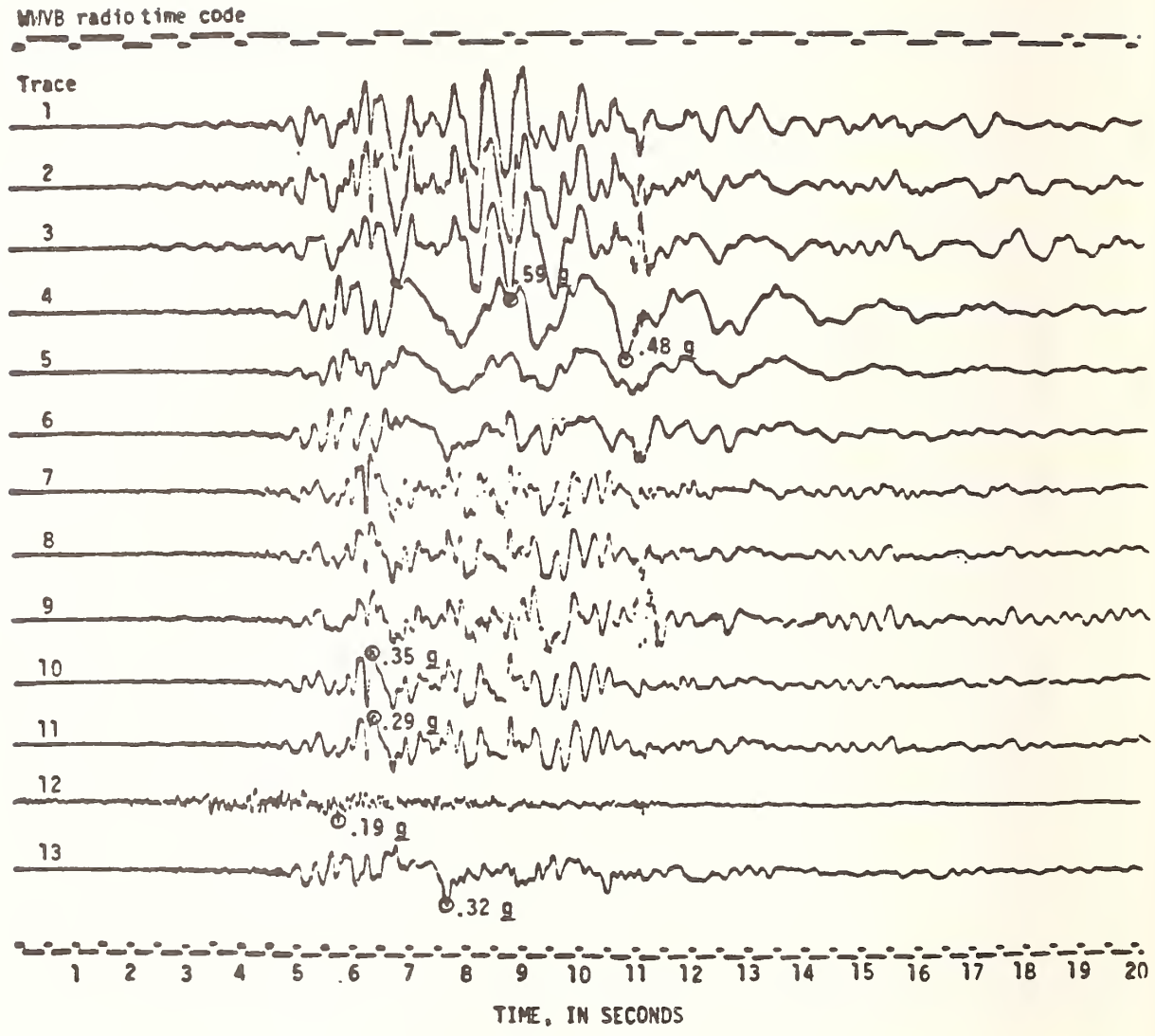

Figure 10.- Part of CRA-1 strong-motion accelerogram recorded on October 15, 1979 in Imperial County Services Building, El Centro, California. Total record length was 90 s. Trace number at start of record (left of figure) corresponds to accelerometers in figure 9 (from Rojahn and Mork, 1981).

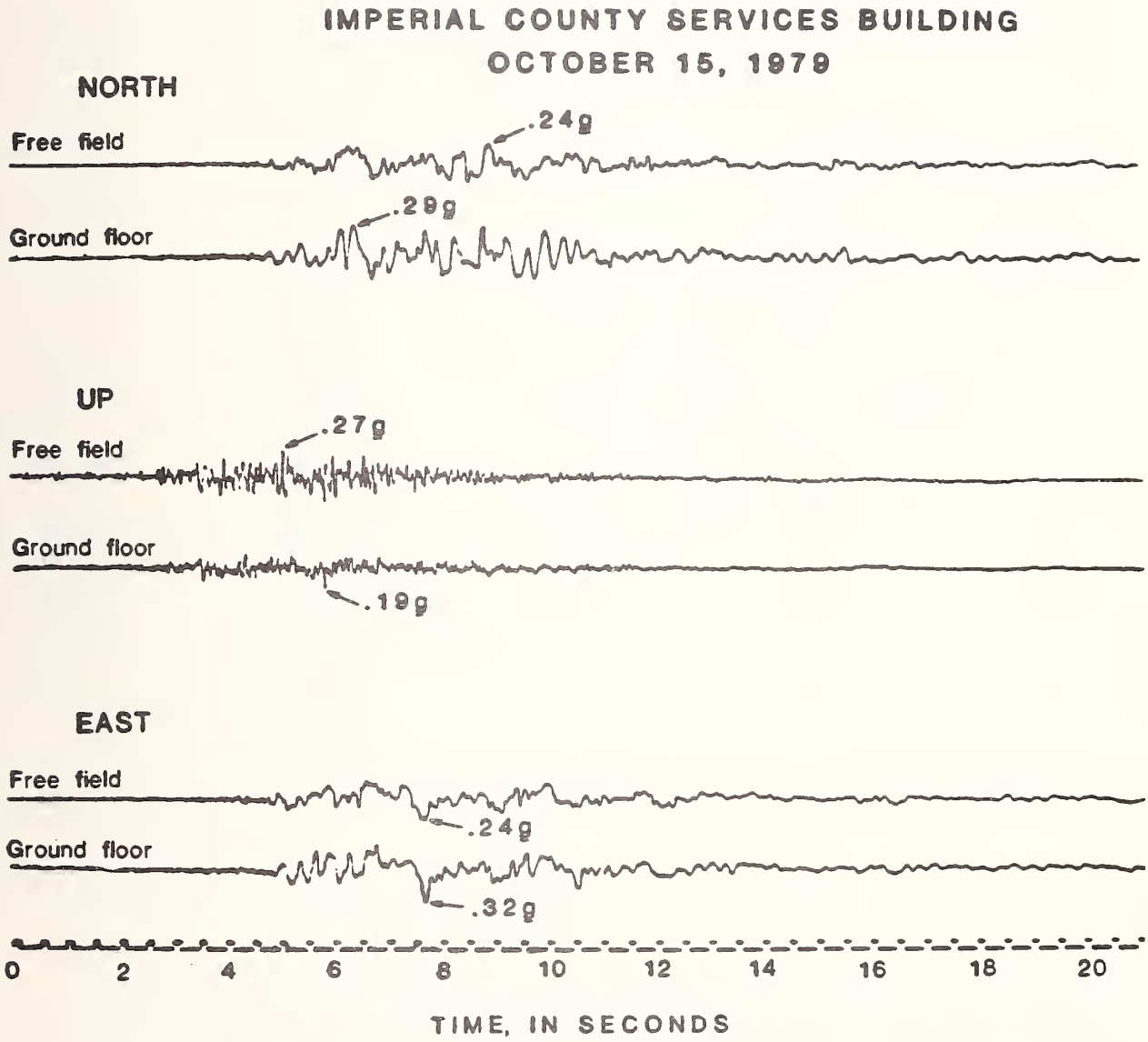

Figure 11.- October 15, 1979 acceleration-time histories recorded at Imperial County Services Building and adjacent free-field site, El Centro, California (from Rojahn and Mork, 1981).

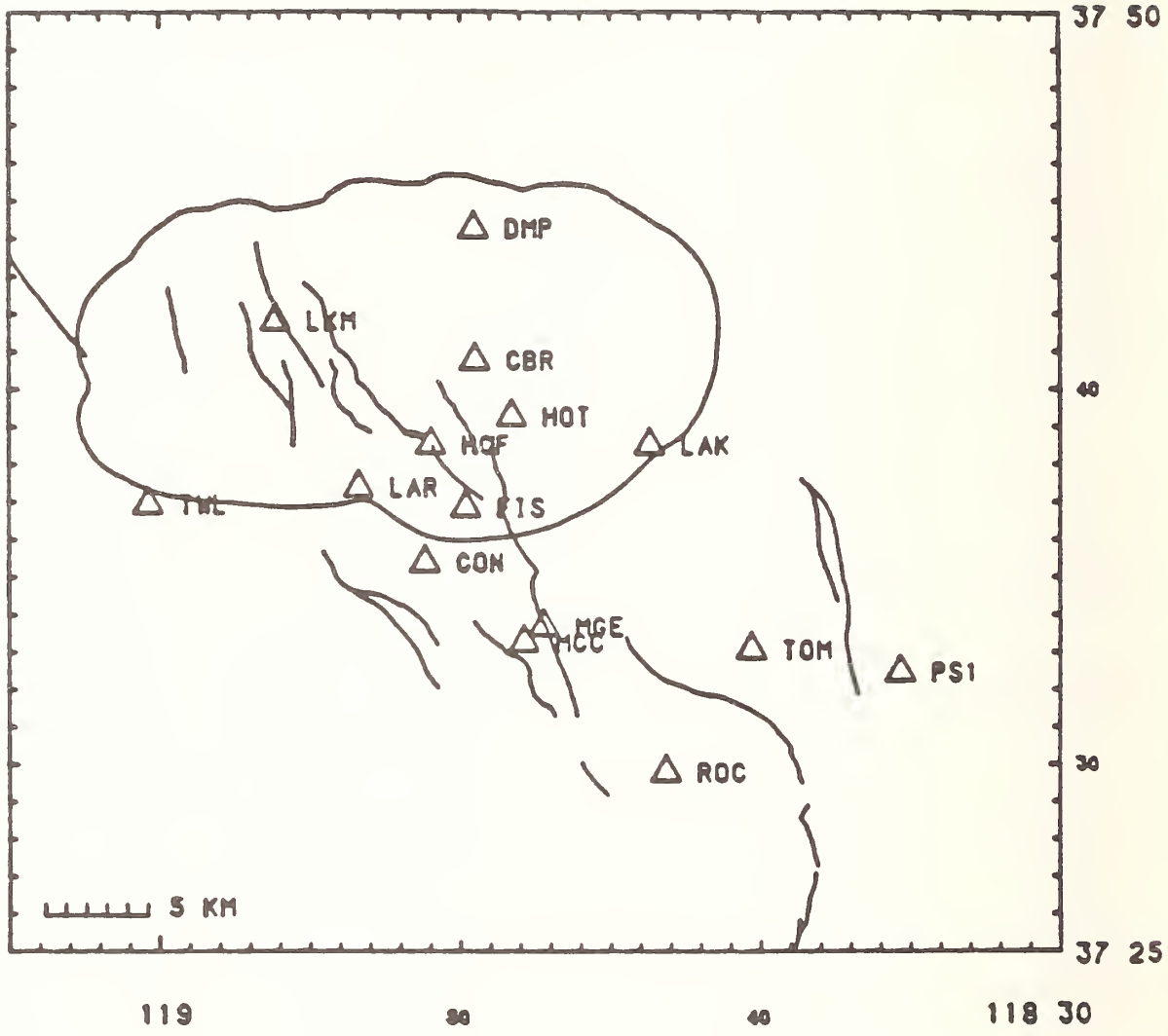

Figure 12.- Locations of digital seismometers which recorded earthquakes during the May 1980 Mammoth Lakes earthquake sequence (from Spudich and others, 1981).

Table 1.--Summary of Ground-Motion Stations in the U.S.

Location	Agency	Number of Station Types*		
		Instrument Shelters	Buildings	Unidentified
		WESTERN U.S.		
Alaska	USGS	12	24	-
	Other	2	3	10
California	CDMG	104	140	-
	USC	-	74	-
	USGS	14	73	-
	VA	-	6	-
	Other	13	16	16
Hawaii	USGS	-	19	-
Nevada	USGS	1	5	-
	VA	-	1	-
Northwest	USGS	2	14	-
	VA	-	6	-
	Other	3	3	-
Rocky Mountain Region	USGS	1	3	-
	VA	-	2	-
Southwest	VA	-	4	-
	Other	2	-	-
Utah	USGS	-	1	-
		CENTRAL U.S.		
North Central	VA	-	2	-
Missippi Valley	USGS	-	16	-
	VA	-	5	-
South Central	VA	-	2	-
		EASTERN U.S.		
Northeast	VA	-	13	-
	Other	-	2	-
Mid-Atlantic	VA	-	6	-
Southeast	USGS	-	3	-
	VA	-	4	-
	Other	-	1	-

*Source: Switzer and others, 1980

Table 2.--Summary of Structures Instrumented to Provide Data for Structural-Reponse Studies

Location	Agency*	Number of Structures with Extensive Instrumentation	Number of Structures with Minimal Instrumentation
		BUILDINGS	
California	CDMG	51	-
	CIT	-	2
	UCLA	3	11
	USGS	1	2
	VA/USGS	4	-
Alaska	USGS	-	2
		BRIDGES	
Alaska	USGS/FHWA	1	-
California	CDMG	3	-
	CDMG/FHWA/USGS	1	-
	CDOT/USGS	-	3
Missouri	USGS/FHWA	1	-
Nevada	UNV	-	1
New York	FHWA/USGS	1	-
Washington	WHD/USGS	3	-
		DAMS	
California	CDMG	5	14

*CDMG--California Division of Mines and Geology, Sacramento
CDOT--California Department of Transportation, Sacramento
CIT--California Institute of Technology, Pasadena
UCLA--University of California, Los Angeles
USGS--U.S. Geological Survey, Menlo Park, California
UNV--University of Nevada, Reno
VA--Veterans Administration, Washington, D.C.
WHD--Washington (State) Highway Department

Table 3a.--Summary of Dams Instrumented to Provide Data for Facility-Evaluation Studies

Location	Number of Structures by Agency*				
	ACOE	CDWR	MWD	WPRS	Other
WESTERN U.S.					
Alaska	2	-	-	-	-
California	17	8	7	6	3
Nevada/Utah	-	-	-	4	-
Northwest	13	-	-	2	1
Southwest	3	-	-	-	-
Rocky Moutain Region	5	-	-	3	-
CENTRAL U.S.					
North Central	16	-	-	-	-
Missippi Valley	1	-	-	-	-
South Central	17	-	-	-	-
EASTERN U.S.					
Northeast	11	-	-	-	-
Mid-Atlantic	6	-	-	-	-
Southeast	7	-	-	-	-

*ACOE--Army Corps of Engineers, Vicksburg, Missippi
CDWR--California Department of Water Resources, Sacramento
MWD--Metropolitan Water District, Los Angeles, California
WPRS--US Water & Power Research Service, Denver, Colorado

Table 3b.--Summary of Buildings Instrumented to Provide Data for Facility-Evaluation Studies

Location	Number of Structures		
	Code-Instrumented	VA Hospitals	Other
	BUILDINGS		
California--Los Angeles	200+	0	0
--San Francisco	0	1	6
--Other Cities	100+	4	2
Utah--Salt Lake City	0	1	0
Washington--Seattle	0	0	1

Table 3c.--Summary of Pumping, Power and Filter Plants Instrumented to Provide Data for Facility-Evaluation Studies

Location	Number of Structures By Agency*		
	CDWR	MWD	Other
California	9	2	1

*CDWR--California Department of Water Resources, Sacramento
MWD--Metropolitan Water District, Los Angeles

Table 4.- Specifications for Digital Strong-Motion Recorders

	DSA-1	DR-100	DCS-302	MCR-600	PDR-2	GEOS
SIGNAL CONDITIONING						
pre-amplification	none	0-120 db/ 6 db steps	x1, 5, 25, 100 with AGC	60 - 120 db/ 6 db steps (42.5 amp)	0-36 db/6 db steps	0-60 db/6 db steps
noise level referred to input	LSB 1.2 mv	<0.3 μv pp	12 μv pp	.2 μv RMS (pass band .2 to 13 Hz)	<9 μv	<0.5 μv RMS
filter (anti-alias)	none	5 pole Butter-worth nominally 50 HZ corner	5 pole Butterworth 30 Hz corner	4 pole-8 corners	2 pole Butter-worth, 7 corners	7 pole Butterworth 4 corners
sensor types	accelerometers (1/4, 1/2, 1, 2g)	geophones, force balance accelerometers	geophones, force balance acceler-ometers	geophones	geophones	geophones, force balance accelerometers
number of inputs	3	1-3	1-3 (6 optional)	1-3	1-3 (6 optional)	1-6
A/D CHARACTERISTICS						
dynamic range	12 bit - 72db	12 bit-72 db	12 bit, 112 db, gain range	12 bit-72 db 3 bit-AGC	12 bit-115 db	16 bit-96 db
resolution	12 bit - 72 db	12 bit-72 db	12 bit-72 db	12 bit-72 db	12 bit-72 db	16 bit-96 db
LSB (input to A/D)	1.2 mv	4.8 mv (FS = 10v)	2.4 mv (FS = 5v)	4.8 mv (FS = 10v)	1.2 mv (FS = 2.5v)	310 μv (FS = 10v)
sample rate (max. sps/chan)	200	600	600	200	500	1200
pre-event memory samples	512, 1024	551 - 1675	192 - 15,360	< 999	3072	2560

Table 4.- Specifications for Digital Strong-Motion Recorders (continued)

	DSA-1	DR-100	DCS-302	MCR-600	PDR-2	GEOS
CLOCK						
stability	TC6-1B, 3×10^{-7}/day 0 - 50°C ageing $5/10^{7}$/yr	±5 x 1^{-8}/day TCXO 0-70°C	5×10^{-6}/day 0 - 50°C ageing 1×10^{-7}/mo	1×10^{-6}day TCXO 0 - 55°C	3×10^{-7} 0 - 50°C ageing 4×10^{-8}/mo	±1 x 10^{-7}/day TCXO-20° - 60°C ageing 8×10^{-8}/mo
slew rate	none	±20 ms/sec	none	5 ms/sec	none	none will have slew
time record	optional record WWVB or TCG	BCD (header/ trailer)	coded BCD each sample	1296 samples/ record	3072 samples/ record	header
clock sync	none/sync to ext via TCG	sync or slew	WWVB	to external time standard	satellite receiver (mounted internally)	sync to WWVB internal receiver sync to ext. time standard
automatic clock correction	none	none	yes	none	yes	yes, CC in header
RECORDING CHARACTERISTICS						
tape medium	cassette	cassette	cassette	cassette	cassette	cartridge
transport	Kinemetrics	phi-dec	Terra-Tech	mFE	Kinemetrics	Kennedy 631
tracks	4	2	2	2	4	4 (serpentine)
density-method	1280 bpi	650 bpi-nrzi	1200 nrzi	800 bpi-ANSI-ECMA	1667 bpi phase encoded	1600 bpi phase encoded (6400 bpi optional)
samples/tape (words)	720,000	167,000	252,000	234,000	921,600	1.2 x 106 (1600 bpi) 4.8 x 106 (16400 bpi)
recording time at 500 to 600 sps	20 minutes	4.6 minutes	7 minutes	6.5 minutes	27 minutes	35 minutes (1600 bpi) 140 minutes (6400 bpi)

Table 4.- Specifications for Digital Strong-Motion Recorders (continued)

	DSA-1	DR-100	DCS-302	MCR-600	PDR-2	GFOS
TRIGGER ALGORITHM	amplitude threshold	STA/LTA analog	STA/LTA digital	STA/LTA-modified on filtered signal	STA/LTA-basic or difference scheme	STA/LTA digital
POWER REQ./PHYSICAL CHARACTERISTICS						
voltage	±12 VDC	+12 VDC	±12 VDC	±12 VDC	±12 VDC	+24 VDC
current drain (600 sps quiescence)	87 ma (pre-event mem.)	36 ma	50 ma	25 ma	95 ma 4 ma-tape	40 ma
operating temp.	0 - 50°	0 - 70°C	-30 - 65°C	0 - 60°C	0 - 50°C	-20 - 60°C
weight (lbs.)	43	28	16.5	28	54	35
size (in.)	10 x 17 x 8.5	15.5 x 9.5 x 10.5	14 x 8 x 10	8.5 x 12 x 18.25	26 x 14.25 x 8.75	21 x 12.5 x 14.25
DESIGN CONCEPTS						
hardware/uprocessor	hardwire	hardwire	hardwire	5 RCA-1802	2-RCA-1802	1-IM6100
chassis design	designated slot	wire wrap - designated slot	wire wrap - designated slot		2 large boards	unibuss (modules)
display - controls	calib (on/off) key	time, clock controls, event reset, trigger calibration record parameters (serial number configuration, event count)	time, trigger controls, clock controls	6 digit display, amplifier controls, keyboard	9 digit display, 2 keyboards, lock-switch	32 character alpha-numeric display, 2 keyboards, test points, interactive English set-up procedures.

Table 5.- Recent U.S. Strong-Motion Data Sets (1978-1982)

Event Name*	Date	M_L	No. of Records <40km	Dist to Closest Station (km)	Maximum Horiz Accel (g)	Responsible Agency**
Santa Barbara, CA	08/13/78	5.1	6	2.9	0.28	CDMG/USGS
Monticello, NC	08/27/78	2.8	1	0.7	0.30	USGS
	10/16/78	3.0	1	0.9	0.35	USGS
St Elias, AK	02/28/79	7.6	2	25.4	0.16	USGS
Coyote Lake, CA	03/06/79	5.9	11	1.2	0.42	USGS/CDMG
Imperial Valley, CA	10/15/79	6.6	34	0.5	0.81	USGS/CDMG
Livermore Valley, CA	01/24/80	5.5	12	10.8	0.24	USGS/CDMG
	01/27/80	5.6	11	4.0	0.28	USGS/CDMG
Horse Canyon, CA	02/25/80	5.3	10	5.8	0.12	CDMG
Mammoth Lakes, CA	05/25/80	6.1	4	1.5	0.46	CDMG/USGS
	05/25/80	6.0	3	3.5	0.43	CDMG/USGS
	05/25/80	6.1	2	6.1	0.49	CDMG/USGS
	05/27/80	6.2	3	11.9	0.52	CDMG/USGS
Mexicalli Valley, CA	06/09/80	6.1	7	2	0.83	UCSD
Westmorland, CA	04/26/81	5.6	10	7	0.49	USGS/CDMG
Franklin Falls, NH	01/19/82	4.7	3	4	0.56	ACOE/VA/USGS

*AK--Alaska
CA--California
NC--North Carolina
NH--New Hampshire

**ACOE--Army Corps of Engineers
CDMG--California Division of Mines and Geology
VA--Veterans Administration
UCSD--University of California at San Diego
USGS--U.S. Geological Survey

STORM SURGE DEFENSE WORKS AND RELATED RESEARCHES IN JAPAN

Yoshimi Goda

Port and Harbor Research Institute
Ministry of Transport

and

Hiroshi Hashimoto

Public Work Research Institute
Ministry of Construction

ABSTRACT

Five typhoons on the average land every year because Japan is located in a typhoon attacking zone of the Western Pacific Ocean. They bring storm surges and high waves along a coast. Once the storm surge causes a flood, damage is enormous. Coastal dikes and gates have been constructed to prevent damage. Storm surge defense works have been carried out on the principle established after the Ise-wan Typhoon which caused heavy damage in 1959. In this regard, research related to the numerical estimation of storm surges and waves were made. Experimental investigations were carried out by universities and governmental institutions to determine the wave run-up and overtopping on a dike. The research stopped after the defense works were almost completed.

INTRODUCTION

Japan is located on the western Pacific Ocean where five typhoons hit every year, on the average. A typhoon brings storm surges and high waves along the coast, which are caused by atmospheric pressure depression and strong winds. Once the storm surge causes a flood in a low topographic plain, damage of life and property become enormous. To prevent such damage, storm surge defense works have been carried out by constructing coastal dikes and gates. This report describes the storm surge defense works and related research activities and organizations.

STORM SURGE DEFENSE WORKS

STORM SURGE

The typhoon is one type of tropical depression like the hurricane and occurs on the south of the Japan Islands. On the average, 26 typhoons are generated each year and five hit the Japan Islands. It brings storm surges and high waves which are generated by atmospheric pressure depression and strong winds. Sea levels become abnormally high in a bay which opens its mouth to the south. Table 1 shows the list of typhoons which brought tides over 2 m and figure 1 shows their tracks.

Storm surges are frequent in Toyko Bay, Ise Bay, Osaka Bay and Ariake Sea. In these bays, large cities lie on deltas formed by the deposition of sand and silt transported by rivers. It is here

that population and property are concentrated. In some areas, land subsidence due to excess pumping of ground water. If storm surges occur and the coastal dikes are broken, the damage is serious.

STORM SURGE DEFENSE WORKS

Although storm surge defense works had been carried out for many years, the Ise-wan Typhoon hit Nagoya City in 1959 and caused the loss of five-thousand lives and five-hundred billion yen's worth of property. As a result of this disaster, the storm surge defense works developed both technically and financially.

At 18:13 hours on September 26, 1959, the center of the typhoon landed near Sionomisaki of Kii Peninsula with a maximum instantanious wind speed of 60 m/sec and a central pressure of 929.5 mb. After the landing, it passed on the west side of Ise Bay and caused extraordinary high tides and waves at 23:15 hours on September 26 in the Port of Nagoya, situated in the recess of the bay. The astronomical tidal level should have been 0.35 m, but the meteorological tide in Nagoya Port was estimated to be 3.55 m. Waves were about 3 m in height and damage by inundation occurred. Figure 2 shows the distribution of the maximum tidal level, the maximum significant wave height and the inundated areas.

After investigations of the typhoon characteristics and the damage conditions, fundamental guidelines on defense works against storm surges were decided upon as follows:

1. Planning should be made considering the various problems of the coast, river, harbor, reclaimed land, road and others.
2. The meteorological tide and the wave height due to the Ise-wan Typhoon plus the mean high water level of the typhoon season should be used as the design weather condition. Precautions should be also taken to minimize damage resulting from conditions exceeding these standards.

With respect to structural embankments, careful attention should be paid to the following:

1. The embankment structure should be as uniform as possible. In places where the embankment is not uniform, such as the connection between a new embankment and an existing one, topographic characteristics and the other conditions, special care must be taken to protect the joints from becoming a weak point.
2. The levee crown and back slope should be protected by concrete-coating even when an embankment is designed not to permit overtopping of waves. When overtopping is designed for, care should be taken to increase the resistance of the face and foot of the back slope against scouring.

3. During construction, care should be taken not to leave any gaps under the coating and not to make any parapets into a structural weak point.

Coastal dikes, gates, and storm surge breakwaters were constructed under the above guidelines. The typical section of embankment is shown in figure 3. Joints were made every 10 m in the sectional direction and every 4 to 5 m in the horizontal direction in the dike surface covering. A cut-off board and a joint bar were used for every joint. The levee crown was covered with asphalt pavement in order to maintain flexibility against settlement.

The embankment by the Nikko River was destroyed by the typhoon, especially near the mouth. As a countermeasure, a high lock gate and a high closing levee were built in the mouth leaving the crown height of the embankment the same height as before the typhoon. The gate is closed when high tides arise and this prevents flooding up to the river.

The Nabeta Reclamation, in construction since 1946, suffered heavy damage by the typhoon. The embankments surrounding it were almost completely destroyed. The main factor leading the embankment to destruction appears to be erosion and scouring of the back slope due to overtopping waves. The reconstruction works are shown in figure 4. The slope of the front surface was designed to be very gentle, 1:10, to take into account the weakness of the foundation and the effect of reduction of wave energy on it. The surface of the slope is covered with asphalt concrete to protect the soil. Five draining pumps were installed.

Storm surge breakwaters were constructed in Nagoya Port. Using breakwaters reduced the crown height of embankments and sea walls inside the breakwaters, so that the embankments and sea walls would not deteriorate the port function and impede the development of reclamation. Figure 5 shows the variations of tidal level at Nagoya with and without the breakwaters in the case of the Ise-wan Typhoon. The tide level was calculated using an electronic computer and assuming the entrance width of the breakwaters to be 500 m as compared with the case of no breakwater. The effect of the breakwaters on the wave height was also calculated by the SMB method. It is shown that the decrease of wave height due to the breakwaters will be 0.5-1.0 m. Therefore, the necessary embankment crown height and sea wall inside of the breakwaters would be expected to be reduced more than one meter as compared with the case of no breakwater. The breakwater consisted of three parts: the Nabeta, Central, and Chita Breakwater cross sections are shown in figure 6.

Based on the guidelines set for the construction of the storm surge defense works in Ise Bay, defense works have been carried out along the coast of Tokyo Bay, Ise Bay, Osaka Bay, Suohonada and Ariake Sea with the design typhoon having the same magnitude as the Ise-wan Typhoon. In other bays and coast locations the maximum tidal level and wave height recorded in the past were used as the

design sea conditions. For storm surge defense works, coastal dikes, revetments, and gates have been constructed.

ADMINISTRATIVE ORGANIZATIONS

Storm surge defense works are administered and executed by the central and local governments. In the central government, the Ministry of Construction, the Ministry of Transport, and the Ministry of Agriculture, Forestry, and Fisheries execute the defense works in accordance with their own jurisdictions. The Ministry of Transport takes care of the coast in the harbor area and the neighboring zone, whereas the coast in the fishing port area and in front of reclaimed land for agriculture is under the control of the Ministry of Agriculture, Forestry, and Fisheries. The rest if managed by the Ministry of Construction.

Usually, the defense works are executed by local governments, namely 47 prefectures and a number of cities, towns, and villages, execute defense works by themselves or with financial support of the central government. The central government is responsible for the coordination of planning and usually executes major projects by a Regional Construction Bureau of each Ministry.

Several organizations of the government other than the three Ministries are related to defense works. The Meteorological Agency has regional observatories along the coast which measures and forecasts wind, wave, storm surges, and tsunami. The Hydrographic Office of the Maritime Safety Agency supplies hydrographic data and marine charts, and the Geographical Survey Institute surveys topography and ground level variation. Figure 7 shows the organization of the central government.

Coastal defense works which include storm surge defense works, depend on the Coast Act, legally. The Act relegates the duty of the manager, assignment of expenses, action to be restricted and so on. In connection with the Act, technical criterion for the design of coastal defense works is laid down and a technical manual has been published.

RESEARCH ACTIVITIES

STORM SURGES

After the Ise-wan Typhoon, a method of storm surge computation was developed for the planning of the defense works in Tokyo Bay, Ise Bay, Osaka Bay and Suohonada. The pressure distribution in a typhoon was modeled and the wind on the sea surface was estimated to be the vector sum of the velocity derived from the atmospheric pressure gradient and the velocity proportional to the typhoon speed. Storm surges generated by the wind were computed numerically by the two-dimensional long water wave equation which consists of momentum and mass conservation equations. The distribution of

storm surge height in a bay, the effect of storm surge breakwaters, and flooding up to a river were analyzed by the model.

The estimation of wind velocity on the sea surface is the most important aspect in the calculation of storm surge levels. Recently, a method was developed to estimate the wind field by considering land forms around a bay. The return period of storm surges is also estimated from empirical typhoon data, since there is more meteorological data compared with the storm surge data. Recent research is not as active as those in the 1960's.

WAVES

Typhoons generate high waves as well as storm surges. The forecasting methods of waves generated by winds have been established. The methods based on the SMB method using a moving fetch and a method which includes bottom friction in shallow water. In a bay, wave heights are estimated on the grid points by the SMB method and a spectral method. In a bay where the mouth opens to the ocean, it is necessary to consider penetration of swells into the bay. In Osaka Bay, swells coming through the strait at the entrance were estimated, but reliable results were not obtained as yet.

Wave refraction, diffraction and dissipation by bottom friction are considered for the forecasting of waves. It is possible to estimate response along a simple coastline but on a complex coastline, hydraulic experiments need to be carried out. In some cases, wave irregularity is also considered by random wave generators. It is necessary to analyze wave deformation not only for storm surge defense works but for the evaluation of the effect and the influence of breakwaters and coastal structures. The development of numerical calculation methods and the analysis of wave nonlinearity are also carried out.

STORM SURGE DEFENSE WORKS

Though breakwaters have been constructed to prevent storm surges, coastal dikes, and revetments are also commonly used for defense works. These latter structures have been constructed to prevent a flood or overtopping of waves. Their height was determined by the run-up height of waves. However, it is rational to estimate the crown height by considering the volume of wave overtopping because of wave irregularity. One of the authors studied experimentally the relation between incident waves and the volume of wave overtopping for coastal dikes and revetments and proposed the relation as shown in figure 8. Wave irregularity is also considered and similar figures are proposed for dikes with artificial blocks in front of them.

The allowance of wave overtopping volume is determined by the function and the stability of the dike. If we need to maintain automobile traffic on a road behind a dike in a storm condition, the

volume should be kept small. Actually, the allowance was estimated by measuring the overtopping volume behind a dike and the possibility of the traffic evaluated. For dike stability, the allowance was made by analyzing past failures of coastal dikes and revetments for several projects.

Research on waves, storm surges, and structures related to storm surge defense works were active while the construction was carried out to defend storm surges. The level of research activities is now somewhat lowered as the works have almost been completed.

RESEARCH ORGANIZATION

Universities and governmental research institutions make investigations for storm surge defense works. Governmental institutions as shown in figure 7 and table 2, include the Meteorological Research Institute, Port and Harbour Research Institute, Public Works Research Institute, National Research Institute of Agricultural Engineering, National Research Institute of Fisheries Engineering, and the National Research Center for Disaster Prevention.

The Meteorological Research Institute performs research to analyze and to forecast climate. In connection with storm surges, the Typhoon Division studies not only the typhoon itself but the phenomenon and forecasting method of storm surges and waves.

The Port and Harbour Research Institute studies harbor planning, the function and the stability of port structures such as breakwaters, hydraulic characteristics of waves and currents, and water pollution. Concerning storm surges, forecasting methods of tidal variation and wave heights, and function and stability of breakwaters and coastal dikes are investigated.

The Public Works Research Institute has responsibility for research work involving flood prevention, sewage treatment, road planning, and structures such as bridges and tunnels. In regard to storm surges, defense work along the coastline and in the river mouth are investigated as well as functions and effects of coastal structures, such as dikes.

The National Research Institute of Agricultural Engineering is mainly conducting research of the improvement and irrigation of farm land. In addition to this, the role and the stability of dikes in reclaimed land is also one of their research problems. The National Research Institute of Fisheries Engineering performs research work on fishing ports and structures for fish farming. Coastal structures are also one of the research subjects.

The National Research Center for Disaster Prevention investigates preventing disasters caused by flooding, earthquake, land slide and snow. Related to the storm surges, investigation of waves is also carried out.

Other than these institutes, the Civil Engineering Research Institute, Hokkaido Development Bureau, and the Central Research Institute of Electric Power Industry are also aiding research on

coastal engineering. Some universities are conducting studies on storm surge problems, but not to the extent as government research.

Research results are presented at the conferences held by the Meteorological Society of Japan, the Oceanographical Society of Japan and the Japan Society of Civil Engineers (JSCE). Especially, research on storm surges and its prevention have been presented at the Japanese conference on coastal engineering of JSCE. The conference has been held every year since the first conference in 1954. In 1981, the 28th Conference was held and 126 papers selected from 166 entry papers were presented. The number of papers related to storm surges and its prevention from disasters is decreasing in recent years.

CONCLUSIONS

Storm surge defense work has been carried out in Tokyo Bay, Ise Bay and Osaka Bay by the guidelines which were established after the heavy damage caused by the Ise-wan Typhoon. As countermeasures, coastal dikes, revetments, gates, and storm surge breakwaters have been constructed. In connection with these works, the numerical calculation method of storm surges and waves has been developed and the effect of coastal dikes for the prevention of wave overtopping has been studied. Research is carried out by universities and governmental research institutions, but their activity is now decreasing because the defense works are almost completed.

REFERENCES

[1] Seminar on Coastal Engineering: Organizing Committee for Seminar on Coastal Engineering, 1964.

[2] Outline of Coastal Engineering in Japan: Organizing Committee of 10th Conference on Coastal Engineering, 1966.

[3] Goda, Y., "Design of Harbour Structure Against Random Sea Waves," Kajima Pub., 1977 (in Japanese).

Table 1. List of Typhoons Causing Meteorological Tide Over 2 m

Date	Bay Attacked	Meteorological Tide Level	Maximum Wind Speed	Atomospheric Pressure
Sept. 13, 1927	Ariake Bay	about 3.0 m		
Sept. 21, 1934 (Typhoon Muroto)	Osaka Bay	3.1	42 m/sec (at Osaka)	954 (912)* mb
Sept. 1, 1938	Tokyo Bay	2.2	31 (at Tokyo)	979 (about 960)*
Sept. 17, 1945 (Typhoon Makurazaki)	Kagoshima Bay	2.0	over 40 (at Kagoshima)	(917)*
Sept. 3, 1950 (Typhoon Jane)	Osaka Bay	2.4	28 (at Osaka)	970 (960)*
Sept. 27, 1957 (Typhoon Ise-wan)	Ise Bay	3.9	36.5 (at Nagoya)	958 (930)*
Sept. 16, 1961 (Typhoon 2nd-Muroto)	Osaka Bay	2.4	33 (at Osaka)	937 (931)*

(* shows the central pressure at the landing time)

Table 2. List of Institutions

Name	Address
Civil Engineering Research Institute, Hokkaido Development Bureau	Hiragishi 1-1, Toyohira-ku, Sapporo Japan
National Research Center for Disaster Prevention	Tennodai 3-1, Sakura, Niihari-gun, Ibaraki, Japan
Port and Harbour Research Institute	Nagase 3-1-1, Yokosuka, Japan
Meteorological Research Institute	Nagamine 1-1, Yatabe, Tsukuba-gun, Ibaraki, Japan
National Research Institute of Agricultural Engineering	Kannondai 2-1-2, Yatabe, Tsukuba-gun, Ibaraki, Japan
National Research Institute of Fisheries Engineering	Ebidai 7620-1, Hazaki, Kashima-gun, Ibaraki Japan
Public Works Research Institute	Asahi 1, Toyosato, Tsukuba-gun, Ibaraki, Japan

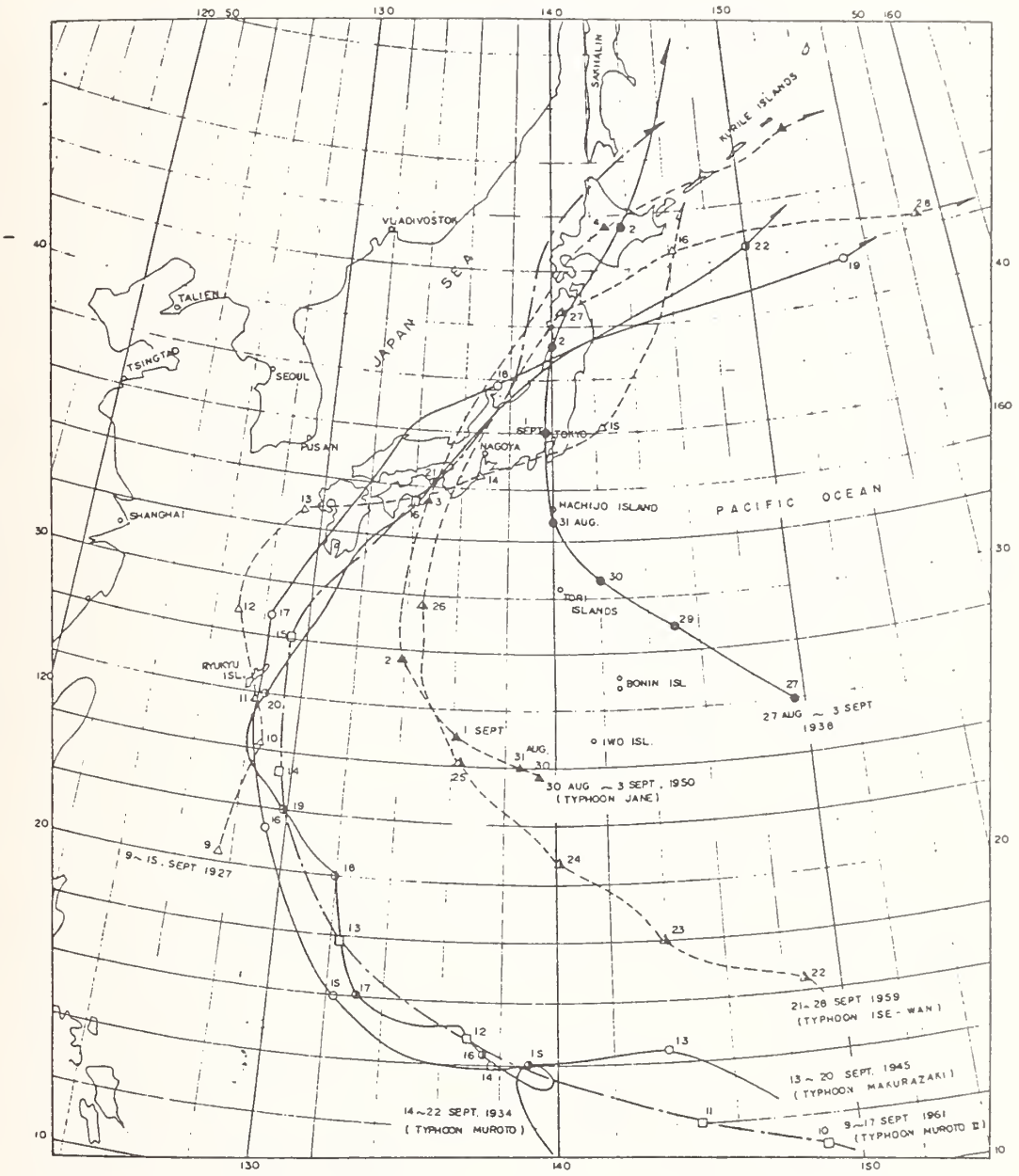

Figure 1. The track of typhoon causing meteorological tide over 2 m

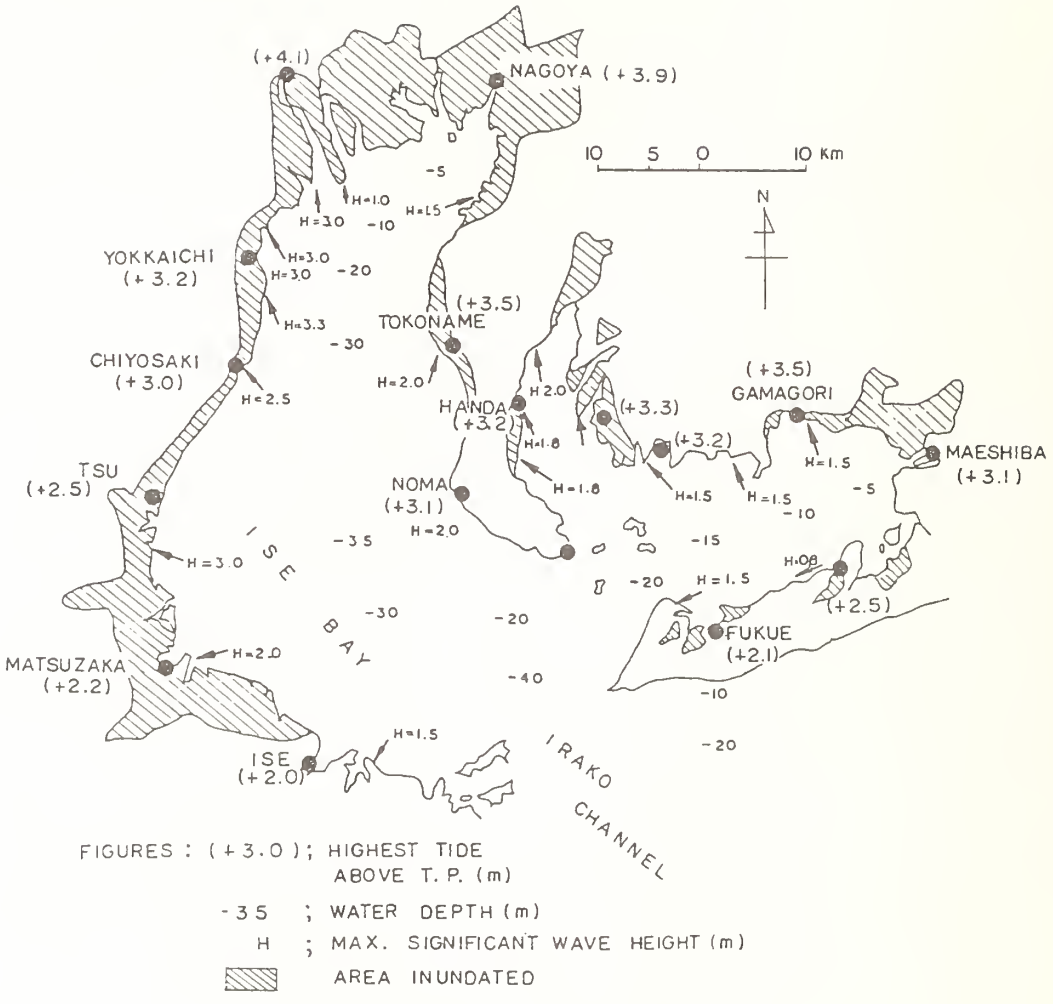

Figure 2. Maximum tide level, maximum significant waves and indundated area along the Ise-Bay coast

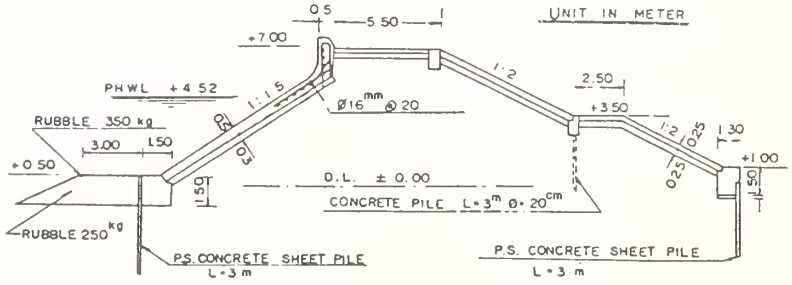

Figure 3. Standard section of coastal dike

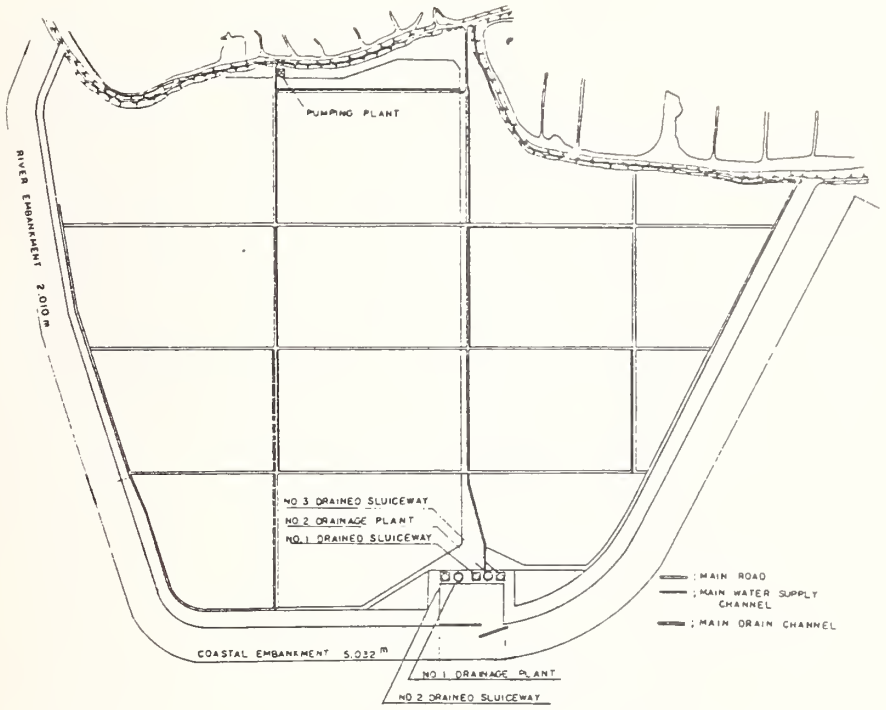

Figure 4. Plan of the coastal embankment of the Nabeta Reclamation

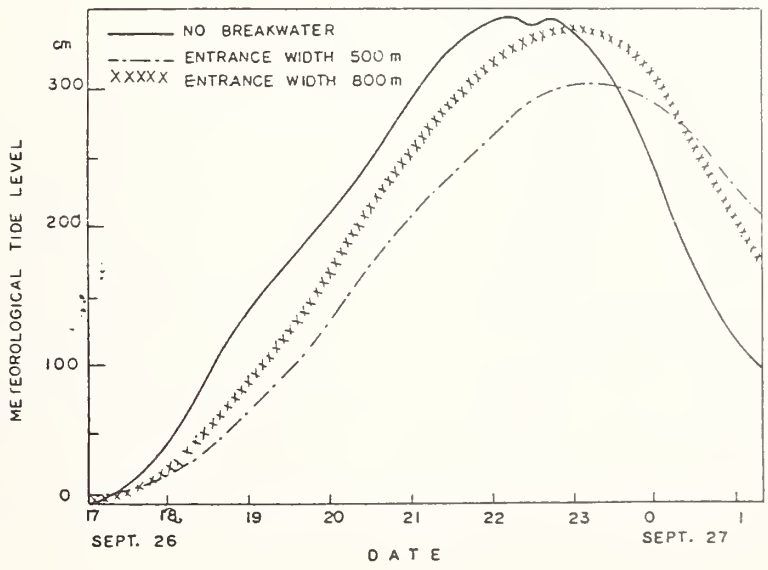

Figure 5. Effect of the storm-surge breakwater on the reduction of tidal level at Nagoya

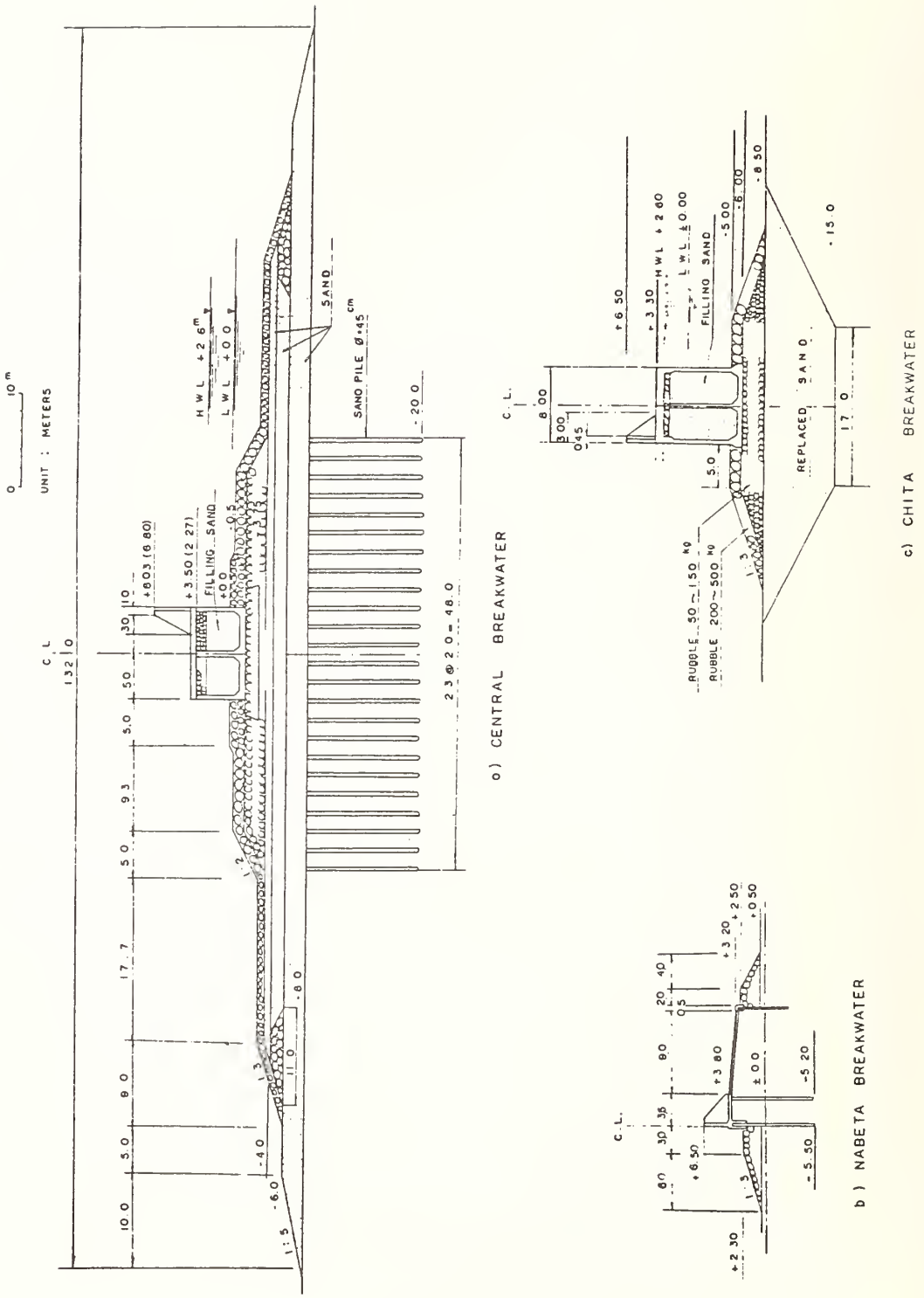

Figure 6. Cross section of the storm-surge breakwater

Figure 7. Administrative system of the central Government

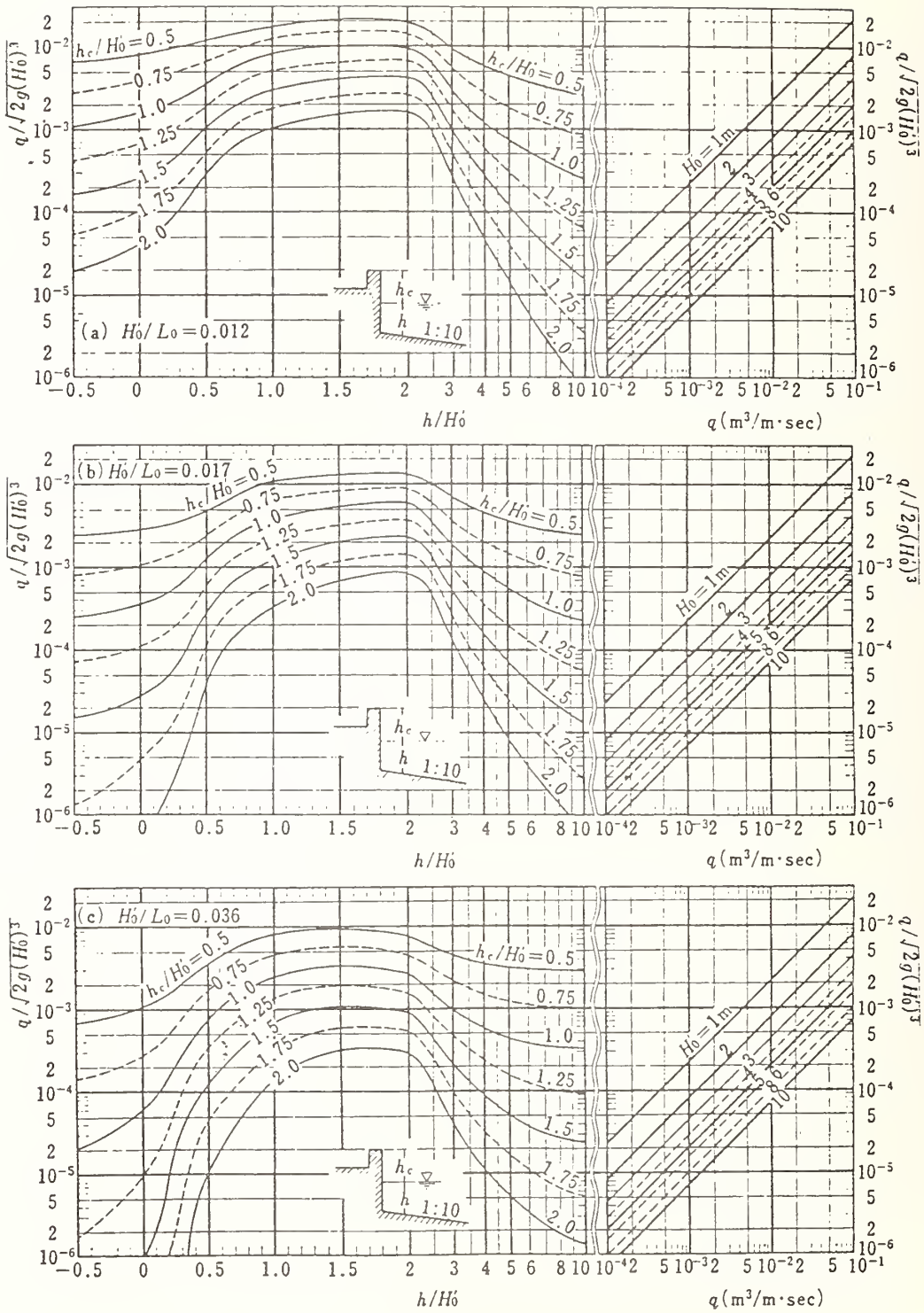

Figure 8. Relation between significant wave height (H_0') and the volume of wave overtopping (q)

Report of Task Committee

(A) STRONG-MOTION INSTRUMENT ARRAYS AND DATA

Date: May 19, 1982

Place: National Bureau of Standards, Washington, D.C., U.S.A.

Attendees: U.S. Side - A. G. Brady (Chairman)
W. B. Joyner
J. F. Lander

Japan Side - Setsuo Node (Chairman, Temporary)
Keiichi Ohtani

(1) Activities and Principal Accomplishments to Date

Catalogs of strong-motion earthquake records observed both in the U.S. and Japan are being exchanged. U.S. data are published in the "Seismic Engineering Program Report," and the Japanese data are reported in the publication, "Strong-Motion Earthquake Records in Japan."

The collection of reports on display at USGS will be forwarded to H. Tsuchida, Chairman, Japanese Task Committee, and Panel members (if available).

Specifications, description, and operator's manual for the USGS's GEOS system will also be exchanged.

Further information on the new JMA accelerograph and the MOC strong-motion accelerographs were exchanged.

We acknowledge the contribution of Exxon's collection of Japanese digitized data, with possibility of comparison studies with U.S. data (i.e., subduction zones vs. shallow earthquakes). Extra copies will be sent to interested members.

(2) Future Programs

Both sides of the task committee plan to continue their respective efforts in the following eight points:

a) After an earthquake which has caused damage to structures or an earthquake during which maximum acceleration exceeding about 0.1 G has been recorded, the task committee of a country where the earthquake has taken place will provide a list of the strong-motion earthquake records for the counterpart of the task committee. The list contains maximum component acceleration of each record. If there is such a list compiled by any organization, the list mentioned above may be replaced by it.

b) Every year the task committee will exchange catalogs of the strong-motion earthquake records in the last year. The catalog contains maximum component accelerations and wave forms of major records. If there is such a catalog compiled by any organization, the catalog mentioned above may be replaced by it.

c) The task committee makes appropriate arrangements to provide digitizable copies of records when they are requested. In addition, arrangements will be made to provide information on the characteristics of the site and structures at the locations where such records are obtained.

d) When the organizations taking part in the Panel publish reports on the strong-motion earthquake records, the organizations will distribute copies of the reports to the organizations of the Panel interested in them. The task committee exchanges lists of the organizations which wish to receive the reports.

e) Every year at the time of the Joint Meeting, the task committee exchanges lists of reports on the strong-motion earthquake records and on analysis of the records published in the last year. The list will cover all the reports on the above mentioned topics published by the organizations taking part in the Panel activities and as many reports as possible published by other organizations and universities.

f) The task committee will continue to exchange lists of digitized data on all the major strong-motion earthquake records in the form of lists, and exchange of digitized records in the form of computer magnetic tapes, cards, and other media will be continued.

g) The task committee plans to assist and cooperate, where possible, in the following areas:

    1) Assistance and cooperation with governmental organizations in other seismic areas, in order to promote high quality strong earthquake motion observations in all seismically active areas of the world.

    2) Assistance and cooperation with any international effort to record strong ground motion close to the source of a large magnitude shock.

h) The task committee feels the UJNR Panel on Wind and Seismic Effects should play a major cooperative role in the implementation of relevant parts of the Resolution of the International Workshop on Strong-Motion Earthquake Instrument Arrays held May 1978, in Honolulu, Hawaii. The exchange of complete information on all aspects of the program, as it develops particularly in Japan and the United States, will be carried out in the manner of our standard exchange when appropriate. Particularly with unique data from arrays, or deep bore-hole instruments in the U.S. and Japan, Task Committee Cochairmen will retain the responsibility of relaying information on their existence and subsequently of transferring the digital data from such institutions as in the U.S., the USGS, CDMG, USC; and, in Japan, PWRI, BRI, PHRI, MRI and NRCDP.

Report of Task Committee

(B) LARGE-SCALE TESTING PROGRAM

Date: May 20, 1982

Place: National Bureau of Standards, Washington, D.C., U.S.A.

Attendees: U.S. Side - Edgar V. Leyendecker (Chairman)
John B. Scalzi

Japan Side - Keiichi Ohtani (Chairman)
Masaya Hirosawa
Shin Okamoto
Shinsuke Nakata
Takashi Kaminosono

(1) Activities and Principal Accomplishments to Date

The main activities related to this task committee during the past year are as follows:

a) According to the recommendation of this task committee report, the Panel Cochairmen endorsed the program of the U.S.-Japan Joint Earthquake Research Program Involving Large-Scale Testing of Steel Structures to the Ministry of Construction and the National Science Foundation on May 22, 1981.

b) The testing of the seven-story reinforced concrete structure was completed in November 1981, at the Building Research Institute, Tsukuba Science City. All support tests to be carried out in Japan were also completed. The support tests in the U.S. are now under way.

c) Active exchange of U.S. and Japanese researchers has occurred under the reinforced concrete program and has been very useful.

d) The program on steel structures has been initiated. Full scale and support tests are being planned or are under way in Japan. In the U.S., the NSF has received proposals for the conduct of support tests. These proposals have been reviewed. Research projects will be funded prior to a scheduled Joint Technical Coordinating Committee (JTCC) meeting in July 1982.

(2) Future Programs

The status of the U.S.-Japan Joint Program of reinforced concrete structures was discussed, and the Joint Program of steel structures was reviewed. The task committee adopted the following resolutions as a result of discussion.

a) The JTCC will meet in Japan on July 14 under the auspices of the UJNR. The research program on steel structures (full-scale test in Japan and support tests in the U.S. and Japan) will be discussed. Experimental results from the reinforced concrete program as well as the exchange of data will be topics for discussion.

b) A more intensive study to understand reinforced concrete test data (full-scale and support tests), including repair and retrofit, should be undertaken in both countries.

c) Exchange of information between the U.S. and Japan on planned tests should take place before the July JTCC meetings.

d) Continuing personnel exchange is encouraged under the steel program.

e) The task committee will review progress of the Joint Research Program and continue to reassess the need for testing of other structures and report its findings and recommendations to the Panel. Increased research needs of masonry in Japan indicate that this construction should be reviewed for a possible coordinated research program. Accordingly, it is expected that related research and development will be actively continued in both countries. Technical exchange should be continued through this task committee. The following information will be exchanged:

    1) bibliography of research reports,
    2) copies of existing reports when possible, and
    3) background papers will be prepared to serve as a basis for developing future plans.

f) Exchange of information on large-scale testing facilities and large-scale testing programs should be encouraged.

Report of Task Committee

(C) REPAIR AND RETROFIT OF EXISTING STRUCTURES

Date: May 19, 1982

Place: National Bureau of Standards, Washington, D.C., U.S.A.

Attendees: U.S. Side - John B. Scalzi (Chairman)
Janina Mirski
Bruce Morgan

Japan Side - Masaya Hirosawa (Chairman)
Shinsuke Nakata

(1) Activities and Principal Accomplishments to Date

During the past three years, the task committee has held three workshops in Los Angeles, Tsukuba/Sendai, and San Francisco. All three workshops were very successful. At each workshop, participants presented technical papers and visited repaired buildings. The papers from the three meetings will be published during the summer of 1982 and distributed to participants and others interested in repair and retrofit of existing and damaged buildings. The cooperative nature of the workshops were very beneficial in the technical presentations, the technical study tours and the social activities which brought our representatives to a better understanding of each other's area of experience.

(2) Future Programs

The current U.S. Project Committee on Repair and Retrofit of Existing Structures will be discontinued for a period of time, and in the meantime the participants have agreed to exchange technical papers. It was agreed at the San Francisco Workshop (resolutions attached) to hold additional workshops after 1984.

Task Committee (C) will continue for future activities as noted below.

Task Committee (C) discussed the possibility of holding workshops on discussions of building codes in the next few years. The objective will be to compare design provisions and criteria for new construction, and the repair and retrofit of damaged and existing buildings. NSF will explore the mechanism of setting up an American project committee with an appropriate organization.

Attachment to Task Committee (C)

3rd U.S./Japan Workshop on
Repair and Retrofit of Structures

San Francisco, California
May 13-15, 1982

RESOLUTIONS

1. This meeting provided an extremely valuable exchange of technical information including:

   a) Research program for assessment method on inspection and repair/retrofiting of structures damaged by earthquakes.

   b) Examples of completed repair and strengthening for existing important structures.

   c) Various basic experiments and analyses on repair and retrofitting techniques.

2. However, it was recognized that many problems remained, especially on the establishing of objective seismic safety. There were few reports which showed the details of repair/retrofitting techniques and methods to evaluate their effect.

3. Accordingly, it is expected that related research and development will be actively continued in both countries. Technical exchange should continue through the task committee of the UJNR Panel on Wind and Seismic Effects. It is recommended that a full cooperative exchange be held after 1984. The following information could be exchanged:

   a) State-of-the-Art reports on:

      i) actual conditions on repair/retrofitting of existing structures,

      ii) actual conditions on repair/retrofitting of structures damaged by earthquakes, and

      iii) actual conditions on inspection of damaged structures.

   b) Data on rehabilitation techniques including their details and methods to evaluate their effectiveness.

   c) Proposals for assessment method on rehabilitation.

4. The reports presented in these three workshops will be published during the summer of 1982 and distributed to the workshop participants and the members of the UJNR Panel on Wind and Seismic Effects.

Report of Task Committee

(D) EVALUATION OF PERFORMANCE OF STRUCTURES

Date: May 20, 1982

Place: National Bureau of Standards, Washington, D.C., U.S.A.

Attendees: U.S. Side - G. Robert Fuller (Chairman)
Peter Gurvin
Stanley Takahashi
Michael Gaus
H. S. Lew
Richard McConnell
Peter Gergely

Japan Side - Shin Okamoto (Chairman, Temporary)
Takashi Kaminosono

(1) Activities and Principal Accomplishment to Date

The following activities have taken place in both countries concerning development of methodologies and procedures to evaluate seismic resistance of existing civil engineering structures and to provide damage assessment predictions for existing buildings and communities.

a) Japanese evaluation and strengthening procedures for reinforced concrete and structural steel building: copies were translated from Japanese into English, by the Office of International Affairs of HUD (OIA/HUD).

b) The set of 108 lecture slides furnished by Dr. Watabe were copied by the National Bureau of Standards. Other copies will be made by the National Science Foundation for distribution to other U.S. Federal agencies and submitted to the National Information Service for Earthquake Engineering at Berkeley, California. The accompanying Japanese narrative was translated into English by OIA/HUD.

c) Copies of "Learning from Earthquake Program" by the Earthquake Engineering Research Institute (EERI) were furnished to each side by Dr. M. Agbabian.

d) The U.S. Federal Interagency Committee on Seismic Safety in Construction (ICSSC) Subcommittee No. 3 on Existing Buildings has developed a draft standard, "Preliminary Evaluation Technique for Determining Seismic Resistance of Existing Buildings." When the final document is prepared, copies will be furnished to the Japanese side.

e) Several other documents were furnished to Mr. Fuller by a representative of the Japanese Ministry of Construction at the 13th Joint Panel Meeting. The following documents were translated into English by OIA/HUD. The National Bureau of Standards furnished copies to the Japanese side.

1) Examination and Improvement of Concrete Block Walls, Shizuoka Prefecture (14 pp.)

2) Necessary Procedures Prior to and During the Existence of the Building, Chapter IV. Based on Provisions of Construction Standard Act and Architects Act (40 pp.)

3) Re-Examination and Reinforcement of Your Home Against Earthquakes, Published by Department of Urban Housing, Shizuoka Prefecture (10 pp.)

4) Seismic Diagnosis of Reinforced Concrete Buildings, Department of Urban Housing, Shizuoka Prefecture (152 pp.)

5) Methods for Determining Earthquake Resistance and Earthquake-Proof Designs of Pre-Existing Steel-Skeleton Structures, Shizuoka Prefecture, December 1, 1979. Part I (107 pp.) and Part II (65 pp.)

(2) Future Programs

a) The task committee discussed the proposal to hold two workshops on "Evaluation of Performance of Existing Buildings for Resistance to Earthquakes." Preliminary plans were developed to hold the first workshop prior to the 15th Joint Panel Meeting, May 1983, in Tsukuba, Japan. Tentative plans are to have 16 papers (8 U.S. and 8 Japanese) presented at a two-day workshop. A draft proposal from Cornell University (Prof. Peter Gergely) to NSF to coordinate the proposed workshops and to publish a final report, was reviewed and discussed. Lists of suggested topics and speakers were also developed. Finally, a resolution was prepared for consideration by the Joint Panel.

b) Activities by U.S. Federal Agencies relative to structural performance evaluation, post-earthquake analysis, and instrumentation of existing buildings were discussed. Pertinent reports from the Veterans Administration and National Science Foundation will be furnished to each side.

c) The task committee reviewed and reaffirmed the 1979 "Scope for Evaluation of Performance of Structures" (attached). Recommendations considered critical will be used to formulate the scope and objectives of the proposed workshops.

Report of Task Committee

(E) LAND USE PROGRAMS FOR CONTROLLING NATURAL HAZARD EFFECTS

Date: May 20, 1982

Place: National Bureau of Standards, Washington, D.C., U.S.A.

Attendees: U.S. Side - G. Robert Fuller (Chairman, Temporary)

Japan Side - Toshio Iwasaki (Chairman)

(1) Activities and Principal Accomplishments to Date

On the activities and principal accomplishments of this task committee, the following were confirmed:

a) The exchange of papers and references on land use programs and the exchange of experts according to the resolutions of this task committee from the 8th through 13th Joint Panel Meetings, have been useful to both countries.

b) The Basic Plan and the Intensified Plan of the Japanese Government Large-Scale Earthquake Countermeasure Act (LSEC Act, Law No. 73, 1978) were presented. These plans are to provide earthquake disaster prevention measures for the Tokai Area, where a large earthquake (Tokai Earthquake) is expected to occur. The Japanese Government also initiated in 1981 a study of earthquake disaster prevention measures for the Southern Kanto Area, together with the Tokai Area.

c) Several earthquake disaster mitigation plans by various U.S. Federal agencies and State organizations were transmitted to Japan.

d) The Geophysical Survey Institute (GSI) of Japan has conducted a land condition survey at the Shizuoka and Enshu areas for use in reduction of highway hazards.

The Public Works Research Institute (PWRI) of Japan has completed maps of liquefaction risk for areas from Tohoku to Kyushu, and also presented procedures for evaluating direct and indirect losses from earthquake disasters.

The Building Research Institute (BRI) of Japan has prepared seismic microzonation maps of Tokyo and other large cities.

The National Research Center for Disaster Prevention (NRCDP) of Japan has studied the possibility of application of satellite remote sensing technology to estimate earthquake damage.

e) The U.S. Geological Survey (USGS) has also prepared similar seismic risk maps for the U.S.

(2) Future Programs

As a result of discussions, the task committee confirmed the following cooperative tasks:

a) The task committee will promote the exchange of the following technical information and materials:

1) earthquake disaster risk maps including socio-economic features, and an example for the case of the Urakawa-oki earthquake of March 21, 1982,

2) planning methodologies for earthquake disaster mitigation for large populated cities, and

3) information and materials on geological condition maps, soil liquefaction potential maps, and earthquake hazard risk maps, listed above.

b) The task committee encourages coordinated research, exchange of information and exchange of experts in the fields of land use programs for mitigating earthquake hazards.

c) The task committee also encourages formal review and commentary, by concerned governmental organizations in both countries, on methodologies and mapping which include earthquake hazard, microzonation, geological conditions and soil liquefaction potential affecting land use planning.

Report of Task Committee

(F) DISASTER PREVENTION METHODS FOR LIFELINE SYSTEMS

Date: May 19, 1982

Place: National Bureau of Standards, Washington, D.C., U.S.A.

Attendees: U.S. Side - C. F. Scheffy (Chairman)
T. Ariman
P. F. Krumpe

Japan Side - T. Okubo (Chairman, Temporary)
E. Nakamura

(1) Activities and Principal Accomplishments to Date

a) Principal activities were accomplished through correspondence between the chairmen during the past year. Especially, cooperative research was conducted through the formal exchange of experts between the U.S. and Japanese sides.

b) Activities on the Japanese Side:

1) Experimental studies on seismic behavior of buried pipes were conducted with the use of research facilities at PWRI.

2) For lifeline facilities, especially for telecommunication and supplying facilities, studies on development of retrofitting methods taking account of importance of the facilities were initiated in the fiscal year of 1981, and are continued.

3) Studies on development of assessment of damage and of restoration methods for seismically damaged lifeline facilities were initiated in the fiscal year of 1981. A survey of literature and examples of damage were conducted this fiscal year. The studies are scheduled to be accomplished in 5 years.

4) Damage investigation on the Urakawa-oki, Hokkaido earthquake of March 21, 1982, was conducted.

c) Activities on the U.S. Side: (primarily sponsored by the National Science Foundation)

1) Investigation of gas and oil pipeline damage caused by large ground deformations.

2) Performance of water supply and sewage lines under seismic excitation and their repair and rehabilitation.

3) Research on response of power and communication lines and equipment to ground shaking.

4) Seismic performance of piping systems in and connected to buildings.

5) General problems in repair and rehabilitation of lifeline systems after earthquakes.

(2) Future Programs

a) Correspondence and cooperative research should be continued through the exchange of experts to promote cooperative research studies of mutual benefit between the U.S. side and the Japanese side.

b) Early restoration of lifeline facilities damaged by earthquake is most basic and important for public life, and from this point of view, both the U.S. and Japanese sides promote research on development of restoration methods of damaged lifeline facilities.

c) Due to the fact that the lifeline facilities have multi-function and that their administration depends on many organizations concerned, Committee Chairmen will complete the establishment of a Planning Committee in each country by October 1, 1982.

Report of Task Committee

(G) WIND CHARACTERISTICS AND STRUCTURAL RESPONSE

Date: May 20, 1982

Place: National Bureau of Standards, Washington, D.C., U.S.A.

Attendees: U.S. Side - Richard Marshall (Chairman)
Michael Gaus
Peter Gurvin

Japan Side - Tadayoshi Okubo (Chairman, Temporary)

(1) Activities and Principal Accomplishments to Date

The task committee notes that:

a) strong winds frequently cause loss of life and extensive property damage,

b) the knowledge derived from the exchange of high wind data and information on wind effects can be useful in reducing loss of life and property damage,

c) insufficient knowledge exists on the effects of strong winds upon structures and methods for modeling these effects, and

d) the needs for wind data for various applications and new projects are increasing.

Several measurements of strong winds in atmospheric boundary layers and responses of structures, to which instruments are mounted, have been recorded.

The following information was agreed to be exchanged at this task committee meeting:

a) establishment of new standards for wind tunnel model test method of buildings in Japan,

b) minimum requirements for wind tunnel modeling as contained in ANSI A58.1-1982,

c) proceedings of the International Workshop on Wind Tunnel Modeling Criteria and Techniques in Wind Engineering Applications which was held in the U.S. in April 1982, and

d) mechanics of glass breakage due to wind loading.

(2) Future Activities

In view of the above items, the task committee hereby resolves to carry out the following programs:

a) Exchange observations and records of high wind data (including remote-sensing reports, i.e., aircraft, satellite) available from the respective national meteorological services and special observation sites.

b) Exchange available reports on high wind data and associated wind pressures. Documentation of instrument characteristics, exposure, and elevation above ground should be included.

c) Encourage the interaction between meteorologists and engineers to identify the types of wind data required for future use in establishing extreme wind distributions; in determining wind loadings on structures; in understanding the urban wind climate; and in considering structural design issues in the wind generation of energy.

d) Encourage the establishment of minimum requirements for the simulation of atmospheric boundary layers in wind tunnels, the exchange of boundary layer wind tunnel test results, and the exchange of information on instrumentation and methods of measurement. Also encourage the exchange of information on measurements made on actual structures and on comparisons with predictions from wind tunnel studies of these structures.

e) Exchange information on techniques and criteria for structural modeling in boundary layer wind tunnels.

f) Continue the exchange of engineers and meteorologists, and make available research facilities for mutual use.

Report of Task Committee

(H) SOIL BEHAVIOR AND STABILITY DURING EARTHQUAKES

Date: May 20, 1982

Place: National Bureau of Standards, Washington, D.C., U.S.A.

Attendees: U.S. Side - Mary Ellen Hynes-Griffin (Chairman, Temporary)
E. O. Pfrang
H. S. Lew
Riley Chung
William Kovacs
Felix Yokel
Stanley Takahashi
J. V. Tyrrell
A. H. Wu
M. Yachnis

Japan Side - Eiichi Taniguchi (Chairman, Temporary)
Toshio Iwasaki
Takahisa Mizuyama

(1) Activities and Principal Accomplishments to Date

a) Exchange of relevant documents on soil behavior during earthquakes, including reports on pile performance under cyclic loading, were made. Four papers were submitted to the Joint Meeting from the Japanese side and two papers were presented by the U.S. side.

b) Review of guidelines for assessing soil liquefaction in the U.S. and Japan will be continued. Reports on liquefaction evaluation for bridge design have been exchanged.

c) Mr. Takahashi of NCEL visited PWRI in September 1981, and had discussions with Japanese Panel Members on the methods to prevent liquefaction.

(2) Future Programs

a) When requested, the task committee will assist in arrangements for visits to earth embankments, including fill dams and foundations which have been subjected to significant ground motions.

b) Discussions and correspondence are being continued concerning soil liquefaction potential, seismically induced permanent displacement estimation of earth structures, standard penetration and cone testing, seismically induced settlements of soils and foundations, and stability of earth structures including tailing dams due to earthquake motions.

c) Efforts for comparing results of Standard Penetration Tests (SPT), as conducted in the U.S. with the results from Japan, will be continued.

d) Task Committee (H) recognizes the importance of the U.S.-Japan Cooperative Program on the response of semi-buried concrete structures due to earthquakes, and therefore recommends the Panel to consider the initiation of the abovementioned cooperative program.

Report of Task Committee

(I) STORM SURGE AND TSUNAMI

Date: May 20, 1982

Place: National Bureau of Standards, Washington, D.C., U.S.A.

Attendees: U.S. Side - Celso S. Barrientos (Chairman)
Eddie N. Bernard
James F. Lander
Gerald T. Hebenstreit

Japan Side - Setsuo Noda (Chairman, Temporary)

(1) Activities and Principal Accomplishments to Date

a) Two new members were added to the task committee:

U.S. Side - James F. Lander
Japan Side - Hideo Watanabe

b) A report on "Tsunami Research Opportunities" prepared by Dr. Bernard from a working group meeting was distributed to the task committee members. Related to this report, an ITSU resolution was approved in a Suva, Fiji meeting in April 1982, endorsing the basic plan of research included in the report.

c) A technical paper by Mr. Tanimoto was given to U.S. members. The paper deals with the hydraulic aspect of breakwater in Japan.

d) The U.S. is conducting a tsunami monitoring program off the Galapagos Islands using a pressure transducer at 4000, 20, and 1 meter depth.

(2) Future Programs

a) The task committee will facilitate the exchange of information related to storm surge and tsunami, such as publications concerning damages and measures to reduce or prevent damages. To enhance the continuation of the cooperative programs, the Chairmen of the task committee will consider taking the following steps:

1) Provide an overview of the activities of the United States and Japan in the area of forecasting, hindcasting, and risk analysis of storm surges and tsunamis as well as the planning and design of disaster prevention works. The overview will include a list of governmental agencies and other institutions concerned with storm surges and tsunamis.

2) Provide a technical review of research accomplishments in storm surges and tsunamis performed by the U.S. and Japan.

3) Exchange information on storm surge models as well as associated meteorological models, which are used for forecasting, planning, design, and disaster prevention purposes.

b) The task committee recommends that a U.S.-Japan tsunami workshop be organized to:

1) describe current research in each country,

2) discuss problems that are tractable with today's knowledge and technology including observations and verification of theory,

3) explore ways and means of increasing U.S.-Japan cooperation in tsunami research and technology transfer, and

4) explore ways of exchanging tsunami data between the U.S. and Japan and other disaster prone areas.

The workshop should be a two day meeting held prior to the 15th UJNR Meeting in Tsukuba, Japan.

Report of Task Committee

(J) WIND AND EARTHQUAKE ENGINEERING FOR TRANSPORTATION SYSTEMS

Date: May 19, 1982

Place: National Bureau of Standards, Washington, D.C., U.S.A.

Attendees: U.S. Side - James D. Cooper (Chairman)
Celso S. Barrientos
Mary Ellen Hynes-Griffin
John F. Fleming
E. V. Leyendecker
John B. Scalzi

Japan Side - Toshio Iwasaki (Chairman, Temporary)
Takahisa Mizuyama
Eiichi Taniguchi

(1) Activities and Principal Accomplishments to Date

Task Committee (J) was formally established at the 13th Joint Meeting held in May 1981, at Tsukuba, Japan. Recognizing the magnitude and scope of wind and earthquake problems relating to transportation structures, initial committee activities will be limited to investigating earthquake engineering problems associated with bridges. Research will be expanded to include wind and earthquake effects on transportation structures at a future date. The principal functions of the task committee are to encourage the performance of coordinated research studies of mutual interest between the Japanese and U.S. sides and exchange research information on a regular basis.

Principal activities during the past year included:

a) The selection of members for the Japanese and U.S. sides. They are:

Japanese Side: Nobuyuki Narita (Chairman), PWRI
Tadashi Arakawa, PWRI
Hideya Asanuma, PWRI
Toshio Iwasaki, PWRI
Shoichi Saeki, PWRI
Kunio Yamamoto, PWRI

U.S. Side: James D. Cooper (Chairman), FHWA
E. V. Leyendecker, NBS
H. S. Lew, NBS
John B. Scalzi, NSF
James H. Gates, CalTrans

b) A visit by Dr. Eiichi Kuribayashi to the U.S. in September 1981, for the purpose of discussing future coordinated research studies on the earthquake response and behavior of bridges.

c) The exchange of research reports on the earthquake vulnerability, design, and construction of bridges.

d) Detailed discussion of proposed coordinated experimental research studies on: (1) the performance of large-scale bridge piers and columns subjected to reversed cyclic loading; (2) model tests on the failure of reinforced concrete piers; and (3) the behavior of concrete-filled steel tubes.

(2) Future Programs

As a result of comprehensive discussions, the task committee hereby resolves to carry forth with the following programs:

a) Continue with experimental activities and studies on the earthquake behavior of reinforced concrete bridge piers and columns. Conduct of studies are to be coordinated through task committee chairmen.

b) Obtain data which are needed to examine the effects of dimension, axial force, shear strength, cross-sectional shape, splice length of bars, dynamic loading, and two dimensional loading on the earthquake performance of bridge columns and piers. Initially, effects of scale factor on axially loaded columns will be examined through the conduct of tests in the U.S. on full, 1/3, and 1/6 scale model columns. Details are to be worked out for the conduct of additional tests.

c) Conduct experimental studies in Japan on:

1) behavior of concrete-filled steel tubes,
2) dynamic behavior of reinforced concrete bridge piers, and
3) behavior of recently failed bridge pier types.

d) Encourage the conduct of coordinated long-range research and the exchange of results in the following areas: 1) design of superstructure details including connections between superstructure and substructure; 2) foundation design; 3) methods of testing (such as pseudo-dynamic vs. dynamic tests); 4) effect of phased ground motion on bridge response; and 5) field measurements of bridge response to dynamic loading.

e) Encourage the continued exchange of information between task committee members and researchers in the U.S. and Japan be carried out through the Panel on Wind and Seismic Effects of UJNR.

NBS-114A (REV. 2-8C)

U.S. DEPT. OF COMM. BIBLIOGRAPHIC DATA SHEET (See instructions)	1. PUBLICATION OR REPORT NO. NBS SP 651	2. Performing Organ. Report No.	3. Publication Date April 1983

4. TITLE AND SUBTITLE

Wind and Seismic Effects, Proceedings of the 14th Joint UJNR Panel Conference

5. AUTHOR(S)

Riley M. Chung, H.S. Lew, and William D. Kovacs, editors

6. PERFORMING ORGANIZATION (If joint or other than NBS, see instructions)

NATIONAL BUREAU OF STANDARDS
DEPARTMENT OF COMMERCE
WASHINGTON, D.C. 20234

7. Contract/Grant No.

8. Type of Report & Period Covered

Final

9. SPONSORING ORGANIZATION NAME AND COMPLETE ADDRESS (Street, City, State, ZIP)

National Science Foundation
Washington, D. C. 20550

10. SUPPLEMENTARY NOTES

Library of Congress Catalog Card Number: 83-600713

☐ Document describes a computer program; SF-185, FIPS Software Summary, is attached.

11. ABSTRACT (A 200-word or less factual summary of most significant information. If document includes a significant bibliography or literature survey, mention it here)

The 14th Joint Meeting of the U.S. – Japan Panel on Wind and Seismic Effects was held in Washington, D.C., United States from May 17 through 20, 1982. This publication, which is the proceedings of the Joint Meeting, includes the program, list of members, formal resolutions, technical papers, and the task committee reports. Subjects covered in the papers presented to the panel include: (1) characteristics of strong winds, (2) wind loads on structures and design criteria, (3) earthquake ground motions and dynamic analysis of embankment dams, (4) soil liquefaction study and methods to improve liquefaction resistance, (5) seismic loads on structures and design criteria, (6) stress analyses of pipelines during earthquakes, (7) full-scale seismic experiments, (8) earthquake hazard reduction program, (9) use of microcomputer for earthquake studies, (10) quantitative evaluation of damages caused by winds and earthquakes, and (11) tsunami research projects.

12. KEY WORDS (Six to twelve entries; alphabetical order; capitalize only proper names; and separate key words by semicolons)

accelerograph; codes; design criteria; disaster; earthquakes; earthquake hazards; geotechnical engineering; ground failure; liquefaction; pipeline; seismicity; solids; standards; structural engineering; structural response; tsunami; wind loads; winds.

13. AVAILABILITY

☒ Unlimited

☐ For Official Distribution. Do Not Release to NTIS

☒ Order From Superintendent of Documents, U.S. Government Printing Office, Washington, D.C. 20402.

☐ Order From National Technical Information Service (NTIS), Springfield, VA. 22161

14. NO. OF PRINTED PAGES

716

15. Price

USCOMM-DC 6043-P80

☆U.S. GOVERNMENT PRINTING OFFICE: 1983-380-997/5010

NBS TECHNICAL PUBLICATIONS

PERIODICALS

JOURNAL OF RESEARCH—The Journal of Research of the National Bureau of Standards reports NBS research and development in those disciplines of the physical and engineering sciences in which the Bureau is active. These include physics, chemistry, engineering, mathematics, and computer sciences. Papers cover a broad range of subjects, with major emphasis on measurement methodology and the basic technology underlying standardization. Also included from time to time are survey articles on topics closely related to the Bureau's technical and scientific programs. As a special service to subscribers each issue contains complete citations to all recent Bureau publications in both NBS and non-NBS media. Issued six times a year. Annual subscription: domestic $18; foreign $22.50. Single copy, $5.50 domestic; $6.90 foreign.

NONPERIODICALS

Monographs—Major contributions to the technical literature on various subjects related to the Bureau's scientific and technical activities.

Handbooks—Recommended codes of engineering and industrial practice (including safety codes) developed in cooperation with interested industries, professional organizations, and regulatory bodies.

Special Publications—Include proceedings of conferences sponsored by NBS, NBS annual reports, and other special publications appropriate to this grouping such as wall charts, pocket cards, and bibliographies.

Applied Mathematics Series—Mathematical tables, manuals, and studies of special interest to physicists, engineers, chemists, biologists, mathematicians, computer programmers, and others engaged in scientific and technical work.

National Standard Reference Data Series—Provides quantitative data on the physical and chemical properties of materials, compiled from the world's literature and critically evaluated. Developed under a worldwide program coordinated by NBS under the authority of the National Standard Data Act (Public Law 90-396).

NOTE: The principal publication outlet for the foregoing data is the Journal of Physical and Chemical Reference Data (JPCRD) published quarterly for NBS by the American Chemical Society (ACS) and the American Institute of Physics (AIP). Subscriptions, reprints, and supplements available from ACS, 1155 Sixteenth St., NW, Washington, DC 20056.

Building Science Series—Disseminates technical information developed at the Bureau on building materials, components, systems, and whole structures. The series presents research results, test methods, and performance criteria related to the structural and environmental functions and the durability and safety characteristics of building elements and systems.

Technical Notes—Studies or reports which are complete in themselves but restrictive in their treatment of a subject. Analogous to monographs but not so comprehensive in scope or definitive in treatment of the subject area. Often serve as a vehicle for final reports of work performed at NBS under the sponsorship of other government agencies.

Voluntary Product Standards—Developed under procedures published by the Department of Commerce in Part 10, Title 15, of the Code of Federal Regulations. The standards establish nationally recognized requirements for products, and provide all concerned interests with a basis for common understanding of the characteristics of the products. NBS administers this program as a supplement to the activities of the private sector standardizing organizations.

Consumer Information Series—Practical information, based on NBS research and experience, covering areas of interest to the consumer. Easily understandable language and illustrations provide useful background knowledge for shopping in today's technological marketplace.

Order the **above** *NBS publications from: Superintendent of Documents, Government Printing Office, Washington, DC 20402.*

Order the **following** *NBS publications—FIPS and NBSIR's—from the National Technical Information Service, Springfield, VA 22161.*

Federal Information Processing Standards Publications (FIPS PUB)—Publications in this series collectively constitute the Federal Information Processing Standards Register. The Register serves as the official source of information in the Federal Government regarding standards issued by NBS pursuant to the Federal Property and Administrative Services Act of 1949 as amended, Public Law 89-306 (79 Stat. 1127), and as implemented by Executive Order 11717 (38 FR 12315, dated May 11, 1973) and Part 6 of Title 15 CFR (Code of Federal Regulations).

NBS Interagency Reports (NBSIR)—A special series of interim or final reports on work performed by NBS for outside sponsors (both government and non-government). In general, initial distribution is handled by the sponsor; public distribution is by the National Technical Information Service, Springfield, VA 22161, in paper copy or microfiche form.

U.S. Department of Commerce
National Bureau of Standards

Washington D.C. 20234
Official Business
Penalty for Private Use $300

POSTAGE AND FEES PAID
U.S. DEPARTMENT OF COMMERCE
COM-215

SPECIAL FOURTH-CLASS RATE
BOOK